50th Anniversary Edition

Edited by:
A. Siegmund, S. Alam, J. Grogan,
U. Kerney, and E. Shibata

TMS

Springer

The Minerals, Metals & Materials Series

GCRIS

A. Siegmund · S. Alam · J. Grogan · U. Kerney · E. Shibata
Editors

PbZn 2020: 9th International Symposium on Lead and Zinc Processing

GCRIS

TMS

Springer

Editors
A. Siegmund
LanMetCon LLC
Lantana, TX, USA

J. Grogan
Gopher Resource
Eagan, MN, USA

E. Shibata
Tohoku University
Sendai, Japan

S. Alam
University of Saskatchewan
Saskatoon, SK, Canada

U. Kerney
Recylex
Nordenham, Germany

ISSN 2367-1181 ISSN 2367-1696 (electronic)
The Minerals, Metals & Materials Series
ISBN 978-3-030-37069-5 ISBN 978-3-030-37070-1 (eBook)
https://doi.org/10.1007/978-3-030-37070-1

© The Minerals, Metals & Materials Society 2020
This work is subject to copyright. All rights are reserved by the Publisher, whether the whole or part of the material is concerned, specifically the rights of translation, reprinting, reuse of illustrations, recitation, broadcasting, reproduction on microfilms or in any other physical way, and transmission or information storage and retrieval, electronic adaptation, computer software, or by similar or dissimilar methodology now known or hereafter developed.
The use of general descriptive names, registered names, trademarks, service marks, etc. in this publication does not imply, even in the absence of a specific statement, that such names are exempt from the relevant protective laws and regulations and therefore free for general use.
The publisher, the authors and the editors are safe to assume that the advice and information in this book are believed to be true and accurate at the date of publication. Neither the publisher nor the authors or the editors give a warranty, expressed or implied, with respect to the material contained herein or for any errors or omissions that may have been made. The publisher remains neutral with regard to jurisdictional claims in published maps and institutional affiliations.

This Springer imprint is published by the registered company Springer Nature Switzerland AG
The registered company address is: Gewerbestrasse 11, 6330 Cham, Switzerland

Preface

Lead–Zinc 2020 (PbZn 2020) is the ninth symposium of the Lead–Zinc conference series organized by multiple metallurgical societies worldwide, which is devoted to the theory and practice of the Lead and Zinc extractive metallurgy. This year's conference celebrates its 50th anniversary and continues a conference series originally initiated as a decennial symposium by the American Institute of Mining, Metallurgical, and Petroleum Engineers (AIME) with the pioneer first meeting in St. Louis in 1970, and subsequent conferences organized by The Minerals, Metals & Materials Society (TMS) in Las Vegas in 1980, Anaheim in 1990, Pittsburgh in 2000, and Vancouver in 2010. Throughout that time, other international societies have also offered major Lead–Zinc meetings, including the Metallurgy & Materials Society of the Canadian Institute of Mining, Metallurgy and Petroleum (MetSoc) in 1998 and 2008, the Mining and Materials Processing Institute of Japan (MMIJ) in 1995 and 2005, and the Gesellschaft der Metallurgen und Bergleute (GDMB) in 2015. The PbZn 2020 symposium is organized by TMS and held in conjunction with the TMS 2020 Annual Meeting & Exhibition, the premier annual event of The Minerals, Metals & Materials Society. It is co-sponsored by the other three international society members of the Lead–Zinc conference series: MetSoc, GDMB, and MMIJ. It is also the first time that the Lead–Zinc conference series received enhanced involvement from the Chinese lead and zinc industry through the active support for the PbZn 2020 symposium by the Nonferrous Society of China (NFSoc). Pooling the resources of TMS and the close sponsorship of MetSoc, GDMB, and MMIJ as well as the co-organization of NFSoc were an imperative and effective approach to offering a meeting of the highest value and quality, and making the PbZn 2020 an efficient, productive, and attractive event. With the global consolidation of the lead and zinc industry, it is important that the different metallurgical societies worldwide are working together in order to avoid conferences scheduled too close together as well as overlapping. Taking into consideration that the market for lead and zinc production and consumption has dramatically shifted during the last two decades, the four society members invited NFSoc to become a permanent member of the Lead–Zinc conference series at the PbZn 2020

symposium. With that, I am happy to announce that the next PbZn symposium in 2023 will be organized and held by NFSoc in China.

Lead–Zinc 2020 will provide an international forum for the lead and zinc processing industries bringing together operators, engineers, and researchers to exchange information regarding all aspects of current processing technologies for primary and secondary lead and zinc, as well as emerging technologies for both metals. The symposium scope extends from process fundamentals to operational practices and also includes the important aspect of environmental issues. At the operation's level, comprehensive reviews of the major applications of both metals are outlined. Emphasis will be placed on the recent commercial developments with less energy intensive technologies which are in harmony with environmental conservation. At the research level, the emphasis is placed on a better understanding of existing technologies and the development of new processing concepts. Environmental concerns that are associated with the processing of both metals are considered, along with acceptable treatment and handling of by-products, wastes, and bleed streams by the industry. A highlight of the conference will be a series of plenary lectures by industry leaders offering overviews of economical, environmental, and marketing topics.

The proceedings volume of the Lead–Zinc symposium is the culmination of more than one year of work, which includes the preparation of the papers by the authors, as well as editing and reviewing by the editors and volunteers. The proceedings volume contains papers from 20 countries divided into three plenary sessions and 20 technical sessions and is a reflection of all aspects of lead and zinc processing, including the global business trends of the metals, plant operations, fundamental developments, emerging technologies, and environmental considerations. It is the editors' sincere hope that the proceedings volume will remain a valuable record of the Lead–Zinc 2020 symposium and that it will become a standard reference for the processing of lead and zinc.

The production of the proceedings volume was a major undertaking, and many individuals were involved over the course of several months. The editors would like to extend their sincere appreciation to Dr. Stuart Nicol, Dr. Alexandra Anderson, and Josh Montenegro (all Gopher Resources); Dr. Christina Meskers and her team at Umicore; Fiseha Tesfaye/Abo Akademi University; Dr. Prabhat Tripathy/Idaho National Laboratory; and Dr. Dean Gregurek/RHI Magnesita GmbH for volunteering and their valuable work in reviewing papers, as well as Kelcy Wagner and Trudi Dunlap from TMS for their assistance in the production of the proceedings volume of the Lead–Zinc 2020 symposium.

Andreas Siegmund
Conference Chair

Contents

Part I Lead and Zinc Future Outlook: Plenary Session

Evolution of Global Secondary Lead Production 3
Huw Roberts

Part II PbZn Process Fundamentals I

Refractory Challenges in Lead and Zinc Furnaces 19
D. Gregurek, K. Reinharter, J. Schmidl and A. Spanring

Numerical Simulation of Gas–Liquid Flow Mixing Effect in Bottom-Blown Bath 31
Dong-bo Li, Peng Li, Xin Yao, Cheng Liu and Ze-shang Dong

Slag Reduction Kinetics of a Lead Slag from a Secondary Lead Smelter 41
Stuart Nicol, Joseph Grogan, Boyd Davis and Trevor Lebel

Phase Evolution During the Oxidation Process of Low Grade Lead–Zinc Oxide Ore 51
Hai-Peng Gou, Kuo-Chih Chou, Zhong-Ye Pei, Song-xuan Chen, Xue-gang Chen and Ming-chuan Li

Part III Secondary Zinc I

A New Era in Smelting Sustainability—Intensification of the Outotec® Ausmelt Top Submerged Lance (TSL) Process for Zinc Production 63
Jacob Wood, David Wilson and Stephen Hughes

Production of SHG Zinc From 100% Recycled Materials 75
John F. Pusateri, J. R. de Wet and Brandon Tirpak

Recent Development of EAF Dust Treating at Shisaka Smelting Co., Ltd. 91
S. Takaya, N. Kubota, H. Watanabe and T. Kudo

Part IV Zinc Electrowinning

Current Efficiency Increase in Zinc Electrodeposition at Cajamarquilla Refinery 101
Juliano Alves de Lima, Eder Lucio Martins, Gian Piero Pajuelo Gonzales and Tone Takayama Filho

To Polarize or Not to Polarize: Practical Advice on How to Control Zinc Electrodeposition 111
Michael Moats and Timothy Hymer

Optimizing Additive Ratios in Alkaline Zincate Electrodeposition 123
Margaret Scott and Michael Moats

Part V Primary Lead I

Lead Metal Production at Paroo Station Mine Using Leach-Electrowinning Process in Methane Sulfonic Acid Solution 135
David Dreisinger, Ken Baxter, Andrew Worland, Tom Cooper, Tony Cau and Nick Waters

Lead Plant Transformations 165
A. Liu, M. E. Reed, R. Close and L. Thompson

Reduction of Lead-Rich Slags with Coke in the Lead Blast Furnace . . . 173
Robin Vanparys, Geoffrey Brooks, M. Akbar Rhamdhani and Tijl Crivits

Installation of a Brown Field Slag Reduction Furnace: State of the Art Off-Gas Treatment with Dry Gas Cleaning for SO_2 Capture 187
Peter Weber, Dirk Behrmann, Thomas Breuer and Rüdiger Margraf

Application of CSC Technology in Nonferrous Metallurgy 201
Xiaosong Wu

Part VI Primary Zinc I

Start-up and Improvements of the New Electrolysis Plant at Annaka Refinery 221
Takuhiro Yamaguchi

Zinc Recovery of Low Grade Concentrate from Vazante Mine by the Waelz Process 231
Fabiana M. Teixeira, Júlia M. Martins, Eder L. C. Martins, Pablo S. Pina, Thiago O. N. Leite, Sérgio A. Penchel Jr. and Tone Takayama

A Dynamic Model of a Submerged Plasma Slag Fuming Process 237
Samant Nagraj, Mathias Chintinne, Muxing Guo and Bart Blanpain

Increase in Zinc Recovery from a Silicate Concentrate by Pre-neutralization Process 247
Maria José Dias, Adelson Dias de Souza, Caio César Spindola de Oliveira, Daniel Dayrell Pereira and Mateus Felipe Lourêdo Araújo

Recovery of Lead from Zinc Plant Residue by Alkaline Leaching Process Followed by Cementation 253
Jonghyun Kim, Min-seuk Kim, Kyeong Woo Chung, Kurniawan and Jae-chun Lee

Zinc Residue Fuming Process in Side-Submerged Combustion Furnace + Fuming Furnace 265
Liang Xu and Shaobin Ma

A Critical Review on Generation, Characteristics, and Utilization of Zinc Slag 275
Yan Song, Weiguo Wu, Liang Xu, Xiangqiang Chen and Ge Zhang

Part VII PbZn Process Technologies

Contributions of Non-ferrous Smelters to Metal Resource Circulation in Japan 285
Etsuro Shibata

The Process and Application of Oxygen-Enriched Air Side Blown Smelting of Lead–Zinc Materials 291
Ling Zhang, L. Zhang and Y. He

New Ideas for the Design of Green Smelting Project of Domestic Lead and Zinc Resources 301
Cui Chen, Xingmin He and Hua Bai

Evaluation and Certification Strategies for Lead–Zinc-Bearing Residues 309
J. Antrekowitsch and G. Hanke

Part VIII Primary Lead II

KCM—Innovator in the Pb Metal Production Through Ausmelt Technology and Variable SO_2 Concentration Off-Gas Utilization 321
Nikolay Starev and Georgi Doganov

The Latest Development of Oxygen Bottom Blowing Lead Smelting Technology 327
Weiguo Wu, Pengfei Xin and Jianming Wang

Characterization of Phase Equilibria and Thermodynamics with Integrated Experimental and Modelling Approach for Complex Lead Primary and Recycling Processing 337
E. Jak, M. Shevchenko, D. Shishin, T. Hidayat and P. C. Hayes

Resource Efficiency Evaluation of Pyrometallurgical Solutions to Minimize Iron-Rich Residues in the Roast-Leach-Electrowinning Process 351
A. Abadías Llamas, N. J. Bartie, M. Heibeck, M. Stelter and M. A. Reuter

Zinc Plant Expansion and Modification for Increased Metals Recovery 365
Björn Saxén, Florentino Estrada, Maciej Wrobel and Marko Lahtinen

Experience with Digital Process Optimization of Zinc Roasting Plants 377
Robert Schiemann, Steffen Haus, Marcus Runkel and Jörg Hammerschmidt

Part IX Zinc Leaching and Fe-Control I

Smelting Jarosite and Sulphur Residue in a Plasma Furnace 391
Justin Salminen, Jens Nyberg, Matej Imris and Bror Magnus Heegaard

Simulation of an Alternative Direct Leaching Process for High Iron Content Zinc Concentrates 405
Caio Cesar Spindola de Oliveira and Daniel Dayrell Pereira

Part X PbZn Process Fundamentals II

Lead and Zinc Extractive Metallurgy Research in the Kroll Institute for Extractive Metallurgy 419
Patrick R. Taylor

Electrochemical Extraction of Pb and Zn from Raw Mineral Materials Using Sulfurgraphite Electrode 429
R. Kh. Sharipov, U. A. Balgimbaeva and E. N. Suleimenov

Characterization and Processing of Residues from Hydrometallurgical Zinc Smelters 437
J. Antrekowitsch and G. Hanke

Leaching of Turkish Oxidized Pb–Zn Flotation Tailings by Inorganic and Organic Acids 447
Muammer Kaya, Sait Kursunoglu, Shokrullah Hussaini and Erkan Gül

Numerical Simulation of Gas-Particle Two-Phase Chemical Reactions and Key Structure Optimization in the Lead Flash Smelting Furnace 469
Kaile Tang, Ling Zhang, Leru Zhang and Fubing Tu

Effect of Alumina Ceramics Surface Condition on the Wetting of Liquid Lead 479
Zhen Qi and Zhang Fu Yuan

Part XI PbZn Sustainability

Material Stewardship for Zinc 491
Sabina Grund and Eric van Genderen

Effect of Deposit Types, Mine Development and Industry Structure on Primary Lead and Zinc Economics in Australia, North America and Europe 507
L. Reemeyer

Part XII By-Product Recovery I

Hydrometallurgical Recovery of Tin from Harris Dross 519
Ryosuke Sato, Koichiro Hirata and Fumito Tanaka

Pb and Other Impurities Recovery from Cu Smelting Residues in JX Nippon Mining & Metals 531
Nobuaki Okajima, Takuma Takei and Shojiro Usui

Pyrometallurgical Recovery of Valuable Metals from Flue Dusts of Copper Smelter Through Lead Alloy 539
Wenzhao Cui, Mao Chen and Baojun Zhao

Part XIII Secondary Lead

Operational Overview of RSR North America Corp. 551
Timothy W. Ellis, Mark A. Drezdzon and Travis Hesterberg

Refractory Solutions by Laboratory Tests and Fieldworks for Lead Recycling Applications 557
K. Reinharter, D. Gregurek, A. Spanring and Camille Fleuriault

Influence of Minor Elements in Waste Lead Battery Recycling 569
Yusuke Sakata

The FAST Pb Process and Its Impact on Secondary Lead Production 581
Massimo Maccagni and Edoardo Guerrini

Recent Improvements at Hosokura Lead Smelter and Refinery 593
H. Nakano, S. Ito, S. Abe and N. Hasegawa

Refractory Corrosion Comparison Through a Rotary Drum Furnace Slag Test for the Lead Industry 605
D. Fonseca, A. Spanring, F. Elias and G. Gonçalves

Part XIV Lead and Zinc Sustainability and Social License: Plenary Session

Regional Changes in Refined Zinc Output and Demand 615
Claire Hassall

Part XV Mineral Processing

A New Innovative Method of Flotation Separation for High Sulfur Lead–Zinc Sulfide Ore 625
Changtao Wang, Runqing Liu, Wei Sun, Yuehua Hu and Zhangyuan Ni

A Novel Collector 5–(Butylthio)–1,3,4–Thiadiazole–2–Thiol: Synthesis and Improved Flotation of Galena and Sphalerite from Pyrite 633
Wanjia Zhang, Zhiyong Gao, Runqing Liu, Haisheng Han, Pan Chen, Yue Yang, Lei Sun, Chenyang, Zhang, Yuehua Hu, Jian Cao and Wei Sun

Part XVI By-Product Recovery II

The Recovery of Pb and Zn in Antimony Smelting Slag 653
Pengfei Xin, Junyan Wei, Liang Xu, Weiguo Wu and Dailong Lan

Studies on the Formation of Intermetallic Compound Layers in Co(W)–Zn Diffusion Couples 661
Tamara Ebner, Nadine Körbler, Stefan Luidold, Christoph Czettl and Christian Storf

Effect of Oxidation of Zinc Powder on Purification of High-Cobalt and High-Germanium Zinc Sulfate Solutions 673
Leixia Zheng, Zhiwei Peng, Liancheng Wang, Lei Yang, Jie Wang, Wenxing Shang, Mingjun Rao, Guanghui Li and Tao Jiang

Part XVII Environmental and Safety Practices I

ILTEC Technology—New Pathways Towards Safe and Effective Cooling 683
Andreas Filzwieser, Martina Hanel, Hans-Jörg Krassnig, Rolf Degel, Timm Lux and Alexander Bergs

Review of Waste Water Treatment Technologies Used in Lead Recycling 695
James Dahlstrom, Joseph Grogan and Benjamin Rodrigue

Optimization of Arsenic Removal Process in Waste Acid from Zinc Smelting Plant Based on Orthogonal Experiment 707
Tianqi Liao, Yongguang Luo, Hongtao Qu, Te Zhang, Jing Li, Yunhao Xi, Jingtian Zou, Libo Zhang and Kaihui Cui

Part XVIII Lead Refining

Driving Innovation in Lead Batteries: The Focus of the Consortium of Battery Innovation 721
Matthew Raiford

New Technology for Copper Removal from Lead by Application of Aluminium: Practical Problems 729
Andrzej Cybulski

Processing of Polymetallic Materials Requires Flexible and Capable Downstream Refining Technology: Aurubis Lead Refinery as Economic, Modern, and Well Integrated Plant at the Site Hamburg 739
Christoph Zschiesche and Ino Bauer

Tin Treatment in Kosaka Lead Smelting 759
K. Miwa, E. Yamaguchi and S. Satoh

True Traceability Enabled by In-Line Laser Marking of Lead and Zinc Ingots 767
Alex Fraser and Jean-Michaël Deschênes

Advanced Technologies Reliant on the Properties of Lead 777
Timothy Ellis, Travis Hesterberg and Mark Drezdzon

Part XIX Secondary Zinc II

The EZINEX® Process for Secondary Zinc Bearing Materials 785
Massimo Maccagni and Edoardo Guerrini

Technologies for Treatment of Zinc-Containing Waste from Metallurgy in KCM AD 799
Stefan Stoychev, Emil Minchev, Aleksander Kyurkchiev and Georgi Radonov

Zinc Reduction/Vaporisation Behaviour from Metallurgical Wastes 811
Timothy Kerry, Alexander Peters, Evangelos Georgakopoulos, Ashkan Hosseini, Erik Offerman and Yongxiang Yang

Recycling of Zinc from Galvanized Steel Scrap 821
Shafiq Alam, V. I. Lakshmanan and R. Sridhar

Part XX Zinc Leaching and Fe-Control II

A New Route for Treating Neutral Leaching Residue 827
Caio César Spindola de Oliveira, Daniel Dayrell Pereira, Felipe Ramos Pereira Mendes and Mateus Felipe Louredo Araujo

Study of a Novel Chloride Volatilization Process for the Treatment of Jarosite Residue 835
H. B. Wang, C. Z. Zheng and S. C. Qin

Magnetic Separation of Iron Ion from Leaching Solution by Magnetic Seeding in Hydrometallurgy 847
Tong Yue, Haisheng Han, Wei Sun, Yuehua Hu, Zhiyong Gao, Runqing Liu, Li Wang, Lei Sun and Honghu Tang

Experimental Study on Pressure Leaching of Zinc Sulfide Concentrate and Discussion on the Latest Relevant Progress 853
Haibei Wang, Shuchen Qin, Kaixi Jiang and Bangsheng Zhang

Recent Operational Improvements of Hematite Plant at Akita Zinc Co., Ltd. 865
Dai Matsuura, Yasuo Usami and Kenji Ichiya

The Analysis of Fe Behavior in Zinc Pressure Leaching 877
Longyi Chen

Part XXI Zinc Hydrometallurgy

Development of the New Zinc-Separation Process for the Blast Furnace Dust 885
Mariko Shinoda, Toyoshi Yamaguchi, Ryota Murai, Goro Okuyama and Ikuhiro Sumi

Outotec Gypsum Removal Circuit and Outotec Cooling Tower Performance in Neutral Solution Cooling 891
Tuomas Hirsi and Björn Saxen

Purification and Comprehensive Recovery Metal Values from Zinc Hydrometallurgical Solution 899
Yue Yang, Shaole Song, Honghu Tang, Li Wang, Wei Sun and Yuehua Hu

Refining of Zinc Chloride by the Combination of Cementation Reaction and Vacuum Distillation 905
Gen Kamimura and Hiroyuki Matsuura

Advanced Concept "Poly Metallurgical Refinery" Developed by Cobre Las Cruces 913
Carlos Frias, Joaquin Gotor, Francisco Sanchez, Jorge Blanco, Natalia Moreno and Edward Vera

Part XXII Environmental and Safety Practices II

A New Lead Cementation Equipment and Lead Recovery Process in Chloride Media Developed by Cobre Las Cruces 925
Carlos Frias, Juan Pedro Soler, Jorge Blanco, Luis Pastor and Natalia Moreno

Performance and Mechanism of Chlorine Removal in Wastewater by Combination of $CuSO_4$ and Zero-Valent Copper 935
Yongguang Luo, Hongtao Qu, Yunhao Xi, Jingtian Zou, Te Zhang, Jing Li, Libo Zhang and Tianqi Liao

A Review on Recycling Technologies and Product Life Cycle Issues of Zinc and Lead 947
Syeda Afsara

Part XXIII Poster Session

Reaction Mechanism on a Novel Enhanced Smelting Technique for Lead-Acid Battery Paste Recycling 961
Wei Jin, Shenghai Yang, Yongming Chen, Yafei Jie, Shufeng Liu, Xinjie Deng, Yan Xi, Di Chang, Fang Hu and Yun Li

Author Index 971

Subject Index 975

GCRIS

About the Editors

Andreas Siegmund studied metallurgical engineering at the Technical University of Berlin, Germany where he received his Masters degree in 1985 and his Doctorate degree in 1989. He then joined Lurgi Metallurgie GmbH where he was involved in the design, commissioning, and operation of non-ferrous metals plants and progressed to Head of Non-ferrous Process Department. In 1998, he joined RSR Technologies, Inc. in Dallas, Texas, as Manager of Research and Development before becoming Vice President focusing on projects for lead recovery from secondary and primary sources and working with anodes for Cu- and Zn-electrowinning. In 2004, he became President of Quemetco Metals Ltd., a company manufacturing permanent lead alloy anodes. In 2008, he established his own consulting company LanMetCon LLC. From 2010 to 2014, he was also the Senior Vice President Process Technology and partner at Gas Cleaning Technologies, providing services to the process design and all aspects of pyrometallurgical and hydrometallurgical applications for primary and secondary metals processing. Since 2015, he has devoted his business activities exclusively to his consulting company LanMetCon LLC. He has worked on multiple pyrometallurgical and hydrometallurgical projects for metal producers and engineering firms related to the copper, lead, zinc, and ferro nickel industry. This includes engineering activities from initial studies to project execution with respect to greenfield projects as well as brownfield plant optimization, modernization, and

expansion. His expertise consists of metal production, gas handling and treatment, by-product recovery, and wastewater treatment. He provides services and advice from operator to executive management level. He is an active member of GDMB in Germany and of TMS in the USA and has served in several committees of both organizations. He also was a co-organizer of PbZn 2000 and PbZn 2005, chairman of PbZn 2010, and has been involved in the organization of other symposia worldwide.

Shafiq Alam is an associate professor at the University of Saskatchewan, Canada. He is an expert in the area of mining and mineral processing with profound experience in industrial operations, management, engineering, design, consulting, teaching, research, and professional services. As a productive researcher, he has secured two patents and has produced over 170 publications. He is the co-editor of eight books and an associate editor of the *International Journal of Mining, Materials and Metallurgical Engineering*. He is the winner of the 2015 Technology Award from the Extraction & Processing Division (EPD) of The Minerals, Metals & Materials Society (TMS).

With extensive relevant industry experience as a registered professional engineer, he has worked on projects with many different mining industries. He is an executive committee member of the Hydrometallurgy Section of the Canadian Institute of Mining, Metallurgy and Petroleum (CIM). During 2015–2017, he served as the Chair of the TMS Hydrometallurgy and Electrometallurgy Committee. He is a co-organizer of many symposia at international conferences through CIM and TMS. He is one of the founding organizers of the Rare Metal Extraction & Processing symposium at TMS. He was involved in organizing the International Nickel–Cobalt 2013 symposium and the TMS 2017 Honorary Symposium on Applications of Process Engineering Principles in Materials Processing, Energy, and Environmental Technologies. He is also involved in organizing the Rare Metal Extraction & Processing Symposium at the TMS 2020 Annual Meeting and Exhibition in San Diego, California.

Joseph Grogan is a metallurgist in the recycling and mining industries. His current role is Vice President of Research and Development at Gopher Resource, one of the largest lead battery recyclers in North America, producing over 300,000 tons of lead alloy per year. There he focuses on improved and more productive technologies to recycle batteries, including furnace technologies and robotic automation.

He was born and raised in Ireland and received his Bachelors (Honors) in Environmental Geochemistry from University College Dublin. Prior to moving to the USA, he worked at SRK Consulting in Wales as a consultant engineer on copper, gold, and uranium projects which were located mostly in Africa. During this time, he earned his Masters in Minerals Engineering from the Camborne School of Mines, England, and was sponsored by the Federation of European Mining Programs where he also studied in Aachen, Wroclaw, and Helsinki. In 2014, he was awarded his Doctorate in Metallurgical Engineering from the Colorado School of Mines, USA, where he researched galvanized scrap recycling and zinc hydrometallurgy.

As an active member of the Minerals & Metallurgical Processing Division of SME and the Extraction and Processing Division of TMS, he is both an associate editor of the SME *Journal of Minerals, Mining and Exploration* and the TMS Pyrometallurgy Committee's advisor for *JOM*. He is a co-author of over twenty journal articles and conference papers.

Ulrich Kerney studied non-ferrous metallurgy at the Technical University of Aachen in Germany between 1977 and 1982. In 1987, he finished his doctoral thesis about the investigations of physical properties of manganese base alloys. In July 1987, he joined Preussag's metallurgical R&D department and became responsible for the department's high purity and special metals production. With the formation of Metaleurop (now Recylex) in 1988, his work focused on environmental technologies especially in metal production and hot dip galvanizing.

In 1995, He left research activities and took over the responsibility for the Waelz kiln operation of Harz-Metall GmbH. In 1999, he became technical director of all Goslarian Zinc activities including the operation of the last New Jersey retorts, the Contop smelter, and the Zinc oxide line in Harlingerode.

In 2003, He switched his activities from zinc to lead and moved to Nordenham. Since then, he has been the technical director of Weser-Metall's Pb smelter first responsible for production, now for maintenance and general services.

His activities for the German Society for Non-Ferrous Metallurgy and Mining (GDMB) cover three expert committee chairs. He started with the presidency of the Expert Group for Special Metals, continued with that for Zinc, and is now the chairman of the Lead Expert Group. He was also the chairman of the PbZn 2015 in Düsseldorf, Germany.

Etsuro Shibata is a professor at the Institute of Multidisciplinary Research for Advanced Materials (IMRAM), Tohoku University, Japan. He has worked in various roles at Tohoku University since 1999 after obtaining his Dr. of Engineering from Kyushu University.

His main research aim is to establish the metal resources circulation system based on the non-ferrous smelting industry. His research activities in non-ferrous metallurgy along with mineral processing beyond the traditional framework are intended to achieve high-efficiency circulation of metal resources and environmental conservation in the future. Research of smelting processes for primary and secondary resources, treatments of by-products, and stabilization of environmental load elements also have been conducted.

PbZn 2020: 9th International Symposium on Lead and Zinc Processing: Plenary Presentations

Lead and Zinc Future Outlook

EPD Distinguished Lecture: "Around the Lead and Zinc Metallurgical World in Eighty Days" A Virtual Tour of World Lead and Zinc Operations and Technologies

Phillip Mackey, P.J. Mackey Technology Inc.

Lead mining and smelting dates back to antiquity, while zinc as an alloying element with copper as brass has a similarly very long history. Today, lead and zinc are produced in large or small tonnages in almost all countries of the world, and lead is the most recycled metal with one of the highest recycling rates of any material. The scale of lead and zinc operations and the type of technologies employed vary widely around the world. The present paper takes the reader on a virtual tour of the major lead and zinc plants throughout the world with a focus on metallurgical facilities. Operations and technology employed at each plant visited are discussed including a brief historical sketch. Future technology trends identified during the world tour are also discussed. The present author needed sufficient time for a thorough study tour and settled on eighty days—the same as that for the celebrated fictional story of world circumnavigation in the 1870s—a time when world lead production far exceeded that of other non-ferrous metals.

Evolution of Global Secondary Lead Production

Huw Roberts, CHR Metals Limited

Secondary lead is recovered from scrapped lead–acid batteries, old lead-sheathed cables and sheets, and a variety of industrial and metallurgical wastes. A significant share of lead output from secondary sources derives from smelters that also treat lead concentrates, so-called primary smelters, which makes the task of estimating the overall scale of secondary lead production more difficult. Estimating the total volume of lead produced from recycling of scrapped batteries is further complicated by the fact that some of this activity still occurs in the informal sector in a number of countries. CHR Metals calculates that secondary lead production accounted for

around 50% of the global total of refined lead production in 1990, but that this share has now risen to just over 75%. This represents an increase from around 3Mt in 1990 to 10Mt in 2018. At the same time, global lead mine production has grown from 3.2Mt (lead in lead and bulk concentrates) to only 3.4Mt in 2018. This paper will trace the development of secondary lead production over the past 30 years highlighting regulatory changes and the shift in regional patterns of output. More particular focus will be on the changes in China over the past 15 years and, more recently, elsewhere in Asia. Reasons for under-reporting of recycled lead production will be examined. International trade in lead–acid battery scrap and other lead-bearing secondary materials will be addressed and consideration given to the environmental concerns and about such trade. CHR Metals' outlook for lead mine and refined lead production to 2030 will be presented.

A Review of Zinc Smelting and Refining in North and South America
Stephen James, Nyrstar

A review of processing of primary and secondary zinc sources in the Americas has been compiled in conjunction with the PbZn 2020 Symposium. This review includes a listing of active processing facilities by location in the Western Hemisphere. Descriptions of key technologies used in these facilities are presented. The review considers trends and changes that have occurred since the PbZn 2010 Symposium. A discussion of likely changes in the medium-term future is also included. This paper follows the examples set by previous authors since 1970 and should serve as a reference for readers interested in the zinc-processing industry.

Lead and Zinc Current Challenges and Opportunities

Our Common Future in Metallurgy
Maurits Van Camp, Umicore

The world is fast transitioning to a sustainable way of living and working to overcome the current societal challenges. This common future is articulated by the UN Sustainable Development Goals. SDGs will pull the metallurgical industry forward, making it an integral participant in the common future. Lead–zinc primary extraction continues to be a key source of technology metals, and lead–zinc metallurgy is enabling the circular economy of a wide range of metals and products. Both mining and metallurgy are essential in realizing the SDGs, although challenges lie ahead. First, the license to operate mines and plants and the license to sell products is provided by society at large. Society will only do so if it considers the lead–zinc industry part of the common future. Second, an industry-wide transition to the innovation economy implies a shared vision on education, research, technology and innovation that includes Industry 4.0 concepts, methods and tools.

Material Stewardship for Zinc
Sabina Grund, International Zinc Association (IZA)

The metals industry is faced with global challenges, among these finding a balance between environmental stewardship, economic development, and social

responsibility, that require full participation by the entire metals value chain. The global zinc industry has a well-established, long-term sustainability program in place providing its customers, regulators, and other stakeholder groups with facts. For example, regular updates of the global zinc mining and smelting Life Cycle Assessment (LCA) provide practitioners with the most representative environmental footprint data for zinc. Furthermore, IZA conducts material stocks and flows analyses to characterize national, regional, and global recycling metrics. IZA's sustainability activities are framed by the SDG Sector Roadmap for the global zinc value chain. It outlines the focus of the global zinc industry's projects linked to Sustainable Development. The presentation provides an overview of the global zinc industries' achievements, goals and actions related and identifies challenges that still lie ahead of this industry.

Lead and Zinc Smelting Technology in China under Green Development
Liu Cheng, China ENFI Engineering Corporation

Lead and Zinc Sustainability and Social License

The Global Zinc Market - Facts, Forecasts and Fundamentals
Paul White, International Lead and Zinc Study Group

In recent years, a number of large zinc-producing mines, most notably the Century mine in Australia, have closed, and this together with a number of production cutbacks resulted in a significant shortage in the market for zinc concentrates in 2016 and 2017. Since that time, both greenfield and brownfield mine capacities have been brought on stream, including a resurrection of Century in the form of New Century Resources, and this has resulted in an alleviation in the supply tightness with a corresponding rebound in the treatment charges levied by zinc refineries. This presentation will examine some of the longer-term trends in mine supply as well as the potential for further new capacity over the next 2–3 years. It will also discuss trends in the refining sector including whether or not a processing bottleneck is developing on an ex-China basis. Finally, it will provide an assessment of the drivers of and outlook for zinc demand.

Developing a Sustainable Global Lead Battery Value Chain
Andy Bush, International Lead Association

Operating responsibly and helping to ensure appropriate management of the materials we produce is critical to meeting society's increasing demands that materials are used responsibly, safely and sustainably. Lead-based batteries represent the vast majority of global demand for lead spanning a wide range of automotive and industrial applications. Their high collection and recycling rate in the developed world is an environmental success story making this battery chemistry one of the most sustainable by meeting the demands of a circular economy. However, the industry is not without its challenges. This presentation we will report on a major new global initiative by the lead and lead battery industries to apply

materials stewardship and responsible sourcing principles to the lead battery value chain. The program is aiming to further enhance the reputation of these industries by adopting a common set of guiding principles, establishing continuous improvement goals and supporting low- and middle-income countries through sharing expertise on the environmentally responsible management of lead.

Regional Changes in Refined Zinc Output and Demand
Claire Hassall, CHR Metals Ltd.

Global refined zinc output has increased from 8.9Mt in 2000 to around 11.8Mt in 2019, an increase of almost 3Mt. Only 530kt of this increase occurred outside China, while China's output increased by over 2.4Mt. The major expansion in China's refined zinc production capacity took place in the ten years to 2010, with some further moderate increase to 2016, but there has been a net decrease in capacity since then. Refined zinc usage globally increased from 8.9Mt in 2000 to 12.2Mt in 2019, an increase of 3.3Mt, but China accounted for more than this total increase, effectively taking away zinc demand from the rest of world. However, China's share of global zinc demand is now changing as its economy matures and, in the last 3 years, China's demand for zinc has stagnated at best, and in some years has fallen significantly. Higher costs, more extensive and better enforced environmental regulations and the effect of trade disputes have seen China's manufacturing industry more constrained, with some Chinese manufacturing companies now basing activities off-shore, and with other countries now better able to compete in world markets than in the initial 10–15 years after China's entry into the WTO at the end of 2002. The last 9 years have seen 13 zinc smelters outside China close, with the loss of close to 1Mt of capacity. The last greenfield zinc smelter ex-China was commissioned in 2010, and capacity expansions have taken place at a number of plants, notably in South Korea, Mexico, India and Norway, compensating for capacity losses, but not adding to capacity overall. The next 5 years are expected to see growth in refined zinc demand concentrated in countries other than China, with South-Eastern and South Asian countries leading the way. This raises the question of where and how the additional requirement for refined zinc will be met and whether China will play any role in supplying zinc to these expanding markets. This presentation will provide an analysis of recent regional changes in zinc demand and supply as outlined above and examine the prospects for future zinc demand and the potential sources of additional refined zinc output globally.

Part I
Lead and Zinc Future Outlook: Plenary Session

GCRIS

Evolution of Global Secondary Lead Production

Huw Roberts

Abstract Secondary lead is recovered from scrapped lead–acid batteries, old lead-sheathed cables, and lead sheet and a variety of industrial and metallurgical wastes. A significant share of lead output from secondary sources derives from smelters that also treat lead concentrates, so-called primary smelters, which make the task of estimating the overall scale of secondary lead production more difficult. Estimating the total volume of lead produced from recycling of scrapped batteries is further complicated by the fact that some of this activity still occurs in the informal sector in a number of countries. CHR Metals calculates that secondary lead production accounted for around 50% of the global total of refined lead production in 1990, but this share has now risen to just over 75%. This represents an increase from around 3 Mt in 1990 to 10 Mt in 2018. At the same time, global lead mine production has grown from 3.2 Mt (lead in lead and bulk concentrates) to only 3.4 Mt in 2018. This paper will trace the development of secondary lead production over the past 30 years highlighting regulatory changes and the shift in regional patterns of output. More particular focus will be on the changes in China over the past 15 years and, more recently, elsewhere in Asia. Reasons for under-reporting of recycled lead production will be examined. International trade in lead–acid battery scrap and other lead-bearing secondary materials will be addressed and consideration given to the environmental concerns and about such trade. The paper will conclude with a brief outlook for secondary lead production.

Keywords Lead recycling · Lead–acid batteries · Lead smelting

Estimating Volume of Secondary Lead Production

There is no accurate data for the volume of refined lead and alloys recovered globally from recycling lead–acid batteries, other lead scrap, and various industrial wastes and metallurgical residues. CHR Metals estimates that 10 Mt of lead were produced

H. Roberts (✉)
CHR Metals Limited, 11 Church Street, Godalming GU7 1EQ, UK
e-mail: huw.roberts@chrmetals.com

© The Minerals, Metals & Materials Society 2020

A. Siegmund et al. (eds.), *PbZn 2020: 9th International Symposium on Lead and Zinc Processing*, The Minerals, Metals & Materials Series,
https://doi.org/10.1007/978-3-030-37070-1_1

globally from sources *other* than lead and bulk concentrates in 2018, almost 50% higher than the total in 2010. In contrast, the International Lead and Zinc Study Group (ILZSG) reports a figure of only 7.3 Mt for secondary lead production in 2018, a total only 25% more than in 2010 and far short of CHR Metals' estimate. A difference of this scale requires explanation, especially as the ILZSG is considered by most in the industry to be the source of reliable, official data.

There are several reasons for the discrepancy between CHR Metals' figure for lead recovered from secondary sources, and that published by the ILZSG. As an international, inter-governmental organisation, the ILZSG relies, in the first instance, on data provided to it by its member states. However, not all countries that produce lead are members of the ILZSG and, even for countries that are members, collection of domestic data may, in some instances, be incomplete and/or inaccurate. For non-member countries, we understand that the ILZSG, aided by advisory committees, will make its own estimates of secondary lead production.

Collection of accurate data about secondary lead production is handicapped owing to the large number of enterprises that are involved in the industry, the almost complete lack of output data published by individual enterprises, even if they are public, listed companies with an obligation to release financial data and the fact that, in many countries, lead recycling may be undertaken within the informal sector. Appropriate government departments may collect production data from operations that are correctly registered and active in the formal sector and are able to report these figures to an organisation such as the ILZSG for collation and publication. By their very nature, informal operations do not report output and are likely to come to the attention of the authorities only when they are found to be a source of excessive pollution. At that point, they may be closed or move to a more remote location. In such cases, none of this output is captured in official data.

Another issue that complicates the collation of data for secondary lead production, and is a further reason for the difference between CHR Metals' figures and those published by the ILZSG, is one of definition, and in particular, as it relates to international trade in lead metal. CHR Metals make extensive use of official trade data to track flows of material and as an aid to identifying where lead is being produced and consumed. If a country providing accurate and timely trade data reports *imports* of lead metal from another country, it is assumed, all other things being equal, that this lead is being produced in the exporting country and, therefore, should be counted as lead production. Given that there are currently few primary smelters outside China and, for most of these, output is reported accurately, the trade data can assist in estimating the amount that could be categorised as secondary output in the exporting country. What may not be known from the trade data is the purity of this lead, especially if it is shipped under codes used for "other alloys" (78019990/1/9). The ILZSG in its definition of refined lead excludes, "remelted lead and lead alloys recovered from secondary materials without undergoing a full refining process." The problem with this quite clear definition is that this unrefined material can be legitimately shipped using the trade code 78019990 which is also used for lead alloys, such as lead–tin and lead–calcium produced from refined lead and today used extensively in the manufacture of maintenance free lead–acid batteries. Trade in lead-antimony

alloys, in the past the key alloy used for battery grids, is reflected in the ILZSG's calculations of apparent consumption and, presumably, estimates of refined output where no actual data is provided or available. However, the international movement of *other* alloys is typically excluded except in those cases where the reporting country does not make any clear distinction between alloys in its trade data. The historical reason for the approach taken by the ILZSG is that the manufacture of alloys, other than lead-antimony alloys, was accounted for as lead consumption in the country making the alloys. In an era where alloys, other than lead-antimony, accounted for a very small share of overall demand and only used in specialist applications, this was a perfectly reasonable way to collate and analyse the data. However, today lead-antinomy alloys account for a relatively small share of total alloy production and the continued use of this old definition introduces distortions in the calculation of both lead consumption and production.

While not an entirely satisfactory solution, CHR Metals has taken the view that, unless lead which is traded internationally can be specifically identified as lead bullion requiring further refining, for example, bullion shipped from the Mt Isa smelter in Australia to the UK's Northfleet lead refinery, this material should be accounted for as lead destined for consumption and, therefore, as lead production in the country of origin. In making this assumption care is taken to ensure that if lead has been counted as being produced in country A, it is not then double-counted as production in country B, even if some further refining and/or alloying takes place in country B before the lead is used.

Collating all available reported production data and detailed analysis of trade flows are two of the methods used by CHR Metals to estimate secondary lead production. A third method involves modelling the demand for lead–acid batteries and, in particular, demand for replacement batteries. This involves making assumptions about battery life in various applications and geographical locations. This provides a figure for the likely generation of battery scrap. From assumptions about local battery recycling rates, it is then possible to estimate the volume of secondary lead recovered from scrap batteries. A small allowance for other lead scrap may also be added in some countries.

However, it is important to note that not all secondary lead production is from operations recycling used lead–acid batteries. Over time, an increasing share of lead output from so-called primary smelters[1] has been derived from lead-bearing wastes, scrap, and residues, in addition to conventional lead and bulk concentrates. The feed mix of primary smelters is not typically disclosed in public but CHR Metals makes an estimate for the recovery of secondary lead by primary smelters based on its own research. This is another area where CHR Metals' data may differ from official sources.

Some of the lead recovered by primary smelters is derived from the lead contained in zinc and other concentrates, so-called second-pass material (Whether or not this

[1]CHR Metals defines all smelters than were originally designed to process lead concentrate as primary smelters. This is the case even where, over time, the principal feed sources have become secondary lead-bearing materials.

should be classified as primary or secondary lead is open for discussion. CHR Metals accounts for this feed as secondary feed). Higher prices since the mid-2000s have encouraged this activity, especially in China, where zinc leach residues are routinely processed in Waelz kilns to enhance overall zinc recoveries and to recover other minor metals, with the resulting slag then sold on to lead smelters for the eventual recovery of the contained lead. Relatively high lead contents in zinc concentrates (and vice versa) were not uncommon in China in the past although, in more recent years, new mills (concentrators) employing modern technology have resulted in an improvement in concentrate quality in China perhaps reducing the availability of second-pass feed. The balance of the secondary lead feed into primary lead smelters, after taking account any allowance for second-pass material, is from true secondary sources. These may be other industrial wastes or residues but also includes battery scrap, especially battery paste. Another source of lead feed which has seen some increase in more recent years has been recovered as a by-product from the processing of electric arc furnace (EAF) dusts undertaken principally for the zinc content which is sold to zinc smelters as crude zinc oxide.

Technology, such as QSL, Kivcet, and TSL (Ausmelt/ISAsmelt), replacing sinter machine/blast furnace operations in the West in the 1990s, was intended to improve environmental performance, compared to more traditional sinter machine/blast furnace operations, and also to widen the range of feed that could be treated, especially secondary lead-bearing materials. In some cases, this was also driven by the need to process related zinc refinery residues with increasing environmental pressures on the long-term storage of zinc leach residues. In China, the adoption of domestically developed flash smelting furnaces using bottom and side-blowing oxygen enrichment, in addition to some limited investment in Western smelting technologies, has been primarily the result of tightening environmental regulations and better enforcement of these rules. This has also meant greater opportunities to utilise a mix of feed materials, including a share of secondaries. In China, zinc smelters can no longer store their leach residues indefinitely. Many have chosen to further process the residues through Waelz kilns which will generate some secondary lead-bearing feeds while some are investing in western flash furnace technologies to directly treat zinc leach residues. All of these developments have added, and will continue to add, to the production of lead from secondary sources which are in addition to lead produced from recycling scrapped batteries.

Global Growth of Secondary Lead Production Since 1990

CHR Metals estimates that global secondary lead output amounted to a little over 2.9 Mt in 1990 and accounted for slightly more than half of all refined lead production. Around 300 kt was accounted for primary smelters processing secondary lead-bearing feed with the balance produced by companies largely recovering lead

from recycling scrapped lead–acid batteries. The ILZSG reports secondary lead production of 2.74 Mt in 1990, a difference of only 5% compared with CHR Metals' estimate.

While most major economies banned the disposal of used lead–acid batteries in landfill during the course of the 1970s and 1980s, it was not until the late 1980s and early 1990s that legislation began to be introduced to set out clearly how scrapped batteries were to be collected and recycled. In the USA, many states published regulations which relied on deposit schemes or mandated that battery manufacturers should be responsible for recycling their products at the end of their useful lives. In Europe, government supported schemes were established in Italy (Cobat) and in Scandinavia (Returbat) and in Japan, battery makers agreed to support a domestic recycling industry by sponsoring the free collection of scrap batteries and delivery to authorised recycling facilities.

From today's perspective, when used lead–acid batteries are being swept up by traders and sometimes shipped halfway around the world for recycling, it may seem odd that there was ever a need for official intervention in the lead–acid battery recycling business. However, that is to forget how the economics of the industry have changed over time. In particular, it is the case that through much of the 1980s and certainly in the 1990s and through to the mid-2000s, recycling a used lead–acid battery, defined in law as a hazardous waste requiring careful handling and processing, returned a negative value if all the proper procedures and environmental regulations were followed. And the costs of meeting ever-stricter environmental standards were also increasing sharply through this period.

With a ban on dumping scrap batteries, but little economic incentive to recycle batteries unless subsidised by a deposit scheme, a government funded organisation or battery manufacturers who were under a legal obligation to take back used batteries and ensure their safe recycling, it is little wonder that there was some accumulation of scrapped batteries in motor service centre yards and domestic garages in this earlier period. In many smaller developing economies where there were relatively few batteries to be recycled in the first instance, scrapped batteries may simply have been broken for the recovery of metallic lead which will then have been remelted, perhaps to be used as fishing weights. Battery cases may have found a second life when filled with earth or concrete and used in retaining walls or other construction. The battery paste is likely to have been dumped.

Figure 1 above charts the increase in secondary lead production through dedicated recycling facilities. In other words, secondary lead-bearing materials processed through so-called primary smelters are not included in the totals shown. CHR Metals estimates that from 2.6 Mt in 1990, with over three quarters accounted for by production in Europe and North America, recycled lead output increased to 4.1 Mt by 2005 with the mature economies of Europe and North America then accounting for just under 60% of the total. This suggests a transformation in the geographical pattern of output being underway.

Another development was also underway. CHR Metals estimates that, in 1990, of the 3 Mt of production from primary lead smelters, which accounted for 54% of total refined lead output at that time, no more than 10% derived from secondary

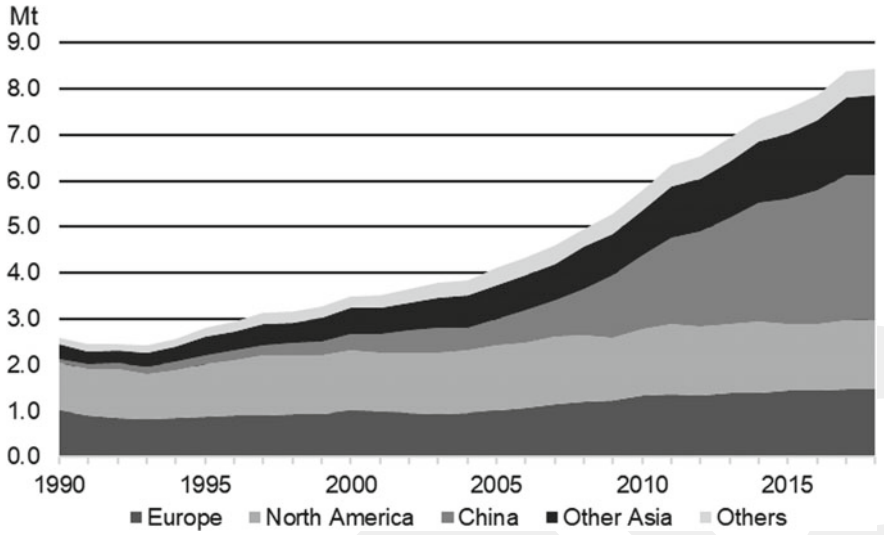

Fig. 1 Global secondary lead production excluding recovery via primary smelters

lead-bearing materials. By 2005, when primary lead smelters produced 3.9 Mt, the share of secondary materials in their feed mix had risen to 20%. Two factors were largely responsible for this. The first was the commissioning of new primary lead smelters outside China in the 1990s, initially in Europe and Korea and subsequently in Canada, that were capable of processing economically a higher share of secondary feed materials than had been possible with the blast furnaces that had been replaced. The second was the sharp decline in treatment charges for processing lead concentrates in the early 2000s as Chinese smelters emerged as significant importers of lead concentrate. This meant that it became uneconomical to run a primary smelter, especially if it was relying on third-party purchases for most of its concentrate. The option, therefore, was to increase the share of cheaper secondary materials, principally battery paste, in the feed mix. Figure 2 charts the evolution of the recovery of lead from secondary feed materials through primary smelters as estimated by CHR Metals.

Both Figs. 1 and 2 reveal significant changes in global secondary lead production from around the mid-2000s. While the clearest change is in China, there are some less obvious developments elsewhere.

For markets outside China, the most significant development affecting the business of secondary lead smelters from the mid-2000s was the sharp increase in LME lead prices. After prices averaged under US$500/t in nominal terms over the six years 1998–2003, they began to rise sharply from 2004 before reaching a peak of almost US$4000/t in October 2007. While LME prices have fallen back from the spike in 2007, and briefly traded back to around US$1000/t during the early stages of the global financial crisis of 2008/2009, the last decade has seen LME lead prices trade mostly above US$2000/t, albeit with some relatively short periods when prices have

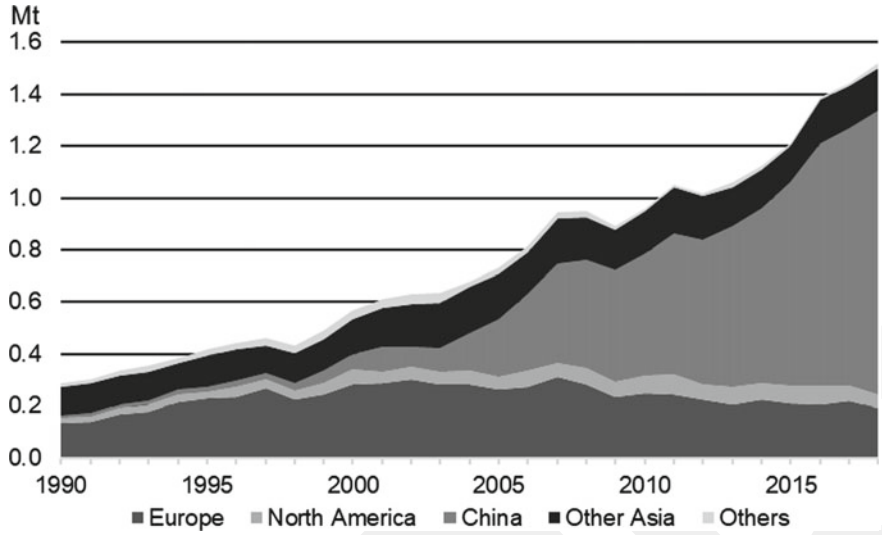

Fig. 2 Global lead production recovered from secondary feed materials via primary smelters

been lower. Higher prices meant that used lead–acid batteries, while still a hazardous waste requiring proper collection and processing to recover the lead, now had a net positive value. Official schemes to ensure collection of scrap batteries were no longer strictly necessary. Scrap merchants were incentivised by the market to re-enter the business to purchase and collect used lead–acid batteries and deliver them to battery recyclers. As a consequence, but also in response to the construction of new capacity to recycle batteries, the price of battery scrap soared. The secondary lead industry, which had enjoyed a brief interlude of enhanced margins and profitability from 2005 through until the global financial crisis, found itself under financial pressure again as competition for scrap feed intensified (Fig. 3).

CHR Metals has a simple model which reflects changes in lead–acid battery recycling rates in all countries excluding China. Although the data is based only on assumptions about the share of lead consumed in SLI and industrial batteries and the useful average lives of these batteries, it does show a clear relationship between the price of lead and the estimated percent of scrapped batteries actually recycled. In the early 2000s, when the price of lead was very low, the volume of lead recovered from scrap batteries appears to have fallen some way below the volume of scrap available to be recycled in used batteries. When, in 2005, the price of lead began to increase, so too did the recycling rate. And with higher prices well established in the years after the global financial crisis and greater capacity to recycle batteries, recycling rates may then have approached 100%.

Although recycling rates this high are to be welcomed, it is probably the case that some of the apparent increase in annual recycling rates may have been accounted for by the mobilisation of scrap generated in earlier years and more particularly in countries which might not previously had much of an industry in collecting and

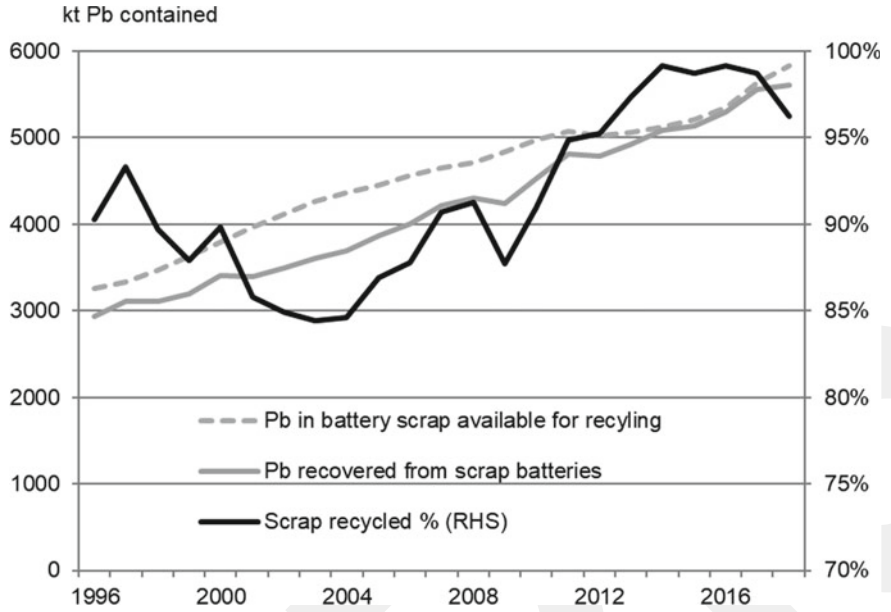

Fig. 3 Estimate of lead recovered from scrap batteries ex-China and recycling rate

processing scrapped batteries. In support of this view is the increase in trade in used lead–acid batteries for recycling in recent years from a wide range of countries in Asia, Africa, South America, and the Caribbean. Battery recyclers in Korea have been especially active in seeking new sources of scrap supply, in addition to importing battery scrap in significant quantities from the USA and Japan. Over the past two years, Korea scrap traders have found themselves competing with buyers from India, particularly in sub-Saharan Africa for battery scrap. The entrance of India into the international trade in battery scrap came after a change in domestic regulations in April 2016 governing the movement of hazardous materials. Hitherto, there had been a formal and more or less blanket ban on importing a wide range of secondary materials into India. This has been revised with new regulations permitting the import of used batteries and other lead scrap provided that the facility that processes these secondary materials is formally registered and licenced. The small dip in Korean imports of lead–acid battery scrap is seen in 2018 in Fig. 4 reflects the competition from Indian traders as well as a fall in imports from Japan as discussed below.

There are concerns that the international trade in scrap batteries, especially from countries where there are well-regulated and mature recycling industries, such as in the USA, Japan, and Europe, to countries where recycling operations may not be as well regulated, is undermining efforts to ensure that, as far as is possible, lead–acid batteries are recycled in a safe and environmentally responsible manner. There is also the risk that, by being prepared to pay more for scrapped batteries than domestic

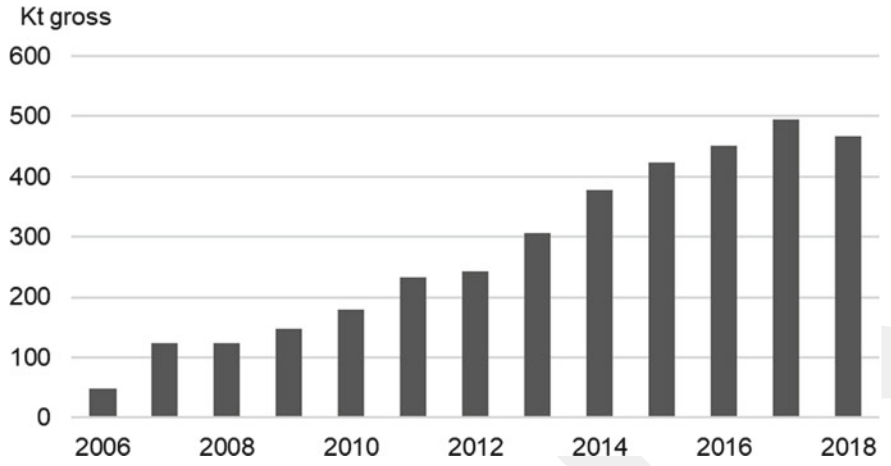

Fig. 4 Korean imports of lead–acid battery scrap

recycling operations, importers of scrapped batteries are making recycling facilities uneconomic in countries where environmental standards are very high.

In order to better regulate the recycling of scrapped lead–acid batteries and to protect its domestic industry, Japan has moved to ban the export of battery scrap to Korea with shipments falling to near zero in 2019. Secondary lead producers in the USA are considering what steps their government could take to provide some protection from foreign buyers of battery scrap.

Secondary Lead Production in China

It is very clear from Figs. 1 and 2 that the greatest changes in secondary lead production since 2005, at least in terms of volume, have been in China. That there are different estimates for secondary lead production in China was discussed earlier, but CHR Metals believes that the actual recycling rate of used lead–acid batteries is significantly higher than is implied by official data. This belief stems from extensive research on the ground which identified as early as 2002 that a well organised system for collecting and recycling batteries existed in China. Moreover, batteries were being recycled even though, at this early date, prices for lead were exceptionally low.

The problem for those collating official data is that much of the recycling activity in China has, until very recently, been in the unregulated and informal sector. This allowed often small-scale operators to continue using outmoded and environmentally unsound methods of used battery storage, collection, breaking, and processing even as China's output grew from around 5% of global secondary lead production in the early 1990s, to 17% by 2005, a little over 30% by 2010 and 40% by 2015. The overall scale of the industry in recent years, with estimated secondary output of 4.2 Mt

in 2018, 3.1 Mt via dedicated recycling operations with the balance coming from secondary materials processed by primary smelters, meant that poor environmental operating conditions could not go unchecked.

The Chinese government began to implement much stricter enforcement of already existing environmental regulations in 2016 and this has resulted in disruption to the secondary lead industry over the past three years. Plants that had installed mechanical battery breaking equipment and were able to separate the component parts but had not yet invested in approved smelting technology were required to sell recovered battery paste to third-party primary smelters while being restricted to remelting and refining/alloying battery grids and posts.

There has been a surge in investment to upgrade battery recycling plants to include smelting technology approved by the authorities. Typically, enterprises are installing oxygen enriched, side-blowing furnaces for the treatment of lead paste. It is notable that, to date, few companies are investing in equipment to desulphurise the battery paste prior to smelting. This means that for most facilities furnace gas emissions require scrubbing.

Plans for new battery recycling plants seen by CHR Metals suggest that the seven largest companies currently involved in the industry could have the capacity to process 6 Mt of scrapped batteries by the end of 2020, an increase of almost 50% from their available capacity in 2018. Following the direction of the central government, most of the larger battery manufacturers are now involved in the collection and processing of used batteries. Government policy is that battery manufacturers collect used batteries equivalent to 40% of their sales by 2020 and 70% by 2025, and that all these batteries must be recycled in a safe and approved manner. Given existing facilities which are already compliant with environmental standards, ongoing investment in new and expanded recycling facilities and a continued effort to eliminate activity in the informal sector, this target is achievable. There are, in addition, reports of several other new/upgraded/expanded plants operated by smaller companies across the country and not directly affiliated with a battery maker which will be commissioned by 2020 and will also meet current environmental standards. The prospect of a glut in battery recycling capacity looks inevitable.

The very rapid growth in China's secondary lead production, especially since 2008, principally reflects the emergence of electric lead–acid battery powered bicycles in the years after 2005, a market that barely existed five years earlier (Fig. 5). By 2005, e-bike sales had reached 13 million a year and more than doubled to almost 30 million a year by 2010. Sales rose at a slower pace thereafter and are reported to have peaked in the years 2012–2014 at around 35 million a year although this may have been an exaggerated figure and also included a small share of e-bikes powered by li–ion batteries. However, with each e-bike on the road carrying a battery pack typically containing 10–11 kg lead in a fleet which has reached a total of at least 160 million (some estimates going as high as 200 million but CHR Metals takes the view that not all of these e-bikes may be in use) this represented a huge market for lead. Moreover, in the early days of e-bikes, batteries typically needed replacing within a year. While battery lives have been extended as quality has improved, regular users of e-bikes still need to replace their batteries at least every two years. This not only

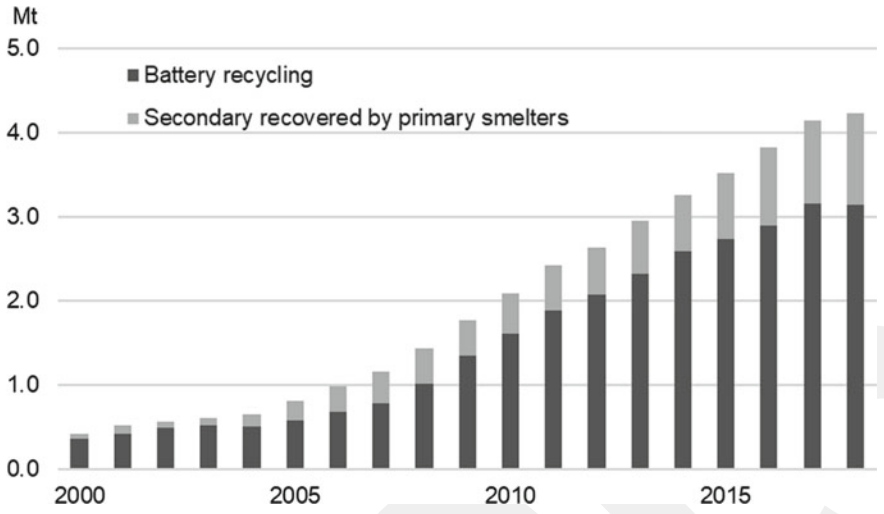

Fig. 5 China's production of secondary lead

creates a huge demand for replacement batteries but also a large supply of battery scrap.

Electric tricycles (e-trikes) also began to appear in China's cities and towns in increasing numbers from 2009/2010. These are mainly used as taxis or short-range delivery vehicles although there are also some smaller models that are used as local run-abouts by pensioners. The battery capacity for each e-trike may be up to four times or more than used on two-wheel e-bikes and, again, need replacing every one to two years depending on use.

CHR Metals estimates that roughly 40% of China's lead demand in 2018 which, in total, amounted to a little over 6 Mt, was accounted for by batteries used by e-bikes/trikes and so-called low-speed vehicles. Growth in this market sector has slowed sharply in recent years and consumption may now be near its peak following the introduction in April 2019 of new standards for e-bikes that will be permitted to be used in cycle lanes. As the new rules begin to be enforced across the country, there may be a shift towards smaller e-bikes powered, in the main, by li–ion batteries. This is certainly the hope of li–ion battery makers. On the other hand, the utility and relatively low cost of larger e-bikes powered by lead–acid batteries may persuade people that it is worthwhile to acquire a motor-cycle licence which will allow them to take a registered and insured e-motorcycle onto main roads although they will not then be allowed to use cycle lanes.

The second largest use of lead in China is, of course, in the manufacture of SLI batteries. This market has also seen rapid growth in recent years with China's conventional vehicle fleet expanding at an astonishing average annual growth rate of 16% over the last 10 years. The number of cars, trucks, and buses on the road has grown from 50 million in 2008 to an estimated 230 million in 2018. Even with

a slowing in the pace of new car sales, China's vehicle fleet is likely to exceed that of the USA in the early years of the next decade. While creating a large market for batteries fitted as original equipment, there is also now a very significant market for replacement batteries which, in turn, generates a large volume of battery scrap.

Closing Comments and Outlook for Secondary Lead Production

The global secondary lead industry has faced significant challenges over the past three decades. These include the low price of lead for many of the first 15 years after 1990 and then, post the global financial crisis, the very high price of battery scrap in relation to price of refined lead. There has been rapid growth in lead recycling capacity in Asia, although much of this has been in China and dependent exclusively on domestic scrap supplies, China has not permitted the import of battery scrap. However, there has also been significant growth in secondary lead production elsewhere in Asia with Korean operations expanding based on scrap imports and India, since April 2016, also allowing some recyclers to import scrap to sustain their operations. On balance, battery scrap imports from countries without viable recycling facilities can be seen as positive as it limits the availability of scrap to very small-scale, informal recycling activities with their attendant environmental issues. However, where battery scrap is moving from countries with the highest environmental standards to areas of the world where standards may not be as stringent or less rigorously enforced, this is clearly an unsatisfactory situation.

Where lead–acid batteries are collected whole and recycled in today's state-of-the art recycling facilities the environmental impact is minimal with negligible emissions of lead into either water or air. Secondary lead producers in North America and Europe, accounting for around 36% of recycled lead output globally, are, for the most part, already meeting very high standards for protecting the environment and the health of their workers. China, producing more secondary lead than North America and Europe combined, is now on the path to improving its environmental performance although the legacy of past weak enforcement of regulations will take time to resolve. And while there may be some good operators in other countries, there are still far too many reports of smaller-scale, unregulated recycling activities which continue to pose significant environmental risks. This remains a key challenge for the industry and its related organisations.

Looking forward, the lead–acid battery industry is also facing challenges to its near ubiquitous use in automobiles, e-bikes and e-trikes in China, and also as the main choice for network and telecom backup power. Any market loss means slower growth in battery scrap available for recycling and, eventually, a gradual contraction in overall output.

In the more immediate future, the industry in China will be watching developments in the e-bike market very closely for signs that consumers are accepting smaller, li–ion powered e-bikes as a substitute for larger e-bikes powered by lead–acid batteries. Even if this is the case there will be a period of transition as most local authorities have put in place temporary registration schemes, in some cases through to 2022, for e-bikes already on the road that do not meet the new standard. However, if a new market for electric motorcycles still powered by lead–acid batteries does not emerge over the next 12–18 months, this will be bad news, not only for battery recyclers in China, but also for the global market for refined lead.

The threat to lead–acid batteries over the next ten years from electric vehicles, in China and elsewhere, is unlikely to be that marked. In the first place, current ambitious forecasts for electric vehicle sales may not be met, just as they have not been met over the past five years, as consumer concern about high vehicle prices and limited charging infrastructure continue to deter the growth of a mass market for these vehicles. This means that the conventional vehicle fleet, powered by internal combustion engine or hybrid power trains, will continue to expand creating demand for lead–acid batteries and the need for used batteries to be recycled.

Figure 6 charts CHR Metals' forecast for global secondary lead production over the period to 2030. From around 10 Mt in 2018, secondary lead production via battery recyclers and from feed processed by primary smelters is expected to rise to a little over 11 Mt by 2030. The major regional areas of production, North America, Europe, and China are forecast to see little overall growth past 2020, with output in China quite possibly dipping towards the end of the forecast period. Modest, but further growth is forecast in other Asian countries, especially India, as well as in parts of South America and Africa.

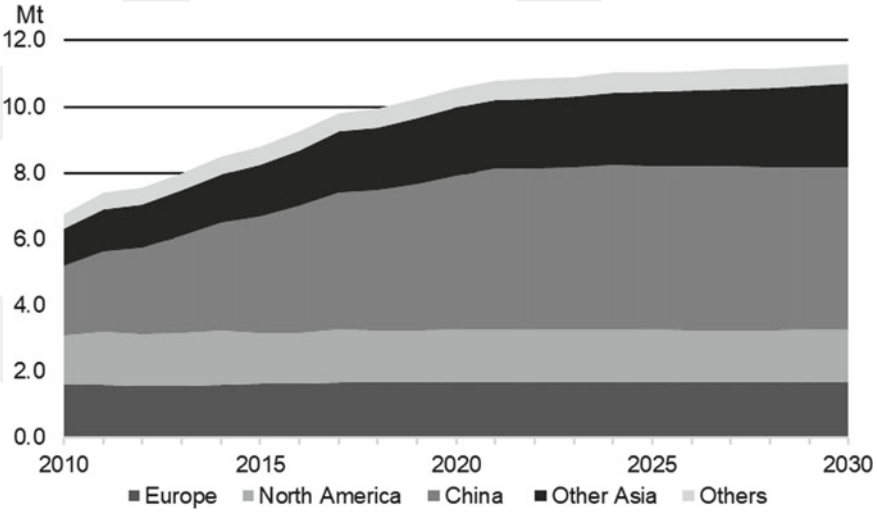

Fig. 6 Global secondary lead production including via primary smelters

Part II
PbZn Process Fundamentals I

GCRIS

Refractory Challenges in Lead and Zinc Furnaces

D. Gregurek, K. Reinharter, J. Schmidl and A. Spanring

Abstract Refractory linings in primary or secondary lead and zinc furnaces like QSL reactor, KIVCET furnace, Top Submerged Lance Technology (Outotec Ausmelt^{TM}/Isasmelter^{TM}), TBRC/Kaldo furnaces, reverberatory furnace, and short rotary furnace, as well as Waelz kiln, are exposed to several stresses rather complex in their interaction. In the present work, the main wear parameters, such as corrosion by slag, high sulfur, soda and iron oxide supply as well as reduction, are briefly introduced and discussed. The extraordinarily high SiO_2 supply results in "forsterite bursting" combined with volume expansion. High operation temperatures in the furnace support microstructural brick degeneration. All mentioned wear phenomena result in severe degradation of brick microstructure and consequently to decreased lining performance. The obtained information and insights serve as a basis for improving refractory materials to provide the best solutions for RHI Magnesita's customers.

Keywords Refractories · Lead and zinc metallurgy · Wear phenomena

Introduction

The profitable primary or secondary pyrometallurgical operation depends on many factors such as furnace type, process conditions, lining design, and selection of refractory types. Depending on the nature of the input materials, various technologies are available for lead production, and generally primary and secondary production routes can be distinguished. The primary route uses mainly sulfidic lead concentrates, also with the addition of zinc plant residues or battery scrap, whereas the secondary route processes only materials from secondary sources, especially batteries. The traditional primary lead route is roasting-reduction/smelting (roast-reduction, i.e.,

D. Gregurek (✉) · K. Reinharter
RHI Magnesita, TC Leoben, Magnesitstrasse 2, Leoben 8700, Austria
e-mail: dean.gregurek@rhimagnesita.com

J. Schmidl · A. Spanring
RHI Magnesita, Kranichberggasse 6, Vienna 1120, Austria

© The Minerals, Metals & Materials Society 2020

A. Siegmund et al. (eds.), *PbZn 2020: 9th International Symposium on Lead and Zinc Processing*, The Minerals, Metals & Materials Series,
https://doi.org/10.1007/978-3-030-37070-1_2

sinter plant and blast furnace); however, over the last decades, the direct smelting reduction processes (roast-reaction) have become more important and are nowadays state of the art [1–5]. The main vessel for zinc production from Zn leaching residues from hydrometallurgical production, EAF dust from steel production and various non-ferrous slags, is the Waelz kiln.

Generally, the process parameters and technology are chosen according to the input material, i.e., present impurities and required metallurgical work. The conditions range from oxidizing for sulfur removal (roasting) to reducing for smelting, including evaporation of metals and metal compounds with alkalis and halogens—sometimes both in one vessel. The process temperature is generally far higher than the metal liquidus temperature which is for lead 327 °C and for zinc 419 °C. The temperature is even high enough for evaporation of certain metals in the form of metals, oxides, sulfides, and halides, namely around 1000 °C. However, these high temperatures are required in order to:

(1) obtain a liquid and reactive slag that is easy to remove in processes dealing with liquid metal and slag, and/or
(2) achieve the desired volatilization of certain input components (slag fuming, Waelz process).

Additionally, slag chemistry is adjusted in a way to minimize metal overheating, as well as enhance the process chemistry and desired reactions.

Consequently, the following challenges arise for the refractory [4, 5] as a result of the:

- Chemistry of liquid slags: varying slag composition within the system $FeO–SiO_2–CaO$ and/or choice of other slag systems and additives (soda slag) causes chemical attack.
- Chemistry of input materials: volatile compounds including metals, halides, alkalis, etc. infiltrate the refractories and react with the refractory components.
- Furnace atmosphere and temperature: repeatedly changing atmospheres (oxidizing/reductive), as well as exposure to hot gases lead to increased refractory damage. Overheated liquid phases (metal and slag) with resulting very low viscosity cause deep refractory infiltration and chemical attack.
- Mechanical forces/abrasion/erosion: the flow of gas and liquid phases also mechanically attacks the refractory lining. Either directly by impact or indirectly by continuously removing protective reaction products formed on the refractory surface. In the case of zinc Waelz kilns dealing with mainly solid materials, moving solid material in a rotating kiln creates different challenges for the refractory lining compared to gas or liquid phases.

A general overview of wear phenomena in lead and zinc furnaces was discussed and introduced in several papers in the past [6–11]. Particularly in the lead industry, a lot of work was done regarding refractory corrosion testing in different pilot-scale and industrial furnaces [10, 11].

This paper gives an overview of the main wear mechanisms affecting the refractory lining from various lead and zinc processing furnaces, such as the QSL reactor, KIVCET furnace, Top Submerged Lance Technology (Outotec Ausmelt^{TM}/Isasmelter^{TM}), TBRC/Kaldo furnace, reverberatory furnace, and short rotary furnace, as well as Waelz kiln.

Wear Phenomena

Slag Attack and Forsterite Bursting

Similar to the copper industry, the refractory lining in the lead industry is highly affected by corrosion due to acidic slag. The main slag types for both industries can be roughly expressed by the system FeO–CaO–SiO_2 (Fig. 1). Nevertheless, in comparison with copper production processes the slag temperatures in the lead industry are lower. Additionally, the production of lead from secondary sources such as battery scrap leads to the formation of different types of slag frequently without or with low content of CaO, SiO_2, and soda containing compounds (e.g., Na_2CO_3). Such modified slag systems allow metallurgical processing at temperatures even below 1000 °C.

In lead furnaces, the low-melting, partly alkali-rich slag penetrates deeply into the brick microstructure. The silica-rich slag and the reaction products formed by the corrosion of the brick-inherent component can be traced up to the cold face. This is a huge difference compared to slag attack and infiltration in copper furnaces, where the infiltration depth is just a few mm from the hot face.

Generally, the corrosion of the refractories by slag attack manifests itself in three ways [9]:

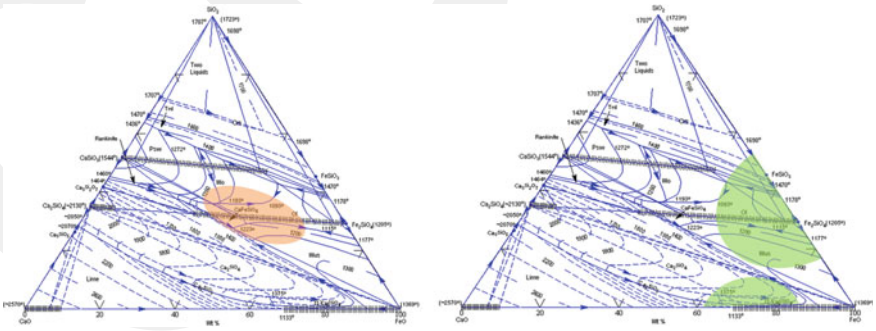

Fig. 1 Typical chemical compositional range of lead (left side) and copper slags (right side) is demonstrated in CaO–FeO–SiO_2 phase diagrams. Modified after [12]

(a) Dissolution reaction occurring at the immediate brick hot face: The driving force here is the lower activity of the refractory oxides like MgO in the slag. The dissolution process, at least in a closed system, will continue until the liquid slag has reached saturation. However, in practice the point of saturation is never reached and dissolution continues until the entire refractory has been consumed.
(b) Dissolution and chemical reaction within the refractory microstructure: Infiltrating slag will dissolve magnesia especially from the fine particles in the brick according to the respective phase equilibrium. This will not directly contribute to corrosive wear which takes place at the immediate refractory hot face. Nevertheless, it will contribute to wear by preparing hot erosion due to a loss of brick bonding.
(c) Kinetics of slag infiltration: Kinetics of slag infiltration causing processes mentioned above depend on several parameters like temperature, viscosity, pore size distribution, and wetting angle.

On microscopic scale, several zones can be distinguished at the brick hot face (Fig. 2):

– Adhering slag coating, frequently covering the immediate brick hot face;
– Reaction zone, below the slag coating showing severe dissolution of the magnesia. Frequently relics of chromite precipitations after magnesia dissolution can be observed;
– Adjacent to the reaction zone infiltrated and corroded brick microstructure.

In the infiltrated brick microstructure, due to corrosion of the coarse magnesia grains and matrix fines, the main reaction products are (Ca)–Mg–silicates, namely monticellite ($CaMgSiO_4$), and forsterite (Mg_2SiO_4), as well as Na–Mg–Fe–Al–silicate. Two minor compounds, (Ca)–Mg–(Fe)–silicate of olivine type and Na–Ca–Ba–silicate glassy phase, can also be detected.

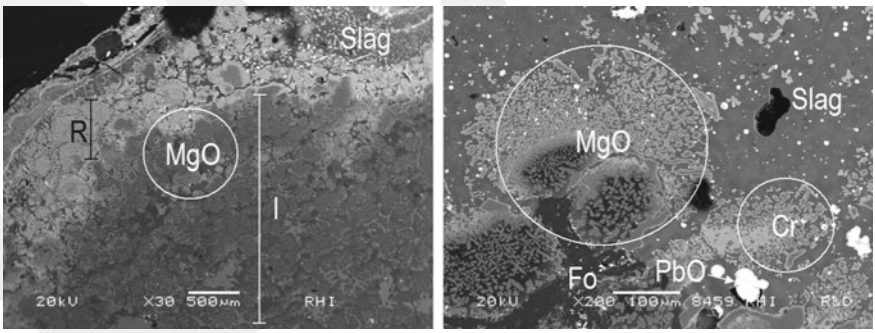

Fig. 2 Magnesia-chromite brick. Mineralogical investigation. Left: slag coating covering the immediate brick hot face. Reaction zone (R). Infiltrated and corroded brick microstructure (I) Corroded magnesia (MgO). Right: detail of the reaction zone. In contact with slag severe corrosion of magnesia (MgO) frequently with relics of primary and secondary chromite precipitations (Cr) after the corrosion of the magnesia. Forsterite (Fo). Lead oxide (PbO)

Fig. 3 Magnesia-chromite bricks out of the lead reverberatory furnace. Macroscopic overview. Left: crack formation and expansion at the brick hot face (arrows). Mineralogical investigation. Right: severely degenerated brick microstructure with coarse pores and crack formation due to forsterite bursting. Massive forsterite formation (Fo). Magnesia (MgO)

Generally, the periclase (MgO) is more basic than chromite and therefore more susceptible to acidic corrosion by slag. The corrosion of MgO is based on the reaction between basic oxide (MgO) and acidic oxides (slag), whereas the chromite is modified in chemical composition due to diffusion phenomena leading to enrichment with iron-, zinc-, antimony-, and tin-oxide.

In lead furnaces, an atypical, exceptionally high SiO_2 supply caused mostly by changes in the processing and/or the uncontrolled addition of silica sand results in the considerable formation of forsterite following contact with periclase (MgO). The associated volume expansion causes forsterite bursting and destruction of the brick structure (Fig. 3).

Sulfur Corrosion

Another very common type of chemical attack is corrosion by sulfur. The latter is frequently observed in metallurgical vessels like KIVCET furnace, Ausmelt^{TM} reactor, and QSL reactor where mainly primary ores are charged. For instance, the magnesia-chromite brick from the KIVCET furnace shows up to 8 wt% SO_3 at the hot face (Table 1).

Table 1 Chemical analysis of magnesia-chromite brick out of KIVCET furnace

wt%	Na_2O	Al_2O_3	MgO	SiO_2	SO_3^a	CaO	Cr_2O_3	$Fe_2O_3^b$	PbO	K_2O
Hot face[c]	0.6	3.0	55.0	0.7	8.0	0.9	7.0	6.0	18.0	0.3
Unused[d]		6.5	58.0	0.6		1.3	19.0	14.0		

[a]sulfur calculated as SO_3
[b]total iron calculated as Fe_2O_3
[c]standardless semiquantitative XRF analysis on original sample
[d]quantitative XRF analysis on ignited sample (1050 °C)

GEORIS

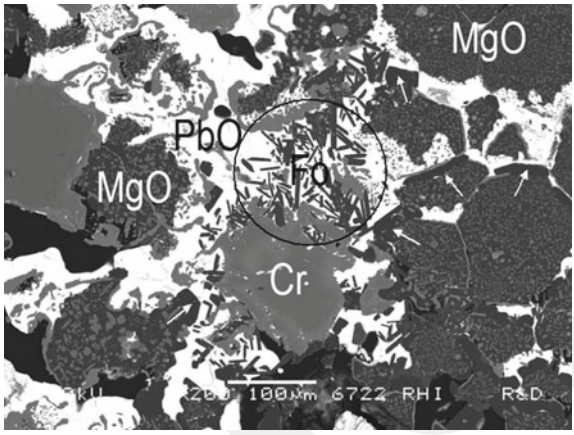

Fig. 4 Magnesia-chromite brick. Mineralogical investigation. Corrosion of the magnesia (MgO) by sulfur attack. Idiomorphic periclase crystals at magnesia rims (arrows). Idiomorphic forsterite crystals (Fo). Chromite (Cr). Lead oxide (PbO)

The penetration of gaseous SO_2 caused by oxidation of sulfidic ore leads to the formation of SO_3, which below temperatures of approximately 1100 °C reacts with the basic oxide of the magnesia-chromite brick leading to the formation of magnesium sulfate ($MgSO_4$) [13].

In case of magnesia-chromite bricks with high CaO/SiO_2 ratio, also the interstitial phase in the magnesia such as dicalcium-silicate (Ca_2SiO_4) is massively corroded. The latter results in formation of Ca-sulfate ($CaSO_4$). Due to a severe corrosion of the brick bonding phase, the initially high CaO/SiO_2 ratio is decreased into the stability area of forsterite. Therefore, numerous single forsterite crystals could additionally form in such a melt (Fig. 4). This is mainly caused by sulfate melt condensated close to the brick cold face. The possible reaction is schematically represented as follows:

$$SO_3 + 2Ca_2SiO_4 + MgO \rightarrow Ca_3MgSi_2O_8 + CaSO_4$$

This means that the CaO/SiO_2 ratio of the silicate phases is shifted to a lower value, and this similarly continues until forsterite is formed. As indicated by the above equation, this reaction takes place only if $CaSO_4$, which is a component of the sulfate melt and not a solid phase, is penetrating to regions more distant from the hot face.

At temperatures above 1100 °C, $MgSO_4$ will dissociate and form fine crystalline MgO at magnesia rims (Fig. 4) [14]. This takes place without adequate rebuilding of the original ceramic bonding of the brick.

Iron Oxide Attack

Either at the interface between the slag coating and the brick hot face or in the first few mm from the hot face the magnesia-chromite brick becomes highly enriched

with iron oxide. This is most frequently observed in magnesia-chromite bricks from the short rotary furnace where iron scrap is used as reducing agent in the processing of lead batteries.

As can be seen from the chemical analysis, up to 26 wt% of Fe_2O_3 (respectively 23.4 wt% FeO) can be determined (Table 2).

The high iron oxide supply results in degeneration of the brick microstructure and formation of Mg–Fe–oxide of magnesia-wuestite type (Fig. 5).

Non-oxide Infiltration

In addition to acidic slag, also other components like metallic lead, PbS, etc. infiltrate the brick microstructure. Generally, non-oxide infiltration only densifies the bricks microstructure without any corrosive attack on the brick components. Similar to the acidic slag, the degree of infiltration depends on the surface tension, the boundary angle in contact with the refractory oxides, the temperature, the bath height, and the size/distribution of the brick pores [14].

Microstructural Changes Due to High Temperature Load

Although the temperatures in lead furnaces are typically well below the maximum service temperature of the as-delivered refractory materials, the temperature plays an important role in the continuous wear of the bricks. The higher degradation rate caused by the reduced viscosity and higher diffusivity associated with an overheated melt clearly demonstrates the effect of temperature.

On the microscopic level, a very characteristic feature for this wear phenomenon is periclase crystal growth and lengthening towards the thermal gradient resulting in several mm long crystals. The crystal size of the single periclase crystals within the original sintered magnesia is usually up to 140 μm [13]. However, in highly degenerated brick microstructure, the single grains, as well as the classical ceramic microstructure with coarse grains and matrix fines, cannot be observed anymore; thus, they have grown into one big crystal. In addition to this, also the supplied oxide components such as zinc-, iron-, and tin-oxide act as mineralizing agents, thus strongly supporting the periclase crystal growth.

Such microstructural changes are typical for ferroalloy furnaces where the operating temperature is much higher than in base metal production. So far in lead processing, this wear phenomenon was observed in the KIVCET furnace only due to the high furnace operation temperature.

Table 2 Chemical analysis of magnesia-chromite brick out of short rotary furnace

wt%	Na_2O	Al_2O_3	MgO	SiO_2	SO_3[a]	CaO	Cr_2O_3	Fe_2O_3[b]	PbO	ZnO
Hot face[c]	2.0	4.0	39.0	4.0	3.0	2.0	11.0	26.0	8.0	0.4
Unused[d]		7.0	60.5	1.5		0.4	19.0	11.6		

[a]sulfur calculated as SO_3
[b]total iron calculated as Fe_2O_3
[c]standardless semiquantitative XRF analysis on original sample
[d]quantitative XRF analysis on ignited sample (1050 °C)

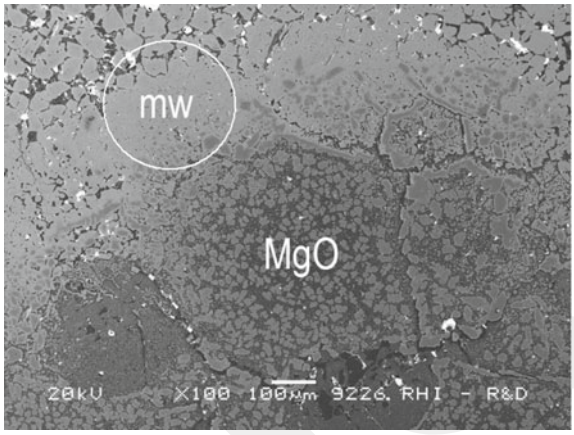

Fig. 5 Magnesia-chromite brick. Mineralogical investigation. Example of microstructural degeneration due to high iron oxide supply. Magnesia (MgO). Formation of magnesia-wuestite (mw)

Reduction/Red-Ox Phenomena

In the KIVCET furnace, Isasmelt™ and in the short rotary furnace, under reducing conditions, caused by low oxygen partial pressure or by the presence of metals, trivalent iron can be reduced to bivalent and further on to metallic iron. In the magnesia-chromite brick, especially the original chromite and newly formed chromite precipitations are sensitive to reduction of iron oxide (Fig. 6). The decrease of the iron valence results in a volume decrease and causes voids between the single grains. In case of a subsequent oxidation, the original brick microstructure will not reform. A frequent repetition of these reactions (Red-Ox) will result in a disintegrated brick microstructure.

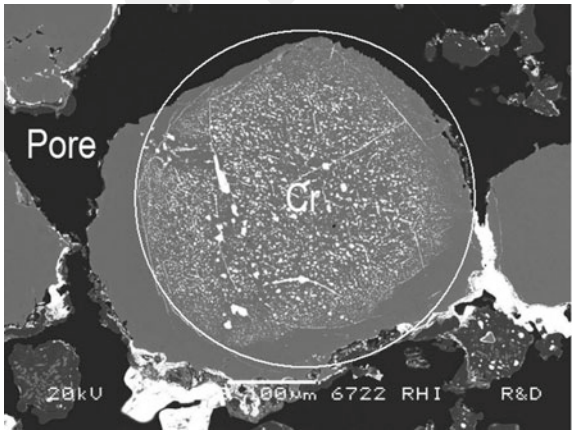

Fig. 6 Magnesia-chromite brick. Mineralogical investigation. Example of highly reduced brick microstructure. Partly bondless, severely reduced chromite (Cr)

High Soda Supply

The high alkali supply in secondary lead production vessels results under oxidizing atmospheric conditions in a formation of chromium (VI) salts. The chromate formation is caused by the key agents like potassium and sodium contained in the furnace feed. According to thermodynamic calculations by FactSage^{TM}, the formation of the chromate phases occurs in a temperature range between 900 and 1000 °C. By the use of the X-ray diffraction, alkali-bearing chromates such as $K_3NaCr_2O_8$ and K_2CrO_4 (tarapacaite) were identified. Both mentioned salts contain toxic chromium (VI).

Conclusion

Post-mortem studies clearly highlight which specific stresses affect the refractory product performance in the lead and zinc processing furnaces. Even though the various wear phenomena in the individual production vessels differ in their nature and cause, their final effect is the same, namely a significant refractory destruction by degeneration of the brick microstructure.

Furthermore, post-mortem studies demonstrated clearly that as consequence of chemical attack (by acidic slag, high supply on SiO_2, sulfur, soda, iron oxide), the infiltration and corrosion of the brick's inherent components lead to a weakening of the refractory microstructure, loss of flexibility, and brick strength. Such weakened microstructure is highly susceptible to continuous wear by hot erosion. Additionally, due to changed (thermo-)mechanical properties, crack formation, primarily at the interface between the infiltrated and non-infiltrated brick microstructure, occurs. Discontinuous wear by spalling is then the final consequence.

Also reduction and Red-Ox phenomena will result in permanent defects. Once the bond between particles and matrix is loosened, the brick microstructure will not reform. This reduces the strength of the brick and increases the susceptibility of the microstructure to further infiltration/corrosion.

The precise knowledge of the wear phenomena and the metallurgical process is an absolutely necessary prerequisite for the refractory producer for providing appropriate brick lining solutions. RHI Magnesita enhances this refractory optimization process through active collaborations with its customers. The post-mortem studies additionally provide an important base for the focused product development, leading to new refractory products for the lead and zinc industry.

References

1. Prengaman RD (2005) Secondary lead production—a survey of smelters and refineries. In: Lead and Zinc'05. Proceedings on the international symposium on lead and zinc processing. Kyoto, Japan, 17–19 Oct 2005
2. Lee YH, Park YM (2003) The experience of lead direct smelting in Korea Zinc's Onsan Refinery. In: Yazawa International symposium on metallurgical and material process. Warrendale, Pennsylvania, USA
3. Spanring A (2010) Refractory applications in the secondary lead industry. RHI Bull 1:56–62
4. Stephens RL (2005) Advances in primary lead smelting. In: Lead and Zinc'05. Proceedings on the international symposium on lead and zinc processing. Kyoto, Japan, 17–19 Oct 2005
5. Sofra J, Hughes R (2005) Ausmelt technology operation at commercial lead smelters. In: Lead and Zinc'05. Proceedings on the international symposium on lead and zinc processing. Kyoto, Japan, 17–19 Oct 2005
6. Wei L (2000) Corrosion of refractories in lead smelting reactors. University of British Columbia, M.Sc. thesis
7. Scheunis L, Mehrjardi AF, Campforts M, Jones PT, Blanpain B, Jak E (2014) The effect of phase formation during use on the chemical corrosion of magnesia-chromite refractories in contact with non-ferrous PbO–SiO_2 based slag. J Eur Ceram Soc 34:1599–1610
8. Kazanbaev LA, Kozlov PA, Kolesnikov AV, Ivakin DA (2004) Wear of basic refractories in the lining of waelz kilns in the production of zinc. Refract Ind Ceram 45:225–227
9. Gregurek D, Reinharter K, Majcenovic C, Wenzl C, Spanring A (2015) Overview of wear phenomena in lead processing furnaces. J Eur Ceram Soc 35:1683–1698
10. Prestes E, Chinelatto ASA, Resende WS (2009) Post mortem analysis of burned magnesia-chromite brick used in short rotary furnace of secondary lead smelting. Ceramica 55:61–66
11. Oprea G (2004) Failure mechanism of refractory linings for non-ferrous flash smelting furnaces. In: Proceedings of Tehran international conference on refractories. Tehran, Iran, 4–6 May 2004
12. Osborn EF, Muan A (1960) Phase equilibrium diagrams of oxide systems. American Ceramic Society with the Edward Orton Jr. Ceramic Foundation, Columbus, Ohio, USA
13. Routschka G (2017) Praxishandbuch Feuerfeste Werkstoffe. Vulkan-Verlag, Essen
14. Barthel H (1981) Wear of chrome magnesite bricks in copper smelting furnaces. Interceram 30:250–255

Numerical Simulation of Gas–Liquid Flow Mixing Effect in Bottom-Blown Bath

Dong-bo Li, Peng Li, Xin Yao, Cheng Liu and Ze-shang Dong

Abstract In order to clarify the stirring mechanism of a bottom-blown bath, the volume of fluid (VOF) multiphase flow model was used to simulate the gas–liquid two-phase flow process. The simulation results were verified by water model test, and the influence of gas–liquid mixed melt process was analyzed. The results show that the separation effect of matte is better when the injection angle is between 15° and 22.5°. When the gas velocity is 70 m/s, the gas stirring radius is 1 m, so the distance between the oxygen lance and the furnace wall is 1–1.5 m, which can ensure that the furnace wall is not washed by excessive melt. The optimum spacing of the oxygen lance is controlled at 2–3 m, the distribution of oxygen lances is more reasonable, the effect of bath agitation is better, and the splash caused by excessive bath agitation is prevented.

Keywords Bottom-blown bath · Gas–liquid mixing · VOF model · Numerical simulation

Introduction

Because of the complicated gas–liquid mixing flow process in a bottom-blown molten bath, there are many difficulties in its theoretical research. However, with the rapid development of computing technology in recent years, the research on the stirring mechanism of bottom-blown molten baths has gradually increased. At present, the research on bottom-blown molten baths is mainly based on numerical simulation to explore the influence of gas flow rate, oxygen lance structure, oxygen lance diameter, and injection angle on the melt flow in the molten bath. For example, Li et al. [1, 2] simulated the gas–liquid-slag three-phase flow process of a bottom blowing ladle based on VOF multiphase flow and standard k-ε turbulence model and explored the relationship between the bottom blowing gas flow rate and the dimensionless area of the slag hole and melt flow near the slag hole. Zhang et al. [3, 4] established a

D. Li · P. Li · X. Yao (✉) · C. Liu · Z. Dong
China ENFI Engineering Technology Co. LTD, Beijing 100038, China
e-mail: yaoxin@enfi.com.cn

© The Minerals, Metals & Materials Society 2020

A. Siegmund et al. (eds.), *PbZn 2020: 9th International Symposium on Lead and Zinc Processing*, The Minerals, Metals & Materials Series,
https://doi.org/10.1007/978-3-030-37070-1_3

three-dimensional mathematical model of gas–liquid two-phase flow in a bottom-blown molten bath by means of numerical simulation. The optimum arrangement of oxygen lances structure was obtained by taking gas holdup, average melt velocity, and average turbulent kinetic energy as optimization indexes. Yan et al. [5] studied the gas–liquid two-phase flow process of a high temperature melt in a bottom-blown molten bath by numerical simulation, discussed the arrangement of oxygen lance and the relationship between the diameter of the oxygen lance and the melting process of molten bath, and obtained the layout and diameter of the oxygen lance under the optimum melting conditions. Zhang et al. [6] used the Eulerian–Eulerian model to describe the gas–liquid two-phase flow in the bottom blowing melting bath and explored the gas–liquid two-phase flow at different injection angles. The simulation results of flow characteristics and gas content show that the surface splashing of molten bath is more serious when the oxygen lance angle is 14°. Yu et al. [7] used the VOF model to explore the relationship between four different nozzle structures and the mixing area and found that the dispersive nozzle structure is more favorable for mixing.

The above papers provide many application examples and model calculation methods for the application of numerical simulation in the molten bath, but there is no in-depth discussion on the oscillation effect, and the content of gas in the molten pool has a great influence on the chemical reaction in the molten pool, so it is necessary to further analyze the change rule of gas content. The model of the bottom-blown smelting furnace is established to simulate the gas–liquid two-phase mixing flow process in a bottom-blown molten bath, which can visually reproduce the swing phenomenon during the process of gas jet injection and can monitor and analyze the disturbance and moment generated in the process, meet the needs of engineering design, and provide a theoretical basis for the development of new equipment.

Physical Model

Taking a horizontal rotary bottom-blown copper smelting furnace as the research object, the external diameter of furnace is 5.8 m, the length is 30 m, and the thickness of furnace body is 0.5 m. The specific structural parameters of the model are shown in Table 1. The gas inlet is located at the bottom of the furnace with 30 cross-arranged oxygen lances. The lance pressure is 0.1 Mpa.

Oxygen is ejected from the nozzle of the lances, and multiple jets are ejected to mix with the surrounding melt. The original static pressure head is transformed into dynamic pressure head to overcome the resistance of pipeline, spray gun, and melt so as to form a uniform diffusion zone of gas in the molten bath. The gas trajectory is controlled by the structure parameters and process parameters of the oxygen lance and furnace body, so that the diffusion zone has its standardized shape and trajectory, which is consistent with the geometry of the furnace body. This gives a relatively uniform diffusion zone, which has no swirl, no splash, and no dead zone.

Table 1 Bottom blowing simulated boundary conditions

Phase	Parameter	Unit	Number
Matte	Density	kg/m^3	5075
	Viscosity	kg/m s	2.5×10^{-3}
	Surface tension	N/m	0.33
Slag	Density	kg/m^3	3200
	Viscosity	kg/m s	0.2
	Surface tension	N/m	3.17×10^{-4}
Oxygen-enriched air	Density	kg/m^3	1.27
	Viscosity	kg/m s	1.982×10^{-5}

Mathematical Model

Model Assumptions

Without affecting the results, and in order to speed up the calculation process, it is necessary to rationally simplify the actual bottom blowing model and set up hypothetical conditions, as follows:

(1) The interface between gas and liquid is a free surface.
(2) Initialize the uniform temperature distribution in the molten bath, without considering the influence of chemical reaction and temperature field on the physical properties of the molten bath.
(3) The initial height of molten bath is 2.5 m, ignoring the influence of feeding and discharging on the height of molten bath.
(4) The wall is considered a non-slip boundary, and the standard wall function is used to deal with the boundary layer near the wall.

Numerical Calculation Model

VOF Model

The VOF model is typically used to simulate a variety of non-mixable fluids, so it is mainly used to simulate the gas–liquid mixing process in this simulation, including stratified flow and free surface flow. VOF model assumes that the multiphase fluid does not exist between each other throughout; in the model every phase, you need to introduce a phase volume fraction in each control volume, all phase volume fraction and 1 in the control volume, if the volume fraction of the q phase fluid for α, then it will be there are three possibilities:

$\alpha = 0$: phase q fluid is empty within the control volume.
$\alpha = 1$: phase q fluid is full within the control volume.
$0 < \alpha < 1$: the unit contains the phase interface between the q phase fluid and other fluids.
The basic equations describing the VOF model are as follows:

(A) Volume fraction equation

$$\frac{\partial \alpha_q}{\partial t} + \overrightarrow{u} \cdot \nabla \alpha_q = \frac{S_{\alpha_q}}{\rho_q} \tag{1}$$

α_q Volume fraction of Q phase (%);
ρ_q Density of Q phase (kg/m3);
$\overrightarrow{u}$ Fluid velocity (m/s);
$S_{\alpha q}$ Source phase.

(B) Momentum equation

In the VOF model, the velocity field is obtained by solving a single momentum equation in the region. The results of the velocity field are shared by all phases. The momentum equation is determined by controlling the fluid density and viscosity of all phases in the computational domain.

$$\frac{\partial}{\partial t}(\rho \overrightarrow{u}) + \nabla \cdot \left(\rho \overrightarrow{u}\,\overrightarrow{u}\right) = -\nabla p + \nabla \cdot [\mu(\nabla \overrightarrow{u} + (\nabla \overrightarrow{u})^T)] + \rho \overrightarrow{g} + \overrightarrow{F} \tag{2}$$

ρ Fluid density (kg/m3);
$\overrightarrow{u}$ Fluid velocity (m/s);
μ Viscosity (Pa. s);
$\overrightarrow{F}$ Volume force (N).

The above densities and viscosities are calculated on the basis of the average volume fraction. The specific expressions are as follows.

$$\rho = \sum \alpha_q \rho_q \tag{3}$$

$$\mu = \sum \alpha_q \mu_q \tag{4}$$

Standard *k-e* Turbulence Model

The standard *k-e* model introduces two unknowns: turbulent kinetic energy k and turbulent dissipation rate E. The expressions of the eddy viscosity coefficient T are as follows.

$$k = \frac{1}{2}(\overline{u'^2} + \overline{v'^2} + \overline{w'^2}) = \frac{1}{2}(\overline{u_i'^2}) \tag{5}$$

$$\varepsilon = \frac{\mu}{\rho}\overline{\left(\frac{\partial u_i'}{\partial x_k}\right)\left(\frac{\partial u_i'}{\partial x_k}\right)} \tag{6}$$

$$\mu_t = \rho C_\mu \frac{k^2}{\varepsilon} \tag{7}$$

k is the sum of the velocity variance divided by 2, C_μ-empirical constant.
The transport equations corresponding to the two unknowns are:

(A) Turbulence kinetic energy k equation:

$$\rho\left[\frac{\partial k}{\partial t} + \frac{\partial}{\partial x_i}(ku_i)\right] = \frac{\partial}{\partial x_j}\left[\left(\mu + \frac{\mu_t}{\sigma_k}\right)\frac{\partial k}{\partial x_j}\right] + G_k + G_b - \rho\varepsilon - Y_M + S_k \tag{8}$$

(B) Turbulent dissipation rate ε equation:

$$\rho\left[\frac{\partial \varepsilon}{\partial t} + \frac{\partial}{\partial x_i}(\varepsilon u_i)\right] = \frac{\partial}{\partial x_j}\left[\left(\mu + \frac{\mu_t}{\sigma_\varepsilon}\right)\frac{\partial \varepsilon}{\partial x_j}\right] + C_{1e}\varepsilon\frac{G_k + C_{3e}G_b}{k} - C_{2e}\rho\frac{\varepsilon^2}{k} + S_\varepsilon \tag{9}$$

$$G_k = \mu_t\left(\frac{\partial u_i}{\partial x_j} + \frac{\partial u_j}{\partial x_i}\right)\frac{\partial u_i}{\partial x_j},\ G_b = \beta g_i\frac{\mu_t}{\mathrm{Pr}_t}\frac{\partial T}{\partial x_i},\ \beta = -\frac{1}{\rho}\frac{\partial \rho}{\partial T},\ Y_M = 2\rho\varepsilon M_t^2 \tag{10}$$

G_k	Turbulent kinetic energy generated by mean velocity gradient;
G_b	Turbulent kinetic energy produced by the effect of melt on buoyancy of bubbles;
Y_M	The effect of fluctuating expansion of compressible turbulence on total dissipation rate;
$C_{1\varepsilon}$, $C_{2\varepsilon}$, $C_{3\varepsilon}$	Empirical constants are 1.44, 1.92, and 0.09, respectively;
∂k, $\partial \varepsilon$	The Prandtl number corresponding to turbulent kinetic energy and turbulent dissipation rate is 1.0 and 1.3, respectively;
Pr_t	Plante number;
g_i	Gravity acceleration component in direction i (m/s^2);
β	The coefficient of thermal expansion (°C^{-1});
M_t	Turbulent Mach number.

Boundary Conditions

There are 30 oxygen lances at the entrance of the matte, and the gas is compressible due to the high inlet velocity (Ma > 0.5). The total oxygen-enriched air volume is 55,415 m^3/h, the inlet velocity of a single oxygen lance is 250 m/s, the turbulent intensity is 5%, the inlet pressure is 0.6 MPa, and the velocity at the wall is zero under the non-slip boundary condition. The specific boundary condition parameters are listed in the table below.

Model Validation

The gas–liquid two-phase flow process in the water model test device was photographed and analyzed. The accuracy of the simulation results was verified by comparing the simulation results with the experimental results. The water model is based on the bottom blowing furnace in Fig. 1 and is designed according to the ratio of 1:10. The design dimensions and experimental parameters are listed in Table 2.

The bubble formation and buoyancy process in the water model were captured by high-speed camera. It can be seen from Fig. 1, the experimental results and the numerical simulation that the shape change of bubbles in the flow process is basically the same. The injection states of single/double guns at different angles are compared. From the comparison of the results of physical water model experiment

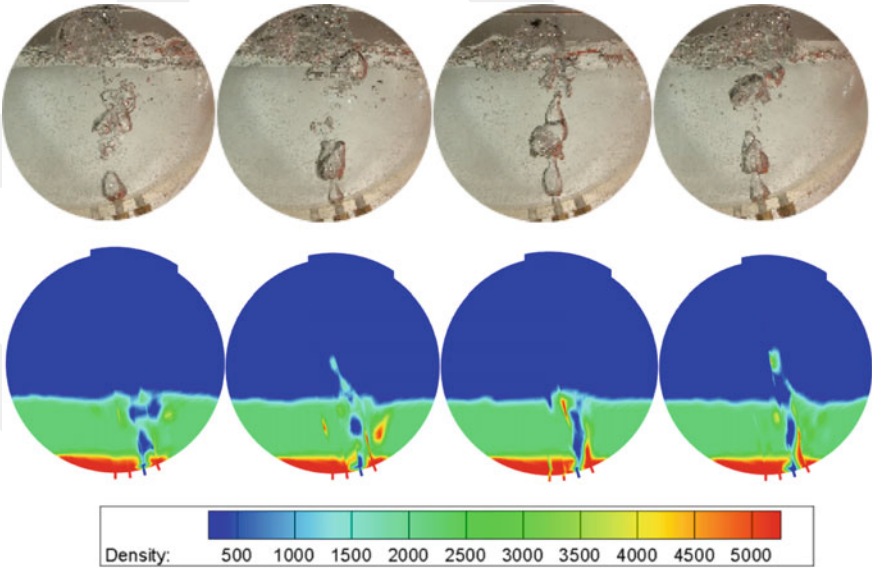

Fig. 1 Comparison of physical (top row) and numerical simulation (bottom row) results

Table 2 Model size and experimental parameters

Furnace diameter (m)	Length (m)	Lance diameter (m)	Liquid level (m)	Viscosity (kg/m s)
0.47	3	0.06	0.25	1.01×10^{-3}

and numerical simulation post-processing, it can be seen that the simulation results in different stages are basically consistent with the experimental results in the shape change of bubbles in the flow process. Therefore, the numerical simulation method adopted in this paper can reflect the results.

Simulation Results and Discussion

Analysis of the Volume Fraction of Oxygen in Melt

The control of oxygen volume fraction in the molten bath can prevent the oxidative of equipment. However, the reaction of mineral particles with too little oxygen content is incomplete, and the less heat released makes it difficult to maintain the smelting process. The change of oxygen volume fraction in molten bath is shown in Fig. 2, the curve of oxygen volume fraction in 10 s.

From the results of the analysis in Fig. 2, it can be seen that the volume fraction of oxygen in the molten bath increases continuously from the beginning of gas injection until 1 s, reaching a peak value of 5.2%. Because part of the gas spilled out, reaction, and at the same time continuously into the molten bath, so in a period of time after the gas content reached equilibrium. The volume fraction of oxygen in the molten bath begins to decrease and finally stabilizes at about 4% after a period of fluctuation. Therefore, it can be considered that 4% of oxygen in the molten bath will exist in the melt and participate in the reaction between mineral particles.

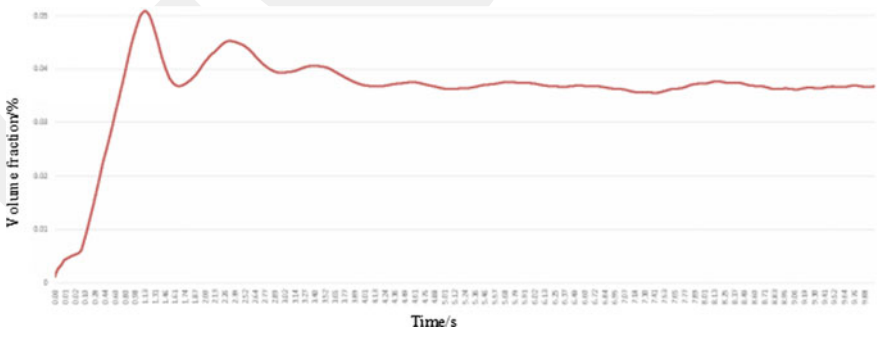

Fig. 2 Volume fraction curve of oxygen in melt

Disturbance Analysis of Gas Jet on Equipment in Furnace Operation

From the above analysis, it can be concluded that the oscillation of melt and gas jets will occur after a period of operation, which will cause the oscillation of the molten bath. The oscillation of the molten bath has adverse effects on the smooth operation of the furnace and the life of the furnace. Therefore, according to the magnitude and variation of disturbance force in each direction of the molten bath in 65 s, the calculation knot can be obtained. As a result, further analysis of the variation of disturbance force in different directions of the furnace body will play a certain role in adjusting the position of oxygen lance nozzle and the size of gas injection to ensure the stability of the molten bath.

From Fig. 3, it can be found that the variation of *X*-direction, i.e. the longitudinal disturbance force of the furnace body, is relatively stable (0–6000 N), but the frequency increases gradually. Therefore, it is considered that the swing amplitude of gas jet in the axial direction of the furnace body is relatively stable, but the swing frequency is gradually accelerated. From Fig. 4, it can be seen that the Y-direction of the furnace body, i.e. the transverse disturbance, presents a relatively obvious increase process (0–150,000 N), but the frequency of change is relatively stable, and there are about four change periods in 10 s. Through the above analysis, it can be concluded that the oscillation of molten bath is directly related to the disturbance force of gas jet in all directions of the furnace body. The gas jet will oscillate in the molten bath, and the size changes regularly. The oscillation frequency along the longitudinal direction accelerates, and the disturbance force along the transverse direction increases gradually. Therefore, adjusting the distribution density and quantity of oxygen lance in the axial direction can play an intuitive role in reducing the oscillation of the molten bath.

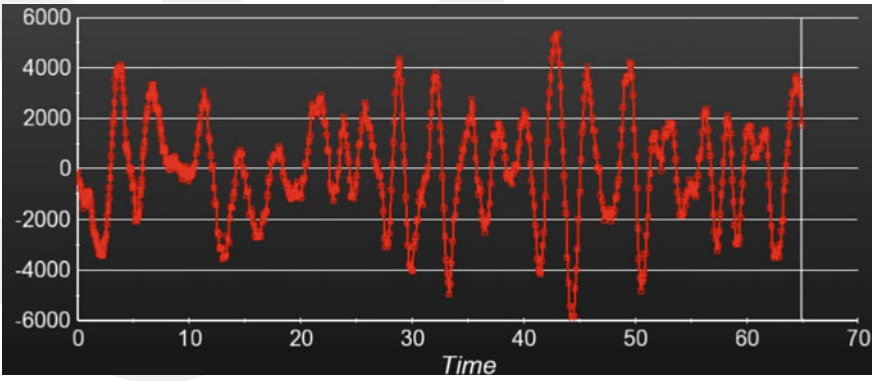

Fig. 3 *X*-directional/longitudinal disturbance analysis of furnace body

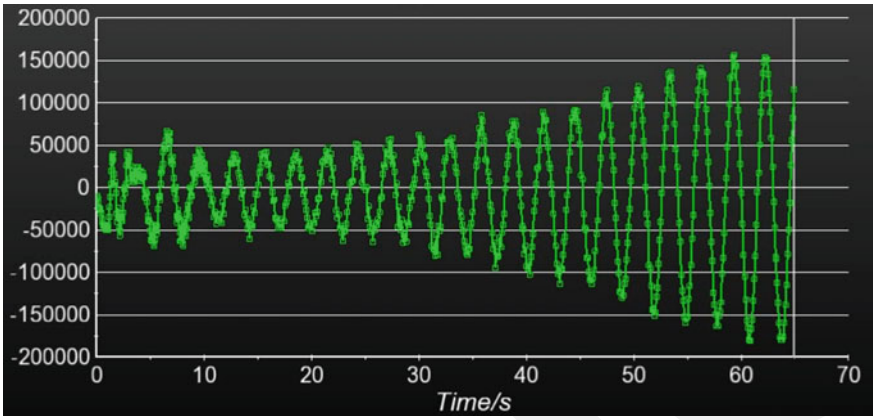

Fig. 4 *Y*-direction/transverse disturbance analysis of furnace body

Conclusion

In this paper, a VOF multiphase flow model is used to simulate the gas–liquid mixing and agitation process in a bottom-blown molten bath. Based on the experimental results from the water model, the flow pattern characteristics and data of bottom-blown gas jet are obtained. The following conclusions can be drawn:

(1) Compared with the results of the water model experiment and numerical simulation, the qualitative analysis images are similar to the numerical simulation of gas jet flow. The bubble flow law and phase characteristics are basically consistent, which verifies the reliability of the VOF multiphase flow model. The simulation results basically reflect the real change of bottom blowing molten bath.

(2) The maximum oxygen content in the molten bath can reach 5.2%, which maintains at about 4% with the stable operation of the furnace, and is mainly in the middle and upper part of the molten bath. Therefore, any excessive oxygen injected does not participate in the oxidation reaction, but follows the flue gas into the flue, and reduces the SO_2 content in the flue gas, which is not conducive to the subsequent acid production process.

(3) The disturbance force of the bottom-blown molten bath has different characteristics in different directions. In the *X*-direction, the disturbance force of the longitudinal jet along the furnace body is relatively stable (0–6000 N), and the swing frequency is accelerated; in the *Y*-direction, the swing amplitude of the transverse jet along the furnace body increases gradually (0–150,000 N), and the swing frequency remains stable (four cycles of 10 s). Therefore, attention should be paid to the spacing and the number of oxygen lances to prevent excessive injection.

References

1. Li B, Yin H, Zhou CQ, Tsukihashi F (2008) Modeling of three-phase flows and behavior of stag steel interface in an argon gas stirred ladle. ISIJ Int 8(12):1704–1711
2. LI B-K, GU M-Y, QI F-S, WANG F, ZHOU Q (2008) Modeling of three-phase (gas/molten steel/slag) flows and slag layer behavior in an argon gas stirred ladle. Acta Metall Sin 44(10):1198–1204
3. Zhang Z, Chen Z, Yan H, Liu F, Liu L, Cui Z, Shen D (2012) Numerical simulation of gas–liquid flows in oxygen enriched bottom-blown furnace. Chin J Nonferrous Met 22(6):1826–1834
4. Zhang Z, Yan H, Liu F, Wang J (2013) Optimization analysis of lance structure parameters in oxygen enriched bottom-blown furnace. Chin J Nonferrous Met 23(5):1471–1477
5. Yan H, Liu F, Zhang Z, Gao Q, Liu L, Cui Z, Shen D (2012) Influence of lance arrangement on bottom-blowing bath smelting process. Chin J Nonferrous Met 22(8):2393–2400
6. Shao P, Zhang Y, Liu Y, Wang D (2012) Numerical simulation of gas liquid flow behavior in a copper matte bottom blowing converter. J Northeast Univ Nat Sci 33(9):22
7. Yu Y, Wen Z, Liu X, Su F, Lan H, Hao X (2014) Simulation and experiment of influence of nozzle structure on bottom-blowing furnace flowing process. J Central South Univ Sci Technol 45(12):4129–4236

GCRIS

Slag Reduction Kinetics of a Lead Slag from a Secondary Lead Smelter

Stuart Nicol, Joseph Grogan, Boyd Davis and Trevor Lebel

Abstract In the classical pyrometallurgy route for lead smelting, the smelter produces a slag containing measurable quantities of lead. The lead in the slag is most often discharged from the smelter, leading to the disposal of significant quantities of lead. The slag needs to be safely stored to prevent the release of lead into the environment. In this work, the recovery of lead, and other deleterious elements, from a lead smelter slag has been investigated experimentally. Thermodynamic simulation was performed to determine the viability of a methane reduction process. Based on the thermodynamic simulation and knowledge of the phases and distribution of elements between the phases in the smelter slag, methane reduction was tested on a bench scale. A comparison between the thermodynamic predictions and observations provides an insight into the processes occurring during reduction and the kinetic limitations of this process.

Keywords Lead slags · Reduction · Slag cleaning

Introduction

In both primary and secondary lead smelters, significant quantities of lead are discharged into the environment each year. Without the use of a settling (or zinc fuming) furnace, slag is discharged from the smelter containing between 0.5 and 3 wt% Pb [1]. This results in a smelter discharging significant quantities of lead into the surrounds each year.

Primary smelter slag is cleaned at some smelters with the zinc fuming furnace, resulting in a discharge slag with less than 0.1 wt% Pb. Other techniques have been used, including settling furnaces and TSL furnaces. However, this slag cleaning is only performed if there is sufficient zinc in the slag to make the process financially

S. Nicol · J. Grogan (✉)
Gopher Resource, 685 Yankee Doodle Road, Eagan, MN 55121, USA
e-mail: joe.grogan@gopherresource.com

B. Davis · T. Lebel
Kingston Process Metallurgy, 759 Progress Avenue, Kingston, ON K7M 6N6, Canada

© The Minerals, Metals & Materials Society 2020

A. Siegmund et al. (eds.), *PbZn 2020: 9th International Symposium on Lead and Zinc Processing*, The Minerals, Metals & Materials Series,
https://doi.org/10.1007/978-3-030-37070-1_4

viable. With increasingly stringent environmental regulations worldwide, there is the need to determine alternative methods to reduce the lead contained in these slags.

Lead is lost to the slag through two mechanisms, entrainment and dissolution. Entrained lead is present in the slag due to insufficient settling prior to the tapping of the slag from the furnace or forehearth. The lead lost through dissolution is commonly classified as either sulfidic or oxidic, with the sulfidic losses incurred by the incorporation of sulfur into the molten oxide solution. The entrained metal is able to be recovered through further settling of the slag. To completely recover the remaining dissolved material, chemical processes are required.

Selective reduction of lead is performed in the lead smelting process. As such, it is reasonable to suggest that further selective reduction has the potential to recover further quantities of lead from the slag. In this experimental work, methane ($CH_{4(g)}$) has been used for this purpose. However, it is possible to use other reductants in industrial processes.

The gaseous reduction of slags has been extensively researched. It has been demonstrated that methane is able to reduce copper containing slags, resulting in slags with about 0.3% Cu before iron begins to reduce to a significant percent [2]. The reduction of slags using methane focused more on copper, but treating lead slags is also important. Fundamental research has been performed on the reduction of PbO from a $CaO–FeO_x–MgO–PbO–SiO_2$ slag with a CO/CO_2 gas mixture [3]. The reducing gas was blown over a slag, with variations in the gas composition, temperature, 'FeO' concentration, PbO concentration, slag agitation, and slag depth. It was shown that, for the slag system and conditions investigated, the reduction of PbO was dependent on the 'FeO' concentration, gas composition, and the slag temperature and composition. The rate-controlling step was suggested to be the formation of the $CO_{2(g)}$ at the slag/gas interface. Diffusion of ionic species within the slag was rapid.

Based on the fundamental research on the kinetics of lead slag reduction, it is proposed that the reduction of lead containing slag by methane injected into the melt is possible. Injecting methane into the slag provides a reducing atmosphere, with the bubbles providing a high surface area for the $CO_{2(g)}$ formation at the slag/gas interface. The aim of this paper is to examine the feasibility of the injection of methane into a molten slag to reduce the lead contained in the slag.

Experimental Study

Characterization of the Slags

The slag used for this study was taken from the Blast Furnace at the Gopher Resource Eagan Smelter. Slag was sampled from the slag pots, after settling of entrained bullion and matte had occurred. The slag bulk composition is summarized in Table 1.

Table 1 Bulk slag composition

	Na_2O (wt%)	SiO_2 (wt%)	'FeO' (wt%)	'Pb' (wt%)	Others (wt%)
Settled slag	18	32	31	0.7	18.3

Note that 'FeO' and 'Pb' are used for presentation purposes. The bulk slag includes Fe^{2+}, Fe^{3+}, and Fe^0 and Pb^{4+}, Pb^{2+}, and Pb^0. The Pb content in the slag can vary significantly and could be up to 3%, depending on the slag. For the thermodynamic calculations, a soluble PbO of 0.7 wt% was assumed. For the test work, since the concern was around reaching low levels of soluble lead, a slag with lower lead (0.17%) was used

Methane Reduction Set Up

The set-up for the reduction is shown in Fig. 1. Slag to be reduced is crushed, ground, and homogenized. Approximately 850 g of ground slag is loaded into the alumina crucible and positioned within a reactor tube with inert gas (N_2 flowing). Samples are heated to 1150 °C at a rate of 4.5 °C/min. After heating, the slag is homogenized by the injection of N_2 into the slag through the lance at 260 ml/min for 5 min. After homogenization, duplicate samples were taken of the melt at ~9 cm above the bottom (approximately half height). Once the melt samples were taken, CH_4 bubbling was started at 160 ml/min (and the N_2 was decreased to 100 ml/min). Bubbling was allowed to continue for a total of 60 min, with a few stops during the test to take pin tube samples of the melt. Sampling was done in duplicate at the mid-height after 2, 5, 20, 40, and 60 min of CH_4 bubbling.

The online infra-red gas analyzer allows for tracking of the CO and CO_2 content in the gas during reduction. The experimental conditions of the inlet gas were such that the reducing gas flow in the melt is delivered as pure methane, increasing the partial pressure of the reducing species in the gas phase and in turn the mass transfer of oxygen containing species to and from the slag-gas interface. For each mole of CH_4 that reacts, between 3 and 4 mol of oxygen are removed from the slag, depending on the CO/CO_2 ratio in the gas phase. Assuming that all of the CH_4 reacts to form $H_2O_{(g)}$, the total amount of oxygen released from the bath can be calculated from the $CO + CO_2$ from the gas analysis, and this corresponds to the reduction of oxide species in the slag.

At the completion of the 60 min of CH_4 bubbling, the methane and nitrogen bubbling was stopped, and the phases entrained in the slag were allowed to settle, while remaining molten for 15 min. The crucible was then lowered in the cold zone for rapid cooling to below the solidus temperature (melting point). After fully cooled, the crucible was sliced to get samples at various heights: 2.5; 7.5; and 12.7 cm from the bottom.

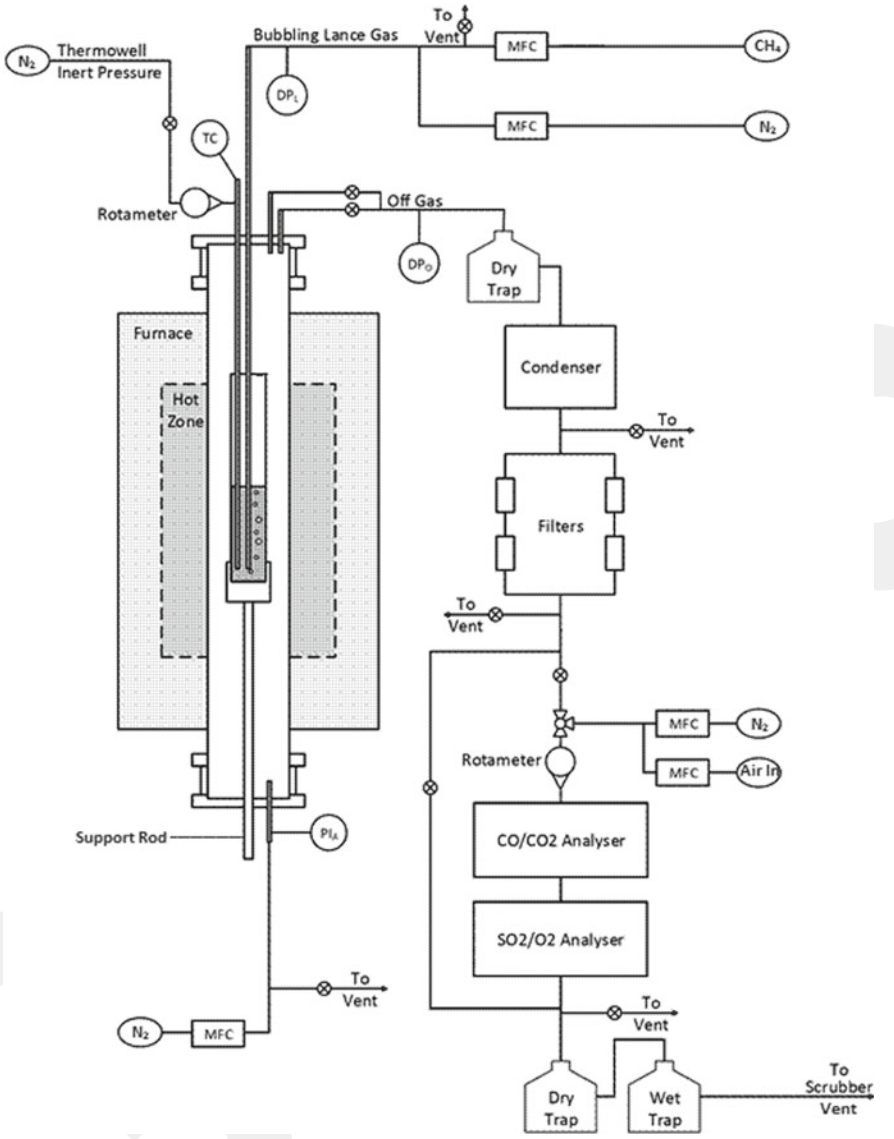

Fig. 1 Schematic for settling experiments

Thermodynamic Simulation

To estimate the impact of methane additions to the slag, thermodynamic simulations were performed with FactSage 7.2. For the thermodynamic simulations, the Pb-liq model was used for the lead phase, the FeS phase used for the sulfide phase, and the

slag model was used for the liquid slag. The FeS phase was selected as this solution model most accurately simulated the matte phase composition generated during the reduction experiments. The oxygen potential (using Fe_2O_3) was adjusted at the start to have an activity of the Pb-liq phase just below 1. The results of the simulation were plotted in Fig. 2, with increasing CH_4 (and decreasing pO_2) versus the percentage of the main metal oxides reduced from the slag, starting at an initial 0 g CH_4.

For the above-mentioned test, about 075 g of CH_4/100 g of slag were added. This degree of reduction for the test is perhaps not 'deep' since there is still significant iron in the slag. However, there is relatively considerable methane injected into the slag, and it is clear that lead is being reduced significantly (almost 90% after 0.75 g/100 g of slag) in the first stage of reduction and that other metal oxides are only slightly reduced.

The thermodynamic simulation provides an indication for what can be reduced from the slag under equilibrium conditions. The accuracy of the simulation is limited by the fundamental phase equilibria data available for solution model fitting, which is extremely lacking in the binary and ternary systems relevant to the slag composition of interest. Under the conditions investigated, it is expected that reaction kinetics are relatively rapid, but there will be a deviation from equilibrium conditions.

The thermodynamic simulations predict that lead in the slag is recovered rapidly, such that after the addition of 5 g CH_4/100 g of slag, the only measurable lead loss to the slag would be as small entrained prills. Entrainment of lead in the slag is reasonable to expect as prills of less than 15 μm are not settled from the slag with the technique used. During the reduction of lead from the slag, other metal species are co-reduced, with zinc rapidly reduced in conjunction with the lead. Iron is reduced

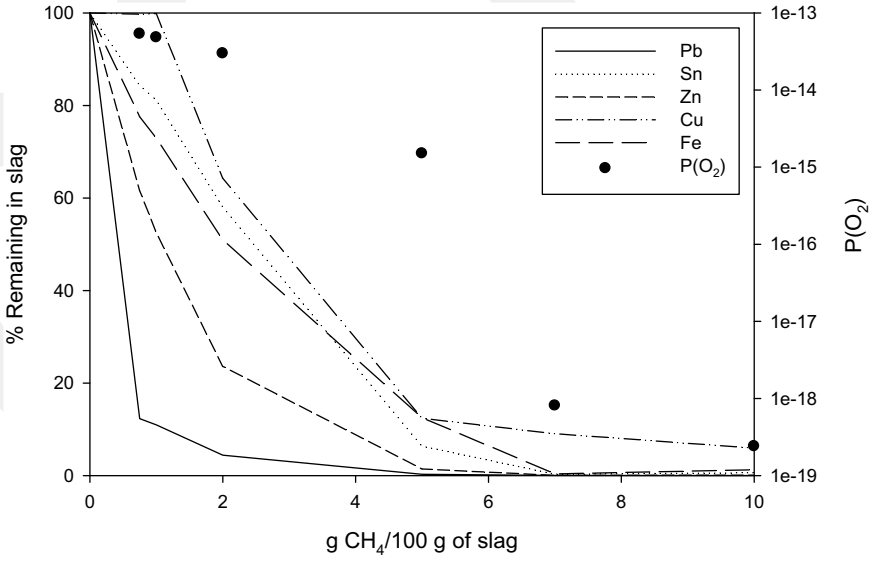

Fig. 2 Percentage of base metals remaining in slag as it is reduced and corresponding $P(O_2)$

throughout the process and will be entirely removed from the slag before copper is fully recovered. The thermodynamic calculations indicated that the copper in the slag is strongly associated with the sulphur in the slag, preventing the recovery of copper until a significant quantity of other metal species has been recovered from the slag. Discussions of exact equilibrium concentrations in the slag are not justified given the uncertainty in the models.

The deep reduction of slags (where iron is reduced) has also been suggested for copper slags. For copper slags, the base slag is an iron silicate, SiO_2–FeO, and the removal of iron requires the addition of another oxide to maintain a molten slag during the reduction process. For the lead slag investigated, the base slag is a sodium silicate, with neither of these species reduced under deep reduction conditions. The binary phase diagram, shown in Fig. 3, shows that for the current 32/18 mass ratio of SiO_2 to Na_2O (65/35 mol ratio), the slag liquidus is below 900 °C, which allows for operability when iron oxide is reduced. Another advantage is that the reduced iron has very limited solubility in the lead and will form solid particles which can grow in the slag [4]. This means that they can either be recovered at the bottom of the slag, or the slag can be crushed and magnetically separated if desired, but they will not contaminate the lead. However, this iron could also cause operational problems in the reduction process and requires significantly more methane to reduce than the small amount of lead in the slag.

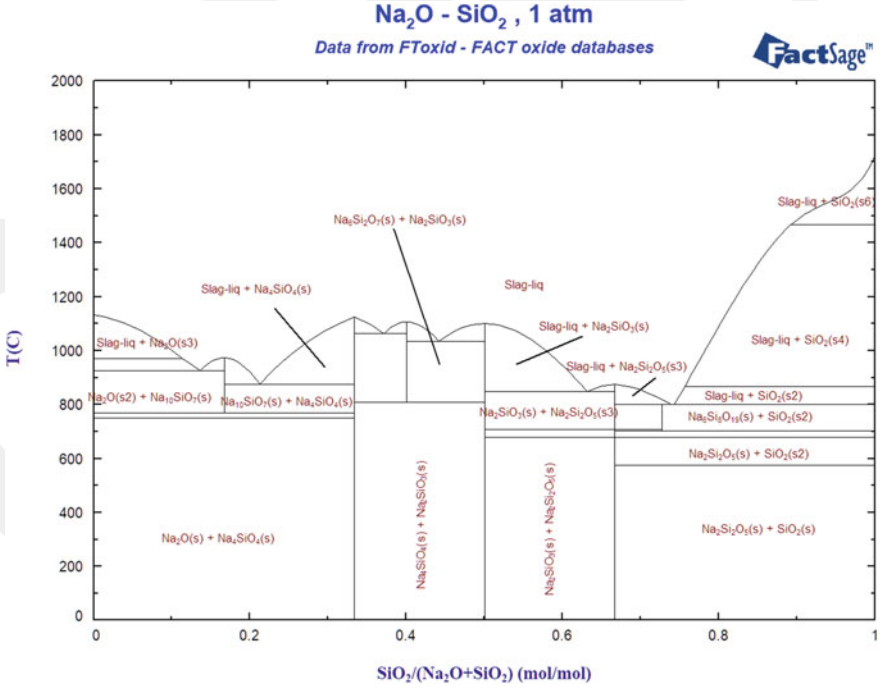

Fig. 3 Sodium silicate phase diagram

Table 2 Slag composition with respect to time during methane reduction

Time (min)	Na_2O (wt%)	SiO_2 (wt%)	S (wt%)	'FeO' (wt%)	Pb (wt%)	Others (wt%)
0	15.8	35.5	3.10	30.3	0.17	15.0
2	15.1	35.8	3.00	30.5	0.14	15.5
5	15.9	35.8	3.03	30.8	0.09	14.4
20	15.2	36.1	3.06	30.2	0.03	15.4
40	14.5	35.8	3.65	30.6	0.04	15.4
60	15.4	36.1	3.01	29.3	0.05	16.3

Methane Reduction

Tests for methane reduction only focused on initial lead removal and did not move in the 'deep reduction' regime. During the methane reduction tests, the lead contained in the slag was observed to decrease from 0.17 to 0.05 wt% during the reduction experiments. This represents a recovery of 71% of the lead in the slag. Other components of the slag are expected to be reduced as well, but the change in concentration for most other elements was outside the limits of the experimental accuracy. A summary of the slag composition as measured during the experiments is summarized in Table 2.

The recovery of lead over time during the experiments is illustrated in Fig. 4. It shows that the initial reduction of lead and zinc is rapid, achieving a recovery of approximately 80% after 20 min. After 20 min, the further reduction of the lead does not result in an increased recovery of lead from the slag. This suggests that the methane is reducing another component of the slag and/or the kinetics of the reduction are dropping as the lead and zinc concentrations decrease, or, as in part, fine lead in the slag is not settling out and leaving a background lead concentration.

The extent and rate of reduction under the experimental conditions were slightly lower than that predicted under equilibrium conditions. This is believed to be related to kinetic effects. Due to the high partial pressure of reducing gas species within the gas bubbles, the main limitations in the reduction processes are the reaction as the slag/gas interface and the diffusion of species within the slag. With a decrease in concentration of a species in the slag, the rate of mass transfer of that species within the slag decreases. As such, it is reasonable to conclude that the rate of reduction is mass transfer limited at low concentrations within the slag.

The off-gas composition measured during the experiments is summarized in Fig. 5. Based on the measured off-gas composition, the partial pressure of oxygen (pO_2) in the off-gas was calculated from the measured CO/CO_2 ratio. This pO_2 is compared to the pO_2 for the Fe/FeO reaction couple assuming an activity of 1 for both condensed phases. The calculated and Fe/FeO reaction pO_2 is shown in Fig. 5.

During reduction, the pO_2 as calculated from the CO/CO_2 reaction couple was initially more oxidizing than the Fe/FeO reaction couple, suggesting that no metallic iron was present at the start of reduction. After the initial 5 mins of reduction, the pO_2

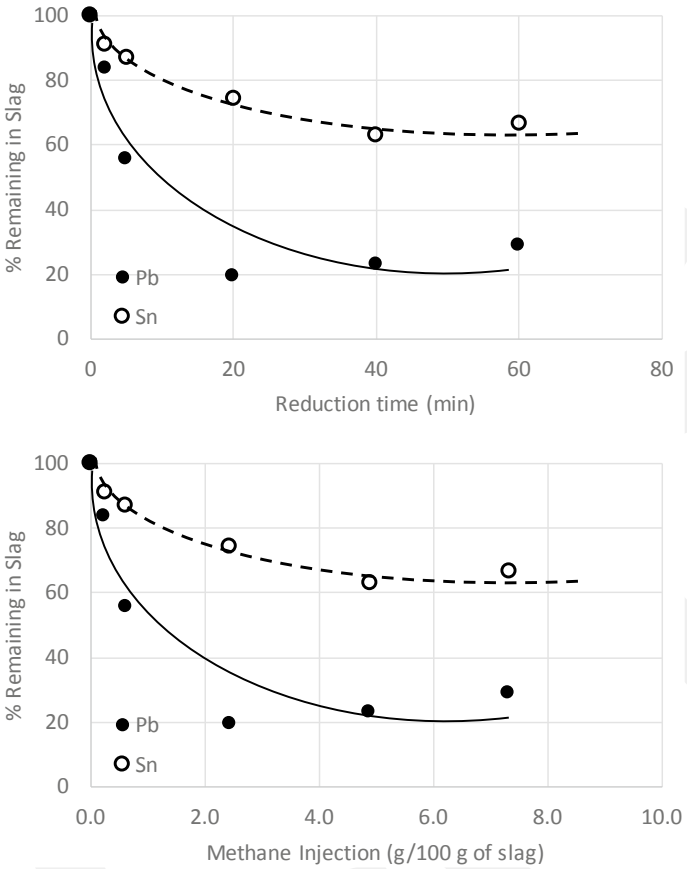

Fig. 4 Reduction of lead with methane injection with respect to time and quantity injected

calculated for the off-gas from the CO/CO_2 reaction couple was more oxidizing than the Fe/FeO reaction couple. This suggests that the dominant reaction after 5 mins of reduction or 0.6 g CH_4/100 g of slag, consuming the majority of the methane, is the reduction of Fe^{2+} in the slag to form an iron phase. This is represented by the reaction;

$$3\,FeO_{(l)} + CH_{4(g)} \rightarrow 3\,Fe_{(s)} + CO_{(g)} + 2\,H_2O_{(g)}$$

This suggests that approximately 40% of the lead in the slag can be recovered prior to the formation of an iron phase. To recover the majority of the lead present in the slag, significant co-reduction of iron is required.

An industrial process using methane to reduce PbO dissolved in the slag will require significant methane addition due to the reduction of iron. Additionally, the

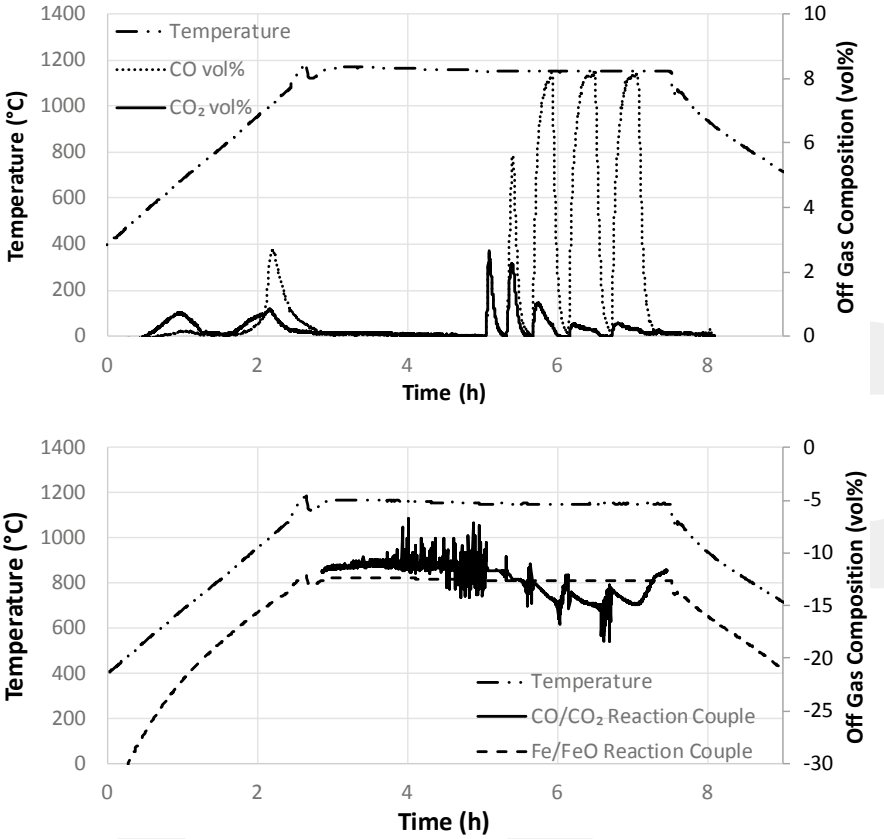

Fig. 5 Off-gas composition and pO_2 with respect to time and temperature and time during reduction

reduced iron is likely to form a solid iron phase, which would settle out of the slag between the slag and any bullion that forms. This would lead to potential issues with slag foaming and accretion formation within the furnace.

Conclusion

Experiments have been performed to reduce the lead dissolved in slag by injecting methane at temperature. It was demonstrated that the lead was able to be partly recovered from the slag, achieving a recover of approximately 80% after 20 min. However, it is suggested that the reduction of Fe^{2+} in the slag to form $Fe_{(s)}$ and other iron phases consumes the majority of the methane. Under deep reduction conditions, it is proposed that the rate of reduction is limited by the diffusion of species within the slag phase and the settling of fine droplets of lead.

References

1. Hayes P et al (2010) Lead smelter survey. In: Paper presented at Pb Zn—2010. Vancouver, British Columbia, Oct 2010
2. Davis B et al (2019) Slag reduction and settling for improved metal recovery. In: Paper presented at the CIM conference of metallurgists. Vancouver, British Columbia, Aug 2019
3. Jahanshahi S, Wright S (2017) Kinetics of reduction of CaO–FeOx–MgO–PbO–SiO_2 slags by CO–CO_2 gas mixtures. Met Trans B 48B:2057–2066
4. Davis B, Lebel T, Parada R, Parra R (2016) Slag reduction kinetics of copper slags from primary copper production. In: Reddy RG, Chaubal P, Pistorius PC, Pal U (eds) Advances in molten slags, fluxes, and salts: proceedings of the 10th international conference on molten slags, fluxes and salts. Springer, Cham

GCRIS

Phase Evolution During the Oxidation Process of Low Grade Lead–Zinc Oxide Ore

Hai-Peng Gou, Kuo-Chih Chou, Zhong-Ye Pei, Song-xuan Chen, Xue-gang Chen and Ming-chuan Li

Abstract The phase evolution during the oxidation process of low grade lead–zinc oxide ore was investigated at 1173–1473 K under air atmosphere. A thermogravimetric and differential thermal analysis was carried out to investigate the oxidation mechanism. The products obtained at different temperatures were analyzed by X-ray diffraction. It was found that the sulfides in the ore were oxidized and the carbonates in the ore decomposed when the temperature was higher than 1173 K. During the oxidation process from 1173 to 1273 K, the main phases in the products were $CaSO_4$, Fe_3O_4, $MgFe_2O_4$, $ZnFe_2O_4$, Zn_2SiO_4, ZnO, and $PbFe_4O_7$. Along with the increase of the reaction temperature, a new phase of $Ca_2Fe_2O_5$ appeared in the products after the decomposition reaction of Zn_2SiO_4 and $CaSO_4$. Based on the formation of the low melting point phase, the sintering phenomenon of the ore occurred obviously at 1473 K. With the increase of the reaction temperature, the content of Pb in the products decreased gradually.

Keywords Low grade lead–zinc oxide ore · Phase evolution · Oxidation mechanism

Introduction

Lead and zinc mineral resources are abundant in the southwest of China. As the primary sources of lead and zinc, the resources of the natural sulfide ores are relatively few in China. With the consumption of the natural sulfide ores, the low grade lead–zinc oxide ore has been receiving more and more attentions, which can be used as an alternative [1]. In the past years, many researches have been studied for treating the oxide ore, such as flotation, hydrometallurgy, and pyrometallurgy [2–5].

H.-P. Gou (✉) · Z.-Y. Pei · S. Chen · X. Chen · M. Li
China ENFI Engineering Corporation, Beijing 100038, China
e-mail: gouhp@enfi.com.cn

K.-C. Chou
State Key Laboratory of Advanced Metallurgy, University of Science and Technology Beijing, Beijing 100083, China

© The Minerals, Metals & Materials Society 2020

A. Siegmund et al. (eds.), *PbZn 2020: 9th International Symposium on Lead and Zinc Processing*, The Minerals, Metals & Materials Series,
https://doi.org/10.1007/978-3-030-37070-1_5

As is known to all, the low grade lead–zinc oxide ore has a higher solubility and an extensive hydration of oxide surfaces. It makes the low grade lead–zinc oxide ore more difficult to float than the sulfide ores [6]. Zhao studied the alkaline leaching of smithsonite ores [7]. It was found that over 85% of both Zn and Pb, and less than 10% of Al could be leached from the ore by using 5 M NaOH solution at 368 K. Meanwhile, the waste water was produced during the hydrometallurgical process. The environmental protection pressure of hydrometallurgy in China is increasing in recent years. It is necessary to find out an effective pyrometallurgy process to obtain lead and zinc from the oxide ore. Thermal decomposition of basic zinc carbonate in the N_2 atmosphere was studied by Liu [8]. It was found that the increase in the sample size caused an increase in the reaction temperature and a decrease in the value of the apparent activation energy.

However, there are few researches reported on the oxidation mechanism of the low grade lead–zinc oxide ore. In this research, the oxidation process of the low grade lead–zinc oxide ore was studied. The aim of the present work was to investigate the phase evolution and reaction mechanism during the oxidation process, which was a foundation for the further pyrometallurgy process.

Materials and Methods

The low grade lead–zinc oxide ore produced in Yunnan Province was used as raw materials, which was characterized by X-ray diffraction (XRD) in a 2θ range of 10°–90°. As shown in Fig. 1, the main mineral phases of the low grade lead–zinc oxide ore are $CaMg(CO_3)_2$, $Zn_{0.776}Fe_{0.224}S$, $CaCO_3$, $PbCO_3$, and $Zn_4Si_2O_7(OH)_2{\cdot}H_2O$. The contents of the main elements in the ore were determined by inductively coupled plasma-mass spectrometry (ICP-MS) and carbon–sulfur analyzer, which are shown

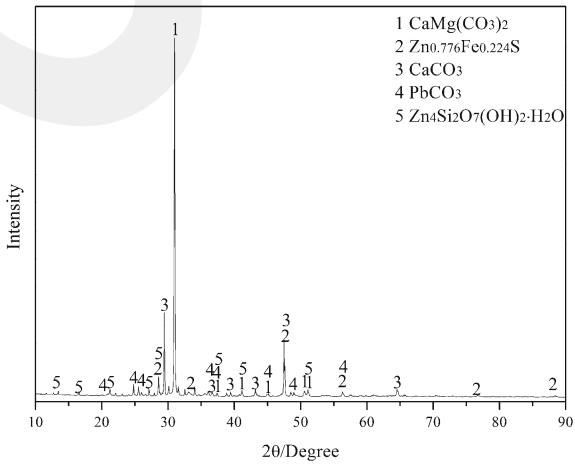

Fig. 1 XRD patterns of the low grade lead–zinc oxide ore

Table 1 Contents of the main metal elements in the ore

Element	Pb	Zn	Fe	Ca	Mg	S	C
Content/%	5.28	11.40	14.50	13.14	3.60	4.95	6.12

Table 2 Main phases in the ore detected the mineralogical analyses

Phase	Content/%	Phase	Content/%
Cerusite	5.00	limonite	18.50
Cechite	0.04	Dolomite	27.20
Galena	0.94	Calcite	17.96
Hemimorphite	9.09	Quartz	1.27
Smithsonite	6.69	Mica	0.97
Sphalerite	4.46	Feldspar	0.86
Pyrite	6.18	Other	0.84

in Table 1. The main phases in the ore were also detected by the mineralogical analyses, which are shown in Table 2. In addition to the phases characterized by XRD, the ore also contains smithsonite, pyrite, limonite, and so on.

A thermogravimetric and differential thermal analysis (HTC-2, Beijing Hengjiu Instrument Ltd., China) was carried out to investigate the reaction mechanism. About 70 mg of the low grade lead–zinc oxide ore was roasted from the room temperature to 1423 K at a heating rate of 10 K min^{-1} in a flowing air atmosphere (40 ml min^{-1}). As shown in Fig. 2, there were both endothermic and exothermic peaks in the TG-DTA curves. The maximum mass loss in the TG curve was 22.3%.

In order to explore the effect of the reaction temperature on the oxidation products, the isothermal experiments were carried out at 1173, 1223, 1273, 1323, 1373, 1423, and 1473 K. About 20 g of the low grade lead–zinc oxide ore was placed in an alumina crucible (50 mm × 28 mm × 14 mm) in each experiment. When the temperature of the muffle furnace reached the desired value, the alumina crucible was put into the furnace quickly. The alumina crucible was taken out from the furnace after 2 h, which was cooled in the room temperature. All the obtained reaction products were examined by XRD. The contents of Zn and Pb in the products were determined by ICP.

Results and Discussion

Thermogravimetric and Differential Thermal Analysis

According to Fig. 1 and Table 2, the main reactions during the oxidation in air atmosphere can be described as Eqs. (1)–(8). ΔG^{θ} of the Eqs. (1–7) are calculated by a thermodynamic database FactSage 7.2. As shown in Fig. 3, Eqs. (1–7) are thermodynamically favorable when the reaction temperature is higher than 1177 K. Since the

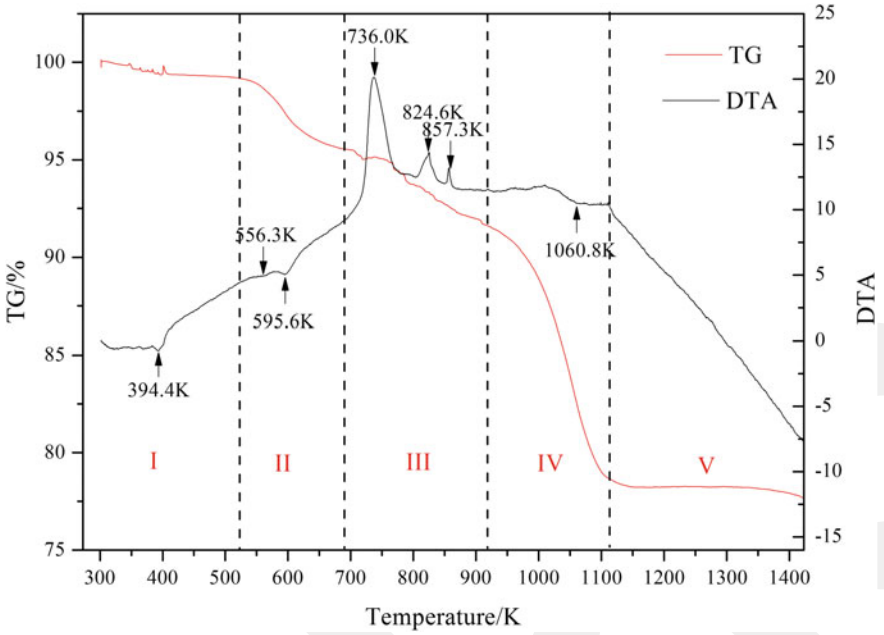

Fig. 2 TG-DTA curves of the low grade lead–zinc oxide ore from room temperature to 1473 K in air atmosphere

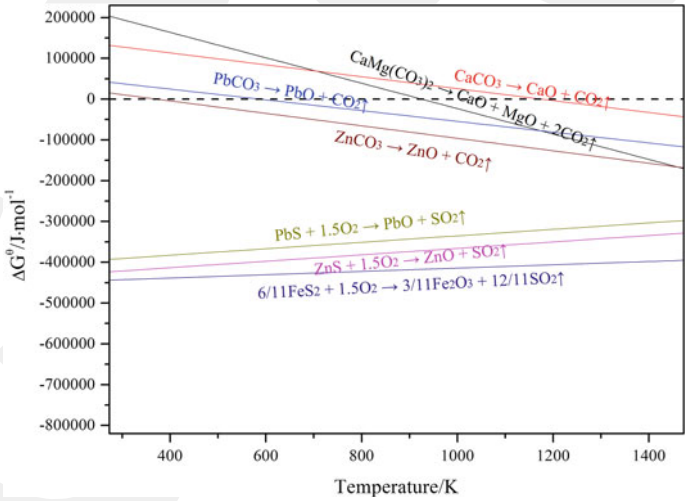

Fig. 3 ΔG^{θ} of the reactions (1)–(7) calculated by FactSage 7.2

database of FactSage do not contain the relevant data of $Zn_4Si_2O_7(OH)_2{\cdot}H_2O$, ΔG^θ of Eq. (8) is not calculated. Equation (8) belongs to dehydration reaction, which can occur at a lower temperature. By comparing ΔG^θ of Eqs. (5–7), it can be seen that the oxygen in the air gives priority to react with FeS_2, which is followed by ZnS and PbS.

$$CaMg(CO_3)_2 \rightarrow CaO + MgO + 2CO_2 \uparrow \quad (1)$$

$$CaCO_3 \rightarrow CaO + CO_2 \uparrow \quad (2)$$

$$ZnCO_3 \rightarrow ZnO + CO_2 \uparrow \quad (3)$$

$$PbCO_3 \rightarrow PbO + CO_2 \uparrow \quad (4)$$

$$ZnS + 1.5\,O_2 \rightarrow ZnO + SO_2 \uparrow \quad (5)$$

$$PbS + 1.5\,O_2 \rightarrow PbO + SO_2 \uparrow \quad (6)$$

$$6/11FeS_2 + 1.5O_2 \rightarrow 3/11Fe_2O_3 + 12/11SO_2 \uparrow \quad (7)$$

$$Zn_4Si_2O_7(OH)_2 \cdot H_2O \rightarrow 2Zn_2SiO_4 + 2H_2O \uparrow \quad (8)$$

According to the results of TG-DTA curves, the oxidation process of the low grade lead–zinc oxide ore was divided into five stages. In the first stage, an obvious endothermic peak appeared at 394.4 K, which was mainly due to the removal of crystal water from the hemimorphite ($Zn_4Si_2O_7(OH)_2{\cdot}H_2O$). In the second stage, there were two endothermic peaks occurred at 556.3 and 595.6 K, which were due to the decomposition of smithsonite ($ZnCO_3$) and cerusite ($PbCO_3$). In the third stage, there were three significant exothermic peaks at 736.0, 824.6, and 857.3 K. The exothermic peaks were, respectively, caused by the oxidation reactions of pyrite (FeS_2), sphalerite (ZnS), and galena (PbS), which were corresponded to Eqs. (7), (5), and (6). As the reaction temperature increased, an endothermic peak appeared at 1060.8 K in the fourth stage. This was caused by the decomposition of dolomite ($CaMg(CO_3)_2$) and calcite ($CaCO_3$). When the reaction temperature was higher than 1150 K, a plateau appeared in the TG curve. There were no obvious endothermic or exothermic peaks in this stage. It is worth noting that a slight loss of weight appeared at the end of the TG curve, which would be further discussed with the results of XRD analyses.

XRD Analyses

XRD patterns of the oxidation products obtained at different reaction temperatures are shown in Fig. 4. When the reaction temperatures were 1173, 1223, and 1273 K, the main phases of the products were $CaSO_4$, Fe_3O_4, $MgFe_2O_4$, $ZnFe_2O_4$, Zn_2SiO_4, ZnO, and $PbFe_4O_7$. It is obviously seen that the element of S did not escape from the ore in the form of SO_2. Since the content of Ca in the ore was 13.14%, the element of S combined with the element of Ca to form $CaSO_4$ during the oxidation process. Therefore, the oxidation reactions of the sulfide occurred as Eqs. (9), (10), and (11). When the reaction temperature was higher than 1173 K, the sulfide in the ore turned into the oxide after 2 h. When the reaction temperature reached 1323 K, the diffraction peaks of Zn_2SiO_4 disappeared. It means that Zn_2SiO_4 decomposed at this temperature. When the reaction temperature was 1373 K, a new phase of $Ca_2(Mg,Fe,Al)_6(Si,Al)_6O_{20}$ appeared in the products. When the reaction temperatures were 1423 K, the diffraction peaks of $Ca_2(Mg,Fe,Al)_6(Si,Al)_6O_{20}$ disappeared and a new phase of $Ca_2Fe_2O_5$ appeared. When the reaction temperatures were 1473 K, the intensities of diffraction peaks of $CaSO_4$ obviously weakened. It is confirmed that the element of S could be removed from the low grade lead–zinc oxide ore when the reaction temperature reached 1473 K. This explained the reason for the slight loss of weight appeared at the end of the TG curve.

$$ZnS + 2O_2 + CaCO_3 \rightarrow ZnO + CaSO_4 + CO_2 \uparrow \quad (9)$$

$$PbS + 2O_2 + CaCO_3 \rightarrow PbO + CaSO_4 + CO_2 \uparrow \quad (10)$$

$$FeS_2 + 3.75O_2 + 2CaCO_3 \rightarrow 0.5Fe_2O_3 + 2CaSO_4 + 2CO_2 \uparrow \quad (11)$$

Figure 5 is the appearance of the products obtained at 1173 K and 1473 K, respectively. It is obvious that the sintering phenomenon of the product obtained at 1473 K was more serious than the other one. It is because that the acicular calcium ferrites (SFCA-I) was quickly formed by the reaction between Fe_2O_3 and CaO, absorbing a small amount of SiO_2 and Al_2O_3. When the reaction temperature was 1473 K, a melt formed and covered the ore surface, which led to the sintering phenomenon [9].

The Percentages of Mass Loss

The percentages of mass loss obtained at different reaction temperatures are shown in Fig. 6. With the increase of reaction temperature, the percentages of mass loss increased obviously. The percentage of mass loss obtained at 1473 K was 29.36%, which was much higher than the maximum mass loss in the TG curve. Combined with the XRD spectrum, it is found that the decomposition of $CaSO_4$ led to the increase of the mass loss.

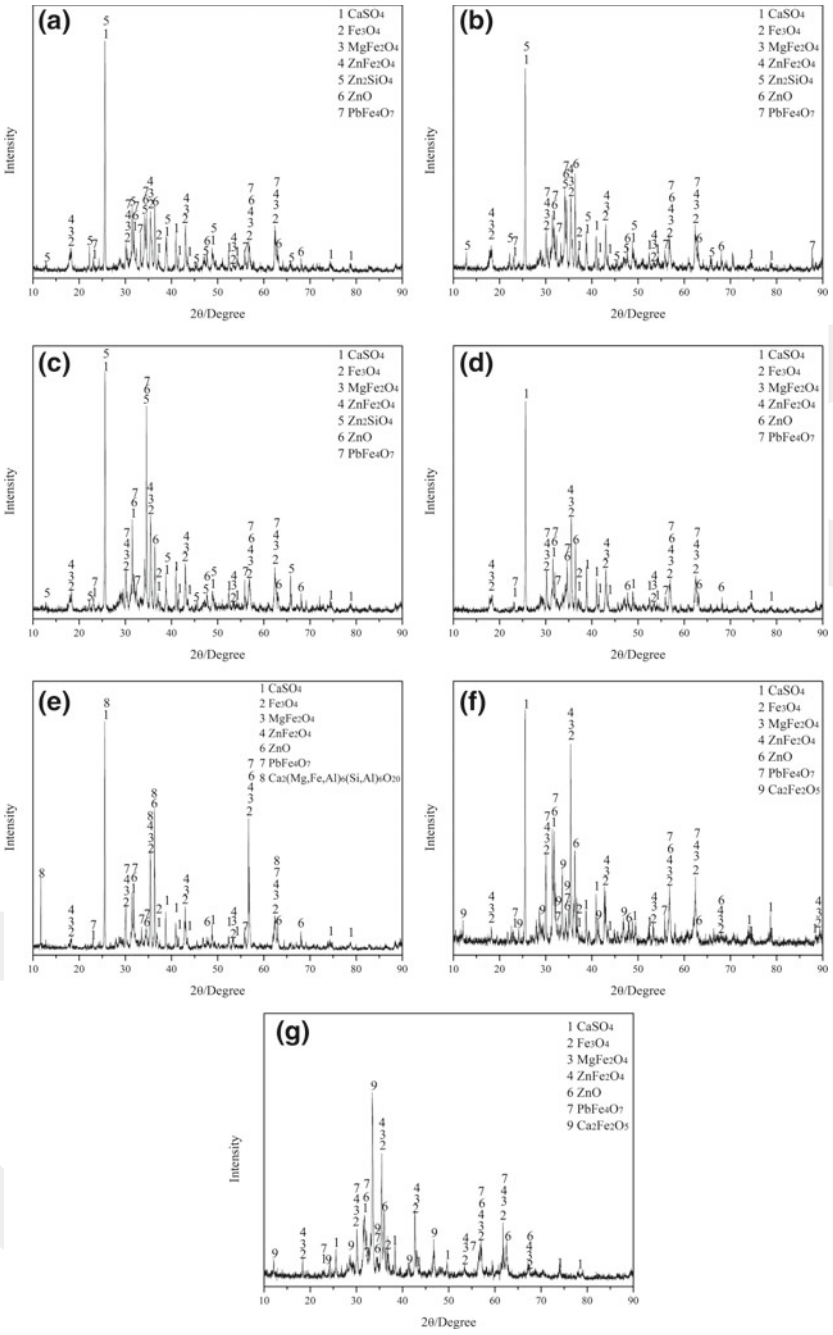

Fig. 4 XRD patterns of the products obtained from 1173 to 1473 K

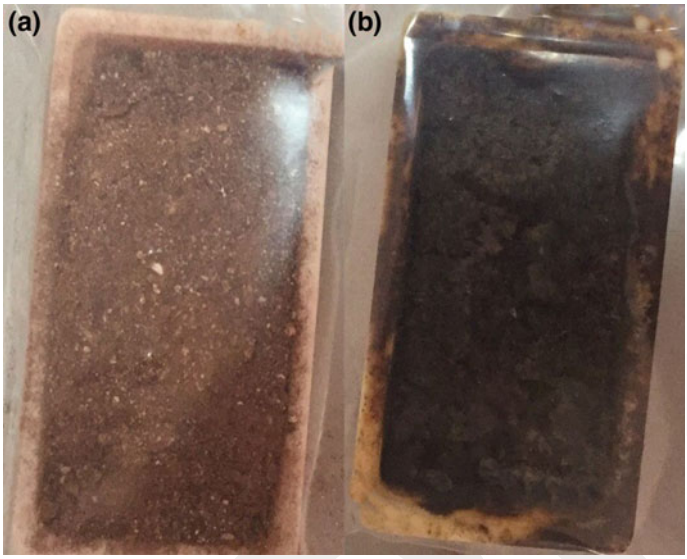

Fig. 5 Morphologies of the products obtained at 1173 and 1473 K

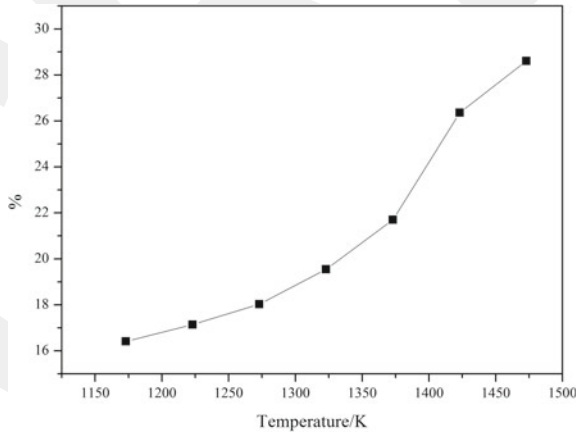

Fig. 6 Percentages of mass loss obtained at different reaction temperatures

Furthermore, the contents of Pb and Zn in the products were also determined by ICP. As shown in Fig. 7, the content of Pb in the products decreased obviously when the reaction temperature increased. The saturated vapor pressure of lead oxide increased with the increase of temperature [10]. Therefore, the element of lead could evaporate from the products in the form of lead oxide at the higher reaction temperatures. The two reasons discussed above ultimately led to the increase of the percentages of mass loss.

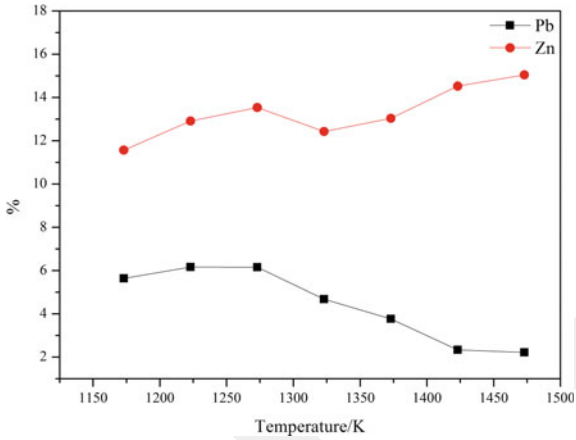

Fig. 7 Contents of Pb and Zn in the products

Conclusions

The oxidation process of the low grade lead–zinc oxide ore was studied at 1173–1473 K. The main phases of the products obtained at 1173–1273 K were $CaSO_4$, Fe_3O_4, $MgFe_2O_4$, $ZnFe_2O_4$, Zn_2SiO_4, ZnO, and $PbFe_4O_7$. When the reaction temperature further increased, the phase of Zn_2SiO_4 decomposed and an intermediate phase of $Ca_2(Mg,Fe,Al)_6(Si,Al)_6O_{20}$ appeared. When the reaction temperature was higher than 1423 K, the phase of $Ca_2Fe_2O_5$ appeared. Based on the formation of the low melting point phase, the sintering phenomenon of the ore occurred obviously at 1473 K. At the same time, the elements of S and Pb evaporated from the products in the form of SO_3 and PbO.

References

1. Liu Q, Zhao Y, Zhao G (2011) Production of zinc and lead concentrates from lean oxidized zinc ores by alkaline leaching followed by two-step precipitation using sulfides. Hydrometallurgy 110:79–84
2. Li Y, Wang JK, Wei C et al (2010) Sulfidation roasting of low grade lead–zinc oxide ore with elemental sulfur. Miner Eng 23:563–566
3. Önal G, Bulut G, Gül A et al (2005) Flotation of Aladag oxide lead–zinc ores. Miner Eng 18:279–282
4. Moradi S, Monhemius AJ (2011) Mixed sulphide–oxide lead and zinc ores: problems and solutions. Miner Eng 24:1062–1076
5. Ejtemaei M, Gharabaghi M, Rannajad M (2014) A review of zinc oxide mineral beneficiation using flotation method. Adv Colloid Interface 206:68–78
6. Frenay J (1985) Leaching of oxidized zinc ores in various media. Hydrometallurgy 15:243–253
7. Zhao Y, Stanforth R (2000) Production of Zn powder by alkaline treatment of smithsonite Zn–Pb ores. Hydrometallurgy 56:237–249
8. Liu Y, Zhao J, Zhang H et al (2004) Thermal decomposition of basic zinc carbonate in nitrogen atmosphere. Thermochim Acta 414:121–123

9. Scarlett NV, Powncebyv MI, Madsen IC et al (2004) Reaction sequences in the formation of silico-ferrites of calcium and aluminum in iron ore sinter. Metall Mater Trans B 35:929–936
10. Holman RL, Fulrath RM (1973) Intrinsic nonstoichiometry in the lead zirconate-lead titanate system determined by Knudsen effusion. J Appl Phys 44:5227–5236

GCRIS

Part III
Secondary Zinc I

GCRIS

A New Era in Smelting Sustainability—Intensification of the Outotec® Ausmelt Top Submerged Lance (TSL) Process for Zinc Production

Jacob Wood, David Wilson and Stephen Hughes

Abstract For almost 30 years, the Outotec® Ausmelt Top Submerged Lance (TSL) process has been applied for the processing of zinc-bearing leach residues, slags, EAF dust and sulphide concentrates. Continual development and evolution of the technology over this period has resulted in a more intense smelting process with higher energy efficiency, lower operating costs and reduced fossil fuel consumption. This paper covers a number of recent technology advances, highlighting their positive impacts on smelter operating costs, CO_2 emissions and metal recoveries for treatment of a range of zinc-bearing feed inputs. It also compares Ausmelt TSL technology against alternatives such as the Waelz kiln, box fumer, Chinese side-blowing process and plasma technology, demonstrating a range of operational and environmental advantages.

Keywords Zinc · Fuming · Recycling · Sustainability · Outotec

Introduction

By far the dominant process for the production of zinc today is the Roast-Leach-Electrowin (RLE) process, which accounts for an estimated 85% of global zinc production [1]. The RLE process is typically applied for the processing of zinc sulphide concentrates, but can also be used to treat a fraction of relatively clean oxide material. Other commercially important processes for the treatment of zinc sulphide concentrates include direct concentrate leaching and the Imperial Smelting Process (ISP). In all of these processes, iron is removed as a separate by-product/waste stream, often characterised by elevated concentrations of not only zinc, but also various minor and precious metals. Untreated, these materials may be physically unstable as they often contain significant levels of lead, zinc and cadmium, and are therefore often

J. Wood (✉) · D. Wilson · S. Hughes
Outotec Pty Ltd, 12 Kitchen Road, Dandenong South, VIC 3175, Australia
e-mail: jacob.wood@outotec.com

© The Minerals, Metals & Materials Society 2020

A. Siegmund et al. (eds.), *PbZn 2020: 9th International Symposium on Lead and Zinc Processing*, The Minerals, Metals & Materials Series,
https://doi.org/10.1007/978-3-030-37070-1_6

classified as hazardous materials [2]. This has presented significant environmental and health challenges in the downstream handling, storage and/or disposal of these waste materials.

In recent years, Outotec has undertaken pilot and commercial-scale development testwork on the direct bath smelting of zinc sulphide concentrates as a potential alternative processing route with lower operating costs and improved recovery of minor and precious metal values. The Outotec® Direct Zinc Smelting (DZS) also eliminates issues around the handling, storage and/or disposal of these waste materials [3]. Whilst such an approach offers promise for future new zinc production capacity, the existing zinc sulphide treatment processes are expected to continue to serve for many decades to come. In addition, zinc is also produced from various primary oxide sources, such as silicate or carbonate ores, where typically direct ore leaching is employed, with inevitable waste/residue generation.

Whilst the majority of zinc production is currently derived directly from the processing of primary ores and concentrates, with modern zinc smelters now capable of achieving >97.5% zinc recovery [4], treatment of the above-mentioned zinc-bearing residues and slags is expected to become increasingly important, particularly as the minimisation of wastes and closed-loop metals recycling comes ever more into focus. The recovery of zinc from secondary materials such as steel plant dusts also represents another important and growing area of interest within the zinc industry.

Despite the development and testing of a range of hydrometallurgical processes for processing these materials, pyrometallurgical front-end processing of such iron and zinc-bearing residues, slags, drosses and dusts has been the dominant processing route prior to electrolytic treatment of the zinc oxide-rich by-products generated. Traditionally, the box fumer (for liquid slag feed) and Waelz kiln (for solid feed) have been the pyrometallurgical zinc fuming workhorses and have been employed over many decades. In more recent years, a range of alternative pyrometallurgical fuming processes have been adopted, such as Top Submerged Lance (TSL), side-blowing and plasma technologies. These can offer benefits such as improved efficiencies, higher minor and precious metal recoveries and generation of a stable slag, suitable for discard or use in construction applications.

Outotec Ausmelt Process Development

Outotec is a leading supplier of technology solutions for the metal production industries, with a long history of developing innovative equipment and processes with strong environmental credentials [5]. This has been enabled by investing in its own research and development facilities as well as through co-operative programs with both its customers and academic institutions. These programs typically employ a combination of theoretical analysis backed up by physical testwork. The use of pilot plant testing has been integral to the successful commercialisation of many processes, including the Ausmelt process. Today, Outotec maintains its own Ausmelt pilot plant

Fig. 1 View of Ausmelt pilot plant

located at its Dandenong office in Australia in addition to other pilot facilities at its major research centres in Pori, Finland and Frankfurt, Germany (Fig. 1).

Outotec's Ausmelt TSL process (Ausmelt process) is currently applied commercially for treatment of a wide range of non-ferrous metals. In the course of testing the capabilities of this process, extensive testwork has been conducted on a wide range of zinc-bearing concentrates, slags, residues and dusts over many years. Compositional data for some of the zinc-bearing materials successfully tested in the Ausmelt pilot plant is provided in Table 1 [6].

Following on from process development and optimisation work conducted in the Ausmelt pilot plant, there have now been some 24 commercial-scale Ausmelt furnaces licensed for the dedicated fuming of zinc-bearing feedstocks, whilst a number of other Ausmelt plants incorporate zinc/lead-bearing residues in their feed mix or employ a fuming process stage. One recent example is the Ausmelt plant operated by Inner Mongolia Xingan Copper and Zinc Smelting Limited (Fig. 2), which provides for the treatment of 160,000 tpa of various zinc-bearing residues for the recovery of zinc, lead, silver, indium and cadmium as part of an oxide fume by-product.

The Ausmelt fuming process has traditionally employed coal as both a fuel and reducing agent, with consequential generation of relatively large amounts of hot offgas. In many plants, energy recovery from the process offgas by the use of waste heat boiler(s) provides for the generation of steam that can be used as a plant utility or for electrical power generation. Whilst this practice has served industry well for many

Table 1 Composition of zinc materials tested at Outotec Ausmelt facilities

	Zinc concentrate	Zinc-Lead concentrate	ISP slag	Lead BF Slag	Neutral leach residue	Jarosite	Goethite	EAF Dust
% Zn	43.6	26.9	12.0	14.3	20.6	2.6	14.3	19.5
% Pb	0.6	18.3	0.9	1.7	5.9	3.3	2.8	2.5
% Fe	12.4	12.5	34.5	22.0	23.5	24.5	36.0	32.0
% As	0.2	0.1	0.1	0.1	0.2	0.1	0.2	0.4
% S	30.4	29.7	–	–	5.9	12.2	4.7	< 0.1
$\%SiO_2$	2.2	8.6	15.2	29.0	4.3	7.6	1.8	3.0
ppm Ag	600	185	–	20	270	100	100	100
ppm In	< 300	–	–	–	–	–	–	–
ppm Ge	< 200	13	–	–	–	–	–	–

Fig. 2 View of Xingan Ausmelt zinc fuming plant

years, today there is a greater focus than ever on minimising energy consumption and CO_2 emissions from industrial processes as part of the sustainability initiatives being promoted by all environmentally responsible companies.

Recent Improvements in the Ausmelt Process for Zinc Fuming

The Ausmelt zinc fuming process as operated commercially to date has typically been characterised by:

- Lance operation with relatively low oxygen enrichment ($\leq$45 vol. %), with cooling required for preservation of the lance tip provided by the injected process gases.
- Use of shrouded lances for efficient afterburning of volatilised compounds within the furnace and consequently, improved heat recovery efficiency to the bath by molten slag splash.
- Use of an intensively cooled, lower furnace construction, incorporating copper cooling elements, due to high slag superheat and intensive splashing.
- Use of a membrane (WHB) upper furnace construction (where economic), due to high freeboard temperatures and to capture waste heat from the process offgas for steam generation.
- Feeding of slag in hot, liquid form, where possible, for maximum energy efficiency.
- Feeding of solid feeds in wet form for simplicity.
- Use of coal as a fuel and reducing agent.

Due to the inherent versatility of the Ausmelt process, fuming has been conducted commercially using either batch or continuous modes, including:

- Batch fuming of liquid slag bath held within the Ausmelt furnace as a process stage.
- Continuous 2 stage fuming, with solid and/or liquid feed to the first Ausmelt fuming furnace followed by continuous liquid flow into the second Ausmelt fuming furnace.
- Continuous single-stage fuming, with solid and/or liquid feed to the Ausmelt fuming furnace.

Improvement 1: Optimising Fuming Process Stages

Given the range of fuming process modes available, selection of the optimum process flow sheet for a particular project must consider not only the feed materials to be treated (composition and throughput) but also constraints around capital investment, target product quality, metals recovery and environmental impacts. For example, continuous processing in either a single or multiple furnaces provides for more stable operation with less variability in lance and offgas conditions. On the other hand, batch fuming can offer savings in capital investment by performing multiple process stages in a single vessel rather than needing separate furnaces for each process stage.

Improvement 2: Increasing Oxygen Enrichment

Oxygen enrichment has long been employed in smelting process applications to reduce fuel consumption, offgas generation rates and to increase productivity. In oxidising processes such as copper smelting, energy liberation from the feed materials, combined with Ausmelt lance operation with high levels of oxygen enrichment, means that little, if any auxiliary fuel introduction is required to regulate the bath temperature. In reducing process applications such as zinc residue fuming, for which there is no energy provided by the feed, fuel introduction via the Ausmelt lance is used to supplement the process heat balance. Fuel combustion at the lance tip ensures higher energy efficiency than in other bath smelting processes and also allows for independent control of the bath temperature and oxygen potential, which is critical in achieving low concentrations of Zn and Pb in the final slag. This method of fuel introduction does, however, impose limitations around the maximum level of oxygen enrichment able to be sustained without impacting lance integrity. Use of oxygen enrichment for the Ausmelt process in fuming applications has typically been limited to approximately 45 vol. % due to elevated combustion/flame temperature at the lance tip and high operating temperatures required in these processes [7].

A key improvement enabling operation with increased enrichment in the Ausmelt fuming process has been the development and commercial-scale implementation of a patented fluid-cooled lance design. By decoupling the lance cooling duty from the energy generation duty, a step change in oxygen enrichment can be achieved.

Improvement 3: Reducing Feed Moisture

Zinc leach residues are quite challenging materials to dewater to low moisture levels by thickening and filtration only, meaning that residue cakes are commonly characterised by moisture levels as high as 35 wt% and only rarely, less than 20 wt%. Due to their fine particle size, these residues often result in significant dust generation when dried to less than 20% moisture. Outotec has considerable experience in the injection of feed materials via the Ausmelt lance, with a good example of where this has been applied being the injection of granulated Ni-PGM matte at the two (2) Anglo Platinum TSL converting furnaces in South Africa [7]. Whilst the introduction of dry feeds via the Ausmelt lance necessitates additional equipment for drying and injection, for the processing of high-moisture content feeds such as zinc leach residues, the benefits are substantial.

Table 2 on the following page illustrates the considerable benefits achievable by tailoring the process configuration and operating conditions for processing a particular feed input (composition and throughput).

Table 2 Impacts of process configuration on key process flows

		Base case	Improvement 1 (process)	Improvement 2 (enrichment)	Improvement 3 (dry Feed)	Combined improvements
Throughput	dry t/y	160,000	160,000	160,000	160,000	160,000
Feed moisture	*%*	*14.0*	*14.0*	*14.0*	*1.0*	*1.0*
Operation	–	Continuous	Batch	Continuous	Continuous	Continuous
Total coal	t/y	100%	71%	84%	78%	44%
O_2 flow	kN m^3/y	100%	93%	124%	80%	82%
O_2 Enrichment	vol. *%*	*40%*	*40%*	*80%*	*40%*	*80%*
Process air	kN m^3/y	100%	93%	8%	80%	5%
Offgas flow	kN m^3/y	100%	68%	74%	74%	27%

Improvement 4: Advanced Fuels and Reductants

Outotec has invested considerable effort examining a range of "advanced" (i.e. non-fossil fuel derived) fuels and reductants for application in the Ausmelt process. Pilot testwork investigating the processing of industrial and consumer wastes such as electronic scrap, automotive shredder residue and automotive tyres under a range of conditions has facilitated an in-depth understanding of how these feeds can be used to offset fuel and reductant usage across a range of non-ferrous processes. Outotec is also actively pursuing efforts to reduce CO_2 emissions through the use of advanced fuels and reductants, leveraging its experience and know-how in the waste-to-energy sector, for the processing of waste materials such as sewerage sludge and other agricultural/biomass by-products.

Zinc Fuming Process Benchmarking

Efforts to improve the competitiveness of the Ausmelt process in zinc fuming applications have also included technology benchmarking against other pyrometallurgical techniques, which are described in the following sections. Further such work is progressing as more data becomes available to examine the relative merits of each process.

Comparison with Waelz Kiln Process

The Waelz kiln process has long been employed for the processing of zinc secondaries [8], primarily:

(i) Neutral leach residues as part of the "classical" RLE plant scheme. Such plants were typically implemented prior to the development of the hot acid leach/jarosite processes to enable improved zinc recoveries.
(ii) Processing of zinc secondaries, most notably steel plant electric arc furnace dusts (EAFD).

The Waelz kiln relies on gas–solid phase reactions under counter current conditions in a rotary kiln. Due to the counter current nature of the process and moderate operating temperatures, the Waelz kiln is thermally efficient and considered reliable and well proven based on its application in the cement industry. The primary disadvantage of leach residue processing in the Waelz kiln, however, is the nature of the final iron-bearing product (clinker) generated, which is considered less stable than fayalite slag produced in the other fuming processes operating with a molten slag bath. This can present a major challenge in terms of long-term disposal of such material, effectively turning one form of metallurgical waste into another. Additionally, the recovery of silver and other valuable minor metals (In, Ge and Ga) is significantly reduced compared with alternatives such as the Ausmelt fuming process. Recovery of these metals is often critical to the economic viability of zinc leach residue processing.

Comparison with Box Fuming Process

The box fuming process is another classical pyrometallurgical technology with many decades of operating history. The process has been widely employed in lead smelters, to recover lead and zinc from molten blast furnace slag. Typically, these furnaces are operated in a batch mode although a continuous zinc fuming process was successfully utilised by KCM at their lead smelter in Bulgaria until 2016 [9]. Primary limitations of the box fuming process include the maximum quantity of solid charge able to treated and level of process air oxygen enrichment able to be employed, making it less well suited to the processing of stockpiled zinc leach residues and more amenable to handling molten, zinc-bearing slags. The box fumer is also limited in its ability to cope with certain impurities, particularly high levels of copper, which may give rise to formation of a matte/metal phase in the furnace.

Comparison with Side-Blowing Process

The side-blowing process, a derivative of the Russian Vanyukov technology, attempts to overcome some of the disadvantages of the box fuming process as a result of its more robust furnace construction, ability to tolerate the presence of matte/metal and capability to operate with oxygen enrichment levels as high as 80% [10]. The process

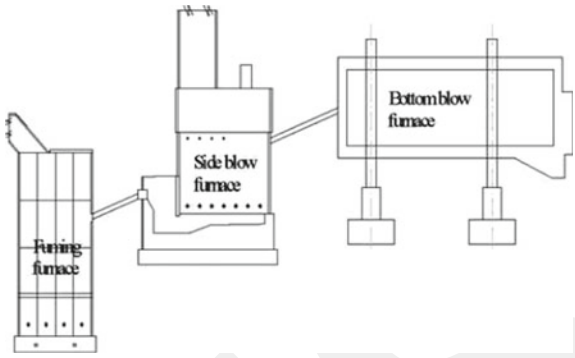

Fig. 3 Typical flowsheet for application of the side-blowing process

has been applied at a number of lead smelting plants for molten slag reduction, as part of a multi-furnace flowsheet operated in series (Fig. 3) [11].

The side-blowing process appears susceptible to suffer from a range of issues, many of which are also inherent to the Vanyukov process, namely:

- Difficulties recovering from a partially or completely solidified bath, due to an inability to provide significant heat input for bath remelting, other than through the installation of roof-mounted burners.
- Low flowsheet availability due to the operation of multiple vessels in series, meaning a complete stop to production in the event of problems with one or more of the processing units.
- Issues with independent regulation of the bath temperature and oxygen potential due to a reliance on efficient oxygen transfer through the bath between the submerged injection points (tuyeres) and roof-fed coal used as both a fuel and reductant.
- Difficulties accessing the injection tuyeres for inspections, maintenance and preventing molten material backflow in the event of a loss in process air/oxygen supply due to the inability to rotate the furnace in the same manner as for PS converter and SKS/QSL vessels.

There is currently limited publicly available literature and data covering application of the process for the treatment of purely solid, zinc-bearing feeds such as leach residues, although a variant of the technology seems to have been used for the batch fuming of zinc from molten slag in a similar manner to the box fuming process.

Comparison with Plasma Process

The plasma furnace has been developed over a number of years, and its potential in zinc fuming applications was recognised, with the implementation of zinc fuming plants at Hoyanger, Norway and Beerse, Belgium [12]. The main apparent advantage of this process is use of a high-temperature plasma “burner” with relatively low gas

injection rates, allowing for low offgas volumes and the potential for "carbon-free" electricity to be employed as the primary energy source. Potential drawbacks for the technology do, however, include:

- A significant electrical energy requirement (c.a. 21.6 MW for the processing of 22.1 t/h (wet) residues [13]) to provide the bulk of the process energy input for melting the feeds and fluxes.
- A significant petroleum coke requirement (c.a. 8—10% of cold feed charge [13]), to act as a reductant for the fuming process.
- Need for competitively priced, "carbon-free" electricity, without which, CO_2 emissions are likely to be equal to, if not higher, than in other fuming processes.
- A relatively high process offgas flow resulting from the treatment of wet feeds and a significant secondary (post-combustion) air input.
- Use of natural gas as a plasma carrier gas, which in some locations, may mean application of the technology is economically prohibitive.

Concluding Remarks

The Ausmelt process has been widely applied for the processing of various zinc-bearing materials, with more than 24 commercial furnaces applied for the zinc fuming process application. Over its history, the process has undergone continued development and improvement to increase its energy efficiency and thus drive down operating costs and fossil fuel consumption. In particular, this development work has centred on a more intense, batch fuming process operated with high levels of process air oxygen enrichment and the introduction of dried feed materials via the Ausmelt Lance. Collectively, these improvements are able to deliver significantly lower utilities and fossil fuel consumptions than alternatives such as the Waelz kiln, box fumer, Chinese side-blowing process and plasma technology.

References

1. Peng N, Peng B, Chali L, Liu W, Li M, Yuan Y, Yan H, Hou D (2012) Decomposition of zinc ferrite in zinc leaching residue by reduction roasting. Procedia Environ Sci 16:705–714
2. Abkhosk E, Jorjani E, Al-Harasheh MS, Raschi F, Naazeri M (2014) Review of the hydrometallurgical processing of non-sulfide zinc ores. Hydrometallurgy 149:153–167
3. Wood J, Dr. Coveney J, Gu H, Lan X, Song X (2015) The Outotec direct zinc smelting process. In: Proceedings of Pb-Zn 2015, vol 2. Dusseldorf, Germany, pp 537–548
4. Moats M, Guerra E, Siegmund A, Manthey J (2010) Primary zinc smelter operating data survey. In: Proceedings of Pb-Zn 2010. Vancouver, Canada. pp 263–282
5. Nykänen P (2016) 150 years' evolution toward a greener future. Outotec Oyj, Espoo, p 240
6. Creedy S, Glinin A, Matusewicz R, Highes S, Reuter M (2013) Ausmelt technology for treating zinc residues—ErzMetall, 66:230–235

7. Wood J, Matusewicz R (2019) Decarbonisation of the Outotec® Ausmelt Process. Proceedings of Copper2019. Vancouver, Canada
8. Sinclair R (2005) The extractive metallurgy of zinc. The Australasian Institute of Mining and Metallurgy Spectrum Series Volume Number 13, 215
9. Sinclair R (2005) The extractive metallurgy of zinc. The Australasian Institute of Mining and Metallurgy Spectrum Series Volume Number 13, 226
10. Chen Lin (2014) An Efficient reactor for high-lead slag reduction process: oxygen-rich side blow furnace. JOM J Miner Met Mater Soc 66:1664–1669
11. Chen L, Bin W, Yang T, Liu W, Bin S (2013) Research and industrial application of oxygen-rich side-blow bath smelting technology. In: 4th International symposium on high-temperature metallurgical processing, pp 49–55
12. Verscheure K, Van Camp M, Blanpain B, Wollants P, Hayes P, Jak E (2005) Investigation of zinc fuming processes for treatment of zinc-containing residues. In: John Floyd international symposium on sustainable developments in metals processing. Melbourne, Australia. pp 237–249
13. Verscheure K, Van Camp M, Blanpain B, Wollants P, Hayes P, Jak E (2007) Continuous fuming of zinc-bearing residues: Part II the submerged-plasma zinc-fuming process. Metall Mater Trans B, 38B:21–33

GCRIS

Production of SHG Zinc From 100% Recycled Materials

John F. Pusateri, J. R. de Wet and Brandon Tirpak

Abstract American Zinc Recycling Corp. operates five recycling plants with a capacity of over 650,000 tons per year for EAF dusts and zinc-containing residues and secondaries. AZR operates nine Waelz kilns at four plants: Chicago, IL, Rockwood, TN, Palmerton, PA and Barnwell, SC, and recovers nickel and zinc through its INMETCO plant (RHF/SAF) near Pittsburgh. Continuous improvements to the Waelzing process have increased productivity, decreased operating costs, enhanced Waelz Oxide quality, and minimized environmental impacts: temperature monitoring, air blast/oxygen-enrichment, feed conditioning, and refractory systems. AZR is reintroducing its **A**dvanced **Z**inc **R**ecovery (aka Flame Reactor) oxy-fuel flash-smelting technology to provide EAF steel producers with on-site dust processing that eliminates the liability and costs associated with EAF dust transportation. Restart of the Mooresboro, NC plant, based on Leach/SX/EW technology, will enable AZR to produce SHG zinc from Waelz Oxide, plus other zinc secondaries, at the rate of 155,000 tons per year. Restart is scheduled for April 2020 (Fig. 1).

Keywords Zinc solvent extraction · Waelz Kiln process · EAF dust recycling · Zinc recycling · Zinc electrolysis · SHG Zinc

J. F. Pusateri (✉) · B. Tirpak
American Zinc Recycling Corp, 3000 GSK Drive, Suite 201, Moon Township, PA 15108, USA
e-mail: jpusateri@azr.com

B. Tirpak
e-mail: btirpak@azr.com

J. R. de Wet
American Zinc Products, 484 Hicks Grove Rd., Mooresboro, NC 28114, USA
e-mail: kdewet@azr.com

© The Minerals, Metals & Materials Society 2020

A. Siegmund et al. (eds.), *PbZn 2020: 9th International Symposium on Lead and Zinc Processing*, The Minerals, Metals & Materials Series,
https://doi.org/10.1007/978-3-030-37070-1_7

Fig. 1 AZR plants and headquarters footprint

AZR History

American Zinc Recycling has its roots in the rich history of two non-ferrous mining companies, St. Joe Lead and New Jersey Zinc, which began operating in the mid-1800s and grew to become major competitors in the zinc industry by the mid-twentieth century. The St. Joe Resources zinc operations and New Jersey Zinc's Waelz kiln recycling assets merged in 1987 to form Horsehead Industries, a fully integrated producer of zinc metal and zinc oxide totaling about 150,000 tons per year of zinc equivalent.

By 2002, Horsehead had expanded its EAF dust recycling capacity through a combination of renovated and expanded kiln plants in Chicago, IL and Rockwood TN, and its novel Flame Reactor operation in Beaumont, TX to a total of about 420,000 tons per year of dust. Low zinc prices and high capital costs to maintain its roasting and acid plant at the Monaca smelter led to a decision in 2001 to cease processing zinc concentrates and file for Chap. 11 bankruptcy protection in late 2002.

The new Horsehead Corp. emerged with renewed competitive strength in early 2004 and went on to add about 220,000 tons per year of net EAF dust capacity with the commissioning of a second kiln at Rockwood in 2008 and start-up of a greenfield two-kiln plant in Barnwell, SC in 2010. These projects and the closure of the Beaumont Flame Reactor plant brought the Company capacity to over 650,000 tons per year of EAF dust. The Company also acquired International Metals Reclamation Company,

LLC (INMETCO) in 2009, adding 70,000 tons per year of specialty steel dust and nickel waste recycling capacity to produce Ni-bearing pig iron. INMETCO generates about 6000 tons per year of flue dusts containing over 1500 tons of zinc that are recovered through the Waelz kilns.

By 2012, the Zinc Corporation of America electrothermic smelter in Monaca, PA was processing over 140,000 tons per year of calcined Waelz Oxide from the Palmerton plant, along with about 40,000 tons per year of Waelz Oxide through its washing plant. These recycle feeds and 50,000 tons per year of purchased zinc secondaries were processed to produce about 80,000 tons per year of zinc metal (PW, CGG and SHG grades) and 80,000 tons per year of high-purity zinc oxide.

Increasing environmental pressures, high operating, maintenance and capital costs, and shrinking markets for Pb-containing zinc metal led Horsehead to make the strategic decision to embrace environmentally-friendly leach, solvent-extraction (SX) and electrowinning technology (EW) to replace its 80-year old Monaca smelter.

Horsehead licensed the Leach/SX technology from Tecnicas Reunidas and EW technology from Asturiana de Zinc to process Waelz Oxide and oxidic zinc secondaries and produce 155,000 tons per year of special high-grade (SHG) zinc metal. The Mooresboro, NC plant produced its first zinc in May 2014, and the Monaca smelter shutdown the same month. While the Mooresboro plant continued operating through January 2016, it was plagued by unit operations capacity and design engineering constraints, which limited throughput to about 40% of design. Horsehead filed for bankruptcy protection in February 2016 and emerged that September with new ownership and a commitment to restart the Mooresboro facility.

With the restart of Mooresboro, AZR is the only producer of SHG zinc metal from 100% recycled feed in the world. With an EAF dust recycling capacity of over 650,000 tons per year, AZR is uniquely positioned among steel scrap re-melters to close the zinc life cycle loop from galvanized and other zinc-rich scrap, to EAF dust and WOX, through to production of CGG and SHG metal ready for steel galvanizing mills. AZR's four regional facilities ensure uninterrupted recycling of EAF steel producers' dust: reclaiming a hazardous waste to produce feed for the company's Mooresboro zinc metal facility with minimal need for secondary zinc units (Fig. 2).

Waelz Kiln Process Improvements

The Waelzing process has been operated by AZR as the EPA-preferred Best Demonstrated Available Technology (BDAT) for nearly 40 years, having survived attempts by as many as 30 other process methods to compete in the EAF dust market. The combination of a robust technical process and equipment design, modest capital, low operating costs, and proven environmental performance have enabled the Waelz process to dominate the world market for recycling of zinc from EAF dust. AZR now operates eight Waelz kilns, one calcining kiln, and one "swing" kiln in four regional plants (see location map in Fig. 1). Details of the Waelzing process have

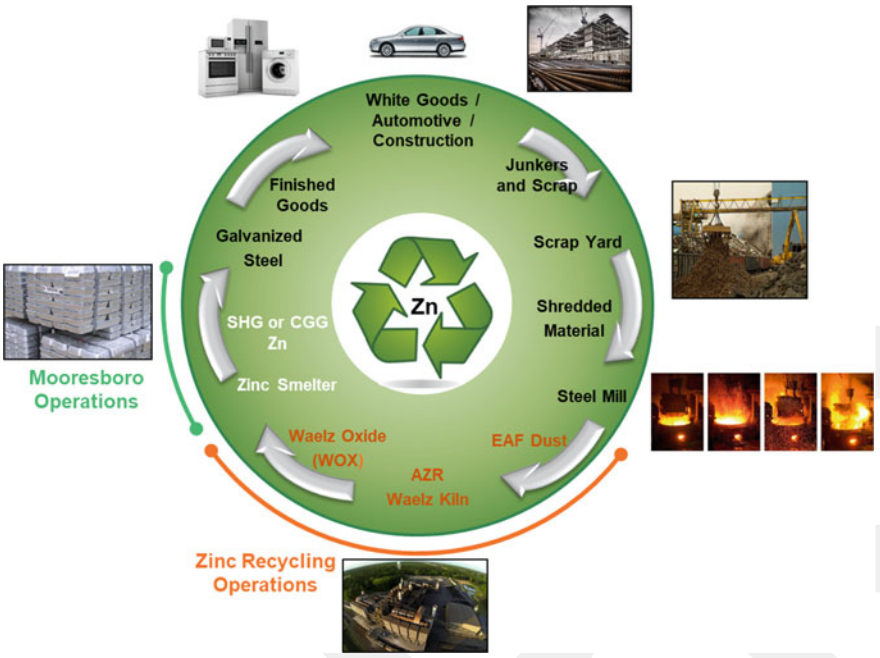

Fig. 2 Zinc lifecycle

been described by others [1–3]. AZR's kilns range in size from 10' ID by 142′ long to 12′ ID by 160′ long.

AZR blends EAF dust from several generators at each plant, adds metallurgical coke or anthracite fines, then conditions this feed blend with moisture and agglomeration before feeding to the kiln. No fluxes are added since the blended EAF dust chemistry maintains a "V4" basicity ratio between 2.0 and 4.0 in the kiln feed without excessive accretions or impacting zinc recovery. AZR's kilns operate with a discharge temperature between 1000-1,100° C, a residence time of 2–2.5 h, kiln rotation of 0.55–0.7 rpm, and zinc recovery of 95–97%. Air-blast is added at the discharge end to oxidize iron and burn residual carbon in the charge bed. A natural gas-air burner at the discharge end is used for cold kiln heat-up and, on occasion, to activate residual carbon in the charge bed and improve kiln thermal balance (Table 1 and Fig. 3).

AZR has continually improved its Waelz process efficiency through development, testing, and application of new technologies for:

Table 1 Typical compositions for EAF dust, Kiln Feed, WOX and IRM

	EAF Dust	Kiln Feed	WOX	IRM
%Zn	10–37	15–23	60–68	0.5–2.4
%Pb	0.3–2.4	0.3–0.8	1.0–2.4	0–0.06
%Fe	14–37	17–25	1.2–5	37–49
V4 Ratio[a]	1.5–10	2.0–4.0	–	1.6–3.2
%Cl-	0.5–3.2	0.8–1.4	3.5–5.3	–
%C	1–4	16–22	0.2–2	1–6

[a]V4 Ratio = $(\%CaO + \%MgO)/(\%Al_2O_3 + \%SiO_2)$

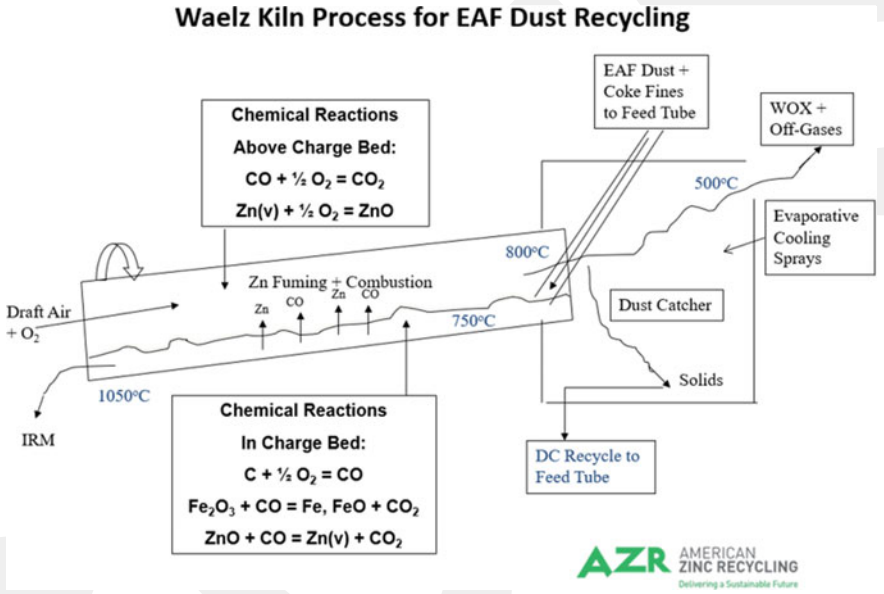

Fig. 3 Waelz kiln process schematic

Kiln Temperatures and Reaction Zone Control

AZR has determined that locating and managing the zinc fuming zone in the kiln have a critical impact on kiln productivity, zinc recovery, feed on-time, and operating costs. AZR employs an "Up-Kiln" thermocouple, which is a through-the-kiln-wall, in-the-charge-bed temperature measurement. AZR has developed a robust protection tube that extends thermocouple life beyond 180 days and avoids accretion buildup. By monitoring and maintaining this temperature between 700 and 900 °C, AZR can identify the "leading edge" of the zinc fuming zone and maintain thermal balance. The resulting benefits include, fewer high-temperature excursions and up-kiln

Table 2 Typical ranges of critical kiln temperatures (°C)

Dust catcher inlet	Up-kiln	Discharge
750–1000	700–900	1000–1150

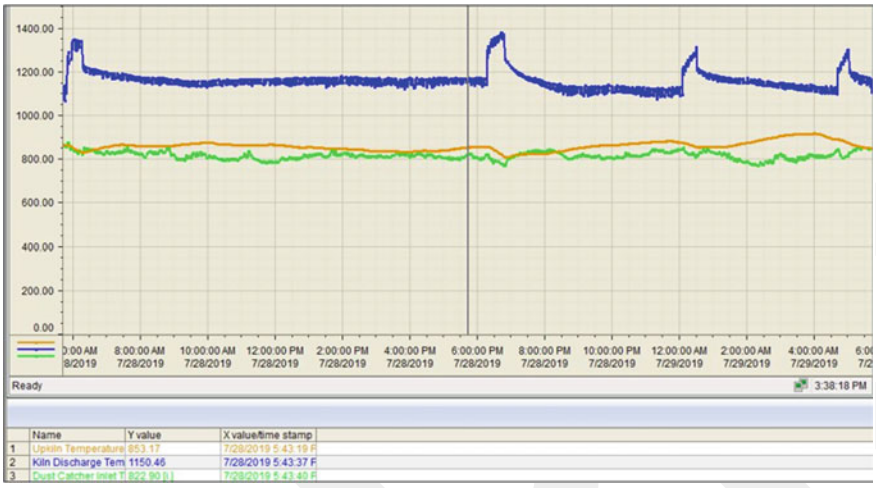

Fig. 4 Typical 24-H trend of critical Kiln temperatures

accretions/rings, longer operating campaigns, improved zinc recovery and increased productivity despite changing feed chemistry.

Table 2 shows the typical ranges of the three critical kiln temperatures (Fig. 4).

Refractory Material, Service Life and Construction

Considerable effort has been made the last several years to improve the service life and performance of the refractory materials used in the Waelz kiln and dust catcher.

For example, AZR has successfully trialed silicon carbide-containing andalusite kiln brick in strategic locations to replace traditional 60% alumina. These bricks resist accretion adhesion, CO and metal vapor penetration, and abrasive wear, leading to increased service life, longer operating campaigns, and ultimately, lower costs.

Dust catcher walls and roofs have evolved from Dietrick hanging brick to monolithic cast and shot-creted non-cement mullite- or andalusite-based refractories with up to 20% SiC. Zoned refractory, panelized construction with ample expansion joints, and insulating light-weight layers have also been incorporated. The service life in the areas that experience the strongest alkali attack and highest temperatures has more than doubled, decreasing overall costs and kiln downtime.

Waelz Kiln Feed Preparation and Control

The critical feed criteria for good Waelz kiln operational control and performance include: (a) blending various sources of EAF dust, (b) conditioning EAF dust with water for lime hydration, (c) agglomeration of EAF dust or EAF dust/carbon blends, (d) accurate proportioning with carbon reductant, and (e) consistent control of kiln feed rate.

AZR's Barnwell facility contains several important features that optimize feed proportioning and control:

- PD & Vacuum Railcar EAF dust unloading to mass-flow silos on load cells
- Independent control of EAF dust silo feed rates for consistent kiln feed zinc content and V4 ratio
- Coal/coke proportioning using a weigh-feeder and PID control to a target %C in kiln feed
- Pre-conditioning of kiln feed with water in a twin-screw blender
- Nuclear and mechanical scales on the pelletizer feed belt downstream of the blender
  - This is the primary point of control for kiln feed rate and coke proportioning
- Agglomeration on a pan pelletizer with multiple independently controlled sprays
- Return of dust catcher recycle material to the kiln feed upstream of the blender.

The results of these feed system improvements include:

- Zinc productivity consistently ~2.2 tons/operating hour or 459 MT Zn/yr/m^3 charge bed volume
- Waelz oxide (WOX) quality at < 2% Fe and > 65% Zn
- Coal/coke consumption ~1.0 tons coke/ton Zn in WOX
- Improved length of campaigns between cleanouts; fewer kiln accretions.

At the Rockwood plant, where feed pelletizing is not available, agglomeration of dust catcher recycle material using a pug mill has resulted in improved WOX quality and fewer feed and temperature excursions.

Oxygen-Enrichment and Productivity

AZR has applied oxygen-enrichment of the air-blast stream to promote iron oxidation and combustion of residual carbon in the charge bed. The system is engineered for safe, controllable application of the oxygen to preheat the kiln draft air, accelerate upstream zinc and iron reduction reactions, and increase kiln productivity all without causing charge melting, entrainment of bed particles, or overheating of the off-gas system (Fig. 5).

The current oxygen-enrichment configuration is improved over the previous generation (early 2000 s) in that (a) enrichment is limited, (b) the air-blast/oxygen mixture

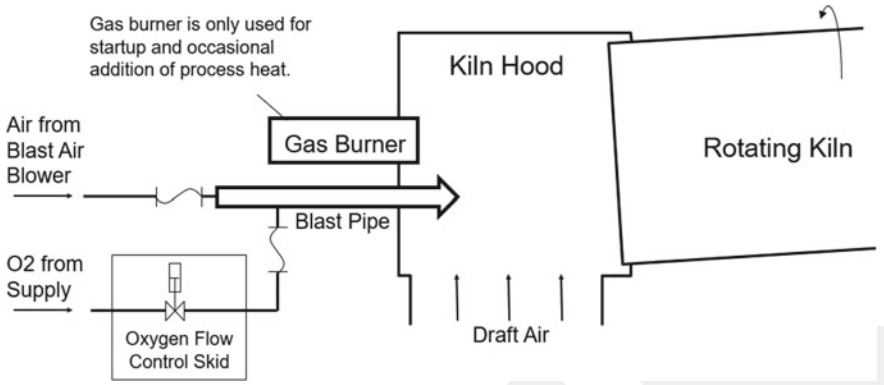

Fig. 5 Waelz kiln oxygen-enrichment schematic

is more tightly targeted near the discharge dam, and (c) process controls and safety interlocks are more sophisticated and extensive.

Kiln productivity gains of 8–10%, zinc recovery improvement of 1–2%, and nearly eliminating the use of the natural gas burner have all been realized during proof-of-concept campaigns at Rockwood in May-September 2019. Optimization and CFD modeling are in process, along with roll-out to all AZR kilns.

AZR Flame Reactor On-Site EAF Dust Recycling Process

AZR operated its Flame Reactor process on the site of the current Optimus Steel melt-shop in Beaumont, TX from 1993 to 2008. This natural gas-fired flash-smelting process operation was shut down due to rising natural gas prices and increasing Waelz kiln capacity. AZR is re-introducing the process to provide cost-competitive, on-site EAF dust processing services for operators looking to eliminate dust transport liabilities.

The **A**dvanced **Z**inc **R**ecovery (AZR) process utilizes a unique oxy-fuel burner that generates a high-temperature (> 2000 °C) reducing atmosphere to "flash" smelt raw EAF dust, separating the volatile metals like zinc from the iron oxides and slag-forming compounds, and producing crude zinc oxide (CZO) and granulated iron-rich slag (IRM).

The AZR process features include:

- Completely enclosed EAF dust receiving, storage and feed systems
- Water-cooled burner, flash-furnace and slag separator modules
- Air-granulated IRM cooling system
- Flash processing residence time of < 0.25 s
- Compact plant footprint of < 4 acres for 60,000 tpy dust capacity

Based on the Beaumont plant operating experience, several improvements have been engineered into the second-generation AZR process. The primary goals are to (a) decrease plant downtime and maintenance costs, (b) improve the quality of the crude zinc oxide and IRM products, and (c) increase zinc recovery (Fig. 6).

The AZR process enables the EAF melt shop operator to transfer EAF dust to receiving silos via direct pneumatic conveying or PD truck/railcar. The dust is then pneumatically conveyed to the flash-furnace feed bins, metered by loss-in-weight screw feeders and air-injected to the furnace just below the burner exit. The dust does not require conditioning, agglomeration or any physical handling which nearly eliminates workplace dust exposures and dramatically decreases chances for spills or releases.

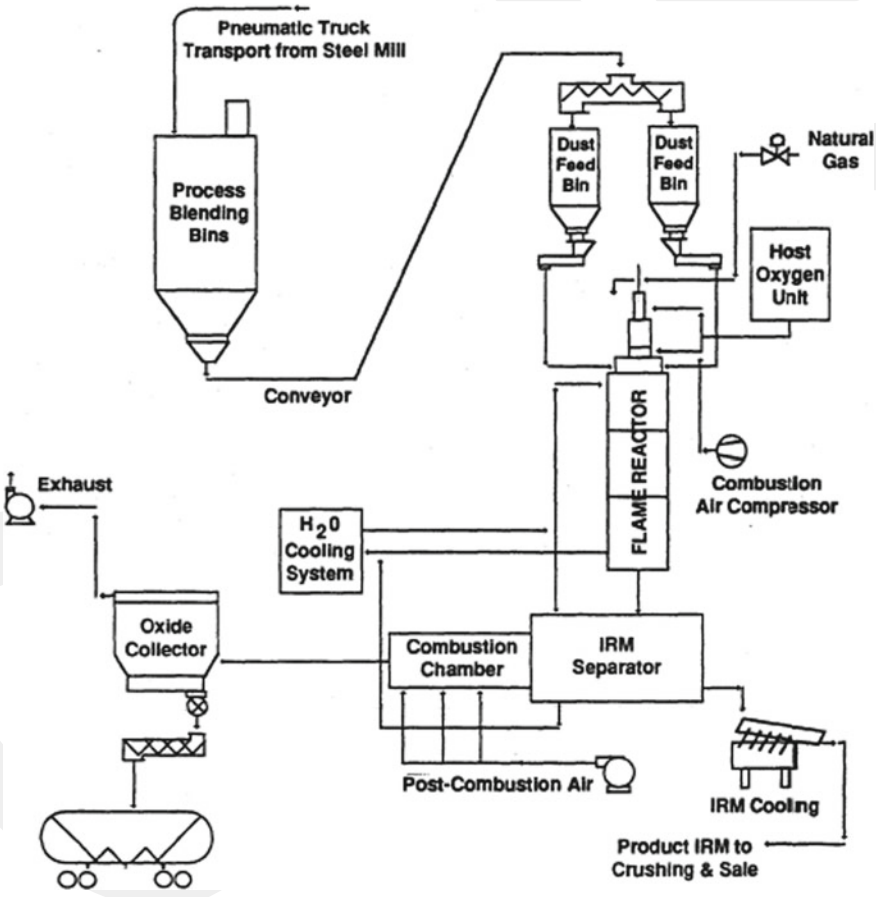

Fig. 6 **A**dvanced **Z**inc **R**ecovery (AZR) process schematic

The AZR process generates CZO and IRM products that are very comparable in quality to their Waelz kiln counterparts. The process meets the strict air-quality emission standards and generates zero contact water discharge [4].

Mooresboro Process Overview

The Mooresboro flow sheet is premised on the state of the art Modified Zincex Process® (MZP), developed by Tecnicas Reunidas, and first implemented in 1997 in a 3000 tons per year spent battery recycling facility near Barcelona [5]. In 2003, the MZP was proven at large industrial scale in the 165,000 tons per year Special High Grade (SHG) Zn Skorpion Zn Refinery (Namibia) and subsequently at Portovesme (Sardinia) and Akita (Japan).

The MZP incorporates atmospheric leaching, impurity precipitation through pH control and solvent extraction (SX), using a 40v/v mixture of Di-2-ethyl-hexyl-phosphoric acid (D_2EHPA) extractant, and a kerosene-based diluent [6]. Figure 7 conceptually illustrates the MZP application in the Mooresboro flow sheet, which comprises the following four main process loops:

- Leach—SX extraction.
- SX extraction—SX washing—SX stripping—SX depletion.
- SX stripping—electrowinning (EW).

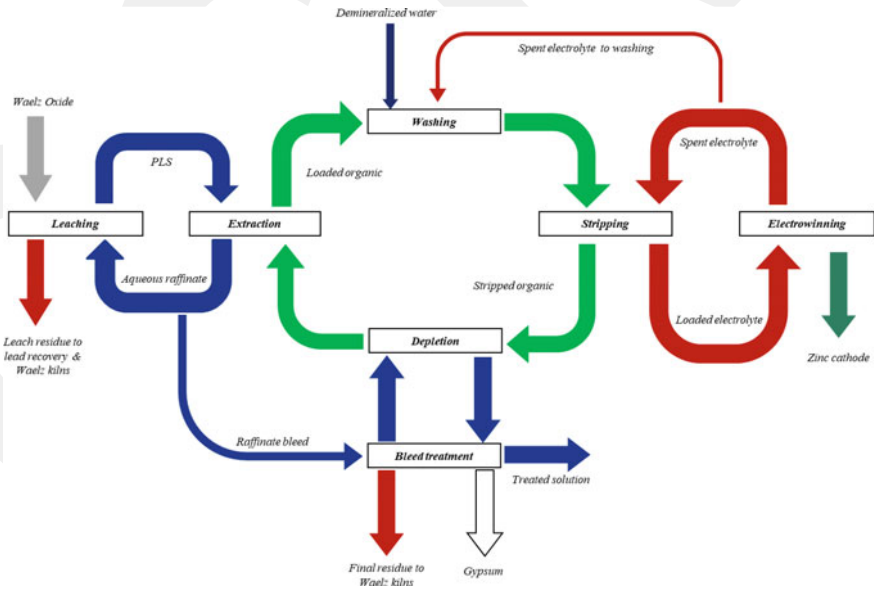

Fig. 7 MZP concept as implemented at Mooresboro (main process flows shown)

- SX depletion—bleed treatment (gypsum precipitation, cadmium cementation, $Zn(OH)_2$ precipitation).

The process loops are separated by the aqueous/organic interface, which offer the following distinct advantages:

- The organic offers a very effective barrier against the classical Zn circuit impurities, such as Cu, Cd, Ni, Co. Moreover, the process provides a barrier against Cl and F, which conventional Zn processing technologies do not, offering the distinct advantage to treat secondary materials, such as WOX, galvanizing ashes, and dross.
- The process yields consistent and predictable electrolyte quality, even at fluctuating impurity levels in feed materials, which further enhances the ability to treat a variety of complex feed materials.
- The SX step allows for the significant upgrading of low concentration Zn solutions, which facilitates the treatment of low Zn grade feed materials, without the requirement to blend with higher grade feed materials.
- The Mooresboro process is designed to yield >90% Zn recovery, and AZR treats leach residue from the Mooresboro facility in its Waelz kilns, which yields an overall Zn recovery of >99% from the AZR business, with no leach residue disposal requirements.

The Mooresboro Restart Project

The Mooresboro Restart Project, recently completed by AZR and its technical partners addressed the following detail design issues, which led to the difficulties experienced during the initial start-up in 2014:

- *Bleed treatment capacity.* Capacity increased by 40% to meet nominal production requirements.
- *Reagent cost reduction.* Limestone will be used instead of lime for neutralization.
- *Gypsum byproduct quality improvements.* Initial operating experience at Mooresboro yielded gypsum which did not meet the specifications for agricultural use, in respect of Zn, Cd and moisture content. Bench scale and piloting work, performed in collaboration with Pocock, confirmed that a 4:1 gypsum seed recycle rate increased thickener underflow solids concentration from 15 to 35% and reduced the required thickener unit area from 40 to 2 m^2/t/day. A hydro cyclone cluster was therefore incorporated into the gypsum flowsheet, to produce the required seed recycle.
- *Electrolyte quality improvements.* The MZP produces excellent quality electrolyte in respect of all the classical Zn impurities, with current efficiency values in the range of 90–92% achievable on a consistent basis. Contamination from external sources and organic entrainment in the electrolyte fed from SX to EW yielded low current efficiencies in the initial operation. Several components were replaced with super duplex stainless steel to minimize electrolyte contamination and improve carbon filter reliability to reduce organic entrainment to specified values.

- *Improved process control.* Although SX presents an effective barrier against most of the classical Zn impurities, Fe is co-extracted with Zn. pH and ORP control in leaching are therefore important to control Fe in the PLS. Unstable pH control, mainly due to blockages in the WOX addition system, yielded highly dissolved Fe values in the PLS, and Fe extracted onto the organic resulted in reduced SX capacity and poor phase separation. The entire WOX addition system was redesigned to eliminate WOX slurry blockages, a standby slurry system was installed, and control valve and take-offs were replaced.
- *Equipment reliability.* As Fe extraction onto the organic is not totally avoidable, HCl is used to strip Fe from the organic, which requires a significant volume of HCl and produces spent $FeCl_3$/HCl solution. Large scale facilities therefore incorporate an HCl recovery process. The corrosive processing conditions of the HCl recovery process necessitates the use of glass-lined process equipment and PTFE-lined piping and mechanical equipment. Piping stress-related leaks yielded low availability of the original Mooresboro HCl recovery circuit. The system was redesigned, based on a detailed piping stress analysis.
- *Leach solid/liquid separation capacity.* Designing an MZP circuit requires great attention to solid/liquid separation equipment design, particularly the leach clarifiers, due to the low tolerance of SX for suspended solids. At Skorpion, CRUD accumulation was caused by total suspended solids (TSS) values in the pregnant leach solution (PLS) averaging 45 mg/l, versus the specified value of 10 mg/l. A CRUD run through SX ultimately led to a hydrogen fire in the EW cell house [7]. A single 41 ft diameter leach clarifier presented one of the most significant capacity constraints in the original Mooresboro leach circuit. The high rise rate of 0.35 ft/min led to significant and varying solids carryover, even at reduced throughput. The Asturiana de Zinc Reverse Leach® process, implemented in the restart project, featured two new and one repurposed clarifier, each of 59 ft diameter, yielding a rise rate to 0.06ft/min, or a capacity increase of 5.8 times.
- *Improved environmental controls.* The Mooresboro Restart Project included the construction of covered product and reagent storage facilities, as well as the construction of sumps and installation of sump pumps to collect process spills and contact stormwater. Process buffer capacity was increased, which minimizes the risk of process spills and improves overall availability. New acid brick and membrane coating of process containments minimize environmental contamination risk.

Project Execution

The project scope included the procurement, fabrication, and installation of 366 pieces of mechanical equipment (mainly pumps, tanks and agitators), the fabrication and installation of 3477 piping spools and 538 tons of structural steel. Foundation and containment construction included 6835 cubic yards of concrete and 612 tons of rebar. Electrical and instrumentation installation included a new E-house, 3640 ft of cable tray, 204,882 ft of cable, the installation of 248 new instruments, and refurbishment of 586 existing instruments.

All construction was performed within the existing refinery, which yielded significant cost and schedule risk due to access issues and potential clashes with existing equipment. The use of high-resolution 3D scanning, modular design, pre-fabrication, and construction methods proved invaluable to minimize construction risk.

The project was approved in Dec 2017, with first Zn produced in April 2019, yielding an overall project schedule of 16.5 months, versus the approved project schedule of 15 months. The final project cost was 4.6% above the original budget, well within the original estimate range of ±25%. A high level of piping construction quality was achieved, evidenced by a thermoplastic weld failure rate of less than 0.1%, experienced during the restart of the facility.

Restart

The cell house rectifier power was achieved within three weeks of feeding WOX to the leach circuit. The start-up proceeded without major process upsets in the leach, SX and bleed treatment sections, and the impact of the various upgrades and modifications were apparent in the early Key Process Indicators (KPI's).

Figure 8 compares the Fe concentration in the PLS during the original Mooresboro commissioning in 2014 and the monthly average for the initial stable operating period from February 2015 to January 2016 with the current restart project. The results illustrate the difficulties with pH and ORP control in the original operation, which have been improved by the modifications and upgrades completed during the restart project, with Fe being consistently within specification.

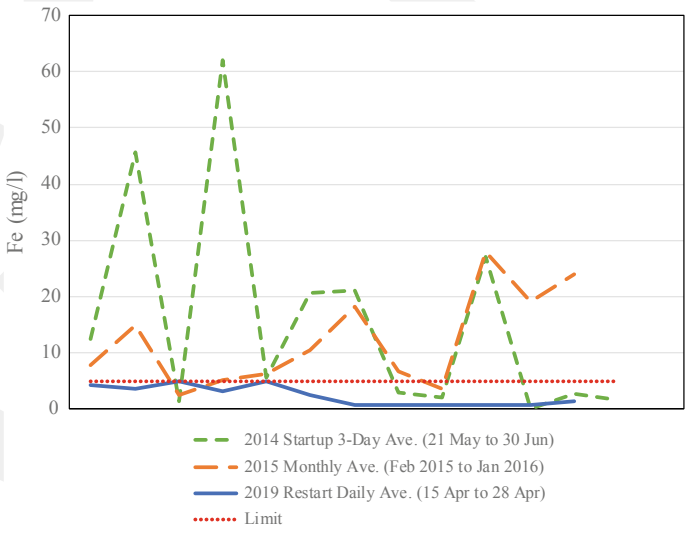

Fig. 8 Improved Fe control in PLS

Increased bleed treatment capacity allowed the Mooresboro team to operate the SX circuit with the required volume of demineralized water flow to the washing circuit, which improved physical washing performance. Figure 9 compares *F* values in the electrolyte for the original steady state operation (Feb 2015 to Jan 2016) with the restart project.

Figure 10 compares Ni in electrolyte for the original project start-up, the steady operation period from February 2015 to January 2016 and the restart project values. The Ni contamination is ascribed mainly to (a) limitations in bleed treatment capacity, which limited the ability to add demineralized water for washing and (b) corrosion of 316 stainless steel components in the cell house, which were replaced in the

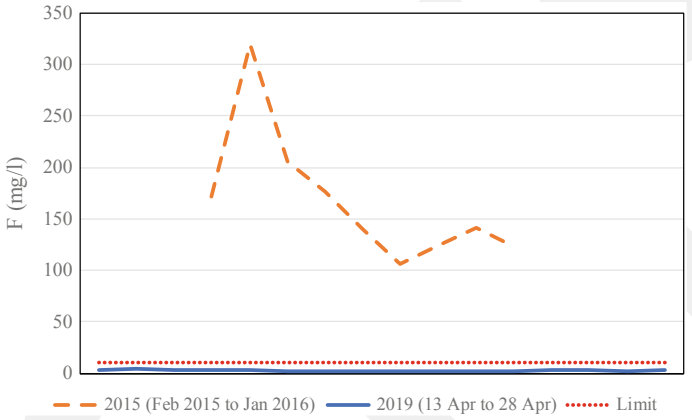

Fig. 9 F in electrolyte

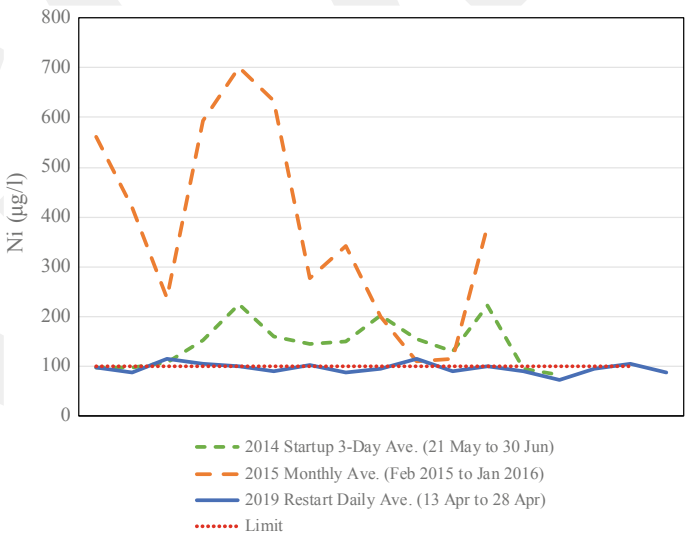

Fig. 10 Ni in electrolyte

Table 3 First Zn produced

	Bay 1	Bay 2	LME
Al (%)	0.0002	ND	0.001
Cd (%)	ND	ND	0.003
Cu (%)	0.001	0.0011	0.001
Fe (%)	0.0059	0.0014	0.002
Pb (%)	0.0146	0.0113	0.003
Sb (%)	ND	ND	0.001
Zn (%)	***99.955***	***99.970***	***99.995***

restart project. The values in the restart project are within specification and are expected to improve as operation proceeds due to the completion of activated carbon washing, which released Ni and Fe into the initial electrolyte inventory in the SX stripping—EW loop.

The first metal from the Restart Project was stripped 30 h after the power was switched on with excellent cathode morphology. Based on experience during the Skorpion start-up, first Zn from the MZP was not expected to be SHG quality due to the use of fresh non-passivated Pb-Ag anodes and the low initial concentration of Mn in the electrolyte. The composition of the metal produced is shown in Table 3, confirming that Pb was out of specification for SHG and Fe slightly over spec for the Zn produced from Bay 1, while Zn from Bay 2 was within spec. The low levels of the remaining classical impurities, often found in SHG Zn, is typical of the quality produced by the MZP and confirms that the facility will produce SHG Zn once passivation of the Pb-Ag anodes is achieved.

Manganese addition system fire and subsequent repair work

One of the upgrades completed during the project involved a first of its kind Mn dissolution system, where high purity Mn metal flakes were dissolved in spent electrolyte to produce $MnSO_4$ which was then fed back to the electrolyte circulation tank. Shortly after the first Zn stripping from the cells, a fire broke out in the Mn dissolution tank, which spread to the cell house, ultimately destroying the cooling towers and electrolyte circulation piping, and causing damage to some concrete components, the electrode cranes, and electrowinning cells. Although the exact cause of the fire is still under investigation, it is generally considered plausible that hydrogen had built up to a level higher than the LEL in the tank and that an external source of ignition had ignited the hydrogen.

Cell house rebuild and resumption of operations

At present the cell house and associated equipment are undergoing refurbishment, while one of the electrode cranes, the cooling towers and associated electrolyte circulation piping are being replaced. The refurbishment work is expected to be completed early in 2020, with Zn production expected to resume before April 2020.

References

1. Gamroth M, Mager K (2010) SDHL Waelz technology: state of the art for recycling of zinc-containing residues. Proc Lead-Zinc 1:861–870
2. Takayama T, Magalhães W, dos Santos FM (2015) Treatment of secondary raw materials at Juiz de fora zinc smelter in Brazil. Proc Pb-Zn 2:931–951
3. Antrekowitsch J, Rösler G, Steinacker S (2015) State of the art in steel mill dust recycling. Chem Ing Tech 1498–1503
4. Clark RK, Pusateri JF, Lherbier Jr. LW (1994) Gas-fired flash-smelting for metals recovery from hazardous solid wastes. Presented at Industrial Energy Technology Conference, Houston, TX
5. Martin D, Diaz G, Garcia MA, Sanchez F (2002) Extending zinc production possibilities through solvent extraction. Jnl SAIMM 463–468
6. Diaz G, Martin D (1994) Modified Zincex process: the clean, safe and profitable solution to the zinc secondaries treatment. Resour Conserv Recycl 10:43–57
7. Gnoinsky J, Sole KC, Swart DR, Maluleke RF, Diaz G, Sanchez F (2008) Highlights and hurdles in zinc production by solvent extraction: the first four years at Skorpion Zinc. Proc ISEC. 1:201–208

GCRIS

Recent Development of EAF Dust Treating at Shisaka Smelting Co., Ltd.

S. Takaya, N. Kubota, H. Watanabe and T. Kudo

Abstract Shisaka Smelting Co., Ltd. has recovered crude zinc oxide from electric arc furnace (EAF) dust using the Waelz kiln process since 1977. When the operation started, malfunctions frequently occurred in a granulation process which was previous process of a reduction roasting process. We stopped this process and shifted to the process directly charging EAF dust in the reduction rotary kiln. As a result, we had been weak in treating high-zinc EAF dust for a long time. To improve the disadvantage, we introduced a new granulation process which is off-line in 2011. Thereby, zinc recovery rate in reduction rotary kiln greatly increases and the capacity treating high-zinc EAF dust reaches 50,000 tons per year.

Keywords EAF dust · Zinc recycling · Waelz kiln process · Pelletizing

Introduction

In 1977, Shisaka Smelting Co., Ltd. of the Sumitomo Metal Mining (SMM) Group started zinc and lead recycling operations using the Waelz process to recover zinc and lead from dust generated in an electric arc furnace (EAF dust) as crude zinc oxide pellets for use in an ISP smelter. As shown in Fig. 1, the EAF dust process in our plant is performed using a reduction rotary kiln (RRK), a Waelz dust washing and dewatering process, and a drying rotary kiln (DRK). Figure 2 shows the yearly amounts of EAF dust treated since we started operations in 1977 using a system with one RRK, washing facilities, and one DRK. At that time, the EAF dust treatment capacity was 50,000 tons per year. The addition of another RRK in 1992 increased the capacity to 120,000 tons per year. Recent economic recessions reduced the amount of incoming EAF dust, resulting in average throughput of about 80,000 tons per year. The residue left upon volatilization and separation of zinc from EAF dust due to the addition of a reducing agent to the RRK is called clinker, which is either recycled as an iron source or disposed of by landfilling. The 2–3% zinc remaining in the clinker

S. Takaya (✉) · N. Kubota · H. Watanabe · T. Kudo
Shisaka Smelting Co., Ltd., 3-5-3, Nishibara-Cho, 792-0011 Niihama, Ehime, Japan
e-mail: satoru.takaya.c3@smm-g.com

© The Minerals, Metals & Materials Society 2020

A. Siegmund et al. (eds.), *PbZn 2020: 9th International Symposium on Lead and Zinc Processing*, The Minerals, Metals & Materials Series,
https://doi.org/10.1007/978-3-030-37070-1_8

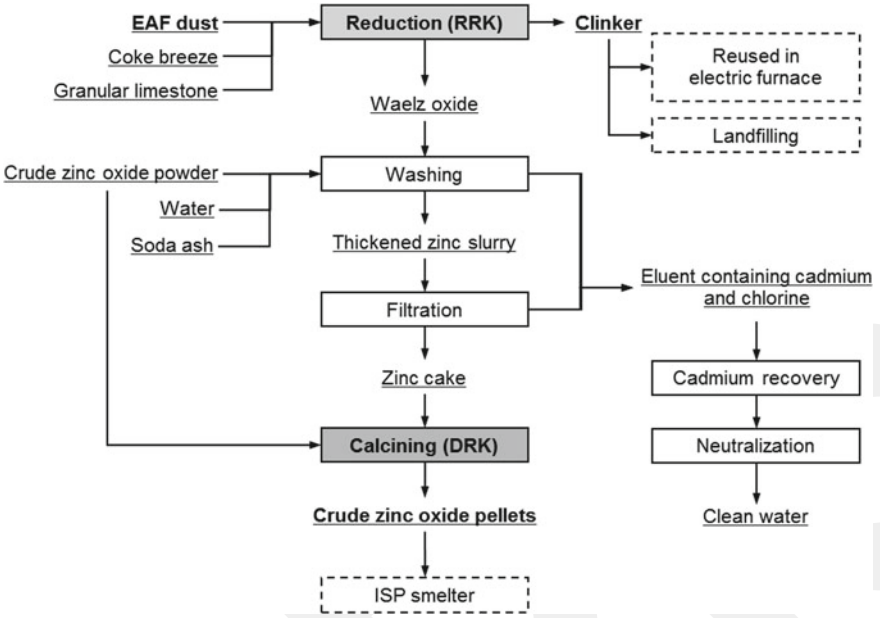

Fig. 1 Process chart of Shisaka smelter

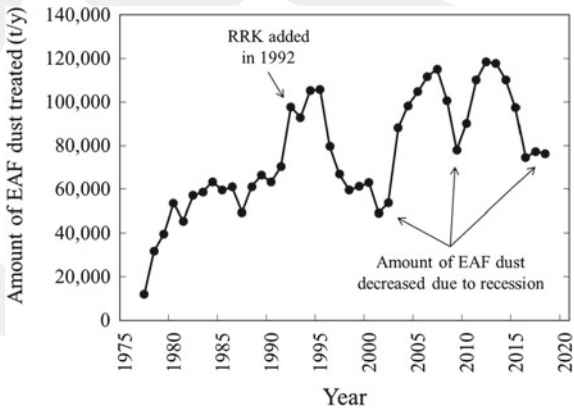

Fig. 2 Changes in amount of EAF dust treated

is a recovery loss, leading to increased processing cost. Under circumstances where the amount of incoming EAF dust is decreasing, it is especially important to improve the zinc recovery rate for cost improvement.

Initially, the granulation process preceding the reduction roasting process was extremely inefficient. It was performed using a crusher with a ball mill, a granulator with a pan-type pelletizer, and a dryer and was connected on-line to the reduction roasting process. However, the pellets were weak and often burst in the RRK, so the granulation process was changed to one in which the EAF dust was directly charged

in the reduction roasting process. As a result, the zinc loss in the clinker increased when EAF dust with a high concentration of zinc was treated, so the treatment of high-zinc EAF dust was inefficient for a long time.

To increase the zinc recovery rate, we introduced a commonly used pan-type pelletizer off-line in 2008. However, the moisture content of pellets is high with this type of pelletizer, so the pellets had to be aged for a long time in the storage yard. The amount of granulation was thus limited to about 2000 tons per month due to the limited capacity of the storage yard. In addition, it was difficult to crush the EAF dust particles and uniformly mix them with a reducing agent, so we were unable to improve the zinc recovery rate. We thus considered introduction of a new granulation process [1–3].

Methods

Introduction of New Granulation Process

To increase the zinc recovery rate when treating high-zinc EAF dust, we introduced a new granulation process in 2011. As shown in Fig. 3, the new granulation process, which is off-line to the reduction roasting process, uses DAW mixer and DAW pelletizer. High-zinc EAF dust particles are crushed in the DAW mixer and mixed with a reducing agent. Next, pelletization is performed in the DAW pelletizer with water added to reach a specific moisture content. Pellets formed with a size of 1–25 mm are stored in the storage yard. After aging for several days, they are processed together with other EAF dust in the RRK.

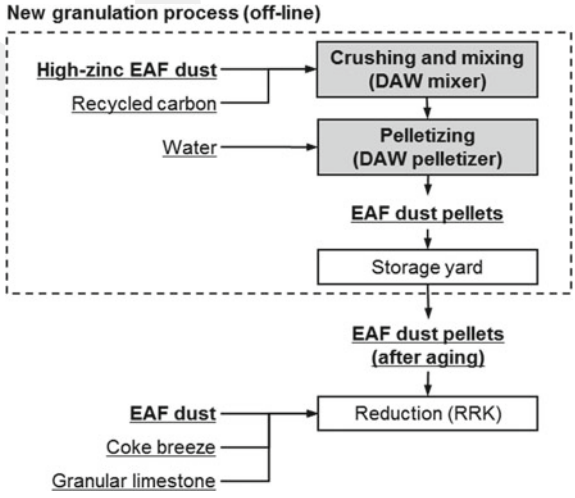

Fig. 3 Process chart of new granulation process

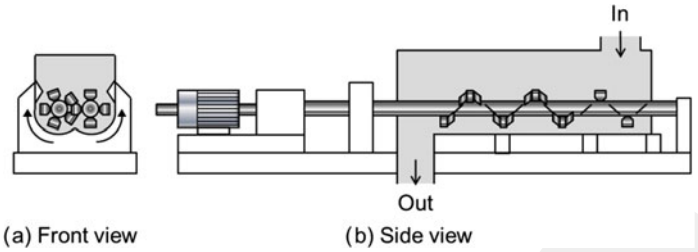

Fig. 4 Diagram of DAW pelletizer

A schematic diagram of the DAW pelletizer is shown in Fig. 4. The DAW mixer is structurally similar. The crushing, mixing, and pelletization are controlled by adjusting the paddle shape. This equipment is characterized by uniform mixing and pelletization due to the unequal-speed 2-axis mechanism (Shin Nichinan Co., Ltd.) and self-cleaning. The drive shaft and driven shaft on which the paddles are arranged in screw form rotate inward with respect to one another. Their unequal speeds enable uniform mixing and pelletization of charged materials. The phase deviation between the two shafts results in mutual scraping of the paddles, which prevents accumulation of the processed materials. In testing, we achieved good pelletization performance when the residence time was 4 min or longer. Therefore, for our facility design, we selected a pelletizer with a total capacity of 1.5 m^3 and specified a total residence time in the DAW mixer and pelletizer of 6 min, giving us a processing capacity of 15 tons per hour. Since the paddles attached to the two shafts are removable, they can be easily replaced in the casing. Initially during introduction, we used paddles with a steel base material made using hardening build-up welding. However, the paddles quickly became worn, and their frequent replacement increased operating cost. We were able to extend their life from 1 month to 1 year or longer by casting a wear-resistant material (iron-base alloy; Hv600 hardness) on their tips. This stabilized the operation of the granulation process.

Results and Discussion

Optimization of Granulation Conditions

The optimal pellet moisture content and the optimal aging period were determined to be 18% and four days, respectively. Introduction of the DAW mixer and DAW pelletizer enabled uniform mixing and pelletizing. Equivalent pelletization performance was maintained even though the moisture content was reduced from 22% (with pan-type pelletizer) to 18% (with DAW pelletizer). Given this result, we shortened the aging period from eight days (when pan-type pelletizer was used) to four days (when DAW pelletizer was used) in order to reach a moisture content of 14%, a level that

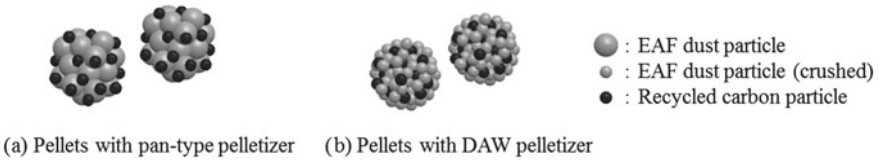

Fig. 5 Diagrams of pellet structures, **b** illustrating improved reducing efficiency with DAW pelletizer due to uniform dispersion of recycled carbon and decrease in EAF dust particle size

does not impair the pellet transfer equipment and RRK charging chute. In addition to shortening the aging period, we increased the capacities of the belt conveyor and other transfer equipment, enabling us to increase the amount of granulation from 2000 to 4200 tons per month.

Improvement in Zinc Recovery Rate

As shown in Fig. 3, in the new granulation process, EAF dust particles and a reducing agent are mixed and pelletized at the same time. The reducing agent is a recycled carbon, which is lower in cost than a coke breeze. The recycled carbon, which is flue dust generated when oil coke is manufactured, is obtained from other companies. It is a powdery reducing agent with a carbon content of 90%. The pellet structures are illustrated in Fig. 5. Pelletization with a pan-type pelletizer causes the recycled carbon to adhere to the surfaces of the pellets formed by the EAF dust particles. In contrast, the DAW mixer and pelletizer crush the EAF dust particles and uniformly mix them with the reducing agent, so the recycled carbon adheres to each piece of dust, resulting in uniform dispersion of the reducing agent. Therefore, compared with those in the pellets made with the pan-type pelletizer, the EAF dust particles and reducing agent are close together in the pellets. Moreover, the dust particles are smaller and their specific surface area is larger. These factors increase the opportunity for contact between the CO gas generated by oxidation of the reducing agent and the ZnO in the EAF dust particles and thereby improve zinc recovery efficiency. The addition rate of the reducing agent is defined as a ratio of the amount of added reducing agent to the amount of EAF dust during granulation. The pellet treatment rate is defined as a ratio of the amount of pellets treated in the RRK to the total amount of EAF dust treated in the RRK. The zinc recovery rate is defined as the amount of zinc recovered to the amount of zinc input to the RRK (i.e., the amount of zinc input minus the amount of zinc loss in clinker). The relationship between the reducing agent addition rate and the zinc recovery rate at a pellet treatment rate of 50% is shown in Fig. 6. When the addition rate was from 0 to 12%, the zinc recovery rate in the RRK improved 1% with a 3% increase in the reducing agent. However, further improvement in zinc reducing efficiency cannot be obtained when the addition rate is 15% or more because the amount of reducing agent carried over (amount expelled into flue gas without contributing to reduction reaction) increases after the pellets

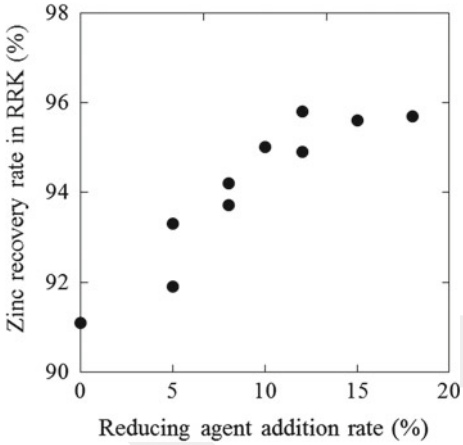

Fig. 6 Zinc recovery rate versus reducing agent addition rate (EAF dust pellet treatment rate: 50%)

are charged in the RRK due to reduced pellet strength and increased amounts of reducing agent adhering to pellet surfaces. Consequently, we set the addition rate of the reducing agent to 12%.

The relationship between the pellet treatment rate and the zinc recovery rate at a reducing agent addition rate of 12% is shown in Fig. 7. With a pellet treatment rate of 0–50%, the zinc recovery rate improved 1% with a 10% increase in the pellet treatment rate. For the granulation amount possible with our current equipment capacity and operation staffing hours, we can now increase the pellet treatment rate to 50%, with a 95% or higher zinc recovery rate. The increase in the pellet treatment rate and improvement in the zinc recovery rate due to the introduction of the new granulation process in 2011 and optimization of the operating conditions resulted in a reduction in the zinc content in the clinker to 1.5% from the conventional 2–3%. Changes in the amount of high-zinc EAF dust treated, requiring pelletization

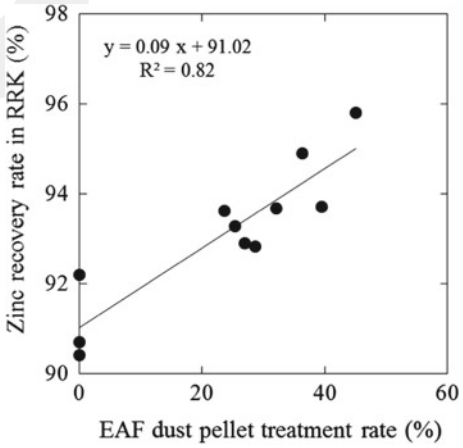

Fig. 7 Zinc recovery rate versus EAF dust pellet treatment rate (reducing agent addition rate: 12%)

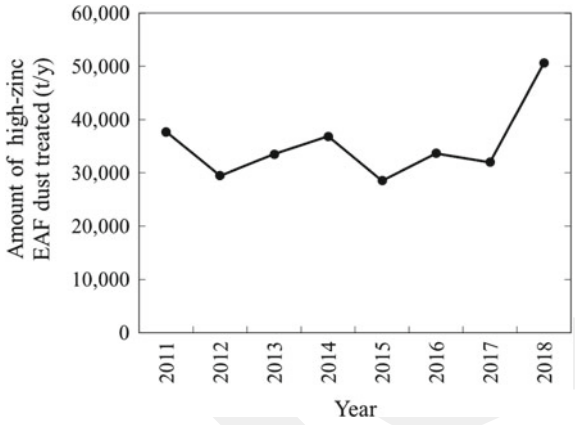

Fig. 8 Changes in amount of high-zinc EAF dust treated

(including powdery EAF dust), are shown in Fig. 8. The increased zinc recovery rate for high-zinc EAF dust enabled us to treat approximately 50,000 tons of high-zinc EAF dust in 2018.

Conclusion

Shisaka Smelting has greatly improved the technology used in its zinc recycling over the 42 years since commencement of EAF dust treatment operation. The high-zinc EAF dust treatment technology described in this report has been indispensable for improving our application performance of raw materials and increase our cost competitiveness. EAF dust treatment is gaining greater attention due to the growing importance of environmental conservation and resource recycling. We will continue to research and implement various improvements to the EAF dust treatment technology to enable even more effective use of resources.

References

1. Yasukawa M, Kuwata H (1981) Zinc and lead recovery from iron and steelmaking intermediates and Shisaka Works. J MMIJ 97:820–821
2. Takewaki M, Ojima Y (1993) Recent operation of EAF dust treatment at Sumitomo Shisaka works. J MMIJ 109(12):1112–1117
3. Nagai K, Takahashi J, Matsumoto Y, Koshino T, Ikeda K (2005) Recent development of EAF dust treatment operation. Lead Zinc '05 1:373–386

Part IV
Zinc Electrowinning

GCRIS

Current Efficiency Increase in Zinc Electrodeposition at Cajamarquilla Refinery

Juliano Alves de Lima, Eder Lucio Martins, Gian Piero Pajuelo Gonzales and Tone Takayama Filho

Abstract The Cajamarquilla Zinc Refinery is a metallurgical unit belonging to Nexa Resources SA; its production capacity is 335 kt of refined zinc. It is an integrated Zinc Refinery that processes Zinc concentrates from the route known as RLE (Roasting–Leaching–Electrowinning). The Electrowinning stage is of fundamental importance because it consumes 80% of all electrical energy and this represents 31% of the entire conversion cost. It also restricts the production capacity of the plant. In the years 2015, 2016, and 2017, there was a significant reduction in the current efficiency of the electrolysis, impacting the transformation cost and also the production capacity of the Refinery. This work includes research studies, actions taken to restore performance, and stability of the process. At present, Cajamarquilla's performance in current efficiency is benchmark against the main world competitors. In addition, the main future developments to increase the competitiveness of the unit are presented.

Keywords Zinc electrowinning · Current efficiency · Cajamarquilla zinc refinery

Introduction

The Zinc Refinery of Cajamarquilla is a metallurgical plant that belongs to Nexa Resources SA and is located in the Lurigancho-Chosica district in Metropolitan Lima. It started operations in 1981 and currently has an annual production capacity of 335 kt of refined zinc. It is an integrated Zinc Refinery that processes Zinc concentrates from

J. A. de Lima (✉) · E. L. Martins · G. P. P. Gonzales
Nexa Resources S.A.—Cajamarquilla, Lima, Peru
e-mail: juliano.lima@nexaresources.com

E. L. Martins
e-mail: eder.martins@nexaresources.com

G. P. P. Gonzales
e-mail: gian.pajuelo@nexaresources.com

T. T. Filho
Nexa Resources S.A.—Juiz de Fora, Juiz de Fora, Brazil
e-mail: tone.takayama@nexaresources.com

© The Minerals, Metals & Materials Society 2020

A. Siegmund et al. (eds.), *PbZn 2020: 9th International Symposium on Lead and Zinc Processing*, The Minerals, Metals & Materials Series,
https://doi.org/10.1007/978-3-030-37070-1_9

the route known as RLE (Roasting–Leaching–Electrowinning). The Electrowinning stage is of fundamental importance because it consumes 80% of all electrical energy and this represents 31% of the entire conversion cost. It also restricts the production capacity of the plant.

During the years of 2015, 2016, and 2017, there was a significant reduction in the current efficiency of the electrolysis in Cajamarquilla, strongly affecting the conversion cost and the production capacity of the Refinery.

This work includes research studies, actions taken to recover the performance, and stability of the process. Currently, the performance in current efficiency in Cajamarquilla is a reference against the main global competitors.

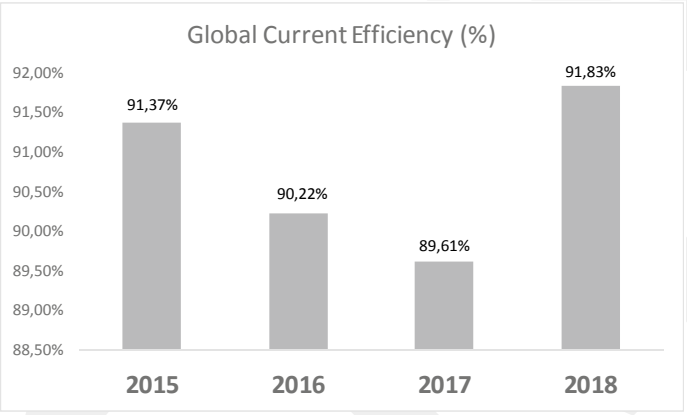

Principles of the Process

Zinc Electrometallurgy

Electrolysis is the unit operation that involves the deposition at the cathode of the metal present in an aqueous solution containing other constituents that can be co-deposited. The feed solution can be used directly from the leaching of the solid, or it can be partially or fully purified before electrodeposition.

Efficient zinc deposition requires the use of high purity zinc sulfate solution [1]. For this, in the Roasting–Leaching and Electrowinning (RLE) process, there are two stages of proper purification. The first stage occurs during the leaching of oxides, where various others elements are leached, in addition to zinc. This leaching occurs in pH of the order of 4.2–4.8, where the Fe^{+3} ions present in the solution precipitate in the form of iron hydroxide. Since the iron hydroxide has an adsorption property similar to a gelatinous solid, several metal ions can be co-precipitated during the

process. The second stage of purification occurs by the cementation of metal ions [2].

The solution fed to the zinc electrolysis proceeds from the recirculation of the cell electrolyte ~50 g/L Zn, which must be enriched with the purified concentrated neutral solution at an order concentration of 150 g/L Zn, raising the concentration of feed electrolyte at order values from 55 to 60 g/L Zn. The energy consumption in this stage varies generally from 3000 to 3500 kWh/t cathodic zinc, whereas about a third becomes heat losses [3]. The potential difference in the cells is from the order of 2.5–3.0 V and the cellroom operates at a current density of 550 A/m^2.

The main reactions involved in the process, as well as the standard potential correspondents, are represented by the cathodic Eqs. (1) and (2) and the anodic Eqs. (3) and (4) [3], with their respective standard potentials of electrode:

$$Zn^{2+}(aq) + 2e^- = Zn^0(s)\ E^0 = -0.76\,V \tag{1}$$

$$H^+(aq) + e^- = 1/2H_2(g)\ E^0 = 0.00\,V \tag{2}$$

$$2H_2O(aq) = 4H^+(aq) + O_2(g) + 4e^-\ E^0 = -1.23V \tag{3}$$

$$Mn^{2+}(aq) + 2H_2O(aq) = MnO_2(s) + 4H^+(aq) + 2e^-\ E^0 = +1.33V \tag{4}$$

At the cathode, the reduction of Zn^{2+} to Zn^0 under standard conditions (Eq. 1) implies a more negative potential than the potential for hydrogen reduction (Eq. 2). Thus, if only thermodynamics is considered of the reaction, the electrolysis of Zn in aqueous medium would not be viable, however, what makes this important reaction possible in the aqueous medium is the slow kinetics of the reaction of the evolution of hydrogen on the surface of zinc. Equation (3) represents the oxidation of water on the anode, with oxygen release, while Eq. (2) represents the oxidation of manganese ion to MnO_2. The formation of a protective layer of MnO_2 on the surface of lead and silver anodes helps to reduce its corrosion rate. As a result, we have less lead contamination in the zinc cathodic deposit as well as reduced costs due to increased service life [1].

Current Efficiency

Current efficiency is one of the most important parameters of the electrolysis process, along with the specific energy consumption. This indicator assesses the relationship between deposited metal mass and theoretical mass, calculated from Faraday's law. For a given applied current, the current efficiency (CE) can be calculated according to Eq. (5)

Table 1 Effect of some metal ions on the loss of zinc current efficiency

Element	Concentration (mg/L)
Ge	0.002
Sb	0.002
Cu	0.12
Tl	0.5
Co	1.0
Ni	1.0
Cd	Without effect
Pb	Minimum

Adapted from [1]

$$EC = \frac{m}{m_f} = \frac{m\,nF}{(i\,t\,M)} \tag{5}$$

where **m** represents the mass of deposited metal, in **g**; $\mathbf{m_f}$ the mass calculated from Faraday's law, in **g**; the current, in A; **t** is the deposition time, in **s**; **M** the atomic mass of the metal, in **g/mol**; **n** the number of electrons involved in the reaction; and **F** the Faraday constant, 96500 °**C/mo**l.

Current efficiency is an indicator of productivity in electrolysis. The main reasons for loss of current efficiency are related to the rate of hydrogen formation and co-deposition of metal impurities in the cathode. In a high purity zinc sulfate solution, the hydrogen ion reduction is very slow and this impact is minimized. However, several metal ions can catalyze the reduction of that ion [1]. With respect to the effect of metallic impurities in the loss of current efficiency, Table 1 demonstrates that the elements Ge and Sb have the greatest impacts, followed by Cu and Tl. There is evidence that the elements Ge and Sb form metal hydrides with zinc, causing the re-dissolution of this metal, which would explain that considerable effect on the deposition process [4]. The elements Cd and Pb, in turn, have no significant effect on the loss of current efficiency, but, when co-deposited, reduce the quality of the zinc deposit.

Manganese in Zinc Electrolysis

In zinc electrolysis, depending on its concentration, the presence of manganese has positive and negative effects [5]. The main positive impacts of manganese are:

- With a concentration between 1 and 3 g/L of Mn^{2+}, reduces the corrosion rate of anodes, which minimizes lead contamination of cathodic zinc.
- The presence of the Mn^{2+} ion reduces the corrosive impact on the anodes of the Cl_2 generation from Cl^- (g) ions [6].
- The main negative effects of the Mn^{2+} ion are:

- Mn^{2+} ions in a concentration greater than 10 g/L significantly reduce current efficiency [7]. This can be explained why as the concentration of the MnO_4 ion increases, the hydrogen evolution reaction becomes dominant [8].
- A high concentration of Mn^{2+} ion generates a large amount of MnO_2 on the anodes, which if not removed in a timely manner causes short circuits since it is an electrical conductor. This also implies a greater generation of anodic sludge, which forces to increase the cleaning frequencies of anodes and cells.

Modifications Made

Minimize Side Reactions (Secondary Reactions)

Zinc Content Increase in Electrolyte

As explained in Sect. 2, one of the factors that impact current efficiency is the rate of generation of H_2 (g). Therefore, tests were conducted in a pilot cell to determine the current efficiency by varying the concentrations of zinc in the electrolyte to define a new specification limit.

For the test, a process electrolyte was used which had a concentration of 60 g/L of Zn, which was diluted using deionized water to obtain concentrations between 30 and 75 g/L of Zn. To keep the concentration of Mn, Mg, and acidity constant, synthetic solutions were used, the electrolyte composition used in the different tests is described in Table 2.

To simulate the operating conditions, a temperature of 40° in electrolyte and current density of 550 A/m^2 were adjusted and the test time was 6 h, obtaining the results shown in Table 3.

In Fig. 1, we can see how the current efficiency increases when the zinc content in the electrolyte increases.

The tests carried out served as a basis for modifying the specification of the zinc content in the spent electrolyte of at least 38 g/L to a new specification between 50 and 55 g/L. Also based on the results obtained, it was decided to change the operational control logic by replacing the [H^+] concentration control by [Zn^{2+}] concentration

Table 2 Concentrations determined for the test

Element	Unit	Value
Zn	Min g/L	30
	Max g/L	70
Acid	g/L	185
Mn	g/L	22
Mg	g/L	10

Data Source Internal Data

Table 3 Results obtained in pilot cell tests

Prueba	$[Zn^{2+}]$	$[H^+]$	E.C
	g/L	g/L	%
1	30	185	84.19
2	30	185	84.04
3	35	185	86.83
4	40	185	88.83
5	40	185	88.64
6	45	185	90.36
7	50	183	91.18
8	50	183	91.20
9	55	184	92.25
10	60	182	92.61
11	60	183	92.76
12	65	185	93.78
13	70	180	93.83
14	70	182	93.89
15	75	182	94.08

Data Source Internal Data

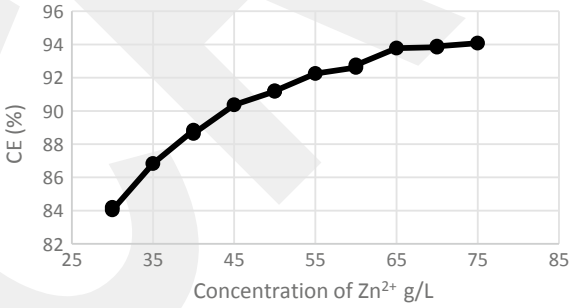

Fig. 1 Current efficiency versus zinc concentration in electrolyte

control, being able to work up to a maximum of 200 g/L of $[H^+]$ in the three CJM 1, CJM 2, and CJM 3 electrolysis cell rooms.

Manganese Reduction in Electrolyte

As mentioned in Sect. 2, the impact of manganese depends on its concentration. In the Cajamarquilla Refinery, given the configuration of the process (Fig. 2), the main outputs of manganese are in the electrolysis process, first through cleaning of anodes and secondly by cell cleaning, laboratory tests determined that 75% of the

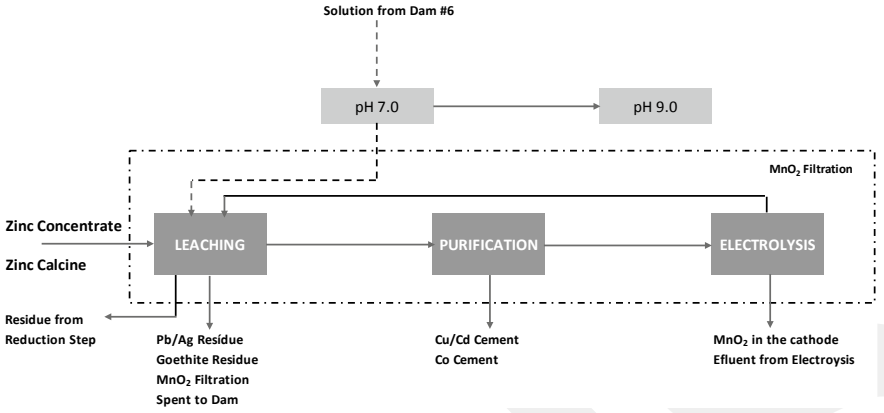

Fig. 2 Diagram of income and exits of manganese in Cajamarquilla

manganese in the anode sludge that is sent to the hot acid leaching stage dissolves and returns to the system.

In Fig. 3, we can see how the concentration of manganese in the Cajamarquilla Refinery has behaved.

To achieve this reduction of manganese in the electrolyte of solution to tailing dam N° 6, this dam is destined to receive the goethite residue which is generated in leaching stage of iron purification process, taking into account that the solutions of this dam will be returned to the plant through the pH 7 stage where 99% of the zinc is precipitated as hydroxide and only 50% of the manganese becoming a manganese purge of the system without impacting the recovery of global zinc. The sludge from this stage known as pH-7 is then used in the goethite stage to neutralize the formation of H^+ ions during precipitation of the Fe^{3+} ion in the form of goethite.

This purge was carried out in three stages as can be seen in Fig. 4, the first stage in September 2017 purging 10,000 m^3 of electrolyte, in November 2017 an additional

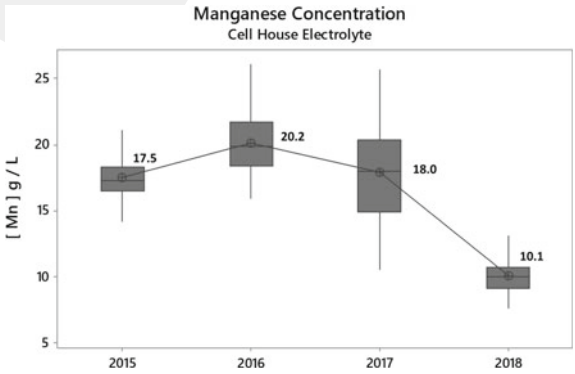

Fig. 3 Historical concentration of manganese in Cajamarquilla

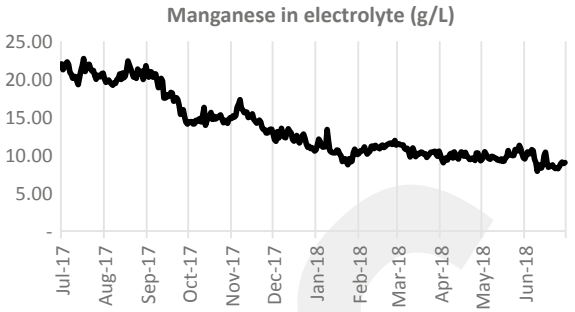

Fig. 4 Reduction and stabilization of the concentration of manganese in electrolyte

5000 m^3 is purged, and finally, in January 2018 5000 m^3. Achieving a concentration of 10 g/L in the electrolyte.

In addition to these electrolyte purges, the following actions were taken to keep the concentration of manganese in stable electrolyte:

- Two press filters were put into operation on the lines that send the anodic sludge from the cell cleaning to avoid leaching of manganese dioxide in the acid leaching circuit.
- The frequency of cleaning of anodes was increased by 30% in each cell house to ensure maximum extraction of manganese dioxide.
- The way in which the anode sludge from the cell is suctioned was modified, previously a compressed air line was used to repel the sludge at the bottom of the cells, obtaining an electrolyte with suspended particles that returned to hydrometallurgy. Now, a third of anodes are removed to suck the sludge from the top of the cell.
- A frequency of anode change was standardized to optimize the generation of manganese dioxide in its first passivation cycles, this also helped reduce the impact by a smaller number of short circuits.

Conclusions

From the modifications made, it was possible to conclude with the results obtained at the industrial level:

- The direct relationship between zinc concentration in the spent electrolyte and current efficiency.
- The indirect relationship between electrolyte manganese concentration and current efficiency.
- Current efficiency results greater than 92.00% were obtained despite working with electrolyte manganese concentrations close to 10 g/L.

Acknowledgements We thank the leadership of Cajamarquilla and the team involved in the work in the development of the project.

We thank co-author Eder Lucio de Castro Martins for allowing us to use excerpts from his master's thesis for the present work.

References

1. Nicol JM (2005) Electrowinning and electrorefining of metals. A course presented to UFMG, Programa de Cooperação UFMG (Depto. Engenharia Metalúrgica e de Materiais)-Murdoch University (Parker Centre), Brasil, pp 1–23
2. Feijo F, Souza AD, Ciminelli VS (2008) Metalurgia extrativa: tecnologias e tendências (Parte I). Brasil Mineral 275:52–59; (Parte Final). 276, p 36–43
3. Umicore (2001) Manual de processo e operação de eletrólise. UM Engineering NR Manual 2102.2-E-700-MBA-9900: p 01–54
4. Robinson DJ, O'keefe TJ, (1976) On the effects of antimony and glue on zinc electrocrystallization behaviour. J Appl Electrochem 6:1–7
5. Krupkowa D, Jurczyk H, Krezel K, Nosel J, Gluszczyszyn A, Mendyka M (1977) Zinc electrowinning. Pl Patent No. 89821
6. Kelsall GH, Guerra E, Li G, Bestetti M (2000) Effects of manganese(II) and chloride ions in zinc electrowinning reactors. In: Proceedings—electrochemical society, 2000–14 (Electrochemistry in mineral and metal processing V), pp 350–361
7. Qi bo Z, Yixin H (2009) Effect of Mn2 + ions on the electrodeposition of zinc from acidic sulphate solutions. Hidrometallurgy 99:249–254
8. Ivanov I, Stefanov Y (2002) Electroextraction of zinc from sulphate electrolytes containing antimony ions and hydroxyethylated-butyne-2-diol-1, 4: Part 3. The influence of manganese ions and a divided cell. Hydrometallurgy 64:181–186
9. Martins EL (2013) Investigation of the effects of organic impurities on the current efficiency of zinc electrolysis and on the quality of metallic deposits (Mastery thesis). Federal University Of Minas Gerais, Brazil

To Polarize or Not to Polarize: Practical Advice on How to Control Zinc Electrodeposition

Michael Moats and Timothy Hymer

Abstract The interaction of impurities and additives on zinc electrodeposition in electrowinning cellhouses are well documented, but generally not well understood. Operators attempt to maximize current efficiency by promoting zinc deposition, while simultaneously inhibiting hydrogen evolution. However, the impacts of impurities and additives are often difficult to understand and predict. Thus, plant personnel are left to ponder whether to polarize (add more gelatin) or not to polarize (add less gelatin). This joint paper by an industrial practitioner and academic scholar attempts to describe the interactions between impurities and additives in simple terms and to offer practical advice on how to control cellhouse operations.

Keywords Zinc · Electrowinning · Polarization · Impurities · Microstructure · Current efficiency

Introduction

This paper is dedicated to the lasting memory of Professor Thomas J. O'Keefe. The authors were privileged to learn from Tom in class and one-on-one as our graduate advisor. In the spring of 1991, Prof. O'Keefe told our metal deposition class that if we understood polarization and how it could be applied to the electrodeposition of metals that we would be far ahead of many people. As students will do, we did not really believe our professor. After all, the concepts of electrochemical reaction polarization were not that difficult to grasp in a classroom setting.

Many years later, we have come to understand the truth that many operators do not really understand polarization. We have also learned that we were a bit naïve to think polarization was easily understood. This is especially true for zinc electrodeposition and the competing hydrogen evolution reaction that occurs in zinc electrowinning.

M. Moats (✉)
Materials Research Center, Missouri University of Science and Technology, Rolla, MO, USA
e-mail: moatsm@mst.edu

T. Hymer
The Doe Run Company, Viburnum, MO, USA

© The Minerals, Metals & Materials Society 2020

A. Siegmund et al. (eds.), *PbZn 2020: 9th International Symposium on Lead and Zinc Processing*, The Minerals, Metals & Materials Series,
https://doi.org/10.1007/978-3-030-37070-1_10

With experience, we believe we have come to learn how to navigate this treacherous terrain. Our hope is that this paper will help operators and academics to understand polarization and use this knowledge to produce optimal deposit structures and maximize the profitability of zinc refineries.

Polarization

Polarization is defined as the deviation of the electrode potential from the reversible value when faradic current flows [1]. As current is applied to an electrolysis cell, the electrode potential deviates from the equilibrium potential. This deviation is called overpotential, η. Thus, overpotential is the difference between the actual electrode potential, E, with current flowing and the reversible equilibrium potential, E_{rev} (Eq. 1). Polarization is, therefore, related to overpotential and the words are occasionally used interchangeably.

$$\eta = |E - E_{\text{rev}}| \tag{1}$$

Polarization would be much easier to understand if there was only one type of overpotential. Unfortunately, there are five different types of polarization listed by Khorüm [2] (1) charge transfer (CT), (2) mass transfer (MT), (3) reaction (Rxn), (4) crystallization (Cry), and (5) resistance (Ω). Therefore, an experimental measured overpotential is really the sum of five individual overpotentials (Eq. 2)

$$\eta = \eta_{CT} + \eta_{MT} + \eta_{\text{Rxn}} + \eta_{\text{Cry}} + \eta_{\Omega} \tag{2}$$

Charge Transfer

Charge transfer overpotential is related to the energy needed to overcome the activation barrier between oxidized and reduced species. The relationship between charge transfer overpotential and current flow (actually current density, i) is not linear. The Butler-Volmer Equation [1] describes the mathematical relationship. If $\eta_{CT} > 0.1$ V, then the simplified Tafel Equation (Eq. 3) applies. The Tafel equation has two constants, a and b. The a constant contains the exchange current density, which indicates how easy/hard the reaction is on the electrode.

$$\eta_{\text{CT}} = a + b \log i \tag{3}$$

The charger transfer overpotential is related to the electrodeposition on zinc and/or hydrogen gas evolution on a metal surface when only the transfer of electrons from the substrate to the reducing specie is considered.

Mass Transfer

Mass transfer polarization is also called concentration polarization. The polarization arises from the change in concentration of a species at the electrode surface as compared to the bulk electrolyte. The equilibrium potential for zinc reduction can be calculated using the well-known Nernst equation (Eq. 4):

$$E_{\text{rev}} = E^{\circ} - \frac{\text{RT}}{nF}\ln\left(\frac{a_{\text{Zn}}}{a_{\text{Zn(II)}}}\right) \tag{4}$$

where $E°$ is the standard state reduction potential, n is the number of electrons transferred in the reaction, F is Faraday's constant, and a_{Zn} and $a_{\text{Zn(II)}}$ are the activities of zinc metal and zinc (II) ion in solution, respectively. As current flows, the concentration of Zn (II) at the electrode surface decreases because the movement of Zn (II) is controlled by the mass transfer of the Zn(II) ion across the Nernst boundary layer. This results in a lower concentration of Zn (II) at the surface than the bulk concentration. This lower Zn (II) concentration causes a shift in potential creating an apparent overpotential. The mass transfer overpotential can be calculated based on the amount of current flowing relative to the limiting current density, i_L, (Eq. 5):

$$\eta_{\text{MT}} = \frac{\text{RT}}{nF}\ln\left(1 + \frac{i}{i_L}\right) \tag{5}$$

Reaction

Reaction polarization is similar to mass transfer polarization except instead of the surface concentration of the reaction species being affected by mass transport through the Nernst boundary layer, a chemical reaction is slowly producing the reducible specie. This mechanism is not thought to be important at the cathode in zinc electrowinning.

Crystallization

Once a zinc atom is reduced on the cathode surface, it may or may not be at an energetically favorable site. The atom will attempt to surface diffuse to a site within an existing crystal lattice. If this process (surface diffusion and/or entry into the crystal lattice) hinders the overall deposition kinetics, then crystallization overpotential is generated. When zinc grains first start to form on an aluminum substrate, we call the crystallization overpotential—the activation [3] or nucleation [4] overpotential.

Resistance

The resistance overpotential is created on a macroscale by electrode misalign and on the microscale by a rough surface, porous surface, or a surface film. This can cause a re-direction of current flow to paths of less resistance or an increase in overpotential. Hence, resistance overpotential may be related to the adsorption of gelatin molecules on zinc surfaces, or misalignment of electrode leading to preferred plating at edges.

Zinc Electrodeposition Versus Hydrogen Evolution

Since polarization is at least a five component value, deciding which components are involved in a single measured overpotential value is where difficulties arise. Polarization is further complicated in zinc electrowinning because there are two competing reduction reactions— zinc electrodeposition and hydrogen reduction. The hydrogen reduction reaction has its own set of polarization values.

Based on the standard reduction potential of hydrogen gas formation from protons ($E^\circ = 0.0$ V), it is highly thermodynamically favored over zinc reduction from Zn(II) ions ($E^\circ = -0.77$ V). However, hydrogen gas evolution is suppressed by the presence of Zn(II) in solution as shown in Fig. 1a [5]. This suppression or polarization of the hydrogen reaction allows zinc to deposit as illustrated by the cyclic voltammogram in Fig. 1b [6].

The driving force to prefer hydrogen gas evolution over zinc deposition still exists. The presence of impurities that have more positive reduction potentials and higher

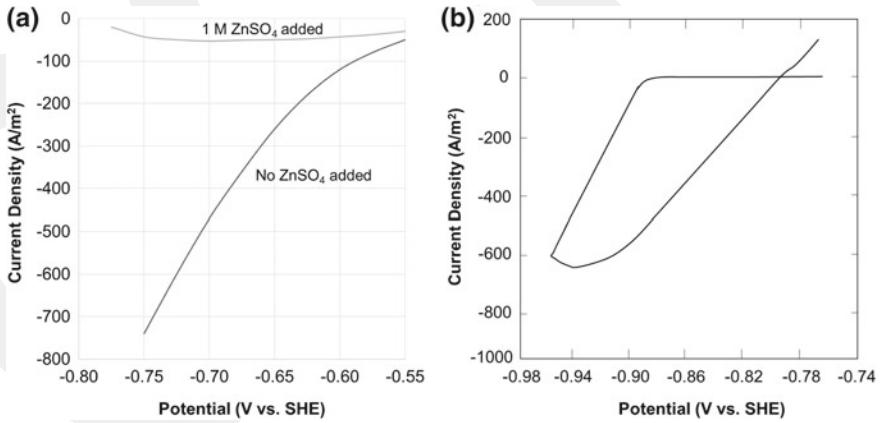

Fig. 1 **a** Hydrogen current density on Al cathode versus electrode potential for electrolytes containing 200 g/L H_2SO_4 with and without zinc(II). $T = 45$ °C; scan rate = 0.5 mV/s [5]. **b** Zinc deposition current density on Al cathode, 55 g/L Zn, 150 g/L H_2SO_4, 0.02 mg/L Sb, $T = 45$ °C, scan rate = 100 mV/min [6]

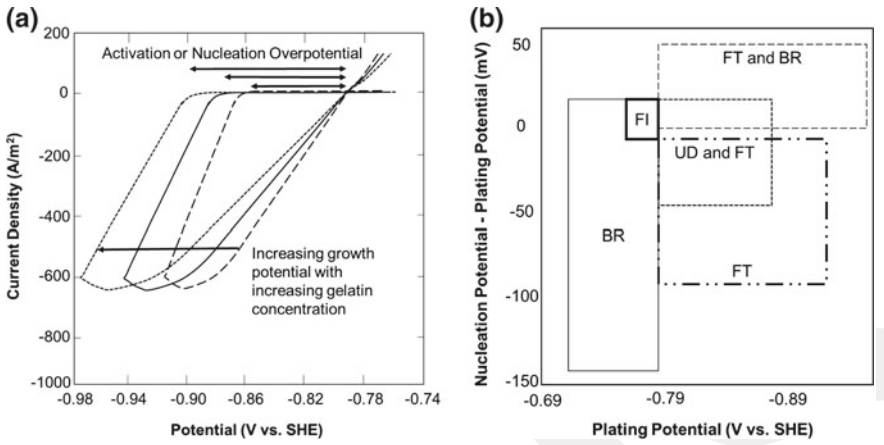

Fig. 2 **a** Cyclic voltammograms illustrating differences in polarization adapted from [3]. **b** Zinc deposit structure as a function of (nucleation potential-plating potential) and plating potential adapted from [8]. BR—Basis reproduced, FI—Field-oriented isolated crystals, FT—Field-oriented texture, UD—Unoriented, dispersed

exchange current densities for hydrogen evolution than zinc can overcome the suppression of the zinc(II) ion. Thus, small concentration of impurities such as Ge, Sb, Co, Ni, and Cu can deposit with time and result in hydrogen evolution and zinc re-solution. These impurities depolarize the hydrogen evolution reaction.

The final piece to the complicated puzzle of polarization is organic additives. Gelatin has been added to zinc electrowinning electrolytes for decades. Gelatin is known to polarize the zinc deposition reaction as shown schematically in Fig. 2a using data from [3]. Many times in the zinc literature, the polarization of gelatin focuses on its effect on activation or nucleation overpotential, which is the added energy needed to nucleate zinc grains on the aluminum substrate. Gelatin also affects the polarization of the growing existing zinc grains.

Adcock and others recognized this phenomenon and theorized that the zinc microstructure should relate to whether the electrolysis conditions favored producing new grains or growing existing grains. Hence, the difference between the nucleation and plating overpotentials should be important [4, 7]. Their work [4, 7] was extended by Chiyangwa et al. [8] and summarized in Fig. 2b. At a relatively negative plating potential (e.g. −0.88 to −0.90 V) which would be observed in industrial practice, the deposit should change from BR/FT to UD/FT to FT as the nucleation potential occurs at more negative values (e.g. increasing activation overpotential).

This trend was observed by Kerby and his co-workers decades previously as shown in Fig. 3a [3]. Kerby et al. also correlated activation overpotential to current efficiency (CE) as shown in Fig. 3b [3]. Long et al. [9] reported the optimum activation overpotential value was not constant between operations. Adcock's theory regarding the difference between plating and nucleation overpotentials may explain why two plants had different optimum activation overpotentials [3, 9].

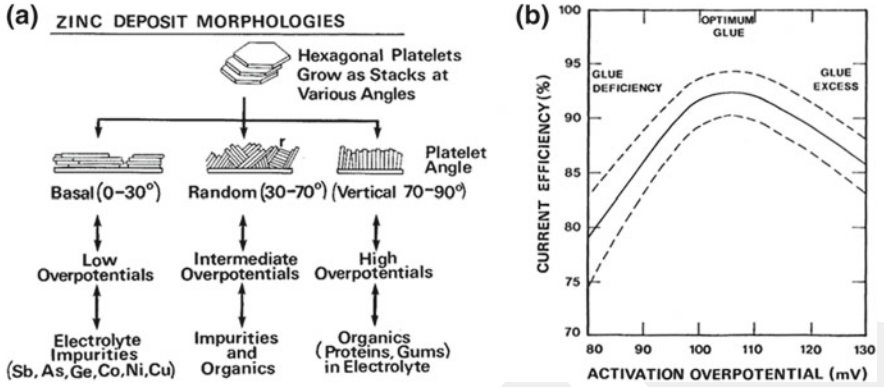

Fig. 3 **a** Zinc structure and **b** current efficiency (CE) as a function of overpotential [3]

The relationship between CE and polarization is one that warrants further discussion. Figure 4 presents three cases similar to those shown in Fig. 3. The zinc and hydrogen polarization curves displayed were calculated using the Butler-Volmer equation to demonstrate how polarization and depolarize from the optimum condition result in a decrease in CE.

The base case (Fig. 4a) is the optimum condition and CE is maximized. Instead of focusing on activation overpotential, the plots in Fig. 4 emphasis the potential needed to sustain an applied current density. This approach is used as cellhouses typically control current to meet production requirements. In Fig. 4a, the optimum glue is present and the CE is 92% (e.g. 92% of total current is used for zinc deposition).

Figure 4b illustrates when excess glue is added, zinc deposition is polarized. The current density versus potential curve for zinc deposition shifts to the right, which in turn shifts the total reaction ($Zn + H_2$) curve to the right. To maintain the applied current density, the cathode potential shifts to a more negative value (right) which causes more hydrogen evolution. Thus, the CE decreases with excess glue or polarization beyond the optimum value.

Figure 4c presents what can result from depolarization. In Fig. 4c, the hydrogen reaction is depolarized (e.g. excess Sb is in the electrolyte). More hydrogen gas evolution occurs at less negative cathode potentials. This shifts the total reaction ($Zn + H_2$) curve to the left. Thus, the cathode potential shifts to a less negative value. Therefore, CE decreases when impurities promote hydrogen evolution and depolarize the cathode potential.

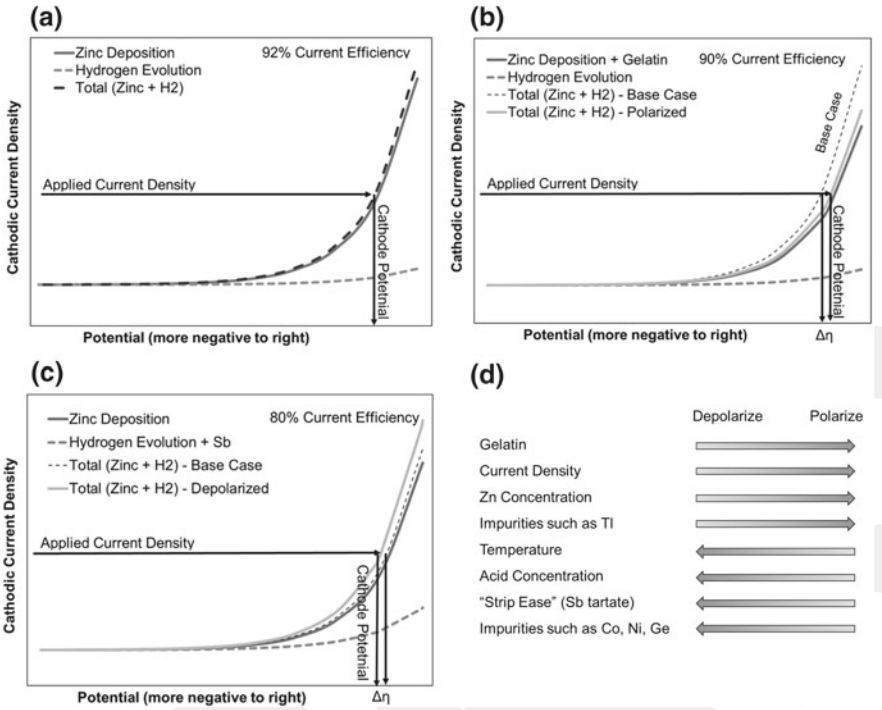

Fig. 4 Schematic polarization curves representing the competing cathodic reactions in a zinc electrowinning cell. **a** Optimum polarization is occurring which produces high CE. **b** Excess glue polarizes the zinc reaction and the total reaction producing a lower CE. **c** Excess Sb depolarizes the hydrogen reaction which leads to a lower cathode potential and a substantial decrease in CE. **d** List of parameters that either polarize or depolarize the cathode by increasing in value as indicated by the arrows

Practical Guide to Zinc Deposits

The science behind the polarizing and depolarizing effects of electrolyte conditions, gelatin and impurities on zinc electrodeposition, and hydrogen evolution are generally accepted. Using this information in practice remains an art. An operator must continually observe a cellhouse to see how the metal changes and learn to "read the metal". The appearance of the zinc deposit structure and morphology will change with operating conditions. The structure can be "read" and demonstrate what is happening in the operation and where the facility is in terms of polarization.

A process engineer should routinely/daily "read the metal" and correlate the observations to the operating conditions of the cellhouse under which the deposits were made. This can require examining the metal deposit after the first few hours or days of deposition. Over time, an understanding of how various process changes impact zinc deposition will develop. Observing the morphology and structure of deposits

will enable a person to make changes to the process. The operational changes will polarize or depolarize the reactions, which in turn will impact the deposit morphology and structure.

Eventually, an operator will come to understand not only the effects of process chemistry and current density, but also the type and frequency of maintenance that will help produce quality deposits that are easy to strip and produce higher in CE. These will ultimately improve the operation's productivity.

These correlations and internalization of lessons learned from "reading the metal" do not happen overnight. It requires time and dedication. The hope is that the following information will inspire operators and engineers to travel a path to gain insight and enable them to apply science to real life situations in a cellhouse and know what to do to improve their bottom line.

Cellhouse Parameters

Within a cellhouse are a variety of different parameters that impact the plating process. Some are readily changeable and others are not. A zinc cellhouse typically has a variety of flow rates that can be changed, temperature control, copper bus bars carrying current that can be changed, Zn and acid concentrations, cell voltage, cathodes, anodes, and additives that are can be added to the system. In addition, the electrolyte will carry impurities from the leaching process that were not fully removed in purification. All of these items can have an impact on the performance of the cellhouse. A good practice is to collect all this information daily to see how the process changes and begin to determine the root causes of deposit structure changes and their impact on performance. A cellhouse is typically designed to have basic operating parameters and certain process design that may or may not be changed by the operator. However, even the parameters that are not readily changeable by an operator can be altered due to improper maintenance or equipment failure and therefore impact other parameters and change the conditions to make a proper deposit. Studying and understanding the intercorrelations between all these items will enable informed decisions on changes in the cellhouse.

Parameters Impacting Polarization

There are certain parameters that are within the control of the operator to increase or decrease polarization which can be changed to improve the structure of the deposit. The main parameters are shown in Fig. 4d. There are two groups—those that increasing their value will polarize and those that depolarize the cathode potential. These parameters can be considered as "levers" that can shift the potential of the cathode. Some of these parameters are more readily changed then others. Variations in impurity concentrations result from changes in solution purification and/or feed to the

refinery. Awareness of these changes enables an operator to prepare to counteract them and maintain high CE.

Some operations use small test cells to determine whether the plant is at the optimum polarization. Usually three cells are run—(1) electrolyte, (2) electrolyte + gelatin, and (3) electrolyte + Sb. The cell conditions are designed to guide an operation in regard how structure and/or current efficiency change with polarization. Test cells, however, are limited because they do not represent the physical condition of the cellhouse (cathode surface, cell maintenance, etc.). While test cells can be helpful in providing guidance about the electrolyte, the information generated can be misleading. It is better to make observations in the cellhouse. "Read the metal" and use the correlations developed over time to determine the direction to go regarding polarization.

It is good to have a polarizing/depolarizing lever to make quick changes if needed. Most zinc cellhouses use gelatin as their lever. The gelatin addition rate can be altered by changing the speed of a pump. Some cellhouses add Sb tartrate (called "strip eaze" in some places) directly to cells. Gelatin and Sb are actually polarizers and depolarizers. They are used to modify the polarization and control the deposit structure. For example, if the zinc deposit is very rough and dendritic, this indicates that the depolarization is needed. This can be done by adding Sb tartrate, decreasing the addition rate of gelatin, increasing the temperature, decreasing the current density, etc. (see Fig. 4d). Changing gelatin and/or Sb concentrations are typically the easiest parameters to modify without disrupting the operation. With that said, there are times when changes in temperature or current density might be warranted.

How to Read a Deposit

This practical guide relies on one's ability to "read the metal" and understand what it is saying. The metal changes structure and morphology as the system shifts in polarizing or depolarizing directions. Observing zinc morphology and structure will provide information to make process changes to counteract what has occurred.

It is best to check multiple samples from different areas in the cellhouse to obtain an overall picture. Observe the morphology (surface appearance), the back of the deposits, and growth structure of the deposits. This will likely require manual stripping of individually pulled cathodes. The structure of the deposit can be observed by breaking the deposit and looking at the cross section. If a cellhouse, due to crane constraints or safety concerns, does not permit manual pulling of cathodes, then observations at the stripping machine and breaking of stripping zinc plates can be used as a substitute. The consequence of using end-of-plating cycle observations is that they reflect what has occurred further in the past then pulling plates with hours of growth.

Different zinc deposit morphologies and structures have been given different names by different authors. Table 1 summarizes some the descriptors used in the

Table 1 Descriptions of zinc structure and morphology used by others and in this paper

Adcock and Ault [10]	Mackinnon et al. [11]	Winand [12]	This Paper
Doughy	Basal	Basis reproduced (or field-oriented isolated crystals)	Coarse sand or spongy
Pin holes	Intermediate	Twining intermediate or field-oriented texture	Pin holes or coarse sand
Compact	Triangular	Unoriented, dispersed	Naugahyde®
Stressed	Vertical	Field-oriented textured	Clam shells

literature with correlation to words used in this guide. We are using names common to most Americans such spongy, lava-ish, spiderwebs, Naugahyde® (imitation leather with bumps like an indoor basketball), coarse sand, clam shells, pin holes, and dendrites.

Figure 5 illustrates the typical relationship between polarization, CE, and ease of stripping with an overlay of the structure observed. Starting at low polarization (e.g. high impurities and low gelatin), the deposit looks spongy with individual grains held loosely together with a significant numbers of voids. This structure typically occurs at low CE and the deposits break easily during stripping. As the polarizing increases, the structure changes to a "lava-ish" or "molten" appearance which corresponds to an increase in CE and strippability. A further increase in polarization produces a spider web looking structure on the surface and a cross section that looks like fine grain sand which again increases the CE and stripping ease. Increasing polarization more creates the "best looking" and easiest to strip deposit which is a fine grain slightly bumpy surface which resembles an imitation leather basketball or "Naugahyde®". The Naugahye® structure is the easiest to strip deposit, but it does not produce the highest CE. The highest CE is produced with a structure that is a mix of spider webs

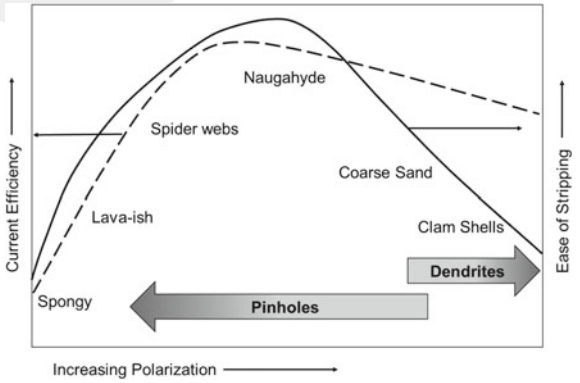

Fig. 5 Schematic diagram correlating the effect of polarization on CE, ease or stripping and zinc structure

and Naugahyde®. Increasing the polarization beyond this point decreases CE and lowers strippability. The deposit structure turns to a coarse sand looking deposit and then clam shells in cross section with polarization beyond the optimal range.

Relatively high polarization can cause dendrites. However, dendrites are more typically associated with electrode misalignment. Misalignment or bent electrodes create high current density regions on a cathode which in turn causes high polarization and dendrites. Thus, dendrites are usually caused by poor maintenance and not excess gelatin.

Pin holes are listed as a structure by several observers. Pin holes are caused by the local accumulation of deposited impurities. This results in local corrosion cells, which fosters hydrogen and zinc re-solution. Usually, pin holes structures are more prevalent at lower polarization conditions (e.g. caused by impurities with lower hydrogen overpotentials, Co, Ni, Ge, and Te) but they can be observed even in structures that are consider higher polarization than the optimum values (e.g. coarse sand structure).

When there are a combination of structures, it can be difficult to determine which "lever" to pull to improve the deposit. It is recommended to take small steps (e.g. small changes in gelatin) and observe the effects in a short time frame. It is important to realize that due to the continuous nature of the cellhouse process, some cathodes are initial growth and some are ready to be harvested that may have experienced different conditions during the plating cycle. Looking at cathodes that have different plating times will provide a more complete picture of whether a problem is starting, has been occurring, or is ending.

Summary

The science of polarization/depolarization is generally accepted in terms of zinc electrodeposition and hydrogen evolution. Applying that science to an operation can be challenging. A processing person needs to understand the fundamentals of polarization, but also cellhouse operations and changeable parameters. The most effective way to understand and control a cellhouse is by "reading the metal". The metal will indicate where on the polarization curves the plant is operating. This information can be used to decide which lever(s) should be used to manipulate the plating conditions to produce the best conditions for a given cellhouse. The best conditions will result in improved productivity and bottom line of the cellhouse. For a given cellhouse, it may be decided that some CE will be sacrificed to maintain a cathode structure that is readily stripped which reduces machine downtime.

Data need to be collected routinely and diligently. The morphology and growth structure data should be correlated to the conditions that produced them. As the relative impacts and intercorrelations of the conditions are learned, it will become apparent whether the optimal conditions are a large target or rather small.

Each cellhouse will not be exactly as others due to differences in design, impurities and other limits imposed by the refinery. Even so, the polarization trends with structure, CE and strippability should be similar between cellhouses.

In closing, some words of wisdom are provided from influential people to the authors. A cellhouse with a "drill sergeant" to maintain operating conditions will find it easier to obtain the best deposit [13]. The zinc cellhouse is "the heart" of the plant and you need to take care of it. If you do not take care of it, it can get out of whack and will take a considerable time to fix [14]. A plant sells zinc and not current efficiency [15]. The answer to whether to polarize or depolarize is, "It depends". [16]

References

1. Bard A, Faulkner L (1980) Electrochemical methods. Wiley, New York
2. Kortüm G (1965) Treatise on electrochemistry. Elsevier, New York
3. Kerby RC (1984) Application of polarization measurements to the control of zinc electrolyte quality for electrowinning. In: Warren IH (ed) Application of polarization measurements in the control of metal deposition. Elsevier, New York, pp 84–132
4. Adcock PA, Adeloju SB, Newman OMG (2002) Measurement of polarization parameters impacting on electrodeposit morphology I: Theory and development of technique. J Appl Electrochem 32(10):1101–1107
5. Fosnacht DR, O'Keefe TJ (1980) Evaluation of zinc sulphate electrolytes containing certain impurities and additives by cyclic voltammetry. J Appl Electrochem 10(4):495–504
6. Kerby RC, Jackson HE, O'Keefe TJ, Wang YM (1977) Evaluation of organic additives for use in zinc electrowinning. Met. Trans. B 8(3):661–668
7. Adcock PA et al (2004) Measurement of polarization parameters impacting on electrodeposit morphology. II: conventional zinc electrowinning solutions. J Appl Electrochem. 34(8):771–780
8. Chiyangwa, E, Sandenbergh, RF, Schoeman, L. (2014) Development and evaluation of polarization parameters as quality predictors for zinc electroplated from acid sulfate electrolytes. In: Hydrometallurgy 2014, vol II. CIM, Montreal, pp 141–152
9. Long G, Meadows, N, Pollard D (1984) Deposit morphology and current efficiency in electrolytic zinc deposition. In: The Aus.I.M.M. Melbourne Branch, Symposium on "Extractive Metallurgy", AUSIMM, pp 179–184
10. Adcock PA, Ault AR (1993) Cathode zinc morphology and effects of changed conditions in electrowinning cells. World Zinc'93. AusIMM, Hobart, Australia, pp 301–306
11. Mackinnon DJ, Brannen JM, Fenn PL (1987) Characterization of impurity effects in zinc electrowinning from industrial acid sulphate electrolyte. J Appl Electrochem 17:1129–1143
12. Winand R (1992) Electrocrystallisation—theory and applications. Hydrometallurgy 29:567–598
13. Personal communication with Floyd Gessford, Big River Zinc
14. Personal communication with Ki Won Jeon, Korea Zinc
15. Personal communication with Stephen James, Nyrstar
16. Personal communication with Thomas J. O'Keefe, UMR

Optimizing Additive Ratios in Alkaline Zincate Electrodeposition

Margaret Scott and Michael Moats

Abstract Alkaline non-cyanide zinc electrogalvanizing is utilized in some plating applications. This study was conducted to evaluate the effects of a commercial carrier, booster, and leveler in a strong zinc (37.5 g/L) and alkaline (210 g/L) plating solution. Hull cell plating was used to assess the roles of each additive on the appearance of the zinc deposits produced from synthetic solutions. Bright white deposits were generated with several different combinations of additives at current densities of 170–420 A/m^2. The zinc structures were characterized using x-ray diffraction and scanning electron microscopy to understand the microstructure which produced the bright deposits in order to determine the optimal conditions leading to mirror-like deposits.

Keywords Zinc · Electrogalvanizing · Alkaline · Zincate · Non-cyanide · Additives · Hull cell

Introduction

Steel is the world's most widely used metal. Unfortunately, steel is highly susceptible to rust, leading to many steel pieces to be coated to prevent corrosion. Galvanizing with zinc is a common method to cover the steel substrate and provide a sacrificial protective layer. Galvanization can be achieved through hot dipping or electroplating. Hot-dip galvanizing has been and continues to be the primary coating method. In a few applications, electrogalvanizing is the preferred method of applying zinc to steel.

In the early 1900s, several industries moved away from hot-dip galvanizing for electrogalvanizing, in favor of a thinner and more controlled coating [1]. Over time, zinc electrogalvanizing baths used cyanide as a means to complex the zinc in solution and form a stable zinc coating bath. Zinc cyanide plating baths produce excellent

M. Scott · M. Moats (✉)
Materials Research Center, Missouri University of Science and Technology, Rolla, MO 65409, USA
e-mail: moatsm@mst.edu

© The Minerals, Metals & Materials Society 2020

A. Siegmund et al. (eds.), *PbZn 2020: 9th International Symposium on Lead and Zinc Processing*, The Minerals, Metals & Materials Series,
https://doi.org/10.1007/978-3-030-37070-1_11

Table 1 Composition of alkaline non-cyanide zinc baths [6]

Component	Low Zinc	High Zinc
Zn (g/L)	6–9	13.5–22.5
NaOH (g/L)	75–105	120–150
Proprietary additives	1–3%	1–3%

coatings with significant throwing power and can tolerate impurities. In more modern times, the presence of cyanide has resulted in significant disposal costs for spent plating baths [2]. The toxicity of the cyanide baths prompted research into low cyanide containing baths as well as cyanide-free baths. The resulting cyanide-free baths (acid zinc and alkaline zincate) can produce acceptable coatings, but are not able to achieve the throwing power or brightness of the cyanide containing baths [3].

Alkaline zincate solutions offer the potential of lower operating costs due to reduced corrosion of steel supports and structures and lower waste disposal costs than acid baths [4]. Zincate baths also exhibit better throwing power than acid baths [5]. The major drawback with zincate baths is inferior plating appearance and properties leading to the need for smaller variations in zinc concentration, temperature, and current density during operation than the other zinc plating baths [4]. The compositions of two typically alkaline non-cyanide zinc baths are presented in Table 1.

In highly alkaline solutions, the proposed zinc reduction reactions are presented in Reactions 1–4 with Reaction 2 being the rate limiting step. As Zn^{2+} prefers to be a tetra or hexa-coordinate species, $Zn(OH)_3^-$ is more likely to exist as $Zn(OH)_3(H2O)^-$ [7] resulting in Reaction 5 instead of Reaction 2. The rate of Reaction 5 is faster than the transport of Zn atoms into the growing zinc lattice. This results in a depletion of zinc ion at the deposit surface which in turn produces dendritic and non-adherent deposits [8]. To overcome this tendency, additives are introduced to facilitate the production of a coherent, compact, and smooth coating [5, 6, 9].

$$Zn(OH)_4{}^{2-}{}_{(aq)} = Zn(OH)_3{}^{-}{}_{(aq)} + OH^-_{(aq)} \tag{1}$$

$$Zn(OH)_3{}^{-}{}_{(aq)} + e^- = Zn(OH)_2{}^{-}{}_{(aq)} + OH^-_{(aq)} \tag{2}$$

$$Zn(OH)_2{}^{-}{}_{(aq)} = Zn(OH) + OH^-_{(aq)} \tag{3}$$

$$Zn(OH) + e^- = Zn + OH^-_{(aq)} \tag{4}$$

$$Zn(OH)_3(H2O)^-{}_{(aq)} + e^- \rightarrow Zn(OH)_2{}^{-}{}_{(aq)} + H2O + OH^-{}_{(aq)} \tag{5}$$

In alkaline zincate baths, three different types of additives can be used—carrier, booster, and leveler. The carrier polarizes the zinc surface which increases the energy available to speed up the transport of Zn atoms into the growing Zn lattice. The booster produces smaller and more faceted grains which leads to a brighter surface.

Finally, the leveler inhibits deposition at high points on a rough deposit and promotes deposition at the low points. Common carriers are polyvinyl alcohol (PVA) [10, 11], polyaliphatic amines, aliphatic polyamines, and heterocyclic amines. Brighteners (booster) tend to be aromatic aldehydes [12]. Vanillin is a common leveler [13]. The correct combination of the plating additives is critical to producing smooth, bright deposits [10, 13].

A common method to evaluate a plating bath's ability to produce a bright and shiny appearance is Hull cell testing [9]. The Hull cell is trapezoidal in shape with the cathode angled away from the anode. The changing distance between the anode and cathode produces a uniform current distribution. This allows the Hull cell to produce an electrodeposit over a range of current densities in one experiment. The resulting plate can be examined to determine if the desired appearance is produced within the current density range exhibited in the plating operation [9].

Experimental

Hull Cell Testing

A standard 267 mL Lucite Hull cell from Kocour was utilized. The anode was a low-carbon steel mesh with dimensions of 8.6 × 0.6 cm. The cathode was a zinc coated stainless steel plate with the zinc removed prior to plating. The zinc coating was removed by immersing the plate in a 50% v/v HCl solution for ~15 s until no gassing was detected. The de-zinced plate was rinsed with de-ionized (D.I.) water prior to placing in the Hull cell.

Synthetic plating solutions were prepared using a commercially available zinc "pre-mix" solution (Technilloy ZN NI 7222). The "pre-mix" solution contained 162–170 g/L Zn and 500 g/L NaOH as determined by titration. The "pre-mix" was diluted using reagent grade NaOH and/or D.I. water to achieve zinc concentrations ranging from 30 to 40 g/L Zn at a NaOH concentration of 210 g/L. Additives were introduced into the electrolyte 20 min prior to each experiment. Three commercially available additives were investigated—a carrier (Eldiem Carrier), a booster (Eldiem Booster), and a leveler (Bright Enhancer 2x). They were examined individually and in combination.

2.0 amps of direct current were supplied from a 20 V Extech, Model #382275 power supply for 5 mins to plate zinc in the Hull cell. No external agitation was used. The plating was performed at elevated temperature. The solution was preheated to 44 °C and then transfer to the Hull cell. The plating test was started immediately without heating. The temperature decreased by approximately 1 °C during the five-minute experiment.

Following the experiment, the zinc-plated cathode was removed from the Hull cell and rinsed with D.I. water. To simulate the actually plating line, the coated part

was dipped in a 0.25% v/v nitric solution for one minute and then rinsed again with D.I. water. Finally, the coated plate was dried with hot air to avoid water spots.

Physical Characterization

Following the Hull cell test, the plate was visually inspected. The appearance was graded using the following terms burnt (blackish in color), matte (gray and non-reflective), white, shiny (gray, reflective, sparkly), or no plating. These appearances were assigned to various areas of the deposit which were correlated to current density using the two-amp scale on a standard Hull cell ruler. The zinc coated plates were sheared to create samples with known current density ranges for further examination.

X-ray diffraction (XRD) was performing using a Philips Panalytical X'Pert Pro Multipurpose Diffractometer to identify the preferred crystal orientation for samples plated at 170–260 A/m^2. The measurements were taken using Cu K-alpha radiation with an angle range in 2 θ of 50–90º and scanning rate of 3º per minute.

Zinc coatings plated at 170 A/m^2 were characterized by scanning electron microscopy (SEM) to observe the deposit morphology. An Aspex Pica 1020 scanning electron microscope was used with 20 kV bias and 34 μA emission current.

Results and Discussion

While other researchers [14–19] have examined the effects of additives on the alkaline zincate plating, this project focused on a unique bath chemistry as the zinc concentration (30–40 g/L) and sodium hydroxide concentration (210–220 g/L) are significantly higher than standard baths in both zinc and NaOH.

To understand the role of each additive, synthetic solutions with constant initial zinc and NaOH concentrations of 37.5 g/L and 210 g/L, respectively, were studied with various additive additions. The resulting zinc coatings produced in the Hull cell were characterized visually, with XRD and microscopically with SEM.

Hull Cell

The results of the visual characterization are presented in Table 2. The addition of individual additives or combinations of additives did not produce any areas with the desired mirror finish. At high current densities, the coating usually had a burnt appearance. At lower current density, the coating generally had a matte appearance.

The surfaces that were closest to the desired appearance were categorized as white. These surfaces were bright but not completely reflective. As expected, plating without additives did not produce any white areas. Several plating conditions yielded

Table 2 Hull cell results from various synthetic solutions

[Zn] g/L	Carrier (mL/L)	Booster (mL/L)	Leveler (mL/L)	Hull cell appearance (80 60 40 30 20 12 4 1)
37.5	0	0	0	b m n
37.5	0	0	0	b m n
37.5	0.75	0	0	b w m
37.5	1.5	0	0	b m b
37.5	0	0.33	0	b m
37.5	0	0.65	0	b w m
37.5	0	0	0.33	b w
37.5	0	0	1.3	b m
37.5	0.75	0.33	0	w m
37.5	1.5	0.65	0	b w m
37.5	0.75	0	0.65	b w m
37.5	1.5	0	1.3	b w m
37.5	0	0.65	1.3	b s w
37.5	0.75	0.33	0.65	b w m
37.5	1.5	0.65	1.3	b m
30	1.5	0.65	1.3	b w m
40	1.5	0.65	1.3	b m

Visual appearance was assigned as b = burnt, m = matte, w = white, s = shiny, and n = no plating. The Hull cell ruler with current densities in A/ft^2 is provided. 1 A/ft^2 = 10.76 A/m^2. Dash lines indicate industrially relevant current density range

white surfaces at the current densities of interest (e.g. 170–430 A/m^2 or 16–40 A/ft^2). The conditions that produced the widest range of a white appearance centered on the target current density range were:

1. [Zn] = 37.5 g/L, Carrier = 0.75 mL/L, Booster = 0.33 mL/L
2. [Zn] = 37.5 g/L, Carrier = 1.5 mL/L, Leveler = 1.3 mL/L
3. [Zn] = 37.5 g/L, Carrier = 0.75 mL/L, Booster = 0.33 mL/L, Leveler = 0.65 mL/L.

The appearance data indicates that in several instances, increasing additive concentrations eliminated the white appearance produced at lower concentrations.

XRD and SEM

To understand the visual observations, XRD and SEM were performed on the samples produced from synthetic solutions. Sample XRD data from 170 to 260 A/m^2 and SEM images from 260 A/m^2 are provided in Table 3 and Fig. 1, respectively. The XRD data was interpreted using the nomenclature used by Mackinnon et al. [20].

The XRD data reveal that without additives, a basal zinc structure is produced at 170 A/m^2. This is confirmed in Fig. 1a where the expected hexagonal plates are observed. The addition of 0.65 mL/L of booster did not change the structure as shown in the XRD and SEM image (Fig. 1c); however, a 0.33 mL/L booster addition did change the structure. Upon the addition of carrier, the structure and morphology changed to yield primarily triangular growth and a nodular/bumpy surface (Fig. 1b). The addition of 0.65 mL/L of leveler did not change the structure, but 1.3 mL/L did to triangular, but the surface morphology revealed a variable appearance which might be caused by the strong secondary vertical growth seen in the XRD data (Fig. 1d).

Carrier and booster additions produced a structure similar (Fig. 1e) to what only carrier addition produced with the nodules being smaller. This is expected result of the grain refining properties of the booster. When leveler and carrier were added, a smooth triangular structure formed (Fig. 1f) with a few large nodules. Booster and leveler additions created a mixed basal/triangular structure which caused a rough faceted surface (Fig. 1g). Upon the addition of all three additives at appropriate concentrations, the structure was more level causing a brighter deposit (Fig. 1h). The structure and surface morphology did not change over the range of 30–40 g/L zinc.

The bright white finish general was produced when the XRD pattern indicates a primary triangular growth with minimal basal growth. Additionally, the vertical growth plane was detected at ~50% of the intensity of the triangular plane.

After consultation with our industrial partner, it was decided that the lack of a mirror finish was perhaps caused by the additives not being allowed to age enough in the Hull cell before current was applied. Based on industrial experience and the SEM images, it was decided to pursue a combination of all three additives in later trails with commercial bath samples.

Summary

This study provides zinc coating data for a unique zincate plating bath with high zinc and caustic concentrations. The effects and interactions of commercial additives (carrier, booster, and leveler) were examined using a Hull cell. Coatings were characterized using visual appearance, XRD and SEM.

Bright white deposits were produced at current densities of 170–420 A/m^2. The conditions that produced bright white deposits generally formed a zinc structure with predominate (101) planes, minimal (002) planes and (100) planes with an intensity ~50% of the (101) planes.

Table 3 Summary of XRD data of zinc coatings produced at 170–260 A/m^2 in a Hull cell

[Zn] g/L	Carrier (mL/L)	Booster (mL/L)	Leveler (mL/L)	Basal		Triangular	Intermediate	Vertical	
				(0 0 2)	(1 0 3)	(1 0 1)	(1 0 2)	(1 0 0)	(1 1 0)
37.5	0	0	0	100.0	0.3	0.5	0.1	0.5	0.1
37.5	0	0	0	100.0	41.2	49.5	16.2	15.3	23.5
37.5	0.75	0	0	4.6	7.8	100.0	9.2	45.9	8.0
37.5	1.5	0	0	10.7	14.5	100.0	18.3	32.8	14.3
37.5	0	0.33	0	8.9	19.1	100.0	24.8	24.6	12.1
37.5	0	0.65	0	100.0	10.4	48.7	10.0	53.4	6.3
37.5	0	0	0.65	100.0	20.1	62.3	14.2	54.7	11.6
37.5	0	0	1.3	9.8	15.7	100.0	14.1	70.1	10.0
37.5	0.75	0.33	0	13.1	37.5	100.0	29.5	34.9	32.5
37.5	1.5	0.65	0	4.0	9.0	100.0	10.1	35.2	6.3
37.5	0.75	0	0.65	3.5	8.3	100.0	10.6	41.0	7.9
37.5	1.5	0	1.3	6.6	12.4	100.0	13.1	46.1	11.2
37.5	0	0.65	1.3	91.3	51.3	100.0	18.7	15.4	31.5
37.5	0.75	0.33	0.65	4.8	7.9	100.0	11.2	35.2	7.1
37.5	1.5	0.65	1.3	18.8	10.6	96.4	6.7	100.0	8.8
30	1.5	0.65	1.3	1.2	2.4	100.0	3.8	75.8	1.8
40	1.5	0.65	1.3	1.8	3.4	100.0	4.7	74.5	2.5

Intensities were normalized, so the maximum crystallographic plan intensity was set equal to 100

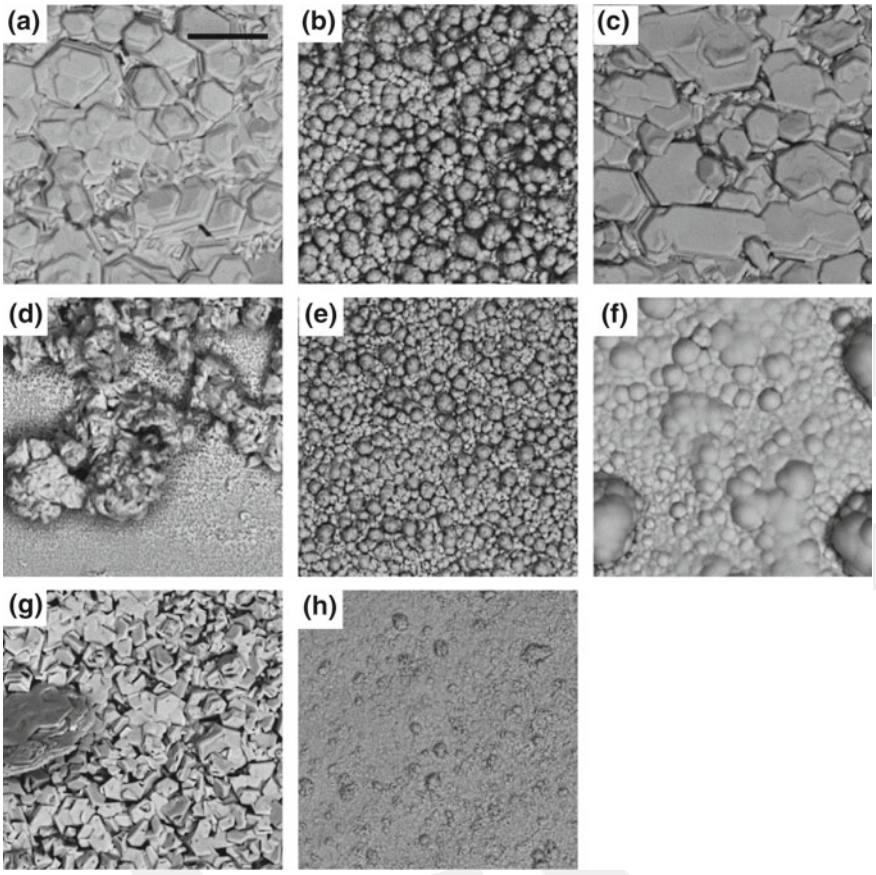

Fig. 1 SEM images of zinc coating surfaces produced in a 267 mL Hull cell with 2 amps of direct current. Images correspond to a current density of 170 A/m^2. Synthetic solution conditions: 37.5 g/L Zn, 210 g/L NaOH and—**a** No additives, **b** 1.5 mL/L carrier, **c** 0.65 mL/L booster, **d** 1.3 mL/L leveler, **e** 1.5 mL/L carrier + 0.65 mL/L booster, **f** 1.5 mL/L carrier + 1.3 mL/L leveler, **g** 0.65 mL/L booster + 1.3 mL/L leveler, **h** 0.75 mL/L carrier + 0.33 mL/L booster + 0.65 mL/L leveler

Surface morphologies correlated with the expected structures indicated from the XRD data. The addition of carrier changed the morphology from hexagonal platelets to compact grains with a knobby surface. Adding booster with carrier appears to refine this structure. Finally, adding all three additives can produce a fairly smooth compact structure.

Despite studying various combinations of additives, no mirror-like deposits were observed as seen in industrial practice. This is believed to be caused by not properly aging prior to plating. Even so, the white deposits formed in the same current density regions as the mirror-like deposits in industrial practice, allowing for electrolyte comparison.

References

1. Mass P, Peissker P (ed) (2011) Handbook of hot-dip galvanization. Wiley-VCH
2. Sierka CE (2015) Industrial zinc plating processes. Ph. D. thesis, Indiana University of Pennsylvania
3. Mccormick M, Kuhn AT (1993) The Haring-Blum Cell. Trans IMF 71(2):74–76. https://doi.org/10.1080/00202967.1993.11870992
4. Wilcox GD, Mitchell PJ (1987) The electrodeposition of zinc from zincate solutions. A Rev Trans IMF 65(1):76–79. https://doi.org/10.1080/00202967.1987.11870775
5. Loto CA (2012) Electrodeposition of zinc from acid based solutions: a review and experimental study. Asian J Appl Sci 5(6):314–326. https://doi.org/10.3923/ajaps.2012.314.326
6. Paunovic M, Schlesinger M (2006) Fundamentals of electrochemical deposition, 2nd edn. Wiley-Interscience, New Jersey
7. Sciscenko I et al (2016) Determination of a typical additive in zinc electroplating baths. Microchem J 127:226–230. https://doi.org/10.1016/j.microc.2016.03.015
8. The Electrochemical Society (1942) Modern electroplating. The Electrochemical Society Inc., New York
9. Geduld H (1988) Zinc plating. ASM International, Great Britain
10. Shanmugasigamani, Puspavanam M (2005) Role of additives in bright zinc deposition from cyanide free alkaline baths. J Appl Electrochem 36(3):315–322. https://doi.org/10.1007/s10800-005-9076-9
11. Ortiz-Aparicio J et al (2014) Electrodeposition of zinc in the presence of quaternary ammonium compounds from alkaline chloride bath. J Appl Electrochem 45(1):67–78. https://doi.org/10.1007/s10800-014-0777-9
12. Paunovic M, Schlesinger M (eds) (2000) Modern electroplating, 4th edn. Wiley, New York
13. Kim SJ et al (2004) Effects of o-vanillin as a brightener on zinc electrodeposition at iron electrodes. J Electrochem Soc 151(12):C850–C854. https://doi.org/10.1149/1.1814033
14. Bapu R et al (1998) Studies on non-cyanide alkaline zinc electrolytes. J Solid State Electrochem 3(1):48–51. https://doi.org/10.1007/s100080050129
15. Kavitha B et al (2006) Role of organic additives on zinc plating. Surf Coat Technol 201(6):3438–3442. https://doi.org/10.1016/j.surfcoat.2006.07.235
16. Ortiz-Aparicio J et al (2013) Effects of organic additives on zinc electrodeposition from alkaline. Electrolytes. J Appl Electrochem 43(3):289–300. https://doi.org/10.1007/s10800-012-0518-x
17. Yuan Liang et al (2017) Effects of additives on zinc electrodeposition from alkaline zincate solution. Trans Nonferrous Met Soc China 27(7):1656–1664. https://doi.org/10.1016/s1003-6326(17)60188-2
18. Nayana KO, Venkatesha TV (2015) Bright zinc electrodeposition and study of influence of synergistic interaction of additives on coating properties. J Ind Eng Chem 26:107–115. https://doi.org/10.1016/j.jiec.2014.11.021
19. Proskurkin EV, Gorbunov NS (1980) Galvanizing sherardizing and other zinc diffusion coatings. Technicopy limited in association with zinc development association, Great Britain
20. Mackinnon DJ, Brannen JM, Fenn PL (1987) Characterization of impurity effects in zinc electrowinning from industrial acid sulphate electrolyte. J Appl Electrochem 17:1129–1143

Part V
Primary Lead I

GCRIS

Lead Metal Production at Paroo Station Mine Using Leach-Electrowinning Process in Methane Sulfonic Acid Solution

David Dreisinger, Ken Baxter, Andrew Worland, Tom Cooper, Tony Cau and Nick Waters

Abstract The Paroo Station lead mine, located in Western Australia and owned by LeadFX, has historically produced a lead flotation concentrate from a lead carbonate (cerussite) orebody. The shipment of the 67% lead concentrate from the mine site to smelters is subject to strict environmental controls and high product handling, logistics, treatment, and refining charges due to the transport distance and the lack of intrinsic fuel value and by-product elements. An innovative solution was required to process the concentrate on-site to reduce environmental risk and cost. A hydrometallurgical process has been studied at bench, pilot, and demonstration plant scale. The process involves leaching and electrowinning of lead in a methane sulfonic acid solution. A Definitive Feasibility Study has been prepared for production of up to 80,000 tonnes per annum of lead metal at Paroo Station lead mine over a 17-year mine life. The results of the testing and the engineering study are presented.

Keywords Lead · Methane sulfonic acid · Electrowinning

Introduction

The Paroo Station lead mine, located in Western Australia and owned by Rosslyn Hill Mining Pty Ltd., has historically produced a lead flotation concentrate from a predominantly lead carbonate (cerussite) containing orebody. The existing flotation plant, which operated intermittently between 2005 and 2015, typically produced a concentrate of 64–71% lead grade from a ~7% lead head grade at 70–80% lead

D. Dreisinger (✉) · K. Baxter · A. Worland · T. Cau · N. Waters
LeadFX Inc., First Canadian Place, 100 King St. West, Suite 5700, Toronto, ON M5X1C7, Canada
e-mail: david.dreisinger@ubc.ca

T. Cooper
Rosslyn Hill Mining Pty Ltd., Parmelia House, 191 St. Georges Terrace, Perth, Western Australia 6000, Australia

© The Minerals, Metals & Materials Society 2020

A. Siegmund et al. (eds.), *PbZn 2020: 9th International Symposium on Lead and Zinc Processing*, The Minerals, Metals & Materials Series,
https://doi.org/10.1007/978-3-030-37070-1_12

recovery. The concentrate was shipped off-site to smelters and the off-site shipment incurred substantial environmental monitoring, was considered high risk, and transport and smelting costs were high. Environmental concerns related to off-site shipment of concentrate have historically led to extended shutdowns while these issues were being addressed.

This scenario set the scene for the development of a hydrometallurgical treatment route to produce lead metal on-site, to improve the project cash costs and to conclusively address the off-site environmental issues.

LeadFX secured rights to a hydrometallurgical process for lead recovery from InCoR Technologies (InCoR), who had earlier secured the process rights from BASF SE and the University of British Columbia (UBC). The technology uses methane sulphonic acid (MSA), produced by BASF, as a lixiviant for cerussite dissolution. The process also employs an anglesite conversion step and recovers the lead by electrowinning to produce lead cathode which is then melted and cast into ingot for sale.

A considerable batch, pilot plant and demonstration plant test work programme were undertaken, predominantly with ALS Global Metallurgical Services at their Balcatta facility in Western Australia, to support the flowsheet and project development. The test programme addressed improving the flotation performance in concert with developing the hydrometallurgical flowsheet. Significant modifications in the flotation reagent regime and flowsheet configuration resulted in improved flotation recovery and concentrate grade compared to historical data. These results were achievable even at lower head grades of 4–5% Pb. The increased recoveries in turn led to a considerable increase in the reserve base for the project, increasing the project life from ~4.5 years (concentrate shipment) to at least 17 years (on-site lead ingot production).

The hydrometallurgical treatment route was developed through batch and pilot plant test work to take the lead concentrate through to produce lead metal, using the concept flowsheet developed by UBC as a basis. The results of the more detailed test work lead to a significant evolution of the flowsheet, which is discussed below, and led to a treatment process capable of recovering 98% of the contained lead in concentrate. The treatment of the concentrate posed significant solid/liquid separation issues which were successfully bypassed and eliminated in the flowsheet development.

The majority of the lead in the concentrate is readily dissolved by rapid leaching with MSA and the flowsheet evolution centered on liquid/solids separation issues and recovering the lead from the minor lead minerals present in the feed. In particular secondary lead sulphide, produced by the sulphidation process used in flotation, needed to be recovered so the overall process now successfully treats both sulphide and oxide lead minerals.

Paroo Station—Operating History

Location

The Paroo Station lead mine is located adjacent the Goldfields Highway, approximately 30 km west of Wiluna and 150 km east of Meekatharra. The owner and operator of the Paroo Station lead mine is Rosslyn Hill Mining Pty Ltd (RHM). The Paroo Station lead mine hosts one of the largest pure lead deposits in the world.

The Paroo Station lead mine discovery dates from the 1980s. The Magellen deposit was discovered in 1991 with a further four local deposits discovered in 1997 and onwards. All deposits are currently held by RHM. The lead mineralogy is predominantly cerussite ($PbCO_3$) with minor anglesite ($PbSO_4$) and other trace lead minerals including galena (PbS).

In 2003, a JV between Lead FX and Sentient Funds arranged for project finance to build a mine and concentrator to produce a lead concentrate for shipment. Construction commenced in 2004 with the first concentrate shipped in 2005 through the port of Esperance.

Historical Operation, Resources, and Challenges

There were three operational phases for the mine. The initial period from 2005 to 2007 produced 181,000 t of Pb concentrate. Mining was stopped due to environmental contamination arising from shipment of bulk lead concentrate through the Esperance port. After a period of formal review and introduction of new shipping and transport protocols, the mine restarted and operated from 2010 to 2011 and shipped a further 81,000 t of Pb concentrate in containers through Fremantle port. This was stopped again to investigate a further issue related to environmental monitoring and analysis before resuming operation and export for the period 2013–2015 (202,000 t of Pb concentrate shipped). The mine and concentrator were placed on care and maintenance in 2015 due to low lead prices and an unfavorable AUD:USD exchange rate. Table 1 shows the historical production from Paroo Station lead mine.

Table 1 Historical production statistics

Operating phase	Unit	2005–2007	2010–2011	2013–2015	Total
Ore milled	kt	2197	1035	2447	5680
Head grade Pb	%	7.3	6.8	7.1	7.1
Recovery Pb	%	71.7	73.8	77.6	74.6
Conc. Pb produced	kt	181	81	202	464
Conc. Pb grade	%	64.0	64.8	66.8	65.4
Sold Pb in conc.	kt	116	52	135	303

All previous environmental permits are still valid for Paroo Station lead mine. A total of 387 ha of 980 ha approved area has currently been disturbed. The mine operates under Ministerial Statement 1083 (Fig. 1).

The mining operation reached 1.7 Mtpa ore treatment rate. A new pebble crusher is to be installed to increase plant throughput to 2 Mt/a ore. The average life of mine waste to ore strip ratio was 3:1. The mining method was conventional open cut drill and blast, load and haul techniques using five 85 t haul trucks and a 120 t excavator. The ore body is shallow (up to 60 m), flat lying, and predominantly above the water table. The concentrator and mine are re-start ready (Table 2).

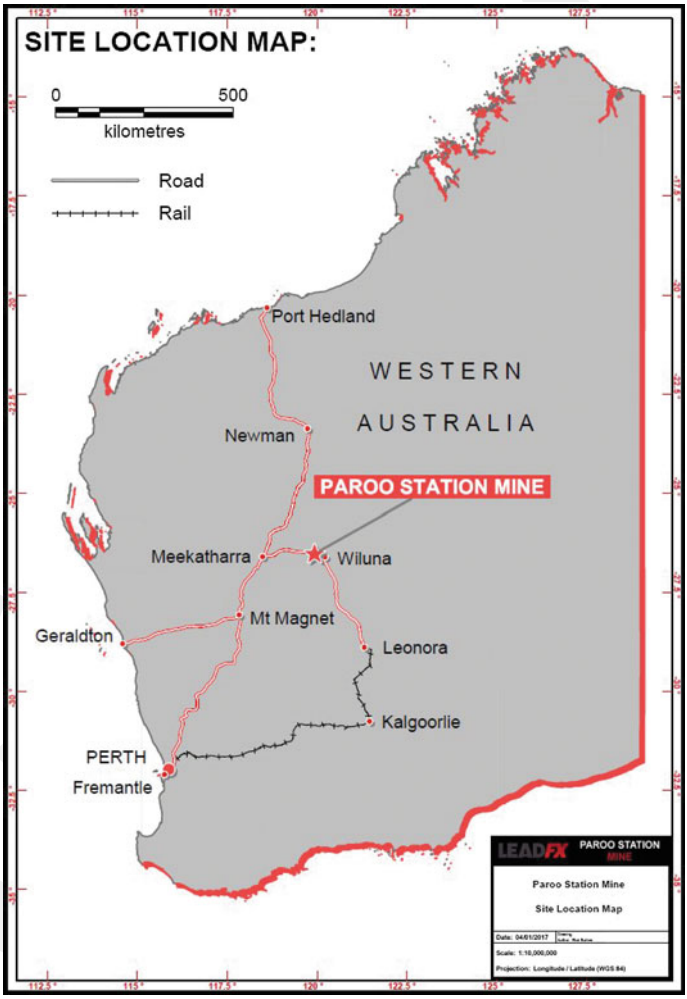

Fig. 1 Paroo station mine location (Western Australia)

Table 2 Paroo station mineral resource statement (February 2019)

	Measured			Indicated			Total M + I			Inferred		
Deposit	(Mt)	Pb %	Pb (kt)	(Mt)	Pb %	Pb (kt)	Tonnes (Mt)	Pb %	Pb (kt)	Tonnes (Mt)	Pb %	Pb (kt)
Magellan	4.5	4.2	185	14.5	4.3	625	19	4.3	810	3.3	3.9	130
Cano	1.6	3.4	55	2.1	2.4	50	3.7	2.9	105	0.8	2.3	15
Pinzon	0.1	6.1	5	9.5	4.1	390	9.5	4.1	395	2.0	3.5	70
Pizarro	–	–	–	4.6	3.1	140	4.6	3.1	140	2.0	2.8	55
Drake	–	–	–	–	–	–	–	–	–	3.7	3.4	125
Stockpiles	2.9	2.4	70	–	–	–	2.9	2.4	70.0	–	–	–
Total	9.1	3.5	315	30.6	3.9	1205	39.7	3.8	1520	11.7	3.4	396

The historical challenges at Paroo Station lead mine were numerous. The mine was at the mercy of offshore lead smelters who set high and variable treatment charges for Paroo Station lead mine concentrate. The concentrate has no intrinsic fuel content (sulphide sulphur) and there are no by-products in the concentrate for smelter credit.

The regulatory compliance imposed by Ministerial Statement 1083 contains many onerous conditions which have the potential to trigger cessation of transportation. The costs associated with compliance include required sampling of air, water, soil, sumps, etc., independent inspection, independent auditing, bagging and containerization of the ~67% Pb concentrate containing +7.5% moisture. A total of 34 people was involved in concentrate handling and shipping. The trucking and railing transport were permitted along a prescribed dangerous goods route.

The economic consequences of these factors resulted in Paroo Station lead mine were numerous:

- High and unpredictable cost operation
- Unable to hedge lead price
- Short mine life treating high grade ore resulting in leaving a large amount of the mineral resource out of the mine plan.

The historical challenges of the Paroo Station lead mine operation provided an ideal situation to consider the implementation of a concentrate to metal hydrometallurgical technology.

Lead Hydrometallurgical Technology

LeadFX secured the rights to use a hydrometallurgical process for lead recovery (1–4) from InCoR Technologies (InCoR), who had earlier secured from BASF SE and the University of British Columbia (UBC) exclusive worldwide rights to two hydrometallurgical lead recovery technologies using methane sulphonic acid (MSA) extraction of lead from "mixed oxide" or "sulphide" concentrates followed by purification and electrowinning of lead [2–4]. The technology uses methane sulphonic acid (MSA), produced by BASF, as a lixiviant for cerussite dissolution. The process also employs an anglesite conversion step and recovers the lead by electrowinning to produce lead cathode for sale.

Methane sulphonic acid (Fig. 2) is an ideal reagent upon which to base the development of a lead hydrometallurgy technology. In water, MSA reacts readily with metal carbonates and oxides to form highly soluble methane sulphonate salts. Lead has a particularly high solubility of ~560 g/l Pb at 23 °C. MSA has a high conductivity, is non-oxidizing and chemically stable. It is odourless, biodegradable, and recyclable. It has a low vapour pressure and a strong acidity (similar to sulphuric acid).

The application of MSA to the Paroo Station lead mine concentrate involves a series of chemical steps.

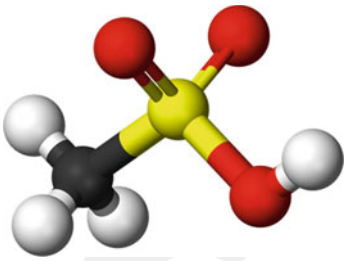

Fig. 2 The structure of methane sulphonic acid (MSA)

Leaching:

$$PbCO_3 + 2CH_3SO_3H = Pb(CH_3SO_3)_2 + CO_2(g) + H_2O$$

$$PbS + 2Fe_2(CH_3SO_3)_3 = Pb(CH_3SO_3)_2 + 4Fe(CH_3SO_3)_2 +$$

$$S_0\ 4Fe(CH_3SO_3)_2 + 2CH_3SO_3H + 1/2O_2 = 2Fe_2(CH_3SO_3)_3 + H_2O$$

Desulphurization: $PbSO_4 + Na_2CO_3 = PbCO_3 + Na_2SO_4$

Electrowinning: $Pb(CH_3SO_3)_2 + H_2O = Pb + 1/2O_2(g) + 2CH_3SO_3H$

Leaching of lead carbonate is very rapid at room temperature (~ 10 min to completion). Desulphurization with sodium carbonate converts lead sulphate to lead carbonate (to return to lead leaching with MSA). The lead methane sulphonate solution is electrowon to produce lead metal cathode and regenerate MSA for recycle to leaching.

The lead sulphide treatment technology is similar except that galena is leached using ferric-MSA and electrowinning may be performed for metal deposition and ferric regeneration.

Flotation Process Development

A significant program of flotation process development was conducted at ALS Global Metallurgical Services (Perth). The existing flotation concentrator comprised a SAG/ball milling circuit followed by two parallel trains of rougher/scavengers and three stages of cleaning to produce the final concentrate. The concentrator treats a plant feed in which the lead minerals are principally lead carbonate (85% of the feed lead), lead sulphate (12% of the feed lead) and minor other lead minerals (3% of the feed lead). The flowsheet has been significantly modified to produce the feed to the hydrometallurgical facility.

The SAG/Ball (SAB) milling circuit will be modified to a SAG/Ball/Crusher (SABC) circuit to address silica pebble buildup in the SAG mill. Screens will replace cyclones to control oversize lead mineral particles from entering flotation. The ore work index is strongly bimodal as the mine is composed of sub-horizontal sedimentary units comprising soft clay horizons to quartz breccias providing a wide range of milling characteristics. Feed blending has historically been successfully used to address this issue.

The milled flotation feed is conditioned with sodium hydrosulphide and a sodium isobutyl xanthate collector (SIBX) and frother reagent scheme is used to recover a lead concentrate. Test work has indicated that significant improvements can be made fairly simply and cost effectively to the existing flotation plant. Rougher flotation kinetics have shown that approximately 60% of the lead can be recovered at a grade of 55–60% lead from rougher cell 1 in each rougher train, bypassing the first mechanical cleaning train directly to final cleaning. The remaining rougher and scavenger concentrate is then pumped to the first cleaner train as per the current circuit, but the first cleaner train is now only required to treat 40% of the lead in the combined rougher scavenger concentrate.

In a similar manner concentrate from cell 1 or the 1st cleaner, train can be bypassed directly to final cleaning and the remaining 1st cleaner concentrate is recycled to the head of the 1st cleaner train and these cells are then run for recovery not grade. 1st cleaner tailings pass directly to the tailing thickener. Concentrates from the 1st cell of the rougher and 1st cleaner banks are then treated in a single stage of column flotation essentially removing the majority of the gangue slimes entrained in the concentrates using a positive bias on the wash water to wash the slimes from the concentrates. Column concentrate gravitates to the concentrate thickener and column tailings are recycled to the head of the 1st cleaner cells.

These changes to the flowsheet configuration plus an improved reagent conditioning regime have produced approximately a 10% improvement in metallurgical recovery at a slightly higher concentrate grade from a lower head grade in comparison to historical data. The predicted life of mine lead flotation recovery is 83% based on a head grade of 3.8% Pb. The flotation concentrates are filtered on an existing plate and frame filter and the concentrate filtration rate has improved by an order of magnitude through removal of the gangue slimes by the inclusion of column flotation in the circuit. The concentrate is dried after filtration in order to minimize water ingress into the hydrometallurgical plant and to remove residual flotation chemicals to minimize foaming issues in leaching.

Hydrometallurgy Process Development

The first stage MSA leach dissolved all of the cerussite in the flotation concentrate with leach extractions typically 100% of the cerussite in less than 10 min of atmospheric leaching at 45 °C, and 84% on average of the lead in the concentrate. Leaching time was typically dictated by the rate at which MSA could be added, while controlling the frothing due to carbon dioxide evolution. A CCD circuit was instituted to recover the lead. The washed MSA leach residue then moved to the anglesite conversion stage.

Recovery of the anglesite in the concentrate was designed as a two-stage process. The washed MSA leach residue was treated with acid (H_2SO_4) to convert all minor lead minerals (e.g. Pyromorphite) to lead sulfate. The acidified residue was

washed and treated with sodium carbonate to convert the lead sulphate to lead carbonate in the DeS leach step (desulphurization). High conversion rates of sulphate to carbonate were achieved in the test work. A large proportion of the anglesite was initially occluded within cerussite grains in the flotation concentrate, so the first MSA leach step was found to be critical to ensuring that the anglesite was exposed to the conversion reaction.

The DeS leach residue was simply floated in a step analogous to the flowsheet used in the flotation concentrator to recover a flotation concentrate comprising the lead carbonate produced in the DeS leach step thus eliminating a difficult solids/liquid separation step. The flotation tailings from this step would be discharged to the main tailings stream in the flotation plant.

The flotation concentrate was then thickened and filtered with the primary flotation concentrate and thus recycled to the MSA leach eliminating a second MSA leach step and subsequent solid/liquid separation step.

It is worth noting at this point that while the ore mineralogy indicates the presence of only minor/trace sulphides, the flotation concentrate contains 2–3% of the lead as lead sulphide, mainly as a result of the sulphidisation step in the flotation concentrator. In a reaction analogous to copper sulphide leaching with the ferrous/ferric sulphate couple, lead sulphide can be leached with the ferrous/ferric methanesulphonate couple. Ferrous methanesulphonate is converted to ferric methanesulphonate in the MSA leach by addition of an oxidant such as air or oxygen. The galena is thus effectively leached in the MSA leach circuit using iron taken into solution from gangue leaching reactions.

The liquor from the MSA leach thickener overflow thus contains all of the lead leached and may pass to an optional impurity removal step ahead of liquor filtration and electrowinning. The solution can be purified by lime addition to form iron and aluminum hydroxide precipitates. In the demonstration plant, this step was not required due to the high quality of concentrate recovered via column flotation.

The electrolyte is filtered and passes to a tank house where the lead is electrowon onto lead started sheets. The tank house and subsequent material handling steps are fully automated to minimize the potential for operator contact with lead solutions. All of the cells are equipped with anode brushes to scrub acid mist from the cell off-gas. Cathodes are recovered at a rate of about 200 kg unit every minute. The lead is melted in an induction furnace and the molten lead is cast into 25 kg ingots and a proportion of the molten lead is cast into starter sheets for recycle to the electrowinning facility.

The target is to produce lead ingot of +99.99% lead purity as demonstrated in test work to date. The majority of the impurity is due to minor metals in the commercial lead sheet used for starter sheets in the pilot plant so reaching the target lead grade is not considered to be an issue.

Refinery residues will be discharged to the existing tailings storage facility and will contain substantially lower residual lead values than the existing flotation tailings.

The flowsheets for the grinding, flotation, and hydrometallurgical plant designs are shown in Figs. 3, 4 and 5.

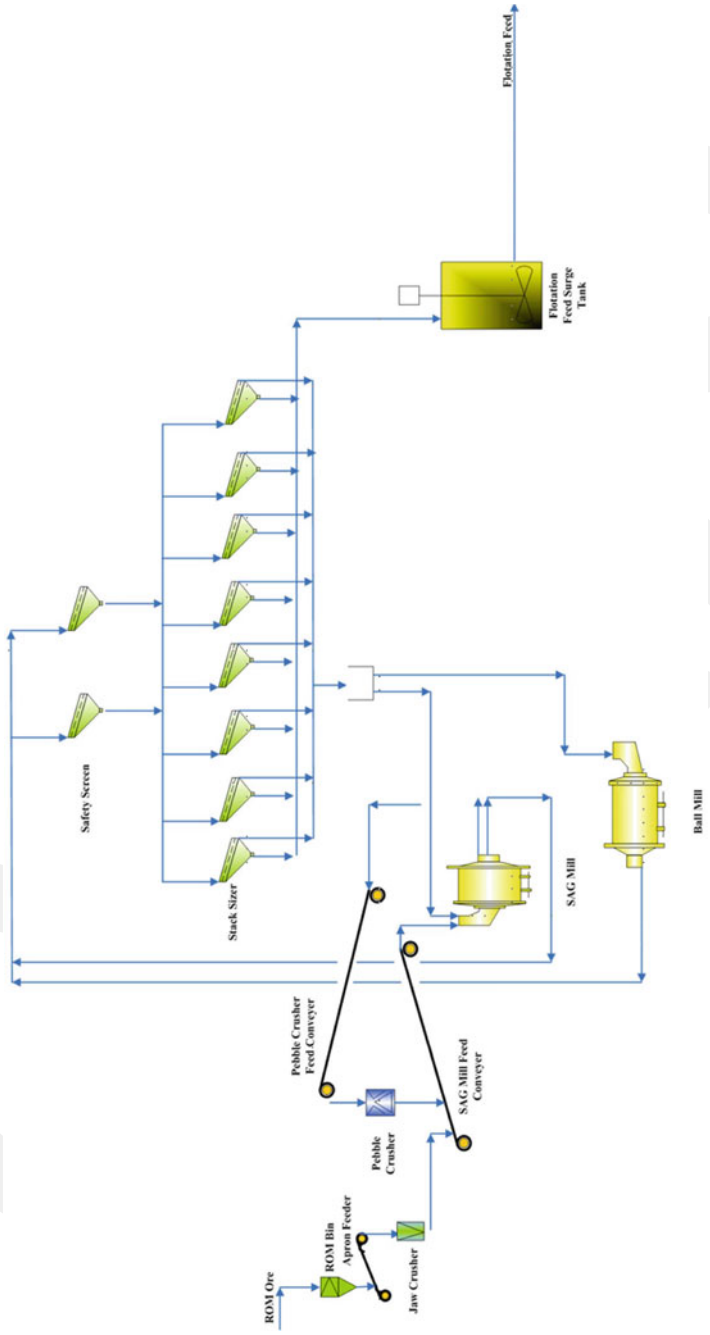

Fig. 3 Paroo station milling circuit

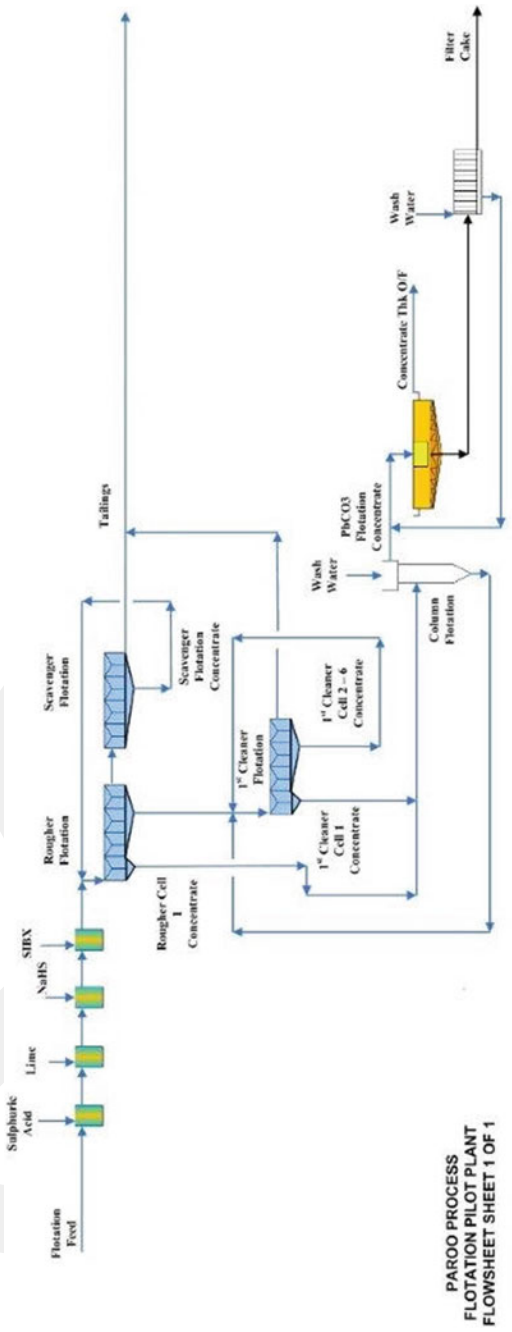

Fig. 4 Paroo station flotation flowsheet

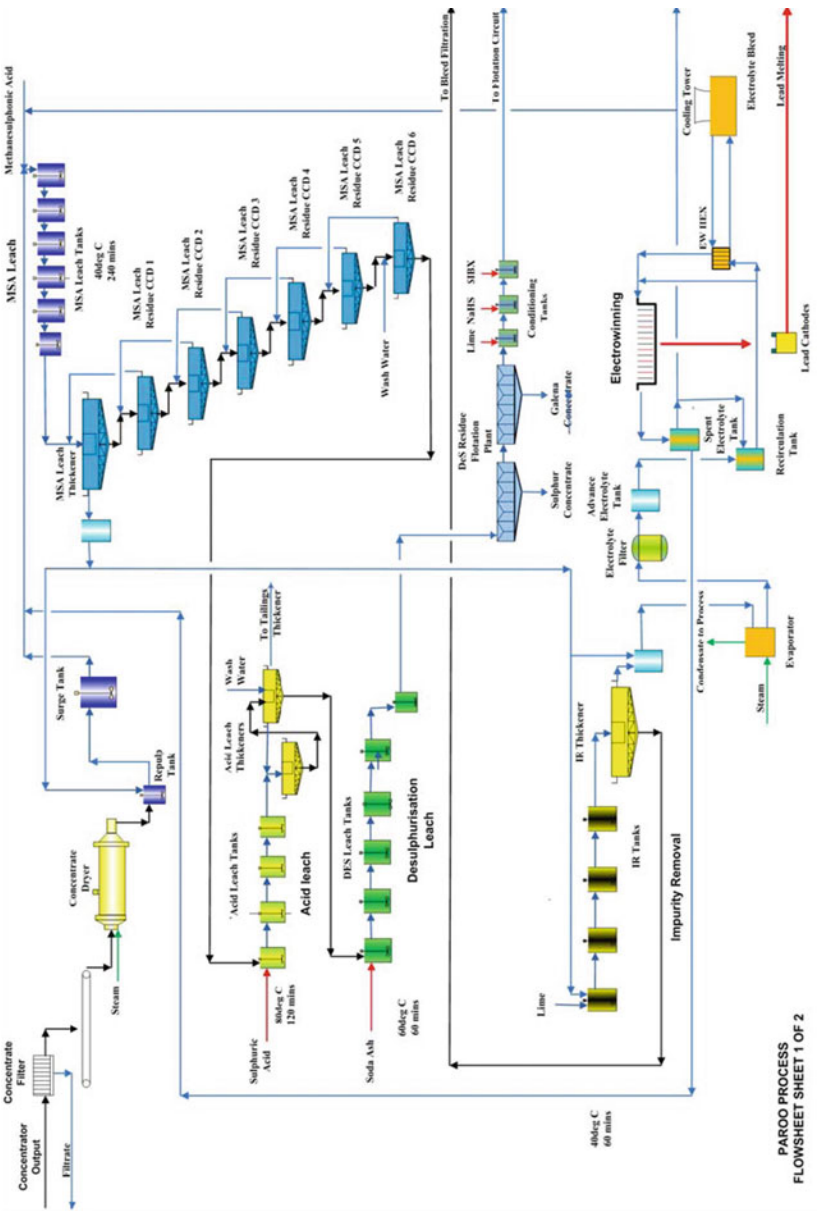

Fig. 5 Paroo station hydrometallurgical flowsheet—part 1

Definitive Feasibility Study

SNC-Lavalin (SNC-L) completed a definitive feasibility study in 2018 and a revised feasibility study in 2019 ('DFS') incorporating the results of various metallurgical test work programs undertaken in 2017 and 2018 for the on-site production of lead ingots. Lead concentrate from the existing concentrator will be processed through a new hydrometallurgical facility which will be located adjacent the existing concentrator.

SNC-L's scope of services for the DFS was the performance of all necessary engineering design and estimation in order to produce a Class 3 estimate in compliance with the AACE International Standard (the "SNC-L Scope"). This includes:

- Confirming (based on testwork results) the technical suitability of the metallurgical process selected to the extent possible;
- Estimating the capital and operating cost of the mineral processing and hydrometallurgical facilities;
- Providing input into RHM financial evaluations as required; and
- Providing an integrated DFS report.

The following work was excluded from the SNC-L scope but data/information provided by others was utilized by SNC-L in its design and estimates where necessary:

- All geology and mining work;
- Proof of concept, variability, and pilot plant testwork;
- Water supply from borefields;
- Tailings storage facility (TSF);
- Environmental work;
- Geotechnical investigation and site survey;
- Regulations, permits, and approvals;
- Upgrades to the existing accommodation village;
- Marketing;
- Exchange rates; and
- All Owner's costs including insurances and import duty.

All information provided to SNC-L by others has been assumed correct and not verified by SNC-L. The battery limits for the SNC-L scope are as follows:

- The underside of the existing concentrate filter discharge chute;
- Existing raw water pond;
- Delivery into existing concentrator tailings disposal system; and
- Delivery of lead ingot into on-site storage.

The hydrometallurgical facility design is based on the 4-phase test program and vendor test work:

- Phase 1—Proof of Concept—ALS;
- Phase 2—Variability—ALS;
- Phase 3—Pilot Plant—ALS;

- Phase 4—Demonstration Plant—ALS
- Solid Liquid Separation—Waterex;
- Filtration Testwork—Metso and Outotec;
- Acid Purification Unit (APU)—Eco-Tec; and
- Electrowinning testwork—University of British Columbia and Murdoch University.

SNC-L interpreted and used the test data in the design of the hydrometallurgical facility.

Existing Operation

The existing facilities comprise:

- Open pit mine;
- Concentrator processing facilities;
- Minesite offices;
- Water supply and waste water treatment;
- Roads, haul roads, and service roads;
- Magazine, heavy equipment workshop, and truck washdown;
- Tailings storage facility;
- Stores, workshop, and laboratory;
- Reagent and fuel storage;
- Accommodation village; and
- Power station and electrical distribution including gas pipeline and gas receival station.

The operating facilities include open pit mining (three major deposits and one satellite deposit) followed by processing through a conventional mineral concentrator with crushing, grinding, flotation, and concentrate dewatering. The total mineral reserve (proven and probable) was developed by AMC (Table 3). Pit designs were generated from the optimizations and a life of mine mining schedule developed. The mine plan reports that the operation has a life of 17 years consisting of 36.3 million tonnes ore feed at 3.71% Pb from both future mining and processing of existing stockpiles (Fig. 6).

Existing Flotation Concentrator Modifications

The flotation plant concentrate requirement moved from producing a 67% grade lead concentrate to 70–72% lead to minimize solid/liquid separation issues in the hydrometallurgical facility. In the process, a revised reagent regime was developed that increased the overall lead recovery at a lower feed head grade.

Table 3 Paroo station mineral reserves statement (February 2019)

	Proven			Probable			Total		
Deposit	(Mt)	Pb (%)	Pb (kt)	(Mt)	Pb (%)	Pb (kt)	(Mt)	Pb (%)	Pb (kt)
Magellan	4.3	4.2	178	13.1	4.1	540	17.4	4.1	718
Cano	1.5	3.3	52	1.2	2.4	29	2.8	2.9	81
Pinzon	0.1	5.9	5	9.2	3.8	350	9.2	3.8	355
Pizaro	–	–	–	3.9	3.1	121	3.9	3.1	121
Stockpiles	2.9	2.4	70	–	–	–	2.9	2.4	70
Total	8.8	3.4	304	27.5	3.8	1041	36.3	3.7	1345

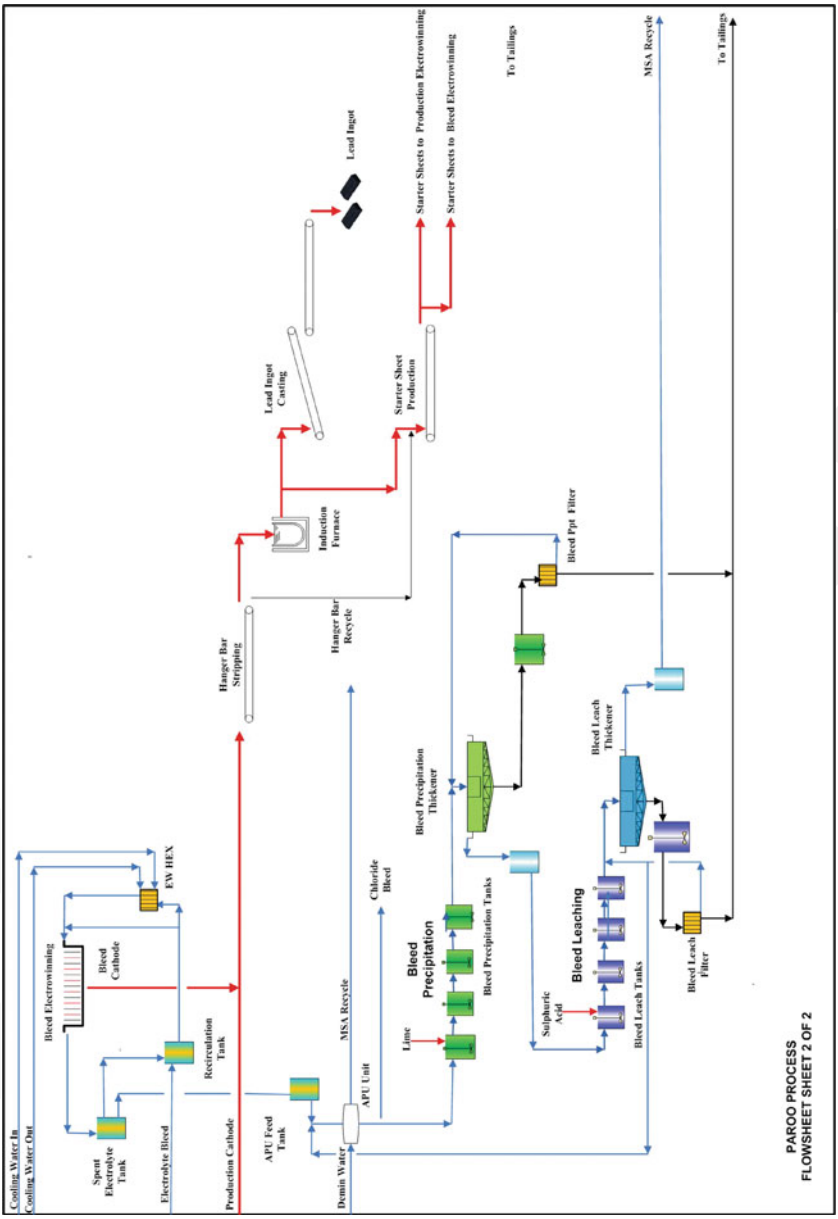

Fig. 6 Paroo station hydrometallurgical flowsheet—part 2

The required concentrator modifications identified by RHM are:

- Inclusion of pebble crushing in the grinding circuit to increase milling capacity to generate +80,000 t/a of lead in concentrate;
- Replacement of cyclones in the milling circuit with sizing screens to minimize coarse material entering flotation;
- Modifications to the flotation circuit including the addition of new conditioning tanks, new column flotation cell and associated pumps and blowers to improve flotation performance; and
- Replacement of the existing flotation thickener with a larger unit to accommodate increased concentrate production.

Hydrometallurgical Facility

The new hydrometallurgical facility will be constructed south of the existing concentrator and include the following:

- New belt feeder under the existing concentrate filter to deliver lead concentrate to a dryer and subsequent repulping and storage facilities ahead of the MSA leaching;
- Three stages of leaching—MSA leach, desulphurisation (DeS) leach, and MSA releach;
- Counter Current Decantation (CCD) circuit on the MSA leach residue;
- A flotation circuit on the DES leach residue (reuse of existing flotation plant);
- Impurity removal, electrolyte filtration, and bleed treatment circuits;
- Lead electrowinning to produce lead cathode;
- Cathode washing and transport to lead melting facility;
- Lead melting, ingot casting and stacking and furnace off-gas handling system;
- Cathode starter sheet production facility with starter cathode returned to the electrowinning circuit;
- All services including water, RO plant, compressed and instrument air and fire services;
- Gas fired power station (to cover total site demand) with heat recovery system to provide steam to the process evaporator and dryer;
- Substation, control room, and control system for the new facilities; and
- Environmental collection/evaporation pond for high rain events from hydrometallurgical facility bunded areas (Fig. 7).

Definitive Feasibility Methodology

The DFS work involved:

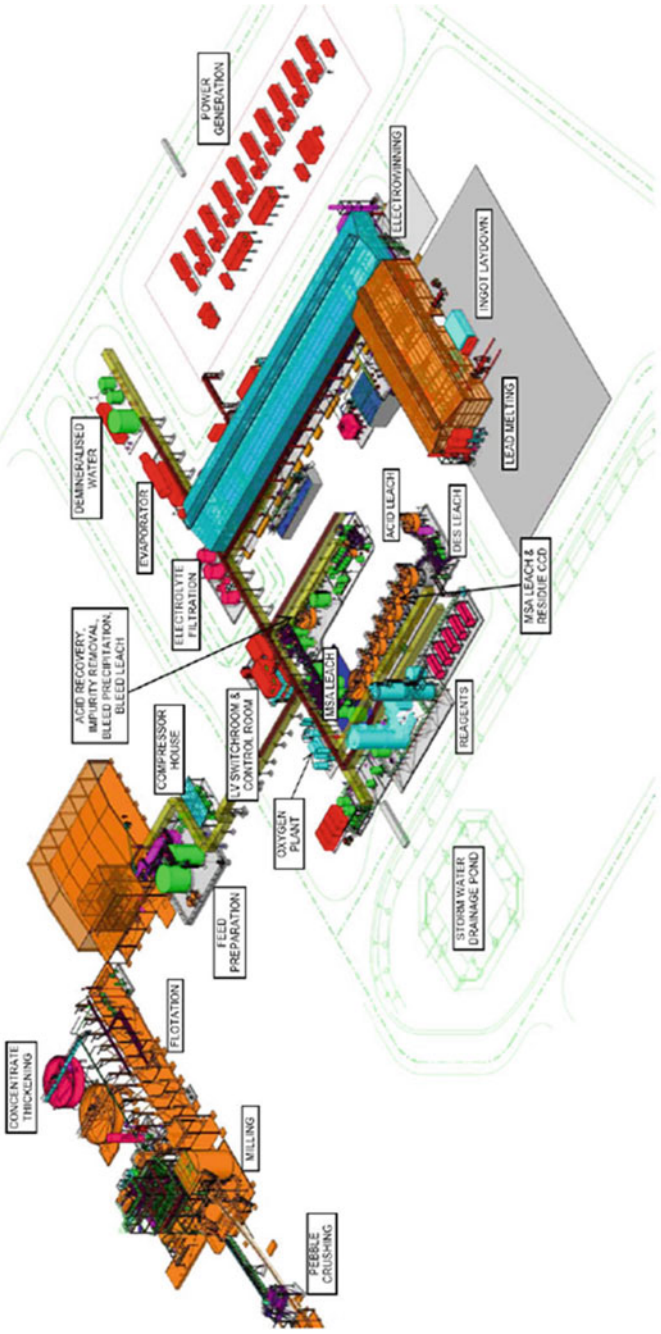

Fig. 7 Paroo station 3D model of the hydrometallurgical facility

- Developing the metallurgical process flowsheet, process design criteria, Metsim model, and plant design based on the results of the test work program;
- Developing engineering designs;
- Obtaining pricing from vendors;
- Developing a project execution strategy and schedule;
- Understanding and mitigating risks; and
- Preparation of capital and operating cost estimates.

The major activities conducted as part of the DFS included:

- Flowsheet development and process design based on the test work information;
- Equipment sizing;
- Development of engineering design criteria;
- Development of specifications and datasheets for equipment;
- Procurement activities to source prices from vendors;
- Planning, scheduling, and project implementation plan; and
- HAZOP, risk assessment, constructability review, and process design peer review.

The work undertaken was to the requirements of AACE Class 3 estimate.

Hydrometallurgical Facility Design Basis

The design capacity for the hydrometallurgical facility was set by RHM at 80,000 tpa lead production. The mine life is expected to be up to 17 years (Table 4).

The concentrate mineralogy was investigated as part of the variability program at ALS Global Metallurgical Services. This gave a range of mineralogy for design (Table 5).

The plant is designed to handle the base case and the minimum and maximum anglesite case. RHM advised that the concentrator will be fed from ore stockpiles to provide a blended feed with mineralogical characteristic to match the design basis range.

For the leaching process:

- Cerussite readily leaches in MSA;
- Anglesite is partially leached by the MSA and the remainder needs to be converted to cerrusite before it can be recovered. This is done in a separate desulphurization (DeS) leach using sodium carbonate;
- The galena also does not readily leach in MSA. It is leached by ferric methane sulphonate which is generated by adding hydrogen peroxide in the MSA leach to obtain soluble lead methane sulphonate and elemental sulphur; and
- Partial leaching of the Pyromorphite and Leadhillite is assumed based on experimental results.
- The MSA used to leach the lead is regenerated in the electrowinning process by precipitating the lead from solution as cathode. The spent electrolyte, typically

Table 4 Hydrometallurgical facility design basis [1]

Production criteria	Units	Parameter
Concentrate feed rate design	Dry tpa	100,000
Concentrate lead grade	%	71.8
Concentrate lead grade—design	%	70–72
Nominal lead in concentrate	tpa	70,000
Nominal lead metal production capacity	tpa	70,000
Maximum lead metal production capacity	tpa	80,000
Lead recovery from concentrate	%	98–99
Operating schedule		
Days per annum		365
Days per week		7
Operating hours per day		24
Process plant		
Design availability	%	92
Operating hours per annum	h	8059

Table 5 Concentrate mineralogy

Mineral	Variability testwork range (%)		Design basis (%)		
			Base case	Minimum anglesite	Maximum anglesite
Cerussite ($PbCO_3$)	59	90	80.8	86.3	69.7
Anglesite ($PbSO_4$)	3	31	9.26	3.32	21.4
Pyromorphite ($Pb_5(PO_4)_3Cl$)	0.4	1.6	1.42	1.33	1.16
Galena (PbS)	0	4	2.33	2.45	2.00
Leadhilite ($Pb_4(CO_3)_2(SO_4)(OH)_2$	0	1.1	0.582	0.6	0.6

containing around 170 g/l MSA is recycled for reuse in the MSA leach operations. The major reactions are:

- Leaching: $PbCO_3 + 2MSA = Pb(MS)_2 + H_2O + CO_2$
- Electrowinning: $Pb(MS)_2 + H_2O = Pb + 2MSA + 0.5O_2$

- Impurity and bleed treatment are used to remove calcium from the circuit and regenerate MSA, which is recycled to the leaching process.

The metallurgical test program proved invaluable in developing and confirming the process flowsheet and design criteria. Unexpected test results resulted in significant flowsheet and equipment changes from original concept flowsheet. The major

outcomes of the test work program in shaping the final DFS flowsheet include the following:

- Changes to the flotation regime to increase overall Pb recoveries from ore to concentrate;
- Inclusion of a flotation columns to limit slimes entrainment and ensure fast filtration and efficient washing of the concentrate prior to introduction into the hydrometallurgical facility;
- Inclusion of a concentrate drying step to overcome frothing issues during the MSA leach;
- Significant variations in mineralogy between variability samples (% Pb in cerrusite ranged between 59 and 90%) resulting in overall predicted lead recoveries from the variability concentrates of 96–99% (Average 98%);
- Introduction of a vacuum degassing step after MSA leach to overcome issues with settling
- Replacing MSA filters with CCD's to ensure good washing efficiency;
- Replacing DeS leach residue filtration with flotation to recover Pb minerals and discard gangue to tailings and reintroduction of the DeS Residue flotation concentrate to the concentrate thickener;
- Optimization of electrowinning performance based on bench scale testing at University of British Columbia, by increasing current density to 400 A/m^2 and optimizing smoothing agent regime and dosing rates; and
- Demonstration of electrowinning on pilot scale and casting of ingots for lead ingot analyses.

The Demonstration Plant operation provided additional confidence on all aspects of the design. A total of 35.5 t of ore was prepared and floated to make 2.95 t of concentrate with 958 kg of lead metal recovered by electrowinning.

In addition, corrosion coupon testing, optimization of desulfurization and acid leach, boiling point elevation, flotation of galena and sulfur and further studies of smoothing agents were investigated.

Three Metsim models comprising a base, and minimum and maximum anglesite cases have been developed by SNC-L. The models have been used to generate heat and mass balances required to size the equipment. Process design criteria have been developed by SNC-L from a combination of test work results and SNC-L experience with similar processing plants. Test work data from the completed programs has been used in the models and other engineering data to verify the equipment selected.

The recovery of lead from concentrate to final ingot has been estimated for the various annual composites using test results, mineralogical analyses, and the Metsim model. An average recovery of 98% is expected across the range of ores to be treated.

The hydrometallurgical facility includes:

- Feed Preparation, Leaching and solid/liquid separation
- Impurity removal and electrolyte preparation
- Lead electrowinning
- Bleed treatment

- Lead melting, casting and load-out
- Utilities and reagents
- Power station, heat recovery, and steam generation.

A brief description of these areas follows.

Feed Preparation, Leaching, and Solid/Liquid Separation

Concentrate from the existing concentrator is filtered and washed on the existing VPA filter press using demineralized water. The filter cake is then dried in a Holoflite® dryer (to drive off flotation reagents), repulped utilizing MSA leach liquor and stored in the hydrometallurgical facility feed storage tank (18 h capacity) from where it fed to the MSA leach facility.

- MSA leach;
- DeS leach; and
- MSA re-leach.

In the MSA leach, the slurry is mixed with recycled spent electrolyte. The process evolves carbon dioxide, which is extracted through a wet scrubber and vented to atmosphere. Hydrogen peroxide is also added to facilitate the generation of ferric methane sulphonate to leach any galena present in the feed. The leach slurry (pH <0.5) passes through a vacuum degasser for removal of dissolved carbon dioxide generated during the leaching process. The degassed slurry is then flocculated and thickened. Thickener U/F (leach Residue) is settled and washed in a six-stage CCD circuit. The final CCD thickener underflow is pumped to the DeS leach tanks. Solution overflow (electrolyte) from the first thickener is pumped to the impurity removal and electrolyte preparation circuit.

In the DES leach, the MSA leach residue is leached with the addition of soda ash which converts the anglesite to cerussite. Slurry from the DeS leach is pumped to the existing flotation plant where the lead minerals are recovered by flotation. The concentrate is washed with demineralized water in a small flotation column and returned to the MSA releach circuit. The releach operates at 65 °C with ferric iron regenerated by hydrogen peroxide addition. The MSA leach extracts nearly 90% of the remaining lead and targets the Galena. The MSA releach discharges into the MSA leach circuit (Fig. 8).

Impurity Removal and Electrolyte Preparation

The impurity removal process ensures the iron and aluminum levels in the MSA leach liquor are acceptable in the electrowinning circuit. MSA leach liquor is mixed with a lime slurry in agitated reactors to precipitate the aluminum and iron. The discharge from the reactors is thickened and a portion of the underflow is recycled to assist in seeding the precipitate. Impurity thickener U/F is recycled in part to the

Fig. 8 Lead cathode samples from the ALS pilot plant operation

head of the MSA leach circuit to supply iron to leach galena contained in the MSA leach feed. A small fraction of the thickener underflow is discharged to the flotation concentrator tailings.

The thickener overflow is treated in a double effect evaporator to recover water as condensate and maintain the circuit water balance. Evaporator discharge is treated through two multimedia filters to ensure that no particulates enter the electrowinning circuit. The solution from these filters (Advance Electrolyte) is delivered to the electrolyte recirculation tank and subsequently fed to the Electrowinning circuit. The Advance Electrolyte contains in excess of 300 g/l of lead.

Electrowinning and Cathode Handling

The lead electrowinning circuit is designed to produce up to 80,000 tpa lead cathode. The tankhouse has 74 production electrowinning cells each fitted with 45 lead cathodes and 46 graphite anodes and operates with a current density of 400 amps/m^2. The tankhouse has one electrical circuit powered by a 195 V, 34,500 A transformer-rectifier.

Lead plating takes place over a 3-day cycle. Cathode thickness will be 18–20 mm and will weigh between 160 and 200 kg. The tankhouse operates with lead starter cathodes that weigh 8 kg which are fabricated in the lead smelting and casting facility.

Each electrowinning cell is provided with a hood and ventilation extraction system to exhaust the acid mist generated by the electrowinning process. The collected acid mist is passed through a scrubber to ensure lead levels to atmosphere do not exceed allowable limits. The solution in the electrowinning circuit is maintained at 40 °C by a heat exchanger.

An automated cathode harvesting and delivery to the furnace system is provided. Cathodes are harvested and melted on a 24-h cycle. Cathodes are removed from the electrowinning cells utilising the automated overhead crane and bale system. One-third (15) of the plated cathodes are removed from each cell at a time. The bale is designed to lift the cathodes and insert a drip tray below the cathodes to collect acid solution. The cathodes are delivered by the crane to storage racks ahead of the cathode wash station. From the storage racks, the cathodes are automatically transported into the cathode wash station and cleaned with hot water sprays and dried. They are then automatically conveyed to storage racks ahead of the lead melting furnace. The storage rack has capacity for 750 cathodes which is sufficient to ensure a 12 h buffer in the event of equipment problems. A robot is used to remove the cathodes from the wash station and to load them onto the storage/transport rack.

Cathodes are removed from the racks (one at a time) by a robot which presents the cathode to a second robot for automatic removal of the copper hanger bar. The bar is then delivered to the cathode starter sheet casting machine for reinsertion in the starter sheet.

Once the hanger bar is removed, the robot delivers the cathode to an induction furnace for melting. Cathodes are delivered to the furnace at the rate of one per minute.

Lead Melting and Casting

A 600 kW induction furnace is provided for melting the lead cathode. The furnace is provided with two sets of metals pumps. One set delivers hot metal to the ingot caster, the other delivers metal for cathode starter sheet fabrication.

The lead ingot caster is made up of multiple moulds which are attached and rotated through the casting cycle by a chain conveyor. The ingot casting is fully automated from receipt of molten lead to the stacking of cast ingots. Cooling water and air are applied to the moulds for cooling the ingot. The ingots are ejected onto a second conveyor and a robot stacks the ingots into bundles on the stacking conveyor where they are banded. A hoist is used to remove the ingot bundles from the stacking conveyor and a forklift is used to the deliver the bundles to a storage area adjacent to the furnace building. The bundles will be shipped off-site by truck.

Cathode Starter Sheet Fabrication

Cathode starter sheets are fabricated form lead from the melting furnace. Hot metal is pumped to a lead starter sheets casting drum. The drum produces lead sheet which is cut to size then has the hanger bar (removed on the way to the furnace) inserted and riveted to make the cathode starter sheet. Finished cathode starter sheets are stored on a storage rack and automatically transported back to the electrowinning plant and reinstated into the cells by the overhead crane in the electrowinning plant. The capacity of the storage rack is 1200 starter cathodes.

Lead Melting/Cathode Handling Ventilation

An extraction system is provided for collecting off-gas from the furnace melting operation. The system comprises of a spark arrestor/cyclone and baghouse for fume extraction and dust collection. It is expected that only small quantities of dust will be collected and this will be manually disposed of back into the leaching system for recovery of any contained lead.

Bleed Treatment

A bleed stream of spent electrolyte (MSA rich) is treated for reagent and lead recovery. The bleed stream treatment removes impurities that build up in the circuit and regenerates MSA for reuse in the process. The major impurities are Mn, Mg, Ca, and Sr. A small "Chloride Bleed Stream" is also treated to remove other trace elements such as sodium, potassium, and chloride ions.

In the first step, lead is recovered from the bleed stream by utilizing 10 electrowinning cells to strip lead over a 16 h cycle. The produced cathodes are harvested and handled in similar manner to the production cells. During this process, the lead concentration in the spent electrolyte solution is reduced to 3 g/L (spent electrolyte Solution). The cells are the same design as the production cells and are provided with hoods and connected to the same ventilation system as the production cells.

An Acid Purification Unit (APU) is used to de-acidify the spent electrolyte in order to recover MSA for reuse in the leach areas. The spent solution is filtered through a media filter and passed through the APU; which absorbs approximately 80% of the MSA. The MSA is stripped with demineralized water and returned to the leach process.

The liquor discharge from the APU containing metallic salts and a small amount of MSA is reacted with lime in agitated reactors to precipitate metal hydroxides and solubilize the calcium methane sulphonates. The solution from the reactors is thickened with the U/F being pumped to the precipitation residue filter, where the precipitate is washed and discarded to tailings.

The liquor (thickener overflow) is fed to a leaching circuit, where it mixed with sulphuric acid to precipitate gypsum and strontium and regenerate MSA. The precipitate is thickened, filtered, and washed before being discarded to tailings. The liquor is returned for reuse in the MSA leach.

Utilities and Reagents

The following utilities are provided for the hydrometallurgical facility:

- Raw Water;
- Fire Water;
- Cooling Water;
- Potable Water;
- Plant and Instrument Air; and
- Environmental collection pond for water from bunded process areas.

Storage, mixing, and pumped distribution facilities are provided for the following reagents:

- Sodium hydrosulfide (NaHS);
- Sodium Isobutyl Xanthate (SIBX);
- Frother;
- MSA;
- Sulphuric Acid;
- Lime;
- Soda ash;
- Flocculants (2);
- Caustic Soda;
- Orthophosphoric acid;
- Aloes; and
- EW50.

Lime and soda ash and acid are delivered in bulk. The other reagents are delivered in isotainers or bulka-bags. A lime slaking plant is provided to produce lime slurry for use in the circuit.

Tailings Disposal

Waste streams from both the flotation concentrator and the hydrometallurgical facility are disposed using the existing concentrator tailings sump and pumps and delivered to the integrated waste landform.

Power and Steam Generation

A power station will be constructed on-site to produce power and steam for the existing concentrator and hydrometallurgical facility. The maximum power draw is 13.7 MW and steam production will be 5.8 tph. The power station will be fed from the existing gas pipeline and receival station, located adjacent the existing diesel power plant. The existing diesel power station will be also be refurbished for emergency events.

The new station will consist of generating units, connected to heat recovery steam generating units (HRSG). The station will operate in an $N + 1$ configuration depending on the load profile. The power station will be provided under a Build, Own, Operate (BOO) basis.

Estimated Capital Cost

The estimate capital cost (CAPEX) for the project (Concentrator and Hydrometallurgy Plants) is shown in Table 6.

The CAPEX complies with the requirements of AACE Class 3 criteria obtained with the following methodology and assumptions:

- Budget quotations for the majority of the equipment;
- Engineering MTO's for earthworks, concrete, steel, platework, piping and electrical and instrumentation for the facility;
- Market rates for fabrication;
- SNC-L labour cost estimate based on current market conditions and rates, and compared to contractor budget quotation.

SNC-L analyzed the CAPEX in a contingency-workshop for uncertainty of quantities, costs, and the variability introduced during execution. The Monte Carlo simulations were run using the @Risk software. The contingency included is based on a P_{80} probability, and the estimate accuracy is $+15/-13\%$.

Table 6 Project CAPEX estimate summary

Description	Capital cost (USD)
Direct costs	114,560,102
Indirect costs	33,390,911
Subtotal base costs	147,951,013
Contingency	14,931,924
Subtotal Inc contingency	162,882,937
Owner's costs	20,833,000
Total (USD)	183,715, 937

Table 7 Operating cost summary

Cost centre	(USD)	Life of mine (USD/t Ore feed)	(USD/t Pb Ingot)
Mining	362,791,836	10.00	332
Flotation concentrator	394,655,986	10.88	361
Hydrometallurgical facility	332,459,946	8.89	295
Supply and logistics	149,702,419	4.13	137
Sustainability	45,657,670	1.26	42
Corporate and G + A	86,411,841	2.38	79
Sustaining capital	32,882,477	0.91	30
Total opex	1,394,562,775	38.43	1276

Operating Cost Estimate

The operating cost for the base design case is shown below. The cost is based on mining material movement costs by RHM, manpower schedule by RHM, all-inclusive labour rates provided by RHM, work cycles provided by RHM, quotations for reagents sourced by SNC-L, reagent usage by SNC-L, power generating costs on a BOO arrangement, RHM quotation for transportation of lead ingots to Fremantle and no contingency. The costs exclude royalties and finished product shipment costs from port to market which are treated as 'net backs' to sales revenue, plant closure and decommissioning costs, Esperance environmental settlement agreement commitment, depreciation, GST, corporate tax, and finance related costs (Table 7).

Conclusions

The DFS provided the following conclusions.

- The capital cost estimate to build the proposed hydrometallurgical facility, make modifications to the existing Flotation Concentrator and associated infrastructure for the Project is US$183.7 M (including Owners costs of US$20.8 M and a contingency of US$14.9 M and growth allowances of US$6.4 M).
- The average operating cost to produce 99.99% lead ingot is US$1276/t (including overhead and sustaining capital over the 17-year life of mine).
- A mineable reserve of 36.3 Mt at 3.71% Pb grade for a 17-year mine life.
- Concentrate grades of the order of 72% lead were achieved over a range of head grades from 3 to 11% lead. An average flotation recovery of 83% lead was achieved at a 3.71% lead head grade.
- Impurity elements within the concentrate were significantly reduced resulting in lower hydrometallurgical facility operating costs.

- Lead extraction in MSA leach average approximately 90% across all lead mineralogy based on a single pass through the leach circuit. The lead extraction from the MSA leach residue average 98% resulting in an overall recovery through the flotation and hydrometallurgy processes of 81.3%.
- Lead cathode was produced at current densities between 300 and 350 A/m^2, which equates to a cathode plating rate of 70,000–80,000 tpa. Cathode quality exceeds 99.995% lead.

References

1. Wu Z, Dreisinger DB, Urch H, Fassbender S (2014) Fundamental study of lead recovery from cerussite concentrate with methanesulphonic acid (MSA). Hydrometallurgy 142:23–35
2. Wu Z, Dreisinger DB, Urch H, Fassbender S (2014) The kinetics of leaching galena concentrates with methanesulphonic acid (MSA). Hydrometallurgy 142:121–130
3. Wu Z, Dreisinger DB, Fassbender S (2016) Recovering lead from a mixed oxidized material. US Patent 9,322,105, April 26, 2016
4. Wu Z, Dreisinger DB, Fassbender S (2016) Recovering lead from a lead material including lead sulphide. US Patent 9,322,104, April 26, 2016

GCRIS

Lead Plant Transformations

A. Liu, M. E. Reed, R. Close and L. Thompson

Abstract Worley has been involved in two major lead transformational projects in the last decade. These projects have involved the replacement of sinter plant and blast furnace operations, with the key initiative relating to improvements in environmental performance for the facilities and to meet tighter global regulations on work place emissions and environmental performance. Worley has been involved in the projects since inception, and the projects involved technology trades offs for both oxidation and reduction processes. A range of options was considered in both cases, and different technology solutions were selected by the two organizations. This paper investigates the selection process and the modelling work that was undertaken to assess both technologies and how the data was used to assist in the final decisions for the two organizations. As a result, Worley has developed a series of comprehensive process models of all lead smelting and reduction technologies that can assist operations assess their performance and to do preliminary assessments on technology selection. Worley also completed wrap around engineering for the balance of plant in both cases and is familiar with total flowsheet solutions for lead smelters globally.

Keywords Lead smelting · Process modelling · Heat balance control · Technology trends

Introduction

Environmental impact and performance have driven lead smelting operations to consider process upgrades and in some cases technology transformations to ensure that they can continue to operate. The lead smelting industry has historically suffered from the stigma of environmental impact and health and safety of operational staff; however, lead remains an important metal that has wide application in a modern

A. Liu · M. E. Reed (✉) · R. Close · L. Thompson
Worley Services Pty Ltd., Level 12, 115 Grenfell Street, Adelaide, SA 5000, Australia
e-mail: michael.reed@worley.com

© The Minerals, Metals & Materials Society 2020

A. Siegmund et al. (eds.), *PbZn 2020: 9th International Symposium on Lead and Zinc Processing*, The Minerals, Metals & Materials Series,
https://doi.org/10.1007/978-3-030-37070-1_13

world. The main application remains in the area of battery manufacture, and approximately, 10–11 Mt/a of lead is consumed. Nearly 60% of this lead is from recycled materials, the remainder from primary production routes.

Worley has been heavily involved in the pyrometallurgy of lead production for many years and has assisted a number of clients' complete brownfield retrofits, upgrades, and process improvements. There a several key technologies that are dominant in the lead smelting industry transformation and, Worley has worked with all of the key vendors in all aspects of project execution.

This paper outlines the approach that Worley has taken in the development of these projects, including the process modelling aspects and data acquisition review and application. This paper reviews two projects that Worley has executed in the last 10 years that have transformed operations. Both have been executed in brownfields environments, with combinations of engineering and execution models.

Blast Furnace and Sinter Plant Operation

The major production route of metallic lead has been the sinter plant and blast furnace. From an environmental perspective, the capture of lead bearing dust and SO_2 containing metallurgical gases has been extremely difficult. Over many years, operations have incrementally improved their operations; however, with tighter global environmental standards and continued pressure from shareholders, lead smelters have had to make investment decisions to replace aging assets. In some cases, the upgrade choices have been uneconomic forcing assets to close.

Historically, much of the lead produced globally was from the sinter plant/blast furnace route. Over the last 15–20 years, there has been a transition from this historic production route to newer technologies including Top Submerged Lance (TSL) technology with both Outotec and Glencore having examples of their technology being adapted to the primary lead smelting industry. More recently, we have seen the rapid introduction and take-up of the SKS technology from China.

In some of these instances, the blast furnace has remained as the key reduction furnace, treating in many cases synthetic sinter in the form of slag from the primary smelting unit. The change in sinter form has meant that incremental changes have been required at the blast furnace to optimise the production of lead bullion. In some cases, bullion can also be produced in the primary smelter; however, in this mode, the majority of the lead continues to come from the blast furnace.

The new primary smelter to replace the sinter plant has increased the ability to recover sulphur bearing gases at a higher SO_2 tenor than typically experienced at the sinter plant, and in addition, the dust capture and feed conditioning have been improved to dramatically decrease airborne lead.

Technology Alternatives

All operations have different drivers for considering a change in process technology. Two of key drivers relate to lead and SO_2 emissions. The operating costs and efficiency of the sinter plant/blast furnace can also be a contributing factor when considering a process change. Also, key feed stock material including internal and external recycles can also contribute to the selection criteria when considering a new technology. The new technology must also be able to integrate with regards the existing equipment and has a suitable capacity to ensure success of the modernisation.

Determining the best alternative technology for a particular operating site involves determining how the technology can be incorporated at the plant and also determining what impact the technology will have on the remaining plant. During this stage, Worley works through a process of collecting the plant data that is relevant to the particular project goals. This can include the following tasks:

1. Review and updating of the process design basis for the area of the plant—including nominating the name plate capacity that the client requires for the future upgraded facility
2. As-building PFDs for the plant—in many cases, a total new plant has not been built, and much of the existing plant infrastructure, for example, feed preparation, feed conditioning, hygiene off gas systems, molten metal handling facilities, and pyrometallurgical refining of the bullion can be re-used with only minor upgrades required
3. Collect plant operating data and assess the plant and equipment performance and condition to ensure that the plant reaches the name plate capacity and that none of the equipment will become a bottleneck for the redeveloped site.

Worley has completed this process by generating area concepts that describe the area of the plant, the issues that are seen in the plant area, condition of the equipment, and the throughput of the plant in its current format. It identifies work that would need to be carried out in the area to overcome the issues in the plant and to determine how the different technology can be implemented and integrated at a particular site. For example, does the facility only install an oxidation process to replace the sinter plant, or do they consider replacement of both the sinter plant and the blast furnace operation.

With the answers to these questions, information on the blend of concentrates and secondaries to be treated, information on the supply of utilities like oxygen, plant air, electricity, and water, a trade-off study can be completed to determine the ideal technology for the plant.

Top Submerged Lance Technology

There are two technology vendors—Outotec and Glencore. Primarily, the technology, however, is a bath smelting process. The Top Submerged Lance consists of an upright

cylindrical refractory lined vessel and a lance to provide process air and oxygen delivery to the bath. Wet feed is added to the process, including solid fuel. The technology was initially developed in the 1970s by CSIRO looking to improve tin smelting operations. The technology was adapted to a range of different applications including copper, lead and nickel smelting.

The advantages of the TSL process are the improved ability to capture process off gases and to minimise fugitive emissions. In addition, the process can take feed materials in a variety of forms and compositions. The process has been used for treating sulphide concentrates, oxide residues, battery scraps, and miscellaneous lead bearing material. The process has been widely accepted in industry with several operations globally.

Typically, the TSL process has been used as a primary smelting furnace to generate a synthetic sinter that can be delivered to the blast furnace for reduction to lead metal. There have been examples when a second TSL is installed, and the slag is reduced in this furnace to lead metal. The TSL furnace can also be used in a batch mode to complete both the oxidation and reduction in a single vessel. This demonstrates the flexibility of the process.

Process and technology selections are dependent on the ultimate name plate capacity, concentrate and secondary mix of feed to the smelter and the customers appetite for technology options and variations. The synthetic slag also preforms differently in the blast furnace, and this can impact the technology selection process. If the blast furnace is of a suitable size with enough flexibility to allow the required process changes, this can be a suitable flowsheet concept.

SKS Technology

The technology was developed in China and has been used now extensively in China over the last 10 years. The technology again is a bath smelting process; however, it takes place in a horizontal bottom blown vessel. Feed is delivered to the furnace via feed conveyor to an opening in the top of the vessel. The furnace is maintained under suction to ensure that there are no fugitive emissions from the feed delivery. Oxygen and process air (and in some cases pulverised coal) are delivered to the process via bottom sonic tuyeres. Slag and some bullion are tapped from the furnace. The slag is cast into small ingots that are used as synthetic sinter for addition to the blast furnace.

The process can be used to produce synthetic sinter for delivery to a blast furnace, or a second reduction SKS can be used to replace the blast furnace. These plants are now producing lead at world class tonnages, and much of the lead produced in China is now from this process. The SKS reduction process is also carried out in a horizontal vessel with bottom blowing tuyeres.

This process has had a significant impact on the Chinese lead smelting and production industry. The number of lead SKS operating units has increased rapidly over

the last few years. Nominally, 3–4 Mt/a of lead is produced using the SKS technology in China. Furnaces as large as 5 m in diameter and over 30 m long have been constructed and operated in China.

All new lead production within China is reportedly to adopt this technology including the new reduction SKS technology to minimise impact of smelting operations on the environment and improve the economics of the operations.

Process Modelling

In many of the studies that Worley has completed, the technology vendor has provided a process model that covers only their core technology. To ensure that the total flowsheet holds together with all the recycle streams and that all the design criteria are consistently used in the development of the process, Worley has built an independent process model of the entire facility.

This assists the client in understanding the interactions with the new plant and can be used to model the impacts of different feed stocks, different recycle configurations. It is also important for the peripheral equipment sizing, like the acid plant, oxygen plant, and the off gas handling process equipment.

Worley uses the Metsim modelling package as the tool to complete this modelling and has built sophisticated models that can be used and adapted for both TSL and SKS technologies. The models can incorporate both the oxidation and reduction process, pyrometallurgical refining processes, and off gas cleaning processes. In some of the project work, these models have been used to complete technology trade-offs and comparisons to allow our customers to make process selections.

Worley works with the client and technology vendor to determine:

- Suitable online time for the process
- Heat loss parameters for the process
- Oxygen enrichment targets
- Feed blends, and
- Target slag compositions and metal grades.

Control parameters are built into the model, like how the plant would be operated, so that it becomes a realistic representation of the process. Other packages have been used at different times; however, Worley has invested significant time in the development of specific process related models that it represents a valuable resource to fast track process modelling and to ensure that our clients have tools that can assist them make decisions. In many cases, the client continues to use the model in same format as the project develops.

Plant A

This plant transformation involved conversion of a sinter plant blast furnace configuration to enhance environmental performance. Trade-off studies involved:

- Replacing only the sinter plant with new technology
- Replacing both the sinter plant and blast furnace.

The process commenced at preliminary process engineering and involved an extensive site visit to collect data, drawings, discuss possible locations for the new plant and to discuss interactions with the existing facility, including how best to incorporate the new plant. The process was interactive with the site technical and development team to ensure that the Worley project team knew all the site-specific limitations that would impact the final process design.

After completing the trade-offs and looking at the condition of the existing equipment on site, the ultimate decision was made to replace both the sinter plant and blast furnace with a single batch TSL facility. This simplified the modifications that were required on the plant. The new TSL feed conditioning plant, TSL facility, and off gas handling could be fitted into the existing facility. The batch operation involved running an oxidation process for a certain period and then changing to reduction. This had downstream impacts on the SO_2 capture plant as for some time, during the reduction process, there were little of no SO_2 laden gases delivered to the off gas handling plant.

The project was a brownfield modification, and Worley worked from process design to advanced basic engineering on the conventional flowsheet and then an advanced basic engineering on flowsheet modifications following a value engineering exercise and part detailed design. Worley also provided management assistance and systems for the Owners Engineering Team, construction assistance completions and commissioning, coordination and support were provided.

Worley, between 2008 and 2014, completed:

- Process (conceptual) design including $\pm$50% CAPEX
- Basic engineering on the conventional flowsheet including $\pm$15% CAPEX
- Cost reduction and value engineering exercise to reduce CAPEX
- Tendering and award of key technology packages
- Advanced basic engineering on the final flowsheet
- Detailed design of hot metals handling and slag granulation systems
- Detailed design of OSBL infrastructure and utilities.

Key management roles and assistance including systems for the Owners Engineering Team, construction assistance completions and commissioning, coordination, and support were provided.

The plant has reached more than name plate capacity, and an additional benefit has been an overall reduction in energy consumption at the plant of over 30%.

Plant B

Worley was engaged to carry out several concept studies (on TSL smelt/reduce and SKS smelt/reduce technology), a pre-feasibility study (on TSL and SKS technology). The technology providers were engaged as part of these studies included ENFI, Outotec, Xstrata, and MECS. Worley also executed the final feasibility study for the replacement and upgrade of the plant (feed preparation, sinter plant, acid plant, blast furnace, and feed system) with process plant based upon non-ferrous TSL oxidation technology.

The studies included TSL oxidation and reduction, TSL oxidation and blast furnace reduction, SKS two stage processing, and SKS oxidation with blast furnace reduction. With the TSL process, both Outotec and Glencore technologies were compared and costed. The various studies were completed over several years as the client developed the business cases to progress to project execution.

The study showed that all processes can treat the various feed blends that were being considered by the client. Parcels of concentrate were sent to China for process testing, and Worley provided technical assistance during the plant trial with ENFI SKS technology. To minimize the capital cost of the project, a strategy to utilise Chinese equipment supply including materials handling, coal grinding, TSL furnace, waste heat boiler, electro-static precipitator, gas cleaning and sulfuric acid, demineralised water, sea water pumps and slag caster, and fabrication where possible in a China based Module Yard fabrication was developed.

On completion of these studies, the customer engaged Worley to undertake part detailed engineering for the preferred option, subsequently engaged to initiate project specific PCM activities, including supplier purchase orders, site establishment, early works construction, and module yard contracts.

Ultimately, the client selected the Outotec TSL technology after completing the trade-off studies that took CAPEX and OPEX to ±30%. The ultimate decision was to install only one TSL furnace to produce synthetic slag to feed the existing modified blast furnace. The facility was constructed in a brownfields location, and the modification included the installation of a new acid plant to incorporate both the TSL and existing blast furnace off gas.

The new facility was developed to unlock a greater proportion of the value contained in a wider range of high margin feed materials including internal zinc smelter residues and concentrates. SO_2 capture was designed to increase from 50 to 98% for the new plant. Acid production was to increase significantly from ~200 to 1000 t/day.

Conclusions

The paper has outlined the approach that Worley has developed to execute lead smelting transformation projects. It discusses two recent projects that have advanced from conceptual studies to executed projects. The approach involves close liaison

with our clients, good understanding of the facility we are working to upgrade, and a good understanding of the project drivers to ensure that the project and process engineering are focused on the ultimate goal.

Acknowledgements We would like to thank Worley for their assistance in preparing this document.

GCRIS

Reduction of Lead-Rich Slags with Coke in the Lead Blast Furnace

Robin Vanparys, Geoffrey Brooks, M. Akbar Rhamdhani and Tijl Crivits

Abstract The reduction of lead-rich slag with metallurgical coke is one of the major reactions in the dripping zone of the lead blast furnace. However, because the conditions of this zone are hard to replicate in a laboratory experiment, previous studies have been limited to simplified reaction geometries. In this work, an experimental study is performed in a laboratory-scale set-up that more closely resembles the conditions inside the dripping zone of the lead blast furnace. A synthetic, lead-rich, $PbO–SiO_2–CaO–Fe_2O_3$ slag, is molten on top of a small-scale metallurgical coke bed with a total bed diameter of 35 mm, by heating for 15–60 min at temperatures of 1200–1300 °C. A multitude of particles, including lead-depleted slag, lead, and iron, were found on the coke surfaces. This illustrates the occurrence of the direct reduction reaction. The importance of coke surface morphology for reactivity with slag is emphasised, as the majority of reduced particles are found in pores and surface depressions.

Keywords Coke · Slag · Reduction · Lead smelting · Blast furnace · Pyrometallurgy

R. Vanparys (✉) · G. Brooks · M. A. Rhamdhani
Swinburne University of Technology, John Street, Hawthorn, VIC 3122, Australia
e-mail: rvanparys@swin.edu.au

G. Brooks
e-mail: gbrooks@swin.edu.au

M. A. Rhamdhani
e-mail: arhamdhani@swin.edu.au

T. Crivits
Umicore Research and Development, Watertorenstraat 33, 2250 Olen, Belgium
e-mail: Tijl.Crivits@eu.umicore.com

© The Minerals, Metals & Materials Society 2020

A. Siegmund et al. (eds.), *PbZn 2020: 9th International Symposium on Lead and Zinc Processing*, The Minerals, Metals & Materials Series,
https://doi.org/10.1007/978-3-030-37070-1_14

Introduction

The lead blast furnace has historically been a staple in the lead smelting process. Its main purpose is the reduction of a PbO-rich feed with metallurgical coke, in order to produce metallic lead. Despite the rise of new technologies over the past decades, it remains highly relevant, as many lead production sites still use a blast furnace in their flow sheets [1, 2]. A schematic illustration of the lead blast furnace is provided in Fig. 1. Different reaction mechanisms for the reduction of lead-rich slags are known, and all of them can occur in parallel in the blast furnace. The main reactions are the indirect reduction reaction and the direct reduction reaction. The former implies that the reductant is a gaseous CO environment (Eq. 1), whereas the latter involves a solid carbon reductant, such as coke, to interact locally with the slag, regardless of the atmosphere present (Eq. 2). The exact mechanism of these reactions is still subject to some debate, but most hypotheses include either a hopping mechanism of O^{2-} species in the slag phase with counter-current electron transport, or the development of a localised bubble of gas containing CO and CO_2, where the CO is regenerated by the Boudouard reaction with coke.

$$\mathrm{PbO(slag, l) + CO(g) \rightarrow Pb(l) + CO_2(g)} \tag{1}$$

$$\mathrm{PbO(slag, l) + C(s) \rightarrow Pb(l) + CO(g)} \tag{2}$$

Several studies on lead blast furnaces, using sinter as feed, indicate that the majority of reduction reactions occur in the region where the temperature exceeds 800 °C, labelled “melting zone” in Fig. 1, since feed material starts to melt there [3–9]. This illustrates the importance of reactions between liquid slags, rich in PbO, and metallurgical coke. However, because the conditions of this zone are hard to replicate in a laboratory experiment and because coke is a very complex material, previous kinetic studies have been limited to simplified reaction geometries. Some examples include sessile drop testing and the submersion of carbonaceous materials, with an accurately specified shape, in liquid slags.

The need for a different test method has been raised in the previous work [10]. In the current work, the first steps towards this new approach are taken. An initial experimental study is performed in a laboratory-scale set-up that more closely resembles the conditions of the dripping zone of the lead blast furnace. In the study, synthetic lead-rich slag is molten on a small-scale bed of metallurgical coke, inside a vertical tube furnace. The mechanism of reduction as well as the flow behaviour of the dripping slag is investigated. Studied parameters include temperature, reaction time, and coke particle size.

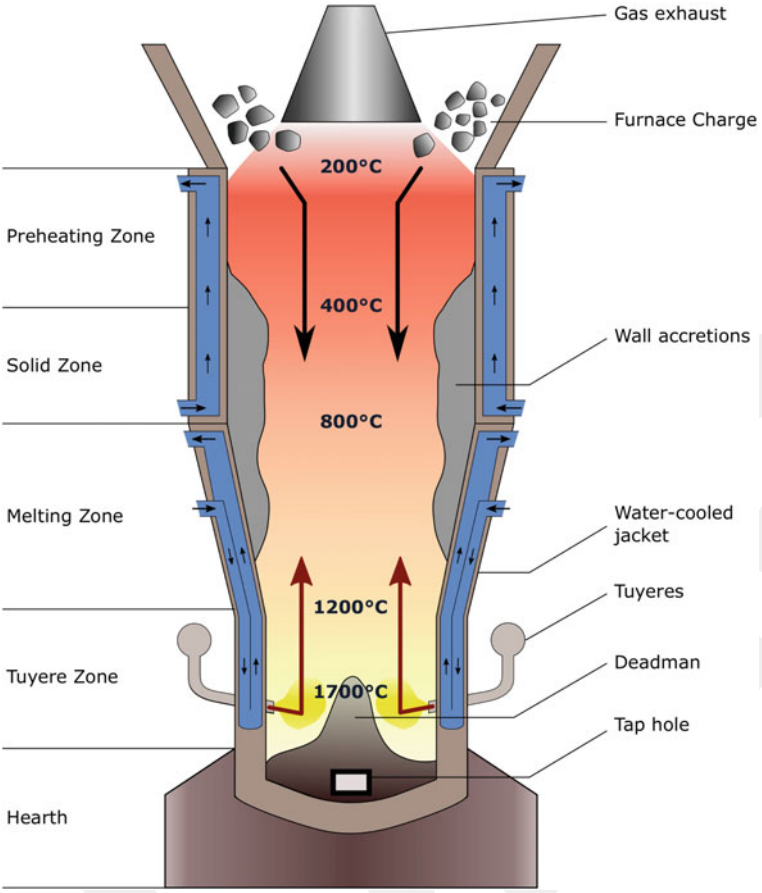

Fig. 1 Schematic illustration of the lead blast furnace with indication of the reaction zones (left), gas temperature at different heights (centre), and other labels (right)

Methodology

The approach used in this study consists of making a synthetic, PbO-rich slag, similar in composition to that found in the lead blast furnace, and to melt them over small-scale coke beds in a vertical tube furnace. In this set-up, the slag drips down through the coke, which will reduce the slag and produce metallic lead. The methodology of these experiments can be subdivided into three categories: the preparation of the materials before melting, the procedure of the dripping experiments, and the analysis of the samples after the experiments. Each will be briefly discussed in subsequent sections.

Slag and Coke Preparation

The chemical properties of the metallurgical coke used for this study are listed in Table 1 and the physical properties in Table 2. The coke size needed to be reduced to allow for use in small-scale experiments. The coke originally had an average lump size larger than 60 mm and it was, therefore, crushed using a hydraulic press. The crushed coke was passed through a series of pan sieves with a square grid, to separate the different size fractions. Doing so, the size fraction with a size between 4.75 and 6.7 mm was isolated, as well as the fraction from 6.7 to 9.5 mm. These fractions will be referred to as the larger and smaller coke size, respectively.

The synthetic slag composition was chosen to resemble a simplified feedstock composition of a secondary lead blast furnace, i.e. a blast furnace using secondary resources rather than ore. In particular, the emphasis is put on a furnace that uses a slag that stems from an oxidative process (such as a copper smelter) as its main feed. Hence, sulphur was not included. The thermodynamic software package FactSage was used to calculate the equilibrium compositions and other important parameters such as liquidus and solidus temperature [11]. High purity powders of PbO (>99.9%), $CaCO_3$ (>99%), Fe_2O_3(>99%), and SiO_2 (>99.5%) were used to prepare the slags. The SiO_2 was sourced from Alfa Aesar, the others from Sigma-Aldrich. Table 3 lists the desired slag composition. The predicted liquidus temperature for this composition was 1235 °C, whereas the predicted solidus temperature was 700 °C. To make the slag, 2 parts by weight of PbO, 2 parts SiO_2, 1 part Fe_2O_3, and 1.785 parts $CaCO_3$ and mixed in a tumble mill for 6 h at 50 RPM. This mixture was then transferred to an alumina crucible, molten in a muffle furnace at 1300 °C for 6 h, and subsequently cast and air quenched. X-ray fluorescence on the cast slag confirmed that the composition

Table 1 Coke chemical properties

Chemical properties	As received	Dry base
Total moisture (%)	5.3	/
Ash (%)	9.2	9.7
Volatile matter (%)	0.55	0.58
Fixed carbon (%)	84.95	89.72
Sulphur (%)	0.64	0.68
Carbon (%)	84	88.7
Hydrogen (%)	0.29	0.31
Gross cal. value (kJ/kg)	28,454	30,046
Net cal. value (kJ/kg)	28,271	29,982

Table 2 Coke physical properties

Physical properties	
Micum M 10 (%)	5.5
Micum M 40 (%)	92.2

Table 3 Synthetic slag composition

Oxide	PbO	SiO_2	Fe_2O_3	CaO	Al_2O_3
Desired (wt%)	33.33	33.33	16.67	16.67	0.00
Measured (wt%)	31.7	30.36	17.28	14.76	5.90

was close to the desired one, as shown in Table 3, with an additional 6 wt% of Al_2O_3 due to the dissolution of the crucible. The quenched slag was crushed to obtain chunks of approximately 5 mm. Slag uniformity was checked and confirmed by EDX analysis.

Experimental Procedure

The set-up of the dripping experiments is illustrated in Fig. 2. This is based on similar experimental procedures used to study the flow of non-reactive slags through coke beds [12–14]. Experimental runs were started by filling an alumina crucible with coke particles to create the bed of coke, after which the slag pieces were positioned on top. In each experimental run, 20 g of coke and 20 g of slag were used, and the crucibles had an internal diameter of 35 mm. For both the smaller and larger coke size, this resulted in a coke bed height of approximately 40 mm. The crucibles were then inserted into a vertical tube furnace on a pedestal. They were left at a height where the temperature would not exceed 700 °C, the FactSage predicted solidus temperature of the slag, while the furnace was heating up. When the desired furnace temperature was reached, the samples were raised to the hot zone, where it was left for a fixed amount of time, depending on the experimental parameters. After this designated time, the sample was lowered again to the zone with a temperature below 700 °C and the furnace was switched off. During the entire experiment, the furnace was kept under an inert atmosphere, using an argon flow rate of 100 ml/min. The varied experimental parameters included the two different coke sizes, temperatures of 1200 and 1300 °C, and time spent at the temperature, ranging from 15 to 30 to 60 min. The temperatures were chosen to represent those in the melting zone of the blast furnace, and to ensure the synthetic slag would be fully (1300 °C) or at least mainly (1200 °C) liquid during the experiments.

Sample Preparation and Characterisation

After the samples cooled down, some coke particles were taken from the top of the crucible, in order to analyse their surface area under a scanning electron microscope (SEM) and perform energy-dispersive X-ray spectroscopy (EDX). The pieces were nano-coated with gold for 45s with a sputter current of 40 mA, to avoid electron

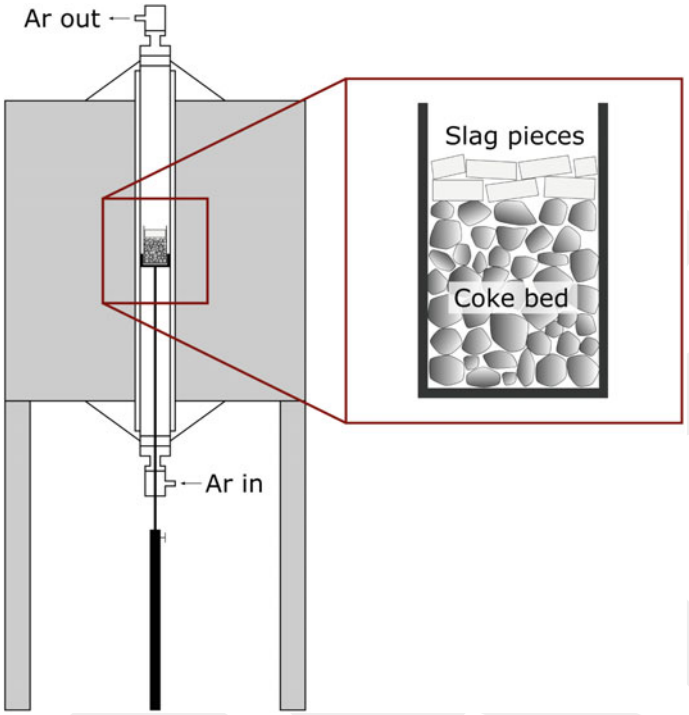

Fig. 2 Illustration of the experimental set-up used in this work, i.e. a vertical tube furnace with an enlarged view of the crucible containing the coke bed and slag pieces

charging. The SEM used for these analyses was a ZEISS SUPRA 40. A working distance (WD) of 10 mm and accelerating voltage (AV) of 10 kV were used for the secondary electron images, and a WD of 14 mm and AV of 20 kV for the EDX mapping. Additionally, the remainder of the crucible was cold mounted by filling it with degassed epoxy. After adding the epoxy, the sample was degassed again under high vacuum, to extract any air from the pores in the coke bed. The crucible was then cross-sectionally cut using a diamond rotary cutter. A cut was made at 10 mm intervals, starting at 2 mm above the bottom of the coke bed. This allows visualisation of the slag flow and reactivity behaviour over the height of the crucible, as well as providing cross-sectional information about the reaction interfaces between coke, slag, and reduced phases. After cutting, these sections were cold mounted under vacuum in 40 mm cups to get consistent sample diameter and to backfill any remaining pores. The surfaces were ground and polished up to a final step with 1 μm diamond paste and analysed under an optical microscope.

Results and Discussion

In the results section, the focus is on the SEM secondary electron images and EDX analysis of coke surfaces after they have been subjected to the dripping experiments. Figures 3, 4, 5, and 6 show a range of surface phenomena observed under the electron microscope, whereas Fig. 7 shows an EDX elemental mapping of some particles which are found on the coke surfaces. The observations will be discussed in more detail the following paragraphs.

In every experimental run performed at 1300 °C, regardless of coke size or reaction time, the slag was fully molten and dripped down through the coke bed. This was also confirmed by optical microscopy of the cross-sectional slices of the bed. Microscopy also demonstrated the presence of two different phases at the bottom of the crucible, most likely the reduced lead and lead-depleted slag. Some very small and shiny spots could be observed on the coke surface. In the experiments performed at 1200 °C, the slag did not fully melt, as it was below the liquidus temperature. The partially molten slag remained on top of the coke bed.

A few pieces of coke from the top of every crucible were taken after the dripping experiments at 1300 °C, before filling the crucible with epoxy. SEM surface analysis of these coke pieces revealed the presence of many spherical particles on the outer

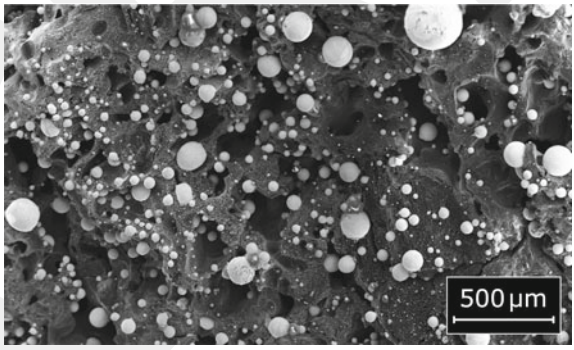

Fig. 3 Secondary electron image of coke surface after dripping experiment for 30 min at 1300 °C, illustrating the large amount of particles on the surface

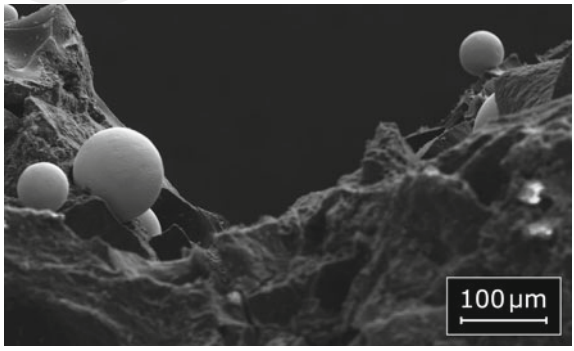

Fig. 4 Secondary electron image of coke surface after the dripping experiment of 60 min at 1300 °C, showing the poor wetting behaviour of the particles

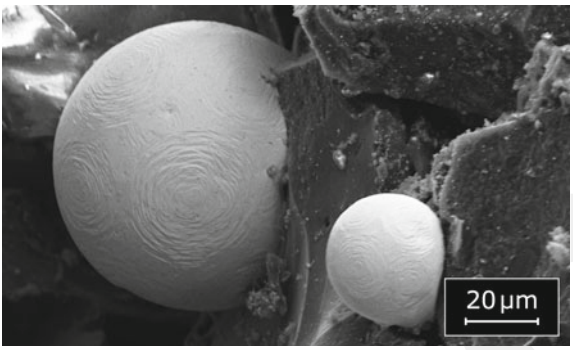

Fig. 5 Secondary electron image of coke surface after the dripping experiment of 60 min at 1300 °C, with emphasis on the ripple-like structure of the particles

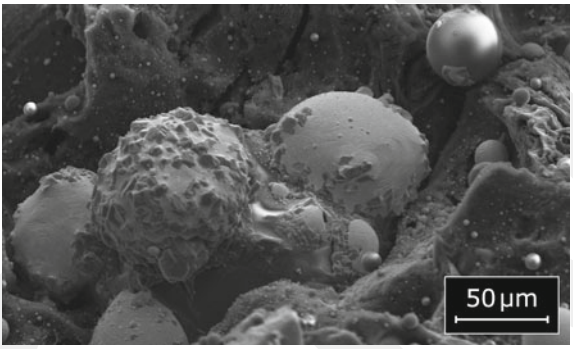

Fig. 6 Secondary electron image of coke surface after the dripping experiment of 60 min at 1300 °C, demonstrating the different types of particles and phases found

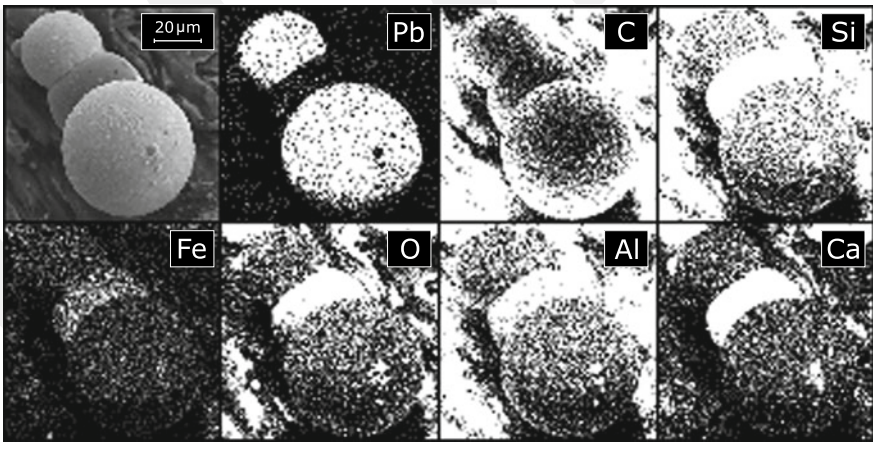

Fig. 7 Secondary electron image of particles found on the coke surface after the dripping experiment of 60 min at 1300 °C with included EDX elemental mappings for Pb, C, Si, Fe, O, Al, and Ca

surface of the coke, as shown in Fig. 3. These cover a large section of the coke surface, but some regions remain uncovered. The uncovered zones did most likely not come in contact with any dripping phases throughout the experiment. The particles appear lighter in colour than the coke substrate and range in size from 5 to 200 μm. EDX analysis was performed to determine the composition and it was found to be a lead-rich phase, presumably the reduced metallic lead. This indicates that initially, the direct reduction reaction (Eq. 2) has taken place, since no air was present throughout the experiment, and hence no CO could have been generated by incomplete coke combustion. The generated CO gas from this direct reduction reaction, however, could in its turn cause further reduction of the slag, by means of the indirect reduction reaction (Eq. 1).

Wetting between the particles and coke is extremely poor, as observed by the spherical, droplet-like shape. This can also be seen in Fig. 4, where the contact angle can be observed to be approximately 180°. When looking more closely at the surface of these spheres, one can observe a ripple-like structure of ledges, as demonstrated in Fig. 5. This structure is likely caused by crystallisation of the lead droplets during cooling, developing facets, as is observed in other studies [15]. Besides the spherical droplets, some other phenomena can be observed. Another type of spherical particle is found, for example, as shown in Fig. 6 on the upper right corner, slightly darker in colour, and smaller in size. This phase proved prone to slight electron charging, despite the gold nano-coating. Its surface is completely smooth and no evidence of crystallisation is found. All of these factors point to a glassy slag phase, which is also confirmed by EDX. EDX also showed that the lead content in this phase was very low, indicating that the reduction of the slag has taken place to a large extent. In Fig. 7, we see one such particle surrounded by two of the lead particles discussed previously. The element mapping supports the hypothesis that the darker particles are lead-depleted slag and the lighter ones are metallic lead.

Additionally, in Fig. 6, one can also see a complex aggregate of different phases. Upon closer inspection, we can see that it is one of the slag particles surrounded by four lead droplets. The lead droplets also have another, polygonally shaped phase dispersed over its surface. These particles are positioned on the top of the lead droplets, indicating they are lighter and hence float. EDX analysis confirmed these to be an iron-rich phase with oxygen. However, EDX analysis cannot reliably quantify oxygen content, so to determine the phases that potentially formed; a thermodynamic calculation was performed using FactSage. This was done by using the actual slag composition, as listed in Table 3, and subjecting it to decreasing oxygen partial pressures, to simulate the reducing environment produced by the coke. This is illustrated in Fig. 8. It shows the production of a spinel phase (almost purely Fe_3O_4, i.e. magnetite), but with decreasing oxygen partial pressure this is reduced to Fe_2O_3, which redissolves into the slag. As the oxygen partial pressure is lowered, the Fe_2O_3 in the slag reduced to FeO before the reduction of liquid lead occurs. Finally, after all the lead is reduced, the FeO starts to reduce to form solid iron. This implies that the phase that was detected is either a spinel phase or solid iron crystals. Since EDX analysis confirms that the slag was fully depleted in lead and its iron content was

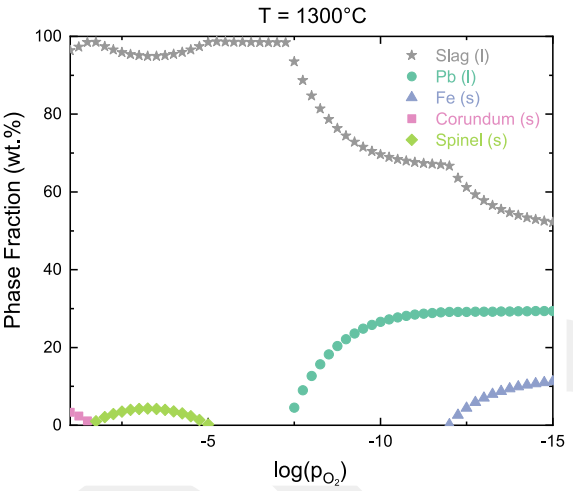

Fig. 8 Phases produced from the reduction of slag, with composition of 31.7 wt% PbO, 30.36 wt% SiO_2, 17.28 wt% Fe_2O_3, 14.76 wt% CaO, and 5.90 wt% Al_2O_3, for varying oxygen partial pressures at 1300 °C. Thermodynamic calculations were performed using FactSage. The gas phase is not included on the figure, but it contains the oxygen that is removed from the slag and makes up the remainder of the weight

significantly lower than the starting concentration, the latter is more likely. The presence of oxygen can in this case be explained by oxidation of the iron after the experiment was complete, by contact with air.

The samples that had reacted for shorter times showed a much higher presence of lead-slag particle agglomerates as well as separate slag particles. This is most likely due to the shorter reaction time, and hence the larger amount of slag that is not yet fully reduced. The presence of these droplets of lead and slag is unexpected due to the non-wetting nature of both phases with coke. If the fixed bed consisted of smooth spheres, which were also non-wetting with both the slag and the lead, one would expect the flow of slag and lead to remain rivulet-like and leave no trace on the spherical bed. Coke is not spherical, however, and not perfectly smooth. Hence, the multitude of crystallised lead-rich droplets should be strongly linked to the morphology of the coke surface. They appear mainly at sites which are in localised depressions, such as pores and crevices. Some hypotheses are provided for these observations.

The first is that lead is reduced from the slag by contact with the coke surface, without any preferential sites for this reaction. As the lead is formed, it gathers in droplets which come in contact with the coke surface, because they are denser than the slag. As they drip downwards, the depressions in the coke provide sites with locally lowered gravitational potential energy, and to get out of them requires to overcome an energy barrier, which proves too great for the smaller droplets. Droplets in these depressions cannot escape because they are trapped in a gravitational potential energy well, like water in a lake above sea level. As the lead particles coalesce and grow in size, they could overcome this and continue dripping downwards, like the lake overflowing after heavy rain. A second theory is that as the slag reacts with the coke, it creates its own local depressions by removing the carbon it is reacting with. The pores would then increase in size as the reaction proceeds. A third hypothesis is that as the slag drips down, it reacts preferentially with cavities such as pores. A possible explanation for this is that the pores allow the formation of a locally stable gas pocket

within the cavity, separating the slag from the coke. The presence of a gas phase has been suggested as an essential part for the reduction of slag with coke, because the gas-ferrying mechanism has been listed as one of the main reaction mechanisms in both reduction of iron and lead from slags [16–18]. It can be summarised as follows:

1. Initial reduction of PbO generates a CO bubble:

$$\mathrm{PbO(slag)} + \mathrm{C(s)} \rightarrow \mathrm{Pb(l)} + \mathrm{CO(g)} \tag{3}$$

2. Mass transfer of PbO through the slag to the gas/slag interface
3. Gaseous (indirect) reduction reaction at the gas/slag interface:

$$\mathrm{PbO(slag)} + \mathrm{CO(g)} \rightarrow \mathrm{Pb(l)} + \mathrm{CO_2(g)} \tag{4}$$

4. Diffusion of gaseous species in the gas phase surrounding the carbon
5. Boudouard reaction at the gas/carbon interface:

$$\mathrm{C(s)} + \mathrm{CO_2(g)} \rightarrow 2\mathrm{CO(g)} \tag{5}$$

Due to the dynamic nature of the melting zone of the blast furnace, it is difficult for stable gas bubbles or films to form and hence to allow this mechanism take place. However, on a localised scale within the pores of coke as just discussed, this is definitely possible. The presence of lead in the pores is in this case not explained because it gets trapped there as it is dripping down, but rather because it is preferentially formed in exactly those locations.

Outlook and Future Work

The results provided in this work are in the early stages of analysis. Further work to verify some results as well as more accurate tests will be performed, such as EPMA to confirm the exact composition of all the phases. Another aspect that will be investigated is how the cooling procedure affects the formed structures. Because the cooling was performed quite slowly in the current work, some surface phenomena can be influenced by the cooling and give a distorted view of the high-temperature reality. A set of duplicate experiments will be performed, in which one sample is quenched to room temperature, and the other is quenched to 700 °C and then oven cooled, like was performed in this study. Another important thing to note is that this is essentially a batch process representation of a continuous process. This way of representation has its limits, as the bottom of the crucible will build up in end products for instance. Another consequence of this is that it is unknown whether the phenomena observed here also hold when a continuous supply of "fresh" slag is added. If the hypothesis of localised gas pockets proves valid, this could also hold under these conditions, as the gas pockets would be shielded from the flow of liquids. These issues and other aspects of the system will be studied by making small modifications to the set-up to make it more closely resemble the blast furnace.

Conclusions

The lead blast furnace remains an important reactor for the production of lead. The reduction reaction between coke and liquid slags is vital towards understanding it. A novel experimental approach is taken in this work to study this reaction in a laboratory-scale experiment that more closely resembles the conditions of the dripping zone of the lead blast furnace. By dripping synthetic lead-rich slag on small-scale beds of metallurgical coke and analysing those beds post-reaction, a lot of interesting surface phenomena were observed. The presence of many lead-rich spherical particles, small iron-rich phases, and lead-depleted slag was observed and verified by EDX. Such observations have, to the author's knowledge, not been reported before. These indicated that initially, the direct reduction reaction did occur, since the experiments were performed under an inert atmosphere. A preferential occurrence of the formed phases was observed near coke porosities and local depressions. Several hypotheses to explain this behaviour were discussed, but overall it indicates the importance of coke surface morphology in the reactivity with reducible slags.

References

1. Siegmund AHJ (2000) Primary lead production—a survey of existing smelters and refineries. In: Lead-zinc 2000, Wiley, pp 53–116
2. Hayes P, Schlesinger M, Steil HU, Siegmund A (2010) Lead smelter survey. In: Lead-zinc 2010. Wiley, pp 345–413
3. Hussain MM, Morris DR (1986) Reduction of lead minerals by CO/CO_2 gas mixtures: application of the grain model. Metall Trans B 17(3):575–586
4. Hussain MM (1987) Ore reduction kinetics and simulation of a lead blast furnace. Ph.D. Thesis, University of New Brunswick
5. Chao JT (1981) Analysis of packed bed processes: I. Simulation of a lead blast furnace. II. Analysis of adsorptive separation processes. Ph.D. Thesis, University of New Brunswick
6. Morris DR, Amero BR, Evans PG, Petruk W, Owens DR (1983) Reactions of sinter in a lead blast furnace. Metall Trans B 14(4):617–623
7. Chao JT (1981) A dynamic simulation of a lead blast furnace. Metall Trans B 12(2):385–402
8. Chao JT, Dugdale PJ, Morris DR, Steward FR (1978) Gas composition, temperature and pressure measurements in a lead blast furnace. Metall Trans B 9(3):293–300
9. Zhao G (1993) Coke performance in lead blast furnaces. Ph.D. Thesis, Monash University
10. Vanparys R, Brooks G, Rhamdhani A, Crivits T (2019) Slag-coke interactions in the lead blast furnace. In: EMC 2019, vol. 1, pp 181–196
11. Bale C, Chartrand P, Degterov S, Eriksson G, Hack K, Mahfoud RB, Melançon J, Pelton A, Petersen S (2002) FactSage thermochemical software and databases. Calphad 26(2):189–228
12. Husslage WM, Reuter MA, Heerema RH, Bakker T, Steeghs AG (2005) Flow of molten slag and iron at 1500 °C to 1600 °C through packed coke beds. Metall Mater Trans B 36:765–776
13. George HL, Longbottom RJ, Chew SJ, Pinson DJ, Monaghan BJ (2014) Characterisation of coke packed beds after liquid slag flow at 1500 °C by image analysis. ISIJ Int 54(8):1790–1796
14. George HL, Longbottom RJ, Chew SJ, Monaghan BJ (2014) Flow of molten slag through a coke packed bed. ISIJ Int 54(4):820–826
15. Chatain D, Galy D (2006) Interfaces between Pb grains and Cu surfaces. J Mater Sci 41(23):7769–7774

16. Teasdale SL, Hayes PC (2005) Kinetics of reduction of FeO from slag by graphite and coal chars. ISIJ Int 45(5):642–650
17. Teasdale SL, Hayes PC (2005) Observations of the reduction of FeO from slag by graphite, coke and coal char. ISIJ Int 45(5):634–641
18. Fun F (1970) Rates and mechanisms of FeO reduction from slags. Metall Trans 1(9):2537–2541

GCRIS

Installation of a Brown Field Slag Reduction Furnace: State of the Art Off-Gas Treatment with Dry Gas Cleaning for SO_2 Capture

Peter Weber, Dirk Behrmann, Thomas Breuer and Rüdiger Margraf

Abstract A new lead slag reduction furnace for the treatment of lead-rich slags from an existing top submerged lance (TSL) furnace has been installed at the Weser-Metall (WMG) lead plant in Nordenham, Germany. With the new reduction furnace, the lead content in the slags is lowered significantly, and lead bullion is produced. A Chinese side-blowing furnace (SBF) was selected for the reduction, and all plant technology around the furnace was engineered and supplied by Germany based company Kuettner. The furnace was integrated and further adopted into a Kuettner process concept to comply with European and clients' standards. The concept includes an off-gas treatment layout with a direct connection from furnace to waste heat boiler and controlled forced-air combustion to mitigate accretion formation in the boiler. Due to environmental requirements, this expansion of the lead operations had to ensure a decrease of the existing emission footprint of the entire plant. To accomplish this, Kuettner has installed a flue gas process line for the slag reduction furnace which integrates several existing emission sources from TSL operations and guarantees dust emissions below 0.2 mg/Nm^3 and SO_2 values below 250 mg/Nm^3 without the need for wet scrubbers.

Keywords Lead · Slag reduction · Side-blowing furnace · Off-gas treatment

Introduction and Actual Situation

At the production site of Weser-Metall GmbH (WMG) Nordenham, lead is produced out of primary and secondary input material. The main unit of this lead production process is a so-called top submerged lance (TSL) furnace.

P. Weber · D. Behrmann (✉) · T. Breuer
Küttner GmbH & Co. KG, Alfredstraße 28, Essen, Germany
e-mail: d.behrmann@kuettner.com
URL: https://www.kuettner.com

R. Margraf
Lühr Filter GmbH, Enzer Str. 26, Stadthagen, Germany

© The Minerals, Metals & Materials Society 2020

A. Siegmund et al. (eds.), *PbZn 2020: 9th International Symposium on Lead and Zinc Processing*, The Minerals, Metals & Materials Series,
https://doi.org/10.1007/978-3-030-37070-1_15

In the TSL process lead bullion, slag and waste gas are produced. The lead bullion is treated in a refining plant to produce lead alloys and crude silver. However, the product slag from the TSL still contains 36–63% Pb. Before the new plant was built, this slag was sold abroad for treatment to recover lead.

With the goal of recovering valuable lead metal from the TSL slag, WMG wanted to expand the site with a lead recovery plant based on the so-called side-blowing furnace (SBF) technology. The furnace shell was sourced by WMG themselves from China, while the rest of the plant equipment supply, the adaptation of the Chinese technology to European standards, and the integration into the existing production site was accomplished by German company Kuettner as an EPC project.

Due to environmental requirements, this expansion of the lead operations had to ensure a decrease of the existing emission footprint of the entire plant. Therefore, a state of the art off-gas system had to be designed to meet most stringent standards not only with respect to dust emissions but even more so when it comes to limit the SO_2 emission to a maximum of 250 mg/Nm^3. This is achieved without using a wet scrubbing system with its inherent cost for effluent treatment. In addition, the new off-gas system integrates several existing emission sources from TSL operations to facilitate the reduction of overall plant emissions.

Process Description

The raw materials to be treated in the SBF are liquid primary slag from the existing TSL, as well as some solid TSL or other furnace slag from stockpile. The function of the SBF reduction furnace is to reduce the lead content in the slag and to recover lead as metal bullion.

The operation of the reduction furnace is in batch mode. Batch duration is 120 min, which means that the reduction furnace requires fresh slag from the TSL furnace every two hours. A general outline of plant data of the new installation is given in Table 1.

Table 1 Plant data of the new SBF plant

	Design	Actual
Throughput	140,000 t/a	Achieved
Input slag	36–63% Pb	Achieved
Process mode	Batch process	Achieved
Tap-to-tap time	120 min.	Achieved
Output slag	<2% Pb	Achieved
Dust emissions	<0.2 mg/Nm^3	Achieved
SO_2 emissions	<250 mg/Nm^3	Achieved

In the SBF furnace, the lead-high input slag is reduced to lead content below 2%. Coke, which is supplied to the furnace with other solid input materials, is used as reducing agent. Air is injected through submerged primary tuyeres to strongly agitate the melt and pre-combust carbon to carbon monoxide. Secondary and tertiary air are injected into the off-gas flow to ensure complete post-combustion and defined off-gas temperature.

The products of the SBF furnace are

- Lead bullion containing Antimony
- Secondary slag at <2% Pb
- Dust rich in Pb and Zn (to be recirculated).

The Kuettner scope as an EPC supplier included the following equipment around the furnace:

- Raw material storage
- Input material conveying and dosing
- Off-gas post-combustion
- Waste heat boiler
- Water quenching
- Filter unit
- Furnace cooling water system
- Complete media supply
- Slag granulation
- Lead decoppering kettles.

A schematic flow diagram of the main plant units is given in Fig. 1

SBF—Side-Blowing Furnace

General

The furnace has a rectangular shape and consists from bottom to the top of mainly three sections, as shown in Fig. 2:

- Furnace hearth zone
- Furnace body/Smelting zone
- Furnace post-combustion zone.

The furnace is equipped with submerged bath tuyeres, so-called primary tuyeres, which are arranged on both long side walls of the furnace in the melting zone. In the post-combustion zone, secondary air tuyeres are arranged along the furnace long side walls.

The furnace top consists of the process gas offtake for the process gas and the material feeding ports in the roof of the furnace. In addition, there is also a feed port

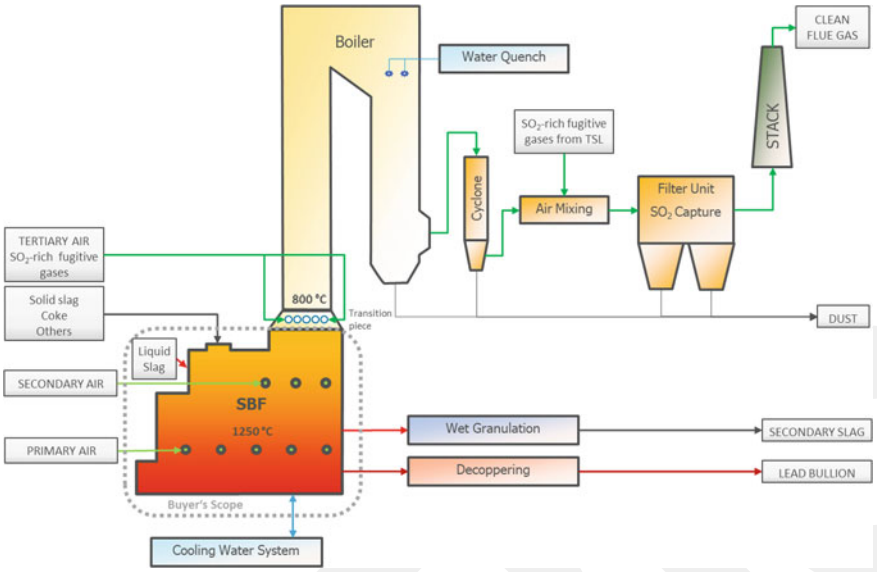

Fig. 1 Schematic flow diagram

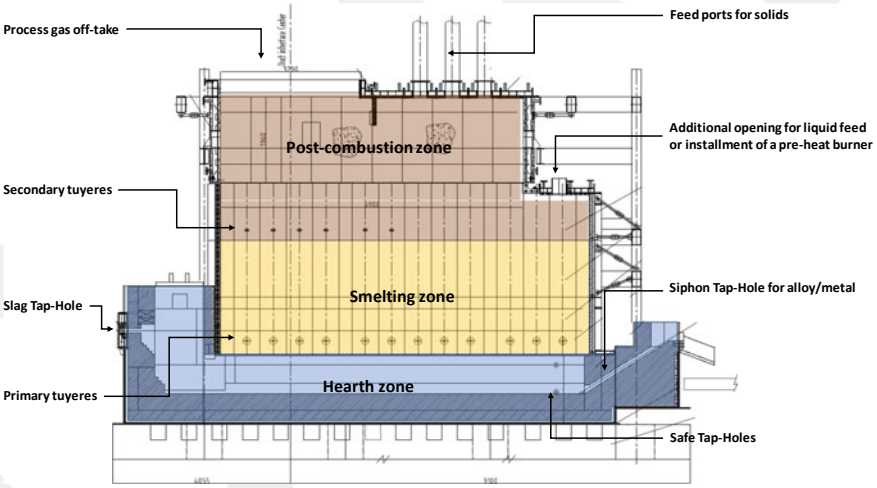

Fig. 2 Schematic side section view of an SBF example with indication of its main zones

in the lower part of the furnace roof for feeding of liquid material. Either port may be used for the installation of a pre-heat burner.

The furnace has four tap-holes:

- An alloy or metal siphon
- One slag tap hole for the produced slag each batch

- One tap hole to remove matte if necessary
- One emergency tap hole for fast discharging.

Furnace Hearth

The rectangular furnace hearth is made of a welded steel construction which is refractory lined, and it is formed as a trough shape with the metal siphon at the lowest point.

Lead will be discharged by this siphon, while slag is discharged by the slag tap hole at the front end of the furnace. In case of matte formation, the matte phase may be discharged from the furnace through the matte tap, which is located at the level of the slag/lead interface. The emergency tap hole is used for complete discharging of the furnace during shutdown.

Furnace Body

The furnace walls in the smelting zone consist of water-cooled panels arranged in three rows. The cooling panels are made of cast electrolytic copper. During furnace operation, cooling water circulates through the panels. At the cold inner surface of the cooling panels, the molten slag freezes and forms a so-called freeze-lining. Kuettner introduced independent cooling water supply and controls for each of the 128 individual circuits, thereby providing detailed monitoring and improved automated controls of the furnace cooling while contributing to operational safety.

Primary air tuyeres are installed at each long side wall in the lower panel row. These primary tuyeres are operating submerged in the molten slag. Oxygen enriched air is blown at high speed via these tuyeres into the melt, vigorously agitating the slag melt and thus ensuring a high degree of intermixing of all reactants.

Upper Furnace

Initial post-combustion takes place above the molten slag. The furnace shell in this area consists of a water-cooled copper panel layer and is covered in the roof by water-cooled steel panels.

Secondary tuyeres are installed on each side wall of the post-combustion zone to enable post-combustion of combustible gases such as CO (carbon monoxide) and metal vapors such as lead and zinc.

Highlighted Equipment

For the WMG installation, Kuettner developed an off-gas treatment concept including the final SBF post-combustion and boiler system with integration of Chinese third-party furnace technology.

Post-Combustion Transition Zone

To ensure full post-combustion of the process gas, so-called tertiary air is supplied to the transition zone between the SBF and the waste heat boiler in controlled form. A defined and controlled extra amount of tertiary air is added to control the temperature of the combusted process gas. The injection of the tertiary air has been modelled and designed to ensure proper mixing and temperature homogeneity of the process gas.

The waste gas generated in the reduction furnace contains a high content of dust, mainly lead oxide. From the thermodynamic point of view, lead oxide will partly form lead sulphate together with sulphur dioxide. This dust from the reduction furnace tends to form sticky accretions at a certain temperature window. This can cause harmful accretions on the boiler walls and heat exchanger tubes. The design of the controlled tertiary air supply accounts for this temperature window and maintains defined process gas temperature at the boiler inlet. This leads to a mitigation of the accretion risk in the boiler.

The gas amount used as tertiary is comprised of process gases with some SO_2 content from suction points in the furnace area.

Waste Heat Boiler/Quench

It is necessary to cool down the process gas and the dust from the SBF furnace. This is achieved in a waste heat boiler consisting of two radiation passes with integrated water quench.

The flue gas passes through the first shaft going up and passes the second shaft going down. At the top of the second shaft, the water quench is installed to cool down the gas further. At the bottom of the second shaft, a dust box with screw conveyor is installed to remove the dust that is separated in the second shaft.

Since the waste gas from the SBF will contain a certain amount of SO_2, it is necessary to account for the acid dew point of the gas. Therefore, the feed water in the steam drum is preheated before it enters the first boiler pass. The boiler is designed as a saturated steam boiler.

Water from the steam drum is fed through the downpipe to the evaporator in the walls of the boiler where it is evaporated partly, cooling the flue gases. The steam–water mixture generated thus is led through the riser back to the steam drum. Due to differences in density (water in downpipe/steam–water mixture in the riser), a natural circulation arises in the cooling circuit.

The generated steam is collected in the steam drum situated on top of the boiler passes. The steam drum is provided with a blow downpipe for partly dewatering in order to reduce the salt content in the feed water.

Off-Gas Treatment

To reduce the dust load in the exhaust gas in a first process step, a cyclone separator designed by Kuettner is installed behind the boiler. The separated dust is removed with water-cooled screw conveyor.

Downstream of the cyclone, further waste gas cooling takes place to maintain the desired filter inlet temperature of approx. 140 °C. It consists of a cooler where SO_2 containing fugitive gases are injected into the gas stream. This cooler has been modelled and designed to ensure proper mixing and temperature homogeneity of the process gas.

As an additional benefit, in this cooler, process gas from existing TSL operations is injected. This, along with the new filter, leads to a decrease of the overall site emissions by the new installation.

Slag Granulation

The wet slag granulation was designed by Kuettner to ensure safe and reliable treatment of hot liquid slag from the SBF furnace. The granulation itself is executed in the granulation box, where hot liquid slag flows from the top into a defined water stream. Upon contact with the water stream, the slag is dispersed into small particles while being rapidly solidified and cooled. The water/granulate mixture is led through the granulation runner from the granulation box to the granulation basin, where the granulate settles at the bottom. The slag granulate is taken out of the basin by an automated crane grab, which serves the whole basin incrementally according to a grid pattern.

The water in the granulation basin flows via an overflow to the so-called hot-water basin. From here, the water is pumped to a cooling tower to reduce the temperature. The cooled-down water from the cooling tower flows to the so-called cold water basin, from where the water is pumped back to the granulation box.

Process Gas Treatment (Filter)

Two filters have been installed for gas cleaning:

- Process gas filter for the separation of SO_2 and particles incl. heavy metals
- Hygiene gas filter for the dedusting of gas from suction points around the new installation.

Both filter lines are executed in multiple chambers: 2 (hygiene gas filter) and 4 (process gas filter). This allows maintenance activities during regular operation of the plant.

The filtration plants are illustrated in Fig. 3. On the left, the hygiene gas filter is shown and on the right the process gas filter with reactor and insulation.

Fig. 3 Hygiene gas filter (left) and process gas filter (right)

Filter Technology

Separation of Particulate Matter

Due to the heavy metals contained in the gas, an extremely low emission limit value totalling 0.2 mg/Nm^3 for particles is required for both filters. To allow the reliable observance of this value, both filters have been realised as two-stage processes. The first stage is a flat-bag filter with compressed air cleaning system, provided with high-efficient needle felt bags. The clean gas values downstream of the first stage are well below 1 mg/Nm^3. In order to observe the requested limit value of 0.2 mg/Nm^3, a second filter stage has each been provided downstream consisting of flat-bag filters, equipped with non-regenerative pocket-type filter units.

SO_2—Removal

The SO_2 contained in the process gas has to be reduced to emission values <250 mg/Nm^3. To avoid a complex waste water treatment system that would be necessary if wet scrubbers were used, a conditioned dry process with the injection of $Ca(OH)_2$ as additive powder has been chosen for this application. The process allows the simultaneous separation of particles, heavy metals, and acid crude gases. It is characterized by a highly efficient separation and a residual product in dry form.

The chosen process variant is the LUEHR FILTER Conditioning Rotor—Recycle Process. Figure 4 shows a schematic view of process which mainly comprises the following component parts:

- Additive powder storage, dosage, and transport
- Entrained flow reactor with conditioning rotor located in the lower reaction chamber elbow
- Flat-bag filter
- Particle re-circulation with wetting of recycled particulate.

The chosen additive powder is commercially available $Ca(OH)_2$. During SO_2-separation, the following reactions are taking place:

$$Ca(OH)_2 + SO_2 \rightarrow CaSO_3 + H_2O$$

$$CaSO_3 + 1/2\,O_2 \rightarrow CaSO_4(\text{partly})$$

The additive powder is injected into the gas flow near the reactor. The process particles, reaction products, and free additives carried along in the gas flow are separated in the flat-bag filter. Prior to discharge out of the filter system, the particles are repeatedly reintroduced into the reactor upstream filter by passing an intermediate storage, a dosing rotary airlock valve, and a moistening mixer.

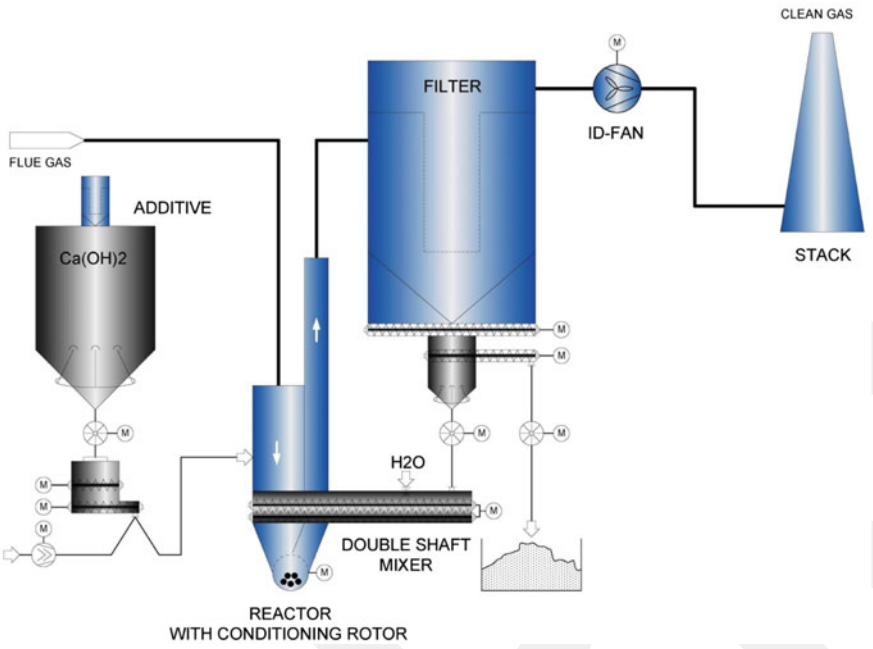

Fig. 4 Scheme of conditioning rotor—recycle process

Particularly, in the case of high particle recycle rates, the particle re-circulation leads to a provable clear improvement of separation efficiency for acid crude gas pollutants and/or to a reduction in additive powder injection quantity because:

- The residence time of additive powder particles in the system is increased
- In the area of the reactor upstream of the filter, a higher additive powder particle density is created at a reaction time inside of reactor of >2 s
- A frequent spatial new orientation with redeposition of the recirculated additive powder particles at the filter fabric is achieved.

This correlation is illustrated in Fig. 5.

With regard to the separation of SO_2, a good additive powder utilization can only be achieved if the water steam partial pressure directly at recycled particles is at least partially near the saturation steam pressure. This is achieved by using the conditioned chemisorption with particle moistening. In this process, the recycled particles are wetted prior to being recirculated into the reactor, thus improving the efficiency in the chemical reaction with the acid crude gas pollutants, particularly with respect to SO_2.

The maximum possible wetting of recycle particulate in the humidifying mixer is subject to the particle features. Before the installation of the SBF, little experience had been available for this particular particle composition. Therefore, laboratory tests

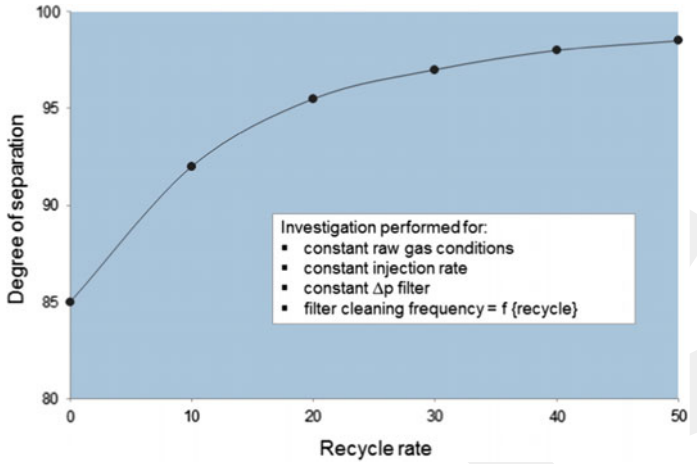

Fig. 5 Influence of particle recycle rate on the sorption efficiency

with mixtures of products of different plants currently in operation have been carried out prior to the design of this filtration plant. The results obtained in the test could be confirmed during the operation of the industrial plant.

Kuettner Thermodynamic Process Model

The furnace process in the SBF and the off-gas treatment are closely linked. During the first start-up of the SBF furnace, it became apparent that for safe and effective hot commissioning of the off-gas treatment, Kuettner had to get involved in the start-up of the furnace process itself. The start-up of the furnace became a success when all parties involved were working closely together.

Quite early in the process, the need for an own detailed thermodynamic furnace model was identified, which was developed completely in-house by Kuettner. This model was refined by actual data from commissioning and start-up. As a foundation, thermodynamic software AsTher was used for the thermal and chemical equilibrium calculations.

In the Kuettner process model, the furnace is divided into different linked zones:

- Bath zone
- Upper furnace
- Post-combustion
- Boiler/Quench.

Calculation of thermal and chemical equilibrium is carried out for each zone individually. Due to the heat and mass transfer between the zones and adaptive boundary conditions such as heat transfer to cooling water, these calculations were carried out iteratively.

Because the SBF process is a batch process, the model had to refine further by dividing the batch into linked phases. The aforementioned iterative approach was carried out for each process phase in succession, while the products were used as initial material for each subsequent phase. After several iterations of the whole cycle, the system reached steady state. From this steady state, output data were generated which includes:

- Mass of products and intermediates
- Compositions of products and intermediates
- Enthalpy of products and intermediates
- Energy Fluxes
- Temperatures
- Elements distributions.

An example of output data from the thermodynamic process model for an SBF process is given in Fig. 6.

The data from the refined model are in very good agreement with real data. The model had nearly no need for corrective variables and seems to be applicable to a range of processes. For the SBF process at WMG, which is somewhat different from traditional established SBF processes in China, the model was able to accurately predict the effects of process modifications.

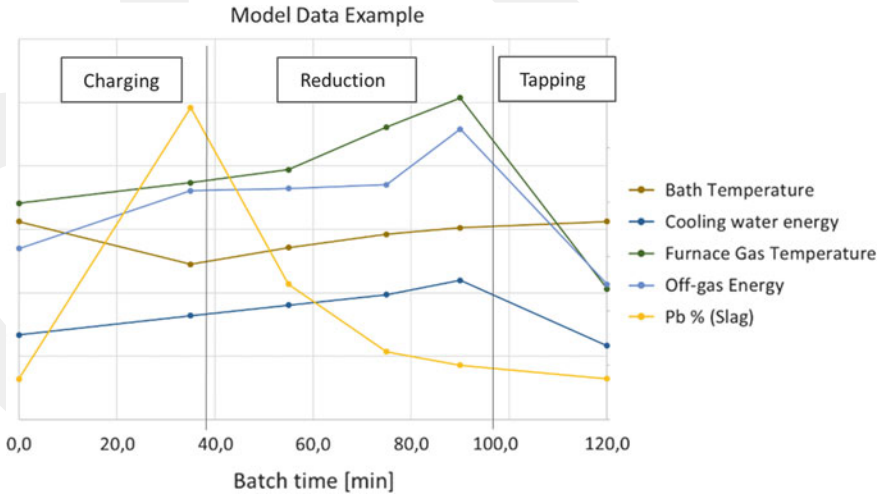

Fig. 6 Model data example

Process Results

The plant was commissioned in summer 2018, and FAC was received still in 2019.

The Kuettner design features together with the LUEHR off-gas filter proved to operate as designed.

Compared to traditional SBF installations, the Kuettner SBF off-gas treatment concept provided a strong improvement in terms of safe and accretion-free operation of the boiler inlet and top.

The key achievements were as follows:

- Stable operation with respective design throughput
- Full post-combustion and safe operation
- No accretion formation of sticky dust in the boiler top
- The required low emission level criteria were achieved without the need for wet scrubbers.

GCRIS

Application of CSC Technology in Nonferrous Metallurgy

Xiaosong Wu

Abstract In recent years, China's requirements for environmental protection and energy conservation have been continuously improved. Nonferrous metallurgy has developed rapidly. Oxygen-enriched air intensified smelting technologies have been fully developed, of which CSC is the most important technology. In this paper, CSC technology development, process mechanism, technical characteristics, and main equipment are discussed, and commercial tests and applications in lead smelting, copper–nickel smelting, antimony smelting, hazardous solid waste treatment, etc., are described, respectively. CSC technology is environmentally friendly energy-saving with strong technological adaptability and has broad application prospects in nonferrous metallurgy.

Keywords Application of CSC technology · Process mechanism · Technical characteristics · Main equipment · CSC smelting furnace

Introduction

CSC technology is a nonferrous metallurgical technology developed on the basis of the Vanukov method. In recent years, a large number of commercial tests and researches on different types of material have been carried out. The furnace structure, process control, and tuyere structure have been developed and optimized. CSC series of key nonferrous metallurgy technologies have been developed, improved, re-innovated and also have been extended to the field of comprehensive recovery of copper, nickel, lead, zinc leaching residues, antimony, and nonferrous metals, with good application results.

X. Wu (✉)
CINF Engineering Co., Ltd., Changsha 410019, Hunan, China
e-mail: wxsdk@126.com

© The Minerals, Metals & Materials Society 2020

A. Siegmund et al. (eds.), *PbZn 2020: 9th International Symposium on Lead and Zinc Processing*, The Minerals, Metals & Materials Series,
https://doi.org/10.1007/978-3-030-37070-1_16

Process Principle

The smelting process mechanism is that oxygen-enriched air is fed into the furnace from a tuyere located about 0.50 m below the plane of the standing melt on the side wall of the smelting furnace, to make the upper melt in the molten bath bubble strongly and stirred violently. Solid furnace charge is added into a molten bath of molten slag stirred at a temperature of 1000–1400 °C, particles or polymers of the furnace charge are wetted by the slag and heated based on the temperature difference between the slag and the furnace charge particles. The fusible components are preferentially melted to form metal droplets in the slag. High melting point components such as flux and coal are strongly stirred or melted into slag, or burned, or reacted with oxygen in slag. The gas blown into the slag melt acts on the slag at the phase interface and changes the composition of the liquid phase and the gaseous phase accordingly until a chemical equilibrium is established between the two phases. Because of the large area of the phase interface and the high stirring energy given by the gas to the molten bath, the heat and mass transfer process in the furnace are accelerated, the composition of each phase tends to be balanced, and the phase separation process is greatly accelerated.

The characteristic of oxygen-enriched air side-blown bath smelting is that the molten bath in the furnace is divided into two layers by air blown in at a certain height. The upper layer is stirred by gas to obtain turbulent motion. The furnace charge is added to the melt layer, and heat and mass transfer processes between the melt and the added furnace charge and between the melt and the blown gas are realized therein. When the uniform distribution of the required stirring energy is formed in the upper stirring layer, the reaction speed in the entire melt will increase many times. This is because stirring the melt will make the added solid, liquid, and gas dispersed rapidly and evenly throughout the upper melt, thus greatly increasing the area of the phase interface.

In the smelting process, the ideal conditions for oxidation, reduction, and any other pyrometallurgical changes are actually created in the stirring layer on the upper part of the melt. The research shows that the material composition of the upper stirring layer is basically consistent with the final equilibrium phase composition of the real system. When the furnace charge to be treated and the gas required by the process is added to the melt, the composition of the molten bath has not changed much due to the extremely high reaction speed, although its composition differs greatly from the material composition of the molten bath in the furnace. Therefore, in continuous operation, what actually exists in the furnace is the final product of the production process.

In addition, below the level at which the melt is blown; there is a lower melt that is less stirring than the upper melt. In this calm area at the lower part, the different liquid droplets forced to grow in the upper layer will rapidly separate according to the difference in specific gravity.

Technical Characteristics

(1) The furnace charge has strong adaptability and is suitable for smelting various metals: Copper, lead, nickel, antimony, zinc, and the like, as well as the treatment of various waste residues, electronic wastes, municipal wastes, and the like;
(2) Simple material preparation: The particle size is not strictly required, and the powder is granulated (15–25 mm) with the moisture content of not more than 15%;
(3) The oxygen-enriched air is blown into the molten bath from the nozzles on both sides of the furnace, and the melt is stirred violently, which intensifies the turning of the upper melt. The mass transfer and heat exchange are rapid, which accelerates the melting speed of refractory components in slag. The productivity of the furnace is high, for example, the lead, copper, and nickel smelting reach 80–100 t/m^2 d, and the specific capacity of slag smelting is generally 50–80 t/m^2 d;
(4) Continuous operation can be realized in the smelting process of metals such as lead, namely charging and slag tapping;
(5) Simple and cheap fuel and reductant: Coal;
(6) Structural characteristics of oxygen-enriched air side-blown tuyere: The tuyere is simple in structure, which can only blow oxygen-enriched air, and also can blow pulverized coal, gas, natural gas, etc., with water-cooled, has a service life of more than 2 years, and is convenient to install and replace; the tuyere is provided with a bott stick. When the furnace stops blowing for some reason, the bott stick is inserted to prevent the melt in the furnace from flowing out, no matter it is the tuyere only for blowing oxygen-enriched air or blowing other fuel at the same time, so as to facilitate the hot shutdown and other operations in the production process. The oxygen-enriched air pressure is 0.06–0.12 MPa, and the oxygen pressure of the oxygen generation station is not more than 0.2 MPa.

Main Equipment—CSC Smelting Furnace

The main equipment of, CSC technology is CSC smelting furnace, whose overall structure is similar to that of Vanukov furnace, but the tuyere structure type under different smelting conditions, the design of tuyere depth is based on the characteristics of processed materials, and optimization of the gap between the tuyeres are better conducive to the agitation of the melting pool, the copper water jacket of the furnace platform is better protected by the back platform design, the upper part adopts the innovative sandwich structure, and the overall furnace life is improved. According to the type of materials, we have innovated and optimized the bosh angle to adapt to the smelting process of different materials such as copper, nickel, lead, and slag treatment. The main structure is shown in Fig. 1.

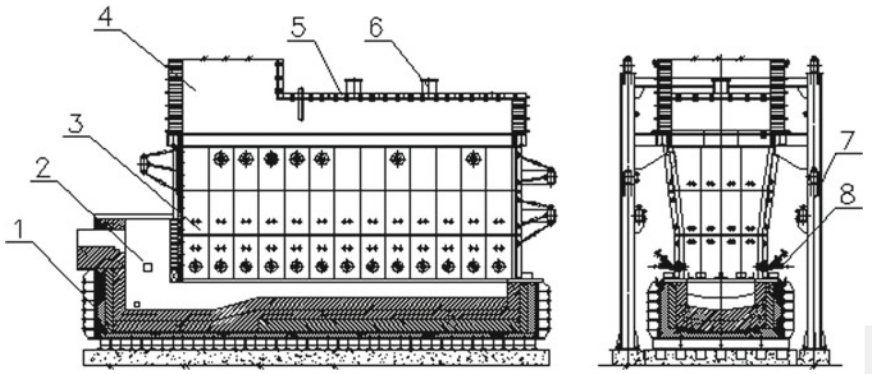

1-hearth; 2-siphon chamber; 3-furnace body; 4-uptake; 5-furnace top; 6-charging opening; 7-steel frame; 8-tuyere

Fig. 1 Structural diagram of CSC smelting furnace

CSC smelting furnace is surrounded by multi-layer cooling water jackets, with a rectangular cross section, and is divided into a hearth, a furnace body, and a furnace top from bottom to top.

(1) Hearth

The hearth is made of magnesia-chrome brick in the steel groove welded by steel plate, the bottom of the hearth is inverted arch, and the edge of the hearth is laid with horizontal steel plate to support the lower layer of the water jacket under the furnace body. The hearth is used to stratify the slag and metal phases and discharge them out through the siphon.

(2) Furnace Body

The furnace body is divided into the molten bath area and reburning area. The two sides of the furnace body are provided with the molten bath tuyere and reburning tuyere. One end of the furnace body is the charging chamber, and the other end is the slag siphon well. The furnace body is provided with the slag outlet and siphon metal outlet. The slag outlet is higher than the lower tuyere to form the molten bath, i.e., the depth of the molten bath can be adjusted by the height of the slag outlet.

① Molten bath area: The smelting area includes lower and middle water jackets, both of which are copper water jackets. The middle water jacket tilts outwards, and it increases the width of the furnace, reduces the airflow velocity and effectively reduces the fine furnace charge carried away by the furnace gas.

② Reburning area: The furnace wall of the reburning area is surrounded by the molten steel jacket (upper water jacket) built with the magnesite-chrome bricks, and reburning tuyeres are installed on both side walls. The S, CO, Sb, and Pb sulfides and others in the furnace gas undergo oxidation reaction in this area.

(3) Furnace Top and Uptake

The furnace top is lined with refractory coating of steel water jacket, and it is provided with a charging opening and an uptake flue surrounded by membrane wall.

Typical Cases of Industrial Application of CSC Technology

Process Copper-Nickel Ore to Produce Low-Grade Matte Nickel [1]

(1) Typical case: Oxygen-enriched Air Side-blown Smelting Project of Copper-Nickel Ore of a Plant in Xinjiang.
(2) Design capacity: Granulated metalized high-grade matte nickel (nickel metal content); 8000 t/a.
(3) Main process: Copper-nickel ore is used as the main raw material, and CSC oxygen-enriched air side-blown bath smelting-depleted electric furnace slag depletion-PS converter blowing technology is adopted to produce granulated metalized high-grade matte nickel, please refer to Fig. 2 for process flow. It was put into operation in March 2011, with good operation effect. It is the first time that China to apply this process to treat copper-nickel ores.

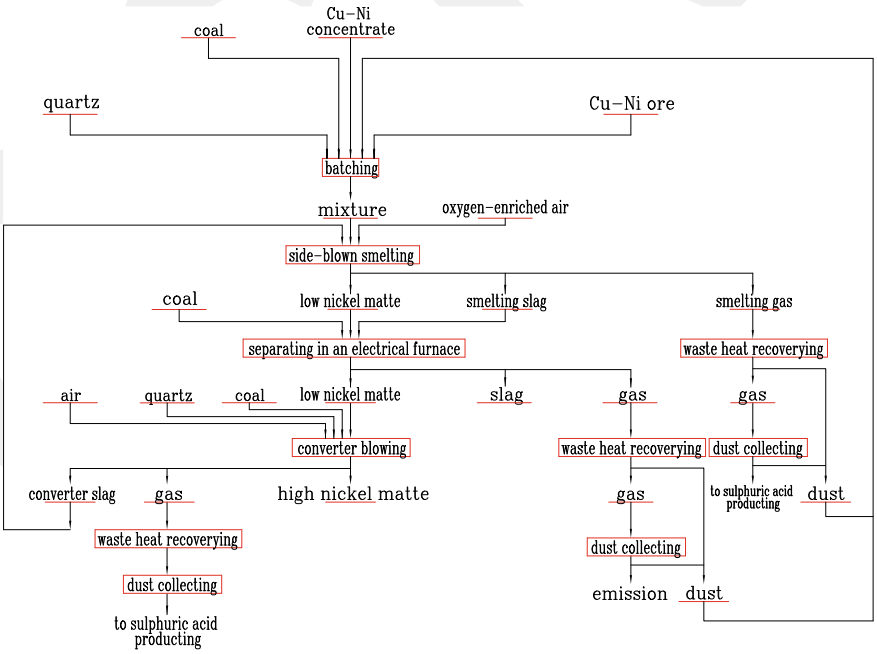

Fig. 2 CSC process flow chart for copper-nickel ore treatment

(4) The brief description of process flow: The annual treatment capacity of copper and nickel ore in this project is 292,728.33 t, including 82,000 t of ultra rich block ore and 210,728.33 t of copper and nickel concentrate. Ultra rich ore, copper-nickel concentrate, quartzite, smoke, and pulverized coal are measured by disc feeder and electronic belt scale, respectively, according to the requirements of proportioning ratio, and then transported to proportioning belt conveyor, and then transferred by belt into oxygen-enriched side blowing furnace for oxygen-enriched matte smelting.

In the oxygen-enriched side blowing furnace and from the Tuyeres on both sides of the furnace body, the charge is blown into the oxygen-enriched air with the oxygen content of ~60% for smelting in the oxygen-enriched molten pool. The height of the tuyere is 0.5 m below the top surface of the slag layer, and the slag layer above the tuyere will generate a bubble layer due to the strong agitation of the oxygen-enriched air, which will melt the added charge and generate a strong oxidation and slagging reaction to generate copper-nickel matte and slag. The heat needed in smelting process mainly comes from the oxidation of sulfur in raw materials and the reaction heat of slagging, and a small part comes from the combustion heat of pulverized coal. The copper-nickel matte produced by smelting and slag is precipitated and separated in a static slag layer 1 m deep below the tuyere. The low matte nickel produced by smelting is deposited in the bottom of furnace, the slag containing low copper-nickel is discharged from the slag mouth in the upper layer of furnace melt; the low matte nickel is discharged from the siphon mouth at the furnace end; the reductive gas discharged from the furnace body is oxidized by the air inhaled in the furnace space to produce high-temperature flue gas containing SO_2 15–25%. After being discharged, it is cooled by waste heat boiler, purified by electric dust collector and sent to sulfuric acid workshop for acid production.

The low ice nickel and slag produced in the smelting process flow into the dilution electric furnace through the launder for reduction, clarification, and separation. The pulverized coal is added above the electric furnace as the reducing agent, and the dosage is 980 kg/h. After the melt is fully clarified and separated in the dilution electric furnace, the upper layer is the dilution slag, which is discharged through the slag mouth, and the water is broken into waste slag. The slag is lifted to the slag bin by the chain bucket raking machine and then transported to the slag yard by the tipper. Low ice nickel is siphoned out and lifted to converter by ladle. The concentration of sulfur dioxide in the flue gas of the dilution electric furnace is less than 0.02%, which is discharged after the waste heat recovery and dust collection. On the one hand, low ice nickel can be used as curing agent, on the other hand, the converter is intermittently charged, and the furnace plays the role of heat preservation.

The low ice nickel of the dilution electric furnace is put into the ladle intermittently and is hoisted by the crane and added into the PS converter for blowing. Converter blowing is an oxidation reaction process. Low ice nickel is mainly composed of Cu_2S, Ni_3S_2, and FES. The task of blowing is to oxidize and slag FES in low ice nickel, remove iron and part of sulfur, and produce high ice nickel composed of Cu_2S and Ni_3S_2 and enriched precious metals. Its grade (Ni + Cu) is about 78%.

Quartz stone should be added to the converter for slag making, and the slag poured out after slag making should be packed in slag ladle and returned to the side blowing furnace for smelting. In the later stage of blowing, in order to control the refractory nickel oxide produced by overblowing, it is necessary to add crushed coal for reduction smelting, and the amount of crushed coal is 160 kg/h. High nickel matte is granulated by high nickel matte in water. The high-temperature flue gas discharged from the furnace mouth during blowing is sent to the acid-making system together with the smelting flue gas after the waste heat recovery and dust collection.

(5) Main equipment and technical parameters of CSC oxygen-enriched side-blown bath smelting process:

- CSC smelting furnace area: 20 m^2
- Specific capacity: 70–80 t/m^2 d
- Smelting temperature: 1300–1400 °C
- Flue temperature: 1400–1500 °C
- Oxygen concentration: 80–85%
- Recovery: Cu 95%, Ni 94.89%.

Lead Smelting with Treatment of Lead and Zinc Slag

(1) Typical case: Project of, Lead Smelting with Lead and Zinc Mixed Furnace Charge in a Plant in Chenzhou.
(2) Design capacity: Low-grade polymetallic materials to be treated; 100 kt/a.
(3) Main process: Lead containing polymetallic materials → side blowing oxidation furnace → side blowing reduction furnace → side blowing fuming furnace. Lead, zinc, precious metals, and other valuable metals are recovered with crude lead and secondary oxidation products. The flue gas is discharged after being treated by waste heat boiler and dust collection. The project was put into operation in June 2014. See Fig. 3 for process flow.
(4) The brief description of process flow: After the lead containing polymetallic materials are batched, they are mixed and granulated. The grain size of the material entering the furnace is about 15 mm, and the water content is controlled within 10%. The oxygen-enriched side blast furnace is added. The oxygen-enriched side blast furnace is injected into the furnace through the air nozzle at the furnace side. The oxygen and the furnace material react chemically. The metal lead is collected by the high lead slag. The smoke is collected by the waste heat boiler and the electric dust collector, and then sent to the batching plant. The high-temperature flue gas is recycled by waste heat to generate steam, which is sent to the residual thermal power station for power generation, and the tail gas is sent to produce acid. The high lead slag enters the oxygen-enriched side blowing reduction furnace through the chute, and the coarse lead is produced from the reduction furnace. After the high-temperature flue gas recovers the waste heat through the waste heat boiler, it is sent to the dust collector for desulfurization, and the flue gas returns to the smelting batching. The reduction slag enters the fuming furnace through the chute, the pulverized coal enters the fuming furnace

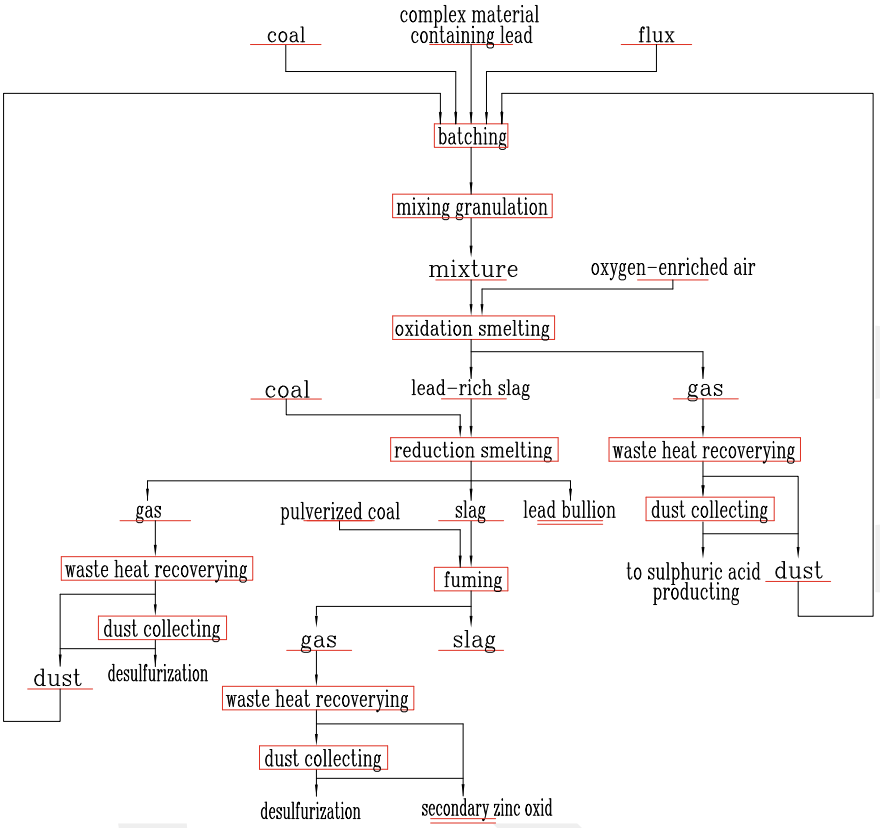

Fig. 3 CSC process flow chart for complex materials containing lead

through the nozzle of the fuming furnace, the metal zinc in the reduction slag is reduced to zinc steam, the zinc steam is oxidized at the third air outlet of the fuming furnace, forming the secondary zinc oxide, the heat energy generated during the period is recovered by the waste heat boiler, and the high-temperature flue gas is sent to desulfurization after passing the waste heat boiler and dust collection. After fuming and converting slag is sent to water for quenching, it will be sold to cement plant. In the actual production process, part of the primary lead is produced in the oxidation furnace, and an intermediate slag port is opened in the hearth of the oxidation furnace to discharge the intermediate slag with high Cu content. The hearth end of the reduction furnace is also provided with an intermediate slag port for discharging the intermediate metal layer in the smelting process.

(5) Main equipment specifications and metal recovery:

- Main equipment: CSC smelting furnace 9 m^2, CSC reduction furnace 7 m^2, and fuming furnace 8 m^2
- Recovery of major metals:

Zinc recovery: 90.27%	Lead recovery: 96.86%
Bismuth recovery: 84.07%	Antimony recovery: 89.11%
Gold recovery: 94.89%	Silver recovery: 95.87%

Lead Continuous Smelting

(1) Typical Case: Lead Smelting Project of a Plant in Guangxi.
(2) Design capacity: Cathode lead; 150 kt/a.
(3) Main process: The Project is the first in China to adopt a three side-blown continuous smelting process for high antimony lead concentrate (with part of leaching residue of zinc system). CSC oxygen-enriched air side-blown oxidation +CSC oxygen-enriched side-blown reduction +CSC oxygen-enriched air side-blown fuming. The Project was completed and put into operation in November 2016. Raw materials are directly fed into an oxidation furnace for oxidation smelting after proportioning and granulation. Oxidized slag continuously enters the reduction furnace through a chute. Reduced slag continuously flows into the fuming furnace through the chute for fuming volatilization, and pulverized coal is used as fuel and reductant to produce secondary zinc oxide smoke dust and waste slag, see Fig. 4 for process flow chart. It was put into production in November 2016.
(4) Process flow:

① Side-blown oxidation smelting

After the mixture from the raw material bin is transferred by the belt conveyor, it will enter the cylinder mixing granulator in the smelting plant to directly add water to mix and granulate. The ball material is metered and then sent to the oxidation furnace. The temperature in the furnace is controlled at 1050 °C, and the oxidation furnace is operated continuously. Two feeding ports are set at the top and nozzles are set at the side for blowing oxygen-rich air for smelting. One end of the oxidation furnace is a siphon slag outlet, and the other side is provided with a siphon antimony silver coarse lead polymetallic outlet. The primary lead is discharged continuously and flows into the fire refining pot through the chute for preliminary fire refining such as copper removal; the high lead slag from the slag outlet flows directly into the reduction furnace through the chute for reduction smelting. A flue gas outlet is arranged above one end of the siphon port. The high-temperature flue gas from the oxidation furnace

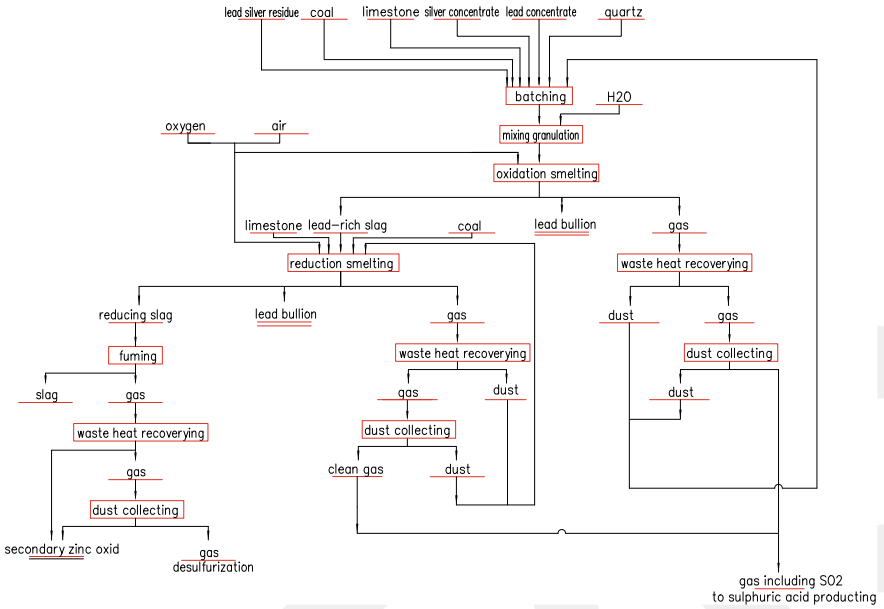

Fig. 4 CSC lead smelting process flow chart

is recycled by the waste heat boiler and collected by the electric dust collector, then combined with the flue gas from the side blow reduction furnace and sent to the sulfuric acid system for sulfuric acid production. The collected oxidation dust is returned to the side blowing oxidation furnace material preparation system on site.

② Side blowing reduction smelting

Limestone, anthracite, and other auxiliary materials from the raw material warehouse are sent to the reduction furnace by belt conveyor. The molten oxide slag produced by the oxidation furnace is discharged continuously and flows directly into the reduction furnace through the chute. The temperature in the furnace is controlled to 1150–1200 °C. Two feeding ports are set at the top of the reduction furnace and nozzles are set at the side for blowing oxygen-rich air for smelting. One end of the reduction furnace is a slag discharge port, and the side part is provided with a siphon antimony silver coarse lead polymetallic port. The secondary lead produced by reduction furnace is discharged continuously and flows into the fire refining pot through chute for preliminary fire refining such as copper removal.

The high-temperature flue gas from the reduction furnace is recycled by the waste heat boiler, cooled, and collected by the bag type dust collector, and then combined with the flue gas from the side blowing oxidation furnace and sent to the sulfuric acid system to produce sulfuric acid. The dust collected by waste heat boiler and bag type dust collector shall be returned to the top material preparation system of side blowing reduction furnace. The slag from reduction furnace is continuously blown into fuming furnace through chute to recover valuable metals such as zinc.

③ Continuous blowing in side blowing fuming furnace

This project adopts the continuous blowing process of side blowing fuming furnace, and the side blowing fuming furnace and smelting furnace are arranged in the same workshop. The hot slag from the reduction furnace is directly and continuously injected into the fuming furnace through the chute, which reacts with the pulverized coal and oxygen-enriched air. The flue gas (dust) produced is recovered by the waste heat boiler and collected by the bag type dust collector. The waste gas is combined with the acid-making tail gas and discharged by the chimney after desulfurization. The smoke and dust (i.e., secondary zinc oxide products) collected by the waste heat boiler and dust collector are pneumatically transmitted to the zinc smelting production system as production raw materials. After the slag from the fuming furnace is precipitated by water crushing, it is grabbed into the car by 5T grab crane, transported by car to the slag yard for temporary storage, and then sold to the cement plant as building materials.

(5) Main characteristics:

① CSC oxygen-enriched air side-blown furnace is adopted for oxidation smelting, reduction smelting, and fuming.
② Continuous operation, i.e., continuous feeding and slagging, improves automation level, avoids low-altitude pollution, improves occupational hygiene environment, and reduces manpower quota.

(6) Main equipment specifications and technical parameters:

- Main equipment: Oxidation furnace: 21 m^2, reduction furnace: 13.5 m^2, fuming furnace: 12 m^2.
- Main technical parameters:

Smelting temperature of oxidation furnace	1050 °C	
Slag type of oxidation furnace	Fe/SiO_2 = 1.1	CaO/SiO_2 = 0.6–0.7
Smoke dust rate of oxidation furnace	8–12%	
Oxygen-enriched air concentration of oxidation furnace	85–95%	
Smelting temperature of reduction furnace	1200 °C	
Smoke dust rate of reduction furnace	10%	
Oxygen-enriched air concentration of reduction furnace	55–75%	
Slag lead of reduction furnace	≤2.5%	
Lead in waste slag of fuming furnace	0.2–0.3%	
Zinc in waste slag of fuming furnace	≤2%	

CSC Technology Commercial Experimental Research

Treatment of Zinc Leaching Residue

(1) Test furnace type: double-area CSC smelting furnace with an area of 3.6 m^2 (smelting area of 2.16 m^2 and fuming area of 1.44 m^2).
(2) Test capacity: 100 t/d.
(3) Test flow: The furnace charge consists of leach slag, coal, flux, etc. It is added from the smelting area. Control the concentration of oxygen enrichment at 60–80%, combustion coefficient at 0.95, and smelting area temperature at 1150–1200 °C. The furnace charge is melted, sulfate decomposed, the produced dust contains 30–40%, which can be sold, and molten slag flows into the fuming area. Using pulverized coal as reducing agent and fuel, the temperature is controlled at 1250 °C, the combustion coefficient is 0.5–0.7, zinc and lead are volatilized in the fuming area to obtain secondary zinc oxide smoke and dust, which are sold out. See Fig. 5 for process flow.
(4) Research results of the test:

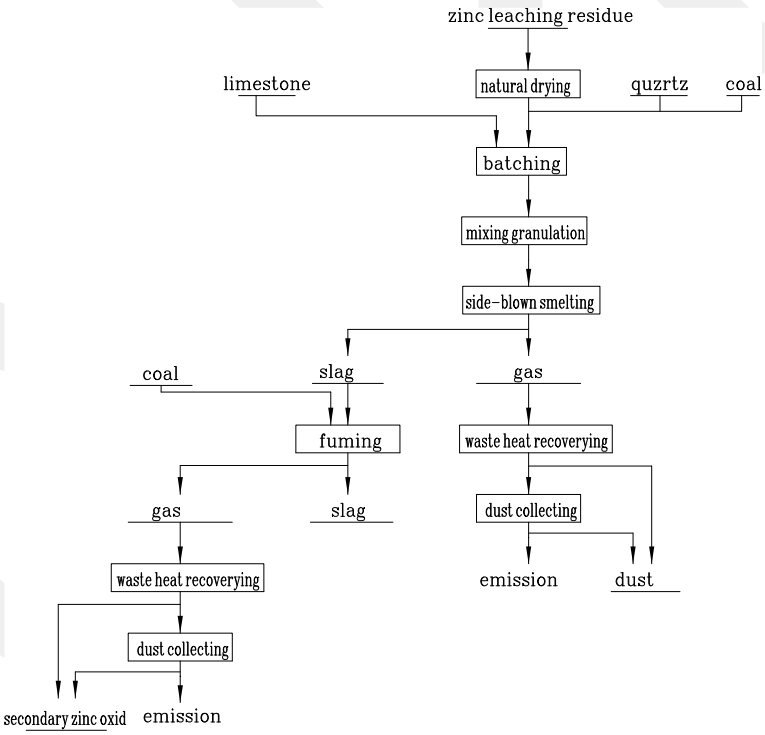

Fig. 5 Process flow chart of CSC technology for zinc leaching residue treatment

Recovery	91% of lead, 91% of zinc, 95.9% of silver, 75% of copper and 72% of indium
Coal rate	30–35%
Oxygen	180 m^3/t of leach residue
Comprehensive energy consumption	291 kgce/t of leach residue, 32% more fuel-efficient than that of the rotary kiln
Waste slag	Zinc $\leq$ 2.5%, Pb $\leq$ 0.5%, Ag $\leq$ 20 g/t

(5) Main features

For the first time, the molten pool smelting method was used to treat leaching slag, compared with the traditional volatilizing kiln [2], the recovery of valuable metals such as copper and silver are improved.

High-concentration oxygen-enriched air $O_2 \geq 60\%$ is used in the treatment of leach residue, which greatly improves smelting strength and reduces flue gas volume. The heat removed by flue gas is reduced and the energy consumption is reduced. The leaching slag is treated by oxygen-enriched side-blown two-zone smelting furnace. The smelting and fuming of the leaching slag are carried out in two different atmosphere and temperature areas of a CSC smelting furnace. At present, the technology has been applied to a factory in Qinghai, China, and put into production in October 2019, with good operation.

Treatment of Lead and Zinc Oxide Ore

(1) Test furnace type: Double-area CSC smelting furnace with an area of 3.6 m^2 (smelting area of 2.16 m^2 and fuming area of 1.44 m^2).
(2) Test capacity: 100 t/d.
(3) Test flow: The furnace charge is composed of lead and zinc oxide ore, coal, flux, etc. It is added from the smelting area. The furnace charge is melted, decomposed, and slagged in the smelting area. The produced melt enters the fuming area through the partition wall, and the lead and zinc volatilize to the smoke and dust for recovery. See Fig. 6 for process flow.
(4) **Test conditions and technical indexes**

Volatilizing furnace capacity of oxygen-enriched side-blown smelting ($T/(M^2 \cdot d)$): 60–80
Zn grade of mixed charge (%): 17.45
Oxygen enrichment concentration (%): 50–70
Oxygen consumption (m^3/T): 100–120
Coal consumption (kg/T): 200–240
Melting temperature (°C): 1100–1200
Zinc content grade of secondary zinc oxide (%): 40–50

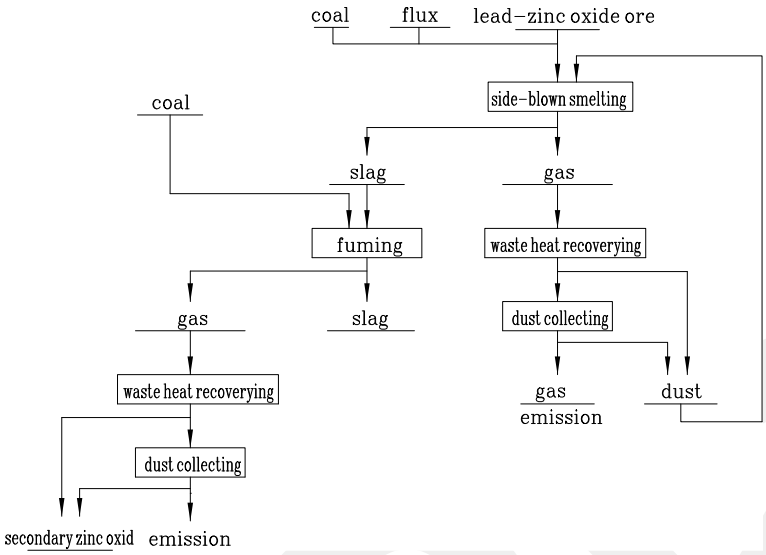

Fig. 6 Process flow chart of CSC technology applied to lead zinc oxide mine

Fuming volatile bed capacity ($T/(M^2 \cdot d)$): 70–90
Oxygen enrichment concentration (%): 30–45
Oxygen consumption (m^3/T): 40–60
Coal consumption (kg/T): 140–180
Melting temperature (°C): 1200–1300
Zinc content grade of secondary zinc oxide (%): 61.61
Total volatilization rate of zinc (%): 97.20
Total volatilization rate of lead (%): 97.44.

(5) **Main features**
It is the first time to use the process of oxygen-enriched side-blown smelting and traditional fuming furnace to treat the lead-zinc oxide ore, which realizes the recovery of valuable metals such as lead-zinc, solves the problems of high energy consumption, poor environment, short life of kiln lining, non-recovery of valuable metals such as gold and silver in traditional rotary kiln process [3–5], and opens up a new technical route for the treatment of lead-zinc oxide ore.

Antimony Smelting

At present, the antimony pyrometallurgy process is the dominant process for antimony smelting, with the most important representative being the "antimony concentrate volatilization and smelting in blast furnace → reduction smelting and refining

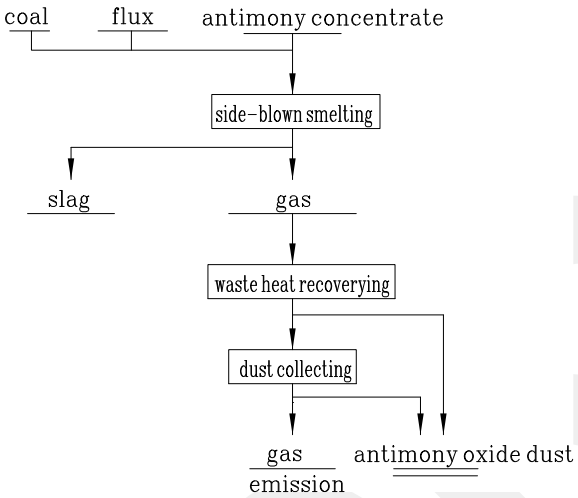

Fig. 7 Process flow chart of using CSC technology in antimony smelting

in reverberatory furnace" process. However, problems such as high energy consumption, difficulty in recycling of SO_2 fume ($SO_2 < 1\%$), and low recovery of antimony are prominent, resulting in serious pollution to the surrounding ecological environment [6]. In order to solve the outstanding problems in the smelting process of antimony, a set of commercial test facilities for antimony concentrate volatilization and smelting with CSC technology were established in 2013. See Fig. 7 for process flow.

Test conditions and technical indexes:

Furnace area (M^2): 2.2
Bed capacity ($T/(M^2 \cdot d)$): 35–60
Concentrate grade (%): 30–50
Antimony in antimony oxide (%): 79–80.9
Antimony content in slag (%): 0.28–0.90
Recovery rate of antimony smelting (%): ≥ 96
Coal rate (%): 13–16
Oxygen enrichment concentration (%): 60–70
SO_2 content in flue gas (%): 10–20
Sulfur capture rate (%): ≥ 99.

Through a dozen of commercial tests, the results show that CSC technology is feasible for treatment of antimony concentrates and has the following advantages over traditional technologies:

- Increasing metal recovery, with less than 0.5% of antimony in waste slag;
- Using the oxygen-enriched air intensive smelting process to ensure the concentration of sulfur dioxide in the flue up to the acid-making requirements;

- Reducing energy consumption, substituting coke with coal, and supplementing small amounts of crushed coals as fuel;
- High sealing performance of the furnace and good on-site environment.

Copper Smelting Waste Treatment

In order to verify the feasibility of CSC technology and equipment to treat copper smelting waste slag, investigate various process parameters and provide basis for the industrialization of CSC technology to treat copper smelting waste slag, a commercial-scale experimental research on recovering copper and cobalt from copper smelting waste slag was carried out in 2014.

(1) Test furnace type: Single-area CSC smelting furnace with an area of 1 m^2.
(2) Test capacity: 40–50 t/d.
(3) Technological process: Copper cobalt slag, flux, and coal are added to CSC smelting furnace after being batched. The temperature in the furnace is controlled to 1400 °C, and the combustion coefficient is 0.5–0.7. Coal is used as fuel and reducing agent. Copper cobalt is reduced to metal phase through reduction reaction, and separated from slag in the furnace, so copper cobalt alloy and smelting slag are produced. The flue gas is discharged after being cooled and collected. See Fig. 8 for process flow.
(4) Test results: The commercial test shows that the commercial test system of CSC technology in copper smelting slag treatment runs continuously and stably. It

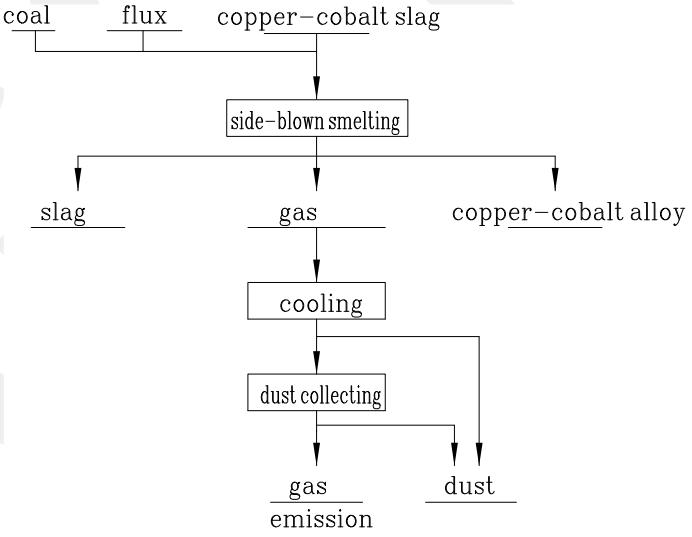

Fig. 8 +CSC process flow chart of copper-cobalt slag treatment

discharges residue and alloys smoothly and produces Cu–Co alloys with the average grade reaching 26.98%. Meanwhile, cooper and cobalt contents in the smelting slag can be reduced to the level of the waste slag. Recovery of copper and cobalt reach above 91% and 80%, respectively. The smoke dust rate is about 1.8%. The copper and cobalt can be efficiently recovered from the slag with significant enrichment effect and low smoke dust rate in Cu–Co slag treatment with CSC technology.

Future Application of CSC Technology

CSC technology has been widely used for reduction in lead smelting process and smelting and converting in copper smelting process and is mature and reliable. In recent years, CSC technology has been gradually popularized in copper-nickel ore treatment, lead smelting redox, miscellaneous material processing, zinc leach residue treatment, Cu–Co residue treatment, and oxide ore treatment. At present, research and development work in the fields of tin smelting, laterite-nickel ore treatment, and the like is underway. It can be seen that CSC technology has a wide application range, and it has a broad application prospect in nonferrous metallurgy due to its advantages of simple material preparation, environmental protection, energy conservation, and excellent smelting indexes.

References

1. Wang Z (2009) Process design of oxygen enriched side blown smelting converter blown production of high nickel matte. Eng Des Res 126:14–19
2. Wang X (2016) Design and analysis of zinc leaching residue system in rotary kiln. Hunan Nonferrous Metals 5:37–38
3. Lan Z, Lan Z, Zhang Q (2015) Research progress in utilization technology of lead zinc oxide ore. Compr Utilization Miner Resour (5):8–12
4. Xu D (2017) The effect of particle size of lead zinc oxide ore on the reduction and volatilization effect of rotary kiln. Compr Utilization Resour China (6):24–26
5. Liu G (2018) Study on the design of oxygen enriched side blast furnace for the treatment of lead-zinc oxide ore. Hunan Nonferrous Metals 6:24–26
6. Wang Z, Yujia Wang (2015) Study on the new smelting process of antimony sulfide concentrate in oxygen enriched side blown melting pool. Hunan Nonferrous Metals 6:41–44

Part VI
Primary Zinc I

GCRIS

Start-up and Improvements of the New Electrolysis Plant at Annaka Refinery

Takuhiro Yamaguchi

Abstract Annaka zinc refinery of Toho Zinc Co., Ltd. produces 100,000 tons of electrolytic zinc per annum with its zinc content over 99.995%, using zinc concentrate as the main raw material. The zinc smelting process in Annaka refinery is the hydrometallurgical method which consists of roasting, leaching, purification, and electrowinning. The environment of zinc smelting business in Japan has been severer due to some operational cost increases. The high electric power price which keeps rising after the Great East Japan Earthquake disaster in 2011 has still been the biggest challenge. Under such circumstances, we renewed the obsolete No. 1 electrowinning plant which had operated for more than 70 years. This report describes the improvement cost effect including the electricity power cost in Annaka refinery and some improvements of the new plant in the start-up stage.

Keywords Zinc smelting process · Electrowinning process · Cooling tower control

Introduction

Overview of Annaka Zinc Refinery

Annaka refinery of Toho Zinc Co., Ltd. produces 100,000 tons of electrolytic zinc per annum with a zinc content over 99.995%, using zinc concentrates as its raw materials. As shown in Table 1, the production method of electrolytic zinc at Annaka refinery is a hydrometallurgical method with a series of processing consisting of roasting, leaching, purification, and electrowinning. An overview flow chart of the process of Annaka refinery is shown in Fig. 1.

T. Yamaguchi (✉)
Toho Zinc Co., Ltd. Annaka Refinery, 1443 Nakajuku, Annaka, Gunma 379-0197, Japan
e-mail: yamaguchi-takuhiro@toho-zinc.co.jp

© The Minerals, Metals & Materials Society 2020

A. Siegmund et al. (eds.), *PbZn 2020: 9th International Symposium on Lead and Zinc Processing*, The Minerals, Metals & Materials Series,
https://doi.org/10.1007/978-3-030-37070-1_17

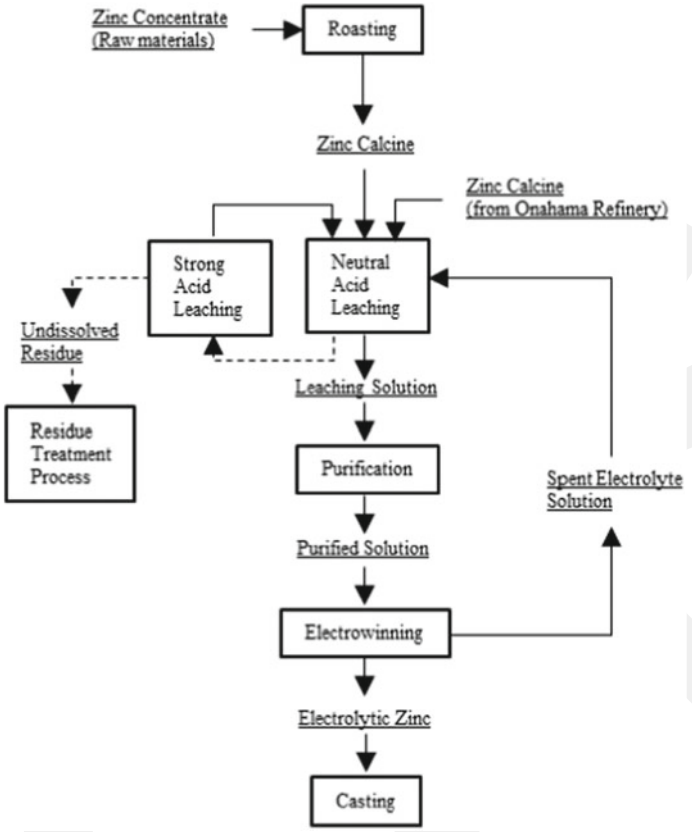

Fig. 1 Flowchart of the process of Annaka refinery

Table 1 Annual production of Annaka refinery

Electrolytic zinc (t/y)	Sulfuric acid (t/y)	Cadmium (t/y)
100,000	60,000	600

As of 2019, we have two electrowinning plants. One is the new No. 3 electrowinning plant (to be described later on this report), and the other is No. 2 electrowinning plant. Each production capacity is 66,000 t/y for the new No. 3 electrowinning plant and 34,000 t/y for the No. 2 electrowinning plant.

The flow of the electrolytic process is shown in Fig. 2, and the overview of the electrolytic operation is shown in Table 2.

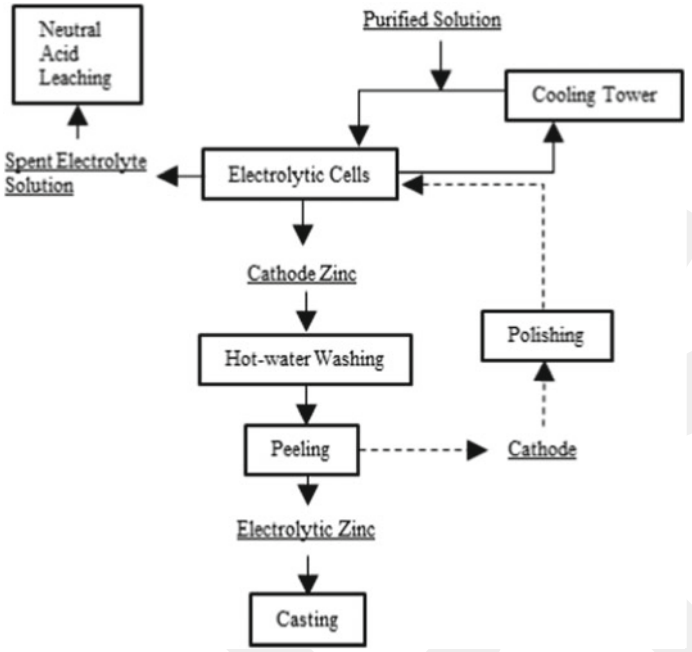

Fig. 2 Flow chart of zinc electrolytic process

Table 2 Zinc electrolytic operation condition in the No. 2 and the new No. 3 electrowinning plant

Items		The No. 2 electrowinning plant	The new No. 3 electrowinning plant	Unit
Electrolyte	Zn	50 + 5		g/L
	Free H_2SO_4	160 + 20		g/L
	Temperature	35–42		°C
	Circulation	40–45	180–200	L/(min · cell)
Electrode plate	Electrode distance	65		mm
	Cathode number	36	108	sheets/cell
	Anode number	37	109	sheets/cell
	Cathode size	660 W × 1100 H × 6 t	710 W × 1325 H × 6.3 t	mm
	Anode size	645 W × 1075 H × 9 t	685 W × 1305 H × 9 t	mm
Energization time	Holidays, weekdays	24, 48		hours

Power Usage Pattern of Electrowinning Plant in Annaka Refinery

In Japan, the electric price of holiday and nighttime of weekdays is significantly cheaper than that of daytime of weekdays. Therefore, as shown in Fig. 3, we use large amounts of electric power during the night and on holidays and try to reduce the electric power as low as possible during the daytime on weekdays. We define the ratio of the cheap nighttime and holiday power used for zinc electrowinning to all the power used as the "nighttime power rate". This rate has a major impact on the production cost of zinc metal. Especially after the Great East Japan Earthquake on March 11, 2011, the electric price rises year by year, and it is getting much more important.

Since the initial electrodeposition after peeling requires a high current density, the peeling work uses a lot of electric power. Therefore, it is ideal to perform the peeling work only at night.

Overview of the New No. 3 Electrowinning Plant

The comparison of the new No. 3 electrowinning plant with the old No. 1 electrowinning plant is shown in Table 3. In the Annaka refinery, the No. 1 electrowinning plant has been in operation for almost 70 years, and its operational efficiency became low. So, we planned to upgrade to a new electrowinning plant. The new electrowinning plant was almost similarly designed based on the proven operational data obtained in the No. 1 electrowinning plant and the No. 2 electrowinning plant.

The concept of the new electrowinning plant is almost the same production capacity of the No. 1 electrowinning plant but designed to be more efficient and rational. The rationalization by increasing the size of the electrolytic cell and the labor saving by automating the electrode plate transport and peeling were studied above all. In addition, automation was expected to reduce peeling time and to improve nighttime rates.

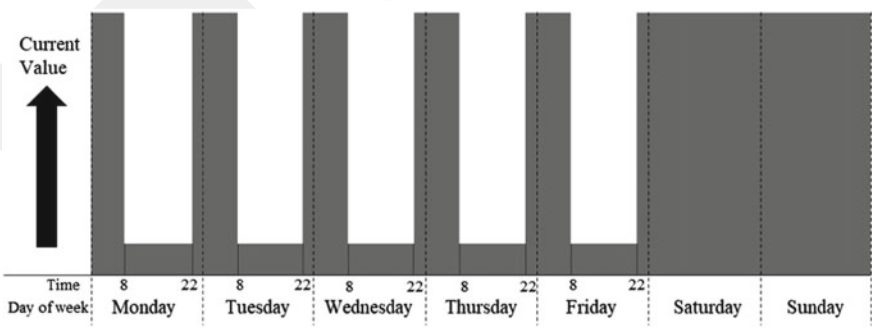

Fig. 3 Electrolytic power usage pattern of a week

Table 3 Comparison of the old No. 1 electrowinning plant and the new No. 3 electrowinning plant

Items	The old No. 1 electrowinning plant	The new No. 3 electrowinning plant
Amount of annual cathode zinc production	66,000 t/y	
Number of series	9	2
Electrode plate transport	Manual hoist · de-insertion	Automatic crane · de-insertion
Electrolytic cell	2.05 L × 0.78 W × 1.19 H (m)	8.0 L × 0.84 W × 1.75–2.05 H (in)
	Steel + PVC	Polymer concrete + FRP
Cathode/cell	32 sheets	108 sheets
Cathode size	640 W × 865 H × 5 t (mm)	710 W × 1325 H × 6.3 t (mm)
Anode size	620 W × 840 H × 71 t (mm)	685 W × 1305 H × 9 t (mm)
Cathode peeling	Hand peeling processing by workers	Peeling machine 54 sheets simultaneous processing
Transport to casting	Truck transport	Automatic conveyor transport
Slime cleaning	Supernatant siphon · bottom unplug	Supernatant siphon · bottom vacuum
Blower system in cooling tower	Induced draft by sirocco fan	Forced draft by axial fan

Construction and Start-up of the New No. 3 Electrowinning Plant

Construction work of the No. 3 electrowinning plant started in October 2009 and completed in July 2011. The picture of the new No. 3 electrowinning plant is shown in Fig. 4

Fig. 4 The new No. 3 electrowinning plant

The cooling tower at the top of the building is a feature of this new plant, and the fan of the cooling tower also serves as ventilation inside the plant. Its operation started in September 2011. Although the construction work and the test operation were interrupted by the Great East Japan Earthquake, some thorough tests in advance and the newly introduced monitoring system worked well, and the start-up operation was so smooth for a while. However, we experienced two major troubles some months later.

Troubles in the Start-up Stage

Electrolyte Temperature Drop and Piping Blockage

The first trouble is an extreme electrolyte temperature drop in winter.

Electrolyte temperature is one of the important factors in electrolytic operation. When the electrolyte temperature drops, the electrolyte resistance and the power cost rise in the meantime. Therefore, it is important to manage it in the appropriate temperature range. The Annaka refinery adjusts the electrolyte temperature to 40–41 °C when the maximum current is used.

The average outside temperature of Annaka drop to around 3 °C in winter evening. In the new plant, piping which bypasses the cooling tower is prepared not to get the electrolyte too cold by circulating in winter. However, since this bypass pipe is a path that goes over the upper part of the cooling tower, the distance is so long, and even if the cooling tower is bypassed, the electrolyte temperature often falls. On weekdays from 8:00 to 22:00, the current is kept to the minimum low level, so the heat generated in the electrolytic cell is so low. As a result, the electrolyte temperature dropped to around 20 °C around 22:00 when a large current was available.

Firstly, in order to keep the electrolyte temperature, its circulation was stopped during the daytime on weekdays, and only purified solution was supplied to the electrolytic cell. This treatment had some effects but was inadequate. After several days, $ZnSO_4$ in the purified solution crystallized, and the supply piping to the electrolytic cell was blocked.

Secondary, new bypass piping was added in the middle of the electrolyte circulation route. As shown in Fig. 5, since this new pipe bypasses the cooling tower through the shortest route, the drop of the electrolyte temperature was greatly suppressed. As a result, as shown in Fig. 6, the electrolyte temperature can be kept over 30 °C.

$ZnSO_4$ Crystal Adhesion to Cooling Fan Casing

This trouble also occurred in the first winter. During the year-end and New Year holidays, electricity prices are cheap all day, so the operation was continued using the

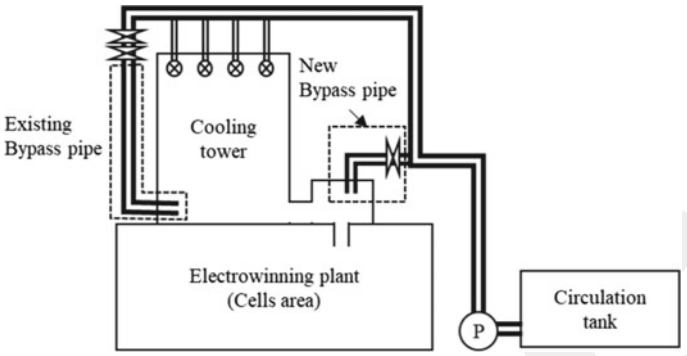

Fig. 5 Schematic diagram of the new bypass pipe

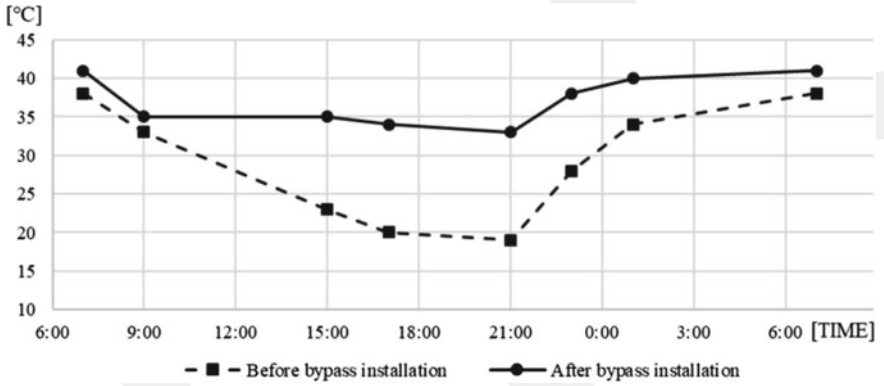

Fig. 6 Electrolyte temperature change before and after installation of new bypass in winter

maximum current for several days. Because of the heat generated by the continuous electrolysis operation, the electrolyte temperature rises abnormally even in winter, so the temperature is adjusted using a cooling tower. Around the end of continuous operation, noise and vibration were seen in the cooling tower fan. Observation of the fan revealed that $ZnSO_4$ crystals were adhered to the fan blades and casing as shown in Fig. 7.

If this is left untreated, there is a risk of operation stoppage due to blade damage. We removed it promptly and examined measures to prevent recurrence.

This crystal adhesion was caused by several factors.

(1) The fan is too close to the cooling tower.
(2) The cooling tower shower nozzle is installed too close to the fan.
(3) The electrolyte temperature was dropped during the winter, and the fan output was lowered.

Fig. 7 Fan blade and casing with $ZnSO_4$ crystals adhesion

To change the fan position, it requires extensive construction cost. So, we decided to stop some nozzles close to the fan and raise the fan output lower limit. The electrolyte temperature drop due to the fan output change was controlled by using a bypass. As a result, this problem was cleared.

Further Improvement of the Nighttime Power Rate

Compared to the old No. 1 electrowinning plant, the new No. 3 electrowinning plant has significantly reduced the time for the peeling work. Therefore, the nighttime power rate has greatly improved from 87.0 to 94.5%. Even so, due to the time constraints for electrode plate transportation, it was not possible to complete the peeling work only at night when the electricity rate was low.

Therefore, we have tried to improve the electrode transport operation to increase the nighttime power rate further. In the new No. 3 plant, 54 cathodes are peeled simultaneously. In the initial plan, in order to peel 54 sheets cleanly, a pre-peeling apparatus was prepared before the peeling procedure. However, in practice, it was found that no pre-peeling is needed. It is possible to perform the peeling without pre-peeling when the zinc electrodeposition height at the edge of the cathode is well controlled.

Therefore, pre-peeling operation was skipped, and we optimized the electrode cathode plate transport route. As a result, the time for the peeling work was shortened by 1 h/day, and the nighttime rate got increased to 95.0%.

Conclusion

By replacing the old No. 1 electrowinning plant with the new No. 3 electrowinning plant, the improvement cost effects were obtained as shown in Table 4. If the nighttime power rate improves by 1%, it will save about $ 125,000. So, 8% improvement results

Table 4 Improvement effect amount by the new No. 3 electrowinning plant

Items	Annual improvement amount (US$)
Labor cost	2,280,000
Nighttime power rate	(87–95%) 1,000,000
Electric power consumption rate	(3110–3014 kWh/t) 290,000
Repair and equipment renewal costs	1,630,000
Other improvements	580,000
Total amount	5,780,000

in a reduction of about $ 1 million. In addition, the effect of the automated peeling work saved the labor cost significantly.

Labor costs, repair and renewal costs, and nighttime power rate were particularly effective, improving about $ 5 million per annum. As of 2019, the new No. 3 electrowinning plant is operating smoothly. However, the business environment is changing rapidly with a focus on the power situation. We will continue to make further cost improvements.

GCRIS

Zinc Recovery of Low Grade Concentrate from Vazante Mine by the Waelz Process

Fabiana M. Teixeira, Júlia M. Martins, Eder L. C. Martins, Pablo S. Pina, Thiago O. N. Leite, Sérgio A. Penchel Jr. and Tone Takayama

Abstract Nexa Resources processes electric arc furnace dusts (EAFD) and other sources of secondary zinc at its Juiz de Fora unit, mainly by the Waelz Process. Aiming to increase the Waelz furnace feed, decrease stocks of the mines, and improve the company's recovery rate, a process to recover zinc from low grade concentrate produced at the Vazante mine that are not suitable for the traditional Roast-Leach-Electrowinning (*RLE*) process, due to the zinc content, were investigated in this study. The zinc concentrates, containing around 18–20% of zinc, were tested in a pilot scale Waelz furnace with the feed portion of 10 and 40% mixed with EAFD. Another input with 100% of this material was also investigated, and all tests were compared to the traditional feed of 100% EAFD. The parameters evaluated were zinc recovery yield and accretion formation inside the furnace. Other parameters of the furnace, such as reduction agent input, temperature, and residence time, were the same as the industrial Waelz process. The proposed process showed good response to accretion formation inside the furnace, such as with the increase in the portion of the low grade concentrate in the feed, and the accretions formation decreased. The technique was also efficient to zinc recovery yield with the feed portion of 10, 20, and 40% resulting around 92% of recovery. However, for the test feeding only the concentrate, the zinc recovery yield was decreased to 82%.

Keywords Base metals recovery · Low grade concentrates · Waelz process · Zinc

Introduction

The Waelz process is the most used route in the world for the treatment of electric arc furnace dust (EAFD) [1]. It is a pyrometallurgical process characterized by the volatilization of metals like zinc, cadmium, and lead in a rotary kiln from a solid mixture by means of reduction by coal or other reduction agent, generating a solid

F. M. Teixeira (✉) · J. M. Martins · E. L. C. Martins · P. S. Pina · T. O. N. Leite · S. A. Penchel Jr. · T. Takayama
Nexa Resources, Br 267, Km 119, Igrejinha, Juiz de Fora, Brazil
e-mail: fabiana.teixeira@nexaresources.com

© The Minerals, Metals & Materials Society 2020

A. Siegmund et al. (eds.), *PbZn 2020: 9th International Symposium on Lead and Zinc Processing*, The Minerals, Metals & Materials Series,
https://doi.org/10.1007/978-3-030-37070-1_18

slag [3]. Nexa Resources has developed the first and only industrial Waelz process in South America in order to recover zinc out of EAFD from steelmaking companies from Brazil.

The Waelz circuit from Juiz de Fora unit has an installed capacity to treat 200,000 tonnes of secondary materials but is currently operating at around 60% of its capacity due to market availability of EAFD [4]. During 2014–2018, the generation of dusts from steel mills in Brazil has varied from 86 to 100 kt.

Considering this idle capacity of the Waelz kiln, the company has investigated other sources of zinc, among them: batteries, effluent treatment sludge, and low grade concentrate from Vazante mine, a non-sulphide zinc orebody.

The objective of the present study was to investigate the performance of the Waelz process feeding low grade concentrate produced at the Vazante mine as a zinc bearing feed material in association to EAFD for the recovery of zinc oxide in a pilot scale Waelz kiln. The optimum conditions and parameters for these processes were also described.

Materials and Methods

The essays to evaluate the performance of the low grade zinc concentrate were conducted in the premisses of Nexa Resources Juiz de Fora, in a pilot scale horizontal rotary kiln seizing 4 m in length and 0.3 m of internal diameter coupled to a gas treatment system containing a dust catcher, cyclone, and bag filters.

Materials

The low grade zinc concentrate utilized in this study is generated on the flotation of carbonates to enrich the main zinc concentrate of Vazante mine. It is a silicate composed mainly of the following minerals: willemite (58.63%), dolomite (24.08%), and quartz (3.64%).

The EAFD sample used on the tests is a typical residue provided by a Brazilian steel mill. The mineralogy of EAFD dusts vary in content from the supplier; however, in all of them the main compounds found are: franklinite, zinc oxide, monticellite, and magnetite. The chemical compositions of both materials are presented in Table 1.

Test Parameters

Each test consumed 306 kg of raw materials and 108 kg of coarse coke charged in the kiln for a period of 36 h using a proportioning scale to guarantee continuous and even charging. The internal and kiln housing temperatures were measured every hour

Table 1 Chemical analysis of the raw materials

Element	Low grade concentrate (%)	EAFD (%)
Fe	10.29	29.24
Zn	16.58	18.34
Pb	0.46	1.58
Al	0.49	0.28
Mg	7.12	2.36
Ca	9.77	2.33
C	6.10	6.72
Cd	0.04	0.18
CaO	13.67	3.26
Al_2O_3	0.91	0.53
SiO_2	12.94	3.02
MgO	11.89	3.95

with an infrared thermometer (model TI-920, Instrutherm), while the temperatures of the dust catcher, cyclone, and bag filter were measured by thermocouples.

For heating the furnace, an LPG gas burner is used; the feed of the coke feedstock is started as soon as the internal temperature of the furnace reaches 600 °C. Figure 1 shows the layout of Nexa Juiz de Fora pilot plant. The range of temperature inside the furnace was 1000–1100 °C, and the residence time was 6–7 h; those parameters meet the industrial process parameters.

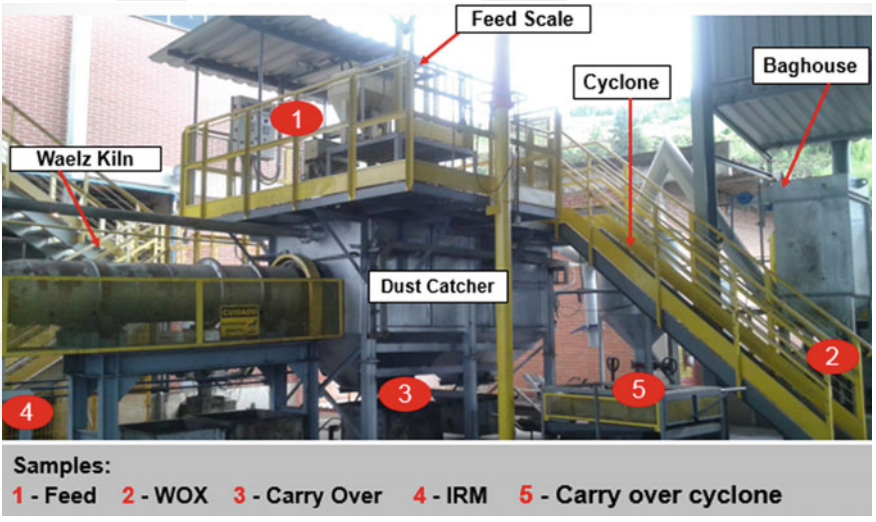

Fig. 1 Picture of the pilot scale Waelz kiln with its main components

Table 2 Tests planning

Test reference	EAFD feed (%)	LGCV feed (%)
Test 1	0	100
Test 2	90	10
Test 3	60	40
Blank test	100	0

When generation of slag starts, samples of the slag and Waelz oxide produced are taken every 4 h. At the end of each test, in addition to the sample of the oxide and slag, the carryover collected from the dust catcher and the material collected from the cyclone were sampled to calculate the mass balance and zinc yield. The evaluation of accretion formation is analysed through photographs taken every hour.

Processing of the low grade concentrate from Vazante mine (here on referred as LGCV) was tested for the following feed proportions: 10 and 40% LGCV mixed with EAFD, and 100% LGCV, with the objective of recovering the zinc contained in these materials and comparing them with the processing of 100% EAFD (Reference Test).

For the purpose of comparison, the yield, the accretion generation, and the quality of the slag generated in each test were analysed. The planning of the tests is shown in Table 2.

Results and Discussion

The pilot scale tests indicate that zinc yield did not decrease for feed of up to 40% LGCV. However, when feeding 100% of this concentrate, the zinc yield was only 82.67 versus 92.2% for the blank test. This may have taken place due to the lower extent of zinc reduction at the temperatures of 1000–1100 °C, present in the LGCV as willemite, a silicate, compared to the degree of zinc reduction in the ferrite, and zincite mineral forms in the EAFD.

Hu et al. [2] verify that zinc volatility is diverse in different carrier minerals, and that zinc in silicate appears lower than that in hematite and carbon, for example. Wu et al. [5] evaluated that all zinc present in ferrites reacts to form metallic zinc vapour at temperatures above 950 °C, which confirms the high performance of zinc recovery from the feed of 100% EAFD, as the main compounds of this material are ferrites. Figure 2 shows the yields obtained in each test.

For the accretion generation, the qualitative analysis of the kiln images indicates that as the percentage of LGCV in the blend is increased, there is a reduction in the formation of accretion, reaching no accretion formation in the test with 100% LGCV. This can be explained by the low iron content present in the material tested; as the accretion formation is mainly related to the formation of fayalite (Fe_2SiO_4), a mineral with low melting temperature (approximately 1000 °C), and a material with a low content of Fe have a tendency to form a minor amount of fayalite. Figure 3

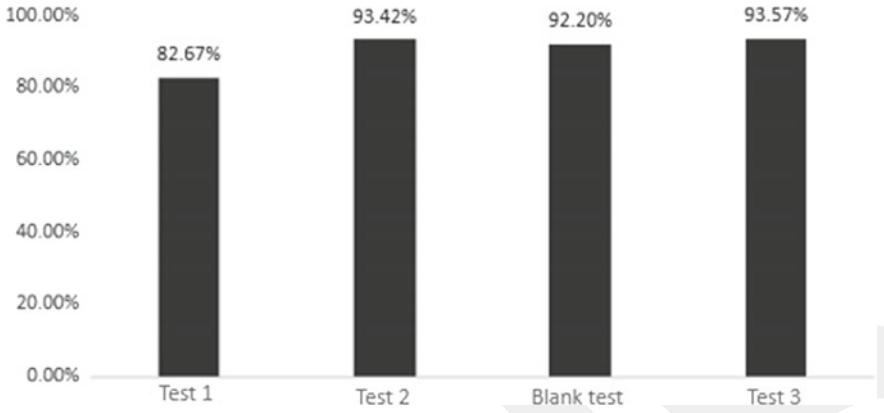

Fig. 2 Tests zinc yield

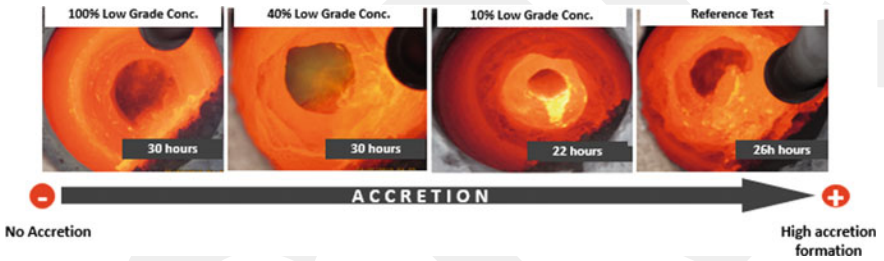

Fig. 3 Pictures of accretion formation inside the kiln during the tests

shows the evolution of accretion generation in the tests.

Regarding the quality of the slag, the tests indicated that the variation in the percentage of LGCV in the feed affects mainly the Fe content. Therefore, as currently the slag generated in the industrial process is applied as an iron source for cement production and also for the production of sinter for steel mills, the percentage of low grade concentrate in the industrial scale feed should be limited to 10%. Table 3 presents the slag quality of each test.

Conclusions and Recommendations

The low grade zinc concentrate from the Vazante mine is suitable for feeding the Waelz kiln for the generation of zinc oxide. Zinc recovery was not reduced up to 40% of the low concentrate in the feed blend. In addition, the accretion formation in the furnace was reduced as the percentage of low feed concentrate increased, which is very desirable as this phenomenon may lead to interruptions in the cleaning process.

Table 3 Chemical composition of the slags of each test

Element	Blank test (%)	Test 1 (%)	Test 2 (%)	Test 3 (%)
Fe	46.35	16.03	45.80	33.15
Zn	3.66	8.39	3.37	3.72
Pb	0.01	0.02	0.01	0.01
Al	0.56	0.76	0.53	0.87
Mg	3.39	11.93	5.54	8.93
Ca	7.05	14.37	7.77	14.47
C	0.13	6.33	0.12	0.02
Cd	0.00	0.00	0.00	0.00
CaO	9.87	20.12	10.88	20.26
Al_2O_3	1.05	1.42	1.00	1.64
SiO_2	5.00	18.34	6.68	12.68
MgO	5.66	19.92	9.25	14.91

There was no significant impact on the chemical composition of the slag when treating up to 10% of the low grade concentrate. The yield of zinc did not decrease with up to 40% of the low grade raw material in the feed blend.

References

1. Antrekowitsch J, Steinlechner S, Unger A, Rösler G, Pichler C, Rumpold R (2014) Handbook of recycling, Chapter 9: Zinc and residue recycling, pp 113–124
2. Hu W, Xia H, Pan D, Wei X, Li J, Dai X, Yang F, Lu X, Wang H (2018) Difference of zinc volatility in diverse carrier minerals: the critical limit of blast furnace dust recycle. Miner Eng:24–31
3. Morcali MH, Yucel O, Aydin A, Derin B (2012) Carbothermic reduction of electric arc furnace dust and calcination of Waelz oxide by semi-pilot scale rotary furnace, pp 173–184
4. Takayama T, Magalhães W, Santos FM (2015) Treatment of secondary raw materials at Juiz de Fora Zinc smelter in Brazil. Proceedings of EMC
5. Wu C, Chang F, Chen W, Tsai M, Wang Y (2014) Reduction behavior of zinc ferrite in EAF-dust recycling with CO gas as a reducing agent. J Environ Manag:208–2013

A Dynamic Model of a Submerged Plasma Slag Fuming Process

Samant Nagraj, Mathias Chintinne, Muxing Guo and Bart Blanpain

Abstract Submerged plasma slag fuming technology is a process intensification of the traditional (coal-fired) slag fuming technology. A general dynamic model of the plasma-driven slag fuming process has been developed in FactSage 7.0 based on Metallo Belgium's industrial scale submerged plasma slag fuming furnace. This model describes the chemical reactions, phase equilibria and heat transfer in each sub-unit operation, and the heat and mass transfer between the subsequent sub-unit operations of the slag fuming process. The model was validated on several process batches. Upon assessing the simulation results, a deviation was found from the industrial process, which can be explained using kinetic factors.

Keywords Metal extraction · Metal recycling · ZnO · FactSage

Introduction

Slag fuming is a reduction process to recover Zn from zinc-rich metallurgical residues such as lead blast furnace slag, secondary copper smelter slag, and electric arc furnace dust. The process involves three steps: (1) heating the slag over Zn vaporization temperature, (2) reducing the ZnO in the slag by a reducing agent and evaporating the Zn from the molten slag bath, and (3) cooling the Zn vapours to collect metallic Zn condensate or oxidizing the Zn vapour with air to produce ZnO precipitates. Several technologies have been developed over the years based on this principle, such as the Waelz-kiln process, the Enviroplas process, and the QSL process [1–3].

In a conventional fuming process, the heating of the slag bath is generally done by injecting product gases of combusted fossil fuel (typically, coal and natural gas) into the reactor through side submerged tuyeres or a top submerged lance. The product

S. Nagraj (✉) · M. Chintinne
Metallo Belgium N.V., Nieuwe Dreef 33, 2340 Beerse, Belgium
e-mail: samant.nagraj@metallo.com

S. Nagraj · M. Guo · B. Blanpain
Department of Materials Engineering (MTM), KU Leuven, Kasteelpark Arenberg 44, 3001 Leuven, Belgium

© The Minerals, Metals & Materials Society 2020

A. Siegmund et al. (eds.), *PbZn 2020: 9th International Symposium on Lead and Zinc Processing*, The Minerals, Metals & Materials Series,
https://doi.org/10.1007/978-3-030-37070-1_19

gases also act as a reductant for the ZnO reduction reaction [4]. Since these technologies require fossil fuel as both an energy source and a reductant, a significant amount is used, thereby emitting a considerable amount of greenhouse gases. Therefore, a new fuming technology has been developed in which fossil fuel burners are replaced with electrically powered non-transferred arc plasma torches as an energy source, and combustion gases are replaced with petroleum-coke pellets as a reductant [5]. Assuming that the electrical energy for the plasma torches is derived from renewable sources, the overall carbon footprint of the process is reduced significantly.

Several mathematical and empirical models of the conventional fuming process have been developed in the past to predict the Zn fuming rate, and to understand the rate-limiting factors of the process. Bell et al., Kellogg et al., and Grant et al. reported that the process happens at thermodynamic equilibrium, and fitted their model by adjusting the activity coefficient of ZnO [4, 6, 7]. On the contrary, the evidence from experimental studies, pilot and industrial tests showed that the fuming rate is limited by kinetic factors. Suzuki et al. investigated the effects of gas and slag composition, gas blast intensity, bath temperature, viscosity and surface tension of the slag on the fuming rate, and found that when the gas blast intensity is increased, the fuming rate also increased. Suzuki et al. also reported that the surface tension and the viscosity of the slag have a significant influence on the fuming rate [8]. Richards et al. conducted measurements of over 11 industrial fuming cycles and found that when coal particles were injected through the tuyeres, 55 wt% of the coal particles were combusted in the tuyere gas column, 33 wt% entrained in the slag, and 12 wt% bypassed the slag bath [9]. Using the industrial data, Richards et al. developed a mathematical model of the fuming process and found that by increasing the amount of entrained coal in the slag, the fuming rate can be enhanced [10, 11]. A study by Floyd et al. on solid reductants for slag fuming supported this idea [12]. Huda et al. developed a CFD model based on the study of Richards et al. to understand the fluid dynamics in the fuming reactor. It was found that there is a significant amount of splashing in the reactor, and the bypassed coal is undergoing a Boudouard reaction above the slag bath to form CO. This newly formed CO is also contributing to the Zn fuming on the slag bath surface [13].

A thermodynamic model of a continuous submerged plasma fuming process constructed by Verscheure et al. showed that the plasma enhances the fuming rate by a factor of 4.6 compared to the conventional fuming process [14, 15]. However, Verscheure's model was a steady state model and did not include kinetics which plays an essential role in the rate of fuming. Therefore, to investigate the thermodynamics and kinetics of the submerged plasma zinc fuming process, a dynamic model is developed based on the industrial scale plasma-driven fuming furnace at Metallo Belgium.

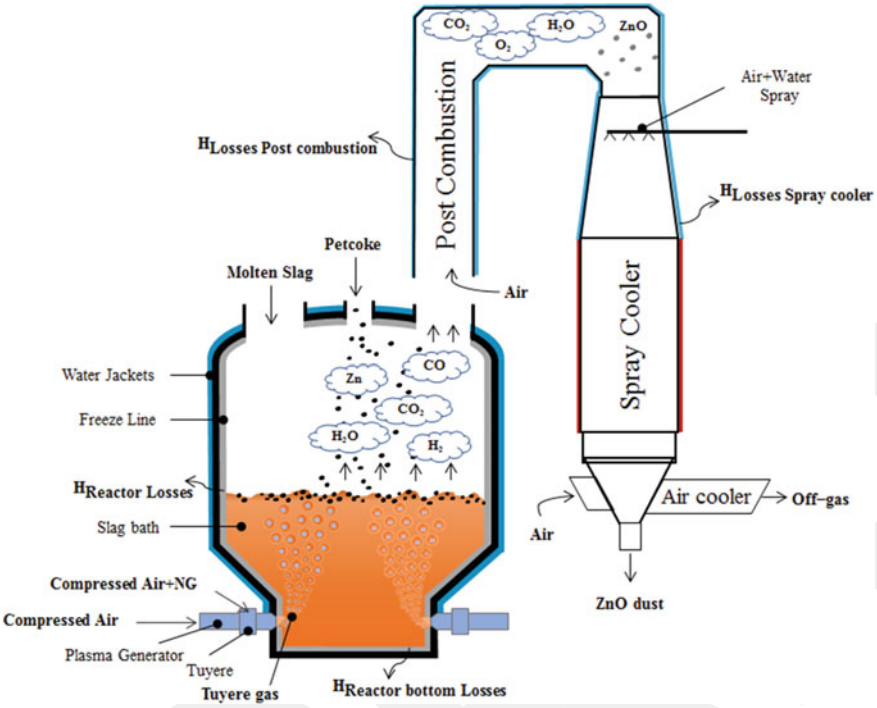

Fig. 1 Schematic of Metallo's submerged plasma slag fuming furnace

Metallo's Fuming Process

Metallo has a batch type fuming process, where a zinc-rich fayalite slag from the secondary copper smelter is treated to recover Zn. The furnace has three non-transferred arc plasma generators (PGs) and tuyeres located at the lower part of the reactor. A maximum of 3 MW can be delivered to each plasma generator. The reactor walls are water-cooled; therefore, the inner surface is covered with a layer of solidified slag called freeze lining. Freeze lining protects the reactor walls from thermal, chemical, and mechanical attacks. The freeze lining thickness influences the reactor heat losses, and it changes depending on slag composition, temperature, and fluid dynamics of the reactor. Figure 1 shows a schematic of Metallo's slag fuming process.

In this process, a molten fayalite slag is fed into the furnace at the beginning of the process. The air plasma is mixed with the natural gas in the tuyeres at a non-stoichiometric ratio. The tuyere gas is then injected into the molten slag bath. Petroleum-coke (petcoke) pellets are continuously added into the reactor to reduce the ZnO and to fume Zn. The interactions between the gas-phase, slag-phase, and petcokes are shown in Fig. 2 (the contours in the figures indicate the thermal gradient between the slag bath, gas bubble, and petcoke). The slag is tapped at the end of the process, and the reactor is prepared for the next batch.

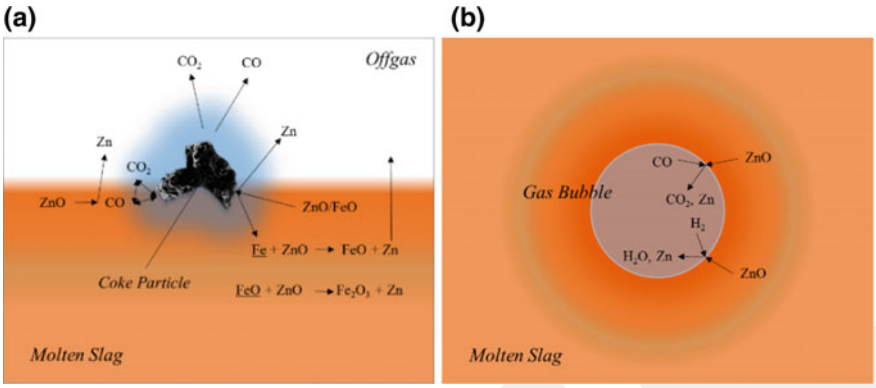

Fig. 2 (left) Petcoke—slag interactions, (right) Tuyere gas—slag interactions

Model Framework

Metallo's fuming process can be divided into five sub-unit operations, namely (1) production of plasma with compressed air in the plasma generators, (2) mixing of the air plasma with natural gas in the tuyeres, (3) reduction reactions between the slag-phase, gas-phase, and the petcoke pellets in the reactor and fuming of Zn, (4) combustion of the Zn fumes along with the off-gas in the post-combustion duct to produce ZnO precipitates, and (5) cooling of the off-gas and the ZnO precipitates in the spray cooler (Fig. 3).

Since, in a batch process, the conditions in the reactor change with time, a dynamic modelling approach is used, which allows determining the changes in process conditions with time. FactSage 7.0's macro processing was used to develop the model, and the databases FactPS, FToxid, and FTmisc were used. The thermodynamic equilibrium is calculated in every sub-unit operation. Each sub-unit is connected by streams

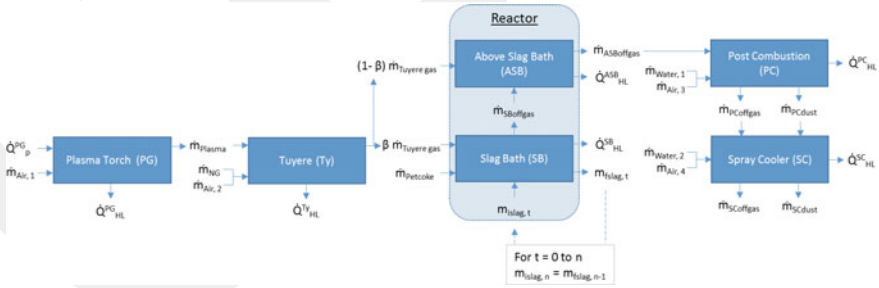

Fig. 3 Flowsheet of the submerged plasma slag fuming process model. PG—Plasma generator, Ty—Tuyere, SB—Slag bath, ASB—Above slag bath, PC—Post combustion, SC—Spray cooler, P—Power (kW), HL—Heat losses, i—Initial, f—Final, $\dot{Q}$—Heat flow rate (kW), $\dot{m}$—Mass flow rate (kg/h), m—Mass (kg), t—Time (s/min/h)

of heat and mass; the heat and mass transfer to the subsequent zones are assumed only after attaining the thermodynamic equilibrium. The heat supplied and lost in each sub-unit operation were also taken into account. Microsoft Excel was used as a user interface to set up the initial conditions for the simulations and to write the results.

The submerged plasma zinc fuming process is a complex process with several reactions between petcoke-slag, gas-slag, and petcoke-gas. Modelling the process and fitting with the reality would be challenging without making assumptions and simplifications. Therefore, the following assumptions and simplifications are made in the model while maintaining the crux of the process. It is assumed that the slag bath is homogenous (uniform in temperature and composition), the slag bath does not splash, the tuyere gas partially bypasses the slag bath, there is no interaction between the slag bath surface and the off-gas, the unreacted slag does not exist in the slag bath, and the freeze lining thickness changes with the process conditions.

Model Predictions

The dynamic model of the submerged plasma slag fuming process includes several aspects of Metallo's slag fuming process, such as change in bath height during fuming, changes in freeze lining thickness, two reaction zones in the reactor (in scenario-2), and heat losses in different reaction zones (in scenario-2). These features helped to predict the fuming rate, slag bath and off-gas temperature, slag bath and off-gas composition, and several other process parameters.

The data for the simulations were taken from Metallo's process database. The batches with a stable fuming cycle were selected for the simulation. For the fuming cycle considered to be stable, the following criteria must be satisfied: the plasma generator power and the under-pressure created at the post-combustion duct must be constant during the fuming, there must be no fluctuations in the reactor heat losses, there must be no outliers in the measured ZnO content of the slag (the coefficient of determination (R^2) of the ZnO content of the slag with time must be greater than 99%), and there must be no solid slag filling during the fuming process.

Two scenarios were simulated using the model to understand the rate-limiting factors of the fuming process. In the first scenario, it is assumed that the process happens at thermodynamic equilibrium, and there are no kinetic factors affecting the process. In the second scenario, it is assumed that the process is affected by kinetic factors. From the literature, it is known that the tuyere gas can partially bypass the slag bath, and it is not in thermal equilibrium. Therefore, the parameter tuyere gas efficiency, which is the amount of tuyere gas in equilibrium with the slag bath, is used to fit the calculated ZnO content with the measured ZnO content in the slag. The initial temperature of the slag bath ($T_{SB,i}$) is not measured and is an unknown. Therefore, it is used as a variable to understand the importance of this parameter on the fuming process.

Scenario 1

In this scenario, it is assumed that the fuming process happens at thermodynamic equilibrium, and no kinetic factors are involved. Ten fuming batches were selected, and three cases were simulated with initial slag temperatures T_{liq} °C (case 1.1), 1170 °C (case 1.2), and 1180 °C (case 1.3). The temperatures 1170 and 1180 °C were chosen as they are close to typical tapping temperatures, and the liquidus temperature of the slag was chosen as most pyro-metallurgical processes occur close to liquidus temperature of the material.

From the simulations, it was found that $T_{SB,i}$ influences the fuming rate. A slower fuming rate was observed when the $T_{SB,i}$ is lower and vice versa. However, a reasonable estimation of the $T_{SB,i}$ resulted in a much closer prediction of ZnO concentration in the slag (Fig. 4). Figure 5 shows the evolution of error between the calculated and measured fuming rate with time in different batches. If the error is positive (the calculated is larger than the measured ZnO fuming rate), the measured fuming rate is slower than the calculated and vice versa. In some batches (1, 2, 6, and 7), the fuming rate was faster than measured at the beginning of the process and slowed down at the end. While in some batches (4, 5, 8, 9, and 10), the fuming rate was slower from the beginning. Since the simulation is dynamic, the error had a snowball effect. However, by adjusting the $T_{SB,i}$, this effect was minimised, but the change was not prominent.

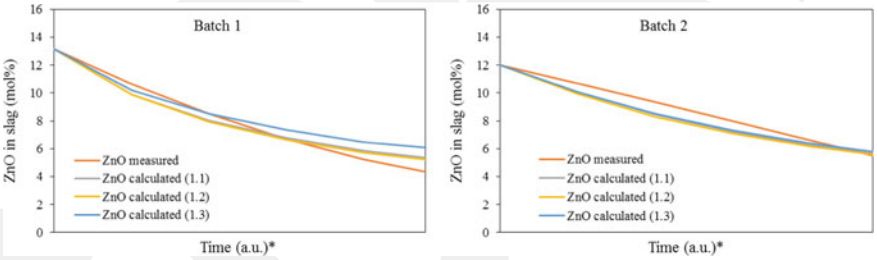

Fig. 4 Evolution of ZnO in slag bath in batches (left) 1 and (right) 2. *x-axis is omitted due to confidentiality

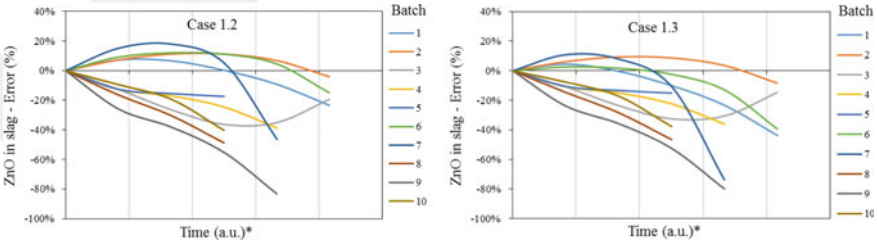

Fig. 5 Evolution of error between measured and calculated ZnO in slag in (left) Case 1.2 and (right) Case 1.3. *x-axis is omitted due to confidentiality

Scenario 2

In this scenario, it is assumed that the process has kinetic limitations. Here, the calculated ZnO content in the slag is fitted to the measured value using a kinetic parameter called tuyere gas efficiency, which is the amount of tuyere gas in equilibrium with the slag bath. The remaining tuyere gas bypasses the slag bath; therefore, the reactor is split into two reaction zones: slag bath and above slag bath. Since the $T_{SB,i}$ is unknown, three cases were simulated where $T_{SB,i}$ is set to T_{liq} (case 2.1), T_{liq}—10 °C (case 2.2), and T_{liq}—20 °C (case 2.3). The $T_{SB,i}$ is chosen close to the liquidus temperature of the slag because most pyro-metallurgical processes occur close to the liquidus temperature of the material.

Figures 6 and 8 show the fitted fuming rates and slag bath's ZnO content at different $T_{SB,i}$ for batches 1 and 2, respectively. The temperature of the slag bath decreased at the beginning and then increased with time in both batches. This is because of the changes in the slag composition in the reactor with time. When the composition of the slag bath changes, the thermal and physical properties of slag bath such as solidus and liquidus temperature, heat capacity and viscosity also change, affecting the slag bath temperature (T_{SB}) and the fuming rate.

The $T_{SB,i}$ also has a significant influence on the tuyere gas efficiency (η_{tuy}) and the T_{SB}, but only at the beginning of the process (Figs. 7 and 9). This phenomenon

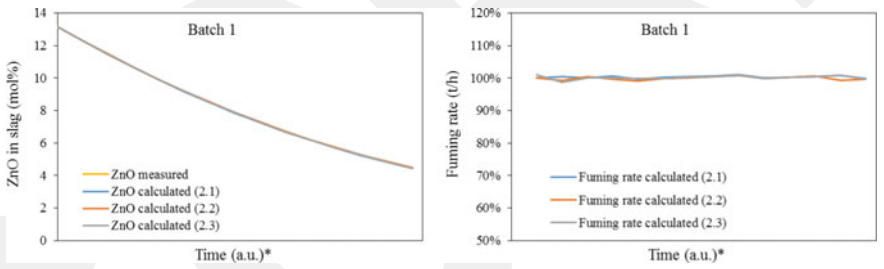

Fig. 6 Evolution of (left) ZnO in slag and (right) fuming rate in batch 1. *x-axis is omitted due to confidentiality

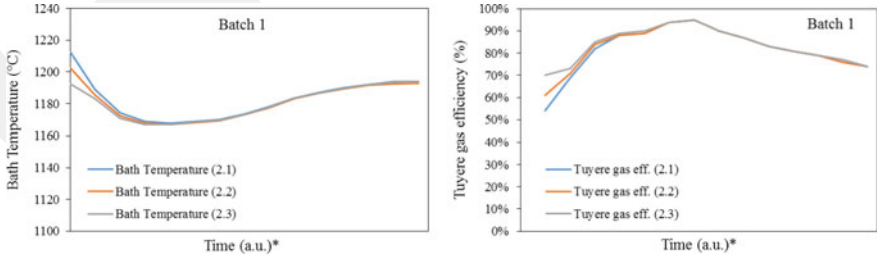

Fig. 7 Evolution of (left) slag bath temperature and (right) tuyere gas efficiency in batch 1. *x-axis is omitted due to confidentiality

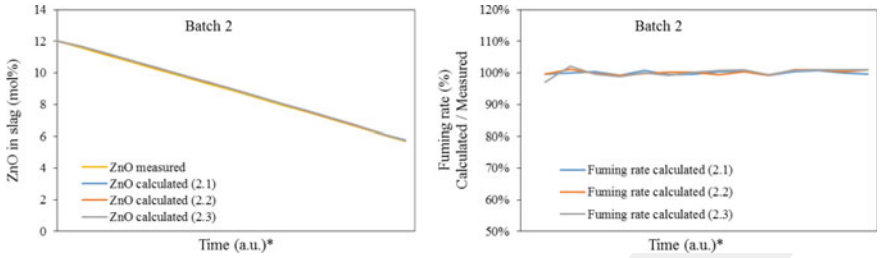

Fig. 8 Evolution of (left) ZnO in slag and (right) fuming rate with time in batch 2. *x-axis is omitted due to confidentiality

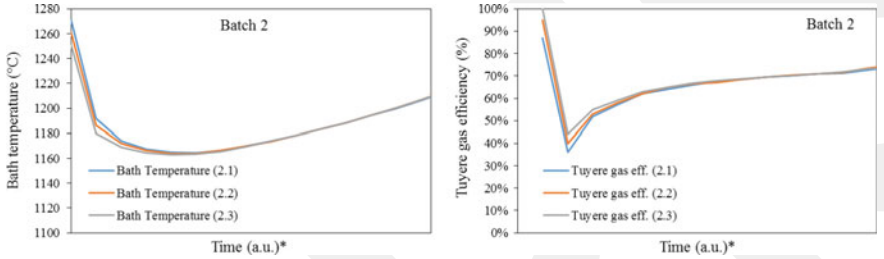

Fig. 9 Evolution of (left) slag bath temperature and (right) tuyere gas efficiency with time in batch 2. *x-axis is omitted due to confidentiality

is observed in all batches. This irregularity in the initial part of the fuming cycle can be minimised by having a good prediction of the $T_{SB,i}$.

From Fig. 7, it is apparent that the η_{tuy} changes with process conditions. For some batches, the η_{tuy} determined by the model is in close agreement with the Richards et al. industrial measurements and Huda et al. CFD model predictions, which is approximately 85%. However, for other batches, the efficiency is as low as 60% despite having similar bath heights. It is hypothesised that the parameters such as slag chemistry, T_{SB}, slag bath height, and slag viscosity influence the η_{tuy}. Therefore, further investigation is needed to understand the correlation between the η_{tuy} and the other process parameters (Figs. 8 and 9).

Conclusion

A dynamic process model of submerged plasma zinc fuming process is developed in FactSage 7.0 based on the industrial scale fuming furnace at Metallo Belgium. Several batches of industrial slag fuming have been simulated using the model. To understand the rate-limiting factors of Metallo's slag fuming process, two scenarios have been modelled. In the first scenario, it is assumed that the fuming process happens at thermodynamic equilibrium, whereas in the second scenario, the model

is fitted with a kinetic parameter called tuyere gas efficiency. It was found that the tuyere gas partially bypasses the slag bath, and the amount of gas bypass predicted by the model was in close agreement with the previous studies.

Moreover, the model predicted the process parameters such as final slag bath temperature, ZnO content of the slag, and the total amount of ZnO dust collected at the end of the process which is in close agreement with the industrial measurements. However, in some batches, the model predicted an abnormal amount of tuyere gas bypass. This abnormality can be explained by studying the correlation between the slag properties and the tuyere gas bypass.

Acknowledgements This research has received funding from the European Union Framework Program for Research and Innovation Horizon 2020 under Grant Agreement No. 721385 (EU MSCA-ETN SOCRATES; project website: http://etn-socrates.eu).

References

1. Clay J, Schoonraad G (1976) Treatment of zinc silicates by the Wealz process. J South Afr Inst Mining Metall 77(1):11–14
2. Abdel-latif M (2002) Fundamentals of zinc recovery from metallurgical wastes in the Enviroplas process. Miner Eng 15(11):945–952
3. Kim M, Lee W, Lee Y (2000) The QSL lead slag fuming process using an Ausmelt furnace. In: Dutrizac JE (ed) Lead-Zinc 2000. Minerals, Metals and Materials Society, Pittsburgh, pp 331–343
4. Bell R, Turner G, Peters E (1955) Fuming of zinc from lead blast furnace slag. JOM 203:472–477
5. Chintinne M, Geenen C, Coletti B, Smets S (2017) Production of clean slag at Metallo Belgium. Paper presented at the 9th European Metallurgical Conference, Leipzig, June 2017
6. Kellogg H (1967) A computer model of the slag fuming process for recovery of zinc oxide. Trans Metall Soc AIME 239:1439–1449
7. Grant R (1980) The derivation of thermodynamic properties of slags from slag fuming plant data. Paper presented at the Australia/Japan extractive metallurgy symposium, Sydney
8. Suzuki R, Goto K, Azuma K (1970) On fuming of zinciferrous slags. J Fac Eng Univ Tokyo, B 30(3):247–288
9. Richards G, Brimacombe J, Toop G (1985) Kinetics of the zinc slag-Fuming process: Part I. Industrial measurements. Metall Trans 16B:513–527
10. Richards G, Brimacombe J (1985) Kinetics of the zinc slag-Fuming process: Part II. Mathematical model. Metall Trans 16B:529–540
11. Richards G, Brimacombe J (1985) Kinetics of the zinc slag-Fuming process: Part III. Model predictions and analysis of process kinetics. Metall Trans 16B:541–549
12. Floyd J, Leahy G, Player R, Wright D (1978) Submerged combustion technology applied to copper slag treatment. Paper presented at the Australia IMM, Queensland
13. Huda N, Naser J, Brooks G, Reuter MA, Matcsewicz RW (2012) Computational fluid dynamics investigation of submerged combustion behaviour in a tuyere blown slag fuming furnace. Metall Mater Trans 43B:1054–1068
14. Verscheure K, Van Camp M, Blanpain B, Wollants P, Hayes P, Jak E (2007) Continuous fuming of zinc bearing residues: Part I. Model development. Metall Mater Trans 38B:13–20
15. Verscheure K, Van Camp M, Blanpain B, Wollants P, Hayes P, Jak E (2007) Continuous fuming of zinc bearing residues: Part II. The submerged plasma zinc fuming process. Metall Mater Trans 38B:21–33

Increase in Zinc Recovery from a Silicate Concentrate by Pre-neutralization Process

Maria José Dias, Adelson Dias de Souza, Caio César Spindola de Oliveira, Daniel Dayrell Pereira and Mateus Felipe Lourêdo Araújo

Abstract The Zinc leaching process of a silicate concentrate is very similar to the sulfide concentrate. One of the differences is the acidity: for the sulfide process (after pyrometallurgical route), it can go up to 60 g/L; for the silicate it is around 10 g/L. However, in order to improve the zinc recovery from the silicate (97.63%), it was necessary to increase the acidity to 25 g/L, without consuming extra neutralizing reagent. To achieve that, the pre-neutralization process was tested where 6% of the zinc silicate concentrate pulp was diverged to the end of the process, while 94% of all the material received the extra acidity, resulting in an increased recovery of 98.47%. However, when adding the diverged flow, the overall recovery falls to 98.27%. These results showed that the pre-neutralization process is applicable to the silicate leaching process and can increase the recovery up to 0.64%.

Keywords Silicate · Pre neutralization · Leaching

M. J. Dias · A. D. de Souza · C. C. S. de Oliveira (✉) · D. D. Pereira · M. F. L. Araújo
Nexa Resources, BR040, km 284, Três Marias 39.205-000, MG, Brazil
e-mail: caio.oliveira@nexaresources.com

M. J. Dias
e-mail: maria.dias.md1@nexaresources.com

A. D. de Souza
e-mail: adelson.souza@nexaresources.com

D. D. Pereira
e-mail: daniel.pereira@nexaresources.com

M. F. L. Araújo
e-mail: mateus.araujo.ma1@nexaresources.com

© The Minerals, Metals & Materials Society 2020

A. Siegmund et al. (eds.), *PbZn 2020: 9th International Symposium on Lead and Zinc Processing*, The Minerals, Metals & Materials Series,
https://doi.org/10.1007/978-3-030-37070-1_20

Introduction

Overall Interest on Zinc Oxidized Ores

Hydrometallurgical extraction of metals from its ore has innumerous advantages over the pyrometalurgical route chiefly because it is more attractive economically, technically and environmentally. Additionally, it costs less and does not emit hazardous gases such as SO_2, for instance [1].

It is known that the production of zinc from sulfide ores has its benefits due to its great separation from gangue as well as to easily concentrate through flotation techniques. Nevertheless, with the decline of zinc sulfide reserves worldwide and the restrictions on SO_2 emissions during its processing, there has been an increased interest in processing reserves of zinc oxide ores [2]. Besides, according to [3], oxidized zinc deposits has such advantages in comparison with non-oxidized deposits:

– High zinc content when compared to sulfide zinc ores (zinc is greater than 10%);
– Low hardness type of ore which demands minor detonations;
– In general, it is exploitable in open cast mines.

Furthermore, the combination of both pyro and hydrometallurgical routes is responsible for the main production of zinc by RLE (Roasting-Leaching-Electrolysis) [4]. One of the oxidized ores containing zinc is named silicate (Zn_2SiO_4), which is found in nature and denominated as willemite, its mineral name given by geologists [5]. This zinc ore is commercially treated and processed through a hydrometallurgical and solvent extraction technology in two places worldwide: Nexa Resources (in Brazil) and Skorpion Zinc (in Namibia), respectively.

Silicate Leaching Process

Regarding silicate concentrate [6]. Três Marias zinc facility has devised an integration of both silicate and sulfide concentrate processes. In this zinc plant, which belongs to Nexa Resources, the silicate treated ore is received from Vazante's mine, which also belongs to the same company. At Vazante's mine, the ore is extracted from an underground mine and goes through such processes as: comminution, flotation, thickening and filtration. The result is a concentrate with 40% zinc content and 15% humidity, on average.

At Três Marias' site, the concentrate is repulped with a solution containing 50 g/L of zinc and feeds the pressure leaching process, which employs autoclaves. In this process, the soluble zinc from the secondary solution precipitates as zinc hydroxide and the calcium and magnesium carbonates contained in the solid are solubilized in the form of sulfates (Eqs. 1 and 2).

$$MgCO_3 + ZnSO_4 + H_2O \rightarrow Zn(OH)_2 + MgSO_4 + CO_2 \quad (1)$$

$$CaCO_3 + ZnSO_4 + 3H_2O \rightarrow Zn(OH)_2 + CaSO_4 \cdot 2H_2O + CO_2 \quad (2)$$

This leached pulp is filtered and the cake is submitted to a leaching process in order to extract the higher zinc content as possible from the solid. The acid dissolution of willemite is best described by (Eq. 3):

$$Zn_2SiO_4 + 2H_2SO_4 \rightarrow 2ZnSO_4 + SiO_2 + 2H_2O \quad (3)$$

In this stage, the leaching agent is called attack solution (recirculated electrolysis spent solution, enriched with concentrated sulfuric acid, containing 50–55 g/L of zinc and 200–210 g/L of H_2SO_4). The usual holding time for this stage is around 7 h. It is also necessary to employ steam throughout this stage once the likelihood of silica gel formation is considerable. For this reason, a range of 90–95 °C temperature is kept, aiming at colloid dehydration (($Si(OH_4)$)) which leads to a gel formation and thus, poor solid-liquid separation and filtration rate of the slurry.

Moreover, silica gel formation during the leaching process has severe effects in the subsequent processing of leach liquor such as great reduction of slurry filterability, which leads to using large quantities of wash water to reach fair recovery of desired metals from the filter cake. In this way, several attempts have been made to counteract this problem. It was found that by coagulating colloidal silica, it is essential to have (i) pH controlling, (ii) increase in temperature, (iii) need of longer holding or conditioning time and (iv) adding an ionic or organic coagulant [1].

Because most of the zinc that is treated in the Três Marias' unit comes from the silicate source, it is fundamental to reach the best recovery in this circuit which highly affects the global zinc recovery.

Basically, by increasing the mass of acid used to leach the silicate, higher recovery is expected once more zinc contained in the solid is extracted. However, after performing solid-liquid separation, the high residual acidity of the generated under flow slurry becomes an issue. Once this material is mixed with the iron removal slurry, the mixture needs to be neutralized for fluorine removal and for filtration purposes. In this way, before mixing, the pre neutralization process is applicable to the high acidity under flow slurry in order to lower the under flow free acidity and not to cause process variables modifications, such as neutralizing consumption.

Results and Discussion

Several pilot plant tests were carried out in order to measure the effective gain adopting the so-called pre neutralization process. Firstly, the leaching process itself was submitted to a higher acidity using higher volume of attack solution. In this case, a range of 1.7–1.75 kg H_2SO_4–/kg Zn was tested. This procedure was aimed at extracting more zinc from the solid and thus achieved a higher recovery. With this, the residual acidity which was 8–12 g/L went up to 20–25 g/L and the usual recovery

Table 1 Chemical characterization of the silicate cake

Element	Content (%)
Zn	40.67
S_iO_2	17.69
Mg	1.30
Ca	3.64
Fe	4.10

of about 97.63% could get up to 98.47%. The amount of silicate cake tested to neutralize the necessary amount of acid followed a ratio of 1.41 kg dry mass/kg H_2SO_4. The mean chemical characterization of the silicate cake is described in Table 1.

Industrially, this process is applied after the pulp sedimentation by diverging approximately 6% of zinc silicate cake repulped with attack solution to the tanks that receive the high acidity under flow slurry (Fig. 1).

The reaction time for this stage was not greater than 1 h. The overall results are summarized in Table 2.

It is important to highlight that by increasing the mass of sulfuric acid during leaching time, the gain in terms of recovery fluctuated at around 0.84% whereas in the pre-neutralization stage, the loss figured at 0.21%. The loss was expected somehow, once the neutralization agent (silicate cake) carries over 40% of zinc content not

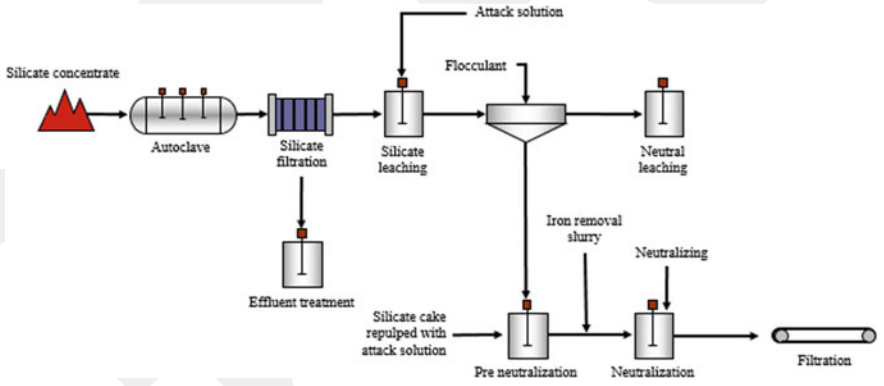

Fig. 1 Três Marias' silicate leaching process with pre-neutralization stage. *Source* Nexa Resources (2019)

Table 2 Overall results comparing process modifications

Leaching process	Residual acidity (1st stage) (g/L)	Final residual acidity (g/L)	Recovery (%)
Conventional	8–12	8–12	97.63
Applying pre-neutralization	20–25	8–12	93.27

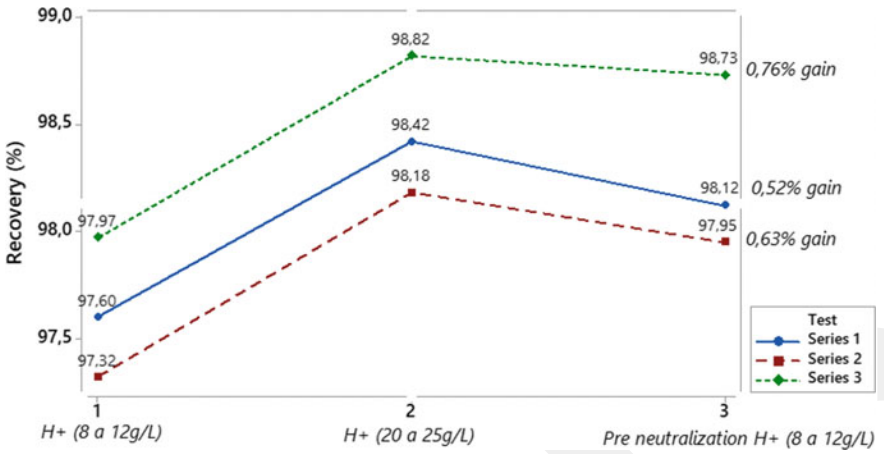

Fig. 2 Overall recovery of silicate leaching steps comprising pre-neutralization

entirely leached under the pre-neutralization process conditions. This fact can be illustrated below (Fig. 2).

By scaling up this process, a high level of automation is needed in order to guarantee process stabilization once the leaching conditions are quite sensible to parameters such as: attack solution flow, temperature, pulp flow and flow of repulped cake for pre-neutralizing the under flow slurry.

Conclusion

The pre-neutralization step applied to the silicate circuit in Três Marias' industrial zinc facility was studied. A simple modification in the silicate leaching process showed a higher zinc recovery which figured at 0.64% on average compared to the current process conditions. This was decisively achieved using the same inlet to the leaching process as the neutralizing agent. Finally, these modifications did not require any other process parameter modification such as extra neutralizing consumption in the subsequent steps.

References

1. Abkhoshk E et al (2014) Review of hydrometallurgical processing of non-sulfide zinc ores. Hydrometallurgy 149
2. Cun-Xiong L et al (2009) Pressure leaching of zinc silicate ore in sulfuric acid medium. Trans Nonferrous Met Soc China 20

3. Boni M (2005) The geology and mineralogy of non-sulfide zinc ore deposits. In: Umetsu Y (ed) Lead & Zinc '05. Kyoto, Japan, TMS, Warrendale, PA, pp 1299–1313
4. Santos FMF et al (2010) The kinetics of zinc silicate leaching in sodium hydroxide. Hydrometallurgy 102
5. Takesue M et al (2009) Thermal and chemical methods for producing zinc silicate (willemite): a review. Prog Cryst Growth Charact Mater 55
6. Sousa AD (2010) Cinética de lixiviação dos concentrados de zinco utilizados na Votorantim Metais. Tese (Doutorado em Engenharia de Materiais). Universidade Federal de Ouro Preto, Ouro Preto

GCRIS

Recovery of Lead from Zinc Plant Residue by Alkaline Leaching Process Followed by Cementation

Jonghyun Kim, Min-seuk Kim, Kyeong Woo Chung, Kurniawan and Jae-chun Lee

Abstract Present work focuses on recovery of lead from a zinc plant residue (ZPR) in alkaline media. Firstly, Zn and Pb were selectively extracted in NaOH from ZPR containing 56.9% Pb, 0.34% Ag, 3.93% Zn, and 0.88% Cu. Lead was effectively leached in a two-step process. The leach-I solubilized 39.5% Pb and 58.5% Zn in 2.0 M NaOH at 25 °C and 10% pulp density in 30 min. Subsequent leaching in 3.0 M NaOH yielded overall extraction of >99% Pb and 67% Zn with stage efficiency of 59.5% Pb and 8.5% Zn. Above 99.9% Pb was recovered from the leach liquor in 30 min at 25 °C and Zn: Pb mole ratio = 1.2:1.0 by cementation using Zn powder. Interestingly silver in the final residue was enriched from 0.3% to 1.17% making it a promising resource of Ag.

Keywords Zinc plant residue · Lead · Zinc · Alkaline leaching · Cementation · Recovery

Introduction

The primary zinc is produced from its sulfide ores such as sphalerite, which accounts for more than 80% of the metal obtained globally using the conventional hydrometallurgical process combining the roasting, leaching, purification, and electrowinning steps [1, 2]. In the hydrometallurgical processing of zinc, the sulfide ore is first converted to the ZnO-rich calcine which is then subjected to the leaching with the sulfuric acid followed by a hot sulfuric acid leach step [3]. After the leaching process is over, the leach liquor after liquid/solid separation is purified and electrowon

J. Kim · M. Kim · Kurniawan · J. Lee (✉)
Resources Recycling, Korea University of Science and Technology (UST), Daejeon 34113, Republic of Korea
e-mail: jclee@kigam.re.kr

J. Kim · M. Kim · K. W. Chung · Kurniawan · J. Lee
Mineral Resources Research Division Korea, Institute of Geoscience and Mineral Resources (KIGAM), Daejeon 34132, Republic of Korea

© The Minerals, Metals & Materials Society 2020

A. Siegmund et al. (eds.), *PbZn 2020: 9th International Symposium on Lead and Zinc Processing*, The Minerals, Metals & Materials Series,
https://doi.org/10.1007/978-3-030-37070-1_21

for the zinc metal production. On the other hand, insoluble lead sulfate formed during the sulfuric leaching, besides the cadmium, silver, etc., are also concentrated in this residue. Therefore, it is worth recovering the valuable metals available in this secondary resource.

With the purpose of comprehensive recovery of valuable metals from the zinc plant residue (ZPR) from leaching step with the stress on the low energy consumption without any pre-treatment process, this study was carried out. The objective is to evaluate the possibility of recovering lead completely through a two-step alkaline leaching followed by cementation. The effects of parameters such as NaOH concentration, leaching time, temperature, and pulp density on the leaching of lead and NaOH concentration on the second step leaching were examined. Finally, the leach liquor after two-step leaching was subjected to the cementation process to obtain cemented Pb using Zn powder in the alkaline media.

Experimental

Material

Zinc plant residue sample used in this study was supplied by Young Poong Company (Kangwon, Korea). The ZPR sample as received contained some moisture, and therefore, it was dried at room temperature and then subjected to grinding to obtain the particle size of <315 μm (−50 mesh sieve). The chemical analysis of the digested sample given in Table 1 shows that the ZPR is mostly composed of 56.9% Pb with 3.93% Zn. Another significant component is that of Ag (0.34%), besides impurities such as Fe, Cu, and Al (0.2–0.8%).

The phase analysis performed by X-ray diffraction (XRD, D/MAX 2200, Rigaku Corp., Japan) is illustrated in Fig. 1. The XRD pattern of ZPR sample shows the presence of anglesite ($PbSO_4$) as the predominant phase, whereas no other phases could be found, perhaps due to unidentifiable low concentrations.

Table 1 Chemical compositions of zinc plant residue used in the study

Elements	Pb	Zn	Ag	Fe	Cu	Al
Wt (%)	56.9	3.93	0.34	0.79	0.88	0.21

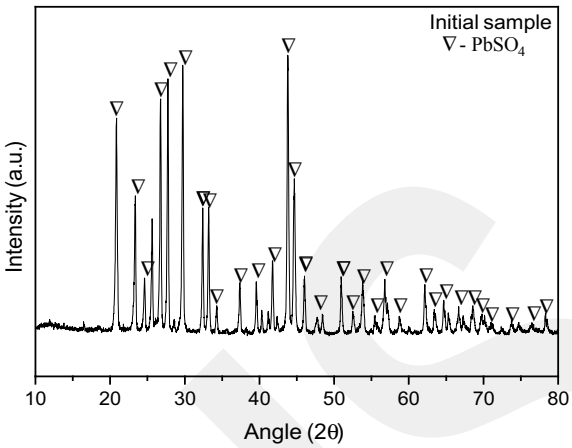

Fig. 1 XRD pattern of the initial ZPR sample

Methods

Leaching

The alkaline leaching was performed in a glass reactor (jacketed) with the magnetic stirrer set up in conjunction with a temperature controlled water bath circulator. After adding the predetermined concentration of NaOH solution to the reactor and setting the leaching temperature, a known amount of sample was added to the reactor. At the desired time intervals, 5 mL of slurry was withdrawn from the reactor, and the filtered solution was analyzed by using the Inductively Coupled Plasma-Atomic Emission Spectroscopy (ICP-AES; JY-38 plus, Jobin Yvon Ltd.).

Cementation

The cementation was also performed in a jacketed reactor set up with a temperature controlled water bath circulator. The leach liquor was transferred to the reaction vessel, and a predetermined weight of Zn powder was added for lead cementation at a desired temperature and agitation speed. The characterization of cemented lead particles was carried out using the scanning electron microscope (SEM) and energy dispersive X-ray (EDX) analyzer (Feico-95 Nova SEM).

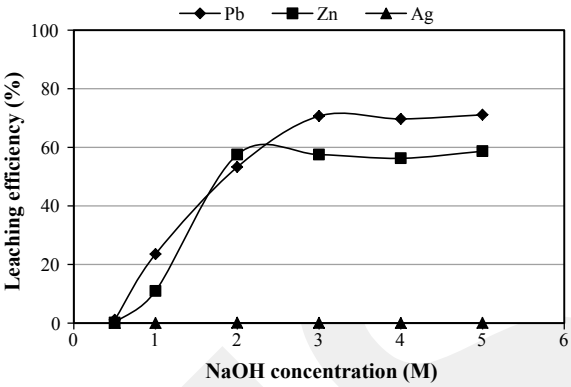

Fig. 2 Effect of NaOH concentration on the leaching of metals from ZPR at 50 °C for 1 h (PD, 10%)

Results and Discussion

First Step Leaching

Effect of NaOH Concentration

Figure 2 shows the effect of NaOH concentration on the leaching behavior of metals for 1 h at 50 °C temperature, 10% pulp density, and 300 rpm stirring speed. As can be seen, the leaching efficiency of the metals increased significantly with increase in NaOH concentration from 0.5 to 3.0 M except for Ag. With 3.0 M NaOH, the leaching efficiencies of Pb, Zn, and Ag after 1 h were found to be 70.7, 57.5, and 0.05%, respectively. The leaching efficiencies of Pb and Zn, however, remained almost constant from 3.0 to 5.0 M NaOH concentration. These results clearly reflect the high selectivity for the leaching of Pb and Zn over other metals when NaOH is used as a lixiviant. This can be attributed to the dissolution of Pb and Zn as complex anions, viz. PbO_2^{2-} and ZnO_2^{2-} in the alkaline media, whereas other impurity metals including Ag exhibit no or limited tendency of forming such soluble anions and hence join the leach residue. Particularly, the low silver leaching may be caused by the lower oxidizing conditions prevailing in the system.

Effect of Leaching Time

Effect of leaching time (2–60 min) on the leaching of metals was investigated in 2.0 M NaOH solution at 50 °C, 10% pulp density, and 300 rpm stirring speed. As can be clearly found in Fig. 3, the leaching time did not affect the extraction of Pb and Zn up to 60 min. To ensure that enough time is given for the complete reaction to proceed, the leaching was, therefore, carried out for 30 min resulting in the leaching efficiency of 52.6, 55.2, and 0.10% for Pb, Zn, and Ag, respectively.

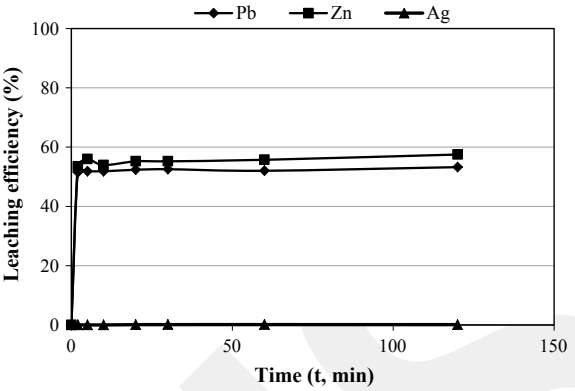

Fig. 3 Effect of time on the leaching of metals from ZPR using 2.0 M NaOH at 50 °C (PD, 10%)

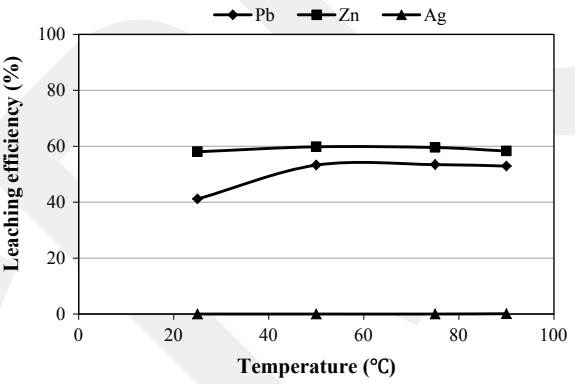

Fig. 4 Effect of temperature on the leaching of metals from ZPR using 2.0 M NaOH for 30 min (PD, 10%)

Effect of Temperature

The leaching behavior of metals versus temperature is illustrated in Fig. 4. The results show that the temperature has no effect on the leaching efficiency of Zn. For an instance, Zn extraction registered hardly any improvement, i.e., from 58.1 to 59.8% with the increase in the temperature from 25 to 90 °C. However, the leaching of Pb increased from 41.1 to 53.3% when the temperature was raised from 25 to 50 °C; the dissolution level remained almost constant beyond 50 °C and till 90 °C. Therefore, with the purpose of saving energy, leaching temperature of 25 °C was chosen as optimum for subsequent tests in the first leaching step.

Effect of Pulp Density

While varying the pulp density, the leaching behavior of metals is shown in Fig. 5. Under the leaching conditions of 2.0 M NaOH concentration, 30 min leaching time, 25 °C leaching temperature, and 300 rpm of stirring speed, the leaching efficiency

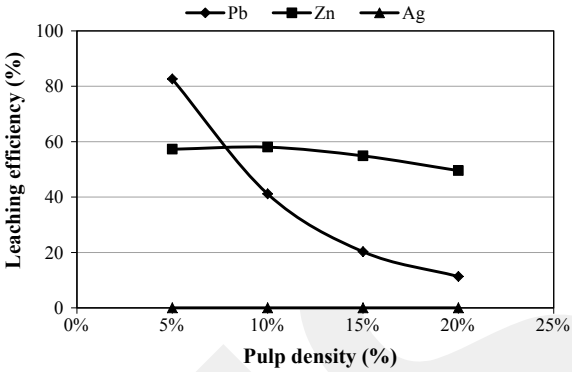

Fig. 5 Effect of pulp density on the leaching of metals from ZPR using 2.0 M at 25 °C for 30 min

of Pb decreased drastically, that is from 82.6 to 11.3% with the increase in the pulp density (PD) from 5 to 20%. The increase in pulp density from 5 to 20% has affected the leaching efficiency of Zn to a lesser extent, which dropped from 57.3 to 49.5%. With the purpose of further investigating the extraction of ZPR in the second step leaching, 10% pulp density was selected as the optimum value in the first step leaching, since Zn dissolution remained the same as that of 5% PD, with some compromise in the leaching of Pb.

Second Step Leaching

After the optimum conditions in the first step leaching, further experiments were performed under the conditions such as 2.0 M NaOH concentration, 25 °C temperature, and 10% of pulp density for 30 min of leaching time. In these conditions, the extraction of metals was found to be 41.1% Pb, 58% Zn, and 0.0% Ag. The purpose of the second step leaching was to increase the overall lead recovery as well as the enrichment of Ag in the leach residue. Table 2 shows the leaching efficiency of Pb, Zn, and other metals with 2.0 M NaOH solution in the first step and variation of NaOH concentrations in the second step.

When the residue from the first leaching step (under the stipulated conditions) was subjected to the second step of leaching using different concentrations of NaOH, the leaching efficiency of Pb improved significantly. Thus, lead dissolution increased from 28.1 to 60.6% with increase in the NaOH concentration from 1.0 to 4.0 M. Total leaching efficiency of Pb could reach ~100% after the leaching with 2.0 M NaOH in the first step (39.5%) and 3.0 M NaOH in the second step (60.6%). Moreover, two-step leaching with 3.0 and 4.0 M NaOH concentration in the first step followed by the second step leaching with 3.0 and 2.0 M NaOH was also carried out.

Notwithstanding the leaching behavior of lead, NaOH leaching in the second step did not have a strong effect on the extraction of Zn. With the increase in the NaOH concentration from 1.0 to 4.0 M, leaching efficiency of Zn just increased in the range

Table 2 Leaching efficiency of metals with 2.0 M NaOH (temperature, 25 °C; time, 30 min; PD, 10%) in the first step and NaOH concentration variation in the second step

NaOH (M)	Leaching efficiency of metals (%)					
2.0 M + 1.0 M	Pb	Zn	Ag	Fe	Cu	Al
1st step	40.4	52.4	0.0	0.1	0.0	2.2
2nd step	28.1	4.1	0.0	0.0	0.0	0.3
Total efficiency	68.5	56.5	0.0	0.1	0.0	2.5
2.0 M + 2.0 M	Pb	Zn	Ag	Fe	Cu	Al
1st step	39.1	55.2	0.2	0.3	0.1	1.3
2nd step	48.7	1.7	0.1	0.1	0.1	1.1
Total efficiency	87.7	56.9	0.2	0.3	0.2	2.3
2.0 M + 3.0 M	Pb	Zn	Ag	Fe	Cu	Al
1st step	39.5	58.5	0.1	0.1	0.1	2.4
2nd step	60.6	8.6	0.2	0.2	0.2	1.4
Total efficiency	100.0	67.1	0.3	0.3	0.2	3.8
2.0 M + 4.0 M	Pb	Zn	Ag	Fe	Cu	Al
1st step	40.8	57.8	0.0	0.1	0.1	2.4
2nd step	~59.2	9.7	0.3	0.4	0.2	1.6
Total efficiency	~100.0	67.4	0.3	0.5	0.3	4.0

1.7–9.7%. Therefore, total leaching efficiency of Zn was observed to be in the range 56.5–67.4% after the first step with 2.0 M NaOH and the second step with 1.0–4.0 M NaOH. The leaching efficiency of Zn compared to lead may be attributed to the presence of ZnS or Zn-ferrite which would be formed in TSL process. On the other hand, the extraction of Ag in the solution was found to be negligible (0.1–0.2%) after following the two-step leaching. Therefore, leaching with 2.0 M NaOH (1st step) followed by that of 3.0 M NaOH concentration in the second step for 30 min at 10% pulp density and 25 °C was selected as the optimum conditions in order to achieve the extraction efficiency of ~100% Pb and 67.1% Zn in the solution.

Cementation

Table 3 shows the chemical composition of the leach liquor after mixing the leach solution from step-I and step-II leaching with 23.6 g/L Pb, 1.21 g/L Zn, and less than 0.01 g/L of other impurities. After the leaching, the cementation process was carried out to investigate the recovery of Pb using Zn powder.

Table 3 Chemical composition of the leach liquor before cementation

Elements	Pb	Zn	Ag	Fe	Cu	Al
Content (g/L)	23.6	1.21	–	0.0013	0.0064	0.0064

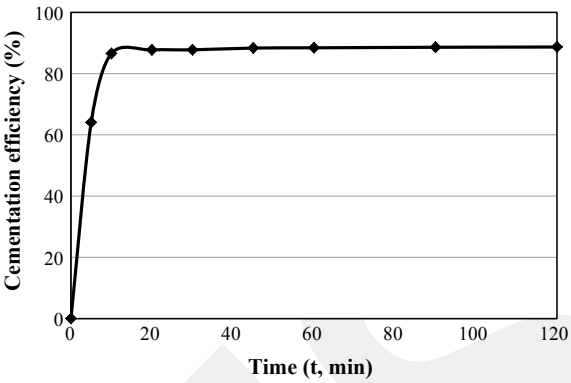

Fig. 6 Effect of time on the lead cementation in alkaline media at 50 °C (Zn:Pb mole ratio = 1.0:1.0)

Effect of Time on the Cementation of Lead

Firstly, the experiments were carried out to investigate the effect of time on the cementation behavior of Pb using the Zn powder. After 10 min, the reaction was almost completed and gave 86.6–88.7% cementation efficiency over a period of 2 h under the conditions mentioned in Fig. 6 at 1.0:1.0 Zn:Pb mole ratio. To ensure the reaction to complete under all conditions, 30 min time was chosen for the subsequent experiments.

Effect of the Quantity of Zn Powder

Figure 7 indicates the effect of quantity of Zn on the lead cementation with the mole stoichiometric value of Zn in the range 1.0–2.0. The results show that the recovery of Pb could reach ~100% at 1.2:1.0 mol ratio at 50 °C and 30 min of cementation time. Therefore, the Zn powder equal to 1.2 times the stoichiometric (mole) requirement was selected as the Zn dose.

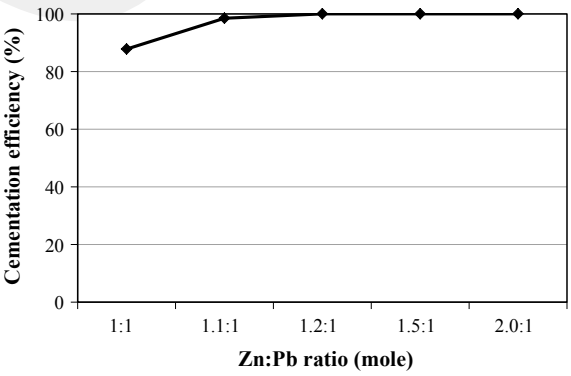

Fig. 7 Effect of quantity of Zn on the lead cementation in alkaline media at 50 °C for 30 min

Effect of Temperature

Effect of temperature (25, 40, and 50 °C) was examined with the purpose of reducing the energy consumption in the Pb cementation. As can be seen in Fig. 8, the change of temperature had no effect on the Pb cementation efficiency. At 25 °C and 30 min of cementation time using 1.2:1.0 Zn:Pb mole ratio, 99.9% of cemented Pb could be recovered with the purity of 97.6% (including 1.2% Zn as a major impurity). Therefore, 25 °C can be fixed as the optimum temperature for the cementation.

The X-ray diffraction pattern illustrated in Fig. 9 indicates the product after cementation using Zn powder under the optimum cementation conditions. Only peaks corresponding to Pb and PbO phases could be identified without any other impurities.

In order to examine the morphology and the trace impurities of the cemented Pb product, SEM analysis has been conducted, and the images are shown in Fig. 10. The uniform globules of lead particles with dark gray color can be clearly seen in Fig. 10a

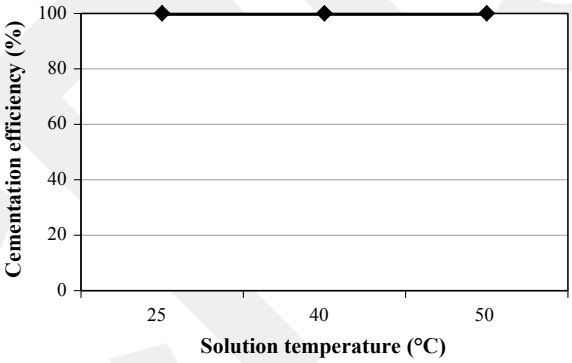

Fig. 8 Effect of time on the lead cementation in alkaline media for 30 min (Zn:Pb mole ratio = 1.2:1.0)

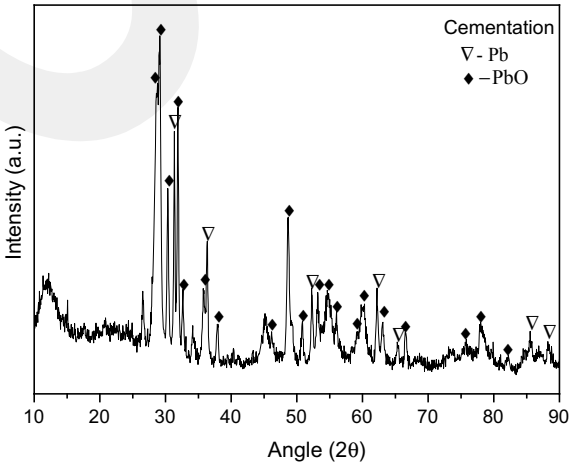

Fig. 9 XRD pattern of lead powders obtained from the leach liquor of ZPR by cementation using Zn powder
(Time, 30 min; Zn:Pb mole ratio = 1.2:1.0; temperature, 25 °C)

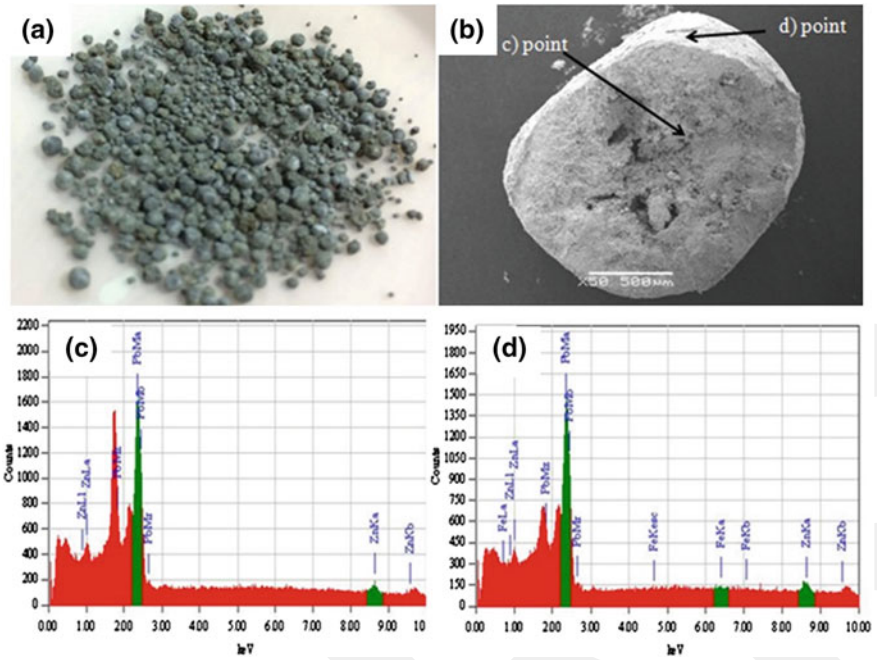

Fig. 10 SEM micrograph and EDS of cementation product using Zn powder (Zn:Pb mole ratio = 1.2:1.0; temperature, 25 °C; time, 30 min)

with the cross-section of one cementation particle shown in Fig. 10b. A comparison of the morphological features of a surface particle and that of the cross-section of the particle shows the uniform distribution of elements (SEM-EDS), which is illustrated in Fig. 10c, d, respectively. These results clearly show that during the reaction, the cemented Pb was agglomerated as the particle, together with unreacted Zn. In that, the elemental Pb was detected as the main component, besides a small amount of Zn; however, no evidence of other impurities was noticed.

Conclusion

A simple process has been developed to treat the zinc plant residue which is considered as a valuable secondary resource, to successfully recover Pb and Zn by following the approach such as alkaline leaching and cementation. While using a two-step process under the conditions of 2.0 M NaOH in the first step, + 3.0 M NaOH in the second step at the leach time of 30 min, temperature of 25 °C, and 10% pulp density, more than 99.9% Pb and 67% Zn could be leached out in the solution. 99.9% Pb could be recovered as the metallic lead (Pb^0) along with some PbO by the cementation with zinc at 25 °C and 1.2:1.0 mol of Zn:Pb ratio in 30 min of cementation

time. An important feature of the development is that it enriched silver the final leach residue turning the material into an economically promising resource for Ag recovery.

Acknowledgements The paper is based on the Basic Research Project (19-3212) of the Korea Institute of Geoscience and Mineral Resources (KIGAM) funded by the Ministry of Science and ICT, Republic of Korea.

References

1. Bahram B, Javad M (2011) Chloride leaching of lead and silver from refractory zinc plant residue. Res J Chem Environ 15(2):1–8
2. Li M, Peng B, Chai L, Peng N, Yan H, Hou D (2012) Recovery of iron from zinc leaching residue by selective reduction roasting with carbon. J Hazard Mater 237–238:323–330
3. Turan MD, Altundogan HS, Tumen F (2004) Recovery of zinc and lead from zinc plant residue. Hydrometallurgy 75(1–4):169–176

GCRIS

Zinc Residue Fuming Process in Side-Submerged Combustion Furnace + Fuming Furnace

Liang Xu and Shaobin Ma

Abstract Zinc hydrometallurgy is the main zinc smelting process in the world. The leaching residues produced by different hydrometallurgical processes have different components, but usually contain valuable metals such as zinc, lead, and silver. In China, the slag is defined as hazardous waste, which needs to be treated harmlessly while recovering valuable metals. This paper introduces the process of treating zinc residue by side-submerged combustion furnace and fuming furnace developed by ENFI and makes a detailed comparison with rotary kiln, top-submerged lance smelting furnace, and fuming furnace which are used in the China.

Keywords Zinc residue · Lance · Side-submerged combustion · Oxygen

Introduction of Zinc Residue Treatment Technology

Zn hydrometallurgy is the main zinc smelting technology in the world. It accounts for more than 85% of the total zinc smelting in the world. The leaching residues produced by different hydrometallurgical processes have different components, but usually contain valuable metals such as Pb, Cd, and As. China has identified leaching residues as hazardous waste. Therefore, zinc smelting smelter needs to dispose of leaching residues harmlessly and recover valuable metals such as zinc, lead, and silver at the same time.

At present, the main technology of zinc residues treatment in China is rotary kiln (Waelz), fuming furnace (FF) and top-submerged lance smelting furnace (TSL).

L. Xu (✉)
China ENFI Engineering Co., Ltd., Beijing 100038, China
e-mail: xuliang@enfi.com.cn

S. Ma
Yunnan Chihong Zn & Ge Co., Ltd., Huize 654200, China
e-mail: 2364310322@qq.com

© The Minerals, Metals & Materials Society 2020

A. Siegmund et al. (eds.), *PbZn 2020: 9th International Symposium on Lead and Zinc Processing*, The Minerals, Metals & Materials Series,
https://doi.org/10.1007/978-3-030-37070-1_22

(1) Waelz

The technology is most widely used. Its advantages are simple operation and mature technology. However, there are some shortcomings, such as large area, high processing cost, easy formation of kiln accretion and difficult to clean up, low silver recovery rate, and high cost of offgas treatment.

(2) FF

There are two smelters in China using the technology. Its advantage is that soft coal is used as fuel, the processing cost is low, and the waste heat recovery efficiency is high. However, there are some problems such as low smelting efficiency, high cost of offgas treatment, and high investment in construction.

(3) TSL

There is only one smelter in China using this technology. Its advantage is that it adopts oxygen-enriched smelting and has smelting efficiency and high waste heat recovery efficiency. However, there are shortcomings such as frequent replacement of spray guns, high cost of offgas treatment, and high investment in construction.

In view of the problems in the above technology, ENFI has developed side-submerged combustion furnace (SSC) + fuming furnace (FF) to treat zinc leaching residue technology, and it was successfully put into operation in July 2019. The technology has the advantages of simple operation, low energy consumption, high recovery rate of valuable metals, and less pollutant discharge. The technology is described below.

SSC + FF Technology

Reaction Principle of Zinc Residues Smelting

Zinc in zinc residues mainly exists in the form of $ZnO \cdot Fe_2O_3$, ZnO, ZnS, $ZnSO_4$, and $ZnO \cdot SiO_2$. Lead is mainly PbSO4. The main chemical reactions in zinc residues smelting are as follows:

$$C + O_{2(g)} = CO_{2(g)} - 393\,\text{kJ/mol} \quad (1)$$

$$C + CO_{2(g)} = 2CO_{(g)} + 172\,\text{kJ/mol} \quad (2)$$

$$ZnO \cdot Fe_2O_3 + SiO_2 + CO_{(g)} = ZnO + 2FeO \cdot SiO_2 + CO_{2(g)} - 23\,\text{kJ/mol} \quad (3)$$

$$ZnO + CO_{(g)} = Zn_{(g)} + CO_{2(g)} + 198\,\text{kJ/mol} \quad (4)$$

$$ZnS + 3/2O_{2(g)} = ZnO + SO_{2(g)} - 444\,kJ/mol \quad (5)$$

$$ZnSO_4 = ZnO + SO_{2(g)} + 1/2O_{2(g)} + 333\,kJ/mol \quad (6)$$

$$ZnO \cdot SiO_2 + CaO = ZnO + CaO \cdot SiO_2 - 88\,kJ/mol \quad (7)$$

$$PbSO_4 = PbO + SO_{2(g)} + 1/2O_{2(g)} + 405\,kJ/mol \quad (8)$$

$$PbO + CO_{(g)} = Pb_{(g)} + CO_{2(g)} + 131\,kJ/mol \quad (9)$$

$$Fe_2O_3 + CO_{(g)} = 2FeO + CO_{2(g)} + 5\,kJ/mol \quad (10)$$

$$FeO + SiO_2 - 2FeO \cdot SiO_2 - 33\,kJ/mol \quad (11)$$

$$SiO_2 + CaO = CaO \cdot SiO_2 - 89\,kJ/mol \quad (12)$$

$$H_2O_{(l)} = H_2O_{(g)} + 44\,kJ/mol \quad (13)$$

Reaction (1) is coal combustion reaction. The heat generated by combustion ensures the temperature of molten pool. The CO produced by reaction (2) maintains a reductive atmosphere in the molten bath area and ensures the reduction and volatilization of metals such as Zn and Pb.

Reactions (3), (4), (8), (9), (10), and (13) are the main reactions in zinc residues smelting, which need to absorb a lot of reaction heat. Reactions (5), (7), (11), and (12) are exothermic reactions, but these substances have less content or exothermic in the leaching residue, which has little influence on the overall thermal balance. In addition, the melting of all kinds of substances needs to absorb a lot of heat.

Therefore, it can be seen from the above reactions that in order to ensure the reduction and volatilization of lead and zinc, the reducing atmosphere and bath temperature must be ensured. The process of zinc residues smelting mainly consists of two steps: melting and reducing volatilization, while the main heat consumption in the whole process is melting. Therefore, the whole smelting process of zinc leaching residues is divided into two stages: SSC melting and fuming furnace fuming. SSC uses high oxygen-enriched combustion. Fuel combustion provides heat while maintaining a weak reductive atmosphere in the furnace, so as to save energy consumption. In the fuming stage, only hot slag is treated, and the heat consumption is mainly lead and zinc reduction,volatilization heat absorption, and furnace heat loss. Therefore, the energy consumption in the fuming stage is low.

Process Flow

Zinc residues are fumed in SSC + FF. As mentioned above, the main energy consumption is the heat absorption of residues melting, and the removal of sulfur is also in the melting stage. The SSC directly injects natural gas or pulverized coal from the side lance into the molten bath for heating and adds some crushed coal into the zinc residues from the top of the furnace. The crushed coal combusts with the oxygen of the lance and participates in the reduction reaction. Oxygen-enriched air concentration in the furnace injected by side lance is more than 50%, and excess oxygen coefficient is controlled from 0.8 to 0.9. The spray gun has multi-channel structure, fast burning speed, and flame temperature over 2000 °C. The combustion flame contacts the melt directly, and the gas injected into the molten bath at high speed ensures the stirring strength of the molten bath, accelerates the heat and mass transfer process in the molten bath, and completes the rapid melting of zinc residues. At the same time, the use of high oxygen-enriched air to combustion reduces the volume of offgas, improves the thermal efficiency of SSC, and significantly reduces the fuel rate. The temperature of the molten bath is controlled from 1200 to 1250 °C. A small part of zinc and most of lead, silver, and germanium volatilize into the offgas. The molten high zinc slag is discharged into the FF regularly through the chute.

The air and pulverized coal injected by the FF from the side tuyere. The incomplete combustion of pulverized coal produces CO and reductive atmosphere at the same time of heating. The excess oxygen coefficient of molten bath is controlled from 0.6 to 0.7. The FF uses air combustion. The blast intensity is greater than 20 $Nm^3/(min\ m^2)$, which provides enough stirring strength for the molten bath. The temperature of molten bath is maintained at 1250–1300 °C, and most of lead and zinc are reduced and volatilized into offgas. The final slag of FF is piled up after water crushing. The final slag contains less than 2% zinc and less than 0.2% lead.

The process flow chart is as in Fig. 1.

Engineering Cases

Overview

Yunnan Chihong Zn & Ge Huize smelter is currently producing 150,000 tons of zinc and 80,000 tons of lead per year. Among them, the original design of lead smelting process is TSL oxidation + SSC reduction, SSC reduction slag into the FF; zinc smelting process is roasting + low acid leaching, leaching residues, and SSC reduction slag of lead into the FF together. Due to the increase of production capacity of zinc system and the increase of zinc residues, the treatment capacity of FF is insufficient. In addition, there are a lot of low-grade lead-zinc oxide ore deposits in the mine of the Yunnan Chihong Zn & Ge. With the normal mining and production of the mine, a lot of lead-zinc oxide ores are still being produced every year and

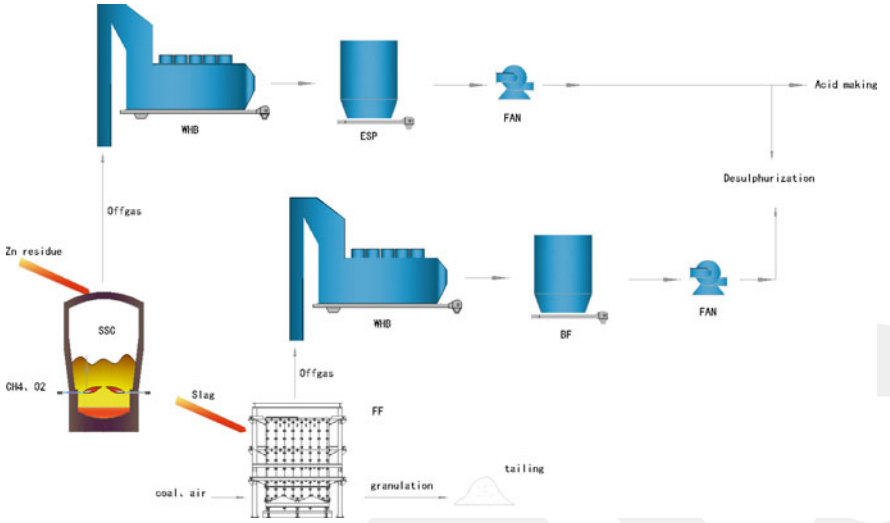

Fig. 1 Process flow of SSC and FF

cannot be effectively disposed of, and valuable metals such as lead and zinc have not been recovered.

Based on the above reasons, Huize smelter intends to build a new SSC in the existing plant, adjust the zinc residues treatment process to SSC + FF, and realize the treatment of 150,000 t/a of zinc residues, while processing a small amount of low-grade lead-zinc oxide ore. The SSC and DCS of the project were contracted by ENFI and started design in January 2018 and completed by the end of July 2019. Up to now, the project has been running continuously for more than two months, and the service life of side lance has exceeded two months.

Process Flow

SSC is used to melt zinc residues. Natural gas is used as fuel, and crushed coal is used to heat up the molten bath and maintain the weak reductive atmosphere in the furnace. Because of the high iron content of zinc residues, quartz is added to reduce the melting point of the slag and form a FeO–SiO_2–CaO slag with low melting point. SSC feeds continuously and discharges slag intermittently. Zinc residues, crushed coal, and quartz are metered and added into the furnace by moving belt. Natural gas and oxygen-enriched air are injected into the side lance to control the temperature of the molten bath from 1200 to 1300 °C. Zinc residues melt in SSC, part of lead and zinc volatilizes into the offgas, and sulfur enters the offgas in the form of SO_2. The offgas of SSC is cooled by the waste heat boiler and purified by the electrostatic precipitator. The SO_2 content of the purified offgas is 3–4%, which is combined with the offgas of the zinc roaster to produce acid. The collected dust is leached.

Table 1 Zinc residues

Element	Zn	Pb	Fe	S	SiO_2	CaO	Ag	Ge
wt%	17–19	5–7	18–22	7–9	3–4	5–7	0.014–0.018	0.016–0.022

Table 2 Production data

Item	Unit	Value
Zn residues	t/h (dry)	~22
Crushed coal	t/h	~2.5
Quartz	t/h	~2.0
Natural Gas	Nm^3/h	~1700
O_2	Nm^3/h, 85% O_2	~4300
Air	Nm^3/h	~5000

SSC slag is discharged into the existing FF through chute and is reduced and volatilized in FF to recover lead and zinc. The hot slag of SSC and reduction furnace of lead system are treated by fuming furnace, and pulverized coal is injected as fuel and reductant. The offgas of FF is cooled by the waste heat boiler, purified by the tube cooler and bag filter, and the collected dust is leached. The purified offgas is sent to the existing desulfurization system. The slag produced by FF contains zinc < 2.0 and lead < 0.2%.

Production Indicators

SSC

(1) Raw materials

Up to now, the treatment of zinc residues by SSC can reach 22 t/h (dry). Due to the large amount of zinc residues in the plant, lead-zinc oxide ore has not been treated. The composition of zinc residues is shown in Table 1.

(2) Input

The production data of SSC are shown in Table 2.

Among them, the calorific value of crushed coal is 5000 kcal/kg and natural gas is 8300 kcal/Nm^3.

According to Table 2, the consumption of natural gas and crushed coal is converted into standard coal, and the consumption of standard coal per ton of zinc residues is ~200 kgce/t.

Table 3 Slag

Element	Zn	Pb	Fe	S	SiO_2	CaO	Ag	Ge
wt%	16–20	0.5–2	24–26	0.1–0.3	18–21	11–13	0.002–0.003	0.004–0.007

Table 4 Dust

Element	Zn	Pb	S	Ag	Ge
wt%	35–45	25–35	4–6	0.06–0.1	0.05–0.09

Table 5 Volatilization rates

Element	Zn	Pb	Ag	Ge
%	25–30	70–80	75–85	70–80

(3) Output

The composition of slag and dust produced by SSC is shown in Tables 3 and 4.

The volatilization rates of Zn, Pb, Ag, and Ge in SSC are shown in Table 5.

The SO_2 content in the offgas of SSC is 3–4% after being treated by waste heat boiler and electrostatic precipitator and mixed with the offgas of zinc roaster to produce acid. The SO_2 content in the offgas after mixing is 5–6%.

FF

(1) Raw materials

FF is used to deal with SSC slag while dealing with some zinc residues. The composition of SSC slag is shown in Table 3.

(2) Input

According to the calculation of treating only SSC slag, the consumption of pulverized coal per ton of SSC slag is about 220 kg, and the calorific value of pulverized coal is 5200 kcal/kg. According to the calculation of 0.65 t SSC slag per ton of zinc residues, the consumption of converted standard coal per ton of zinc residues in FF is ~110 kgce/t.

(3) Output

The composition of slag and dust produced by FF is shown in Tables 6 and 7.

The volatilization rates of Zn, Pb, Ag, and Ge in FF are shown in Table 8.

The SO_2 content in the offgas is less than 0.2% after being treated by waste heat boiler, tube cooler, and bag filter, which is sent to the existing desulfurization system for treatment.

Table 6 Slag

Element	Zn	Pb	Ag	Ge
wt%	1–2	0.05–0.2	0.001–0.002	0.001–0.002

Table 7 Dust

Element	Zn	Pb	Ag	Ge
wt%	55–65	3–8	0.004–0.006	0.01–0.02

Table 8 Volatilization rates

Element	Zn	Pb	Ag	Ge
%	90–95	90–95	45–55	75–85

Table 9 Recovery rate of various metals

Element	Zn	Pb	Ag	Ge
%	92–96	95–98	92–96	92–96

Summary

The current trial production results show that the system of SSC + FF system works well.

The standard coal consumption per ton of zinc residues is ~310 kgce/t.

The recovery rate of various metals is shown in Table 9.

Contrast of Indexes of Zinc Residues Treatment

The indexes of zinc residues treatment technology, such as rotary kiln, TSL, FF, and SSC + FF, are analyzed and compared. The results are shown in Table 10.

From the above data, the following conclusions can be drawn:

(1) The volatilization rate of lead and zinc in all processes is similar, but the recovery rate of silver in TSL, FF, and SSC + FF is much higher than that in rotary kiln.
(2) Soft coal can be used in TSL, FF, and SSC + FF, and coke or anthracite is used in rotary kiln.
(3) SSC is rich in oxygen, while SSC + FF consumes the least fuel, but the most oxygen. TSL consumes the most fuel if it uses a single furnace to fume directly.
(4) SSC + FF tail gas emissions are the least, and the SO_2 content of SSC offgas is the highest, which can be mixed with other high concentration offgas to produce acid. The process has the lowest cost of offgas treatment.

Table 10 Contrast of indexes

Item	Waelz	TSL(in China)	FF	SSC + FF
Zn recovery rate (%)	>90	>80	>90	>90
Pb recovery rate (%)	>90	>90	>90	>90
Ag recovery rate (%)	<40	>85	>85	>90
Fuel type	Coke/anthracite coal	Soft coal	Soft coal	Soft coal
Standard coal consumption in tons of residue (kgce/t) (%)	40–45	50–55	45–50	30–35
O_2 (v%)	21–25%	21–40%	21–25%	40–80%(SSC) 21% (FF)
O_2 consumption in tons of residue (Nm^3/t)	0–50	100–150	0–50	180–250
Offgas in tons of residue (Nm^3/t)	4000–4500	4500–5000	5000–5500	3500–4000
SO_2 in offgas (v%)	<1%	<1%	<1%	3–4%(SSC) < 0.1%(FF)
Steam production in tons of standard coal (t/t)	~1.5	~6	~5.5	~6.5
Processing capacity of single unit ($\times 10^3$ t/a)	100–150	100–160	50–80	100–200

(5) The steam consumption per ton of standard coal produced by rotary kiln is the least, and the utilization rate of waste heat is low. SSC + FF produced the most steam per ton of standard coal and has high utilization rate of waste heat.
(6) The treatment capacity of single FF is the smallest, while that of SSC + FF is the largest.

Conclusion

SSC + FF has been running for more than two months at Yunnan Chihong Zn & Ge Huize smelter. The standard coal consumption per ton of zinc residues is ~310 kg, which is 30–50% less than that of other existing residues treatment technologies. The recoveries of Zn, Pb, Ag, and Ge all exceed 92%. Its energy consumption index and recovery rate of valuable metals have reached the leading level in China. SSC + FF has less tail gas emissions and high SO_2 content in the offgas of SSC, which can be mixed with other high concentration offgas to produce acid with low cost of offgas treatment.

At present, zinc residues treatment projects in Northwest Lead-Zinc Smelter and Sihuan Zn & Ge Smelter in China all adopt this technology, and are expected to be put into operation in 2020–2021.

Practice shows that SSC + FF technology reduces the cost of zinc residues treatment, improves the recovery of metals, and raises the zinc slag treatment technology to a new stage. The technology can be applied to new construction and renovation projects.

GCRIS

A Critical Review on Generation, Characteristics, and Utilization of Zinc Slag

Yan Song, Weiguo Wu, Liang Xu, Xiangqiang Chen and Ge Zhang

Abstract Zinc slag (including zinc smelting slag and zinc leach residue) belongs to solid waste from the zinc pyrometallurgical and hydrometallurgical industry. Generated by the pyrometallurgical process, zinc smelting slag contains a high content of zinc, lead, and cobalt as secondary resource. And zinc leach residue, generated in the zinc hydrometallurgical process, usually contains zinc, germanium, and indium. The large amount of zinc slag discharge causes environmental pollution and resource waste. Reducing the toxicity and increasing utilization of zinc slag are important measures to solve the negative impact of zinc slag on the environment. The review focuses on the utilization of zinc slag. Pyrometallurgical and hydrometallurgical methods for metal recovery are summarized. The utilization of zinc slag in construction materials is also discussed. Eventually, the related technological challenges and their possible solutions are described and discussed.

Keywords Zinc slag · Metal recovery · Utilization · Construction materials · Technological challenges

Introduction

Zinc is a versatile and strategically important metal resource for the industrial development and global economy. It is intrinsically associated with galvanizing, zinc alloy, and instrument battery [1–3]. From the consumption perspective, zinc products are widely used in the fields of automotive, household appliances, construction, and infrastructure. The global and Chinese zinc terminal consumptions are shown in Figs. 1 and 2, respectively [4, 5]. Global zinc consumption exceeds 13 million tons annually. And the global zinc demand is predicted to continuously increase in the coming years [6]. As shown in Fig. 3, the global refined zinc production is out of

Y. Song (✉) · W. Wu · L. Xu · X. Chen · G. Zhang
China ENFI Engineering Corporation, 12 Fuxing Road, Haidian District, Beijing 100038, People's Republic of China
e-mail: SONGYANNEU@139.com

© The Minerals, Metals & Materials Society 2020

A. Siegmund et al. (eds.), *PbZn 2020: 9th International Symposium on Lead and Zinc Processing*, The Minerals, Metals & Materials Series,
https://doi.org/10.1007/978-3-030-37070-1_23

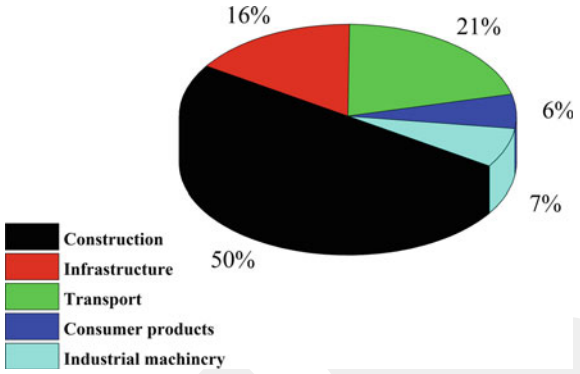

Fig. 1 Global zinc terminal consumption

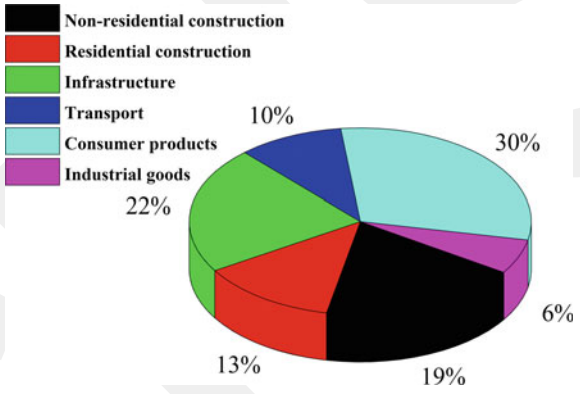

Fig. 2 Chinese zinc terminal consumption

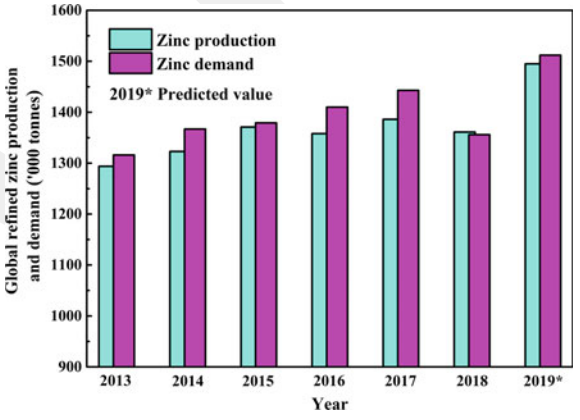

Fig. 3 Global refined zinc production and demand

balance with demand. In 2019, the global refined zinc production is forecast to reach 14.95 million tons. And the predicted zinc demand is up to 15.12 million tons [4, 5].

Zinc production process generally can be divided into pyrometallurgical and hydrometallurgical process. 90% of global zinc is produced by hydrometallurgical process. And 40% of global zinc is produced by high-acid leaching, oxygen pressure leaching, and oxygen atmospheric leaching [7]. The zinc production lines using the pyrometallurgical process are mainly in China, which include zinc smelting by horizontal retorting, vertical retorting, electric furnace, and imperial smelting furnace [8]. Zinc hydrometallurgical process can be divided into two categories. The traditional hydrometallurgical process consists of the roasting of zinc concentrate, extraction, purification, and electrowinning. And the other one is composed by the direct extraction of zinc concentrate, purification, and electrowinning [9].

Zinc Smelting Slag and Zinc Leach Residue

Zinc smelting slag is generated by the zinc pyrometallurgical process. In general, total contents of zinc and lead of the zinc smelting slag are about 5–15%, while the contents of rare and noble metals are very low [10]. Therefore, it is not economic for the recovery of valuable metals from the zinc smelting slag by the traditional hydrometallurgical processes (including acid curing and alkali leaching) and pyrometallurgical processes. Moreover, if the zinc smelting slag is treated using a traditional hydrometallurgical process, the leaching agent (acid or alkali) will be left in the residues, and the gangue components in the slag are turned into a secondary slag without utilization, which results in a secondary pollution [11–13].

Zinc leach residue, generated in the zinc hydrometallurgical process, belongs to hazardous solid waste [14]. The composition of the leach residue is very complex, especially the high-temperature and high-acid leach residue, which contains zinc and other valuable metals (such as lead, copper, indium, and silver) [15, 16]. Using the traditional pyrometallurgical or hydrometallurgical process, the treatment cost of zinc leach residue is high. Therefore, how to utilize the leach residue is an urgent task, including recycling valuable metals and reutilizing the rest slag.

Progress of Zinc Smelting Slag Recovery and Recycling

Traditional progress of zinc smelting slag recovery and recycling focuses on zinc and lead recovery. Nowadays more and more attention has been paid to the recovery and recycling of other valuable metals in zinc smelting slag. The hydrometallurgical technology has been used to recover rare and noble metals. By step-by-step removal of impurities from the leaching solution of zinc smelting slag, Zinc and cobalt were extracted [17].

The sintered process has been applied to recycle and reutilize the zinc smelting slag [18]. In the first stage, zinc and lead were reduced by the carbon and volatilized into the dust as a secondary zinc resource. In the second stage, a lightweight brick was produced.

Ferro-silicate slag produced from zinc smelting by imperial smelting furnace (ISF). Some occasional research attempts seen in the literature are to its use as a replacement for aggregates in construction related applications, such as the sand in cementitious mixes [19]. The latest research shows that ISF zinc smelting slag can be used as a building material using geopolymerization process, which involves formation of a new rock like species from various aluminosilicate minerals under strong alkaline environment [20].

Progress of Zinc Leach Slag Recovery and Recycling

For the efficient treatment of zinc leach residue, the pulverized coal injection system of rotary kiln has been reformed and improved by a zinc smelting plant in Yunnan province [21]. Different from the traditional coal injection way, 15% of the pulverized coal is injected from the head of rotary kiln. The ratio of zinc leach residue to coal is only 100:20. By the technology, 40% of coal can be saved. The product quality is improved and the number of nodulations becomes smaller.

Side-submerged combustion smelting process (SSC) is a new technology to treat zinc leach residue, which is designed and developed by China ENFI Engineering Corporation. By multi-channel side-submerged spray guns, the oxygen-enriched air and fuel are injected into the melt at high speed. The melt is stirred and heated directly. After the furnace charge added, carbonate or sulfate materials are rapidly dispersed into the melt. The heat and mass transfer occur rapidly. The heating, decomposition, and melting of the furnace charge are promoted. After more than ten years of design and development, the technology has been applied by Yunnan Chihong Zn & Ge Co., Ltd to treat 350 t/d zinc leach residue in 2019.

In this program, the electric heating fore well is replaced by a melting furnace using the side-submerged combustion smelting technology. 350 t/d zinc leach residue and 250 t/d lead-zinc oxidized ore are treated. The compositions of the zinc leach residue and the lead-zinc oxidized ore are shown in Tables 1 and 2, respectively.

The hearth area of the side-submerged combustion melting furnace is 16.6 m^2. The schematic diagram of the melting furnace is shown in Fig. 4.

The main technical and economic indexes of the melting furnace process are shown in Table 3.

Table 1 Composition of the zinc leach residue (dry basis, wt%)

Element	Zn	Pb	Cu	Fe	S	As	Sb	Ag[a]	Ge[a]	SiO_2	CaO
%	18	7.7	0.09	23.2	8.31	0.31	0.01	100	200	3.2	4.16

[a]Represents g/t

Table 2 Composition of the lead-zinc oxidized ore (dry basis, wt%)

Element	Zn	Pb	Cu	Fe	S	As	Sb	Ag[a]	Ge[a]	SiO_2	CaO
%	17.82	4.98	0.01	11.6	4.25	0.16	0.01	44	33	4.8	15.5

[a]Represents g/t

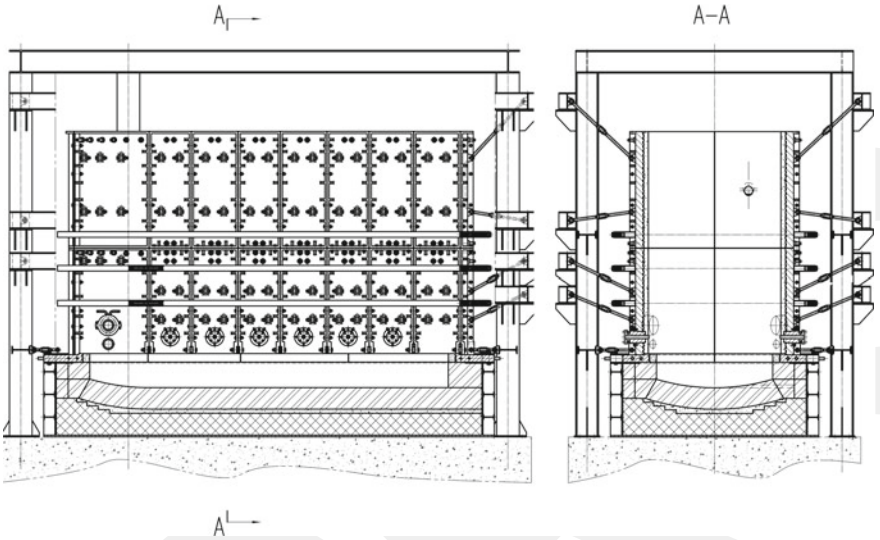

Fig. 4 Schematic diagram of the side-submerged combustion melting furnace

Table 3 Main technical and economic indexes of the melting furnace process

No.	Item	Unit	Value
1	Total day work	d/a	330
2	Hearth area of the side-submerged combustion melting furnace	m^2	16.6
3	Number of melting furnaces		1
4	Processing capacity of zinc leach residue	kt/a	115.5 (dry basis)
5	Processing capacity of lead-zinc oxidized ore	kt/a	82.5 (dry basis)
6	Coal consumption	t/a	2.11×10^4
7	Industrial oxygen consumption	Nm^3/a	4.97×10^7 (85%)
8	Natural gas consumption	Nm^3/a	1.58×10^7
9	Annual production of zinc oxide dust	t/a	2.45×10^4
	Zn content	%	28.99
	Pb content	%	33.88

By the side-submerged combustion smelting technology, the smelting temperature increases from 1200 to 1300–1400 °C. The actual standard of coal consumption is 30–40% lower than other treatment processes.

Conclusions

(1) In the coming years, the global zinc demand will continue to exceed the zinc production. The treatment of zinc slag (including zinc smelting slag and zinc leach residue) is more and more important to improve global zinc production and environmental protection.
(2) Due to the complex composition of zinc smelting slag and the low content of valuable metals, the economic and efficient recovery of polymetallic elements can be realized by the hydrometallurgical process. Zinc smelting slag produced by ISF can be used as a building material by the geopolymerization process.
(3) Side-submerged combustion smelting technology has been successfully industrialized to treat the zinc leach residue. The technology can simplify the process of zinc leach residue treatment, save energy, and reduce consumption. And it has a broad application prospect.

References

1. Jun M, Jing G, Chuan X, Wenxi W, Husam NA (2016) Zinc-ion batteries: materials, mechanisms, and applications. Mater Sci Eng 135:58–84
2. Shibli SMA, Meena BN, Remya R (2015) A review on recent approaches in the field of hot dip zinc galvanizing process. Surf Coat Technol 262:210–215
3. Jia L, Shichun J, Yan S, Cong N, Junke C, Genzhe H (2015) Effects of zinc on the laser welding of an aluminum alloy and galvanized steel. J Mater Process Technol 224:49–59
4. Tao D, Qishen C, Wenjia Y (2015) Global zinc consumption and demand forecast and development of China's zinc industry. Resour Sci 37(5):951–960 [in Chinese]
5. Chuanyao S, Zhenguo S, Yangge Z, Xiqun W (2019) Exploitation and utilization status and safe supply strategy of copper, aluminum, lead, and zinc resources in China. Eng Sci 21(1). https://doi.org/10.15302/j-sscae-2019.01.019 [in Chinese]
6. Taoze L, Feili L, Zhisheng J, Yuangen Y (2018) Acidic leaching of potentially toxic metals cadmium, cobalt, chromium, copper, nickel, lead, and zinc from two Zn smelting slag materials incubated in an acidic soil. Environ Pollut 238:359–368
7. Dongbo L, Jimu J (2015) Current situation and development trend of zinc smelting technology at home and abroad. China Met Bull 6:41–44 [in Chinese]
8. Jimu J (2012) Review of lead and zinc smelting technology in China. China Nonferrous Met 3:32–33 [in Chinese]
9. Cheng W, Xiaode J (2011) Brief analysis of zinc smelting wet oxygen pressure leaching technology. Qinghai Sci Technol 5:21–24 [in Chinese]
10. Almela A, Elizalde M, Daplusmn I, Obeitia (1998) Quid-liquid extraction applied to metals separation from Waelz oxide. Sep Sci Technol 33:2411–2422
11. Jha MK, Kumar V, Singh RJ (2001) Review of hydrometallurgical recovery of zinc from industrial wastes. Resour Conserv Recycl 33:1–22

12. Harvey TG (2006) The hydrometallurgical extraction of zinc by ammonium carbonate: a review of the Schnabel process. Miner Process Extr Metall Rev 27:231–279
13. Yang SH (2001) Making high-purity zinc from zinc oxide fume dusts. Chin J Nonferr Metall 11:1110–1113
14. Coruh S, Ergun ON (2010) Use of fly ash, phosphogypsum and red mud as a liner material for the disposal of hazardous zinc leach residue waste. J Hazard Mater 173(1):468–473
15. Vahidi E, Rashchi F, Moradkhani D (2009) Recovery of zinc from an industrial zinc leach residue by solvent extraction using D2EHPA. Miner Eng 22(2):204–206
16. Raghavan R, Mohanan PK, Patnaik SC (1998) Innovative processing technique to produce zinc concentrate from zinc leach residue with simultaneous recovery of lead and silver. Hydrometallurgy 48(2):225–237
17. Shaole S, Wei S, Li W, Runqing L, Haisheng H, Yuehua H, Yue Y (2019) Recovery of cobalt and zinc from the leaching solution of zinc smelting slag. J Environ Chem Eng 7(1). https://doi.org/10.1016/j.jece.2018.11.022
18. Huiping H, Qiufeng D, Chao L, Yue X, Zeqin D, Wei Z (2014) The recovery of Zn and Pb and the manufacture of lightweight bricks from zinc smelting slag and clay. J Hazard Mater 271:220–227
19. Morrison C, Hooper R, Lardner K (2003) The use of ferro-silicate slag from ISF zinc production as a sand replacement in concrete. Cem Concr Res 33(12):2085–2089
20. Alex TC, Kalinkin AM, Nath SK, Gurevich BI, Kalinkina EV, Tyukavkina VV, Kumar S (2013) Utilization of zinc slag through geopolymerization: Influence of milling atmosphere. Int J Miner Process 123:102–107
21. Yufei L, Guohuang X, Yanming H (2014) Analysis on resource utilization of zinc leaching residue. Yunnan Metall 43(1):93–96 [in Chinese]

Part VII
PbZn Process Technologies

GCRIS

Contributions of Non-ferrous Smelters to Metal Resource Circulation in Japan

Etsuro Shibata

Abstract As contributions of non-ferrous smelters to metal resource circulation, ores and secondary raw materials, such as scrap and waste, are treated to recover base metals such as copper, lead, and zinc, as well as other precious and minor metals. One crucial factor that makes this metal recovery possible is the creation of an organic link among copper, lead, and zinc smelters. In recent years, the specialization of non-ferrous smelting companies has been promoted in Japan, and it has become difficult to maintain this close organic link. In addition, in the field of metal resource circulation, the importance of lead smelters should be recognized again. For example, lead smelting acts as an essential destination for copper smelting by-products, such as smelting dusts. Additionally, printed circuit boards that have been treated in large quantities in copper smelters contain metal impurities, such as lead and tin in solder and antimony in flame-retardant auxiliaries. When printed circuit boards are treated in copper smelters, these excess impurities may interfere with the copper smelting process and accumulate in by-products. These impurity metals can be recovered effectively in lead smelters.

Keywords Non-ferrous smelter · Resource circulation · Recycling · Secondary raw materials · E-scrap · Waste treatment

Introduction

Non-ferrous smelting industry (copper, lead, zinc smelters) in Japan is making use of the advantages of having technologies for recovering various minor metals and precious metals from complex raw materials that are characteristic of non-ferrous smelter. The social role of smelters is not only smelting and refining of concentrates but also recycling treatments of various secondary raw materials (scraps, solid

E. Shibata (✉)
Institute of Multidisciplinary Research for Advanced Materials, Tohoku University, 1,1 Katahira, 2-Chome, Aobaku, Sendai 980-8577, Japan
e-mail: etsuro.shibata.e3@tohoku.ac.jp

© The Minerals, Metals & Materials Society 2020

A. Siegmund et al. (eds.), *PbZn 2020: 9th International Symposium on Lead and Zinc Processing*, The Minerals, Metals & Materials Series,
https://doi.org/10.1007/978-3-030-37070-1_24

wastes, etc.). Pyro-treatments enable separation and concentration of various elements by controlling multiple phases such as molten metal, slag, matte, speiss, and gas phases. By combining pyro-treatments with various hydro-treatments (leaching, precipitation, solvent extraction, ion exchange, electrolytic refining, etc.), various metals are separated and recovered. Environmental load elements are also controlled in smelters.

However, the continuous development of smelting and refining technologies is indispensable due to social constraints such as strengthening of environmental regulations and increases in impurities derived from secondary raw materials. In addition, by treating the concentrate and secondary raw materials, environmental load elements such as arsenic (As), mercury (Hg), and cadmium (Cd) are inevitably introduced and concentrated in the smelting processes. In this way, the non-ferrous smelting industry is responsible for the recovery of valuable metals, as well as the concentration and stabilization of environmental load elements. The non-ferrous smelting industry is socially indispensable for the recycling of metal resources and the controlling of environmental load elements. It has the potential to turn into a growth industry by extending this advantage in the future.

In this review, the present status and contributions of Japanese non-ferrous smelting industry for metal resource circulation are introduced with a summary of the technologies, features, and problems in smelters [1].

Treatments of Secondary Raw Materials and Associated Problems in Non-ferrous Smelters

The non-ferrous smelting industry in Japan has been reorganized and each company is generally focusing on copper, lead, or zinc smelting. However, to recover various metals from each smelting residue, such as dust, sludge, and dross, it is necessary to recharge them into a proper smelting process or individually treat them by considering the chemical components of each residue. In addition, regarding the treatments of secondary raw materials such as industrial wastes, it is also indispensable to charge them into a proper smelting process according to their form and contents. Under the situation where the ratio of secondary raw materials has been increasing, it should be emphasized that valuable metals such as precious metals (Au, Ag, Pt, Pd, Rh), selenium (Se), tellurium (Te), nickel (Ni), cobalt (Co), antimony (Sb), bismuth (Bi), tin (Sn), cadmium (Cd), gallium (Ga), and indium (In) can be recovered by efficiently using an organic linkage among copper, lead, and zinc smelters related to exchanges of various smelting residues.

However, the metals that can be recovered through the organic linkage among smelters are limited to the above, and the so-called active metals, such as rare earth elements (Nd, Dy, etc.), tantalum (Ta), and tungsten (W), cannot be recovered in the non-ferrous smelting process because they become diluted in the slag as their oxides. Therefore, to recover these active metals, it is necessary to separate components

containing the active metals by pretreatment of E-scrap such as printed circuit boards, particularly by physical separation techniques. In copper smelters in particular, the influence of increased charging of secondary raw materials such as printed circuit boards has been highlighted, and there is an urgent need to appropriately cope with an excess increase in impurities.

Due to a limitation of the removal of impurities in the smelting process constructed for the concentrates, the physical selection techniques of E-scrap such as printed circuit boards should be focused and developed with the aim of removing impurities that impede the smelting processes. In addition, for improving the process to withstand impurities in main smelting processes, for example, it is necessary to consider introducing a new smelting process such as the TSL (top submerged lance), a furnace specialized in treatments of secondary raw materials.

Features and Technologies of Non-ferrous Smelters in Japan

Usually, printed circuit boards are incinerated, roasted [2, 3], or melted [4, 5] prior to being charged into copper smelting furnaces in the form of metal-containing ash, or slag and metal, along with concentrates. In copper smelters, Se, Te, and precious metals are recovered from the anode slime; however, the excess increase in other impurities such as Ni, Sb, Sn, and Bi derived from secondary raw materials such as printed circuit boards is a serious problem.

Ni is originally recovered as crude nickel sulfate from copper electrolyte; however, Sn, Sb, and Bi should essentially be recovered in lead smelting processes as they are impurities that copper smelters find difficult to treat properly. Although the technology for removing Sb in copper electrolyte with a chelate resin has been used in copper smelters [6], it is also important to appropriately treat the residue accumulated with these impurities in lead smelters. It is also important to separate beforehand various mounting components and solder containing impurities from the printed circuit board by physical separation techniques. Generally, when components are separated from the printed circuit board, precious metals tend to be distributed there, but by introducing these separated components into the lead smelting process, precious metals could be recovered along with other minor metals such as Sb, Sn, and Bi.

In the general copper smelting process consisting of flash smelting furnace and converter, the limit of the secondary raw material ratio to concentrate is expected to be about 20% due to impurities and heat balance. In order to increase the charging amount of secondary raw materials, it is necessary to fundamentally change the main smelting processes. In Japan, a copper smelter that treats only secondary raw materials, mainly printed circuit boards, is already in operation based on a TSL furnace [7]. In addition, the treatment of shredder residues using a copper smelting facility [8] and also sulfurization process [2] for converting copper-containing secondary materials into copper matte are also operated in Japan. They are very interesting

technologies in terms of recycling of solid wastes. However, as secondary raw materials containing waste plastics such as printed circuit boards and shredder residues contain bromine flame retardants and polyvinylchloride, it is necessary to deal with associated corrosion problems for exhaust gas treatment facilities.

Effective Use of Lead Smelters

Unlike copper smelting, lead smelting is a process that can operate with only secondary raw materials using existing facilities such as lead blast furnaces (originally operated for concentrates). At present, it is estimated that about half of the lead bullion is produced from secondary raw materials in Japan [9]. In a lead smelting furnace, it is possible to control multiple phases such as gaseous components, slag, matte, speiss, and molten lead. From this point, it is obvious that the lead smelting process can separate and recover various metals efficiently [10–14].

In lead smelting process, precious metals, Sb, and Bi can be recovered from anode slime generated by electrorefining. Copper matte generated in the furnaces and the dross recovered by decopperization of lead bullion can be used as copper raw materials. Sn is also recovered by Harris treatment of lead bullion [10–14]. Lead smelters are also responsible for treating smelting residues from other non-ferrous smelters. In addition, lead smelters must play a vital role in treating solder and various mounting components generated by physical separation treatments of printed circuit boards. By charging these components into the lead smelter, Sn, Sb, Bi, and precious metals can be recovered without serious problems. Thus, the lead smelter plays a central role in the construction of a metal resource circulation system based on the non-ferrous smelting industry. The lead smelters are indispensable for waste treatments in Japan. For example, a CRT glass that contains lead was efficiently treated as a substitute for flux in lead smelting furnaces [15]. As an example from overseas, Umicore process in Hoboken is a typical process that combines a lead smelting furnace (blast furnace) and a copper smelting furnace (TSL furnace) [16].

The Importance of ISP

There are two processes involved zinc smelting and refining: hydrometallurgical zinc smelting [17–20], which is the main zinc production process, and ISP (Imperial Smelting Process) [21] in Japan. An important secondary raw material for zinc is EAF (electric arc furnace) dust generated from an electric furnace for recycling iron scrap. As EAF dust contains zinc from the galvanization of steel, crude zinc oxide is produced using EAF dust as a raw material. A typical process for producing crude zinc oxide is the Waelz kiln method [22, 23]. In addition, the MF (Mitsui Furnace) process, which uses a characteristic blast furnace [24], is also operated in Japan. The MF process produces crude zinc oxide from EAF dust and molten fly ash as a

unique waste, which is generated from the melting treatment of incineration ash of municipal solid wastes in Japan.

Zinc in EAF dust is concentrated and recovered in the crude zinc oxide. At the same time, fluorine (F), which is considered to be derived from the flux in the EAF process, is also mixed in the crude zinc oxide. As fluorine impedes the zinc electrowinning process, a high-cost halogen removal treatment is required when charging crude zinc oxide into a hydrometallurgical zinc smelter process. Therefore, the ISP method, which is resistant to halogen impurities, is responsible for the treatment of secondary raw materials of zinc [21]. Although this process is declining outside of China, one smelter is still in operation in Japan. Thus, it is important to maintain the ISP smelter as the central base for zinc recycling in Japan. However, secondary raw materials containing low-boiling zinc tend to be accompanied by other low-boiling metals, particularly mercury (Hg). In Japan, mercury is recovered and refined from various mercury-containing wastes including smelting residues at the Itomuka plant [25], but more efficient mercury recovery will be necessary through collaboration between non-ferrous smelters and the Itomuka plant in future.

Conclusions

The following summarizes the topics that should be considered in the future for the construction of a metal resource circulation system based on the non-ferrous smelting industry in Japan. For copper smelters, physical separation techniques of secondary raw materials such as E-scrap for the purpose of separating and removing impurities are important as pretreatment. Furthermore, impurities such as solder, mounted components and iron scrap mixed with precious metals should be treated properly in lead smelters. In addition, for the treatment of flame-retardant plastics generated in large quantities after the physical separation of secondary raw materials, thermal recycling and halogen removal are conducted simultaneously using smelting facilities. If possible, low-temperature volatilization technique for heavy metals by halogenation should be also considered.

Combining copper and lead smelters is ideal for the treatment of various secondary raw materials by exchange of intermediate by-products (smelting residues), as well as the recovery of valuable metals. The secondary smelting industry such as lead smelters is considered to occupy an important position as a social infrastructure industry in the treatment of solid wastes containing heavy metals, particularly by playing an important part in waste disposal. In addition, it is possible to concentrate and recover environmental load elements such as Hg and As in the smelting processes. However, their chemical stabilization and the construction of a system for their final disposal are important issues to be considered by the entire non-ferrous smelting industry across the globe.

References

1. Shibata E (2016) Bull "Kozan" 69:9–17 (in Japanese)
2. Akagi S, Aoki T, Yoneda J, Narisako M, Hino J (2007) J MMIJ 123:763–767 (in Japanese)
3. Ikeda R, Hoshi M, Takahashi K, Ikuta Y (2010) J MMIJ 126:292–295 (in Japanese)
4. Igarashi T, Shimizu T (2007) J MMIJ 123:377–385 (in Japanese)
5. Shimizu T (2007) J MMIJ 123:614–619 (in Japanese)
6. For example, Japanese Unexamined Patent Application Publication (JP-A) No. Hei 9-67627
7. Morise T, Naka M, Shiratori T (2007) J MMIJ 123:758–762 (in Japanese)
8. Hirano M, Iida M, Sakai T (2012) J MMIJ 128:495–499 (in Japanese)
9. JOGMEC (2011) Mineral resources material flow 2010, July, pp 20–34 (in Japanese)
10. Mine Y (2007) J MMIJ 123:672–674 (in Japanese)
11. Mitsune Y, Satoh S (2007) J MMIJ 123:630–633 (in Japanese)
12. Takayanagi S, Abe S (2007) J MMIJ 123:719–722 (in Japanese)
13. Inoue Y (2007) J MMIJ 123:634–638 (in Japanese)
14. Sasaoka H, Kobayashi D, Sasaki Y (2013) Proceedings of copper 2013, vol IV, pp 93–105
15. Tohoku Bureau of Economy, Trade and Industry (METI Tohoku) (2009) Report of survey commission fee to resource circulation promotion (Recycling of CRT TV), 31 March, pp 3–23 (in Japanese)
16. For example, Alvear Flores GRF, Nikolic S, Mackey PJ (2014) JOM 66:823–832
17. Togashi R (2007) J MMIJ 123:642–645 (in Japanese)
18. Kusuda Y, Morita E (2007) J MMIJ 123:646–650 (in Japanese)
19. Yaoka T, Nishijima A (2007) J MMIJ 123:657–660 (in Japanese)
20. Yanagisawa H (2007) J MMIJ 123:651–656 (in Japanese)
21. Azuma S (2007) J MMIJ 123:661–665 (in Japanese)
22. Nagai K, Matsumoto Y, Watanabe H (2007) J MMIJ 123:726–729 (in Japanese)
23. Sugimoto H, Takizawa H, Ueda H (2007) J MMIJ 123:723–725 (in Japanese)
24. Nakamura K, Fujikawa M, Hatae S, Ishito T (2013) J MMIJ 129:333–340 (in Japanese)
25. Tamura N, Miura H (2007) J MMIJ 123:747–750 (in Japanese)

The Process and Application of Oxygen-Enriched Air Side Blown Smelting of Lead–Zinc Materials

Ling Zhang, L. Zhang and Y. He

Abstract The paper has discussed smelting process and application of oxygen-rich side blown for lead–zinc materials. This process includes three steps: oxidation melting, reduction melting, and slag fuming which are continuously conducted in three oxygen-rich side blown furnaces connected by chute. The lead–zinc materials fed into the first furnace for oxidation melting and desulfurization produce lead-rich slag which flows into the second furnace to produce crude lead and reduction slag which flows into the third furnace to fume and produce zinc oxide dust. The result of application indicates that the process can treat materials with 22–40% lead and about 10% zinc content in furnace charge. The specific capacity of the furnace is about 60 t/m^2 d. Oxygen concentration in oxygen-enriched air side blown oxidation furnace reached 90%. Desulfurization rate of oxidation furnace reached 99.5%. The coal rate of reduction reached 8.6%. The furnace life is up to 5 years. Lead and zinc. Recovery are over 97% and 92%, respectively.

Keywords Lead smelting · Oxygen-enriched air side blown · Oxidation reduction · Fuming

Lead-bearing polymetallic materials exist mainly as metal oxides and sulfates. At present, the blast furnace is widely applied in China for processing the lead-bearing polymetallic materials after briquetting. This process is characterized by low investment for per unit output and high direct recovery, yet low SO_2 concentration in off-gas, impossible for direct acid production, resulting in unsatisfactory environmental protection effect. The oxygen-enriched side blown process is based on the enriched oxygen-enriched smelting; the off-gas contains high concentration of SO_2, which can be directly used for acid making with good environmental protection effect. This process can make full use of chemical reaction heat of the charge and consume less fuel with wide adaptability of the raw materials, it can process powder

L. Zhang (✉) · L. Zhang · Y. He
CINF Engineering Co., Ltd., Changsha 410011, Hunan, People's Republic of China
e-mail: zlingcinf@126.com

© The Minerals, Metals & Materials Society 2020

A. Siegmund et al. (eds.), *PbZn 2020: 9th International Symposium on Lead and Zinc Processing*, The Minerals, Metals & Materials Series,
https://doi.org/10.1007/978-3-030-37070-1_25

material, and also the lump material with no need for the flux or coal needs preparation and drying. In addition, it is characterized by low investment, large specific throughput of the furnace, flexible capacity, and convenient operation.

Description of Oxygen-Enriched Air Side Blown Furnace

The oxygen-enriched air side blown process is developed based on the Vanyukov process invented by the former Soviet Union, which is an oxygen-enriched air side blown bath smelting process. The furnace hearth is made of refractory materials, and the furnace body is made of copper jacket and steel jacket. A copper water jacket is provided with several primary tuyeres for blowing oxygen-enriched into the melt slag layer. The furnace charge is fed from the upper feeding port, and the blown oxygen-enriched strongly agitates the upper melt to quickly complete the smelting process. Since 1976, this process has been widely used for copper and nickel smelting in the former Soviet Union. China has conducted the improvement re-innovation on the basis of Vanukov furnace; the commercial-scale test on the Pb smelting by oxygen-enriched air side blown process was started in 2001, and in 2009, it was successfully applied for the reduction in hot high-Pb slag. The research on the processing of lead-bearing polymetallic materials by this process began in July 2012, and the commissioning was conducted successfully at one go on June 1, 2014 (Fig. 1).

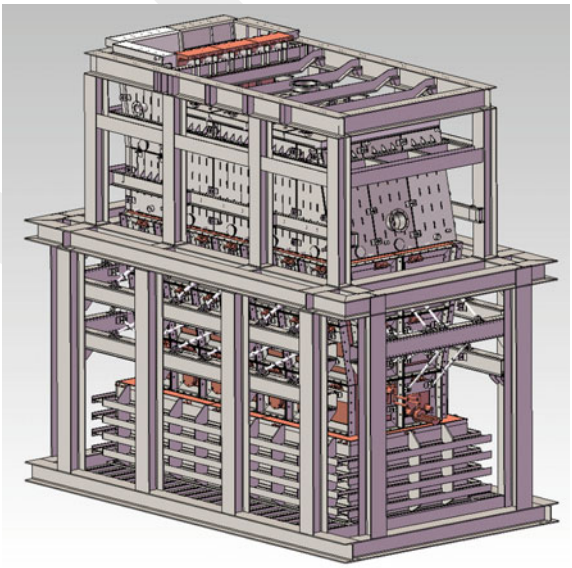

Fig. 1 Oxygen-enriched air side blown furnace

Process Flow for Processing of Lead-Bearing Polymetallic Materials

The process flow diagram for processing of lead-bearing polymetallic materials by oxygen-enriched side blown oxidation, oxygen-enriched side blown reduction and fuming with fuming furnace is shown in Fig. 2. After proportioning, the lead-bearing polymetallic materials are mixed and granulated, with input charge particle size of around 15 mm, water controlled within 10% before fed to the oxygen-enriched side blown smelting furnace, where the enriched oxygen is blown via the furnace side tuyere to the furnace for chemical reaction with the furnace charge. The metal lead is captured through the high-Pb slag, while the dust goes through the waste heat boiler and electrostatic precipitator for dust collection to the proportioning operation. The high-temperature fume generates steam through waste heat recovery, which is sent to the waste heat power station for power generation, before the off-gas is sent to acid-making operation. High-lead slag enters via the chute into the oxygen-enriched side blown reduction furnace; the crude lead is produced from the reduction furnace. The high-temperature fume goes to the waste heat boiler for heat recovery before

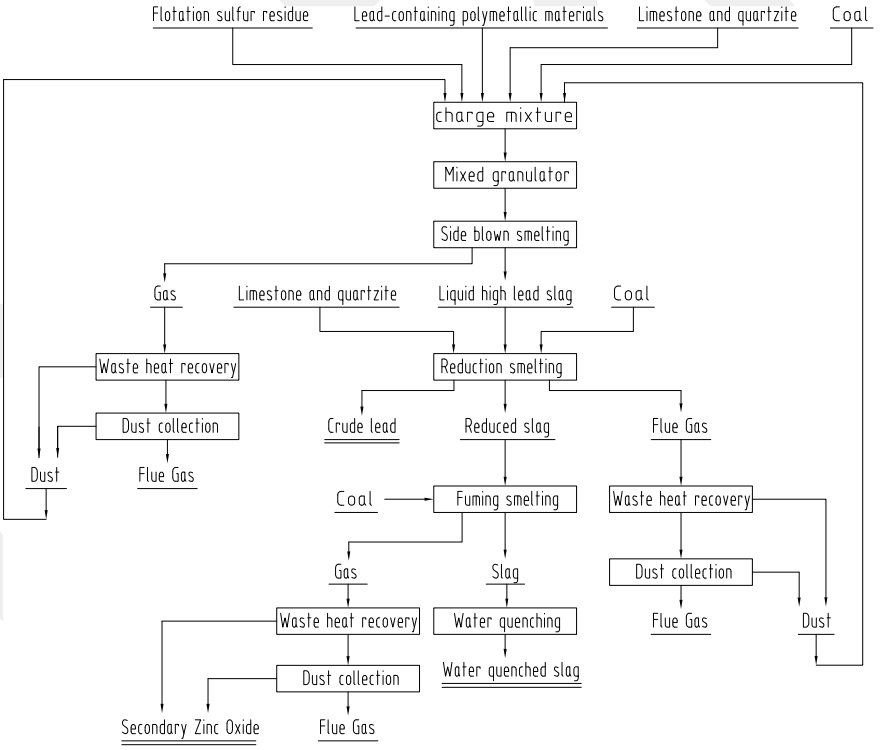

Fig. 2 Process flow diagram of processing of lead-bearing polymetallic materials in oxygen-enriched side blown furnace

reported to the dust collector for desulfurization, while the dust is returned to the smelting proportioning operation. The reduction slag enters through the chute to the fuming furnace, where the pulverized coal is added through the nozzle of the fuming furnace. The metal zinc in the reduction slag is reduced into zinc steam, which is oxidized in the tertiary tuyere of the fuming furnace to form secondary zinc oxide. The resultant heat energy is recovered by the waste heat boiler. High-temperature fume is sent to desulfurization process after heat recovery in the waste heat boiler and dust collection. The fuming and converting slag are reported to the granulation process before sold to the cement factory. In the actual production process, some crude lead is produced in the oxidation furnace. The oxidation furnace hearth is provided with an intermediate slag tap to discharge intermediate slag with high content of Cu. The end of the reduction furnace hearth is also provided with an intermediate slag tap to discharge the intermediate metal layer in the smelting process.

Principle of the Smelting Process

Oxidation Stage

Lead in Pb-bearing polymetallic materials exists mainly in the form of lead oxide or lead sulfate.

The melting point of lead sulfate ($PbSO_4$) is 1170 °C, which is a relatively stable compound. According to the thermal spectrum experiment of $PbSO_4$, $PbSO_4$ initial decomposition temperature is 850 °C, while $PbSO_4$ intense decomposition temperature is 905 °C.

$$2PbSO_4 = 2PbO + SO_2 + 2O_2 \tag{1}$$

Coal is added mainly to provide heat.

$$C + O_2 = CO_2 \tag{2}$$

When a small amount of lead concentrate is added in production, PbS can promote the decomposition of $PbSO_4$, that is, the initial decomposition temperature of lead sulfate can be lowered. $PbSO_4$ and PbO can react with PbS to form metallic lead. For example, the initial reaction temperature in $PbSO_4 + PbS$ system is 630 °C. The main reaction equations are as follows:

$$2PbS + 3O_2 = 2PbO + 2SO_2 \tag{3}$$

$$PbSO_4 + PbS = Pb + SO_2 \tag{4}$$

$$PbS + 2PbO = 3Pb + SO_2 \tag{5}$$

Heat can be provided by adding flotation sulfur slag to improve the concentration of SO_2 in the fume and meet the requirement of acid-making system. The main reaction is as follows:

$$S + O_2 = SO_2 \tag{6}$$

Smelting process: Lead-bearing polymetallic materials, flotation sulfur slag, quartz sand, and crushed coal are fed by disc feeder and measured through the electronic belt scale in accordance with the requirements of the proportioning process, before charged via the belt conveyer into the oxygen-enriched side blown oxidation furnace for oxidation smelting. The charge is smelted in the furnace with oxygen-enriched air blown in from the tuyeres on both sides of the furnace. The input charge reacts strongly with oxygen to form lead alloy and slag. The heat required in the smelting process comes from the combustion heat of crushed coal, flotation sulfur slag, and the slagging reaction heat. The lead alloy formed from the smelting is precipitated and separated from the slag in the static slag layer below the tuyere with Pb alloy settled in the hearth bottom and slag in the top layer of the hearth melt. The slag flows from the slag tap into the reducing furnace for reduction; the lead alloy is discharged out from the flat head of the furnace end before the casting by the disc casting machine. Carbon monoxide and elemental sulfur are oxidized by secondary air blown in the hearth space. The resultant high-temperature fume will be cooled in the waste heat boiler, purified and dedusted by ESP and bag filter before sent to the sulfuric acid-making workshop. The dust from the waste heat boiler and ESP dust will be returned to the smelting process, while the bag filter dust will be sent to the metal arsenic recovery process.

Reduction Stage

The main reaction equations of the reduction section are as follows:

$$2C + O_2 = 2CO \tag{7}$$

$$CaCO_3 = CO_2 + CaO \tag{8}$$

$$C + 2PbO \cdot SiO_2 + CaO = 2Pb + CO_2 + SiO_2 \cdot CaO \tag{9}$$

$$CO + PbO \cdot SiO_2 + CaO = Pb + CO_2 + SiO_2 \cdot CaO \tag{10}$$

Smelting process: Limestone and crushed coal are measured by electronic belt scale based on the proportioning ratio before transferred via the belt conveyer to the oxygen-enriched air side blown reduction furnace, the slag with higher lead content flows into the oxygen-enriched side blown reduction furnace, and then, is reduced and smelted with the blown oxygen-enriched air. The heat required for the reduction process comes from the combustion heat of the crushed coal. The lead alloy produced by smelting is precipitated and separated from the slag in the static slag layer below the tuyere. The slag is discharged from the slag tap into the fuming furnace, and the lead alloy is discharged from the siphon mouth at the end of the furnace. The carbon monoxide produced in the furnace is oxidized by the secondary air blown in hearth the space. The high-temperature fume is cooled in waste heat boiler, purified and dedusted by the bag filter before sent to desulfurization process. The waste heat boiler dust and bag filter dust are returned to the smelting process.

Fuming Stage

The main reaction equations of the fuming area are as follows:

$$2C + O_2 = 2CO \tag{11}$$

$$C + ZnO = Zn\ (\text{vapour}) + CO \tag{12}$$

In the upper part of the fuming furnace, the tertiary air is suctioned under negative pressure; zinc vapor and carbon monoxide are burned together.

$$2Zn + O_2 = 2ZnO \tag{13}$$

$$2CO + O_2 = 2CO_2 \tag{14}$$

Smelting process: The pulverized coal is prepared in the pulverized coal preparation area from the raw coal stored in the concentrated bin. The pulverized coal is transported via the single spiral pump with compressed air as the carrier to the pulverized coal receiving bin of the fuming furnace workshop. The molten slag from the reduction furnace flows into the fuming furnace and reacts with the pulverized coal and air. The produced fume (dust) is recovered through the waste heat boiler and dedusted by the bag filter, the collected dust is the secondary zinc oxide, and the off-gas is emitted after desulfurization; the furnace slag is granulated before sent to the slag dump or for sale.

Main Equipment

List of main equipment

No.	Equipment title	Specifications	Qty.
1	Oxygen-enriched air side blown oxidation furnace	9 m^2	1 pc
2	Oxygen-enriched air side blown reduction furnace	7 m^2	1 pc
3	Fuming furnace	6 m^2	1 pc
4	Centrifugal blower	Q = 390 m^3/min, P = 120 kPa	2 pcs
5	Oxygen station	Q = 5000 m^3/h, deep cooling method	1 set
6	Drum mixing granulator	φ1.5 × 6 m	1 pc

Main Techno-economic Indicators

Summary of main techno-economic indicators

Item		Unit	Design indicators	Production indicators
Oxidation stage	Hearth area	m^2	9	9
	Throughput	t/d	395	550–600
	Pb content in the raw material	%	26.74	22–40
	Primary lead quantity	t/d	42.9	15–20
	Primary lead rate	%	35	~10
	Oxygen consumption	m^3/t charge	263.93	100
	Oxygen concentration	%	70	~90
	Coal rate	%	16.34	1.05
	Dust rate	%	30.37	18–20
	Desulfurization rate	%	96.84	99.5
	Specific capacity of the furnace	t/m^2 d	43.89	61.11–66.66
	Slag output	t/a	220	380–420

(continued)

(continued)

Item		Unit	Design indicators	Production indicators
	Pb content in the slag	%	20.32	30–40
	Cooling water temperature difference	°C	5	1.9
	Slag temperature	°C	1100	1050–1200
	Tuyere life	Year	2	>2
Reduction stage	Area	m^2	7	7
	Slag yield	t/d	220	380–420
	Secondary lead	t/d	42	110
	Oxygen consumption	m^3/t 渣	79.15	86
	Oxygen concentration	%	60	55–60
	Coal rate	%	11.16	8.6
	Flux rate	%	0.95	9
	Dust rate	%	8.71	12
	Specific capacity of the furnace	t/m^2d	31.43	54.29–58.57
	Slag yield	t/a	151	228–252
	Pb in the slag	%	1.98	1.5–2.4
	Zn in the slag	%	14.7	15–17
	Cooling water temperature difference	°C	5	3.5
	Tuyere life	Year	2	≥2
Fuming state	Area	m^2	6	6
	Slag throughput	t/d	150.77	228–252
	Zn in secondary Zn oxide	%	59.11	>60
	Specific hearth throughput	t/m^2 d	25.13	38–42
	Pulverized coal rate	%	23.27	~21.5
	Lead in slag	%	0.21	<0.1
	Zn in slag	%	1.54	<1

Conclusions

In the oxidation stage, slag contains low sulfur; desulfurization rate is higher than the design value. In production, higher oxygen concentration is applied, the temperature difference of cooling water is lower than the design value, the daily throughput is higher than the design value, and the coal rate is much lower than the design value. The slag throughput in the reduction stage increases; the reduction dust is returned to the reduction furnace, resulting in increase of the cold material. In addition, the consumption of flux limestone and the heat required for limestone heating decomposition and heating are increased. The temperature rise of cooling return water is lower than the design value with little heat carried off by the water jacket. In the fuming stage, the slag throughput increases, and the pulverized coal rate is close to the design value. The lead and zinc content in the slag are lower than the design value, and the recovery is higher than the design value. In general, the process of oxygen-enriched air side blown oxidation, oxygen- enriched air side blown reduction, and zinc extraction by fuming furnace for the processing of lead-bearing polymetallic materials is characterized by high desulfurization rate, high overall sulfur recovery, good environmental protection effect, low energy consumption, and high recovery. It is an environment-friendly new process worth popularizing.

GCRI

New Ideas for the Design of Green Smelting Project of Domestic Lead and Zinc Resources

Cui Chen, Xingmin He and Hua Bai

Abstract During the past 15 years, through independent research and development and innovation, a thorough review and assimilating information of this industry showed that the lead and zinc smelting technology in China's non-ferrous industry has experienced many historical turning points. Especially in the past five years, under the dual pressure of resources and environmental protection, the lead and zinc smelting industry has continuously upgraded and reformed the existing technologies and equipment, greatly improving the level of technical equipment in the industry, with the enhancement of sustainable developments in the industry. This is demonstrated in this paper through the following lead–zinc smelting process examples: the innovative and industrialized zinc–oxygen pressure leaching process and associated equipment; the research and development and upgrading of three-continuous furnace bath smelting technologies, and associated equipment and by the introduction and adjustment of lead smelting technologies and equipment from abroad. All of above have the intention to establish the twofold transformation between gold mine and green mine, as quoted by Xi Jinping, who focuses on the synergy of environmental and industrial effect. For this purpose, this paper summarizes and analyses the whole life cycle of the project from investigation and establishment to design and construction, and then to commissioning and operation, and puts forward new ideas for the design of green smelting project of domestic lead and zinc resources.

Keywords Demonstrative lead–zinc smelting process · Three-continuous furnace bath smelting technology · Zinc–oxygen pressure leaching · Two-way transformation · Design of green smelting project

Introduction

China is rich in Pb and Zn mineral resources and globally the largest country in smelting and consumption of both metals. With the rapid economic development,

C. Chen (✉) · X. He · H. Bai
Nanjing, China
e-mail: thomaxchen@126.com

© The Minerals, Metals & Materials Society 2020

A. Siegmund et al. (eds.), *PbZn 2020: 9th International Symposium on Lead and Zinc Processing*, The Minerals, Metals & Materials Series,
https://doi.org/10.1007/978-3-030-37070-1_26

more emphasis has been placed on its environment protection, especially with respect to air pollution, heavy metal pollution, scattered pollution, and other problems. The Chinese government has always been highlighting environmental protection in their governance. So, it is an important developing target for metallurgical enterprises to ensure stable and efficient development by means of modern reforms and plant upgrades considering the entire life cycle. Wastewater, waste gas, and waste residue are by-products of metallurgical enterprises and have become critical obstacles to resolve for "green" metallic products.

The Project Cases

Lead Bullion Production at Zhuzhou Smelter

Zhuzhou smelter is located in Zhuzhou City, Hunan Province, which is a large-scale Cu and Pb and Zn smelter built in 1981. Since the plant was put into operation in January 2013, it has been in good operation for now 6 continuous years with excellent performance at both domestic and international level and demonstrated its outstanding features.

Raw Material Management

Through the modernization and updating of the production mode and process, the high requirements from variations in raw materials on the main furnace operations in the early stage of production have been lowered by selecting a wider range of different types of slag. The proportion of lead in the concentrates has been reduced to 30%. The fluxes used for slag making (river sand and limestone) have been changed to more efficient materials.

Main Process and Production Management

Process control is the core part of flash smelting. During six months of operation, a manual for process control of the flash smelting furnace was developed, which provides a foundation for sound production management as well as safety and environmental protection. The maintenance shut down in September 2013 during which also improvement modifications were implemented and enabled the furnace system to distinctively raise its production efficiency. This operating level was maintained for 10 months.

Production Process Control

Zhuzhou smelter consolidated a number of production process control operation methods to ensure the economic operation of the system. One example is the no insulation operation for the reaction tower when the flash melting furnace stops for a short time. During the shutdown of the flash melting furnace, the insulation for the reaction tower is turned off resulting in lower consumption of energy. Another example is the accelerated start and restart of the electric furnace production, taking only 72 h for the electric furnace to reach normal operating mode.

During the years of stable operation, the Zhuzhou smelter has continuously increased the percentage of secondary materials charged to the smelting process in form of solid wastes and hazardous wastes, including purchased materials such as lead floating dressing, lead raw ore, lead–zinc mixed ore, high gold ore, lead mud, lead sand as well as in-house recirculated materials such as high acid slag, sulfur slag, lead slag, silver flotation slag, and various types of dusts. The treatment of these materials is truly green and environment-friendly with zero emission of waste residue and increased the economic benefits of the enterprise, and also bringing good social benefits.

Industrial Application of Oxygen Pressure Leaching Combined with Pyrometallurgical Smelting Process and Equipment

The Danxia oxygen pressure leaching plant is located in Dong Tang town, Renhua County, Guangdong province. In order to take full advantage of the high contents of rare metals in Fankou zinc concentrate, the project comprehensively recycles gallium, germanium, silver, and other valuable elements. In September 2009, the plant operating with these types of materials was commissioned.

Compared with other oxygen pressure leaching projects, this project has several remarkable features.

Systematic Acid Equilibrium

In the oxygen leaching process of zinc concentrate, different raw materials have different requirements on acidity, which may lead to problems with the acid balance in the system. The process at Danxia is designed and constructed based on treating seven water zinc sulfate. Fundamentally, this solved a series of problems caused by the concentration of sulfate ions in the leaching process and ensured the good operation of the entire system producing high value-added by-products and enlarging the product portfolio of the company.

New Technology for Particle Size Control of Oxygen Pressure Leaching Products

Due to the improper control of reactor operating conditions during operation, the elemental sulfur generated in the leaching process and the unreacted sulfide form an enveloping polymer, which affects achieving high leaching rates of the reaction. The application of two kinds of additive instead of one single not only effectively avoids the leaching requirement of molten zinc sulfide and other sulfide sulfur package agglomerate but also takes good control of the output material particle size and eliminates employing a pressure tank. Overall, it lowers the overall additive cost consumption and significantly improving the efficiency of leaching of ore concentrate obtaining leaching rates of 98–98.5%.

Upgrading of Main Equipment

One of the refractory lining materials in the high-pressure autoclave was replaced by a new patented product in China that meets the requirements of long service life and greatly reduces the cost of the autoclave. Furthermore, adjusting the tank lining in the flash tank in conjunction with a structural form transformation effectively enhanced the anti-abrasion and anti-corrosion performance of the equipment. Manufacturing and installation cost were significantly decreased with equipment operating availability at above 90%.

Zinc Electrowinning Cellhouse

For the first time, the employment of glass fiber reinforced plastic wind fans installed on the roof was adopted for cellhouse ventilation. The acid mist is removed by means of cooling tower fan and ventilation and exhaust fan, which effectively lowered the potential severe equipment corrosion rate caused by acid mist over long-term operation. In addition, a comparison with the conventional ventilation method showed that ventilation air change and energy consumption could be reduced.

The oxygen pressure leaching system at Danxia smelter greatly improved the level of available zinc smelting technologies and equipment in China. At the same time, the stable operation of ten years played a positive role in promoting the transformation and improvement of the existing zinc smelting technologies in China. At present, in order to improve the overall smelting process for lead and zinc, it is planned during the relocation of Shaoguan smelting plant, an affiliation of the company, to design and put into production a set of flash smelting systems matching the output of secondary slag in the existing lead–zinc process, so as to realize zero discharge and zero storage of waste slag.

Research, Development, and Application of Smelting Technology and Equipment of Side Blown Triple Furnace with Oxygen Enrichment

This project of GXHC company consists of a production line with a capacity of processing annually 300,000 tons of concentrates. Design objectives were to collaboratively treat complex multi-metal raw materials, to recycle valuable elements such as antimony, silver, zinc, copper, bismuth, and sulfur in addition to producing electrical lead, and to develop a complete set of key processes and equipment for collaboratively smelting lead–antimony and silver. The plant was commissioned in 2016.

Compared with the existing lead-related process, the project has the following features:

CSCC Process—The First Set of Side Blown Triplex Furnace Involving Lead Oxygen Enrichment in the World

Continuous production of three metallurgical furnaces has been tried for the first time. Continuous production has always been a development direction for metallurgical workers, which is not only beneficial to the collection and utilization of residual heat of high-temperature flue gas in metallurgical furnaces, but also greatly reduces the labor intensity.

By means of cold model testing and numerical simulation, the basic laws of momentum transfer, i.e. heat transfer and mass transfer in bubbling combustion conditions in the molten pool are investigated.

The structure and material of the three furnaces were innovated and transformed into design, which greatly improved the stability and service life of the furnace in production.

For the first time, three furnaces were used in a linear configuration, and the liquid slag could be self-flowing by using the height difference. In order to meet the environmental standards for disposing waste slag, the fuming furnace is designed with a choice for both continuous slag discharge and intermittent slag discharge.

Anodic Mud Treatment and Integration of Rare and Precious Metals

The anodic mud with high antimony and low silver lead concentrations is treated by oxygen-enriched side blowing smelting process. The whole process is clean and efficient, and valuable metals such as lead, copper, gold, silver, antimony, bismuth, and tellurium are effectively recovered. The recovery rate of the main metals such as gold and silver is more than or equal to 99% and that of antimony is more than 95%.

Summary and Analysis

(1) The development of the overall life cycle of non-ferrous metal smelting projects in China is still in its infancy. Among the three mentioned demonstration projects, two are the general contracting projects of our company, CINF. We have continuously participated in, followed up, and paid a return visit to each stage of the project: from the preliminary investigation and project approval, conceptual comparison and selection, design, procurement, construction, to the production standard completement.
(2) For the purpose of reducing sulfur dioxide emission pollution and improving recycle rates of rare metals, Danxia smelter implemented a technology adopting the oxygen leaching process to convert sulfur compounds in the concentrate generating elemental sulfur. This prevents air pollution caused by sulfur dioxide by pyrometallurgical smelting processes and greatly improved recycle rate of rare metals. In the process of leaching, all kinds of secondary residue materials can be subsequently treated in a flash smelting process to achieve zero discharge of waste slag pollution.
(3) The Zhuzhou smelter project takes the original system of smelting technology in conjunction with equipment upgrades as a starting point, to reduce the waste residue discharge and operating cost, along with efficiency increasing. It not only processed almost all of the secondary materials from the old conventional leaching system, but in addition a variety of purchased low grade raw materials can be treated. It assisted Zhuzhou in solving the problems about existing methods of secondary stockpiling of the excavated debris and resulted in considerable economic benefits.

In Hechi Southern's triple furnace project, the continuous operation of side blown oxygen-rich smelting furnace in lead-related smelting process was implemented for the first time on a commercial scale, and the treatment of antimony anode slime with low silver lead was accomplished. The furnace system effectively reduces the operating intensity for workers and improves the operating environment, which is of great reference significance to other smelting operations.

The above three demonstration projects all focus on comprehensive utilization of secondary materials, reduction of waste emissions, reduction of consumption, and efficiency increasing. In the design and operation stage, the basic process flow and equipment have been upgraded to different degrees. To realize environmentally friendly smelting projects and improving the companies' economic situation, the entire process including equipment performance, product quality, product structure, and other factors cannot be accomplished by ordinary process changes starting from raw materials and ending with crude metal production and subsequent refining processing. The entire process chain needs to be adjusted and synchronized, as one of the key points of the entire life cycle.

(4) On the basis of the study of the project case data obtained, it can be concluded that establishing the overall life cycle emission reduction model to lead–zinc smelting processes will be the focus for green smelting projects. Secondary material recycling, waste heat recycling system, and value chain extension should be taken as the main parts of smelting project design. The energy use, resource utilization, and automation degree, to establish information database in accordance with the actual production situation should be studied and analyzed, to update the database in the application process. This can also help companies to explore any potential and to establish their own way to green development.

Through the establishment of the full life cycle emission reduction model, negative pollution benefits of enterprises can be changed into positive economic benefits, and a two-way transformation channel between "gold and silver mountains" and "clear water and green mountains" can be established to keep companies competitive throughout their whole life cycle.

GCRIS

Evaluation and Certification Strategies for Lead–Zinc-Bearing Residues

J. Antrekowitsch and G. Hanke

Abstract While the recycling of metallic scrap is nowadays state of the art, metal-containing by-products from the metallurgical industry represent a new potential secondary resource. Huge amounts of such materials are available worldwide either on dumps or continuously produced. However, their complex composition renders a detailed characterization difficult, resulting in few and weakly developed recycling concepts available to date. To realize this potential in the future, more bundled competence is necessary. Montanuniversität Leoben has already developed some expertise in the field of typical by-products such as dust, slags, and sludge. Due to the genesis of the primary polymetallic ores, it is especially the metallurgical processes used in the copper, lead, and zinc industries that offer a high potential in their by-products. To allow an assessment of these materials, a certification system similar to the ones already existing for primary resources needs to be established. This, in turn, will be of major use as a basis for investment decisions and relevant feasibility studies turning these often untouched materials into valuable resources.

Introduction

Investigating the development of primary metal resources a tendency becomes obvious nowadays that can be summarized by two trends, the decrease of metal grades and the increase of unwanted impurities. The following statistics (Fig. 1) illustrates the metal grade decrease with the example zinc and lead ores.

This development for zinc and lead (Fig. 1, left) clearly shows a decrease from about 10% in 1972 to about 4–6% in 2016. This must be seen as relevant change, especially facing only a moderate development of smelting technologies within this

J. Antrekowitsch (✉)
Chair of Nonferrous Metallurgy, University of Leoben, Leoben, Austria
e-mail: juergen.antrekowitsch@unileoben.ac.at

G. Hanke
Chair of Geology and Economic Geology, University of Leoben, Leoben, Austria

© The Minerals, Metals & Materials Society 2020

A. Siegmund et al. (eds.), *PbZn 2020: 9th International Symposium on Lead and Zinc Processing*, The Minerals, Metals & Materials Series,
https://doi.org/10.1007/978-3-030-37070-1_27

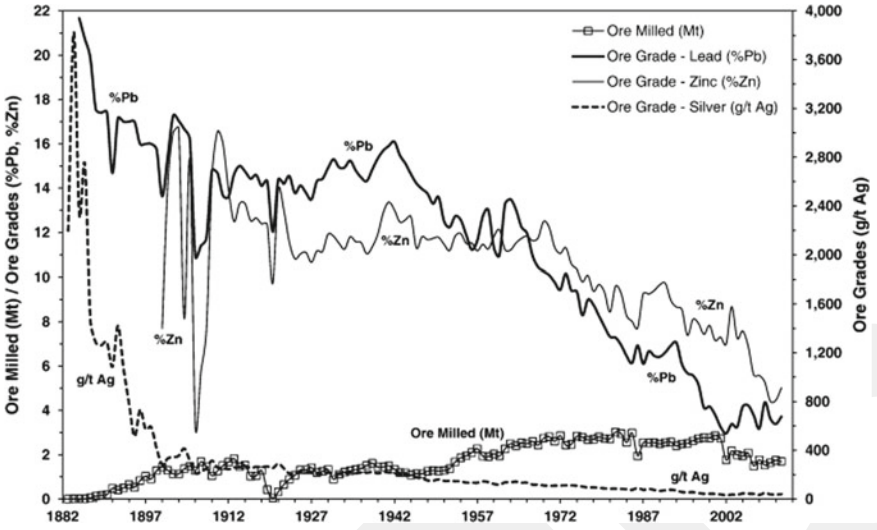

Fig. 1 Decrease of metal grades in lead and ores [1]

time span. The same is true for gold resources that dropped from the well-known 10 ppm content in the past to 2–4 ppm within the same period [2].

In parallel, increasing iron values in zinc ores become apparent, leading to much higher amounts of residues which currently have to be landfilled due to missing reprocessing methods causing an environmental problem that has to be solved in the future. In case of gold, the multi-metal-containing resources make an economic gold-winning difficult often caused by a lack of efficient recovery methods for the associated valuable metals. Additionally, more and more refractory-type gold ores, often associated with arsenic, show a reduced gold recovery due to missing concepts of suitable liberation technologies.

Alternative metal supply by recycling might offer a certain compensation for declining ore qualities. However, as it can be seen from Fig. 2, the recycling rates of most of the metals are still relatively low. The illustration indicates the fact that the recycling rates of most of the important metals are far below 50%, raising the question why there seems to be a certain limit in secondary metal production even though recycling especially of metallic scrap is highly developed and applied in most regions of the world.

When having a closer look into metal processing circuits, it becomes obvious that the following circumstances avoid higher recycling rates and make the dream of a circular economy, which is quite popular at present time, unrealistic for this field of industry:

– The process used for metal production always produces a not so small amount of residues, often called by-products, which are often landfilled, even though they contain interesting amounts of valuable elements.

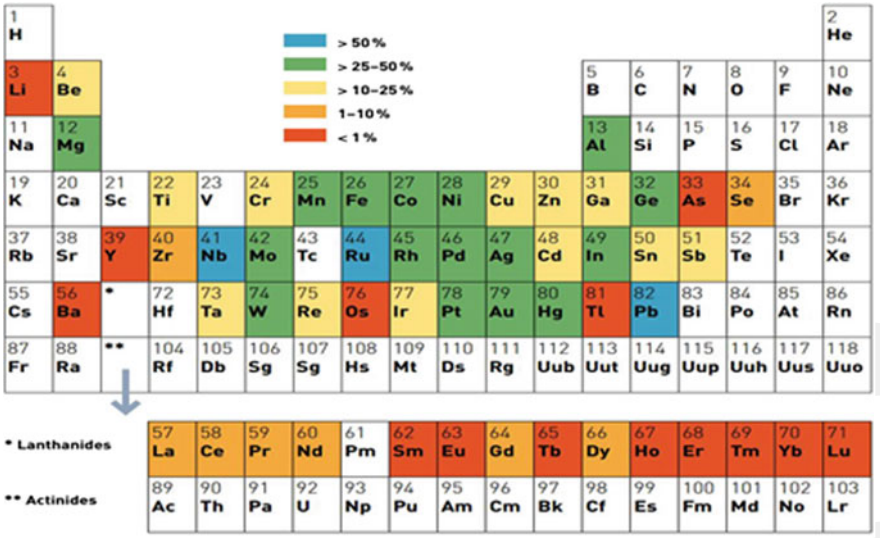

Fig. 2 Recycling rates of various metals [3]

– Collection of the materials is difficult. Especially in Europe, many scraps and other secondary raw materials leave the continent via legal and illegal ways and cannot be seriously implemented into recycling circuits.
– Also, during recycling processes wastes are generated, containing valuable metals.
– During processing, part of the targeted metal is transferred into a form (e.g. low metal-containing slag, etc.) out of which no recovery is possible due to energetic issues and as a direct consequence ultimately economic reasons.

Raw Materials in Europe

Europe nowadays faces the difficulty that even when raw materials are present, no matter if primary or secondary ones, they often leave Europe and are not available any more for metal production. Typical examples are automobile scrap, electronic scrap, residues from lead and zinc industry but also copper and gold concentrates to name just a few.

This means Europe on the one hand hardly searches for own raw materials to become more independent but on the other hand available raw materials cannot be kept in Europe and are treated elsewhere.

The reasons for this strange situation can be listed as follows:

– high costs for energy
– high costs for labor

– strict environmental legislations
– strict safety regulations
– complicate approval and permission procedures
– lack of new or improved processing concepts that might be able to compensate for the above difficulties.

Of course, European citizens must be happy to live in a region of the world with highest safety and environment standards but it also has to be realized that this contributes to a missing competitiveness with countries in Africa or Asia. With this, many of European raw materials are treated outside Europe, which ultimately cannot be the strategy for the future.

In this context, a relatively new metal source, industrial by-products, has to be discussed asking the question if they could represent an interesting raw material for Europe.

By-products

For many decades, residues from metal production, such as slags, dust, and sludge, have often been qualified as waste that was simply dumped. This fact was—at least at that time—accepted by industry and involved authorities. Except for metal-producing companies, no market participant really recognized that metal-bearing wastes were often landfilled to an amount that was more or less as high as the metal production itself. In the eighties and nineties of the last century, first environmental concerns triggered more attention on such dumps and residues. Nevertheless, due to missing technologies and low metal prices the interest in processing residues to recover valuables was still very low.

During the past few years, multi-metal recovery from concentrates has been developed for both, primary ores and secondary materials. In addition, minor metals contained in such residues became important for daily life in industry. In other words, metals that did not have a real value in the past nowadays may essentially contribute to the economic viability when recovered from residues.

In combination with increased metal prices and the need for special and rare metals in various highly sophisticated technologies (e.g. the electronics industry), more attention must be paid to such residues which often represent a potential secondary resource. Currently, recycling rates are still low and huge amounts of residues are dumped annually.

Recycling is mainly based on scraps, where the elements in focus are available as pure metals.

However, scraps have a defined volumetric limit and their treatment is already optimized to a certain level. As a matter of fact, recycling rates must be improved in the near future considering continuously dropping grades in primary ores, implying that new sources need to be exploited as described above.

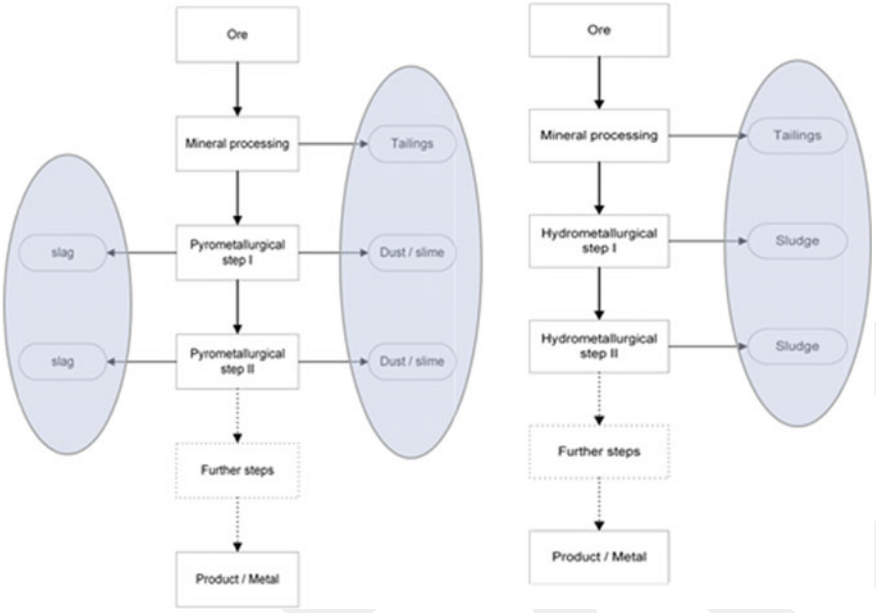

Fig. 3 By-products out of mineral processing and metallurgy (pyrometallurgical route—left; hydrometallurgical route—right)

As an important solution to this problem, by-products of various metallurgical processes (see Fig. 3), already dumped or continuously being produced, started to move into the focus of interest of both industry and research.

Screening the metallurgical area, residues emerging from the lead, zinc, and copper industries must be considered. Processed ores commonly contain a high number of critical and valuable metals at the same time. Typical by-products are produced either in hydrometallurgical or in pyrometallurgical process routes as shown in Fig. 3.

Some of the contained metals are recovered to a certain amount by primary metallurgical processes, but the bulk ends up in different waste streams.

Very often sludge from hydrometallurgical operations and dust from pyrometallurgical operations offer a significant number of metals at concentration levels that might be of economic interest. In addition, some recycling processes of highly diversified and contaminated scraps (e.g. car bodies or waste electric and electronic equipment) generate complex by-products.

Figure 4 illustrates the possible recoverable elements but also shows the high overall metal content available in currently produced residues.

These residues can be found worldwide in huge quantities either on dumps dating from the end of the last century or being currently produced and form an interesting secondary resource of metals with high availability. Due to the long European history in mining and metallurgy, such landfilling sites and producing mills are still present and have to be considered as “part of the market” [4, 5].

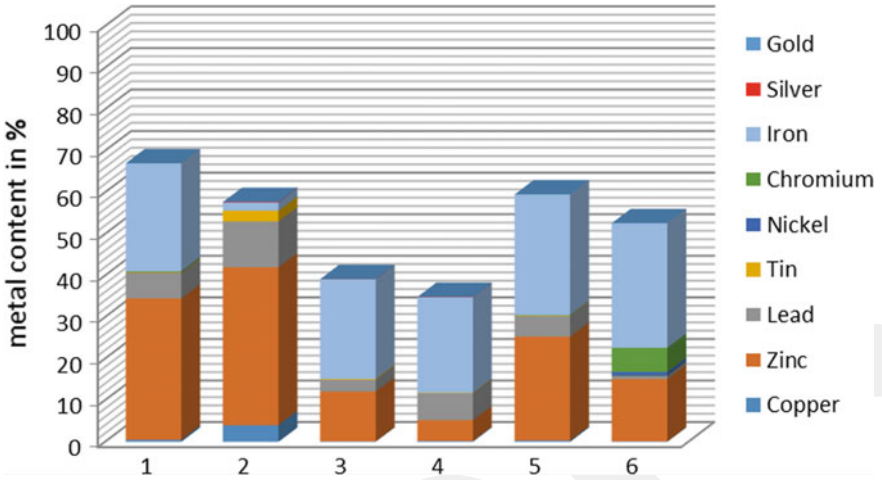

Fig. 4 Examples for different residues and their metal content (1: electric arc furnace steel mill dust; 2: dust from copper recycling; 3: slags from lead industry; 4: jarosite from zinc industry; 5: dust from cupola furnaces; 6: stainless steel production dust)

Some of the residues described in Fig. 4 are already recycled to a certain extent. However, also for these secondary materials the worldwide recycling rates are still below well 50% due to two main reasons:

– the lack of optimized processes
– missing information and data about the materials.

Both factors are responsible for the inefficiently utilized potential on secondary resources [4].

Another reason for the weak exploration and use of residues is the lack of any guideline or competence describing how to evaluate residual materials. This is partly due to non-existent adequate databases. For primary materials like metal ores, codes do exist that serve as accepted and applied guidelines for a qualified evaluation by following pre-defined steps, leading to a "bankable feasibility study". Such guidelines currently do not exist for secondary materials.

A consequent "stepwise approach" must be applied right from the beginning of the project.

Assessment of Metal-Bearing By-products

Montanuniversitaet Leoben has started to develop a guideline for the assessment of specific metal-bearing by-products to allow a clear perspective on how valuable typical materials are. Two main areas are important from the technical point of view, described in the following chapters.

Characterization

Depending on the feed material used and the treatment technology applied, various residues with different properties emerge that can be discriminated by their origin or properties. Some of the above-described residues have already been investigated to a certain extent with respect to characterization and a first evaluation.

Detailed geochemical and mineralogical characterization of metallurgical residues is of highest importance in order to develop appropriate mineral processing recipes and further on appropriate metallurgical methods to recover all metals of interest. Hence, the following questions need to be answered:

(1) Which particles contain the metals to be recovered?
(2) What is their particle size, shape, and texture, i.e. zoned grains, coated grains?
(3) How intensive/complex are incorporated phases intergrown in different particle fractions?
(4) What is the concentration level of metals in the major particles?
(5) Presence and concentration of deleterious elements (such as As, Cd, Hg)?

In order to separate minerals or metallurgical phases by means of mineral processing techniques with physical, physical–chemical, and/or chemical methods, it is necessary to know the relevant phases regarding the key aspects mentioned above. In the end, the size, shape, structure, and the chemical and mineralogical composition define a particle [6].

Deriving from these parameters, the density, optical, electrochemical, thermal, chemical, and mechanical characteristics of any particle can be determined. As the way of managing a metallurgical process and its actual parameters highly affect the residues not only in composition but also in structure, the variance of the residues' properties with regard to mineral processing characteristics is large, even for an existing plant in operation. In analogy to primary mineral deposits, processing results may vary widely if these changes are not taken into account. Thus, the residue has to be investigated and characterized properly.

Based on that, the main goal is to generate a basis for assessing possible metal or metal compound recycling methods. Additionally, the different metallurgical possibilities for a treatment—hydro- or pyrometallurgical—need to be determined. These results are mandatory for evaluating possible process steps that are required to generate products from the residues. To generate this information, the main properties such as melting behavior, volatilization behavior, reducibility, and solubility need to be determined in advance by using special metallurgical characterization procedures.

Process Development and Product Quality

To cope with the continuously stricter environmental legislation next to a shortage of critical metals in Europe, especially the process development for a treatment

of secondary resources and the optimization of existing processes are two major concerns. The challenge of the years to come is, at the same time, to minimize newly generated residues and to achieve maximum product quality within the recycling process. In addition, the quality of the products influences the targeted market and achievable revenues. Therefore, the state-of-the-art processes have to be continuously adapted regarding energy consumption, mass-balancing, and further improvement of the product quality.

A specific geochemical, mineralogical, and metallurgical characterization creates the basis for improving such existing processes. Thus, it will be possible to obtain higher product qualities and lower amounts of newly generated waste streams.

As demonstrated by several investigations carried out at Montanuniversität Leoben, the residues are not at all homogenous. Hence, it is not possible to recycle such residues as one combined single input stream. In order to increase the recoverable metal grade and to reduce the content of substances that hinder the metallurgical process, some separation by physical/mechanical techniques is required. If such a process shall be developed systematically rather than by trial-and-error, the residue must be characterized properly in terms of its properties relevant to a separation process. Fractional analysis is the standard tool in mineral processing for assessing the amenability of primary mineral resources to be upgraded to saleable products of defined and consistent quality. Taking into account the heterogeneity of the residues, it is expected that some upgrading is possible which may pay off during recycling. Fractional analysis yields the optimum results for separating a given feed material by assuming perfect separation. Thus, it also serves as a benchmark for assessing the performance of an existing process. The possible benefits of assessing and processing the residues in a similar way to primary mineral resources are obvious. As some common properties of the residues (e.g. the generally fine particle size distribution of dusts, just to name one) are problematic in fractional analysis, the methods require further adaptations.

In order to find the suitable processing chain, test work needs to be carried out. Once done for a residue, the obtained data will be collected and condensed in a database, which acts in future assessments as a decision support tool. Although similarities within the same type of material (e.g. slags and dust) can be found, each residue is generated in slightly different processing routes with varying input material. This leads to variable extraction yields, consumable consumption, energy input, obtained product quality, etc. Based on the experimental results, the database will grow, and the more materials are cataloged, the more accurate the data for the assessment becomes.

One major disadvantage of past attempts in recycling by-products was that often just one single metal was recovered while possible further valuable metals distributed into newly generated wastes and were therefore lost for production. Pyrometallurgical concepts allow the recovery of valuable metals by applying different basic operations: forming a volatile phase, where, e.g., zinc or lead can be collected as oxides in the

off-gas; forming a liquid metal phase, where, e.g., iron or lead acts as an efficient collector for various minor metals. In combination with mineral processing steps, where a separation of metal-containing fractions could be realized prior or subsequent to a metallurgical step, the targeted multi-metal recovery can be realized.

For hydrometallurgical concepts, the dissolution of a larger number of elements followed by a selective precipitation, again combined with mineral processing, would offer a multi-metal recycling. However, also a combination of hydro- and pyrometallurgy could lead to appropriate solutions [6].

Facing the situation that for some by-products recycling concepts do not exist and for those which are already partly recycled but with the majority recovering only one metal, this approach must be regarded as one of the essential novelties.

Economic Considerations

Within the investigations, also a model for economic verification was established and different dumps worldwide have been investigated. With this evaluation, high promising dump sites as well as residues of poor quality have been detected.

Economics were done for different materials and metal prices. As already mentioned above, gold and silver contribute in a very important way to the overall revenues. However, the key message is that a multi-metal recovery is essential for the economic stability of a recycling process and allows a higher flexibility regarding varying metal prices.

Summary

By-products from metallurgical industry can play an important role as secondary resource for different metals in the future. Important for the successful utilization is a detailed evaluation and assessment of the materials, offering interested parties a reliable information tool similar to already existing guidelines for primary resources. Important steps to such an assessment concept are an advanced characterization of the by-products combined with sophisticated processing concepts which in certain cases might be already available but might be also subjected to new developments. Especially, the idea of recovering more than only one metal from described by-products would allow an economic and ecologic utilization of such wastes that will play an important strategy for the future.

References

1. Mudd G (2007) An analysis of historic production trends in Australian base metal mining. Ore Geol Rev 32(1–2):227–261
2. Development of gold grades. http://www.wikiwand.com/en/Gold_mining. Accessed Feb 2019
3. Reuter MA (2013) Metal recycling, United Nations Environment Programme
4. Antrekowitsch J, Steinlechner S (2011) The recycling of heavy-metal containing wastes: mass balances and economical estimations. JOM 63(1):68–72
5. Mineral Yearbooks. http://minerals.usgs.gov/minerals/pubs/country/index.html#pubs. Accessed June 2018
6. Antrekowitsch J (2016) Recycling of poly-metallic residues from metal industry—current status and future developments. In: Proceedings of TMS 2016, 145 annual meeting & exhibition—REWAS, Nashville, USA

GCRIS

Part VIII
Primary Lead II

GCRIS

KCM—Innovator in the Pb Metal Production Through Ausmelt Technology and Variable SO_2 Concentration Off-Gas Utilization

Nikolay Starev and Georgi Doganov

Abstract KCM 2000 Group is the principal of the non-ferrous smelter located near Plovdiv, Bulgaria, with an annual production of 70,000 tpy lead and 75,000 tpy zinc including their alloys and compounds. As part of a large-scale renovation plan, a new brown field lead smelting plant was commissioned in the middle of 2014. It was designed to produce 75,000 tpy crude lead and 55,000 tpy sulphuric acids in an economically feasible and environmentally friendly way of substituting the old sintering–blast furnace technology. The New Lead Plant (NLP) compiles the best available techniques (BAT) in the metallurgical industry such as the Ausmelt top submerged lance (TSL) smelting and wet gas sulphuric acid process. At the end of 2016, the New Lead Plant reached its design capacity and proved to perform better than designed regarding utility consumption. Since the beginning of 2017, the plant has been operating steadily with increasing results.

Keywords Ausmelt smelting · Lead production · TSL

The Process

The metallurgical process is organized in cycles with the duration of around 9 h each. Every batch consists of two stages—smelting of around 7 h when the furnace is fed with raw materials and subsequent 1.5 h of slag reduction with lump coal. Both stages take place in a single vessel. At the end of the batch, the slag is tapped, granulated, and stockpiled for zinc recovery. All utilities, such as air, oxygen, and natural gas are injected through the lance submerged in the bath.

The feed material mixture is prepared in a new preparation department equipped with day bins for each kind of feed, weight belt feeders controlled by a furnace control system and a mixing drum for conditioning moisture and particle size. The structure of the raw materials is primary lead concentrates mined locally and secondary materials such as lead paste from KCM's Spent Lead–Acid Batteries Plant, lead cakes from

N. Starev · G. Doganov (✉)
KCM 2000 Group, Asenovgradsko shose, 4009 Plovdiv, Bulgaria
e-mail: georgi.doganov@kcm.bg

© The Minerals, Metals & Materials Society 2020

A. Siegmund et al. (eds.), *PbZn 2020: 9th International Symposium on Lead and Zinc Processing*, The Minerals, Metals & Materials Series,
https://doi.org/10.1007/978-3-030-37070-1_28

the zinc plant, as well as the recycled dust in the form of cake, generated by the metallurgical process in the TSL Furnace. Fluxes added for slag chemistry control includes iron-containing material (roasted iron pyrites), silica, and lime-ash.

The feed rates are as follows: lead concentrates 16–19, lead cakes 3–4, and lead paste around 4 t/h. The chemical analysis of the feed materials is shown in Table 1.

Recycled dust from the process of around 14% moisture is fed at a rate of 4–8 t/h. The average analysis is shown in Table 2.

The average flux additions are approximately 2 t/h.

Since the beginning of 2018, the share of secondary feeds has steadily increased from 20 to 27%.

The average direct lead recovery achieved in the first quarter of 2018 is 74.4%. Monthly lead bullion production has steadily increased. The average specific lead productivity expressed as produced lead per m^2 of the furnace per day for the first four months of 2019 is displayed in Fig. 1.

Table 1 Typical feed material analysis in %

	Pb	Cu	Zn	Bi	Sb	As
Lead concentrates	71	1.6	4	0.19	0.06	0.20
Lead cake I	40	0.4	7	0.20	0.05	0.13
Lead cake II	22	0.4	12	0.07	0.13	0.25
Lead paste	75	<0.1	–	0.01	0.10	0.01

Table 2 Recycled dust composition in %

Pb	Cu	Zn	Sb	As
64	0.05	5	0.3	0.9

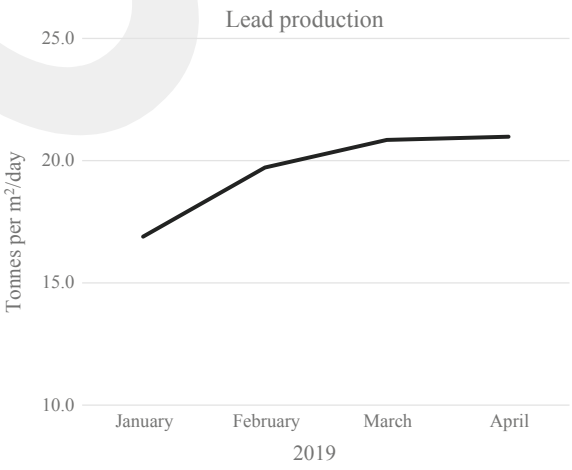

Fig. 1 Average specific lead productivity in 2019

Table 3 Slag content during smelting stage in %

Pb	Zn	Fe	SiO_2	CaO
40–45	10–12	11–13	10–12	6–8

Table 4 Typical granulated slag chemistry in %

Pb	Zn	Fe	SiO_2	CaO	Sb	As
4–5	17–18	~22	19–21	8–10	0.4	0.2

Table 5 Typical lead bullion analysis in %

	Pb	Cu	As	Sb	Bi
Smelting	99.0	0.5	0.02	0.2	0.3
Reduction	97.5	0.7	0.3	1.3	0.1

Slag chemistry during the smelting stage is controlled by regular sampling and adjustment of flux rates. The average slag content during this stage is shown in Table 3.

Slag granulation is carried out by a water jet system. After being dewatered in a bin, the slag is transferred for zinc recovery in the existing waelz kilns. The chemical content of the granulated slag is shown in Table 4.

Average slag tapped per one batch is 35 t with around 6% moisture.

Frequently tapped lead during the batch is cast into moulds and is transported to the existing pyrorefining department in 4 ton ingots in solid state. The lead bullion analysis is shown in Table 5.

All transfer points are equipped with individual dust extraction units, which operate only during material supply.

Downstream the furnace the off-gas is cooled to the temperature of 650 °C in a waste heat boiler with radiation section only. Steam production is 14 t/h in the smelting stage and 16 t/h in the reduction stage. The steam is utilized for common plant needs, and the surplus is condensed and polished for reuse.

At the boiler exit, SO_2 content is around 10 vol.% during the smelting stage and nearly 0 vol.% during the reduction stage. Dust generation is around 5,000 kg/h for both stages.

Before entering the sulphuric acid plant, the gas is conditioned in a wet gas cleaning section. Cooling and dust extraction take place in a series of units: quench tower, radial flow scrubber, packed cooling tower, and two wet electrostatic precipitators. Two ID fans (1 standby) maintain furnace draught. The dust slurry is clarified, and the underflow at an average density of 1200–1300 is transferred to the feed preparation area and is dewatered by a filter press. The cake is added to the mixture of feed materials during the smelting stage. The purified gas contains less than 1 mg/Nm^3 dust and around 10% SO_2 during smelting. At the exit of the wet gas cleaning section, the gas temperature is maintained within 40–45 °C, acid mist at less than 20 mg/Nm^3, and

HF at less than 0.25 mg/Nm^3. Gas properties, e.g. fluctuating SO_2 content depending on the stages in the furnace, are the main challenge of the batch TSL process. The technology adopted in KCM's New Lead Plant is based on the wet gas sulphuric acid process, which does not require any sulphur burning during the furnace stages with low SO_2. The operation temperature in the converter is maintained by natural gas burning in a direct-fired preheater controlled by the converter inlet temperature.

At the acid plant inlet, the gas is diluted by fresh air to 5.5–6% SO_2 before entering the direct-fired preheater. After pre-heating to 390–400 °C, the gas enters the reactor, which consists of three catalyst beds loaded with vanadium–caesium catalyst. The heat generated by the exothermal catalytic process is recovered by a liquid salt system using two interpass heat exchangers. The gas temperature at the third bed outlet is around 400 °C and has to be decreased for the next step—acid condensation. The cooling to 265 °C is carried out in a heat exchanger with molten salt as a heat transfer media. Downstream the SO_3–water vapour–acid mist mixture is condensed in a condensation column through glass tubes heat exchangers. Additional cooling downstream to 60 °C is applied by blowing ambient air into the glass tubes. Product acid with concentration of 97–98% is collected in a tank and is further cooled down to 40 °C by flowing through a plate heat exchanger. Acid production is as low as 0.5 t per 1 t lead bullion. After condensation, the process gas still contains some acid aerosols, which are removed in a wet electrostatic precipitator downstream. The weak acid, collected in the precipitator sump, is sprayed in the condensation column head over the glass tubes in counter-current to the gas flow.

Final SO_2 capture to 99.8% is performed in a tail gas scrubber by hydrated lime solution sprayed in counter-current to the gas flow. The generated 20% gypsum solution is periodically transferred and mixed with the slurry from the wet gas cleaning plant and is recycled with the raw material feed. By utilizing the calcium from the gypsum, the total demand for fresh lime-ash required as a flux is decreased by almost 30%. Final gas prior to releasing to the atmosphere contains less than 300 mg/Nm^3 of SO_2.

Conclusion

The New Lead Plant commissioned in KCM represents a unique combination of subsystems and applies the best available techniques. The smelting technology allows treatment of primary and secondary lead-containing materials in a wide range of ratios. The TSL furnace process off-gas with SO_2 content varying from 0 to 10% is treated in the wet gas sulphuric acid plant. This process allows versatility in choosing raw materials and corresponds to the challenges of the raw materials market. Sulfuric acid production is reduced to the lowest possible rates and depends solely on sulphur content in the TSL input. The specific acid production is as low as 0.5 tons acid per ton of lead bullion produced. The residual gypsum solution, generated in the final gas-purifying unit, is recycled in the smelting stage allowing reduction of the

amount of calcium fluxes needed for slag content corrections. The technology creates no other products than lead bullion, low Pb slag, and sulphuric acid.

The specific energy consumption per ton of lead bullion produced in the New Lead Plant proved to be around 40% less than in the old sintering and blast furnace smelting department.

GCRIS

The Latest Development of Oxygen Bottom Blowing Lead Smelting Technology

Weiguo Wu, Pengfei Xin and Jianming Wang

Abstract The world's largest lead smelting plant using oxygen bottom blowing (SKS) lead smelting technology under construction is introduced in the paper. The most advanced smelting and environmental protection technologies are applied in the design and construction of the plant, representing the latest development level of SKS lead smelting technology. The secondary bullion is produced by the process of oxygen bottom blowing reduction (RSKS) furnace. Zinc oxide is recovered from the RSKS furnace slag by fuming furnace. The refined lead is produced by continuous refining furnace, anode formwork erection cast, and large plate electrolysis process. The world's largest single series lead smelting plant is introduced from five aspects including treatment scale raw materials, technological process, furnace and the main technical specifications.

Keywords SKS lead smelting technology · RSKS smelting technology · Single series · Largest scale

Introduction

SKS lead smelting technology is one of the world's most advanced lead smelting technologies. More than 80% lead production is adapt SKS technology. The application of SKS lead smelting technology greatly increases the automation degree of the lead smelting process, improves the operating environment, and reduces the three wastes emission and the production cost, which has become the world's most widely used lead smelting process.

Since the first SKS furnace was put into industrial application, the SKS lead smelting technology has made great progress after nearly 20 years of production practice and application. The reduction process of blast furnace is gradually replaced by the reduction process of bottom blowing melting furnace. The annual production

W. Wu (✉) · P. Xin · J. Wang
China ENFI Engineering Corporation, 12 Fuxing Road, Haidian district, Beijing 100089, People's Republic of China
e-mail: Wuwg@enfi.com.cn

© The Minerals, Metals & Materials Society 2020

A. Siegmund et al. (eds.), *PbZn 2020: 9th International Symposium on Lead and Zinc Processing*, The Minerals, Metals & Materials Series,
https://doi.org/10.1007/978-3-030-37070-1_29

capacity of the SKS furnace has developed from 60,000 to 800,000 tons. Not only the lead concentrate, but also the high silver low lead silver concentrate and solid waste including zinc leaching residue, lead paste, copper ash, steel dust and lead glass can be treated by the SKS furnace. The lead concentrate is treated with the gold concentrate to made matte for capturing gold, which has changed the traditional smelting process of gold concentrate.

Plant Composition

The plant is designed to process 800 kt tons of lead concentrate and secondary lead materials annually. The main product is lead ingots. Sulfuric acid, zinc oxide dust and copper matte are the by-products. Zinc oxide dust and copper matte are treated by zinc plant and copper plant respectively.

The factory consists of waste lead battery pretreatment system, lead smelting system, and common auxiliary system. The waste lead battery pretreatment system is composed of three parts including crushing and sorting system, lead-based alloy production system, and waste plastic modified granulation comprehensive utilization system. The lead smelting system includes raw material storage and proportion system, mixing granulation workshop, smelting workshop, bullion refining, sulfuric acid, and desulfurization. The utility system consists of soft water and desalination preparation, pulverized coal preparation station, blower and air compressor station, oxygen plant, circulating water station, waste heat power plant, sewage treatment plant, acid storage, etc.

Raw Materials

The raw materials treated by SKS furnace are the mixed lead bearing materials including lead concentrate, lead paste, sulfur gold ore, and lead silver residue. The processing scale is 800 kt/a. The composition of the mixed lead bearing materials is shown in Table 1.

Table 1 Composition of the mixed lead bearing materials (dry basis, wt%)

Element	Pb	Zn	Cu	Fe	S	SiO_2	CaO	As	Sb	Ag*	Au*
%	40–45	4–6	0.8–1.2	8–12	15–18	5–6	0.5–1	0.4–0.6	0.4–0.6	1000–1200	3–4

Note: *Represents g/t

Technological Process

Pretreatment of Waste Lead Acid Battery

The waste lead acid battery is caught into the hopper by multi-lobe grab crane, which is uniformly added to the belt conveyor through the vibrating feeder and transported to the crusher for crushing. The crushed accumulator is continuously sent to the hydraulic grading box by the screw conveyor. The heavy parts with large density (i.e. metal particles) sink to the bottom of the grading box, which are taken away by the screw conveyor. And the qualified metal particles after washing are sent to the lead-based alloy production system by the belt conveyor. The light parts with low density are sent to the horizontal sieve with the water flow. The material under the screen is the oxide with small particle size (lead paste), which is sent to the filter press by pump. The filter cake is sent to the melting system for processing, and the filtrate is sent to the circulation tank for recycling. The organic matter on the screen flows into another hydraulic grading box for grading. The plastic parts with low density and the rubber parts with high density are separated and unloaded, respectively, by the corresponding screw machine. The plastic and rubber parts are sent to the waste plastic modified granulation comprehensive utilization system.

Using the natural gas as fuel, the lead alloy is smelted by the regenerative melting pot. After added appropriate amount of antimony powder, the lead antimony alloy is produced for sale.

Bullion Smelting

SKS Smelting

After proportion, the lead concentrate, lead paste, sulfur gold ore, and lead silver residue sent to the mixing granulation workshop, which are mixed with the weighed returning dust to be granulated. After granulation, the mixed lead bearing materials are sent to the front furnace bin of smelting workshop by belt conveyor, which are added into the SKS furnace by belt conveyor after measuring by the constant feeder. Oxygen is sprayed into the furnace from the bottom. The rich slag, primary bullion, dust and offgas are produced. The molten SKS slag flows directly into the RSKS furnace through the launder for reduction smelting. The primary bullion is fed into the molten lead pot through the tundish and chute for copper removal. The dust is returned to the smelting system for through the scraper conveyor. After recovering waste heat from waste heat boiler and collecting dust from electric dust collector, the offgas is delivered to the sulfuric acid delivery plant to produce acid by the double contact sulphuric acid process. And the tail gas after acid making is sent to the offgas desulfurization system.

Bottom Blowing Reduction Smelting

In the process of bottom blowing reduction smelting, limestone needs to be added to adjust the slag type and the pulverized coal is used as the reducing agent. After quantitative weighing, limestone, pulverized coal, and return product are added into the bottom blowing reduction smelting furnace by the belt conveyor. Oxygen and pulverized coal are sprayed into the furnace from the bottom. The reducing slags, secondary bullion, dust, and offgas are produced by reduction smelting furnace. The reducing slags flow into the fuming furnace through the slag chute to recover zinc. The secondary bullion is fed into the plumbum smelter through the tundish and chute for initial fire refining. The dust is returned to the smelting system for batching via the airtight scraper conveyor. After recovering waste heat from waste heat boiler and collecting dust from electric dust collector, the high-temperature offgas is delivered to the offgas desulfurization system.

Fuming Furnace Blowing Smelting

Pulverized coal is used as fuel and reducing agent in the process of fuming furnace blowing smelting, which is blown into the fuming furnace by the compressed wind after weighed. Zinc oxide dust, slag, and offgas are produced. The zinc oxide dust is collected by the waste heat boiler and dust collector for the recovery of zinc. After water quenching in the granulation tower, the slag flows into the drum for water-slag separation and is sent to the slag bin through the belt. After recovering waste heat from waste heat boiler and collecting dust from electric dust collector, the high-temperature offgas is delivered to the offgas desulfurization system.

The bullion produced by the SKS furnace and the RSKS furnace flows into the continuous copper removal furnace through the tundish and chute for initial fire refining. After removing the copper, the bullion is cast into the anode plate and sent for electrolytic refining. Large plate is used for electrolysis. The copper matte produced by the continuous copper removal furnace is delivered to copper plant for processing.

The steam from waste heat boiler of the SKS furnace, the bottom blowing reduction smelting furnace and the fuming furnace are for waste heat power generation. The saturated steam is used for waste heat power generation system.

The ionic liquid process and low temperature in slurry phase chelating and reduction denitrogenation process are applied for offgas desulfurization.

Bullion Refining

Continuous Removal of Copper in Bullion

The bullion from RSKS furnace is discharged through siphon and added to the continuous refined copper furnace in a molten state for copper removal. And then the

bullion is added to the lead pot for further refining. Copper, tin, and other impurities are removed, which are harmful to electrolysis in bullion. And then the content of antimony is adjusted to meet the requirements of lead electrolysis.

After refining, the molten lead is pumped into the anode casting pot through the lead pump and then transferred to the lead holding furnace of anode casting machine with the lead pump. The molten lead is fed into the quantitative casting ladle and then sent to the metal casting machine. And the rest is returned to the lead holding furnace. The lead anode plate is transported to the lead electrolysis workshop by the automatic crane.

Electrolytic Refining

After primary pyro metallurgy refining and casting the anode, the bullion needs to be purified by electrolytic refining. Antimony, gold, silver, bismuth, and other valuable metals are recovered from anode slime by lead electrolysis.

Electrolytic refining of lead process consists of cathode plate making, anode and cathode automatic spacing, lead electrolysis, anode scrap washing, precipitation of drawing bars for lead washing, copper bar grinding, electrolyte circulation, and slime washing and filtration.

Cathode lead obtained from electrolyzing is sent to Lead melting pot for casting before it is cast to lead ingot by castor. Anode scrap obtained from electrolyzing is washed in washing tank before it returns to smelting process to be recast to anode plate. After washing, anode slime is obtained and sent to the existing copper smelter after pulping and filtering, so as to recover valuable metals like Au, Ag and Bi. Washing solution and filtrate returns separately to anode scrap washing tank and electrolyte circulating tank. During refining process, circulating electrolyte flows into circulating tank. Appropriate amount of H2SiF6 and additive needs to be supplemented regularly into circulating tank. The solution in circulating pump is pumped to overhead tank for recycling.

Main Equipment

SKS Furnace

The type structure of the SKS furnace is in closed, rotary, and horizontal cylinder.

The specification of the SKS furnace is ø5 × 28 m, which includes three feed ports, fifteen oxygen injector, one siphon, two slag tapping holes, and one offgas outlet on the siphon side.

The refractory brick life of the SKS furnace is more than three years.

The schematic diagram of the SKS furnace is shown in Fig. 1.

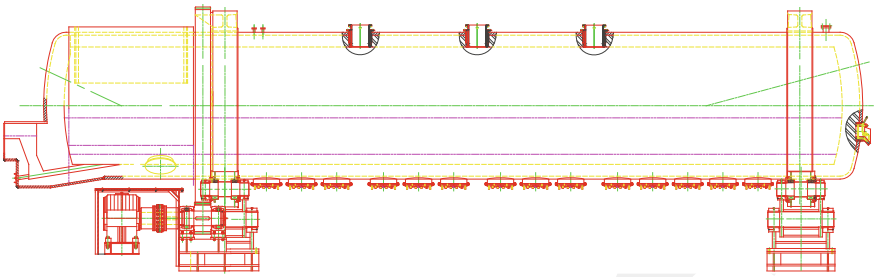

Fig. 1 Schematic diagram of the SKS furnace

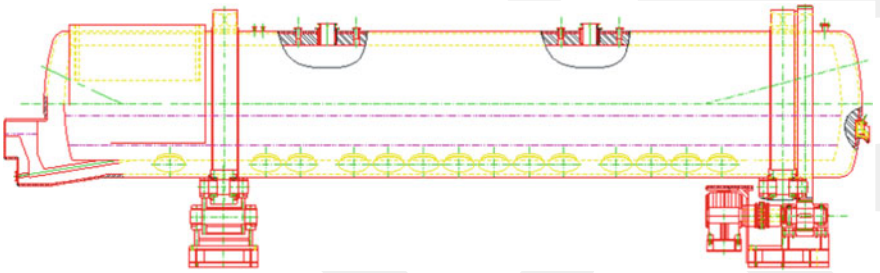

Fig. 2 Schematic diagram of the RSKS furnace

RSKS Furnace

The type structure of the SKS furnace is in closed, rotary, and horizontal cylinder.

The specification of the oxygen bottom blowing smelting furnace is ø5 × 28 m, which consists of two feed ports, fourteen oxygen injector, positions on the bottom of the furnace, four lance on the top, one siphon, two slag tapping holes, and one offgas outlet near each siphon mouth.

High lead slag is added to the reducing furnace from the offgas outlet.

The refractory brick life of the RSKS furnace is more than two years.

The schematic diagram of the RSKS furnace is shown in Fig. 2.

Fuming Furnace

Consisting of water jackets, the type structure of the fuming furnace is a square shaft furnace, which is inclosed and settled.

The specification of the fuming furnace is 32 m^2, which consists of one feed opening for hot materials, two slag tapping holes and one emergency slag tapping holes, and one offgas outlet directly connected to membrane wall of waste heat boiler.

The schematic diagram of the fuming furnace is shown in Fig. 3.

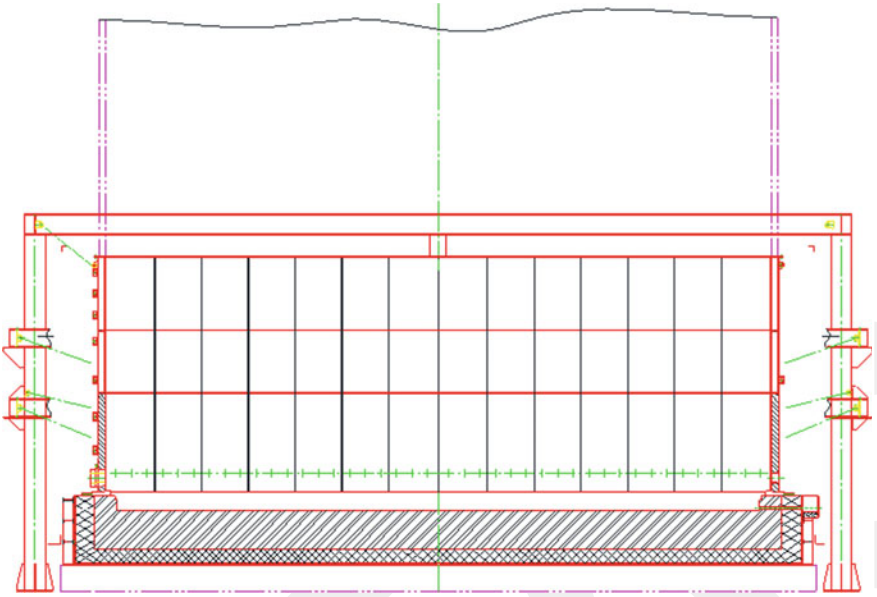

Fig. 3 Schematic diagram of the fuming furnace

Continuous Copper Removal Furnace

Continuous de-coppering furnace is a fixed horizontal furnace. The furnace is arranged with four auxiliary pots: recycling pot, cooling pot, return pot, distribution pot. They are connected to the furnace through pipes. The lead liquid flows between the furnace and the auxiliary pot in the same system.

An off-gas outlet, a slag outlet, a copper matte outlet and a lead outlet are set in the continuous de-coppering furnace. Two burners are set at both ends of the furnace for heat supply.

The continuous copper removal furnace is shown in Fig. 4.

Technical and Economic Index

The main technical and economic indexes of bullion smelting are shown in Table 2.

The main technical and economic indexes of bullion electrolytic refining are shown in Table 3.

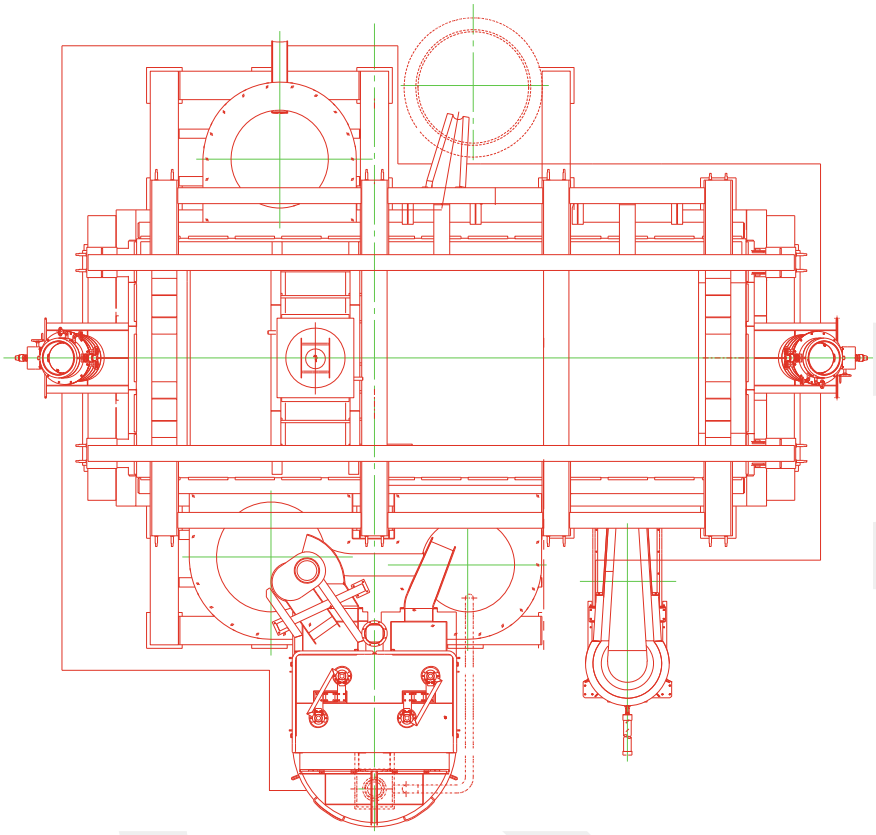

Fig. 4 The schematic diagram of the copper removal furnace

Conclusion

(1) The oxygen bottom blowing lead smelting technology is a green energy-saving smelting technology
(2) The oxygen bottom blowing lead smelting technology is applied by the lead smelter, which is characterized by low construction cost, excellent index, good environmental protection, high efficiency, strong competitiveness, energy-saving, and low pollution
(3) The development trends of oxygen bottom blowing lead smelting technology are as follows: firstly, the technology is developing towards the direction of large-scale production, energy-saving and emission reduction, improving labor production efficiency; secondly, the technology is applied to treat various solid wastes comprehensively for achieving comprehensive utilization of resources and maximizing economic and social environmental benefits.

Table 2 The Main technical and economic indexes of bullion smelting

No.	Item	Unit	Value
SKS section			
1	Specifications of the bottom blowing furnace	m	ø5 × 28
2	Working days	d/a	330
3	Processing capacity of concentrate	kt/a	800
4	Lead grade of the mixed materials	%	40–45
5	Sulfur grade of the mixed materials	%	15–18
6	Industrial oxygen consumption	Nm^3/t	100–110
7	Ash rate	%	12–15
8	SKS Slag	t/a	~740
9	Lead content in SKS oxide slag	%	40–48
10	Steam quantity of waste heat boiler	t/h	30–35
11	Operating pressure of waste heat boiler	MPa	5.0
RSKS section			
1	Specifications of the reduction smelting furnace	m	ø5 × 28
2	Working days	d/a	330
3	Processing capacity of RSKS slag	kt/a	~740
4	Ratio of oxygen to coal	Nm^3/kg	0.4–0.5
5	Rate of pulverized coal	%	8–10
6	Ash rate	%	8–12
7	Secondary bullion porduction	kt/a	~410
8	Pb in bullion	%	94–96
9	Slag quantity	kt/a	~350
10	Lead content of reducing slag	t/a	2–3
11	Zinc content of reducing slag	t/a	12–15
12	Steam quantity of waste heat boiler	t/h	35–40
13	Operating pressure of waste heat boiler	MPa	5.0
Fuming furnace smelting section			
1	Specifications of the fuming furnace	m^2	32
2	Working days	d/a	330
3	Processing capacity of reducing slag	kt/a	~350
4	Zin oxide dust production	%	15–18
5	Zinc in zinc oxide dust	%	55–60
6	Ability of fumer	t/m^2 d	30–35
7	Percentage of coal powder	%	16–20
8	Pb in fumer slag	%	0.2–0.5
9	Zn in fumer slag	%	2–3

(continued)

Table 2 (continued)

No.	Item	Unit	Value
10	Slag quantity	kt/a	300
11	Steam quantity of waste heat boiler	t/h	65–70
12	Operating pressure of waste heat boiler	MPa	5.0

Table 3 Main technical and economic indexes of bullion electrolytic refining

No.	Item	Unit	Value
1	Lead ingot capacity (Pb: 99.994)	kt/a	400
2	Working days	d/a	330
3	Specifications of the continuous copper removal furnace	m^2	20
4	The number of the continuous copper removal furnace	pic	2
5	Industrial oxygen consumption	Nm^3/t Pb	20–25
6	Natural gas consumption	Nm3/t Pb	10–12
7	Residual anode ratio	%	38–40
8	Average electrolysis current density	A/m^2	140
9	Current efficiency	%	93
10	Electrobath voltage	V	0.35–5
11	Recovery rate		
	Pb	%	99
	Ag	%	99.5
	Au	%	99.5
	Sb	%	99

References

1. Editorial committee of Lead-Zinc Metallurgy (2003) Lead-Zinc Metallurgy [M]. Beijing Science Press
2. Dongbo L, et al. (2003) The application of oxygen Bottom Blowing and Blasting Furnace smelting for Pb &Zn smelting [J]. Non-Ferrous Metals (Smelting)
3. Weifeng L, et al. (2010) Current status and progress of Pb smelting technology in China [J]. China Nonferrous Metallurgy
4. Rong Z (2015) The application of continuous de-coppering furnace in lead bullion pyrometallurgical refining [J]. Shanxi Metallurgy

Characterization of Phase Equilibria and Thermodynamics with Integrated Experimental and Modelling Approach for Complex Lead Primary and Recycling Processing

E. Jak, M. Shevchenko, D. Shishin, T. Hidayat and P. C. Hayes

Abstract Substantial advances have been made in the characterization of phase equilibria and thermodynamic properties of complex multi-phase equilibria in gas—slag—matte—metal—speiss—solids systems directly relevant to primary and recycling lead smelting. The present review summarizes some of the outcomes of recent studies of the multi-component and multi-phase system containing PbO–ZnO–"Cu_2O"–FeO–Fe_2O_3–CaO–SiO_2–S as major components, Al_2O_3–MgO–Cr_2O_3 as minor slagging components, and As–Bi–Ni–Sb–Sn–Ag–Au–Co as other minor components. The research methodology that has been employed involves the integration of experimental measurement and thermodynamic database development. The target of these fundamental studies is to characterize phase equilibria and thermodynamics of this multi-component system and to develop a thermodynamic database as part of a computer package that can be used to assist in optimization of all stages of the value chain from sintering, smelting, and zinc fuming in primary production to complex chemistry processing in recycling. A summary and examples of research outcomes and applications are presented.

Keywords Phase equilibria · Thermodynamic modelling · Primary lead · Secondary lead · Matte formation · Minor elements · Lead refining · Speiss formation

E. Jak (✉) · M. Shevchenko · D. Shishin · T. Hidayat · P. C. Hayes
School of Chemical Engineering, PYROSEARCH, Pyrometallurgy Innovation Centre, The University of Queensland, Brisbane, QLD 4072, Australia
e-mail: e.jak@uq.edu.au

T. Hidayat
Department of Metallurgical Engineering, Bandung University of Science and Technology, Bandung, Indonesia

© The Minerals, Metals & Materials Society 2020

A. Siegmund et al. (eds.), *PbZn 2020: 9th International Symposium on Lead and Zinc Processing*, The Minerals, Metals & Materials Series,
https://doi.org/10.1007/978-3-030-37070-1_30

Introduction

In the survey of global lead smelter operations reported in the Pb/Zn 2010 symposium [1], two major trends were noted: (i) the relatively rapid changes to process technologies and (ii) the increasingly diverse range of source materials, the use of mixtures of primary ores, complex process wastes and recycled materials by industry in their feed materials. These trends have continued at an accelerating pace. The task of optimizing process design and operation of modern metallurgical plants has become more complex. Accurate and reliable descriptions of phase equilibria and thermodynamics properties are required to describe these multi-component systems over wide ranges of bulk compositions and process conditions. In the previous review of phase chemistry of lead smelting systems [2], some of the advances that had been made in characterizing the PbO–ZnO–FeO–Fe_2O_3–CaO–SiO_2 system and the development of a thermodynamic database describing this base slag system were highlighted. The accuracy of the database at that time was reliant on experimental data available at two extremes in process conditions, in air and in equilibrium with metallic iron. Phase equilibrium data were available on the majority of PbO- and ZnO-containing low-order SiO_2-containing sub-systems, on selected multi-component systems in PbO–ZnO–"Fe_2O_3"–CaO–SiO_2 in air and ZnO–"FeO"–CaO–SiO_2 in equilibrium with metallic iron.

Since that time, with the financial support from major lead primary and recycling companies, this research program has further progressed and significant advances have been made to increase the range of chemical systems that can be experimentally characterized in these lead-containing systems. With the development of an integrated experimental and thermodynamic modelling research methodology, a program on development of the thermodynamic database for the complex multi-component and multi-phase gas—slag—matte—speiss—metal—solids PbO–ZnO–"Cu_2O"–FeO–Fe_2O_3–SiO_2–S–Al_2O_3–CaO–MgO–Cr_2O_3–(As–Bi–Ni–Sb–Sn–Ag–Au–Co) system is currently underway.

The strategic target of the program is to be able to produce sophisticated computer-based tools that can be used to predict the outcomes from industrial reactor systems, to support the introduction of feed-forward control systems, to increase the productivities and efficiencies of pyrometallurgical processes, and, ultimately, to develop and implement the use of computer-based virtual reactor models of these systems. These tools have the potential to deliver substantial economic and productivity benefits to industry as well as improve metal recycling and energy efficiency.

The present paper provides a brief outline of the following:

- The extensive experimental and thermodynamic database development research capability that has been established.

- Selected examples demonstrating recent research progress on phase equilibria in the development of the 19-component database, including equilibria in high-PbO-containing low-silica systems, equilibria with Pb metal; equilibria with Cu–Pb metal alloys; S-containing systems; minor elements distributions; refining conditions with speiss.
- Examples of industrial applications of the database to the analysis of complex multi-component systems.

A more detailed review of the information available in the literature of phase equilibria in high-temperature lead smelting and refining systems, and the corresponding references, will be given in a forthcoming journal version of the paper [3].

Outline of Research Techniques

An overview of the latest advances in the integrated experimental and modelling research approach to the thermodynamic database development for these pyrometallurgical systems has been provided in [4]. The unambiguous determination of the unique set of binary and ternary model parameters accurately describing a whole range of conditions from low- to high-order systems is critical for the accuracy and predictive power of the tool, and requires experimental data for all binary and ternary sub-systems, and for selected quaternary sub-systems. If there are no experimental data—there can be no unique reliable accurate parameters and therefore no reliable model.

Recently, significant advances in experimental techniques and capabilities have been achieved due to the development and availability of advanced microanalytical techniques including (i) electron probe X-ray microanalysis (EPMA) and (ii) laser ablation inductively coupled plasma mass spectrometry (LAICPMS). These microanalysis techniques provide breakthrough capabilities in phase equilibrium studies for pyrometallurgical applications greatly extending the range of systems that can be studied, and the accuracy of characterization with very few limitations on the range of bulk compositions and conditions that can be characterised. Details of the experimental technique based on the equilibration at fixed conditions, quenching, and direct measurement of phase compositions using microanalysis techniques EPMA and LAICPMS developed by the authors are outlined in the previous publications.

Thermodynamic modelling is performed with the FactSage computer package. The methodology used for the development of the database involves, first, developing a preliminary database using experimental data available in the literature data, the identification of key areas of disagreement or thermodynamic inconsistency, and the selection of critical experiments required to resolve these inconsistencies or omissions. The databases are developed so as to achieve a self-consistent set of parameters for the thermodynamic models, accurately describing phase equilibria and all other thermodynamic properties for all phases over the complete range of conditions in terms of temperature, composition, and atmospheric conditions. The

Table 1 Summary of phases and elements described in the current internal PYROSEARCH solution databases (UQPY-2019) important for Pb–Cu–Zn pyrometallurgical processing. Further detailed description is provided in [5]

Slag:(Cu^{1+}, Fe^{2+}, Fe^{3+}, Si^{4+}, Al^{3+}, Ca^{2+}, Mg^{2+}, Pb^{2+}, Zn^{2+}, Ni^{2+}, Sn^{2+}, Sb^{3+}, As^{3+}, Bi^{3+}, Ag^{1+}, Au^{1+})(O^{2-}, S^{2-}), modified quasichemical formalism in quadruplet approximation
Spinel: [Cu^{2+}, Fe^{2+}, Fe^{3+}, Ni^{2+}, Al^{3+}, Mg^{2+}, Zn^{2+}]^{tetr}[Cu^{2+}, Fe^{2+}, Fe^{3+}, Ni^{2+}, Al^{3+}, Ca^{2+}, Mg^{2+}, Zn^{2+}, $vacancy^0$]$_2^{oct}O_4$, compound energy formalism
Liquid matte/metal/speiss: (Cu^{I}, Cu^{II}, Fe^{II}, Fe^{III}, Pb^{II}, Zn^{II}, Ni^{II}, Sn^{II}, Sb^{III}, As^{III}, Bi^{III}, Ag^{I}, Au^{I}, O^{II+}, S^{II+}), modified quasichemical formalism in pair approximation
Monoxide: (CuO, FeO, $FeO_{1.5}$, NiO, $AlO_{1.5}$, CaO, MgO), Bragg-Williams formalism
Mullite: (Al^{3+}, Fe^{3+})$_2$(Al^{3+}, Si^{4+})(O^{2-}, $vacancy^0$)$_5$, compound energy formalism
Olivine: [Fe^{2+}, Ni^{2+}, Ca^{2+}, Mg^{2+}, Zn^{2+}]^{M2}[Fe^{2+}, Ni^{2+}, Ca^{2+}, Mg^{2+}, Zn^{2+}]$^{M1}SiO_4$, compound energy formalism
Melilite: [Ca^{2+}, Pb^{2+}]$_2$[Fe^{2+}, Fe^{3+}, Al^{3+}, Zn^{2+}][Fe^{3+}, Al^{3+}, Si^{4+}] $_2O_7$, compound energy formalism
Pyroxenes: [Fe^{2+}, Ca^{2+}, Mg^{2+}, Ni^{2+}]^{M2}[Fe^{2+}, Fe^{3+}, Mg^{2+}, Al^{3+}, Ni^{2+}]^{M1}[Fe^{3+}, Al^{3+}, Si^{4+}]$^{B}Si^{A}O_6$, compound energy formalism
Dicalcium silicates: (Ca_2SiO_4, Fe_2SiO_4, Mg_2SiO_4, Pb_2SiO_4, Zn_2SiO_4), Bragg-Williams formalism
Wollastonite: ($CaSiO_3$, $FeSiO_3$, $MgSiO_3$, $ZnSiO_3$), Bragg-Williams formalism
Willemite: [Zn^{2+}, Fe^{2+}, Mg^{2+}][Zn^{2+}, Fe^{2+}, Mg^{2+}]SiO_4
Corundum: ($FeO_{1.5}$, $AlO_{1.5}$, NiO), Bragg-Williams formalism
Fcc and bcc solids alloys: (Fe, Cu, Ni, O, S, Pb, Zn, As, Sb), Bragg-Williams formalism
Digenite-bornite: (Cu_2S, FeS, PbS, ZnS, Ni_2S, $vacancy_2S$), Bragg-Williams formalism
MeS cubic: (FeS, PbS, CaS, MgS, vacancyS), Bragg-Williams formalism
Solid stoichiometric compounds: (over 150 phases) including solid oxide, metal, sulfide, and sulfate solids
Ideal gas: >100 species including N_2, H_2O, CO, CO_2, SO_2, SO, As_2, AsS, AsO, Zn, ZnS, ZnO, AgS, Pb, PbS, PbO, Bi, Bi_2, BiO, BiS, Sn, SnO, SnS, Ag, AgO, AgS, Sb, Sb_2, SbO, SbS

overview of solution phases and thermodynamic models developed to date is given in Table 1.

Overview of Recent Results

The following section presents selected examples demonstrating recent research progress on the characterization of phase equilibria in the 19-component system of importance for Pb and Zn pyrometallurgy.

Phase Equilibria in High-PbO Slag Systems in Air, with Pb Metal and with Pb–Cu Metal Alloys

There are major experimental difficulties in measuring phase equilibria in high-PbO slag systems in oxidizing conditions and particularly in equilibrium with Pb and Pb–Cu metal alloys. The slags and liquid metal alloys are chemically aggressive, dissolving conventional refractory and metal containment materials resulting in contamination of the system with unwanted chemical components, difficulties in retaining the original liquid phase as a uniform amorphous phase on quenching due to low viscosity, fast crystallization, and high vapor pressures leading to selective vaporization of metal and metal oxide species. These difficulties have been overcome in recent research [6], which has resulted in important advances in experimental technique. These improved techniques include the use of primary phase substrates and closed system experiments in which samples are sealed in evacuated silica ampoules. Using these approaches, many PbO-containing systems have been characterized; some examples are listed below:

In air, the liquidus and phase equilibria for the systems, the PbO–"$FeO_{1.5}$"–CaO [6] and PbO–"$FeO_{1.5}$"–SiO_2 [7].
In equilibrium with metallic Pb, the liquidus and phase equilibria for the system PbO–"FeO"–SiO_2 [8].
In equilibrium with Cu–Pb metal alloys, new information on the liquidus surface for the PbO–"Cu_2O"–SiO_2 system in equilibrium with Pb–Cu metal and the distribution of copper between slag and bullion [9]. Note that the Pb–Cu metal alloy present in this system is in the solid state for a range of Pb/Cu ratios.

In summary, with the development of improved experimental techniques, many low-order oxide and oxide-metal sub-systems of high importance for Pb and Zn complex pyrometallurgy have been accurately characterized over the last decade. These include many Pb- and Zn-containing oxide sub-systems. Using the same methodology and similar research techniques, a great deal of new fundamental data on phase equilibria in Cu-containing oxide-metal sub-systems has also recently become available.

Slag-Matte Equilibria

The distribution of elements between slag and matte is one of the key factors in lead smelting and refining. No systematic studies were found in the open literature describing the equilibria between the lead slag, matte, and metal. The problems associated with characterizing phase equilibria in lead matte systems are even more challenging than those with metal due to the high vapor pressures of PbS gas species. With the recent advances in experimental capability, it is now possible to obtain accurate measurements of metal distributions in multi-phase systems containing sulfur.

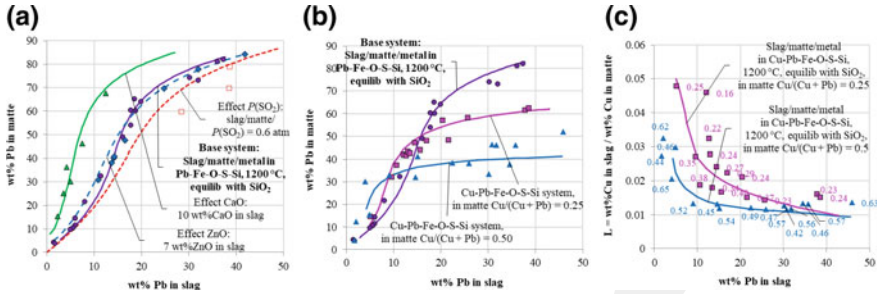

Fig. 1 Slag-matte-metal-SiO_2 equilibria in the Pb–Fe–O–S–Si–(Ca, Zn, Cu) system at 1200 °C showing **a** effects of CaO [4], ZnO, $P(SO_2)$, and Cu, including, **b** %Pb in slag and in, **c** the distribution coefficient of Cu between PbO-containing slag and matte. The lines represent FactSage calculations with current internal PYROSEARCH database. The symbols represent experimental data from PYROSEARCH (2016–2019). For $P(SO_2) = 0.6$ atm, the metal phase is not present

At PYROSEARCH, investigation of the equilibria between lead slag, matte, and metal in the Pb–Fe–O–S–Si system has started; the effects of temperature, $P(SO_2)$, CaO, Al_2O_3, ZnO, and Cu_2O, on the three phase equilibria have been measured. The distribution of lead and copper between matte and slag phases in the Pb–Fe–O–S–Si system with addition of CaO, ZnO, and Cu_2O over a range of conditions is shown in Fig. 1.

Slag-matte systems are important in processing of complex Cu–Pb–Zn materials. Most of the previous studies have been focused on Cu and Cu–Ni slag-matte systems. Almost no data in laboratory-controlled conditions were found in the literature for the Pb–Cu–Zn slag-matte systems. The new experimental techniques developed in PYROSEARCH enable experimental investigations in these systems to be undertaken. The availability of these new data greatly improves the accuracy and reliability of the thermodynamic database for predictions relevant to Cu–Pb–Zn smelting.

Minor Element Distributions

By combining improved experimental techniques, electron probe X-ray microanalysis (EPMA) and laser ablation inductively coupled plasma mass spectrometer (LAICPMS) microanalysis techniques and experiments in closed system in ampoules, minor element distributions between phases can now be accurately measured. The effective partial pressures of $P(O_2)$ and $P(S_2)$ in these systems can be derived from the microanalytical measurement of trace metal concentrations in the condensed phases, e.g. "Cu_2O" concentrations in ZnO–"FeO"–SiO_2 slags. The experimental data available to date as well as new experimental data obtained recently at PYROSEARCH have been used to develop the thermodynamic database describing these systems. The predictions presented in Fig. 2a–d provide a summary and

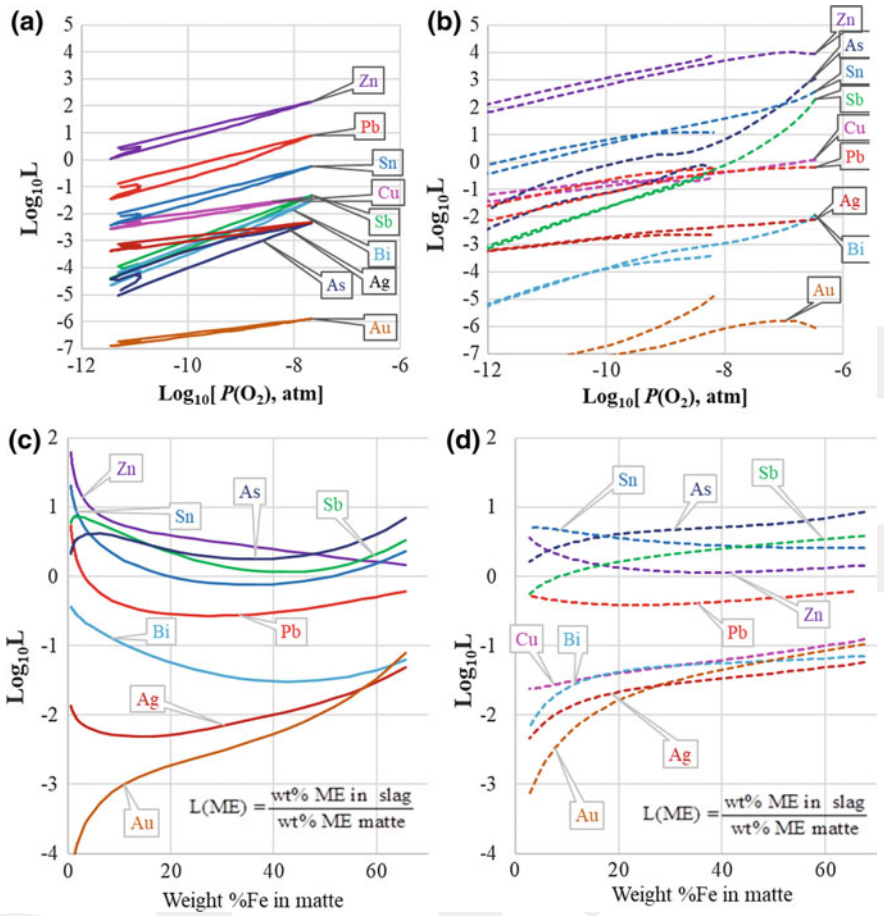

Fig. 2 Summary of distribution coefficients of minor elements (ME) between slag and liquid metal in equilibrium with solid SiO_2 at 1200 °C in the following systems **a** Cu–Fe–O–Si–(ME), slag/liquid copper, **b** Pb–Fe–O–Si–(ME), slag/liquid lead, and between slag and matte in equilibrium with solid SiO_2, at $P(SO_2) = 0.25$ atm and 1200 °C in the following systems, **c** Cu–Fe–O–S–Si–(ME), slag/Cu_2S–FeS matte, and **d** Pb–Fe–O–S–Si–(ME), slag/PbS–FeS matte. The lines represent FactSage calculations with current internal PYROSEARCH database

comparison of slag/metal and slag/matte distribution coefficients of a number of minor elements in copper and lead systems.

Most of the previous studies on minor element distributions reported in the literature on non-ferrous systems are focused on Cu– or Cu–Ni–systems. Very limited data are available for the Pb– and Pb–Cu–systems. Examples of recent experimental measurements of distributions of As, Sb, Cu, and Ag between PbO–FeO–Fe_2O_3–CaO–SiO_2 slag and liquid Pb as a function of $P(O_2)$ and slag composition are given in [10]. The distributions of Ag, Au, Bi, and Zn between Pb metal and Pb–Fe–O–Si slag are reported in [11]. The distribution coefficients between slag/liquid lead and

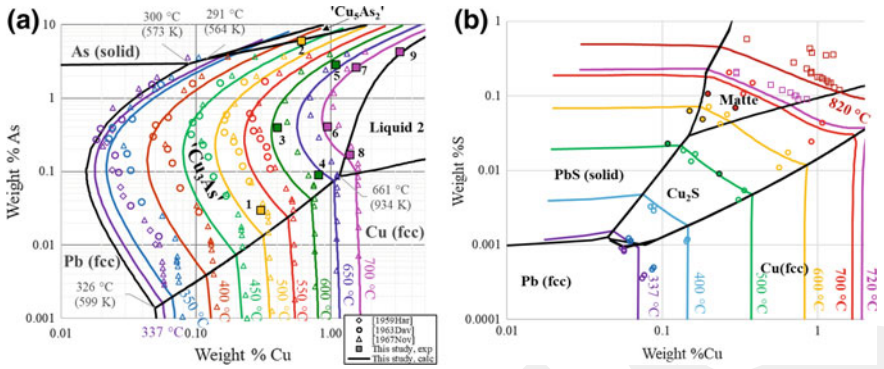

Fig. 3 The Pb-corner of the liquidus surface in the **a** Cu–Pb–As and **b** Cu–Pb–S systems. The lines represent FactSage calculations with current internal PYROSEARCH database. Symbols represent experimental data

slag/PbS–FeS matte are measured and also integrated into the database describing copper smelting systems.

Metal-Speiss Equilibria

During the refining stages of lead processing copper–arsenic and sulfur-containing phases are formed. Figure 3 demonstrates experimental data and thermodynamic database predictions for the key refining systems of Pb–Cu–As and Pb–Cu–S.

The availability of accurate data for the binary systems is critical for the development of accurate thermodynamic databases for systems in which the speiss phase is formed. Critical assessments are available for the Cu–Sb, Cu–Sn, and Cu–As systems. The solubilities of the elements in liquid lead at low temperatures have been given in the following Pb–Cu–As, Pb–Cu–S, Pb–Cu–Sb, and Pb–Cu–Sn systems. Even fewer results are available for the multi-component systems, where solid solutions may form between solid As- and Sb-containing compounds. Some kinetic aspects of copper removal in the presence of speiss-forming elements were reported.

Overview of Industrial Applications

Systematic Analysis of Pb–Cu–Fe Matte/Slag Equilibria

Having obtained new experimental data and incorporated these into the optimized thermodynamic database, it is possible to use these powerful predictive tools to systematically analyze the trends in phase formation and chemical compositions of

these phases in complex chemical systems. The availability of the thermodynamic database enables the systems to be presented and viewed in different ways depending on the needs of the user.

The example presented in Fig. 4a shows a projection of the matte compositions in the Pb–Cu–Fe–O–S–Si slag-matte-metal system in equilibrium with SiO_2 on to the Cu–Fe–Pb composition triangle. Figure 4b contains information on the %PbO in slag corresponding to these matte compositions. The lines drawn on the figure correspond to the data provided previously in Fig. 1a for selected compositions of Cu/(Cu + Pb) in matte. By constructing information in this way, the trends in chemical behavior can be visualized and more efficiently analyzed. This type of calculation and representation can be undertaken for any set of process conditions and bulk chemical compositions to assess the potential outcomes of these multi-phase equilibrium reactions. For instance, the formation of the matte phase can be a problem during the bullion tapping in the Kivcet process. Thermodynamic calculations can provide better understanding of desulfurization reactions in the shaft.

Multi-component Fluxing Diagrams

The thermodynamic database can also be used to construct diagrams that can be used to assist in the selection of optimum flux additions to slags. Examples of the application of these diagrams to the optimization of flux additions to complex lead smelting slags are given in Fig. 5a–d. The effect of the CaO/SiO_2 ratio on the liquidus temperatures of Pb–Zn–Fe–Al–Ca–Mg–Si–O slags for a given PbO concentration and Zn/Fe ratio in the slag is given in Fig. 5a. Here, it can be clearly seen that the slag is fully liquid below 1200 °C for the CaO/SiO_2 weight ratios between 0.1 and 0.6. The liquidus temperature at low flux additions in the spinel primary phase field corresponds to a Fe/SiO_2 ratio of approximately 0.33–0.37 for the above range of CaO/SiO_2 ratios. If the flux addition results in sub-liquidus phase assemblage at these operating conditions, the % solids in the slag can be estimated from Fig. 5c. Excessive % solids in the slag can lead a practical operating issues, such as difficulties in tapping due to increased slag viscosity and the loss of operating volume due to the build-up of solids on the reactor lining. The effect of variable Zn/Fe ratio in slag can be assessed through the use of a pseudo-ternary section ZnO–"FeO"–(CaO + SiO_2), an example of which is shown in Fig. 5b. Here, the liquidus temperature is shown to vary with Zn/Fe ratio with the minimum liquidus temperatures occurring at the join between the zincite, (Zn, Fe) O, and spinel, $ZnO \cdot Fe_2O_3$, primary phase fields.

Process Modelling

Important principles of using thermodynamics in process modelling were outlined in recent publications. Reliable model predications are important for navigating the

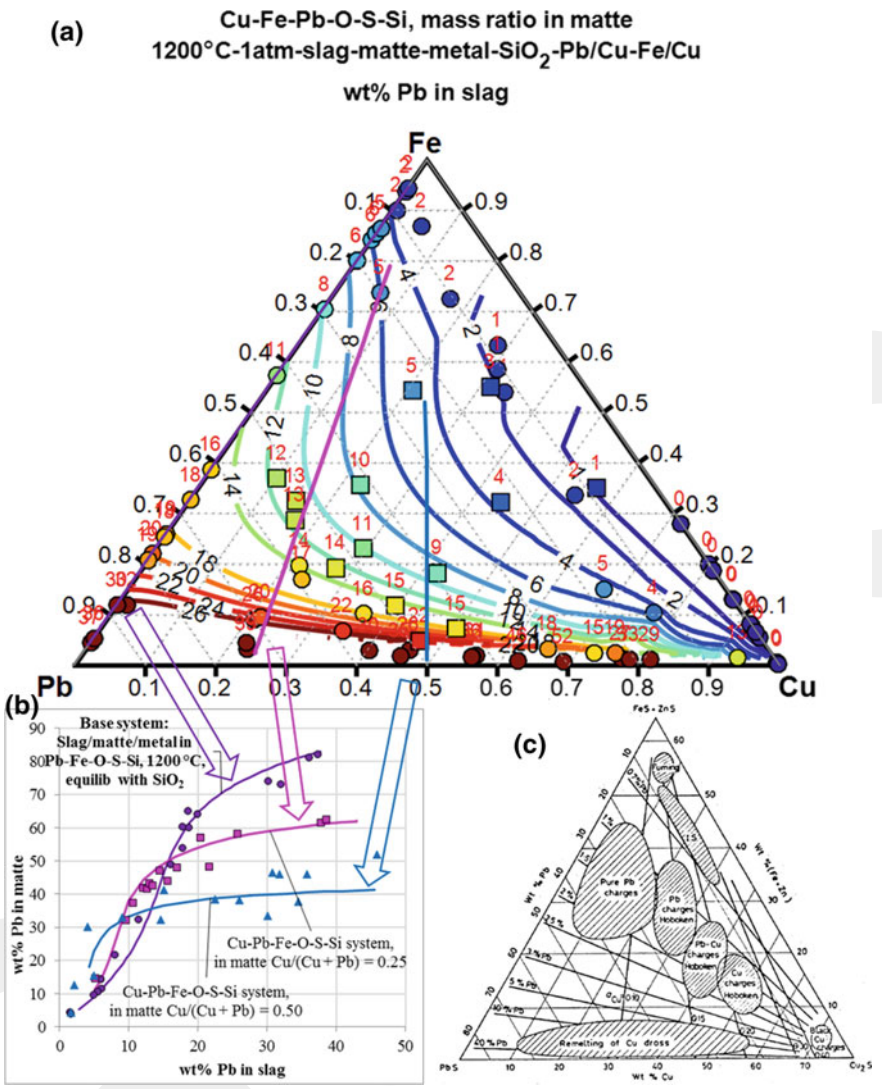

Fig. 4 Slag-matte-metal-SiO_2 equilibria in the Pb–Fe–O–S–Si–(Cu) system at 1200 °C. **a** Projection of the matte compositions on to the Cu–Fe–Pb composition triangle (mass fractions). Iso-lines and labels next to experimental points show %Pb in slag as a function of matte composition. **b** Three sections through the triangle showing the effect of Cu/(Cu + Pb) ratio in matte on the distribution of lead between slag and matte, and **c** the diagram from Fontainas et al. [12], which inspired the systematic study of slag-matte-metal equilibria. Lines in (**a**) and (**b**) represent FactSage calculations with current internal PYROSEARCH database. Symbols represent experimental data

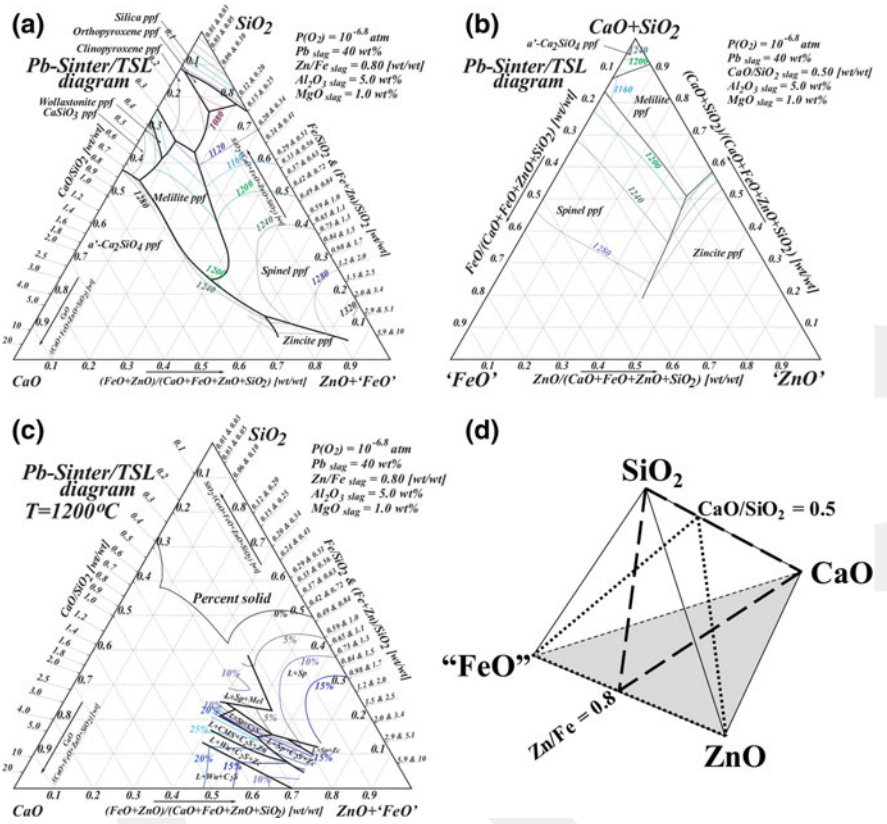

Fig. 5 Fluxing diagrams for multi-component lead slag smelting systems at fixed %PbO in slag. **a** The pseudo-ternary section (ZnO + "FeO")–CaO–SiO_2 showing the effect of CaO/SiO_2 on liquidus temperature for a given Zn/Fe ratio in feed, **b** pseudo-ternary section ZnO–"FeO"–(CaO + SiO_2) showing the variation of liquidus temperature with CaO/SiO_2 ratio in slag for a fixed Zn/Fe ratio, **c** % solids at a 1200 °C for the process conditions given in (**a**), and **d** pseudo-ternary sections of the ZnO–"FeO"–CaO–SiO_2 quaternary

complex reality of modern pyrometallurgical processes. Thermodynamics and phase equilibria are the foundation of sophisticated models. Earlier thermodynamic simulations of lead processes are using the simplified thermodynamic database available for copper drossing and the lead blast furnace.

The thermodynamic database developed by PYROSEARCH can be used together with software products, such as FactSage, ChemApp, ChemSheet, and SimuSage. Several examples of the use of thermodynamic modeling in copper systems are reported. Again full details of references will be provided in [3].

Concluding Statements

Advances in the research methodologies used in high-temperature phase equilibrium studies, improved experimental measurement techniques, and the integration of experimental and thermodynamic database studies have resulted in:

- significant increases in the ranges of process conditions temperature, oxygen and sulfur partial pressures, that can be characterized,
- considerable extension of the number and complexity of chemical systems that can be characterized, and
- improvements in the accuracy of the thermodynamic databases relevant to lead smelting and refining systems.

These fundamental studies have led to the development of sophisticated thermodynamic databases that can be used to predict the outcomes of high-temperature reactions. These databases are particularly important for the optimization of complex process flowsheets that contain multi-element, multi-phase separation systems. The development of these databases is particularly relevant to lead smelting and refining technologies, which are increasingly used as a means of recovering and recycling metals form the end of life of electrical and electronic devices. In these processes, elemental separation can be achieved through the controlled partitioning between gas—slag—matte—metal—speiss—solid phases.

Acknowledgements The authors acknowledge the financial support and technical guidance by the consortium of lead producers: Aurubis, Kazzinc, Glencore, Umicore, Nystar, Peñoles, and Boliden through Australian Research Council Linkage program, LP180100028. The experimental studies cited here would not be possible without the facilities and technical assistance of the Australian Microscopy and Microanalysis Research Facility at the Centre for Microscopy and Microanalysis, The University of Queensland. Dr. Charlotte Allen at the Centre of Analytical Research Facilities at Queensland University of Technology, Brisbane, Australia, provided valuable contribution to the development of the LAICPMS technique.

References

1. Hayes PC, Schlesinger ME, Steil H-U, Siegmund A (2010) Lead smelter survey. In: Lead-zinc 2010, TMS, Warrendale, pp 345–413
2. Jak E, Hayes PC (2010) Phase chemistry of lead smelting slags. In: Lead-zinc 2010, TMS, Warrendale, pp 1161–1176
3. Jak E, Shevchenko M, Shishin D, Hayes PC (2020) Review of phase equilibria in lead smelting and refining systems, Submitted to JOM
4. Jak E, Hidayat T, Shishin D, Prostakova V, Shevchenko M, Hayes PC (2019) Complex copper pyrometallurgy challenges and opportunities—integrated experimental phase equilibria and thermodynamic modelling research and implementation. In: Copper '19 conference, Vancouver, Canada, TMS, Warrendale
5. Shishin D, Hayes PC, Jak E (2019) Development and applications of thermodynamic database in copper smelting. In: Copper '19. Vancouver, Canada, COM, Met Soc CIM, Montreal

6. Shevchenko M (2019) Integrated experimental and thermodynamic modelling research on the multicomponent Pb–Cu–Fe–Zn–Ca–Si–O system. PhD thesis, School of Chemical Engineering, The University of Queensland
7. Shevchenko M, Jak E (2019) Experimental liquidus studies of the Pb–Fe–Ca–O system in air. J Phase Equilib Diff 40:128–137. https://doi.org/10.1007/s11669-018-0703-7
8. Shevchenko M, Jak E (2019) Experimental liquidus studies of the Pb–Fe–Si–O system in air. J Phase Equilib Diff 40:319–355. https://doi.org/10.1007/s11669-019-00727-x
9. Shevchenko M, Nicol S, Hayes PC, Jak E (2018) Experimental liquidus studies of the Pb–Cu–Si–O system in equilibrium with metallic Pb–Cu alloy. Metall Mater Trans B 49B:1690–1698. https://doi.org/10.1007/s11663-018-1249-0
10. Moon N, Hino M, Lee Y, Itagaki K (1998) Distribution of minor elements between metallic lead and PbO–FeO_x–CaO–SiO_2 or PbO–FeO_x–CaO–SiO_2–ZnO slag. Shigen to Sozai 114:121–126. https://doi.org/10.2473/shigentosozai.114.121
11. Shishin D, Hidayat T, Sultana U, Shevchenko M, Jak E (2019) Experimental study and thermodynamic calculations of the distribution of Ag, Au, Bi and Zn between Pb metal and Pb–Fe–O–Si slag. J Sustain Metal, accepted
12. Fontainas L, Coussement M, Maes R (1978) Some metallurgical principles in the smelting of complex materials. In: Complex Metallurgy '78, Proceedings of International Symposium, pp 13–23

GCRIS

Resource Efficiency Evaluation of Pyrometallurgical Solutions to Minimize Iron-Rich Residues in the Roast-Leach-Electrowinning Process

A. Abadías Llamas, N. J. Bartie, M. Heibeck, M. Stelter and M. A. Reuter

Abstract The Roast-Leach-Electrowinning process generates considerable quantities of iron-rich precipitates that must be landfilled, potentially causing a problem for the zinc smelters as well as negatively affecting the society and the environment. The integration of pyrometallurgical flowsheets into existing Roast-Leach-Electrowinning plants is evaluated in this paper. Ten different cases, including Direct Zinc Smelting, ferrite fuming or pyrometallurgical treatment of iron-rich residue, are assessed to find the most resource efficient and environmentally friendly solution to minimize the hydrometallurgical precipitates of the electrolytic process for the zinc production. The simulation-based methodology used provides indicators to evaluate the material recovery and losses, residue production, resource consumption, exergy destruction, and environmental impacts, which are used to find the best alternative that improves the resource efficiency and the environmental impact of the Roast-Leach-Electrowinning process. Furthermore, the social, environmental, and economic impacts associated to the different alternatives are discussed based on the indicators provided by the simulation.

Keywords Exergy · Thermoeconomics · Process simulation · Sustainability evaluation · Jarosite treatment

A. Abadías Llamas (✉) · M. Stelter
Technische Universität Bergakademie Freiberg, Institute for Nonferrous Metallurgy and Purest Materials, Leipziger Str. 34, 09599 Freiberg, Germany
e-mail: a.abadias@hzdr.de

M. Stelter
e-mail: stelter@inemet.tu-freiberg.de

A. Abadías Llamas · N. J. Bartie · M. Heibeck · M. A. Reuter (✉)
Helmholtz-Zentrum Dresden-Rossendorf, Helmholtz Institute Freiberg for Resource Technology, Chemnitzer Str. 40, 09599 Freiberg, Germany
e-mail: m.reuter@hzdr.de

N. J. Bartie
e-mail: n.bartie@hzdr.de

M. Heibeck
e-mail: m.heibeck@hzdr.de

© The Minerals, Metals & Materials Society 2020

A. Siegmund et al. (eds.), *PbZn 2020: 9th International Symposium on Lead and Zinc Processing*, The Minerals, Metals & Materials Series,
https://doi.org/10.1007/978-3-030-37070-1_31

Introduction

The metallurgical infrastructure is a key for the circular economy (CE) since it provides solutions for the metal production, processing, and recycling. However, this infrastructure has material losses and generates residues [1]. One of the base metals within the metallurgical infrastructure composing the CE is zinc. This zinc production process generates iron-rich precipitates, e.g. jarosite, goethite or hematite. For instance, 88.33 kt of jarosite are generated in a plant with an annual zinc production of 200 kt of zinc [2]. Therefore, zinc smelters have been researching possibilities of dealing with these residues, since they require a large ponding area for their disposal. One of these alternatives is the Direct Zinc Smelting (DZS) technology, which is a process preventing the iron precipitate from being produced [3].

DZS is composed by two stages. In the first one, concentrate is smelted to eliminate the sulfur as sulfur dioxides through the off-gases, at the same time that elements such as Zn, Pb, Ag, In or Ge volatilize partially and are collected as oxide dust. In the second stage, the slag produced in the first smelting stage (25 wt% of Zn) is reduced to fume zinc, along with Cd, Pb, Sb or Ge to produce a clean iron-rich slag (2–3% of Zn) [3]. This slag can be safely disposed or used as construction material if it is cleaned enough to comply with the specifications for metals in these materials. Additionally, as the zinc content of the smelting slag must be below 25% due to viscosity issues, part of the clean slag can be circulated to the smelting stage to mitigate these situations.

However, if DZS is integrated with a Roast-Leach-Electrowinning (RLE) plant, the iron residue produced during the RLE can be fed to the DZS smelting stage to control its slag chemistry, while the zinc oxide rich dust can be leached in the neutral and weak acid leach stages of the RLE. This would free the land occupied by residue dumps and recover co-precipitated elements during jarosite process such as indium and germanium. Additionally, this option would extend the life of the current RLE plants [3] as jarosite dumping is minimized. Recent industrial trails [4] have shown that >90% of zinc is already recovered during the smelting stage.

Another alternative is to use a reactive approach, i.e. the treatment of these iron residues once they are produced through the RLE process [2, 5]. One of these reactive alternatives can be, for instance, the pyrometallurgical treatment of the jarosite produced [6]. This alternative would transform the jarosite into a slag, which requires less landfill volume since it is a dry and high density by-product.

These pyrometallurgical alternatives and their integration into the current RLE plants are quite promising from the point of view of decreasing the hydrometallurgical iron-rich precipitates. However, they require high temperatures and the use of reducing agents to be conducted. Therefore, the resource consumption, material recovery and losses, environmental impact, and residue production of these circular actions must be carefully evaluated so that the resource efficiency of the integrated system can be assessed objectively [7, 8]. For this reason, ten scenarios integrating

pyrometallurgical flowsheets into the current RLE process to decrease or eliminate the generation of iron precipitates are studied and their resource efficiency and environmental impact are quantified.

Simulation-Based Evaluation of the Resource Efficiency of the Zinc Production

The first step required to evaluate the resource efficiency of the zinc production is to have a good overview of the system. This can be done by using the simulation-based approach developed by Reuter et al. in HSC Sim [9, 10] to quantify the resource efficiency of metallurgical, recycling, and CE systems [1]. This methodology is based on the development of simulation models which will provide the required indicators to evaluate the material recovery and losses, residue production, resource consumption, and environmental impact of the studied process.

Simulation of the Considered Zinc Production Flowsheets

An integrated RLE-DZS system has been modelled with the simulation platform HSC Sim (HSC Chemistry 9.9 [11]), whose simulation pane is shown in Fig. 1. This

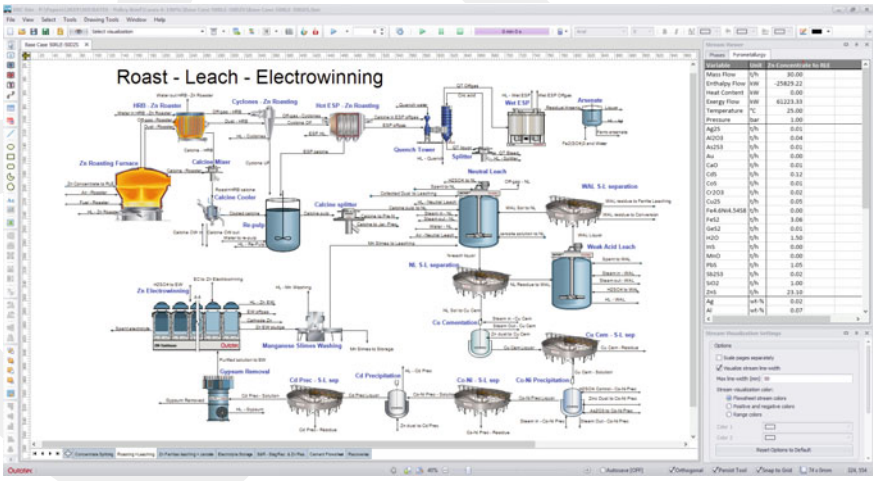

Fig. 1 HSC Sim pane showing the simulated roast-leach-electrowinning (RLE) flowsheet. The tabs at the bottom of the simulation pane contain different flowsheets within the complete system (i) zinc concentrate splitting between RLE and DZS, (ii) RLE flowsheet, (iii) zinc ferrites leaching, and jarosite precipitation, (iv) electrolyte storage and distribution, (v) DZS flowsheet, and (vi) material recoveries of the system

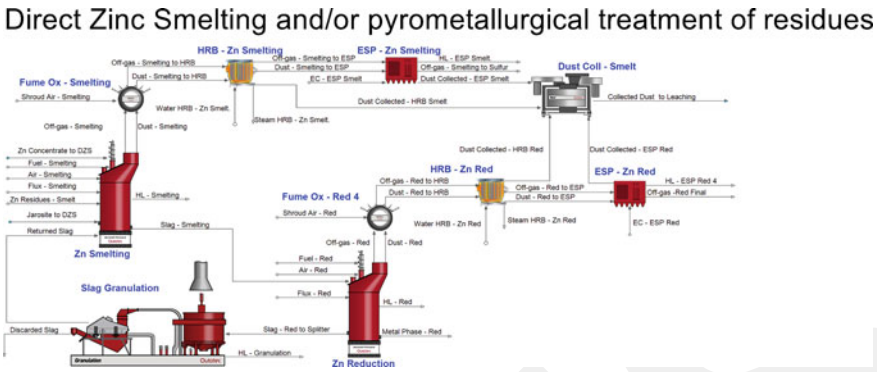

Fig. 2 Direct zinc smelting flowsheet modelled in HSC Sim (fifth tab of the simulation pane in Fig. 1) showing the smelting and reduction stages. During the first stage, a fume containing volatile metals under smelting conditions such as Ag, e.g. as AgO(g) [3], Pb, Zn, As or In, and a slag which will be cleaned in a second stage under reducing conditions are produced. During the reduction stage, volatile metals are fumed, while non-volatile and reducible metals such as Cu or residual Ag and As can form a speiss/alloy phase. A clean slag (less than 3% Zn) is produced and the fumes are processed in a neutral leaching stage of the RLE [3]

model is composed of 58 unit operations, 222 streams, and over 20 elements (and all compounds). The input of the process is an average zinc concentrate with a flow rate of 60 t/h, which is composed by 51% Zn, 5% Fe, 3% Pb, and minor elements, such as silver, indium, germanium or arsenic in their average concentration in zinc concentrates, while its water content is 5%.

Eight scenarios of a preventive alternative such as DZS have been evaluated, whose flowsheet simulated in HSC is shown in Fig. 2. Six of them correspond to different zinc concentrate feed ratios between the RLE and the DZS flowsheets, i.e. from 100% RLE–0% DZS to 0% RLE–100% DZS. Furthermore, the other two cases are 100% DZS with different operation parameters considered. The fuming of the zinc ferrites and the pyrometallurgical treatment of jarosite have been also considered as they are not preventive solutions to avoid the generation of jarosite, but reactive, i.e. the jarosite is generated and then treated.

Material Recovery, Losses and Residue Production

Through the mass balances provided by the simulation of the integrated zinc production system, the recovery rates of all the elements (through their various compounds) can be evaluated, as well as where from the system and in which form they are recovered [12]. Furthermore, the unavoidable material losses can be identified and tracked along the flowsheet. Figure 3 shows the material recoveries for three different scenarios. In the considered 100% RLE scenario, metals such as indium, germanium or antimony are lost in the jarosite residue. Additionally, as the jarosite is not treated,

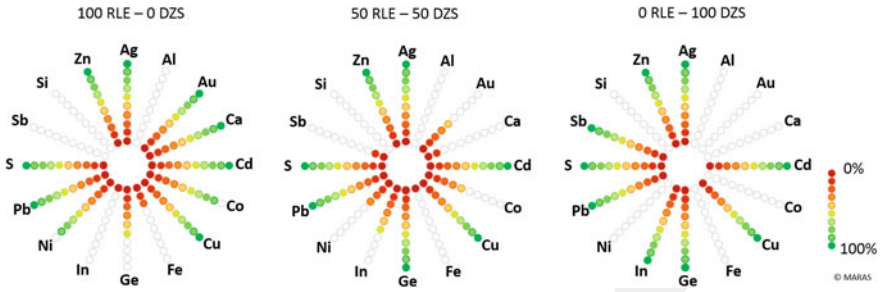

Fig. 3 Metal recovery flowers showing the recovery rates of different elements considered in the simulation model, both in pure or as by-product form. Three different configurations of the integrated RLE-DZS are depicted (i) 100% of the concentrate going to the RLE, (ii) concentrate split equally between RLE and DZS, where the jarosite residue is partially fed to the DZS flowsheet to control the slag chemistry, and (iii) 100% DZS, where zinc dust is produced and leached in neutral and weak acid leach stages of the RLE and iron reports mainly to slag

the lead, silver, and zinc recoveries are lower since these metals contained into the jarosite are landfilled. Usually, the total recovery of these three elements in a 100% RLE scenario is over 90% (99% in the case of zinc), as Fig. 3 shows. Furthermore, metals like cobalt, nickel, or cadmium are recovered during the purification of the electrolyte, as well as the calcium as gypsum, which is filtered and washed to ensure its safe disposal.

When more concentrate is fed to the DZS flowsheet, i.e. "50 RLE–50 DZS" and "0 RLE–100 DZS" scenarios, the recoveries of indium and germanium increase since they are collected through the DZS dust. Additionally, the zinc, lead, or silver contained in the jarosite residue will be recovered too. However, nickel and cobalt are lost through the slag, thus their recoveries would be lower than the current RLE process. The performance of cadmium is independent on the processing route since it is recovered through the fumes in the DZS. As the cadmium is leached with zinc in the neutral leaching stage, it is recovered in the solution purification.

In terms of residue production, the integration of the DZS and RLE transforms the problematic hydrometallurgical iron precipitate into a clean disposable slag, which could be used as construction material if it is sufficiently clean. Through this integration, the clean slag may become a valuable product for the plant, while freeing landfill space around zinc smelters, which would help to improve the society's perception of zinc metallurgy.

Resource Consumption—Thermoeconomics

Exergy can be used to evaluate the resource consumption in metallurgical systems [7, 13–15]. In the same way, the resource consumption of the ten considered scenarios for the zinc production has been evaluated through exergy. The six scenarios

evaluating how the fraction of concentrate introduced to the DZS flowsheet affects to the resource consumption of the system are depicted in Fig. 4a. The DZS operation parameters of these six scenarios are defined according to Hoang et al. [3] with an oxygen enrichment of 60%, which reports zinc fuming rates of 62% in the smelting stage. However, improved zinc fuming rates have been recently estimated during the smelting stage of the DZS on a commercial scale in one plant located in China, where 93% of the zinc is fumed during this stage [4]. Therefore, a 100% DZS scenario considering these fuming rates has been also evaluated ("0 RLE–100 DZS (Smelt.)" scenario), as well as a scenario where no oxygen enrichment was considered ("0 RLE–100 DZS (No O_2 Enr.)"). The other two scenarios, whose resource consumption is depicted in Fig. 4b correspond to (i) roasting, neutral leaching (R+NL), and ferrites fuming to extract the zinc of the ferrites as an iron-free zinc dust and (ii) jarosite treatment through smelting and reduction stages for material recovery and the conversion of the residue into a slag that, if the composition complies the specifications, can be used as building material [6].

As shown in Fig. 4, the total resource consumption of the current RLE process and a 100% DZS scenario with an oxygen enrichment of 60% and the zinc fuming rates of the smelting stage reported by Wood et al. [4] (93% of Zn fumed in smelting), i.e. the "0 RLE–100 DZS (Smelt.)" scenario are practically equal. The reason is that the resources required to operate the DZS flowsheet are compensated with the lower resources consumed in the RLE since the roasting, hot acid leaching, and iron precipitation stages are eliminated. The high oxygen enrichment DZS has the additional advantage that exergy destruction can be balanced between hydro- and pyrometallurgical operation. The RLE route is much more limited in this regard.

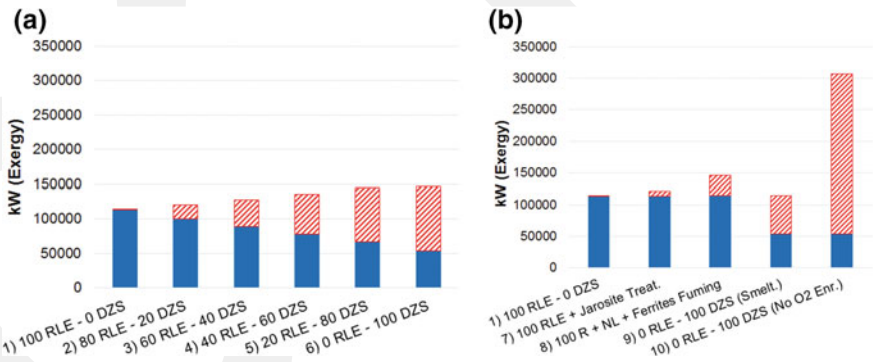

Fig. 4 Exergy destruction of the ten different cases representing their resource consumption. "100 RLE–0 DZS" is the reference case. **a** represents the exergy destruction from a 100% RLE scenario to 100% DZS, while **b** depicts the resource consumption associated to the treatment of jarosite and the fuming of ferrites, as well as two 100% DZS scenarios with different operation parameters from the DZS cases represented in (**a**). Resource consumption allocated to the hydrometallurgical route, i.e. RLE, is represented as a solid-blue color. Exergy destruction allocated to the pyrometallurgical flowsheet, i.e. DZS and pyrometallurgical treatment of RLE residues, is depicted as striped-red

However, if the zinc fuming rates of the DZS plant were lower than the reported rates by Wood et al., the high zinc concentration in the smelting slag would cause viscosity issues. Therefore, the zinc in the smelting slag would need to be reduced by recirculating clean slag and feeding iron residues to the smelter. This would increase the material circulating along the DZS, thus the resource consumption would be larger, as Fig. 4a shows for the cases 2–6. Furthermore, the use of oxygen-enriched air in DZS reduces the resource consumption as the quantity of nitrogen introduced to the furnace decreases, as the "0 RLE–100 DZS (No O_2 Enr.)" shows.

If the zinc ferrites are treated in a fumer instead of leaching them in the hot acid leach, the jarosite precipitation process is avoided. This case, represented in the scenario 8, has a resource consumption that is comparable to treating 80% of the concentrate in a DZS flowsheet. The reason for this high resource consumption is that the zinc ferrites would be fumed together with the precipitated lead-silver residue increasing the amount of material to fume. This action would also increase the lead circulation load since the lead-silver residue to which lead reports, is not produced.

The scenario 7 represents the pyrometallurgical treatment of the jarosite residue produced during the RLE. This option would convert the jarosite residue into a slag through two stages, jarosite smelting and reduction. Obviously, these extra stages would require extra resource consumption; however, it is not as high as the other options evaluated. The required energy and the reductant feed in this scenario would be lower in comparison to the consumptions of the DZS or ferrites fuming since a slag recirculation would not be required, i.e. the zinc content in the jarosite is low enough to avoid problems associated to a high viscous slag.

Emissions and Their Associated Environmental Impact

The simulation of the system provides a good characterization of the emissions and residues in terms of composition and flow rates. Therefore, by linking the results of the simulation to a life cycle assessment (LCA) software, the environmental impact of the system can be evaluated. It can be done through the dedicated LCA tool of HSC Sim, which connects the simulation platform with GaBi [16]. This methodology has been applied to evaluate the environmental impact of primary copper production, e-waste recycling, and nickel pig iron using the HSC Sim process simulation tool [11]. By using the same methodology, the environmental impact of the ten scenarios defined has been obtained.

Within all the environmental impact indicators, the global warming potential (GWP), measured in kg of CO_2 equivalent, will be discussed in this case. As depicted in Fig. 5, the GWP shows a similar increasing trend that the resource consumption. The CO_2 emissions associated with the RLE flowsheet, which are mainly generated when the electricity required for the zinc electrowinning is produced, remains constant since the amount of zinc cathodes produced in all the studied scenarios is the same (30 t/h). However, the CO_2 emissions increase with the use of the DZS

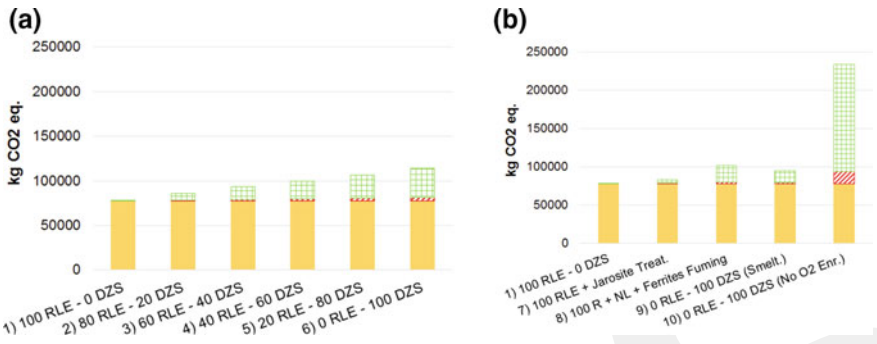

Fig. 5 Global warming potential (GWP) is represented as kg of CO_2 equivalent, for the ten studied scenarios. The solid-yellow part represents the CO_2 emissions associated to the RLE process, which come mostly from the production of electricity required to electrowinning the zinc from the solution (electricity mix from China chosen for this study as representative zinc producer). The striped-red area represents the emissions related to the production of the metallurgical coke required for the pyrometallurgical operations, while the plaid-green part shows the CO_2 emissions produced in the pyrometallurgical flowsheet, both during DZS or pyrometallurgical treatment of RLE residues

technology due to the use of fuels as energy carriers and reductants, while the RLE consumption is considerable lower since the lower temperatures and input material required in comparison with the smelting stage of the DZS.

The pyrometallurgical treatment of jarosite appears as the best alternative to the RLE in terms of GWP, since the emissions associated to the direct fuming of the zinc ferrites are considerable because of the fuel and reductant requirements for the fuming process. However, improved zinc fuming rates during DZS and oxygen enrichment decreases the difference to the pyrometallurgical treatment of jarosite.

The Most Resource Efficient Route for Zinc Production and Its Effect on Sustainable Development—Social, Environmental, and Economic Impacts

Based on the indicators provided by the simulation and studied previously, the most resource efficient and environmentally friendly alternative to reduce the hydrometallurgical iron residues produced in the RLE process for the zinc production can be selected. From the point of view of resource consumption, the 100% DZS with high zinc fuming rates (scenario 9) is the best option. However, the cobalt and nickel entering the DZS flowsheet would be lost in the slag. Furthermore, CO_2 emissions would increase in comparison with the base case.

A 100% RLE followed by a pyrometallurgical treatment of the jarosite residue, i.e. case 7, would have a slightly larger resource consumption. However, the CO_2 emissions would be lower than in comparison to case 9. Additionally, cobalt and nickel would be recovered through the electrolyte purification circuit. Therefore, it

would be the most suitable option to avoid the generation of a wet hydrometallurgical residue. An existing RLE plant and the infrastructure required for the DZS could create this integrated system, with the difference of, instead of splitting the concentrate and feeding it to the DZS, only the produced jarosite residue would be fed to the pyrometallurgical flowsheet; thus, the concentrate would be entirely fed to the RLE flowsheet (scenario "100 RLE + jarosite treatment").

In terms of material recovery, elements co-precipitated with the jarosite residue, e.g. indium, germanium, or antimony, could be recovered through the fumes generated during the pyrometallurgical treatment of the jarosite, if these were not recovered during the typical RLE operations. Additionally, the copper, cobalt, nickel, cadmium, and lead-silver residues would be still produced; thus, the recovery of these elements through further treatment would be possible. Therefore, the material recovery would improve with respect to the base scenario, while in addition, the jarosite residue is converted into a clean slag with the potential of being commercialized as construction material.

Obviously, the resource consumption of the integrated system would increase in comparison to the base case and the high-fuming DZS. The reason is simple, the 2LT dictates that every extra process performed will require extra resources to be used or destroyed. However, the extra resources required to conduct this pyrometallurgical treatment are not much larger than the options shown in Fig. 4. Furthermore, the same occurs with the GWP of the integrated system. An increase in the CO_2 emissions is expected when the system is integrated because of the fuel and reductant required for the thermal treatment, however, the CO_2 emissions of this scenario are the lowest of all the considered alternatives.

The considered alternatives for a lower generation of residues within the zinc production must guarantee a sustainable development. It can only be achieved if the social, environmental, and economic sustainability are fulfilled, as they are the three pillars of sustainability [17]. A first quantification of the factors affecting these three pillars can be done by normalizing the indicators provided by the simulation. For instance, the CO_2 emissions, which affect to the environmental sustainability, can be normalized with respect to the lowest emissions value of all the evaluated alternatives (best-case scenario), or even to the emission limit, to evaluate the deviation of the emission values for every scenario. The same can be done for resource consumption, land use, or CAPEX/OPEX. If the normalized values are calculated in a scale from 0 to 100%, where 0 is the scenario with the most negative impact and 100 is the best-case scenario (positive one), a good view of all the evaluated factors affecting society, environment, and economics can be obtained, thus a first conclusion about the effect of the different solutions in the resource efficiency of each solution can be obtained. The effects of the CE solutions for the reduction of iron-rich precipitate during hydrometallurgical zinc production on these three pillars are discussed, with a few examples on how the impact of some factors affecting them can be quantified.

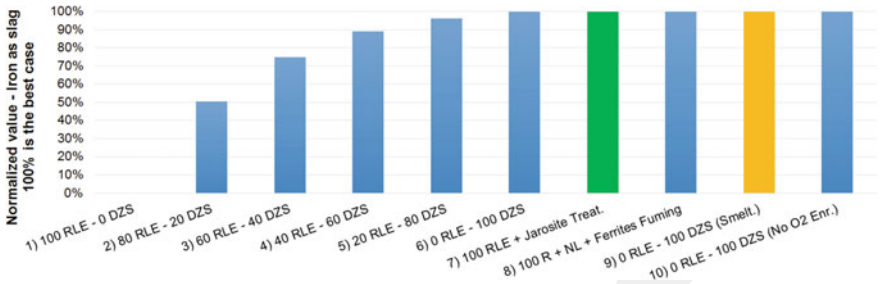

Fig. 6 Normalized value of iron removed as slag (highest density and land freeing) respect to the best-case scenario, i.e. 100% iron removed as slag during 100% DZS operation. This indicator can be used to discuss how land is freed up, being 100% the best case. Green represents the pyrometallurgical treatment of jarosite, while yellow depicts the iron removed as slag during DZS, whose values are the maximum

Effects on Society

Improving the human well-being and having a more sustainable industry, and land use are three of the United Nation's Sustainable Development Goals (SDGs) [18]. Reducing pond volume and creating high density and dry slag from jarosite, which is suitable for safe disposal, or even as building material if the slag is clean enough, helps to achieve these goals, implying a positive development for the society. For instance, a proxy for the impacts on society would be the land use reduction. By using the simulation results, the amount of iron removed as slag can be studied and normalized with respect to the best scenario, i.e. 100% of the iron removed through a slag (represents the highest density and cleanest of products). The deviations of each of the ten scenarios evaluated with respect to the ideal case to freeing up land can be obtained, as represented in Fig. 6. In summary, this means, 0% is the worst scenario, i.e. all the iron is disposed of as jarosite as happens during a 100% RLE case, and 100% the best one, where all the iron is removed as a slag. As Fig. 6 shows, the more concentrate is treated in the DZS flowsheet, the more land will be released. This relationship is not linear since the quantity of iron removed as slag depends on several factors such as the concentrate feed ratio or the quantity of jarosite the DZS flowsheet can treat (the lower concentrate feed to DZS, the lower jarosite can be treated since the DZS facilities would be smaller). In the same way, the ferrite fuming and jarosite treatment cases do not require a large land use since the iron is transformed into a clean slag through these two alternatives.

Effects on the Environment

As previously discussed, the resource consumption, mainly energy resources as coal or pet coke, and the GWP associated with the pyrometallurgical treatment of jarosite

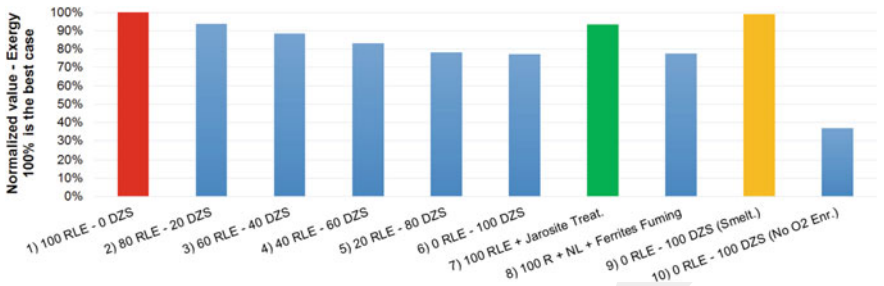

Fig. 7 Normalized value of resource consumption, measured by exergy destruction, respect the minimum resource consumption value. The closer to 100%, the lower resource consumption. Red represents the base case, green the pyrometallurgical treatment of the jarosite, and yellow the DZS with high zinc fuming rates

in the zinc smelters increases. Therefore, this supposes a trade-off that the environment must accept if the production of jarosite wants to be eliminated. For this reason, a quantitative evaluation of factors affecting the environmental sustainability of the system can be also done in the same way that the land use indicator used to start discussing the social impacts. In this case, the resource consumption increases in every evaluated alternative. Therefore, by normalizing the resource consumption with respect to the base scenario, i.e. dividing the exergy destruction of the base case by the exergy destruction of every case, an indicator of how close the alternative is to the minimum exergy destruction, on a scale from 0 to 100%, can be obtained as represented in Fig. 7. As the results show, the 100% DZS with high zinc fuming rates alternative (represented in yellow) accounts for the lowest resource consumption within the alternatives to the RLE. The largest resource consumption, as discussed before, happens when the DZS is operated without oxygen enrichment, while the pyrometallurgical treatment of jarosite accounts for the second lowest resource consumption within the alternatives.

Another indicator of the effects of the system on the environment is the CO_2 emissions. As done with the exergy indicator, the CO_2 emissions of the system can be normalized with respect of the 100% RLE scenario, which accounts for the lowest CO_2 emissions of all the cases, as explained before. The results of Fig. 8 show that the alternative that is closer to the minimum of CO_2 emissions is the pyrometallurgical treatment of the jarosite with a deviation of 9% on its relative value with respect to the minimum CO_2 emission (best case represented as 100%) as depicted by the green bar.

Effects on Economics

The pyrometallurgical flowsheets evaluated as alternatives in this paper would require considerable investment for the RLE plants, even if the smelting and reduction stages

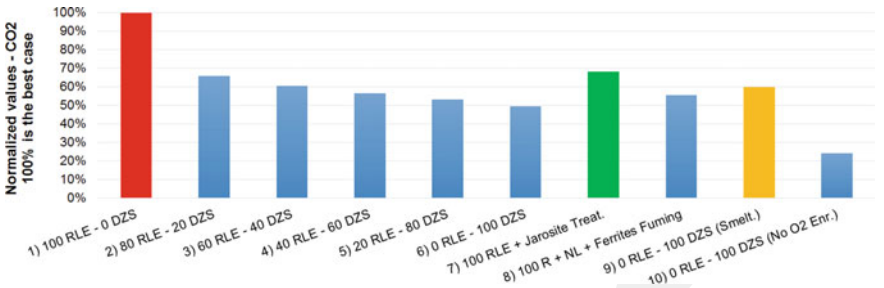

Fig. 8 Normalized value CO_2 emissions respect to the minimum emission value, which happens in the base case. The closer to 100%, the lower CO_2 emission of the alternative, red represents the base case, green the pyrometallurgical treatment of the jarosite, and yellow the DZS with high zinc fuming rates

can be performed in one reactor, e.g. top submerged lance technology. Additionally, larger operational costs are expected since the larger resource consumption is required, whose normalized value with respect to the minimum has been depicted in Fig. 7 and discussed previously. Therefore, these economic requirements for the operation of the CE action imply that a compromise between cost/benefit must be achieved to guarantee its economic sustainability.

The economic benefits of the pyrometallurgical treatment of jarosite include that the products of the RLE plant would increase, e.g. germanium and indium-rich dust or a potentially marketable slag if it is cleaned enough. Furthermore, the problems related to the jarosite landfilling and its cost would be avoided, which can also imply an economic saving and a more circular and environmentally friendly image for the smelter. This is very important for RLE plants located in countries where the restrictions on residue landfilling are strict or the space available for residue deposition is small, since they could keep operating if the legislation for residue production or landfilling becomes more restrictive, e.g. the Directive 2018/851 on waste of the European Union, which suggest the state members restrictions or economic penalties for the landfill of waste [19]. This must be confirmed through a CAPEX/OPEX analysis so that all the factors affecting the economics of the solution are considered, e.g. metal prices, downstream refining costs or avoided landfilled costs. However, a CAPEX/OPEX analysis is outside the objective of this study.

Conclusions

Having a more circular society implies that the residue generation must be reduced. In case of the zinc production, several pyrometallurgical alternatives to avoid or treat the iron-rich precipitates generated during the RLE process have been studied over the years. The integration of pyrometallurgical flowsheets within the RLE reduces or even eliminates the jarosite generation. However, the metal recoveries change,

and the resource consumption and CO_2 emissions increases. Ten different configurations of pyrometallurgical flowsheets combined with the traditional hydrometallurgical zinc production route have been evaluated to find the most resource efficient and environmentally friendly alternative. This alternative is the pyrometallurgical treatment of jarosite through smelting and reduction stages. As this solution requires high temperatures and reducing agents, its resource consumption and CO_2 emissions increase. This supposes a trade-off between the positive effect on society, because of the lower ponding volume required, and the impact on economics and environment, which will be larger than the current RLE process for the zinc production. However, the quantified economic, through thermoeconomics, and environmental impacts are close to the best scenario.

This simulation-based approach can be extrapolated to other metallurgical processes to evaluate their resource efficiency from a systemic perspective. The process simulation platform provides a good view of the resources consumed, produced, lost, or exchanged within the system. Additionally, as mass, energy and exergy balances are performed by the simulation platform, it can predict and show all material recoveries and losses, generation of residues, resource consumption, and environmental impacts. On this basis, different options to move the system towards a more resource efficient and circular scenario can be assessed and selected. This systemic approach can be also used to inform society and policy makers about the best possible way to achieve circularity, at the same time that a good perspective to discuss the possible trade-offs between society, environment, and economics is provided.

Acknowledgements This research has received funding from the European Commission's H2020—Marie Sklodowska-Curie actions (MSCA)—Innovative training Networks within SOCRATES (Website: http://etn-socrates.eu) project under the grant agreement no. 721385. This work reflects only the author's view, exempting the Community from any liability.

References

1. Reuter MA, van Schaik A, Gutzmer J, Bartie N, Abadías Llamas A (2019) Challenges of the circular economy—a metallurgical and product design perspective. Annu Rev Mater Res 49:10.1–10.22
2. Sinclair RJ (2005) The extractive metallurgy of zinc, vol 13. The Australasian Institute of Mining and Metallurgy, Melbourne
3. Hoang J, Reuter MA, Matusewicz R, Hughes S, Piret N (2009) Top submerged lance direct zinc smelting. Miner Eng 22(9–10):742–751
4. Wood J, Coveney J, Helin G, Xu L, Xincheng S (2015) The Outotec® direct zinc smelting process. Proc Pb-Zn 2015(2):537–548
5. Creedy S, Glinin A, Matusewicz R, Hughes S, Reuter MA (2013) Outotec® Ausmelt technology for treating zinc residues. World Metall ERZMETALL 66(4):230–235
6. Rämä M, Nurmi S, Jokilaakso A, Klemettinen L, Taskinen P, Salminen J (2018) Thermal processing of jarosite leach residue for a safe disposable slag and valuable metals recovery. Metals (Basel) 8(10):744
7. Abadías Llamas A et al (2019) Simulation-based exergy, thermo-economic and environmental footprint analysis of primary copper production. Miner Eng 131:51–65

8. Reuter MA, Hudson C, van Schaik A, Heiskanen K, Meskers C, Hagelüken C (2013) Metal recycling: opportunities, limits, infrastructure. United nations environmental protection (UNEP) report [online]. Available http://www.resourcepanel.org/reports/metal-recycling. Accessed 26 July 2018
9. Reuter MA, van Schaik A, Gediga J (2015) Simulation-based design for resource efficiency of metal production and recycling systems: cases—copper production and recycling, e-waste (LED lamps) and nickel pig iron. Int J Life Cycle Assess 20(5):671–693
10. Reuter MA, (2016) Digitalizing the circular economy: circular economy engineering defined by the metallurgical internet of things. Metall Mater Trans B Process Metall Mater Process Sci 47(6):3194–3220
11. Outotec (2019) HSC chemistry 9 [online]. Available https://www.outotec.com/. Accessed 28 Feb 2019
12. van Schaik A, Reuter MA (2016) Recycling indices visualizing the performance of the circular economy. World Metall ERZMETALL 69(4):201–216
13. Castro MBG, Remmerswaal JAM, Brezet JC, Reuter MA (2007) Exergy losses during recycling and the resource efficiency of product systems. Resour Conserv Recycl 52(2):219–233
14. Ignatenko O, van Schaik A, Reuter MA (2007) Exergy as a tool for evaluation of the resource efficiency of recycling systems. Miner Eng 20(9):862–874 (Spec. ISS.)
15. Ayres RU, Ayres LW, Masini A (2006) An application of exergy accounting to five basic metal industries. In: Sustainable metals management: securing our future—steps towards a closed loop economy. Springer, pp 141–194
16. Thinkstep (2019) GaBi LCA software [online]. Available https://www.thinkstep.com/. Accessed 28 Feb 2019
17. Purvis B, Mao Y, Robinson D (2019) Three pillars of sustainability: in search of conceptual origins. Sustain Sci 14(3):681–695
18. United Nations (2015) Transforming our world: the 2030 agenda for sustainable development. Working paper no. A/RES/70/1 [online]. Available https://sustainabledevelopment.un.org/content/documents/21252030%20Agenda%20for%20Sustainable%20Development%20web.pdf. Accessed 15 Jul 2019
19. European Union (2018) Directive (EU) 2018/851 of the European Parliament and of the council of 30 May 2018 amending directive 2008/98/EC on waste. Official journal of the European union [online]. Available https://eur-lex.europa.eu/legal-content/EN/TXT/PDF/?uri=CELEX:32018L0851&from=EN. Accessed 16 Jun 2019

Zinc Plant Expansion and Modification for Increased Metals Recovery

Björn Saxén, Florentino Estrada, Maciej Wrobel and Marko Lahtinen

Abstract Met-Mex Peñoles recently increased its zinc production capacity by 120,000 ton per annum at Torreón plant in Mexico. The expansion was based on Outotec atmospheric Direct concentrate Leaching (DL) technology integrated to the calcine leaching circuit. Also, new solution purification and electrowinning sections were added for the increased capacity. As a continuation to the expansion, there is an ongoing project aiming at improving recovery of silver and lead by new flowsheet modifications and technology from Outotec. The pure jarosite process minimizing metal losses to iron residue will be introduced in the leaching circuit. Sulfur cake from iron reduction step of pure jarosite process will be recycled to the fluidized bed roasting through a new feed pre-treatment system (FPS). Expected additional benefits of FPS are reduced dust entrainment and more homogeneous temperature distribution in roaster. This paper presents results and observations from the DL expansion and describes the new flowsheet.

Keywords Zinc · Concentrate leaching · Roasting · Plant expansion · Silver · Jarosite

B. Saxén (✉)
Outotec (Finland) Oy, PO Box 69 28101 Pori, Finland
e-mail: bjorn.saxen@outotec.com

F. Estrada
Metalúrgica Met-Mex Peñoles S.A. De C.V., Blvd. Laguna Poniente 3200, Col. Metalúrgica, Torreón Coah, Mexico
e-mail: florentino_estrada@penoles.com.mx

M. Wrobel
Outotec GmbH & Co. KG, Ludwig-Erhard-Strasse 21, D-61440 Oberursel, Germany
e-mail: maciej.wrobel@outotec.com

M. Lahtinen
Outotec (Finland) Oy, PO Box 1000 02231 Espoo, Finland
e-mail: marko.lahtinen@outotec.com

© The Minerals, Metals & Materials Society 2020

A. Siegmund et al. (eds.), *PbZn 2020: 9th International Symposium on Lead and Zinc Processing*, The Minerals, Metals & Materials Series,
https://doi.org/10.1007/978-3-030-37070-1_32

Introduction

Industrias Peñoles is a Mexican company founded in 1887 constituted by the mines and metals—chemicals divisions. The metals division operates the most important non-ferrous metallurgical complex in Latin America and one of the most important worldwide, which is located in northern Mexico in the city of Torreón Coahuila. Metallurgica Met-Mex Peñoles has a lead smelter, a lead–silver refinery, and an electrolytic zinc refinery where lead and zinc concentrates from Peñoles and Fresnillo groups are processed. The main products of the metallurgical complex are refined zinc, lead, silver, and gold as well as a series of by-products such as sulfuric acid, cadmium, bismuth, ammonium sulfate, and liquid sulfur dioxide.

The zinc refinery began operations in 1973, with an annual installed capacity of 105,000 ton. Due to increasing demand for this metal, the plant annual capacity was increased to 240,000 ton in 2006. The production of zinc concentrates with high iron content by Peñoles mines also increased; however, the main characteristic of these materials is the lower recovery of zinc in the roasting–leaching–electrowinning process. An alternative to process these materials without sulphuric acid production and high zinc recovery was searched, and the direct leaching (DL) technology met the requirements established by Peñoles. The first steps in the DL project were taken already in 2004 with concentrate leaching tests at Outotec laboratories. As the first tests showed good results, bigger scale tests including continuous piloting of both leaching and residue treatment steps were carried out, and engineering studies were executed. After also some inactive periods, Peñoles made the decision for DL expansion early 2015 followed by detail engineering, delivery, installations, and finally process start-up late 2018.

In the coming years the quality of zinc concentrates available in Mexico will be lower due to the increase in impurities content, as well as the variation in mineralogical composition and the decrease in particle size. One of the main objectives of Industrias Peñoles is the processing of all the concentrates produced by Fresnillo group in Met-Mex Peñoles metallurgical complex, to achieve this goal a strategic plan with the objective of defining technological alternatives for the processing of zinc concentrates of Fresnillo group was done.

An analysis of the technologies available for the purge of iron showed Outotec Pure Jarosite precipitation process being the best option. With this technology Peñoles will be able to process zinc concentrates with high content of values (Au, Ag and Zn), as well as impurities. The Pure Jarosite process, including also the roaster feed pretreatment system (FPS), was piloted at Outotec in parallel with basic engineering during 2016. This provided necessary information for the investment decision which was made early 2017. The implementation of these process changes is now going on.

This paper presents the DL process and its implementation at Torreón plant. In addition, the features and application of Pure Jarosite process and the roaster FPS are described.

Expansion by Atmospheric Direct Leaching

The zinc plant expansion is depicted below with a description of the DL process and its integration into existing plant, an outline of the implementation as well as some first operational results.

Process Description

Outotec atmospheric direct leaching of zinc concentrates was originally developed by Outokumpu for Kokkola zinc plant (today Boliden Kokkola) in Finland during the 1990s and has later been applied at Odda in Norway (today Boliden Odda) and at Zhuzhou in China [1, 2]. The key feature of the process is the oxidative leaching of sphalerite and other metal sulfides in the concentrate by means of ferric iron in sulphate solution according to

$$2Fe^{3+}(aq) + MeS(s) \rightarrow 2Fe^{2+}(aq) + Me^{2+}(aq) + S^{0}(s) \quad (Me = Zn, Fe, Cu, Cd) \tag{1}$$

In parallel, the ferrous iron formed in leaching is re-oxidized by oxygen gas:

$$2Fe^{2+}(aq) + 2H^{+}(aq) + 0.5O_2(g) \rightarrow 2Fe^{3+}(aq) + H_2O(aq) \tag{2}$$

As seen from the reactions, iron ions are needed in solution, and sulfuric acid is consumed. The sulfur of the metal sulfides is converted into elemental form. Excellent zinc leaching recovery of 98% or more is normally achieved after 20–25 h retention time. For providing the needed volume and at the same time ensuring efficient oxygen utilization, tall reactors with internal down-flow tubes are used for the leaching [1]. With proper adjustment of process conditions, iron can be precipitated as jarosite towards the end of the direct leaching step, where the acidity is lower and iron concentration is higher. The jarosite precipitation reaction (3) is given in a later section of the paper.

Prior to the DL expansion, the Torreón zinc plant was based on the roasting–leaching–electrowinning route having an annual zinc production capacity of 240,000 ton. The expansion for increasing the annual zinc production to 360,000 ton was integrated into the existing leaching plant according to the flowsheet outlined in Fig. 1. In addition to capacity, the DL addition gives higher flexibility in terms of raw materials for the total zinc plant. For instance, concentrates with high Si and Cu can be problematic in roasting but are easily treated in DL, while concentrates rich in Ag are better recovered through roasting–leaching.

The calcine leaching consists of three stages: neutral leaching, acid leaching, and hot acid leaching. The lead–silver residue from hot acid leaching goes further to the lead smelter for recovery. Iron is removed as jarosite, and there is an acid wash stage

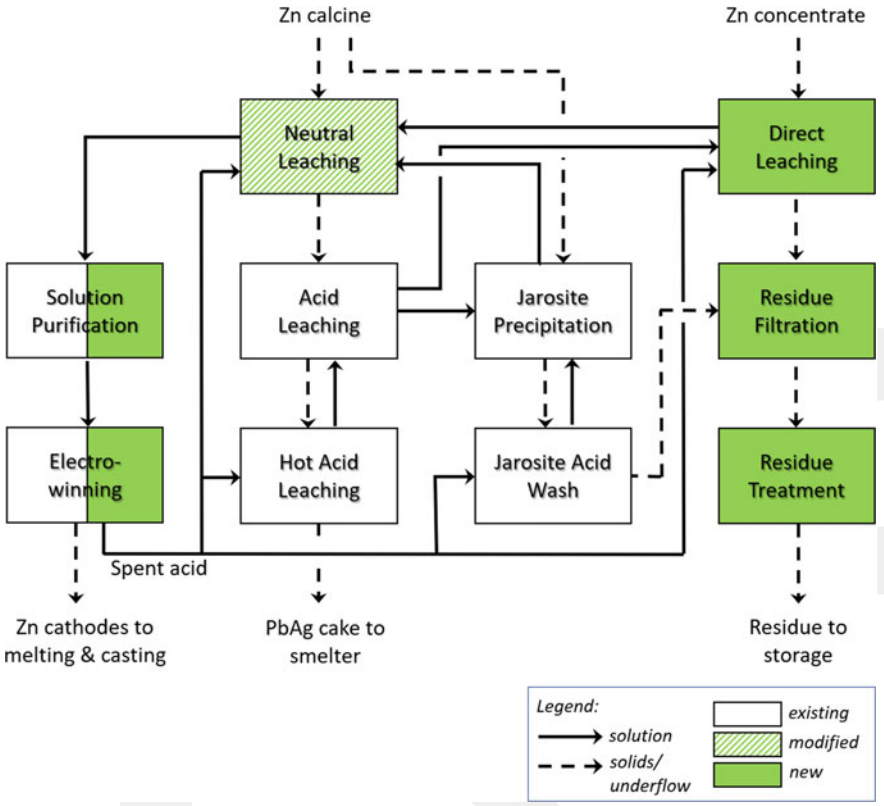

Fig. 1 Simplified flowsheet of the DL integration to Torreón zinc plant

for leaching zinc from the calcine remainders in jarosite. The new DL was integrated to the plant keeping existing calcine leaching as before, although some changes were needed in the neutral leaching stage due to the increased flow.

The DL step consists of two smaller reactors for concentrate pulping, eight main leaching reactors in series followed by a thickener. Off-gases are led through a pre-heater for utilizing excess heat for warming up the feed slurry. After that, the gases are led to a scrubber before exiting to atmosphere. The DL step was designed for precipitating all iron leached from the concentrate as jarosite, and thus, the capacity of existing jarosite precipitation was kept unchanged.

A new vacuum belt filtration plant was added for separating the jarosite and the DL residue from the leach solution, replacing old press filters for jarosite. The residue treatment stage before storage was renewed to a slurry/paste based process including neutralization with magnesium oxide and stabilization with limestone.

To treat the additional PLS flow caused by the expansion, a new solution purification plant was added in parallel with the existing one. The new solution purification is based on same three-stage chemical concept as in the old plant: (1) copper removal,

(2) cobalt, nickel, and cadmium removal, and (3) polishing. All steps utilize zinc powder for the cementation reaction, whereas antimony trioxide is added as activator to the second stage for efficient cobalt removal. To control the chloride leached from concentrates, a chloride removal step is integrated to the new solution purification plant. The chloride removal is based on Outotec technology utilizing cuprous oxide formed in the copper removal step. After the polishing stage, there is a gypsum removal step for lowering the Ca concentration in solution by cooling and precipitation [3]. The last step in the expanded process is a new zinc electrowinning plant. The zinc cathodes from the new electrowinning are transported to the Aleazin facility of Peñoles for melting and casting.

Some nominal flow figures are given for reference: The concentrate feed to DL is around 31 ton/h of dry mass, and the total flow to solution purification is around 450 m^3/h. The calcine feed, being approx. 53 ton/h, was not affected by the expansion.

Implementation

Peñoles consulted Outotec for the conceptual and basic engineering of the total leaching and solution purification expansion. Leaching tests both in batch and continuous mode with several concentrates of Peñoles proved the suitability of DL and formed the basis for the design. Several stages of conceptual process engineering were executed, focusing mainly on how to integrate the new sections optimally in the existing plant. The basic engineering including process, equipment, layout, piping, electrification, instrumentation, and automation design provided data for cost calculations and offers, leading finally to the investment decision by Peñoles.

All the key process equipment of the new leaching and purification areas were in Outotec delivery scope; 57 reactors, five thickeners, 15 filter presses, eight vacuum belt filters, three cooling towers. In addition, off-gas scrubbers, chemical analyzers and certain tanks, pumps, and feeders were delivered by Outotec. The delivery scope included detail engineering, manufacturing, and erection supervision, whereas the construction activities were carried out by other contractors. Figure 2 shows two photographs of the installed equipment.

Along with completing installations, wet commissioning activities started gradually during 2018. These included water tests, instrument and loop testing, calibrations, field training, etc. The leaching and purification process areas were started up late 2018 and ramped up towards nominal production during the first half of 2019. Outotec was present with mechanical, process, and automation support at the plant during the start-up and ramp-up periods.

Fig. 2 DL reactors with off-gas treatment (upper) and Cl removal thickener and gypsum removal cooling tower installations close to the new solution purification building (lower)

First Operational Results

Direct leaching was started at 50% capacity at the very end of 2018, at that time utilizing five of totally eight leaching reactors. The capacity was then gradually increased as all reactors were taken into use. Shorter periods with nominal capacity were run from March 2019 onwards; however, there were limitations from other plant areas as the stabilization of the integrated plant still needed time. At the time of writing, nominal DL capacity is mostly reached. The leaching recovery of zinc has been at a very good level, approx. 98%. Some issues with extensive foaming in reactors and launder were experienced in the start-up, but the situation is now controlled by increased dosing of anti-foaming agent.

The new solution purification plant was started up simultaneous with DL at the end of 2018. The solution feed was initially around half of nominal. There were some challenges in reaching the required Co removal efficiency in the start-up, which in turn lead to high zinc powder use. The situation was improved by tuning some operational parameters, and zinc powder use is now at designed level when operating roughly with nominal feed capacity.

Modifications for Improved Metals Recovery

This section presents the ongoing modifications aiming at higher metal recoveries, especially for silver. The calcine leaching sections are modified to a process for precipitating pure jarosite. A feed pre-treatment system for the roaster furnaces is installed, partly because of a new intermediate from the pure jarosite process that is to be fed to the roaster. Differently from the DL project, these changes will not significantly affect zinc production capacity.

Pure Jarosite Process

The traditional process for precipitating jarosite starts with iron in the ferric (Fe^{3+}) form according to

$$3Fe^{3+}(aq) + X^{+}(aq) + 2SO_4^{2-}(aq) + 6H_2O \rightarrow XFe_3(SO_4)_2(OH)_6(s) + 6H^{+}(aq) \quad (X = Na, NH_3, K) \tag{3}$$

For each mole of iron precipitated, there are two moles of hydrogen ions (H^+) formed. As jarosite formation occurs favorably only in a certain acidity range, typically 10–20 g/l H_2SO_4, there is a need to neutralize the produced acid during the precipitation. Typically, and as well at Torreón plant, the neutralizing agent is ZnO of zinc calcine. However, the calcine also contains components that will contaminate

the precipitated jarosite. Zinc ferrite ($ZnOFe_2O_3$) in the calcine is problematic, as this will not leach under the conditions used for jarosite precipitation and needs an acid washing stage for recovering zinc. Even more important, silver and lead in the calcine used for neutralization will be lost to the jarosite residue because they are not soluble in sulphuric acid. Typically, around 20% of the Ag and Pb in the feed is lost this way.

In the process for precipitation of pure jarosite developed by Outotec, iron is brought to ferrous (Fe^{2+}) form by reduction with zinc concentrate prior to jarosite precipitation. In the jarosite precipitation stage, oxidation is carried out to transform iron to ferric form (Fe^{3+}) to enable precipitation:

$$3Fe^{2+}(aq) + Na^{+}(aq) + 2SO_4^{2-}(aq) + 0.75O_2(g) + 4.5H_2O \rightarrow NaFe_3(SO4)_2(OH)_6(s) + 3H^{+}(aq) \quad (4)$$

The formation of sulphuric acid is only half of that in the traditional process. This significantly reduces the need for neutralization and enables jarosite precipitation without zinc calcine feed, thus leading to a pure jarosite obtained without separate acid washing stage. Simultaneously, no silver and lead from neutralizing calcine will be lost in the jarosite. In addition to the renewed jarosite precipitation step, there is a new step for reducing ferric iron to ferrous form with zinc concentrate and a step for neutralizing the reduced solution with neutral leaching underflow. Details of the chemistry involved are found in an earlier publication [4].

Figure 3 outlines the flowsheet for pure jarosite implementation at Torreón plant. As can be seen, all calcines are directed to leaching, and the components not leached, like silver and lead, will report to the PbAg cake. Elemental sulphur (S-cake) from the reduction step is mixed with concentrates in the roaster feed pre-treatment system described later in this paper. Direct leaching is not affected by the pure jarosite implementation and is still connected to calcine leaching as shown earlier in Fig. 1.

The change to pure jarosite emphasizes the requirements for reactor performance. The required efficient mixing and oxygen dispersion capabilities are realized by new Outotec OKTOP® reactors for the jarosite precipitation. Equipment from old jarosite precipitation and acid wash stages becoming redundant is reused and partly revamped for the new neutralization and reduction steps.

Roaster Feed Pre-treatment System

The sulfur cake from a leaching process is in many cases a problematic waste with significant costs of disposal. Due to its rheologic characteristic, sulfur cake requires extensive dumping areas. Attempts to upgrade sulfur cake into a saleable product have not been successful so far. Co-combustion of sulfur cake with zinc concentrate in fluid bed roasting furnaces frequently causes operation difficulties in downstream plant equipment. Sulfur cake lumps evaporate partially in the furnace and condense in colder plant sections forming sticky coatings in gas cleaning equipment. For proper

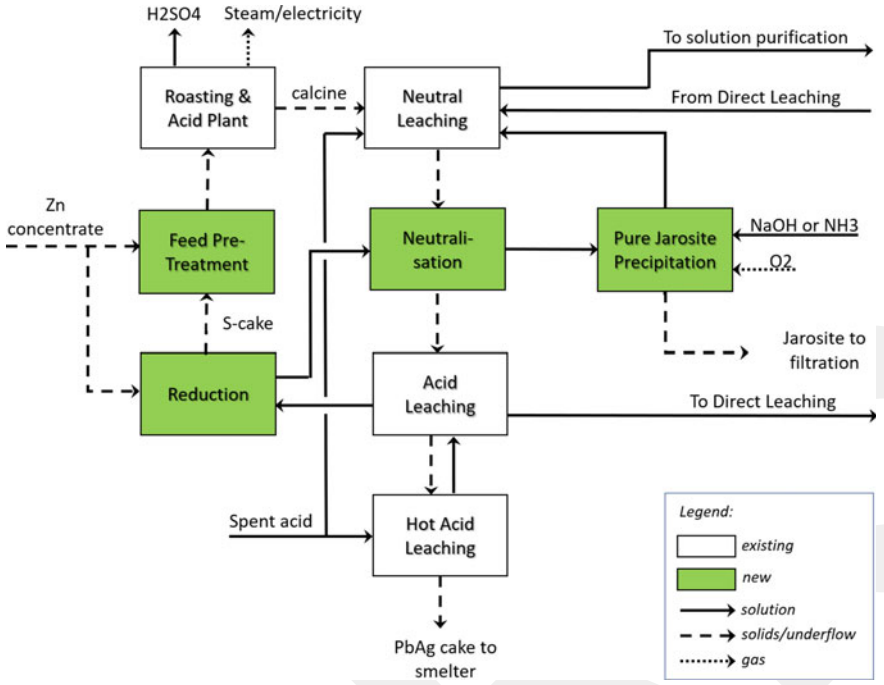

Fig. 3 Flowsheet of pure jarosite and roaster feed pre-treatment integrated to the roasting–leaching circuit

operation of fluid bed roaster and full combustion of the sulphur cake, a homogeneous feed blend is also required. Pilot test work at Outotec's R&D center in Frankfurt has proven that full oxidation can be achieved with blend produced by feed pre-treatment system and that the calcine quality is not affected by simultaneous oxidation of sulphur cake and concentrate. Moreover, the dust entrainment to the roaster freeboard could be reduced significantly compared to roasting of untreated concentrate as it is practiced nowadays. Based on test result obtained in pilot plant, it was decided to install the FPS as part of the modification project. In the FPS, the sulphur cake from the pure jarosite process is blended with Zn concentrates. The new feed pre-treatment system can proceed the total concentrate feed stream, feeding all three roasters with 51 tph of concentrate (on dry basis). The plant design is based on a mass flow of 5 tph of sulfur cake on dry basis.

FPS designed by Outotec consists of transportation, dosing granulation, feeding, and discharge of material. It will be possible to operate each of the two parallel granulators in a flexible range between 50 and 100% of the design capacity, and each installed system is also able to handle the full capacity of all three roasters. If the entire FPS section is out of operation for any reason, the full roasting capacity would be kept by bypassing the zinc concentrate stream around the FPS section.

The FPS is located upstream of the roasters close to the existing concentrate bins and the new sulphur cake filtration station. It produces a homogeneous feed blend for all three roasters. The core area of the FPS comprises granulator, dosing, feeding, and discharge systems for the feed materials and the FPS product as well as a control unit for the batch operated system. The FPS receives concentrate from the existing belt conveyor running through the concentrate storage and sulphur cake from the new sulphur cake filter presses. Both feed streams are dosed in an exact mass ratio into the feed hoppers. The separate zinc concentrate and sulfur cake conveyor systems convey a preset amount of materials, which is weighed on belt conveyor. A batch cycle starts with discharge of an exact measured amount from the feed hopper into the dedicated granulator. The operation of the granulator is a sequential treatment scheme, which was developed during the pilot test work at Outotec R&D center. The FPS product is finally conveyed to the existing roaster feed bins and fed into the roasters via the existing table feeders and slinger belts.

Important process parameters have been analyzed and defined during the pilot plant test work in Outotec R&D center. The FPS product is a homogeneous mixture of sulphur cake and concentrate. Figure 4 shows the final product after roasting. Contained fines were successfully turned into very small granules, and the bulk of the product has a perfect grain size for the fluid bed roasters.

FPS eliminates the necessity of dumping of hazardous sulfur cake, and all valuable metals contained in the sulfur cake can be recycled in the subsequent hydrometallurgical process. These valuable metals are typically e.g. silver and lead. But this is not the only one benefit of feed pre-treatment system. In many roasters, fine feed materials are entrained in the process gas and are oxidized in the upper furnace section (freeboard) instead of the fluidized bed. This displacement of the combustion causes high temperatures at the furnace top. The temperature spread between the default roasting temperature in the bed and the furnace top easily reaches 100 °C and often

Fig. 4 Typical zinc calcine from roasting of FPS product

is necessary to reduce the feed rate to protect the furnace dome against overheating. The Outotec FPS technology solves this problem. Most of the fines are kept in the fluidized bed, and the full furnace capacity can be used. The reduced dust entrainment from the fluid bed reactor after implementation of FPS should be beneficial for the off-gas treatment. During the cooling, the fine dust reacts with SO_2 and forms easily hard sulfates (agglomerates) on the surface of the heat exchangers. The cleaning of bundles is in many cases challenging, and often, it is required to stop the whole operation for the purpose of the boiler cleaning. Thus, the reduced dust amount after implantation of FPS should reduce also the required cleaning frequency and improve the general performance of waste heat boiler.

Conclusions

The direct leaching expansion at Torreón zinc plant is now operating at close to nominal capacity. The concept for integrating DL to the roasting–leaching plant has been shown functional. The integration of several new process steps to an operating plant is by nature challenging, and certain parts of the process operation still need fine-tuning and stabilization.

At the time of writing, the new process equipment of pure jarosite and roaster FPS is mostly installed, whereas piping, electrification, and automation installations of the modification project are still ongoing. The start-up of these areas is planned for 2020.

References

1. Lahtinen M et al (2005) Atmospheric zinc concentrate leaching technology of Outokumpu. Paper presented at lead & zinc '05. Kyoto, 17–19 Oct 2005
2. Haakana T et al (2008) Outotec direct leaching application in China. J South Afr Inst Min Metall 108(5):245–251
3. Hirsi T, Saxen B (2020) Outotec gypsum removal circuit and Outotec cooling tower performance in neutral solution cooling. Paper to be presented at PbZn 2020. San Diego, California, 23–27 Feb 2020
4. Saxen B, Lahtinen M, Savikangas J (2017) Higher metal recovery by Outotec pure jarosite process. Paper presented at European metallurgical conference, Leipzig, 25–28 June 2017

Experience with Digital Process Optimization of Zinc Roasting Plants

Robert Schiemann, Steffen Haus, Marcus Runkel and Jörg Hammerschmidt

Abstract Operation of zinc roasting plants has always been a challenge for changing feed mixtures and difficult concentrate qualities. Especially very fine particle sizes and increased amount of impurities like Pb and Cu require a higher attention of the control room operator to run the plant in stable conditions. As a result of this manual roasting plant control, the operation campaigns get interrupted by unplanned shutdowns due to poor roaster bed fluidization. In addition, the production targets and product quality are difficult to reach. Therefore, plant availability becomes more of a focus than other key production indicators (KPI). Operating the complete process chain consisting of zinc roasting furnace-gas cleaning and acid plants in desirable operating conditions is subject to many factors such as feed, air, and oxygen flow as well as water addition at different positions and many more. Operating the roaster in a stable and profitable operating window requires careful, regular, and anticipatory adjustment of these parameters. To support the operation of such plants, Outotec has developed and commissioned the Pretium Roaster Optimizer, a system that continuously leverages embedded process know-how to operate the roaster in an optimal way for high process efficiency, a consistently high product quality and improved economical KPIs. This chapter gives a short review on the application of modern advanced automation and optimization methods to improve metallurgical process plant operations and in specific the zinc roasting process.

Keywords Roasting · Digitalization · Zinc · Digital know-how

R. Schiemann (✉) · S. Haus · J. Hammerschmidt
Outotec GmbH & Co. KG, Ludwig-Erhard-Straße 21, 61440 Oberursel, Germany
e-mail: robert.schiemann@outotec.com

S. Haus
e-mail: steffen.haus@outotec.com

J. Hammerschmidt
e-mail: joerg.hammerschmidt@outotec.com

M. Runkel
Outotec (USA) Inc., 8280 Stayton Dr. Ste. M, Jessup, MD 20794, USA
e-mail: marcus.runkel@outotec.com

© The Minerals, Metals & Materials Society 2020

A. Siegmund et al. (eds.), *PbZn 2020: 9th International Symposium on Lead and Zinc Processing*, The Minerals, Metals & Materials Series,
https://doi.org/10.1007/978-3-030-37070-1_33

Introduction

Roasting of sulfide ores (such as zinc ores) in fluidized bed plants is a commercially available process route and has been since the 1950s. While the number of greenfield roasting projects had reached its peak in the 1970s and has been declining since the concentrate processing capacity for fluidized bed plants is still increasing today. This trend was mainly achieved by larger sized plants, whereas in recent years the focus is shifting towards more efficient usage of digitalization tools. Plant size seems to have reached their optimum in terms of feasible design and cost efficiency. Metallurgical and process principles of the roasting process remain unchanged and are based on the fluidization behavior of the feed material, produced calcine and the chemical main and side reaction as the oxidation of Zinc sulfide. Over time, technological advances took place impacting availability, maintenance, effectivity, and profitability in many positive ways.

While environment and safety standards are still as important as ever, plant efficiency and optimization remain an active area of further research and improvement. Additionally, with today's challenges such as declining ore grades, further refinements of processing, and operating principles become necessary to maintain high plant profitability and to comply with environmental regulations. This transition also impacts the operability of the roasting process so that more and more process control is required. The control room operator of today faces a different skill set as the operator two decades ago. In order to reach the high level of new production targets, these new operators must adapt to the new technology where process know-how is an integral part of the control philosophy.

In that regard, a shift in operating philosophies can be observed: Operating decisions and plant control have long been the responsibility of human operators alone. Today, however, more and more advanced plant automation is introduced, especially digital solutions with embedded process know-how by technology providing companies. This can be seen from the earliest design stages through commissioning and into production as evidenced by roasting plants in Mexico, Brazil, and Turkey.

This paper will describe the need and benefits of optimizing roasting plant operations as discussed. It explains how digital process know-how can be used to great advantage to achieve such optimizations. This is further exemplified in an approach for an advanced control system, combining an expert system based on process know-how and modern digitalization tools as described in the following chapters. The conclusion will also describe the outlook in the fast-developing technology.

Optimization of Roasting Plant Operation

Control philosophy of traditional roasting plants has long been straight forward with clear instructions and rules for the operators. Such rules would, for example, involve increasing air by a certain amount for a certain throughput increase or an

increased water injection into the furnace in case of too high temperatures. Such simple operating instructions often lack proper consideration of cross-effects as well as mid-term anticipation of operating effects. It does not serve necessary control requirements of today's roasters which have undergone substantial technical evolution since large-scale roasting technology adoption in the last decades.

The simple roasting concept of the past has become increasingly complicated with a much wider variation of operating parameters. This necessitates advanced expert systems combined with multivariable optimization to achieve desirable operating conditions. It is apparent that a high number of process parameters must be taken into consideration at once in order to achieve a desirable roaster operation. This is a complex task that human operators cannot easily achieve. Modern optimization systems connected to a traditional DCS can fulfill many of the control room operator tasks, freeing up mental resources to shift operator focus from the simple monitoring of the process more towards process analysis and emergency prevention. Additionally, digitized process know-how integrated in such systems can support operators in their decision-making process and continuously make situation-dependent operating decisions to improve stability, availability, and profitability of roasting plants.

If carried out appropriately, such optimizations can yield very desirable results such as:

- Improved operational safety for human beings,
- Protection of downstream equipment, reducing the need for maintenance,
- Enhanced environmental performance due to in-spec operating windows,
- Increased throughput, pushing the plant to its limits,
- Improved and homogenized product quality by process stabilization.

Digital Evolutions in the Process Industry

In recent years, more digital approaches can be observed in the minerals processing industry. A general target of such approaches is optimization of process plant performance.

More operating data of processes and equipment are collected than ever before. Accordingly, a need for analysis and leverage approaches and tools arises. Intelligent monitoring and analysis systems can open up the field for a wide range of advanced control and optimization approaches.

Usually, the following drivers for digitalization can be observed [1]:

- Investment risk avoidance: Debottlenecking plant sections and equipment to achieve maximum impact on performance with lowest risk involved
- Productivity challenge: Customer focus on optimizing the operation of existing equipment and maximizing profits without high investment costs
- Shortage of skilled labor: Many production sites are in remote locations, making them an unattractive working place for operating personnel. Thus, a more

autonomous operation with improved level of equipment monitoring can maximize availability for a production site
- Sustainability: With environmental regulations becoming increasingly strict, operators face the challenge of reducing their emissions to avoid financial penalties
- Declining ore grades: Plant operation at its highest efficiency faces greater challenge with declining ore grades
- Technology push: Digitalization allows information to be made available in real time, practically anywhere in the world, providing a solid basis for improved decision-making supported by the experts.

The challenges mentioned above prevail especially in the metallurgical production sector. Thus, there are many drivers for digital technologies to become more apparent.

It is anticipated that in the future, digitalization and digital technology innovations will play a key role in overcoming challenges in productivity, profitability, and compliance with environmental regulations. Digital solutions will be able to provide round-the-clock assistance to the operating personnel, thus facilitating proper processing of lower-grade ore types. As a problem-solution approach featuring relatively low investment with comparatively large possible benefits, low investment risks and quick return on investments can be expected.

Know-How and Data as a Source of Information in Digital Systems

Digital solutions in the industry typically follow either a know-how-based or a data-based approach. The two approaches have the common target of exploiting known information in order to improve operating conditions with respect to profitability, efficiency, environmental aspects, maintenance, and safety. Despite this common target, the two methods are vastly different from each other. In this section, the key differences between them are addressed.

By definition, the primary source of information is very different for the two approaches. While know-how-based approaches draw their exploitable information about physical phenomena from a human being's knowledge and experience, data-based approaches rely on evidence of these phenomena in a set of data measured in the plant. This major methodical distinction gives rise to certain limitations to be aware of.

Any conclusion drawn from previously acquired data can be due to apparent correlations present in the data with no underlying causal relationship. This is a real threat, especially in plant operations, because it can lead to false decisions and hence to plant maloperation and potentially threatening plant availability. For example, if the bed temperature of fluidized bed zinc roaster drops due to furnace overfeeding, a

pure data-based approach would recommend a feed increase to bring the temperature backup. This conclusion is based on the positive correlation of feed flow and bed temperature usually observed in roasting plant data but obviously wrong, potentially even hazardous, because the complex reality of roasting phenomena is not sufficiently captured by the data. Methods for decision-making based on process know-how take an entirely different approach by analyzing causes and effects based on the laws of physics and thermodynamics. This way, much more effects and complexity are captured than with the data-based approach. In the aforementioned example, process know-how would dictate that something is wrong with the oxygen/feed ratio and that further feed increase will not lead to a restored bed temperature.

The same fundamental issue with data-based approaches also lead to difficult, sometimes even impossible traceability of results. Origins of results and made decisions are often not clear and understandable because the approach abstracts interpretable data and thus greatly reduces interpretability. In contrast, approaches based on process know-how draw conclusions with clear relationships between causes and effects, which maintain interpretability of the results. This way, digital systems can also give situation-dependent operational advice and explanations to the operator to avoid decay of operator know-how for example. Data-based methods struggle to achieve this.

Data-based methods rely on previously acquired data about the process to learn the inherent behavior of reality. In practice, although large amounts of data are more and more available, these data are often shallow with respect to covered operating ranges, different feed materials processed, operating philosophy, plant modifications, and so on. Each of these aspects has a strong influence on plant behavior. If the data does not contain meaningful ranges and variations for all of them, data-based methods struggle to achieve a necessary degree of predictive capability. Approaches based on know-how can overcome this difficulty because the knowledge can be extrapolated and applied to new situations.

Finally, extensibility of digital systems is very important. Operational priorities, plant setups, plant automation, feed materials but also process insight can change over time and digital solutions need to consider these variations in order to be successful. Introducing this additional information or knowledge into an existing know-how-based system is usually easily done. If a pure data-based approach is followed, inclusion of the new information into the existing set of data-based information can be difficult to achieve. For that reason, it is also difficult to include new customer requirements into existing solutions.

All in all, approaches including process know-how are favorable over pure data-based approaches because they feature many benefits. Despite the drawbacks of purely data-based methods, they can help close gaps between know-how and reality and are hence a good complementation of know-how-based approaches.

Digital Process Know-How and Its Usage in Advanced Plant Operation

With process know-how being the identified key success factor in digital solutions, the remainder of this paper will focus on describing a digital system that integrates extensive process know-how, design experience, and advanced operational control into one holistic solution. The pure advanced automation aspect of such a solution alone can quickly achieve process stabilization, but true long-term optimization of plant production, availability, and profitability is only achievable through the embedded know-how of process thermodynamics and equipment design details.

As the technology provider for a certain process must have a comprehensive know-how on all aspects of this technology regarding the design, construction, commissioning, and operation of the plant, it is a logical step to integrate an advanced control philosophy into this scope and responsibility. This serves as a basis for potential operational improvements and is hence integrated into digital optimization solutions.

The process know-how can be integrated into different model-based digital systems, such as heat and mass balance calculation models [2], dynamic process models [3], or equipment and process level continuous monitoring systems [4]. Making these models available to the plant site enables short- and long-term improvement of the operating conditions. For sulfide ore roasting applications, automatic recognition of sulphur input to the furnace and accordingly prevention of bed overfeeding is a very good example of how a digital system can prevent highly undesired, potentially hazardous operating conditions. A further beneficial integration of process know-how is in automated operational sequences, which are especially common during plant load changes or start-ups and shutdowns. This reduces the risk of human errors potentially leading to an abortion of the load change, reducing overall plant availability and lifetime of the plant equipment.

Roaster Optimizer as Part of a Digital Solution Concept

As discussed in this paper, the integration of process and equipment know-how is a key success factor in complementing advanced automation, leading to optimizing solutions at a plant level. Figure 1 shows the general scheme of process know-how integration. As depicted, the Pretium suite includes different product classes (Advisor, Optimizer, Training simulator, Plant performance monitor), each of which has its own benefit realization approach and set of features. All of them have in common that the process knowledge, operating data, laboratory results, design data, and process models are combined and transferred to a virtual plant, which forms the backbone for all mentioned products. Such a system can also be used for a real-time comparison between measured data and the data expected by the know-how enabled software system. By performing such a so-called gap analysis, untapped potential in the plant can be revealed and equipment or process issues can be identified.

Fig. 1 General scheme of process know-how integration in digital systems

Overall, a digital solution concept as the one shown should not only span individual process areas but whole process lines. In the frame of zinc processing, this translates into a solution covering roasting, gas cleaning and sulfuric acid production. Two examples contributing to such an overall solution are introduced in the following.

The Plant Operability, Reliability and Safety (PORS) system is an example of a plant performance monitor targeting at safety and availability relevant focus areas in the process [5]. It continuously monitors plant operation in the sulfuric acid plant with respect to potentially harmful damages in the plant such as leakages in heat exchangers. The basis for this analysis is the usage of plant operational data and process know-how which allows to draw fact-based conclusions of the current state of the plant. The key task of the system is to recognize abnormal, potentially hazardous conditions which are not part of the normal operating conditions. These operational situations arise only rarely in normal plant operation, and hence, data-based approaches will have difficulties to draw the right conclusions. For this reason, process know-how is the methodology of choice for such products.

The Roaster Optimizer as another product of the Pretium family is going to be focused on in this chapter. It is currently in operation in several zinc roasting plants as well as other pyrometallurgical plants worldwide, improving the plant operation on a continuous basis. After a further description of the solution and approaches, the achievements in these worldwide applications are reported.

Implementation in Customer Plant Level

Digital systems as discussed in this paper are integrated or interfaced with an existing distributed control system (DCS). This approach requires several steps. The DCS is connected to an advanced control tool (ACT) system. ACT can provide the platform and includes the automation intelligence as well as the embedded process know-how, such as advanced heat and mass balances, for example. Additionally, the platform reads process measurements from DCS and can write data back. In doing so, digital optimization systems stabilize the process and operate it within safe and desirable limits by taking process limitations and constraints into account. Trade-offs between

different, sometimes conflicting, process targets are made. This results in a more stable process operation with comparatively gentle operating conditions. Additionally, plant operation is less prone to human errors and decreases operator workload.

To keep the digital solution performant over its whole life cycle, continuous optimization improvement is suggested, which consists of the following aspects:

- The process models included in the system need to be adjusted from time to time. While varying plant behavior on short time scales, such as due to load changes can be taken into account, long-term aging effects need to be accounted for in model updates. Model changes are required when equipment is modified or modernized.
- Functionality upgrades are done when new digitized process know-how becomes available. Close monitoring of the digital system can reveal further improvements and new functionalities that, upon implementation, will enhance the overall solution.
- Periodic reports focusing on operation and utilization of the digital system are generated and made available to the system users. Such reports typically include the views of Outotec process experts to enable a deeper understanding of process bottlenecks and potential plant improvements.
- A remote connection from Outotec back-office to the Outotec hardware on site through secure and proven technology allows the described adaptations and improvements as well as inclusion of new features and ensures fast response time in case of any change in customer requirements.

Features

If set up and maintained as mentioned in the sections above, the described optimizing systems offer many valuable features, such as:

- *Advanced control loops* on top of classical PID controllers at DCS level for stabilization of the plant.
- *Operational advice* for digital know-how assistance for operators. The system compares many process variables, analyses them, and creates warnings and advice in case of inconsistencies, dangerous levels, or unhealthy signals such as due to measurement faults. Combinations of many different sensors are considered, whereas human operators tend to focus mainly on single variables, comparing them against constraints. With this approach, plant-wide comprehensive situational awareness of the operator is improved. Additionally, the system also informs the operators on the actions taken and the reasons for them. This way, operator know-how is preserved and maybe even improved over long-term operation of the system.
- The *process optimization system* includes mathematical routines for finding the best possible operating conditions for the feed mixtures and allow for near automatic plant operation close to the possible optimum. These logics provide the guidelines for the advanced control loops.

Fig. 2 Typical user interface of the Outotec Pretium Roaster Optimizer

- *Health monitoring* modules in the digital system carry out online comparisons of measured process data with theoretical, model-based values which are derived from first principle laws of thermodynamics or advanced equipment models. This way, indications of malfunctioning equipment and sensors are obtained. Additionally, drifts in signals are captured as evidence of aging or degradation effects.
- *Soft sensors* produce additional information normally not available to neither the operator nor the advanced automation system based on process simulation models. An example is the effluent amount that is calculated based on a roasting plant model. Another example would be the estimation of product quality in dependence on different operating parameters.

The graphical user interface of the digital system is shown in Fig. 2. Typically, the interface is shown on a dedicated screen in the control room, independently of the DCS screens. Operators can turn the system on and off in the DCS, in their familiar environment, via optional buttons on their screen. On the supervisor level, further tuning and monitoring of the digital system can be done from the ACT operator/supervisor interface. It is recommended that the monitor is positioned in a central location in the control room so that operational awareness for the operator is triggered. Although the layout of the user interface is a proven and well-accepted solution, it can be adjusted from one application to the next.

Solution Implementation Steps

A complex and multifunctional digital system like the Roaster Optimizer is typically implemented at customer sites in multiple steps, as illustrated in Fig. 3.

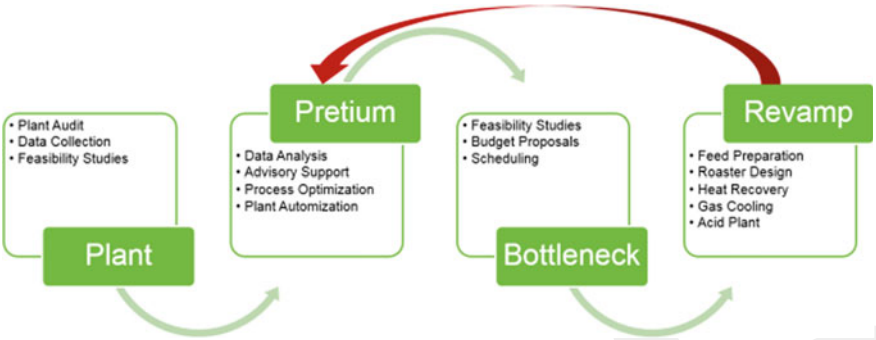

Fig. 3 Typical solution life cycle of Pretium digital systems

The first step comprises clarification and implementation of IT structure and solution. This includes IT setup, security aspects as well as agreement on remote access. The mentioned remote connection only provides external access to the PC, server or virtual machine that has the ACT platform installed.

The implementation of the Pretium Optimizer is the next step and involves a deployment, commissioning and tailoring of the digital solution: Connection to specific and selected DCS tags and measurements is set up, simulation models are tailored to the specific plant, and safety checks are configured. When that is done, a stepwise commissioning of the system during a site visit from process and digitalization experts is carried out.

Next, during the early operation period of the system, the Optimizer usage typically increases up to 100%. The system performance is closely monitored and fine-tuned remotely. If necessary, adjustments to models and graphical interface are made. The frequency of remote adjustments and updates typically declines with the system becoming more and more utilized and performant.

Finally, a transition to the last lifetime phase of the product is taking place where it is kept in automatic operation but still monitored remotely. Functional upgrades are made as required. In this phase, process know-how is continuously used to debottleneck the plant to further improve performance. In this sense, digitalization is part of a modernization journey for a process plant. The combination of digital systems, process know-how and manufacturing capability allows to deliver the best level of support on the roadmap to achieve operational excellence.

Worldwide Applications

Today, multiple Pretium digital systems are in place in Zinc and other metal roasting plants in the world, continuously exploiting the integrated digital know-how to run the plant in a stable, profitable, and availability-preserving way. In each application,

individual requirements, limitations, and potentials exist. For example, for some customers, a stable roasting process is the main issue, whereas at other sites, the process train is bottlenecked by the sulfuric acid plant, imposing to operating constraints to the roasting section. Throughout the different applications, observed improvements in process operations are:

- Production increase of more than 5% (Fig. 4)
- Significant reduction of SO_2 emissions
- Significant improvement and homogenization in product quality (Fig. 5).

While the production increase typically is a result of plant stabilization and optimization, product quality improvements are due to product quality included models into optimization. Reduction in emissions of the whole roasting, gas cleaning, and sulfuric acid plant train is possible through the inclusion of a site process model including downstream plant sections.

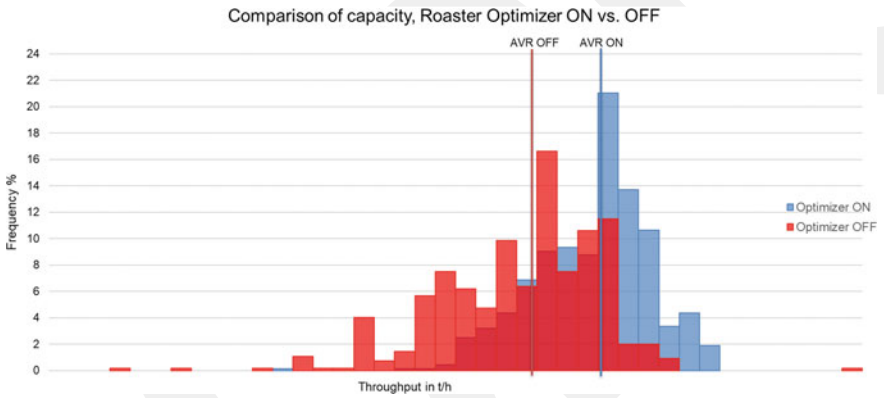

Fig. 4 Comparison of plant capacity with and without Roaster Optimizer in operation

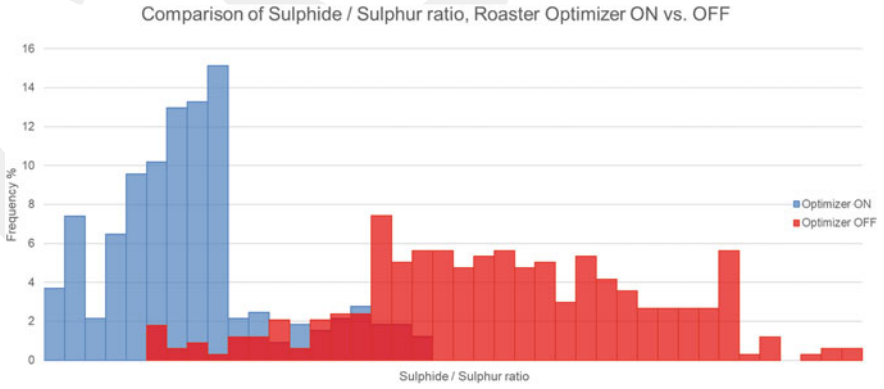

Fig. 5 Comparison of product quality with and without Roaster Optimizer in operation

Conclusion and Outlook

A growing demand for increased automation and operational optimization of process plants is observed in the minerals processing industry.

To meet this demand for metallurgical roasting plants, a Roaster Optimizer has been developed, which is a digital system applying advanced automation methods in combination with digitized process know-how as well as decades of experience with plant design and operation. The resulting combination is a powerful tool continuously controlling the plant in a close to optimal way, taking care of stable and profitable operation while respecting process limits and protecting downstream equipment for reduced maintenance. One of the backbones is constituted by detailed thermodynamic process models on a plant level as well as equipment-specific special models. This combination provides insight and operational awareness on multiple levels of plant operation, which can be leveraged by the underlying optimization routines.

Several Pretium advanced control systems such as digital systems are currently rolled out for various processes including zinc and pyrite roasting, alumina calcination as well as iron ore pelletizing plants. Analyses show a high potential for energy consumption optimization in all of these technologies.

References

1. Runkel M, Haus S, Kauvosaari S, Hammerschmidt J (2019) Digitalization to maximize performance of metallurgical roasting plants. Paper presented at EMC 2019, Düsseldorf, 23–26 June 2019
2. Haus S, Mehl S, Lagerstedt A (2015) Optimizing iron ore agglomeration plant performance—Outotec's solutions for plant monitoring and sustainable operation. https://www.outotec.com/globalassets/products/sintering–pelletizing/optimus_whitepaper_2018.pdf. Accessed 2 Sept 2019
3. Schiemann R, Haus S, Orth A (2018) Dynamic training simulators for the process industry: an application to power plants. Heat Process 4:57–66
4. Schlautmann M et al (2011) Dynamic process models for on-line control of steelmaking processes, exemplified for the VOD process. Stahl und Eisen 2011(10)
5. Kemmerich M, Storch H (2015) Process heat recovery and digitalization in sulphuric acid plants. Paper presented at 3rd international symposium on innovation and technology in the phosphate industry, Marrakech, Morocco, 18–20 May 2015

Part IX
Zinc Leaching and Fe-Control I

GCRIS

Smelting Jarosite and Sulphur Residue in a Plasma Furnace

Justin Salminen, Jens Nyberg, Matej Imris and Bror Magnus Heegaard

Abstract Jarosite and sulphur residues are formed during electrolytic recovery of zinc at Boliden Kokkola. In order to minimize the waste generation as well as promote better recovery of metals, pyrometallurgical options have been studied to treat this material. In addition to recovering more metals, another goal was to obtain clean stable slag that could be used in construction. Pilot test work was carried out using an ArcFume plasma process for directly smelting and fuming several combined residues, i.e. jarosite plus sulphur residue from Boliden Kokkola zinc plant. The tests were carried out in two stages, including a smelting stage and a reduction stage. The obtained slag compositions after smelting were typically 1–2 wt% of Zn and 0.1–0.3 wt% of Pb. The smelting stage was followed by a shorter reducing stage to further decrease volatile metals in the slag. Very low compositions of Zn < 1 and Pb < 0.03 wt% were reached. In the smelting stage, no coke was added. In the reducing stage however, coke was added to ensure sufficient reductive conditions for fuming volatile metals such as Zn, Pb, Ag, In, and Ge and obtain good recovery. Heavy metals and elements such as As, Sb, Cd, and Cl reports into fume oxide as well. Consequently, the overall direct CO_2 emissions were lower than expected due to avoiding coke use in the smelting stage. The allowed contents of heavy metals in the slag are determined by legislation and the targeted use of the slag.

Keywords Jarosite · Sulphur · Smelting · Plasma · Fume · Slag

J. Salminen (✉) · J. Nyberg
Boliden Kokkola, Sinkkiaukio 1, 67101 Kokkola, Finland
e-mail: justin.salminen@boliden.com

J. Nyberg
e-mail: jens.nyberg@boliden.com

M. Imris · B. M. Heegaard
ScanArc, PO Box 41 SE 81321 Hofors, Sweden
e-mail: Matej@scanarc.se

B. M. Heegaard
e-mail: Bror.Magnus.Heegaard@scanarc.se

© The Minerals, Metals & Materials Society 2020

A. Siegmund et al. (eds.), *PbZn 2020: 9th International Symposium on Lead and Zinc Processing*, The Minerals, Metals & Materials Series,
https://doi.org/10.1007/978-3-030-37070-1_34

Introduction

In non-ferrous industries, the trend is going towards producing less waste and recovering more metals. That is in line with circular economic targets but involves large investments as well as investigations on how to best integrate the material flows into existing processes [1–4] (Fig. 1).

If the iron residues are treated pyrometallurgically, it requires energy either by fossil fuel or by electricity. That opens new possibilities in the zinc industry for better recoveries of Zn, Pb, and Ag as well as recovery of new by-product metals such as In and Ge. Furthermore, one must find safe final disposal options for elements of concern such as As. There is also a dilemma with the slag quality and how to deal with CO_2 emissions caused by coal use in smelting (if needed) and reduction stages.

In zinc production, the standard way of operating is to remove the iron in the leaching stage by producing an iron precipitate (jarosite, goethite, paragoethite, Jarofix, etc.) and then landfill the precipitate after chemical stabilization.

Boliden Kokkola uses two leaching lines; leaching of calcine after roasting and direct leaching of zinc concentrates. Elemental sulphur is formed in the direct leaching stage. In Kokkola case, the jarosite is also precipitated in the direct leaching stage. The residue is chemically stabilized by sulphidation and double filtrated prior to landfilling (Fig. 2).

Currently, the landfilled material contains more than 6 Mdmt. The landfilled material is a stabilized mixture of jarosite and elemental sulphur called as combined residue. The yearly amount of combined residue at Boliden Kokkola is about

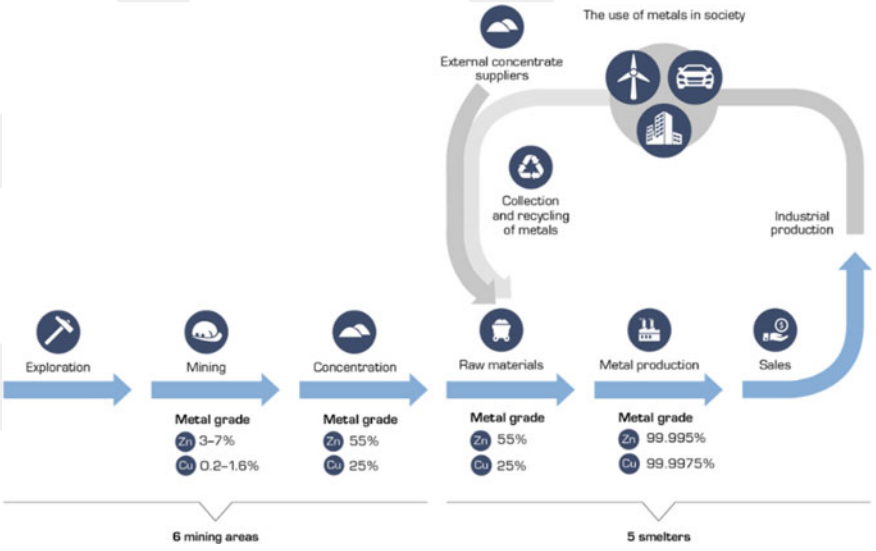

Fig. 1 Circularity in the mining and metals refining. The treatment of residues adds into raw material supply and opens up by-product metals recovery

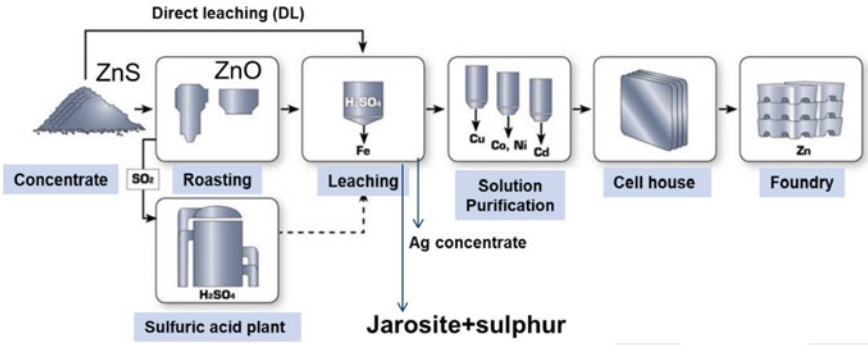

Fig. 2 Boliden Kokkola roasting, leaching, electrowinning (RLE) flowsheet

230,000 dmt/a (jarosite 160,000 dmt/a and sulphur residue 70,000 dmt/a). Typical analysis of the combined residue shows following compositions: Zn 2.9%, Pb 2.7%, Fe 15.2%, Ca 3.2%, S 31.7%, Si 2.0%, Na 1.6%, Cu 1.3%, As 0.7%, Al 0.6%, Cd 0.1%, etc. The chemical composition of elements can vary significantly based on the feed mixture into the zinc processing (Fig. 3).

Iron residues are formed deliberately in electrolytic production of zinc because the amount of iron needs to be controlled and removed from the solution. Precipitation of iron removes many impurities that are detrimental for zinc electrolysis such as As, Sb, F, Hg, In, Ge, and Al. The unrecoverable portion of Zn, Pb, and Ag ends up in the landfill.

Iron removal is a crucial part of solution purification prior to electrolytic recovery of 99,995% pure zinc metal. Typically, half of the amount of concentrate feed ends up

Fig. 3 Landfilled combined residue at Boliden Kokkola

in the landfill in zinc production. However due to large space requirements, tightening legislation, and loss of valuable metals, landfilling is not perhaps the best option in the medium- and long-term future.

Investigations to minimize the waste generation and possibilities on how to process them in the best way have been carried out in this work. Smelting the residues like jarosite, goethite, ferrites, etc. is widely in use in non-ferrous industries instead of landfilling of stabilized waste like Jarofix. The motivation of processing iron residues can be legislation, direct ban of landfilling, scarcity of available land area, and targets to achieve better yields and recoveries of critical by-product metals.

Generally, the pyrometallurgical residue smelting processes work in the same way. After smelting at temperatures around 1250–1350 °C, the residue is decomposed and volatile compounds such as Zn, Pb, Ag, In, Ge, As, Sb, Hg, Se, Cd, F, Cl, and S are evaporated. The outcome is mixed metal oxide-containing dust (fume) and iron silicate base slag. Slag forming materials include Fe, Si, Ca, Mg, Al, Mn, Na, and K. Portion of Cu and Co will report into slag, and the distribution depends mainly on the content of these metals in the feed material.

Boliden Kokkola has made several pilot tests with jarosite, combined residue as well as with other feeds. The target has been to recover Zn, Pb, Ag, In, Ge, and producing a slag for further utilisation. Moreover, the final safe disposal of elements of concern such as As, Hg, and Cd needs to be in place.

The ScanArc plasma process marketed under the name ArcFume has been successfully demonstrated for smelting other types of zinc residues [5]. In this work ScanArc plasma pilot plant in Hofors, Sweden has been piloted.

The recoveries of the valuable metals have been high, and good stable slag has been obtained. The final slag has been low in target metals like Zn, Pb, and Ag. In addition, the standard leaching tests have also given promising results.

Challenges

Jarosite and combined residue material is a sludge-like, fine material that needs to be pre-treated prior to the smelting stage. The moisture content should be lowered down to 25 wt% or less to avoid stickiness in the conveyer belt. In addition, the material cannot be too dry as it becomes dusty. Suitable levels of moisture are within 10–25 wt%.

Smelting combined waste, i.e. jarosite plus sulphur residue, is challenging due to the high level of elemental sulphur in the residue (30–40 wt%). Therefore, the right oxidising conditions in the furnace are required during the smelting stage. Sufficient amount of air must be fed into the reactor to avoid formation of FeS matte in the smelting stage. In the smelting stage, the sulphur is burned out as SO_2 gas and jarosite is decomposed into FeO and forms $FeSiO_4$ with SiO_2 present in the feed. Most of the volatile metals are vaporized and recovered as oxide dust in the smelting stage. Still, significant amount of Zn (2.5–1 wt%, typically about 1 wt%) and Pb (<0.3 wt%, typically under 0.1 wt%) is left after the smelting stage. Subsequent steps in the

reductive stage or further reduction in the same reactor are still required to fume Zn and Pb into acceptable levels. However based on the experience from this work, it could be possible to reach acceptable levels of Pb and Zn only using one stage after further optimization of the process. Length of the fuming period depends on final slag composition requirements as well on legislation. In this work, the target was set as Zn < 1% and Pb < 0.03%.

The leaching test target has been to reach inert criteria status according to standard leaching test (CEN).

In the reducing stage, coke is used to enable fuming, further volatilization of Zn and Pb. Consequently, CO_2 emissions are created. Firstly, in the test work, it was noticed that no coke was required in the smelting stage, avoiding a significant part of the direct CO_2 emissions. In the fuming stage on the other hand, a reductant such as coke is required. Further studies have been carried out in laboratory scale and comparing bio-based reducing agents such as bio-coal. Thermochemical models have been developed, and laboratory studies are being carried out to further investigate different phenomena [5, 6].

It should be noted that it will be more and more important to avoid direct and indirect CO_2 emissions in the future. Sufficient amount of electrical energy with reasonable prices is required for plasma operation with as low as possible CO_2 footprint.

Principles of ScanArc Plasma Process

The plasma reactor itself is a twin-shelled water-cooled steel construction with a number of openings for feed, plasma generators, slag tapping, sampling, and gas outlet [7].

Energy is added to the process by plasma generators (PGs). Oxygen potential in the PG gas is controlled by addition of hydrocarbon into the water-cooled tuyeres in front of the PG. In the pilot plant, LPG (propane) is used for this purpose. By not using a combustion reaction to provide heat, temperature and oxygen potential is decoupled allowing to separate the heat from chemistry, a feature that is not possible in a process with energy supplied by conventional fossil fuels.

Heat generation by a PG is simple and straight forward and is presented in Fig. 4. Compressed air flows through the PG where it is heated to a temperature of about 3000–5000 °C by the rotating electric arc between up- and downstream electrodes. The energy content in the outgoing PG gas is about 3.5–4.5 kWh/Nm^3.

The superhot PG air is mixed with propane in the tuyere in front of the PG to control the oxygen potential in the gas. NOx formation is controlled by keeping the gas composition at a low level of free oxygen. The very hot gas is thereafter injected into the slag bath where its heat is transferred to the slag. In the pilot plant, the reactor is equipped with two PGs, a lower submerged PG1 (1 MW) that supplies heat and

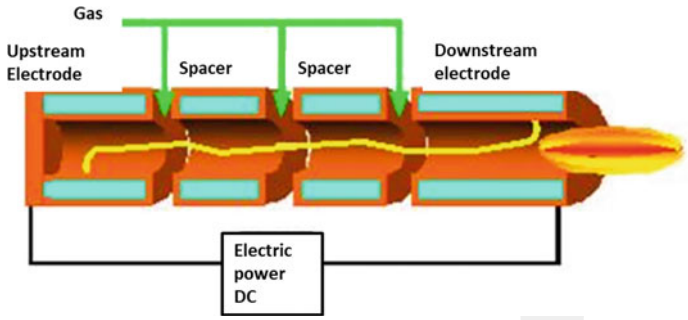

Fig. 4 Principle of ScanArc's plasma torch

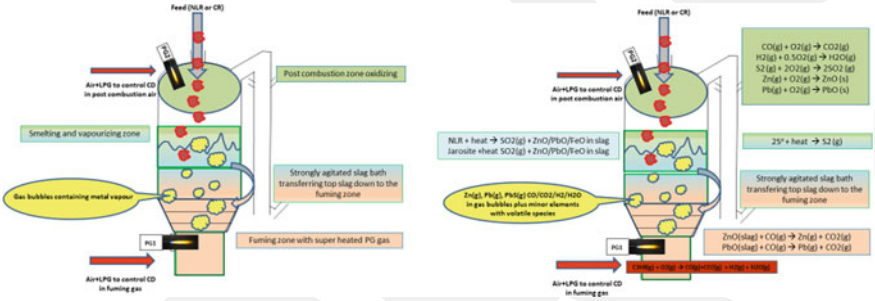

Fig. 5 Principles of ScanArc and ArcFume plasma reactor

turbulence to the liquid slag and an upper smaller PG2 (200 kW) that helps to keep the heat balance of the reactor and helps the kinetics of the reactions. Air/LPG = 27 was typically used in the test work (Fig. 5).

Smelting Tests of Boliden Kokkola Residues Using ArcFume Plasma Reactor

The idea of testing combined residue as a feed was first seen as risky and challenging. The main foreseen risk lied in the slightly unknown dynamics of sulphur vaporization and reactions in the plasma furnace and unwanted solidification of sulphur in the off-gas lines. Tests were first carried out with jarosite after flotation that still contained significant amounts of sulphur. Good clean slag was produced with flotated jarosite, and no matte (FeS) formation was observed. That gave confidence using combined residue as a feed into plasma reactor. The results shown in this work looks promising, and as an outcome, one can state that the ArcFume plasma process can handle the most difficult feeds such as Boliden Kokkola's combined residue.

Figure 6 shows the preliminary idea for the smelting and fuming process. Com-

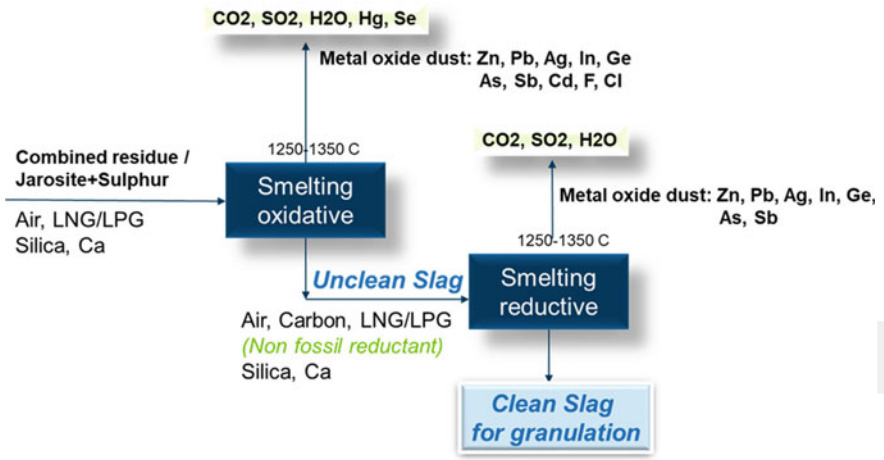

Fig. 6 Flowsheet for smelting and fuming of jarosite and/or combined residue

bined residue, jarosite or other feeds like neutral leach residue or even zinc concentrates could be fed into flexible plasma process. All these feeds mixed or individually will form a slag, fume oxide, and off-gases. In the case of sulphur-containing combined residue, the off-gases would go into acid plant with efficient weak acid treatment and Hg removal for final deposition. The metal oxide fume contains valuable metals Zn, Pb, Ag, In, Ge, and Sb as well as impurities As, Cd, Tl, F, and Cl. On the other hand, by recovering the toxic elements into metal fume, the slag results in a clean and usable material. The goal of the test work was to show if combined residue could be smelted and produce good quality slag and enable multi-metal recovery. The oxide fume can then be treated hydrometallurgically with known processes including halide washing, selective leaching stages obtaining Pb–Ag residue, and separate extraction of In and Ge. Zn stream would go into the zinc plant circuit, As is precipitated as ferrous arsenate making it the final waste for final deposition.

The combined residue (CR) used is a filter cake with a typical moisture of 25%. The actual target value is a moisture content that gives a non-sticky feed to the reactor. CR was fed with and without lime or alumina addition to achieve best fuming conditions. Coke was added to the feed only in the reducing stage. The CR mix was then transported from the feed preparation area to the ArcFume reactor by a conveyor belt and fed to the reactor through feeding port at the top of ArcFume reactor. The conditions in the furnace have been strongly oxidising during the smelting stage and reducing during the reduction stage. Several smelting and fuming tests have been carried out for combined residue. In the largest test, 20 wmt of combined residue was fed into the reactor for oxidative smelting. After smelting, the obtained slag was water granulated. This intermediate slag was then fed again into the plasma reactor into reductive conditions in order to decrease the content of the volatile metals even more. The temperature in the furnace has been in the range of 1250–1350 °C. During the smelting stage, no pet coke addition was needed to reach suitable levels for Zn

and Pb in the intermediated slag. Coke has only been added during the reduction stage to further evaporate volatiles and obtain clean slag. Figure 7 shows ternary phase diagram of the system FeO–SiO_2–CaO and the respective operational area of the slag obtained from combined residue.

The ArcFume process and combined residue reactions are further discussed. Sulphur in any chemical form must be converted into SO_2(g) or elemental sulphur gas, S^o(g), to avoid formation of matte, a liquid phase consisting of base metal sulphides, including FeS, ZnS, PbS, and Cu_2S. Elemental sulphur forms elemental sulphur gas, S^o(g), while sulphate sulphur decomposes into SO_2(g) at the high temperature in the ArcFume reactor. Formation of matte must be avoided since its presence makes it very difficult, if not impossible, to reduce the content of zinc to very low levels and remaining ZnS and Cu_2S will also reduce the slag stability during test leaching.

Results from the test work indicate that most of the sulphur decomposition and volatilization takes place instantly when the CR mix is fed to the reactor. Fuming of zinc and lead is favored by a high slag temperature (preferably 1250–1300 °C), amount of gas blown through the slag bath, right oxygen potential, slag with relatively

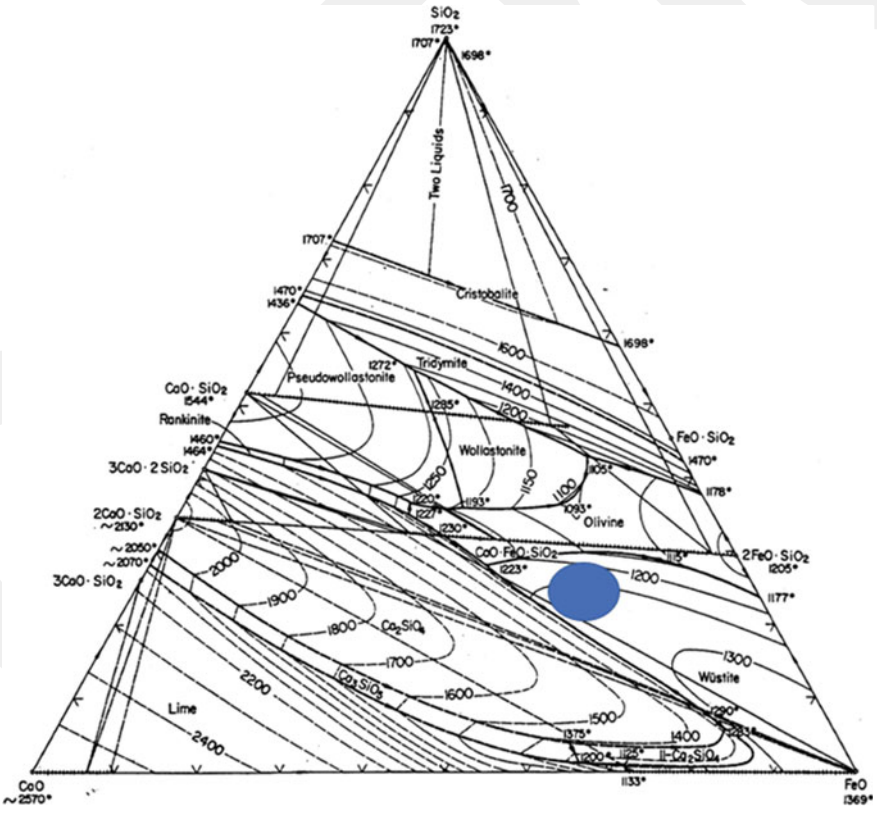

Fig. 7 Phase diagram and slag composition operation region in the test work

Fig. 8 Pilot ScanArc furnace at Hofors, Sweden. In the middle tapping of jarosite slag and on the right water granulated slag after fuming. The slag volume is around 1/7 of the feed volume and around 1/2 of the weight of the feed

higher lime or alumina content, and somewhat lower silica content. These parameters are controlled by addition of lime/alumina, addition of LPG/coke and PG-power in combination with feed rate.

The reactor gas is a mixture of CO/CO_2, H_2/H_2O, elemental sulphur $S^o(g)$, $SO_2(g)$, vapour of lead, zinc, and other volatilized elements.

Post-combustion of reactor gas will ensure complete oxidation of sulphur and other species. Cooling of oxidized process gas will solidify the fume into fine-grained mixed metal oxides that follow the gas stream into the gas cleaning system where the fume product is separated from the gas. The fully combusted gas then leaves the process via a stack into the atmosphere.

Figure 8 shows the Pilot ScanArc furnace and water granulated fumed slag.

Table 1 shows typical analysis after smelting stage and fuming stage, and Table 2 shows the average distributions of elements into the fume and slag after smelting and fuming.

The slag shows surprisingly low levels of Zn and Pb already after the smelting stage. Slag analysis after step 1 was Zn 1–3% and Pb about 0.1–0.3% and after step 2: Zn < 1%, Pb < 0.03% target levels have been achieved consistently in several tests. The chemical composition of elements can vary significantly based on the feed mixture into the zinc processing and thus has effect into final slag and fume dust compositions after smelting and fuming.

Recoveries of valuable metals from the combined waste and jarosite have been: Zn > 90%, Pb > 99%, Ag 75–85%, In 60–70%, and Ge 80–90%. Many of the impurities end up in the fume or gas phase: As > 98%, Hg 100%, Cd 98%, and Sb 97%. Most of the F and Cl reports to the fume as well. CEN leaching tests were carried out of the produced final fumed slag. Three samples á 5 kg were taken from the final tapping.

Table 3 shows the leaching test results together with acceptance criteria for inert landfill. Highlighted in red is the element Sb that did not pass the acceptance criteria

Table 1 Slag analysis after smelting and fuming of combined residue from 20 wmt test

Slag/wt%	Ag	Al	As	Ca	Co	Cr	Cu	Fe	Ge	In	Mg	Mn	Na	Pb	S	Sb	Si	Zn
After smelting	0.010	3.35	0.03	9.25	0.03	0.05	0.48	32.03	<0.001	0.01	1.02	0.59	3.56	0.12	0.42	0.04	9.81	1.30
After fuming	0.005	3.93	0.01	9.43	0.03	0.05	0.34	33.37	<0.001	0.003	0.92	0.48	3.71	0.004	0.32	0.02	9.19	0.10

Table 2 Average distributions of some elements into the fume and slag after smelting and fuming stages

Element	Distribution to slag, wt%	Distribution to fume, wt%	Typical residual content in slag, wt%	Comments
Zn	5 ~ 10	90 ~ 95	<1	Target < 1wt%
Pb	1	>99	<0.03	Target < 0.03 wt%
Cd	2	98	<0.001	
Ge	<20	>80	<0.001	Feed content has effect on the distribution
In	30	70	0.005	
Ag	<20	>80	<0.005	
As	1	99	<0.01	
Sb	3	97	<0.02	

Table 3 Results from leaching tests and acceptance criteria for inert landfill

Element	Leach test 1 mg/kg	Leach test 2 mg/kg	Leach test 3 mg/kg	Average mg/kg	Criteria for inert landfill mg/kg
As	0.10	0.20	0.20	0.17	0.5
Ba	1.2	1.6	1.5	1.43	20
Cd	<0.02	<0.02	<0.02	<0.02	0.04
Cr	<0.1	<0.1	<0.1	<0.1	0.5
Cu	0.1	<0.1	0.2	0.15	2
Hg	<0.01	<0.01	<0.01	<0.01	0.01
Mo	<0.1	<0.1	<0.1	<0.1	0.5
Ni	<0.1	<0.1	<0.1	<0.1	0.4
Pb	<0.4	<0.4	<0.4	<0.4	0.5
Sb	0.17	0.07	0.13	0.12	0.06
Zn	0.7	0.4	0.9	0.67	4
Cl	5.1	3.1	3.0	3.73	800
F	2.8	2.4	2.5	2.57	10
SO_4	12.3	7.8	8.4	9.50	1000
S	4.1	2.6	2.8	3.17	n/a

for inert landfill. The slag passes all acceptance criteria for the disposal of non-hazardous waste and for all components except antimony, which is slightly above the strict limit.

Since energy for the process is supplied via plasma generators which are powered by electricity, the CO_2 emission of the process depends on the energy mix used for electricity production. The only "direct" CO_2 emission from the process originates

from LPG gas and coke, which is used in the reduction stage. About 5 wt% coke addition was used in the feed for the final reduction stage. In the following test works, the behaviour and efficiency of bio-coal and other non-fossil reductants will be studied.

Conclusion

The idea of testing combined residue as a feed was at first seen as risky and challenging. The risks were foreseen in the slightly unknown dynamics of sulphur vaporization and reactions in the plasma furnace. First tests were indeed carried out with jarosite after flotation that still contained significant amount of sulphur. Tests with jarosite, including combined residue, containing variable sulphur content delivered excellent results with slag composition and metal recoveries as desired. The CEN leaching tests showed promising results as well. Only Sb content in the final slag was slightly above inert landfill criteria. The results presented in this work look promising and give technical confirmation that the process is feasible. The ArcFume process was able to handle a feed with very high content of sulphur, being elemental sulphur, sulphate sulphur, as well as sulphides. Smelting only jarosite or neutral leach residue is easier because smaller off-gas handling is required. The fuming stage that follows the smelting is similar for all these cases. The results from the combined residue tests however indicate that a separate fuming stage operated under reducing conditions might not be necessary. Treating combined waste in a one-stage plasma process is a possible solution for treating residues from zinc industry. Further investigations will be carried out using non-fossil reductants like bio-coal. The use of slag in construction is also being studied.

References

1. Salminen J (2018) Overcoming challenges in the circular economy: a thermodynamic reality-check. Socrates policy brief. www.socrates.com. Accessed 20 Aug 2019
2. Reuter et al (2019) Challenges of the circular economy: a material metallurgical and product design perspective. Annu Rev Mat Res 49:253–274
3. Salminen J et al (2018) Challenges and possibilities in zinc residue treatment. Paper presented at Extraction 2018. Ottawa, ON, 26–29 Aug 2018
4. Nyberg J (2019) Challenges for non-ferrous industry—less waste and recovering more metals. Paper presented at Emc 2019 plenary lecture in Düsseldorf. ERZMETALL 72(3):158–166
5. Rämä M et al (2018) Thermal processing of jarosite leach residue for a safe disposable slag and valuable metals recovery. Metals 8:744–748

6. Helsten N et al (2019) Slag cleaning equilibria in iron silicate slag—copper systems. J Sust Met. https://rd.springer.com/article/10.1007/s40831-019-00237-7. Accessed 20 Aug 2019
7. Heegard BM, Swartling M, Imris M (2015) Submerged plasma technology and work within Zn/Pb recovery. In: PbZn 2015, vol 2. Düsseldorf, Germany, pp 807–816

GCRIS

Simulation of an Alternative Direct Leaching Process for High Iron Content Zinc Concentrates

Caio Cesar Spindola de Oliveira and Daniel Dayrell Pereira

Abstract Conventional RLE process (Roasting, Leaching, and Electrowinning) usually avoids high iron content zinc concentrates due to roaster heat limitations and high zinc ferrite formation, causing losses in zinc recovery. Alternatively, direct leaching processes may recover zinc from this undesired type of concentrate with high yields. In this work, we evaluate the sulfatation process (staged roasting process at lower temperature that favorites the oxidation of sulfides to sulfates) as an alternative and compare it with traditional direct leaching and roasting processes. The simulation showed that sulfatation process might be a good alternative for treating high iron content zinc concentrates in future investments, reducing consumables and generating an extra amount of steam.

Keywords Simulation · Sulfatation · Direct leaching

Introduction

The RLE Process

In the past decades, the RLE process (Roasting, Leaching, and Electrowinning) have become the predominant route to obtain zinc from sulfide concentrates. Each company has its variations to optimize their opportunities, but they all follow these three basic steps. They are economical and reliable stages in order to produce competitive zinc in Special High Grade (SHG) specification.

The roasting step comprises of a fluidized bed reactor that converts ZnS to ZnO, at approximately 950 °C, by blowing an intense flow of air (most of the time enriched with pure O_2) to promote de reaction and fluidization. With the outlet gas, enriched

C. C. S. de Oliveira (✉) · D. D. Pereira
Nexa Resources, BR040, Km 284, Tres Marias, MG 39206-000, Brazil
e-mail: caio.oliveira@nexaresources.com

D. D. Pereira
e-mail: daniel.pereira@nexaresources.com

© The Minerals, Metals & Materials Society 2020

A. Siegmund et al. (eds.), *PbZn 2020: 9th International Symposium on Lead and Zinc Processing*, The Minerals, Metals & Materials Series,
https://doi.org/10.1007/978-3-030-37070-1_35

with SO_2 from the reaction, it produced sulfuric acid. At the leaching phase, the ZnO (often called calcine) reacts with sulfuric acid (most from the spent solution from the electrolysis, and some recently produced—the surplus is sold), becoming $ZnSO_4$. Usually, the leaching process is divided into two stages, neutral and acid stages. At the neutral stage, most of the ZnO is converted to zinc sulfate. At the acid stage, a hard to leach zinc formed at the roaster is recovered by adding excess sulfuric acid. The solution is then purified and electrolyzed, producing a cathode of pure zinc.

Usually recovering 97–98% of the zinc contained in the concentrate, the RLE process has achieved a major acceptance in the Zn production world; its operations are well established, and its operations can almost be purchased as shelf items.

Impurities in Zn Concentrates

Despite the beneficiation process that usually takes place in the mine sites and aims to reduce impurities, concentrating the zinc and reducing logistics costs, the Zn concentrate contains several impurities (averaging 15% of the concentrate mass). These impurities also react with the roaster airflow, producing their respective oxides or sulfates. Furthermore, depending on the contamination element, it produces an enormous amount of heat while oxidizing, compromising the roaster capacity. Besides that, many elements combine to form spinel components: $A^{2+}B_2{}^{3+}X_4{}^{2-}$, "A" usually been Ca, Zn, Mg, and Cu among others; "B" can be Fe or Al and "X" predominantly O. As zinc is the most abundant element in the concentrate, it reacts with iron to produce zinc ferrites, the hard to leach compounds mentioned previously (Eq. 1) [1].

Equation 1: Zinc sulfide oxidation and hard to leach zinc compound formation.

$$\begin{aligned}
&ZnS(s) + 1.5O_2(g) \rightarrow ZnO(s) + SO_2(g)\\
&\quad \Delta H = -442.958\,\text{kJ/mol} \quad \Delta G = -347.594\,\text{kJ/mol}\\
&FeS_2(s) + 2.75O_2(g) \rightarrow 0.5Fe_2O_3(s) + 2SO_2(g)\\
&\quad \Delta H = -828.241\,\text{kJ/mol} \quad \Delta G = -741.458\,\text{kJ/mol}\\
&ZnO(s) + Fe_2O_3(s) \rightarrow ZnFe_2O_4(s)\\
&\quad \Delta H = -23.707\,\text{kJ/mol} \quad \Delta G = -33.811\,\text{kJ/mol}
\end{aligned} \tag{1}$$

As it can be seen in Eq. 1, iron contamination produces de double of heat per mol as compared to zinc. Beyond that, the iron oxide formed in the roaster reacts with the zinc oxide resulting in zinc ferrites, a very hard species to leach.

Because of the restrictions caused by impurities (production decreased due to heat limitations, costs involved in purification, and Zn recovery diminishing), these types of concentrates receive price penalties, according to the type and amount of contamination [2, 3]. These discounts are fundamental in order to make these concentrates as attractive as pure ones and can persuade some smelter to buy them, regardless of the consequences (Fig. 1).

Common Zinc Concentrate Penalties

Element or Compound	Chemical Symbol	Threshold for penalty to apply	Penalty Examples	Chinese Limits
Arsenic	As	0.2%-0.3%	US$1.50-$2/dmt for each 0.1% above 0.2-0.3%	0.5% (Import), 2-3% (Domestic)
Antimony	Sb	0.2%-0.3%	US$1.50-$2/dmt for each 0.1% above 0.2-0.3%	1%
Bismuth	Bi	0.02%-0.03%	US$1.80-$2/dmt for each 0.1% above 0.02-0.03%	
Mercury	Hg	0.005%-0.01%	1.US$1/dmt for each 0.001% above 0.005% 2.US$1.75/dmt for each 0.01% above 0.01%.	0.06%
Cadmium	Cd	0.25%-0.3%	1.US$1/dmt for each 0.01% above 0.03% 2.US$2.00/dmt for each 0.1% above 0.25%	0.3%
Iron	Fe	8%	US$1.50/dmt for each 1% above 8%	12%
Fluorine	F	0.02%	US$1.50/dmt for each 0.01% above 0.02%	
Silica	SiO_2	3.00%-4.00%	US$1.00-US$1.80/dmt for each 1% above threshold	
Magnesium Oxide	MgO	0.3%	US$1.50 for each 0.1% above the threshold to a maximum of US$5/t.	

Source: AME, Company Reports

Fig. 1 Common zinc concentrate penalties

As we exhaust superficial and concentrated zinc mines, we need to move deeper and to more impure sites, usually producing dirtier concentrates (Fig. 2). Because of that, it is fundamental that the future of Zn extraction and production be able to process this type of material without detriments. Furthermore, new techniques are been developed each day to contemplate this future, like TSL and Waelz process, both able to treat secondary sources of Zn with high degrees of impurities.

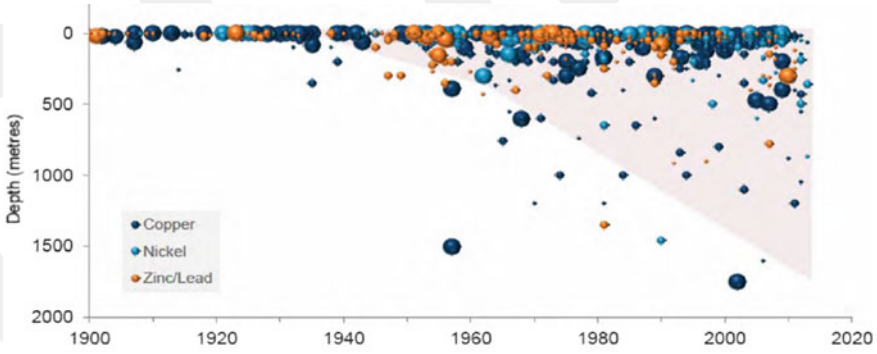

Source: Newcrest, R. Schodde, MinEx Consulting, The Global Shift to Undercover Exploration, 2014. NB. Size of bubble refers to 'Moderate', 'Major' and 'Giant' sized deposits. Excludes nickel laterite deposits.

Fig. 2 Tendency of mines size and depth as a function of time

Direct Leaching Processes

Alternatively to the RLE process, the direct leaching (DL) mechanisms can recover zinc from its concentrates without the need of a roaster. Under the DL category, we can find the bioleaching process (in which bacteria converts ZnS to $ZnSO_4$) and the inorganic routes: In an autoclave or high water column tank (Albion leaching process), ZnS is mixed with Fe^{3+} to oxidize the sulfide, precipitating as elementary sulfur, and leaving the zinc soluble. The produced Fe^{2+} must now go to an oxidizing stage (usually with pure O_2), in order to return to the begging of the process or for precipitation (Eq. 2).

Equation 2: Process of direct leaching of zinc concentrates with high iron content at 100 °C.

$$\begin{aligned} &ZnS(s) + Fe_2(SO_4)_3(aq) \rightarrow ZnSO_4(aq) + 2FeSO_4(aq) + S(s) \\ &\quad \Delta H = -17.586\,kJ/mol \quad \Delta G = -133.480\,kJ/mol \\ &FeSO_4(aq) + 0.25O_2(aq) + 0.50H_2SO_4(aq) \rightarrow 0.5Fe_2(SO_4)_3(aq) + H_2O(l) \\ &\quad \Delta H = -90.925\,kJ/mol \quad \Delta G = -36.703\,kJ/mol \end{aligned} \tag{2}$$

The non-formation of spinel zinc ferrite is one of the major recovery rate (97.5%) advantages, while roasting promotes the formation of this very stable oxide, the direct leaching solubilizes everything, improving the recovery [4, 5]. Although these processes are efficient, they require special attention in order to work: (1) Elevated costs with the iron removal process (including the disposal of it). (2) Separation and drying of the elemental sulfur (required to produce sulfuric acid). (3) Operation stability control, preventing the contamination of iron in the cell house. (4) Usually, direct leaching plants are less efficient with acid, as a great part of it is spent with the iron. (5) Larger retention time: As the solubility of O_2 is limited, the direct leaching process requires higher reaction residence time.

Aware of the future need to treat high iron concentrates and exploring beyond the direct conventional leaching processes, we aimed at this work to evaluate the sulfatation process and compare it with the previously mentioned ones.

Sulfatation, Leaching, and Electrowinning (SLE)

The sulfatation process was well described by Willard Mitchell, in 1930 [6]. At that time, Mitchell developed an integrated process for treating zinc sulfide concentrates (for Anaconda Mining Company, the largest at that time), based on the RLE concept. He used a wedge furnace (staged rotate plates) instead of the fluidized bed reactor for roasting. However, the most significant difference was the iron removal stage (goethite) and the subsequent zinc recovery treatment: a sulfatation process (with another wedge furnace) [7]. At the first plate of the reactor, the goethite was dried.

Then, the co-precipitated sulfate in the goethite was thermally decomposed at 480 °C, producing SO_2 and hematite; after that, the gases were carried to the bottom of the reactor, where at 650 °C reacts with the hard to leach zinc, producing easily washable zinc sulfate. These reactions can better be seen in Eq. 3.

Equation 3: Zinc tailings treatment with sulfatation process, Anaconda Mining Company, 1930.

$$
\begin{aligned}
&480^{\circ}\mathrm{C}.\\
&\mathrm{Fe_2O(SO_4)_2(s)} \rightarrow \mathrm{Fe_2O_3(s)} + 2\mathrm{SO_2(g)} + \mathrm{O_2(g)}\\
&\quad \Delta H = 25.487\,\mathrm{kJ/mol} \quad \Delta G = -33.131\,\mathrm{kJ/mol}\\
&\mathrm{Fe_2O_2SO_4(s)} \rightarrow \mathrm{Fe_2O_3(s)} + \mathrm{SO_2(g)} + 0.5\mathrm{O_2(g)}\\
&\quad \Delta H = 22.547\,\mathrm{kJ/mol} \quad \Delta G = -29.388\,\mathrm{kJ/mol}\\
&650^{\circ}\mathrm{C}.\\
&\mathrm{ZnO(s)} + \mathrm{SO_2(g)} + 0.5\mathrm{O_2(g)} \rightarrow \mathrm{ZnSO_4(s)}\\
&\quad \Delta H = -319.209\,\mathrm{kJ/mol} \quad \Delta G = -82.087\,\mathrm{kJ/mol}\\
&\mathrm{ZnFe_2O_4(s)} + \mathrm{SO_2(g)} + 0.5\mathrm{O_2(g)} \rightarrow \mathrm{ZnSO_4(s)} + \mathrm{Fe_2O_3(S)}\\
&\quad \Delta H = -297.406\,\mathrm{kJ/mol} \quad \Delta G = -50.808\,\mathrm{kJ/mol} \qquad (3)
\end{aligned}
$$

By the time the sulfatation process was designed (right after the great depression), Anaconda Company was going to some financial difficulties, aggravated in the following years. The zinc reserves were becoming scares and impure (increasing production cost), specialized labor was becoming more expansive, environmental laws more restrict, etc. The sulfatation project and the patent were developed with proposes to increase zinc recovery and diminish waste generation. However, the implementation required further equipment development and enormous CAPEX, but the company was not whiling to invest anymore in the zinc market, so the idea never took off [8].

Based on Mitchell's idea, the sulfatation process for high iron zinc concentrates was simulated. At the wedge furnace, the concentrate would go first to an oxidation stage, releasing the SO_2. Later, the gases would be captured in a sulfatation reaction, at 650 °C. We tested this idea in the HSC Outotec Software®, and the results are discussed hereafter.

Results and Discussion

Zinc Concentrate with High in Iron Percentage

Considering the following composition of typical zinc concentrate with low and high iron content (Table 1).

Table 1 Composition of a typical zinc concentrate with low and high iron content and zinc sulfide concentrate variability (not a complete survey on possible compositions, but a mere analysis on 36 concentrates available)

Low iron content				High iron content				Concentrate variability		
Element	%	Mineral	%	Element	%	Mineral	%	Element	% min.	% max.
Ag	0.0057	Ag_2S	0.0065	Ag	0.0002	Ag_2S	0.0002	Ag	0.0001	0.0070
Al	0.25	Al_2O_3	0.48	Al	0.31	Al_2O_3	0.59	Al	0.08	0.50
As	0.024	AsS	0.017	As	0.016	AsS	0.011	As	0.0001	0.0360
Ca	0.66	$CaCO_3$	1.63	Ca	0.50	$CaCO_3$	1.23	Ca	0.07	0.70
Cd	0.39	CdS	0.51	Cd	0.15	CdS	0.20	Cd	0.085	0.960
Cl	0.0047	$CaCl_2$	0.0074	Cl	0.0032	$CaCl_2$	0.0050	Cl	0.0047	0.0032
Co	0.00077	CoS_2	0.0016	Co	0.00383	CoS_2	0.0080	Co	0.0008	0.0210
Cu	0.50	Cu_2S	0.63	Cu	0.65	Cu_2S	0.81	Cu	0.10	0.70
Fe	4.85	FeS_2	9.56	Fe	12.77	FeS_2	14.10	Fe	9.00	14.00
		Fe_2O_3	0.58			Fe_2O_3	8.88			
Ge	0.00053	GeS	0.00076	Ge	0.00050	GeS	0.00072	Ge	0.0005	0.0008
Hg	0.0083	HgS	0.0097	Hg	0.0007	HgS	0.0008	Hg	0.0005	0.0100
In	0.0067	InS	0.0086	In	0.0146	InS	0.0187	In	0.0067	0.0170
Mg	0.16	$MgCO_3$	0.55	Mg	0.10	$MgCO_3$	0.35	Mg	0.08	0.60
Mn	0.18	MnS	0.29	Mn	1.12	MnS	1.77	Mn	0.18	2.90
Ni	0.0014	NiS	0.0021	Ni	0.0018	NiS	0.0028	Ni	0.0007	0.0300
Pb	0.70	PbS	0.80	Pb	0.49	PbS	0.57	Pb	0.05	4.00
S	32.74	–		S	31.88	–		S	30.00	40.00
Sb	0.013	Sb_2S_3	0.0187	Sb	0.002	Sb_2S_3	0.0025	Sb	0.0003	0.0020
SiO_2	2.37	SiO_2	2.37	SiO_2	0.34	SiO_2	0.34	SiO_2	0.15	3.50

(continued)

Table 1 (continued)

Low iron content				High iron content				Concentrate variability		
Element	%	Mineral	%	Element	%	Mineral	%	Element	% min.	% max.
Tl	0.0013	TlS_2	0.0017	Tl	0.0014	TiS_2	0.0018	Tl	0.0009	0.0050
Zn	55.38	ZnS	82.53	Zn	47.71	ZnS	71.11	Zn	46.00	55.00
		SUM	100.00			SUM	100.00			

GCRIS

Table 2 Composition of the simulated calcined from high and low iron content zinc concentrate (low concentration species were taking into account for calculation, but for simplicity, not represented here)

	Low iron content (%)	High iron content (%)
Fe_2O_3	0.34	1.03
$CaSO_4$	2.56	1.94
$CuO*Al_2O_3$	0.91	1.18
FeO	0.70	1.16
Fe_3O_4	0.0015	0.0075
$PbSO_4$	1.15	0.82
$ZnFe_2O_4$	10.45	28.46
ZnO	65.79	55.03
$ZnSO_4$	6.98	5.92
Zn_2SiO_4	8.53	1.20
Mass change	−13.09	−13.37

Both compositions were simulated in a roaster operation: 1 ton of low iron concentrate, and 1.16 ton of high iron content, for an equal amount of Zn production. They demanded a different amount of air: For the low iron content, it was used 2109 Nm^3 with 22% O_2 and for the high iron content 2262 Nm^3. At 950 °C, and same product species (but in different proportions—Table 2). The energy balance of the high iron content concentrate produced an extra 10.45% of heat, meaning that a roaster treating this concentrate would have its capacity reduced or heat removal demand increased by this value.

The simulation predicted that 5.1% of the Zn from the low iron content would be in the form of ferrite, while the high iron content, this proportion goes to 16.2%. That would require a significant increase in the acid leaching and iron removal phase, for a conventional RLE process.

Regarding iron oxidation, different products are possible. However, the spinel form (zinc ferrite) is by far the most stable, becoming the most abundant.

Equation 4: Oxidation of pyrite (FeS_2) in a roaster at 950 °C.

$$\begin{aligned}
&FeS_2(s) + 2.50O_2(g) \rightarrow FeO(s) + 2SO_2(g)\\
&\quad \Delta H = -686.730\,\text{kJ/mol} \quad \Delta G = -673.425\,\text{kJ/mol}\\
&FeS_2(s) + 2.66O_2(g) \rightarrow 0.33Fe_3O_4(s) + 2SO_2(g)\\
&\quad \Delta H = -786.029\,\text{kJ/mol} \quad \Delta G = -729.373\,\text{kJ/mol}\\
&FeS_2(s) + 2.75O_2(g) \rightarrow 0.50Fe_2O_3(s) + 2SO_2(g)\\
&\quad \Delta H = -828.241\,\text{kJ/mol} \quad \Delta G = -741.458\,\text{kJ/mol}\\
&FeS_2(s) + 3.50O_2(g) + 0.5ZnS(s) \rightarrow 0.50ZnFe_2O_4(s) + 2.5SO_2(g)\\
&\quad \Delta H = -1061.573\,\text{kJ/mol} \quad \Delta G = -932.161\,\text{kJ/mol} \qquad (4)
\end{aligned}$$

Table 3 Composition of the simulated sulfatation products from high and low iron content zinc concentrate

	Low iron content (%)	High iron content (%)
Fe_2O_3	2.44	6.73
SiO_2	1.39	0.16
$CaSO_4$	1.44	1.12
$FeSO_4$	1.50	2.99
$Fe_2(SO_4)_3$	1.08	5.61
$ZnFe_2O_4$	0.68	1.39
$ZnSO_4$	87.74	76.90
Mass change	+54.51	+162.49

Furthermore, the obtained iron products wüstite (FeO) and magnetite (Fe_3O_4) can further oxide to hematite (Fe_2O_3), dislocating the final composition (Eq. 5).

Equation 5: Conversion of wüstite (FeO) and magnetite (Fe_3O_4) to hematite (Fe_2O_3) at 950 °C.

$$\begin{aligned} &FeO(s) + 0.25O_2(g) \rightarrow 0.50Fe_2O_3(s) \\ &\quad \Delta H = -141.511\,\text{kJ/mol} \quad \Delta G = -68.033\,\text{kJ/mol} \\ &Fe_3O_4(s) + 0.25O_2(g) \rightarrow 1.50Fe_2O_3(s) \\ &\quad \Delta H = -125.650\,\text{kJ/mol} \quad \Delta G = -35.357\,\text{kJ/mol} \end{aligned} \tag{5}$$

The Sulfatation Process

By taking the same concentrates composition, amount, and airflow mentioned above, we now simulated the sulfatation process, at 600 °C. The product composition is shown in Table 3.

Differently from the calcination process, the zinc at the sulfatation process is less than 1% in the ferrite form (0.33% and 0.79% low iron content and high iron content, respectively). Furthermore, most of the zinc is in an easy to wash form, zinc sulfate.

Regarding the choice of reactor, it is not possible to do sulfatation in a conventional fluidized bed roaster. The sulfates formed in the reaction would stick in the reactor walls, causing constant maintenance problems, and making the fluidized system impractical. The sulfatation requires a wedge furnace (or similar), in order to control the reaction in stages and continuously brush the walls, avoiding impregnation.

Another concern regarding the sulfatation process is the SO_2 gas outlet concentration. In a normal roasting process, the concentration of this gas is between 6.5 and 9%, which is the minimum for a conventional sulfuric acid plant to work. In the sulfatation process, the concentration hardly reaches 1%.

This process requires strict temperature control: If the sulfatation temperature is too low, most of the iron assumes the sulfate form, including any iron that was

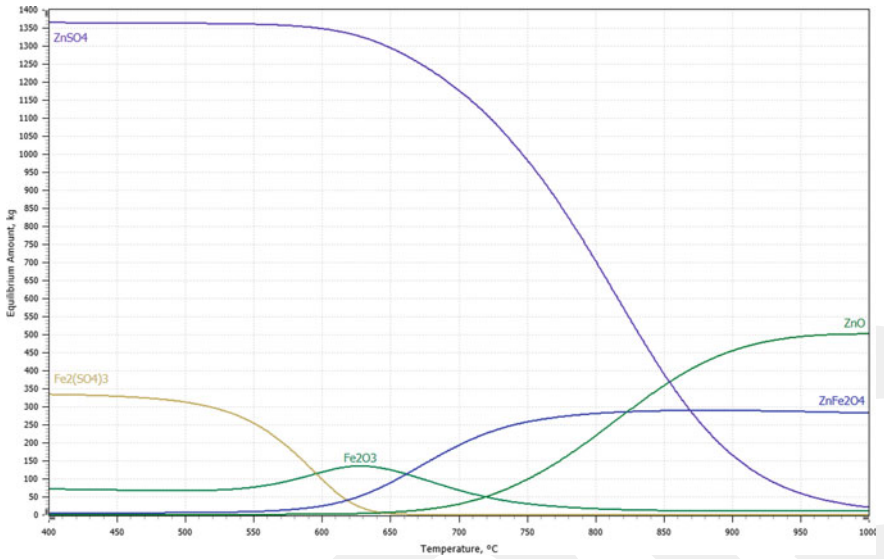

Fig. 3 Equilibrium composition as a function of temperature for a high iron content zinc concentrate

Table 4 Excess heat comparison for low and high iron content in different process

	Roasting, 900 °C (MJ/ton ZnC)	Sulfatation, 600 °C (MJ/ton ZnC)
Low iron content	−2.535	−9.868
High iron content	−2.800	−10.919

previously in the form of hematite. This consumes excessively the SO_2. On the other hand, if the temperature is too high, the ferrite formation becomes predominant, diminishing the zinc recovery, as it can be seen in Fig. 3.

Regarding the heat balance, the sulfatation process is significantly more exothermic than the calcination process. This means that this process can produce more steam compared to a common roaster. Table 4 shows this excess heat generated comparison.

Conclusion

In this work, we performed a series of simulations in order to evaluate the sulfatation process for treating high iron content zinc concentrates. The simulation showed less zinc in the ferrites form, allowing an easier recovery zinc. However, the sulfatation would require specific operations: (1) a wedge furnace, as an example, for stage reaction control and reactor wall sulfatation prevention, (2) higher heat retreat, and

(3) specific gas treatment for low SO_2 concentration (e.g., by liquefying it). This implies that new smelters could evaluate these operations, but hardly an installed one would be able to adapt its operations.

References

1. Crundwell FK (1988) Effect of iron impurity in zinc sulfide concentrates on the rate of dissolution. AIChE J 34(7):1128–1134
2. Ulf Söderström—President BA Market (2008) Zinc smelters revenue stream. https://www.boliden.com/globalassets/investor-relations/reports-and-presentations/capital-markets-day/2008/cmd/12-zinc-smelters-revenue-stream-ulf-soderstrom-president-ba-market.pdf. Accessed 8 Aug 2019
3. Introduction to zinc and lead smelting business. https://www.nyrstar.com/~/media/Files/N/Nyrstar/results-reports-and-presentations/english/2009/zincleadsmelting.pdf. Accessed 8 Aug 2019
4. Svens K, Kerstiens B, Runkel M (2003) Recent experiences with modern zinc processing technology. Erzmetall J Explor Min Metall 56:94–103
5. Turner DW, Hourn M (2013) Albion Process^{TM}. Simplicity in leaching—introduction to Albion Process. Xtrata Technology, XTT 2149
6. Mitchell WE (1931) Treating zinc concentrate and plant residue. US. Patent 1,834,960
7. Wedge U (1914) Metallurgical furnace. US. Patent 1,086,494. 10 Feb 1914
8. McNamara DC (1972) Analysis of the factors leading to the announced closure of the Anaconda zinc plant at Great Falls. Graduate student theses, Dissertations, and Professional Papers. 1546

Part X
PbZn Process Fundamentals II

GCRIS

Lead and Zinc Extractive Metallurgy Research in the Kroll Institute for Extractive Metallurgy

Patrick R. Taylor

Abstract The Kroll Institute for Extractive Metallurgy has performed graduate research in zinc and lead extractive metallurgy over its history. Presented is an overview of some of the past and current research on this topic, and this includes as follows: galena leaching with fluosilicic acid; soda ash reduction of galena; characteristics of sodium-iron-silicate slags; computational fluid dynamic modeling of a secondary lead reverberatory furnace; vacuum distillation of complex lead bullion; hydrogen partial reduction of zinc ferrites; and evaluation of zinc process jarosite, ferrites, and leach precipitates for by-product recovery.

Keywords Extractive metallurgy · Galena leaching · Soda ash reduction · Slags · Computational fluid dynamic modeling · Vacuum distillation · Zinc ferrites · By-product recovery

Introduction

The Kroll Institute for Extractive Metallurgy (KIEM) was established at the Colorado School of Mines in 1974 using a bequest from William J. Kroll. Dr. Kroll was the inventor of the processes for recovering titanium and zirconium metals from their ores, among other process metallurgy inventions. Over the past 45 years, KIEM has trained numerous extractive and process metallurgists for work in industry and academia. Many have gone on to be leaders in industry. The objectives of KIEM are to provide education, research, and service in extractive metallurgy, mineral processing, recycling, and waste minimization. The laboratories for research in these fields are among the best in a university in the USA. This paper discusses some of the current, recent, and past research performed by graduate students and faculty in our program.

P. R. Taylor (✉)
Colorado School of Mines, Kroll Institute for Extractive Metallurgy, Golden, CO 80401, USA
e-mail: prtaylor@mines.edu

© The Minerals, Metals & Materials Society 2020

A. Siegmund et al. (eds.), *PbZn 2020: 9th International Symposium on Lead and Zinc Processing*, The Minerals, Metals & Materials Series,
https://doi.org/10.1007/978-3-030-37070-1_36

Current Research

There are currently four graduate students working on research projects related to the extractive metallurgy of lead or zinc. One student [1] is looking at the vacuum distillation of lead bullion for her Ph.D. project. The Center for Resource Recovery and Recycling funds this research. The experimental system is shown in Fig. 1. The system is used to evaluate the effects of temperature, vacuum pressure, and time on the removal of arsenic and antimony by selective volatilization. The work includes detailed thermodynamic modeling in an attempt to describe the experimental results. The overall objective is to see if it is possible to simplify lead refining using vacuum distillation and produce a pure volatile product.

Another research project [2] is on the controlled hydrogen reduction of zinc ferrites to zinc oxide and magnetite. The objective is to recover the zinc and any contained gallium, germanium, or indium. The Critical Materials Institute funds this research. The tube furnace roasting experimental system is shown in Fig. 2. The student is evaluating the effects of time, temperature, and hydrogen concentration of the roast reduction reaction and the leaching, purification, and recovery of the desired elements.

Fig. 1 Vacuum distillation reactor

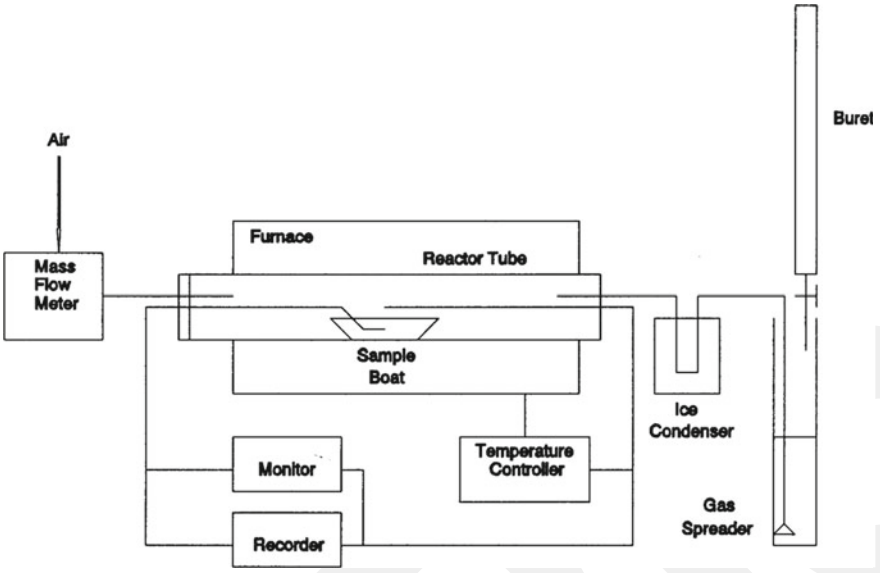

Fig. 2 Tube furnace schematic

The reaction of interest is shown as:

$$3ZnFe_2O_4 + H_2(g) = 2Fe_3O_4 + 3ZnO + H_2O(g)$$

This roast reaction is followed by leaching to solubilize the zinc and minor impurities, followed by solution purification and metal recovery (Fig. 3).

A third current project is being evaluating new methods to recover gallium and germanium from a zinc leach precipitate [3]. A preliminary flow sheet is given in Fig. 4. The Critical Materials Institute funds this research. The work includes leaching, solution purification, and metal recovery. In addition, the student is investigating new chemical methods to regenerate sulfuric acid and sodium hydroxide from spent leach solutions.

A fourth project has just started, funded by the Center for Resource Recovery and Recycling, on alternatives for lead softening [4]. The concepts are outlined in Fig. 5 (prepared by Dr. Tom Boundy). The overall objectives are to evaluate various methods for lead softening and to explore the possibilities for NaOH regeneration and antimony recovery.

Recent Research

A lead battery recycling company has funded two Ph.D. students in KIEM. One student looked at computational fluid dynamic modeling of a lead reverberatory

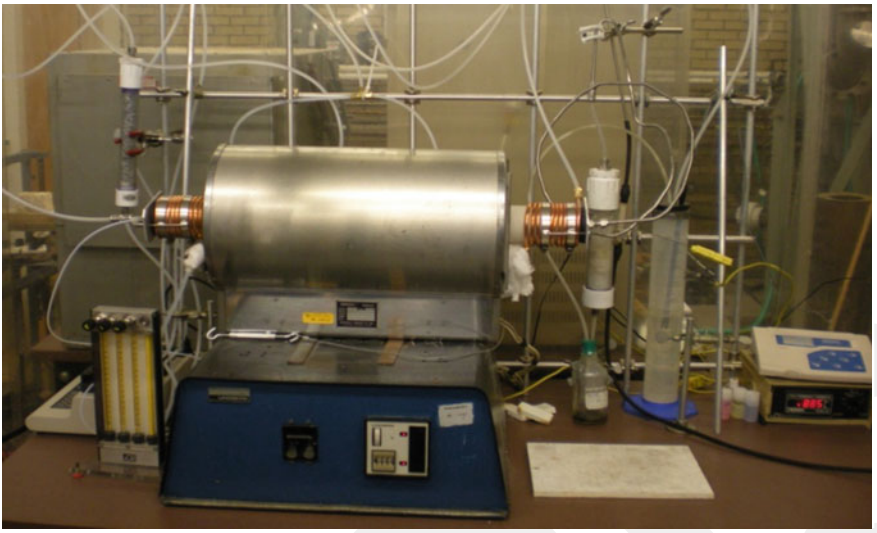

Fig. 3 Laboratory tube furnace

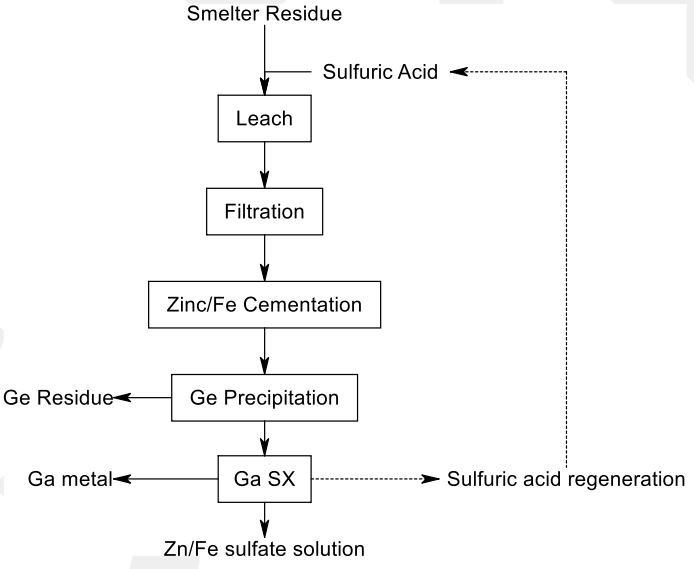

Fig. 4 Preliminary flow sheet

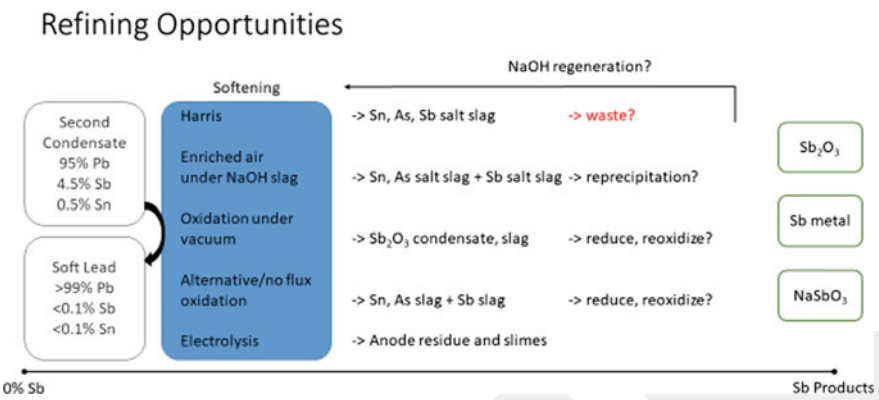

Fig. 5 Lead softening concepts

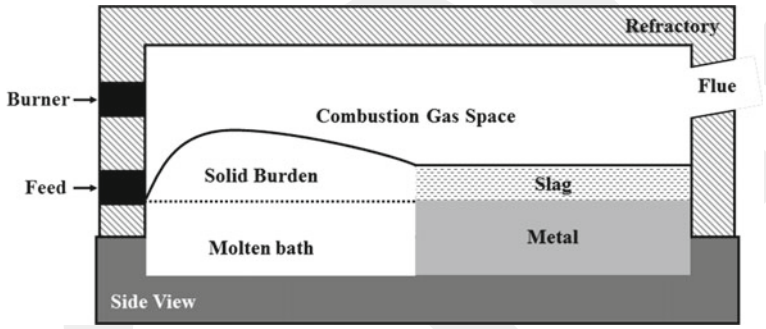

Fig. 6 Computational domain

furnace for her research [5, 6]. The objectives were to improve energy transfer and reduce wear in the furnace. The computational domain is shown in Fig. 6.

Another student looked at the chemistry and properties of secondary lead blast furnace slags [7, 8]. He measured density, viscosity, and leaching characteristics as a function of composition and temperature. The experimental system is shown in Fig. 7.

Past Research

Another student worked to develop a method to selectively extract zinc from galvanized steel [9, 10] (Fig. 8). The work was funded by the Center for Resource Recovery and Recycling. This work was patented [11].

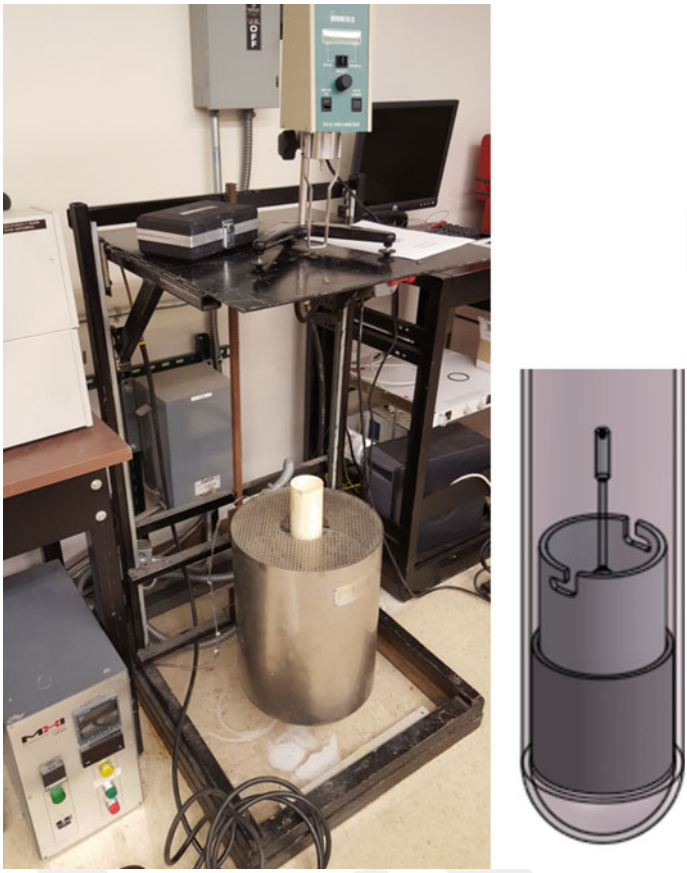

Fig. 7 Viscosity and density measurement system for high temperatures

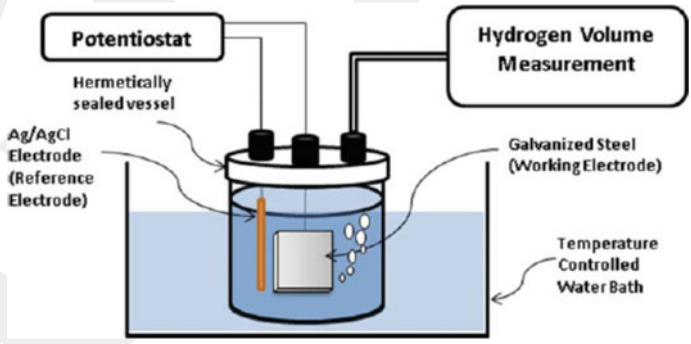

Fig. 8 Lab scale de-zincing experimental system

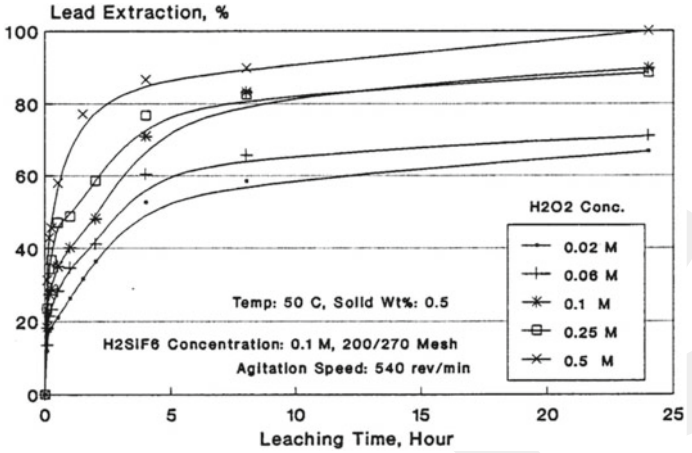

Fig. 9 Kinetic curves for galena leaching

Work started at the University of Idaho and continued at Colorado School of Mines, evaluated fluosilicic acid leaching of galena [12]. Example results are shown in Fig. 9. This demonstrated the need for an oxidizing agent to eliminate the effect of elemental sulfur coating of the particles on the leach kinetics.

Another project carried over from the University of Idaho was the caustic reduction of galena [13]. The reaction of interest is:

$$PbS(s) + Na_2CO_3(l) + 3/2\,O_2(g) = Pb(l) + Na_2SO_4(l) + CO_2(g)$$

Experiments were conducted in a crucible furnace at temperatures between 923 and 1133 K. NaCl was added to help in the fluidity and melting point of the slag. This work is continuing to evaluate methods to regenerate the sodium carbonate from the slag. The reactor schematic is given in Fig. 10. Example results are given in Fig. 11.

Conclusion

Examples of current and past research on the extractive metallurgy of zinc and lead performed by graduate students in the Kroll Institute for Extractive Metallurgy have been presented.

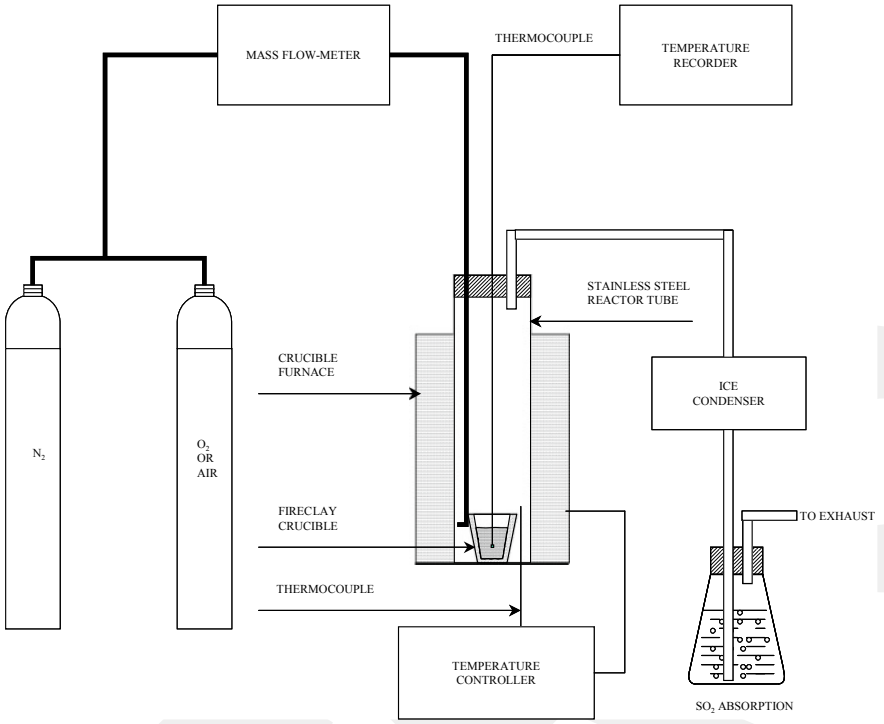

Fig. 10 Tube furnace schematic

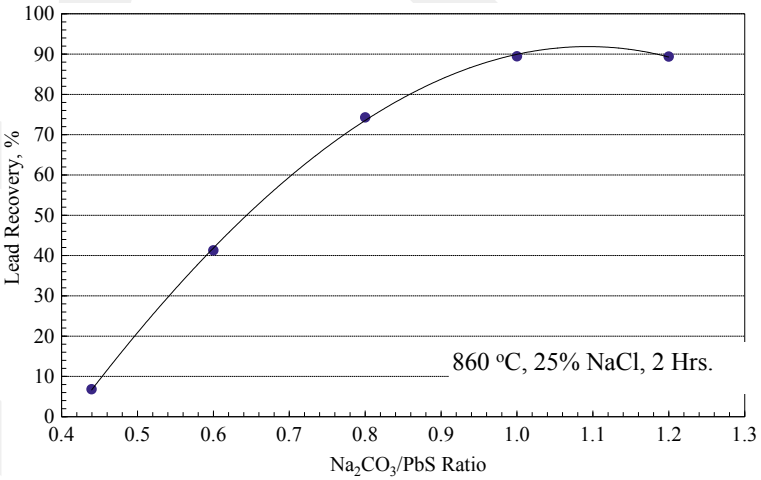

Fig. 11 Effect of soda ash to lead sulfide ratio on lead recovery

References

1. Karumb TE (2019) Vacuum distillation of lead bullion, Ph.D. thesis in progress, Colorado School of Mines
2. Kayshap V (2019) Minor metal and zinc recovery from zinc ferrites, Ph.D. thesis in progress, Colorado School of Mines
3. Ott B (2019) Gallium and germanium recovery from zinc plant resides, Ph.D. thesis in progress, Colorado School of Mines
4. Asante S (2019) Alternatives for lead softening and antimony recovery, Ph.D. thesis in progress, Colorado School of Mines
5. Anderson A, Grogan J, Bogin B, Taylor PR (2018) Computational fluid dynamic modeling of a secondary lead reverberatory furnace. In: Extraction 2018, Peter Hayes symposium on pyrometallurgical processing, TMS
6. Anderson A (2017) Computational fluid dynamic modeling of a secondary lead reverberatory furnace. Ph.D. thesis, Colorado School of Mines
7. Schriner D, Taylor PR, Grogan J (2016) A review of slag chemistry in lead recycling. In: Reddy RG, Chaubal P, Pistorius PC, Pal U (eds) Advances in molten slags, fluxes, and salts: proceedings of the 10th international conference on molten slags, fluxes and salts (MOLTEN16), TMS
8. Schriner D (2018) Experimental investigation of fundamental viscosity, density and leaching characteristics of sodium-iron-silicate slags, Ph.D. thesis, Colorado School of Mines
9. Grogan J, Martins GP, Anderson CG (2018) Dezincing of galvanized steel by sulfuric acid leaching. Extraction 2018 B. Davis Ed. TMS 2018:1733–1742
10. Grogan J (2015) Dezincing of galvanized steel. Ph.D. thesis, Colorado School of Mines
11. Grogan J, Anderson CG, Martins GP (2018) Decoating of coated materials, US. Patent 10,087,503 B2, 2 Oct 2018
12. Taylor PR, Choi Y, Vidal EE (2003) Fluosilic acid leaching of galena. Hydrometallurgy 1:461–468
13. Taylor PR, Omofoma MA, Wang W (2019) Direct smelting of complex galena-sphalerite-precious metal concentrates by the soda ash process. Internal Report, Colorado School of Mines

Electrochemical Extraction of Pb and Zn from Raw Mineral Materials Using Sulfurgraphite Electrode

R. Kh. Sharipov, U. A. Balgimbaeva and E. N. Suleimenov

Abstract This paper presents the results of electro-leaching of lead and zinc by an electrochemical method from raw mineral materials using a sulfurgraphite electrode as a cathode. Extraction of metals from the hardly refractory sulfide intermediate product requires a change in technological conditions in accordance with the structure and physicochemical state of compounds containing the base metal. The result of X-ray phase analysis showed that the metals contained in the raw mineral materials are in the form of sulfides. The initial concentration of sodium hydroxide during leaching in solutions was 0.1 and 0.5 M. The duration of the electrochemical leaching was 5 h. The maximum extraction during leaching of the concentrate for zinc is 42.15% and for lead 61.65% in 5 h. A brief description of the raw mineral materials used in the Shalkiya deposit is given. It has been established that the use of a sulfurgraphite electrode as a cathode has a positive effect in the electrochemical leaching of lead and zinc from the concentrate.

Keywords Collective concentrate · Electrochemical leaching · Sulfur-graphite electrode

Introduction

Waste management is the weakest point in modern metallurgical industry. A feature of the modern mineral resource base of the Republic of Kazakhstan is the complexity of both chemical and material compositions. In addition, difficulties are caused by the lack of real ideas on the formation of the material composition of metallurgical waste, which occurs as a result of the impact of technological regimes on processed raw materials. In most cases, stable chemical formations are formed (e.g., eutectic reactions of slag formation of pyrometallurgical processes), which are very difficult

R. Kh. Sharipov (✉) · U. A. Balgimbaeva · E. N. Suleimenov
Kazakh-British Technical University, Almaty 05000, Republic of Kazakhstan
e-mail: freedom.k@mail.ru

© The Minerals, Metals & Materials Society 2020

A. Siegmund et al. (eds.), *PbZn 2020: 9th International Symposium on Lead and Zinc Processing*, The Minerals, Metals & Materials Series,
https://doi.org/10.1007/978-3-030-37070-1_37

to chemically convert and which prevent their use without physicochemical transformations of their structure. A change in the physicochemical state of the dumps sometimes leads to the possibility of their successful processing.

Refractory ores make up 75–80% of the mineral resource base of non-ferrous metallurgy in Kazakhstan. Existing technologies cannot ensure the efficiency of extraction of precious and non-ferrous metals from these ores which would be comparable with technological indicators in the processing of such raw mineral materials for which traditional technologies were created. The need for new scientific approaches to creating technical solutions and technologies adapted to the changing mineral resource base is obvious. In this case, it is necessary to study issues related to the structural features of not only minerals containing recoverable metals, but also the mineralogical features of the rocks included. The formation of minerals during the processes of ore formation under various thermobarogeochemical conditions determines the features of the material composition of ores, the energy characteristics of ore minerals, their geochemical specialization, and the form in which metals are found in the structure of minerals.

As is known, the processes of electrochemical dissolution and reduction of metals are widely used in hydrometallurgical technologies [1]. The scientific research results on combined electrochemical reactions that we found in literary sources take place only when studying corrosion processes. However, published data in this scientific direction show that it is possible to use combined electrochemical reactions to develop innovative technical solutions in hydrometallurgy, including to reduce the technological chain of raw materials—the final product [2].

We have developed a method for the use of combined electrochemical reactions to carry out the process of obtaining a leaching agent and reactions of the transfer of metals into solution in the volume of one unit [3, 4]. The proposed method is very complicated and it is necessary to provide knowledge of the processes in the following areas for successful development of technologies: (i) the mineral-electrolyte interface, (ii) the solution–solution interface, (iii) structure of the studied inorganic aqueous solutions, (iv) structural changes in solid systems after treatment with a leaching agent, and (v) influence of physicochemical factors on the change in the structure of the studied systems.

Experimental

The Shalkiya deposit is one of the largest lead-zinc deposits in the world and takes fifth place in the world in terms of zinc reserves. The ore of this deposit is classified as difficult to ore due to the thin dissemination of minerals, their close intergrowth among themselves and with rock-forming minerals, and the presence of thin carbonaceous inclusions. The high dispersion of minerals (galena, sphalerite, pyrite, etc.), their close intergrowth with minerals of the rock and with each other, the presence of small carbonaceous inclusions, the presence of easily grinding minerals along with high-strength mineral formations lead to many difficulties, both in enrichment

and in during hydrometallurgical processing. A collective concentrate of the following chemical composition was used as an object of research: % (mass fraction.): Si-14.94; Pb-5.68; Zn-14.57; Fe-6.26; S-14.96; C-6.94; and Ca-2.11.

The experiments were carried out in a reaction cell. The cell had a three-electrode system consisting of a working electrode, a reference electrode, and an auxiliary electrode. A sulfur-graphite electrode was used as a working electrode, in which the ratio of sulfur to graphite was 65:35%. The silver chloride electrode served as the reference electrode, and the graphite electrode served as the auxiliary electrode (anode). The volume of alkaline solution in the reaction vessel contained a volume of 150 ml. A sample was placed in a vessel with a ratio of T:W = 1:10, (sample 15 g: sodium hydroxide 150 ml). The current density is from i-100 A/m^2, the mixing speed is 480 rpm, and the leaching time is 5–6 h. The alkali concentration in the solution is 0.1, 0.2, 0.3, and 0.5 M.

In parallel with the experiment, the physicochemical characteristics of the solutions were determined, which changed as the leaching reagent formed and metal compounds formed in the aqueous solution. Samples were taken every hour for analysis, the pH of the medium was determined, the potential of the cathode (sulfur graphite electrode) was E^0k, the electrical conductivity was Eh of the solution, and the concentration of dissolved oxygen (DO) using the 856 Conductivity Module, 867 pH Module "Metrohm" (Switzerland), SensIon 156 handheld analyzer manufactured by HACH (USA). The amount of metals transferred to the solution was determined on a contrAA 300 atomic absorption spectrometer. The concentrate was leached for 300 min at concentrations of sodium hydroxide in the initial solution of 0.1 and 0.5 M NaOH.

Results and Discussion

The corresponding data are shown in Figs. 1, 2, 3, 4, and 5. As can be seen from Figs. 1 and 2, a distinctive feature of the extraction of zinc and lead into solution is a gradual increase in recovery followed by reverse deposition of metals. In this case, lead begins to pass into solution only after 60 min of leaching, while zinc goes into solution almost at the beginning of the experiment. It should be noted that, as in the case of lead, zinc is extracted into the solution at a low rate during the first 60 min of leaching. After 60 min of leaching, the rate of transition of lead and zinc into solution increases significantly. Moreover, the transition of lead into solution is characterized by an increased rate. The most characteristic indicator is the effect of the concentration of sodium hydroxide in the initial solution on the transition of lead and zinc into the solution.

As can be seen from Figs. 1 and 2, an increase in the concentration from 0.1 to 0.5 M NaOH leads to the fact that both zinc and lead go into solution.

Figures 3 and 4 show the data on the change in pH and electrical conductivity of solutions during leaching of sodium hydroxide 0.1 and 0.5 M in the course of leaching decrease from 11.99 to 6.99 and from 13.047 to 10.39, respectively. The electrical

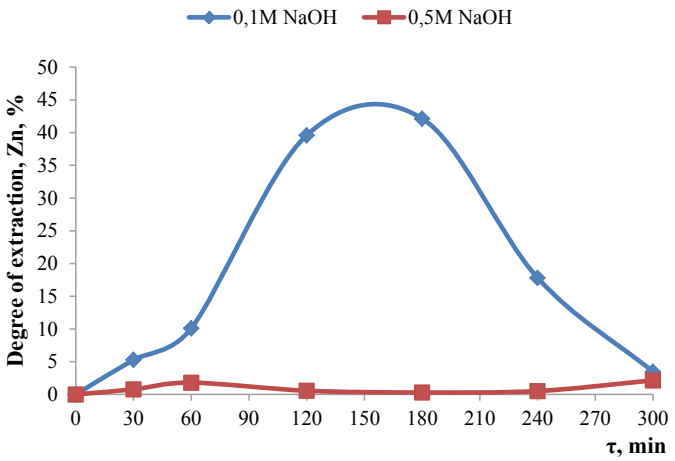

T = 25˚C; Current density i = 100 A / m^2; S: L (1:10); cathode - SGE; anode - graphite;

Fig. 1 Degree of zinc extraction by electroleaching collective concentrate depending on the concentration of sodium hydroxide

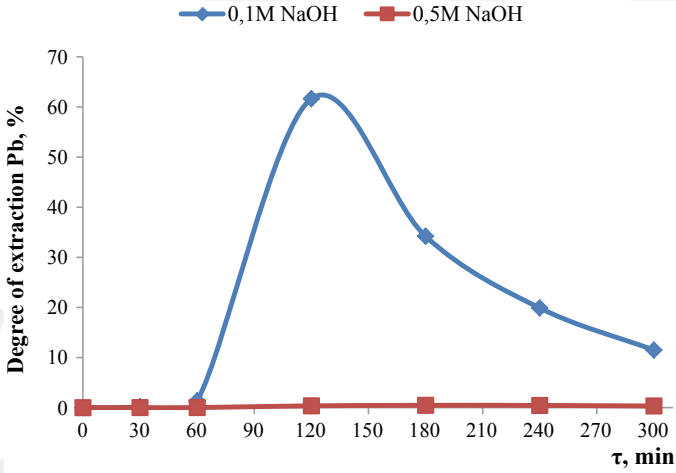

T = 25˚C; Current density i = 100 A / m^2; S: L (1:10); cathode - SGE; anode - graphite;

Fig. 2 Degree of lead extraction by electroleaching collective concentrate depending on the concentration of sodium hydroxide

conductivity of the solution decreases markedly and the nature of the change in electrical conductivity does not meet the generally accepted point of view which is to say that the mechanism of the electrical conductivity of inorganic aqueous solutions of which an increase in the concentration of cations and anions increases the electrical conductivity of the inorganic aqueous solution.

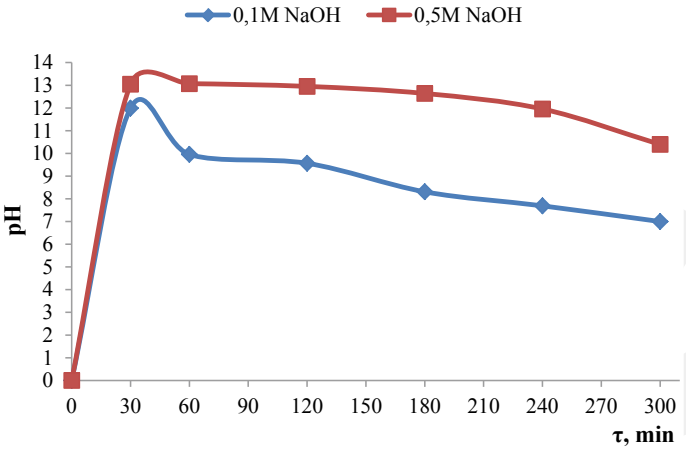

T = 25˚C; Current density i = 100 A / m2; S: L (1:10); cathode - SGE; anode - graphite;

Fig. 3 Change in pH of solutions in the process of leaching of the concentrate depending on the concentration

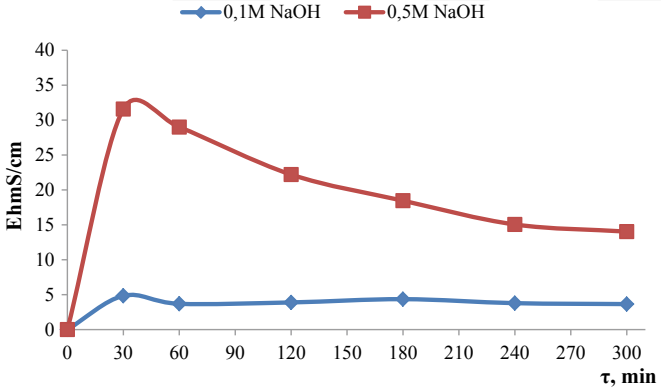

T = 25˚C; Current density i = 100 A / m2; S:L (1:10); cathode - SGE; anode - graphite;

Fig. 4 Change in the electrical conductivity of solutions in the process of leaching of the concentrate depending on the concentration of NaOH

It is shown that the features of leaching solutions can lead to the reverse deposition of metals in the precipitate.

Figure 5 shows the change in oxygen concentration in the solution during leaching. It can be assumed that an increase in the concentration of sodium hydroxide in the initial solution prevents the oxidation of the metal, which precedes the conversion of the metal into the solution. A change in the oxygen concentration in the leaching

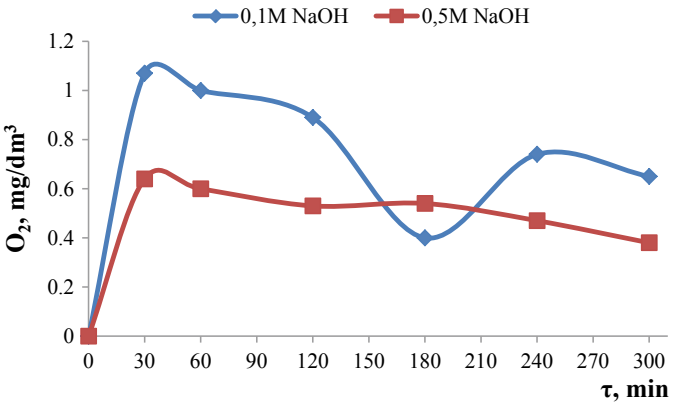

T = 25˚C; Current density i = 100 A / m2; S:L (1:10); cathode - SGE; anode - graphite;

Fig. 5 Change in the oxygen concentration of solutions in the process of leaching of the concentrate depending on the concentration

solution shows that the oxygen concentration decreases: when the concentration of sodium hydroxide is 0.1 M from 1.07 to 0.4 mg/dm^3 for 3 h, then it increases to 0.74 mg/dm^3, at 0.5 M—oxygen concentration from 0.64 to 0.38 mg/dm^3, decreases monotonously.

Conclusion

It was found that the extraction of metals into solution using the combined electrochemical reaction method can be applied to raw mineral materials of any mineralogical composition, but it is necessary to develop leaching parameters adapted to the properties of the feedstock.

The degree of extraction of zinc and lead by electrolytic leaching from collective concentrates obtained from ore from the Shalkiya deposit by this method can be quite effective.

The degree of zinc extraction by electrically leaching up to 3 h increases with a concentration of sodium hydroxide of 0.1 M to 42.15%, then there is a reverse deposition of zinc up to 5 h 3.47%, at 0.5 M the maximum recovery is 2.15%. For lead, these indicators are, respectively: at a concentration of sodium hydroxide of 0.1 M—61.65% in 2 h, then the process of precipitation may occur, and at 0.5 M the maximum recovery of lead is 0.33% in 5 h.

References

1. Deutsch JL, Dreisinger David B (2013) Silver sulfide leaching with thiosulfate in the presence of additives, Part II: ferric complexes and the application to silver sulfide orePart II: ferric complexes and the application to silver sulfide ore. Hydrometallurgy 137:156–164
2. Kenzhaliyev BK et al (2016) Using the composite electrode for the organization of aligned electrochemical reactions during the extraction of metals from raw materials. In: Paper presented at the 48 international October conference on mining and metallurgy, University of Belgrade—Technical Faculty in Bor, Serbia, 28 Sept to 01 Oct 2016
3. Sharipov RH, Berkinbayeva AN, Kenzhalyiev BK, Dosymbayeva ZD, Suleimenov EN (2016) The influence of the dynamics of the formation of a leaching agent on the parameters of aqueous alkaline solutions when using combined electrochemical reactions for leaching brass. J Kompleksnoe Ispol'zovanie Mineral'nogo Syr'a 2:83–87
4. Sharipov R, Kenzhaliyev B, Berkinbayeva A (2015) Oxidized nickel-cobalt-containing raw materials electro-chemical leaching. Metall Mining Ind 5:146–152

GCRIS

Characterization and Processing of Residues from Hydrometallurgical Zinc Smelters

J. Antrekowitsch and G. Hanke

Abstract Leaching residues out of primary zinc industry like the so-called jarosite, move more and more into the focus of research and development, due to environmental reasons and the potential to recover zinc, lead, silver as well as other valuables. Even though values of lead and zinc can be found in a range of 2–8% sometimes accompanied by up to 500 ppm of silver, missing concepts for concentration, e.g. by flotation, and failing hydrometallurgical approaches, make an economic treatment difficult to realize. At the University of Leoben, together with associated R&D-companies, a pyrometallurgical process for jarosite treatment has been developed, realizing a multi-metal recovery and the formation of slag, allowing utilization in construction or cement industry. However, to avoid high specific energy consumption, at least a certain grade of concentration would be beneficial. The paper describes the general process idea, the characterization of the material, and the first results of mineral beneficiation trials and how they could influence the economy of the concept.

Keywords Recycling · Zinc · Lead · Mineral processing · Characterization

Introduction

Zinc ores nowadays often suffer from decreasing zinc and lead grades going along with increasing iron contents. The iron, which follows the valuables into the concentrate, has to be removed during the leaching process, creating huge volumes of waste which are, in the majority of cases, dumped worldwide. Considering that for every ton of zinc produced in zinc smelters operating a jarosite or goethite precipitations, 600–1000 kg of leaching residue is generated alongside; globally, the amount of slurry generated per year lies somewhere between 7 and 10 million tons.

J. Antrekowitsch (✉)
Chair of Nonferrous Metallurgy, University of Leoben, Leoben, Austria
e-mail: juergen.antrekowitsch@unileoben.ac.at

G. Hanke
Chair of Geology and Economic Geology, University of Leoben, Leoben, Austria

© The Minerals, Metals & Materials Society 2020

A. Siegmund et al. (eds.), *PbZn 2020: 9th International Symposium on Lead and Zinc Processing*, The Minerals, Metals & Materials Series,
https://doi.org/10.1007/978-3-030-37070-1_38

It was estimated that these residues contain metal values of one to two billion USD [1]. Important to note is that these numbers are steadily growing and merely represent the amount of newly created jarosite every year.

In general, only a few concepts for reprocessing are existing, showing various disadvantages like high energy consumption, the recovery of only one metal, or complex process flow sheets leading to high operational costs [2].

The morphology of the material is of high importance for possible processing steps. Therefore, the characterization of typical zinc smelter leach residues is described in the following chapter.

Characterization

The complexity of zinc leach residues and the small grain size makes a detailed and clear characterization difficult. Often, jarosite or goethite residues do not only contain the iron compound, responsible for its name but also different other materials. Examples are remaining solids, not separated by filtration, leaching residues containing lead and silver, not dissolved calcine, added for pH-adjustment, etc. Out of this, residues from hydrometallurgical zinc smelters can vary a lot, even though the underlying procedures and basics should be quite similar. As the development of any kind of treatment needs detailed knowledge of the materials' properties, characterization is of major importance. Most of all, the particles of very small grain size, which are very common, cause problems. Amorphous phases are additionally difficult to handle with some methods like x-ray diffraction analysis for mineralogical analysis [3].

Samples from different zinc plants were collected. Strew samples were used to get basic information about the morphology and grain size. For detailed measurements, it is necessary to use polished sections. Various methods like scanning electron microscopy, microprobe analysis, x-ray diffraction analysis, ICP-MS/OES (inductively coupled plasma-mass spectrometry/optical emission spectrometry), and fire assay were employed to investigate the material.

Twelve different jarosite samples from all over the world were analysed leading to the values shown in Table 1.

Table 1 Chemical analysis of different jarosites

	wt%		wt%
Zn	1.5–8.4	Fe	15.2–32.4
Pb	0.5–7.8	Si	0.8–7.2
Ag	0–0.05	Cu	0.1–0.8
Au	0–3 (ppm)	Ca	3.2–10.3
In	0–0.03	Ge	0–0.04
Ga	0–0.03	S	10.4–16.5

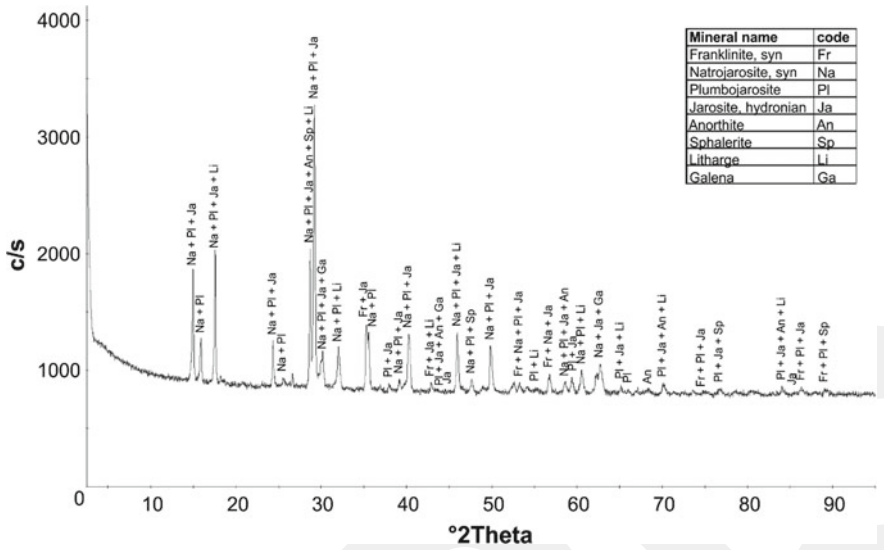

Fig. 1 XRD-pattern of the jarosite material (Na-jarosite)

The particle size distribution of the samples received was determined by wet screening using standard analytical test screens. Usually, more than 60% of the grains are found to be below 10 μm.

The material is very versatile and consists of many different phases. As expected, the XRD-analysis shows a clear dominance of jarosite (Fig. 1).

Many other phases, found using a SEM, were not detected by XRD-analysis due to their small amount. The appearance of lead is very interesting, as it is found as sulphide, sulphate, and oxide.

The jarosite crystals show often areas which are richer in lead than others. Most likely, this is caused by appearance of plumbojarosite within another type of jarosite (mostly, natro- or hydronium jarosite).

Lead and silver are the main elements of interest. Unfortunately, especially, these two seem to be present in various compounds, making a concentration by physical separation difficult.

Additionally, one specific jarosite material was found to be very rich in gypsum.

Process Concepts

As already mentioned, University of Leoben together with associated companies developed a multi-metal recovery concept on pyrometallurgical basis. In a first step, the calcination, sulphates, and hydroxides are split under oxidizing conditions and SO_2 as well as H_2O escapes through the off-gas. A rotary kiln, short drum furnace, or

top blown rotary converters are the furnaces of choice, dependent, if a continuous or batch process is preferred. In the case of homogeneous dumps, a continuous operating rotary kiln would be favorable due to positive aspects for the off-gas treatment and higher throughputs. In the case of inhomogeneous material, a batch process would help to treat the material under more flexible and therefore optimized conditions.

The calcine is then charged, preferably in hot stage, into an electric furnace where it is molten and reduced on a lead bath. Quartz and carbon carriers are added. The metal bath collects most of the lead, copper as well as silver and gold, if present. Zinc oxide is reduced, zinc evaporates and re-oxidizes in the off-gas. If indium is also part of the jarosite, it most likely follows the zinc into the dust. A simplified process scheme is shown in Fig. 2.

Trials in laboratory scale as well as technical scale (50–100 kg/batch) showed high recovery rates for the important metals. Figure 3 shows the different metal yields; Table 2 shows the composition of the received metal product and the remaining slag, summarizing 12 trials on a technical scale.

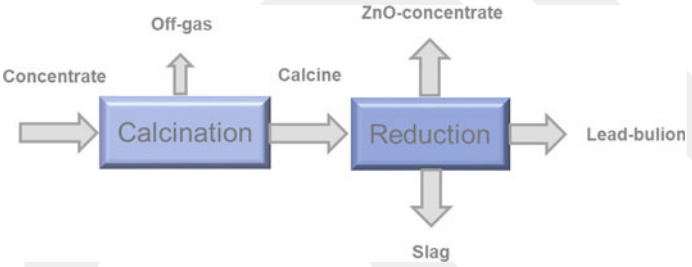

Fig. 2 Simplified scheme of the developed process

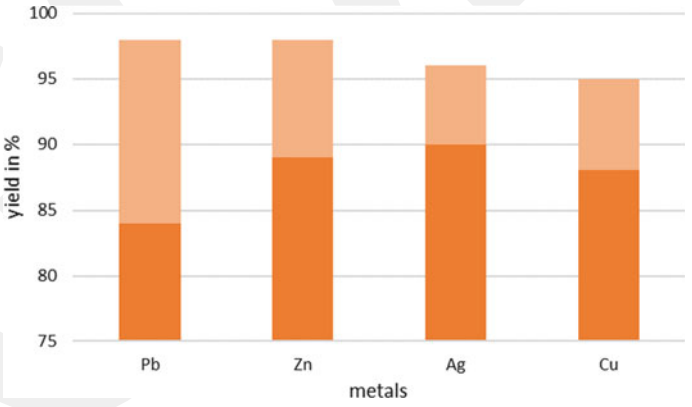

Fig. 3 Minimum and maximum recovery yields for different metals

Table 2 Typical compositions of resulting lead alloy and slag phase

Slag	**SiO_2**	**FeO**	**CaO**	**ZnO**	**Pb(O)**	**Al_2O_3**	**Na_2O/K_2O**
%	21.4–29.6	58.2–65.9	1.8–3.7	1.0–2.8	0.8–3.1	2.7–3.9	1.3–3.1
Metal	**Pb**	**Cu**	**Ag**	**Au**	**Sn**	**As**	
%	91.4–96.9	2.5–8.2	0.1–0.6	0–60 ppm	<0.1	<0.1	

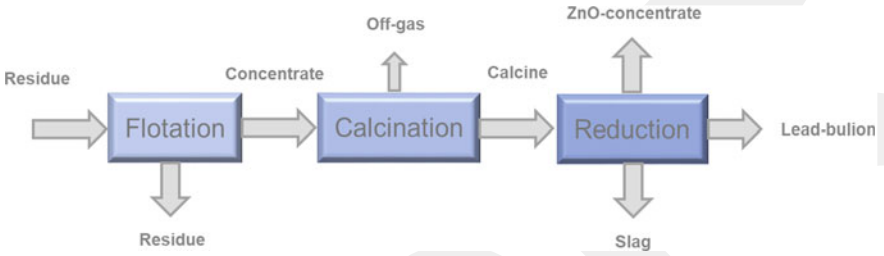

Fig. 4 Adapted scheme of the developed process including a beneficiation step

The big gap between the minimum and maximum yield for lead results out of the fact that in some trials lead was not successfully separated and formed small droplets in the resulting slag.

Together with specialists in building and construction materials, various tests have been started to evaluate the possibility to utilize the resulting slag. First tests were done on replacing up to 25% of sand in concrete by the produced slag. Mechanical properties showed similar or even improved values compared with standard concrete mixtures. Leaching tests were satisfying with the exemption of lead, which resulted in values above the permissible limit for slags with high remaining lead contents. Optimization of the slag properties to meet such requirements is ongoing.

One important step that would increase considerably the economy of such a concept is the possible concentration of valuable metals by means of beneficiation. An example of an adapted process scheme can be found in Fig. 4.

Mineral Processing

As already described in the chapter characterization, a serious intergrowth of the material is present. Also, lead as one of the metals of interest, in many samples, seems to be well distributed between the different phases.

One concept could be the separation of the jarosite particles to increase the valuables in the rest. However, this is only possible, if only a small part of lead and/or silver is present in the formed jarosite.

The second strategy is to remove gangue compounds like silicon oxide, calcium oxide, etc. and/or gypsum, which can be often found in higher amounts, due to the addition of lime, which was done in the past for neutralization.

After investigation of different beneficiation methods, the following conclusions could be drawn.

- Most of the valuables are evenly distributed over the grain size fractions, produced by screening. There is a certain concentration in the bigger grains. However, this fraction is less than 10% of the overall material and its separation does not lead to an economic benefit. This leads to the fact that no concentration via separation into different corn fractions is possible.
- Standard magnetic separation was without any effect on concentration.
- The use of a high gradient magnetic separator (HGMS) allowed a certain concentration of copper and zinc but left lead and silver in the remaining fraction. Due to high costs for the facility itself and the necessity to have all valuables in one concentrate, this option has not been pursued.
- Flotation showed the option to remove gangue material, and in case the jarosite mineral itself does not contain too much valuables, a separation between the jarosite mineral and the rest could be possible.

Flotation—Tests

Flotation tests were performed on different samples out of various dumps.

Due to the fineness of the jarosite precipitates, flotation is seen to represent the most promising beneficiation technique. To successfully apply flotation, several challenges must be overcome, such as

- operating flotation in an extremely high ionic strength environment. It is known that high salinity of the pulp significantly affects the flotation process
- due to the fine particle size distribution of the solids, long residence times might be required to achieve a satisfying recovery of the material to be floated. The application of pneumatic flotation cells might increase the overall flotation performance and in particular the grade of the froth product
- due to the complex chemistry in the pulp, changes of the surface chemistry of the particle are very likely to appear by the forming of layers of undefined structure and chemistry on the “mineral” surface caused by precipitation
- the forming of microflocs is an issue as non-floating particles will be locked in flocs built up by hydrophobic particles resulting in a depressed concentrate grade
- the development of a reagent regime which allows to achieve the highest possible selectivity between “gangue minerals” and “ore minerals” and which is applicable for a process being fed with a highly variable feed in terms of “mineralogy” and taking place in an aqueous phase of undefined chemistry.

The testwork was performed in a standard Denver D12 flotation machine. As the flotation cell is self-aerated, the rotational speed of the rotor was adjusted so that the superficial gas velocity in the laboratory cell is comparable to industrial scale flotation machines. The chemical grades of Pb, Zn, Cu, Fe, and Ag were analysed by means of atomic absorption spectroscopy (AAS).

Flotation—Results

First tests on a jarosite, trying to separate the jarosite mineral itself from the rest, failed. Lead seems to be evenly distributed over the different phases, and especially, the jarosite mineral seems to host lead, e.g. in form of plumbojarosite. Figure 5 shows how the lead recovery follows the weight recovery to the concentrate, and what finally makes a separation impossible.

Similar results were achieved for silver, while copper and zinc showed a certain but still inefficient concentration. Materials from other dumps gave slightly better results, maybe because they host less lead and other metals in the jarosite mineral. However, concentration was low and needs to be greatly improved, if possible, before the procedure can be considered as successful.

In case gangue material is present in higher extent, what might be caused by a mixture with leaching residue, or if gypsum is high, the residue shows a good potential to be concentrated by separating such compounds. Flotation tests with such materials allowed especially the concentration of lead, silver, and copper. Zinc was also concentrated but less successful compared to the other metals.

Figure 6 illustrates the results for one zinc smelter residue that contained around 4% zinc, 7.5% lead, 0.7% copper, and 250 ppm silver before flotation.

From Fig. 6 it can be seen that around 85% of lead, silver, and copper were collected in the concentrate, which amount was 58% of the overall mass. As mentioned,

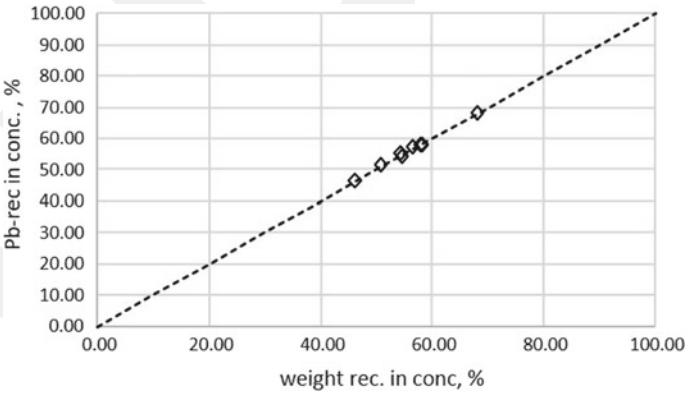

Fig. 5 Summary of the lead recovery achieved with different reagent regimes and parameter settings

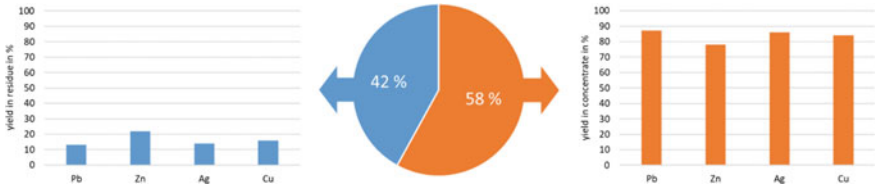

Fig. 6 Separation of metals into concentrate (58 wt%, right) and residue (42 wt%, left) by flotation

zinc with 77% was less successful but is anyway present in a smaller amount in the charged material. Considering that only first tentative trials have been performed and there is definitely room for improvement, the result for this type of material is quite satisfying.

Economic Considerations

As mentioned in the introduction, different valuables could be recovered from residues out of hydrometallurgical zinc winning. Additional value could be generated by saving landfilling costs, where applicable. In Europe, for example, landfilling costs between 15 and 40 USD per ton of jarosite residue are reported. Figure 7 shows theoretically recoverable values, considering a residue with 5% zinc, 6.5% lead, 0.5% copper, and 250 ppm silver. The diagram on the left shows the metal content multiplied with the London Metal Exchange (LME) notation in one bar. The second lower bar shows the same corrected by a factor that takes into account the reduced value of an intermediate product which has to be sold to primary industry (e.g. zinc oxide, lead bouillon containing impurities, etc.). The diagram on the right gives the split between the different values and illustrates their contribution to the overall revenue.

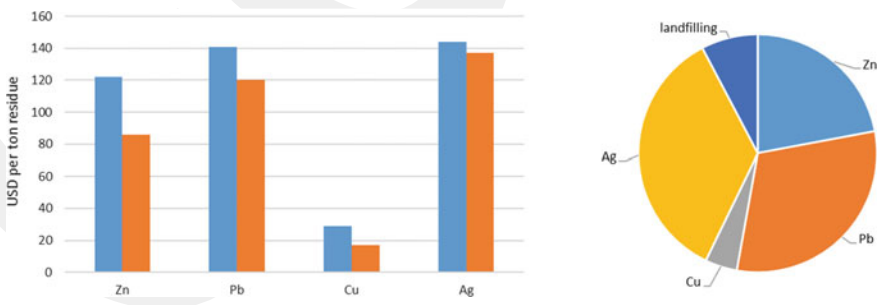

Fig. 7 Calculation of possible revenues out of an investigated jarosite residue (left), and split of possible revenue values (right)

Including landfilling, the overall revenue of 390 USD per ton of residue can be calculated. Due to current metal prices, silver is of main importance. In all the calculations, the metal yield of the process has not been considered. Taking about 90% into consideration, the value is reduced to 350 USD per ton. This would allow an economic treatment using the described pyrometallurgical process. However, there are of course dumps with lower amounts of valuable elements. In this case, a beneficiation would help to reduce energy costs and allow an economic processing also with lower metal concentrations. Gold could play an important role. If only 2 ppm is collected, additional 100 USD can be added to the revenue.

Summary

Zinc leach residues, often called jarosite, are dumped worldwide. University of Leoben together with industry has developed a process for the recovery of valuable metals. The process has been tested and up-scaled. Furthermore, detailed characterization has been carried out for different dumpsites. To allow better economic conditions by saving energy, the first tests for possible beneficiation have been performed. Only for some residues, a concentration of valuables was possible. Economics showed positive values for metal rich leach residue types while for lower metal, especially lower silver concentrations, a concentration by flotation is mandatory.

References

1. Reuter MA, UNEP (2013) Metal recycling: opportunities, limits, infrastructure, international resource panel
2. Patino F, Salinas E, Cruells M, Roca A (1998) Alkaline decomposition–cyanidation kinetics of argentian natrojarosite. Hydrometallurgy 49:323–336
3. Hanke G, Melcher F, Antrekowitsch J (2016) Characterisation of by-products of the zinc industry. In: OPMR 2016 Opportunities in processing of metal resources in South East Europe, pp 184–190

Leaching of Turkish Oxidized Pb–Zn Flotation Tailings by Inorganic and Organic Acids

Muammer Kaya, Sait Kursunoglu, Shokrullah Hussaini and Erkan Gül

Abstract An eco-friendly approach and simultaneous recovery of metals from mine tailings is still a significant challenge. This study investigates the extraction of zinc metal from the Kayseri region oxidized lead-zinc (Pb–Zn) flotation tailings by leaching using three different inorganic acids (HNO_3, HCl, and H_2SO_4) and six different organic acids (citric (CA), oxalic (OA), formic (FA), ascorbic (AA), malic (MA), and tartaric (TA) acids). The effects of acid type and concentration, leaching temperature and time, and solid/liquid (S/L) ratio were studied for maximum Zn dissolution and minimum Pb, Fe, and As co-dissolution at lowest temperature and leaching time. For inorganic acids at 1/10 S/L ratio, 1.0 M H_2SO_4 and HCl concentrations achieved 92% Zn + 0% Pb + 12% Fe at 40 °C leaching temperature and 60 min leaching time and 92% Zn + 10% Pb + 0% Fe at 80 °C leaching temperature and 30 min leaching time, respectively. For organic acids, at 1/10 S/L ratio and 1.0 M concentration, 92% Zn + 8.3% Pb with malic acid at 80 °C leaching temperature and 180 min leaching time and 91% Zn + 12% Pb with citric acid at 60 °C leaching temperature and 180 min leaching time were achieved. 1.0 M formic acid dissolved about 83% Zn + 2.8% Pb at 80 °C and 180 min leaching time. More than 90% Zn dissolution can be succeeded by using either inorganic acids at 40 °C for 30–60 min leaching time or organic acids at 60–80 °C for 180 min leaching time. Oxalic acid significantly dissolved Fe and As without Zn and Pb dissolution.

Keywords Oxidized Pb–Zn flotation tails · Leaching · Inorganic acids · Organic acids · Zn extraction

M. Kaya (✉) · S. Hussaini · E. Gül
Mining Engineering Department, Eskisehir Osmangazi University, Eskişehir, Turkey
e-mail: mkaya@ogu.edu.tr

S. Kursunoglu
Material Science and Nanotechnology Engineering Department, Abdullah Gül University, Kayseri, Turkey

© The Minerals, Metals & Materials Society 2020

A. Siegmund et al. (eds.), *PbZn 2020: 9th International Symposium on Lead and Zinc Processing*, The Minerals, Metals & Materials Series,
https://doi.org/10.1007/978-3-030-37070-1_39

Introduction

Strengthened environmental legislation has prompted Pb–Zn producers to consider at least three approaches to the problem: (1) Disposal of the oxidized Pb–Zn flotation tails in environmentally stabilized forms. This is accomplished through mixing with cement-forming or silicate-binding additives. (2) Recycling of tailings to recover Zn and Pb units and to produce higher grade concentrates (with minimum impurities such as Fe and As) in smaller quantities for further treatment. (3) Recovery of valuable metals from the tails for economic recovery and detoxification of the residues [1].

Zn is one of the most important non-ferrous metals after aluminum and copper. There is an increasing demand for Zn in the world. Primary (ores) and secondary (tailings, waste) production of Zn can be achieved by hydro- and/or pyro-metallurgical processes. Hydrometallurgical methods mainly contain acid, alkaline, or ammonia leaching. An acid dissociation constant, K_a, (also known as acidity constant or acid-ionization constant) is a quantitative measure of the strength of an acid in solution. It is the equilibrium constant for a chemical reaction known as dissociation in the context of acid–base reactions:

$$K_a = [A^-]^*[H^+]/[HA] \quad (1)$$

For many practical purposes, it is more convenient to discuss the logarithmic constant, pK_a:

$$pK_a = -\log_{10}[K_a] \quad (2)$$

The more positive the value of pK_a, the smaller the extent of dissociation at any given pH—that is, the weaker the acid. A weak acid has a pK_a value in the approximate range -2 to 12 in water. Acids with a pK_a value of less than about -2 are said to be strong acids. Strength of an acid is defined by its pK_a value; the smaller the number, the stronger the acid. The pK_a value of HCl is approximately -7, the pK_a value of H_2SO_4 is approximately -2, and the pK_a value of HNO_3 is approximately 1.3. Acidity constants of inorganic acids tested in this study are in the range of 10^{-3} and 10^{-5}. So HCl is the strongest of all inorganic and organic acids tested. HNO_3 is the weakest inorganic acid. From an environmental point of view, HNO_3 and organic acids should be tested to dissolve flotation tailings. Inorganic sulphuric acid (SA) leaching is the most commonly used process in the Zn–Pb industry today.

In general, leaching efficiency increases with increasing fineness of particles. Flotation tails are ground, and if there is already fine material, then there is no need for further grinding other then deagglomeration. However, fine particles may produce aggregation and cause reduced dispersion problems during leaching. Gravity pre-concentration and/or further flotation concentration of these fine tails are very difficult and not feasible. The increasing demand for Zn and Pb has required intensive studies on new hydrometallurgical processes for extraction of these metals from low grade primary oxide ores or secondary tails. Surface composition, oxidation,

mineralogical alterations, and dissolved ions also affect the floatability of particles. But it seems that the best way to recover the fine valuable metals from Turkish waste material is hydrometallurgical leaching.

Larba et al. (2) used CA as an alternative lixiviant in the presence of NaCl for zinc oxide dissolution [2]. They obtained 70% Zn dissolution at 25 °C, 0.5 M CA concentration, 350 rpm impeller speed, 60 min leaching time, and 50 mL/g L/S ratio. At 50 °C, 90.4% Zn dissolution was obtained at 60 min leaching period with 0.05 M CA concentration. Larba et al. (2) also found that mixtures of 0.05 M CA with 0.05 M chloride anion increased Zn dissolution to 98% at 40 °C in 10 min [2]. Larba et al. (2) found that NaCl or chloride ions both increased the Zn dissolution by 8.6% and significantly reduced leaching time from 60 min to 10 min at 40 °C leaching temperature [2]. Since Larba et al. (2) used pure chemical substance (5%ZnO/αAl_2O_3) in their study, they dissolved only Zn with very dilute CA in 60 min [2]. The presence of chloride anions along with H^+ from CA catalysed the dissolution of Zn and was involved in the rate controlling step. Larba et al. (2) calculated the activation energies for ZnO-citric acid leaching as 45.7 kJ/mol and ZnO-citric acid-chlorides leaching as 96.9 kJ/mol [2].

Boukerche et al. (3) found that 2.0 M nitrates ($NaNO_3$) with 0.5 M citric acid dissolved Zn totally after 30 min while 92% were dissolved in the presence of 2.0 M chlorides (NaCl) after 270 min [3]. SEM analyses have shown the surface morphology corroded/pitted with nitrate anions. Among three anions tested in this study, only sulfates (Na_2SO_4) gave very low Zn dissolution. Furrer and Stumm (4) explained the dissolution process by low molecular weight organic acids as follows: The adsorption of chelating anion (citrate) will transfer a considerable electron density into the coordination sphere of the Zn metal cation (citrate contains several donor atoms that are able of forming mononuclear bi- and polydentate surface chelates) [4]. As a result, Zn metal-oxygen bonds are polarized and weakened consequently lowering the energy barrier for the dissolution of Zn metal atoms. The explanation given above indicates clearly the importance of the anionic species of organic acid (ligand) in the dissolution process. Thus, two kinds of positive species (protons and the positively charged surface of Zn) and two negative species [citrates and anions (Cl^-, NO_3^- and SO_4^{2-})] may react together and simultaneously in several ways: (1) H^+ attack (protons with Zn surface species), (2) anions reactions (Cl^-, NO_3^-, SO_4^{2-} with Zn surface species), (3) citrate complexation with Zn surface species, and (4) H^+ combination with citrates to form molecular citric acid. This shows the complexity of the system studied.

Leaching by organic acids is an attractive alternative that is emerging in green technology for the removal of metals due to the biodegradability of the organic acids and the toxicity of inorganic leaching agents. Organic acids are weak and usually have –COOH. Green organic acid leaching results with CA with and without NaCl, OA, AA, TA, MA, and FA are presented. Reagent type, reagent dosage, leaching temperature, leaching time, and S/L ratio are optimized in the leaching tests. Table 1 shows basic inorganic and tested organic acid properties and chemical bond structures. For inorganic acids acidity changes, $HCl > H_2SO_4 > HNO_3$ and organic acids ascorbic < formic < malic < citric < tartaric < oxalic acids.

Table 1 Inorganic and organic acids molecular structure and properties used in this study Adapted from [6, 7]

Acids	Molecular structure
Common inorganic acids	
Name: **Hydrochloric acid (monoprotic acid)** Formula: HCl Molecular mass: 36.46 g/mol Density: 1.18 g/cm^3 Acidity constant: >1.10^7 (pK_a: −7)	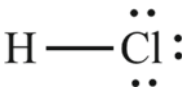
Name: **Sulphuric acid (polyprotic acid)** Formula: H_2SO_4 Molecular mass: 98.079 g/mol Density: 1.83 g/cm^3 Acidity constant: 1 × 10^2 and 1 × 10^{-2} (pK_a: −2)	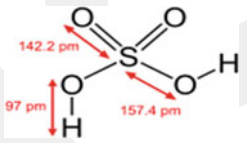
Name: **Nitric acid (monoprotic acid)** Formula: HNO_3 Molecular mass: 63.01 g/mol Density: 1.512 g/cm^3 Acidity constant: 2.3 × 10^1 (pK_a: 1.3)	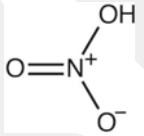
Heteroatom inorganic acids	
Name: **Citric acid—(CA)** Formula: $C_6H_8O_7$ Molecular mass: 192.12 g/mol Density: 1.66 g/cm^3 Solubility in water: 133 g/100 mL at 20 °C Acidity constant: 8.4 × 10^{-4} (pK_{a1}: 3.13)	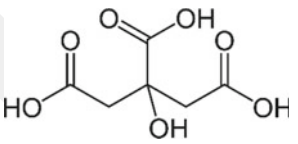
Name: **Malic acid—(MA)** Formula: $C_4H_6O_5$ Molecular mass: 134.09 g/mol Density: 1.609 g/cm^3 Solubility in water: 55.8 g/100 mL at 20 °C Acidity constant: 3.9 × 10^{-4}	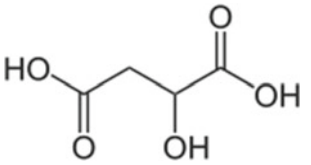

(continued)

Table 1 (continued)

Acids	Molecular structure
Name: **Formic acid—(FA)** Formula: HCOOH Molecular mass: 46.03 g/mol Density: 1.22 g/cm^3 Solubility in water: 10 g/100 mL at 20 °C Acidity constant: 1.78 × 10^{-4} (pK_a: 3.74)	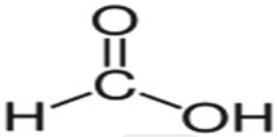
Name: **Tartaric acid—(TA)** Formula: $C_4H_6O_6$ Molecular mass: 150.09 g/mol Density: 1.79 g/cm^3 Solubility in water: 20.6 g/100 mL at 20 °C Acidity constant: 1.0 × 10^{-3}	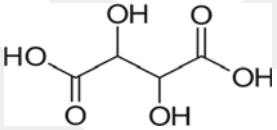
Name: **Oxalic acid—(OA)** Formula: $C_2H_2O_4$ Molecular mass: 90.03 g/mol Density: 1.90 g/cm^3 Solubility in water: 9.0–10.0 g/100/mL at 20 °C Acidity constant: 5.9 × 10^{-2} (pK_a: 1.23)	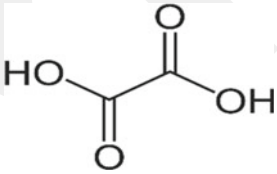
Name: **Ascorbic acid—(AA)** Formula: $C_6H_8O_6$ Molecular mass: 176.12 g/mol Density: 1.65 g/cm^3 Solubility in water: 33.0 g/100 mL at 20 °C Acidity constant: 6.7 × 10^{-5} (pK_{a1}: 4.17)	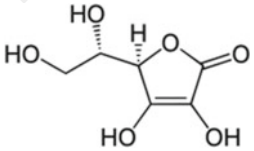

Materials and Methods

Material and Its Characterisation

For this study, 100 kg representative Pb–Zn oxide flotation tailing samples were taken from Kayseri region of Turkey. Dry tailings were collected from tailing dam.

Tailing samples were roll crushed, dried, sieved (−3.175 mm), ball milled 5 min for deagglomeration and dispersion, and then homogenized by mixing. Sample contains 5.3% moisture and has specific density of 3.46 g/cm^3 and surface area of 3456 g/cm^3 [5]. The particle size distribution of the tailing material was determined by Malvern Inst. Mastersizer 2000. d_{10} of Oreks tailing sample was around 1 μm, d_{50} 13 μm, d_{80} 57 μm, and d_{90} 100 μm. As can be seen from the results, almost half of the sample is less than 10 μm in size. Major oxides in the flotation tailing sample were determined using Panalytical Zetium WDXRF. Mineralogical composition and phases of flotation tailing sample were examined using XRD. The major mineral peaks were from smithsonite ($ZnCO_3$) (4%), cerrussite ($PbSO_4$) (0.8%), goethite (FeO(OH)) (2.4%), calcite ($CaCO_3$) (32.2%), quartz (SiO_2) (13.8%), corkite [$PbFe_3[(OH)_6:SO_4:PO_4]$] (7.8%), and beudantite ($PbFe_3(OH)_6SO_4AsO_4$). Flotation tails also contain hemimorphite ($Zn_2SiO_4{\cdot}H_2O$), quartz, dolomite, zinc sulphite hydrate ($ZnSO_4{\cdot}7H_2O$), gypsium, and melanterite ($FeSO_4{\cdot}7H_2O$) as minor phases. In this tailing, smithsonite and cerrussite (i.e. Zn and Pb) are the important and abundant base metals. Major gangue minerals can be goethite, quartz, calcite, and kaolinite. ICP-AES analysis of tailing sample contained 7.50% Pb; 5.77% Zn; 21.3% Fe; 3.91% Ca; 1.92% Al; 1.85% S; 0.66% K; 0.45% Mg; 0.10% Ti; 101 ppm Ag; 101 ppm As > 10,000 ppm Ba; 376 ppm St; 306 ppm Cu; 279 ppm Sb; 245 ppm Cd; 63 ppm Cr; 43 ppm V; 20 ppm Tl, U, and W; <20 ppm Th; 10 ppm Ga, La, and Ni; 9 ppm Mo; <2 ppm Bi; <1 ppm Co, and 0.6 ppm Be. Major metals in flotation tail sample are Pb, Zn, Fe, and As [5]. The particle morphology and surface composition of flotation tails were detected by SEM-EDX analyses. Surface morphology of particles is very rough, porous, and complex. Different shapes and sizes are observed [5].

Method

The sample was not exposed to any metallurgical pre-treatment operations before leaching. Analytical grade Merck/Sigma acids were used in this study. Deionized water was used throughout experimental tests. All leaching experiments were conducted at atmospheric pressure. The leaching experiments were conducted in a magnetically stirred three-necked Pyrex reactor (0.5 dm^3) equipped with a glass reflux condenser inside a temperature controlled extraction mantle (MTops) (Fig. 1).

For each laboratory scale batch leach test, 25 g of solid tailing samples are used with S/L ratio of 1/10 (w/v). Constant 400 rpm stirring speed was used. Particle size was also constant for all tests. In this study sample, the withdrawal method is mainly used. At certain time intervals, 5–10 mL of samples are withdrawn from leach medium and analyzed for dissolved metals while leaching continues until final leaching period. This method is faster and requires less time, samples, and reagents. Samples were immediately vacuum filtered, centrifuged at 5000 rpm, diluted, and stored at 4 °C before Zn, Pb, and Fe (three elements) analyses with AAS at ESOGU and/or Zn, Pb, Fe, As, and Ag (five elements) analyses with ICP at ALS (İzmir). During sample withdrawal, pH of the solution and at the end of leaching test PLS

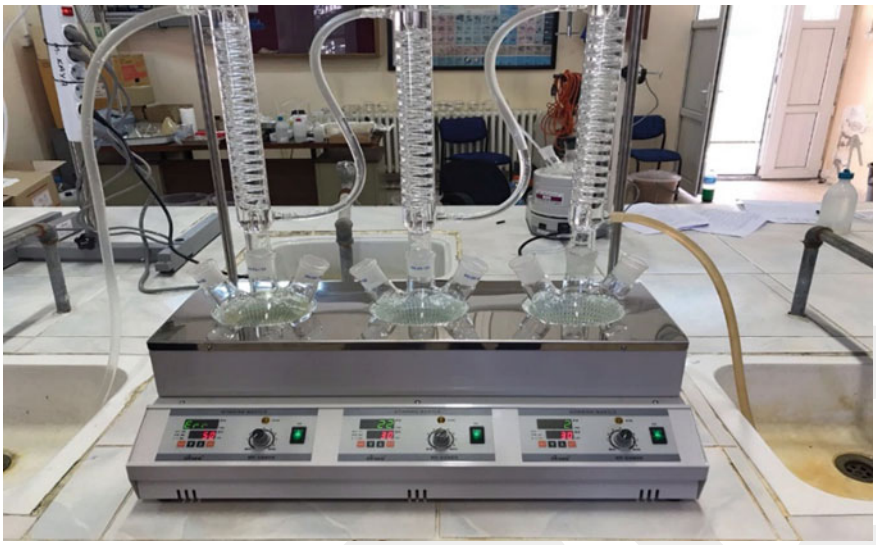

Fig. 1 Digital leaching experimental set-up

of the solution were taken and analyzed for Zn, Pb, and Fe with AAS at ESOGU. Dissolutions of Zn, Pb, As, Ag, and Fe metals were determined as a function of S/L ratio (1:10–1:30 g/mL), acid concentration (0.25–1.0 M), and temperature (40–80 °C) using most common inorganic acids (H_2SO_4, HNO_3, and HCl) and organic acids (CA, MA, OA, FA, AA, and TA). The leaching tests were triplicated to assess the reproducibility of the test results and given 95% confidence interval. The leaching rate/efficiency of metals/metal extraction was calculated from solution analyses (5).

In this study, desired metals will be Zn, Pb, and Ag. Impurities will be As and/or Fe, if Fe is not concentrated (<50%) as a saleable product. Two-step leaching will be performed. Selective dissolution of base metals of Zn and/or Pb will be considered as desired/optimum. In the first stage, optimal dissolution aims to maximize Zn dissolution and minimize the Fe, As, and Pb dissolutions in leach solution. Ag will be dissolved and recovered at the end of the process as much as possible.

Results and Discussion

Inorganic Acid Leach (HCl, H_2SO_4, and HNO_3)

Table 2 shows the effect of leaching temperature from 40 to 80 °C and leaching time from 30 to 120 min on base metal dissolutions using 0.25–1.0 M HCl, H_2SO_4, and HNO_3 as lixiviant at S/L ratio of 1/10 and 400 rpm mixing speed. With HCl and HNO_3, metal dissolution order was Zn > Pb without Fe. With H_2SO_4, metal

Table 2 Optimum metal dissolution results obtained with inorganic acids at 1/10 S/L ratio

HCl	Zn (%)			Pb (%)			Fe (%)		
0.50 M	40 °C	60 °C	80 °C	40 °C	60 °C	80 °C	40 °C	60 °C	80 °C
30 min	78	82	90	10	10	10	0	0	0
1.0 M	40 °C	60 °C	80 °C	40 °C	60 °C	80 °C	40 °C	60 °C	80 °C
30 min	86	90	92	8	10	10	2	5	10
H_2SO_4	Zn (%)			Pb (%)			Fe (%)		
0.5 M	40 °C	60 °C	80 °C	40 °C	60 °C	80 °C	40 °C	60 °C	80 °C
120 min	91	84	90	0	0	0	5	7	9
1.0 M	40 °C	60 °C	80 °C	40 °C	60 °C	80 °C	40 °C	60 °C	80 °C
60 min	92	95	97	0	0	0	12	15	26
HNO_3	Zn (%)			Pb (%)			Fe (%)		
0.25 M	40 °C	60 °C	80 °C	40 °C	60 °C	80 °C	40 °C	60 °C	80 °C
30 min	70	55	42	23	22	22	0	0	0

dissolution order was Zn > Fe without Pb (Kaya et al. 5). At 1/10 S/L ratio, HNO_3 achieved 70% Zn + 23% Pb and 0% Fe dissolutions at 1.0 M dosage, 40 °C leaching temperature, and 30 min leaching time; HCl succeeded 92% Zn + 10% Pb + 10% Fe at 1.0 M dosage, 80 °C leaching temperature, and 30 min leaching time, and 90% Zn + 10% Pb and 0% Fe at 0.5 M dosage, 80 °C leaching temperature, and 30 min leaching time and H_2SO_4 achieved 92% Zn + 0% Pb + 12% Fe at 1.0 M dosage, 40 °C leaching temperature, and 60 min leaching time and 91% Zn + 5% Fe + 0% Pb at 0.5 M dosage, 40 °C leaching temperature, 120 min leaching time. Optimum leaching reagent was 1.0 M H_2SO_4. From three tested inorganic acids, H_2SO_4 achieved the maximum Zn dissolution without Pb co-dissolution at 40 °C and 60 min leaching time.

Citric Acid ($C_6H_8O_7$) Leach in Absence of NaCl

Citric acid ($C_6H_8O_7$ or $CH_2COOH–C(OH)COOH–CH_2COOH$) is a natural weak organic acid with low molecular weight. It is colorless and odorless and has crystalline structure. At room temperature, CA is a white hygroscopic crystalline powder. The pH of the CA is 3.5. Citric acid is an excellent chelating agent, binding metals by making them soluble (i.e. Cu). A citrate is a derivative of CA ($C_3H_5O(COO)_3^{3-}$). Solubility of CA in 100 mL water is 147.76 g at 20 °C, 220 g at 40 °C, and 382.48 g at 80 °C. CA is also considered as non-persistent biodegradable organic product, and its half-life in soil suspension is close to 8 days [2]. These characteristics are considered as advantageous since alone, and at low concentration, it can dissolve effectively ZnO without the risk of pollution or post-treatment. This makes it as a good choice for a more ecological treatment of Zn. The reaction steps between zinc oxide/Zn and CA can be written as follows:

$$C_6H_8O_7(s) + H_2O(l) \leftrightarrow H_3O^+(aq) + C_6H_7O_7^-(aq) \quad (3)$$

$$C_6H_7O_7^-(aq) + H_2O(l) \leftrightarrow H_3O^+(aq) + C_6H_6O_7^{2-}(aq) \quad (4)$$

$$C_6H_6O_7^{2-}(aq) + H_2O(1) \leftrightarrow H_3O^+(aq) + C_6H_5O_7^{3-}(aq) \quad (5)$$

$$3ZnO(s) + 2C_6H_8O_7(aq) \rightarrow 3Zn^{2+}(aq) + 2C_6H_5O_7^3 - (aq) + 3H_2O(l) \quad (6)$$

$$3Zn + 2C_6H_8O_7(aq) \rightarrow 3Zn^{2+} + 3H_2(g) + 2C_6H_5O_7^{3-}(aq) \quad (7)$$

The pK_a values presented in the literature are $pK_1 = 3.128$, $pK_2 = 4.761$, and $pK_3 = 6.396$. Because the pH of the reaction medium was less than 3, a basic reaction was carried out with respect to Eq. 3. Pb-citrate ($Pb_3(C_6H_5O_7)_2$) is almost insoluble. CA is often used because of high efficiency in binding Zn cations [3]. The first group

of CA leaching tests were performed using 0.5 M CA concentration with 25 g Oreks tails at S/L ratio of 1/10. The second group tests were carried out using 0.5 M CA and 0.05 M NaCl. The third group tests were performed under the optimum Zn dissolution results obtained from previous two tests at 1.0 M CA concentration to further increase the Zn dissolution. Pulp temperature was 25, 40, and 60 °C. Leaching time was 30, 60, and 120 min. At the end of leaching tests, one PLS solution was also taken.

Table 3 shows metal dissolutions with 0.5 M citric acid at 1/10 S/L ratio and 400 rpm at different leaching temperatures. Zn dissolution always increased with increasing leaching time and temperature from 44 to 90%. At 25 °C leaching time, Zn dissolution increased from 44 to 50%; at 40 °C, 50 to 61%; at 60 °C, 61 to 75%, and 80 °C 75 to 90% within the tested leaching times. Arsenic is the second most co-dissolved metal up to 80 °C leaching temperature. Fe is the third most co-dissolved metal except for 25 °C. Pb is the least co-dissolved metal except for 25 °C leaching temperature. As co-dissolved from 6.8% up to 14.4%, Fe co-dissolved from 3.6% up to 17.4% and Pb co-dissolved from 4.2% up to 7%. Optimum Zn

Table 3 Metal dissolutions with 0.5 M CA at 1/10 S/L ratio and 400 rpm at different leaching temperatures

Citric acid	Zn (%)	As (%)	Fe (%)	Pb (%)
Time	**25 °C**	**0.5 M**	**1/10 S/L**	**400 rpm**
30 min	44	6.8	3.6	4.2
60 min	47	7.2	4.0	4.4
120 min	50	7.9	4.3	4.6
	Metal	**Dissolution**	**Order**	**Zn > As > Pb > Fe**
Time	**40 °C**	**0.5 M**	**1/10 S/L**	**400 rpm**
30 min	50.1	8.1	4.7	4.9
60 min	55.0	9.0	5.6	5.2
120 min	61.2	9.7	6.6	5.4
	Metal	**Dissolution**	**Order**	**Zn > As > Fe > Pb**
Time	**60 °C**	**0.5 M**	**1/10 S/L**	**400 rpm**
30 min	60.7	10.4	7.7	5.8
60 min	67.7	11.6	9.6	6.0
120 min	74.7	12.7	11.5	6.3
	Metal	**Dissolution**	**Order**	**Zn > As > Fe > Pb**
Time	**80 °C**	**0.5 M**	**1/10 S/L**	**400 rpm**
30 min	74.5	12.8	11.5	6.6
60 min	81.5	13.7	13.9	6.8
120 min	89.6	14.4	16.3	7.0
180 min	**90.1**	**14.2**	**17.4**	**6.8**
	Metal	**Dissolution**	**Order**	**Zn > Fe > As > Pb**

dissolution was obtained at 0.5 M CA concentration, 80 °C leaching temperature, and 1/10 S/L ratio under tested conditions with Oreks flotation tails. More than 90% Zn dissolution was achieved with 17.4% Fe, 14.2% As, and 7% Pb co-dissolutions. Up to 80 °C leaching time and 120 min leaching time, there was an increase in Zn dissolution; but at 180 min leaching time, Zn dissolution almost reaches a plateau. With increasing temperature, Fe > As > Pb co-dissolutions increase. Up to 60 °C leaching temperature, As is the second most co-dissolved metal. At 80 °C and 60 min leaching time, Fe co-dissolution exceeds As co-dissolution. At 80 °C leaching time, Pb co-dissolution remains almost constant at 7% for 3 h leaching period. Maximum 90.1% Zn dissolution with 14.2% As, 17.4% Fe, and 6.8% Pb co-dissolutions was obtained using 0.5 M citric acid concentration at 80 °C leaching temperature and 180 min leaching time. Metal dissolution selectivity difference between Zn and As was 75.9%, between Zn and Fe 72.7%, and Zn and Pb 83.3%.

As the leaching time and temperature increase, Zn dissolution increases significantly, and As, Fe, and Pb dissolutions slightly increased. Most of the organic acids solubility increases with increasing temperature. Increase in Zn dissolution was highest in the first 30 min, and after that, there was a slight increase in the Zn dissolution. pH values of the solution increase in the first 30 min indicating the consumption of H^+ ions. After 30 min, pH values reach a plateau suggesting very slight contribution of H^+ ions in the dissolution reactions. After 30 min leaching, anions in the solution interact with solid surface for dissolution.

Table 4 compares the effect of % solid on metal extractions at the 0.5 M CA concentration and 80 °C leaching temperature for different leaching times. Under these test conditions, as the leaching time increases Zn dissolution increases significantly. With increasing S/L ratio, Zn dissolution slightly decreases at 2/10 and significantly decreases at 3/10 S/L ratio. As % solid increases, As, Fe, and Pb co-dissolutions also decrease. Ag dissolution was zero with CA for all conditions. At S/L ratio of 1/10, 75%; at 2/10, 53%, and 3/10 41% Zn dissolution was obtained for 30 min leaching time. At S/L ratio of 1/10, 90%; at 2/10, 88%; and at 3/10, 34% Zn dissolution was obtained for 180 min leaching time. At S/L ratio of 3/10, Zn dissolution drastically decreased along with very low Pb, As, and Fe co-dissolutions. Table 4 also shows the PLS analyses results after 180 min leaching time. Metal dissolution rates for 1/10 S/L ratio is much closer to 180 min leaching results than 2/10 S/L ratio. The decrease in metal dissolutions with increasing solid % is due to less lixiviant in the medium. The best condition was 0.5 M CA concentration, at 80 °C leaching temperature, and 1/10 S/L ratio. 1/10 S/L ratio requires about 40 g/L CA usage.

Since higher quantities of Zn are leached at higher S/L ratios, the ionic strength (concentration of total ions in the solution) of the resultant solution increases. Solubility is affected by the ionic strength of the solution in that, as the solution's ionic strength increases, the solubility will be decreased (if the ions are like ions). Thus, in the case of higher S/L ratios, the solubility decreases as the ions are leached from the solids. Since there are more ions to be leached (due to the presence of more solids), a lower percentage of the ions can be leached, because the ionic strength and viscosity of the solution will increase as more ions are leached [8]. Herrero et al. (9) found that decreasing the S/L ratio increased the percentage of metal leached, due to the

Table 4 Effect of S/L ratio on metal dissolution at 0.5 M CA concentration and 80 °C leaching temperature

Citric acid (CA)	Zn (%)	As (%)	Fe (%)	Pb (%)
S/L ratio: 1/10, time	**80 °C**	**0.5 M**	**1/10 S/L**	**400 rpm**
30 min	74.5	12.8	11.5	6.6
60 min	81.5	13.7	13.9	6.8
120 min	89.9	14.4	16.3	7.0
180 min	**90.1**	**14.2**	**17.4**	**6.8**
	Metal	**Dissolution**	**Order**	**Zn > As > Pb > Fe**
S/L ratio: 2/10, time	**80 °C**	**0.5 M**	**2/10 S/L**	**400 rpm**
30 min	53.3	10.2	10.6	4.3
60 min	63.0	10.8	12.5	4.4
120 min	74.8	11.7	14.8	4.6
180 min	88.0	12.4	17.2	4.8
PLS	70.9	10.3	14.5	4.8
	Metal	**Dissolution**	**Order**	**Zn > Fe > As > Pb**
S/L ratio: 3/10, time	**80 °C**	**0.5 M**	**3/10 S/L**	**400 rpm**
60 min	41.3	7.3	10.1	3.0
120 min	49.5	7.3	11.6	1.5
180 min	46.9	7.3	11.1	0.9
240 min	34.0	6.5	11.1	0.6
PLS	30.4	6.5	11.8	0.6
	Metal	**Dissolution**	**Order**	**Zn > Fe > As > Pb**

presence of a greater amount of lixiviant per unit of solids and, therefore, a greater chance of solid-liquid contact [9]. In addition, at higher S/L ratios, because of the high Zn quantities leached for the amount of solution available, the solution became saturated with Zn, preventing more Zn from being leached and limiting the overall Zn recovery. Studies involving the leaching of electric arc furnace dust (EAFD) have shown that increasing the solution density decreases the percentage of the Zn that is dissolved [10]. Decreasing S/L ratio, not only decreases the suspension density, but also reduces the viscosity of the whole system and therefore decreases the mass transfer resistance at the solid-liquid interface [11]. Metal dissolution decreases with increasing S/L ratio due to the faster saturation of the liquid. Ruşen et al. [12], on the other hand, found that decreasing slurry density had little effect on Zn extraction, resulting in only about 3% increase in Zn extraction, when the density was lowered by 100 g/l [12].

Increasing CA concentration from 0.5 to 1.0 M at 1/10 S/L ratio at 60 °C and 80 °C significantly increased Zn dissolution (Table 5). 1.0 M CA dissolved maximum 84.4% Zn as opposed to 74.7% with 0.5 M CA dosage at 120 min leaching time and 60 °C leaching temperature. At 80 °C leaching temperature, maximum Zn dissolution

Table 5 Metal dissolution with 1.0 M CA concentration at 1/10 S/L ratio at 60 and 80 °C leaching temperatures

Citric acid (CA)	Zn (%)	As (%)	Fe (%)	Pb (%)
Time	**60 °C**	**1.0 M**	**1/10 S/L**	**400 rpm**
30 min	72.6	12.5	9.2	9.9
60 min	80.0	13.2	11.1	10.5
120 min	**84.4**	14.7	12.8	10.9
	Metal	**Dissolution**	**Order**	**Zn > As > Fe > Pb**
Time	**80 °C**	**1.0 M**	**1/10 S/L**	**400 rpm**
30 min	83.5	14.0	11.0	10.0
60 min	89.1	15.0	13.0	11.0
120 min	90.6	16.0	17.0	11.0
180 min	**91.0**	**17.0**	**19.0**	**12.0**
	Metal	**Dissolution**	**Order**	**Zn > Fe > As > Pb**

of 91% was obtained with 1.0 M CA concentration which is slightly higher than 0.5 M CA dosage. Increasing CA concentration also increases As, Fe, and Pb co-dissolutions. Metal dissolution order was Zn > As > Fe > Pb at 1.0 M CA dosage and 60 °C and Zn > Fe > As > Pb at 80 °C leaching temperatures. At 1.0 M CA dosage, maximum 91% Zn dissolution was achieved with 17% As, 19% Fe and 12% Pb co-dissolutions. Selectivity between Zn and As dissolutions was 74%, between Zn and Fe 72%, and between Zn and Pb 79%. Increase in CA concentration has positive effect on Zn dissolution at the expense of more Pb, As, and Fe co-dissolution.

Table 6 shows the effect of S/L ratio on metal dissolution at 1.0 M CA concentration and 80 °C leaching temperature. Similar results obtained for 0.5 M CA concentration was obtained for 1.0 M CA dosage. 1/10 and 2/10 S/L ratios gave similar Zn extraction at slightly different Fe, As, and Pb co-dissolutions. Zn dissolution was low at 3/10 S/L ratio. At 1.0 M CA concentration, 80 °C leaching time, different S/L ratios and leaching times, pH of the medium was changed between 2 and 3. As the S/L ratio increased, pH of the medium increased, but Zn dissolution and Fe, As, and Pb co-dissolutions decreased. pH of the medium is less acidic with organic CA than inorganic H_2SO_4 leach (0.5–1.0). Theoretically, since Zn is leached Zn^{2+} at the low pH values involved in acid leaching, the solution would become saturated with Zn ions, if the S/L ratio was too high.

Figure 2 shows the colour difference of PLS using CA and H_2SO_4. CA-leached PLS is green and H_2SO_4-leached PLS is yellowish. Our Zn dissolution was 47% at 25 °C and 68% at 60 °C with 0.5 M CA concentration which are lower than Larba et al. (2) results. In our flotation tailing samples, we have carbonate, oxide, and hydroxide minerals of Zn, Pb, Fe, As, etc. So our Zn dissolution was lower than their results.

Table 6 Effect of S/L ratio on metal dissolution at 1.0 M CA concentration and 80 °C leaching temperature

Citric acid (CA)	Zn (%)	As (%)	Fe (%)	Pb (%)
S/L ratio: 1/10, time	**80 °C**	**1.0 M**	**1/10 S/L**	**400 rpm**
30 min	83.5	14.0	11.0	10.0
60 min	89.1	15.0	13.0	11.0
120 min	90.6	16.0	17.0	11.0
180 min	**91.0**	**17.0**	**19.0**	**12.0**
	Metal	**Dissolution**	**Order**	**Zn > Fe > As > Pb**
S/L ratio: 2/10, time	**80 °C**	**1.0 M**	**2/10 S/L**	**400 rpm**
30 min	72.0	12.0	11.0	8.0
60 min	79.4	13.0	14.0	8.0
120 min	88.0	14.0	17.0	9.0
180 min	**90.6**	**15.0**	**20.0**	**10.0**
	Metal	**Dissolution**	**Order**	**Zn > Fe > As > Pb**
S/L ratio: 3/10, time	**80 °C**	**1.0 M**	**3/10 S/L**	**400 rpm**
60 min	64.7	11.0	11.0	6.0
120 min	69.0	12.0	13.0	7.0
180 min	80.0	13.0	16.0	7.0
240 min	82.6	13.0	18.0	7.0
PLS	78.3	11.2	17.8	7.0
	Metal	**Dissolution**	**Order**	**Zn > Fe > As > Pb**

Fig. 2 PLS of citric (left) and H_2SO_4 (right) leach solutions

Citric Acid ($C_6H_8O_7$) Leach in Presence of NaCl

The effects of 0.5 M CA and 0.05 M and 2.0 M NaCl mixtures on metal dissolutions were determined. At 0.5 M CA and 0.05 M NaCl concentrations and 25 °C leaching temperature, Zn dissolution was 41.6% at 30 min and 48.6% at 120 min Pb co-dissolution was 4.3% at 30 min and 5.3% at 120 min Fe co-dissolution was 6.4% at 30 min and 7.9% at 120 min. As co-dissolution was 9.5% at 30 min and 11.3% at 120 min (Table 7). As co-dissolution was again higher than both Fe and Pb with CA+NaCl mixture addition. Metal extraction order changed as Zn > As > Fe > Pb under these conditions for all tested temperatures. At the highest Zn extraction of 48.6, 11.3% As, 7.9% Fe, and 5.3% Pb were co-dissolved. Presence of NaCl decreased the Zn dissolution from 49.6 to 48.6% and increased As co-dissolution from 7.9 to 11.3%, Fe co-dissolution from 4.3 to 7.9%, and Pb co-dissolution from 4.6 to 5.3%. For our tails, NaCl addition to CA had negative effect on both Zn dissolution and impurity co-dissolutions. Increasing leaching temperature to 40 and 60 °C increased both Zn dissolution and As, Fe, and Pb co-dissolutions with increasing leaching time. Maximum 74% Zn dissolution with 16.5% Fe, 15.9% As, and 7.5% Pb co-dissolutions at 60 °C for 120 min leaching time was achieved using 0.5 M CA + 0.05 M NaCl addition. Without NaCl addition, 74.7% Zn dissolution with 12.7% As,

Table 7 Comparison of metal dissolutions with CA in the presence and absence of NaCl at 1/10 S/L ratio

Citric acid + NaCl	Zn (%)	As (%)	Fe (%)	Pb (%)
0.5 M CA + 0.05 M NaCl	**25 °C**		**1/10 S/L**	**400 rpm**
30 min	41.6	9.5	6.4	4.3
60 min	45.0	10.0	7.0	4.8
120 min	48.6	11.3	7.9	5.3
Only 0.5 M CA	49.6	7.9	4.3	4.6
	Metal	**Dissolution**	**Order**	**Zn > As > Fe > Pb**
0.5 M CA + 0.05 M NaCl	**40 °C**		**1/10 S/L**	**400 rpm**
30 min	49.1	11.5	8.3	5.6
60 min	53.0	13.0	10.0	6.0
120 min	58.4	14.2	11.3	6.5
Only 0.5 M CA	61.26	9.7	6.6	5.4
	Metal	**Dissolution**	**Order**	**Zn > As > Fe > Pb**
0.5 M CA+ 0.05 M NaCl	**60 °C**		**1/10 S/L**	**400 rpm**
30 min 60 min 120 min	58.1 65.0 74.0	14.5 15.2 15.9	11.9 13.0 16.5	7.2 7.4 7.5
Only 0.5 M CA	74.7	12.7	11.5	6.3
	Metal	**Dissolution**	**Order**	**Zn > As > Fe > Pb**

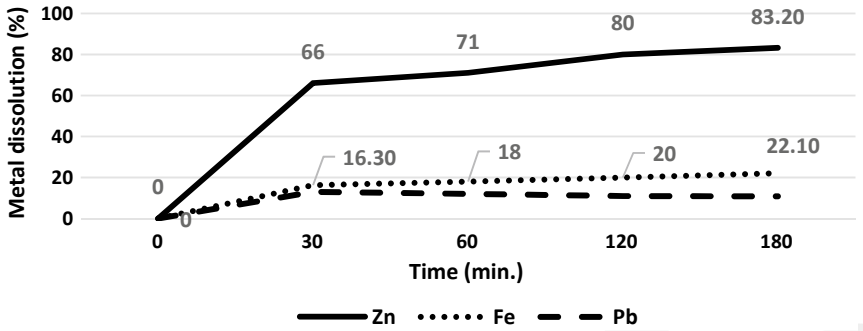

Fig. 3 Metal dissolutions with 0.5 M CA + 2.0 M NaCl at 80 °C and 2/10 S/L ratio

11.5% Fe, and 6.3% Pb was obtained. Thus, the addition of NaCl to citric acid was not used any more.

Since Zn dissolution was lower than 75%, NaCl dosage was increased to 2.0 M, leach temperature 80 °C, and S/L ratio 2/10 at 0.5 M CA concentration. Figure 3 shows metal dissolutions at 0.5 M CA and 2.0 M NaCl mixture at 80 °C leaching temperature and 2/10 S/L ratio. Metal dissolution order was Zn > Fe > Pb. As the leaching time increases, Zn and Fe metal dissolutions increase, but Pb dissolutions decrease. At 30 min leaching time, Zn, Fe, and Pb dissolutions were 66, 16.3, and 13%, respectively. At 180 min leaching time, Zn, Fe, and Pb dissolutions were 83.2, 22.1, and 10.8%, respectively. About 28.2% of the feed material was leached and medium pH was between 2.5 and 2.6. Increasing NaCl dosage and leach temperature along with solid ratio did not improve Zn dissolution more than 83% with much higher Fe and Pb co-dissolutions. Therefore, the addition of NaCl into CA was neglected. For our samples, addition of NaCl into CA reduced the Zn dissolution and significantly increased impurity Fe and As co-dissolutions. Therefore, addition of NaCl to CA to leach our samples is not desirable. Maximum 75% Zn dissolution with 0.5 M CA at 2 h and 60 °C was not sufficient for our objectives.

Oxalic Acid (OA) Leach

Oxalic acid undergoes many of the reactions characteristic of other carboxylic acids. It forms esters such as dimethyl oxalate. It forms an acid chloride called oxalyl chloride. Oxalate, the conjugate base of OA, is an excellent ligand for metal ions. The dissolution of Fe complexes in OA can be expressed as follows:

$$H_2C_2O_4 \rightarrow H^+ + HC_2O_4^- \rightarrow 2H^+ + C_2O_4^{2-} \tag{8}$$

$$Fe^{2+} + C_2O_4^{2-} + 2H_2O \rightarrow FeC_2O_4 \cdot 2H_2O \tag{9}$$

$$Fe_2O_3 + 2HC_2O_4^- + 4H^+ \rightarrow 2Fe(C_2O_4)^+ + 3H_2O \quad (10)$$

The OA acts as a strong complexing agent for the metallic cations. OA has the strongest capacity to dissolve Fe and As. Acidification, complexation, and reductive dissolution play a critical role in dissolution of Fe, As, and other trace metals in the presence of OA. For Zn, Cu, and Mn, acidification-driven dissolution is likely to be dominant while complexation might play a major role in Pb dissolution. The formation of soluble Fe and Pb oxalate complexes effectively prevent solid Fe and Pb arsenate or arsenite [13]. Dissolution of As and trace metals by six organic acids (citric, acetic, formic, malic, oxalic, and tartaric) was determined. OA dissolved metals in the following order Fe > As > Mn > Pb > Cu > Zn. Zn-oxalate ($ZnC_2O_4 \cdot 2H_2O$) has a very low solubility of 1.38×10^{-9} at 20 °C. Pb-oxalate (PbC_2O_4/($Pb(C(COO)_2)_2$)) solubility product at 18 °C is 2.74×10^{-11}, which is insoluble.

The effects of 1.0 M OA on metal dissolutions at 25, 40, and 60 °C leaching temperatures were determined at 1/10 S/L ratio. Figures 4a, b, and c show metal dissolutions as a function of leaching time. Fe and As dissolve while Zn, Pb, and Ag did not dissolve with OA. Fe and As dissolutions are about 50% in the first 30 min and then remained almost constant up to 180 min at 25 °C. With increasing leaching temperature to 40 °C, Fe and As dissolutions slightly increased between 50 and 70%. At 60 °C, 96% Fe and 69% As dissolutions were obtained at 180 min with 2.9% Zn and 3.2% Pb co-dissolutions. Generally, increasing both leaching temperature and time increased Fe and As dissolutions. At ambient leaching temperature, Fe and As dissolutions were similar. With increasing leaching temperature and time, Fe dissolution increases more than As. At 60 °C, dissolution difference between Fe and As was more than 25% at 180 min leaching time. There was no significant pH variation in the solution medium at different leaching temperatures with OA. pH was changed between 0.7 and 0.9. OA can be used to dissolve impurities Fe and As without dissolving valuable Zn, Pb, and Ag metals. Optimum results with OA were obtained at 1.0 M concentration at 60 °C leaching temperature, 180 min leaching time, and S/L ratio of 1/10.

The effect of % solid was determined at 60 °C leaching temperature at 1.0 M OA dosage. Table 8 shows the comparison of the metal dissolutions at different S/L ratios for 180 min leaching time. Fe and As dissolutions significantly decrease with increasing S/L ratio. In dilute solution, 96% Fe and in high percentage solid solution, only 30% Fe dissolves. Arsenic dissolution also dropped from 69 to 25% with S/L ratio of 3/10. Increasing S/L ratio slightly increased Zn dissolution at almost constant Pb dissolution without any Ag dissolution. Zn-oxalate is more soluble than Pb-oxalate. The best S/L ratio at 60 °C and 1.0 M OA is 1/10.

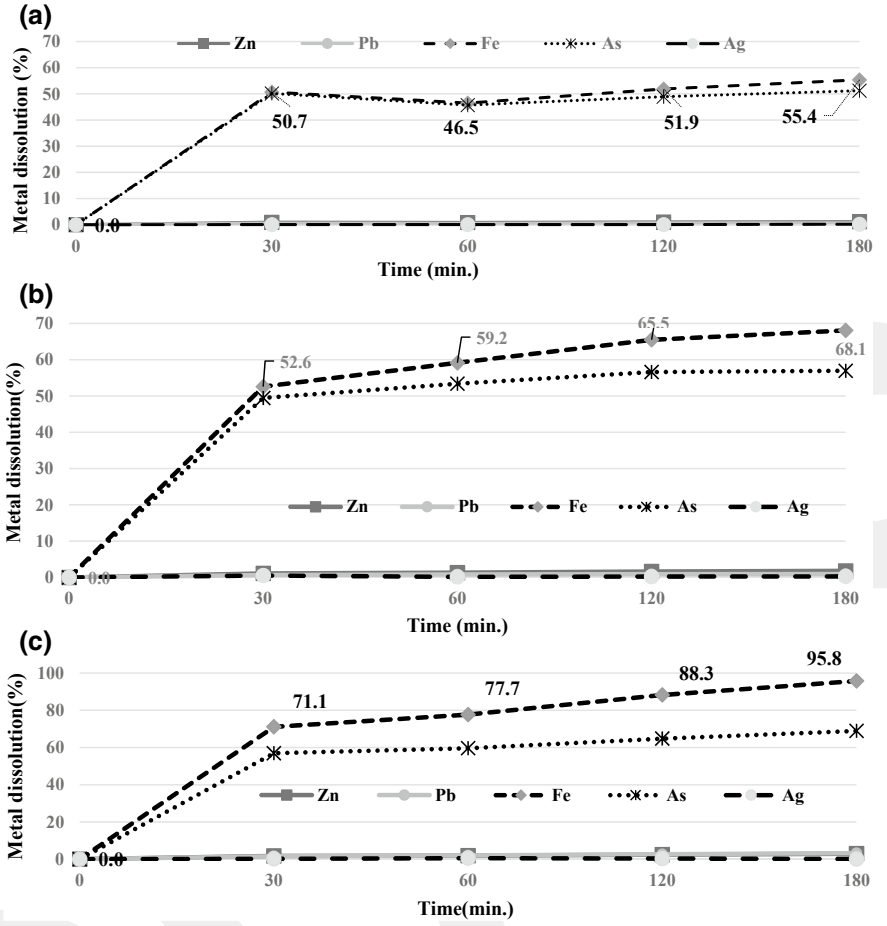

Fig. 4 Metal dissolutions with 1.0 M oxalic acid at S/L ratio of 1/10, **a** 25 °C, **b** 40 °C, and **c** 60 °C

Table 8 Comparison of metal dissolutions at different S/L ratios with OA at 60 °C leaching temperature and 180 min leaching time

1.0 M OA, 60 °C, 180 min	S/L: 1/10	S/L: 2/10	S/L: 3/10
Fe (%)	96.0	55.9	30.0
As (%)	69.0	45.4	25.2
Zn (%)	2.9	3.5	9.0
Pb (%)	3.2	3.4	3.0
Ag (%)	0.0	0.0	0.0

Formic Acid (FA) Leach

Leaching with FA at 1.0 M concentration at 40, 60, and 80 °C was performed at S/L: 1/10 ratio. For 40 °C leaching temperature, at 30 min leaching time 62%, and at 120 min leaching time, 78% Zn dissolution was obtained. At 180 min leaching time, Zn dissolution was 76%. Metal dissolution order was Zn > Pb > Fe. Solution pH changed between 2.8 and 3.0 with formic acid (Table 9). For 60 °C leaching temperature, Zn dissolution increased with increasing leaching time from 74 to 83% at 2.8% Pb co-dissolution. Solution pH was around 3.0. At 80 °C leaching temperature, Zn dissolution increased from 76 to 82% at 4.3% Pb co-dissolution with increasing leaching time from 30 min to 180 min Solution pH was around 3.0. FA achieved maximum 83% Zn dissolution with 3% Pb and without Fe co-dissolution at 60 °C leaching temperature using 1.0 M FA which seems to be selective to only dissolve Zn without Fe and Pb co-dissolutions.

Malic Acid (MA) Leach

Metal dissolutions with 1.0 M MA at 80 °C and 1/10 S/L ratio were given in Fig. 5. Metal dissolution order was Zn > Pb > Fe. Zn and Pb dissolutions were 72.1 and 13.3%, respectively, at 30 min leaching time. 91.6% Zn and 8.1% Pb dissolutions were achieved at 180 min leaching time. 6.4% Fe co-dissolution was maximum at 180 min leaching time. Zn dissolution increased from 30 min to 180 min leaching time. While there was a maximum at 30 min for Pb dissolution, Fe dissolution increases with time up to 6.5% at 180 min pH of the leach medium increased from 2.04 at 30 min to 2.39 at 180 min. The dissolution selectivity difference between Zn and Pb was 84% and between Zn and Fe was 85% at 180 min.

Ascorbic Acid (AA) Leach

The effects of 1.0 M ascorbic acid at 60 °C and 1/10 S/L ratio on metal dissolutions were determined. Metal dissolution order is Zn > Fe > As > Pb > Ag. As the leaching time increases Zn dissolution increased up to 34% at 60 min leaching time and then slightly decreased to about 30% at 180 min. There is a slight increase in Fe, As, and Pb co-dissolutions with increasing leaching time. pH of the leach solution changed from 3.5 to 3.7 with increasing leaching time from 30 min to 180 min. At 1.0 M AA dosage, Zn dissolution was very low and selectivity between Zn and impurity metals for our purposes.

Table 9 Comparison of metal dissolutions with 1.0 M FA at S/L ratio of 1/10 for different leaching temperatures

Formic acid (FA)	40 °C	1.0 M	1/10	60 °C	1.0 M	1/10	80 °C	1.0 M	1/10
Time	**Zn**	**Pb**	**Fe**	**Zn**	**Pb**	**Fe**	**Zn**	**Pb**	**Fe**
30 min	62.1	3	0	74.0	2	0	75.9	2	0
60 min	65.4	4	0	80.1	2	0	78.3	3	0
120 min	78.1	2	0	82.3	3	0	80.2	4	0
180 min	76.3	2	0	**82.6**	**2.8**	**0**	82.3	4.3	0
PLS	73.2	1	0	78.5	3	0	77.9	3	0

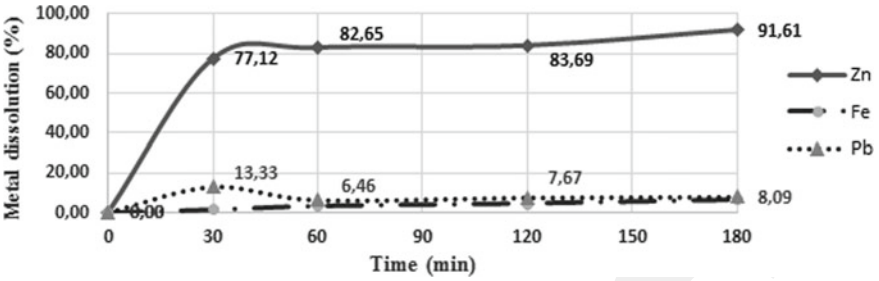

Fig. 5 Metal dissolutions with 1.0 M malic acid at 80 °C and 1/10 S/L ratio

Tartaric Acid (TA) Leach

The effects of 1.0 M TA at 80 °C leaching temperature and 1/10 S/L ratio were determined. 34% Zn dissolution at 30 min and 32% Zn dissolution at 180 min were obtained. Metal dissolution order was Zn > Pb > Fe. Maximum Zn dissolution was achieved at 30 min with 10% Pb and 4.2% Fe dissolutions. Tartaric acid was not a good leach reagent for our purposes. pH was almost constant at 2 for all leaching times.

Conclusions

Table 10 compares and summarizes the optimum leaching results and conditions with respect to maximum Zn dissolution and minimum impurity co-dissolutions using inorganic and organic acids tested in this study. At 1.0 M H_2SO_4, HCl, citric, and

Table 10 Summary and comparison of optimum leaching results

Reagent Metal Dissol. Order	pH	Max. Zn Dissol.	Pb/Ag Dissol.	Selectivity (Zn-Fe) / (Fe-Zn)	Selectivity (Zn-As) / (As-Zn)	Optim. Conditions Conc., S/L, T, t
H_2SO_4 Zn>Fe>As>Pb	**0.5-1.0**	**92 %**	**0%Pb 0%Ag**	**80%**	**72%**	**1M, 1/10, 40°C, 60 min**
HCl Zn>Pb>Fe		**92%**	**10% Pb 0% Ag**	**82%**		**1M, 1/10, 80°C, 30 min**
Malic acid Zn>Pb>Fe	**2.3**	**91.6%**	**8.1%**	**85%**		**1M, 1/10, 80°C, 180 min**
Citric acid Zn>Fe>As>Pb	**2.0-3.0**	**91.0%**	**12%**	**72%**	**74%**	**1M, 1/10, 80°C, 180 min**
Formic acid Zn>Pb>Fe	**3.0**	**82.6%**	**2.8%**	**82%**		**1M, 1/10, 60°C, 180 min**
Oxalic acid Fe>As>Pb>Zn	0.7-0.9	2.9%	3.2%	93.1%	66.1%	1M, 1/10, 60°C, 180 min
Tartaric acid Zn>Pb>Fe	2.0	34.4%	10%	30.2%		1M, 1/10, 80°C, 30 min
Ascorbic acid Zn>Fe>As>Pb	3.5-3.7	32%	3%	19%	23%	1M, 1/10, 60°C, 60 min

malic acids achieved more than 90% Zn dissolution with significant Zn–Fe or Zn–As dissolution difference selectivity at 1/10 S/L ratio for Oreks flotation tails. H_2SO_4 dissolved Zn, As, and Fe without Pb and Ag at 40 °C and 60 min. HCl dissolved similar percent Zn at 10% Pb co-dissolution at higher temperature (80 °C) and shorter time (30 min). 1.0 M malic and citric acids at 1/10 S/L ratio achieves more than 91.6 and 91% Pb and 8 and 12% Pb co-dissolutions respectively at 80 °C and 180 min. Formic acid dissolves about 83% Zn with less than 3% Pb at 60 °C and 180 min leaching time. Zn dissolutions with tartaric, ascorbic, and oxalic acids were very low for 180 min. leaching time and up to 80 °C leaching temperature. Interestingly, oxalic acid dissolved more than 93% Fe and 66% As impurities without significant Zn and Pb dissolution at 60 °C and 180 min leaching time.

Acknowledgements This project was supported by European Union ERA-MIN2-Minteco Project and Turkish Tübitak 217M959.

References

1. Dreisinger DB, Peters E, Morgan G (1990) The hydrometallurgical treatment of carbon steel EAF dust by the UBC-Chaparral process. Hydrometallurgy 25:137–152
2. Larba R, Boukerche I, Alane N, Djerad S, Tifouti L (2013) Citric acid as an alternative lixiviant for zinc oxide dissolution. Hydrometallurgy 134–135:117–123
3. Boukerche I, Djerad S, Larba R, Benmansour L, Tifouti L (2018) Dissolution behavior of metallic zinc in organic acid. Env Res Tech 1(3):11–18
4. Furrer G, Stumm W (1986) The coordination chemistry of weathering: I. dissolution kinetics of δAl_2O_3 and BeO. Geochim Cosmochim Acta 50:1847–1860
5. Kaya M, Gul E, Kursunoglu S, Hussaini S (2019) Leaching of oxidized Turkish Pb–Zn flotation tails by inorganic acids, IMPC-Eurasia-2019 Congress, Antalya-Turkey
6. https://www2.chemistry.msu.edu/faculty/reusch/VirtTxtJml/acidity2.html
7. https://www.wikipedia.org
8. Lottering C (2016) Leaching of secondary zinc oxides using sulphuric acid, M. Eng. Thesis. University of Stellenbosch, S.A., 116 p
9. Herroro D, Arias PL, Güemaz B, Barrio VL, Cambra JF, Requies J (2010) Hydrometallurgical process development fort he production of a zinc sulphate liquor suitable for electrowinning. Miners Eng 23:511–517
10. Havlik T, Souza BV, Bernardes AM, Schneider IA, Miškufová H (2006) Hydrometallurgical processing of carbon steel EAF dust. J Hazard Mater 53(1–3):311–318
11. Wang L, Mu W, Shen H, Liu S, Zhai Y (2015) Leaching of lead from zinc leach residue in acidic calcium chloride aqueous solution. Int J Miner Metal Mater 22(5):460–465
12. Ruşen A, Sunkar AA, Topkaya Y (2008) Zinc and lead extraction from Çinkur leach residues by using hydrometallurgical method. Hydrometallurgy 93:45–50
13. Nworie OE, Qin J, Lin C (2017) Differential effects of low molecular weight organic acids on th mobility of soil-borne arsenic and trace metals. Toxics 5:18. https://doi.org/10.3390/toxics5030

Numerical Simulation of Gas-Particle Two-Phase Chemical Reactions and Key Structure Optimization in the Lead Flash Smelting Furnace

Kaile Tang, Ling Zhang, Leru Zhang and Fubing Tu

Abstract In this paper, the numerical simulation of the temperature field and the velocity field of the reaction tower in the lead flash smelting furnace was carried out by the numerical simulation. The concentrate particles were tracked by the DPM model, and the particle reaction model was used to trace the particle combustion. The numerical model was verified with the thermocouple data in the industrial furnace, and the percentage error was within 4.5%. The study found that the highest temperature zone located at about 1.5 m from the top of the tower. The highest SO_2 concentration was in 2.5 m below the nozzle. In addition, this paper uses a central single nozzle to analyze the coke area distribution in the furnace which greatly simplified the lead smelting process. It is found that the single nozzle arrangement could have the uniform distribution of coke, which could use in the future design of the furnace.

Keywords Flash smelting · Numerical simulation · Lead smelting furnace

Introduction

The flash lead smelting process [1] has been considered to be the most advanced, mature, and most effective direct lead smelting method in the world today. From the point of view of metallurgical principles, the most important feature of the flash smelting method is the oxidation and reduction atmosphere combined in one furnace. A partition wall is used to divide the flash smelting furnace into the smelting shaft oxidation melting zone and an electric furnace reduction zone. The smelting process is completed in a closed, compact furnace, eliminating the need for a sintering process. Process is continuous and can achieve a high degree of automation, significantly reducing worker operations and reducing production costs the above.

K. Tang (✉) · L. Zhang · L. Zhang
CINF Engineering Co., Ltd., Changsha 410011, Hunan, People's Republic of China
e-mail: 373731806@163.com

F. Tu
Central South University, Changsha 410011, Hunan, People's Republic of China

© The Minerals, Metals & Materials Society 2020

A. Siegmund et al. (eds.), *PbZn 2020: 9th International Symposium on Lead and Zinc Processing*, The Minerals, Metals & Materials Series,
https://doi.org/10.1007/978-3-030-37070-1_40

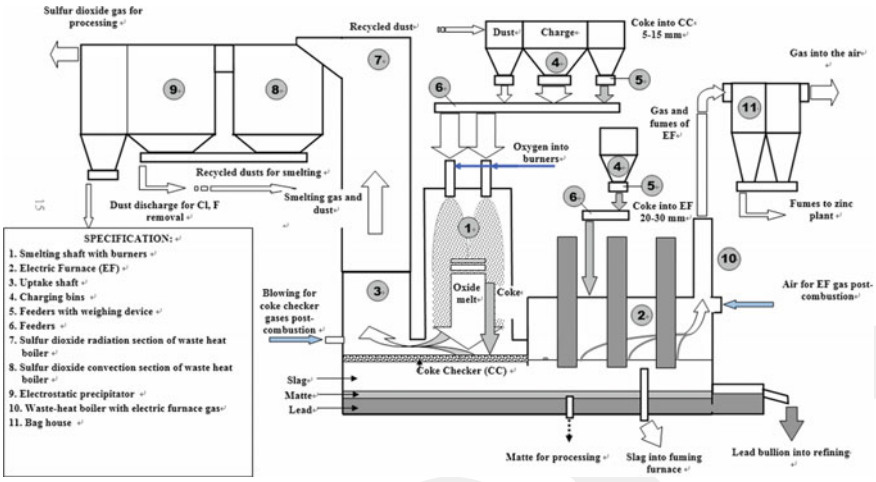

Fig. 1 Schematic of Flash smelting process

The whole process has low energy consumption, low coke consumption, low smoke rate, and high production.

The key component of the flash lead smelting furnace is the top nozzle which used to add the lead concentrate and the coke, and the oxygen-riched air also injected through this nozzle.

The arrangement and the structure of the top nozzle play important role in the whole lead smelting process.

Numerical Models and Boundary Conditions

Geometry and Mesh

The major reaction is happened in the lead flash smelting shaft (as shown in Fig. 1, specification 1). Figure 2 shows the computational domain, concluding the feed burner at the top of the furnace and the uptake shaft connecting the gas flue outlet.

The total mesh number is 2.4 million. The structured mesh was used for the shaft.

Mathematics Model

(1) Continuity equation

Basic control equation for industrial oxygen transfer process, in order to describe the flow and heat transfer between industrial oxygen and material particles in the furnace, is necessary to establish related differential equations, including mass and energy

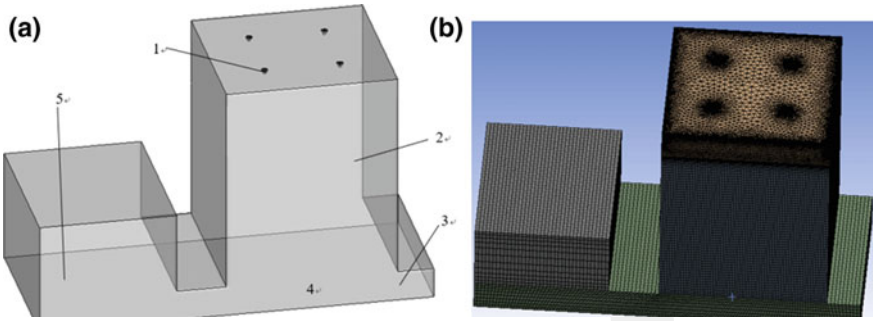

Fig. 2 Geometry and mesh, **a** smelting shaft geometry 1—Nozzle; 2—Shaft; 3—Gas space; 4—melting surface; 5—uptake shaft, **b** mesh

conservation equations, momentum balance equations, and chemical composition equations. These equations can be used in the following general forms:

$$\frac{\partial \rho\varphi}{\partial t} + \frac{\partial}{\partial x_i}(\rho\varphi u_i) = \frac{\partial}{\partial x_i}\left(\Gamma_\varphi \frac{\partial \varphi}{\partial x_i}\right) + S_\varphi + S_{p\varphi}$$

ρ is the density of the fluid; t is the time;
u_i is the velocity in the direction I;
φ is the universal variable;
u_i is the viscosity;
Γ_φ is the index of the transport process.

(2) Discrete phase model

The particle motion uses the discrete phase model (DPM) to track, and the governing equation can be showed as follows:

$$\frac{\mathrm{d}v_p}{\mathrm{d}t} = F_D(v_g - v_p) + \frac{g(\rho_p - \rho_g)}{\rho_p} + F$$

v is the velocity vector;
g gravity acceleration;
F depicts the other force exerted on the particle;
$F_D(v - v_p)$ is the drag force.

(3) Chemical reactions

The flash smelting raw material has complex species in it. As shown in Table 1, the species mass fractions were listed. The major reactions considered in the simulation are listed in Table 2.

Table 1 Phase compositions

Phase compositions	Mass fractions (%)
PbS	37
ZnS	5
$CuFeS_2$	1
FeS_2	4
Fe_7S_8	10
CaO	30
$CaCO_3$	1
SiO_2	9
C (coke)	3
Total	100

Table 2 Major reactions

Chemical reaction formula	
$2PbS + 3O_2 = 2PbO + 2SO_2$	$2ZnS + 3O_2 = 2ZnO + 2SO_2$
$FeS_2 + O_2 = FeS + SO_2$	$2FeS + 3O_2 = 2FeO + 2SO_2$
$Fe7S8 + O_2 = 7FeS + SO_2$	$4CuFeS_2 + 5O_2 = 2Cu_2S + 2FeS + 4SO_2 + 2FeO$
$2Cu_2S + 3O_2 = 2Cu_2O + 2SO_2$	$C + O_2 = CO_2$
$CaCO_3 = CaO + CO_2$	$2FeO + SiO_2 = 2FeO \cdot SiO_2$

The local mass fraction of each species, Y_i, through the solution of a convection-diffusion equation for the ith species. This conservation equation takes the following general form:

$$\frac{\partial}{\partial t}(\rho Y_i) + \nabla \cdot (\rho v Y_i) = -\nabla \cdot J_i + R_i + S_i \tag{7.1}$$

where R_i is the net rate of production of species by chemical reaction (described later in this section) and S_i is the rate of creation by addition from the dispersed phase plus any user-defined sources.

The reaction rate: $R_{i,r}$ is given by the smaller of the two expressions below:

$$R_{i,r} = v'_{i,r} M_{w,i} A \rho \frac{\varepsilon}{k} \min_R \left(\frac{Y_R}{v'_{R,r} M_{w,R}} \right)$$

$$R_{i,r} = v'_{i,r} M_{w,i} A B \rho \frac{\varepsilon}{k} \frac{\sum_p^N Y_P}{\sum_j^N v'_{j,r} M_{w,j}} \tag{4.24}$$

Table 3 Temperature validation

Measurement point	Measurement temperature/°C	Simulation results/°C	Relative error/%
Shaft	1380	1445	4.5
Flue gas outlet	1301	1356	4.1

where Y_p is the mass fraction of any product species, $M_{w,i}$ is the mass fraction of a particular reactant, A is an empirical constant equal to 4.0, and B is an empirical constant equal to 0.5 [2].

Boundary Conditions

The geometry is built base on the smelting shaft of the flash smelting furnace.

(1) Inlet boundary condition

There are four nozzles in the top of the furnace, as it is shown in Fig. 2. There are two types of the inlet condition: velocity inlet for the gas phase and surface injection for the lead concentrate particles. The total charging rate is 48.45 t/h. The oxygen flow rate is 584 m^3 h^{-1}.

(2) Outlet boundary condition

The uptake shaft is connected with the heat boiler. The pressure outlet is used and the pressure is −50 Pa.

Model Validation

In the smelting process, the temperature was measured by using the thermal couple. The temperature within the smelting shaft and the temperature of the flue gas outlet were measured in the smelting process. The measurement data were compared with the baseline case simulation results, and the relative error is within 5% (Table 3).

Results

Velocity Field

Figure 4 shows the flow field distribution on the Y_1 section. It can be seen that the high-speed air blows into the reaction tower strongly impact with the molten

pool which at the bottom of the furnace. The recirculation will be formed when the recirculated air contacts with the wall surface. The mainstream of the airflow will exit from the vertical flue tunnel.

Temperature Field

Figure 5 shows the temperature distribution of the cross-sections. It can be seen that the temperature distribution under each nozzle is basically similar, and the high temperature region in the furnace first opens in a trumpet shape. At a position of about 6 m from the top of the shaft, the radius of the high temperature region is reduced because of the recirculation causes the high temperature zone to gather in the middle; the industrial temperature at room temperature will rapidly heat up from the nozzle into the reaction tower, reaching a maximum temperature of about 2000 K from about 1.5 m from the top of the tower and within 1–2 m from the top of the tower. For the high temperature region, the exothermic reaction in this region is very intense; as the mass fraction of sulfide particles in the concentrate decreases and the oxygen concentration decreases, the oxidation reaction rate slows down, and the temperature below 2 m from the top of the tower decreases slowly.

Species Distribution

Figure 6 shows the SO_2 concentration distribution. Figures 3, 4, 5, and 6 show the distribution of sulfur dioxide in the X_1 and Y_1 sections. It can be found that the concentration of SO_2 is higher in 2.5 m below the nozzle because the desulfurization reaction is very intense in this area, and a large amount of SO_2 is released. The region with the most intense lead oxidation reaction; the concentration of SO_2 in the shaft is basically stable from about 2.5 m below the top of the furnace surface, and the desulfurization reaction has been basically completed.

Figure 5 shows the O_2 concentration contour on the X_1 and Y_1 cross-sections. It can be observed that the industrial oxygen enters the reaction tower and exchanges energy momentum with the charge particles. The oxidation reaction occurs, so that the O_2 concentration decreases rapidly near the nozzle. The average O_2 mass fraction is less than 0.07, indicating that the gas-particle mixture in the furnace is better, and O_2 is fully utilized.

Single Nozzle Simulation

Base on the numerical model of the baseline case. This study changes the four nozzle design and does the single central nozzle simulation as it is shown in Fig. 7. The

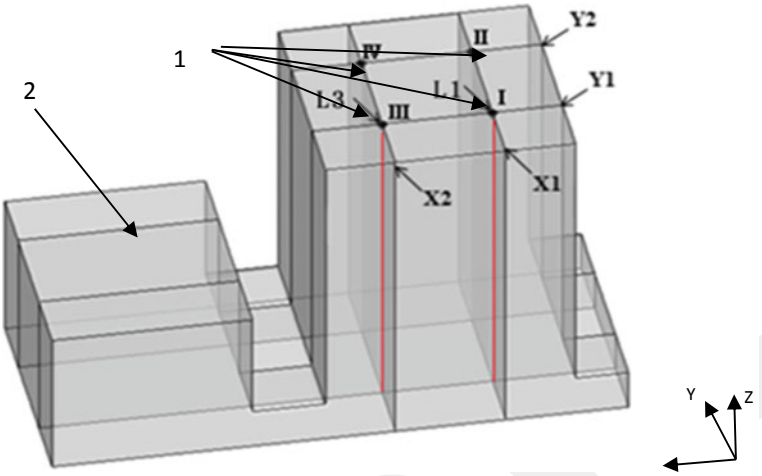

Fig. 3 Numerical smelting shaft

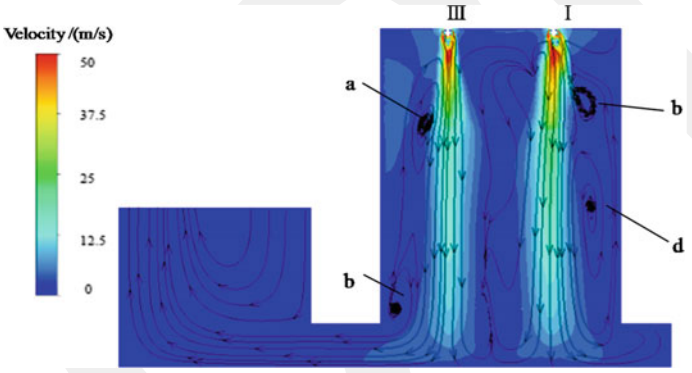

Fig. 4 Velocity distribution

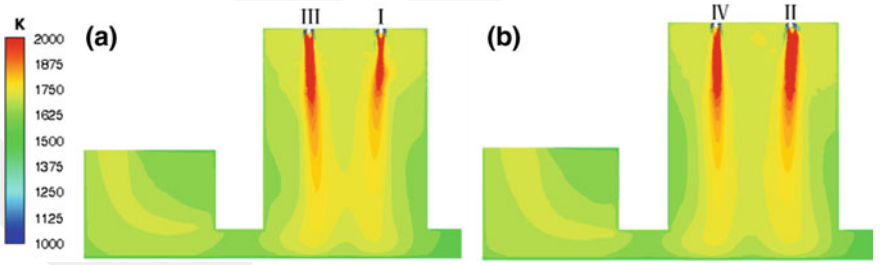

Fig. 5 Temperature distribution

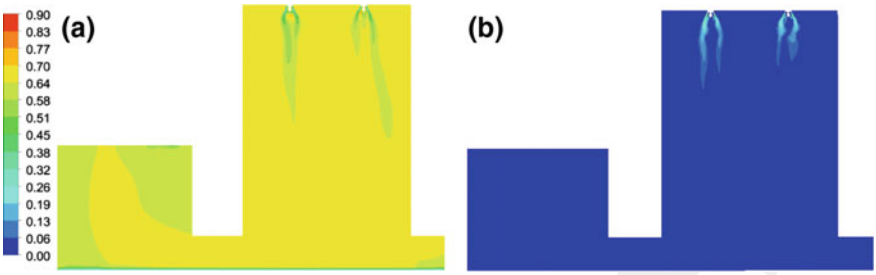

Fig. 6 Species distribution, **a** SO_2 distribution, **b** O_2 distribution

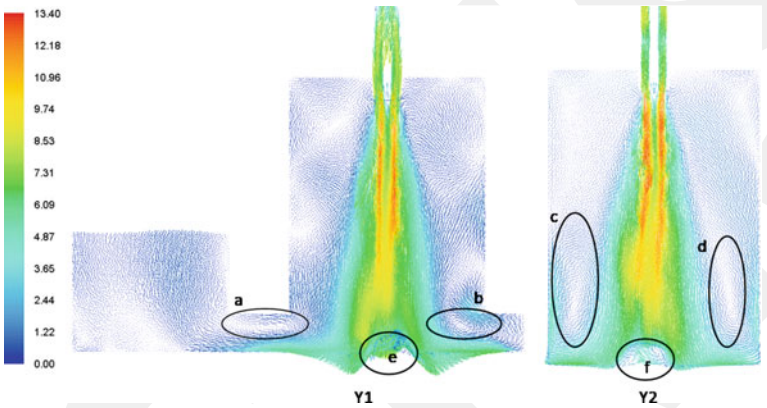

Fig. 7 Velocity field

air dispersed in the shaft, and the recirculation phenomenon is greatly reduced. The operation conditions will be more stable compared to the four nozzle design.

Conclusions

1. The baseline case results show that after the industrial oxygen enters the smelting shaft from the nozzle, a distinct horn-shaped high-speed airflow is formed under the nozzle; the high temperature zone is 1.5 m away from the top of the shaft.
2. When four nozzles were replaced by one nozzle, the results showed that industrial oxygen was entered by the central nozzle. The scale of the air recirculation in the smelting shaft is significantly reduced, the gas flow in the shaft is more stable and uniform, and the flow rate is low; the high temperature zone is mainly distributed in the range of 3–6.5 m from the top of the shaft indicating that the one nozzle replacement is feasible.

References

1. Chaudhuri KB, Melcher G (1978) How kivcet lead smelting compares with other direct reduction processes for lead. Eng Min J 179(4):88–91
2. Brian Spalding D (1977) Development of the eddy-break-up model of turbulent combustion. Symp Combust 16:1657–1663

GCRIS

Effect of Alumina Ceramics Surface Condition on the Wetting of Liquid Lead

Zhen Qi and Zhang Fu Yuan

Abstract The effect of alumina ceramics surface roughness on the wetting characteristics of liquid lead was investigated by the sessile drop method. The surface 3D appearance and surface roughness of the alumina substrate were measured by confocal laser scanning microscope (CLSM). The interface micrographs of lead and alumina substrates were characterized by scanning electron microscope (SEM). The results show that as the alumina substrate surface roughness increases, the contact angle of the lead drop increases, the drop height increases, the contact diameter decreases, and the adsorption work decreases. An obvious pinning effect was observed during the wetting process, and the potential mechanism of the wetting behavior was described on the basis of Wenzel equation. This work provides a theoretical basis for the application of alumina ceramics in the lead industry.

Keywords Surface roughness · Wetting · Adsorption work · Lead

Introduction

The surface properties of materials have been of great influence in many studies and have received widespread attention. In particular, alumina ceramics are widely used in many fields such as self-cleaning, coating, optoelectronic devices, and composite materials because of their excellent wear resistance, corrosion resistance, and high temperature resistance [1–3].

The wetting of gas-liquid-solid systems is mainly affected by the chemical composition of solid and liquid phases, liquid-solid interface reaction, the substrate surface roughness, and other factors [4–6]. The research on surface roughness of materials was mainly carried out at room temperature, such as mechanical processing and laser texture are used to change the surface roughness and anisotropy in order to improve the hydrophilicity or hydrophobicity of the surface [7–9]. The wetting of

Z. Qi · Z. F. Yuan (✉)
Collaborative Innovation Center of Steel Technology, University of Science and Technology Beijing, Beijing, China
e-mail: zfyuan2016@ustb.edu.cn

© The Minerals, Metals & Materials Society 2020

A. Siegmund et al. (eds.), *PbZn 2020: 9th International Symposium on Lead and Zinc Processing*, The Minerals, Metals & Materials Series,
https://doi.org/10.1007/978-3-030-37070-1_41

the metal/ceramic system at high temperature has also been studied extensively, but it mainly concentrates on the chemical composition of solid or liquid phases, liquid-solid interface reaction, and the experimental furnace conditions. Ma et al. [10] investigated the wetting between molten tin and CuFeNiCoCr high-entropy alloy substrate at 573–973 K. The wetting process was divided into three stages. The first stage occurs in the temperature range of 573–673 K. The wetting between molten tin and substrate was poor due to the oxidation of the substrate surface. In the second stage, the oxidation film was dissolved by the reaction between molten tin and the Cu-rich phase in the substrate, which improved the wetting at 673–723 K. The temperature of the third stage was 723–973 K. Tin atoms passed through the Cu-rich phase and initiated a variety of chemical reactions; therefore, the equilibrium contact angle further decreased with the increasing temperature. The surface roughness of most materials varies greatly in practical application; however, the theory about the effect of roughness on the wettability of metal/ceramic non-reactive wetting system is not perfect. Therefore, it is of great significance to study the influence of surface roughness on interfacial wettability of molten metals at high temperature.

In this paper, lead with low melting point, good stability, and strong anti-oxidation ability were selected as the research object. The surface roughness of alumina substrate was taken as the variable, and the wetting behavior of liquid lead on the surface of alumina substrate was studied in detail. The mechanism of roughness affecting wetting behavior was illustrated on the basis of the Wenzel equation, and the effect of roughness on surface tension was studied which provided a theoretical basis for improving the wettability of metal and alumina.

Experimental Materials and Methods

Surface Roughness Measurements of Alumina Substrate

Alumina with a purity of 99.95% was chosen as the substrate to study the relationship between surface roughness and liquid lead wettability. The alumina substrate was processed into four sets of sheets having different roughness, and the size was $20 \times 20 \times 2$ mm. It was pre-acid cleaned by ultrasonic cleaner for 3–5 min, then ultrasonically cleaned in acetone, absolute ethanol, and deionized water for 20 min in sequence, dried and placed in a drying cabinet to remove water vapor from the surface. The 3D morphology and roughness parameters (*Ra* indicates the height of peaks and the depth of valleys along a mean line, which was used as a measure of surface roughness.) of alumina substrate surface were measured by confocal laser scanning microscope (CLSM).

The Wetting Measurements of Lead Drop

The wetting of liquid lead on different roughness alumina substrates was measured by a sessile drop method. Details of the experimental apparatus and procedure can be referenced in our previous work [11, 12]. The apparatus consists of a furnace (Kanthal line heated), photographic equipment, a digitizer, and a computer analysis system. A quartz tube was sealed with a quartz cap (inner diameter, 30 mm; outer diameter, 34 mm; length, 560 mm) as a heating chamber. The tip of the thermocouple (Fe–CuNi) between quartz pipes was located directly under the alumina substrate and lead drop. The temperature difference of measurement was negligible. Ar–H_2 5% functioned as protective gas.

The lead block (purity, 99.99 mass%) was cut into a cylinder ($\Phi 5.5 \times 5.5$ mm). The polishing cloth was used to remove the oxide layer on the lead surface and cleaned with acetone using an ultrasonic automatic washer for 20 min. Then the sample was rinsed with deionized water and dried. The lead cylindrical sample was set on the alumina substrate, which was made horizontal by two water levels, and then put into the quartz tube of the furnace by a quartz support. The quartz tube was sealed and evacuated to 10–3 Pa, then filled with Ar–H_2 5% and evacuated again. After repeated operations for three times, heating was started, and the flow rate of gas was maintained at 0.2 L/min. After reaching the target temperature, photographs of the molten lead drop were taken every 3 min and the corresponding time was recorded for measuring contact angle, droplet height, contact diameter, and adsorption work. After cooling, the samples were prepared for microscopic characterization of the interface.

Results and Discussion

Surface Roughness of Alumina Substrate

Figure 1 shows the 3D morphology map of CLSM analysis for the 1# to 4# alumina substrates, which shows the mean values of *Ra*. The surface roughness of four substrates can be easily compared by 3D morphology map, and the roughness value of four alumina substrates was calibrated by *Ra*. The surface roughness then increases in turn. The surface of 1# substrates is a smooth mirror, and there are many pits with different depths on the surface of other substrates.

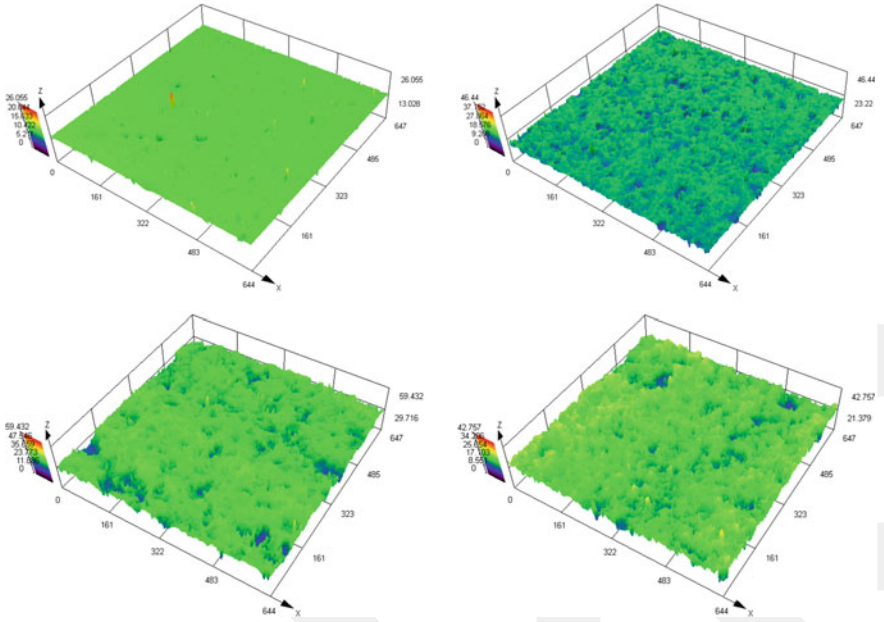

Fig. 1 3D morphology map for different alumina substrates surface

The Wetting of Lead Drop on Alumina Substrates with Different Roughness

The key of this work was to study the wetting behavior of molten lead on alumina substrates with different roughness [13–15]. Figure 2 shows the micrographs and linear scanning analysis of the interface between solidified lead and alumina substrates. The contact line between the lead and the smooth substrate is gentle, and the contact line with the rough substrate fluctuates greatly. Moreover, in all cases, lead filled the pits on the surface of alumina and the interface was clear. This phenomenon indicates that the wetting process of lead on alumina substrate was the same as Wenzel wetting model. Linear scanning analysis showed that there was no reaction between the lead and alumina substrates.

Figure 3a shows the heating curve for this experiment. It was a preheat zone before 473 K to eliminate the gas molecules and stress on the surface of the alumina substrate. After 473 K, the temperature was rapidly increased. From 923 to 1123 K, at the thermal insulation zone, the temperature was kept at 50 K for 15 min at intervals and the photos were taken every 3 min. Figure 3b shows the changes for contact angle of lead drop on alumina substrate of different roughness at various temperatures. Obviously, the contact angle slightly decreased as the temperature increased, and the increase in the surface roughness of the alumina substrate resulted in the contact angle increase. The contact angle of the smooth substrate was different from that of

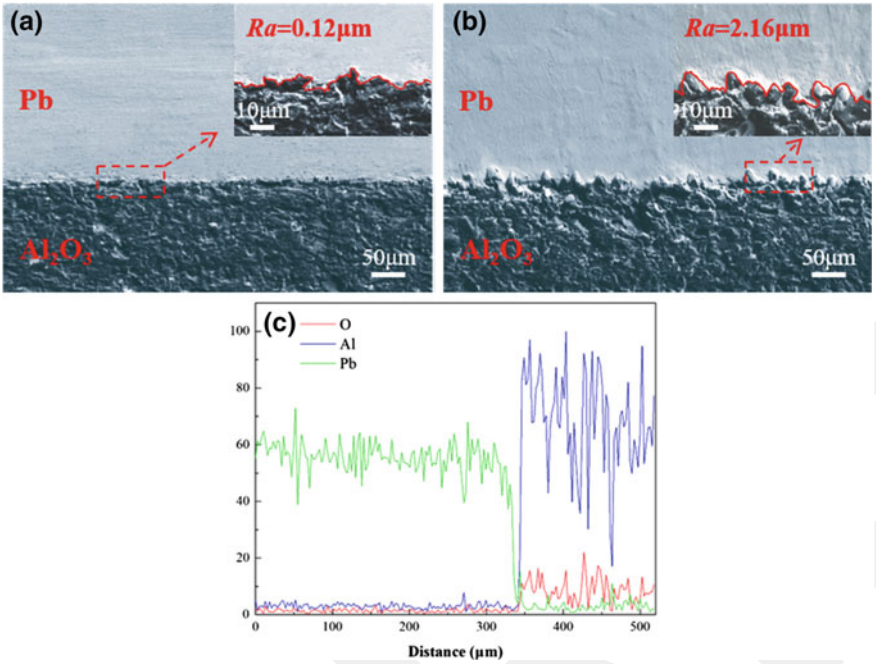

Fig. 2 SEM micrographs of interface between lead and alumina substrates: **a** $Ra = 0.12$ μm alumina substrate, **b** $Ra = 2.16$ μm alumina substrate, and **c** linear scanning analysis of interface between lead and alumina substrates

the rough substrate, which indicated that the surface roughness of the substrate had a great influence on the wetting of droplets. The relationship between the contact angle of molten lead and the surface roughness of the substrate conformed to Wenzel equation [16].

$$\cos\theta_w = r\cos\theta_y \tag{1}$$

where θ_w is the apparent contact angle, θ_y is defined for an ideal surface, and r is the roughness factor. According to the Wenzel equation, when the contact angle is greater than 90°, the contact angle increases as the surface roughness increases.

Figure 4 shows the changes for contact diameter and drop height of lead drop on alumina substrate of different roughness at various temperatures. As the roughness of the substrate increases, the lead drop contact diameter increases and the drop height decreases. The results show that the contact angle (Fig. 3b), the contact diameter (Fig. 4a), and the drop height (Fig. 4b) are interdependently related. At the same temperature, with the increase of Ra, the increase or decrease of the above three variables is initially large and then small; when Ra is unchanged, the contact diameter increases, and the contact angle and drop height decrease. In Fig. 4a, the contact

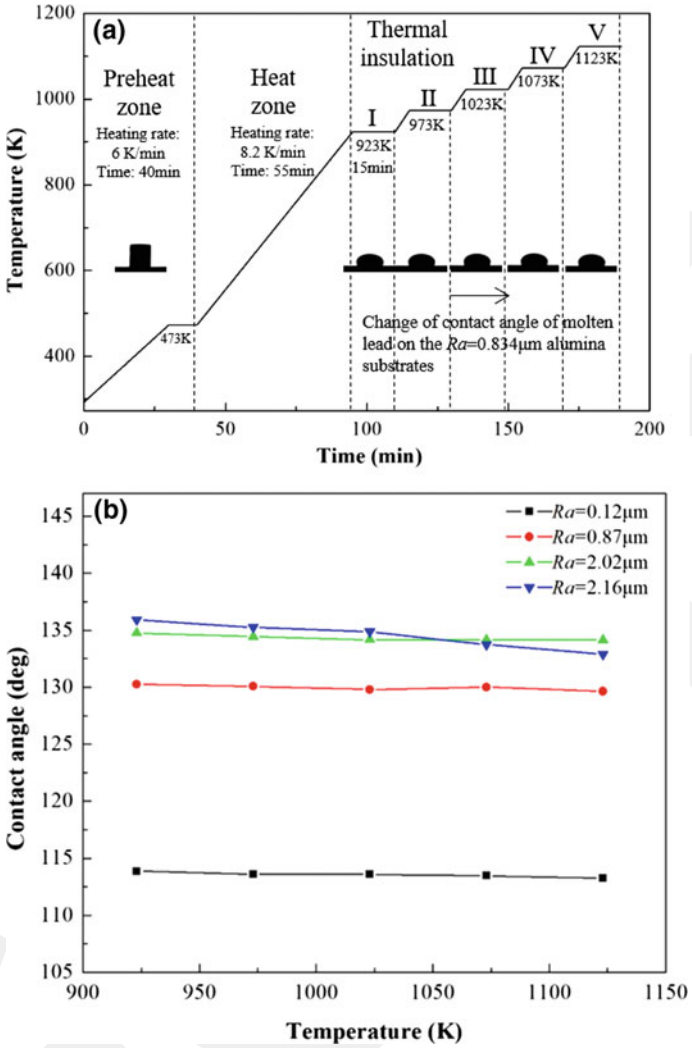

Fig. 3 **a** Heating curve for wetting experiment of molten lead and **b** changes for contact angle of lead drop on alumina substrate of different roughness at various temperatures

diameter of $Ra = 2.02$ μm exceeds that of $Ra = 2.16$ μm. At the same time, the contact angle (Fig. 3b) and the drop height (Fig. 4b) also change correspondingly.

On the basis of Wenzel equation [16], according to the above results, the increase of surface roughness of alumina substrates means that the actual surface area of alumina substrates increases. In molten lead/alumina systems, lead tends to reduce the contact area with alumina substrates. At the same time, the pits on the surface of the substrate hindered the movement of the three-phase line, forming a pinning

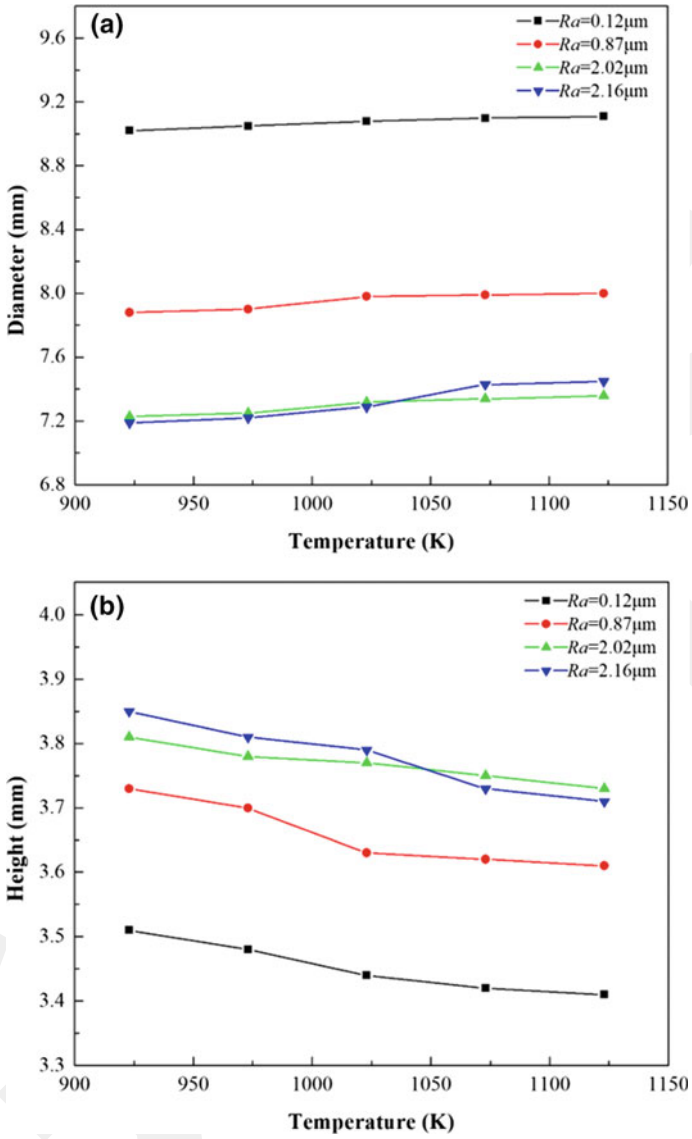

Fig. 4 Changes for **a** contact diameter and **b** drop height of lead drop on alumina substrate of different roughness at various temperatures

effect [17]. Therefore, the contact diameter of the molten lead was reduced, and the drop height and the contact angle were increased.

Figure 5 shows the changes for adsorption work of lead drop on alumina substrate of different roughness at various temperatures. After roughening the surface of the smooth alumina substrate, the adsorption work between the liquid lead and

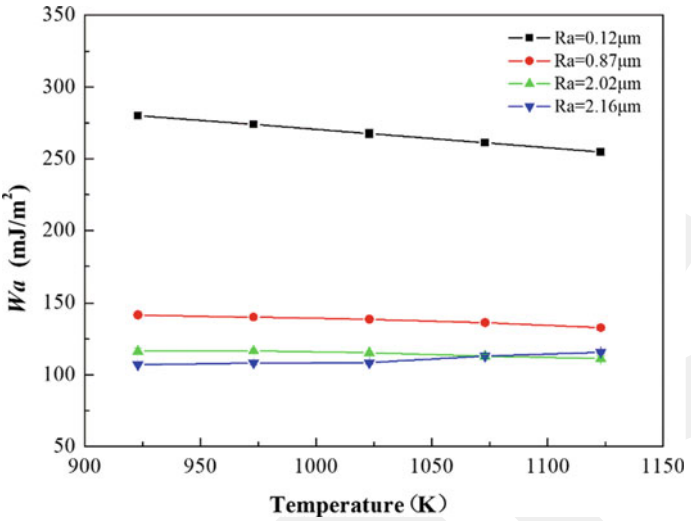

Fig. 5 Changes for adsorption work of lead drop on alumina substrate of different roughness at various temperatures

the alumina substrates can be greatly reduced. Therefore, the surface roughening of the substrate can reduce the wettability between the molten lead and the alumina substrates. It has fundamental significance for the application of alumina ceramics in lead production or recycling.

Conclusion

The effect of surface roughness of alumina substrates on wetting behavior and adsorption work of liquid lead was studied, and the micrographs of interface between condensed lead and alumina were observed. The molten lead maintains Wenzel wetting state on the surface of alumina substrate. Increasing the surface roughness of the substrate means that the actual area increases, which leads to the spontaneous reduction of the contact area between molten lead and the substrate. Therefore, the contact diameter of molten lead on the alumina substrate decreases, and the drop height and the contact angle increase, which leads to the decrease of the adsorption work and the deterioration of wetting between molten lead and the substrate.

Acknowledgements This work was supported by the Natural Science Foundation of China (Grant No. U1738101) and Fundamental Research Funds for the Central Universities (Grant Nos. FRF-TP-18-007A1).

References

1. Xu P, Coyle TW, Pershin L, Mostaghimi J (2018) Superhydrophobic ceramic coating: Fabrication by solution precursor plasma spray and investigation of wetting behavior. J Colloid Interface Sci 523:35–44
2. Wu M, He X, Ren S, Qin M, Qu X (2009) Effect of various Ni plating layers and aging on microstructure and shear strength of Sn–2.5 Ag–2.0 Ni solder joint. Surf Coat Technol 203:3011–3018
3. Protsenko P, Terlain A, Traskine V, Eustathopoulos N (2001) The role of intermetallics in wetting in metallic systems. Scr Mater 45:1439–1445
4. Cong XS, Shen P, Wang Y, Jiang Q (2014) Wetting of polycrystalline SiC by molten Al and Al–Si alloys. Appl Surf Sci 317:140–146
5. Sangghaleh A, Halali M (2009) Effect of magnesium addition on the wetting of alumina by aluminium. Appl Surf Sci 255:8202–8206
6. Wang J, Matsuda N, Shinozaki N, Miyoshi N, Shiraishi T (2015) Effect of SUS316L stainless steel surface conditions on the wetting of molten multi-component oxides ceramic. Appl Surf Sci 327:470–477
7. Singh AK, Singh JK (2017) Fabrication of durable super-repellent surfaces on cotton fabric with liquids of varying surface tension: low surface energy and high roughness. Appl Surf Sci 416:639–648
8. Liang Y, Shu L, Natsu W, He F (2015) Anisotropic wetting characteristics versus roughness on machined surfaces of hydrophilic and hydrophobic materials. Appl Surf Sci 331:41–49
9. Riahi S, Niroumand B, Moghadam AD, Rohatgi PK (2018) Effect of microstructure and surface features on wetting angle of a Fe-3.2 wt% CE cast iron with water. Appl Surf Sci 440:341–350
10. Ma GF, Li ZK, Ye H, He CL, Zhang HF, Hu ZQ (2015) Wetting and interface phenomena in the molten Sn/CuFeNiCoCr high-entropy alloy system. Appl Surf Sci 356:460–466
11. Yuan ZF, Mukai K, Huang WL (2002) Surface tension and its temperature coefficient of molten silicon at different oxygen potentials. Langmuir 18:2054–2062
12. Yuan ZF, Mukai K, Takagi K, Ohtaka M, Huang WL, Liu QS (2002) Surface tension and its temperature coefficient of molten tin determined with the sessile drop method at different oxygen partial pressures. J Colloid Interface Sci 254:338–345
13. Zou X, Zhao D, Sun J, Wang C, Matsuura H (2018) An integrated study on the evolution of inclusions in EH36 shipbuilding steel with Mg addition: from casting to welding. Metall Mater Trans B 49:481–489
14. Volceanov E, Volceanov A, Stoleriu Ş (2007) Assessment on mechanical properties controlling of alumina ceramics for harsh service conditions. J Eur Ceram Soc 27:759–762
15. Yuan ZF, Fan J, Li J, Ke J, Mukai K (2004) Surface tension of molten bismuth at different oxygen partial pressure with the sessile drop method. Scandinavian J Metall 33:338–346
16. Wenzel RN (1936) Resistance of solid surfaces to wetting by water. J Ind Eng Chem 28:988–994
17. Kumar G, Prabhu KN (2007) Review of non-reactive and reactive wetting of liquids on surfaces. Adv Colloid Interface Sci 133:61–89

Part XI
PbZn Sustainability

GCRIS

Material Stewardship for Zinc

Sabina Grund and Eric van Genderen

Abstract The metals industry is faced with global challenges linked to sustainable development, among these finding a balance between environmental stewardship, economic development, and social responsibility that require full participation by the entire metal value chain. The global zinc industry has a well-established, long-term sustainability program in place providing its customers, regulators, and other stakeholder groups with facts. For example, regular updates of the global zinc mining and smelting life cycle assessment (LCA) provide practitioners with the most representative environmental footprint data for zinc. In addition, IZA conducts material stocks and flows analyses to characterize national, regional, and global recycling metrics. Furthermore, IZA's sustainability activities are framed by the SDG Sector Roadmap for the global zinc value chain, which outlines today's impacts and future impact opportunities on sustainable development as related to the United Nations' Sustainable Development Goals (UN SDGs). This paper provides an overview of the global zinc industries' achievements, goals and related actions and identifies challenges that still lie ahead of this industry.

Keywords Zinc · Responsible sourcing · Circular economy · Circularity · UN SDG roadmap · Sustainable development · Climate change · Recycling · Material stewardship

Introduction

Sustainable development according to the often-cited definition by Brundtland is "development that meets the needs of the present without compromising the ability of future generations to meet their own needs." [1]. Typically, the three pillars of sustainable development are described as social, environmental, and economical. Today, sustainability is the foundation for the leading global framework for international cooperation—the United Nations' 2030 Agenda for Sustainable Development

S. Grund (✉) · E. van Genderen
International Zinc Association, Brussels, Belgium
e-mail: sgrund@zinc.org

© The Minerals, Metals & Materials Society 2020

A. Siegmund et al. (eds.), *PbZn 2020: 9th International Symposium on Lead and Zinc Processing*, The Minerals, Metals & Materials Series,
https://doi.org/10.1007/978-3-030-37070-1_42

Fig. 1 United Nation's Sustainable Development Goals (UN SDGs) define the pathway towards sustainable development based on targets [2]

and its Sustainable Development Goals (SDGs) [2]. The 17 goals defined in the agenda and the underlying targets in fact can be interpreted as the detailed pathway reflecting all three pillars (Fig. 1).

All 17 goals are of similar importance. Three of the most dominant challenges today are reflected in the goals:

- Climate Change (reflected in SDGs 7 and 13): The Intergovernmental Panel on Climate Change (IPCC) confirmed the need to meaningfully reduce CO_2 emissions in order to remain within the boundaries of the Paris Agreement [3].
- Circularity (reflected in SDGs 9, 11, 12): The OECD projects the global metals use to triple from 8 Gt in 2011 to 20 Gt in 2060: "Recycling will grow faster than mining and become more competitive, but it will not be sufficient." [4].
- Responsible Sourcing (links to most SDGs): Customer driven evolution from a niche activity into the mainstream procurement strategy of global companies providing goods and services across sectors. Users and end users today demand information on the conditions under which products have been produced including the sourcing of the raw materials needed for the products. Often referred to are the OECD Guidelines for Multinational Enterprises. These are recommendations from governments to multinational enterprises on responsible business conduct [5].

The numerous requirements that a responsible metals industry needs to fulfill are complex and demanding in order to provide all the information needed and to manage engagement in innovation, initiatives, frameworks, and standards. Much needs to be done at company level, which can, in part, be facilitated by targeted material stewardship programs coordinated within commodity associations to support companies' progress towards meeting obligations linked to sustainable development and to the UN SDGs.

For the zinc industry, the International Zinc Association (IZA) is the focal point for joint material stewardship actions. Through its global programs, IZA ensures that necessary information is objectively collected and communicated to users, regulators, and other stakeholders. IZA also provides the zinc industry a forum to develop strategies and co-ordinate activities that productively and efficiently contribute to the UN SDGs.

Zinc Production, Use, and Recycling

Zinc is a material of versatile properties and thus of a broad variety of uses. Due to its electrochemical properties, zinc's major use—more than 50% of the global zinc production—is protecting steel from corrosion by galvanizing. Use span the breadth of first use sectors, including automotive and transportation infrastructure, agricultural, industrial and consumer goods, electronics, and building and construction. The life-extension and finishing options made possible by modern zinc coatings are unique. Zinc is used as the base alloy or an alloying element (~35% of the global zinc production) in die casting and brass. Zinc sheet for roofings, facades, gutters, and downpipes are produced from 6% of the global zinc production, as well as with another 6% used for the production of zinc compounds (e.g., zinc oxide in rubber, medicines, and fertilizers) and other semi-manufactured products (Fig. 2).

In 2017, 13 million-tons (Mt) of zinc were mined globally, with the top three mining countries being China (40%), Australia (7%), India, and Mexico (5% each) [6]. 99% of zinc mining are done in large scale mining operations. This type of operation allows for a higher degree of control and automation. It is estimated that only up to one percent of the globally mined zinc originates from artisanal and small-scale mines (ASM) [7].

Also, in 2017, 13 Mt of zinc have been produced in primary zinc smelters, the top three being China (46%), South Korea (6,6%), and Canada (5%) [6]. Primary

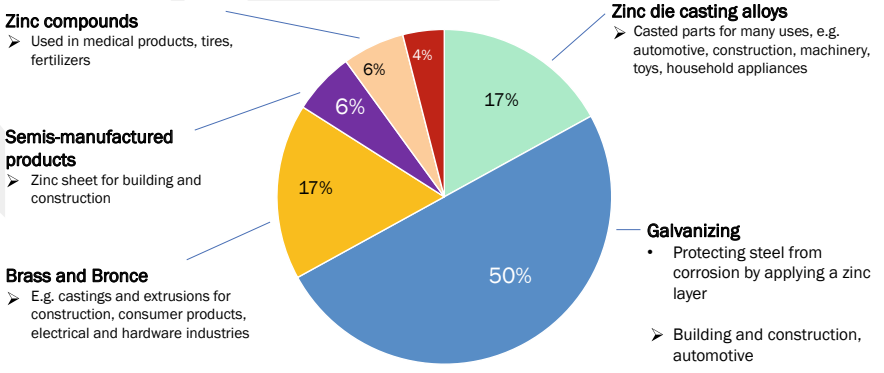

Fig. 2 Zinc is versatile: its numerous uses reflect the variety of properties [6]

zinc smelters mainly produce zinc from ore concentrates. In addition to the ore concentrate, zinc smelters feed an average of 10–15% secondary raw materials into their processes. Mostly these are so-called crude oxides (Waelz oxides), which are enriched zinc containing flue dusts from steel production from galvanized steel. In some cases, the recycled zinc content in the smelter feed can be higher—in specific cases up to 100%.

An additional tonnage of 4–5 Mt of zinc is recycled in re-melt processes, in the copper or in the zinc compound industry without passing through the zinc smelters. Different from many other metals, there is not one single technology for zinc recycling. Instead for the most important zinc uses, tailor made recycling technologies are well-established:

- Zinc sheet and zinc die casted parts are re-melted. Over 95% of zinc sheet scrap is recycled in Europe [8]. Re-melting zinc requires only 5% of the energy that is needed to produce primary zinc from ores [9].
- Galvanized steel is re-melted in the steel industry, e.g., electric arc furnace. Zinc ends up in the flue dust (EAF dust) and is further concentrated in the Waelz process. The Waelz/crude oxide is a welcome raw material for primary zinc production at less costs than concentrates supply, its use often being limited by the available tonnage. Other potential technologies for zinc recycling from galvanized steel are being tested at pilot plant or conceptual phase. 11% of steel scrap from building and construction is reused, e.g., in Germany, while 88% are recycled in the steel industry [10]. All EAF dusts that are produced in Europe are recycled. With the emerging markets for galvanized steel a significant growth at global scale is expected [11, 12, 13].
- Zinc as an alloying element in brass is recycled by the copper industry. There it is used for brass production or alternatively returned to the zinc industry.
- Various technologies are applied to recycle zinc from residues, wastes, and by-products. Often zinc in these recycling loops is directly used to produce zinc compounds without passing through zinc smelters, thus saving costs, energy and raw materials.

Two approaches commonly used to assess recycling rates for zinc are the Recycled Content (RC), the fraction of secondary zinc in use, and End of Life (EoL) recycling rate, the fraction of zinc recycled relative to the amount available at EoL. For zinc, as for metals in general, the EoL recycling rate provides the most informative information on the success of recycling. Higher EoL recycling rates relate to effective waste management systems and capacity for recycling products at the end of their useful life (Fig. 3).

The recycled content for zinc, as for other metals, will continue to increase over time but will remain below 100% due to dynamics of market growth and durability of zinc metal products. For example, it may require decades before zinc metal that is used today, e.g., as sheet for roofing or to galvanize steel, becomes available for recycling [14]. Moreover, the tonnage of zinc that is used today is much higher than what has been put into use decades ago.

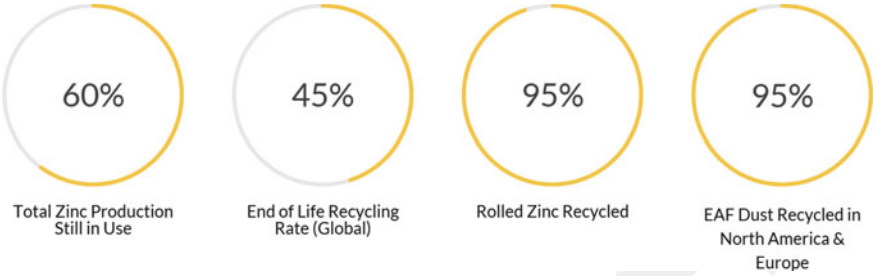

Fig. 3 Recycling characteristics [8]

Tools of Material Stewardship

General information on zinc production, use, and recycling requires the development and application of robust tools related to material stewardship. Material stewardship has been defined by the International Council on Mining and Metals (ICMM) as "the concept to embody the range of activities required for optimal and appropriate use of minerals and metals in society" [15]. Among the meaningful tools commonly used in material stewardship are mass flow analyses (MFA), life cycle assessment (LCA), and the guidance, standards, and frameworks linked to responsible sourcing.

Mass Flow Analysis (MFA)

Resource availability is one of today's major concerns [4] leading to an increased focus on circularizing economies [2]. MFA enables us to calculate how much zinc enters the use phase today, the tonnage that is added to the in-use stocks or becomes available for recycling. Recycling rates usually are calculated based on MFA analysis. For zinc, Yale University has developed an MFA model [16, 17, 18] based on mass flow data until 2010. Often the MFA models are mono-metal models, thus on the one hand giving easy answers to regulators' questions, but at the same time not reflecting the complex interlinkage of the material flows in the metals industry [19]. Detailed, multi-metal metallurgical models are available, that support MFA with information based on metallurgical science that is needed to answer more complex questions that occur linked to circularity and the interlinkage of zinc with other metals [10]. In 2020, IZA will update the MFA model for zinc (Fig. 4).

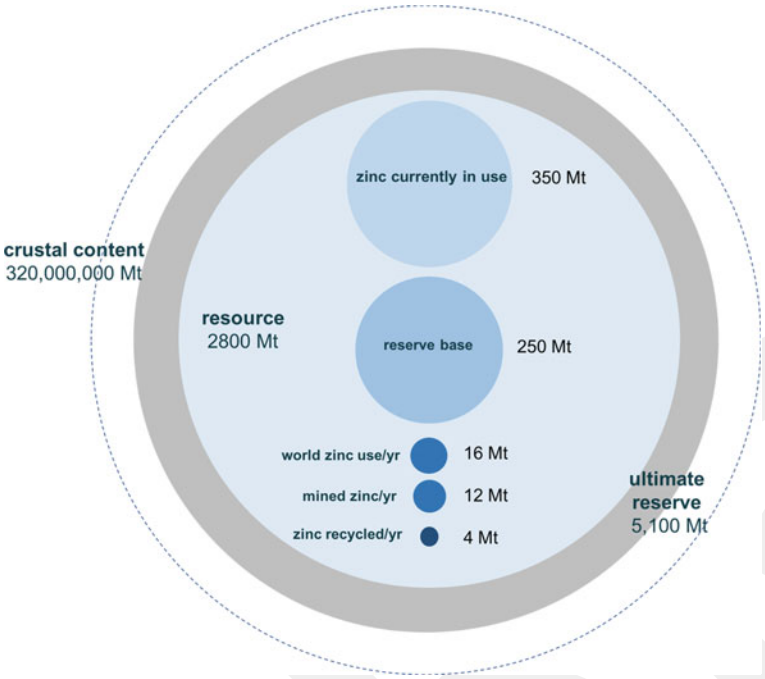

Fig. 4 Based on mass flow analysis and geographical data, the long-term availability of zinc is visualized [43]

Life Cycle Assessment (LCA)

Material stewardship product design based on life cycle analysis (LCA) has become common practice. Initially having been applied in the automotive industry, LCA today is widely used in building and construction and a variety of other sectors. LCA methodologies are standardized (ISO 14040, [20]) and there is a strong push from within the EU Commission to harmonize foot-printing methodologies for products and organizations in addition to providing a common basis for product comparisons and "green" claims (product environmental footprint, PEF) [21].

Commercial databases and calculation tools such as GaBi or ecoinvent are available. These are used by LCA practitioners when quantifying and evaluating the impact of alternative product designs on environmental impact categories, such as the carbon footprint, water footprint, or ozone depletion potential. Designers use these tools to optimize the product design under specific framework conditions, e.g., minimize the carbon footprint. Crucial for reliable results from LCA is a high quality of the data based on which the LCA has been generated. That is, industry data must remain up to date, be geographically representative, and generated under well-documented conditions. For zinc mining and smelting, the IZA has published the second global LCA based on data provided by participating companies in 2016 [22,

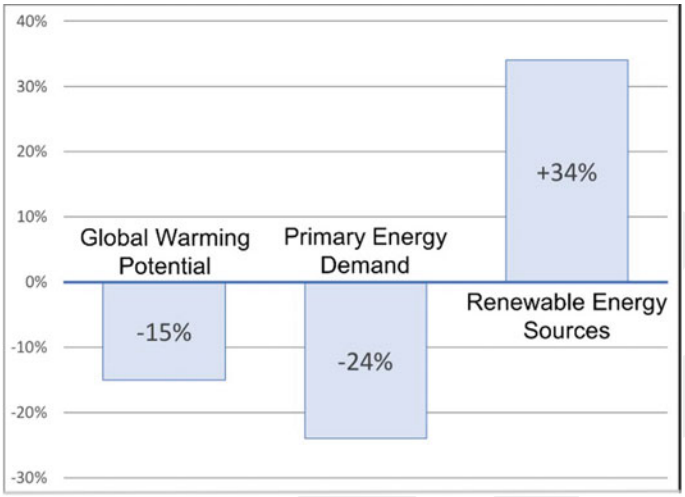

Fig. 5 Comparison of impact categories for zinc mining and smelting (global average): between 2006 and 2012, the global warming potential decreased by 15%. The primary energy demand decreased by 24%, while the use of energy from renewable sources increased by 34%

9]. In 2020, the next update will be published and introduced into relevant databases such as GaBi, PEF, and ecoinvent, among others (Fig. 5).

While LCA delivers useful information on environmental impacts, other impacts, such as resource use (Abiotic Depletion Potential, ADP) do not seem to be fit for purpose yet, e.g., because circularity of metals is not reflected [23]. To express circularity either separately or linked to LCA, indicators have been developed that reflect not only the use of primary material, but also the durability of a product, the recycled content in the materials used to produce it and the recyclability of the product at the end of its use phase [24, 25, 26]. Thorough analysis of LCA and circularity indicators reveals often conflicting goals of lower carbon emissions and increased recycling rates.

Responsible Sourcing

More recently, the life cycle community explores ways to introduce social aspects into LCA (s-LCA). Quantifying adverse aspects linked to, e.g., bribery or child labor seems to be a way to consider these already in the design phase of a product by designing materials under suspicion out of products. While the success of this approach still needs to be proven, the meaning of responsibility across whole value chains is already translated into standards, initiatives, and frameworks.

Many of the zinc mining and producing companies worldwide are members of the IZA or of the ICMM. They recognize the principles of sustainable development

through their respective programs such as the IZA Sustainability Charter [27] or the ICMM Performance Expectations [28]. Since 2019, IZA represents its member companies in the International Responsible Business Conduct (IRBC) for the Metal Sector in the Netherlands [29] and in the Responsible Steel Standard [30]. Furthermore, companies belonging to the zinc value chain support sustainability and responsibility initiatives, such as the UN Global Compact [31], the Global Reporting Initiative (GRI) [32], or the Extractive Industries Transparency Initiative (EITI) [33].

Zinc Contributes to the UN SDGs

Embedded in IZA's material stewardship activities, the global zinc industry in 2019 has worked on the SDG sector roadmap for the global zinc industry supported by ERM [34, 35]. The concept of SDG sector roadmaps has been developed by the World Business Council for Sustainable Development (WBCSD) in cooperation with ERM [34]. It consists of three main steps:

1. Establish the current position (Fig. 6);
2. Identify key impact opportunities;
3. Agree on actions to advance SDG impact opportunities.

In order to understand where the sector can make a meaningful and effective impact, a comprehensive review and assessment of all 17 SDGs were conducted, and impact priorities were determined. Various sources of publicly available information and company insights were also reviewed and analyzed to understand sector interactions with the SDGs. This included looking at leading think tanks and insight reports, UN and WBCSD developed SDG reports, industry reports, and IZA member

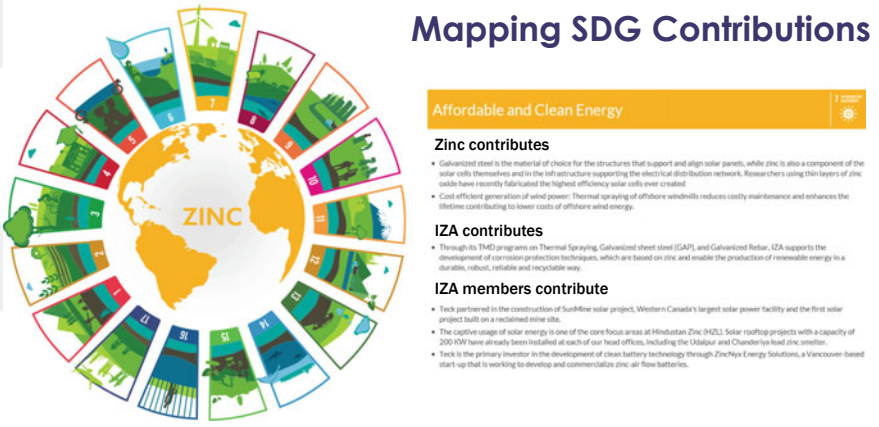

Fig. 6 Step 1 of the SDG sector roadmap: zinc products, the zinc industry, and the International Zinc Association already contribute in numerous ways to the UN SDGs [27]

companies' corporate sustainability reports. The findings allowed to identify priority SDGs, which were grouped under four themes [35]:

1. Health and wellbeing;
2. Energy and climate resilience;
3. Employment and operations along the value chain;
4. Sustainable cities and circular economy.

Health and Wellbeing

Zinc is an essential element and plays a critical role in plant-, animal-, and human health. Zinc deficiency is one of the most common nutrient deficiency problems worldwide and affects not only humans, but also animals, soils, and crops. Almost 50% of wheat-cultivated soils in the world—often located in developing countries—contain low amounts of zinc leading to crops poor in zinc and subsequently to zinc deficiency among humans that depend on these crops in their diet. Zinc in fertilizers can contribute to the realization of SDG 2 "Zero Hunger" by ensuring crops are productive and have the appropriate nutrition to nourish the people that depend on them.

Zinc is also an integral part of human health and the body's ability to function properly. It assists with producing new cells and enzymes, healing wounds, and processing the nutrients in food. Zinc deficiency affects about a third of the global population by weakening the immune system and leaving the body vulnerable to infection and disease and is particularly affecting young children. Approximately, half a million children die every year from causes related to zinc deficiency. Zinc supplements have shown to improve growth in children in developing countries and reduce total deaths in children under five years old by 18% [36].

The zinc sector initiates and supports initiatives in high-risk regions to address zinc deficiency of people and in soils. Through improving nutrient content in soils around the world and providing micronutrients needed to keep the population's bodies balanced and healthy, the zinc sector contributes to SDGs 2 "Zero Hunger" and 3 "Good health and Well-Being". Consecutively, the zinc sector's contributions to SDG 2 and 3 also contribute to SDG 1 "No Poverty" [35].

Impact opportunities linked to theme 1 aim at eliminating zinc deficiency worldwide. Actions, the zinc sector undertakes to reach this ambitious goal are, e.g., the zinc saves kids program in cooperation with UNICEF and the recently started project with wordbank in India.

With Theme 1, the zinc sector contributes to those SDGs that according to a study by PWC matter most to citizens [37] (Fig. 7).

Fig. 7 Because of zinc being an essential element, impact opportunities for the zinc sector are linked to SDGs 1–3: health and wellbeing, zero hunger and indirectly no poverty [35, 37]

Energy and Climate Resilience

Zinc primary production is an energy intensive process. The majority of zinc's carbon footprint is attributed to energy use, with smelting being the most energy intensive stage of the value chain. The energy mix powering each stage of the value chain, and smelting in particular, is a critical part of addressing the zinc sector's impact on SDG 7 "Affordable and Clean Energy" and 13 "Climate Action". By implementing major technological changes, the zinc sector has already contributed to the reduction of CO_2 emissions over the last 25 years. The zinc sector already is electrified to a high degree and has made progress in innovation and development of new, more efficient technologies [38]. Most of the energy needed for zinc melting is required for the electrolysis. If available zinc smelters could switch to sustainable energy for this process.

The zinc sector has been an important part of infrastructure due to zinc's many inherent, beneficial properties such as durability and recyclability. These properties are also increasingly important for zinc's growing role in contributing towards SDG 7 "Affordable and Clean Energy" through the provision of raw materials to support technologies for renewable energy recovery. For example, zinc is used for galvanizing

supporting structures for solar panels and towers for off-shore windmills, ensuring a maintenance-free service life over decades. Zinc based energy storage systems will play a major role in providing constant energy supply from non-constant energy sources (wind and solar power).

Zinc through the galvanization of steel will also play a role in climate resilience, when this material is used instead of other, more vulnerable materials, such as wood, e.g., for utility poles in North America. The use of galvanized steel in urban infrastructure, particularly in developed countries, will significantly contribute to infrastructural integrity facing more extreme weather patterns and make cities safer for growing urban populations [35].

Employment and Operations Along the Value Chain

The zinc industry, through the entire value chain from mining operations to manufacturing, has the responsibility to make a positive contribution, to the communities in which it operates, including job creation and investment in host countries. Within this context, the diverse nature of zinc and its global sector footprint contribute significantly to the zinc sector's importance as a source of employment and potential to enhance the quality of life for people around the world. Through compliance with labor standards and ensuring human rights throughout the sector and in all geographies, the zinc sector can contribute to human development goals around the world.

Through its enhanced activities linked to responsible sourcing, the zinc sector focuses on upholding and respecting human rights throughout their operations. While this is already high on the radar of mining companies, this is a crucial issue that warrants ongoing focus, as it is fundamental to protecting companies', and the broader mining sector's social license to operate. Protecting human rights is also central to achieving all the SDGs. The zinc sector's role as a major employer and contributor to the local economies of the regions it operates in contributes significantly to SDG 8 "Decent Work and Economic Growth" and can also contribute to SDGs 5 "Gender Equality" and 10 "Reduced Inequalities", which focus on gender and broader economic inequalities. Furthermore, the sector can also contribute to human development in the geographies in which it operates through company initiatives with local communities.

Mining and its associated infrastructure by its nature have the potential to adversely affect ecosystems, demonstrating clear links to SDG 15 "Life on Land". The mining sector has a strong potential role to play in the sustainable stewardship of the land that it manages, and the people that rely on these natural resources.

Mining organizations are reducing their operation carbon footprint through partnerships with organizations such as ICMM. Overall, mining organizations are taking steps to reduce their resource use along their value chains and steward the local environments in which they operate. These partnership efforts acknowledge that SDG 15 remains a key SDG of relevance to all mining operations [35].

Sustainable Cities and Circular Economy

The construction and transportation sectors account for 70% of zinc product applications. Zinc contributes to the longevity of steel infrastructure by protecting it from corrosion and extending the useful life of buildings, cars, public transport, and many other types of societal infrastructure that is crucial to everyday life. This strength therefore adds to the safety element of sustainable cities and communities. About 60% of total zinc production is still in use today. The use of hot-dip galvanized steel has been shown to be characterized by lower consumption of resources and less pollution throughout its service life in comparison with an equivalent paint system [39, 40].

While galvanized steel is used widely in developed countries and across a variety of sectors, there is still considerable growth to be realized in new growth economies where the markets are underdeveloped, and where significant population growth and subsequent rapid urbanization is expected into 2050 [41]. More than three billion people are estimated to be in need of adequate housing by 2030 [42]. Without safe, long-lasting infrastructure, some of the world's most vulnerable people will be further at risk of exposure to increasingly frequent and volatile climatic events. The construction of high-rise buildings typically aims to address population growth by maximizing the use of space, especially in areas of rapid urbanization. Specifically, high-rise buildings classed as skyscrapers are constructed using steel. As such, the housing and construction sector is the largest consumer of steel, using around 50% of steel produced. At this scale, the requisite of steel galvanization illustrates the magnitude of zinc's role in SDG 9 "Industry Innovation and Infrastructure", 11 "Sustainable Cities and Communities" and 12 "Responsible Consumption and Production".

While zinc contributes to SDG 9 and 11 by keeping infrastructure durable and more resilient in the face of climatic uncertainty, it also contributes to SDG 12 as zinc has an extremely high recycling potential. Zinc metal can be infinitely recycled without losing its essential properties. About 35% of current zinc production comes from zinc-bearing materials that have come out of use and been recycled. While it's estimated that at a global scale about 45% of all available zinc at the end of life is actually recovered and recycled, recycling rates vary depending the maturity of recycling networks and regulatory incentives for industrial waste reduction of different regions.

Moving forward, there are significant opportunities to scale up the recycling of zinc products through innovative recovery technologies and engagement with regulators in order to close the loop for zinc's life cycle [35].

Conclusions

The metals industry is faced with global challenges linked to sustainable development, such as climate change, circular economy, and responsible sourcing. Of course, there are responsibilities that companies have to deal with at enterprise or at site level.

In addition, success of material stewardship initiatives relies on coordination by commodity associations for the sustainable long-term success of an industry sector. For the global zinc industry, IZA is the home of material stewardship along the whole zinc metal value chain.

The tools of material stewardship, e.g., life cycle assessment, mass flow analysis, and the vast field of responsible sourcing are the basis for credible information and analysis of the current position and developments as well as for strategical action planning to ensure the sector's sustainable development.

IZA is and has been the source of credible information on LCA data on global zinc mining and production, mass flows, availability, and recycling rates. By design, the zinc sector's responsible sourcing activities are influenced by the various materials stewardship activities.

The global zinc industry evaluated its current position in the "Zinc Sector SDG Roadmap". Impact opportunities and actions were agreed, that ensure a sustainable development in the coming years that is in line with the goals defined by the United Nations in 2015 (the UN SDGs). These focus on four themes including health and wellbeing, energy and climate resilience, employment and operations, and sustainable cities and circular economy, reflecting the strengths of zinc as a critical raw material along the global zinc industry value chain:

- Zinc is an essential element for human beings as well as for plants and animals;
- Zinc protects steel from corrosion, specifically in infrastructure and renewable energy recovery;
- Innovative zinc uses contribute to climate resilience;
- Zinc mining and production sites impact on employment, communities and reduced inequalities; and
- Zinc metal is recycled from its uses over and over again.

With the actions derived from the zinc sector SDG roadmap, the global zinc industry ensures its continued and increased contributions to many of the UN SDGs.

Finally, IZA contributes to SDG 17 "Partnerships for the Goals" which is a pillar of achieving all other SDGs, as these cannot be achieved in isolation. IZA coordinates the global zinc industries' joint activities linked to sustainable development and ensures that the experts of the zinc world are connected with relevant networks of other experts to enhance its positive impact.

References

1. Brundtland commission: report of the world commission on environment and development: "our common future". Oslo, 20 Mar 1987. Available online at http://www.un-documents.net/our-common-future.pdf
2. Resolution by the United Nation General Assembly: "transforming our world: the 2030 agenda for sustainable development", adopted 21 Oct 2015. Available online at https://www.un.org/ga/search/view_doc.asp?symbol=A/RES/70/1&Lang=E, https://sustainabledevelopment.un.org/?menu=1300

3. United Nations “Paris Agreement” (2015) Available online at https://unfccc.int/sites/default/files/english_paris_agreement.pdf
4. OECD (2019) Global material resources outlook to 2060: economic drivers and environmental consequences. OECD Publishing, Paris. Available online at https://doi.org/10.1787/9789264307452-en
5. OECD (2011) OECD guidelines for multinational enterprises. Available online at http://www.oecd.org/daf/inv/mne/48004323.pdf
6. ILZSG (2019) Statistical data base. http://www.ilzsg.org/static/statistics.aspx?from=1, downloaded at 27.9.2019
7. Maréchal L (2019) OECD due diligence guidance on responsible supply chains of minerals. In: Presentation at Eurometaux Trade Committee. 7 May 2019
8. IZA (2018) About cycles, recycling, and circular economy. Available online at https://sustainability.zinc.org/recycling/
9. Krüger J et al Sachbilanz Zink. Aachen 2001, Mainz-Verlag 2002, ISBN 3-89653-939-6
10. Reuter MA, van Schaik A, Gutzmer J, Bartie N, Abadías-Llamas A (2019) Challenges of the circular economy: a material, metallurgical, and product design perspective. Annu Rev Mater Res 49:253–274
11. Bergische Unversität Wuppertal/bauforumstahl (2015) Sachstandsbericht zum Stahlrecycling im Bauwesen. Manfred Helmus. Available online at https://bauforumstahl.de/upload/documents/nachhaltigkeit/Sachstandsbericht.pdf
12. Piret NL (2012) EAF dust processing: rotary hearth a potential substitute for the waelz kiln? World Metall Erzmetall 65(5):306–316
13. Jorge J (2015) Secondary zinc as part of the supply chain and the rise of EAF dust recycling. In: ILZSG 19th zinc & its markets seminar. Helsinki, Finland. 6 May 2015
14. Grund S, Schönnenbeck M (2011) “Lebenslänglich“, Dachbaumagazin 12/2011, pp 48–49
15. Maximizing value: guidance on implementing materials stewardship in the minerals and metals value chain. Available online at https://www.icmm.com/en-gb/publications/materials-stewardship/maximizing-value-guidance-on-implementing-materials-stewardship-in-the-minerals-and-metals-value-chain
16. IZA (2018) Resources and guiding principles. https://sustainability.zinc.org/resources/
17. Meylan G, Reck BK (2017) The anthropogenic cycle of zinc: status quo and perspectives. Resour Conserv Recycl 123:1–10
18. Meylan G, Reck BK (2017) The anthropogenic cycle of zinc: status quo and perspectives. Res Conserv Recycl 123:1–10
19. Blanpain B, Reuter M, Malfliet A (2019) Lead metallurgy is fundamental to the circular economy. Socrates Policy Brief, Feb 2019
20. ISO 14040 (2006) Environmental management—life cycle assessment—principles and framework. Available online at https://www.iso.org/standard/37456.html
21. EU Single Market for Green Products Initiative. Available online at http://ec.europa.eu/environment/eussd/smgp/index.htm. Status Jan 2019
22. Van Genderen E et al (2016) A global life cycle assessment for primary zinc production. Int J Life Cycle Assess 21:1580–1593
23. Johannes A. Drielsma et al (2016) Mineral resources in life cycle impact assessment—defining the path forward. Int J Life Cycle Assess 21(1):85–105. Available online at https://link.springer.com/article/10.1007/s11367-015-0991-7
24. Grund S, van Genderen E, van Leeuwen M (2019) Circular economy—recycling at all costs? Zinc: unleashing valuable resources. In: Proceedings of EMC2019, published by GDMB in 2019
25. Ellen McArthur Foundation (2015) Granata design and life: circularity indicators—an approach to measuring circularity. Available online at https://www.ellenmacarthurfoundation.org/resources/apply/circularity-indicators
26. van Schaik A, Reuter MA (2016) Recycling indices visualizing the performance of the circular economy. World Metall Erzmetall 69(4):5–20

27. IZA (2018) How zinc, the zinc industry and IZA contribute to the UN SGDs. Available online at https://sustainability.zinc.org/
28. ICMM Performance Expectations. Available online at https://www.icmm.com/icmm-10-principles, downloaded on 27.9.2019
29. Dutch IRBC. Available online at https://www.imvoconvenanten.nl/metallurgisch?sc_lang=en, downloaded on 27.9.2019
30. Responsible Steel Standard. Available online at https://www.responsiblesteel.org/, downloaded on 27.9.2019
31. UN Global Compact. Available online at https://www.unglobalcompact.org/
32. GRI. Available online at https://www.globalreporting.org/Pages/default.aspx
33. EITI. Available online at https://eiti.org/homepage
34. wbcsd and ERM: "SDG sector roadmaps". Available online under https://www.wbcsd.org/Programs/People/Sustainable-Development-Goals/SDG-Sector-Roadmaps/Resources/SDG-Sector-Roadmaps
35. Street L, Andrade A, Hartlin B, Roberts G (2020) Zinc sector SDG roadmap, to be published by IZA, Jan 2020
36. Black RE, Fischer CW (2012) Role of zinc in child health and survival. Nestle Nutr Inst Workshop Ser 70:37–42
37. PWC, presentation at EM SD Committee, June 2018
38. IZA: "Sectoral roadmap zinc 2050" (2012) Available online at https://eurometaux.eu/media/1907/sectoral-roadmap-zinc-2050.pdf
39. Wolley T (2014) Galvanizing and sustainable construction- a specifier's guide. European General Galvanizing Association. Available online at https://www.egga.com/wp-content/uploads/2014/06/6.-ga_sustain_eng_lr.pdf
40. Rossi B, Marquart S, Rossi G (2017) Comparative life cycle cost assessment of painted and hot-dip galvanized bridges. J Environ Manage 197:41–49
41. United Nations (2018) World population prospects: the 2018 revision: key facts. Available online at https://population.un.org/wup/Publications/Files/WUP2018-KeyFacts.pdf, https://population.un.org/wpp/Publications/Files/WPP2019_Highlights.pdf
42. UN Habitat (2018) Sustainable cities and communities. Available online at https://unhabitat.org/wp-content/uploads/2018/07/UN-Habitat-Brochure.pdf
43. IZA (2015) Material supply. IZA fact sheet. Available online at https://www.zinc.org/wp-content/uploads/sites/4/2015/04/RecyclingMaterialSupply_July2015_Final.pdf
44. Intergovernmental Panel on Climate Change (IPCC) special report, 25 Sept 2019. Available online at https://www.ipcc.ch/2019/, downloaded on 27.9.2019
45. UNEP (2011) Recycling rates of metals—a status report. In: Gradel TE, Allwood J, Birat J-P, Reck BK, Sibley SF, Sonnemann G, Buchert M, Hagelüken CH (eds) A report of the working group on the global metal flows to the international resource panel

Effect of Deposit Types, Mine Development and Industry Structure on Primary Lead and Zinc Economics in Australia, North America and Europe

L. Reemeyer

Abstract The economics of primary lead and zinc production are influenced by geological attributes of deposits and geographical factors such as access to transport infrastructure and markets. Characteristics of deposit types such as SEDEX, VMS, CRD and MVT influence both revenue and costs. Resulting mine economics are reviewed with focus on Australia, Canada, USA and Europe. Mine development and depletion and changes in smelting due to tightening environmental standards and changing concentrate availability are reviewed for the last 25 years. This includes major changes in smelting flowsheets to adapt to feedstock supply shifts. Changes in industry structure including consolidation, changes in vertical integration and the rise of Chinese production are examined. The role of byproduct recovery, particularly silver, on economics of both mines and smelters is reviewed. A future outlook on lead-zinc industry structure in Australia, Canada, USA and Europe to 2040 is included.

Keywords Lead · Zinc · Mineralogy · Smelting · Economics

Introduction

Mine production of lead and zinc comes primarily from sulphide deposits that contain lead, zinc and silver. Lead is typically present as galena and zinc as sphalerite. Silver is often associated with galena but may also be present in a range of silver minerals such as tetrahedrite or pyrargyrite. Most ores are processed using grinding and flotation.

Historically, Australia and Canada were major mine producers of zinc and lead, but their production has waned in the last 20 years. This is particularly true for Canada, which was the world's largest zinc mine producer in 1996 but had fallen to 8th by 2017. Canadian lead mine production virtually disappeared by 2017. This was due to the depletion of two major mines (Sullivan and Brunswick). Australian zinc production peaked in 2015, but fell dramatically the following year, due to the closure of the large Century mine. USA, Mexico and the European Union have also

L. Reemeyer (✉)
Resourceful Paths, Vancouver, BC, Canada
e-mail: laurie@resourcefulpaths.com

© The Minerals, Metals & Materials Society 2020

A. Siegmund et al. (eds.), *PbZn 2020: 9th International Symposium on Lead and Zinc Processing*, The Minerals, Metals & Materials Series,
https://doi.org/10.1007/978-3-030-37070-1_43

been significant historical producers. Zinc production in USA and the EU have been relatively consistent, while some decline in lead production occurred. Lead and zinc production in Mexico have increased since the late 1990's, largely due to the start-up of Penasquito mine. As Australian and Canadian production declined, Chinese and Indian production increased (Figs. 1 and 2; Table 1). By 2017, China was by far the largest producer of mined lead and zinc. Indian production has centered on a single large zinc mine (Rampura Agucha).

In 2018, MMG's Dugald River mine has achieved commercial production, and New Century resources has commenced reprocessing of historical Century tailings for recovery of zinc concentrate. The combination of these developments is less than the historical production from Century mine but has allowed some rebound in Australian zinc concentrate production.

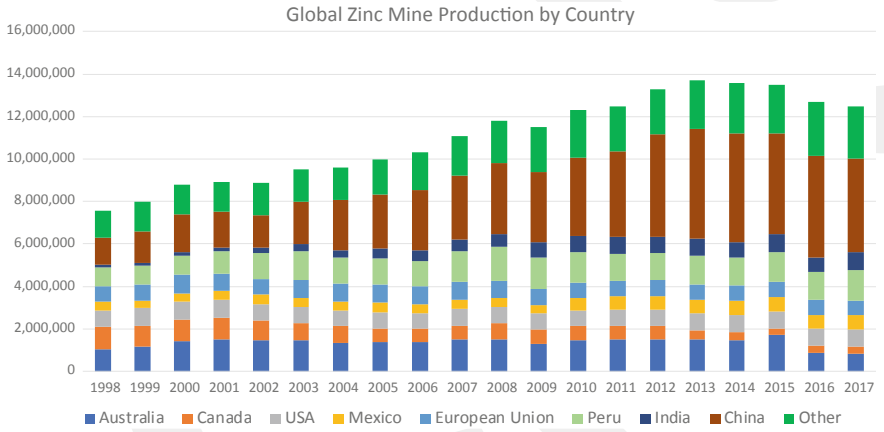

Fig. 1 Global zinc mine production by country [1]

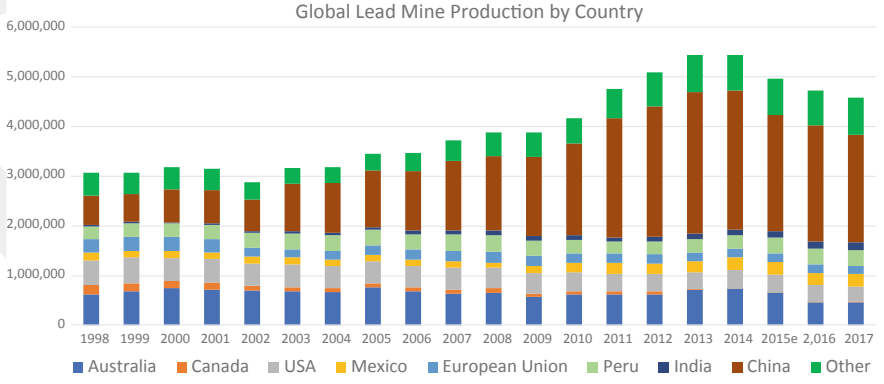

Fig. 2 Global lead mine production by country [2]

Table 1 Changes in zinc and lead production by country between 1998 and 2017

	Zinc ('000 t)			Lead ('000 t)		
Country	1998	2017	Change (%)	1998	2017	Change (%)
Australia	1059	842	−20	618	459	−26
Canada	1062	344	−68	190	14	−93
USA	755	774	3	493	310	−37
Mexico	395	674	71	166	243	46
European Union	743	683	−8	259	169	−35
Peru	869	1473	70	258	307	19
India	143	833	483	39	170	333
China	1270	4400	246	580	2150	271
Other	1274	2476	94	457	758	66
Total	7570	12,500	65	3060	4580	50
Proportion Australia, Nth America, EU	53.0%	26.5%	−50	56.4%	26.1%	−54
Proportion China	16.8%	35.2%	110	19.0%	46.9%	148
Proportion India	1.9%	6.7%	253	1.3%	3.7%	189

Lead-Zinc Deposit Types

Major lead-zinc deposit types found in North America, Europe and Australia are shown in Table 2.

Broken Hill Type deposits tend to be coarse grained, allowing coarser grinds and higher metal recoveries than other Pb-Zn deposits. They are also typically high in

Table 2 Lead-zinc deposit types in North America, Europe and Australia [3]

Deposit type	Example	Country
SEDEX	McArthur River, Mt Isa, Century Red Dog Selwyn	Australia USA Canada
Broken hill type (high grade metamorphic)	Broken Hill Cannington	Australia
Mississippi Valley Type/Irish Type/carbonate Replacement deposit	Missouri Lead Belt, Tennessee, Taylor Pine Point Tara	USA Canada Ireland
VMS	Manitoba operations, Izok, Kidd Greens Creek Rosebery	Canada USA Australia
Epithermal	Penasquito Elura (Endeavour)	Mexico Australia

Ag, resulting in Ag-rich lead concentrates. Fine grained SEDEX deposits (e.g. Century, McArthur River, Mt Isa) typically require fine regrinding to maximize lead and zinc recovery and concentrate quality, increasing processing costs. MVT/Irish/CRD tend to have high proportions of carbonate in gangue minerals, and therefore have significantly less challenges with acid-rock drainage issues from tailings than other deposit (e.g. VMS, SEDEX). In some cases, it is possible to produce saleable agricultural lime by-product from MVT flotation tailings (e.g. Tennessee). Epithermal deposits, such as those in Mexico typically have high precious metal content, resulting in high-value lead concentrates with elevated Ag and Au. Such concentrates may also be enriched in impurities such as Bi and Sb. Therefore smelters (e.g. Penoles) may tailor their processes to manage both high precious metals and impurities. VMS deposits can contain economic quantities of copper and precious metals, although the head grades of these can vary considerably. For example, in some zinc containing VMS deposits, copper dominates economic value (e.g. Neves Corvo, Portugal), some are gold rich (e.g. LaRonde, Canada, Rosebery, Australia) and some are very rich in silver (e.g. Greens Creek, USA). Figure 3 shows estimated net smelter return for different deposit types in North America, Europe and Australia.

Other mineralogical aspects of Pb-Zn deposits may also affect concentrate quality, which in turn can affect marketability of zinc concentrates. For example:

- Pb in Zn concentrates—affected by grain size and mineral textures between galena and sphalerite. For very fine-grained ores (e.g. McArthur River), it may be necessary to produce bulk concentrates containing relatively low Zn grade and relatively high Pb grade. Such concentrates attract less favourable terms (payable factors, treatment charges) from smelters, reducing economic attractiveness of mines.

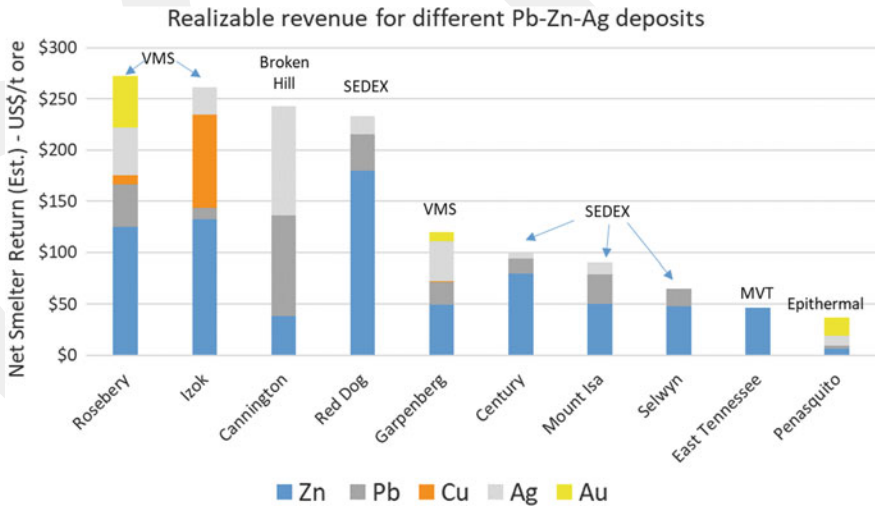

Fig. 3 NSR for different lead-zinc deposit types

- Fe in sphalerite—the level of Fe in sphalerites can vary considerably by deposit. Some zinc mines have very low iron in sphalerite (e.g. Century, Tennessee), which allows production of high Zn grade concentrates and low residue formation in smelters. Other deposits have much higher iron in sphalerite such as Broken Hill (which contains a high iron form of sphalerite called marmatite) and Dugald River.
- Mn in sphalerite—Dugald River also has elevated levels of Mn in sphalerite. This affects concentrate quality and marketability. Mn causes operational challenges in the cell houses of electrolytic zinc refineries (Mn mud build up).
- Fine grained silica—some SEDEX deposits (e.g. Century, McArthur River) have fine grained silica intergrowths with sphalerite that results in elevated silica in concentrate. This can affect the settling properties of residues in the smelter. Smelters can apply penalties for silica above 4%.
- Organic carbon, which can be present.
- Fluorine—which is present in Cannington ore can cause problems with corrosion in the gas handling system of smelters. An acid leach using aluminium sulphate is used to leach fluorine minerals from lead and zinc concentrates.
- Dolomite (MgO, CaO)—Irish mines (e.g. Tara, Galmoy) have sometimes leached concentrates with sulphuric acid to improve concentrate grades [4]. Applicable to Irish/MVT type deposits.

Smelting

Sinclair [5] estimated that in 2003, 89% of primary zinc smelter production was from the electrolytic process. Most of the remaining capacity was from plants using the Imperial Smelting Process (ISP). Major changes in lead and zinc smelting by country have also occurred since 2000. There has been a major increase in lead and zinc smelting in China. In the meantime, smelters in North America, Europe and Australia have closed (Table 3). Many of these closures were hastened by tightening environmental standards for lead, particularly those plants using sinter plant flowsheets (Cockle Creek, Herculaneum, Avonmouth and Duisburg). In addition, Glencore closed the Portovesme ISP plant in Italy, focusing instead on improving its electrolytic zinc smelter, Kivcet lead smelter and zinc solvent extraction plant. The decline in ISP plants has made it more difficult for mines producing zinc concentrates with elevated lead to market their concentrates. This has affected McArthur River (MIM/Xstrata/Glencore), which produces a low-grade zinc concentrate with significant lead.

Table 3 Lead and zinc smelter closures in North America, Europe and Australia since 2003 [6]

Name	Country	Metal	Process	Capacity	Year closed
Cockle Creek	Australia	Pb–Zn	ISP	90,000 tpa Zn, 35,000 tpa Pb	2003
Kidd	Canada	Zn	Electrolytic	145,000 tpa Zn	2010
Big River Zinc	USA	Zn	Electrolytic	90,00 tpa Zn	2006
Herculaneum	USA	Pb	Sinter plant blast furnace	115,000 tpa Pb	2013
Avonmouth	UK	Pb–Zn	ISP	90,000 tpa Zn, 35,000 tpa Pb	2003
Duisburg	Germany	Pb–Zn	ISP	100,000 tpa Zn, 35,000 Pb	2005
Ruhr Zink	Germany	Zn	Electrolytic	140,000 tpa Zn	2008

Industry Structure

Around 2000, the industry structure of lead and zinc mining industry in North America, Europe and Australia included several major vertically integrated companies (Table 4). In the 1990's, vertical integration strategies by MIM and Pasminco had focused on acquiring smelters compatible with concentrates produced from the major McArthur River and Century mines. Pasminco sold the Avonmouth ISF smelter to MIM to allow treatment of McArthur River bulk concentrates and purchased the Budel smelter in the Netherlands as it was compatible with the low iron, low residue forming Century concentrates.

Major waves of consolidation occurred from 2002 to 2013, including:

- Xstrata acquiring MIM and Falconbridge to form a major vertically integrated zinc and lead mining, smelting and refining company, with subsequent acquisition by Glencore
- Zinc asset swaps between Outokumpu and New Boliden in Europe resulting in Boliden controlling vertically integrated zinc assets in Europe
- Pasminco refloating as Zinifex, offloading mines in NSW, Australia and then splitting off its smelting business into Nyrstar in conjunction with Umicore's European zinc smelters
- The breakup of former Zinifex, with sale of Australian zinc mining assets to Chinese controlled MMG
- Acquisition of Breakwater Resources (incorporating several North American zinc mines) by Nyrstar
- Sale of Anglo American zinc assets to Hudbay and Vedanta
- Partial float of precious metals rich mining operations by Penoles into Fresnillo PLC.

In addition, Teck and Glencore now hold significant zinc mining assets in Peru (e.g. stakes in Antamina mine), which provide feed to their smelters in North America. In

Table 4 Lead and zinc industry structure in North America, Europe and Australia in 2000

Company	Mining assets		Smelting and refining assets	
	Asset	Country	Asset	Country
MIM holdings	Mount Isa Mines	Australia	Mount Isa Pb smelter	Australia
	McArthur River Mine		Northfleet Pb refinery	UK
			Avonmouth ISP	
			Duisburg ISP	Germany
Pasminco	Rosebery	Australia	Hobart Zn smelter	Australia
	Broken Hill		Port Pirie Pb smelter	
	Elura		Cockle Creek ISP	
	Century		Budel Zn smelter	Netherlands
	Tennessee	USA	Clarksville Zn smelter	USA
BHP	Cannington	Australia	N/A	
Western metals	Pilara	Australia	N/A	
Teck-Cominco (Teck)	Sullivan, Polaris	Canada	Trail Zn and Pb smelter	Canada
	Red Dog	USA		
Noranda-Falconbridge	Brunswick	Canada	Brunswick Pb smelter	Canada
	Kidd		Kidd Zn smelter	
			CEZinc smelter	
Anglo American (inc. Hudson Bay Mining and Smelting)	Manitoba Operations	Canada	Flin Flon Zn smelter	Canada
	Lisheen	Ireland		
Penoles	Fresnillo, Cienega	Mexico	Torreon Zn and Pb smelter	Mexico
Xstrata	N/A		Asturiana Zn smelter	Spain
Outokumpu	Tara	Ireland	Kokkola Zn smelter	Finland
Boliden	Garpenberg	Sweden	Odda Zn smelter	Sweden
Umicore	N/A		Balen Zn smelter	Belgium
			Auby Zn smelter	France

2019, Trafigura took control of Nyrstar, resulting in two metals trading companies (it and Glencore) controlling a significant proportion of zinc mining and smelting. In 2018, Glencore zinc mine production was 1.07 Mt, and smelter production was 0.80 Mt. Glencore is also operator of the CEZinc refinery in Canada, with capacity of 270,000 t refined Zn. Therefore, Glencore's overall mine and smelting capacity is quite evenly balanced. In 2018, Teck mine production was 705,000 t, and refined production was 303,000 t [7]. In 2018, Nyrstar zinc mine production was 139,000 t and refined production was 1.06 Mt.

The closure of the Brunswick mine in 2013 led to conversion of the Brunswick lead smelter from a vertically integrated internal smelter to a custom smelter treating both Pb concentrates from mines and recycled Pb-bearing materials. Similarly, CEZinc is currently going through a transition to a more custom feeds, as zinc concentrate supply from Glencore's Canadian zinc mines continues to decline. In 2012, Glencore reported 506,000 t Zn in concentrate from its Canadian Zn mines (Brunswick, Perseverance and Kidd). By 2018, production had fallen to 101,000 t [8]. Hudbay has announced the impending closure of the Flin Flon zinc refinery in 2021 as its Manitoba zinc mines decline in coming years [9]. In contrast, Korea Zinc is expanding its Townsville refinery in Australia given the secure long term outlook for zinc concentrate production from mines in NW Queensland [10].

The dynamics of lead smelting are much different to zinc, as the majority of the world's refined lead supply is now met from the recycling of lead from lead-acid batteries. In 2018, ILZSG [11] estimated that mined lead production was 4.7 Mt of contained metal and refined production was 11.6 Mt metal, indicating approximately 60% of supply came from secondary sources.

Economics of Lead and Zinc Mine Production in North America, Europe and Australia

Mines and smelters in North America, Europe and Australia follow typical negotiations for payable fractions, treatment and refining charges for lead and zinc concentrates. Typical terms are as follows:

- Zinc concentrates are paid at the minimum of 85% of contained Zn, or 8% deduction on grade units
- Lead concentrates are paid at minimum of 95% of contained Pb or 3% deduction on grade units
- Silver in lead concentrates are paid at 90–95% depending on grade (higher grades are paid at higher proportions)
- Silver in zinc concentrates are usually subject to a 90 g/t deduction and are only paid at 65% of Ag content above that
- Gold in Pb concentrates are paid at approximately 90% for high Au concentrates, this mainly applies to mines in Mexico

- Treatment charges are set annually for zinc and lead concentrates (per t concentrate) depending on the balance of supply and demand between miners and smelters
- Mining companies pay for transport of concentrates to customers.

Companies with integrated mines and smelters (e.g. Glencore, Teck, Boliden, Penoles) also have opportunities to realize the value of minor metals across the vertical lead-zinc processing chain. This can include metals such as Bi, Cd, Cu, Ge, In and Sb. The Nyrstar Tennessee mines and Clarksville smelter is an additional pair of integrated assets that benefit from such byproduct recovery (Ge). However, these byproducts produce relatively low revenue compared with the main payable metals (Zn, Pb, Ag).

The rapid rise in Chinese lead and zinc smelting capacity and since 2000 has dramatically changed the international flows of lead and zinc concentrates. This coupled with the decline in vertical integration of mines and smelters, especially in Canada and Australia has led to a changing dynamic and increased volatility in treatment charges for concentrates.

MVT deposits, which often contain relatively low head grades and byproduct silver, have typically been swing producers during periods of low zinc prices. This is because their margins change dramatically as zinc prices change.

Locational proximity of mines and smelters can be a strategic advantage, e.g. Hobart smelter and Rosebery mine, Townsville smelter and Zn mines in NW Queensland, Penoles mines and Torreon smelter in Mexico, Clarksville smelter and Tennessee mines in USA, Boliden mines and smelters in Europe. Mine depletion and smelter closures in Australia and North America have weakened these location advantages in some cases (e.g. Brunswick, Kidd in Canada, closure of Herculaneaum smelter adjacent Missouri lead mines in USA). In the past, vertically integrated smelters and mines were tailored to the characteristics of local concentrates, which derived from deposit types. The global trend in lead and zinc smelting and refining has instead been towards increased economies of scale for strategically located smelters, flexible flowsheets for a range of concentrate feeds, and technologies that allow increased recycled material feeds (e.g. lead bearing residues, Zn-bearing EAF dusts). This trend can be expected to continue, especially for smelters in North America and Europe.

Outlook for Next 40 Years

In general, the pipeline of future lead-zinc projects has not been strong and lead and zinc have attracted less exploration investment than copper and gold. There are several large, long life SEDEX deposits in North America and Australia that will continue to provide a supply of metal including George Fisher, Dugald River, McArthur River and Red Dog. There are considerable Pb–Zn resources in Canada that could be developed in Yukon, NWT and Nunavut. These include the MacMillan

Pass and Selwyn SEDEX deposits in Yukon Territory, the Pine Point MVT deposit (restart) in North West Territories and the Izok and Hackett River VMS deposits in Nunavut [12]. All of these but these are remote from ports and have significant infrastructure requirements. Therefore, they would require high lead and zinc metal prices to justify development. The Taylor deposit in Arizona is being developed by South32 and would likely export concentrates to world markets. Glencore controls a large Irish style carbonate deposit in Ireland, Pallas Green, which could replace declining reserves of zinc concentrates from other European mines to feed European smelters. The availability of significant lead and zinc resources in North America, Europe and Australia suggests that these regions can continue to be significant long term producers of these metals, but the viability of individual mining projects will depend on geographical location and deposit type and characteristics [13–15].

References

1. USGS, Mineral Commodity Summaries, Zinc (2001, 2004, 2007, 2010, 2013, 2016, 2019)
2. USGS, Mineral Commodity Summaries, Lead (2001, 2004, 2007, 2010, 2013, 2016, 2019)
3. Laznicka P (2010) Giant metallic deposits: future sources of industrial metals, 2nd edn. Springer, Heidelberg
4. Glencore, Q4 2012 Production Report
5. CBC (28 Nov 2018) https://www.cbc.ca/news/canada/manitoba/800-jobs-flin-flon-mine-shutters-1.4924774. Accessed 1 October 2019
6. http://www.sulphuric-acid.com/sulphuric-acid-on-the-web/acid%20plants/Ruhr-Zink%20-%20Datteln.htm. Accessed 14 Oct 2019
7. https://www.teck.com/investors/five-year-production/. Accessed 13 Oct 2019
8. Glencore, Q4 2018 Production Report
9. Reemeyer L (2018) Mining and metals industry structure and interaction with the circular economy. SME Annual Meeting, Minneapolis
10. Queensland Government (2019) Refinery expansion a jobs bonanza for Townsville. 7 Dec 2018. http://statements.qld.gov.au/Statement/2018/12/7/refinery-expansion-a-jobs-bonanza-for-townsville. Accessed 15 Oct 2019
11. Noranda Income Fund, Annual Information Form (2018)
12. Galley A, Hannington M, Jonasson I (2007) Volcanogenic massive sulphide deposits, in mineral deposits of Canada, Geological Association of Canada, Mineral deposits division special publication no. 5. St John's Canada
13. Irish EPA (2013) Tara mine attachment D: infrastructure and operation. http://www.epa.ie/licences/lic_eDMS/090151b2803b7387.pdf
14. Sinclair R (2005) The extractive metallurgy of zinc. AusIMM, Melbourne
15. International Lead Zinc Study Group (2019) press release: world lead and zinc supply and demand. 21 August 2019

Part XII
By-Product Recovery I

GCRIS

Hydrometallurgical Recovery of Tin from Harris Dross

Ryosuke Sato, Koichiro Hirata and Fumito Tanaka

Abstract Emerged businesses in recycling have been causing the accumulation of impurities in by-processes in base metal smelters. In lead smelters, such impurities are basically removed by drossing. Since drosses comprise several impurity elements of approximately 20 mass% each as well as lead, they require further treatment to separate into each element. Conventional pyrotreatments are, however, not effective due to affinity of impurity elements at high temperatures. The authors have developed a hydrometallurgical process to recover tin and lead separately from Harris dross which is composed mainly of tin, arsenic, and lead. In the process developed, Harris dross is leached to separate lead-bearing residue, then the leachate is mixed with limestone to precipitate burtite ($CaSn(OH)_6$) selectively, and the effluent is mixed with slaked lime to precipitate calcium arsenate. Lead-bearing residue can be recycled to the blast furnace while burtite can be payable for tin smelters because impurities in burtite are negligible.

Keywords Harris dross · Tin leaching · Burtite

Introduction

Hosokura Metal Mining Company (Hosokura), which is a subsidiary of Mitsubishi Materials Corp., refines bullion by conventional Harris process in which caustic soda and sodium nitrate are added to bullion of the temperature between 400 and 500 °C to remove impurities as "Harris dross" [1]. After that, the dross is separated into lead bullion and caustic copper matte by pyrotreatments since the bullion adheres to the dross. Recovered bullion is recycled to the blast furnace and caustic matte is sent to

R. Sato (✉)
Mitsubishi Materials Corporation, Kagawa, Japan
e-mail: satoryo@mmc.co.jp

K. Hirata
Mitsubishi Materials Corporation, Fukushima, Japan

F. Tanaka
Mitsubishi Materials Corporation, Tokyo, Japan

© The Minerals, Metals & Materials Society 2020

A. Siegmund et al. (eds.), *PbZn 2020: 9th International Symposium on Lead and Zinc Processing*, The Minerals, Metals & Materials Series,
https://doi.org/10.1007/978-3-030-37070-1_44

Table 1 Chemical composition of Harris dross

Element	Pb	Sn	Sb	As	Te	Se
Concentrations (%)	21.9	19.3	8.2	1.8	1.2	0.3

the copper smelter at Naoshima (NSR). In lead smelting processes, Harris process aims to remove arsenic into caustic matte while, on the contrary, arsenic is a burden on NSR. Furthermore, the tin content of raw materials received from copper smelters has been increasing due to intentional recycling business. Incremental tin has resulted in the accumulation of tin in Hosokura because tin concentrates into Harris dross, then transfers to bullion which returned to the blast furnace. Therefore, an innovative process to remove arsenic and tin separately has been desired strongly. Seeking the optimal solution to the problem, the authors have developed a hydrometallurgical process to remove arsenic and to recover tin from Harris dross.

Experimental

Raw Materials

The chemical composition of the Harris dross used in the present experiments is shown in Table 1. Na and O are contained as elements other than those listed in the table. The auxiliary materials were selected from commercial products of reagent grade or industrials grade. All experiments were conducted at the temperature of 25 °C unless otherwise noted. Samples were analyzed by inductively coupled plasma-atomic emission spectroscopy (ICP-AES) for the chemical composition, X-Ray diffraction (XRD) for identifying mineralogy, and scanning electron microscope-energy dispersive X-ray spectroscopy (SEM-EDS) for observing morphology.

Conceptual Process Design

The authors have developed a conceptual design of the new process as illustrated in Fig. 1. Major elements included in Harris dross can be separated optimum ways for recycling to the blast furnace, recovering for further treatment in the tin smelter, or discharged to the wastewater treatment plant. Each step will be defined in subsequent sections.

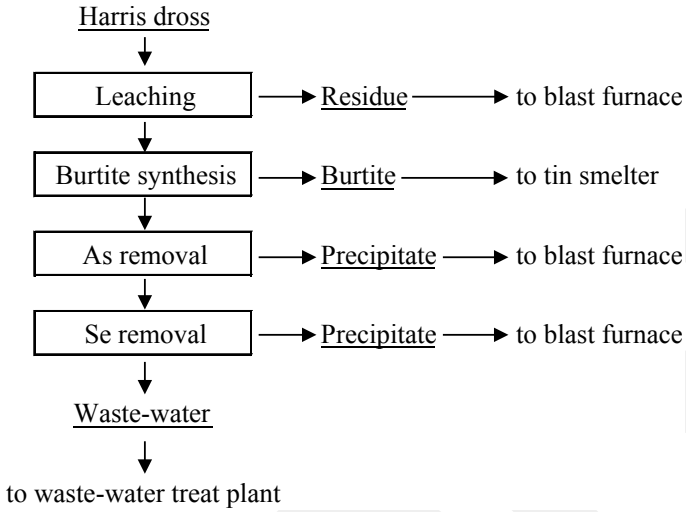

Fig. 1 Block flow diagram of the developed process

Tin Leaching

In the first step, Harris dross is charged into distilled water to leach out tin while copper and lead are remained in the residue. Since lead and tin have similar thermodynamic properties, the present study was focused on the evaluation of conditions where tin is solely soluble to the leachate. For the sake of this objective, the concentration of tin and lead in leachate was examined by the change of pH and leaching time. The initial pulp density was fixed to 25% through whole series of the experiments. Sulfuric acid of 98% was used for pH adjustment.

Burtite Synthesis

Tin is precipitated out of the leachate as burtite ($CaSn(OH)_6$) in the second step. In order to determine the conditions for the burtite synthesis, Pourbaix diagram of Ca–Sn–H_2O system at 298 K was determined as illustrated in Fig. 2. Thermodynamic data used for the calculation was basically quoted from HSC Chemistry by Outotec and ΔG_f^0 of $CaSn(OH)_6$ from Hunter et al. [2]. The stable neutralization form of tin to be crystalized out of the liquid was estimated as hydroxide, and the concentration of the stable solution component of tin was set to 1 mol/L. The stable region of burtite extends in pH from 10.4 to 13.2 as indicated by the shaded area. In the present experiments, pH was controlled to 12.5 during the burtite synthesis.

The authors examined the optimal calcium compounds added for burtite synthesis. At first, a predetermined amount of each calcium compound was added to the

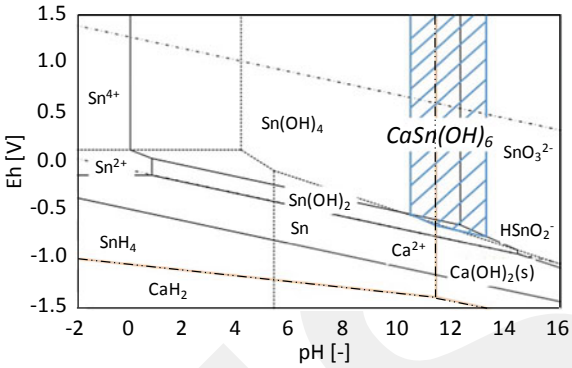

Fig. 2 Pourbaix diagram of Sn–Ca–H_2O system at 298 K

leachate, and then, after stirring for three hours, solid–liquid separation was performed by vacuum filtration, and tin and arsenic of the filtrate were analyzed to select the optimal additive. Subsequently, the amount of the selected additive and the synthesis time were changed to investigate the conditions under which the tin recovery can be maximized. The Ca/Sn ratio was changed between 0.5 and 2.0, and the tin concentration of the leachate was examined at predetermined intervals.

Removal of Arsenic and Selenium

Since the effluent from the burtite synthesis step must be acceptable for the smelter's wastewater treatment plant, the conventional techniques for the removal of arsenic and selenium were applied. Calcium chloride was used to remove arsenic and ferrous sulfate ($FeSO_4 \cdot 7H_2O$) was used to remove selenium. For arsenic removal, pH was adjusted to 12.5 with the caustic soda solution of 24% and added calcium chloride. In this process, not only $Ca_3(AsO_4)_2$, but also $CaSeO_3$ and Ca_3TeO_6 are precipitated, and the amount of added calcium was determined after accounting for the amounts of arsenic, tellurium, and selenium in the solution. For selenium removal, pH was adjusted to 9.0 with caustic soda and added ferrous sulfate.

Results and Discussion

Optimal Conditions for Tin Leaching

As pH decreases, both tin and lead concentrations in the leachate decrease as shown in Fig. 3. When leaching is conducted at pH = 13, it is possible to reduce the lead concentration of the leachate to 500 mg/L or less. The tin leaching ratio under this condition is about 76%. With increasing the leaching time, the tin concentration of

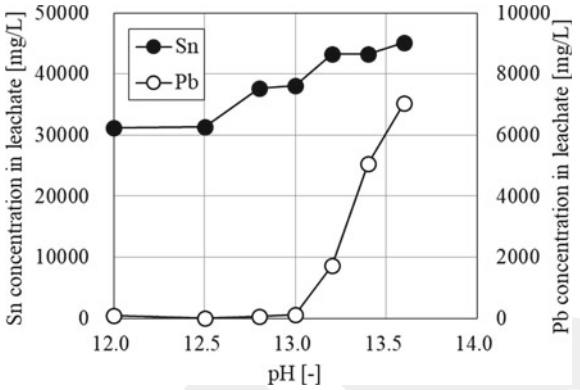

Fig. 3 pH and Sn, Pb concentration of leachate

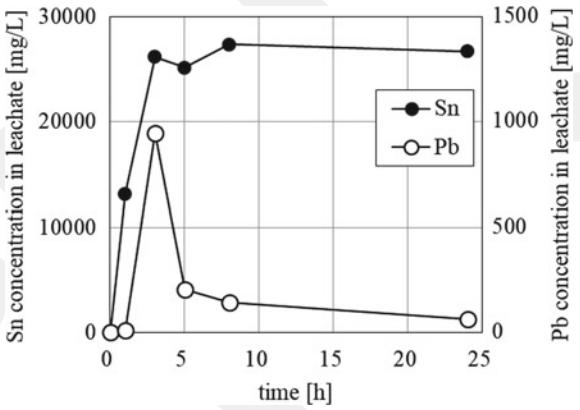

Fig. 4 Temporal change of Sn, Pb concentration of leachate

Table 2 Typical composition of leachate

Element	Sn	As	Te	Se	Pb	Sb
Concentrations (mg/L)	25,000	10,000	230	79	66	24

the leachate increases the maximum at 8 h and remains constant after that while the lead concentration stays at the same level as shown in Fig. 4. Typical assay of the leachate obtained by the present experiments is listed in Table 2, showing rich tin and arsenic have eluted into the leachate.

Stable Burtite Synthesis

Ca/Sn (molar ratio) in this section indicates the molar ratio of the amount of added calcium to the amount of tin in the leachate. Any calcium compound examined

can be used to recover tin completely while arsenic behavior depends strongly on the calcium compound added. The arsenic concentration decreased when calcium chloride or calcium hydroxide were added, on the contrary, did not decrease when calcium carbonate was added as shown in Fig. 5. Such difference is attributable to the solubility of each calcium compound in alkaline solutions. Calcium chloride and calcium hydroxide dissolve to form calcium arsenate via reaction (1), resulting in the precipitation of calcium arsenate with burtite. As calcium carbonate hardly dissolves in alkaline solution, calcium arsenate precipitated with burtite is negligible. Therefore, calcium carbonate was selected for the burtite synthesis.

$$3Ca^{2+} + 2AsO_4^{3-} = Ca_3(AsO_4)_2 \quad (1)$$

The predominant reaction of the burtite synthesis with calcium carbonate is presumed to be reaction (2). The reaction equivalent based on stoichiometry is Ca/Sn = 1.

$$CaCO_3 + SnO_3^{2-} + 3H_2O = CaSn(OH)_6 + CO_3^{2-} \quad (2)$$

Figure 6 demonstrates time-dependent changes of the tin concentration of the leachate during burtite synthesis. The tin concentration was stable after five hours at any Ca/Sn ratio and 98% or more of tin can be recovered under the condition of Ca/Sn = 2 after 5 h have passed. Table 3 shows the Ca/Sn and calcium reaction efficiency using data after 24 h reaction. The calcium reaction efficiency is defined as the ratio of consumed to added calcium carbonate, which is calculated on the assumption that the reduction in tin concentration of the leachate is consumed for the burtite synthesis by reaction (2). At any Ca/Sn ratio, the calcium reaction efficiency was approximately 50%. According to this reaction efficiency, Ca/Sn = 2 calcium carbonate is required to recover the whole amount of tin.

Another half of calcium added remains as calcite ($CaCO_3$) because burtite and calcite were identified from the XRD analysis of the precipitates after the synthesis

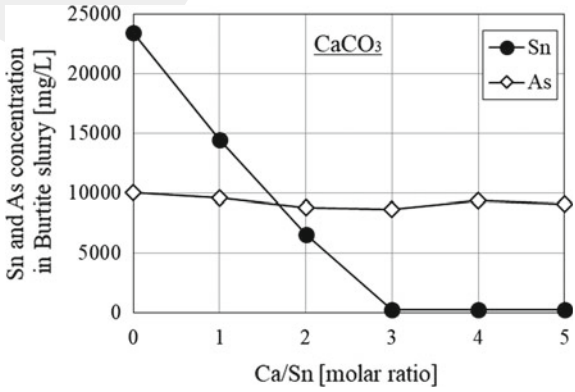

Fig. 5 Effect of molar ratio (Ca/Sn) on Sn and As concentration ($CaCO_3$)

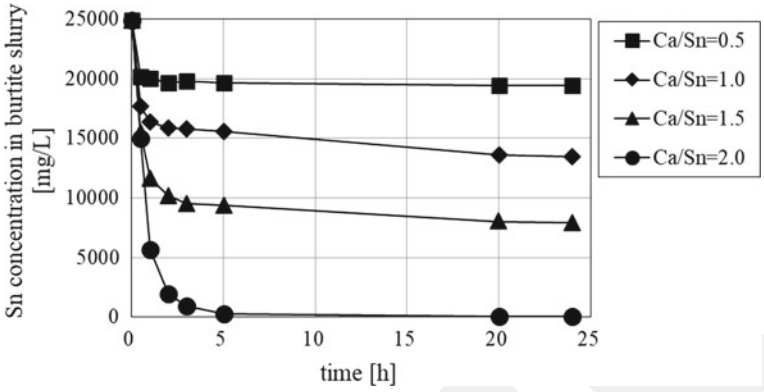

Fig. 6 Time-dependent changes of Sn concentration in the leachate during the burtite synthesis

Table 3 Ca/Sn ratio and Ca reaction efficiency

Ca/Sn (molar ratio)	0.5	1.0	1.5	2.0
Ca reaction efficiency (%)	43.5	45.9	45.4	49.9

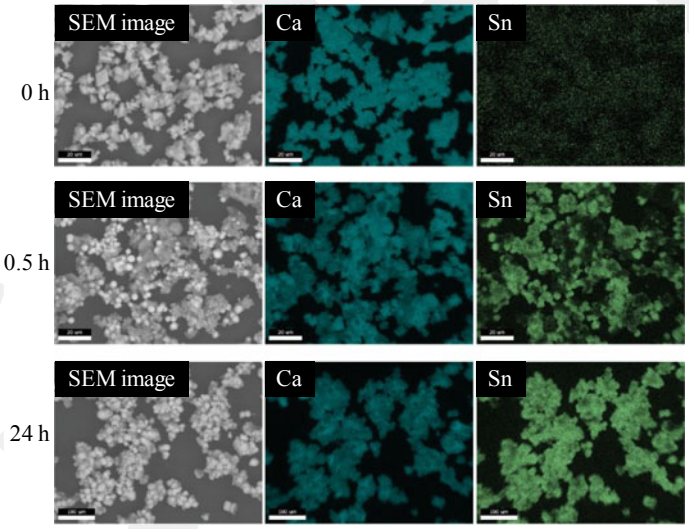

Fig. 7 SEM-EDS analysis of burtite

at Ca/Sn = 2 for 24 h. Composite morphology of the precipitates was observed using SEM-EDS. Figure 7 illustrates the surface morphology of the calcite indicated as "0 h" and the precipitates indicated as "0.5 h" and "24 h." Sequential pictures demonstrate that tin distribution on the calcite surface grows wider and thicker as

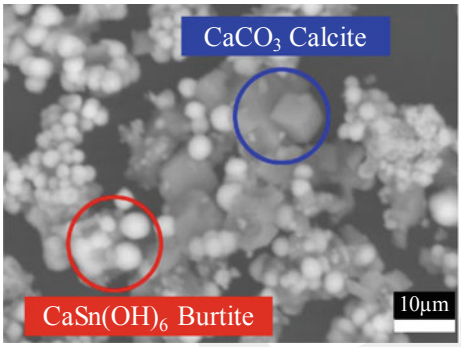

Fig. 8 Burtite growing on the surface of calcium carbonate (Ca/Sn = 2, reaction time is 0.5 h)

Table 4 Chemical composition of burtite precipitates

Element	Sn	Ca	As	Pb	Te	Sb
Concentrations (%)	28.0	24.9	0.9	0.1	<0.1	<0.1

time passes. Figure 8 shows the expanded picture of the precipitates after 0.5 h where the surface of angular calcite is covered with spherical burtite. These observations indicate that SnO_3^{2-} ion and solid calcium carbonate react heterogeneously to form burtite on the surface of the calcite. Since, in general, diffusion through product layer retards strongly as the product layer grows, unreacted core of approximately 50% is estimated to stop shrinking after 5 h have passed. Table 4 shows the chemical composition of burtite precipitates. Elements other than those listed in the table include C, O, and H.

Commercially available calcium carbonate is roughly classified into heavy calcium carbonate and light calcium carbonate. Heavy calcium carbonate is a product obtained by crushing and classifying natural limestone, and the shape of particles is amorphous. Light calcium carbonate is a wet synthesized product [3] which has a large specific surface area and excellent surface reactivity [4]. The calcium carbonate used in the experiments above was light calcium carbonate of reagent grade. Thus, calcium carbonate of industrial grade was selected from commercial products below whose purity were 99% or more.

Heavy calcium carbonate

- 150 μm under in Hosokura: calcium carbonate used in the wastewater treatment plant in Hosokura
- 44 μm under in Hosokura: granules which is a product of the same manufacturers as the product above.

Light calcium carbonate

- Industrial: light calcium carbonate for industrial use
- Reagent: same product as calcium carbonate used in laboratory test.

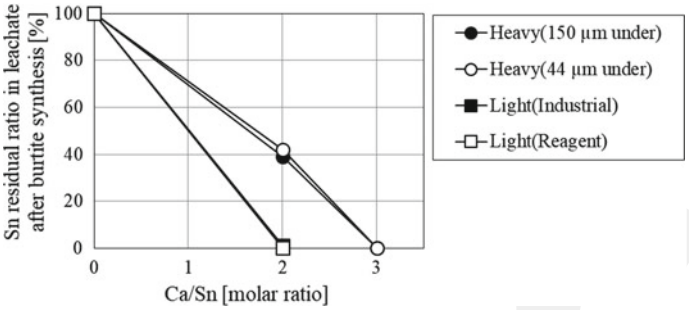

Fig. 9 Residual ratio of tin in leachate after burtite synthesis using several calcium carbonates

The results of the burtite synthesis test using the above four types of calcium carbonate are shown in Fig. 9. The ground calcium carbonate recovered tin of at most 60% when Ca/Sn was adjusted to 2, irrespective of the particle size, while the industrial light calcium carbonate captured tin of more than 99% when Ca/Sn = 2 even though it was in the industrial grade. Although heavy calcium carbonate is less expensive than light calcium carbonate, the use of heavy calcium carbonate leads to an increase in the unit cost of burtite and a dilution of the product being less attractive to the tin smelter. As a result of economic evaluation, light calcium carbonate was selected for the commercial process.

Removal of Arsenic and Selenium

The chemistry of effluent from the burtite synthesis is shown in Table 5 and the results of the arsenic removal tests are shown in Fig. 10. The concentration of arsenic of the effluent decreases with increasing the amount of calcium chloride added. Since calcium added is consumed by tellurium and selenium as well as arsenic, Ca/(1.5As + 3.0Te + 1.0Se) has provided consistent estimations even though the chemistry of the effluent changes depending of batches. Ca/(1.5As + 3.0Te + 1.0Se) should be controlled to 2 or more.

The liquid composition after arsenic removal is shown in Table 6, and the results of the selenium removal tests are shown in Figs. 11 and 12. The target can be achieved when the Fe/Se ratio is 100 or more.

Table 5 Chemical composition of leachate after burtite synthesis

Element	As	Te	Se	Sn	Pb	Sb
Concentrations (mg/L)	11,000	1800	310	140	<10	<10

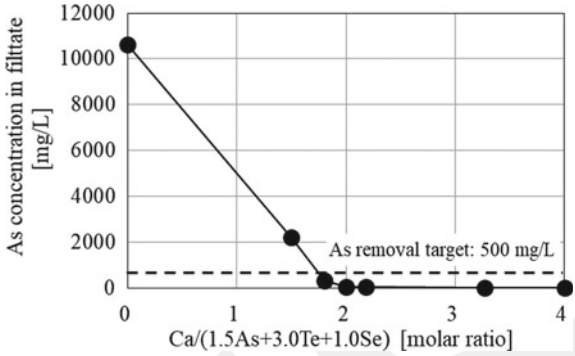

Fig. 10 Effect of molar ratio [Ca/(1.5As + 3.0Te + 1.0Se)] on As concentration in filtrate

Table 6 Chemical composition of leachate after removal arsenic

Element	As	Te	Se	Sn	Pb	Sb
Concentrations (mg/L)	41	29	97	<10	<10	<10

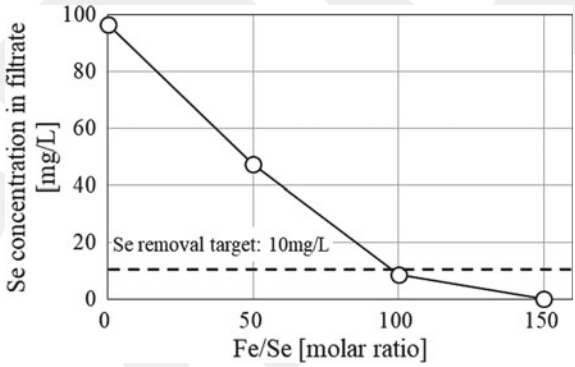

Fig. 11 Effect of molar ratio (Fe/Se) on Se concentration in filtrate

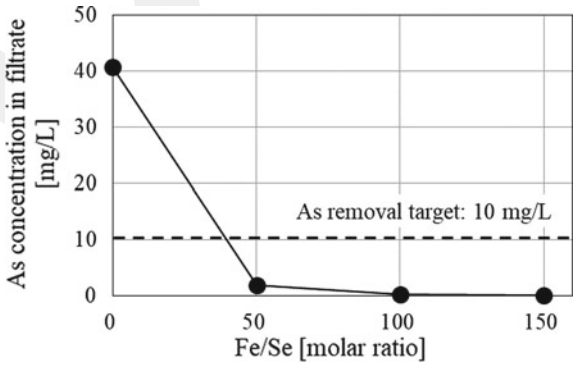

Fig. 12 Effect of molar ratio (Fe/Se) on As concentration in filtrate

Conclusions

A hydrometallurgical process to treat Harris dross has been developed by which lead, tin, and arsenic are separated each other and 76% of tin included in Harris dross is recovered as burtite ($CaSn(OH)_6$). The process developed has already been proven by the pilot-scale tests. The commercial plant has been constructed at Hosokura for starting-up in the next fiscal year. Burtite produced will be smelted and refined into electrolytic tin in a tin smelter of Mitsubishi Materials Corp. This innovative business has required the close and flexible network between group smelters of Mitsubishi Materials Corp.

References

1. Wright PA (1982) Extractive metallurgy of tin. Elsevier Scientific Pub. Co., New York
2. Hunter F, Heeath T, Holton D (2013) Update of thermodynamic data for tin in the HATCHES database. https://rwm.nda.gov.uk/publication/update-of-thermodynamic-data-for-tin-in-the-hatches-database/. Accessed 9 Aug 2019
3. Kumasaka T, Shimono K, Tanaka K (1990) Precipitated calcium carbonate for paper industry. J Jpn Tech Assoc Pulp Paper Ind 44(10):1067–1077
4. Agnihotri R, Mahuli SK, Chauk SS, Fan L (1999) Influence of surface modifiers on the structure of precipitated calcium carbonate. Ind Eng Chem Res 38(6):2283–2291

GCRIS

Pb and Other Impurities Recovery from Cu Smelting Residues in JX Nippon Mining & Metals

Nobuaki Okajima, Takuma Takei and Shojiro Usui

Abstract The amount of impurities, such as Pb, Sn, Sb, Bi, had increased in the copper smelting process of JX Nippon Mining & Metals Group, because of its active recycling from the urban mine. Accordingly, it became a critical issue to bleed off such impurities from its Cu smelting circuit and recover them as products. The company constructed the plant to treat the residues from Cu smelters in the Hitachi Works in 2008. The plant, named as HMC (Hitachi Metal-Recycling Complex), has been playing an important role to bleed off and recover 11 kinds of precious metals and impurity elements, and to stabilize the Cu smelting operation with recycling activities. This report describes about the role of HMC process, especially on Pb and Sb recovery.

Keywords Lead · Antimony · Copper smelting · Urban mine · Recycling

Introduction

Business Segments of JX Nippon Mining & Metals Group

The JX Nippon Mining & Metals Group engages in a wide range of operations, which are centered around copper, and cover upstream (resources development), midstream (smelting and refining), and downstream (electronic materials, and recycling and environmental services) activities (Fig. 1).

Figure 2 provides an outline of the copper smelting process. Copper concentrate is processed in the flash smelting, converter and anode furnaces and is refined in the tankhouse to produce electrolytic copper. Sulfuric acid is produced from the exhaust gas of the flash smelting furnace and converter furnace. Pb is distributed into the converter dust from the converter furnace and is recovered as Pb sulfate.

N. Okajima (✉) · T. Takei · S. Usui
HMC Department, Manufacturing Section 1, 1-1-2 Shirogane-cho, Hitachi-shi, Ibaraki, Japan
e-mail: okajima.nobuaki@jxgr.com

© The Minerals, Metals & Materials Society 2020

A. Siegmund et al. (eds.), *PbZn 2020: 9th International Symposium on Lead and Zinc Processing*, The Minerals, Metals & Materials Series,
https://doi.org/10.1007/978-3-030-37070-1_45

Fig. 1 Business segments of JX Mining & Metals Group

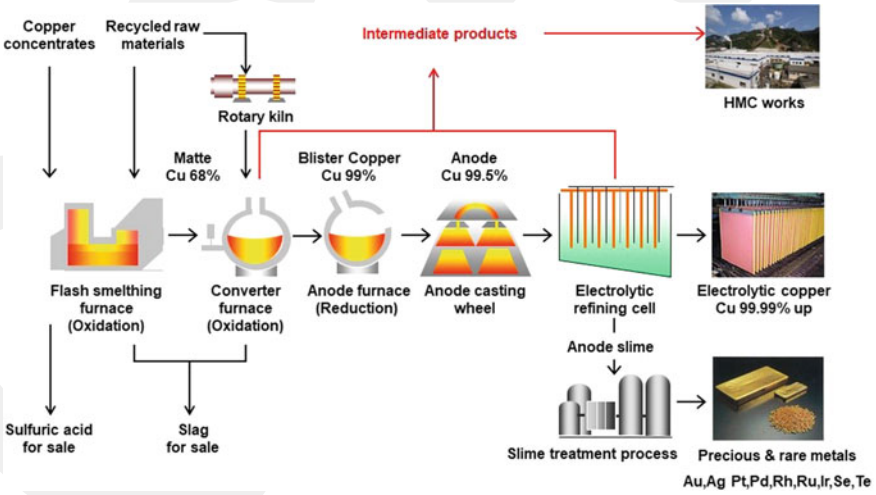

Fig. 2 Outline of the copper smelting process

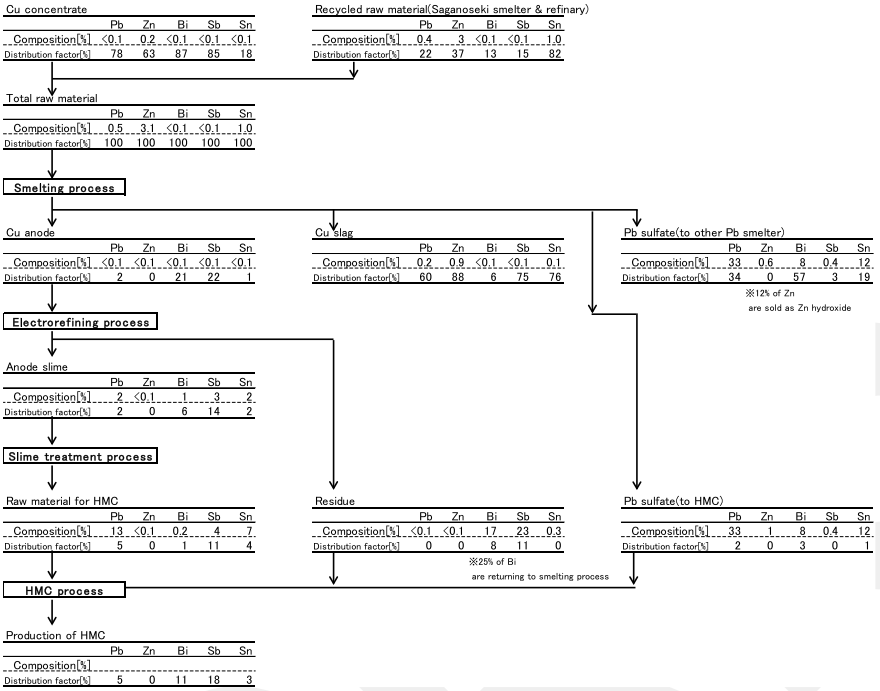

Fig. 3 Material balance for Pb, Zn, Bi, Sb, and Sn

Dusts in the smelting exhaust gas and tankhouse residue are examples of impurity discharge routes in the copper smelting process. These intermediate products are processed further to recover Pb and Sb. In this way, Pb and Sb are bled off from copper smelting process.

Figure 3 shows the distribution from the smelting process to each metal product. Pb, Sn, and Bi are made into products as metal ingots. Sb is made into product as oxide powder. During smelting, ~60% of the Pb is distributed to slag, and ~40% is distributed to Pb sulfate. In Japan, non-ferrous refining industry operates in various forms. Each company takes advantage of its strengths within the smelter network. As for Pb sulfate, it is sold to Pb smelter along with impurities. In this way, metal resources are effectively used. Approximately 75% of the Sb is distributed to the slag and ~22% is distributed to the anode. The anode is refined in the tankhouse to produce electrolytic copper. The anode slime is treated in the slime treatment process. Au is made into a product as the ingot or shot. Sb and Bi are removed as the tankhouse residue and the slime treatment residue.

Role of the HMC in Copper Smelting

An outline of the Cu smelter and HMC flowsheet is shown in Fig. 4. In this process, eleven non-ferrous metals are recovered efficiently from recycled raw materials and intermediates of copper smelting by combining pyro- and hydrometallurgical processes with technologies that have been developed in our non-ferrous smelting and refining businesses [1].

The compositions of the intermediates of copper smelting, i.e., Pb sulfate and a residue from copper electrolyte purification, are shown in Table 1. Sb is an inhibitor of the electrorefining process. Increases in antimony concentrations in the anode and electrolyte cause the formation of suspended solids in the electrolyte and Pb decreases the current efficiency [2].

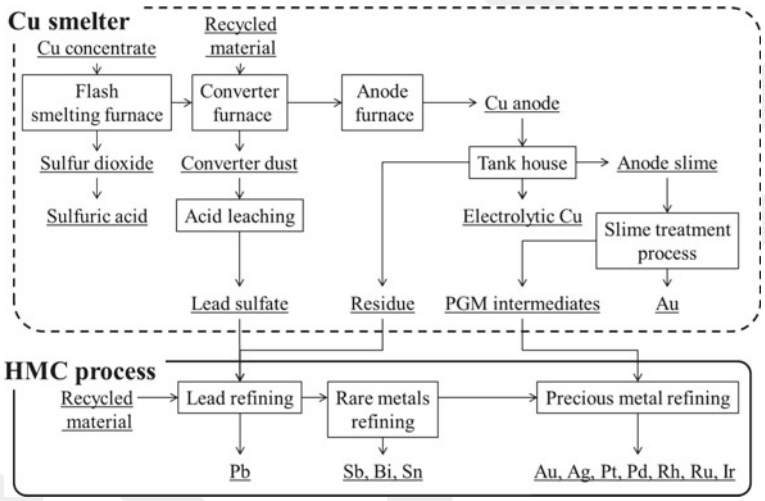

Fig. 4 Relationship between copper smelter and HMC

Table 1 Composition of intermediates of copper smelting process (%)

	Pb	Sn	Sb	Bi	Cu
Pb sulfate	23–30	8–14	0.3–0.6	5–8	0.7–0.9
Residue from Tankhouse	–	–	20–27	20–22	<1

Pb Recovery in JX Nippon Mining & Metals

Pb Recovery in Saganoseki Copper Smelter

In the copper smelter, approximately 40% of Pb is distributed into the converter dust from the raw material, and some Cu is contaminated in the dust. Therefore, a two-stage Cu removal technology was installed at the Sagaseki Smelter [3, 4]. The flowsheet for Pb recovery is shown in Fig. 5. Table 2 shows changes in the quality of each intermediate. In the first stage, Cu is removed by specific gravity separation from the slurry from the leaching of the converter dust with sulfuric acid. The removed Cu is sent to the neutralization process and returned to the flash smelting furnace with neutralized residue. The specific gravity separation of Cu reduces the Cu grade in the Pb sulfate from 12–14 to 8.4%. In the second stage, the Cu is leached and removed by ferric leaching from the converter dust to the leaching solution as shown in Eq. (1).

$$Cu_2S + 4Fe_2(SO_4)_3 \rightarrow CuSO_4 + 4FeSO_4 + S \quad (1)$$

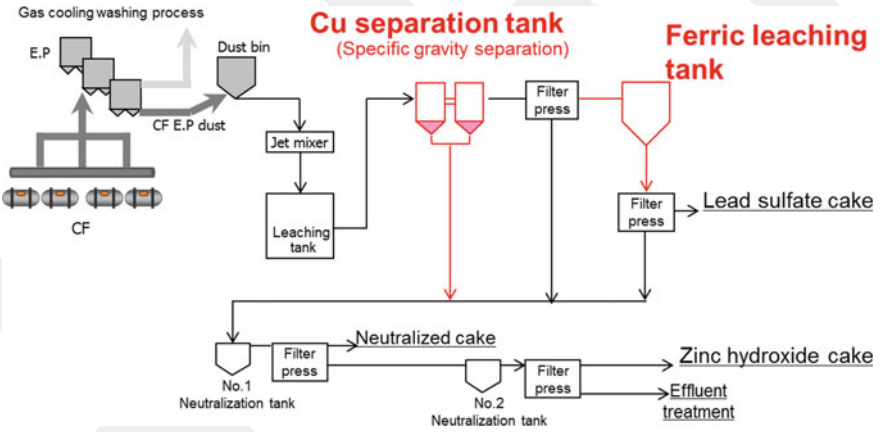

Fig. 5 Flowsheet for Pb recovery in the Cu smelter

Table 2 Change in intermediate composition (%)

	CF dust		Lead sulfate	
	Cu	Pb	Cu	Pb
Before the installations	16–22	5–10	12–14	16–20
After installation of Cu separation tank (2011/11~)	16–22	5–10	8.4	18–24
After installation of ferric leaching (2014/4~)	16–22	5–10	<1	20–30

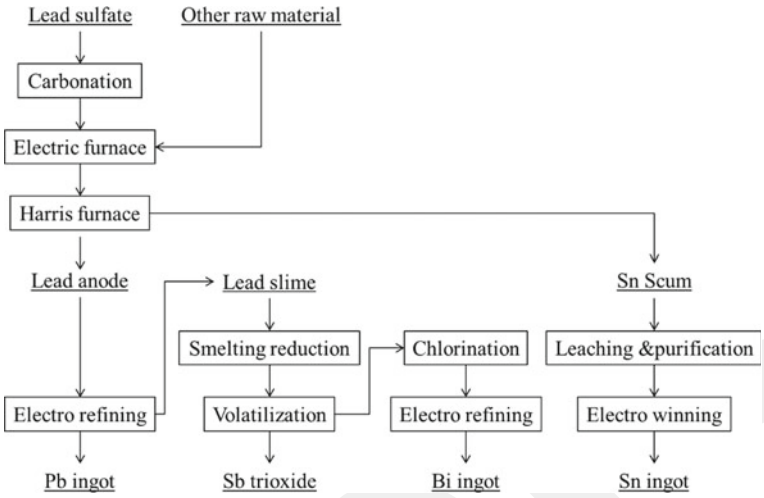

Fig. 6 Flowsheet for Pb, Sb, Bi, and Sn, recovery from Pb sulfate in the HMC

This removal reduces the Cu grade in Pb sulfate to <1%. Some residues that contain Zn hydroxide or Pb sulfate are raw materials for HMC and may be sold to other companies.

Pb Recovery in the HMC

The flowsheet for Pb, Sb, Bi, and Sn recovery from Pb sulfate in the HMC is shown in Fig. 6. The process comprises carbonation, an electric furnace, a Harris furnace, electrorefining, and Pb anode slime treatment [5]. One of the main feeds to the HMC is Pb sulfate from the copper smelter. Examples of the chemical compositions of other raw materials, tankhouse residue, and slime treatment residue, are shown in Table 3. Lead is contained as lead sulfate in it, and it is converted to lead carbonate by carbonation, and sulfur is removed from the raw material as shown in Eq. (2).

$$3PbSO_4 + 3Na_2CO_3 + H_2O \rightarrow 2PbCO_3 \cdot Pb(OH)_2 + CO_2 + 3Na_2SO_4 \qquad (2)$$

Table 3 Raw material composition for the HMC (%)

	Pb	Zn	Bi	Sb	Sn
Tank house residue	<0.1	<0.1	17	23	0.3
Slime treatment residue	12	<0.1	<0.1	38	–

This prevents the generation of sulfurous acid gas at electric furnace and reduces the risk of environmental pollution. Lead carbonate and other raw material are treated with electric furnace. Afterward, Sn is removed into Sn scum with Harris furnace as shown in Eq. (3).

$$\begin{aligned} 5Sn + 6NaOH + 4NaNO_3 &\rightarrow 5Na_2SnO_3 + N_2 + 3H_2O \\ 2Sn + NaNO_3 + 3NaOH &\rightarrow 2Na_2SnO_3 + NH_3 \end{aligned} \quad (3)$$

Even though Pb can be oxidized to Na_2PbO_2 with $NaNO_3$, it can be reduced to Pb with Sn as shown in Eq. (4) [6]. Pb can be prevented from the distribution to Sn scum.

$$Sn + 2Na_2PbO_2 + H_2O \rightarrow Na_2SnO_3 + 2Pb + 2NaOH \quad (4)$$

Electrolytic refining purification of Pb increases the purity from 75–85 to 99.99%. Sulfamate is used as the electrolyte. Compared with the Betts process that uses hexafluorosilicate, it is possible to maintain a comfortable working environment and reduce the environmental risk. Bi and Sb are higher in the Pb anode compared with that of conventional processes, and we could achieve a Pb purity of 99.99%.

Sb Recovery in the HMC

As shown in Fig. 3, Sb is discharged from the Cu smelting process to the HMC as a tankhouse residue and slime treatment residue.

Sb raw materials and Pb anode slime are treated in a reduction furnace. The Pb anode slime is an HMC intermediate. Se and Te are removed from the crude metal as scum. When sufficient Te has been removed ($\leq$0.2%), Sb is volatilized by air oxidation and recovered as Sb oxide. By such treatment, Se and Te can be reduced to <10 ppm in the products as shown in Table 4.

Pb and Bi remain after Sb volatilization. Pb is recovered as a chloride by reaction with chlorine and is processed in an electric furnace in an upstream process. Bi is cast as an anode and is refined electrolytically for electrolytic Bi.

Table 4 Sb product composition

	Purity (%)	Te (ppm)	Se (ppm)
Sb_2O_3 (products)	>99.5	<10	<10

Conclusions

We reported the removal process of Pb and Sb in the copper smelting business. Both metals have been made as products with a quality that have been acceptable in the market. HMC is an indispensable process in copper smelting, and to develop the recycling business further, it is important to remove impurities efficiently, whilst maintaining safety and the environment. HMC stabilizes the copper smelting business by removing impurities.

References

1. Sasaoka H (2013) A novel ferric leaching process to recover copper from converter dust. Copper IV:79–90
2. Atsuki S, Akira U, Kunio W, Kazuaki T (2019) Recent operational improvements at Saganoseki electrorefinery. Copper
3. Shinya S (2011) Processing method of copper converter dust. Japan patent, JP2011-32516a
4. Shinya S (2013) Separation method and separator of copper converter dust. Japan Patent, JP2013-209717a
5. Shojiro U, Eiki O (2019) A refining of minor elements in copper smelting process. Paper presented at the MMIJ Annual Meeting 2019, Vol. 6, No. 1
6. Motoo W (1960) Lead Smelting (Translated from Japanese) Asakura Publishing Co., Ltd

GCRIS

Pyrometallurgical Recovery of Valuable Metals from Flue Dusts of Copper Smelter Through Lead Alloy

Wenzhao Cui, Mao Chen and Baojun Zhao

Abstract Low-grade copper concentrates containing increased impurities such as As, Pb, and Zn are used in copper production. In copper smelting and converting processes, large amounts of flue dusts are collected from the waste heat boiler (WHB) and the electrostatic precipitator (ESP). The dusts consisting of Cu, Pb, Zn, As, Fe, Bi, and Ag are presented in the forms of sulphate, sulphide, and oxide. The complex combination of these minerals makes it difficult to recover the valuable metals from a single lead-reduction process. Different approaches have been compared through experimental studies and thermodynamic calculations to efficiently recover most of the valuable metals and obtain clean slag. It was found that leaching, oxidation, and reduction are essential steps to fix arsenic and recover valuable metals. Optimum conditions for high-temperature processes of oxidation and reduction have been proposed. Most of the Ag and Bi can be recovered from lead alloy.

Keywords Flue dust · Copper smelter · Lead reduction · Pyrometallurgical recovery

Introduction

Flue dusts are generated during all stages of pyrometallurgical processing of copper concentrates, including roasting, smelting, converting, and slag cleaning. The mass of dust can be 1–10 wt% of the feed to the furnace. These dusts are collected by waste heat boiler (WHB), electrostatic precipitator (ESP), or baghouses. The dusts can be classified into two types depending on how it is formed during the gas cleaning process [1]. The first type is the chemically formed one which is a product of vaporization and condensation in the gas cleaning system. The other type is the physically formed dust generated as a result of movement of small solid and/or liquid

W. Cui
Dongying Fangyuan Nonferrous Metals Co. Ltd, Dongying, China

M. Chen · B. Zhao (✉)
The University of Queensland, Brisbane, Australia
e-mail: baojun@uq.edu.au

© The Minerals, Metals & Materials Society 2020

A. Siegmund et al. (eds.), *PbZn 2020: 9th International Symposium on Lead and Zinc Processing*, The Minerals, Metals & Materials Series,
https://doi.org/10.1007/978-3-030-37070-1_46

particles carried by the process gas into the gas cleaning system. With more and more restricted environmental legislations, copper smelter dusts are getting serious attention due to their high concentrations of toxic elements such as As, Bi, Pb, and Sb.

The flue dusts consist of valuable metals including Cu, Bi, Zn, and Pb that need to be recovered. Common practice has been to recycle these dusts to the smelting and converting furnaces to recover the copper content [2]. However, this approach also recycles and concentrates the harmful impurities. The levels of these impurities increase as well and this eventually results in high impurity levels in the blister copper and makes electrolytic refining more difficult. In addition, the recycling of these dusts also decreases the productivity. As impurity levels in copper concentrates increase, numerous hydrometallurgical processes mainly acid leaching have been developed to treat copper smelter dusts [3–6]. Ammoniacal leaching was also proposed for pelletised and roasted flue dusts [7]. However, these hydrometallurgy-based approaches are not suitable for high-Pb dusts. Pb can be as high as 26 wt% in the ESP dust [8]. Lead sulfide from the copper concentrates is converted to oxide and sulphate in the dusts collected during smelting and converting processes and they are difficult to be leached and filtered. The pyrometallurgical approach has been confirmed to be the only way to efficiently treat the high-Pb dusts. Noranda treated their high-Pb flue dusts from the copper smelters by adding the dusts to the lead sinter plant [9]. However, the capacity to treat the dust was limited due to heat balance and minor elements control. Moldabayeva et al. [10] did a laboratory study to treat Pb-containing dusts from copper smelters at 1100–1175 °C. They used charcoal and coke as reducing agents, Na_2SO_4 and Na_2CO_3 as flux. The products were crude lead, soda-based slag containing copper, lead and zinc, and secondary dust containing Cd, Pb, Zn, and Re. Lead was not fully recovered, and the slag and dust generated were required for further treatment. A combined hydro- and pyrometallurgy two-stage process was proposed to treat copper converter dust [11]. The hydrometallurgical treatment by NaOH solution was undertaken for removal of sulfate sulfur and then carbothermal reduction of desulphated dust at 900 °C in a soda ash melt to recover valuable elements. However, 80% of the copper was reported to the secondary dust which is not acceptable. Xu et al. [12] also proposed a combined hydro- and pyrometallurgy two-stage process to treat high-As and high-Pb dust generated from copper IsaSmelting furnace. The dust was first leached by H_2SO_4 to dissolve Cu, Zn, and As with Cd, Pb, and Bi remained in the residue. The residue was treated in a blast furnace with additions of coke, lime, and iron ore. Pb and Bi were recovered in the alloy and a large amount of secondary dust was generated for further treatment.

Dongying Fangyuan Nonferrous Metals successfully developed bottom-blown copper smelting technology in 2008 which demonstrated a number of advantages [13, 14]. It is suitable for a wide range of copper, gold, and silver concentrates with minimal feed preparation. Low-temperature operation and high-pressure gas injection enable high energy efficiency and productivity. This technology was further developed to a simplified copper-making process including two furnaces which is again the first process of this kind in the world [15]. Based on the deep understanding and extensive operating experience of the new bath smelting furnace, the

company proposed to treat the flue dusts from the copper smelter by a combination of hydro- and pyrometallurgy. Thermodynamic considerations and plant trial results are presented in this paper.

Results and Discussion

Description and Results of the Plant Trials

The dusts from smelting and converting furnaces at Dongying Fangyuan were mixed and treated by leaching and smelting reduction. The typical compositions of the mixed dusts are given in Table 1. It can be seen that Pb and Cu concentrations varied significantly due to the different sources of the copper concentrates and the furnaces used. In addition to the Pb and Cu, valuable Ag and Bi are also present that need to be recovered. Most of the Pb, Bi, Cu, and Zn were present in the dusts as sulphate and oxide. Significant amount of arsenic present in the dust needs to be treated and fixed in the stable form. The dust was mixed with water and H_2SO_4 to control liquid: solid = 3:1 and pH $\approx$ 1. The leaching was conducted at 50–60 °C heated by steam. It was expected that most of the Cu, Zn, sulphur, and arsenic would be dissolved into the solution. Cu and Zn will be recovered following the standard hydrometallurgical process. The arsenic will be fixed as ferric arsenate precipitate which is a stable phase acceptable environmentally. The residue was dried for pyrometallurgical processing.

The residue from the leaching process, after drying, was fed into a bottom-blown furnace together with silica, lime, and coke according to the required ratios. Oxygen-enriched air and natural gas were injected through three lances on the bottom of the furnace to provide reductant and heat, and to stir the bath. The Pb-based alloy and slag were tapped separately. The dust from the furnace was recycled to the furnace. The alloy contains approximately 85 wt% Pb and 10 wt% Bi with small amounts of Cu, Sb, As, and Ag. Matte containing Cu, Pb, Fe, and S was also observed from time to time indicating that copper and arsenic were not completely removed in the leaching process.

The quenched slag samples were mounted and polished for analyses. The microstructures and compositions of the phases present in the slags were determined by a JEOL JXA 8200 Electron Probe X-Ray Micro-analyser (EPMA) with wavelength dispersive detectors. (JEOL is a trademark of Japan Electron Optics Ltd., Tokyo). An accelerating voltage of 15 kV and a probe current of 15 Amps were used. The Duncumb-Philibert ZAF correction procedure supplied with JXA-8200 was applied. The average accuracy of the EPMA measurements was estimated to be within $\pm$1 weight percent. Typical microstructures and phase compositions are given in Fig. 1 and Table 2, respectively, for two slag samples FY183 and FY186. It can be seen that liquid and melilite [$2CaO.(Zn,Fe)O.2SiO_2$] were present in both slag samples. No significant alloy droplets were present in the slag indicating complete separation of the alloy from the slag. 16.8 wt% PbO was present in the liquid of

Table 1 Typical dust compositions from Dongying Fangyuan copper smelter (wt%)

Pb	Bi	Cu	Zn	S	As	SiO_2	CaO	Fe	Ag (g/t)	Au (g/t)
27–41	2–5	3–5	4–6	8–10	3–6	2–4	1.5–2	2	520	5–10
10–20	2–5	6–10	4–6	5–7	6–9	2–4	1.5–2	2	520	5–10

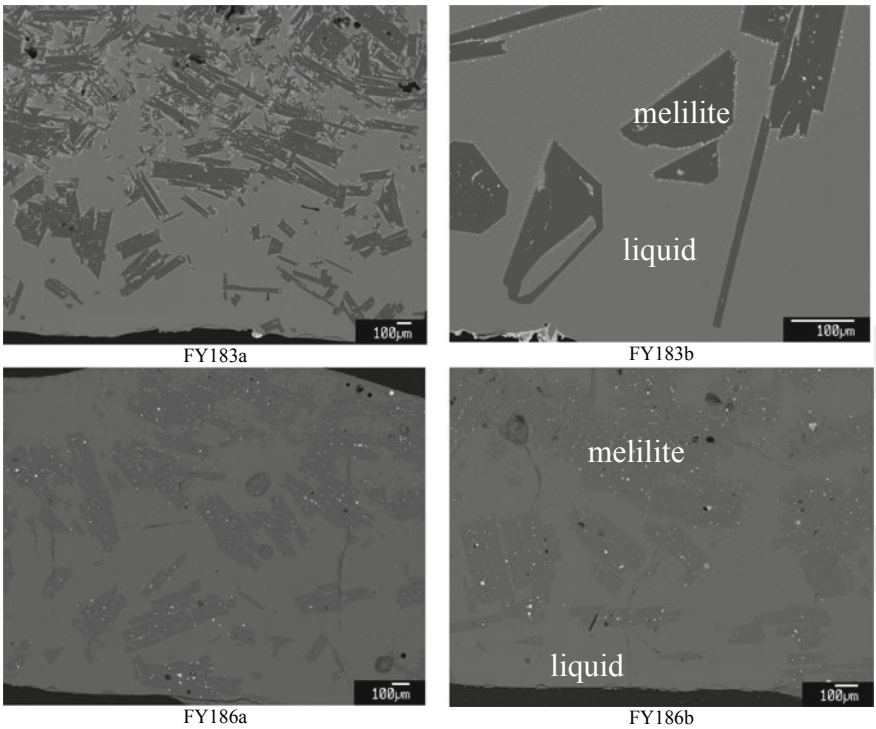

Fig. 1 Typical microstructures of the reduction slags

slag FY183 and only 2.7 wt% PbO was present in the liquid of slag FY186. Higher As_2O_3 (9.1 wt%), Cu_2O (0.7 wt%), and Sb_2O_3 (1.7 wt%) were also present in slag FY183. It is clear that the reductant was not enough to reduce the oxides during the smelting reduction of slag FY183. It is noticed that the "FeO" concentration in FY183 (9.6 wt%) is lower than that in FY186 (14 wt%) which might be responsible for different reduction degree. The plant trials were not stable to achieve high lead recovery and low PbO in the slag. The processing parameters need to be optimized to obtain acceptable and stable operations.

Thermodynamic Considerations for New Process to Treat Copper Smelter Dust

It can be seen from Table 1 that $PbSO_4$ is the major component in the copper smelter dust which is also the major component in lead batteries. If $PbSO_4$ is used for reduction directly, a large amount of PbS will be formed under reducing conditions and vaporized to form dust again. In the lead battery recycling process, a number of

Table 2 Compositions of the phases present in the lead smelting slags measured by EPMA (wt%)

	"FeO"	SiO_2	Cu_2O	CaO	Al_2O_3	MgO	S	ZnO	As_2O_3	Na_2O	PbO	Sb_2O_5	Bi_2O_3
FY183L	7.6	27.2	0.7	24.5	2.5	0.0	0.0	8.5	9.1	1.1	16.8	1.7	0.1
FY183M	2.9	39.7	0.0	35.5	2.2	1.4	0.0	17.3	0.0	0.0	0.8	0.0	0.0
FY186L	14.0	32.8	0.2	30.5	3.8	0.3	0.1	9.9	3.0	2.3	2.7	0.4	0.0
FY186M	3.6	39.6	0.0	35.6	2.1	1.1	0.0	17.4	0.0	0.0	0.4	0.1	0.0

reactions are involved to produce Pb metal from $PbSO_4$. The first reaction is to desulfurize $PbSO_4$ with soda ash to form a marketable sodium sulfate product (1). The lead carbonate continues to the reverb (2) and blast furnaces (3) for two-step reduction [16]:

$$2PbSO_4 + 2Na_2CO_3 + 2H_2O \rightarrow Pb_3(CO_3)_2(OH)_2 + 2Na_2SO_4 + H_2SO_4 \quad (1)$$

$$2Pb_3(CO_3)_2(OH)_2 + C + 2SiO_2 \rightarrow 2Pb + 2Pb_2SiO_4 + 2H_2O + 5CO_2 \quad (2)$$

$$Pb_2SiO_4 + C + 2FeO \rightarrow 2Pb + Fe_2SiO_4 + CO_2 \quad (3)$$

However, copper smelter dusts are different from the lead battery paste. In addition to $PbSO_4$, $CuSO_4$, $ZnSO_4$, and arsenic are also present in the dusts that can be easily removed by water or acid. $CuSO_4$ will form sulfide matte, zinc and arsenic will form dust during the reduction process if they are treated directly with $PbSO_4$ by following the reactions above. On the other hand, it can be seen from Table 2 that one-step reduction may result in higher PbO in the slag (FY183) which requires further treatment to obtain discarded slag with low PbO. Large amount of PbS-containing dust generated during the process also reduces the productivity. Two-step reactions are necessary to fully recover Pb and Bi and produce environmentally friendly slag. This can be explained in detail by the thermodynamic considerations below.

FactSage 7.3 is used to predict the reactions for the treatment of leaching residue of the dust [17]. The databases selected were "FactPS", "FToxide", and "FTmisc. Certain amounts of flux such as CaO, FeO, and SiO_2 are added into the leaching residue to make a low-liquidus slag.

It can be seen from Fig. 2 that at 1000 °C, Bi can be easily formed at relatively high Po_2. At Po_2 10^{-8} atm, nearly 99 wt% Bi is present as liquid metal where all lead is present in the oxide slag. Metallic lead will start to form when the oxygen partial

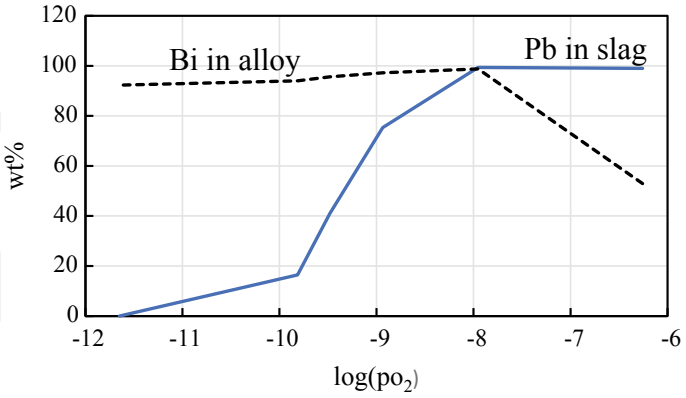

Fig. 2 Distributions of Bi and Pb between alloy and slag at 1000 °C calculated by FactSage 7.3

pressure is lower than 10^{-8} atm. Further reduction can increase direct recovery of Pb in the alloy, but the recovery of Bi will be reduced due to the vaporization of Bi. For example, at Po_2 10^{-10} atm, approximately 86% lead will be reported to the alloy. However, the recovery of Bi to the alloy is only 94%. Lower oxygen partial pressure also results in formation and vaporization of PbS causing the loss of lead. If the temperature is higher for rapid reaction and better separation of the alloy from the slag, the recovery of Bi will be even lower. Therefore, optimum temperature, Po_2, and slag composition will need to be identified to balance the direct recovery rates of Bi and Pb in the first reduction stage. The most important aims for the first reduction stage is to (1) remove sulphur from the condensed system; (2) keep valuable elements in the condensed system; (3) maximizing reduction of Bi and Pb reduction. The main reactions include

$$2PbSO_4 + SiO_2 + C \rightarrow Pb_2SiO_4 + 2SO_2 + CO_2 \tag{4}$$

$$Pb_2SiO_4 + C + 2FeO \rightarrow 2Pb + Fe_2SiO_4 + CO_2 \tag{5}$$

$$2Bi_2O_3 + 3C \rightarrow 4Bi + 3CO_2 \tag{6}$$

The lead-rich slag produced from the first stage is used for further reduction to completely recover Pb and produce a discarded slag containing CaO, "FeO", and SiO_2. The dusts generated in the 1st and 2nd stage reduction, if any, will be sent to the leaching process. Differently from the first stage reduction, no SO_2 is formed in the second stage reduction so that the gas handling system is relatively simpler. Higher temperature and more reducing condition are required for deep reduction of lead oxide.

Conclusions

Plant trials on treatment of copper smelter dusts have been conducted in Dongying Fangyuan Nonferrous Metals. It was found that one-step reduction of the leaching residue cannot recover all valuable metals and produce discarded slag. Optimum leaching condition, proper washing, and two-stage reduction are required to treat the copper smelter dusts properly.

References

1. Okanigbe DO, Popoola API, Adeleke AA (2016) Characterization of copper smelter dust for copper recovery. Proc Manuf 7:121–126
2. Montenegro V, Sano H, Fujisawa T (2013) Recirculation of high arsenic content copper smelting dust to smelting and converting processes. Miner Eng 40:184–189

3. Morales A, Cruells M, Roca A, Bergó R (2010) Treatment of copper flash smelter flue dusts for copper and zinc extraction and arsenic stabilization. Hydrometallurgy 105:148–154
4. Tomitia M, Higashi M, Oto S, Okamoto H (1992) Hydrometallurgical process of copper converter dust at the Saganoseki smelter and refinery, residues and effluents. In: Reddy RG, Imrie WP, Queneau PB, Warrendale PA (eds) Processing and environmental considerations. The Metallurgical Society, pp 283–293
5. Hagni RD, Karakus M (1991) Mineral variation in flash furnace particles produced under varying furnace conditions, in EPD Congress 91:811–819
6. Kunter RS, Bedal WE (1992) The Cashman process treatment of smelter flue dusts and residues, residues and effluents. In: Reddy RG, Imrie WP, Queneau PB, Warrendale PA (eds) Processing and environmental considerations. The Metallurgical Society, pp 269–282
7. Yin ZB, Caba E, Barron L, Belin D, Morris W, Vosika M, Bartlett R (1992) Copper extraction from smelter flue dust by lime-roast/ammoniacal heap leaching, residues and effluents. In: Reddy RG, Imrie WP, Queneau PB, Warrendale PA (eds) Processing and environmental considerations. The Metallurgical Society, pp 255–267
8. Swinbourne DR, Simak E, Yazawa A (2002) Accretion and dust formation in copper smelting—thermodynamic considerations. In: Stephens RL, Sohn HY (eds) Sulfide smelting. TMS, pp 247–259
9. Hancock PJ, Peacey JG (1994) Review of pyrometallurgical processes for treating non-ferrous complex materials and wastes. In: Nilmani M, Lehner T, Rankin WJ (eds) Pyrometallurgy for complex materials & wastes. TMS, pp 27–48
10. Moldabayeva GZ, Akilbekova SK, Mamyrbayeva KK, Mishra B (2015) Electrosmelting of lead-containing dusts from copper smelters. J Sustain Metall 1:286–296
11. Lucheva B, Iliev P, Kolev D (2017) Hydro-pyrometallurgical treatment of copper converter flue dust. J Chem Technol Metall 52:320–325
12. Xu Y, Li Y, Ding K, Kong Q (2005) A new process for comprehensive utilization of high-As dust from Isa furnace. China Nonferrous Metall 5:16–18
13. Cui Z, Wang Z, Zhao B (2014) Features of the bottom blown oxygen copper smelting technology. In: Bassa R, Parra R, Luraschi A, Demetrio S (eds) Proceedings of Nickolas Themelis Symposium on pyrometallurgy and process engineering. The Chilean Institute of Mining Engineers, Santiago, Chile, pp 351–360, ISBN: 978-956-7180-10-3
14. Zhao B, Cui Z, Wang Z (2013) A new copper smelting technology—bottom blown oxygen furnace developed at Dongying Fangyuan nonferrous metals. In: Jiang T, Hwang J-Y, Mackey PJ, Yucel O, Zhou G (eds) Proceedings of 4th international symposium on high-temperature metallurgical processing. Wiley, pp 3–10, ISBN: 978-1-118-60569-1
15. Wang Z, Wang H, Guo X, Cui Z, Zhao B (2018) Simplified process for making anode copper. In: Hwang J-Y, Jiang T, Kennedy MW, Gregurek D, Wang S, Zhao B, Yucel O, Keskinkilic E, Downey JP, Peng Z, Padilla R (eds) 9th international symposium on high-temperature metallurgical processing. Springer International Publishing, pp 3–12, ISBN: 978-3-319-72137-8
16. Schriner D, Taylor P, Grogan J (2016) A review of slag chemistry in lead recycling. In: Reddy RG, Chaubal P, Chris Pistorius P, Pal U (eds) Advances in molten slags, fluxes, and salts: proceedings of the 10th international conference on molten slags, fluxes and salts (MOLTEN16). TMS (The Minerals, Metals & Materials Society), pp 879–888
17. Bale CW, Bélisle E, Chartrand P, Decterov SA, Eriksson G, Gheribi AE, Hack K, Jung IH, Kang YB, Melançon J, Pelton AD, Petersen S, Robelin C, Sangster J, Spencer P, Van Ende MA (2016) FactSage thermochemical software and databases. CALPHAD 54:35–53

Part XIII
Secondary Lead

GCRIS

Operational Overview of RSR North America Corp.

Timothy W. Ellis, Mark A. Drezdzon and Travis Hesterberg

Abstract RSR North America Corp. (RSRNA) is the second largest secondary lead (Pb) producers in North America with smelting operations in Middletown, NY, Indianapolis, IN, and City of Industry, CA. Over the last several decades, RSRNA has focused on sustainability, becoming an industry leader in environmental performance by the installation of Wet Electrostatic Precipitators (WESPs) at all three operations. Also, average blood lead levels of plant personnel are well below 10 micrograms per deciliter, approaching background levels for non-industry personnel. With the industry's need to improve Pb battery performance to maintain sustainability in the marketplace, RSRNA has developed state-of-the-art analytical capabilities, including Inductively Coupled Plasma-Mass Spectroscopy (ICP-MS), to better quantify key elements crucial to Pb battery operation. This has led to the development of several new alloys, including the soft Pb micro-alloyed SUPERSOFT-HYCYCLE® and the high-temperature grid alloy 009-PERFORMANCE GRID™, which independently and together improve batter performance (e.g. cycle life).

Keywords Blood lead (Pb's) · WESP · Battery · Recycling

Introduction

Lead batteries continue to be the primary rechargeable energy storage technology for automotive, telecommunications, industrial, and power backup markets. However, lead batteries are being challenged by competition from other battery chemistries and by environmental regulations. Pb is one of the most heavily regulated elements on the planet even though it has the highest recycling rate of any metal in the world economy [1]. Production of secondary lead now exceeds primary lead production and lead batteries currently account for over 80% of the market for Pb. In the USA, recycling rates of lead batteries exceed 99% [1]. Lead batteries have become a valuable resource and efficient collection streams and salvage values of the spent lead batteries make

T. W. Ellis · M. A. Drezdzon · T. Hesterberg (✉)
RSR Technologies, Inc., 4828 Calvert St., Dallas, TX, USA
e-mail: THesterberg@rsrtechnologies.com

© The Minerals, Metals & Materials Society 2020

A. Siegmund et al. (eds.), *PbZn 2020: 9th International Symposium on Lead and Zinc Processing*, The Minerals, Metals & Materials Series,
https://doi.org/10.1007/978-3-030-37070-1_47

the recycling process economically profitable and sustainable. RSR North America (RSRNA) is the second largest secondary Pb producer in North America, with three smelting operations in the USA.

Environmental Management in Smelting Operations

Lead smelting operations in worldwide are under enhanced scrutiny by government regulations, with standards becoming more and more strict in certain areas of the USA and the world. Environmental management is an ever-growing challenge to the lead smelting industry and is an important factor for those operating the smelters, the employees who work in the facilities and the communities around them. Minimization of the exposure of Pb to the workforce and to the environment are issues of extremely high importance to RSR North America and an area where large amounts of effort and capital have been placed on facility improvements to ensure sustainability of the circular economy of Pb.

RSRNA smelters have achieved world class blood lead levels and are among those with the lowest Pb emission levels of any smelting operation. All three smelting facilities in the USA have now installed Wet Electrostatic Precipitators (WESP) in their off-gas stream. Each facility produces over 120 kilo tons of Pb metal and Pb alloys each year and has achieved a total Pb process emission of <5 lb per year. The WESP technology utilizes an aqueous aerosol to capture particulate from the off-gas stream after conventional bag house filtration. The aerosol particles with absorbed species (i.e. Pb and As) are then removed electrostatically. The electrostatic chambers are washed down and the resulting aqueous solution is reused in process or sent to the on-site water treatment facility for processing. Capital cost of the WESP equipment is quite high, about 25–30 million USD. However, without this technology in place meeting the strict air emission requirements in the USA and specifically in the state of California would be very difficult if not impossible. Figure 1 shows the recent history of Pb ambient on-site monitor levels from the City of Industry, CA smelter.

Much effort has been focused on improving employee hygiene in the smelters to reduce blood Pb levels in the workforce. Each of RSRNA's smelting operations has shown a continual reduction in blood Pb over the last decade. Through monitoring of employee hygiene, improved safety practices, and increased point of source ventilation in the Pb handling facilities, average blood Pb averages have been reduced to <10 ug/dL. Efforts are ongoing to continue to further improve this reduction in blood Pb levels, in hopes of making the smelter workforce's blood Pb levels indistinguishable from those of non-exposed adults in the general population. Figure 2 shows the reduction trend in average blood lead levels per smelter over the last decade.

Ensuring safe and responsible recycling of Pb batteries is and will continue to be a major goal of RSRNA's smelters. Responsible recycling starts with proper battery collection and shipment to the smelter. Nearly, 25% of spent lead batteries collected in the USA are exported to other countries for recycling in order to avoid the strict environmental regulations in place in the USA. This is a practice that should

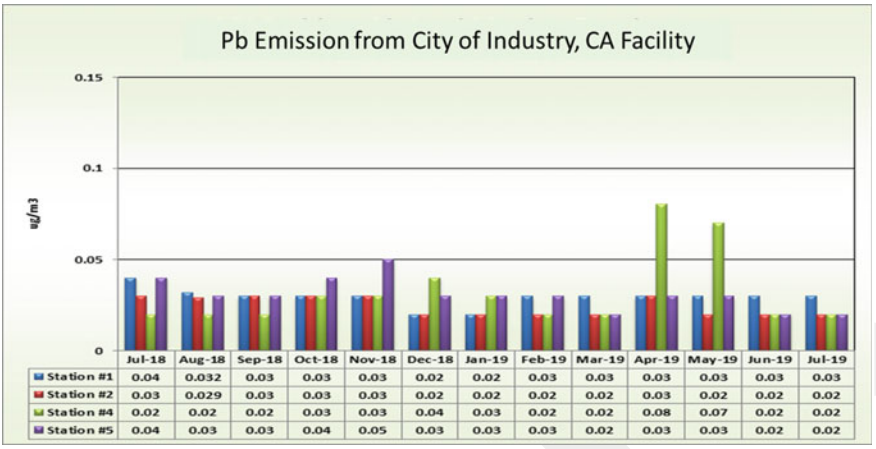

	Jul-18	Aug-18	Sep-18	Oct-18	Nov-18	Dec-18	Jan-19	Feb-19	Mar-19	Apr-19	May-19	Jun-19	Jul-19
Station #1	0.04	0.032	0.03	0.03	0.03	0.02	0.02	0.03	0.03	0.03	0.03	0.03	0.03
Station #2	0.03	0.029	0.03	0.03	0.03	0.02	0.02	0.02	0.02	0.03	0.02	0.02	0.02
Station #4	0.02	0.02	0.02	0.03	0.03	0.04	0.03	0.02	0.02	0.08	0.07	0.02	0.02
Station #5	0.04	0.03	0.03	0.04	0.05	0.03	0.03	0.03	0.02	0.03	0.03	0.02	0.02

Fig. 1 Pb Emission for the Quemetco Metal Facility, City of Industry, CA

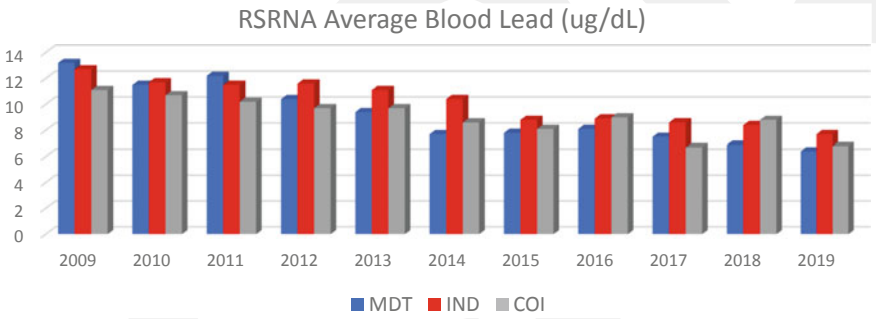

Fig. 2 Average RSRNA smelter employee blood lead levels (ug/dL)

be monitored and controlled, as batteries used within the USA can be responsibly recycled in the USA. Also, with batteries of different chemistries (i.e. Li-ion) showing up in the battery collection stream, sorting of batteries is another key component to safe recycling. Pushing the message of responsible recycling will be a key to RSRNA and the Pb industry moving forward.

Improved Pb Materials for Lead Batteries

New and emerging uses of lead batteries in stop/start and hybrid vehicles and renewable energy grid management have increased the requirements for partial state of charge (PSOC), cycle life, dynamic charge acceptance (DCA), performance at high temperature and increased utilization rates of active material. Current Pb batteries can

be designed to fit specific applications, allowing the manufactures and Pb suppliers, like RSRNA, to modify the components to provide the best performance for a given application. Due to these new requirements, the smelting and refining processes with RSRNA's facilities are being pushed to produce higher quality pure Pb and Pb alloys with more stringent requirements on product specifications. Understanding the effect of each element within the Pb, whether at impurity or alloying concentration levels, is critical to the overall performance of the Pb battery. Improved analytical capabilities within the smelters and in the research and development laboratories of RSRNA have allowed for more accurate analysis and control of trace impurities known to cause gassing issues within lead batteries. Highly refined secondary Pb has shown similar performance to primary Pb for battery applications, providing a recycled product that meets the requirements for applications traditionally requiring the use of a mined source of material.

Utilizing improved smelting and refining processes and combining those with the use of core quality tools, advanced analytical techniques and collaboration projects with Argonne National Laboratory, RSRNA have developed several new alloys to improve battery performance in the areas of increased cycle life and high-temperature performance. SUPERSOFT-HYCYCLE® was developed as a micro-alloyed active material Pb containing antimony and arsenic at controlled levels designed to improve capacity and cycle life of the battery. Understanding the roles of micro-alloyed elements on the crystal growth and dissolution of PbO_2 and $PbSO_4$ was a key in the development of this alloy. Battery testing at the 2 V test cell and on 12 V batteries demonstrates the cycle life improvement from SUPERSOFT-HYCYCLE® compared to normal leady oxide active material [2]. 009-PERFORMANCE GRID™ alloy has shown enhanced mechanical testing properties and improved corrosion resistance over traditional PbSnCa grid alloys, especially at elevated temperatures. This alloy has increased levels of Ag and the addition of Ba which has shown to inhibit grid pit corrosion and increase cycle life at 60 °C [2].

Conclusions

Ensuring the safe and responsible recycling of Pb batteries is RSRNA's priority. Challenges will continue to rise from regulatory bodies and from other battery chemistries in the market. Continuous improvement in handling Pb emissions and reducing workforce exposure are key priorities to the long-term company strategy. Developing and producing quality Pb and Pb alloys that improve battery performance will help to ensure the lead battery stays the dominant technology in the energy storage market.

References

1. Lead Action 21, International Lead Association, Bravington House, 2 Bravingtons Walk, London, N19AF
2. Raiford M, Ellis TW (2019) Microalloyed control of lead battery active materials and resulting improvements in battery performance through in situ electrochemical techniques. In: Presented at European Lead Battery Conference, Vienna, Austria, International Lead Association

GCRIS

Refractory Solutions by Laboratory Tests and Fieldworks for Lead Recycling Applications

K. Reinharter, D. Gregurek, A. Spanring and Camille Fleuriault

Abstract The most common route for secondary lead recycling from battery scrap in the USA is the reverberatory smelting furnace. Detailed knowledge of operating conditions is important for selecting and developing the most suitable refractory materials for such a process route as they influence the refractory performance. This paper describes detailed mineralogical investigations on selected slag samples from a secondary lead smelter followed by laboratory test work (corrosion test with an induction furnace and a crucible test) with magnesia-chromite bricks. Based on the results of those tests, refractory bricks with the highest corrosion resistance were selected for use in field trials. Investigations of post-mortem samples are carried out to understand the operational practice-orientated wear mechanism. This work was done to increase the refractory application knowledge of the lead smelting industry as well as providing customized refractory solution to RHI Magnesita's customers.

Keywords Reverberatory furnace · Laboratory tests · Post-mortem study

Introduction

Lead production is divided into primary production where the raw materials are predominantly derived from sulfidic lead concentrates and secondary materials mainly originating from the recycling of spent lead acid batteries [1]. Recycling of spent lead acid batteries plays a very important role within the nonferrous metals industry.

The secondary lead production process is quite straightforward, and with the present technology, it is possible to recycle without any loss of quality. The pyrometallurgical route is the most common, and the processing can be classified in one-

K. Reinharter (✉) · D. Gregurek
RHI Magnesita AG; TC Leoben, Magnesitstrasse 2, 8700 Leoben, Austria
e-mail: katja.reinharter@rhimagnesita.com

A. Spanring
RHI Magnesita, Kranichberggasse 6, 1120 Vienna, Austria

C. Fleuriault
Gopher Resource, Yankee Doodle Road 685, Eagan, MN 55121, USA

© The Minerals, Metals & Materials Society 2020

A. Siegmund et al. (eds.), *PbZn 2020: 9th International Symposium on Lead and Zinc Processing*, The Minerals, Metals & Materials Series,
https://doi.org/10.1007/978-3-030-37070-1_48

or two-stage smelting, which mainly differs on implemented process flow sheet in combination with used furnace types and technologies. For one-stage smelting, the typical furnaces are reverberatory, blast, and rotary furnace. For two-stage processing, common furnace combinations are reverberatory + blast, rotary or electric arc furnace, and bottom-blown oxygen furnace + blast furnace [2–6].

This paper deals with laboratory test and industrial field trials of customized refractory materials for the reverberatory furnace process. Stationary reverb furnaces have been historically used in North America for the production of secondary lead. They are reliable, highly productive furnaces allowing for continuous smelting.

The main input of the reverberatory furnace is battery scrap combined with reductants such as metallurgical coke. The furnace is operated with a gas-air burner, and under oxidizing atmosphere for oxidation of the carbonaceous materials, sulfur and other alloying elements like Ca, Al, Sb, As, Sn, etc. contained in battery scrap [2]. In fuel-fired furnaces, which are most common in the secondary lead industry, flames extend from the end wall to the furnace hearth or from the roof to the bath. The role of the refractory is paramount as part of the heat is also reverberated by radiation from the roof and the side walls. Reverberatory furnaces produce a soft lead (99% + Pb) and slag which is very rich in lead (30–50% + PbO) and other metallics. This slag needs to be further processed for optimal lead recovery as well as production of a product that is environmentally safe and accepted for disposal (Table 1).

From the melting and thermal decomposition of desulfurized battery paste, oxidizing conditions participate in the formation of a stable slag phase. Desulfurization has for direct consequence to enrich the slag in sodium oxide. Combined with lead oxide, these species have the ability to form a low melting, low viscosity, highly corrosive slag system. Usually, secondary lead reverberatory furnaces are lined with magnesia-chromite bricks to achieve necessary chemical resistance in combination with mechanical and thermal stresses. Magnesia provides stability against high temperatures and the compatible chemistry to withstand basic slags. Chrome is added to MgO-based refractories to enhance properties such as corrosion or thermal shock resistance. The slag chemistry of secondary lead furnaces, thermal cycling, and high-intensity burner regimes creates challenging conditions leading to refractory wear (see Fig. 1).

Table 1 Typical composition of battery material feeding reverberatory furnaces (after draining) [7]

Description	wt%	Components
Grid	20	(Pb,Sb) and (Pb,Ca) alloys (Sn, As, Se)
Paste	35	55–60% $PbSO_4$, 30–35% PbO_2, 1–4% Pb
Acid	25	H_2SO_4
Plastics	5	PP
Other (separators, posts, etc.)	15	Glass fiber mats, Pb alloys, rubber…

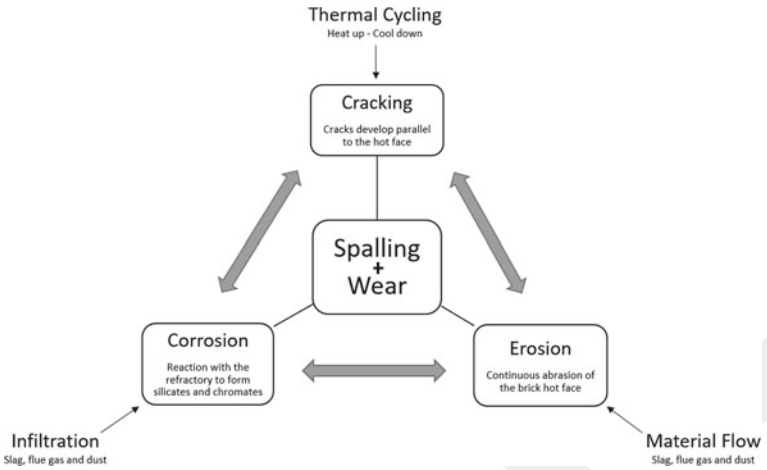

Fig. 1 Overview of wear influences to refractory material

Laboratory Testwork

To provide the most appropriate refractory solution in order to fulfill the customer needs in regard to increase service lifetime and optimize cost-benefit. Therefore, a series of laboratory tests are carried out at RHI Magnesita's Technology Center, Leoben.

As this paper describes the lead reverberatory process, a slag sample out of this furnace is characterized to investigate properties about the chemical and mineralogical composition (see Section "Slag Characterization").

With this information, two special corrosion tests were carried out on chosen refractory grades: The high-frequency induction furnace test (HF-IF) (see Section "High-Frequency Induction Furnace (HF-IF)") is a dynamical test, where theoretically infiltration of the slag, corrosion of the brick components, and hot erosion of the sample takes place. The crucible test (see Section "Crucible Test".) is a stationary test, where mainly infiltration and corrosion of the samples can be observed. For those testings, three different magnesia-chromite bricks were chosen. Brick 1 was specially developed for this furnace type, based on past field test experience, containing out of pre-reacted material in combination with chromite material. Bricks 2 and 3 consist of different magnesia material with chromite addition.

Slag Characterization

The reverberatory slag characterization was done chemically and mineralogically. According to the XRD, the main phases found were metallic lead, lead sulfide,

Pb–Sb–Sn oxide, and a high amount of amorphic phases. Based on the optical microscopy and SEM investigations, those amorphic phases are mainly Ba–Ca–Na sulfate. Additionally, Na–Pb–Sb–Sn–Fe–Si oxide, $PbSbNi_{met}$ and in minor amounts nitrogen-containing Sn–Pb oxide, CuS, PbNiCuS, and $SbNiPb_{met}$ could be detected (Fig. 2; Tables 2 and 3).

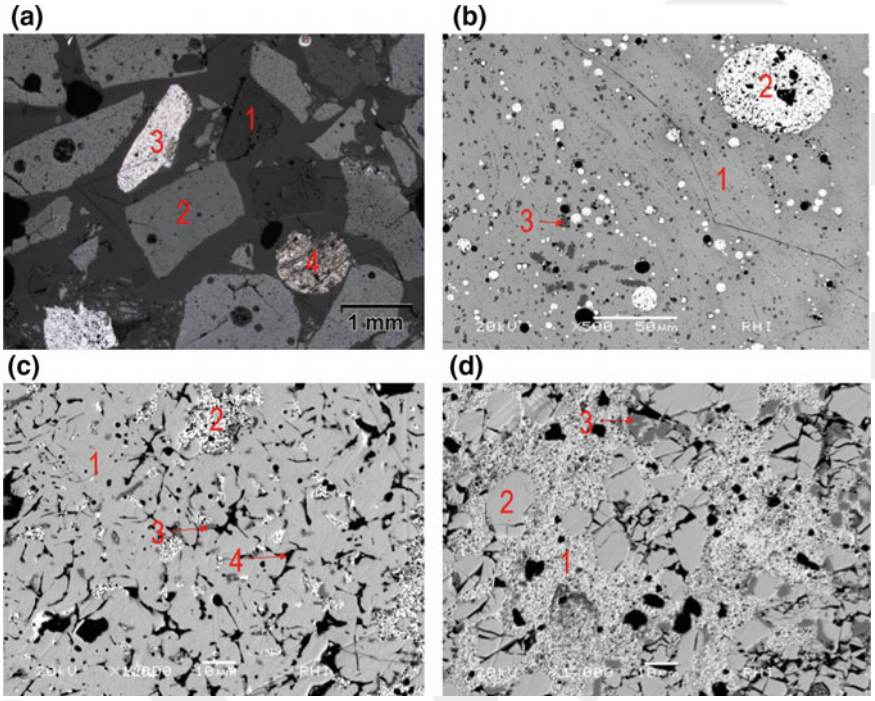

Fig. 2 Mineralogical slag characterization with help of scanning electron microscope (SEM). **a** Overview. The slag consists of different components. Grain 1—Ba–Ca–Na sulfate. **b** Detail grain 2 of (**a**). Na–Pb–Sb–Sn–Fe–Si oxide (1). Pb_{met} (2). Nitrogen-containing Sn–Pb oxide (3). **c** Detail grain 3 of (**a**). PbS (1). $PbSbNi_{met}$ (2). PbNiCuS (3). CuS (4). **d** Detail grain 4 of (**a**). Pb_{met} (1). PbS (2). $SbNiPb_{met}$ (3)

Table 2 Phase analysis by x-ray diffraction

Lead	Pb	10–50%
Galena	PbS	10–50%
Lead tin antimony oxide	$Pb_2SnSbO_{6.5}$	10–50%
Amorphous	Amorphous	10–50%

Table 3 SEM/EDX-analysis in wt%

Figure 2	Spot	N	O	Na	Mg	Al	Si	S	K	Ca	Fe	Ni	Cu	Sn	Sb	Ba	Pb
a	1		43.4	28.6				23.3	0.3	1.4						3.1	
b	1		17.4	1.6	0.4	0.4	4.9				3.0			3.6	3.2		65.5
	2		2.0														98.0
	3	1.3	29.9				0.2							67.5			1.1
c	1							9.6					0.8				89.6
	2		2.8									1.2			3.5		92.5
	3							8.0				19.1	2.5				70.4
	4							22.0					78.0				
d	3		1.0		0.5							29.0			58.1		11.5

High-Frequency Induction Furnace (HF-IF)

To get an advanced information about the corrosion behavior, a high-frequency induction furnace (HF-IF) corrosion test is carried out on three different magnesia-chromite brick samples (labeled as bricks 1–3).

Every brick brand was prepared with a dimension of 20 × 25 × 115 mm. As soon as test temperature was reached (in this case, 1500 °C under controlled atmosphere), the samples were immersed by 30 mm into the liquid slag melt. During the test, the sample holder rotates with a frequency of 0.15 Hz (corresponds to approximately 9 rotations per min). After the pre-defined test duration (240 min), the samples were lifted out of the melt and were subjected to a controlled cooling procedure, followed by a macroscopic and mineralogical examination (Fig. 3). Based on the investigation, brick 1 showed the highest corrosion resistance. At all samples, mainly the magnesia component was corroded due to SiO_2 supply under formation of sulfur-containing Na–Mg–Ca–Ba silicate. Remarkable is that no lead containing phases could be found

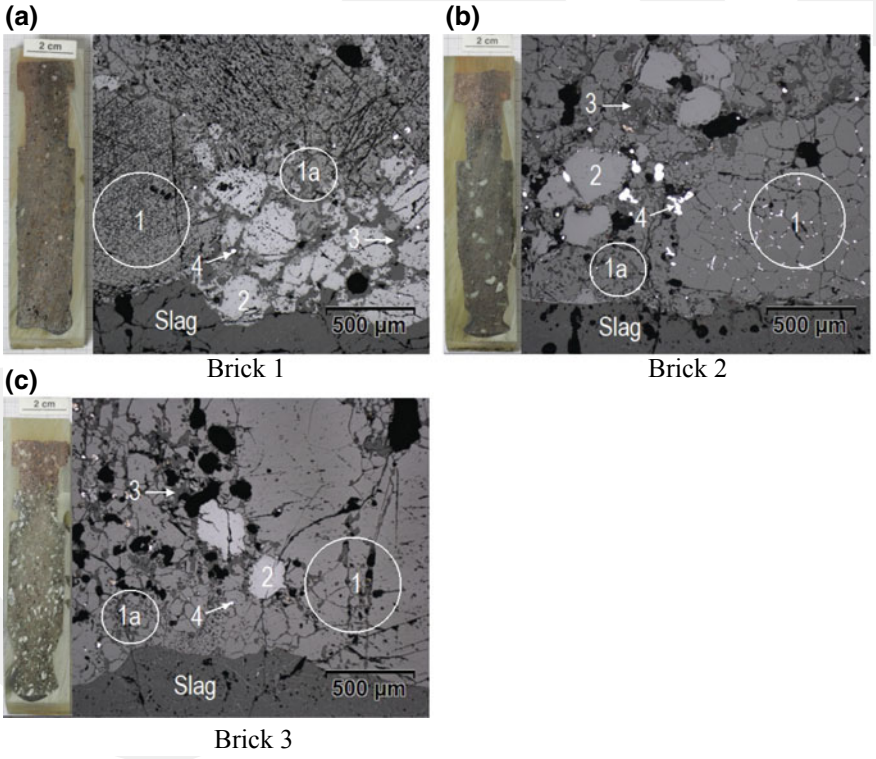

Fig. 3 Macroscopic and mineralogical documentation. The corrosion mechanism of all samples is the same: Mainly corrosion of the magnesia component—coarse grains (1) as well as the matrix (1a). Chromite (2). Infiltration of sulfur-containing Na–Mg–Ca–Ba silicate (3). $FeSnSb_{met}$ (4)

in the bottom area of all investigated samples (0–25 mm). A yellow/greenish coating was formed due to volatilization and precipitation of slag components at the upper part of the samples. Based on SEM-analyses, this coating consists of sodium, sulfur, tin, antimony, and lead.

Crucible Test

Another important laboratory test is the crucible test. Therefore, the same magnesia-chromite brick brands tested in the HF-IF, with a dimension of 80 × 80 × 70 mm and a drill hole with 45 mm depth and 40 mm diameter, were prepared and filled with a defined amount of slag material. Afterwards, a cover consisting of the same brick brand was fixed with mortar material on the crucible. The crucibles were placed inside the furnace and heated up to the defined temperature (1500 °C under controlled atmosphere). After the defined test duration of 480 min, the furnace cooled down and the crucibles were cut through diagonally. The evaluation of the samples and their corrosion behaviour is again done on a macro- and microscopical view (Fig. 3). Macroscopically, there is no difference between the samples in corrosion resistance; however, no remaining slag was found in the crucibles after the tests, probably due to volatilization of several compounds due to low vapor pressure of slag components and in combination with the high test temperature. Hence, just slight corrosion by the slag was detected (Fig. 4). The magnesia component was corroded due to SiO_2 supply of the slag under formation of forsterite (Mg_2SiO_4) and monticellite ($CaMgSiO_4$). Chromites are highly enriched with Sb and Sn oxides.

A difference can be seen in the infiltration—brick 1 shows a lower infiltration depth of approx. 1.5 cm compared to approx. 3 cm for bricks 2 and 3.

Post-Mortem Study

Magnesia-Chromite Brick

Due to the results of the laboratory tests, brick 1 was chosen for practical test in a lead reverberatory furnace.

In general, a post-mortem study starts with a macroscopical investigation of the sample, followed by chemical analysis and microscopical investigation.

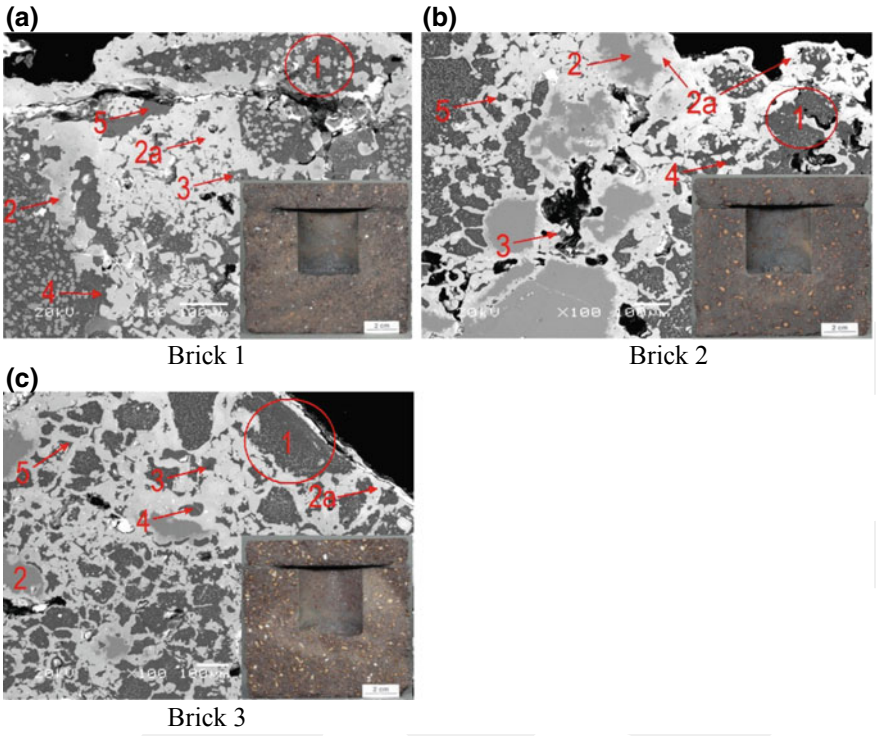

Fig. 4 Slight corrosion of the magnesia component (1). Chromites (2) are highly enriched with Sn and Sb oxides at the rims (2a). Na–Mg–Al–Fe silicate (3). Forsterite enriched with Sn and Sb oxides (4) and monticellite (5) as reaction products

Macroscopic Overview

The residual brick thickness of the investigated sample is about 220–230 mm (the original thickness was 342.9 mm). Parallel to the hot face running, non-filled cracks can be observed which is an indication that cracks are formed during cooling down phase of the smelter (Fig. 5).

Chemical Analyses

Chemically, the hot face of the brick is highly enriched with Na_2O, SiO_2, CaO, sulfur, and PbO and in minor with BaO, Sb_2O_3, and SnO_2. The cold end represents a typical chemical composition of this brick brand type (Table 4).

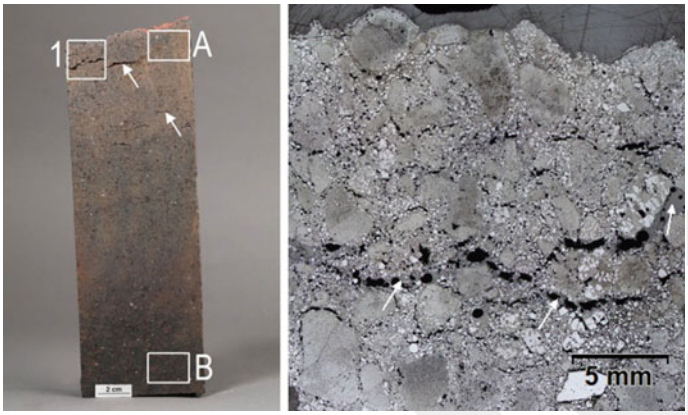

Fig. 5 Samples out of the slag line area. Left: Cut sectional view of the whole sample. Right: Polished sample of the hot side area. Cracks (arrows). Samples for chemical investigation (A) (B). Sample for polished sections (1)

Mineralogical Investigation

The immediate brick hot face is covered with a 0.5–1 mm thin reaction layer consisting of chromite highly enriched with Fe–Sb–Sn oxide, Na–Mg–Al–Fe silicate, Na–Ca–Mg silicate, and Na–(Cr)–(Si) sulfate. Below the reaction layer over the whole polished section (0–25 mm from the hot face), an infiltrated and corroded brick microstructure can be observed. Within this brick area, the magnesia component is severely corroded due to mainly the SiO_2 of the slag. The main reaction products include forsterite (Mg_2SiO_4), monticellite ($Ca_3Mg(SiO_4)_2$), and Na–Mg–Al–Fe silicate. Additionally, the rims of chromites are enriched with Fe–Sb–Sn oxide. The whole polished section is infiltrated by Na–Ba–Pb–(Ca) silicate. Additionally, at approx. 2 mm from hot face Na–Ba sulfate has been detected (up to 25 mm from hot face). At 10 mm, Pb oxide can be detected up to 165 mm. In a depth of approx. 20 mm from the hot face, newly precipitated MgO crystals formed at rims of the magnesia component (Fig. 6).

Table 4 Chemical analyses of investigated sample (in wt%)

	Na_2O	MgO	Al_2O_3	SiO_2	CaO	SO_3[a]	Cr_2O_3	Fe_2O_3[a]	BaO	PbO	Sb_2O_3	SnO_2
Hot face	7.2	41	5.8	7	1.3	1	18	12.7	1	3	0.4	0.3
Cold end	0.15	48.4	7.6	1.2	0.9	0.06	25.5	15.6				

[a]Total iron/sulfur calculated as Fe_2O_3/SO_3

GCDIS

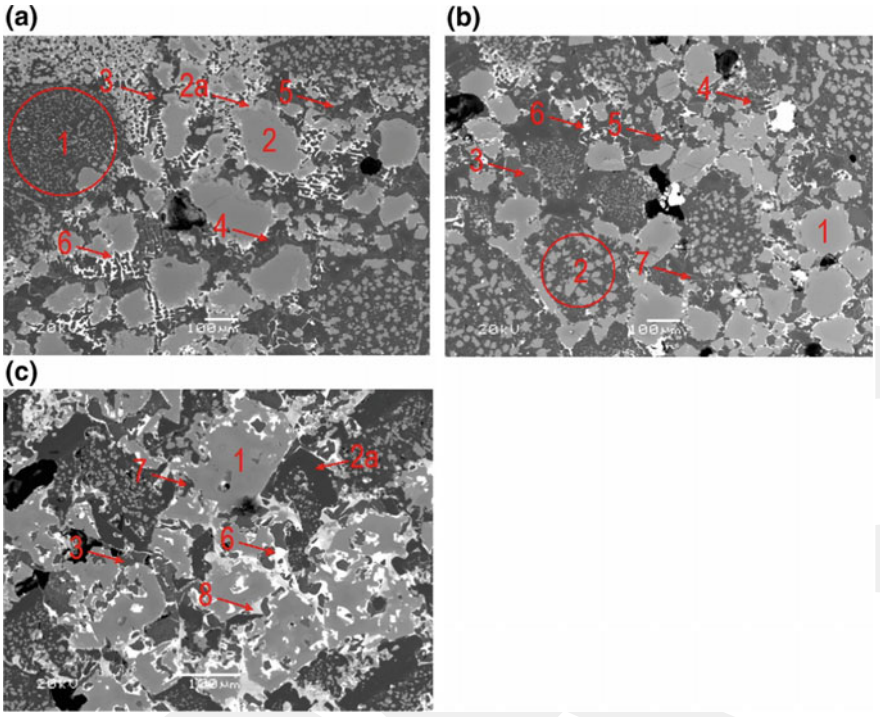

Fig. 6 **a** Detail of the reaction layer. Corroded magnesia (1). Chromite (2) enriched with Fe and Sn and Sb oxides (2a). Forsterite (3). Na–Ma–Al–Fe silicate (4). Monticellite (5). Na–Ba–Pb–silicate (6). **b**, **c** 10 and 20 mm from hot face—still corroded microstructure. Chromite (1). Magnesia (2). Newly precipitated MgO crystals formed at rims of the magnesia component (2a) (at 20 mm from hot face). Na–Ba sulfate (3). Monticellite (4). Forsterite (5). Pb oxide (6). Na–Mg–Al–Fe silicate (7). At 20 mm from hot face Ba-rich monticellite was detected (8)

Conclusion

To provide the most appropriate refractory solution, laboratory corrosion tests carried out with a reverberatory furnace process slag (lead and sodium sulfate-based slag) are done at RHI Magnesita's Technology Center, Leoben. The mineralogical investigation of the HF-IF test reveals that all tested brick brands show very similar corrosion phenomena, namely corrosion of the magnesia component, but differences in the infiltration depth. Due to the controlled atmosphere and long test duration at the crucible test, volatilization of the main slag components took place as no remaining slag was detected in the crucibles after the test. Therefore, only slight corrosion of the chosen refractory brand was observed—only minor corrosion of the magnesia component, but highly enrichment of the chromite with Sb and Sn oxides. Based on the results of the corrosion tests, the lowest wear has been observed for the specially developed magnesia-chromite brick 1, due to the used pre-reacted material in this brick. This brick was chosen for further field trials.

The post-mortem study carried out on the chosen magnesia-chromite brick demonstrated that as a consequence of chemical attack by slag, the infiltration and corrosion of the brick's inherent components led to a softening of the brick's microstructure, loss of flexibility, and brick strength. This weakened microstructure is then susceptible to continuous wear by hot erosion. Additionally, such degenerated brick microstructure is susceptible to spalling off.

To sum up, laboratory tests carried out on different refractory brands, followed by fieldwork trials at the customer itself, represent an important prerequisite to find the most suitable refractory choice for lead reverberatory smelting furnaces. This is the general approach for a defined and engineered lining concept and requires a high level of trust between supplier and customer—if this is the case, we can also contribute and bring in our full expertise to increase the performance of the wear lining in a pyrometallurgical vessel.

References

1. ILA International Lead Association, August 2014, www.ila-lead.org, https://www.ila-lead.org/UserFiles/File/ILA9927%20FS_Recycling_V06.pdf
2. Prengaman RD (2005). Secondary lead production—A survey of smelters and refineries. In: Lead & Zinc '05. Proceedings on the international symposium on lead and zinc processing 17–19 October, Kyoto, Japan, 2005
3. Lee YH, Park YM (2003) The experience of lead direct smelting in Korea Zinc's Onsan Refinery. In: Yazawa international symposium on metallurgical and material process, Warrendale, Pennsylvania, USA, 2003
4. Spanring A (2010) Refractory applications in the secondary lead industry. RHI Bull 1:56–62
5. Stephens RL (2005) Advances in primary lead smelting. In: Lead & Zinc '05. Proceedings on the international symposium on lead and zinc processing 17–19 October, Kyoto, Japan, 2005
6. Sofra J, Hughes R (2005) Ausmelt technology operation at commercial lead smelters. In: Lead & Zinc '05. Proceedings on the international symposium on lead and zinc processing 17–19 October, Kyoto, Japan, 2005
7. Gregurek D, Reinharter K, Reiter V, Wenzl C, Spanring A (2015) Postmortem study of a magnesia-chromite brick from a lead recycling furnace. JOM 67(9)

Influence of Minor Elements in Waste Lead Battery Recycling

Yusuke Sakata

Abstract Chigirishima Refinery of Toho Zinc Co., Ltd., started its lead smelting and refining operation in 1951 and now produces 95,000 tons of electrolytic lead per annum. At Chigirishima Refinery, the conventional smelting and refining method was adopted, with a series of process of sintering—blast furnace—electrolytic process. We recover some valuable by-product metals such as silver from lead concentrate and also utilize the cupola furnace to recycle the lead electrode in the waste battery. This paper describes the influences of minor elements in the lead electrode treatment such as Sb, Ca, Sn, sulfuric acid, and organic substances with its measures against them.

Keywords Waste lead battery recycling · Minor elements (Ca, Sb, Sn) · Sulfuric acid · Organic substance

Introduction

In Chigirishima Refinery smelting process, lead concentrate and waste lead battery are used as raw materials to produce the lead metal ingot.

Figure 1 shows the smelting flow of Chigirishima Refinery. The lead concentrate is put into the sintering machine with small amount of miscellaneous secondary raw materials. They are sintered and agglomerated and we obtain the massive sinter. The sinter is reduced in the blast furnace (BF) using coke to produce crude lead. The copper in crude lead is removed as the copper dross in the copper removal casting process and the anode for the electrolytic process are obtained.

The waste lead batteries are treated in the cut/separation operation, and the lead electrode in the waste lead battery is separated from plastic components. After that, the lead electrode is processed in a cupola furnace (CF). And the molten CF crude

Y. Sakata (✉)
Toho Zinc Co., Ltd, Chigirishima Refinery, 5562-1 Higashino Osakikamijima-cho, Toyota-gun, Hiroshima-pref. 725-0231, Japan
e-mail: sakata-yusuke@toho-zinc.co.jp

© The Minerals, Metals & Materials Society 2020

A. Siegmund et al. (eds.), *PbZn 2020: 9th International Symposium on Lead and Zinc Processing*, The Minerals, Metals & Materials Series,
https://doi.org/10.1007/978-3-030-37070-1_49

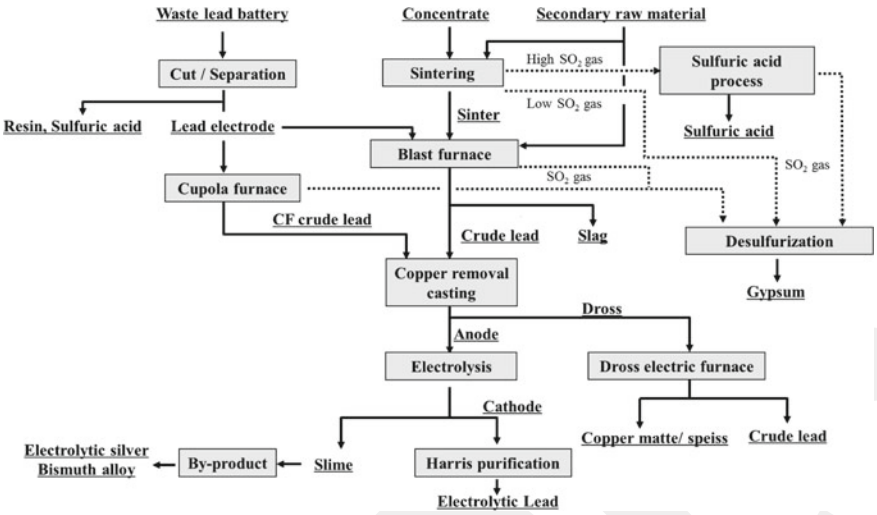

Fig. 1 Flow chart of Chigirishima Refinery

lead is mixed with crude lead from the blast furnace and treated in the copper removal casting process.

The casted lead anode is refined in the electrolysis process (the Betts method), and 99.995% pure electrolytic lead is obtained. The anode slime containing silver, gold, and bismuth is treated, and each element is recovered in the by-product process.

As for exhaust gas treatment, the SO_2 gas from the main reaction part of the sintering process with high SO_2 concentration (>5%–SO_2) is treated in the sulfuric acid process to produce sulfuric acid. The low SO_2 gas generated in the blast furnace, cupola furnace, and cooling part of the sintering process is treated, and the gypsum is produced in the desulfurization process.

The Minor Elements in the Waste Lead Battery

The Structure of the Waste Lead Battery and the Disassembling Line

As shown in Fig. 2, the lead battery can be taken apart into six main parts:

- Lead alloy electrode grid,
- Strap lead alloy connecting the electrodes,
- Top part (the lead alloy external terminal),
- Lead paste (PbO_2, $PbSO_4$),
- Dilute sulfuric acid electrolyte, and
- Plastic resin case.

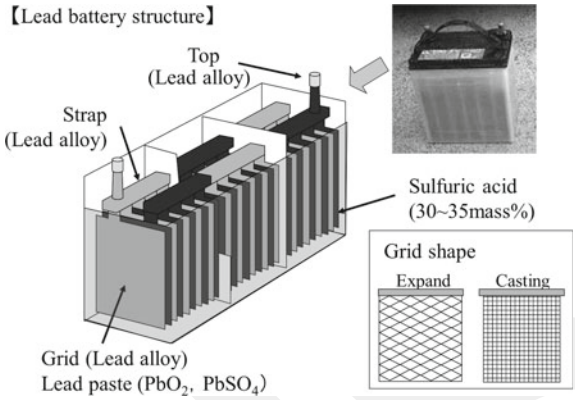

Fig. 2 Lead battery structure

Lead alloy electrode grid, other lead alloy parts, and lead dioxide paste can be evaluated as the source for the lead recycle. But dilute sulfuric acid and plastic resin case should be removed carefully to enhance the value of the lead material parts.

Figure 3 shows the waste lead battery disassembling line in Toho Zinc. As a method of separating the waste lead battery, the top parts of the lead battery are cut and separated from the battery body firstly. Then, the top parts with the strap lead alloy are removed, crushed, water-washed, and separated from the plastic resin lid. The lead alloy of the top parts is crushed, and strap parts can be used as the lead source.

Regarding the body separated from top parts, the liquid dilute sulfuric acid is separated from other case parts at the reversing step. The sulfuric acid contains some

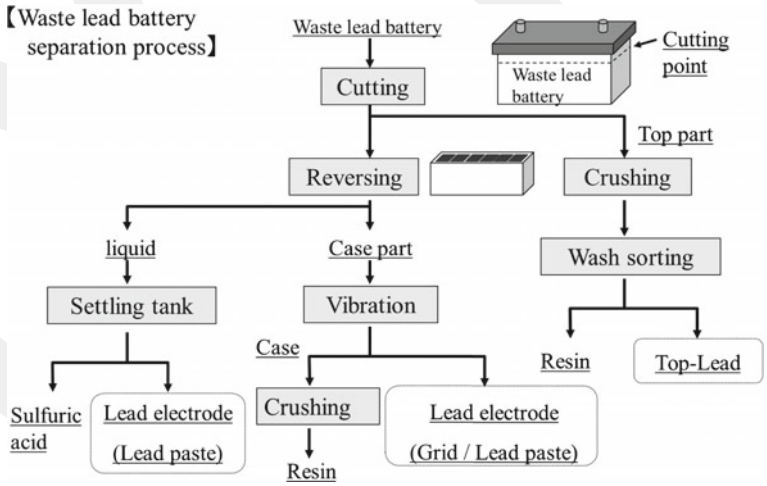

Fig. 3 Waste lead battery disassembling line

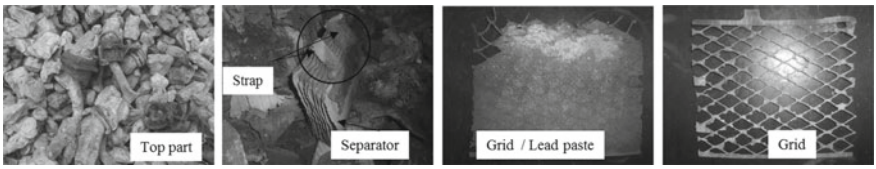

Fig. 4 Appearance of various lead components for the waste lead battery recycle

lead paste which should be recovered at the settling step to secure the quality of the acid. The case part is treated in the vibration step and the lead electrode (grid and paste) is separated from the plastic resin case. The plastic resin case is crushed, water-washed, and recovered as the resin for sale. The separated top part, grid, and lead paste are treated as the lead raw material. Figure 4 shows the appearance of them.

Minor Elements in the Waste Lead Battery

The recovered lead components such as the top part, grid, and lead paste are well-valued materials in lead recycle, but it contains some minor elements such as antimony, calcium, and tin which cause some troubles in the lead processing or some contaminants such as sulfates and resin caused by the imperfect separation. The Sb and Sn in top alloy parts and the Ca, Sb, and Sn in lead grid are added to improve those mechanical and chemical properties of the lead battery. In the lead paste in the waste lead battery, not only lead dioxide but some lead sulfate is also generated by the repeated usage. The lead sulfate increases the sulfur input to the process with the sulfuric acid adhered to the lead components. Also, most of the resin parts of the waste battery can be removed as the crushed resin, but it is not perfect. And also the resin bag is used as the separator to prevent the short circuit between the electrodes. That fraction of the weight of the separator is shown in Fig. 5, and it is hardly separated from the grid and paste.

These minor elements can influence our process in different ways. Those troubles are not always critical, but it is getting more important in recent years to treat in order to meet the requirements of the products quality and the surrounding's environment.

Table 1 shows the minor elements contained in the recovered lead components from the waste lead battery and their effects on the smelting process.

The lead electrode grid and strap contain Sb, Ca, and Sn in order to improve battery characteristics. In the smelting process, Sb increases the hardness of the anode slime in the electrolysis process, and sometimes, it causes the difficulty to separate the slime from the anode. Ca influences the slag composition formed in the CF process. As for Sn, it is bled to some by-products such as Fe slag and copper matte but relatively hard to be removed from the lead refining circuits. We apply Harris refining method

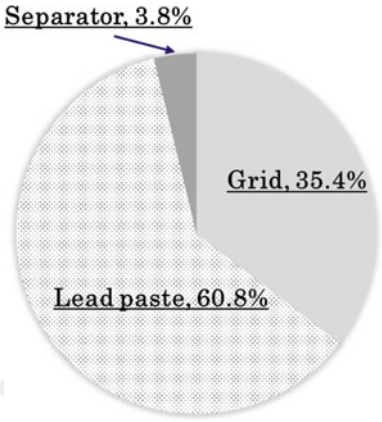

Fig. 5 Lead electrode composition

for Sn separation, but if the Sn load on our Harris refining exceeds the capacity, it can impact the quality and production of the lead products.

The sulfuric acid component (sulfur) adhered to the recovered lead components and lead sulfide component in the lead paste corrode the water cooling jacket of the cupola furnace. In addition, SO_2 gas generated by the thermal decomposition of sulfuric acid in the cupola furnace increases the load on the desulfurization process.

Regarding the organic part originated in the resin separator, if it is put and processed in the cupola furnace, most of it is combusted, but some unburnt carbon fraction is recovered as the flue dust in the exhaust gas process of CF. This generated dust is recycled together with other raw materials in a sintering machine, and the unburnt volatile organic component enters in the sulfuric acid process and causes the quality problem, such as coloring of the product acid.

Figure 6 shows the transition of the amount of lead components from the waste lead battery processed at Chigirishima Refinery, which started to treat it only in the BF in 1983. The current cupola furnace treating the lead components solely started operation in 1991, and the processing throughput of them was increased. The combined treatment in the blast furnace and cupola furnace has recorded close to 50,000 ton/year in 2004. However, the throughput decreased due to various economic factors such as the soared waste lead battery price caused by the increasing oversea outflow, the fallen silvery lead concentrate price, and the promotion of silver production. Then, in 2009, we stopped to put the lead components from the waste lead battery into BF but keep it only in CF.

Table 1 Minor elements contained in the lead electrode and effects on the process

Minor elements contained in lead electrodes		Impact on process						
		CF process	Sulfuric acid process	Blast furnace process	Electrolytic process	Casting process	By-product process	Desulfurization process
Sb [%]	0.26				○ Increase slime strength			
CaO [%]	0.12	○ Flux component						
Sn [%]	0.29				× Electrodeposition on the cathode	× Increased Harris purification load		
S [%]	3.80	× Corrosion of water cooling jacket						× Increased desulfurization load
Organic component			× Coloring to product acid					

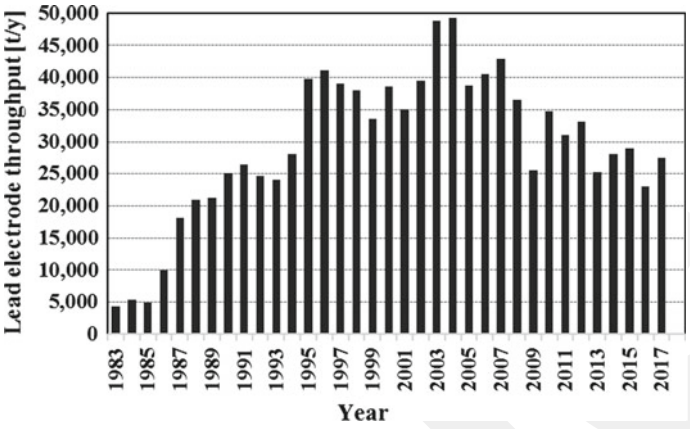

Fig. 6 Transition of lead electrode throughput

Influence of Minor Elements

Influence of Metallic Elements

As mentioned in the previous section and Table 1, the lead components recovered from the waste lead battery contains Sb, Ca, and Sn. Table 2 shows the distribution behavior of them in the CF.

Almost all of Ca is processed in the CF and then BF and transferred to the slag. Most of Sb is dispersed in the crude lead. Ca and Sb affect those processes in different ways in the refining circuit but they are controllable mainly by blending the raw material carefully. We do not utilize only the lead components from the waste lead battery but also the lead concentrate, so it is easier to decrease the impact of those elements. Adversely, in recent 5 years, the Sb content of the lead concentrate is getting less, so more Sb input from the lead recycling can be an effective additive element to keep the current efficiency better in the electrolysis process, maintaining the proper hardness of the anode slime. However, the situation of Sn is different and hard to clear it by blending.

As shown in Fig. 7, Sn derived from the lead components from the waste lead battery occupies 67% of the total input. Since Sn can be oxidized easier than Pb, it

Table 2 Distribution ratio of various additive metals in the CF

Out put	Pb [%]	CaO [%]	Sb [%]	Sn [%]
CF crude lead	92.7	0.0	84	21
CF slag	1.2	98.6	5.0	29
CF dross	3.9	0.0	9.0	47
CF dust	2.2	1.4	1.5	2.7

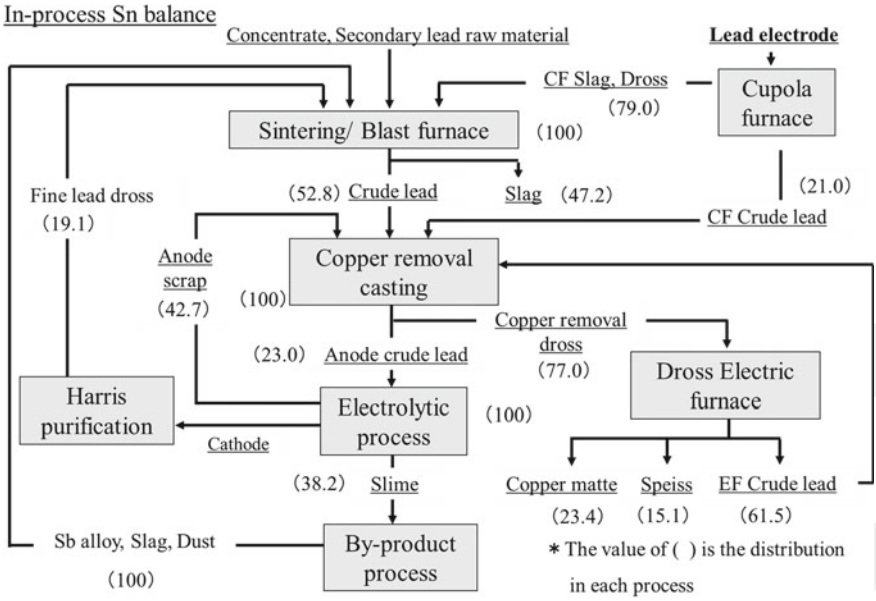

Sn balance					
Input			Output		
Name	Sn [t/y]	Distribution[%]	Name	Sn [t/y]	Distribution[%]
Concentrate/ Secondary Lead raw	56	33	Slag	86	51
			Cupper matte	50	30
Lead electrode	112	67	Speiss	32	19
Input total	168	100.0	Output total	168	100.0

Fig. 7 Behavior of Sn in the smelting process

tends to be transferred to the slag. But a part of Sn is also going to the crude lead and other by-products. Sn is recycled to all over the lead refining circuit including the sintering process and blast furnace by a certain amount. Eventually, Sn is distributed 51% to the slag, 30% to copper matte, and 19% to speiss and discharged outside the process.

Sn impacts various processes and has major influence on the purity of electric lead in the electrolysis process. Since Sn cannot be removed completely in the copper removal casting process at our refinery, Sn contained in the anode is partially transferred to the cathode in the electrolysis process. In our recent operation, the Sn content in the cathode is higher than 100 ppm. Sn shall be removed in order to keep the quality of the electric lead>99.99% as the final product. Harris purification method shown in reaction (1) is used in the electric lead purification process.

$$\mathrm{Sn} + \mathrm{O_2} + 2\mathrm{NaOH} \rightarrow \mathrm{Na_2SnO_3} + \mathrm{H_2O} \quad (1)$$

If the Sn content in the cathode increases, the operation cost is increased by the higher cost of caustic soda used for purification and the extension of the purification

time. At the same time, refined lead dross generated during the Harris refining is transferred to the sintering and smelting process.

Effect of Adhered Sulfuric Acid

Corrosive Damage on the CF Water Cooling Jacket

Figure 8 shows a schematic diagram of the CF. The crude lead, slag, and dross are discharged from the hearth to the bottom of the furnace. And, the CF also has tuyeres, water cooling jacket for cooling the furnace, and the shaft portion. The raw material is charged using the bucket and filled into the furnace. Coke, iron source, and the lead components from the lead waste are put layer by layer.

Dilute sulfuric acid, which is an electrolytic solution for a lead battery, adheres to the lead components from the lead waste. Figure 9 shows the simulated result for the thermal decomposition of dilute sulfuric acid in the CF, which is created using HSC simulation software, with 30 wt% dilute sulfuric acid, 1 kmol sulfuric acid, and an activity coefficient of 1 for each compound for simplification. The behavior is that the sulfuric acid component is pyrolyzed to SO_2 by pyrolysis in the cupola furnace. At a lower temperature than 800 °C, it is not decomposed sufficiently and becomes sulfuric acid, sulfuric acid vapor, or SO_3 gas. The low-concentration sulfuric acid generated from these components and moisture in the lead components from the lead waste can corrode the metal material of the cupola exhaust duct. The cupola furnace

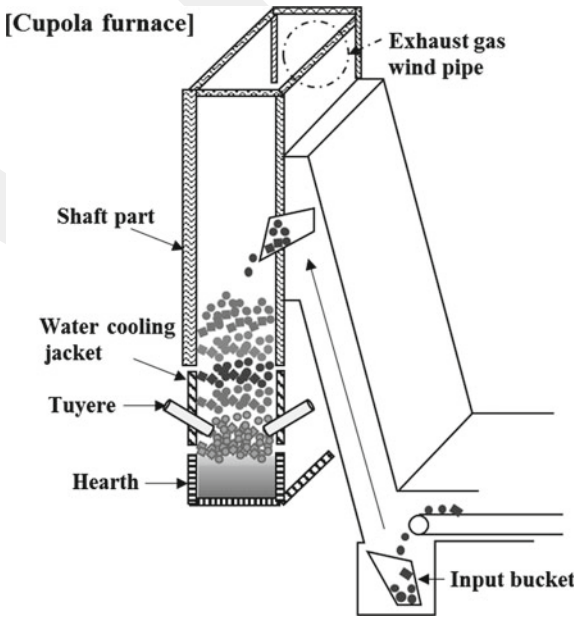

Fig. 8 Schematic diagram of cupola furnace

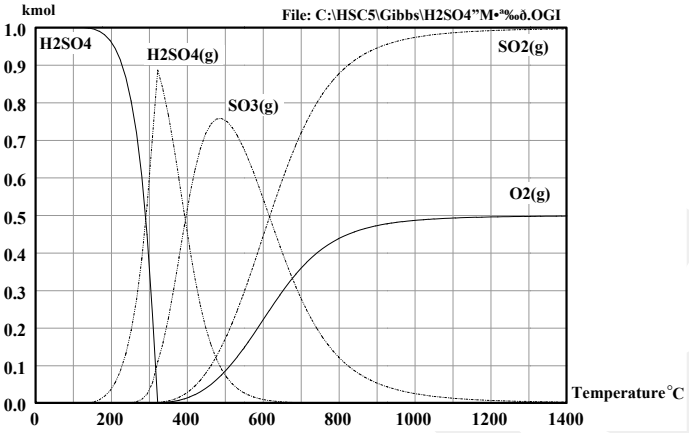

Fig. 9 Thermal decomposition behavior model of dilute sulfuric acid

body is made of steel plate and water-cooled. The surface of the water cooling jacket tends to be in a low temperature state, and in particular, the upper part in the raw material preheating stage is easily affected by the above-mentioned corrosion by low-concentration sulfuric acid.

Figure 10 shows the configuration of the water-cooled jacket for the cupola furnace and the photograph of the wear-resistant welding for the water cooling jacket. The adhered sulfuric acid mainly corroded the upper part of the water cooling jacket (SS 16 mm thickness) and caused water leakage. As a countermeasure, for the part where the thinning is remarkable, 3 mm overlay was constructed by high Cr wear-resistant welding. In addition, we started to reduce the amount of attached sulfuric acid as much as possible to keep the lead components from the lead waste temporarily stored for a while in a storage yard when we receive them. As a result, problem of corrosion and leakage of the water cooling jacket in the cupola furnace are cleared.

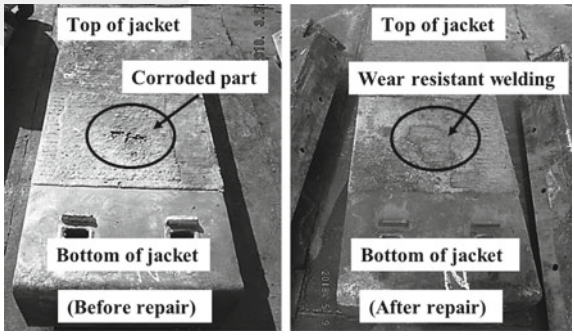

Fig. 10 Photograph of the wear-resistant welding for the water cooling jacket

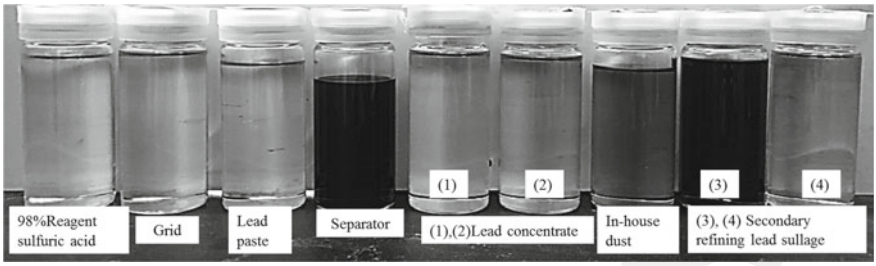

Fig. 11 Results of sulfuric acid coloring test by calcination of lead electrode components

Influence of Organic Substances (Separator)

As shown in Fig. 4, a separator is used for the lead battery. The separator has a role of preventing a short circuit between the positive electrode and the negative electrode, allowing each ion related to the reaction to pass through and holding the electrolytic solution in the separator. As a material for the separator, generally, a mixture of hydrophilic PE fibers and SiO_2 powder is used. In our refinery, sulfuric acid is produced from SO_2 gas generated in the sintering process. In-house dust containing organic components recovered from the cupola furnace exhaust gas is processed in the sintering process. As a characteristic of the furnace of the sintering machine, there is a preheating process of raw materials at the raw material charging stage. The organic substances are not completely burned in the furnace, and the gaseous organic components that cannot be washed in the sulfuric acid gas refining equipment are transferred to the sulfuric acid process. As a result, the gaseous organic matter is absorbed and carbonized in an absorption tower in the sulfuric acid process, and the product acid becomes brown. Figure 11 shows the photograph of the various test results of the coloring condition when the combustion conditions in the sintering machine are simulated. In the case of a gas produced from a lead electrode plate separator and from in-house dust including dust generated from cupola exhaust gas sulfuric acid, the acid is colored, while in the case of concentrate, which is the main raw material of a sintering machine, sulfuric acid is less colored. From the above results, the cause of sulfuric acid coloring is considered to be due to the influence of organic substances due to the lead electrode plate treatment.

Conclusion

In this paper, the influence of the minor elements in waste lead battery such as adhered sulfuric acid, organic matter, and alloy components was described. Regarding the attached sulfuric acid, the corrosion of the water cooling jacket in the cupola furnace is caused and the generated SO_2 gas causes an increase in the desulfurization load in the desulfurization process. As for the separator (organic substance), coloring of the

product acid in the sulfuric acid process is caused. Almost all of Ca is processed in the CF and BF and transferred to the slag. Most of Sb is dispersed in the crude lead. They affect those processes in different ways in the refining circuit, but Ca and Sb are controllable mainly by blending the raw material carefully. The alloy component Sn is an element that circulates in the process, and there is a problem that the load increases in the Harris refining process as lead electrode treatment increases.

Currently, in Japan, the supply and demand situation for the waste lead battery has changed significantly, and the waste lead battery has become available at much cheaper price than concentrate. Therefore, we are in need of increasing the waste lead battery usage as soon as possible. We would like to clear these problems by promoting research, minimizing the impact on quality and the surrounding environment.

GCRIS

The FAST Pb Process and Its Impact on Secondary Lead Production

Massimo Maccagni and Edoardo Guerrini

Abstract Today, all lead is produced in pyrometallurgical plants. Secondary lead production is assuming a growing importance but requires to be updated to comply with the more and more stringent regulation that is going to be implemented in the future. Engitec, involved for a long time in the development of an hydrometallurgical lead production, finally, has demonstrated that the recovery of lead from battery paste through electrochemistry is technically and economically viable through campaigns run on the FAST Pb Process demo plant. The latest development was based on the use of non-desulphurized paste learning that the presence of sulphates in the electrolyte can be controlled and is not causing any additional technical problem if not the consequent removal of sulphates from the electrolyte. This new approach heavily impacts on the new way of operating the whole battery recycling process simplifying the flowsheet through the removal of some problematic units and achieving a further reduction in the environmental impact.

Keywords Lead · Battery · Recycling · Electrolysis · Ammonium chloride

Introduction

We are living in the time of the "Circular Economy", of which one of the most challenging aspects is the energy production and storage. Lead acid battery technology is one of the oldest technologies and has a bad reputation public opinion but it was, is, and will be one of the most important players in energy storage because of some unquestionable advantages versus competing systems: it is well known, inexpensive, reliable, and fully recyclable. Furthermore, the existing lead output and mine reserves, also because of the high lead recycling rates, guarantee sufficient material for future growth.

M. Maccagni (✉) · E. Guerrini
Engitec Technologies S.p.A., Via Borsellino e Falcone, 31, 20026 Novate Milanese (MI), Italy
e-mail: m.maccagni@engitec.com

E. Guerrini
e-mail: e.guerrini@engitec.com

© The Minerals, Metals & Materials Society 2020

A. Siegmund et al. (eds.), *PbZn 2020: 9th International Symposium on Lead and Zinc Processing*, The Minerals, Metals & Materials Series,
https://doi.org/10.1007/978-3-030-37070-1_50

In lead production, secondary lead production overtook primary production and both the technologies had to face a lot of environmental constraints that pushed these technologies to go through significant improvements becoming safer and more environmentally friendly. The strong reduction in emissions data, as well as blood lead data within lead production plants, demonstrates that a properly operated lead production plant is no more dangerous than other metals having an infinitely better reputation than the lead. This result was possible because of the steady introduction of new processes, new equipment, and new concepts to continuously update the existing processes that, currently, are only pyrometallurgical.

Hydrometallurgical/electrochemical processes are welcome as they are more selective, more environmentally friendly, and able to reduce the emissions and the generation of wastes typical of a pyrometallurgical process.

Engitec started investigating this kind of processes since thirty years ago trying different systems and different chemical approaches till, a few years ago, the FAST Pb Process was patented.

The FAST Pb Process is a way to produce metallic lead from oxidized Pb bearing materials, in particular from lead acid battery paste, through an innovative and unconventional approach. The first application for this electrolysis was an electrochemical pre-removal of lead within Engitec's chloride zinc electrowinning EZINEX® Process. This electrolysis was first performed in a tubular cell and was never fully developed. Unfortunately, the EZINEX® Process was limited to the first plant and was decommissioned for non-technical reasons after 4 years operation.

At the beginning, the FAST Pb Process was supposed to be used only on desulphurized paste. Paste desulphurization is a common unit in Engitec's battery recycling process, the CX® Integrate Process, used to remove the sulphur before feeding the paste to the furnace to avoid, or at least minimize, SO_2 emissions. We were concerned about building up sulphates in solution that, sooner or later, were supposed to create problems in the electrochemical system. However, after extended test campaigns, the viability of the same process using undesulphurized paste was demonstrated. Some further considerations and studies, caused us to realize this new approach, could deeply change and improve the lead acid battery recycling process.

Some other oxidized lead bearing materials were successfully tested in the demo plant built at Engitec's laboratory demonstrating the robustness of the process.

The FAST Pb Process

The process is based on an ammonium chloride electrolyte and a flow cell, which is the true novelty of the process, where Pb is not plated in the traditional form of a sheet but in a non-adherent flake form. These Pb flakes are stripped off the cathode and transported out of the cell by the electrolyte flow. This electrolysis uses a chloride electrolyte that usually produces anodic chlorine. Engitec's EZINEX® experience demonstrated that in the presence of ammonium/ammonia in a buffered solution, the chlorine will immediately react with ammonium producing nitrogen.

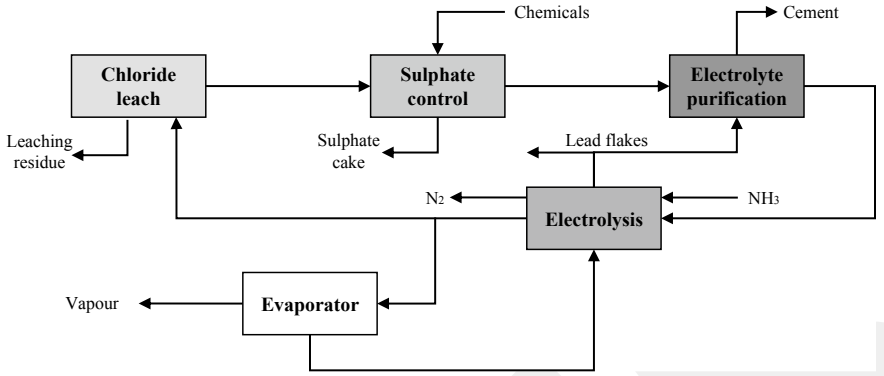

Fig. 1 FAST Pb Process block diagram

The new process is shown in the block diagram of Fig. 1.

Going through the units, in the leaching unit, in a stirred reactor, the oxidized lead compounds, including lead dioxide, are leached according to the following reactions:

$$PbSO_4 + 3NH_4Cl \rightarrow NH_4PbCl_3 + (NH_4)_2SO_4 \quad (1)$$

$$PbCO_3 + 3NH_4Cl \rightarrow NH_4PbCl_3 + CO_2 + 2NH_3 + H_2O \quad (2)$$

$$PbO + 3NH_4Cl \rightarrow NH_4PbCl_3 + 2NH_3 + H_2O \quad (3)$$

$$PbO_2 + H_2O_2 + 3NH_4Cl \rightarrow NH_4PbCl_3 + 2NH_3 + 2H_2O + O_2 \quad (4)$$

$PbSO_4$ is completely leached because of the chloride complexation. PbO_2, which is not leachable in the Pb depleted solution, requires the presence of a reducing agent such as hydrogen peroxide. Concentration of ammonium chloride and temperature is fixed according to the solubility of the Pb complex. The extraction rate for the above-mentioned compounds is usually very high, quite often reaching a value higher than 98%. The kinetics depends on the grain size and the hydraulics of the reactor.

The sulphates leached and converted to $(NH_4)_2SO_4$ have to be taken out of the process to avoid their build-up that will create some solubility problems as well as the development of scales along the process lines. There are some chemicals usable for this task. The most common is lime that reacts through the following reactions:

$$(NH_4)_2SO_4 + CaO + H_2O = CaSO_4.2H_2O + 2NH_3 \quad (5)$$

$$(NH_4)_2SO_4 + Ca(OH)_2 = CaSO_4.2H_2O + 2NH_3 \quad (6)$$

Through this reaction, we reach an equilibrium calcium-sulphate in solution that has to be controlled to avoid, or at least minimize, the possible formation of $CaSO_4$ scales, mainly into the heat exchangers, which need a careful work to be removed.

We demonstrated in our demo plant the possibility to produce very pure lead (Pb > 99.99%). To reach this high purity, we need to remove all the impurities nobler than lead to avoid their co-plating with lead. This can be achieved through cementation using, in the cementation reactor, the electrolytic produced Pb flakes as the reactant or any kind of Pb scrap. The relevant chemical reaction is shown here below.

$$Me^{n+} + n/2\ Pb = Me + n/2\ Pb^{2+} \quad (Me = Ag, Cu, Cd, \ldots) \tag{7}$$

After the cementation, the solution now is pure enough to be fed to the electrolytic unit but needs a careful polishing filtration to remove even any particle of cement that, in the electrolytic unit, can be incorporated into the deposit decreasing its quality.

The electrowinning flow cell unit is the core of the process; it is unique and very different from the typical cells used in the traditional electrowinning.

The plating mechanism is the opposite of the traditional electrowinning cells: instead of trying to plate a very smooth lead cathode plate, in the FAST cell, we would like to produce flakes that do not strongly adhere to the cathode. These plated flakes are easily stripped off the cathode and transported out of the cell by the electrolyte flow that has to be higher than 1.5 m/s.

The cell design is very peculiar. The most important feature is the gap between the two electrodes that is very narrow for the following reasons:

- having to reach a high linear velocity of the electrolyte, a narrow gap helps to achieve the required velocity with a reasonable pump flow rate;
- having to reduce the ohmic drop in solution to reasonable value and being it function of the gap between the electrodes, a narrow gap reduces this ohmic drop keeping low the cell voltage and, consequently, the energy cost.

Of course, this gap has to be "big" enough to avoid the formation of short circuits that can occur when the plated Pb contacts the anode before being stripped to avoid the re-dissolution of lead decreasing the faradic efficiency.

The FAST cell was proven capable of operating at very high current densities (up to 50,000 A/m^2). The best compromise for an industrial application seems to be in the range of 8000–12,000 A/m^2. Due to the lead solubility, the temperature of the electrolyte in the cell, as well as one of the solutions in any other unit of the process, has to be kept quite high.

Another important peculiarity of the cell is the use of bipolar electrodes: on one face, they work as a cathode, and on the other one, they work as an anode. Some different material candidates such as graphite and some metallic electrodes were tested. These different electrode materials proved to have a strong impact on the cell design, on the adhesion to the cathode, and on the formation of anodic PbO_2. For this last mentioned problem, the appropriate working conditions through the control of the free ammonia concentration of the electrolyte play a very important role.

The reactions in the cell are very similar to the ones of the EZINEX® Process. On the cathodic side of the electrode, the following reaction takes place:

$$NH_4PbCl_3 + 2e^- \rightarrow Pb + NH_4Cl + 2Cl^- \quad (8)$$

producing the metallic flakes that are the product of this electrolysis. On the anodic side of the electrode, the following reaction takes place:

$$2Cl^- \rightarrow Cl_2 + 2e^- \quad (9)$$

The chlorine management is, fortunately, not required because the anodic reaction is followed by the following very fast chemical reaction:

$$\text{Chemical reaction} : 2/3\ NH_3 + Cl_2 \rightarrow 1/3\ N_2 + 2HCl \quad (10)$$

Some recent test on different anodes seems to demonstrate that on some of them the direct de-hydrogenation of ammonia is also possible as a competing reaction having, in any case, no impact on the process.

The overall cell reaction (8 + 9 + 10):

$$NH_4PbCl_3 + 8/3\ NH_3 \rightarrow Pb + 1/3\ N_2 + 3NH_4Cl \quad (11)$$

shows that, in the cell, the process is able to regenerate the leaching reactant to make a closed loop system. Some NH_3 is consumed in the chemical reaction following the anodic reaction, and the Pb/NH_3 molar ratio is the same for all the possible battery paste components.

Several factors, such as the operative current density, the solution temperature, and the electrolyte composition, impact the cell voltage. In optimized working conditions, cell voltage is in the range 2.9–3.1 V at current densities ranging between 8000 and 10,000 A/m^2. The current efficiency does not depend substantially on the current density and it is between 85 and 90%, and one of the main factors for this is the narrow working gap between the anode and cathode. Some flakes can contact the anode and re-dissolve. The direct current energy consumption is between 870 and 900 kW/t of produced lead.

The flakes produced take with them some electrolyte that needs to be squeezed out, for instance by rolling or briquetting, before feeding them to a crucible for converting them into a commercial cast ingot.

Engitec's long demonstration plant campaigns, lasting more than three years during which more than 15 tons of sulphurized paste have been treated, have provided all the data and parameters required to design the industrial cell and the complete industrial plant.

Impact of the FAST Pb Process on the Lead Acid Battery Recycling Process

Despite the tests on a lot of different lead bearing materials, this new technology was developed to take care of the lead acid battery paste because we have learned that it will have a significant impact on the overall battery recycling process, deeply impacting several unit operations in terms of future efficiency, economics, and environmental impact.

The most evolved current recycling process is the Engitec CX® Process that is highly simplified in the block diagram shown in Fig. 2.

This is a highly refined and consolidated process that has undergone extensive changes and continuous process updates. But there are still some areas to be further improved to obtain an even cleaner and environmental sound process. The most important issues are:

- the paste smelting unit, along with slag and fumes management, which is the bigger problem as far as concerns the environmental impact;
- the desulphurization unit where that cost of reactants is much higher than the revenues for the sulphate salt selling, and the evaporation cost is high and continuously growing;
- not to be forgotten, the challenging market for the crystallized sulphate salt.

The introduction of the new FAST Pb Process can significantly change the entire battery recycling approach. Some of the operations indicated in the previous block diagram can be reduced, cut, and/or minimized by the introduction of this hydrometallurgical process. The process becomes simpler and more environmentally friendly as shown in Fig. 3.

As you can understand looking at Fig. 3, the process changes where it needs to change. In fact, desulphurization is not required anymore and this means to consequently cut also the sulphate solution purification and the big crystallization unit. This also means to have not anymore the problem of selling the sulphate salt.

The other big change is that the big rotary furnace used for the smelting of the paste is not required being the recovery of lead from the paste performed by the FAST Pb Process. This means also that the big baghouse taking care of the foundry is not anymore required.

There are several additional benefits to the FAST Pb Process not yet mentioned. The sulphate removal can be carried out in a dedicated unit where, using a high quality lime, a saleable gypsum can be produced. The final leaching residue contains all the antimony from the paste, so it does not transfer through to the refinery. There is a small amount of unleached lead also contained in the residue that can be treated by campaign in a small furnace where the metallic grids fraction is also recovered. The final amount of slag and ashes is very highly reduced compared to current operating techniques. There is an evaporator for the FAST Pb Process, but the capacity is much less than for desulphurization, and it is only to maintain the water balance in the FAST unit, not to produce any products.

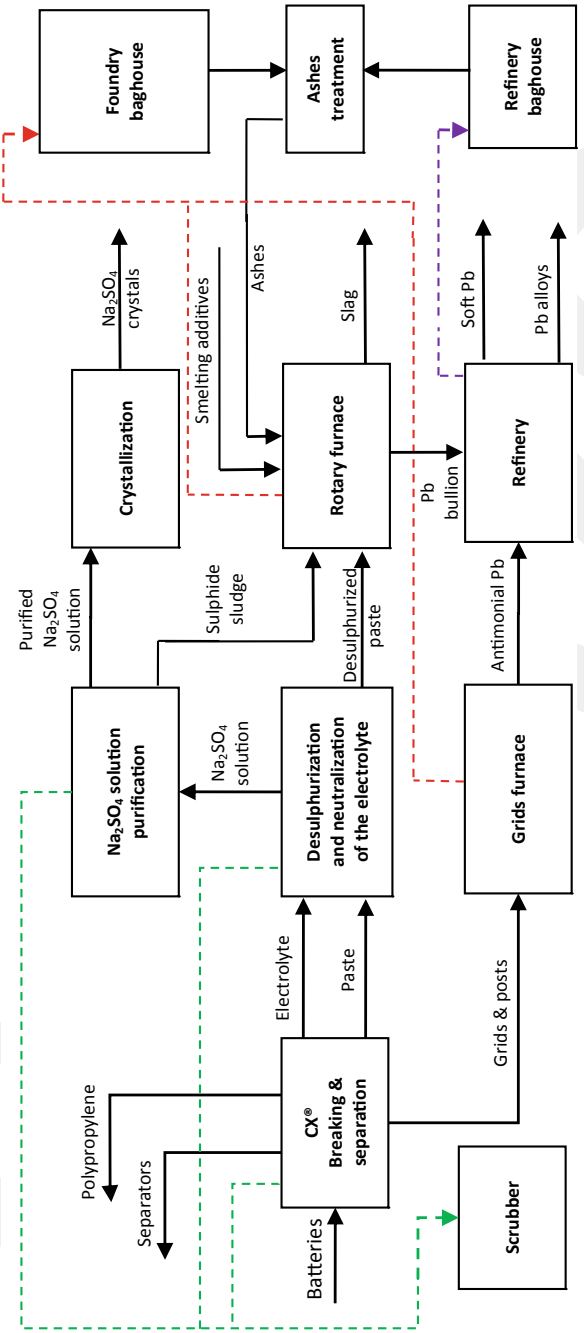

Fig. 2 CX® simplified process block diagram

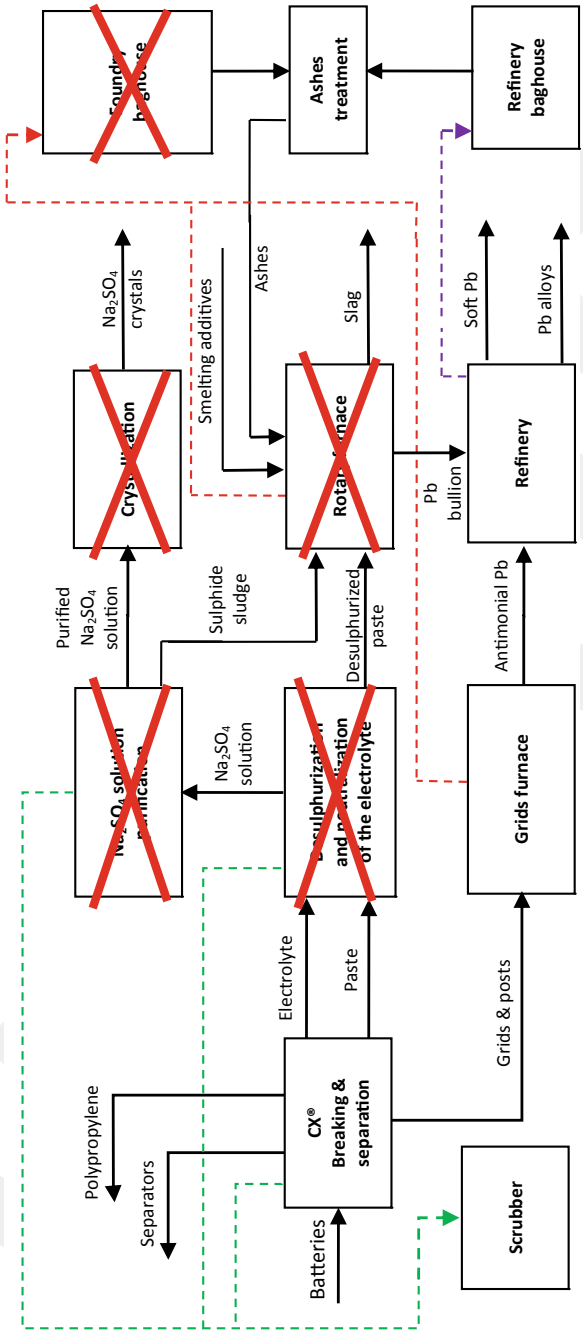

Fig. 3 CX® simplified process block diagram: possible simplification

The FAST electrowinning system is fully automated and requires a very limited labor. The process is also enclosed providing a much better workplace environment than the traditional foundry.

The process configuration for the "future" new and modern battery recycling plant is shown in the block diagram in Fig. 4.

Economics

The new configuration of a recycling plant based on the FAST Pb Process is more capital intensive than the conventional lead smelter equipped with desulphurization, rotary furnaces, and refinery kettles. The electrowinning cells themselves are not disproportionately expensive but the processes for the lead compounds leaching, the solution filtration, and purification units each require additional equipment.

However, the operational cost of the FAST Pb Process appears to be much better than conventional smelting and refinery, even when considering only the direct costs. Depending mainly upon the cost of the electric energy, the direct cost ranges between 240 and 280 Euro/ton of refined lead. The major cost savings are the labor and the logistics due to the continuous operation of the FAST versus the batch operations of conventional smelting.

While the direct cost for the operation of the health and environmental protection units has been included in the above specific cost, the fixed cost for the management of the lead fume bag houses and for the human health protection in the plant is incomparably lower for the FAST Pb Process than the cost for the conventional smelters.

Lastly, the image and respective community acceptance management are a cost for any smelter. Cleaner lead production through electrowinning is expected to be a welcome improvement by the neighbourhood as well as local and federal regulating agencies.

Conclusion

Even though lead is always considered a "dead man walking", its importance in the energy storage market is vital and it is not likely to lose standing in the future. Of course, the image and public opinion of lead impose the need for research into safer and more environmentally friendly production methods. Electrochemistry can provide a big hand in changing this opinion.

Engitec started to study lead electrochemical recovery decades ago and has investigated many different options to treat both primary and secondary lead sources. The FAST Pb Process for secondary sources is a unique and challenging electrochemical process. Extensive laboratory, pilot, and demo plant development operations have

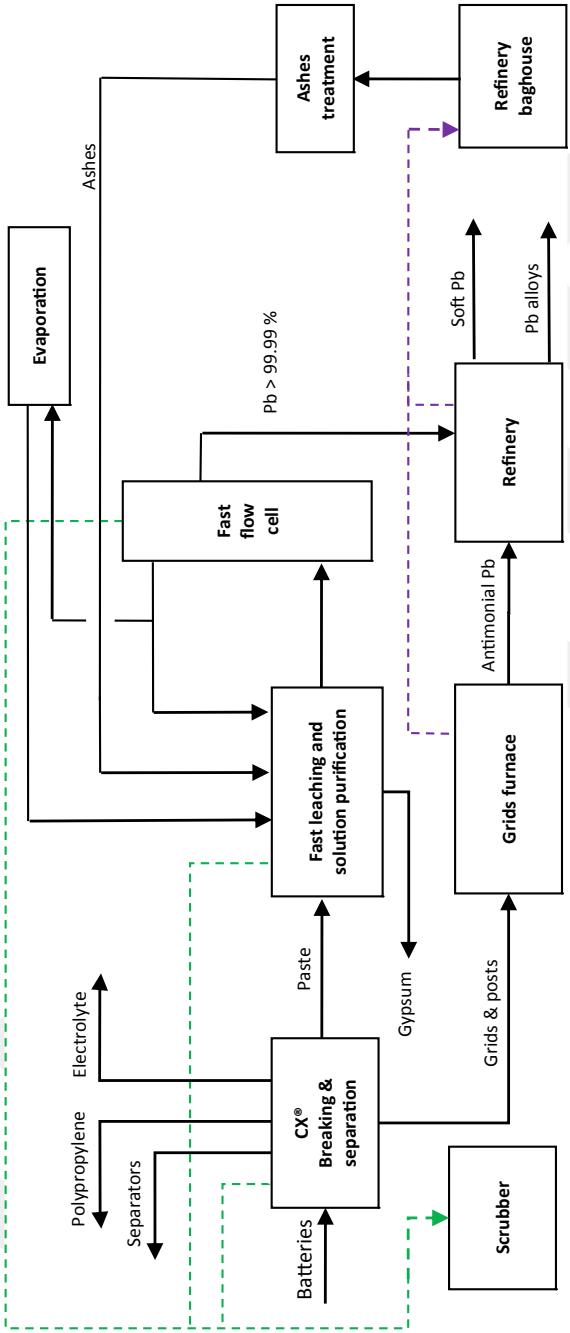

Fig. 4 CX® simplified process block diagram: possible simplification

allowed Engitec to study the system, collect the data, and reach the point of industrial plant design.

The lead acid battery was, is, and will long be the most important use of lead, the most important source for lead production, and the most important system for energy storage. The Engitec FAST Pb Process, as shown in this paper, will have a tremendous technical, economic, and environmental impact on the overall lead acid battery recycling process.

GCRIS

Recent Improvements at Hosokura Lead Smelter and Refinery

H. Nakano, S. Ito, S. Abe and N. Hasegawa

Abstract Hosokura Metal Mining Co., Ltd., operates as a secondary lead smelter and refinery, which produces about 30,000 tons of electric lead per year from waste lead-acid batteries and lead residue generated in copper smelters and refineries. Wastewater from the closed lead and zinc mines and tailing dams is also treated. Since 2017, our company has carried out a 10-year future plan, which focuses on themes such as safe working environment, compliance, and optimization of lead smelting and refining business. This paper reports on major topics about the plan, such as "Improvement of working environment around furnaces", "Treatment of wastewater containing fluorine at high concentration", "Rationalization of the closed mines monitoring", and "Improvements of separation work of waste lead-acid battery".

Keywords Fluorine wastewater treatment · Closed mine monitoring · Secondary lead smelting

Introduction

Hosokura mine had been operated as a lead and zinc mine for approximately 1200 years. Hosokura mine was closed in 1987 due to a great appreciation in the yen and a remarkable rise in personnel expenses. Hosokura Metal Mining Co., Ltd., has been operated as a lead smelter and refinery for 32 years. The company has important roles as the position for metal recovery such as lead, antimony, bismuth, gold, and silver from copper smelters and refineries of Mitsubishi Materials Group. Hosokura planed the next 10-year future plan in 2017. The plan focuses on themes such as safe working environment, compliance, and optimization of lead smelting and refining business.

H. Nakano (✉) · S. Ito · S. Abe · N. Hasegawa
Hosokura Metal Mining Co., Ltd., 48 Uguisuzawa-Nangouaramachi, 989-5402 Kurihara, Miyagi Pref., Japan
e-mail: hinakano@hosokura.co.jp

© The Minerals, Metals & Materials Society 2020

A. Siegmund et al. (eds.), *PbZn 2020: 9th International Symposium on Lead and Zinc Processing*, The Minerals, Metals & Materials Series,
https://doi.org/10.1007/978-3-030-37070-1_51

This paper reports major topics about the plan, such as “Improvement of working environment around furnaces”, “Rationalization of the closed mines monitoring”, “Treatment of high concentration fluorine wastewater”, and “Improvements of separation work of waste lead-acid battery”.

Process Description of Hosokura Smelter

The process flow for recycling spent lead-acid batteries in Hosokura smelter is shown in Fig. 1.

At first, the spent lead-acid batteries are collected to the pre-treatment plant and separated into three parts: electrolyte, grids and pastes, and plastic cases. The grids and pastes are then charged into a blast furnace with coke, fluxes, and iron scraps and reduced to bullion. Lead containing residues from copper smelters are also fed to the furnace in order to recover gold and silver as well as lead. The bullion is refined in kettles by copper drossing and Harris softening, and then molded into anodes. The anodes are transferred to the tank house equipped with 180 cells and finally electrorefined by Betts process.

Various by-products are produced from the anode slimes and the copper drosses. The anode slimes are charged into a short rotary furnace and reduced into black metal. The black metal is, then, transferred to a kettle and oxidized to burn-down metal with vaporizing of Sb_2O_3. The burn-down metal is transferred to a cupel and further oxidized to dore metal with top blown air. A Bi-rich phase is also recovered in cupellation and processed to metallic bismuth. Dore metal is finally treated in the anode furnace and molded into silver anodes. On the other hand, the copper-bearing drosses are smelted to recover lead and copper matte in another short rotary furnace. Both the silver anodes and the copper mattes are sent to a copper smelter equipped with a precious metal plant.

Improvement of Working Environment Around Furnaces

Problems in the Working Environment Around Furnaces

Working environment around the blast furnace and the short rotary furnaces used to be very dusty by lead fumes and dusts, and so the blood lead concentrations of the workers were risen. For this reason, it was necessary to improve the working environment around furnaces and to reduce the dust concentration in the air around furnaces.

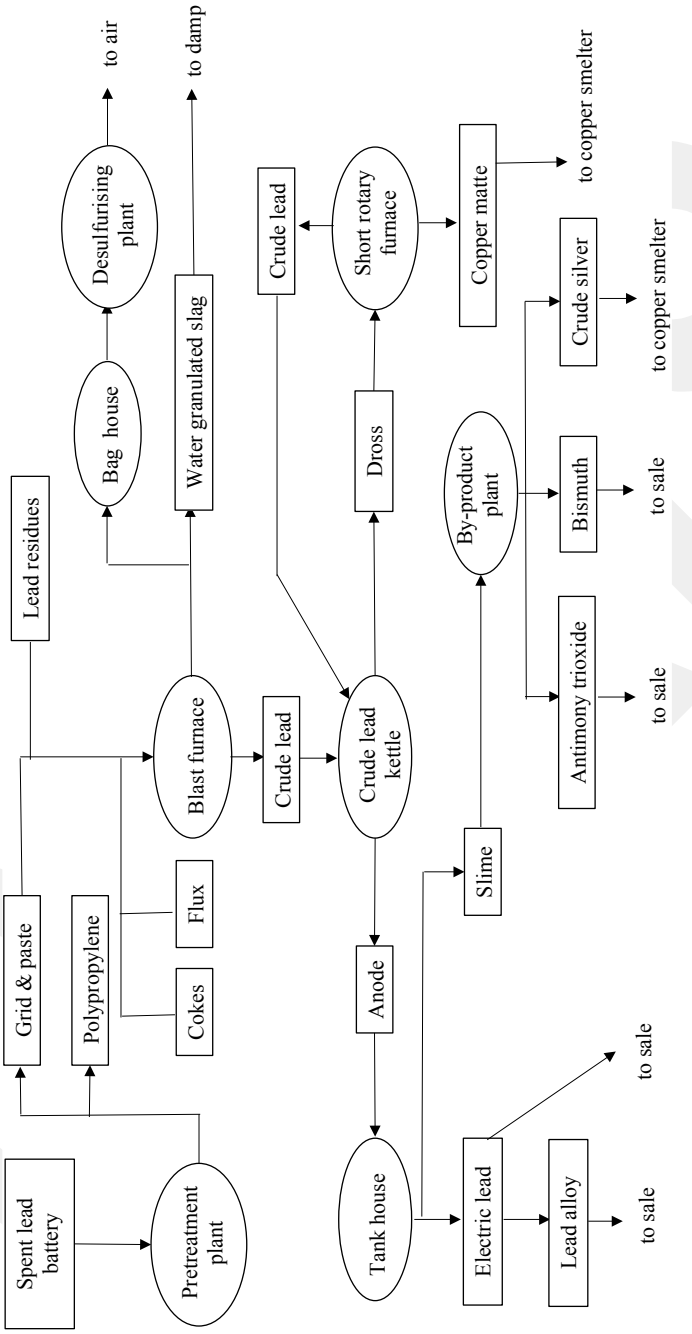

Fig. 1 Process flow of Hosokura smelter

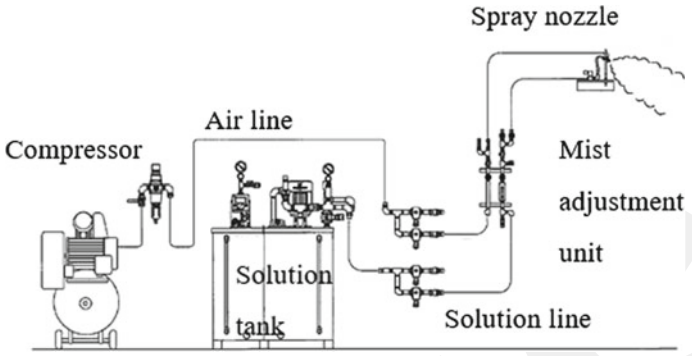

Fig. 2 Mist spraying system

Mist Spraying System Around Blast Furnace

Mist spray system was selected to collect fumes and dusts around the blast furnace. Foamed mist is sprayed around the blast furnace, and the suspended fumes and dusts are collected by the mist.

The system is shown in Fig. 2.

Spray solution and compressor air are sprayed through mist nozzles. Spray solution is a mixture of a chemical solution containing a surfactant and water. As the surfactant improves wettability of the dusts, the dusts can be collected efficiently with a small amount of water. And the floor around furnaces is kept dry.

Improvement of Hoods of Short Rotary Furnaces

Hoods over short rotary furnaces were improved as a countermeasure against leakage of fumes and dusts. On implementing relocation of the short rotary furnaces to a new plant, which is one of the items of the 10-year future plan, the hoods were newly designed and installed. The hood of short rotary furnace is shown in Fig. 3.

Each front area of the short rotary furnaces is completely covered with a hood to prevent from leakage of exhaust gas from the furnace. The shutter is opened only when the raw materials are charged and the products are discharged, and it is closed during blowing and holding periods.

Results

Owing to those countermeasures, the dust concentration in the working environment around the blast furnace and the rotary furnaces could be much reduced. In addition,

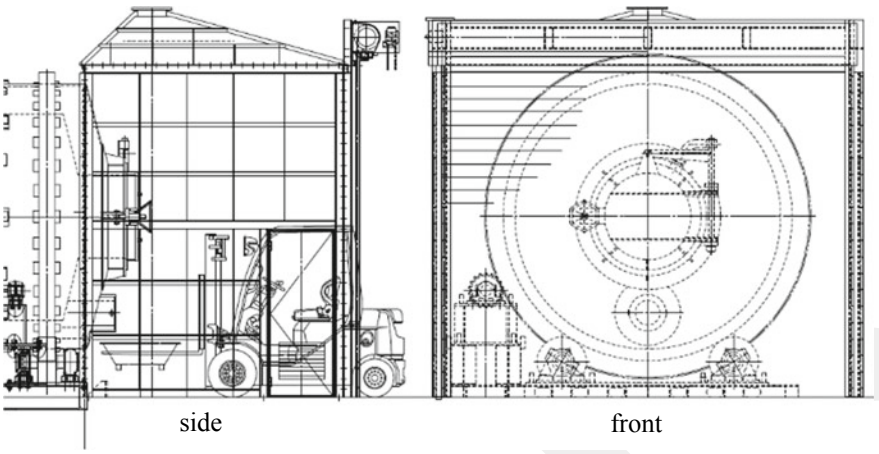

Fig. 3 Hood of short rotary furnace

the floor around the short rotary furnaces is kept much cleaner compared to the previous dusty environment. As a result, the blood lead concentrations of the workers are decreasing.

Treatment of Wastewater Containing Fluorine at High Concentration

Regulation of Fluorine in Hosokura Wastewater Treatment

Careful attention must be paid to the fluorine concentration in wastewater in Hosokura area. Japanese standard of fluorine concentration of effluent water discharged from the plant is 8 mg/L. But in Hosokura area, stricter regulation, 6 mg/L, is established by regional ordinance.

Wastewater Containing Fluorine at High Concentration in Lead Smelting

Figure 4 shows the process flow of the anode slime treatment. The anode slimes generated in the lead electrorefining process contain H_2SiF_6 (hydrofluorosilicic acid) as the electrolyte. The anode slimes are melted and reduced in a short rotary furnace, where H_2SiF_6 is decomposed. HF (hydrogen fluoride) is transferred to exhaust gas.

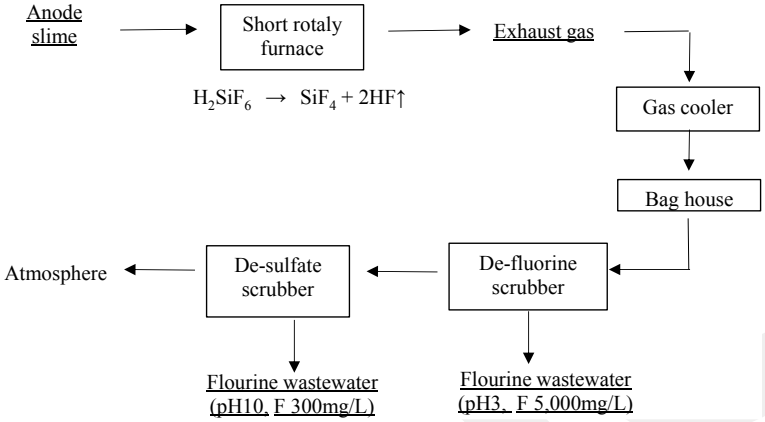

Fig. 4 Process flow of the anode slime treatment

The exhaust gas is washed in a water scrubber, and wastewater containing fluorine at high concentration (around 5000 mg/L) is generated.

Previous Treatment of Wastewater Containing Fluorine at High Concentration

The wastewater containing fluorine at high concentration is treated by using the following chemical reactions and coprecipitation method.

$$2HF + Ca(OH)_2 \rightarrow CaF_2 \downarrow + 2H_2O \quad (1)$$

$$nAl_3{}^+ + 3n(OH)^- + F^- \rightarrow (Al(OH)_3)_nF^- \downarrow \quad (2)$$

It is generally reported that in the calcium fluoride coprecipitation method (1), calcium hydroxide milk is added to fluorine wastewater, but the fluorine concentration of treated water cannot be reduced enough. Therefore, fluorine is further removed by using a hydroxide coprecipitation method (2) in which aluminum sulfate is added. Fluorine can be removed at lower concentration by agglomeration and precipitation with an aluminum salt [1].

In our company, wastewater was treated by the following process as shown in Fig. 5. The wastewater containing fluorine at high concentration was pretreated in lead smelter. Aluminum sulfate and calcium hydroxide milk were together added to the wastewater, and pH is adjusted at 7, in reaction tank for fluorine wastewater. The fluorine concentration of wastewater could be reduced to approximately 50 mg/L. Overflow of the tank was mixed with other wastewaters from lead smelter, and polymer flocculant was added in the thickener. The overflow of the thickener reduced

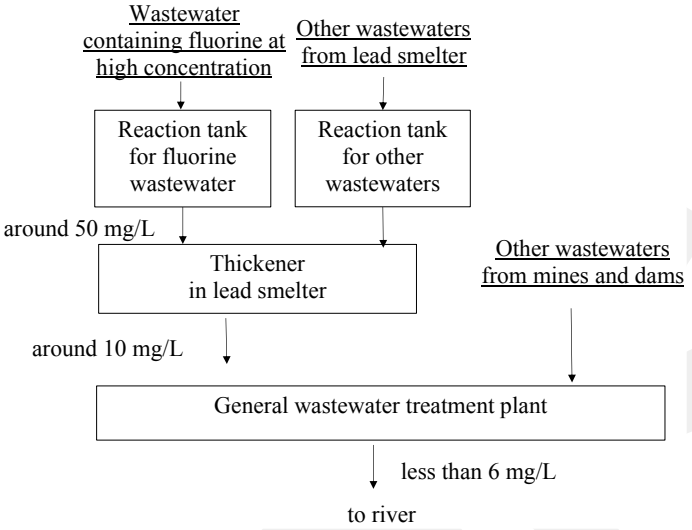

Fig. 5 Wastewater containing fluorine at high concentration treatment in Hosokura

lower than 10 mg/L. The wastewater passed general wastewater treatment plant and finally reduced to less than 6 mg/L of fluorine concentration. However, the fluorine concentration in effluent water was fluctuated and sometimes exceeded 4 mg/L.

Examination of Two-Stage Neutralization Treatment

In order to reduce the fluorine concentration, two-stage neutralization treatment was examined and was found to reduce fluorine sufficiently. Adopted chemical processes are similar to the previous one mentioned above, but in the new method neutralization is carried out in the two stages. The results in a laboratory test are shown in Fig. 6. The fluorine concentration can be reduced from 5000 mg/L to less than 1 mg/L by two-stage neutralization.

Introduction of Equipment

The flowchart of the treatment for the wastewater containing fluorine at high concentration is shown in Fig. 7. Aluminum sulfate and calcium hydroxide milk are added to the wastewater to adjust to pH 7. Next, polymer flocculant is added, and the suspended solids are condensed in a primary thickener (first-stage neutralization treatment). The primary thickener overflow is neutralized again, and the newly generated solids are separated in a secondary thickener (second-stage neutralization

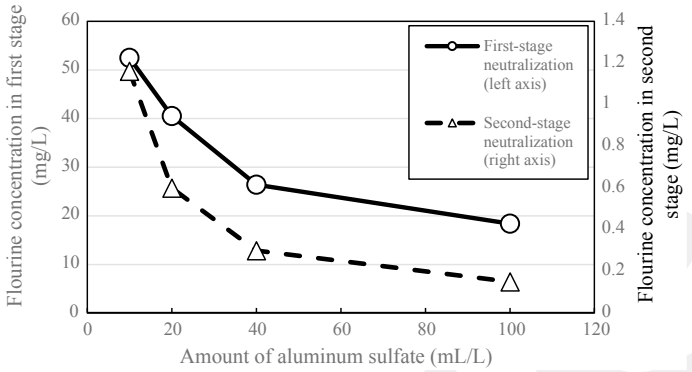

Fig. 6 Examination of two-stage neutralization treatment

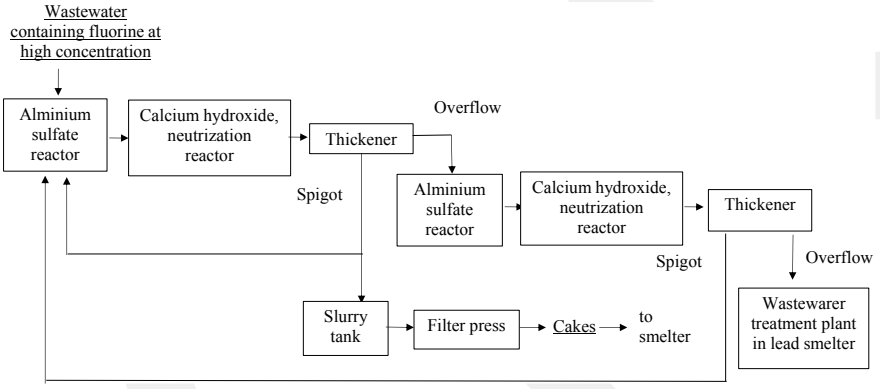

Fig. 7 Process flow for the high fluorine water

treatment). The spigots (sediment from under the thickener) of the primary and secondary thickeners are transferred to the primary neutralization tank to make use of the unreacted calcium hydroxides and also condense the spigots further. The condensed spigots are filtered by the filter press.

Results

By the two-stage of neutralization, fluorine concentration is decreased to less than 10 mg/L, and by the wastewater treatment in the smelter, the concentration is reduced to 3–4 mg/L. Now, fluorine concentration of effluent water discharged from the plant is very stable, 2–3 mg/L.

Rationalization of the Closed Dam Monitoring

Management of Hosokura Mines

Hosokura Metal Mining Co., Ltd., is responsible for the management of the closed mines and the closed dams where deposited lead slags and discharged tailings are piled. Previously, it was difficult to patrol several dams by two workers because they are wide in the mountains and far from the smelter. In particular, in case of emergency due to heavy rain, especially at night, the patrol was very difficult and dangerous, because the roads and ways are very slippery and sometimes closed by landslides.

For safer and easier patrol, installation of automatic monitoring camera system was considered. But the dams are located in the mountains, and the problem was to supply electric power at a low cost.

Remote Monitoring Camera System

Remote monitoring camera system is consisted of a solar panel, lead-acid battery, power controller, router, and network camera with night vision function. The system can be continuously monitored from PC and mobile terminals and has no electric power line. The lead-acid batteries have many advantages such as safe, stable performance, low cost, and established recycling technology. The lithium ion batteries have a risk of ignition in the mountain and are expensive.

Results

Now, it is possible to monitor the closed dams from operator's mobile terminals and increase the frequency of monitoring, from once to three times per day. With the new monitoring system, it is no longer necessary to go to the dams for monitoring in heavy rain, and the risk of patrol could be much reduced. The company has increased the number of remote monitoring camera systems, totally four.

Improvements of Separation Work of Waste Lead-Acid Battery

Problem

The company treats used lead-acid batteries from automobiles as raw materials for lead smelting. These batteries are manually separated into three parts: electrolyte, grids and pastes, and plastic cases, in the pre-treatment plant. The work of the battery separation was interrupted frequently by several reasons and becomes the production limiting step in the smelter.

Analysis Results and Countermeasures

Video cameras were set at the pre-treatment plant. By analyzing the video data of the work, the longest waiting time was found to be the line workers waiting time for the transportation of batteries from storage, about one hour. As line workers and batteries transport workers started the work at the same time, line workers had to wait for a long time until batteries were on the line. So start time of batteries transportation work was changed 20–30 min earlier than before.

The next longest waiting time was the stoppage of the line in order to remove garbage such as the packing materials of batteries. As a countermeasure, the manual garbage removal facility was installed. And the batteries with a lot of garbage are pretreated by the new facility before put into the line.

Results

As a result of these improvements, the amount of throughput per unit man-hour increased by 20%. The work is now not the production limiting step.

Conclusion

This paper reports on “Improvement of working environment around furnaces”, “Treatment of high concentration fluorine wastewater”, “Rationalization of the closed dam monitoring”, and “Improvements of separation work of waste lead-acid battery”. These are the important topics of the improvements of the next future 10-year plan. Hosokura Metal Mine Co., Ltd., will continue to improve safety of workers, environment, and stable operation and profits.

Reference

1. Yokoyama et al (2016) New pollution prevention technology and regulations 2016 water quality technology. Japan Environmental Management Association for Industry, Japan, pp 254–258

GCRIS

Refractory Corrosion Comparison Through a Rotary Drum Furnace Slag Test for the Lead Industry

D. Fonseca, A. Spanring, F. Elias and G. Gonçalves

Abstract RHI Magnesita performs a variety of corrosion tests to simulate the operating conditions in lead smelters and compare the performance of different refractories. In this study, six refractory grades were submitted to corrosion tests in a rotary drum furnace using six Fe_2O_3–SiO_2–CaO synthetic slags with varying contents of sodium carbonate or anhydrous borax. This study aims to gather information about the relationship between different sodium levels in the slag and the corrosion resistance of bricks used in the lead industry. The rebonded magnesia-chromite grade showed the highest overall wear resistance. High sodium content in the slag ($\geq$20% $NaCO_3$ or $Na_2B_4O_7$) favored the corrosion of the alumina-chromia brick, while low sodium content led to higher corrosion of the direct-bonded magnesia-chromite grades due to increased amounts of CaO and SiO_2 in the slag. The results obtained in this study can be used to recommend refractory grades based on the slag chemical analysis.

Keywords Refractory corrosion · Slag test · Wear mechanism

Introduction

In 1995, the global secondary lead production surpassed primary lead production, accounting for 52.6% of the total metal production worldwide. The total lead production has doubled since 1995, reaching 11.6 million tons in 2017, 58% of which corresponds to secondary lead [1]. Currently, more than 80% of smelted North American lead and over 60% of the lead produced in Europe comes from secondary sources

D. Fonseca (✉)
RHI Magnesita, TC Leoben, Magnesitstrasse 2, Leoben, Austria
e-mail: daniela.fonseca@rhimagnesita.com

A. Spanring
RHI Magnesita, Kranichberggasse 6, 1120 Vienna, Austria

F. Elias · G. Gonçalves
RHI Magnesita, Praça Louis Ensch, Contagem 240, Brazil

© The Minerals, Metals & Materials Society 2020

A. Siegmund et al. (eds.), *PbZn 2020: 9th International Symposium on Lead and Zinc Processing*, The Minerals, Metals & Materials Series,
https://doi.org/10.1007/978-3-030-37070-1_52

[1, 2]. Reasons for this are that most lead is used in easily recyclable and economically viable applications, such as lead-acid batteries, and the energy consumption is almost 50% lower compared to primary production [3].

Short rotary furnaces (SRF) used for secondary lead production are highly versatile and have become popular in Europe. These kilns can perform similar functions compared to the blast furnace, however with higher flexibility due to the possibility of handling fine material. Its main disadvantage is the short life of the refractory lining [4].

Common fluxes used in rotary furnace smelting are shredded iron scrap or steel turnings and sodium carbonate (soda ash). A high sodium slag is used in many cases due to its low melting point and low viscosity, promoting good separation of slag and bullion [4]. In addition, the amount of volatilized lead could be reduced by operating at lower temperatures, and sulfur can be easily captured into the slag through the formation of sodium sulfide:

$$PbSO_4 + 4CO \rightarrow PbS + 4CO_2 \quad (1)$$

$$PbS + CO + Na_2CO_3 \rightarrow Pb + Na_2S + 2CO_2 \quad (2)$$

$$CO_2 + C \rightarrow 2CO \quad (3)$$

Owing to the increased fuel consumption (Eq. 3) and the high cost of soda ash, a higher proportion of iron in the flux material is commonly employed [4]. In addition, restrictive environmental legislations hamper the disposal of high soda slags due to their high toxic compound content. Thus, new slags based on low soda and increased calcium and silica contents are being adopted [3].

In the case of lead-acid battery recycling, SRF are typically used. The refractories in the furnace lining suffer severe wear, and the service life generally varies between 12 and 14 months, depending on the operation process and thickness of the working lining [3]. Magnesia-chromite bricks (60–80% MgO) are the preferred choice for the furnace lining due to their high resistance to extreme chemical attack. However, the use of alternative CaO-rich slags accelerates refractory wear and significantly reduces lining lifetime of magnesia-chromite bricks [3, 5].

The present study attempts to simulate the SRF environment in a laboratory scale rotary drum furnace and provides a comparison of the slag wear resistance of six different refractory grades. The main goal is to deepen the knowledge of the wear phenomena of refractories exposed to different slag chemistries employed in secondary lead production. This would allow refractory producers to provide optimal brick lining solutions based on the slag chemistry of each furnace.

Methods

Six refractory corrosion resistance tests were performed in a laboratory scale rotary drum furnace (Fig. 1) using synthetic lead-free slags. The base slag composition was kept constant (26% SiO_2, 57% Fe_2O_3, 12% CaO, 5% Al_2O_3) and different amounts of sodium carbonate (Na_2CO_3) or anhydrous sodium tetraborate ($Na_2B_4O_7$), commonly used as flux agents, were added to the slag in each corrosion test (Table 1). The amount of Na in each slag was calculated based on the molar masses of Na_2CO_3 and $Na_2B_4O_7$ and is shown in the last line of Table 1. Although the lead-bearing components usually present in the slag clearly affect refractory corrosion, this study was mainly focused on the effect of CaO, SiO_2, and Na_2O.

The rotary drum furnace used in this study had an inner diameter of 265 mm and length of 150 mm. The lining of the furnace was composed of six refractory bricks cut in trapezoidal prism shaped specimens size 90 × 50 × 60—115 mm. One sample of each refractory grade (Table 2) was used in each test.

Fig. 1 Rotary drum furnace used in the refractory corrosion tests

Table 1 Chemical composition of the slags used in the rotary drum furnace slag tests

wt%/Test #	1	2	3	4	5	6
SiO_2	25	23	21	18	23	18
$Fe_2O_3^a$	54	51	46	40	51	40
CaO	11	11	10	8	11	8
Al_2O_3	5	5	4	4	5	4
Na_2CO_3	5	10	20	30	–	–
$Na_2B_4O_7$	–	–	–	–	10	30
Total Na	2.2	4.3	8.6	12.9	2.3	6.9

[a]Total iron calculated as Fe_2O_3

Table 2 Refractory grades used in the rotary drum furnace slag tests

Abbreviation	Description	Main oxides
A	Alumina-chromia product type ACr80/10 ISO 10081-4	91% Al_2O_3, 9% Cr_2O_3
DB	Magnesia-chromite product type MCr60 ISO 10081-2, direct bonded (sintered grains)	67% MgO, 18% Cr_2O_3
DBP	Magnesia-chromite product type MCr60 ISO 10081-2, direct bonded, premium	65% MgO, 20% Cr_2O_3
DBL	Magnesia-chromite product type MCr60 ISO 10081-2, direct bonded, low permeability	68% MgO, 17% Cr_2O_3
DB7	Magnesia-chromite product type MCr70 ISO 10081-2, direct bonded	72% MgO, 14% Cr_2O_3
R	Magnesia-chromite product type MCr60 ISO 10081-2, rebonded (pre-reacted grains)	61% MgO, 22% Cr_2O_3

The slag tests were performed at approximately 1710 °C for 3 h, with slag renewal every 30 min. The test temperature was significantly above the operating temperature of lead furnaces (generally up to 1300 °C maximum) in order to accelerate the corrosion of the refractory specimens. The corrosion resistance of the refractory grades was compared by measuring the difference in the thickness of each specimen before and after the tests (wear %). Refractory grades A and DB (one magnesia-chromite and one alumina-chromia grade) were chosen to be analyzed through optical microscopy after the slag tests 4 and 6. In addition, the polished sections corresponding to refractory A used in test 4 and DB used in test 6 were analyzed through scanning electron microscopy (SEM).

Results and Discussion

The results from each corrosion test are shown in Table 3 and illustrated in the diagram in Fig. 2. Figure 3 shows the visual aspect of the specimens (cross section) after test 4. Due to the high number of refractory grades (6) and slags (6) tested in

Table 3 Results of the slag corrosion tests performed in the rotary drum furnace (wear %)

Test #	A	DB	DBP	DBL	DB7	R
1	2.66	4.87	4.58	5.69	4.63	2.65
2	2.84	1.82	2.91	4.16	3.80	1.35
3	4.52	2.73	3.48	2.82	2.87	2.12
4	4.63	3.75	2.95	2.67	2.86	3.11
5	2.15	3.90	2.96	3.36	3.81	2.07
6	2.85	2.63	2.37	1.72	2.53	0.97

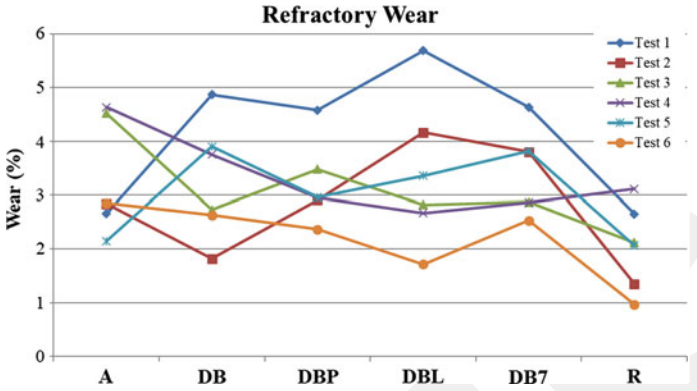

Fig. 2 Comparison of the wear of each specimen used in the rotary drum furnace slag tests

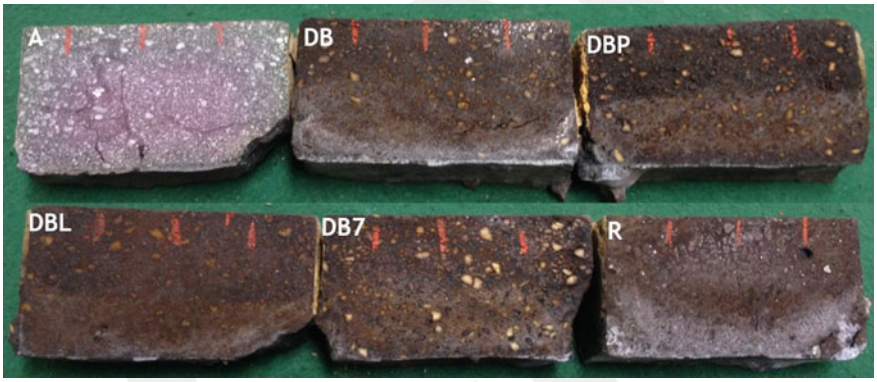

Fig. 3 Cross section of the refractory specimens used in test 4

this study, each brick was tested with each slag composition only once. The most relevant tests should be repeated for more representative findings.

The slag test results suggest that brick R is the most resistant to refractory wear when in contact with the slags used in tests 1, 2, 3, 5, and 6. The slag used in test 4 had the highest amount of sodium, and all magnesia-chromite bricks, except for DB, showed similar wear in this test. DBL and DB7 showed similar wear resistance compared to brick DB in all tests, except for test 2. This suggests that low permeability and higher MgO content did not significantly affect the brick's corrosion resistance in this study. When comparing tests 1 and 5, with similar Na contents in the slag, test 1 showed overall higher wear, which suggests that slags containing sodium tetraborate are slightly less aggressive to the refractories than slags containing soda ash. This might be related to the increased viscosity of the liquid phases formed in the systems containing boron. Thermodynamic calculations using Factsage^{TM} have shown that 7% B_2O_3 addition to slag 1 can lead to a 30% increase in its viscosity at 1710 °C. The

magnesia-chromite specimens showed the highest wear in tests 1, 2, and 5, probably due to the higher amount of CaO and SiO_2 in these slags. In addition, DBP presented the highest resistance among the direct-bonded bricks in tests 1 and 5, most likely due to its higher Cr_2O_3 content.

Brick A showed lower wear resistance to slags with relatively high Na content (tests 3 and 4 and 6) and higher resistance in tests 1, 2, and 5 compared to the direct-bonded bricks. This suggests that sodium plays an important role in the corrosion mechanism of non-basic bricks under these test conditions.

Apart from A and DB, the specimens showed the lowest overall wear during test 6, probably because this slag had the highest viscosity. The optical microscopy images of bricks A and DB after tests 4 (30% Na_2CO_3) and 6 (30% $Na_2B_4O_7$) were compared and are shown in Figs. 4 and 5, respectively. These specimens were chosen for microscopical analysis because they showed the highest wear in the tests with the highest flux content (4 and 6).

There was significant slag infiltration in the microstructure of brick A in both tests; however, the corundum grains have apparently resisted well to slag attack. A

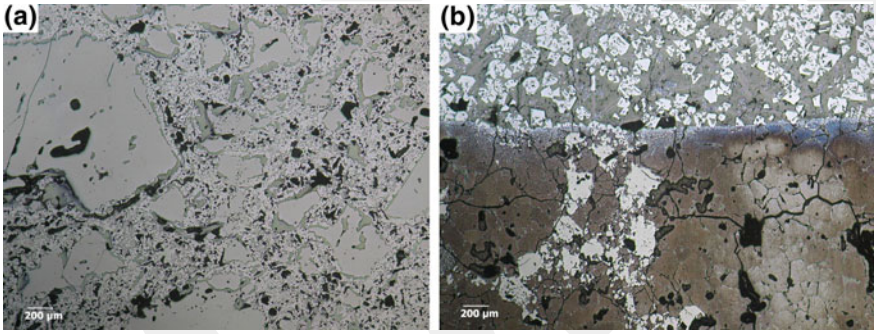

Fig. 4 Optical microscopy images of the hot face of the specimens after slag test 4. **a** Brick A; **b** Brick DB

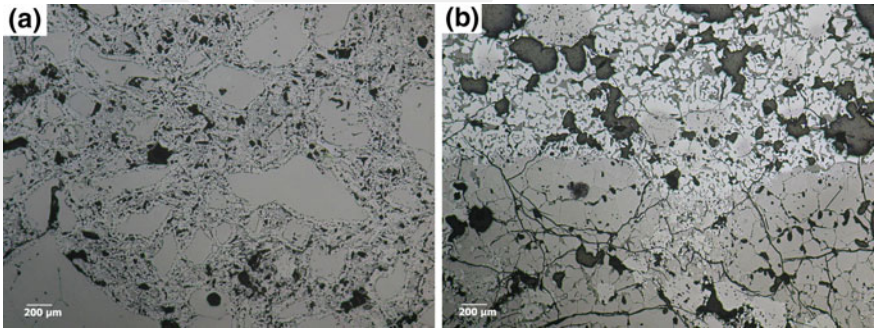

Fig. 5 Optical microscopy images of the hot face of the specimens after slag test 6. **a** Brick A; **b** Brick DB

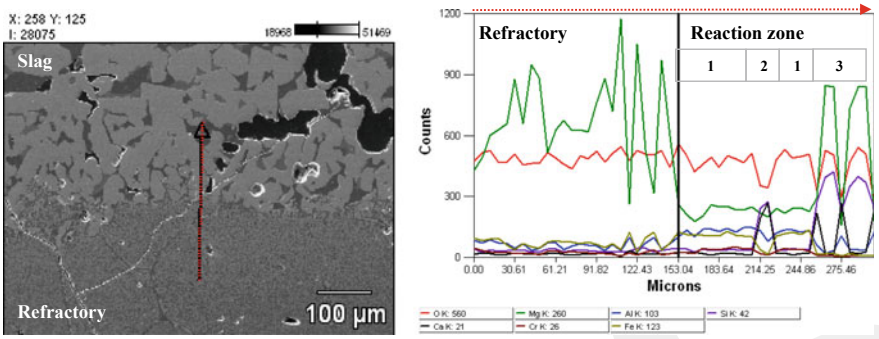

Fig. 6 Slag-refractory interface composition of brick DB after test 6 analyzed by SEM with coupled EDS. Possible phases: 1: Mg–Al–Fe spinel; 2: Monticellite/Merwinite; 3: Forsterite

layer of Al_2O_3–Cr_2O_3 solid solution was detected surrounding the corundum grains, which could have protected them against corrosion. SEM confirmed the presence of a liquid phase resulting from the reaction of the brick's matrix with Na, Si, and Ca oxides present in the slag. The slag components reacted preferentially with pure alumina as opposed to alumina-chrome solid solution.

The DB specimen was not significantly infiltrated with slag after test 4: A well-defined line is shown in Fig. 5b separating the reaction zone from the refractory. However, the brick's microstructure presented several cracks after both tests. During test 6, the slag infiltrated in the brick to a certain extent. The MgO in the refractory dissolved into the slag and formed a liquid phase surrounding the solid parts consisted in Ca, Si, and Mg oxides, with small amounts of Na_2O. Chromite rims were enriched in iron oxide. The slag-refractory interface analyzed by SEM is shown in Fig. 6. The corrosion of the magnesia-chromite grades in this test was mainly through the reaction of the MgO component with the CaO and SiO_2 in the slag under formation of Ca–Mg-silicates and forsterite. Chromite was not corroded; however, its chemical composition was modified due to the diffusion of iron oxides.

Conclusion

In general, slags containing Na_2CO_3 lead to higher refractory wear than slags containing $Na_2B_4O_7$, probably due to the higher viscosity of the latter. In non-basic refractories, the corrosion happened through the formation of a liquid phase containing Na, Al, Si, and Ca oxides. An alumina-chrome solid solution detected around the coarse alumina grains potentially protected them against slag corrosion. The slag corrosion of magnesia-chromite refractories involved mainly the reaction of MgO with CaO and SiO_2 present in the slag, resulting in forsterite and Ca–Mg-silicates formation. The high Na content in the slag was more detrimental to the non-basic brick grade than to the magnesia-chromite grades, due to the significant participation

of sodium in this brick's corrosion mechanism, while the higher amounts of CaO and SiO_2 in slags with lower Na content were more harmful to the basic bricks. The rebonded magnesia-chromite grade showed the highest overall wear resistance. The interaction between the refractory and lead-containing compounds is an additional aspect to be considered when applying the findings of this study to the refractory lining optimization in secondary lead production.

References

1. Data from the International Lead and Zinc Study Group: www.ilzsg.org
2. Schriner D, Taylor P, Grogan J (2016) A review of slag chemistry in lead recycling. In: Lead & Zinc '05. Proceedings of the 10th international conference on molten slags, fluxes and salts 22–25 May, Washington, USA, 2016
3. Spanring A (2010) Refractory applications in the secondary lead industry. RHI Bull 1:56–62
4. Sinclair RJ (2009) Extractive metallurgy of lead. The Australasian Institute of Mining and Metallurgy (The AusIMM)
5. Gregurek D, Reinharter K, Majcenovic C, Wenzl C, Spanring A (2015) Overview of wear phenomena in lead processing furnaces. J Eur Ceram Soc 35:1683–1698

GCRIS

Part XIV
Lead and Zinc Sustainability and Social License: Plenary Session

GCRIS

Regional Changes in Refined Zinc Output and Demand

Claire Hassall

Abstract Global refined zinc output has grown from 8.9 Mt in 2000 to around 11.8 Mt in 2019, an increase of almost 3 Mt. Only 530 kt of this increase occurred outside China, while China's output rose by over 2.4 Mt. The major expansion in China's refined zinc production capacity took place in the ten years to 2010, with some further moderate increase to 2016, but there has been a net decrease in capacity since then. Refined zinc usage globally grew from 8.9 Mt in 2000 to 12.2 Mt in 2019, an increase of 3.3 Mt, but China accounted for more than this total rise, effectively taking away zinc demand from the rest of world. However, China's share of global zinc demand is now changing as its economy matures and, in the last 3 years, China's demand for zinc has stagnated at best, and in some years has fallen significantly. Higher costs, more extensive and better enforced environmental regulations, and the effect of trade disputes have seen China's manufacturing industry more constrained, with some Chinese manufacturing companies now basing activities off-shore, and with other countries now better able to compete in world markets than in the initial 10–15 years after China's entry into the WTO at the end of 2002. The last nine years have seen 13 zinc smelters outside China close, with the loss of close to 1 Mt of annual capacity. The last greenfield zinc smelter ex-China was commissioned in 2010, and capacity expansions have taken place at a number of plants, notably in South Korea, Mexico, India, and Norway, compensating for capacity losses, but not adding to capacity overall. The next five years are expected to see growth in refined zinc demand concentrated in countries other than China, with South-Eastern and South Asian countries leading the way. This raises the question of where and how the additional requirement for refined zinc will be met and whether China will play any role in supplying zinc to these expanding markets. This presentation will provide an analysis of recent regional changes in zinc demand and supply as outlined above and examine the prospects for future zinc demand and the potential sources of additional refined zinc output globally.

Keywords Refined zinc demand · Refined zinc production · Chinese zinc market

C. Hassall (✉)
CHR Metals Limited, 11 Church Street, Godalming GU7 1EQ, UK
e-mail: claire.hassall@chrmetals.com

© The Minerals, Metals & Materials Society 2020

A. Siegmund et al. (eds.), *PbZn 2020: 9th International Symposium on Lead and Zinc Processing*, The Minerals, Metals & Materials Series,
https://doi.org/10.1007/978-3-030-37070-1_53

Regional Changes in Refined Zinc Output and Demand

The global zinc market has been in deficit since 2012, drawing down inventories from the high levels accumulated after the global financial crisis of 2008/2009 when both China and the world excluding China saw substantial annual refined zinc market surpluses. Refined zinc usage globally grew from 8.9 Mt in 2000 to 12.2 Mt in 2019, an increase of 3.3 Mt, but China accounted for more than this total rise, effectively taking away zinc demand from the rest of world. While growth in Chinese demand supported strong annual average global demand growth through to 2015, more recently structural changes in Chinese zinc demand and the geographic distribution of demand growth have led to a recovery in zinc consumption in the world outside China (Fig. 1).

Annual global zinc usage fell by an estimated 1.5–2%—200 kt) between 2015 and 2018 entirely because of a significant downturn in Chinese zinc consumption. The decline in Chinese usage is structural, but unsurprising, reflecting the maturity now of the economy. Growth in other Asian countries is a reflection of increased manufacturing competitiveness vis-à-vis China, and growing investment in infrastructure. China's share of global zinc demand, therefore, is changing with this increasing economic maturity and, in the last three years, consumption of zinc in China has stagnated at best, and in some years has fallen significantly. Higher costs, more extensive and better enforced environmental regulations, and the effect of trade disputes have constrained the profitability of China's domestic manufacturing industry, with some Chinese companies now basing their manufacturing activities off-shore. With these changes inside China, other countries are now better able to compete in world markets than was the case in the initial 10–15 years after China's entry into the WTO at the end of 2002. Furthermore, the impact of China's intense focus on fixed asset investment since 2002, if not before, particularly in relation to the development

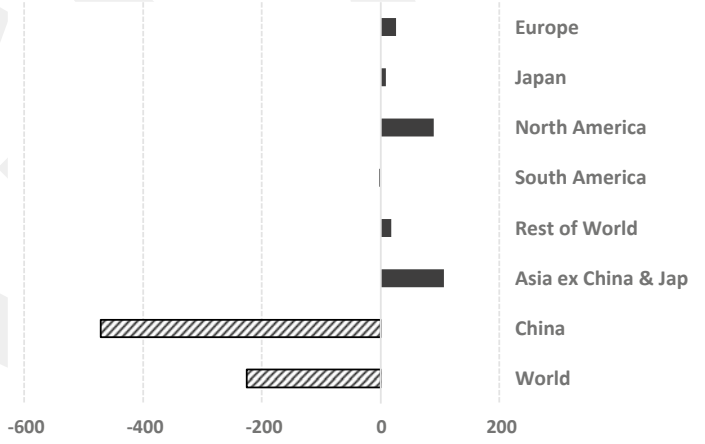

Fig. 1 Change in regional zinc demand: Difference between 2015 and 2018 ('000s tonnes)

of extensive and world-class infrastructure in the transport, communications, and power transmission networks, was a major factor in the rapid increase observed in zinc demand. Rising exports of semi-manufactured and manufactured goods after its accession to the WTO also boosted China's zinc demand. China now possesses extensive modern infrastructure and, though investment continues, net annual additions to road, rail, and power distributions networks are on a declining trend.

Also significant in the overall reduction in zinc demand globally since 2015 has been the impact of subdued economic activity, especially as measured by industrial production, in the OECD, in spite of low interest rates and, at times, extensive monetary easing (quantitative easing) which has generally not been matched by government fiscal stimulus. Very accommodative monetary policy has played a part in high commodity prices, including zinc, which has encouraged efforts to find lower cost substitutes and to reduce per unit usage. However, growth of demand in recent years in North America has been boosted by the impact of tax cuts in the USA, while increased consumption in a number of Asian countries has been supported by increased infrastructure spending, in which China's Belt and Road initiative (BRI) has played a part in funding.

With a global business cycle trough experienced in 2018/2019, some upturn in activity from 2020 is expected with South and South East Asia likely to be major growth areas. Europe overall is also forecast to benefit as Turkey is expected to register continuing robust economic growth in the medium to longer-term, barring any disruptive geopolitical developments. Some recovery in Chinese demand is possible but not to previous peak levels seen in 2015 and 2016. However, disputes over trade (the so-called Trump tariffs) could lead to a move away from China as a supplier to the USA, in favour of countries such as Vietnam. At present, with the outcome of Chinese/USA trade negotiations uncertain, there remains considerable downside risk to trade and the global economy in the event that the trade war escalates (Fig. 2).

These changes in the growth of regional demand raise questions as to where the incremental requirement for refined zinc will be produced in the future. Global zinc

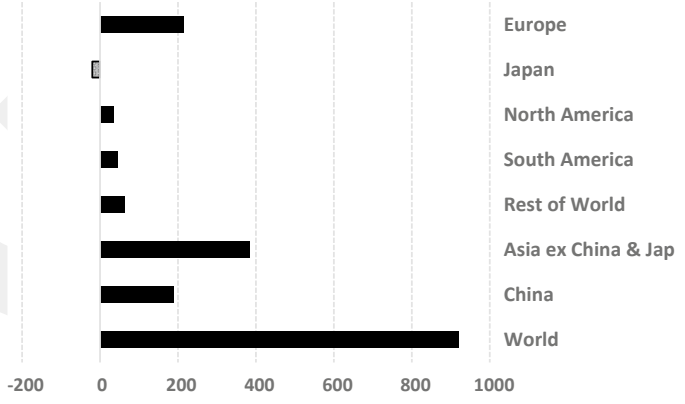

Fig. 2 Forecast change in regional zinc demand: Difference between 2018 and 2023 ('000s tonnes)

demand in 2018 was ~3.3 Mt higher than it was in 2000, but all of this growth took place in China, with Chinese demand 3.4 Mt higher in 2018 than in 2000.

Global refined zinc output grew from 8.9 Mt/year in 2000 to around 11.8 Mt in 2019, an increase of almost 3 Mt in annual production between these two years. However, only 530 kt of this rise occurred outside China, while China's output increased by over 2.4 Mt, the additional requirement for zinc in China being met by rising imports from the rest of the world. Indeed, up to 2007, China was at times a net exporter of refined zinc to the rest of the world but, since the cancellation of value-added tax (VAT) rebates on exports of special high grade (SHG) zinc in August 2008, China has been a net refined zinc importer of an average of 500 kt/a since 2009, peaking at net imports of over 700 kt in 2018.

The major expansion in China's refined zinc production capacity took place in the ten years to 2010, with some further moderate increase to 2016, but there has been a net decrease in capacity since then. Refined zinc output in China grew by ~138% between 2000 and 2010, was roughly stable through to 2017 but then fell by 7% in 2018. Processing and transportation of zinc smelting residues, largely from leaching, have been a focus of environmental authorities for some years, with some variation between provinces a feature. For example, there have been some restrictions imposed on shipping residues between provinces for treatment and there is now a need for treatment facilities to be properly licensed. But the widespread enforcement of regulations intensified in 2018 and a number of zinc smelters were significantly impacted, e.g. Hanzhong (360 kt/a refined zinc capacity) in Shaanxi and Luoping (120 kt/a) in Yunnan. Not all smelters coming under increased environmental scrutiny had to cut output, e.g. Laibin (60 kt/a) in Guangxi. And not all production losses in 2018 were associated solely with tighter environmental regulation and enforcement on smelting. Some production was lost in Hunan Province with environmental upgrades undertaken at the smelters, but principally because of the prolonged closure of local mines as major consolidation and re-organisation were undertaken, against the background of tighter regulation of health, safety, and environmental standards in mining nationally. There was a rundown of output at the Zhuzhou smelter prior to its move to a new site as the original smelter had, as the city expanded, come within the city limits and was no longer permitted to operate in such a location. Generally, across China, some shortage of raw materials for smelting may have played a minor role in early 2018 in lower output, but environmental regulation was the main reason for lower Chinese output in 2018.

In 2019, there has been a recovery in refined output in China, mainly as smelters affected in 2018 were able to resume normal operations having satisfied the need to assure compliant treatment of smelting residues, in effect largely by installing residue treatment facilities at their own plants. However, smelting residues are just one facet of tighter environmental requirements. The Chinese industry is now subject to much more stringent emissions standards which are now closely monitored and enforced. At times, lengthy shutdowns have been required, while remedial systems and measures are put in place and official approval obtained. In H1 2019, for instance, a 100 kt/a smelter in Gansu experienced an SO_2 leak on one of its two lines due to a fan failure, but the whole operation remained closed for the balance of the year.

Bearing in mind the outlook for development of refined zinc demand regionally, it is noteworthy that the last nine years have seen 13 zinc smelters outside China close, with the loss of close to 1 Mt of capacity. The last greenfield zinc smelter outside China was commissioned in 2010, but capacity expansions have taken place at a number of plants, notably in South Korea, Mexico, India, and Norway, compensating for capacity losses since 2010, but not adding to capacity overall. Over the next five years, there are some further expansions of smelting capacity planned and already in the process of ramping up to higher output, namely in India, Australia, Norway, Mexico, Poland, and Japan. There are also two greenfield projects, namely at AZR Mooresboro in the USA where commissioning of the new operation, now anticipated for early 2020, has been subject to a number of delays but which represents replacement capacity for a plant closed in 2014 and a new multi-metal smelting complex in Saudi Arabia being constructed in a joint venture between Trafigura and Modern Mining Holdings, though as yet no exact timing for the start-up this project has been announced. These projects have the ability to raise annual refined zinc production outside China from 7.5 Mt in 2018 to 8.3 Mt by 2023, a net increase of 0.8 Mt.

While refined zinc production capacity outside China appears, on the surface, sufficient to meet anticipated demand growth outside China, this assumes output is at full capacity at all zinc smelters and that there are no further closures of zinc smelting capacity. The first assumption is clearly unrealistic and the second assumption cannot be fully relied upon. It also does not take into account the fact that current refined zinc inventories outside China are at historically low levels in relation to demand, a factor that may not matter, while the global economy is experiencing a cyclical business downturn but may become a major issue when refined zinc demand starts to pick up more significantly from 2020/2021. And, most importantly, it takes no account of the fact that both the global, and the world excluding China, markets were in substantial deficit in 2018. Indeed, following four years of large refined zinc annual surpluses from 2008, these markets moved into supply deficits in 2012 and have been in deficit every year since 2012, leaving inventories now at historically low levels. In other words, this means that some of the demand for zinc in each year since 2012 has been met from inventory.

Therefore, in addition to the 0.8 Mt increase in annual zinc smelting capacity outside China expected by 2023, a further 0.3–0.5 Mt of new annual capacity will be needed to meet anticipated increases in demand. Stringent environmental policies, coupled with local objections, make expanding capacity in many OECD locations (e.g. Europe, North America, and Japan) more costly and may not be economically viable. However, there are a number of locations where new capacity is being evaluated (e.g. at Gamsberg in South Africa) and we would expect to see further new capacity perhaps also being considered in the Middle East, Central Asia, and India. But there remains the question of how soon any such new projects, particularly greenfield plants, could be commissioned.

One feature which may ease anticipated pressure on refined zinc supplies outside China over the next 2–3 years would be a decline in Chinese imports of refined zinc from the rest of the world. We have discussed reasons to expect only very modest

growth in Chinese zinc demand earlier in this paper but, though there are zinc smelting projects on the drawing board in China at present, these may be subject to delays or cancellation, and further closure of existing smelting capacity cannot be ruled out. This means that there is significant potential for Chinese refined zinc imports to be little changed from recent average levels over the next 4–5 years.

Chinese zinc producers are not an integrated part of the supply network for manufacturers using zinc in the rest of the world, thereby reducing supplier choice for these non-Chinese first-use consumers. There are, to the very best of our knowledge, no long-term supply contracts between Chinese refined zinc producers and zinc consumers outside China. The Chinese zinc market is effectively ring-fenced by the imposition of VAT on exports, which makes exporting zinc commercially non-viable for Chinese producers, unless LME zinc trades at a significant premium (~ + 13%) to Chinese domestic prices. This means that, at times when the Chinese zinc market is in surplus and/or the LME price is less than 13% higher than the domestic price, the option to export zinc to the rest of the world is effectively closed. China imports a certain amount of zinc to meet domestic demand, but further imports may be made for purely financial reasons related to the differential between domestic prices and LME prices plus regional premia. These differences at times may simply reflect market (speculative) sentiment, with little grounding in supply/demand fundamentals.

However, this does not imply that Chinese-produced zinc does not leave China. Indeed the opposite is true but the exports take place as zinc used in semi-manufactured and manufactured goods, such as a multitude of zinc diecastings (the majority as parts in other final manufactured goods), galvanized sheet, and other galvanized steel products, a very important factor in reducing zinc demand outside China since the early 2000s. With slowing of fixed asset investment in China, including infrastructure build, and a loss of competitiveness to other countries for many manufactured goods, Chinese industry has begun to move its production offshore to lower cost locations such as Vietnam, while the Chinese government, through initiatives such as Belt and Road projects outside China, has sought, amongst many other things, to provide alternative markets for domestic industries previously largely engaged in meeting local infrastructure needs. For instance, Chinese funding has been instrumental in widespread investment in developing rail and power transmission networks in Africa and this is reflected in Chinese exports to various African countries of steel towers, rail, and other products associated with these projects. Though this has provided markets for Chinese producers of these steel products, rather than creating opportunities for domestic suppliers of steel products in the countries in receipt of the infrastructure, there are undeniably also huge benefits for African economic development (Fig. 3).

In many instances, provision of Chinese galvanized steel products to BRI projects may be necessary if there is no local capability to produce them. But for many countries, particularly in Asia, this is not the case. Following the April 2019 BRI forum in Beijing, there has been some renegotiation of projects taking place, both scaling down project size to reduce project debt and increasing pressure for local production of inputs into projects where there is already local capacity to do this. Essentially, what this means is that Chinese funding of offshore BRI projects is

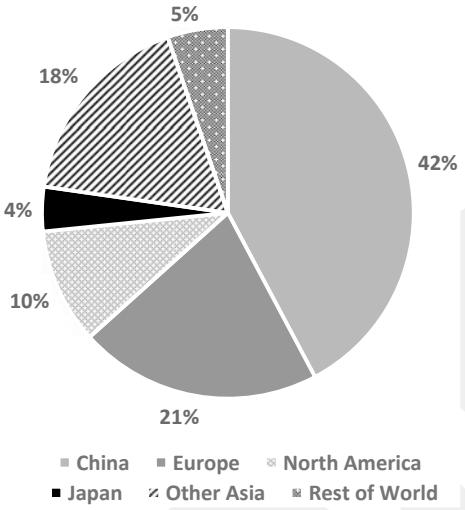

Fig. 3 Regional share of global refined zinc consumption in 2015

already promoting demand for zinc outside China and will continue to do so. China's BRI is by no means the only source of funding for infrastructure projects in the rest of the world, with Japanese funding for such projects in the six largest South East countries somewhat higher than BRI financing. Regional development banks and various government agencies are also playing a major role in promoting infrastructure development in many countries (Fig. 4).

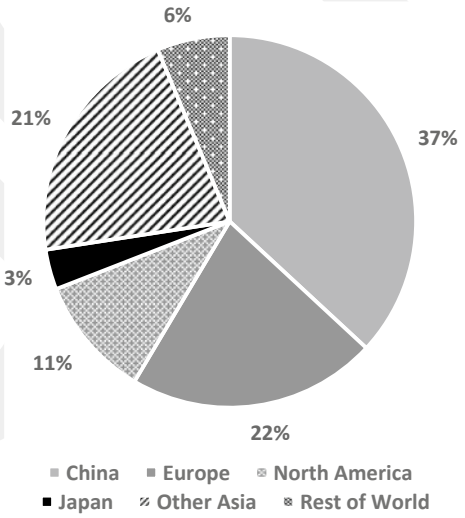

Fig. 4 Regional share of global refined zinc consumption in 2023

Over the next five years, we see a shortage of refined zinc production capacity as the major issue facing the industry, perhaps no surprise given the acute, though short-lived, shortage of raw material supplies following the permanent closure of the Century and Lisheen mines in 2015/16, and Glencore's temporary cuts in 2015 which took close to 1 Mt of zinc in concentrate production out of the supply chain in 2016, compared with 2014. Zinc treatment charges were pushed down to historically low levels as a consequence, though higher zinc prices did compensate smelters for some of the revenue lost as a result through the higher value of the free zinc component of their revenue streams. Nonetheless, the narrative at the time of a prolonged period of low zinc TCs may have delayed much needed zinc smelting projects.

Looking ahead over the next 3–4 years, we do not see a shortage of raw materials restricting refined zinc supplies, with the global zinc concentrate market now in substantial surplus. Zinc, lead, copper, and silver prices are still high enough to ensure ongoing profitability (albeit at considerably lower levels than enjoyed in 2015–2018) even with higher treatment charges. Only a major weakening of metal prices would likely lead to significant mine closures. However, for more marginal mines, losses may emerge forcing cutbacks and there remains the question of whether all zinc concentrates now being produced are able to secure customers on acceptable, or indeed, any terms. Concentrate quality and the ability or willingness of the existing zinc smelting capacity to treat more complex materials is increasingly a factor in determining treatment terms.

In conclusion, we expect to see some significant changes in the pattern of regional demand over the next 4–5 years, necessitating increased investment in expanding zinc smelting/refining capacity outside China. In addition to expanding capacity, more complex raw materials, the need to comply with tightening environmental standards, and enhance smelter revenues will necessitate investment in equipment upgrades and greater ability to recover a wider range of saleable by-products.

Part XV
Mineral Processing

GCRIS

A New Innovative Method of Flotation Separation for High Sulfur Lead–Zinc Sulfide Ore

Changtao Wang, Runqing Liu, Wei Sun, Yuehua Hu and Zhangyuan Ni

Abstract In response to the environment and economic problems attributed to the usage of large amount of lime and sulfuric acid in high alkaline preferential process (HAPP), this research systematically investigated a new, environment friendly and cost-effective flotation approach for the selective separation of galena, sphalerite, and pyrite from a high sulfur lead–zinc sulfide ore. In this study, the sample was obtained from Fankou Mine in Guangdong Province. With the new scheme, it was found that most of galena ($Pb_{Recovery}$: 93.5%) and pyrite ($S_{Recovery}$: 87.5%) were gathered through galena–pyrite mixed flotation without the usage of lime, and then galena and pyrite were effectively separated using a little amount of lime (2000 g/t). More important, the product of high-grade pyrite (S_{Grade}: 46.8%) was recovered without sulfuric acid. Totally, the new innovative method can reduce the amount of lime and eliminate sulfuric acid requirement. At the same time, the closed circuit flotation results can be obtained with $Pb_{Recovery}$: 82.60%, $Zn_{Recovery}$: 95.26%, and $S_{Recovery}$: 64.47%. Besides, both the reagents' costs and power requirements were minimized, and 4.5 million RMB could be saved annually in Fankou plant of China. Therefore, the developed approach has significant environmental and economic benefits possessing a broad prospect in the mineral industry.

Keywords Flotation · High alkaline preferential process (HAPP) · Lead–zinc ore · Lime · Sulfuric acid

C. Wang · R. Liu (✉) · W. Sun · Y. Hu · Z. Ni
School of Minerals Processing and Bioengineering, Central South University, Changsha 410083, China
e-mail: liurunqing@126.com

C. Wang
e-mail: 1044004190@qq.com

W. Sun
e-mail: sunmenghu@126.com

Y. Hu
e-mail: hyh@csu.edu.cn

Z. Ni
e-mail: 1402460314@qq.com

© The Minerals, Metals & Materials Society 2020

A. Siegmund et al. (eds.), *PbZn 2020: 9th International Symposium on Lead and Zinc Processing*, The Minerals, Metals & Materials Series,
https://doi.org/10.1007/978-3-030-37070-1_54

Introduction

With the rapid development in the modern manufacturing industries such as automobile, electrical, chemical, and medical, the demand of lead and zinc is increasing continuously based on its good physical and chemical properties. Most mined of lead and zinc are extracted from lead and zinc sulfide minerals, such as galena and sphalerite. However, in nature, most galena and sphalerite are commonly finely disseminated and intimately associated with each other or coexist with other sulfide minerals, such as pyrite, chalcopyrite, molybdenite, and precious metals, gold or and silver. Given the complex symbiotic relationship, the similar natural floatability, and the inadvertent activation of metal ions, e.g., Pb^{2+}, Cu^{2+}, dissolved in the pulp, the selective separation of galena, sphalerite, and pyrite is very challenging in the production of high sulfur lead–zinc ore.

High alkaline preferential process (HAPP) is the most popular conventional flotation flowsheet for the beneficiation of high sulfur lead–zinc ores. In this process, high alkaline conditions are required to recover the galena first and then sphalerite from pyrite and other gangue minerals. Subsequently, the acidic process is usually used for the recovery of pyrite. This method is very effective but has some disadvantages. In high alkaline conditions, the froth is sticky and easier to carry slime and further affect the concentrate grade. The recovery of previous metals is significantly reduced by high alkaline pulp pH. The pipe is usually choked that can be attributed to the generation of $CaSO_4$ by the reaction between Ca^{2+} and $SO_4{}^{2-}$. Besides, some environment and economic problems are also inevitable. This method requires a large amount of lime and sulfuric acid, which not only increase the reagents costs but also increase the toxicity in the environment. In addition, a large amount of dust, acid, NO_2/SO_2 and greenhouse gases will be produced during the production, transportation and use of lime, which will be released into the atmosphere. Sulfuric acid, as a highly corrosive chemical, is dangerous for operator's safety. In addition, in fields of mineral processing, lots of acidic wastewater, heavy metal irons, residues, and harmful gases, such as SO_2, SO_3, or H_2S are generated from the usage of H_2SO_4 that further destroyed the environment. Therefore, it is of various environmental and economic benefits of introducing an alternative process flowsheet for the beneficiation of high sulfur lead–zinc sulfide ores.

Facing above shortcomings of HAPP, Fankou mine has investigated many methods to reduce lime and sulfuric acid dosage, including galena–sphalerite mixed flotation and iso-flotation flowsheet. However, considering those results and conclusions, none of them was succeeded completely. In this study, a galena–pyrite mixed flotation flowsheet was tested as a novel scheme to effectively recover lead, zinc, and sulfur with a relatively low lime doses and without the addition of sulfuric acid.

Figure 1 shows the process flowsheets for new and old schemes. In the new scheme, galena–pyrite bulk flotation was conducted with the depression of sphalerite followed by galena/pyrite separation and the re-flotation of sphalerite.

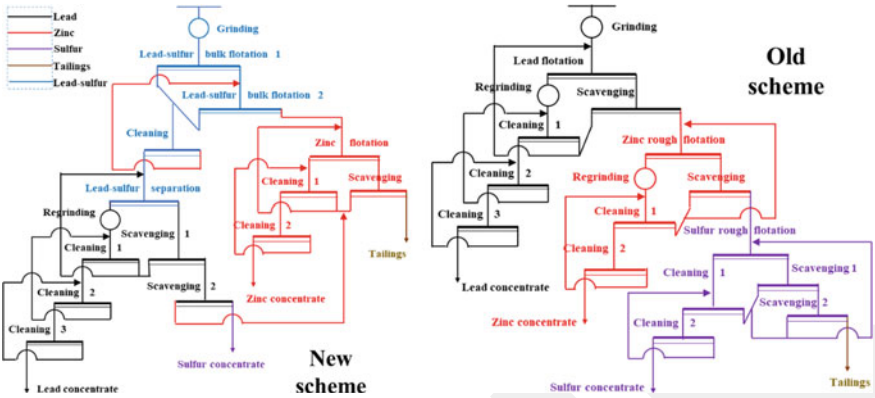

Fig. 1 Closed circuit flotation flowsheet for old and new schemes

Results and Discussion

Galena–Pyrite Bulk Flotation

The particle size has a significant effect on the flotation behaviors of minerals; therefore, the effect of grinding fineness (−0.074 mm) on galena-pyrite bulk flotation was firstly investigated and the results are shown in Fig. 2a. As can be noted that the recovery of lead, zinc, and sulfur was increased simultaneously as the proportion of −0.074 mm particles increased from 70 to 85%. However, their flotation behaviors enhanced slightly at much particles finer than −0.074 mm. Thus, the optimum grinding condition was determined as 85% particles finer than −0.074 mm. Figure 2b–d shows the flotation performance of galena, sphalerite, and pyrite under the different collector systems. It is clear from the results that good flotation behavior was not achieved by adopting individual collector. Contrary, the highest recovery of lead (93.5%), sulfur (87%), and relatively low recovery of zinc (22%) could be realized by using the combined collectors BX and DDTC at BX to DDTC ratio of 1:1. When collector dosage increased to 100 g/t from 60 g/t, the recoveries of lead, zinc and sulfur were raised obviously from 82, 15, and 72 to 93, 21, and 77% respectively. and then remained almost unchanged, while their grades began to fall gradually. Zinc sulfate and sodium carbonate acted as zinc depressant; their depression effects are depicted in Fig. 2e, f. After the conditional tests, the optimum reagent conditions for galena–pyrite bulk flotation were determined as follows: combined collector (BX: DDTC=1:1) 100 g/t, zinc sulfate and sodium carbonate dosage 600 and 1000 g/t, respectively. Above results indicated that galena and pyrite have good flotation performance without adding lime. In galena–pyrite mixed flotation, the recoveries of galena and pyrite are 93.5% and 87.5%, respectively. The phase analysis results are close to the ideal recoveries (not shown). Besides, the recovery of sphalerite (not

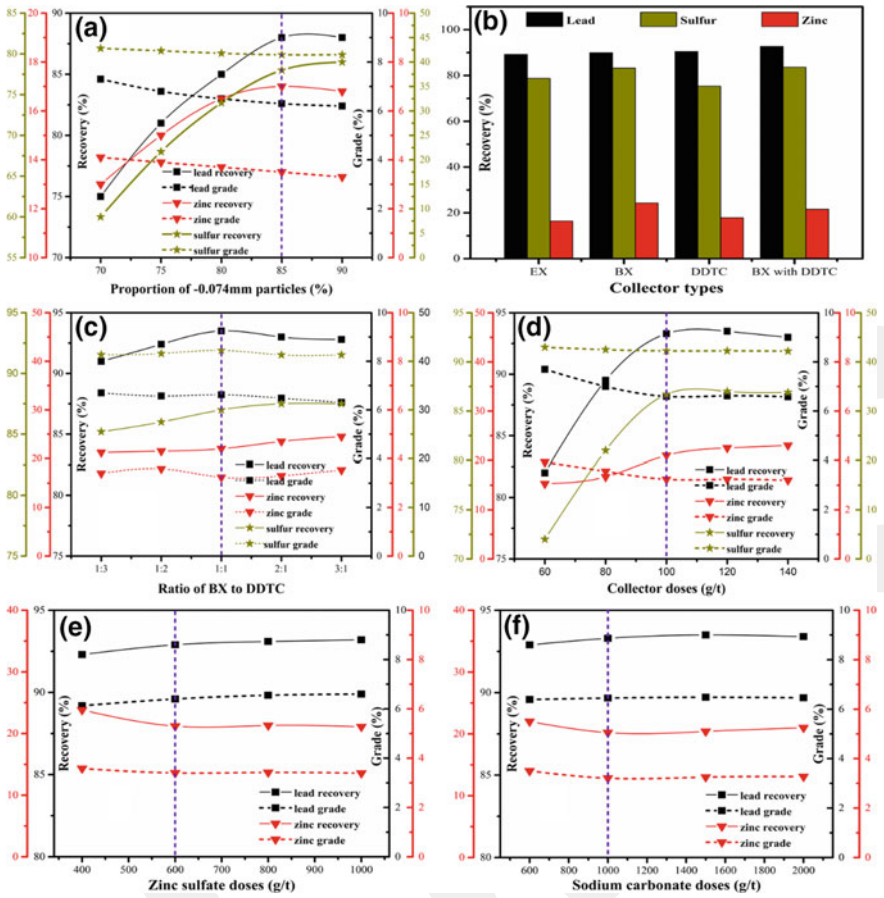

Fig. 2 Conditional experiments for lead–sulfur bulk flotation **a** grinding fineness; **b** collector types; **c** ratio of BX to DDTC; **d** collector doses; **e** zinc sulfate doses; and **f** sodium carbonate doses

activated by activator) is poor and utilizes sodium carbonate and zinc sulfate can strongly depress its flotation.

Galena–Pyrite Separation

Based on the previous studies, lime and calcium hypochlorite are good depressants for pyrite flotation. These reagents were applied individually in this research for the selective separation of galena from pyrite, and the results are displayed in Fig. 3a, b. Results show that both depressants could inhibit the pyrite flotation; however, as can be seen, more lime were required to achieve a good level of pyrite depression. The pyrite flotation remained strongly depressed with a maximum recovery

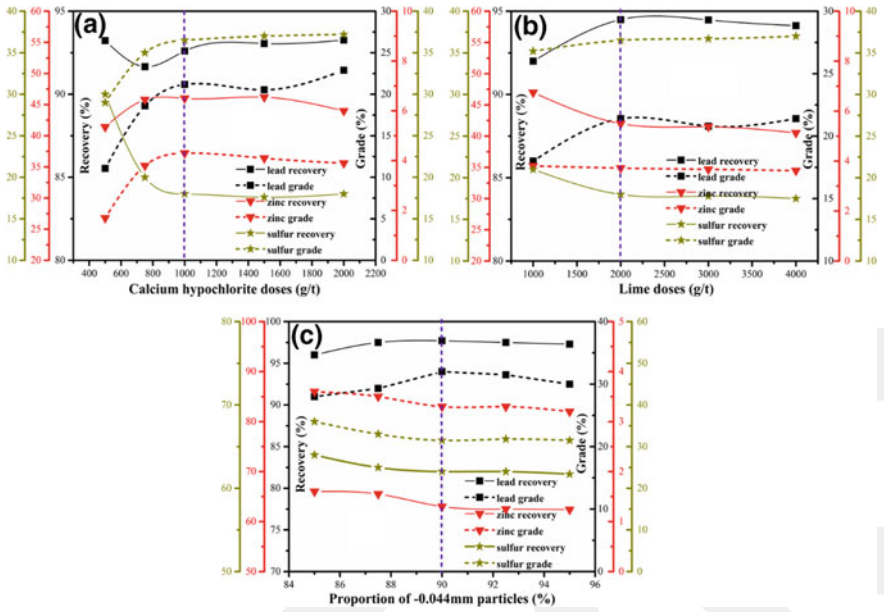

Fig. 3 Conditional experiments for lead–sulfur separation **a** calcium hypochlorite doses; **b** lime doses; and **c** regrinding fineness of bulk lead concentrate

of approximately 17.5% under the conditions of calcium hypochlorite 1000 g/t and lime 2000 g/t. Moreover, under the same experimental conditions, the lead recovery with calcium hypochlorite was 92.5% lower than the 94.5% with lime as inhibitor, and thus, lime was selected as pyrite depressant in lead–sulfur separation.

In order to improve the liberation degree and obtain high-grade lead concentrate, bulk lead concentrate was reground and the flotation performance corresponding to milling fineness is shown in Fig. 3c. After regrinding, the recoveries of both sulfur and zinc were decreased and the grade and recovery of lead increased progressively with higher regrinding fineness up to 90% particles finer than 0.044 mm. However, the grade of lead subsequently decreased with increasing fineness, which may be attributed to over-grinding of galena.

In this flotation stage, galena and pyrite were effectively separated with 2000 g/t lime. 94.5% of lead was obtained in lead bulk concentrate, and most importantly, bulk pyrite concentrate with 85% recovery was gathered by reverse flotation without the addition of sulfuric acid.

Zinc Rejection from Sulfur Concentrate

Another key to the success of galena–pyrite mixed flotation is to remove zinc from sulfur concentrate and recycle it to zinc flotation. Copper sulfate and butyl xanthate

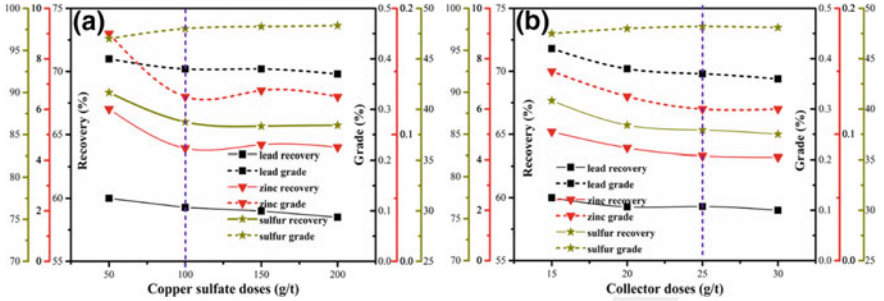

Fig. 4 Conditional experiments for removing zinc from sulfur concentrate **a** copper sulfate doses; **b** collector doses

as the most popular sphalerite activator and collector were induced in this study, and Fig. 4 shows the flotation results. As can be seen, at lower concentrations of copper sulfate (100 g/t) and butyl xanthate (25 g/t), the zinc content from sulfur concentrate was reduced to about 4.3% and the grade was as low as 0.12%. Therefore, zinc removal is very successful, its recovery in the total flowsheet can be guaranteed, and it is comparable to HAPP. Besides, the sulfur grade was 48.3%, which indicated the concentrate belongs to high-grade products and possesses higher economic values.

Zinc Flotation

After the preferential recovery of galena and pyrite, the remaining minerals existing in the flotation pulp are sphalerite and other gangue minerals. These minerals have a significant floatability difference, and thus, the selective flotation of sphalerite from the pulp is quite easier. Lime is also a kind of dispersant and regulator, which can disperse the slime and improve the adsorption of collector onto the mineral surface. Therefore, a certain amount of lime addition was beneficial for the sphalerite flotation, as it improved the zinc flotation recovery as shown in Fig. 5. Under the optimum conditions with lime 1000 g/t, copper sulfate 300 g/t and butyl xanthate 100 g/t, the zinc recovery and grade were reached to 98% and 34.5%, respectively.

Closed Circuit Flotation Index

Based on the conditional experiments, closed circuit flotation was carried out and the results of old (HAPP) and new (galena–pyrite mixed flotation) flowsheet were compared in Table 1. As illustrated in Table 1, in old system (HAPP), lead and zinc concentrates were gathered with Pb grade of 60.70%, recovery of 83.39% and Zn grade of 55.19%, recovery of 94.52%. While high-grade Pb (60.84%), Zn (56.22%),

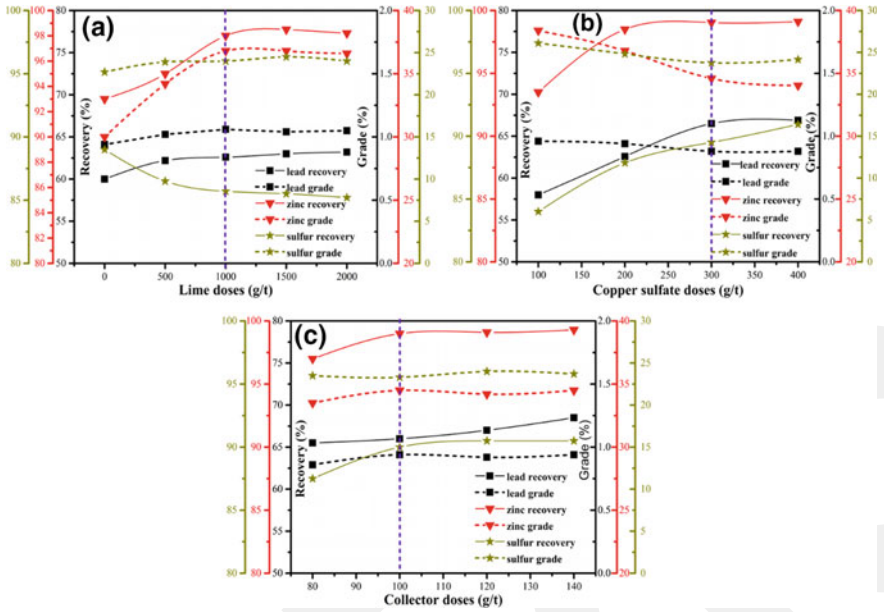

Fig. 5 Conditional experiments for zinc flotation **a** Lime doses; **b** copper sulfate doses, and **c** collector doses

Table 1 Closed circuit flotation results of old and new technologies

System	Product	Grade/%			Recovery/%		
		Pb	Zn	S	Pb	Zn	S
Old	Lead concentrate	60.70	2.57	23.50	83.39	1.49	4.38
	Zinc concentrate	0.91	55.19	30.70	3.69	94.52	16.84
	Sulfur concentrate	0.45	0.22	47.30	4.44	0.91	62.98
	Tailings	0.76	0.66	10.52	8.48	3.08	15.84
	Feed	3.78	8.97	28.00	100.00	100.00	100.00
New	Lead concentrate	60.84	2.34	22.00	82.60	1.40	4.30
	Zinc concentrate	1.20	56.22	30.46	4.61	95.26	16.85
	Sulfur concentrate	0.51	0.25	46.78	4.92	1.07	64.47
	Tailings	0.76	0.50	9.67	7.87	2.27	14.37
	Feed	3.98	9.04	27.68	100.00	100.00	100.00

and S (46.78%) concentrations were obtained in the new flotation flowsheet with recovery rates of 82.60%, 95.26%, and 64.47%, respectively. In new system, the recoveries of primary minerals galena and sphalerite remained as high as that in HAPP, and pyrite was successfully recovered through reverse flotation in the absence

of sulfuric acid. Considering the comprehensive results, the flotation index of new scheme is as good as that of HAPP.

Conclusions

In this research, an environment friendly and cost-effective approach was developed for the beneficiation of high sulfur lead–zinc sulfide ore from Fankou mine, Guangdong Province, China. The closed circuit flotation generates concentrates with Pb grade of 60.84%, recovery of 82.60% and Zn grade of 56.22%, recovery of 95.26%, S grade of 46.78, recovery of 64.47 by new method. Both the reagents' costs and power requirements were minimized, resulting in 4.5 million RMB annual savings for the Fankou mine.

GCRIS

A Novel Collector 5–(Butylthio)–1,3,4–Thiadiazole–2–Thiol: Synthesis and Improved Flotation of Galena and Sphalerite from Pyrite

Wanjia Zhang, Zhiyong Gao, Runqing Liu, Haisheng Han, Pan Chen, Yue Yang, Lei Sun, Chenyang, Zhang, Yuehua Hu, Jian Cao and Wei Sun

Abstract The introduction of aza-blocks into α-site of thiocarbonyl represents a semiempirical strategy to impart exotic selectivity into collector molecules for sulfide mineral flotation. In this work, a novel thiadiazole derivative (5–(butylthio)–1,3,4–thiadiazole–2–thiol, CSC-1) was atom-economically synthesized using easily sourced raw materials (CS_2, $N_2H_4{\cdot}H_2O$, and haloalkane) and then used for the flotation of galena and sphalerite from pyrite. Flotation results showed that, compared with ethyl xanthate, using CSC-1 as the collector, higher flotation recoveries of sphalerite and galena with improved selectivity against pyrite were obtained. Furthermore, the results of contact angle and zeta potential measurements revealed that CSC-1 molecule preferred to absorb on the surfaces of sphalerite and galena, rather than that of pyrite. DFT calculations demonstrated that nitrogen heterocyclic ring (conjugated thiocarbonyl and diazole structure), paralleled electron pairs location lobes, and ring tension provided CSC-1 collector with preferable chelating selectivity towards Pb^{2+} and Zn^{2+} and deserved it to possess better flotation selectivity for sphalerite and galena against pyrite than ethyl xanthate. This study indicates that CSC-1 has a great industrial application potential in sulfide mineral flotation.

Keywords Collector · Flotation · Galena · Sphalerite · Pyrite

W. Zhang · Z. Gao (✉) · R. Liu · H. Han · P. Chen · Y. Yang · L. Sun · Chenyang · Zhang · Y. Hu · J. Cao · W. Sun (✉)
School of Minerals Processing and Bioengineering, Central South University, Changsha, China
e-mail: zhiyong.gao@csu.edu.com

W. Sun
e-mail: sunmenghu@126.com

Y. Hu
e-mail: hyh@csu.edu.cn

Key Laboratory of Hunan Province for Clean and Efficient Utilization of Strategic Calcium-Containing Mineral Resources, Central South University, Changsha, China

© The Minerals, Metals & Materials Society 2020

A. Siegmund et al. (eds.), *PbZn 2020: 9th International Symposium on Lead and Zinc Processing*, The Minerals, Metals & Materials Series,
https://doi.org/10.1007/978-3-030-37070-1_55

Introduction

Controlling the selectivity in heterogeneous system is critical to reduce undesired byproducts and improve energy efficiency and material utilization [1]. In mineral processing, selective collectors are indispensable reagents to arbitrate the interfacial reaction of different mineral surfaces for selective separation [2]. Commonly, selective collector is composed of polar and non-polar groups; the polar portion affords the selective affinity to mineral surfaces, while the non-polar portion is termed as hydrophobic group [3]. Most selective collectors are chelating reagents. The key to the selectivity is the selective chemical affinity between collector molecules and specific metal ions on mineral surfaces [4], which benefits from the lone pair of electrons in heteroatoms of collector molecules. In fact, in this process, the chelating heteroatoms in collector molecules serve as "selective active sites" to bind target sites on mineral surfaces, offering the same functionality similar to enzymes [5, 6].

In general, chelation donor atoms (heteroatoms) endow collector molecule with stronger selective chemical affinity towards specific metal ions [7]. For example, xanthates are the predominant collectors for the flotation of sulfide minerals [8–10], while those conventional collectors suffer from the inferior selectivity in a complex system involving pyrite (Fe^{2+}) (Fig. 1a) [11]. Considering that ionic bonds attenuate selectivity during the adsorption process, nonionic thiocarbamate (TC) collectors are developed based on the molecular structure of xanthates, by replacing the sulfhydryl anions in xanthate molecules with tertiary amines (Fig. 1b, in α-site of thiocarbonyl). As a consequence, TC collectors eliminate the nonselective bonding caused by ionic bonds and boast a strong collecting ability similar to xanthates [12].

At present, the utilization of chelate-forming collector is a powerful strategy for the selective flotation against pyrite [4]. Although numerous efforts have been made to develop chelate-forming collectors, successful precedents used in flotation separation for pyrite rejection are still limited. For further development of selective collectors against pyrite, a reasonable molecular modification using xanthates as an initial model was proposed here.

The first factor considered is that the undesired anions cannot be "shielded" due to the tautomerism of thiocarbonyl and sulfydryl (Fig. 2, 1 and 1') in xanthate structures. However, if the methanedithioate core fragment is embedded into a heterocycle, tautomerism transformation will take place between thiocarbonyl and the secondary amine at α-position of thiocarbonyl (Fig. 2, 2 and 2'). Further, the construction

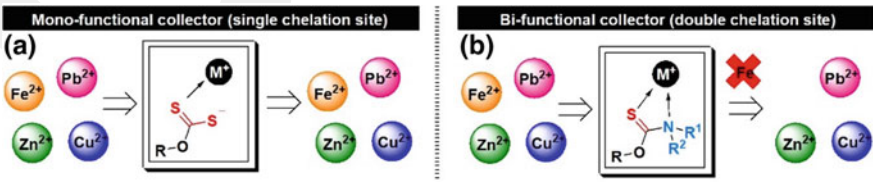

Fig. 1 Different coordination effects to metal cations by **a** xanthates and **b** thiocarbamates

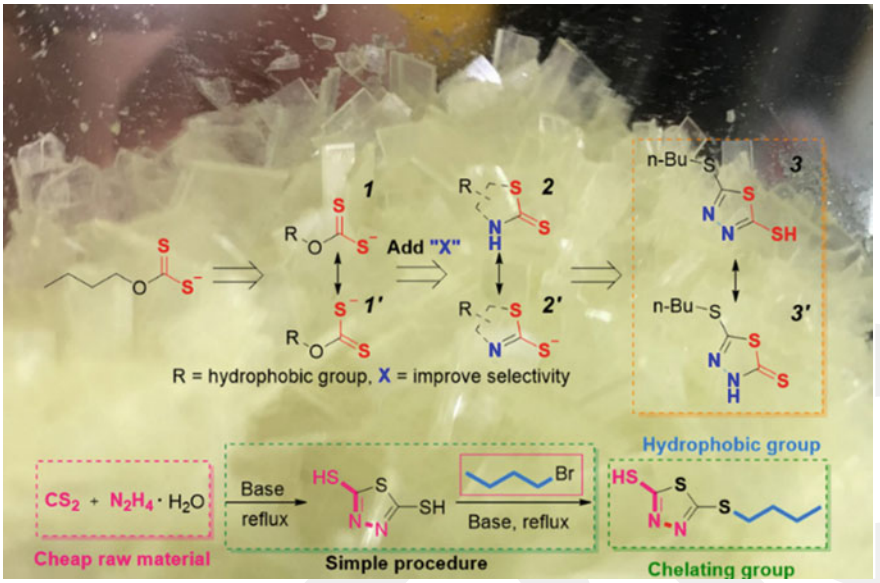

Fig. 2 Design and synthesis of CSC-1 collector

of heterocycle skeleton by introducing diazole building-block conduces to enhance the contribution of atomic orbitals of two nitrogen atoms to the HOMO orbital of collector. Finally, *n*-butyl was selected as a hydrophobic group and inserted through a concise nucleophilic substitution reaction (Fig. 2, 3 and 3'). It is envisaged that the flotation separation of galena and sphalerite from pyrite can be achieved by using such a bismuthiol derivative–5–(butylthio)–1,3,4–thiadiazole–2–thiol (CSC-1).

In this study, 5–(butylthio)–1,3,4–thiadiazole–2–thiol (CSC-1) was synthesized, for the first time. CSC-1 was then evaluated as a collector for the flotation separation of Pb/Zn sulfide minerals from pyrite by flotation experiments using single mineral, artificial mixed minerals, and actual ore. Ethyl xanthate (EX) was chosen as a comparison collector. The mechanism of selective adsorption of CSC-1 on those sulfide minerals was experimentally and theoretically unveiled through contact angle measurements, zeta potential measurements, and DFT simulations.

Materials and Methods

Materials and Reagents

Pure pyrite, sphalerite, and galena samples were obtained from Hubei and Hunan Province, China. To obtain the samples for contact angle tests, the commonly exposed

Table 1 Grades and origins of samples

Mineral species	Grade (%)			Origins
	Fe	Zn	Pb	
Pyrite	45.18	0	0	Hubei, China
Sphalerite	0.63	65.01	0	Hunan, China
Galena	0	0.08	85.52	Hunan, China
Artificial mixed minerals	22.59	16.25	21.38	–
Actual ore	28.33	5.45	3.83	Guangdong, China

cleavage surfaces were carefully selected and cleaved. For further grinding and polishing, the required surfaces were embedded in the resin and exposed. The preferred surfaces of pyrite, sphalerite, and galena were grounded successively by sandpaper at roughness of 90, 38, 18, 6.5, and 2.5 μm to obtain a flat surface. Using 1.0, 0.5, and 0.05 μm alumina powder solution in sequence, ground surfaces were successively polished on a polishing cloth [13, 14].

In preparation of the required flotation samples, pure pyrite, sphalerite, galena crystal samples, and actual ore (Table 1) were grounded in a ceramic ball mill and screened to the size of $-74 + 37$ μm. Furthermore, to prepare the samples for zeta potential measurements, flotation samples were finely grounded in an agate mortar to the size of -5 μm. As shown in Table 1, pyrite, sphalerite, and galena samples are pure and the artificial mixed minerals consisted of pyrite, sphalerite, and galena with a ratio of 2: 1: 1.

5–(butylthio)–1,3,4–thiadiazole–2–thiol (CSC-1) was synthesized according to the described method (Supplementary Material 1.1) [15]. Ethyl xanthate (EX) was used as the control collector (90%, available from Macklin Chemical Reagent Co., Ltd., China) and terpineol (90%, available from Tianjin Kermil Chemical Reagent Centre, Tianjin, China) as a frother. The solution pH was adjusted with NaOH and HCl stock solutions (0.1 mol/L). All experiments were carried out in deionized (DI) water at a resistivity of over 18 MΩ × cm.

Micro-Flotation Tests of Single Mineral and Artificial Mixed Minerals

Micro-flotation tests were carried out in an XFG flotation machine with a 40-mL Plexiglass [16, 17] at a spindle speed of 1600 rpm. In each flotation test, firstly, the mineral suspension was obtained by adding the single mineral sample (2.0 g) or artificial mixed minerals sample (1.0 g pyrite, 0.5 g sphalerite, and 0.5 g galena) to a micro-flotation cell (with 40 mL DI water). Secondly, if necessary, NaOH or HCl stock solution (0.1 mol/L) was added to regulate pulp pH. Then, CSC-1/EX and terpineol with desired dosage were added in sequence, and floated products were collected for 3 min. Finally, flotation concentrates and tailings were filtered, dried,

weighed, and assayed for flotation recoveries and metal grades. Each flotation test was repeated three times, and the average value was obtained.

Actual Ore Flotation Tests

Actual ore flotation tests were conducted on an XFG flotation machine with a 1.5-L Plexiglass [18] at a spindle speed of 1600 rpm. In each flotation test, firstly, the mineral suspension was prepared by adding actual ore (500 g) to the flotation cell (with 1.5 L tap water). Secondly, if necessary, NaOH or HCl stock solution (0.1 mol/L) was added to regulate pulp pH. Then, CSC-1 (or EX) and terpineol of desired concentration were added in sequence, and floatation products were collected for 3 min after inflating (8 L/min) for 3 min. Finally, flotation concentrates and tailings were collected, filtered, dried, and weighed. Flotation recoveries and metal grades were calculated and assessed by weighing and chemical analysis, respectively. The recovery and grade were averaged from three repeated actual ore flotation tests in a certain condition.

Contact Angle Measurement

Contact angle measurement is a common method to detect the wettability on mineral surface [19, 20]. Contact angles of pyrite, sphalerite, and galena in DI water, EX solution (1×10^{-5} mol/L), and CSC-1 collector solution (1×10^{-5} mol/L) were measured by Zetasizer Nano contact angle tester (England). The prepared samples of pyrite, sphalerite, and galena were initially immersed and stirred for 20 min in a beaker (250 mL) filled with a given solution (150 mL) at 20 °C. Subsequently, the samples were taken out, gently washed with DI water, and dried in a vacuum oven (40 °C). The contact angles were measured by suspension droplet method. At each contact angle test, droplets of 3.5 μL DI water were added to reach a stable state after 30 s. Then, the contact angle was calculated based on the shape of the droplet (Windrop++ Software). Under various test conditions, three contact angle tests were performed to obtain the average value. After each measurement, sample surfaces were washed repeatedly with alcohol and DI water. Finally, samples were polished with 0.05 μm alumina powder solution for the next measurement.

Zeta Potential Measurement

Zeta potential measurement is another method to further investigate the mechanism of flotation separation [21, 22]. Zeta potential measurements were carried out at 20 °C by Malvern Zeta Sizer Nano Series. In each measurement, the mineral suspension was

prepared by adding 30 mg single sample (−5 μm) to 60 mL KCl electrolyte solution (0.01 mol/L) in a beaker (100 mL) at a given pH and required solution. Then, the suspension was used for zeta potential measurement after being magnetically stirred for 20 min and left for 5 min. Under each test condition, zeta potential was tested for three times and the average value was obtained.

DFT Calculation and Wavefunction Analysis of Simplified Coordination Model

DFT calculation [23] is a suitable method to analyze the interaction between the collectors and the metal ions on mineral surfaces [24, 25]. In this work, high-precision DFT calculation was carried out to explore the properties of the coordination model (between collectors and metal ions), using Gaussian 09 software and under M06-D3/6-311++G (d, p) (SDD) (SMD, water) level of theory. In the calculation process, we simplified the metal ions on mineral surfaces as isolated metal ions in water because such simplification could decrease the computational costs and ensure an almost identical simulation of the experiments [26, 27]. Visualization of coordination structures was done using ChemDraw. Energy decomposition method was utilized to quantify the distortion energy that the collector molecules have to overcome.

To further probe into the electronic structure of CSC-1, several wavefunction analysis methods were performed using Multiwfn [28], including electrostatic potential surface (EPS), natural population analysis (NPA), and electron localization function (ELF). EPS and NPA charge are both qualitative tools to plot and elucidate the electron distribution of the molecule and thus provide us insight into its interaction with metal ions. ELF plot, on the other hand, is a promising way to describe how localized or delocalized the electrons are; thus, we can analyze the alignment of the lone pairs and how they affect the distortion energy.

Results

Micro-Flotation Tests of Single Mineral

To examine the feasibility of the envisaged selectivity of CSC-1, individual micro-flotation tests were selected as a model experiment to optimize the reagent scheme. In initial studies, the flotation recoveries of pyrite, sphalerite, and galena were compared by using EX or CSC-1 with different collector concentrations (show in Fig. 3). Results of single mineral flotation tests using EX as a collector indicate that flotation recoveries of three kinds of minerals are almost indistinctive, especially at ultra-low collector concentrations (below 1×10^{-5} mol/L). However, using CSC-1 as the collector, flotation recoveries of sphalerite and galena turn remarkably higher than

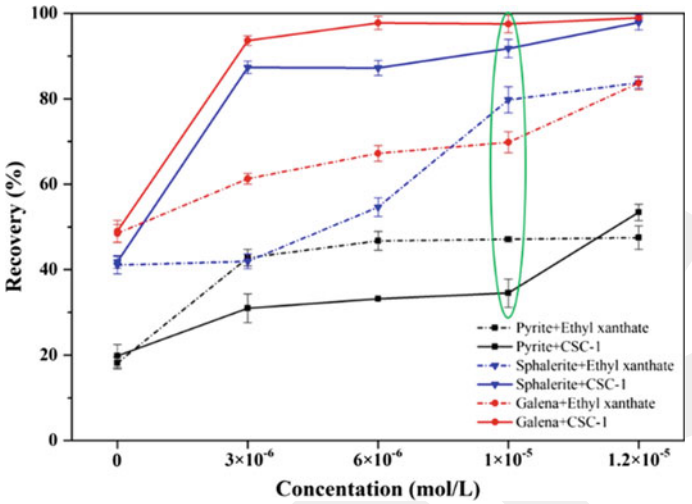

Fig. 3 Flotation recoveries of pyrite, sphalerite, and galena as a function of collector concentration ([terpineol] = 5×10^{-6} mol/L)

that of pyrite. 1×10^{-5} mol/L of CSC-1 is enough to improve the flotation recoveries of sphalerite and galena to 91.76% and 97.52%, respectively, whereas that of pyrite is only 34.52%. According to the results of single mineral micro-flotation tests, the optimal reagent scheme of 1×10^{-5} mol/L collector and 5×10^{-6} mol/L terpineol as the frother was used in the follow-up tests.

Next, various pulp pH values were screened, with results shown in Fig. 4. Under the optimal reagent scheme, flotation recoveries of pyrite, sphalerite, and galena vary slightly within a pH range of 4–10. In particular, flotation recoveries of sphalerite and galena collected by CSC-1 stand as high as 75.66% and 88.05%, respectively in a wide pH range (pH 4–10), while that of pyrite is below 33.55%. Moreover, flotation recovery difference values between sphalerite/galena and pyrite are 50.08% and 61.90%, respectively, at pulp pH 8. Hence, according to the trend in Fig. 4 and the value of original pulp pH, pH 8 was employed in subsequent flotation experiments.

Micro-Flotation Tests of Artificial Mixed Minerals and Batch-Flotations Tests of Actual Ore

In order to further investigate the flotation behaviors of EX and CSC-1 in complex flotation system involving pyrite, sphalerite and galena, flotation experiments of artificial mixed minerals and actual ore were conducted. The results of artificial mixed minerals flotation tests in Fig. 5a shows that, using CSC-1 as the collector and under optimized flotation condition, the flotation grades and recoveries of Zn and Pb are much higher than that of Fe in flotation concentrates whereas Fe shows the

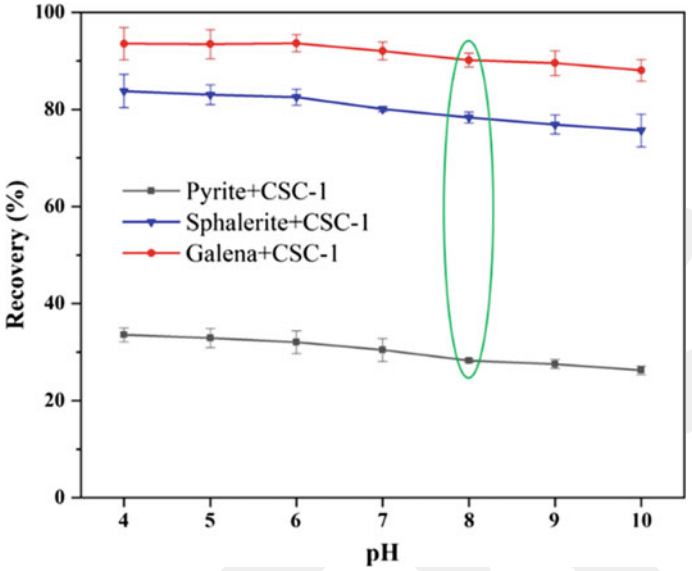

Fig. 4 Effects of pulp pH on the flotation recoveries of pyrite, sphalerite, and galena with CSC-1 as a collector ([CSC-1] = 1×10^{-5} mol/L; [terpineol] = 5×10^{-6} mol/L)

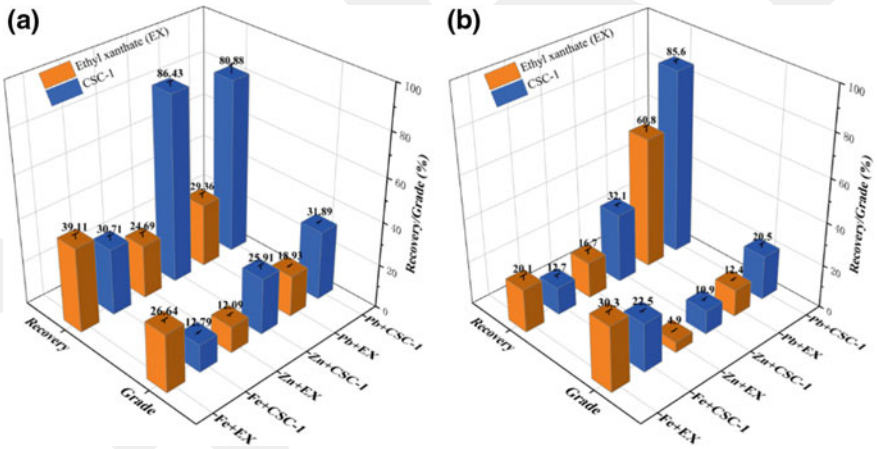

Fig. 5 Flotation recoveries and metal grades of **a** artificial mixed minerals and **b** actual ore with ethyl xanthate (EX) or CSC-1 acted as a collector ([EX/CSC-1] = 1×10^{-5} mol/L; [terpineol] = 5×10^{-6} mol/L; pH = 8)

ascendancy for the grades and recoveries of flotation concentrates than that of Zn and Pb, when EX is the collector. Furthermore, the results of actual ore flotation tests (Fig. 5b) indicate the satisfactory flotation recovery (85.6%), and moderate flotation grade (20.5%) of Pb are obtained by CSC-1 collector, while other metal recoveries are inferior with poor metal grades.

Contact Angle Measurement

In this study, the flotation results obtained are investigated by using the contact angle measurements as the criterion. In Fig. 6, the contact angles of pyrite, sphalerite, and galena in DI water stand at 65.8°, 67.4°, and 71.6°, respectively. In the presence of CSC-1/EX (1×10^{-5} mol/L), contact angle values on the surfaces of pyrite, sphalerite. and galena all increase to varying degrees (at pH 8). In the presence of EX, the contact angles of pyrite, sphalerite, and galena increase similarly by 9.3°, 10.3°, and 10.6°, respectively. However, in the CSC-1 measurement system, the contact angles of sphalerite and galena increase significantly by 16.1° and 16.6°, respectively, while that of pyrite increases slightly by 1.6°. In brief, the change of contact angle values of sphalerite and galena with CSC-1 is greater than that with EX, while that of pyrite with CSC-1 is smaller than that with EX.

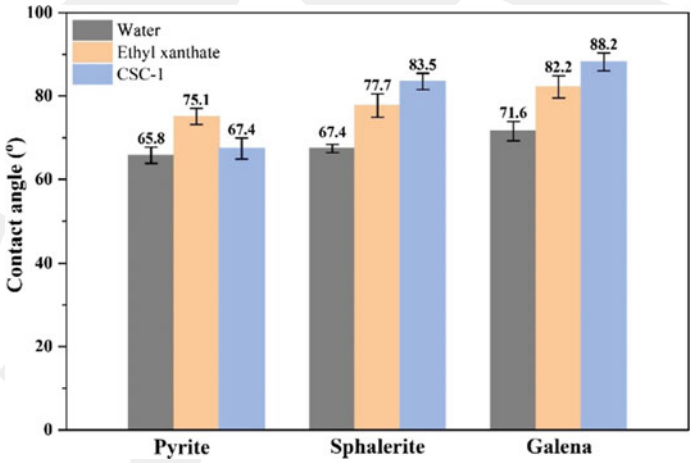

Fig. 6 Surface contact angles of pyrite, sphalerite, and galena at pH 8 in the presence and absence of EX/CSC-1 (1×10^{-5} mol/L; Experiments times = 3)

Zeta Potential Measurement

Next, zeta potential measurement was carried out to further explore the mechanism of flotation separation, with results shown in Fig. 7a–c. Zeta potential curves of pyrite, sphalerite, and galena in DI water (the gray curve) at different pH were measured. Furthermore, the points of zero charge (PZC) of pyrite, sphalerite, and galena are 3, 2, and 3, respectively, which is consistent with the previous work [7, 9, 29–32].

Figure 7 shows that compared with the zeta potential curves in DI water, using 1×10^{-5} mol/L EX at the same pH, the zeta potential curves of pyrite, sphalerite, and galena undergo similar negative shifts. However, using 1×10^{-5} mol/L CSC-1 at the same pH, the zeta potential curves of sphalerite and galena exhibit remarkable negative shifts, while that of pyrite, a slight negative shift. In particular, Table 2 shows that using 1×10^{-5} mol/L of EX at pH 8, zeta potentials of pyrite, sphalerite, and galena decrease by 8.5 mV, 8.0 mV, and 12.0 mV, respectively, with little difference in their downward trend. Contrarily, using 1×10^{-5} mol/L of CSC-1 at pH 8, the

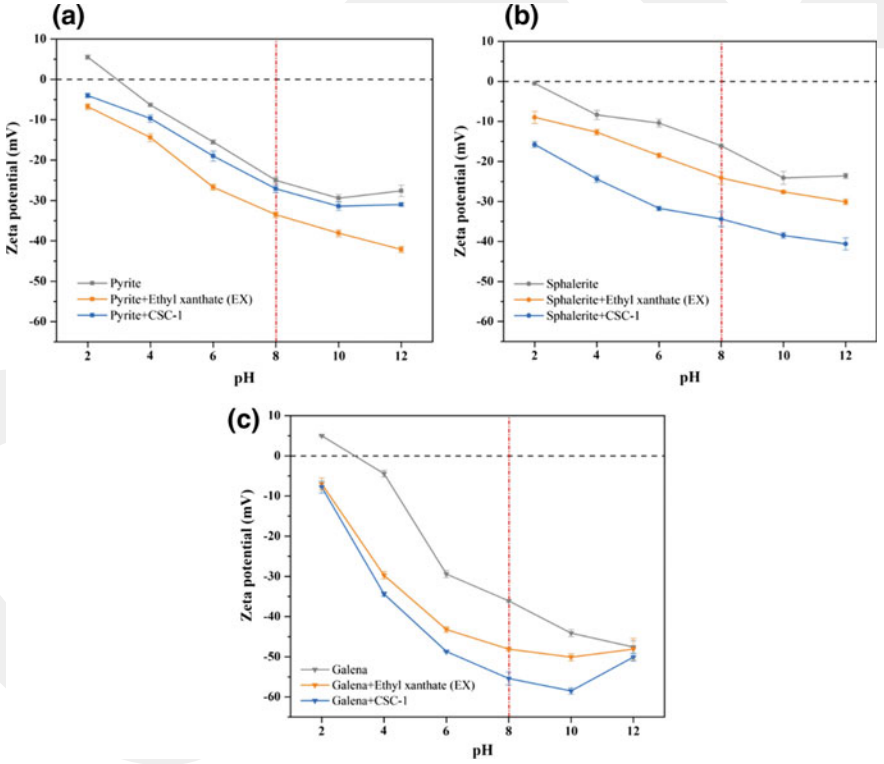

Fig. 7 Zeta potentials of **a** pyrite, **b** sphalerite, and **c** galena as a function of pH in the presence and absence of EX/CSC-1 (1×10^{-5} mol/L)

Table 2 Zeta potential variations (mV) of pyrite, sphalerite, and galena in the presence of ethyl xanthate (EX)/CSC-1 (1×10^{-5} mol/L) at pH 8

	Pyrite	Sphalerite	Galena
Ethyl xanthate (EX)	−8.5	−8.0	−12.0
CSC-1	−2.1	−18.3	−19.3

zeta potentials of sphalerite and galena significantly drop by 18.3 mV and 19.3 mV, respectively, while that of pyrite trivially decrease by 2.1 mV.

DFT Calculations

Selective collecting ability of CSC-1 collector has been proven by flotation tests, contact angle measurements, and zeta potential measurements. In order to understand the mechanism of the selectivity of CSC-1 collector, DFT calculations were carried out. First of all, the electrostatic potential surface (EPS) and natural charge population (NCP) of EX (Fig. 8a) and CSC-1 (Fig. 8b) were calculated by DFT to investigate the distribution of negative charges and the reactive sites. The different values of the electrostatic potential are symbolized by different colours at the EPS. Red, blue, and green represent the regions of the most negative (electrophilic reactivity), most positive (nucleophilic reactivity), and zero electrostatic potential, respectively. The electrostatic potential decreases in the order blue > green > yellow > orange > red. It can be seen that the negative potential is located at the tautomeric thiocarbonyl and sulfydryl in EX molecule [33], while commensurate negative potential prefers to delocalization in thiocarbonyl and conjugated diazole structure in CSC-1 molecule. As a result, the equalizations of electrostatic potentials of EX molecule and CSC-1 are different: in EX molecule, S1 and S2 share approximate a negative charge (−0.553 and −0.585, respectively), while N1, N2, and S1' are co-possessors of comparable

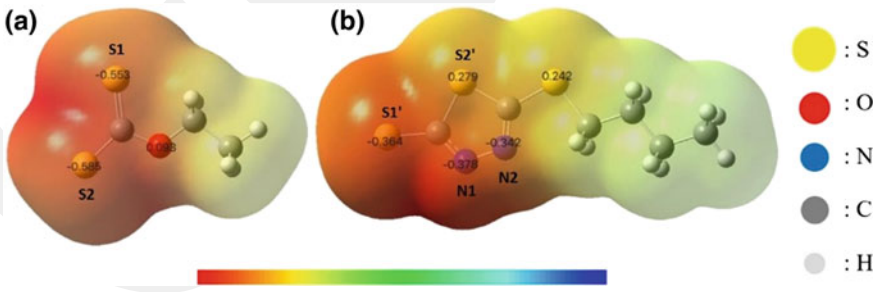

Fig. 8 Electrostatic potential surface (EPS) and natural charge population of **a** EX and **b** CSC-1 (The dark red region has negative potential, and the light green region has positive potential)

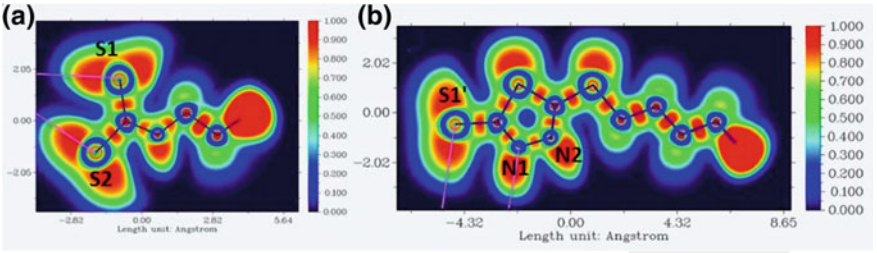

Fig. 9 Electron localization function (ELF) plots of **a** EX and **b** CSC-1. Higher value (red color) indicates a larger electron density around the atom in (**a**) and (**b**)

negative charge (−0.378, −0.342, and −0.364, respectively). This regard is in accordance with our molecular design: Firstly, embedding the methanedithioate fragment is into the heterocycle, sulfydryl (S2) is transformed into electropositive thioether (S2'); therefore, S2' is no longer a reaction site in CSC-1 collector, and as a result, the plausible reactive sites are S1' and N1. Secondly, conjugated thiocarbonyl and diazole structure is responsible for bonding metal ions because of methanedithioate fragment acts as the dipole for the concentration of negative charges. That means, negatively charged N2 occupy a considerable proportion in the frontier molecular orbital of CSC-1collector, from the perspective of molecular orbital theory.

The morphology of electron lone pairs inside ligand molecules plays an important role in coordination reaction [34], so the electron localization function (ELF) was carried out to study the electron densities associated with electron lone pairs and core regions in EX and CSC-1 molecules. The localisation mode of EX and CSC-1 molecule was established, respectively (Fig. 9). ELF is measured between 0 and 1, where perfect localization of an electron is equal to 1, and 0 is no probability of localization [35]. For the bonding atoms in EX and CSC-1 collectors, symmetric electron pairs location in S atoms (S1, S2, and S1') and asymmetric electron pairs location in N atoms (N1) could be distinguished. Observing the location lobes of electron pairs and its orientation, there is an evident angle between the electron pairs of S1 and S2 (EX), while the electron pairs of S1' and N1 are almost parallel (CSC-1).

After elucidating the EPS, NCP, and ELF of EX and CSC-1 molecule, finally we optimized the molecular geometry of six metal ion–collector anion complexes to obtain further inspiration for understanding the superior selectivity of CSC-1 (Fig. 10). From the optimized molecular geometry of EX and CSC-1, some important information can be obtained. Firstly, the bidentate angles of EX (S–C = S) and CSC-1 (S–C = N) increase as the increased cation radius. Secondly, there is an indistinctive difference in the ΔG of EX–M^{2+}, while the difference in the ΔG of CSC-1–M^{2+} is obvious. Additionally, cation radius is closely correlated with distortion energy: for two kinds of collector, larger cation radius contributes to reducing the distortion energy of coordination compound.

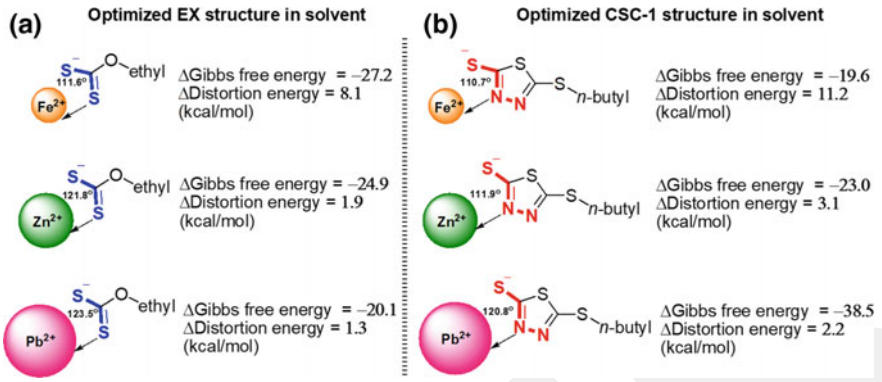

Fig. 10 Optimized molecular geometry and energy profile of the EX–M^{2+} (**a**) and CSC-1–M^{2+} (**b**) in solvent. *Note* Optimized geometry of EX/CSC-1-metal ion model at M06-D3/6-311++G(d, p) (SDD) level [36]. Solvation was taken into consideration with SMD model (water, $\varepsilon = 1.78$ [37])

Discussion

Collector CSC-1 was synthesized and applied in the selective flotation of galena and sphalerite from pyrite. The results of single mineral flotation tests demonstrate that flotation recoveries of three kinds of minerals are almost indistinctive using EX as the collector, while satisfactory flotation recoveries of sphalerite and galena and inferior flotation recovery of pyrite could be obtained with CSC-1. Moreover, in a wide range of pH values, CSC-1 operates normally with maintaining the distinctive gap of the flotation recoveries of galena/sphalerite and pyrite. This proves CSC-1 is a potential selective collector for galena and sphalerite with pyrite rejection ability. Next, the results of artificial mixed minerals flotation tests prove again that CSC-1 collector possesses powerful collecting ability for galena and sphalerite and excellent selectivity against pyrite. Batch-flotations tests are the best simulator of flotation industry. In the last part of the flotation tests, the results of batch-flotation tests employing actual ore decide that CSC-1 collector recognized and collected PbS (galena) efficiently and selectively in complex flotation system involving FeS_2 (pyrite), fully demonstrating the excellent flotation efficiency and selectivity of CSC-1 collector towards PbS (galena).

Contact angle results prove that addition of collectors could increase contact angles (hydrophobicity) of minerals. CSC-1 collector could significantly increase the hydrophobicity of sphalerite and galena, rather than pyrite. But the increasing ranges of three kinds of contact angles (sphalerite, galena, and pyrite) are approximately equal by EX collector. According to the previous studies, increased contact angles (hydrophobicity) means a stronger adsorption between collectors and sulphide minerals [2, 38], which was the reason for the excellent flotation separation of sphalerite (Zn) and galena (Pb) from pyrite (Fe) when CSC-1 acted as collector (the results from Figs. 3, 4, and 5).

Additionally, zeta potential results show the same trend as contact angle measurements: there are obvious negative changes of zeta potential values of sphalerite and galena but slight changes of pyrite in CSC-1 test system. Using EX as the collector, however, the changes of zeta potential values of three kinds of minerals is minor and similar. Zeta potential results further confirm the inferences from contact angle: CSC-1 has a stronger adsorption on sphalerite and galena but weaker adsorption on pyrite, compared with EX, consistent with the experimental results shown in Figs. 3, 4, 5, and 6.

On the basis of the above discussions, CSC-1 molecule prefers to absorb on the surface of sphalerite and galena rather than pyrite surface. This is the reason for the efficient and selective flotation separation for sphalerite and galena against pyrite by using CSC-1 collector. As a comparison, EX collector mediates these three minerals poorly and non-selectively.

EPS and NCP studies of collectors confirm that the bonding groups of CSC-1with metal ions are conjugated thiocarbonyl and diazole structure, while that of EX is tautomeric thiocarbonyl and sulfydryl. Noteworthy, sulphur atom is a softer Lewis base and better electron-donating than nitrogen atom, which binds with most transition metal ions rapidly and stably. As a consequence, the "all-sulfur-composed" bidentate ligand (EX collector) is not performing as selective as the aza-collector CSC-1. In addition, negatively charged N2 occupy a considerable proportion in the HOMO orbital of CSC-1 molecule; this is the supplementary reason for the excellent selectivity of CSC-1 collector.

Lone pair electron is the key factor for selective chelation. ELF study reveals that there is an evident angle between the location lobes of electron pairs in EX molecule (S1 and S2), while the located electron pairs in CSC-1 molecule are almost parallel (S1' and N1). This suggests that CSC-1 molecule is more likely to bind to Pb^{2+} with larger radius, while EX molecule prefers to Pb^{2+} with smaller radius, because of the match relationship between the located electron pairs of collectors and the empty orbital of metal ions. The result of ELF is consistent with flotation tests, EPS, and NCP studies.

The optimized ΔGibbs free energy of molecular geometries demonstrates that CSC-1–Pb^{2+} coordination is the most stable chelation modes of CSC-1–M^{2+} complexes. This is the primary reason why the flotation recovery of galena is the highest compared with sphalerite and pyrite in batch-flotations tests. And this point also provides us with one question: why does Pb^{2+} become the decisive factor for the stabilization of EX–M^{2+} and CSC-1–M^{2+} The answer is ring tension. EX–M^{2+} chelation forms a monocyclic complex, and CSC-1–M^{2+} chelation incorporates two atoms (C and N) into different rings, enforcing monocyclic and fused ring tension, respectively. As shown in Fig. 10, Pb^{2+}, Zn^{2+}, and Fe^{2+} take their turn to hold the position in the collector–M^{2+} complexes, but Fe^{2+} is not favorable to be the coordinative metal center because there are obvious distortions in the bidentate angles of EX–Fe^{2+} (S–C = S, 111.6°) and CSC-1–Fe^{2+} (S–C = N, 110.7°). According to Δdistortion energy, Pb^{2+} is the optimum metal ion to reduce fused ring tension of collector–M^{2+}

complexes. We can also confirm the excellent selectivity again of CSC-1 collector towards galena in flotation separation by obvious difference value of ΔGibbs free energy and Δdistortion energy in CSC-1–M^{2+} complex.

Conclusions

In this study, a novel selective collector 5–(butylthio)–1,3,4–thiadiazole–2–thiol (CSC-1) was synthesized by modifying the molecular structure of xanthate. The results of the flotation tests prove that under the optimized reagent scheme, CSC-1 collector could significantly improve the flotation recoveries and the grades of Zn and Pb rather than Fe, while EX collector mediates these three minerals poorly and non-selectively. Next, the results of flotation tests were demonstrated by contact angle and zeta potential measurements: using CSC-1 as the collector, the adsorption on sphalerite and galena surfaces is much stronger than that on pyrite surface. However, using EX as the collector, the adsorption on pyrite, sphalerite, and galena surfaces is minor and similar. Furthermore, DFT calculation results provided insight into the mechanism. EPS and NCP studies of collectors proved that aza-framework of CSC-1 molecule are responsible for the excellent flotation selectivity. ELF study reveals that CSC-1 molecule is more likely to bind to Pb^{2+} and these inferences were further proven by Δdistortion energy and ΔGibbs free energy in optimized molecular geometry: Pb^{2+} is the optimum metal ion to reduce fused ring tension of collector–M^{2+} complexes, and CSC-1–Pb^{2+} coordination is also the most stable chelation modes in CSC-1–M^{2+} complexes. In summary, CSC-1 can be used for flotation separation of galena and sphalerite from pyrite and has a great potential for industrial application.

References

1. Christopher P, Linic S (2008) Engineering selectivity in heterogeneous catalysis: Ag nanowires as selective ethylene epoxidation catalysts. J Am Chem Soc 130:11264–11265
2. Liu G, Yang X, Zhong H (2017) Molecular design of flotation collectors: a recent progress. Adv Colloid Interface Sci 246:181–195
3. Mu Y, Peng Y, Lauten RA (2016) The depression of pyrite in selective flotation by different reagent systems—a literature review. Miner Eng 96–97:143–156
4. Ghirlanda G (2008) Old enzymes, new tricks. Nature 453:164–166
5. Kaiser ET (2010) Catalytic activity of enzymes altered at their active sites. Angew Chem Int Ed 27:913–922
6. Pecina Treviño ET, Uribe Salas A, Nava Alonso F et al (2003) On the sodium-diisobutyl dithiophosphinate (Aerophine 3418A) interaction with activated and unactivated galena and pyrite. Int J Miner Process 71:201–217
7. Huang Z, Wang J, Sun W et al (2019) Selective flotation of chalcopyrite from pyrite using diphosphonic acid as collector. Miner Eng 140:105890
8. Nowak P, Laajalehto K (2007) On the interpretation of the XPS spectra of adsorbed layers of flotation collectors—ethyl xanthate on metallic lead. Physicochem Probl Miner Process 41:107–116

9. Porento M, Hirva P (2002) Theoretical studies on the interaction of anionic collectors with Cu^{+}, Cu^{2+}, Zn^{2+} and Pb^{2+} ions. Theor Chem Acc 107:200–205
10. Ackerman PK, Harris GH, Klimpel RR (2000) Use of xanthogen formates as collectors in the flotation of copper sulfides and pyrite. Int J Miner Process 1–13
11. Gao Z, Sun W, Hu Y (2015) New insights into the dodecylamine adsorption on scheelite and calcite: an adsorption model. Miner Eng 79:54–61
12. Hu Y, Gao Z, Sun W et al (2012) Anisotropic surface energies and adsorption behaviors of scheelite crystal. Colloids and Surf A: Physicochem Eng Aspects 415:439–448
13. Katritzky AR, Wang Z, offerman RJ (1990) S–S'– and S,N–Disubstituted derivatives of 1,3,4–thiadiazoledithiones. J Heterocyclic Chem 27:139–142
14. Gao Y, Gao Z, Sun W et al (2016) Selective flotation of scheelite from calcite: a novel reagent scheme. Int J Miner Process 154:10–15
15. Gao Z, Gao Y, Zhu Y et al (2016) Selective flotation of calcite from fluorite: a novel reagent schedule. Minerals 6:114
16. Huangfu Z, Khoso SA, SUN W (2018) Utilization of petrochemical by-products as a new frother in flotation separation of molybdenum. J Clean Prod 204:501–510
17. Chau TT (2009) A review of techniques for measurement of contact angles and their applicability on mineral surfaces. Miner Eng 22:213–219
18. Zhang W, Sun W, Hu Y et al (2019) Selective flotation of pyrite from galena using chitosan with different molecular weights. Minerals 9:549
19. Liu C, Hu Y, Feng A et al (2011) The behavior of N, N–dipropyl dodecyl amine as a collector in the flotation of kaolinite and diaspore. Miner Eng 24:737–740
20. Mitchell TK, Nguyen AV, Evans GM (2005) Heterocoagulation of chalcopyrite and pyrite minerals in flotation separation. Adv Colloid Interface Sci 114–115:227–237
21. Tan X, He F-Y, Shang YB et al (2016) Flotation behavior and adsorption mechanism of (1–hydroxy–2–methyl–2–octenyl) phosphonic acid to cassiterite. Trans Nonferrous Met Soc China 26:2469–2478
22. Zhao G, Zhong H, Qiu X et al (2013) The DFT study of cyclohexyl hydroxamic acid as a collector in scheelite flotation. Miner Eng 49:54–60
23. Kendall TA, Hochella MF, Becker U (2005) Computational modeling of azotobactin–goethite/diaspore interactions: applications to molecular force measurements and siderophore–mineral reactivity. Chem Geol 216:17–35
24. Liu G, Ren H, Zhan J et al (2013) Synthesis, characterization and properties of 3,3′–diethyl–1,1′–oxydiethylenedicarbonyl bis(thiourea). Res Chem Intermed 40:2025–2038
25. Lu T, Chen F (2012) Multiwfn: a multifunctional wavefunction analyzer. J Comput Chem 33:580–592
26. Difeo A, Finch JA, XU Z (2001) Sphalerite–silica interactions: effect of pH and calcium ions. Int J Miner Process 61:57–71
27. Shall HEE, Elgillani DA, Khalek NAA (2000) Role of zinc sulfate in depression of lead-activated sphalerite. Int J Miner Process 58:67–75
28. Ikumapayi F, Makitalo M, Johansson B et al (2012) Recycling of process water in sulphide flotation: effect of calcium and sulphate ions on flotation of galena. Miner Eng 39:77–88
29. Zhang C, Liu C, Feng Q et al (2017) Utilization of N-carboxymethyl chitosan as selective depressants for serpentine on the flotation of pyrite. Int J Miner Process 163:45–47
30. Fornasiero D, Ralston J (2006) Effect of surface oxide/hydroxide products on the collectorless flotation of copper-activated sphalerite. Int J Miner Process 78:231–237
31. Khrenova MG, Krivitskaya AV, Tsirelson VG (2019) The QM/MM-QTAIM approach reveals the nature of the different reactivity of cephalosporins in the active site of L1 metallo-β-lactamase. New J Chem 43:7329–7338
32. Osborne DA, Morishita T, Tawfik SA (2019) Adsorption of toxic gases on silicene/Ag(111). Phys Chem Chem Phys 21:17521–17537
33. Zhao Y, Truhlar DG (2008) The M06 suite of density functionals for main group thermochemistry, thermochemical kinetics, noncovalent interactions, excited states, and transition elements: two new functionals and systematic testing of four M06 functionals and twelve other functionals. Theor Chem Acc 120:215–241

34. Marenich AV, Cramer CJ, Truhlar DG (2009) Universal solvation model based on solute electron density and on a continuum model of the solvent defined by the bulk dielectric constant and atomic surface tensions. J Phys Chem B 113
35. Drzymala J, Mielczarski E, Mielczarski JA (2007) Adsorption and flotation of hydrophilic and hydrophobic materials in the presence of hydrocarbon polyethylene glycol ethers. Colloids Surf A: Physicochem Eng Aspects 308:111–117
36. Xiao J, Liu G, Zhong H (2017) The adsorption mechanism of N–butoxypropyl–S–[2–(hydroxyimino) propyl] dithiocarbamate ester to copper minerals flotation. Int J Miner Process 166:53–61
37. Liu S, Zhong H, Liu G et al (2018) Cu(I)/Cu(II) mixed-valence surface complexes of S–[(2–hydroxyamino)–2–oxoethyl]–N, N–dibutyldithiocarbamate: Hydrophobic mechanism to malachite flotation. J Colloid Interface Sci 512:701–712
38. Si G, Zhang L, Han B et al (2016) Chromium complexes containing a tetradentate [OSSO]-type bisphenolate ligand as a novel family of catalysts for the copolymerization of carbon dioxide and 4-vinylcyclohexene oxide. RSC Adv 6:22821–22826

GCRIS

Part XVI
By-Product Recovery II

GCRIS

The Recovery of Pb and Zn in Antimony Smelting Slag

Pengfei Xin, Junyan Wei, Liang Xu, Weiguo Wu and Dailong Lan

Abstract This paper studies the recovery of metals Pb, Zn, and Sb in antimony smelting slag by fuming furnace. The study focuses on volatile mechanism of Pb, Zn, and Sb, metal distribution, metal recovery, and fuel consumption in the process of slag fuming. It is concluded in this report that the Pb, Zn, and Sb from reduction reaction in the molten bath during the process of fuming will be oxidized in the offgas zone and collected by dust collection. When the antimony smelting slag contains Pb ~1.2%, Zn ~6.9%, and Sb ~1.4%, the metal recovery of Pb, Zn, and Sb after fuming and volatile process will be 95%, 88%, and 60%, respectively. Meanwhile, the coal consumption is ~0.3 t per ton antimony smelting slag, when the pulverized coal with 59.92% fixed carbon is utilized as reductant and fuel.

Keywords Fuming furnace · Zinc · Lead · Antimony smelting slag

Overview

Guangxi province is a major place to produce metal antimony in China. In accordance with statistics, the metal antimony produced in Guangxi in 2018 accounts for 33% of the total output in China. The antimony ore mainly occurs as jamesonite ($4PbS{\cdot}FeS{\cdot}3Sb_2S_3$). The process of sinter + blast furnace reduction—reverberatory refining—is utilized for metal antimony smelting. With regard to such process, amounts of smelting slag are produced during blast furnace reduction. However, the treatment of such antimony smelting slag will cost a lot. Therefore, such quantities of smelting slag are stored. However, Zn, Pb, Sb, and other metals remain in such antimony smelting slag due to the characteristics of jamesonite, which will cause some negative impact on the environment due to long term storage. Therefore, it will

P. Xin (✉) · L. Xu · W. Wu
China ENFI Engineering Co., Ltd., Beijing 100038, China
e-mail: xinpf@enfi.com.cn

J. Wei · D. Lan
Guangxi Raw Antimony Rich Polytron Technologies Inc, Hechi 547000, China
e-mail: gxldl3158@163.com

© The Minerals, Metals & Materials Society 2020

A. Siegmund et al. (eds.), *PbZn 2020: 9th International Symposium on Lead and Zinc Processing*, The Minerals, Metals & Materials Series,
https://doi.org/10.1007/978-3-030-37070-1_56

have a great significance on antimony smelting industry development in Guangxi if an applicable and feasible technology of such antimony smelting slag treatment can be utilized in the plant.

There are some smelting slag treatment technologies utilized in China at present, which are rotary kiln process and fuming furnace process. Rotary kiln process is widely utilized for zinc leaching residue treatment. The equipment and facilities of rotary kiln process are easy to operate. However, zinc recovery is low when the low zinc content slag is treated with rotary kiln process, because the effective contact area between reductant and slag in rotary kiln is small, and the slag in rotary kiln is not totally in molten. At the same time, a large amount of metallurgical coke is consumed during the process, which will increase the operation cost [1]. Fuming furnace process is a kind of molten bath smelting technology, and pulverized coal is utilized as reductant. The pulverized coal and CO produced by pulverized coal combustion will have reaction with metallic oxide in the molten bath. This technology can be utilized to treat various raw materials and has high recovery of zinc and lead. Currently, this technology has been widely utilized for the treatment of antimony smelting slag, lead smelting slag, and zinc leaching residue. Based on research study on antimony smelting slag and operation experiences, the fuming furnace process is utilized by Guangxi Shengfu Antimony to treat such antimony smelting slag. The factory has been in operation for two years. This paper introduces the actual production situation. Finally, it is proved that Zn, Pb, and Sb are effectively recovered by fuming furnace process after a period of operation. Therefore, the fuming furnace technology solves the problem of antimony slag storage which containing Zn, Pb, and Sb and effectively recovers the valuable resources as well.

Process Theory

Antimony smelting slag is produced from blast furnace during antimony oxides reduction. The slag composition of such antimony smelting slag is FeO–SiO_2–CaO, and Pb, Zn, and Sb in slag appears as complicated oxides. In the antimony smelting slag, part of Pb exists in the form of PbS. In the heating stage, PbS is oxidized into oxide PbO, and a small part of PbO, ZnO, and Sb_2O_3 volatilizes into dust. Most lead, zinc, and antimony oxides in the slag will have reaction with pulverized coal and CO produced from pulverized coal combustion to recover metals lead, zinc, and antimony. The major chemical reaction in the molten bath is as follows [2] (Fig. 1):

$$C(s) + O_2(g) = CO_2(g)$$

$$2C(s) + O_2(g) = 2CO(g)$$

$$ZnO(1) + CO(g) = Zn(1) + CO_2(g)$$

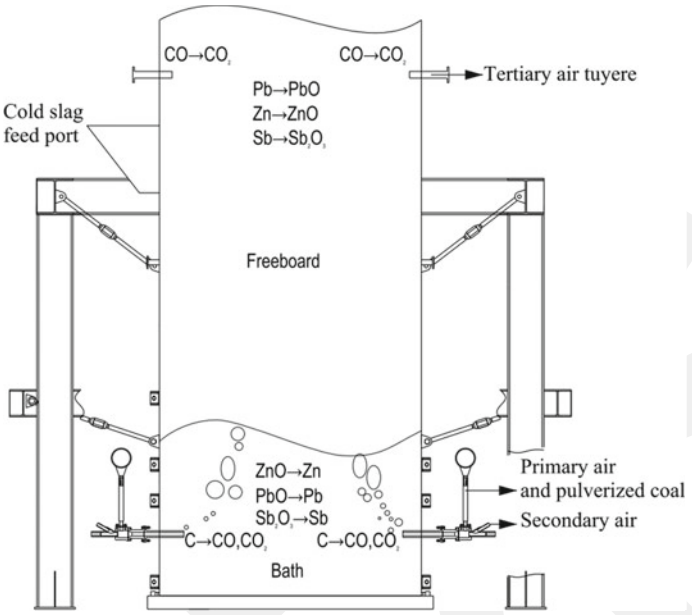

Fig. 1 Schematic diagram of fuming furnace reactions

$$PbO(1) + CO(g) = Pb(g) + CO_2(g)$$

$$Sb_2O_3(1) + 3CO(g) = 2Sb(1) + 3CO_2(g)$$

The molten bath in fuming furnace is agitated by process air, which makes metal zinc, metal lead, and metal antimony volatilize from molten bath and go to offgas. The metals lead, zinc, and antimony in the offgas will have reaction with unreacted O_2 and tertiary air blown from tertiary air tuyere to produce ZnO, PbO, and Sb_2O_3. To ensure reduction reaction in the molten bath, there will be excess CO in the offgas, which will be combusted in the freeboard. The major reaction in the freeboard is as follows:

$$2CO(g) + O_2(g) = 2CO_2(g)$$

$$2Zn(1) + O_2(g) = 2ZnO(s)$$

$$2Pb(g) + O_2(g) = 2PbO(g)$$

$$4Sb(1) + 3O_2(g) = 2Sb_2O_3(1)$$

The dust produced during such reaction will go to dust collection system together with offgas. After dust collection, the offgas will be sent to desulphurization system.

Process Description

Antimony smelting slag produced from blast furnace will be fed to fuming furnace via belt conveyor after weighting. Since fuming process is satisfied with antimony smelting slag, no flux is required for slag composition adjustment during the process. The operation of fuming furnace is in batch, and certain molten bath should be remained in accordance with process requirement. The slag will be tapped out when one campaign is completed, but certain molten bath should be kept, and then cold materials will be fed to molten bath of fuming furnace via belt conveyor. Process air and pulverized coal will be injected into fuming furnace via tuyeres located at the side of fuming furnace. Pulverized coal is delivered to constant coal feeder by double cyclones for pulverized coal feeding. Primary air and secondary air as process air are blown into fuming furnace via injectors. Primary air as coal handle carrier is mixed with pulverized coal and then injected into injector passage. The primary air carrying with pulverized coal together with secondary air within injector passage will be injected into fuming furnace. The cold materials are fed into fuming furnace during melting stage in batch. The period of melting is around 70–75 min. During melting stage, the λ (λ = actual air supply/required air for fed coal fully combustion) should be controlled within 0.9–1.0 to speed up cold slag melting and ensure most coal completely combustion. For fuming stage, the reducing atmosphere will be created by adjusting the amount of process air blown from tuyeres and that of coal. Zinc and lead will be reduced in the molten bath, when λ is controlled within 0.6–0.8. When the fuming stage is completed, the final slag will be tapped out, and the process will go to next campaign (Fig. 2).

Major Equipment

The fuming system of antimony smelting slag includes circulation water cooling system, pulverized coal preparation system, materials feeding system, desulphurization system, and fuming furnace system. For fuming furnace system, the major equipment covers fuming furnace, waste heat boiler for fuming furnace, surface cooler, bagfilter, ID fan, process blower, and pulverized coal feeder. The specification of major equipment in such system is shown in Table 1.

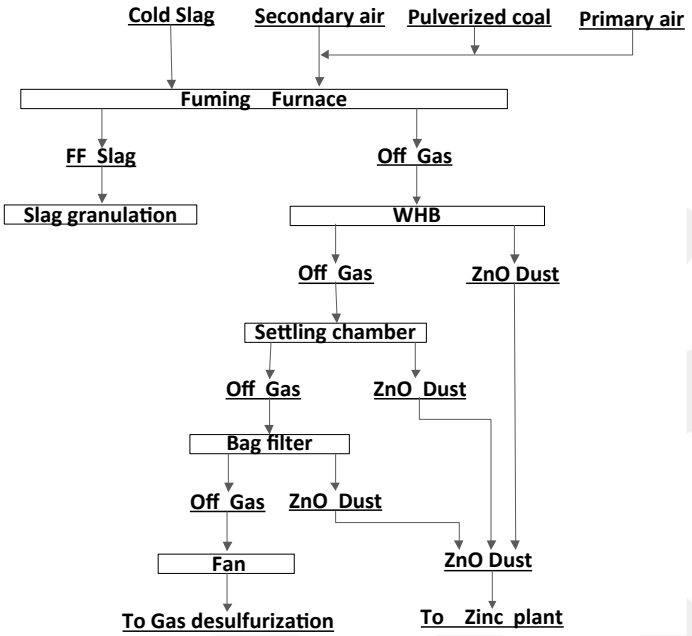

Fig. 2 Process block diagram of fuming furnace

Table 1 Major equipment specification

Equipment	Unit	Specification
Fuming furnace	m^2	7.0
Blower	m^3/min	300
Waste heat boiler	t/h	~15 t/h
Surface cooler	m^2	1000
Bag filter	m^2	2200
Pulverized coal feeder	t/h	3*2
Pulverized coal preparation system	t/h	10

Major Production Data and Process Data

The antimony smelting slag treated is the slag stored during antimony production, so the composition of slag has few variation. The composition of antimony smelting slag is shown in Table 2.

Table 2 states that Pb in the slag is almost similar to that from blast furnace of lead smelting, which shows that zinc in slag is low, antimony content and lead content are almost same, and $Fe/SiO_2 = 0.93$ and $CaO/SiO_2 = 0.86$.

Table 2 Antimony smelting slag composition (wt%)

	Pb	Zn	Sb	S	Fe	SiO_2	CaO
Sample 1	1.16	5.59	1.2	1.65	20.15	22.18	17.52
Sample 2	1.32	7.56	1.42	1.42	21.03	22.32	20.66
Average	1.24	6.58	1.31	1.54	20.59	22.25	19.09

Table 3 Production data

	Duration (min)	Boiler evaporation (t/h)	Air (m^3/h)	Pulverized coal (t/h)	λ
Feeding and melting	70–75	7.6–7.7	12,000–12,500	~1.7	0.89
Fuming	60	9.5–10	11,500–12,000	~2.0	0.72
Slag tapping	12–20	7.1–7.2	11,500–12,500	~1.6	0.94

In operation, 15–16 t will be fed into fuming furnace per campaign. According to the production process experience,the duration of materials feeding is around 70–75 min. The period of fuming is around 60 min, and the slag tapping duration is 15–20 min. The temperature of molten bath is 1250–1300 °C. The other production data is shown in Table 3.

The atmosphere within fuming furnace is controlled by adjusting the amount of coal fed to fuming furnace to ensure the speed of melting and reduction reaction. In Table 3, production data shows cycle of fuming furnace boiler operation. For fuming stage, more coal is fed into fuming furnace and more reaction heat is produced, so boiler evaporation is more. The coal consumption is ~0.3 t per ton antimony smelting slag.

ZnO dust is the main product of fuming reaction. ZnO dust will go to waste heater boiler, surface cooler, and bag filter and be collected by these facilities. The composition of dust collected by such three facilities is shown in Table 4.

In accordance with production data, Pb content in the dust collected from waste heat boiler, surface cooler, and bag filter is reduced gradually; the reduced percentage is 0.12% and 0.13%, respectively. However, zinc content in the dust collected from bag filter is higher than that dust collected from boiler and surface cooler. The reason is that dust collected from boiler and surface cooler is by gravity and lead oxides are heavier than zinc oxides. The assays of dust in above table show that Fe, SiO_2, and

Table 4 Composition of dust collected by waste heater boiler, surface cooler, and bag filter

	Pb	Zn	Sb	S	Fe	SiO_2	CaO
WHB	9.38	43.53	2.77	2.41	4.57	7.61	2.76
SC	9.29	42.13	8.42	3.13	1.24	2.19	0.68
BF	9.16	46.55	8.03	3.62	0.98	1.73	0.57

CaO content in the dust collected from boiler is higher, which does not appear during molten slag treatment. The reason is that some slag goes to waste heat boiler directly rather than falls into bath when they are fed into fuming furnace during cold slag treatment due to small particle size of granulated slag. The melting point of Fe, SiO_2, and CaO is high, and such compound is with lower volatilization, so they appear as solids in the offgas and collected by gravity from waste heat boiler.

The slag from fuming furnace will be sold out after granulation. The slag assay is shown in Table 5.

In accordance with slag assay, zinc and lead in fuming furnace slag are largely reduced comparing with feeding materials. When 16 t (dry base) materials are fed into fuming furnace for each campaign, 13 t slag is produced, 1.3 t dust is collected from bag filter and surface cooler, and 0.6 t dust is collected from boiler.

The mass balance is shown in Table 6.

In accordance with mass balance, the major metal output distribution is shown in Table 7.

Table 5 Composition of final slag

	Pb	Zn	Sb	S	Fe	SiO_2	CaO
Antimony smelting slag	0.08	1.01	0.70	0.83	23.25	29.86	23.52

Table 6 Mass balance

	Pb	Zn	Sb	S
Input (t)				
Antimony smelting slag	0.198	1.053	0.210	0.246
Output (t)				
WHB dust	0.056	0.261	0.017	0.014
BF dust and SC dust	0.120	0.576	0.107	0.044
Slag	0.010	0.131	0.085	0.108
Other loss	0.012	0.085	0.002	0.080
Total	0.198	1.053	0.210	0.246

Table 7 Major output distribution (%)

	Pb	Zn	Sb	S
WHB dust	28.28	24.79	8.10	5.69
BF dust and SC dust	60.61	54.70	50.95	17.89
Slag	5.05	12.44	40.48	43.90
Other loss	6.06	8.07	0.48	32.52
Total	100.00	100.00	100.00	100.00

In accordance with above table, Pb, Zn, and Sb can be collected and recovered from bag filter, but sulfur goes to offgas in the form of other loss. It can be seen that lead and zinc can be effectively collected and recovered during antimony smelting slag treatment by fuming furnace process, Pb recovery is about 95%, Zn recovery is about 88%, but Sb recovery is comparatively low which is impacted by low saturated steam pressure of antimony. When the operation temperature is 1250 °C, metals Pb and Sb are both in liquids, and metal Zn is volatilized in gas. In addition, saturated steam pressure of Sb is lower than that of Pb, so Pb is easier to volatile than Sb.

Conclusion

Zn, Pb, and Sb in antimony smelting slag can be effectively collected and recovered by fuming furnace process. The zinc recovery is around 88%, the lead recovery is about 95%, and the antimony recovery is about 60%. The fuming furnace process can help the plant to treat with such stored antimony smelting slag and can further collect and recover some zinc, lead, and antimony as well.

When cold slag is directly fed into fuming furnace, some cold slag goes to following dust collection system rather than falls into bath for reaction due to small particles. Therefore, agglomeration or screening should be considered to ensure the particle size of feeding materials. On the other hand, if the particle size of feeding materials is oversize or too big, the melting speed will slow down, which will have negative impact on production capacity. Therefore, the range of feeding materials particle size should be researched and studied during following operation.

If only cold slag is fed into fuming furnace, less cold slag should be fed into fuming furnace at the first half feeding period to avoid cold slag heaping up at the bottom of fuming furnace. In accordance with operation experiences in Guangxi raw antimony rich Polytron Technologies Inc, the feeding speed at the first half hour of feeding period should be controlled at 12 t/h, and the second half hour should be controlled at 20 t/h, which can keep normal operation.

References

1. He Q-X, Qin Y-L (2008) On zinc and indium recycle from blast furnace slag by fuming process. Jiangxi Nonferrous Met 22(2):29–32
2. Richards GG, Brimacombe JK, Toop GW (1985) Kinetics of the zinc slag-fuming process: part I. Industrial measurements. Metall Trans B 16(B):513–526

Studies on the Formation of Intermetallic Compound Layers in Co(W)–Zn Diffusion Couples

Tamara Ebner, Nadine Körbler, Stefan Luidold, Christoph Czettl and Christian Storf

Abstract Cemented carbides are a composite material which consists of a hard phase and a binder metal. At the end of their product lifecycle, these commodities can be recycled by the zinc process. In the first step of this method, the scrap reacts with molten zinc at elevated temperatures, which forms intermetallic phases with the binder (Co) resulting in a disintegration of the material. By now, the exact mechanism of this technique is not fully understood. Therefore, this research focuses on the transactions between the binder and the liquid zinc by analysing the formation of intermetallic phases via simultaneously varying decisive process parameters and the composition of the binder metal. Hence, this study provides information regarding the growth of intermetallic Co–Zn phases and emphasises the effect of dissolved tungsten in the binder on the formation of these compounds.

Keywords Cemented carbide · Recycling · Zinc process · Co–Zn phases · Tungsten

Introduction

Due to the high hardness, thermal and wear resistances, cemented carbides are applied in machining of metallic and non-metallic materials, chipless forming, wear parts, nozzels, etc., and therefore, are an indispensable tool in the machining and mining industries. The combination of metallic carbides or carbonitrides and a metallic binder results in a composite material, which exhibits a wide range of unique properties. In general, tungsten carbide (WC) serves as hard, wear-resistant and high-melting phase and is embedded in a tough and ductile metallic binder, such as Co. The microstructure is defined by the WC grain size as well as the content of the binder

T. Ebner (✉) · N. Körbler · S. Luidold
CD Laboratory for Extractive Metallurgy of Technological Metals, Montanuniversitaet Leoben, Franz-Josef-Straße 18, 8700 Leoben, Austria
e-mail: tamara.ebner@unileoben.ac.at

C. Czettl · C. Storf
CERATIZIT Austria GmbH, Metallwerk-Plansee-Straße, 6600 Breitenwang, Austria

© The Minerals, Metals & Materials Society 2020

A. Siegmund et al. (eds.), *PbZn 2020: 9th International Symposium on Lead and Zinc Processing*, The Minerals, Metals & Materials Series,
https://doi.org/10.1007/978-3-030-37070-1_57

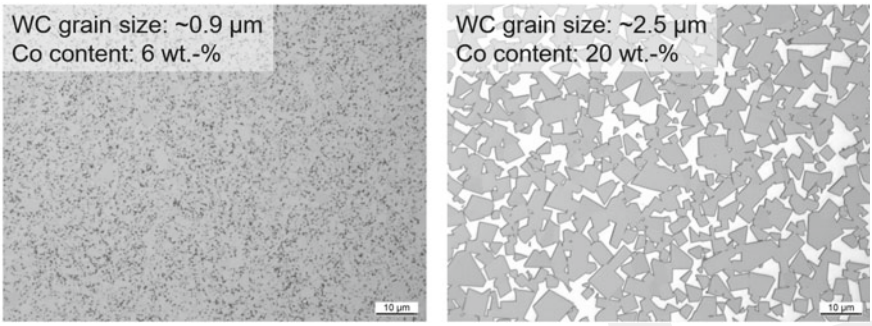

Fig. 1 Microstructure of straight WC-Co grades with different Co contents (Co: white area) and WC grain sizes (WC: gray area) [9]

material and strongly affects the characteristics of the composite. In commercially available WC-Co grades 4–16 wt% binder metal is applied typically. The grain size of tungsten carbides commonly accounts to values between submicron to tens of micrometers. Figure 1 depicts the microstructure of two different cemented carbide grades [1–8].

Cemented carbides are manufactured by a powder metallurgical route. At first, the required amounts of tungsten carbide and cobalt powders are blended and milled. Subsequently, a consolidation of the mixtures into various shapes by a wide range of methods takes place. The further processing of these green parts exhibits particular importance for the investigations of the present study, therefore, a more detailed description of the sintering is given subsequently [5, 10].

Sintering converts the pressed powder into a dense and compact material by treating the green parts at temperatures far below the melting point of the high-melting hard phase (WC, $T_{M,WC} = 2870$ °C) exceeding the eutectic point between WC and the binder material (Co, $T_{M,Co} = 1493$ °C) under vacuum conditions. A typical, commercially applied WC-10%Co cemented carbide is sintered at 1400 °C, because according to the WC-Co binary system, a liquid phase appears at temperatures above 1320 °C due to the occurrence of a low-melting eutectic. At these temperatures solid WC and liquid cobalt, in which WC is dissolved, are present. Upon cooling, the liquid phase solidifies containing 20–25% WC in solid solution. With decreasing temperature, the WC content of the binder declines, because WC precipitates on the surface of the undissolved hard phase resulting in a growth of the WC grains. In principle, the binder contains less than 1% WC in solid solution at room temperature [5, 10, 11].

The amount of remaining WC in the binder strongly depends on the carbon balance of the cemented carbide. Only in a narrow range of a molar W:C ratio of about 1, WC precipitates upon cooling. At a W:C ratio < 1, the formation of WC and C as graphite occurs, at ratios > 1 Co_3W_3C, the so-called η phase, forms. Both cases lead to undesired changes of the mechanical properties of the manufactured product. Hence, it is of particular importance to control the carbon content and keep it within

an optimum of 6–6.13 wt% C. Lower levels of carbon result in a higher amount of dissolved W in the binder phase, which increases the density of Co and furthermore leads to a deceleration of the solution-reprecipitation process during the sintering step. Therefore, the grain size of these cemented carbides remains smaller. Higher amounts of W in cobalt result in a stabilization of the cubic structure, which can not be converted to the hexagonal form by extensive annealing. Hence, cemented carbides with smaller grain sizes exhibit a higher content of fcc-Co in the binder [5, 12, 13].

At the end of their product life cycle, cemented carbides like inserts, drills, compacts from mining, oil and gas industry, wear parts, and hot rolls are recycled for example by the so-called zinc process. Due to the low energy consumption, high tungsten recovery, eco-friendliness, and high amount of treated scrap (12,000 t/a in 2010), these methods offer a number of advantages. In this study, we concerned ourselves with the fundamental mechanisms within the zinc process. Thus, a detailed description will be provided [14–16].

In the first step of the zinc process, the scrap is treated with molten or vaporous zinc at temperatures of 800–1050 °C in graphite crucibles under Ar or N_2 atmosphere, whereas the ratio of masses of cemented carbide to zinc typically corresponds to 1:1.3. The zinc infiltrates the material and forms various intermetallic phases with the Co binder according to the Co–Zn binary phase diagram. Compared to Co, these intermetallic compounds exhibit a higher volume. As a result, the initially compact and solid material swells and disintegrates to a porous cake. The reaction between Co and Zn corresponds to a diffusion controlled process, which proceeds from the cemented carbide surface inwards. The second step includes the removal of zinc from the disintegrated material by distillation based on elevating the temperature to 1000–1050 °C and applying of a vacuum in the range of 10 Pa. The product of the zinc process constitutes a porous and spongy cake with a zinc content < 10 ppm, which is milled and homogenized to obtain a high quality WC-Co powder. This zinc reclaim serves as feed material in the production of ready-to-press powder for cemented carbides [14, 15, 17, 18].

The exact mechanism of the progress of disintegration of the cemented carbides in the first stage of the zinc process is not known yet, therefore, the purpose of this investigation was to generate fundamental knowledge regarding the formation and growth of the intermetallic Co–Zn phases. As aforementioned, a wide range of cemented carbide grades with varying Co content and WC grain size exists. Since the structure of the feed material affects the disintegration of the material significantly, this study takes a step back and puts the focus on the interactions between the two main components Co and Zn, in order to gain basic understanding of the phase formation by avoiding the challenges arising from the application of WC-Co composite material. The tungsten content of the binder material strongly depends on the structure of the cemented carbide, the carbon balance, sintering process, etc.; hence, this study intended to describe the influence of the W content in Co on the Co–Zn phase formation and to allow conclusions regarding the impact on the recyclability of certain cemented carbide grades. Therefore, this article provides basic information concerning the growth of intermetallic Co–Zn phases and the effect of dissolved

tungsten in the binder on the formation of these alloys by contacting Co(W) testing material with liquid zinc at 600–750 °C for 0.5–8 h.

Experimental

To investigate the formation of intermetallic phases in the Co(W)–Zn system, tungsten containing Co testing material was contacted with liquid zinc at a certain temperature for various durations. Figure 2 depicts electron images, element distributions, and chemical analyses of the Co(W) staring materials (M1, M2 and M3) by scanning electron microscopy with energy dispersive spectroscopy (SEM/EDS). The measurements were performed with a JEOL JSM-IT300 SEM. The EDS analyses reveal W contents of 3.77 wt% in M2 and 4.01 wt% in M3. Since the testing material M1 only consists of cobalt, no mapping is given in this case. The solid metals were sliced into cubes with an edge length of 10 mm, which served as starting materials for this study.

The application of the statistical software Modde 12 assisted the creation of a design of experiments by a full factorial model according to the response surface methodology (RSM) and the generation of reliable data from the tests, which were conducted at different temperatures (600, 675, 750 °C), durations (0.5, 4.25, 8 h), and Co(W) testing materials (M1, M2, M3). The sliced Co(W) cubes were placed in a quartz crucible. Subsequently, 99.9999% pure zinc, heated to the target temperature was casted on the cube. The average ratio of Zn:Co accounted for 116:1, which allows an observation of the intermetallic Co–Zn layer formation far off the chemical equilibrium, since an excess of zinc is available for the reaction with cobalt. Afterwards, the crucibles were held for a certain duration in a nitrogen flushed resistance furnace at the desired temperature, followed by a cooling at ambient temperature and a metallographic preparation to enable the analyses by SEM/EDS and light optical microscopy (LOM) via the application of a Zeiss Axio Imager M1M. Figure 3 dis-

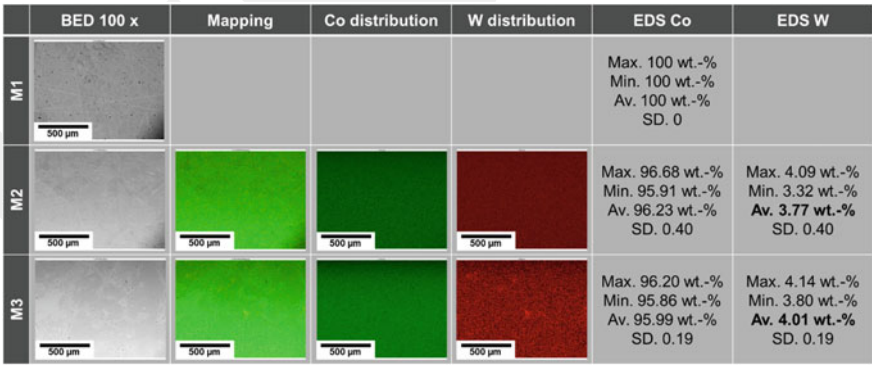

Fig. 2 SEM/EDS analyses of the three different testing materials (M1, M2, and M3)

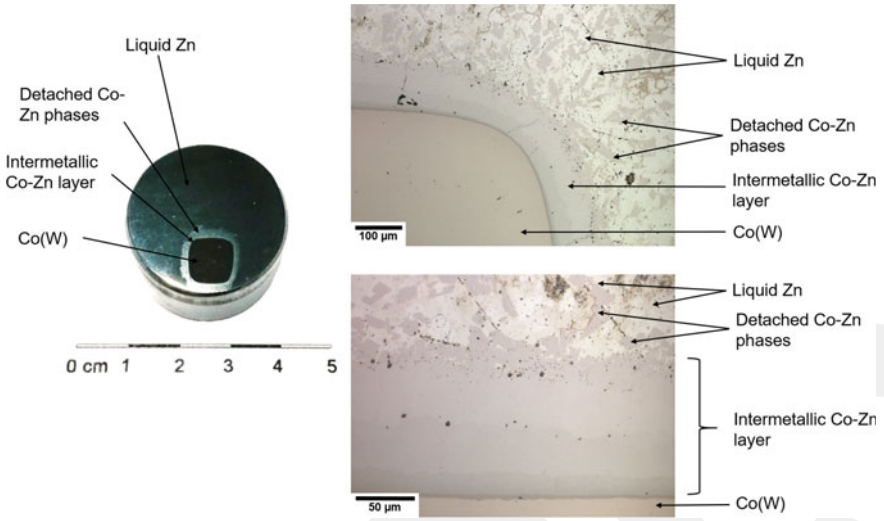

Fig. 3 Co(W)–Zn specimen [19] (left) and the resulting intermetallic Co–Zn layer at the interface of Co(W) and the solidified zinc with assignation of the different zones (right)

plays the resulting specimen, in which the remaining Co(W) cube and the intermetallic transition zone are visible (left), furthermore, light optical microscope images of the interface between Co(W) and the solidified zinc are given (right).

To provide basic information concerning the growth of intermetallic Co–Zn phases and the effect of dissolved tungsten in the binder on the formation of these alloys, the layer thickness of the transition zone was measured by LOM at various positions within a homogeneous area over the whole edge length of the remaining Co(W) cube, as shown in Fig. 4, to ensure a statistically representative result. The average of the individual lengths, also given in Fig. 4, was evaluated by the statistic software

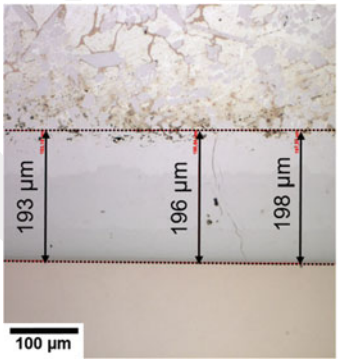

Test designation	Layer thickness [µm]	Test designation	Layer thickness, [µm]
600 0.5 M1	56.0	600 8 M2	190
675 0.5 M1	69.0	675 8 M2	121
750 0.5 M1	93.0	750 8 M2	47.0
600 4.25 M1	207	600 0.5 M3	63.0
675 4.25 M1	154	675 0.5 M3	65.0
750 4.25 M1	97.0	750 0.5 M3	115
600 8 M1	212	600 4.25 M3	76.0
675 8 M1	133	675 4.25 M3	130
750 8 M1	94.0	750 4.25 M3	105
600 0.5 M2	43.0	600 8 M3	101
675 0.5 M2	85.0	675 8 M3	112
750 0.5 M2	96.0	750 8 M3	180
600 4.25 M2	54.0	675 4.25 M2_2	211
675 4.25 M2_1	112	675 4.25 M2_3	192
750 4.25 M2	45.0	675 4.25 M2_4	213

Fig. 4 Extract for the thickness measurement of the resulting intermetallic layer (left) and average thickness of the resulting Co–Zn alloy layer (right) analysed and measured by LOM [19]

MODDE 12 Pro®. The test designation covers the applied temperature, duration, and testing material, thus, M1 was treated for 0.5 h at 600 °C in the experiment 600 0.5 M1. Since the transition zone between Co(W) and Zn exhibits an irregular surface, the measurement is afflicted with a certain error, which should be taken into consideration while evaluating the results.

Beyond that, SEM/EDS analyses of the transition zones were performed in order to determine the distribution of the elements Co, Zn, and especially W and to describe the behavior and the impact of the W content in Co on the Co–Zn phase formation. This allows us to draw conclusions regarding its impact on the recyclability of certain cemented carbide grades.

Results and Discussion

During the treatment of the Co(W) testing material with liquid zinc for a certain duration at a distinct temperature, the formation of Co–Zn phases occurs at the interface due to mutual diffusion processes of Co and Zn. At a certain point, these phases detach into the molten zinc. The simultaneously occurring growth and detaching of the intermetallic compounds affects the total layer thickness. In order to describe the growth of intermetallic Co–Zn compounds and the effect of dissolved tungsten in the binder on the formation of these phases, the average of the total layer thicknesses was evaluated by the statistic software MODDE 12 Pro®. The resulting prediction plots, given in Fig. 5, depict the effect of each parameter (temperature, duration, and W content) on the total layer thickness in µm. One of the parameters is varied, whereas the others are held constant at their average values regarding the experimental limits. Furthermore, the graphs display the lower and upper limits of the 95 ppm confidence interval for the model equation. The first plot in Fig. 5 displays the impact of the temperature on the total layer thickness at an average W content of 2.5 wt%. Each of the three curves shows a maximum at a certain temperature, which indicates, that the detaching of the Co–Zn phases into the liquid zinc overlaps the growth of the layers

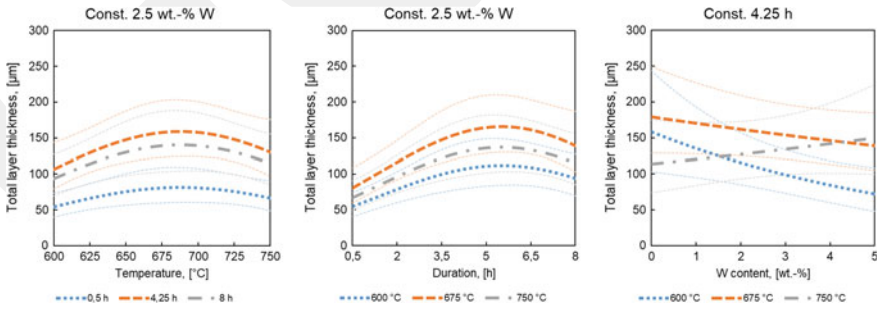

Fig. 5 Influence of the temperature (left), duration (middle), and W content (right) on the total layer thickness

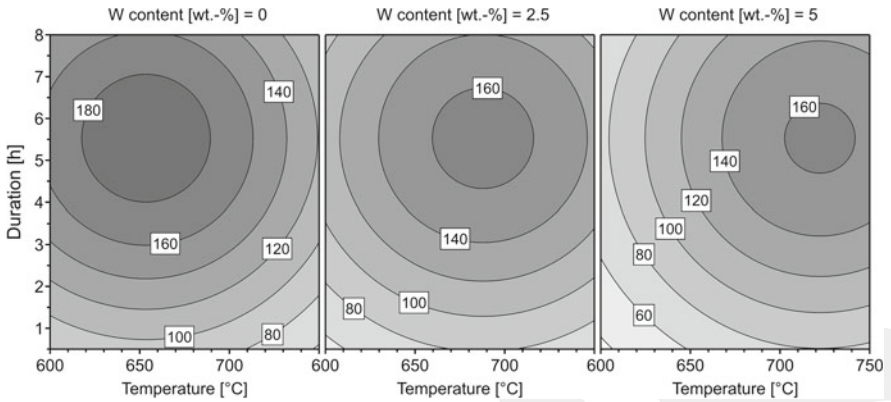

Fig. 6 Total layer thickness given in μm depending on temperature, duration, and W content of the testing material generated by Modde 12 Pro®

at the interface at a certain point and therefore, leads to a reduction of the thickness. The influence of the duration on the Co–Zn layer thickness (middle) shows a maximum between 5–6.5 h. Later on the detaching of intermetallic compounds constitutes the predominating process in the system compared to the growth of these phases at the interface. The last graph in Fig. 5 illustrates the impact of the W content of the starting material on the total layer thickness. The rising W content negatively affects the layer width at 600 and 675 °C, whereas this effect is more pronounces at 600 °C. Higher temperatures of 750 °C lead to a shift of the curve progression, resulting in a higher layer thickness with increasing W content.

The contour plot, given in Fig. 6, depicts the total layer thickness within the investigated limits and mirrors the impact of the investigated parameters displayed in Fig. 5. The influence of the temperature and the duration in the prediction plots showed peaks in the trends due to the interactions of the growth and detaching of the intermetallic compounds, which lead to round areas of maximum layer thicknesses. These maxima approximately lie at 5.5 h and shift to higher temperatures with increasing W content. This compilation presents a useful overview of the development of the layer thickness within the total parameter range, but pushes the effect of the individual parameters into the background. Therefore, this graph could lead to the assumption that a rising W content results in lower layer widths, whereas Fig. 5 describes the impact of tungsten in more detail and shows that its positive or negative effect on the outcome depends on the temperature at which the specimen is treated.

In order to describe the behavior and effect of tungsten in detail, SEM/EDS scans of the transition zones were performed. A chemical analysis of the interface enables the determination of the element distribution. The compilation in Fig. 7 depicts an example of a SEM image of the transition zone and the according element distribution for Zn (pink), Co (green), and W (cyan). The transition zone consists of different Co–Zn phases, which overlap each other and coexist in certain areas. As a result, a layered structure of Co and Zn is apparent in the mapping. Based on the element distribution,

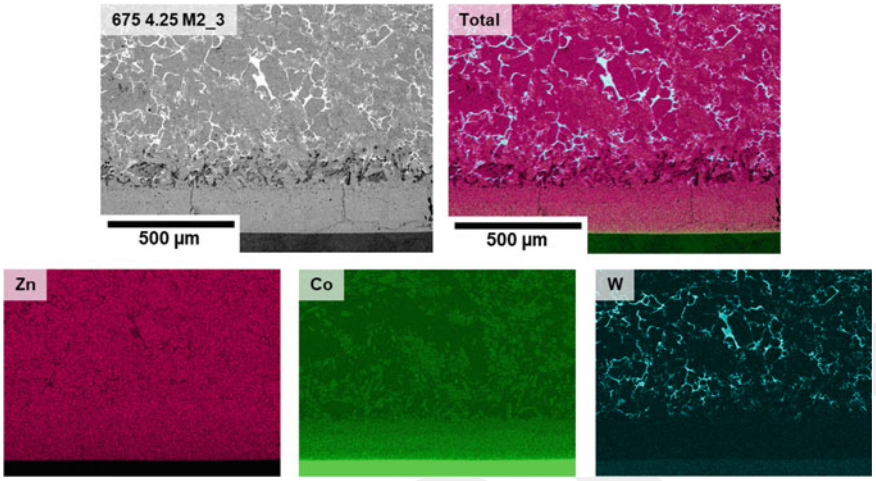

Fig. 7 SEM image and element distribution in the transition zone analysed by EDS

the detached Co–Zn phases outside of the adherent compound layer are also visible. Tungsten is homogeneously distributed in the starting material but it is striking, that it does not exist in the Co–Zn intermetallic layer. In contrast, tungsten accumulates outside of the compound layer in the area of liquid zinc. Figure 8 combines the images of the W distribution of the specimen, in which M3 served as starting material and underlines the fact that tungsten is practically nonexistent in the compound layer, but can be found in the outer areas.

By means of the generated SEM/EDS data, we conclude that the basis for the behavior of tungsten is explained by the fact that W and Zn do not form any intermetallic compounds, as, for example, stated by Köster and Schmid [20], but various phases exist between pure Co and Zn. Thus, as simplified given in Fig. 9, if the Co(W) starting material came into contact with liquid zinc, Zn atoms reach the interface at which Co and W atoms are available. The zinc atoms will react with the Co atoms to a Co–Zn compound and the W atoms stay unaffected. Due to the volume expansion and the progressive compound formation the W atoms are pushed together and transported outside of the Co–Zn phase leading to the development of a seam on the interface between the Co–Zn and the "liquid" zinc and to the observed W accumulations in outer areas. The SEM/EDS analyses given in Fig. 10 depict examples of the resulting W rich areas at the surface of the Co–Zn phases (600 0.5 M2) and W enrichments outside of the alloy layer (600 8 M2).

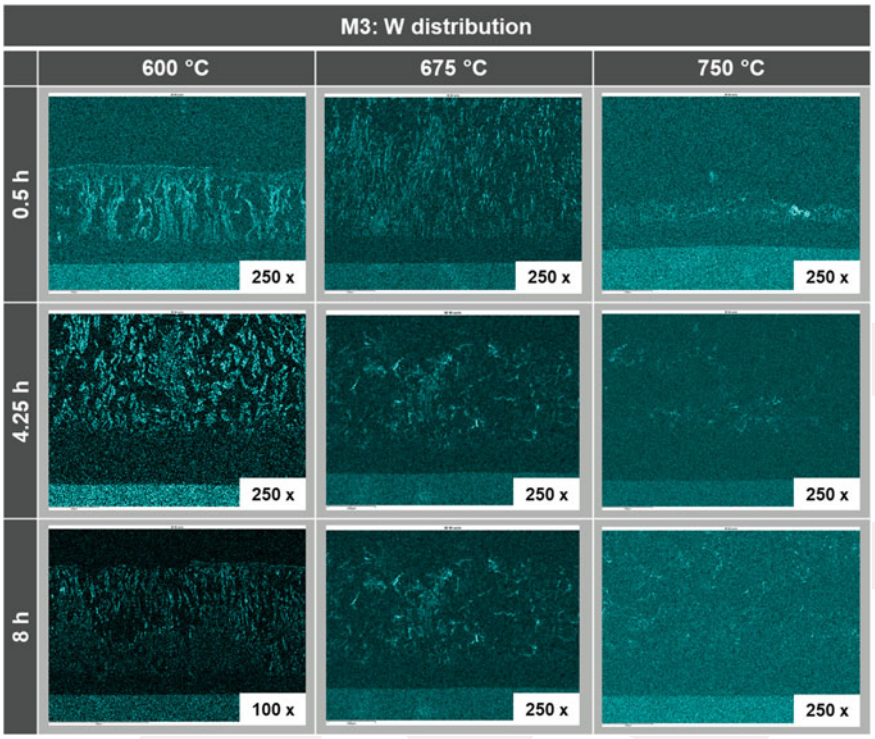

Fig. 8 W distribution in the transition zones of the experiments in which M3 served as starting material

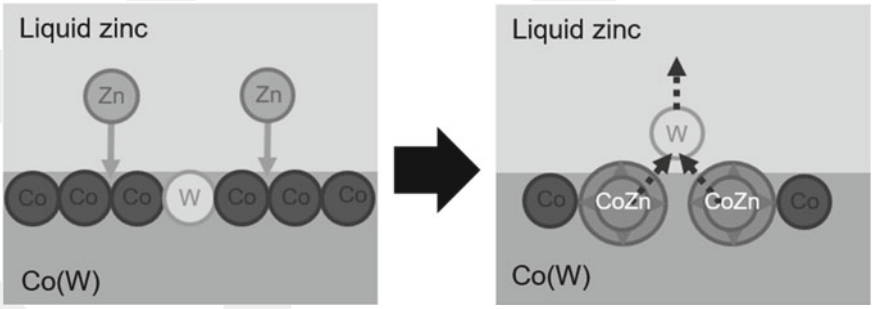

Fig. 9 Ongoing activities at the interface between Co(W) and liquid Zn

Conclusion and Prospects

The zinc process constitutes the most important direct recycling method for cemented carbides due to the low energy consumption, high tungsten recovery, eco-friendliness,

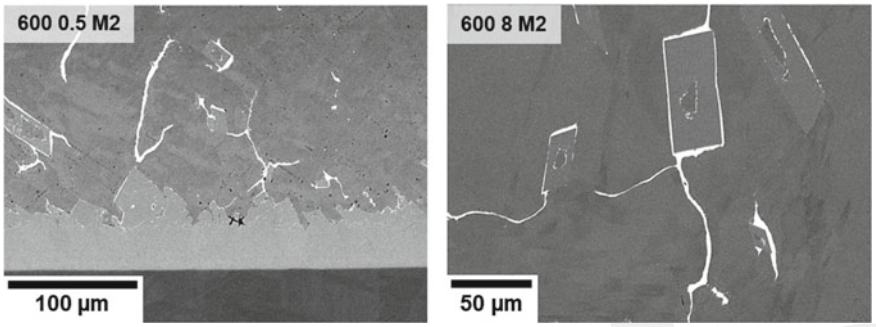

Fig. 10 SEM images of W accumulations (white) outside of the Co–Zn compound layer

and accordingly high amount of treated scrap. Since the exact mechanism of the progress of disintegration in the first step of the zinc process is not known yet, this study focused on the transactions between the binder and the liquid zinc by investigating the growth of intermetallic Co–Zn phases at 600–750 °C for durations of 0.5–8 h. In addition, we aimed to describe the effect of the W content in the binder material on the recyclability of certain cemented carbide grades by varying the W amount in the starting material (0, 3.77 and 4.01 wt% W).

The formation of intermetallic phases in the Co(W)–Zn system was examined by contacting Co(W) testing material with zinc according to a full factorial design of experiments. During the treatment of the binder material with liquid zinc, the formation of Co–Zn phases occurs at the interface due to mutual diffusion processes of Co and Zn. At a certain point, these compounds detach into the molten zinc. Both effects, the growth and detaching of the phases affect the adherent layer at the Co(W) interface. The thickness of this compound layer, consisting of different and overlapping Co–Zn phases, was measured by light optical microscopy and evaluated by assistance of the statistical software Modde 12 Pro®. Our study yielded that highest layer thicknesses occur at durations of approximately 5.5 h. Later on the detaching of the Co–Zn phases constitutes the predominant process in the system, leading to increasing layer widths with rising durations. In addition, we encountered high compound layer thicknesses at average temperatures of 675 °C. Concerning the optimal layer widths for the treatment of cemented carbides within the zinc process, it can be hypothesised that thicker compound layers decelerate the intrusion of the zinc into the material. As a result, the disintegration of the material slows down. In contrast, a certain layer thickness is required to enable the chipping of lamellar WC structures, which positively affects the speed of the reaction. On the one hand, thinner layers accelerate the intrusion of Zn into the binder because of a smaller diffusion resistance; on the other hand, they will not promote the chipping of the WC structures. The results of this study should provide the basis for the follow up study, which will focus on the disintegration of cemented carbides by liquid zinc, highlighting the effect of different microstructures by varying the tungsten carbide grain size, and cobalt content at temperatures of 600–750 °C.

As aforementioned, the tungsten content of the binder material in the cemented carbides strongly depends on its structure, the carbon balance, sintering process, etc. Therefore, a further purpose of this study was to investigate the influence of the W content in Co on the Co–Zn phase formation and draw conclusions concerning the recyclability of certain cemented carbide grades. Extensive SEM/EDS analyses revealed that the transition zone consists of different and overlapping Co–Zn phases resulting in a layered structure in which tungsten is practically nonexistent. However, tungsten accumulates outside of the Co–Zn layer in the area of liquid zinc. The ability of Zn to form alloys with Co and not with W allowed us to conclude that if Zn atoms reach the interface, they will react with Co atoms to a Co–Zn compound and the W atoms stay unaffected. As a result of the volume expansion and the progressive Co–Zn formation due to the mutual diffusion processes of Co and Zn, the W atoms are pushed together and transported outwards of the adherent layer. This process leads to the development of a W seam on the interface between the Co–Zn layer and the surrounding Zn as well as to tungsten accumulations in outer areas.

These locally higher W concentrations can constitute certain challenges regarding the recyclability of cemented carbides throughout the zinc process. If cemented carbides with a higher W content in the binder are treated by this method, these remaining W accumulations will stay in the material. As a consequence, these enrichments can lead to a blocking of pores between the WC grains, which impedes the distillation of Zn in the second stage of the process, especially for cemented carbides with low Co contents. Moreover, the remaining W enrichments may result in a higher stability of the generated product and cause problems in crushing and milling. Since the W and C content in the binder of cemented carbides rises with decreasing grain size and are enriched in a narrow seam in the binder in the vicinity of the WC/Co interface [13], the occurrence of W accumulations and challenges in recyclability are more likely to arise for cemented carbides with lower grain size. Future studies should provide further insight concerning the composition of W enrichments since tungsten can form various compounds with cobalt like Co_3W or Co_7W_6. If Co(W) came into contact with liquid zinc, it is assumed that Co partly reacts with Zn resulting in an enrichment of W until the exceeding of the solubility of tungsten in cobalt Co. Subsequently, the formation of Co–W phases takes place according to $Co_3W \rightarrow Co_7W_6 \rightarrow W$ with decreasing Co supply. Follow up investigations aim to clarify on which side of the reaction $3Zn + Co_3W \leftrightarrow 3CoZn + W$ the system is located, whereas Co_3W and CoZn represent arbitrary Co–Zn and Co–W phases, respectively. This study will involve thermodynamical approaches as well as XRD measurements for phase identification. Furthermore, the disintegration behavior of cemented carbides with higher W content in the binder throughout the zinc process needs to be focused since the current study indicates certain challenges regarding the recyclability due to the occurrence of W enrichments.

Acknowledgements The financial support by the Austrian Federal Ministry for Digital and Economic Affairs and the National Foundation for Research, Technology and Development is gratefully acknowledged.

References

1. Böhlke W (2002) Hartmetall—Ein moderner Hochleistungswerkstoff. Materialwiss Werkstofftech 33:575–580
2. Liedtke M, Schmidt M (2014) Rohstoffrisikobewertung—Wolfram. Deutsche Rohstoffagentur (DERA) in der Bundesanstalt für Geowissenschaften, Berlin
3. Prakash L (2014) Fundamentals and general applications of hardmetals. Comprehensive Hard Mater 1:29–90
4. Schubert WD, Lassner E, Böhlke W (2010) Cemented carbides—a success story. Internet: http://www.itia.info/assets/files/Newsletter_2010_06.pdf. Access 14 Jan 2015
5. Fang ZZ, Koopman MC, Wang H (2014) Cemented tungsten carbide hardmetal-an introduction. Compr Hard Mater 1:123–137
6. Bose A (2011) A perspective on the earliest commercial PM metal-ceramic composite: cemented tungsten carbide. Int J Powder Metall 47:31–50
7. Ceratizit Austria SA (2016) Rods performs. Internet: http://www.ceratizit.com/services/downloads/. Access 13 Oct 2016
8. Ceratizit SA (2016) Cutting tools. Internet: http://www.ceratizit.com/services/downloads/. Access 13 Oct 2016
9. Ebner T (2016) Konzepte zur Optimierung des Hartmetallrecyclings. Dissertation, Montanuniversität Leoben, Leoben
10. Franken E (2004) Handbuch der Gewindetechnik und Frästechnik. Publicis Corporate Publishing, Erlangen
11. Upadhyaya GS (1998) Cemented tungsten carbides. In: Materials science and process technology series. Ceramic and other materials–processing and technology. Noyes Publications, Westwood, NJ
12. Schedler W (1988) Hartmetall für den Praktiker. VDI-Verlag, Düsseldorf
13. Kellner FJJ, Hildebrand H, Virtanen S (2009) Effect of WC grain size on the corrosion behavior of WC–Co based hardmetals in alkaline solutions. Int J Refract Metal Hard Mater 27:806–812
14. Karhumaa T, Kurkela M (2013) Review of the hardmetal recycling market and the role of the zinc process as a recycling option. In: Proceedings of the 18th planseeseminar 1.138–1.148
15. Angerer T, Luidold S, Antrekowitsch H (2011) Technologien zum recycling von Hartmetall. World Metall ERZMETALL 64:5–14
16. Leal-Ayala DR et al (2015) Mapping the global flow of tungsten to identify key material efficiency and supply security opportunities. Resour Conserv Recycl 103:19–28
17. Lassner E, Schubert WD (1999) Tungsten: properties, chemistry, technology of the elements, alloys, and chemical compounds. Springer, US
18. Karhumaa T et al (2017) Effect of powder particle size distribution on the properties of submicron hard metal made of WC–Co zinc reclaim powders. In: Proceedings of the 19th Plansee Seminar (2017), RC2/1-RC2-12
19. Körbler Nadine (2019) Untersuchung des Schichtwachstums im Co(W)-Zn-System. Masterarbeit, Montanuniversität Leoben, Leoben
20. Köster W, Schmid H (1955) Über die Legierungsfähigkeit von Zink mit Wolfram und Molybdän. Zeitschrift für Metallkunde, 462–463

Effect of Oxidation of Zinc Powder on Purification of High-Cobalt and High-Germanium Zinc Sulfate Solutions

Leixia Zheng, Zhiwei Peng, Liancheng Wang, Lei Yang, Jie Wang, Wenxing Shang, Mingjun Rao, Guanghui Li and Tao Jiang

Abstract It is popular to use zinc powder to purify electrolytic zinc sulfate solution via replacement reactions between zinc and other metals in the solution. In view of easy oxidation of zinc that affects its purification performance, in this study, the influence of oxidation of zinc powder on the purification of high-cobalt and high-germanium zinc sulfate solutions was explored. The oxidation of zinc powder was simulated by adding ZnO. It was demonstrated that the oxidation percentages of fine and coarse zinc powders should not exceed 2.5% and 1.0%, respectively, for sufficient removal of cobalt from the solution, while for removal of germanium, the corresponding values were 0.5% and 0.2%. The results can be used for guiding purification of zinc sulfate solution to meet the requirements of subsequent operation.

Keywords Zinc sulfate solution · Purification · Zinc powder · Cobalt · Germanium

Introduction

The industrial application of metals has been increasing in the past decades, with about 60 metallic elements in use today [1]. Zinc is the fourth most widely used metal after iron, aluminum, and copper [2]. The production of refined zinc in 2017 was approximately 13 million tons [3], and the demand for zinc is expected to remain strong in the coming years due to the development of zinc-consuming industries [4]. Currently, more than 85% of zinc is produced by hydrometallurgical processes [5]. One of them is the roasting-leaching-electrowinning process [6].

The presence of metallic impurities in the zinc electrolyte is a major problem for the zinc electrodeposition process [7]. The existence of impurities greatly impacts the cathodic deposition of zinc, leading to a decrease in zinc current efficiency and to

L. Zheng · Z. Peng (✉) · L. Wang · L. Yang · J. Wang · W. Shang · M. Rao · G. Li · T. Jiang
School of Minerals Processing and Bioengineering, Central South University, Changsha 410083, Hunan, China
e-mail: zwpeng@csu.edu.cn

National Engineering Laboratory for High Efficiency Recovery of Refractory Nonferrous Metals, Changsha 410083, Hunan, China

© The Minerals, Metals & Materials Society 2020

A. Siegmund et al. (eds.), *PbZn 2020: 9th International Symposium on Lead and Zinc Processing*, The Minerals, Metals & Materials Series,
https://doi.org/10.1007/978-3-030-37070-1_58

changes in deposit morphology [8]. Cobalt and germanium impurities often remain during the zinc leaching process. They affect the quality of cathode zinc obviously and cause low current efficiency with high power consumption [9]. At present, the zinc-antimony salt purification method is widely used for removal of cobalt and germanium in the second-stage purification of zinc sulfate solution. Various parameters, such as cementation time, temperature, solution pH, concentration of activators, and concentration of zinc ions in the electrolyte, may have influence in this process [10].

Metallic zinc is a good reactant for purification of zinc sulfate solutions. In humid air, zinc powders stored in the natural state are easily oxidized to form dense oxide films on their surfaces. These oxide films will change the kinetic reaction characteristics during the two-stage solution purification process, thereby increasing difficulties in removing cobalt and germanium by zinc itself. Also, the zinc oxidation often causes increase of zinc consumption, difficult hydraulic filtration after purification, high filtration fabric consumption, and rapid accumulation of residue in the purification container which needs proper treatment in time.

The aim of this study was to determine the effect of oxidation of zinc powder on the purification of high-cobalt and high-germanium zinc sulfate solutions by adding zinc powder with different amounts of zinc oxide powder to the solutions for test.

Experimental

Materials

The main materials for the study, zinc powders and zinc sulfate solutions, were collected from a plant in China. Table 1 shows the main compositions of the two types of zinc powder samples. Their zinc contents were more than 95%, and the lead contents were higher than 1.5%. Figure 1 shows the phase compositions of the zinc powders. It was obvious that they were mainly consisted of metallic lead and zinc. The zinc sulfate solutions had the following compositions: 112.7 g/L Zn^{2+}, 3.1 mg/L Co^{2+}, 0.1 mg/L Ge^{4+}, 0.49 g/L Cd^{2+}, and 0.17 g/L Cu^{2+}. The other raw materials used for purification are summarized in Table 2.

Method

The zinc powders and zinc oxide were firstly pre-dried and then grounded using a ball mill. The Co^{2+} and Ge^{4+} concentrations were adjusted to 25 mg/L and 1 mg/L, respectively, using $CoSO_4 \cdot 7H_2O$ and GeO in the zinc sulfate solution. A 4 g/L zinc A with particle size less than 0.05 mm or zinc B with particle size between 0.074 and 0.1 mm, as well as 0.3 g/L $CuSO_4$ and 7.5 mg/L Sb_2O_3 were used for purification with the stirring speed of 300 r/min and pH 5.0. The addition of ZnO (0.5 wt%, 1

Table 1 Chemical compositions of zinc powders (wt%)

Zinc powder	O	Mg	Al	Si	S	Cl	Fe	Ni	Sb	Cu	Zn	Pb
A	2.35	0.07	0.03	0.03	0.03	0.005	0.01	0.001	0.01	0.01	95.98	1.47
B	2.89	0.06	0.03	0.02	0.02	0.005	0.02	0.001	0.01	0.01	95.43	1.50

GCRIS

wt%, 1.5 wt%, 2 wt%, and 2.5 wt%) was varied for purification of the solutions. The spectrophotometric method was used for measuring the cobalt and germanium ion concentrations to determine the purification percentages.

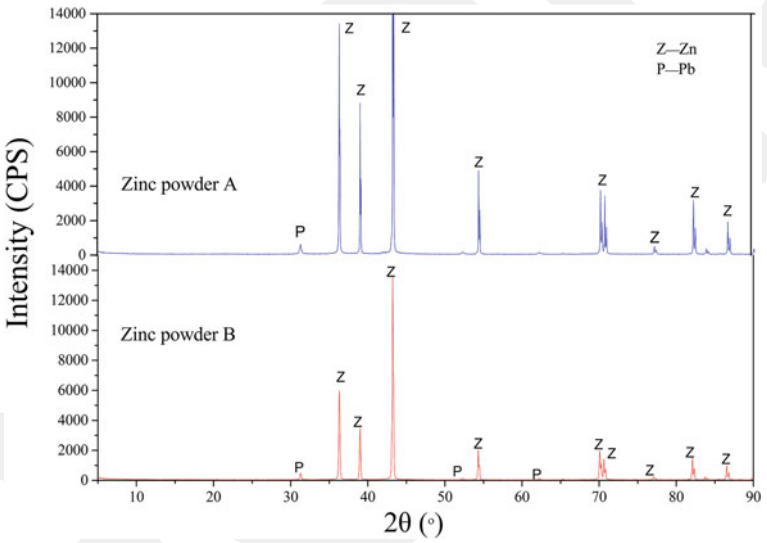

Fig. 1 XRD pattern of zinc powder

Table 2 Chemical reagents for purification

Material	Purity	Provider
Sb_2O_3	≥99.5%	Aladdin
$CuSO_4 \cdot 5H_2O$	AR	Sinopharm Chemical Reagent Co., Ltd.
$CoSO_4 \cdot 7H_2O$	≥99%	Aladdin
GeO	≥99.99%	Sinopharm Chemical Reagent Co., Ltd.
ZnO	AR	Ron Reagent Company

Results and Discussion

φ-pH Diagram of Zn-H_2O System Concerning Zinc Powder Replacement

The φ-pH diagram of the Zn-H_2O system is shown in Fig. 2. It is divided into three stable regions, namely Zn, Zn^{2+}, and $Zn(OH)_2$, which are involved in leaching, hydrolysis, purification, and electrolysis of zinc hydrometallurgy. Because the standard electrode potentials of Co and Ge are more positive compared with Zn, thermodynamically, Zn can replace Co and Ge in an acidic environment, and the replacement reaction product, Zn^{2+} does not cause secondary pollution. Therefore, almost all zinc hydrometallurgy plants choose zinc powder as a displacer.

In the Zn^{2+} ion stable region, when the solution temperature increases from 25 to 80 °C, the Zn^{2+} ion stable region decreases. In other words, the starting pH value of Zn^{2+} ion starts to decrease. When the Zn^{2+} ion concentration is 150 g/L, or 2.294 mol/L, the activity of zinc α_{Zn}^{2+} is 0.0853. The pH of the solution in contact with the zinc powder is higher than that of the bulk of the solution during the purification process. According to the literature, its value is generally 2–3. It was mainly attributed to the hydrogen ion consumption by zinc oxide, which changes the properties of zinc sulfate. Figure 2 shows that Zn^{2+} ions can hydrolyze on the surface

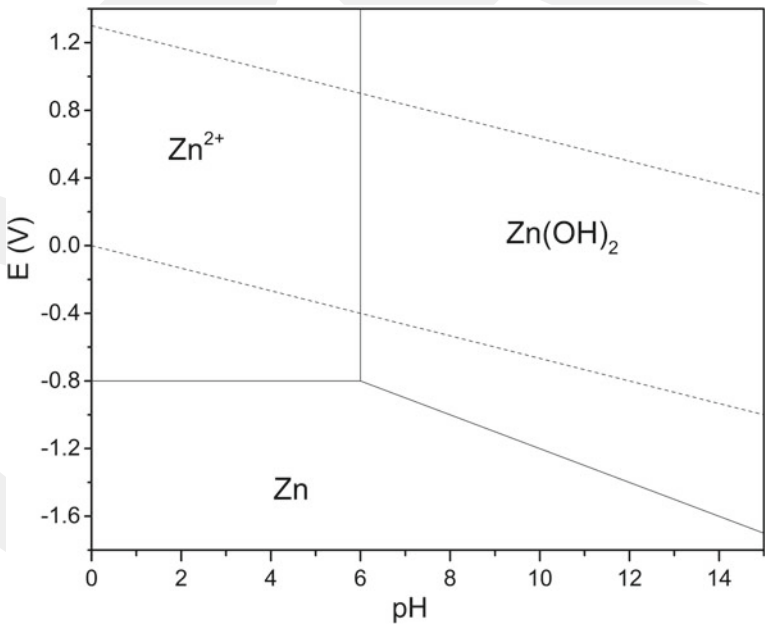

Fig. 2 φ-pH diagram of Zn-H_2O system

of zinc powder to form $Zn(OH)_2$, which will cover the zinc powder surface, inhibiting the discharge of cobalt and germanium ions and the diffusion of Zn^{2+} ions from the surface of zinc powder to the bulk of the solution. For this reason, the removal of cobalt and germanium is restrained.

Effect of Oxidation of Zinc Powder on Purification of High-Cobalt Zinc Sulfate Solution

In the acidic zinc sulfate solution, the zinc oxide film on the surface of the zinc powder can consume hydrogen ions in the solution, thereby changing the physicochemical properties of the solution. As the amount of zinc oxide increases, the zinc concentration in the solution increases. Figure 3 shows that with the increase of the oxidation of zinc powder A, the concentration of cobalt ions in the zinc sulfate solution gradually increased. When the oxidation percentage of zinc powder A was 2.5%, the concentration of cobalt ions in the solution was more than 0.8 mg/L after purification, which could not meet the requirement of subsequent electrolysis. When the oxidation of zinc powder B increased, the cobalt ion concentration in the zinc sulfate solution increased after purification. When the oxidation percentage of zinc powder B exceeded 1.0%, the cobalt ion concentration in the solution exceeded 0.8 mg/L. The use of zinc B for purification was more susceptible to oxidation which affected the removal of cobalt more seriously.

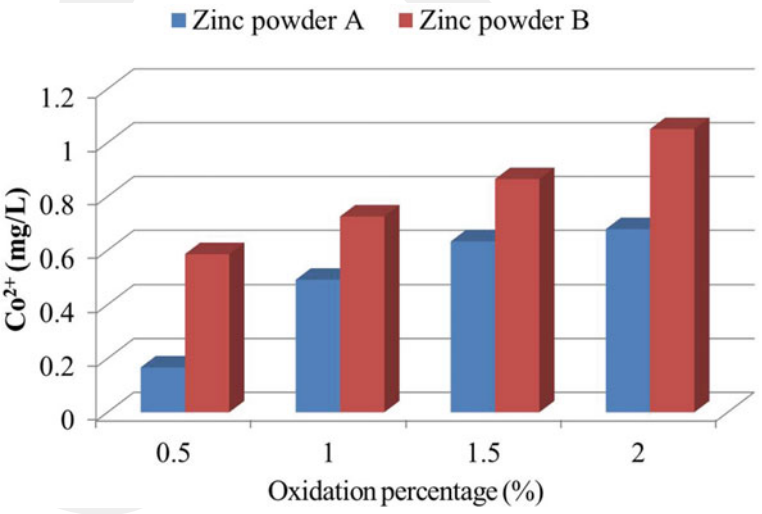

Fig. 3 Effect of oxidation of zinc powder on purification of high-cobalt zinc sulfate solution

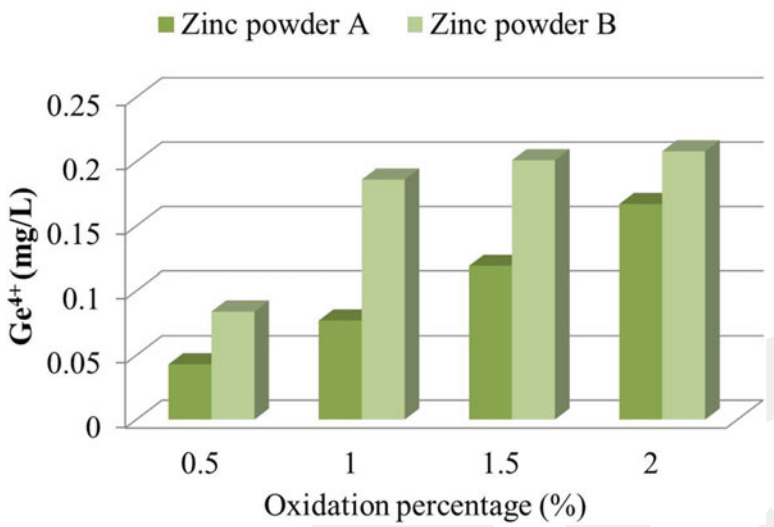

Fig. 4 Effect of zinc powder oxidation on purification of high-germanium zinc sulfate solution

Effect of Oxidation of Zinc Powder on Purification of High-Germanium Zinc Sulfate Solution

Figure 4 shows that with the increase of the oxidation of zinc powder A the concentration of germanium ions in zinc sulfate solution gradually increased. When the oxidation percentage of zinc powder A was 0.5%, the germanium ion concentration in the solution after purification was higher than 0.064 mg/L, which did not meet the requirement of electrolysis. Figure 4 also shows that as the oxidation of zinc powder B increased, the germanium ion concentration increased in the zinc sulfate solution after purification. When the oxidation percentage of zinc powder B exceeded 0.2%, the geranium ion concentration in the purified solution was higher than 0.064 mg/L. The oxidation of zinc powder B resulted in consumption of hydrogen ions. It inhibited the removal of germanium ions from the zinc sulfate solution. Meanwhile, the decrease of hydrogen ions hindered the formation of intermediates between hydrogen and germanium, affecting the removal of germanium from the solution.

Conclusions

In this study, the effect of zinc powder oxidation on the removal of cobalt and germanium from zinc sulfate solution was studied. When the amount of zinc powder is excessive, the removal of cobalt and germanium showed a downward trend with increasing proportion of zinc oxide. In the acidic zinc sulfate solution, the zinc oxide

film on the surface of the zinc powder can consume hydrogen ions in the solution, thereby changing the physiochemical properties of the solution. The oxidation percentages of fine and coarse zinc powders should not exceed 2.5% and 1.0% for removal of cobalt from the solution, respectively, while for removal of germanium, the corresponding values were 0.5% and 0.2%. When the zinc oxidation percentage was more than 2.5%, both zinc powders could not meet the requirement of purification.

Acknowledgements This work was partially supported by the Science and Technology Planning Project of Hunan Province, China, under Grant 2019RS2008 and the Fundamental Research Funds for the Central Universities of Central South University under Grant 2018zzts901.

References

1. Callister Jr. WD, Rethwisch DG (2018) Materials science and engineering: an introduction. Wiley, Hoboken, New Jersey, USA
2. Peng R (2005) Zinc metallurgy. Central South University Press, Changsha, Hunan, China
3. CNMIA (China Nonferrous Metals Industry Association) (2018) Website. Available online http://www.chinania.org.cn. Accessed on 7 June, 2019
4. Abkhoshk E, Jorjani E, Al-Harahsheh MS, Rashchi F, Naazeri M (2014) Review of the hydrometallurgical processing of non-sulfide zinc ores. Hydrometallurgy 149:153–167
5. NDRC (National Development and Reform Commission of the People's Republic of China) (2016) Zinc smelting industry cleaner production evaluation index system-compiling description 2017
6. Fuls HF, Petersen J (2011) Evaluation of processing options for the treatment of zinc sulphide concentrates at skorpion zinc. J S Afr Inst Min Metall 113:423–434
7. Luo J, Duan N, Fuyuan X, Jiang L, Zhang C, Ye W (2019) System-level analysis of the generation and distribution for Pb, Cu, and Ag in the process network of zinc hydrometallurgy: implications for sustainability. J Clean Prod 234:755–766
8. Sorour N, Zhang W, Ghali E, Houlach G (2017) A review of organic additives in zinc electrodeposition process (performance and evaluation). Hydrometallurgy 171:320–332
9. Mureşana L, Maurin G, Oniciu L, Gaga D (1996) Influence of metallic impurities on zinc electrowinning from sulfate electrolyte. Hydrometallurgy 43:345–354
10. Karlsson T, Cao Y, Colombus Y, Steenari B-M (2018) Investigation of the kinetics and the morphology of cementation products formed during purification of a synthetic zinc sulfate electrolyte. Hydrometallurgy 181:169–179

Part XVII
Environmental and Safety Practices I

GCRIS

ILTEC Technology—New Pathways Towards Safe and Effective Cooling

Andreas Filzwieser, Martina Hanel, Hans-Jörg Krassnig, Rolf Degel, Timm Lux and Alexander Bergs

Abstract It is the increasing demand for an economic and cost saving operation mode that requires effective cooling in order to achieve low refractory wear and good furnace lifetime, which is making cooling technology an important aspect of furnace operation. In addition, the requirements for safety are getting more and more into focus. However, the use of water—today's standard cooling medium—has major drawbacks as it can cause problems both during furnace start-up and operation, namely hydration problems, corrosion, and explosion. Not to forget the severe risks for the operators as well as economical damage in case of a malfunctioning water cooling system. With this new and patented cooling technology ILTEC and the ionic liquid IL-B2001 as the cooling medium, it is possible to realise a water-free cooling solution, and therefore, the door is wide open to rethink existing and conventional cooling solutions. Furthermore, there is also the chance to recover heat from the process in a more efficient way. However, since the technology is novel and unique, there are a lot of concerns and doubts regarding safety for plant operators and employees. The paper is intended to cover both: highlighting the enormous potential of the technology but also eliminating concerns mainly caused by rumour and unawareness.

A. Filzwieser (✉) · M. Hanel
Mettop GmbH, Peter-Tunner-Strasse 4, 8700 Leoben, Austria
e-mail: andreas.filzwieser@mettop.com

M. Hanel
e-mail: martina.hanel@mettop.com

R. Degel · T. Lux · A. Bergs
SMS Group GmbH, Eduard-Schloemann-Strasse 4, 40237 Düsseldorf, Germany
e-mail: rolf.degel@sms-group.com

T. Lux
e-mail: timm.lux@sms-group.com

A. Bergs
e-mail: alexander.bergs@sms-group.com

A. Filzwieser · H.-J. Krassnig · R. Degel
PolyMet Solutions GmbH, Peter-Tunner-Strasse 4, 8700 Leoben, Austria
e-mail: hans-joerg.krassnig@polymet-solutions.com

© The Minerals, Metals & Materials Society 2020

A. Siegmund et al. (eds.), *PbZn 2020: 9th International Symposium on Lead and Zinc Processing*, The Minerals, Metals & Materials Series,
https://doi.org/10.1007/978-3-030-37070-1_59

Keywords Cooling elements · Ionic liquid · Safe cooling · Safety · Steel making · Ferro-alloy · Electric furnace · Non-ferrous metals · Water-free cooling · Increased furnace availability · Novel cooling options · ILTEC

Introduction

All of us are aware of the risks when water is used as a coolant and placed in the vicinity of the liquid metal phase. Unsuitable design solutions or wrong operation modes of the furnaces or failures of refractories can cause a direct contact of water with liquid metal. The consequences can lead to equipment failures and vessel destruction but even worse to injuries and even fatalities. Over the past decades, countless incidences were reported. Fatal accidents caused by water coming into contact with liquid metal happen every year [1, 2]. With the novel ionic liquid cooling technology, virtually all negative effects of a water cooled system regarding safety are eliminated, and even additional benefits can be provided [3–5]. The fact that no explosion occurs when IL-B2001 gets in contact with molten metal results in a revolutionary solution for the metallurgical industry in terms of safety—new safety standards can be achieved.

History and Milestones of ILTEC

For the cooling application, the ionic liquid IL-B2001 was designed as a medium for meeting the typical requirements for this application. It took years of intensive research and a multitude of different ionic liquids to find the most suitable composition to meet the requirements for metallurgical aggregates. The major milestones of this patented cooling principle are as follows:

- 2009 The idea was born by Mettop
- 2009 Preliminary tests and patent application by Mettop
- 2009 Design of characteristic and creation of various ionic liquids
- 2012 Completion of laboratory tests and final launch of IL-B2001
- 2012 Industrial scale trials in Austria (Fig. 1)
- 2012 European certification for industrial application
- 2015 First reference at Nyrstar, Norway
- 2016 JV PolyMet Solutions of Mettop and SMS group
- 2017 Exclusive cooperation agreement with SMS group.

Fig. 1 Ionic liquid as being injected into a copper bath (for demonstration purposes)

Safety Aspects

After these years of research activities, the technology was matured and finally brought to industrial scale. The specially designed ionic liquid IL-B2001 combines several superior properties, and together with Mettop's knowhow in the field of cooling technology and cooler designs, a tailor-made solution can be provided for every customer. The ILTEC Technology is characterized by the following: Instead of water, the ionic liquid IL-B2001 is being used as cooling medium, which is liquid at room temperature and can be used at an operating temperature of up to 250 °C on a short-term basis and 200 °C on long term use. In case of a leak in the cooling system, the IL-B2001 will disintegrate into its components without a sudden increase in volume and without the formation of hydrogen. There will be no explosion when getting in contact with liquid metal, and so, safety can be guaranteed even in case of breakdowns. Furthermore, no cooler corrosion problems will occur, as the IL-B2001 can be used at higher temperatures (above the dew point of the exhaust gases). Due to the higher temperature (up to 250 °C), the dissipated heat can be recovered. This advantage will play a particularly important role in the future, not only in case of local legal requirements.

The two diagrams in Fig. 2 show the distribution of reported (!) accidents in the metallurgical industry [2]. It can be seen that almost three quarters of all accidents happening are related to the non-ferrous and ferro-alloy industry, which is an enormous number compared to the overall worldwide production from non-ferrous and ferro-alloy products compared to iron and steel industry. And furthermore, more than two-thirds of the accidents can be related to water as the cause of the accident.

When substituting water by the ionic liquid, damages will decrease dramatically, given in Fig. 3. Due to the lack of explosions, the economic damage, the environmental damage, and finally the personal damage will be substantially decreased, and the area of acceptable risk will move towards lowering the acceptability of consequences.

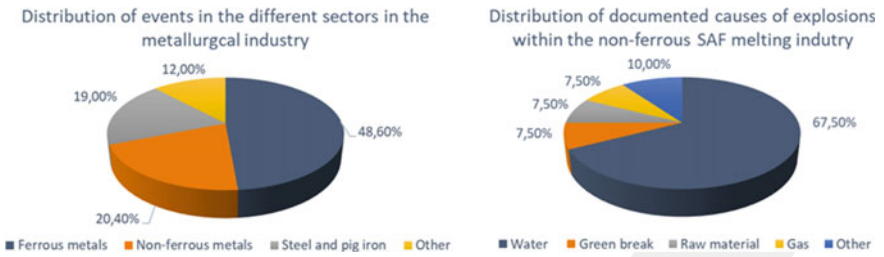

Fig. 2 Accidents happened, divided by sectors and reasons [2]

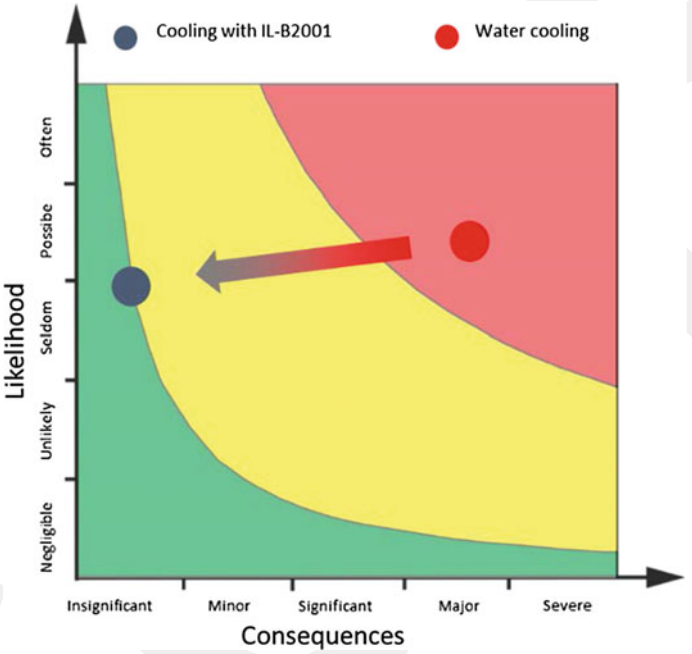

Fig. 3 Two-dimensional risk matrix and diminishment of fatal consequences by replacing water

Properties of the Cooling Medium IL-B2001

Basically, ionic liquids are salts, meaning that they consist solely of anions and cations. Caused by their poorly coordinated ions, many of them are liquid even at room temperature [6–8]. After years of intensive research, the most optimised ionic liquid for the use as a coolant was developed. The main properties of this special and unique ionic liquid, with the trade name IL-B2001, are given in Fig. 4.

Property	Symbol	Value	Unit	Range
Operation temperature		50 – 200	°C	ΔT = 150 °C
Short term stability		250	°C	
Decomposition temperature		450	°C	
Minimum operation temperature		< -10	°C	
Crystallization temperature		-30 – -40	°C	
Specific heat capacity	c_p	1.38 – 1.70	J/gK	50 – 200 °C
Density	ρ	1.25 – 1.14	kg/dm^3	50 – 200 °C
Dynamic viscosity	η	20 – 5	mPa·s	50 – 200 °C
Electrical conductivity	K	30 – 130	mS/cm	

Fig. 4 Physical properties (left) and optical appearance (right) of the cooling medium IL-B2001

Non-explosive

Whenever the decomposition temperature of 450 °C is reached and exceeded, the ionic liquid will completely decompose into its gaseous components. In order to demonstrate that there is no explosive reaction occurring when IL-B2001 gets in contact with hot liquid melt, tests have been performed at industrial scale operating furnaces. The ionic liquid was brought in contact with molten copper (at 1250 °C) as well as liquid steel (at 1750 °C) by pumping it beneath the bath level with a lance. In both instances, it could be seen that there is virtually no reaction. Only slight bubbling of the melt was apparent.

Non-corrosive

An essential characteristic of IL-B2001 is its chemical composition and the production procedure. A special and patented production process ensures that this ionic liquid is free of chlorine. As a direct consequence, IL-B2001 can be employed as a coolant in every conventional cooling element and most of common sealing materials. A variety of materials (steel grades, copper, aluminium, and nickel-base alloy) have been investigated at room temperature but also at higher temperatures comparable to the maximum operation temperature. Different construction and piping materials were brought in contact with the ionic liquid for 30 days and at temperatures of 200 and 250 °C. All results showed only a negligible weight loss indicating high corrosion resistance. These results are meanwhile proven at an industrial scale installation where the ionic liquid is used since more than 17 months at operation temperature between 150 and 180 °C. Ever since the start-up, there is no corrosion at the furnace shaft wall at all.

Non-flammable

When comparing the ionic liquid with thermal oils, as an example of an alternative cooling medium, in particular the different characteristic at high temperatures has to be emphasized. Some thermal oils are defined as non-flammable. However, once the oil temperature reaches and exceeds its ignition temperature, it starts to burn, and burning cannot be stopped even when the heat source is removed. This is in stark contrast to the behaviour of IL-B2001. Once the heat source is removed, the decomposition stops immediately.

Non-toxic, Not Harmful

Since the ionic liquid is used at industrial scale in plants, an uncomplicated handling and simultaneously guaranteeing health and safety of the operators are strongly desired. In this context, all the information is collected and described in the manual as well as the technical and safety data sheets and can be summarized as follows. The ionic liquid is REACH certified (registration number 01-2120086816-43-0000) and has a CAS number (143314-16-3). It is classified as a non-dangerous good and can be stored and transported without any special restrictions except preventing contact with water and open atmosphere. It shall not be classified as acutely toxic, the hazard class and category is 2, meaning skin irritating.

IL-B2001 shall not be classified as hazardous to the aquatic environment, but it is not biodegradable.

Broad Operation Temperature Range

The operation temperature is 50–200 °C, and hence, the temperature difference between inlet and outlet temperature of up to 150 °C is advantageous in terms of heat recovery as well as operational practice.

Cooling within this temperature range enables an adjustable intensity of cooling. A higher cooling element temperature can prevent the condensation of water vapour and, as a direct consequence, can minimize the risk of refractory hydration during heating up or due to leakages. Furthermore, a sufficiently high cooling element surface temperature avoids the formation of condensed corrosive compounds and dew point corrosion, respectively.

The fact that the IL-B2001 allows an outlet temperature of up to 200 °C makes the process suitable to be combined with a heat recovery system for direct usage or power generation under feasible conditions. This high absolute temperature and the extensive temperature range permit a heat recovery in an efficient way rather than being lost (creating steam instead of warm water). In case of continuously provided heat, the possibility of heat recovery through an Organic Rankine Circle (ORC)

exists, which is a technology not suitable for water as cooling medium. Under these circumstances, primary energy resources can be saved.

Heat Removal and Specific Heat Capacity

Considering properties like heat capacity, heat transfer coefficients, Reynolds number, and Prandtl number, it may be assumed that the amount of heat removed is less compared to a water cooled system. But comparing an IL-B2001 cooled application with the same application cooled by water, the entire system has to be taken into account. From industrial scale trials, it is known that the same amount of heat can be removed, either with water or with IL-B2001.

High Electrical Conductivity

Since the ionic liquid is per definition a salt and hence consisting of cations and anions the electrical conductivity is several orders of magnitude higher compared to water. This restricts the application of substituting water within induction furnaces or wherever a minimum electrical conductivity is required. To overcome this issue within induction furnaces, a special design of the cooling circuit has to be considered.

No Altering, Non-consumable

In contrast to other cooling media, IL-B2001 shows no ageing phenomena whenever the cooling circuit is closed, and the liquid does not get in contact with water or open atmosphere. This makes it a non-consumable good.

Hardware

In principle, the hardware consists of a tank, heat exchangers, and pumps as well as the necessary piping and instrumentation. The tank is filled with IL-B2001; the freeboard volume above the liquid level is purged with nitrogen in order to prevent hydration of the liquid through humidity in the air. Two identical pumps (one for redundancy) guarantee the flow of the IL through the entire pipe system, and two heat exchangers (one for redundancy) remove the heat into the secondary cooling circuit. Numerous measuring devices for temperature, flow, pressure, and differential pressure throughout the entire system guarantee fast leak detection. A variety of valves, adjusting wheels and shut-off devices, provide the necessary flexibility for all different operation modes. Assembly, installation, and start-up on site can be conducted within a few days (Fig. 5).

Fig. 5 3D model and picture of ILTEC facilities

General Application Overview for ILTEC in Metallurgical Plants

Basically, the ILTEC technology opens new windows for metallurgical furnaces for all the metallurgical fields of interest in both iron and steel technology as well as non-ferrous industry (Fig. 6).

Whenever water-cooled components are prevailing, the water cooling can be substituted by a closed loop ILTEC system and IL-B2001. The same amount of heat can be removed, and the prevailing piping and instrumentation system can be used. Hence, with the same cooling effect, a perfectly safe operation mode can be achieved. Research activities, and even more commercial operations, have proven that the ionic liquid IL-B2001 and the ILTEC Technology can lead to an industrial change regarding safety standards (Fig. 6).

Increasing Safety

Over the past years, more than 200 incidences with fatal damages in terms of health and equipment had been officially reported [9]. However, the real number is even higher. The elimination of the water in critical areas of furnaces, such as the cooling of metal bath area of smelters, will not essentially eliminate the risks for break downs but it greatly diminishes the consequential damages caused by explosions. Typical applications for improved safety are the furnace tapping areas, sidewall cooling, and cooled parts, which are exposed to the hot face and liquid metal.

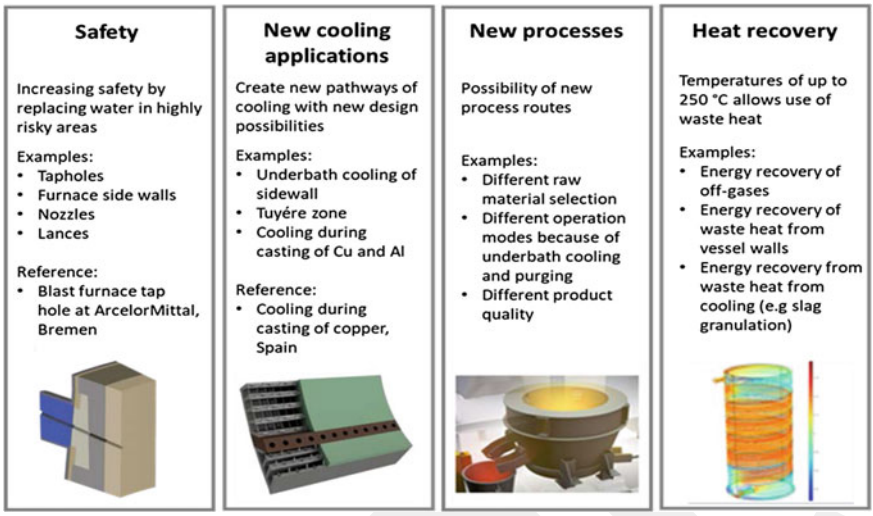

Fig. 6 Possible applications for the ILTEC Technology divided in four major topics

New Cooling Options

This revolutionary new approach allows cooling of areas where water cooling was hard to imagine so far, creating new solution paths. Cooling beneath bath level within side walls and cooling of tap holes and parts beneath liquid metal and slag levels in reaction vessels can now be realized. Combined with a new design of coolers and the concept of high intensity coolers working based on the freeze-lining concept [10–13], this technology allows novel and innovative cooling solutions. The refractory consumption is significantly reduced or stopped. This was successfully demonstrated in steel making electric arc furnaces and copper Pierce Smith converters. Furthermore, instruments, lances, etc., can be designed for continuous under-bath operation in metallurgical vessels.

New Processes, Equipment, and Instruments

ILTEC allows the design of new processes and furnace types as well as a new generation of equipment and instruments. Processes can be designed for higher temperature ranges. One example is the development for a new type of electronic scrap smelter, developed by Mettop/UrbanGold, which can take a much higher organic load (up to 50%) in the input material. We are currently involved in the development of new type of induction furnaces, to prevent explosion risks in the water-cooled induction loops. Additionally, new generation of instruments for on-line under-bath temperature measurements and chemical analysis is in the development phase.

Heat Recovery

The fact that ILTEC Technology with the ionic liquid IL-B2001 allows a temperature difference of 150 °C between inlet and outlet combined with the higher level of outlet temperature makes the process suitable to be combined with a heat recovery system for direct usage or power generation under feasible conditions. In conjunction with the higher absolute temperature, the extensive temperature range permits a heat recovery in an efficient way rather than being lost (creating steam instead of warm water).

In case of continuously provided heat, the possibility of heat recovery through an Organic Rankine Circle (ORC) exists, which is a technology not suitable for water as cooling medium. Under these circumstances, primary energy resources and hence CO_2 can be saved.

Industrial Scale Application

Several industrial scale applications have been realized or are in the stage of finalization (date of January 2019). The ILTEC Technology means improved safety in certain areas, and subsequently, this will have a positive influence on insurance policies (Table 1).

Summary and Outlook

The opportunities to increase furnace safety and operational efficiency by an industrially proven alternative cooling method are widely spread. It substantially improves the operation economically by increasing the life time of refractory lining, corrosion prevention, while offering the potential of high-quality heat recovery. The described examples demonstrate that it is possible to employ the new cooling technology as an alternative for replacing water in existing cooling circuits for different reasons. The replacement of the water in a tap hole is more or less driven exclusively by safety considerations. The approach of replacing the water in the side wall cooling combined with a new design of the cooler of an electric arc furnace (for example) is driven by the increase in lifetime of the refractory and an increase in furnace availability. This technology is, however, not only limited to these specific applications but could be used in multiple other applications where cooling with water is not possible mainly due to safety reasons.

Table 1 List of industrial scale applications (selection)

Application	Benefit	Supply lines	Overall flow capacity (m^3/h)	Country	Start-up
Cooling of shaft part of **plasma furnace**	Guaranteeing higher temperature inside the furnace for preventing corrosion from sulfuric acid	3	30	Norway	January 2015
Blast furnace tap hole	Increasing safety	2	30	Germany	October 2015
Test for cooling **EAF bottom shell**	Increasing the lifetime of refractory beneath bath level	2	20	Germany	Tests performed in Summer 2017
Cooling of **pipes of copper coolers** during the casting process	Increasing process safety and improve copper cooler quality	4	50	Spain	January 2018
Cooling of connection flanges at the **RH degassing vessel**	Increasing process safety and prevent warping	2	15	Austria	June 2018
Side wall cooling in cyclone furnace	Side wall cooling for improved lifetime in highly stressed burner area	2	10	Denmark	Test in May 2019

References

1. Filzwieser A, Konetschnik S, Filzwieser I, Wallner S, Preiss R (2014) Mettop's new cooling technology is the safest way to cool a furnace. In: COM 2014: 53rd annual conference of metallurgists, Vancouver, Canada, 28 Sept–1 Oct 2014, Paper No. 8622
2. Oterdoom HJ (2014) Furnace explosions with a focus on water. In: COM 2014: 53rd annual conference of metallurgists, Vancouver, Canada, 28 Sept–1 Oct 2014, Paper No. 8647
3. Verscheure K, Kyllo AK, Filzwieser A, Blanpain B, Wollants P (2006) Furnace cooling technology in pyrometallurgical processes. In: Sohn international symposium: advanced processing

of metals and materials, proceedings non-ferrous materials extraction and processing, vol 4
4. Voermann V, Ham F, Merry J, Veenstra R, Hutchinson K (1999) Furnace cooling design for modern high-intensity pyrometallurgical processes. In: TMS—the minerals, metals and materials society, 4th international conference, Copper, COBRE 99, Phoenix, AZ, pp 573–582
5. Wallner S, Filzwieser A, Kleicker J (2003) Some aspects for the use of water cooled furnace walls—water the best refractory? In: Proceedings Copper Cobre, vol 4, Book 1, pp 667–679
6. IoLiTec (2013) Wärmeträgermedien, Thermofluide. http://www.iolitec.de/Warmespeicherung-Transport/waermetraegermedien-thermofluide.html. Access on 20 Mar 2013
7. Joglekar H, Rahman I, Kulkarni B (2007) The path ahead for ionic liquids. Chem Eng Technol 7:153–168
8. Wasserscheid P, Welton T (2008) Ionic liquid in synthesis, vol 1. Wiley-VCH Verlag GmbH & Co. KGaA, Weinheim, Germany
9. Kobernuss DN (2015) Case studies of 23 workplace accidents and their causes. In: AISTech 2015 Proceedings, D&B Kobernuss Consultants, P.O. Box 440, Taberg, New York, 13471
10. Fallah-Mehrjardi A, Hayes PC, Vervynckt S, Jak E (2014) Investigation of freeze-linings in a nonferrous industrial slag. Metall Mater Trans B 45:850
11. Fallah-Mehrjardi A, Hayes PC, Jak J (2014) Understanding slag freeze linings. JOM 66(9):1654
12. Kyllo AK, Gray NB (2005) Composite furnace module cooling systems in the electric slag cleaning furnace. In: Proceedings of the EMC, p 1027
13. Nelson LR, Sullivan R, Jacobs P, Munnik E, Lewarne P, Roos E, Uys MJN, Salt B, de Vries M, McKenna K, Voermann N, Wasmund BO (2004) Application of a high-intensity cooling system to a DC-ARC furnace production of ferrocobalt at Chambishi. In: Proceedings: tenth international ferroalloys congress, Cape Town, South Africa, p 508

GCRIS

Review of Waste Water Treatment Technologies Used in Lead Recycling

James Dahlstrom, Joseph Grogan and Benjamin Rodrigue

Abstract Lead is one of the most highly recycled and regulated metals. Environmental controls around the processing of lead are extremely important to the continued success of lead as a means of energy storage in the circular economy. This paper describes the different chemistries and technologies used to control waste water emissions from secondary lead facilities. Commonly used technologies include iron co-precipitation, sulfide precipitation, and gypsum precipitation. Alternative technologies with future potential are also discussed.

Keywords ZVI · Cementation · Waste water · Selenium

Background

Secondary lead facilities in North America mainly produce lead alloys by recycling end of life lead bearing materials, primarily lead acid batteries. Throughout the lifecycle, these batteries undergo thousands of charge–discharge cycles that cause degradation of the electrically active components. As a result, lead and the alloying elements leach into the battery electrolytes, typically sulfuric acid. In battery recycling facilities, the electrolytes, along with process water introduced to the classification system, are collected and sent to an onsite water treatment process before discharging to a municipal water treatment center. Due to different processes upstream of the water treatment site, each recycler will have varying concentrations of lead, antimony, arsenic, selenium, and cadmium that must be removed from their waste water in order to meet compliance limits. All but cadmium are found in typical lead acid batteries. Lead-Cadmium alloys are not common in batteries, and instead cadmium enters the process when undesirable battery chemistries such a nickel-cadmium (NiCd) are comingled with the lead bearing materials and mistakenly enter the process in small quantities. The following metallic species are generally present in the treatable waste water circuit:

J. Dahlstrom · J. Grogan (✉) · B. Rodrigue
Gopher Resource, 685 Yankee Doodle Rd., Eagan, MN, USA
e-mail: joe.grogan@gopherresource.com

© The Minerals, Metals & Materials Society 2020

A. Siegmund et al. (eds.), *PbZn 2020: 9th International Symposium on Lead and Zinc Processing*, The Minerals, Metals & Materials Series,
https://doi.org/10.1007/978-3-030-37070-1_60

Pb(II), As(III), As(IV), Sb(III), Sb(IV), Se(IV), Se(VI), and Cd(II)

During discharge, the battery forms lead sulfate ($PbSO_4$) according to the following mechanism:

$$Pb + PbO_2 + 2HSO_4^- + 3H^+ \rightleftarrows 2PbSO_4 + 2H_2O \quad (1)$$

Over a battery's life, the charging process will become less efficient, leading to an increase in the concentration of lead sulfate that no longer participates in the electrochemical reaction. Eventually, this sulfate accumulation renders the battery unable to fulfill the application demand, and it is sent off for recycling. Some recyclers opt to desulfurize the battery's active materials in order to reduce the total SO_2 emissions that would result from the downstream smelting operations. The lead sulfate and sulfuric acid are typically converted in the desulfurization process using either sodium carbonate or sodium hydroxide:

$$PbSO_4 + Na_2CO_3 \rightarrow PbCO_3 + Na_2SO_4 \quad (2)$$

$$PbSO_4 + 2NaOH \rightarrow PbOH + Na_2SO_4 \quad (3)$$

$$H_2SO_4 + Na_2CO_3 \rightarrow Na_2SO_4 + H_2O + CO_2 \quad (4)$$

$$H_2SO_4 + 2NaOH \rightarrow Na_2SO_4 + 2H_2O \quad (5)$$

This results in an insoluble lead byproduct ($PbCO_3$ or PbOH) and soluble sodium sulfate (Na_2SO_4). The products are filtered to capture the lead bearing materials, with the sulfates sent downstream to the water treatment process.

Industrial Treatment Technologies

Most secondary lead operations rely on chemical precipitation techniques to remove heavy metals from solution. Chemical precipitation occurs by converting soluble metals to insoluble products via the addition of chemical reagents. In practice, recyclers employ one of three technologies:

(1) Iron co-precipitation
(2) Metal-sulfide precipitation
(3) Hydroxide precipitation via lime slaking.

Iron Co-precipitation

In an iron co-precipitation process, the pH of the waste stream is first lowered in conjunction with the addition of ferric salts to preferentially form ferric hydroxide $Fe(OH)_2^+$ [1]. This typically occurs at a pH around 3.0 with ORPs greater than 800 mV SHE as seen in Fig. 1. Under these conditions, arsenic and antimony will form the oxyanions $H_2AsO_4^-$ and SbO_3^-, which adsorb onto the iron surface (Fig. 2).

After oxyanion adsorption occurs, an alkali is added, usually sodium hydroxide, allowing for hydroxide precipitation of the remaining lead and cadmium [1]. The solution pH is controlled to minimize metal solubility. Solubility curves for common metal hydroxides are shown in Fig. 3.

Often times, environmental permit limits forbid recyclers from discharging waste water above certain pH levels. As a result, most lead recyclers operate their processes below a pH of 10 and instead increase reactor residence time to achieve the desired metal precipitation efficiency. Lastly, coagulants are added to increase precipitate mass and allow for better flocculation. The precipitates are then settled, and the resultant sludge is either dried for landfill, or recirculated in process.

Iron co-precipitation has advantages in the secondary lead industry because the process is relatively simple to control and the removal of arsenic/antimony can be

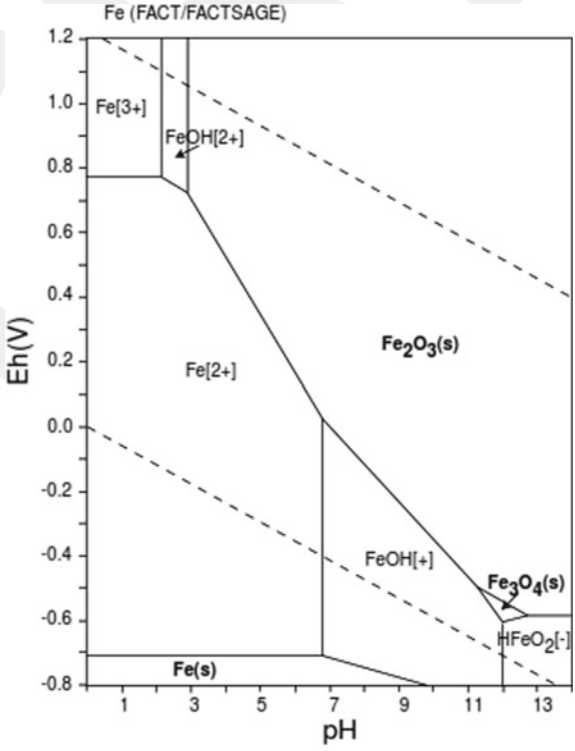

Fig. 1 Eh-pH diagram of iron species [2]

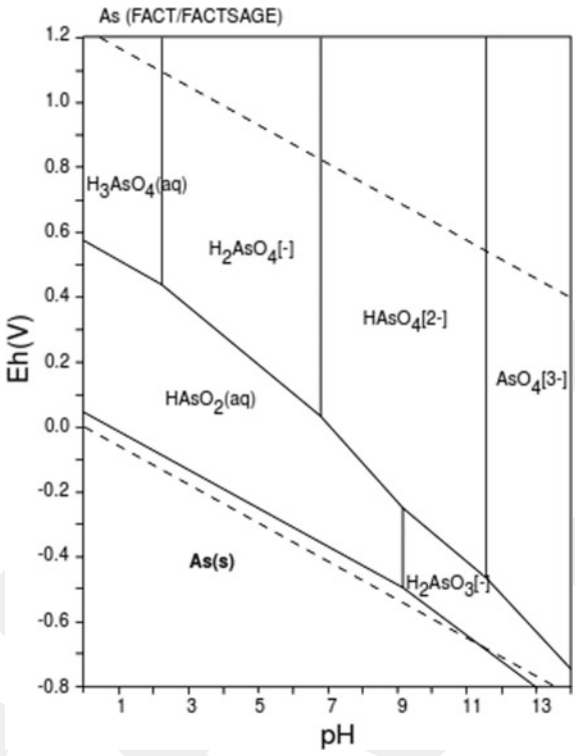

Fig. 2 Eh-pH diagram of arsenic species [2]

accomplished with lower reagent concentrations compared with alternative hydroxide precipitation systems. Overall, reactor volumes can be greater than competing technologies to enable longer residence times, ensuring metals can be reduced to desired levels [3].

Sulfide Precipitation

Sulfide precipitation treatment technologies operate with a similar concept to hydroxide precipitation, in reducing metal solubility through the introduction of sulfides, generally sodium sulfide, directly to the waste stream. An example of soluble lead precipitation by sulfide is shown below:

$$Pb^{2+} + S^{2-} \rightarrow PbS \tag{6}$$

For the majority of industrial applications, this is accomplished by a multi-stage treatment process that begins with increasing the waste water pH, generally above

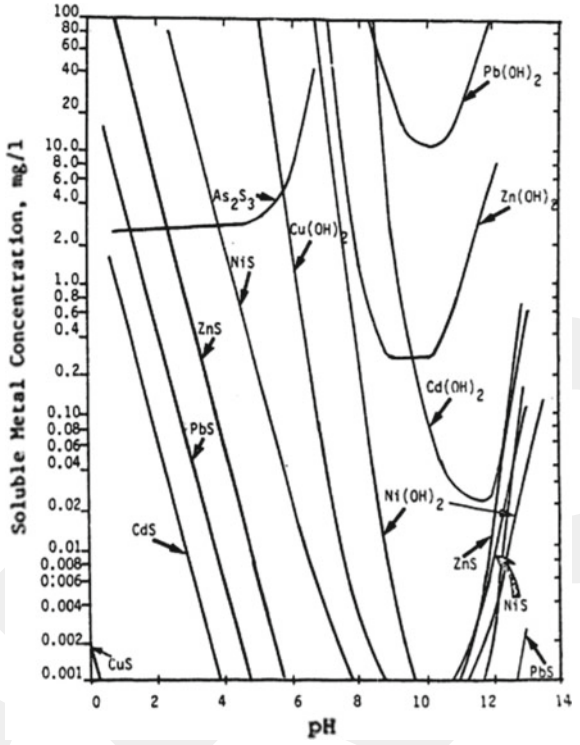

Fig. 3 Solubility of metal sulfides and hydroxides as a function of pH [3]

9.0. Next, sodium sulfide is added to react with the metal cations, forming a metal-sulfide precipitate [4]. Lastly, the precipitates are allowed to coagulate/flocculate, before being concentrated for disposal. The initial pH step is necessary for two main reasons. First, the metal-sulfide solubility of the major metal contaminants is minimized, as indicated in Fig. 3. Second, the sulfuric acid electrolytes, if not neutralized first, can react to form hydrogen sulfide as shown by the mechanism below [3]:

$$Na_2S + H_2SO_4 \rightarrow Na_2SO_4 + H_2S \tag{7}$$

Sulfide speciation as a function of pH is indicated in Fig. 4. The generation of hydrogen sulfide is negligible a higher pH's, however given its toxicity safety measures including localized ventilation are prudent when operating these types of systems.

Sulfide precipitation is able to remove metals quickly due to high nucleation rates and can be beneficial where residence times are short. System performance is less impacted by chelating agents than other technologies [6], and it is effective over a wide range of pHs. The main deterrent from selecting this technology is the potential for H_2S off-gassing [3].

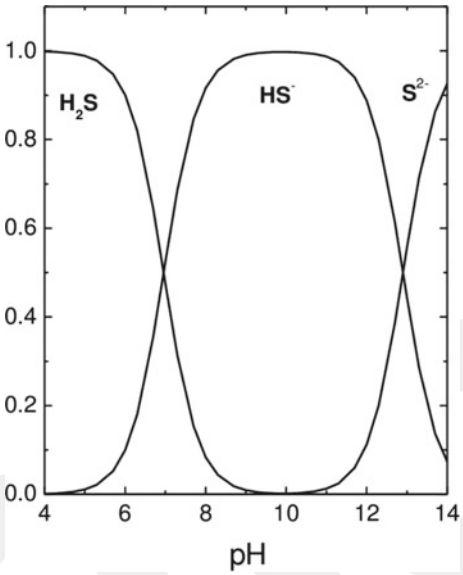

Fig. 4 Sulfide speciation as a function of pH [5]

In either the sulfide or iron co-precipitation processes, sodium sulfate is a major soluble byproduct. Typical effluent concentrations are in the range of 5–12 wt% [7], and depending on the facility location may require treatment to maintain compliance prior to discharge. Sodium sulfate is commonly used in the production of powdered laundry detergents, glass, and textiles. In order for it to be used in these applications, metal contaminants must first be separated.

Hydroxide Precipitation (Lime Slaking)

Lime slaking is a version of hydroxide precipitation that relies on large doses of hydrated lime, $Ca(OH)_2$, to precipitate the desired metals. An example of this is shown below:

$$Pb^{2+} + Ca(OH)_2 + H_2SO_4 \rightarrow Pb(OH)_2 + CaSO_4 + H_2 \quad (8)$$

Unlike iron co-precipitation, where antimony and arsenic are rapidly precipitated at lower pHs, aided by the use of ferric salts, hydroxide precipitation of these metals requires relatively large concentrations of alkali at longer residence times to effectively lower their solubility, and achieve similar treatment concentrations. Once precipitated, the metals are flocculated and thickened.

Lime slaking is advantageous because the treatment plants are easy to operate, and the primary reagent is not only inexpensive, but commercially available throughout North America. Unfortunately, the large lime concentrations needed to remove some

metals lead to large sludge volumes that can be problematic to dispose of [3]. In most cases, the sludge is dried to form gypsum, and either landfilled or valorized where possible.

Selenium Removal in Conventional Secondary Lead Iron Co-precipitation Systems

Of the metals discussed previously, all can be removed to a high degree with the exception of selenium. Although selenium has four potential valence states, secondary lead smelters are primarily concerned with the soluble species, selenite (4+) and selenate (6+) [7]. Selenium is a grain refiner in lead acid batteries and through various upstream separation and smelting processes, will eventually end up in the facilities waste water, with concentrations ranging from 1 mg Se/L [1] to 10 mg Se/L [8], with 40–60% of this being selenate [7].

Selenium can be removed via adsorption onto iron oxides and is regarded as the best demonstrated available technology by the USEPA for industrial waste waters [9]. Unfortunately, the mechanisms necessary to adsorb selenate onto the iron surface are impeded by similar reactions with sulfates [7]. Because of the high sulfate concentrations seen at secondary lead facilities, the removal of selenium from treatment waters is greatly limited by the selenate concentration.

Zero Valent Iron (ZVI) Reduction of Selenate

Gopher Resource, who currently utilize an iron co-precipitation system, began exploring alternative methods for selenate removal that would function under high sulfate concentrations. Table 1 indicates proven methods for the reduction of selenite and selenate.

Comparatively, the use of ZVI poses less physical and environmental risk than the alternative methods and as a result was selected for further testing. Under low

Table 1 Various reductants for aqueous selenium species [7]

Reductant	Selenite reduction	Selenate reduction
Sulfur dioxide [10]	X	Limited effectiveness
Ferrous salts [11]	X	Limited effectiveness
Hydrazine salts [10]	X	X
Chlorides in acidic medias [10]	X	X
Hydrogen peroxide in hot sulfuric acid [10]	X	X
Zerovalent iron [12]	X	X

pH, oxidizing conditions, sodium selenate and sodium biselenite are mainly present as shown in Fig. 5.

Proposed reduction reactions using ZVI for selenite and selenate are shown in Eqs. 9 and 10 [12]:

$$\text{Selenite:} \quad 3Fe^0 + SeO_3{}^{2-} + 6H^+ \rightarrow 3Fe^{2+} + Se^0 + 4H_2O \tag{9}$$

$$\text{Selenate:} \quad 3Fe^0 + SeO_4{}^{2-} + 8H^+ \rightarrow 3Fe^{2+} + Se^0 + 4H_2O \tag{10}$$

Laboratory scale experiments demonstrated selenate could be removed from high sulfate influents, and a pilot system was built to identify and resolve scalability problems. The pilot system consisted of five 55 G (208 L) continuously stirred tank reactors (CSTR), connected in series. The system was operated at an influent rate

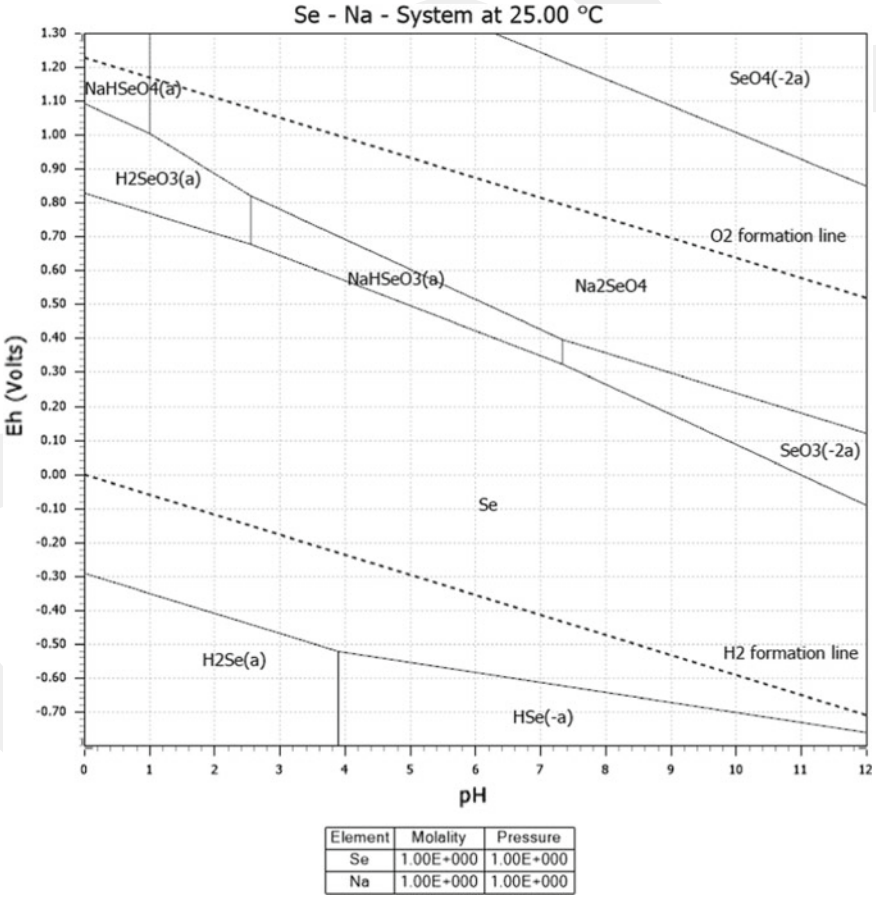

Fig. 5 Eh-pH diagram of the Na-Se-O system. Plotted using HSC 8 [7]

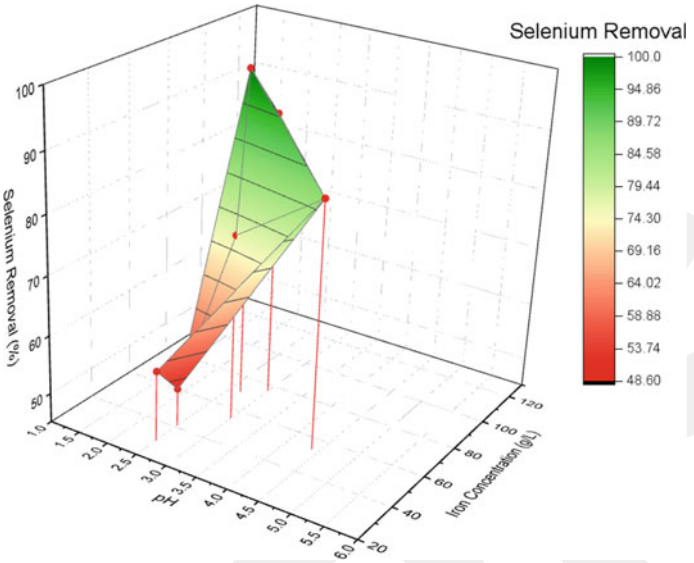

Fig. 6 Model response for selenium removal at different pH's and iron powder concentrations [7]

of 1 G (3.78 L) per minute (gpm), with ZVI introduced to the first CSTR using a volumetric feeder. Reactors 1–3 were operated under varying pH conditions, with reactors 4–5 at a pH of 9.5 to ensure remaining dissolved solids could precipitate, and be captured prior to discharge [7].

Throughout 2016 and 2017, pilot experiments were performed to determine the effectiveness of ZVI on selenium reduction. Results of the study indicate that ZVI concentration, ZVI particle surface area, and solution proton concentration have the greatest impact on selenate reduction [7]. Figure 6 shows the response model for selenium removal demonstrated through short duration pilot testing.

Longer duration, 5 day (100 h), testing was executed and found to reduce selenium (60% selenate) from an average concentration of 5.6 mg Se/L to <0.015 mg Se/L with peaks of 10+ mg Se/L under the following conditions [7]:

- ZVI suspended concentration—100 g Fe/L
- pH approximately—3.0
- Reactor residence time—60 min
- ZVI surface area—0.38 m^2/g

During this time period, the system demonstrated ZVI can also remove 100% arsenic, 98% lead, 69% cadmium, and 50% antimony. The addition of sodium hydroxide in reactors 4–5 ensured the remaining cadmium and antimony were precipitated before discharge (Table 2).

Table 2 Metals removal measured at critical stages in ZVI pilot [7]

Removal %	As (%)	Cd (%)	Pb (%)	Sb (%)	Se (%)
R1 Influent	0	0	0	0	0
R3 Effluent	100	69	98	50	64
R5 Effluent	98.9	96.3	99.9	99.6	99.7

Conclusions

Of the three technologies currently in use throughout the secondary lead industry, all are effective at removing lead, arsenic, antimony, and cadmium from high-sulfate waste water streams. Iron co-precipitation has the advantage of doing so with relatively low sludge volumes, and without the potential risk for noxious gas generation. Sulfide precipitation is a viable solution, especially where reactor volumes and residence times must be kept to a minimum. Lime slaking, while effective, is the least palatable of the options due to the generation of large sludge/gypsum volumes that are typically landfilled at great expense.

In areas where selenium discharge is a concern, iron cementation has been demonstrated effective at removing upwards of 100% selenate under appropriate operating conditions. As ZVI surface area can have a dramatic impact on the overall rate of selenium reduction, it is important to understand material consumption and availability when considering this type of system.

References

1. Bagby EL, West CM (1995) Treatment of an anionic metal by adsorption on iron oxides. In: Emerging technologies in hazardous waste management V, vol 607. American Chemical Society, pp 64–73
2. Research Center for Deep Geological Environments, “Atlas of Eh-pH diagrams”, National Institute of Advanced Industrial Science and Technology, Report No. 419, May 2005
3. Peters RW, Shem L (1993) Separation of heavy metals: removal from industrial wastewaters and contaminated soil. Argonne National Laboratories Energy Systems Division
4. Robinson AK, Sum JC (1980) Sulfide precipitation of heavy metals. United States Environmental Protection Agency, June 1980
5. Miloshova M, Baltes D, Bychkov E (2003) New chalcogenide glass chemical sensors for S^{2-} and dissolved H_2S monitoring. Water Sci Technol 47:135–140
6. Ku Y (1982) Sulfide precipitation of heavy metals: development of reaction equilibrium model and establishment of chelating agents effect on precipitation. M.S. thesis, University of Kentucky, Lexington KY
7. Grogan J, Dahlstrom J, Rodrigue B (2019) Removal of selenium as selenate from high sulfate brine waste waters. In: European metallurgical conference, vol 4, June 2019, pp 1359–1372
8. RMT (2009) Selenium in lead recycling wastewater. Presented at the Association of Battery Recyclers, Las Vegas, Nevada
9. Sandy T, Disante C (2010) Review of available technologies for the removal of selenium from water. North American Metals Council, June 2010

10. Bye R (1983) Critical examination of some common reagents for reducing selenium species in chemical analysis. Talanta 30(12):993–996
11. Sharrad MOM, Liu H, Fan M (2012) Evaluation of FeOOH performance on selenium reduction. Sep Purif Technol 84:29–34
12. McCloskey J, Twidwell L, Park B, Fallon M (2008) Removal of selenium oxyanions from industrial scrubber waters utilizing elemental iron. In: Proceedings of the sixth international symposium hydrometallurgy, pp 140–148

GCRIS

Optimization of Arsenic Removal Process in Waste Acid from Zinc Smelting Plant Based on Orthogonal Experiment

Tianqi Liao, Yongguang Luo, Hongtao Qu, Te Zhang, Jing Li, Yunhao Xi, Jingtian Zou, Libo Zhang and Kaihui Cui

Abstract In this paper, a method is determined, removing arsenic from waste acid by adding Fe and $CuSO_4$. Through orthogonal experiment, further analyze the effect of different factors on the removal rate of arsenic in this method. $L_{16}(4^4)$ orthogonal experiments were employed to optimize the process parameters such as temperature, the reaction time, pH, and the molar ratio of Fe/As. Based on the results of the orthogonal experiment, the optimum experimental conditions were that: pH was 8, temperature was 80 °C, the reaction time was 30 min, and the molar ratio of Fe/As was 8. Through range analysis, it was found that the order of significant factors for the removal rate of arsenic in waste acid is the reaction time > pH > temperature > the molar ratio of Fe/As. The optimized technological parameter was selected for verification experiment. Forming iron oxides and hydroxides via Fe powder corroded, which adopt adsorption coprecipitation mechanism to remove arsenic from waste acid. Besides that, the most important point is that Cu–Fe battery is formed by adding $CuSO_4$ to accelerate the corrosion of Fe powder, which could indirectly increase the efficiency of arsenic removal. From the above, the Cu–Fe battery and the adsorption

T. Liao · Y. Luo · J. Li (✉) · Y. Xi · J. Zou · L. Zhang (✉) · K. Cui
Faculty of Metallurgical and Energy Engineering, Kunming University of Science and Technology, Kunming 650093, Yunnan, China
e-mail: lijingkind@163.com

L. Zhang
e-mail: zhanglibopaper@126.com

T. Liao · J. Li · Y. Xi · J. Zou · L. Zhang · K. Cui
Kunming Key Laboratory of Special Metallurgy, Kunming University of Science and Technology, Kunming 650093, China

State Key Laboratory of Complex Nonferrous Metal Resources Clean Utilization, Kunming University of Science and Technology, Kunming 650093, Yunnan, China

National Local Joint Laboratory of Engineering Application of Microwave Energy and Equipment Technology, Kunming 650093, Yunnan, China

Key Laboratory of Unconventional Metallurgy, Ministry of Education, Kunming 650093, China

Y. Luo · H. Qu · T. Zhang
Yunnan Chihong Zn&Ge Co., Ltd., Qujing, Yunnan 655011, China

© The Minerals, Metals & Materials Society 2020

A. Siegmund et al. (eds.), *PbZn 2020: 9th International Symposium on Lead and Zinc Processing*, The Minerals, Metals & Materials Series,
https://doi.org/10.1007/978-3-030-37070-1_61

process are very important to arsenic removal, which have close connection with the reaction time and pH. It is consistent with range analysis of orthogonal experiment.

Keywords Waste acid · Orthogonal experiment · Adsorption coprecipitation

Introduction

Arsenic is an acutely harmful element, chronic exposure to as causes severe illness such as cancer. Arsenic contained in minerals enters metallurgical system, during the smelting process of metal. Acidic wastewater containing arsenic known as waste acid is obtained from washing and purifying smelting flue gas [1–4]. Waste acid directly drained without removal arsenic has considerable damage to the ecological environment and could cause irreversible harm to the human. Effective treatment of removal arsenic from waste acid is imperative [5–8].

At present, a variety of methods have been used to remove arsenic from waste acid, absorption, sedimentation, ion exchange, filtration, and so on [9, 10]. In the industrial, two common methods of removing arsenic from waste acid are precipitation method and sulfurized method. Precipitation method is safe and economical but produces a large amount of sludge needing further disposal. Sulfurized method reduces the amount of reagent added. But it produces toxic gases and is costly. Both two methods are multi-stage processes [11–14]. In the paper, the method of removing arsenic from waste acid by adding Fe and $CuSO_4$, is used for study.

Orthogonal test design is a design method for studying multi-factor and multi-level. It is based on the orthogonality to select some representative points from the comprehensive test. These representative points are uniformly dispersed and neatly comparable. The orthogonal design can study factors simultaneously in a single set of experiments with fewer experimental units. By analyzing the results of orthogonal experiments, the main influencing factors and optimal experimental conditions can be obtained. It has been extensively used in various fields due to its efficiency and analysis result [15, 16]. Therefore, orthogonal experiment was used in this paper to analyze the effects of different factors on the method. By analyzing the results of orthogonal experiments, the primary and secondary factors were distinguished and the optimal experimental conditions were determined in this paper. The experimental mechanism was also explored in this paper, which laid the foundation for practical application.

Experimental Section

Experimental Materials

The waste acid used in the experiment was obtained from zinc smelting plant located in Yunnan, containing heavy metal ions and harmful elements such as cadmium, lead, fluorine, chlorine, and arsenic. The concentration of waste acid from a zinc smelting plant in Yunnan was shown in Table 1, and the initial pH of waste acid was 2.1.

Orthogonal Array Experimental Design

Concerning relevant literature and combined with preliminary research, temperature (factor *A*), the reaction time (factor *B*), pH (factor *C*), and the molar ratio of Fe/As (factor *D*) were chosen for the present study. Four different levels were selected for each factor. There have been no reports of the interaction among the four parameters in the literature which we have read, and we have not found the interaction among the four parameters in our previous studies. Therefore, the interaction among the four parameters has not been considered in this paper. An orthogonal array of $L_{16}(4^4)$ was used to assign the considered factors and levels in this study. The experimental factors and their corresponding levels were illustrated in Table 2. The designed orthogonal array was described in Table 3.

Table 1 Concentrations of waste acid elements

Composition	Cd	Cl	Pb	As	F
Concentration (mg/L)	101.7	829	116	629	456

Table 2 Orthogonal experimental factors and levels

Level	Factors			
	A Temperature (°C)	*B* The reaction time (min)	*C* pH	*D* The molar ratio of Fe/As
1	20	15	6	4
2	40	30	8	6
3	60	45	10	8
4	80	60	12	10

Table 3 Orthogonal array $L_{16}(4^4)$

No.	*A* Temperature (°C)	*B* The reaction time (min)	*C* pH	*D* The molar ratio of Fe/As	The residual concentration of As (mg/L)	The removal rate of As (%)
1	1	1	1	1	219	65.2
2	1	2	2	2	77	87.8
3	1	3	3	3	187	70.3
4	1	4	4	4	254	59.6
5	2	1	2	3	82	87
6	2	2	1	4	156	75.2
7	2	3	4	1	308	51
8	2	4	3	2	298	52.6
9	3	1	3	4	212	66.3
10	3	2	4	3	112	82.2
11	3	3	1	2	187	70.3
12	3	4	2	1	178	71.7
13	4	1	4	2	145	76.9
14	4	2	3	1	89	85.9
15	4	3	2	4	68	89.2
16	4	4	1	3	246	60.9

Results and Discussion

Range Analysis

In a range analysis, there are three parameters, K_{ij}, $\overline{K}_{ij}$, and R_j. K_{ij} is defined as the sum of the indexes of all levels in each factor j. $\overline{K}_{ij}$ is the average value of each experimental factor at the same level i. R_j is defined as the range between the maximum and minimum value of $\overline{K}_{ij}$. $\overline{K}_{ij}$ is used for evaluating the importance of the factors, and a large R_j means a crucial factor.

$$R_j = \max(\overline{K}_{ij}, \overline{K}_{ij}, \overline{K}_{ij}, \overline{K}_{ij}) - \min(\overline{K}_{ij}, \overline{K}_{ij}, \overline{K}_{ij}, \overline{K}_{ij})$$

According to the orthogonal array $L_{16}(4^4)$, sixteen experiments were carried out and when the experimental index was lower, the experimental effect was reversed. Experimental indicators mean the residual concentration of arsenic. The results of residual concentration of arsenic are in Table 3. Range analysis results were shown in Table 4. As mentioned that the experimental indicators as small as possible, the value of $\overline{K}_{ij}$ was smaller, the better the effect of arsenic removal.

Therefore, the best level for the four factors is as follows: temperature was 80 °C, the reaction time was 30 min, pH was 8, and the molar ratio of Fe/As was 8, since

Table 4 Range analysis table

$\overline{K}$	Control factors			
	A	*B*	*C*	*D*
$\overline{K}_{1j}$	184.25	164.5	202	198.5
$\overline{K}_{2j}$	211	86.8	101.25	176.75
$\overline{K}_{3j}$	172.25	187.5	196.5	156.75
$\overline{K}_{4j}$	137	244	204.75	172.5
R_j	74	158	103.49	41.75

the min $\overline{K}_{ij}$ was ($A_4B_2C_2D_3$). Meanwhile, a larger R_j means the factor has a bigger impact on the removal of arsenic. In Table 4, the decreasing order $R_B > R_C > R_A > R_D$ indicates that importance of factors is as follows: the reaction time > pH > temperature > the molar ratio of Fe/As. In addition, due to the reaction time and pH had little difference in extremum analysis, those two elements were the main influencing factors. The temperature and the molar ratio of Fe/As had little influence on the removal rate of arsenic. This could also be proved from Fig. 6. Overall, the change in temperature has little effect on ΔG^{θ} in the chemical Eqs. (1, 2 and 3) of iron.

To further explore the influence of various factors on the method, the relationship between the levels of each factors and the removal rate of arsenic was shown in Fig. 1. Figure 1a was effects of temperature on the rate of arsenic removal. With the temperature rose, increased the electron exchange per unit time and speeded up the corrosion rate of Cu–Fe battery. The removal rate of arsenic also has slight increase in general. Final confirmation of the optimal temperature was 80 °C, but the effect was not significant.

As can be seen from Fig. 1b, Fig. 1b was effects of the reaction time on the rate of arsenic removal. The arsenic removal rate increased from 73.85 to 82.78% with the reaction time increasing from 15 to 30 min, then fell after more than 30 min, and the fluctuation range was extensive. The reaction time was the main element affecting the arsenic removal rate. In the adsorption process, the adsorption capacity increases rapidly with the reaction time. After more than 30 min, the adsorption speed decreases, the resolution speed increases, and the resolution value exceeds the adsorption value, so the optimal arsenic removal rate was reached at 30 minutes.

From Fig. 1c effects of pH on the rate of arsenic removal showed that with the rise of pH, the removal rate of arsenic reaches a maximum value at pH value 8. Because of different pH, iron existed in different forms in solution, Fe(II) and Fe(III) at pH 7.6 and 2.7, respectively, formed iron oxides and hydroxides precipitation. When the pH is 8, more precipitates can be formed, thereby increasing the adsorption coprecipitation effect are increased. For another, since the pH was neutral, iron powder corrosion was more likely to form hydroxide adsorption. In a strong acidity or strongly alkaline solution environment, existed the phenomenon of mutual repulsion of charges, which negatively affects the adsorption process. In addition, Fe reduces H instead of Cu under acidic conditions, preventing the formation of Cu–Fe battery. pH of 8 was

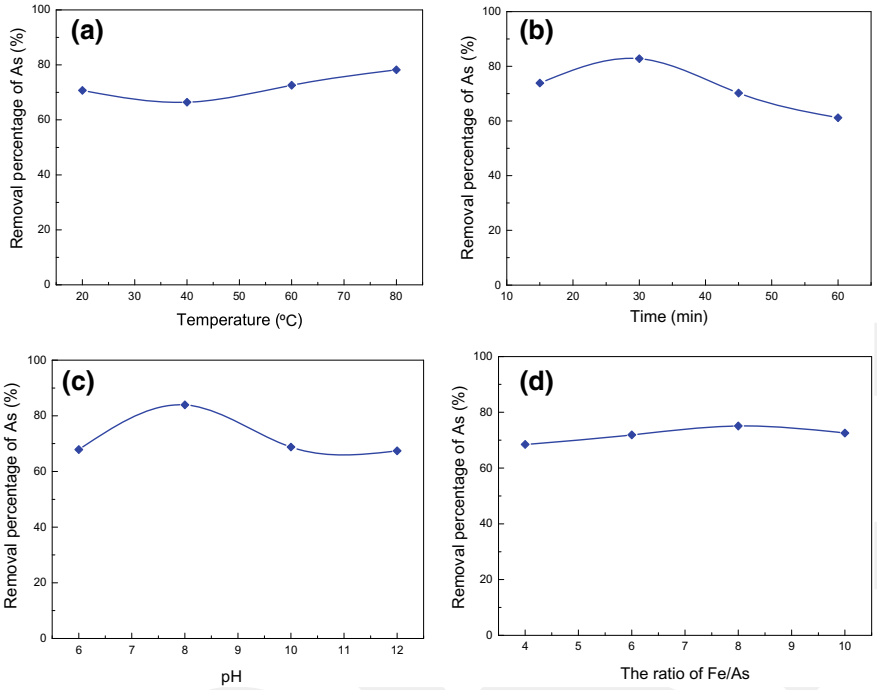

Fig. 1 Effects of various factors on the rate of arsenic removal. **a** Temperature, **b** the reaction time, **c** pH, and **d** the molar ratio of Fe/As

the best experimental condition. pH has a great influence on the effect of the rate of arsenic removal. Figure 5 was the pourbaix diagram of Fe, which was also found that the elemental iron was more converted to iron hydroxide after pH reaches 8.

Figure 1d was effects of the molar ratio of Fe/As on the rate of arsenic removal. It can be seen from Fig. 1d that as the Fe/As ratio increases, when the Fe/As molar ratio was 8, the removal rate of arsenic reached the optimal value. However, it had little effect on the removal rate of arsenic.

Verified Experiment

The comprehensive consideration of extremum analysis, operation index, economic benefit, and the optimal condition of this method was determined to be $A_4B_2C_2D_3$. Verification experiment was carried out under these conditions. According to the requirements of the enterprise, the residual concentration of arsenic in the waste acid reaches the reuse standard when it is less than 80 mg/L. The result shows that the removal rate of arsenic was satisfactory. Experimental result was shown in Table 5.

Table 5 Results of the proving experiment

As concentration of raw materials (mg/L)	The residual concentration of As (mg/L)	The removal rate of As (%)
629	52	91.73

The image and data of SEM analysis were shown in Fig. 2 and Table 6, and XRD spectrum was shown in Fig. 3. Based on two main factors and above analysis data, the elements of a high concentration of filter residue were Fe, As, S, O, and Cu, and the concentration of Cu element was less than that of the other four items. Cu element existed in both point 2 and point 3. Fe, As_2O_3, and Fe_2O_3 exist. Iron was residual unreacted iron powder. As_2O_3 was As^{3+} generated, respectively, after drying. Fe_2O_3 was generated during the corrosion process.

From the above, based on the main factors affecting the arsenic removal rate, the experimental mechanism was further studied, as shown in Fig. 4. Adding $CuSO_4$, displacement reaction between Fe and $CuSO_4$ forms Cu. Then Cu and Fe are formed Cu–Fe battery, which accelerated the corrosion of Fe to form Fe(II) and Fe(III). The change of pH generated iron oxides and hydroxides. Finally, As^{3+} was adsorbed by iron oxides and hydroxides, and the adsorption coprecipitation mechanism was used to get rid of the arsenic. The main reaction equations in the mechanism are as follows [17–20] (Figs. 4, 5 and 6).

$$Fe + Cu^{2+} = Cu + Fe^{2+} \tag{1}$$

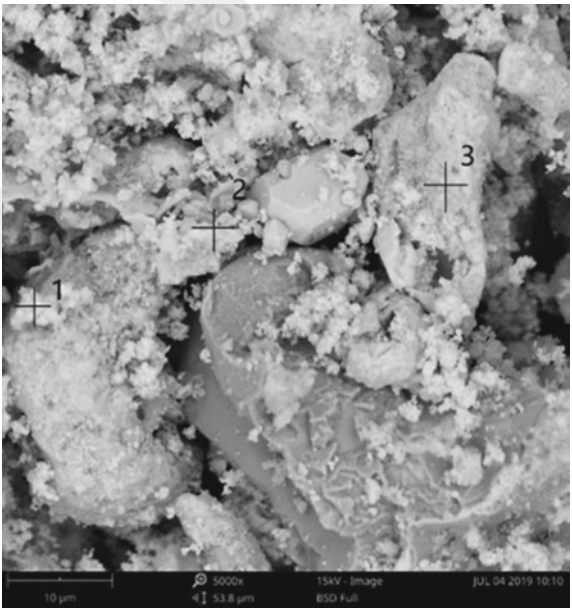

Fig. 2 SEM analysis of filter residue was verified

Table 6 SEM element concentration table of filter residue

		Sopt 1	Sopt 2	Sopt
As	Atomic conc.	31.18	12.00	29.36
	Weight conc.	52.95	16.56	37.52
S	Atomic conc.	14.54	3.34	15.10
	Weight conc.	10.57	1.97	8.26
Fe	Atomic conc.	18.60	65.42	45.42
	Weight conc.	23.54	67.28	43.26
O	Atomic conc.	35.67	9.51	0.00
	Weight conc.	12.94	2.80	0.00
Cu	Atomic conc.	0.00	9.72	10.12
	Weight conc.	0.00	11.38	10.96

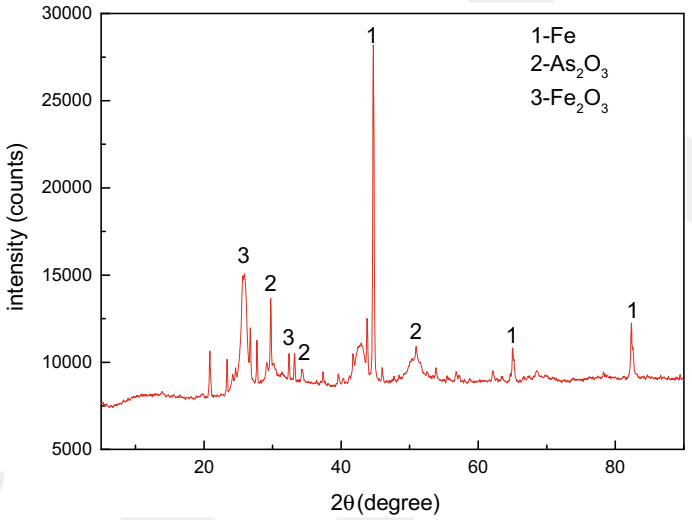

Fig. 3 XRD pattern of filter residue was verified

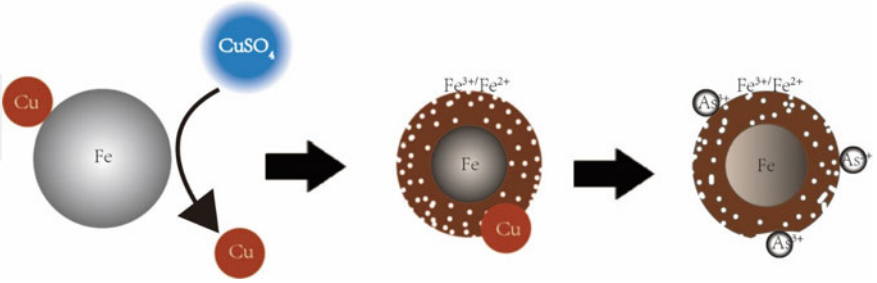

Fig. 4 Experimental schematic diagram

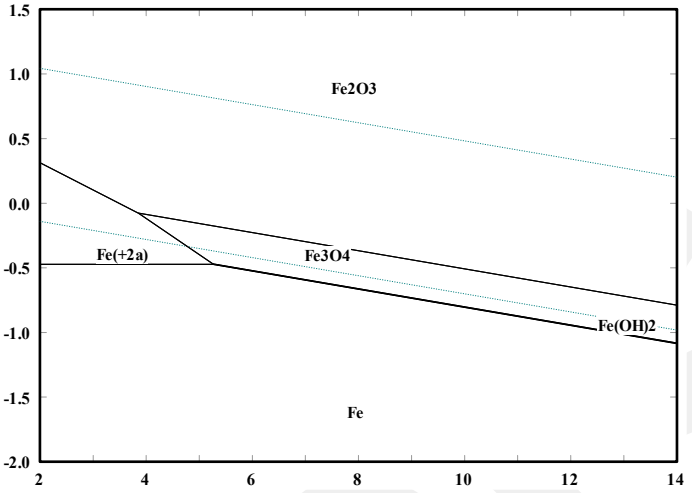

Fig. 5 Pourbaix diagram of Fe, the abscissa and ordinate are pH and $E(V)$

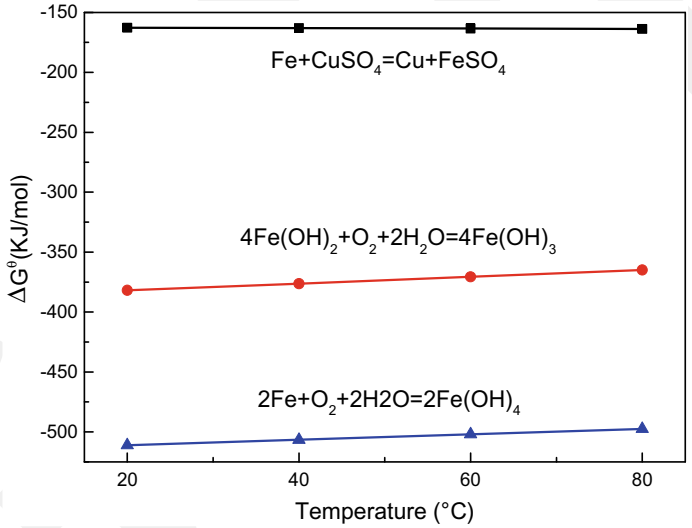

Fig. 6 Dependency of ΔG^{θ} on temperatures for the main reactions of iron

$$2Fe + O_2 + 2H_2O = 2Fe(OH)_2 \tag{2}$$

$$4Fe(OH)_2 + O_2 + 2H_2O = 4Fe(OH)_3 \downarrow \tag{3}$$

$$2Fe(OH)_3 \triangleq Fe_2O_3 + 3H_2O \tag{4}$$

Conclusion

The conclusions of this study can be drawn as follows. (1) Based on orthogonal experiment, the influences of four factors *A* (temperature), *B* (the reaction time), *C* (pH), and *D* (the molar ratio of Fe/As) on the method of treating as in waste acid by Fe and $CuSO_4$ were analyzed, and the reaction time and pH were the main factors affecting the removal rate of arsenic. The reaction time has a great influence on the adsorption effect, and pH plays an important role in the displacement reaction, the adsorption process, and the formation of iron oxides and hydroxides. (2) Based on the orthogonal experiment, the best process of treating arsenic in waste acid by adding Fe and $CuSO_4$ are as follows: temperature was 80 °C, the reaction time was 30 min, pH was 8, and the molar ratio of Fe/As was 8. The removal rate of arsenic reached 91.73%. (3) By analyzing the main factors obtained through orthogonal experiment and researching the results of the verification experiment from verified experiment, the experimental mechanism was further studied. The mechanism was that $CuSO_4$ was added, and the substitution reaction occurred between Fe and $CuSO_4$ to formed Cu. Then, forming Cu–Fe battery to accelerate the corrosion of iron powder to form Fe(II) and Fe(III) (iron oxides and hydroxides) which adopt adsorption coprecipitation mechanism is to remove arsenic from waste acid.

Acknowledgements This work was supported by a Yunnan Provincial Science and Technology Key Project (No. 2017FA026); Yunnan Ten Thousand Talents Plan Young & Elite Talents Project; National Natural Science Foundation of China (No. 51404115), Yunnan Ten Thousand Talents Plan Young & Elite Talents Project. The authors are grateful to the Kunming Key Laboratory of Special Metallurgy, Kunming Academician Workstation of Advanced Preparation for Super hard Materials Field, and Kunming Academician Workstation of Metallurgical Process Intensification.

Foundation support by the Yunnan Provincial Science and technology key project (NO. 2017FA026).

References

1. Bhattacharya P, Welch AH, Stollenwerk KG, Mclaughlin MJ, Bundschuh J, Panaullah G (2007) Arsenic in the environment: biology and chemistry. Sci Total Environ 379(2):109–120
2. Woolson EA, Axley JH, Kearney PC, Woolson EA, Axley JH, Kearney PC (1971) The chemistry and phytotoxicity of arsenic in soils: I. Contaminated field soils. Soil Scisocamerproc 35(6):938–943
3. Papassiopi N, Virčiková E, Nenov V, Kontopoulos A, Molnár L (1996) Removal and fixation of arsenic in the form of ferric arsenates. Three parallel experimental studies. Hydrometallurgy 41(2–3):243–253
4. Oh C, Rhee S, Oh M, Park J (2012) Removal characteristics of As(III) and As(V) from acidic aqueous solution by steel making slag. J Hazard Mater 213–214(213–214):147–155
5. Riveros PA, Dutrizac JE, Spencer P (2001) Arsenic disposal practices in the metallurgical industry. Can Metall Q 40(4):395–420
6. Fei J, Wang T, Zhou Y, Wang Z, Min X, Ke Y, Hu W, Chai L (2018) Aromatic organoarsenic compounds (AOCs) occurrence and remediation methods. Chemosphere 207:665–675

7. Ma J, Lei M, Weng L, Li Y, Chen Y, Islam MS, Zhao J, Chen T (2019) Fractions and colloidal distribution of arsenic associated with iron oxide minerals in lead-zinc mine-contaminated soils: comparison of tailings and smelter pollution. Comparison of tailings and smelter pollution. Chemosphere 227:614–623
8. Nazari AM, Radzinski R, Ghahreman A (2016) Review of arsenic metallurgy: treatment of arsenical minerals and the immobilization of arsenic. Hydrometallurgy 174:S0304386X16307095
9. Ying G, Li Q, Yin S, Chen W (2016) The present situation and the developing trend of processing technology for copper smelting contaminated acid. Min Metall 25(4):68–72
10. Wang Y, Zhang L, Han H, Zhang L (2019) Production practice of lead smelting wastewater treatment process. Jiangxi Build Mater 6:19–20 + 22
11. Xie H, Zhao ZW, Cao CF, Liang Y, Jiang-Tao LI (2012) Behavior of arsenic in process of removing molybdenum by sulfide method. J Central South Univ 43(2):435–439
12. Yi Q (2012) Three-stage lime-ferric salt process for treating high-arsenic waste acid. Sulphuric Acid Ind 1:46–48
13. Fu F, Wang Q (2011) Removal of heavy metal ions from wastewaters: a review. J Environ Manage 92(3):407–418
14. Xi Y, Zou J, Luo Y, Li J, Li X, Liao T, Zhang L, Wang C, Lin G (2019) Performance and mechanism of arsenic removal in waste acid by combination of $CuSO_4$ and zero-valent iron. Chem Eng J 375
15. Zhou WK, Peng YL, Zheng YJ, Yu-Tian MA (2011) Reduction and deposition of arsenic in copper electrolyte. Trans Nonferrous Metals Soc China 21(12):2772–2777
16. Shen Q, Zheng Y, Li S, Ding H, Xu Y, Zheng C, Thern M (2016) Optimize process parameters of microwave-assisted EDTA method using orthogonal experiment for novel $BaCoO_{3-\delta}$ perovskite. J Alloy Compd 658:125–131
17. Guo X, Yang Z, Dong H, Guan X, Ren Q, Lv X, Jin X (2016) Simple combination of oxidants with zero-valent-iron (ZVI) achieved very rapid and highly efficient removal of heavy metals from water. Water Res 88:671–680
18. Wang S, Zhang D, Li X, Zhang G, Wang Y, Wang X, Gomez MA, Jia Y (2018) Arsenic associated with gypsum produced from Fe(III)-As(V) coprecipitation: implications for the stability of industrial As-bearing waste. J Hazard Mater 360:S0304389418306964
19. Luong VT, Kurz EEC, Hellriegel U, Luu TL, Hoinkis J, Bundschuh J (2018) Iron-based subsurface arsenic removal technologies by aeration: a review of the current state and future prospects. Water Res 133:S0043135418300071
20. Shao W, Xiaomin LI, Cao Q, Luo F, Jianmei LI, Yangyang DU (2008) Adsorption of arsenate and arsenite anions from aqueous medium by using metal(III)-loaded amberlite resins. Hydrometallurgy 91(1):138–143

Part XVIII
Lead Refining

GCRIS

Driving Innovation in Lead Batteries: The Focus of the Consortium of Battery Innovation

Matthew Raiford

Abstract Energy storage is paramount to the electrification and hybridization of society, and aggressive adoption of batteries into many different environments has created significant challenges for the grid and for batteries. Lead battery energy storage provides a unique solution to these issues, offering a high performing technology with near-complete sustainability, intrinsically safe, cost-effective, and reliable. The Consortium for Battery Innovation (CBI) focuses on increasing the effectiveness of lead batteries in current and new applications. CBI has developed an innovation roadmap aimed at driving performance enhancement in automotive, industrial, and renewable energy storage lead battery applications. A new technical program has started featuring projects around the world aimed at improving some aspects of lead battery performance. The program covers a broad array of research areas, from crystallization/dissolution of lead species in battery electrodes to controlled energy throughput analysis of a lead battery energy storage system (ESS). Main drivers in the program, covered in the roadmap, are centered on increasing capacity turnovers of lead batteries in all applications and also creating lead batteries that charge quickly at various states of charge (DCA). This paper will focus on the performance enhancements observed in commercially advanced lead batteries and how innovation has opened up new pathways for improvement.

Keywords Lead batteries · Energy storage · Performance enhancements

Introduction

Balancing modernization of the grid with decarbonization goals and an increasing population requires clear stewardship plans and an increased reliance on the sustainability of natural resources and energy production. Regions across the world, from Germany to California, from Indonesia to Chile, are forecasting the need for cheaper and more stable energy production and transfer. Energy storage can be used

M. Raiford (✉)
Consortium for Battery Innovation, 2530 Meridian Parkway, Suite 115, Durham, NC 27713, USA
e-mail: matt.raiford@batteryinnovation.org

© The Minerals, Metals & Materials Society 2020

A. Siegmund et al. (eds.), *PbZn 2020: 9th International Symposium on Lead and Zinc Processing*, The Minerals, Metals & Materials Series,
https://doi.org/10.1007/978-3-030-37070-1_62

in many ways in front of or behind the meter. Frequency regulation, microgrid services, demand charge response, load leveling, and emergency backup are just a few of the ways that energy storage is vital to grid stabilization and the hybridization of the world electrical grid. Electrochemical energy storage is key to implementing solutions for the impending energy needs for the world. The lead battery industry has established an unprecedented recycling rate of 99.3% for lead battery technologies [1]. High recycling rates are complemented by the fact that over 80% of lead in use is sourced from secondary recycling streams [1, 2].

Lead batteries are used widely in automotive applications, as starter-light-ignition (SLI) batteries and as auxiliary safety (SLA) batteries, present in internal combustion engine vehicles as a major component to the electrical system, but also serve vital irreplaceable safety functions in hybridized and electric vehicles. Stop-start lead batteries in mild hybrids have been highly adopted in the automotive industry at ~35% implementation in new US ICE vehicles and over 95% in new European ICE vehicles [3–5]. In the USA, an estimated 4.5 million tons of CO_2 is saved through the use of lead battery stop-start systems. Supporting automotive focused batteries are large amounts of infrastructure, from lead producing smelters to state-of-the-art lead battery production facilities, are present in every region of the world. Lead batteries are not restricted to the automotive sector, and industrial, ESS, and UPS lead batteries are produced in the tens of millions of units every year. Lead battery technology is already poised to provide a sustainable, commercially available, and cost-effective solution for ESS needs.

The US Department of Energy (DOE) has set clear goals for renewable and utility grid ESS systems based on a combination of technical and economic indicators. These goals are summarized on a $/kW h and $/energy throughput basis. Lead batteries must improve in total cycle life, and several projects are underway to explore both the fundamental aspects of lead battery electrode failure in ESS conditions and also understanding the benefits of using battery management systems (BMS) and suitable recuperative charging schemes, as well as the effect of morphological changes of $PbSO_4$ on battery life. This paper will aim to summarize current research in lead batteries in automotive and ESS applications, as well as some of the advanced batteries utilized currently [7–16]. Furthermore, the paper will outline the areas of research that are strategically important to improving lead battery performance [17].

Results and Discussion

The CBI has outlined key performance indicators that must improve in automotive and ESS lead batteries. Automotive SLI and stop-start batteries must increase in both recharge capability and high temperature durability. Improvements in these performance metrics equate to more dynamic charge acceptance (DCA) (approaching 2A/Ah) and low cumulative damage of lead battery electrodes at sustain temperatures of 75 °C. ESS batteries must cycle highly at 100% DOD, or the ESS system must be sized to cycle appropriately. Cycle life or total capacity turnovers are crucial to

Indicator	2019	2022	2025
DCA. A/Ah	0.4	2.0	2.0
PSoC, 17.5% DoD	1500 EFB	2000 EFB	3000 EFB
Water loss, g/Ah	< 3	< 3	< 3
Corrosion, J2801, Units	12	18	22

Fig. 1 Needed improvements for lead batteries in terms of cycle life and DCA in automotive applications. Items in red have been deemed most important. Adapted from Ref. [17]

Indicator	2019	2022	2025
Service life, Y	12+	12-15	15-20
PSoC, PV	1500	2000	2500
Cycle life	1000 - 3000	5000	6000
Charge efficiency	85 – 90%	90 – 95%	> 95%

Fig. 2 Key performance indicators for lead batteries in industrial and utility services applications. Highlighted items are integral to the operation cost of ESS, and are important metrics for lead batteries in ESS applications. Adapted from Ref. [17]

the economics of these systems. Figures 1 and 2 summarize the target performance indicators for utility grid energy storage and automotive lead batteries.

Advanced Automotive Lead Batteries

CO_2 emissions from ICE and hybrid vehicles are under heavy scrutiny, and every component of the drive-train and electrical systems are being optimized for additional increases in fuel efficiency. Batteries have become an important pathway for CO_2 savings in all levels of hybridization. Stop-start systems powered by lead battery technology present in mild hybrid vehicles are saving approximately 4.5 million tons of CO_2 emissions [3–5]. The advanced lead batteries present in stop-start systems have superior performance provided by new electrode designs, absorbent glass mat technology, and carbon and ionic additives in the electrolyte and active material. Superior performance from advanced lead batteries is commonly measured via electrical testing following closely governed standards. The effect of new electrode configurations and additives on the crystal growth and dissolution processes has been

published [9–13]. However, a deeper look into the changes in morphology and preferred growth planes could yield vital understanding of the most effective $PbSO_4$ crystal form for dissolution during charge. Dynamic charge acceptance (DCA) must increase in lead batteries to the point where the electrical system is alternator limited (approximately 3 kW charge power) [18]. Determining effective ways to improve DCA has yielded entire families of additives, and lead batteries have demonstrated large gains in recharge capability (0.2 A/Ah for standard SLI to current advanced lead batteries possessing 1.5 A/Ah recharge current) [17, 18].

High temperature durability of lead batteries in automotive applications dictates the longevity of the battery in the field. Lead batteries in mild hybrids must be robust from −30 to 80 °C [18, 19]. New grid and active materials have increased durability in this range, with current automotive specification being met by the micro-alloyed materials [20].

Energy Storage Systems for Grid Services

ESS uses are manifold and are effective assets in many different areas in the electrical grid. In the past, lead batteries have served in frequency regulation, demand response, microgrids, and other applications [10, 21, 22].

Lead batteries offer many advantages in ESS systems, mainly good safety, high reliability, and sustainability [10, 21]. Maximum number of capacity turnovers must increase for lead batteries to stay competitive in this sector, however, with desired 2500 cycles at 100% depth of discharge (DOD) being required to enter the market. There are many commercial lead batteries that can attain this performance, with some exceptional battery products operating in the 5000–6000 cycle range [23].

Fundamental Studies to Improve Lead Battery Performance

In an effort to understand the processes occurring in basic and advanced lead batteries, in situ and in-operando synchrotron X-ray experiments have been utilized to explore the crystallization/dissolution mechanistic of $PbSO_4$, Pb, and PbO_2 phases [24, 25]. There are severe complications studying lead species using X-rays due to the high density and poor penetration and interaction volume. Past literature has focused on compositional analysis after exposure to air and water, as covered by seminal work by Detchko Pavlov et al. $PbSO_4$ growth in the negative electrode is accommodated through the transformation of $3PbO \cdot PbSO_4$, $4PbO \cdot PbSO_4$, and PbO. These relationships serve as the framework for understanding not only the fundamental changes in the phases present in both electrodes, but are used as a fingerprint for premature failure modes. However, morphological changes that eventually lead to the concentration of species along the surface and near surface have only been studied in ex situ samples that have experienced significant phase changes related

to water and air exposure. In depth exploration of the surface and through thickness of lead battery, electrodes have been conducted through a combination of electron microscopy of mounted, aged lead battery cross sections using microprobe analysis [24]. Intense light sources utilized in synchrotron beamlines offer the ability to penetrate millimeters through a lead battery electrode. New information regarding the morphology of $PbSO_4$ during discharge is beginning to provide key insights into the effect of additives on the preferred growth faces of the orthorhombic (Pnma, 62). Highly polar faces, such as the <111> and <101>, grow rapidly in $PbSO_4$ facilitating dendritic growth processes responsible for electrical shorts in later stages of battery life [26].

The synchrotron-facilitate high-energy X-ray experiments provide key structural insight into nucleation processes and morphology changes due to different additives. The high penetration depth and array of X-ray techniques allow for intensive study of lead battery electrodes during operation, overcoming negative and false information observed in ex situ studies. Multiple techniques have been employed to not only look at the crystal behavior of the electrodes, but also the kinetics of the growth processes and the extensive electrochemical changes present in lead batteries [24]. Visualizing the growth processes have also been studied by in situ liquid TEM in electrochemical conditions and in situ ICP-MS combined with rotating disk electrode configuration. Regan et al. utilized LQ-TEM experiments to visualize dendritic growth of Pb in negative electrodes in micron and nanometer regimes. This study yielded unprecedented observations on the behavior of harmful Pb dendrites during discharge and charge [27]. Uncontrolled $PbSO_4$ crystal growth is the main progenerate to failure modes in the positive and negative electrodes, utilizing techniques that observe these processes in a native environment at crucial to inhibiting these failure modes.

Conclusion

Lead batteries have been constantly improving to fit societies' performance needs in automotive and utility grid applications. CBI has created attainable performance enhancement goals based on new research pathways for lead batteries. Lead batteries provide high sustainability and reliable energy storage, and offer unique advantages when compared to other electrochemical storage technologies, such as Li-ion. Inhibiting failure modes must occur to prolong battery life, and a higher understanding of the crystal growth and dissolution process and the electrochemical kinetics is yielding definitive information to be used in the next generation of advanced lead batteries. Failure modes such as positive paste shedding and negative sulfation can be engineered to occur at a slower rate, once there is a stronger grasp of the preferred crystal faces for dissolution and growth in $PbSO_4$ in lead battery electrodes. The lead battery industry has introduced a league of advancements to push lead battery performance further and further advancements are underway.

References

1. SmithBucklin Statistics Group (2017) BCI National recycling rate study. Battery Council International. https://cdn.ymaws.com/batterycouncil.org/resource/resmgr/Recycling_Rate/BCI_201212-17_FinalRecycling. Accessed 1 Oct 2019
2. International Lead Association (2013) Lead recycling: as good as new. International Lead Association. https://www.ila-lead.org/UserFiles/File/FS_Recycling.pdf. Accessed 1 Oct 2019
3. Environmental Protection Agency (2018) Greenhouse gas emissions from a typical passenger vehicle. https://nepis.epa.gov/Exe/ZyPDF.cgi?Dockey=P100U8YT.pdf. Accessed 1 Oct 2019
4. Hedges & Company (2019) U.S. vehicle registration statistics. https://hedgescompany.com/automotive-market-research-statistics/auto-mailing-lists-and-marketing/. Accessed 1 Oct 2019
5. Environmental Protection Agency (2018) The 2018 EPA automotive trends report: greenhouse gas emissions, fuel economy, and technology since 1975. https://nepis.epa.gov/Exe/ZyPDF.cgi?Dockey=P100W3WO.pdf. Accessed 1 Oct 2019
6. Sugumaran N, Everill P, Swogger SW, Dubey DP (2015) Lead acid battery performance and cycle life increased through addition of discrete carbon nanotubes to both electrodes. J Power Sour 279:281–293
7. Boden DP, Loosemore DV, Spence MA, Wojcinski TD (2010) Optimization studies of carbon additives to negative active material for the purpose of extending the life of VRLA batteries in high-rate partial-state-of-charge operation. J Power Sour 195(14):4470–4493
8. Pavlov D, Nikolov P (2013) Capacitive carbon and electrochemical lead electrode systems at the negative plates of lead-acid batteries and elementary processes on cycling. J Power Sour 242:380–399
9. Fernández M, Valenciano J, Trinidad F, Muñoz N (2010) The use of activated carbon and graphite for the development of lead-acid batteries for hybrid vehicle applications. J. Power Sour 195(14):4458–4469
10. Bullock KR (2010) Carbon reactions and effects on valve-regulated lead-acid (VRLA) battery cycle life in high-rate, partial state-of-charge cycling. J Power Sour 195(14):4513–4519
11. Pavlov D, Nikolov P, Rogachev T (2010) Influence of expander components on the processes at the negative plates of lead-acid cells on high-rate partial-state-of-charge cycling. Part I: Effect of lignosulfonates and $BaSO_4$ on the processes of charge and discharge of negative plates. J Power Sour 195(14):4435–4443
12. Pavlov D, Nikolov P (2012) Lead-carbon electrode with inhibitor of sulfation for lead-acid batteries operating in the HRPSoC duty. J Electrochem Soc 159(8):A1215–A1225
13. Naresh V, Elias L, Gaffoor SA, Martha SK (2019) Corrosion resistant polypyrrole coated lead-alloy positive grids for advanced lead-acid batteries. J Electrochem Soc 166(2):A74–A81
14. Foudia M, Matrakova M, Zerroual L (2015) Effect of a mineral additive on the electrical performances of the positive plate of lead acid battery. J Power Sour 279:146–150
15. Lam LT, Louey R, Haigh NP, Lim OV, Vella DG, Phyland CG, Vu LH, Furukawa J, Takada T, Monma D, Kano T (2007) VRLA Ultrabattery for high-rate partial-state-of-charge operation. J Power Sour 174(1):16–29
16. Moseley PT, Prengaman RD (2002) In pursuit of high specific energy, high specific power valve-regulated lead-acid batteries. J Power Sour 107(2):240–244
17. May GJ, Raiford MT, Davidson AJ (2019) An innovation roadmap for advanced lead batteries. Consortium for Battery Innovation. https://batteryinnovation.org/wp-content/uploads/2019/09/CBIRoadmap_FINAL.pdf. Accessed 1 Oct 2019
18. Garche J, Karden E, Moseley PT, Rand DAJ (2017) Lead-acid batteries for future automobiles. Elsevier, Amsterdam
19. Karden E, Nagata Y (2019) Future of micro-hybrid automotive applications from an OEM perspective. Paper presented at the BCI Convention 2019, New Orleans, Louisiana, 26–28th Apr 2019
20. Prengaman RD (2000) Alloy for thin positive grid for lead acid batteries and method for manufacture of grid. US patent 6649306, 26 Dec 2000

21. May GJ, Davidson AJ, Monahov B (2018) Lead batteries for utility energy storage: a review. J Energy Storage 15:145–157
22. Huck M, Badeda J, Sauer DU (2015) Modeling the crystal distribution of lead-sulfate in lead-acid batteries with 3D spatial resolution. J Power Sour 279:351–357
23. Zipp K (2016) GS Battery technical report: developing a long cycle life valve regulated lead acid battery. Solar Power World. https://www.solarpowerworldonline.com/2016/10/gs-battery-technical-report-developing-long-cycle-life-valve-regulated-lead-acid-battery/. Accessed 1 Oct 2019
24. Pavlov D (2017) Lead-acid batteries: science and technology, 2nd edn. Elsevier, Amsterdam
25. Moseley PT, Garche J, Parker CD, Rand DAJ (2004) Valve regulated lead-acid batteries, 1st edn. Elsevier, Amsterdam
26. Fister TT (2018) Real-time studies of sulfate growth and dissolution on negative electrode materials using high energy X-ray diffraction. Paper presented at the European lead battery conference in Vienna, Austria, Sept 2018
27. White E, Singer S, Augustyn V, Hubbard WA, Mecklenburg M, Dunn B, Regan BC (2013) Imaging lead dendrite formation and ion diffusion in aqueous solution with scanning transmission electron microscopy. ACS Nano 6(7):6308–6317

GCRIS

New Technology for Copper Removal from Lead by Application of Aluminium: Practical Problems

Andrzej Cybulski

Abstract The widely known and used worldwide method for copper removal from lead by application of sulfur cannot always be effective since a part of the sulfur becomes oxidized. The process is often repeated which results in higher costs and longer process duration. Application of sulfur in copper removal from lead and subsequent smelting of Cu dross has negative influence on environment because of SO_2 emission to atmosphere. Łukasiewicz—Instytut Metali Nieżelaznych in Gliwice—developed a new technology for copper removal from lead with application of aluminum, which is used in industrial conditions with a good result. The advantages of this technology are elimination of sulfur compounds, low quantity of the formed semi-finished products, reduction of Pb losses, process stability, guaranteed removal of copper below 5 ppm in each case, and ease of fabrication. However, this technology, in the case of lack of technological regime, may cause the loose Al–Cu dross to burn and glow. The paper shows methods for copper removal from lead with the use of aluminium, as well as problems resulting from application of this technology in industrial conditions.

Keywords Refining · Lead · Decoppering · Aluminium

Introduction

A commonly known and used worldwide process of lead decoppering with sulfur does not always provide the effective copper removal due to the partial oxidation of the sulfur supplied to the process. Frequently, lead decoppering by dosing sulfur requires repetition, what increases the costs and elongates the lead refining process. The application of sulfur in lead decoppering and the following processing of the produced Cu drosses requires the utilization of the process gases in order to avoid their negative impact on the natural environment due to the SO_2 emission.

A. Cybulski (✉)
Łukasiewicz Research Network, Institute of Non-Ferrous Metals, Gliwice, Poland
e-mail: andrzejcy@imn.gliwice.pl

© The Minerals, Metals & Materials Society 2020

A. Siegmund et al. (eds.), *PbZn 2020: 9th International Symposium on Lead and Zinc Processing*, The Minerals, Metals & Materials Series,
https://doi.org/10.1007/978-3-030-37070-1_63

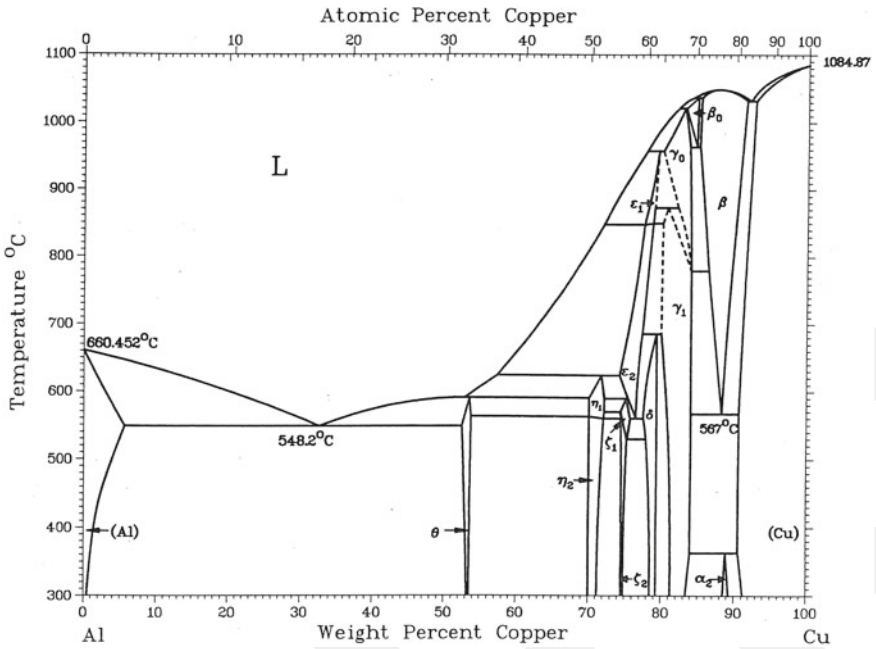

Fig. 1 Al–Cu phase equilibrium diagram [1]

This paper includes information on an innovative and ecological lead decoppering process performed with the application of aluminum. The technology is based on the formation of intermetallic copper and aluminum compounds, according to the Al–Cu phase equilibrium shown in Fig. 1, based on the Eq. (1):

$$nAl + mCu = Al_nCu_m \tag{1}$$

Lead decoppering with the application of aluminum can be performed in two ways. One is based on a short and intensive mixing of lead and the refining agent at 660 °C. Then, lead is cooled to the temperature close to the solidification temperature. The Al–Cu foam formed on top of lead, that contains intermetallic compounds, can be collected in the metallic form or dried, i.e. with sawdust, and collected in the form of loose Al–Cu drosses.

The second method is based on melting of aluminum on the lead surface and slow mixing. Thereby, the obtained liquid Al phase with high Cu and low Pb content can be collected from the liquid lead in the metallic form after solidification. The liquid Al–Cu alloy solidifies at the eutectic point at approx. 540 °C.

The Al–Cu–Pb phase diagram presented in Fig. 2 confirms this and presents the existing separation of two liquids with a limited miscibility: a liquid rich in Pb with low Al and Cu contents and Al–Cu liquid with low Pb content. As can be observed

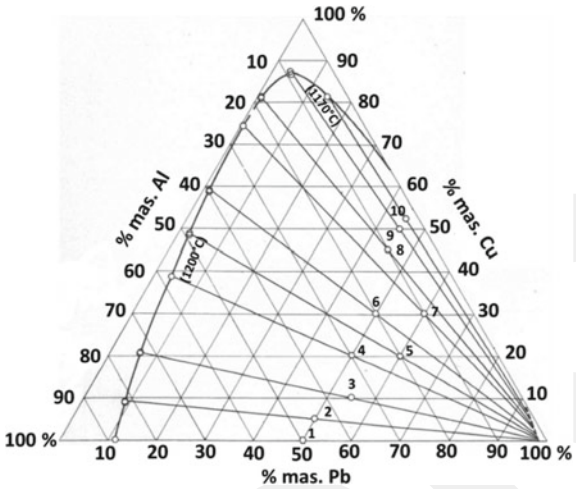

Fig. 2 Al–Cu–Pb phase equilibrium diagram at 1020 and 1070 °C [2]

in the diagram (Fig. 2), it is possible to produce Al–Cu alloy containing 30 wt% Cu, approx. 65 wt% Al and low Pb content approximately 5–7 wt%.

A Method of Lead Decoppering and Production of Metallic Al–Cu Foam and Al–Cu Drosses

On the industrial scale, the procedure of lead decoppering with aluminum is based on heating lead to 660 °C after the lead oxidation process. Next, aluminum is added in the fragmented form on the lead surface with intensive mixing. After aluminum is blended, lead is cooled to 450 °C. The produced metallic Al–Cu foam (Fig. 3a), containing intermetallic Al–Cu phases, is collected from the lead surface or dried, i.e. with the application of battery spacers, and the Al–Cu drosses are collected in the powdery form (Fig. 3b).

The first lead decoppering method was implemented in the industrial conditions with an excellent result. The technology was implemented by a company which is the leading refined lead producer in Poland, within a project funded by the Ministry of Science and Higher Education in 2011. At the end of 2015, patent PL 219840 B1 was granted for the developed lead decoppering technology with the application of aluminum and Al–Zn alloys.

An example of the parameters of the decoppering with aluminum applied in the industrial scale is presented in Table 1.

The chemical compositions of lead at different temperatures of lead decoppering process with aluminum are presented in Table 2.

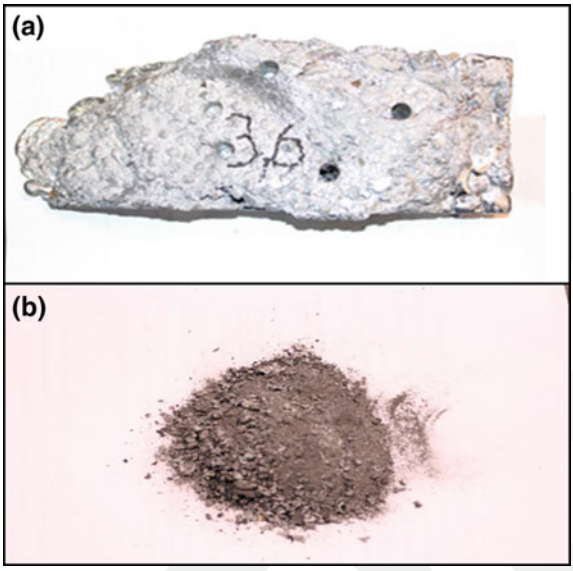

Fig. 3 Refining semi-products: **a** metallic Al–Cu foam, and **b** Al–Cu drosses

Table 1 Parameters of the process of decoppering with the application of aluminum

Technological parameters					
Lead mass (kg)	Initial temperature (°C)	Aluminum mass (kg)	Cooling time (h)	Final temperature (°C)	Al–Cu drosses (kg)
110,000	660	110	10	450	1200

Table 2 Chemical composition of lead during the exemplary industrial sample

Operation	Temperature (°C)	Chemical composition of lead (%)					
		Sb	As	Sn	Ag	Cu	Al
Sb removal	660	0.053	0.0002	0.00072	0.0027	0.0664	0.00001
Decoppering	660	0.029	0.0001	0.00001	0.0026	0.0058	0.01363
Decoppering	450	0.036	0.0002	0.00002	0.0026	0.0006	0.00460

The exemplary chemical composition of Al–Cu drosses produced in the industrial conditions during lead decoppering with aluminum is presented in Table 3.

The application of a new lead decoppering technology with the application of aluminum results in the total elimination of the sulfur compounds from the refining process, what improves the environmental protection conditions.

Comparing the sulfur and aluminum technology, in terms of the amount of by-products, it can be stated that:

Table 3 Chemical composition of Al–Cu drosses during the exemplary industrial test

Chemical composition of Al–Cu drosses (%)				
Al	S	Cu	Sb	Pb
4.90	0.20	4.16	4.86	85.88

- The amount of the Cu drosses generated by the technology that uses sulfur is approx. 2–3% of the lead mass,
- For the aluminum technology, the amount of by-products in case of Al–Cu dross formation is 1.1, and 0.86% of lead mass for Al–Cu alloy production, that is approx. 50% less by-products, therefore this technology is more efficient and also more cost-effective.

The decoppering technology with sulfur causes the fact that the operation is often repeated due to the oxidation of sulfur during batching. Each additional decoppering with sulfur causes the formation of additional amount of Cu drosses that increase the lead losses. The technology that uses aluminum eliminates this problem because after a single batching of aluminum, low copper content (below 5 ppm) as well as a constant amount of generated by-products is guaranteed.

Due to the utilization of the final temperature of the previous operation (lead oxidation), no additional heating of the refining kettle is required to process aluminum. Therefore, the energy efficiency increases.

Practical Problems of Lead Decoppering with the Application of Aluminum

The lead decoppering technology with the application of aluminum has been functioning in the industry since 2011, without any significant issues. This technology has been constantly improved and was easily incorporated into lead refining process. In 2016, after 5 years of utilization of this technology, a problem of ignition of Al–Cu drosses, which were a huge problem due to the safety standards, was reported. The incandescent Al–Cu drosses in the refining kettle are presented in Fig. 4.

Both laboratory and industrial scale tests have been performed in order to eliminate this problem. The factors that could cause these problems were analyzed. The Al–Cu drosses have a powdery form and contain fine metallic particles. The reaction between aluminum and oxygen is a strong exothermic reaction. The very fine particles are characterized with a large specific surface area; therefore, the oxidation proceeds rapidly and generates a large amount of heat that can be manifested with incandescence or even explosions. The additional factor that may influence the ignition of drosses is the application of aluminum scrap, that contains flammable components, i.e. magnesium and sulfur, which have a greater affinity to oxygen than aluminum, and the reaction is even more rapid and generates larger amounts of heat. Another factor which may initiate the ignition of drosses is the substance used to dry

Fig. 4 Incandescent Al–Cu drosses in the refining kettle

the metallic Al–Cu foam—usually battery spacers or sawdust, which are pyrolyzed at higher temperatures. The solid product of pyrolysis—char—easily ignites and incandescents.

Al–Cu drosses from the refining kettle, before ignition and after burnout, were subjected to the microscopic and chemical analysis and the elemental distribution was determined. The microstructure of Al–Cu drosses before and after burnout is presented in Fig. 5.

Comparison of the samples before and after burnout of Al–Cu drosses:

The chemical analysis shows that after the burnout process the amounts of oxygen and aluminum are higher, and carbon and lead are lower. Based on the elemental distribution map, in the sample after burnout, Cu, Ni, and Sn are more scattered. This sample also contains clusters (order of magnitude of the diameter 1 μm) of those elements, wherein it can be observed that in many cases, copper is accompanied by nickel. In the burnt out sample, aluminum and oxygen are present in the same regions, which indicates aluminum oxidation.

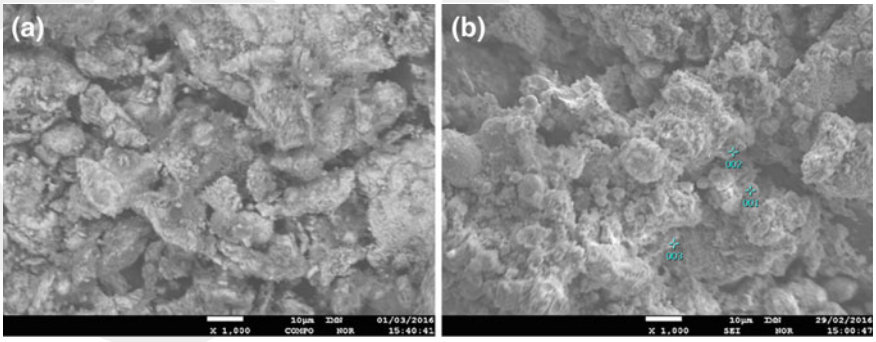

Fig. 5 Al–Cu dross microstructure, **a** before ignition, and **b** after burnout. Secondary electron images (SEI), 1000× magnification

The chemical analysis of the Al–Cu drosses performed during the microscopic analysis shows a large increase in the sulfur content. For the analysed Al–Cu drosses, sulfur content was approx. 4% and was two times higher than for Al–Cu drosses obtained in the previous years, which was not higher than 2% sulfur.

Such high sulfur content in Al–Cu drosses may initiate thermite reaction—reduction of metal oxides with aluminum. Sulfur, magnesium, and saltpeters, i.e. $NaNO_3$, are also used as catalyst. Therefore, it is desirable to reduce the sulfur content in Al–Cu drosses.

The tests of drying of Al–Cu drosses with different drying agents have been performed in order to eliminate the flammable materials, i.e. battery spacers and sawdust. The main suitability criterion during the selection of the drying material for the drying process was to obtain loose Al–Cu drosses which will not ignite inside the furnace. The following materials have been analyzed:

- milled limestone $CaCO_3$,
- slaked lime—$Ca(OH)_2$,
- quicklime—CaO,
- sodium carbonate Na_2CO_3.

The Al–Cu drosses produced in the process of lead decoppering dried with slaked lime, quicklime, and sodium carbonate are presented in Fig. 6.

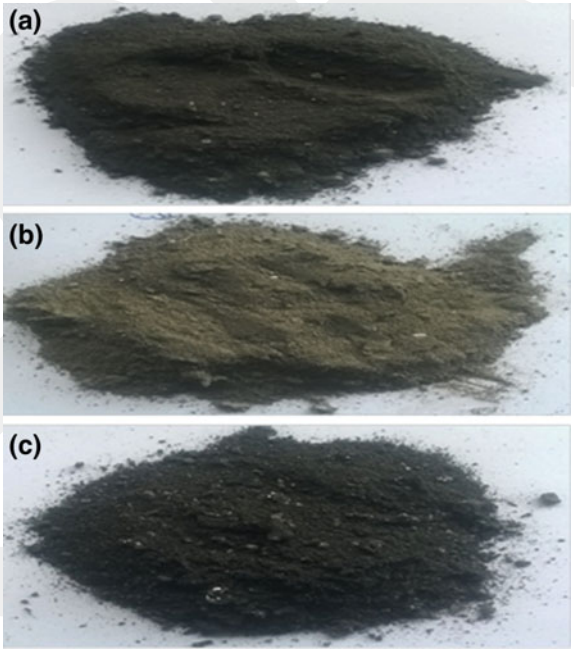

Fig. 6 Al–Cu drosses after drying with: **a** slaked lime, **b** quicklime, **c** sodium carbonate

Unfortunately, drying of metallic Al–Cu foam with milled limestone did not give a positive result in a form of the production of loose Al–Cu drosses. During drying with slaked lime, the incandescence was observed on the produced powdery Al–Cu drosses and small flames of burning hydrogen from the decomposition of $Ca(OH)_2$ could be observed.

The most favorable results in terms of the possibility to dry the metallic Al–Cu foam and provide safety during drying were obtained for the process performed with the application of sodium carbonate and quicklime.

The analysis of the lead decoppering process with the application of aluminum shows that the main factors that may cause the ignition of Al–Cu drosses are:

- too long drying of the metallic Al–Cu foam causing high level of oxygen saturation of the produced Al–Cu drosses,
- application of aluminum scrap with high content of flammable compounds,
- application of flammable battery spacers for the process of drying of metallic Al–Cu foam,
- large surplus of aluminum added to the lead decoppering process,
- high sulfur content in the produced Al–Cu drosses.

Conclusions

In order to eliminate the problem of Al–Cu dross ignition, it is necessary to strictly and rigorously follow the instructions for the process of lead decoppering with application of aluminum in technical and technological terms, with a particular regard to occupational health and safety regulations. The instructions include all the factors that may lead to the spontaneous combustion as well as their storage.

Another alternative that may eliminate this undesirable phenomenon is the application of the second lead decoppering method with the application of aluminum, where Al–Cu alloy is produced. This alloy is collected from the lead surface in the metallic form after the decoppering process. The second lead decoppering method with application of aluminum does not produce the metallic Al–Cu foam which requires drying. Even when it is formed, the amounts are very small. The produced Al–Cu alloys are more valuable by-product that contains approx. 32 wt% Cu and small amount of Pb. This alloy, after the initial refining, can be used as a ready by-product, i.e. for the production of copper-aluminum radiators. In a process conducted in this way, the amount of by-products is below 1% of the mass of refined lead, which significantly increases the refining efficiency and lead yield. The application of lead decoppering process with application of aluminum that produces Al–Cu alloy results in a significant financial profit when compared to the sulfur technology or the first lead decoppering method that generates Al–Cu drosses.

References

1. Murray JL (1985) The aluminium-copper system. Int Met Rev 30(1):211–234
2. Claus W, Herrmann I (1939) Zur Kenntnis der systeme Al-Cu-Pb und Al-Pb, vol XVIII, no 48. Metallwissenschaft Reine und angewandte Metallkunde, Berlin

GCRIS

Processing of Polymetallic Materials Requires Flexible and Capable Downstream Refining Technology: Aurubis Lead Refinery as Economic, Modern, and Well Integrated Plant at the Site Hamburg

Christoph Zschiesche and Ino Bauer

Abstract Synergies between copper and lead metallurgy are essential to ensure efficient processing of polymetallic complex materials. The required process efficiencies along with environmental demands have been common elements behind technological transformations in the non-ferrous industry. In case of Aurubis, firstly modernization of its copper plant in 1972 followed by the lead plant in 1992, are clear examples of drastic transformations implemented to achieve. Continuing with these goals, Aurubis commissioned a new lead refinery in 2014 in order to achieve a more efficient refining process that could deal with the increasing complexity of materials and improve emission control. This was achieved by the implementation of a smart ventilation system instead of common ridge turret systems. This paper describes Aurubis's lead refinery operation adaptation to meet the challenges imposed by the increasing complexity of raw materials and the environmental aspects required to operate a sustainable urban metallurgical facility.

Keywords Polymetallic · Lead refinery · Operations · Crude lead

Introduction

Aurubis has a long tradition in the processing of non-ferrous metals. Since its establishment in 1866 as Norddeutsche Affinerie in the field of precious metals' refining, the company gradually evolved, as well as the primary copper processing business also the refining of lead has also a long standing tradition in Aurubis. In 1912, the first lead refinery with a reverberatory furnace was operated at the Peute (Hamburg, Veddel). The well-described Harris process was introduced in 1925 which means

C. Zschiesche (✉)
Aurubis AG (Research & Development), Hamburg, Germany
e-mail: c.zschiesche@aurubis.com

I. Bauer
Aurubis AG (Operations Hamburg), Hamburg, Germany

© The Minerals, Metals & Materials Society 2020

A. Siegmund et al. (eds.), *PbZn 2020: 9th International Symposium on Lead and Zinc Processing*, The Minerals, Metals & Materials Series,
https://doi.org/10.1007/978-3-030-37070-1_64

up to now, an operational experience of nearly 100 years [1]. While Norddeutsche Affinerie shaped its company profile and became an important custom smelter for copper concentrates, the lead smelter and refinery were adapted to the demand for treating crude lead bullions with varying impurity concentrations. As expressed in Aurubis's 2025 vision, it is the target to expand and improve the flowsheet in terms of a multi-metal recovery strategy.

The lead smelter in Hamburg allows Aurubis to have a more efficient processing of copper complex materials, extracting other valuable metals than the only Cu, precious metals or platinum group metals such as Bi, Sb, Sn, and Te. The execution of the project "new lead refinery" was an important step ahead towards to a sustainable commitment to refine crude lead in a facility which is capable to cope with varying bullion concentrations and production of intermediates which fit to the further purification processes to make those metals useable for urbanization and digitalization.

The current paper provides a description of the improvements which were achieved by executing the project "new lead refinery" gathered during the first four years of production.

The Lead Smelter and Refinery

Figure 1 shows the current metallurgical flowsheet combining copper and lead metallurgy. At the site of the lead production line, the core equipment is the electric furnace.

With its capability to process various secondary raw materials and intermediates, the secondary smelting process is a key pillar of Aurubis recycling business on the market of Cu-, Pb-, and precious metals'-bearing materials. In this process, Cu is recovered in a matte phase which is converted before sent back to the primary copper operations. Crude lead is utilized as a carrier to manage the flow of minor elements, such as Bi, Sb, Sn, and Te. As and Ni-bearing raw material could be processed while producing a concentrated metal alloy—called speiss. The produced slag is utilized as construction material. The connectivity of the electric furnace and the lead refinery is given by the crude lead stream and a couple of intermediates produced in the lead refinery (dross) which will be then recycled back.

Commissioning of the New Lead Refinery in 2014

With the project "new lead refinery," Aurubis generated the basement for a sustainable lead refining operation according to recent standards to operate such a metallurgical plant in the near of one of the most attractive cities in Germany. The main goals of this project were:

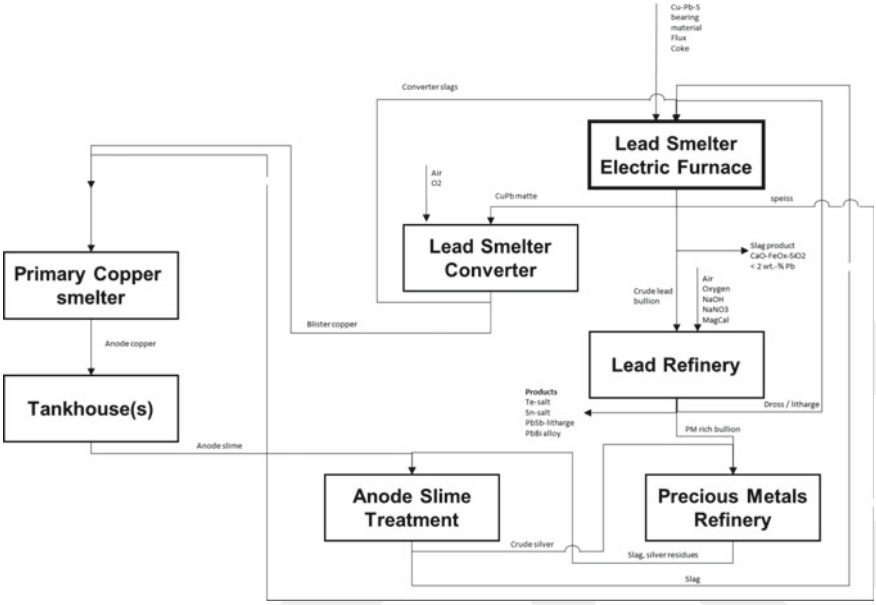

Fig. 1 Aurubis metallurgical flowsheet combining copper and lead metallurgy

- Improve emission control,
- Provide suitable working conditions to achieve a minimization of blood lead concentration,
- Achieve a more efficient refining process that could deal with the increasing complexity of materials indicating an expansion of refining capacities,
- Optimize the overall performance of the plant (logistic, plant layout, handling of intermediates) (Fig. 2).

Fig. 2 Left: Old lead refining facility; Right: New lead refining capacity with offices for site administration

The project was approved in 2012, and the erection time was approximately 1.5 years. The hot commissioning was finished in December 2014. For the first phase, the utilization of 8 kettles was aimed, whereas the facility was already prepared to install four further kettles as required.

The main objectives to enhance the environmental performance and occupational health and safety of the lead refinery were carefully defined and considered as key aspects during the conceptualization and execution of the project. These are summarized as follows:

- Reduce the emissions at their source (the kettle) by an improved sealing with a proper ventilation system,
- Reduce the emissions which could leave the facility by planning the right position for the ridge turret system to ensure a proper circulation of the air,
- Design a plant layout which allows a proper access to all kettles for cleaning and maintenance and which allocate solutions to minimize the storage of intermediate bullions or dross on the kettle floor,
- Plan an energy efficient kettle heating system to minimize the heat losses while increasing the contact area [2].

Improvement of Occupational Health and Safety and Environmental Protection

The old lead refinery with its capacity of 30,000 t/a crude lead processing had 8 kettles in operation, arranged in a very busy environment. As can be noted from Fig. 3, the kettles had a secondary ventilation system which was placed at the outer corner of each kettle. The suction was limited with 80,000 N m^3/h filtered in a baghouse. The valid limits in air circulation were critically reviewed and had to be improved during planning of the new facility. Also according to the strive for minimization of fugitive emissions, the new refinery was planned with a different concepts of ridge turret system. Figure 3 shows the plant layout of the new refinery if all 12 kettles

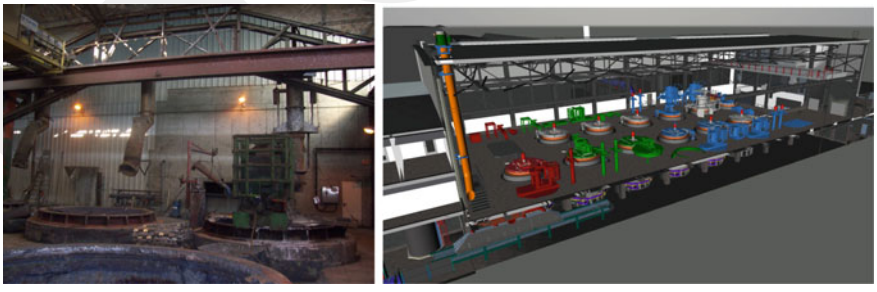

Fig. 3 Left: Old lead refining facility; Right: New lead refining capacity with expansion setup where 12 kettles could be utilized

are installed including their respective hood system (Fig. 4) which is connected to a baghouse with the capacity of 120,000 N m^3/h.

To minimize the utilization of a heating system supplied by fossils, a couple of CFD simulations were performed in order to identify, if adequate working conditions concerning temperature can be realized without an active ventilation concept. Due to that, a model of the plant (Fig. 5) was developed taking into account the heated kettles, pipes, the active exhaust at the kettles and a variation of openings like a ridge turret, windows and gates. In the done simulations, the heating caused by radiation

Fig. 4 Sealed kettle with an installed stirring device, an access point for a dross removal equipment (drag chain conveyor) and the connected duct to the secondary ventilation

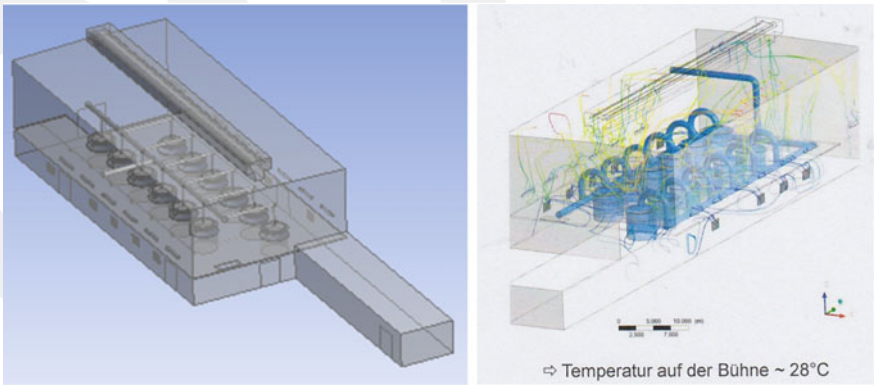

Fig. 5 CFD simulation of the planned building to simulate the temperature on the working platform during summer and winter days in order to avoid an active ventilation system

and convection at the furnaces and pipes and the cooling effect by air getting into the plant at the openings were considered.

The goal of these simulations was the identification of a ventilation concept which provides a temperature range of 17–28 °C at the working area during the whole year. It has to be mentioned that in Hamburg the minimum temperature in winter was assumed with −12 °C and a maximum temperature for summer was considered with 32 °C. For this high peak in summer, which is statistically only the case for less than 10 days per year, the ambient air could not be cooled sufficiently with the foreseen technical measures which demand organizational measures, e.g. gate open, time restriction for permanent workspace, cold beverages).

For an average outside temperature of 18 °C (summer), an adequate temperature can be achieved by opening the gates and the windows in the working area floor and in the ground level. The ridge turret is used for the controlled emission of gas from the plant.

According to the results of the simulations for winter times, all windows and gates should be closed at a low outer temperature. Fresh air will be provided by the ridge turret and will be sufficiently preheated by thermal lift. With a very low outer temperature of −12 °C, the thermal effect does not heat up adequately on the whole working area, if the ridge turret is fully opened (Fig. 6). A simulation of this case showed that a division of the ridge turret into two parts can help (Fig. 6), if one of the parts will be closed during extremely cold days.

In respect of a sustainable operation, a relevant aspect is the commitment for a continuous improvement of working conditions. In the case of operating a lead smelter or lead refinery, this improvement is mainly tracked via the development of the lead in blood concentration of the employees. Since 1999, the limit was reduced from 700 to 400 µg/l, Aurubis progressed in the execution of a couple of measures which are explained in Table 1. Furthermore, an incentive program was launched in 1999 which is based on individual values since 2012 and continues until today. Currently, Aurubis is committed to a maximum lead concentration in the blood for

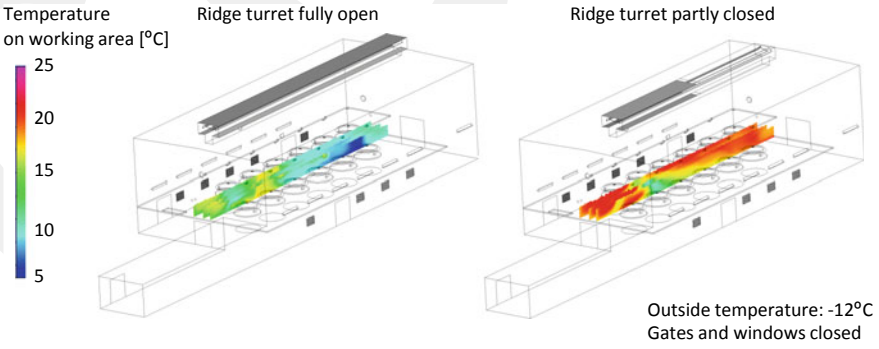

Fig. 6 CFD simulation results for a fully open ridge turret and a partially open ridge turret to manage the ambient temperature on the working platform during winter days

Table 1 Measures to minimize the lead concentration in lead according to the TRGS 505

Criteria/Measures	Technical	Organizational
Plant layout	• Black and white separation for control room, social rooms • Air overpressure in white areas • Several double door locks • Washing facilities next to the production site	
Behavior based safety		• Agreement with workers and union for discussion of values classified in "traffic light" ranges and on individual basis (in a closed group) • Instructions, rules, training people, understanding lead • Incentive program on individual values
PPE (Personal protective equipment)	• Different masks and especially air-stream or air-flow helmets (3 M) with daily cleaning in a special workshop • Daily change of working clothes after shift, including T-Shirt	
Tracking	• Traffic light system for lead in blood values: green/yellow/red for each plant manager	

men with 300 µg/l and for women with 100 µg/l. Therefore, an investigation in the medical department is scheduled minimum twice a year. The limit of 300 µg/l was undercut for the first time in 2016.

Equipment Design Improvements

During the engineering phase, the equipment design of the kettle heating system was challenged in order to improve the efficiency of used natural gas. This could be achieved by applying a new process control system and a failsafe control which shut down the burner in case of a possible overheating of the kettles. All in all, the heating is significantly improved because of the installed thermocouples which have direct contact to the melt and will allow to reach the set temperature without overheating. The new lining of the kettle stations (Fig. 7) allows a faster cooling of the melt which

Fig. 7 Lining of a kettle station with openings for maintenance and the burner equipment

accelerates the period time during cooling, e.g. immediately after antimony removal ($T > 600$ °C).

The step of Zn-removal and Bi-removal takes a relevant portion of the total processing time. Facing the current development of growing complexity in bullion composition, this process step could be de-coupled by the implementation (2018) of a new kettle K7 (Fig. 8).

This new kettle which has also a volume of 200 t is now fully dedicated for the Bi-removal step and received the crude lead after Zn-removal. During the Zn-removal, the lead level is decreasing which is mitigated with the addition of crude lead bullions to this new kettle to manage the bath levels and keep the initial Bi-content before refining on the desired level. All in all, this had a quite positive effect on the Bi concentration Bi-product which is an PbBi alloy.

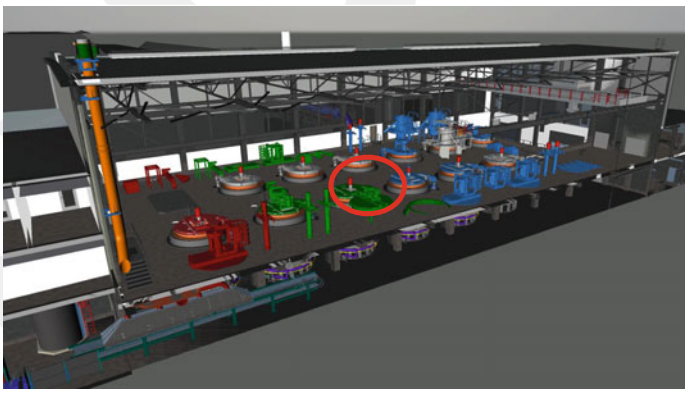

Fig. 8 Implementation of a new kettle to de-couple Zn-removal and Bi-removal stage

Fig. 9 Improved access for Harris cylinder

As a result of the improved overall plant layout, there was more space to implement a new platform which allows the operator to get a safer access to the Harris cylinder (Fig. 9). The whole equipment is made of one part, so that the time in between equipment removal and installation could be shortened.

For the floor of the working platform (Fig. 10), a standard concrete according to DIN EN 206-1/DIN 1045-2 was prepared according to a special recipe. At elevated temperatures, this generates a porosity which then takes the produced water vapor and avoids cracking of concrete by releasing the additional volume into those porous spaces. For the lead refinery, a massive concrete plate was used for the platform, and

Fig. 10 Developed concrete mix for metallurgical applications

above this, a quite large layer of this special concrete mix was added. To address the daily work with heavy equipment, the mechanical resistance was realized by implementing steel needles for a proper reinforcement.

Process Control Improvements

A fundamental knowledge for end-point control for the subsequent refining procedures is from the importance to improve the overall efficiency of the lead refinery. Especially during the Harris process, the oxidation behavior of As, Te, Sn, and Sb is quite important and is influenced by the fluxing strategy. During this study, a plot (Fig. 11) was prepared which shows the point where Sb is significantly oxidized out of the crude lead and will report to the Sn salt. For end-point control, a proper calculation is needed which take the initial Sn concentration in lead and the targeted Sn concentration into account. As derived in this study it seems, that this target of remaining Sn concentration in lead could be at approximately 2000 g/t.

Emicke described a linear function of Sn extraction via the Harris process. This equation was confirmed in this study (Fig. 12) [1]. Using this, equation allows a proper calculation of required refining time, demand for fluxes, and number of used refining cylinder cycles. Furthermore in combination with the finding from Fig. 12, the end-point could be predicted.

In analogy to Fig. 12, the extraction of antimony follows a linear relationship (Fig. 13) regarding the required refining time. The mentioned interruption due to charging additional bullion, the determined equation represents the linear tendency. Following this, the Sb-refining speed is approximately 0.09 wt% per hour.

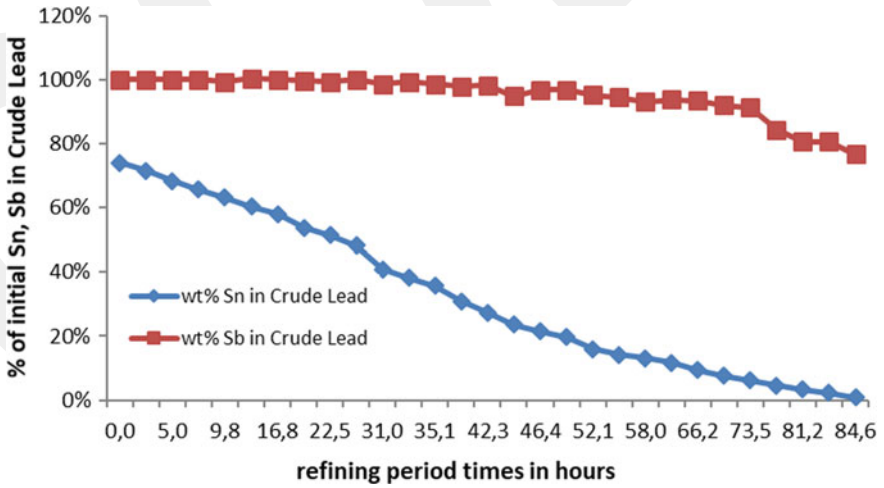

Fig. 11 Comparison of Sn and Sb content in crude lead during the Harris Sn-refining process

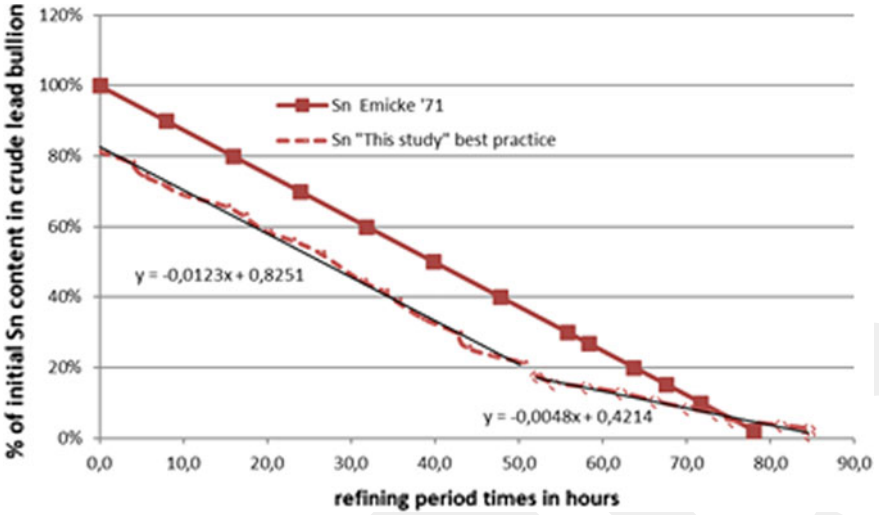

Fig. 12 Forecast for Harris process of Sn-refining

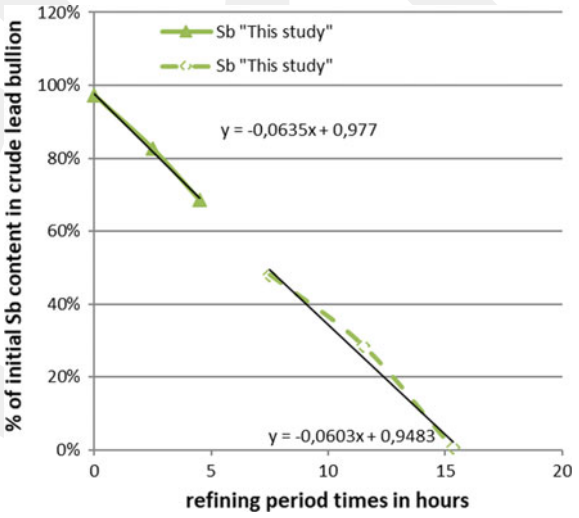

Fig. 13 Forecast for Sb-refining (oxidation process)

Design Criteria for the New Lead Refinery

From metallurgical perspective, the main goal was the expansion of existing refining capacities for those elements which were expected to be increased in raw materials for the primary smelter or secondary smelter. With the increasing complexity, the requirement for flexible process design is demanded from the smelter as well as from the downstream refining operations. This was a key task for the project team during

Table 2 Design data for the old lead refinery versus the new facility [2, 3]

Criteria of comparison	Old lead refinery	2014 commissioned lead refinery
Capacity for crude lead (t/a)	20,000–30,000	24,000–50,000
No. of kettles	8	8 installed, 4 spare capacity 9 installed since 2018
Volume of kettles	200 t kettles 90 t kettle Total = 1490 t molten lead	250 t melting kettle 200 t all others Total = 1850 t molten lead
Refining procedure	As, Te, and Sn—Harris process Cu removal—Colcord process Sb—Harris process/oxidation Bi—formation of CaMgBi-crystal Precious metals—Parkes process Zinc—vacuum de-zinking	As, Te, and Sn—Harris process Cu removal—Colcord process Sb—oxidation Bi—formation of CaMgBi-crystal Precious metals—Parkes process Zinc—vacuum de-zinking
Fine lead casting capacity (t/h)	25–30	>40
Baghouse capacity (N m^3/h)	80,000	120,000
Secondary ventilation system	10,000 N m^3/h per kettle and 20,000 N m^3/h for drossing unit	13,000 N m^3/h per kettle (9 pcs.) and 20,000 N m^3/h for drossing unit

the planning phase. Within this period, the full refining procedures were critically reviewed, especially regarding their efficiency and quality. Calculating different scenarios for crude lead bullion annual production and elemental concentration, the new design capacities for the most relevant elements (As, Te, Sn, Sb, Bi, Ag) were defined. A comparison of the procedures and equipment is summarized in Table 2.

Figure 14 illustrates the development of refining capacity for crude lead processing, silver, arsenic, bismuth, antimony, tin, and tellurium. The baseline is the blue bar which represents the capacity of the old lead refinery. The grey bars are the additional capacities that were used as design criteria for the new plant. It becomes obvious that the complexity of the bullion will limit the maximum input of total crude lead capacity due to expected effort for refining procedure. For the mentioned elements especially Sn and Sb are the most demanding refining operations in terms of processing time (Table 3 and Fig. 15).

The most time consuming process step is the extraction of Te, As, Sn, and Cu in the kettle K2. Extracting of tellurium via Harris process is a very fast step due to the fast chemical reaction of tellurium and sodium to form the Te-salt. The Te-refining requires only 6% of the total refining period time to extract both, Te and Sn. So it could be stated that the Sn-removal step takes the major share of the time. The required time depends mainly on the Sn initial content in crude lead and can be optimized by using

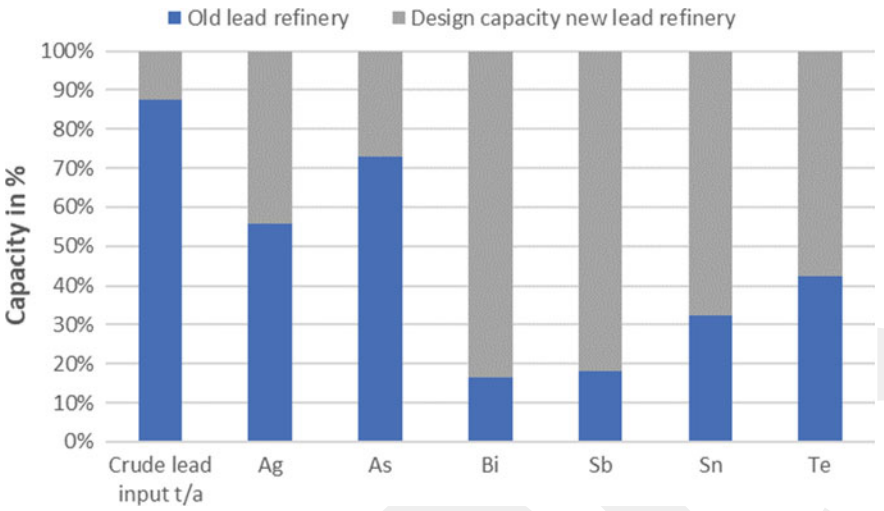

Fig. 14 Comparison of the developed capacities for crude lead processing and respective impurities enabled with the commissioning of the new lead refinery

a parallel Harris cylinder setup and process control for the viscosity management of the produced salt melt. Last but not least, the de-copperization with the addition of elemental sulfur needs a cooling down period to lower the temperature and avoid excess sulfur vaporization. The next step is the Sb removal, which takes place at kettle K3. For the established formation of PbSb litharge, a heating period is required which lengthen the refining time a bit. As "pure" refining time where injected oxygen is in contact with lead only 30% could be specified. In comparison with the well-described Harris process, this method for Sb extraction (Table 4) is much faster in terms of reaction time.

The de-silvering of the lead required approximately 10% of total process time. For de-zincing of lead as well as for removal of bismuth, approximately 13% of total time is consumed. The final softening will adjust the lead regarding to the given specifications of fine lead before fine lead will be casted, and in this calculation, 7% of total processing time was measured to cast approximately 120 t of fine lead.

Operational Experience During First Years of Operation

The ramp-up of the new lead refinery was planned according to the well-known McNulty approach [4]. As Fig. 16 shows, the performance curve for crude lead processing fits to the series-2 curve from McNulty. In the first year, approximately 72% of the annual design capacity could be achieved. In the following years, the actual processed amounts of crude lead were close to the design capacity. With increasing complexity in raw materials, somehow the total lead volume which flows

Table 3 Kettle setup for subsequent refining step

Kettle	K1	K2	K3	K4	K5	K6	K7 (2018)	K8	K9
Step	Melting—de-drossing	Te/Sn-removal De-copperization	Antimony removal	Buffer	De-silvering	De-zincing	De-bismuthing	Softening preparation and casting of fine lead	Oxidation of bi-foam Casting of PbBi alloy

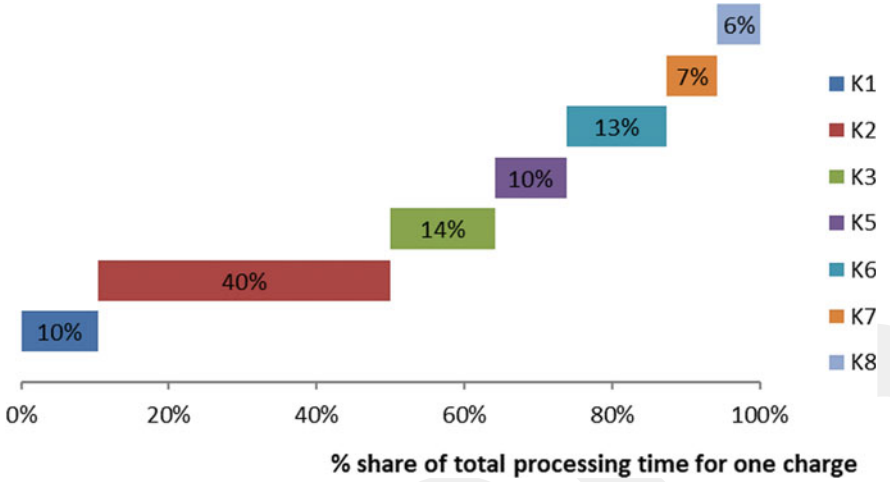

Fig. 15 Period time for a whole batch of a charge crude lead

Table 4 Comparison of methods to extract Sb from lead phase within the refining process

	Harris process (NA-Emicke 1970) [1]	Aurubis process (Sb-removal)
Initial Sb content (wt%) in lead phase to compare both processes	1.5 wt%	1.5 wt%
Equipment	Kettle with Harris cylinder including a tank to granulate the salt + filter + regeneration of process solution	Stirred kettle with an oxygen lance and a launder system to overflow the formed PbSb litharge
Oxygen delivery/Additives	NaOH/$NaNO_3$	99.5% O_2 from lance
Process time	52 h	39 h
Product	White antimonite 77.5 wt% Sb Grey antimonite 19.3 wt% Sb	PbSb litharge with >30 wt% Sb

from the lead smelter to the refinery was not further increased. The composition of the bullion demanded more refining time which is the explanation for the performance in year four and five.

Figure 17 demonstrates the large capacities for fine lead casting which were not fully utilized during first years after commissioning. This plot is in-line with the argumentation of growing complexity of raw materials at constant level of lead volume as carrier originated at the lead smelter.

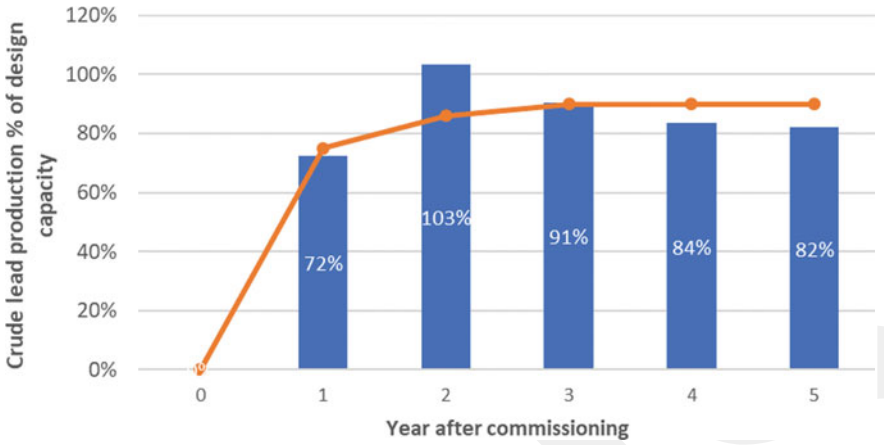

Fig. 16 Ramp-up curve after commissioning and comparison with approach from Terry McNulty's curve series 2 [4]

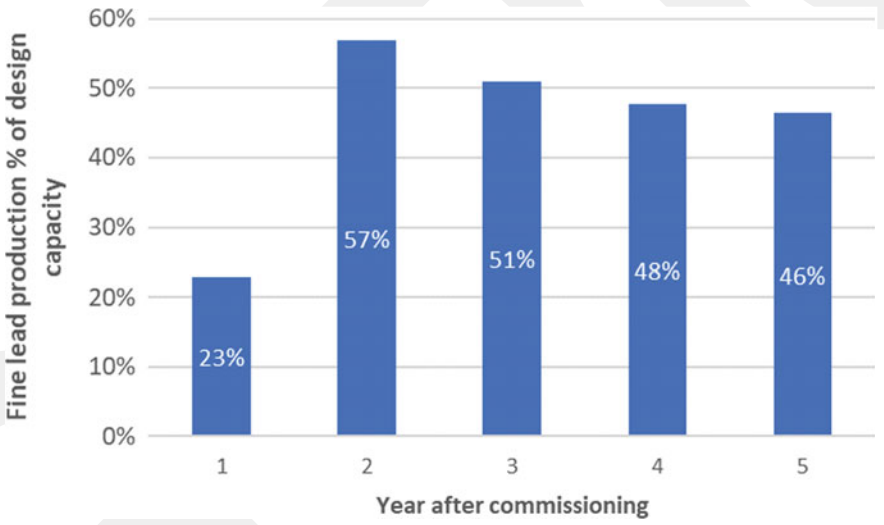

Fig. 17 Ramp-up curve for fine lead casting after commissioning of the new lead refinery

Summary of Compiled Operational Experience

Five years of operation showed up a lot of improvements but as well as raised up challenges what has to be improved further. In Table 5, there is a compilation of the most relevant findings. Following this table, some selected examples are discussed in detail referring to plant layout and process control strategy.

Table 5 Operational experience and taken actions during first years after commissioning

Positive	Need improvement	Measures/Actions
• Better suction of kettles and de-drossing units due to better cover of kettles, increased off-gas volume and separate baghouse • Less level handling at kettles, reduced the casting of intermediate blocks • Better temperature control due to kettle design, two burners for each stand • Frequency control for each stirrer and pump • Parallel de-drossing of kettles possible • Improved removal of Zn deposit from vacuum lid instead of vacuum bell • Shorter ways on the shop floor for crane works (parking stands for pumps, covers, and stirrers next to kettles) • Safer access to Harris cylinder and working platform • Plugs next to every kettle • Shop floor ground made of special concrete, heat resistant • Casting speed approximately 40 t/h • Crane can reach all necessary positions in the refinery • Possibility of installing a second crane if required	• Quality of welding and sealing at vacuum kettle and lid in the beginning • Time consuming procedure to protect the cooling edge of vacuum kettle by installing a protection shield at each batch during removal of bismuth foam	
	• Temperature changes during bismuth removal process caused cracks at cooling edge later on	• Installation of additional kettle (No. 9) in 2018 to separate de-zincing and de-bismuthing process • Due to the installation of a separate de-bismuthing kettle the de-zincing process runs very stable
	• No experience in de-zincing parameters with lid, no chance to take samples	• Time controlled procedure is preferred

(continued)

GCRIS

Table 5 (continued)

Positive	Need improvement	Measures/Actions
	• Installation of dross transportation system under the roof of basement with bad accessibility • Solid dross particles block the dross transportation system	• Installation of additional sieve
	• No segments in dross and kettle suction pipes	• Installation of valves and blanking plates became necessary afterwards
	• Moulds were too cold in winter time	• Optimization of burners at casting machine
	• Double work for the installation of equipment	• Cover and equipment have to be moved separately due to size and load

Conclusions

The main aspects associated with the conceptualization, development, implementation, and further operation of Aurubis "new lead refinery" have been presented.

The new lead refinery has been a key pillar supporting the implementation of Aurubis multi-metal strategy, allowing a sustainable processing of complex materials, and acting as a key enabler to support synergies between the copper and lead lines.

With the successful commissioning of the plant, Aurubis expanded the refining capacities for As, Te, Sn, Sb, Bi, and Ag. In addition, Aurubis was also committed to significantly improve in environmental and occupational health and safety aspects. The results of this phrased project goals could be seen from the last years of operation which showed significant improvements as follows:

- lowering the lead concentration in the blood (sealing of equipment, layout for separation of black/white areas),
- an improved efficiency for the use of fossils (natural gas) by implementing a well-working burner control system and lining concept of the kettle stations,
- an improved secondary ventilation system (kettle sealing, design of ridge turrets),
- use of refining capacities (lead bath level management, process control/end-point detection, improved equipment design).

From the operational point of view, it can also be shared that the operation benefits from the well-planned plant layout providing a quite better access to the kettles, allowed to reduce the required casting of intermediate bullions which limits the space on the platform, and the significant improved dross handling. This accurate planning of the project was also shown with the help of the well-done ramp-up phase which was nearly according to the McNulty series-2 approach.

With this facility, integrated into a quite complex infrastructure at the site in Hamburg, Aurubis placed the basement for a sustainable downstream lead refining operation which is able to cope with state of the art demand in occupational health and safety, environmental protection and is well-prepared for up-coming challenges in terms of growing complexity.

Acknowledgements The authors gratefully acknowledge the management of Aurubis for the possibility to work on this particular topic and the permission to publish this. Also, the authors would like to thank Gerardo Alvear for his support to improve the quality of the paper.

References

1. Emicke K, Holzapfel G, Kniprath E (1970) Lead refinery and auxiliary by-product recoveries at Norddeutsche Affinerie (N.A.). Extractive metallurgy of lead and zinc. In: AIME World symposium on mining and metallurgy of lead and zinc, vol 2. The American Institute of Mining, Metallurgical and Petroleum Engineers, New York, pp 867–890
2. Bauer I, Dammann B (2016) New lead refinery at Aurubis Hamburg. Presentation GDMB Lead Expert Committee 2016, Plovdiv Bulgaria
3. Plitzko C (2017) Complex lead refinery in a secondary copper lead smelter. In: EMC 2007, Düsseldorf, Presentation
4. McNulty T (2004) Minimization of delays in plant startups. Improving and optimizing operations. Plant operators forum 2004, Society of Mining, Metallurgy, and Exploration, Inc., Littleton, pp 113–120

GCRIS

Tin Treatment in Kosaka Lead Smelting

K. Miwa, E. Yamaguchi and S. Satoh

Abstract In Kosaka Smelting and Refining Co., Ltd., tin input increases rapidly from around 2008, because of TSL furnace starting up and raw materials change from ores to E-scraps. With tin increase, more dross was produced in lead purification process, and the dross became deadstock. To recover metals in stocked dross, new tin recovery process has been installed. At first, in the tin smelting, dross is reduced with coke in electric furnace and metal consist of tin and lead is produced. The obtained metal is pulverized under 200 μm diameter and sent to leaching process with NaOH. After passing through purification processes, the tin containing liquid is sent to electrowinning process and tin metal is recovered. Thanks to these recovery processes installation, dross stock has been decreased to zero and other metals in the dross have also been recovered. Currently, tin metal itself also becomes one of the main products of Kosaka. In this paper, these tin recovery processes are described.

Keywords Sn · Lead refining · Pyrometallurgical refining

Introduction of Kosaka Flow

Kosaka Smelting and Refining Co., Ltd. is a smelter in northern part of Japan. The main products are electrolytic copper and lead. In addition, some metals—including tin, the theme of this paper—are recovered as by-products.

The recent production is shown in Table 1.

As a part of Kosaka process, the process of lead smelting section is shown in Fig. 1. The main raw material for the lead smelting is lead sulfate, which is composed of dusts from copper smelting and residues from zinc refinery.

K. Miwa (✉) · E. Yamaguchi · S. Satoh
Kosaka Smelting and Refining Co., Ltd., 60-1 Otarube Kosaka-machi Kazuno-gun, Akita 017-0202, Japan
e-mail: miwak@dowa.co.jp

© The Minerals, Metals & Materials Society 2020

A. Siegmund et al. (eds.), *PbZn 2020: 9th International Symposium on Lead and Zinc Processing*, The Minerals, Metals & Materials Series,
https://doi.org/10.1007/978-3-030-37070-1_65

Table 1 Annual production of Kosaka (2018fy)

Product	Production
Gold	5569 kg
Silver	432 t
Copper	9061 t
Lead	21,499 t
Tin	487 t

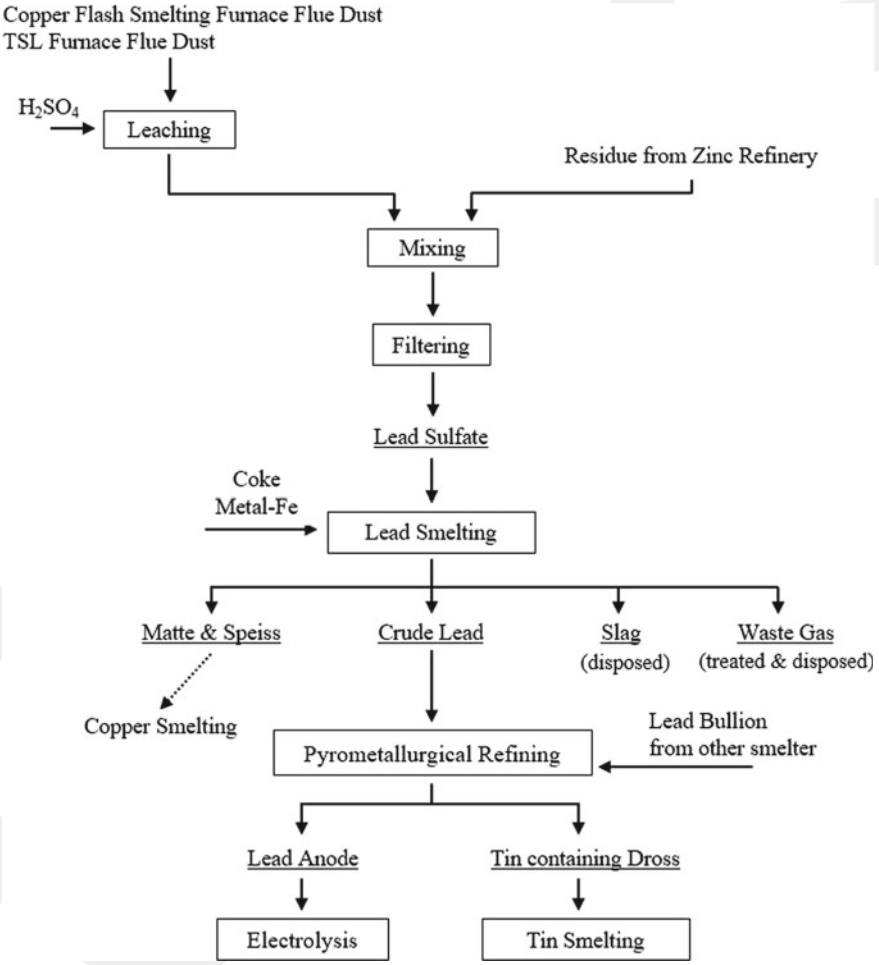

Fig. 1 Flow sheet of lead smelting

Increase of Sn Input

In recent years, tin input to lead smelting section has been increased.

For copper smelting section, the main smelter was changed from flush smelting furnace to TSL furnace on 2008, focusing on recycled materials. The dust from copper smelting section became containing more tin because of raw material shift from ores to E-scraps. And the characteristics of Kosaka's TSL furnace also led to tin increase: both oxidation and reduction processes are continuously conducted at one furnace.

In addition, zinc concentrate also contains more tin as impurities because of tight zinc concentrate market.

From these reasons, lead sulfate, the first material of lead smelting, was containing more and more tin as shown in Fig. 2.

This increase mainly affected lead purification process. The purification process is softening method: molten crude lead is stirred at 600 °C and tin in the crude lead is preferentially oxidized with air at this condition. The product is tin-enriched-dross: the typical composition is shown in Table 2.

The more tin inserted, the more dross produced. As a result, the stock of tin-enriched-dross grew rapidly as shown in Fig. 3.

In the purification process, gold, silver, and other valuable metals are partly distributed to dross. Dross stock increase meant valuable metals were stacked in remaining dross and became deadstock. These precious metals should be recovered.

In addition, too much tin input extended the lead purification process time, and lead productivity got worse. These phenomena had negative effects on lead smelting section.

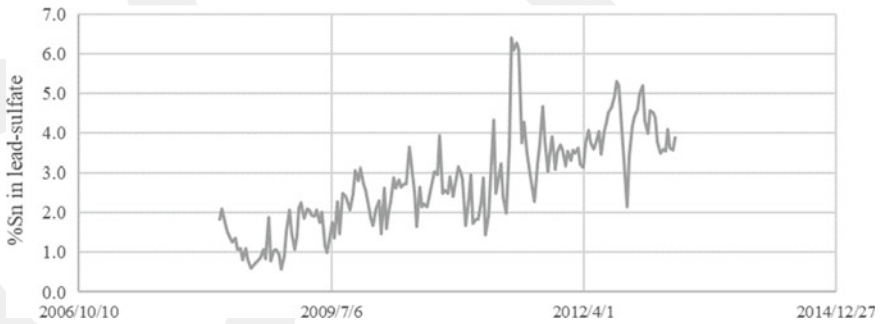

Fig. 2 Increase of %Sn in lead sulfate

Table 2 Typical composition of tin-enriched-dross

Au (g/t)	Ag (g/t)	Pb (%)	Sn (%)	Sb (%)	Bi (%)
15	3000	35	45	5	0.5

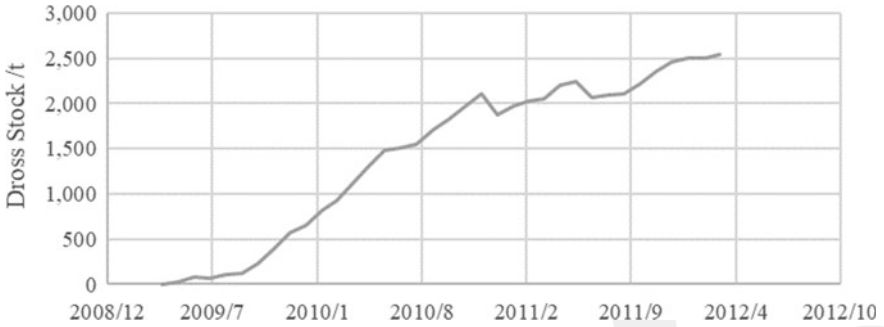

Fig. 3 Stock of tin-enriched-dross (before recovery system installed)

Sn Recovery System

To deal with the tin increase, new recovery system has been installed. Figure 4 shows the process of tin recovery and metal tin production.

Tin Smelting (Reduction)

Tin-enriched-dross from lead purification process is fed to tin smelting section. The main facility is electric furnace, having a 1.8 m diameter and 1.6 m height. The outlook of the furnace is shown in Fig. 5.

Coke and dross are together inserted into the furnace and following reduction reactions occur.

$$SnO_2 + 2C = Sn + 2CO$$

$$PbO + C = Pb + CO$$

The product is called "Sn–Pb metal". The typical content of the metal is shown in Table 3.

Molten Sn–Pb metal is tapped from the furnace and casted into ingots having about 500 kg weight. The ingot is transported to the next process, leaching section.

Leaching

At the beginning of leaching section, Sn–Pb metal ingot is again melt and pulverized into powder style having 200 μm diameter. This process is aimed at dissolving tin effectively.

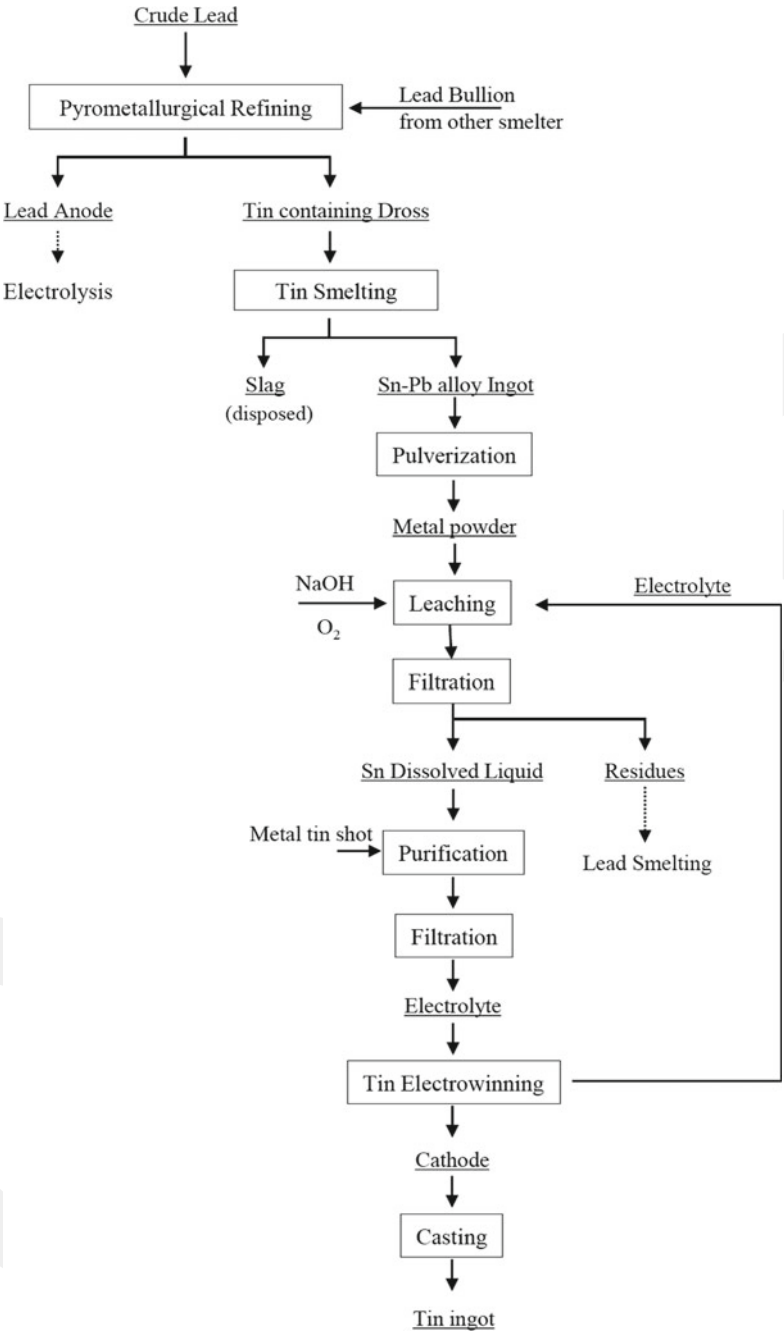

Fig. 4 Flow sheet of tin recovery

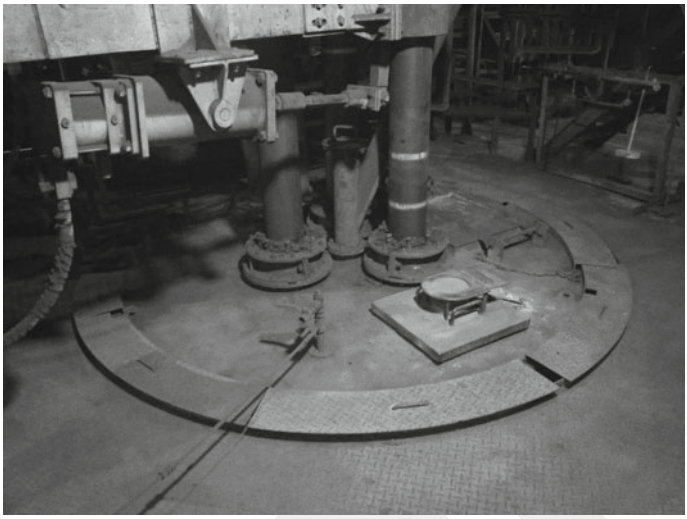

Fig. 5 Sn smelting furnace (outlook)

Table 3 Typical composition of Sn–Pb metal

Au (g/t)	Ag (g/t)	Pb (%)	Sn (%)	Sb (%)	Bi (%)
20	4500	50	45	3.5	0.5

In the leaching process, tin dissolves with the following reaction.

$$Sn + 2NaOH + O_2 + 2H_2O = Na_2Sn(OH)_6$$

In the alkaline condition, tin is preferentially dissolved into aqueous liquid than lead. However, if too much free NaOH remained after tin leaching, lead would be also leached and would affect the electrowinning. So, to avoid lead leaching, NaOH feed is calculated based on tin composition of each Sn–Pb ingot: target-free NaOH content after tin leaching is under 25 g/L.

Purification

In the purification process, at first, metal tin shot (about 99%-Sn) is fed and remaining lead is substituted by tin with the following reaction.

$$NaHPbO_2 + H_2O + \frac{1}{2}Sn = \frac{1}{2}Na_2Sn(OH)_6 + Pb$$

Table 4 Operating conditions of tin electrowinning

Current density	100 A/m^2
Current efficiency	80–90%
Electrolyte temperature	60–80 °C
Electrolyte composition Sn	30–50 g/L

Next, antimony is excluded by feeding Na_2S. The main mechanism seems to be also substitution, but in antimony case, sulfur addition is necessary to accelerate the reaction. Remaining lead also consumes sulfur, so Na_2S addition is conducted after lead is removed. Precipitated impurities are separated by filtration.

Electrowinning and Casting

After filtration, the electrolyte is sent to electrowinning cells. Table 4 shows operating conditions of tin electrowinning, and Fig. 6 shows the outlook of cells.

Metal tin electrodeposited on cathode is split, melt, and casted into ingot of 18 kg each. Table 5 shows the typical composition of final product tin: the product is

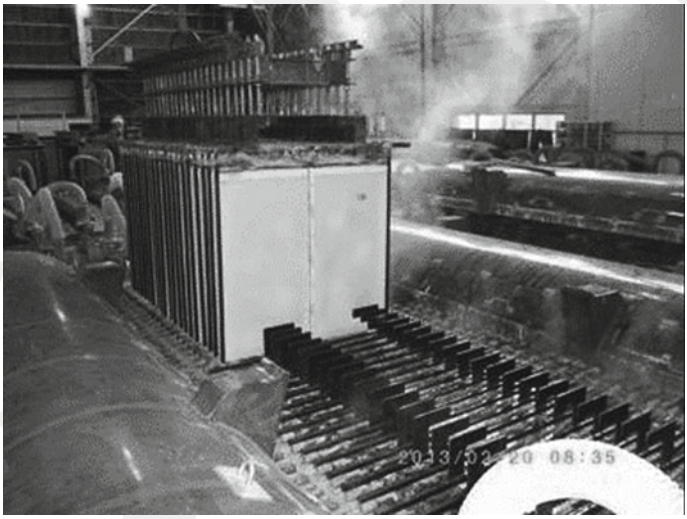

Fig. 6 Electrowinning cells (outlook)

Table 5 Components of Kosaka tin metal

Sn (%)	Fe (ppm)	Cu (ppm)	Sb (ppm)	Pb (ppm)	Zn (ppm)	Cd (ppm)
>99.99	30	2.5	1.5	1.5	<0.5	<0.5

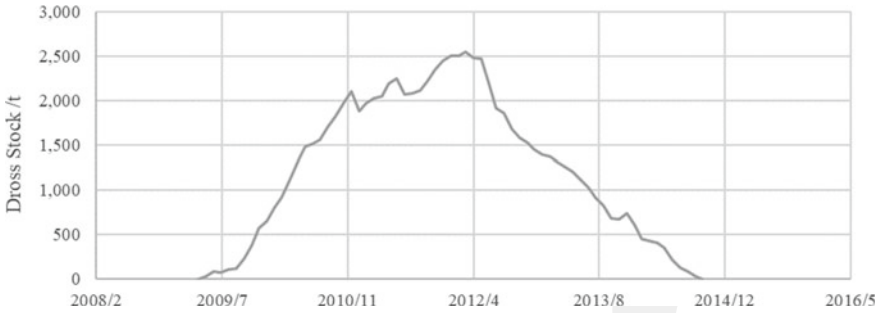

Fig. 7 Stock of tin-enriched-dross (after recovery systems installed)

4N-grade tin metal.

The primary impurity is iron from SUS cathode and anode.

Current Challenges About Tin Metal Production

Currently, the technical topic in tin production is additional purification. As shown in Table 5, current electric tin metal has 4N grade. To achieve 5N grade product for electronics regions, electrodes of new materials and coat of the pool wall are tested to eliminate iron contamination.

Conclusion

To treat tin input increase, the tin recovery process was installed in Kosaka Smelting and Refining.

Smelting section with electric furnace convert the purification product dross into metal, that is easy to dissolve into aqueous liquid. By alkaline electrowinning, dissolved tin is recovered as product.

Thanks to this tin recovery system, dross stock was decreased, and nowadays no deadstock is remained, as shown in Fig. 7.

By increasing the ability of treating impurities, we are continuing to accept wide range of materials and recover many types of elements.

Acknowledgements The authors wish to thank the Kosaka Smelting and Refining Co., Ltd. and DOWA Metals & Mining Co., Ltd. for granting permission to publish this paper.

True Traceability Enabled by In-Line Laser Marking of Lead and Zinc Ingots

Alex Fraser and Jean-Michaël Deschênes

Abstract In the last few years, traceability has become an important asset for improvement of manufacturing processes and logistics in the primary metal industries. One of the key elements to obtain true traceability is the ability to consistently apply an identifier on the metal product, as early as possible in the manufacturing process. This often implies marking on very hot metal in harsh foundry environment, conditions that are far from ideal for traditional labelling or inkjet printing systems. In this paper, we discuss the feasibility of laser marking of lead and zinc ingots directly in the production line. Such laser marked identifiers are very robust and the marking machines require much less maintenance than traditional technologies. Emphasis is put on the process speed and contrast level. Dynamic compensation for the inaccurate part positioning is also explained, which makes the system capable of handling most real-world industrial conditions.

Keywords Laser marking · Lead · Zinc · Traceability · Identifiers

Introduction

Traceability systems have become a key asset in the primary metal industry within the last few years. They help improve the production process as well as eliminating the risk of shipping the wrong alloy, which is of huge value for producers. In order to work, the traceability process requires a reliable way to apply durable unique identifiers on the ingots and to maintain their readability over their entire lifecycle. Old technologies used such as paper labelling, inkjet marking, and dot peen marking all have some drawbacks related to low reliability and/or high maintenance costs, so most producers are looking at laser technologies to replace them. Indeed, laser direct part marking is known has a mature technology that is very efficient, reliable and with very low operational costs. In addition, the laser marked identifiers have high contrasts and are etched permanently in the material, which makes them very

A. Fraser (✉) · J.-M. Deschênes
Laserax Inc, 2811 Avenue Watt, Québec, QC G1X 4S8, Canada
e-mail: afraser@laserax.com

© The Minerals, Metals & Materials Society 2020

A. Siegmund et al. (eds.), *PbZn 2020: 9th International Symposium on Lead and Zinc Processing*, The Minerals, Metals & Materials Series,
https://doi.org/10.1007/978-3-030-37070-1_66

suitable for long-term, durable readability. In this paper, we are presenting the results of a laser marking solution that is suitable to mark either lead or zinc ingots. The marking time to produce the identifier is optimized for both lead and zinc, and the depth of focus is precisely measured. The details of the implementation of a laser marking system into an in-line machine are also explained.

Laser Marking Process

Laser marking of metals like lead and zinc allows generating a high contrast identifier and black marking on white background. We used the experimental setup shown in Fig. 1 to study laser marking on zinc and lead. A laser controller is used to synchronize the emission of a pulse fiber laser with the movements of a galvanometer scanning system. The focused laser beam is then precisely adjusted on the workpiece surface using a motorized elevation stage.

The laser characteristics are presented in Table 1.

Figure 2 shows an example of the laser marked Data Matrix Code (DMC) on these two materials. Both metals can be efficiently laser marked with high contrast identifiers, zinc, and lead exhibiting 84 and 77% contrast values, respectively. The contrast measurements are done by a Cognex reader, model DM8072.

This change in coloration is caused by the laser modifying the microstructure of the surface, thus changing its light reflection and absorption properties [1]. Figures 3

Fig. 1 Schematic of the experimental setup used (left) and photograph of the LXQ-20W laser marking system (right)

Table 1 Pulsed fiber laser characteristics

Laser type	Pulsed fiber laser
Max. pulse energy	1 mJ
Max average power	20 W
Pulse repetition rate	5–200 kHz
Pulse duration	100 ns
Wavelength	1064 ± 2 nm
Lens	420 mm
Focused pulsed diameter	~100 μm (@ $1/e^2$)

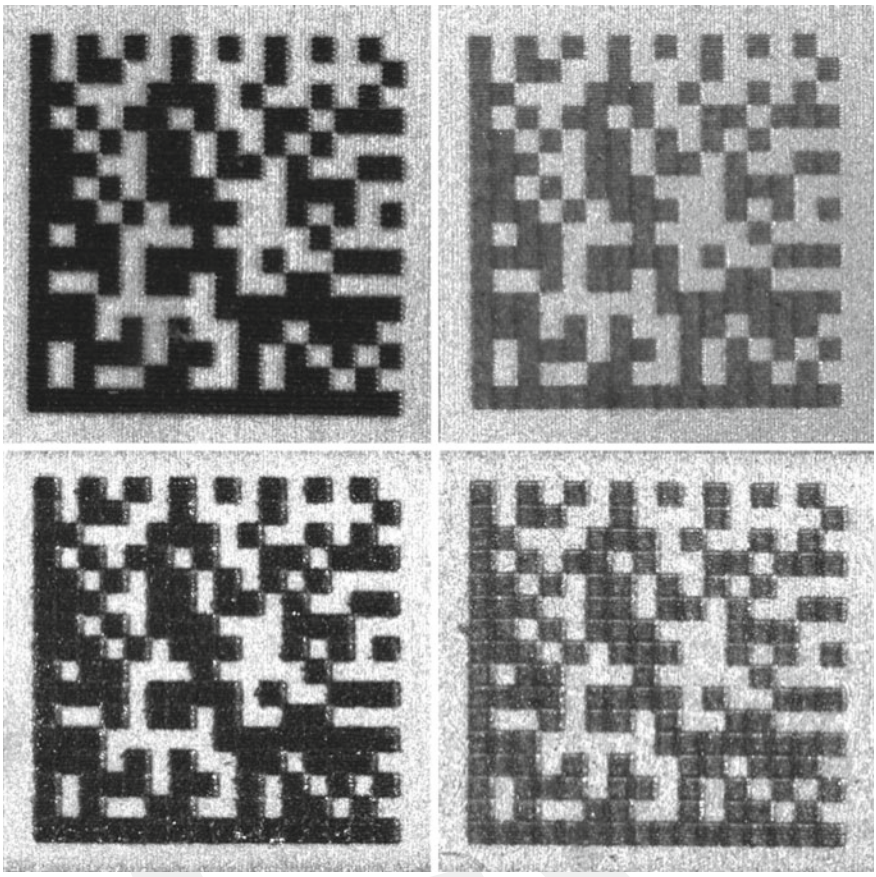

Fig. 2 Laser marking of a 10 mm DMC on zinc (top left: 84% contrast and top right: 47% contrast) and lead (bottom left: 77% contrast and bottom right: 55% contrast)

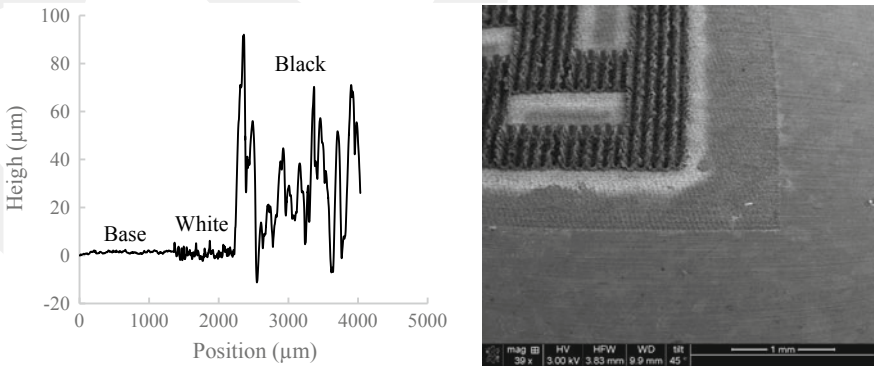

Fig. 3 Surface profile measurement (left) and SEM image (right) of a portion of a DMC mark on zinc that includes base material (not laser treated), white background, and blackened portion

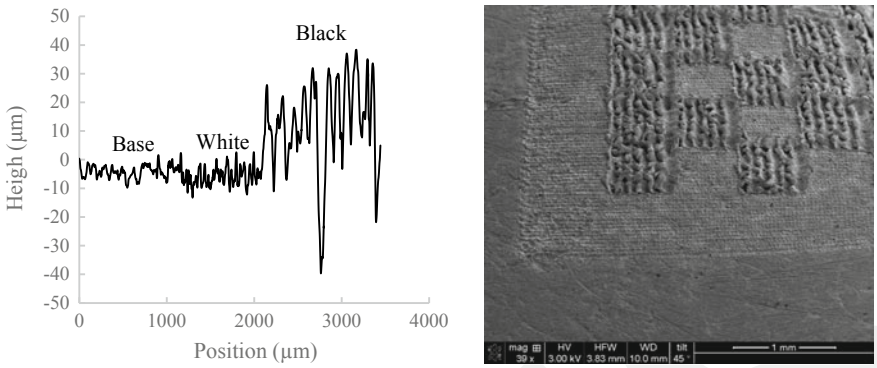

Fig. 4 Surface profile measurement (left) and SEM image (right) of a portion of a DMC mark on lead that includes base material (not laser treated), white background, and blackened portion

and 4 show SEM images and surface profiles of the black and white surface on zinc and lead, respectively.

A previous published study shows the marking speed and contrast achievable for several non-ferrous metals including lead and zinc [2]. Figure 5 shows the marking speed obtained with a 100 W laser to reach a grey level of 100 (on a 256 grey level scale).

We performed a similar experiment, but this time the contrasts and readability of DMCs were measured with a Cognex code reader model DM8072 for different set of parameters. The results are shown in Fig. 6 where we can see the contrast level for a 10 $\times$ 10 mm DMC marked on lead and zinc. Each point represents the optimum set of parameters that gives the higher contrast for a given time.

These results show that the contrast attainable is similar for both lead and zinc. However, the marking speed is much higher for lead, as it can be understood from

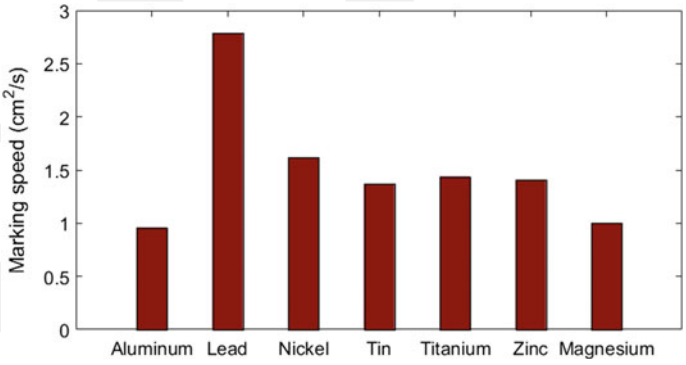

Fig. 5 Marking speed for different non-ferrous metals to obtain a 100/256 contrast level [2]

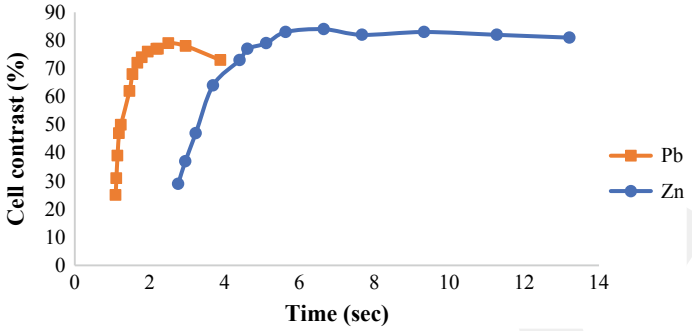

Fig. 6 Cell contrast (%) with respect to marking time for a 10 mm DMC mark on lead (squares) and zinc (circles) with the LXQ-20 2D (20W) laser marking system

the much shorter time required to get the maximum contrast value (approx. 2.4 s compared to approx. 6 s).

In addition to having the right parameters set to achieve the highest contrast, another very important aspect of a laser marking process is the focal range. As we move away from the focal point, the laser beam diverges and the pulse diameter increase. As the pulse diameter increases, the energy density decreases up to a point where it is too small to mark the metal surface. The focal range refers to the position interval where it is still possible to do laser marking. A bigger focal range allows to have a greater sample positioning tolerance relative to the laser head. We studied in detail the focal range for zinc and lead. To do that, we used the same setup shown in Fig. 1.

DMCs with the optimal cell contrast on lead and zinc (see Fig. 6) were marked at different positions with respect to the focal spot position, and the contrast was measured with a Cognex DM8072 code reader and grader. Figure 7 shows the evolution of the marking contrast for both metals.

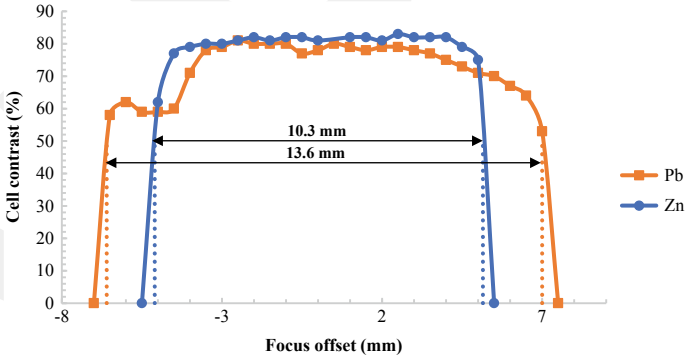

Fig. 7 Contrast value with respect to focus offset for lead (squares) and zinc (circles) obtained with the LXQ-20 2D (20W) laser marking system

These measurements indicate that the marking system can accommodate part positioning variation of 13.6 mm for lead and 10.3 mm for zinc while keeping a contrast value above 50%. If the positioning precision of the surface to mark is within that range, a 2D laser head is an appropriate option. On the other hand, if the part positioning process does not allow to be within that range, the solution must include a 3D laser heads with dynamic part positioning compensation with integrated distance sensors. Next section presents how to implement this.

Integration

Marking needs of lead and zinc smelters are typically either for large ingots (jumbos), individual small ingots or small ingot bundles. All these needs are addressed by the laser marking solution presented in this paper.

As shown in Fig. 7 of the previous section, in order to create a high contrast mark, the focal spot needs to be within a few millimeters of the surface to mark (10.3 mm for zinc, 13.6 mm for lead). Often this is not the case and we then must use a 3D head combined with a laser distance sensor. The 3D head includes a moving lens that allows to move the focus distance to keep it precisely on the surface. With this feature, the allowable distance variation is much higher and reaches approximately 200 mm. Integrated solution to mark jumbos or bundles is shown in Fig. 8.

These machines have doors that open and close to let the part to mark go in and out while keeping the laser beam enclosed for safety. The mounting position of the laser head and sensors depends on the side of the part to which the marking is to be applied.

If a marking is to be applied on either the front or back side relative to the part movement, the laser is mounted at 45° and the sensors are mounted in the door (see

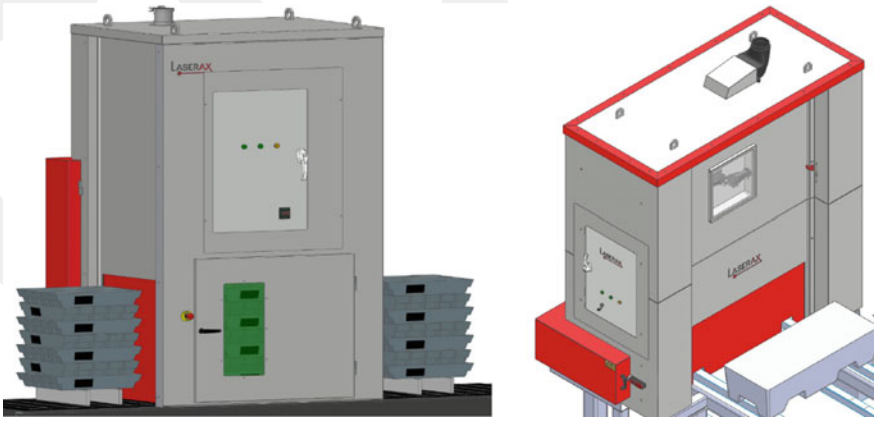

Fig. 8 Laser marking machine for bundles (left) and jumbos (right)

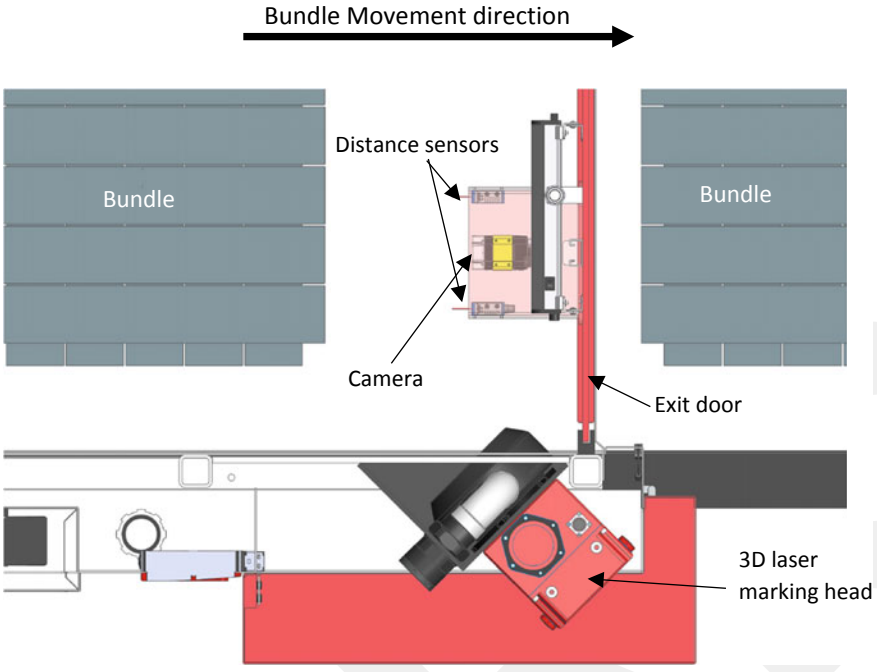

Fig. 9 Top sectional view of the laser marking machine to mark front or back side of the parts

Fig. 9). While the door is closing, the sensors measure the part profile; the shape and position of the part are then transferred to the 3D lasers which adapt the marking according to the measurement.

If the marking is to be done on the sides (see Fig. 10), then the lasers are mounted perpendicular to the surface and both sensors on each side of the laser head. Again, the sensors transfer the information of the distance of the part so the laser can compensate for offset and angle of the surface with respect to the laser head.

A camera (model Cognex DataMan 262X) is integrated to the systems to read the laser marked code (either 1D or 2D) right after marking and save read data and contrast for user reference and preventive maintenance. An additional distance sensor can also be mounted in the enclosure roof, pointing down to measure the part height, that helps to the laser marking position adjustment (especially for bundles).

To mark on individual ingots on a moving conveyor, the machine shown in Fig. 11 is used.

This machine can include either 2D or a 3D head, depending on the surface height variation that the system needs to handle.

All machines presented in this section are Class 1 certified laser equipment compliant with both ANSI1040.10 and IEC 60825-1, which are the American and international standards for safe use of lasers.

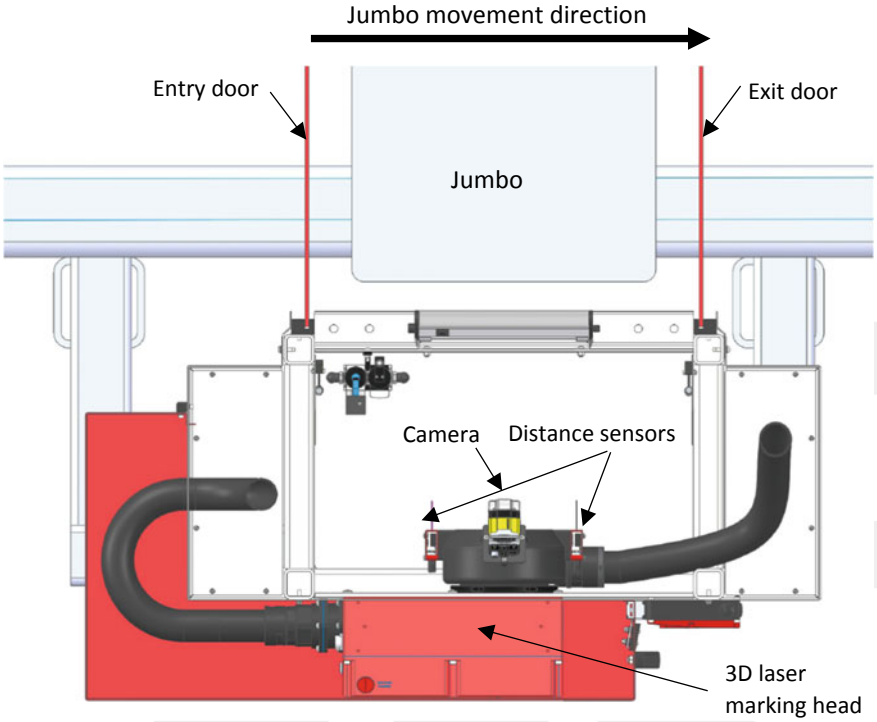

Fig. 10 Top sectional view of the laser marking machine to mark the sides of the parts

Conclusion

Laser marking of lead and zinc can be accomplished with single-mode fiber lasers. High contrast identifiers such as human readable characters, 1D or 2D codes, and logos can be rapidly marked on lead and zinc surfaces to enable traceability of the parts. Two-dimensional or three-dimensional laser marking systems can be used depending on the precision of the positioning of the part with respect to the laser marking head.

Machines are available to mark either individual ingots moving continuously on a conveyor or bundles and jumbos inside an enclosure that is integrated on an indexing conveyor. Integrated reading cameras allow live monitoring of the laser marking process and can guarantee that the part is correctly marked and readable. With their high reliability and low maintenance, these machines pave the way to true in-line traceability for the lead and zinc primary and secondary metal industries.

Fig. 11 Laser marking machine for individual ingots in movement on a conveyor

References

1. Maltais J, Brochu V, Frayssinous C, Vallée R, Godmaire X, Fraser A (2016) Surface analysis study of laser marking of aluminum. In: Proceedings of ICSOBA
2. Fraser A, Maltais J, Godmaire XP (2018) Analysis of laser marking performance on various non-ferrous metals. In: Light metals 2018. Springer, Cham, pp 937–941

Advanced Technologies Reliant on the Properties of Lead

Timothy Ellis, Travis Hesterberg and Mark Drezdzon

Abstract Over the past several years, great strides have been made in the fundamental understanding of the processes at play in a lead (Pb) battery. Using modern analytical opportunities such as high energy X-rays available at the Advanced Photon Source at the Argonne National Laboratory and Scanning Laser Mass Spectrometry, new features of Pb battery processes are being uncovered. And though the Pb battery is the largest application of Pb in the modern economy, other technologies take advantage of the unique properties of Pb. New battery types such as Li/PbS and solar cells/thermoelectrics based on the perovskite structures on materials contain Pb which are emerging as important technologies. These applications not only represent new opportunities for Pb in the economy, but also will motivate the industries continued need to maintain its societal license to operate through continuous improvement to sustainability.

Keywords Batteries · Solar cells · Thermoelectric · Perovskite · Lithium ion

Introduction

RSR Technologies (RSRT), a member of the ECOBAT group, is a research and development company engaged in the non-ferrous smelting and refining industries. The company provides services to battery, mining, and smelting companies. RSR Technologies is focused on achieving innovations in material science to help companies develop batteries achieving the highest standards for health, safety, and the environment. The company provides R&D services to its worldwide secondary lead producers and is headquartered in Dallas, Texas.

RSRT has been engaged in lead alloy developed for the active material of Pb-acid batteries in three areas, active material utilization, dynamic charge acceptance, and cycle life. Batteries tested with the new alloy can approach the performance level of some lithium batteries, while keeping low costs and maintaining recyclability. With

T. Ellis (✉) · T. Hesterberg · M. Drezdzon
RSR Technologies, Dallas, TX, USA
e-mail: tellis@rsrtechnologies.com

© The Minerals, Metals & Materials Society 2020

A. Siegmund et al. (eds.), *PbZn 2020: 9th International Symposium on Lead and Zinc Processing*, The Minerals, Metals & Materials Series,
https://doi.org/10.1007/978-3-030-37070-1_67

the aid of real-time X-ray imaging, technology has gone into commercial production following tests that show it doubles the cycling life of lead batteries.

Pb batteries offer a unique cross section of performance, cost, and sustainability. These advantages are accessed because of the very materials that make up lead batteries, mainly lead, plastic, and electrolyte. However, performance enhancement in lead batteries must keep pace with the added requirements demanded by an increasingly energy storage dependent world. RSRT's view of this issue is the best way to change how lead batteries perform is to start from the very beginning: lead.

Experimental Program for Batteries

The role of common elements found in lead alloys on the growth and crystal habit of the many species ($PbSO_4$ and PbO_2 for instance) in Pb batteries is not understood. Each element has an effect, and we are studying how each can benefit or limit the dynamic charge acceptance and cycle life of lead active material. For instance, electron microscopy has shown that the $PbSO_4$ crystal behavior can change drastically based on the elements present in the active material or electrolyte (Fig. 1).

The slow dissolution behavior of $PbSO_4$ is of key importance due to its negative effect on charge acceptance and cycle life. The focus on $PbSO_4$ crystal behavior has been fruitful, yielding a new alloy for higher performing lead battery active material, SUPERSOFT-HYCYCLE®. Trace elements in this alloy help govern the crystallization of $PbSO_4$ in the positive and negative electrode. Smaller $PbSO_4$ crystallites with a more easily dissolved crystal habit are formed using SUPERSOFT-HYCYCLE®. The

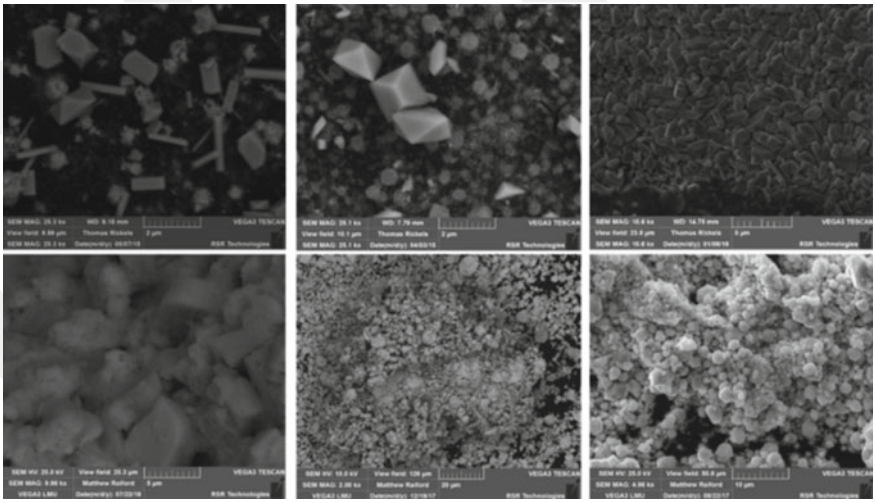

Fig. 1 $PbSO_4$ morphological change due to minor element contaminate variation

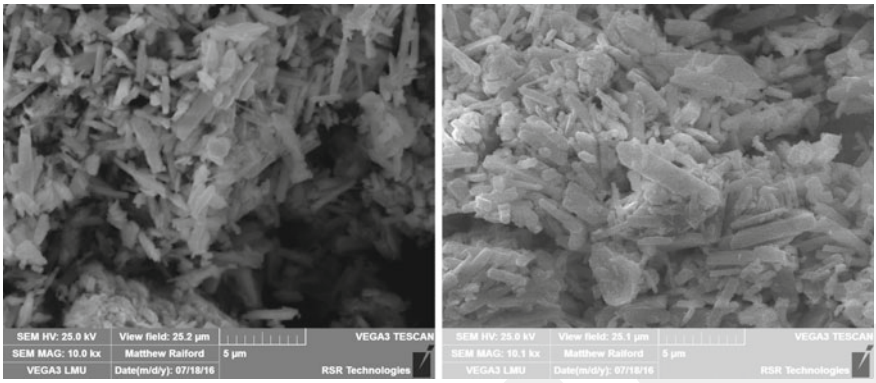

Fig. 2 Morphological differences between convention active material (left) and SUPERSOFT-HYCYCLE® micro-alloy active material (right)

faster dissolution in turn facilitates high charge acceptance and cycle life provided they remain in electrical contact within the active material (Fig. 2).

The breakthrough SUPERSOFT-HYCYCLE® material contains a carefully engineered suite of micro-alloying additions which have been shown to enhance the cycling and charge acceptance of the active material in a Pb-acid battery combination of antimony, arsenic, and lead. The effect of the micro-alloying addition on the micro-structure of the active material was determined with the use of the Advanced Photon Source at the Argonne National Laboratory (ANL), a synchrotron used in a wide range of scientific disciplines. This has allowed far more accurate analysis of dynamics of crystallization phenomena that occur in the battery during charge/discharge cycling, Fig. 3.

When the SUPERSOFT-HYCYCLE® alloy was placed against a "control" lead element typical of standard lead batteries, careful selection of antimony (~100 ppm) and arsenic (~100 ppm) micro-alloying additions and removal of specific contaminants were found to directly aid in changing the $PbSO_4$ to a more easily solubilized crystal form, thus prolonging battery life shown in Fig. 3. For reference, the control is oxide produced with standard 99.9% Pb, SUPERSOFT-ULTRA® is refined control material with Cu < 2 ppm, Ni < 1 ppm, and Te reduced to <0.3 ppm, and SUPERSOFT-HYCYCLE® as stated is micro-alloyed. This test was done under the EN 50342 Micro-Hybrid Test (MHT) protocol (Fig. 4).

An interesting new technology is the use of Pb based materials as anode in a lithium (Li) ion battery [1]. Li–Pb alloy anodes have a theoretical capacity advantage over the commonly used graphite, 582 mAh g^{-1} for Pb versus 372 mAh g^{-1} for graphite. Cycling at C/20 cycle of the electrodes reached 455 mAh g^{-1} using a 1.0 V cutoff close to the theoretical maximum which increases to 689 mAh g^{-1} for the 3.0 V cutoff. Research in this arena may lead to interesting new opportunities for Pb in electrochemical storage.

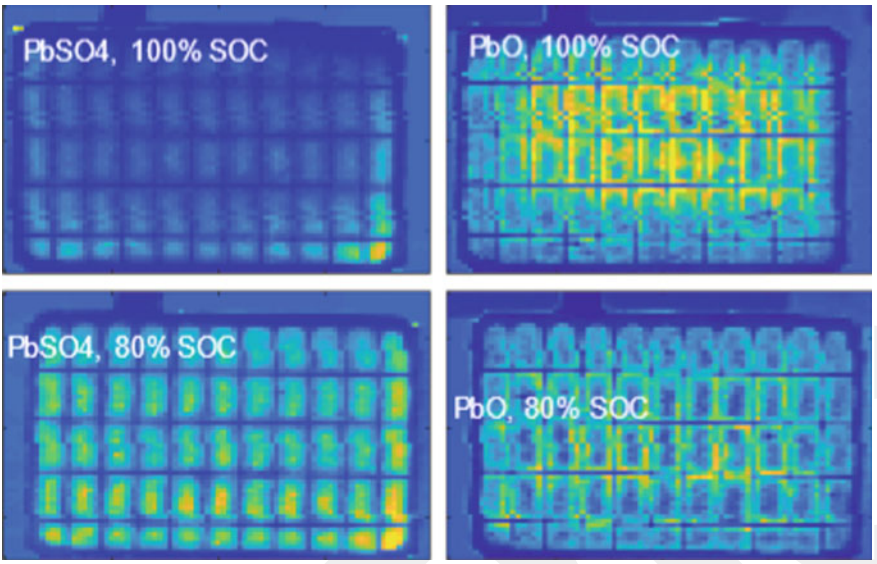

Fig. 3 X-ray diffraction imaging of Pb battery plates on cycling

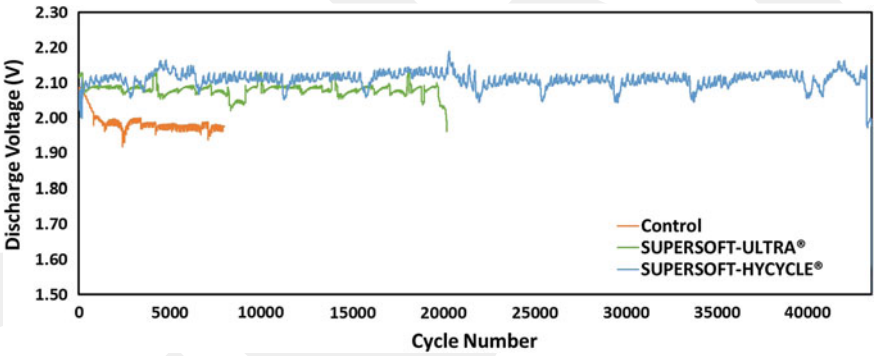

Fig. 4 Cycle life comparison of three active material Pb's

Applications of Pb in Energy Harvesting

One cannot over-emphasize the importance of the Pb based battery to the overall Pb market. And though Pb is still used for roofing, cable sheathing, electrowinning anodes, and other fabricated products, the 150-year history of the Pb battery is of paramount importance to the industry. However, several new applications have emerged based on the unique properties of the Pb atom with its relativistic effects which make it somewhat unique. In truth without relativity, lead would be expected

to behave much like tin, but calculations indicate that 10 V of a 12 V are due to relativistic effects [2]. The relativistic properties of Pb have been used in the development of organic–inorganic hybrid perovskite materials to produce solar cells. Generally, these materials have a chemical formula of AMX_3, where A=Cs, CH_3NH_3; M=Pb, Sn; X=Halide, for example. One great attribute of this chemistry is the band gap 1.15–3.06 eV, and one great advantage of the methylammonium Pb iodide is its band gap 1.55–1.62 eV which is ideal for single junction photovoltaic solar cells [3, 4].

For quite a while, Pb chalcogenides, e.g. PbTe, PbSe, PbS, have been known to have interesting properties for thermoelectric device for heating or cooling [5]. Thermoelectrics are rated by their figure of merit, ZT, which helped determine the thermodynamic efficiency of the material. The value of ZT is a ratioing of the Seebeck coefficient which is the thermopower, r the electrical resistivity, k the thermoconductivity, and the temperature of the device T. Since these devices are band gap materials with the thermal gradient across them, which generates the electron/hole carrier distribution across the material. Carrier concentration may also be tuned by doping or alloying the materials to form molecular composites to tune them to the temperature range of operation. Of interest to Pb producers is that tellurium (Te), selenium (Se), and sulfur (S) are all very common elements in the smelters. Particularly in the case of Te and Se finding, an outlet for these elements may be interesting as modern specifications for Pb active materials in batteries remove these to very low levels.

Conclusion

The unique chemistry of Pb opens many new opportunities for technical innovation in the realm. As Pb has an already established recycling industry in the support of the drive for a circular materials economy, Pb will continue to be a vital part of the energy portfolio.

References

1. Woods SM, Powell EJ, Heller A, Mullins CB (2015) Lithiation and de-lithiation of lead sulfide (PbS). J Electrochem Soc 162(7)
2. Ahuja R, Blomqvist A, Larsson P, Pyykkö P, Zaleski-Ejgierd P (2011) Relativity and the lead-acid battery. Phys Rev Lett 106(1):018301
3. Green MA, Ho-Baillie A, Snaith HJ (2014) The emergence of perovskite solar cells. Nat Photonics 8(7):506
4. Saila M, Graetzel M, Correa-Baena J, Hagefeldt A (2017) Perovskite solar cells from the atomic to the film level. Angew Chem https://doi.org/10.1002/ange.201703226
5. He J, Tritt TM (2017) Advances in thermoelectric materials research: looking back and moving forward. Science 357(6358)

Part XIX
Secondary Zinc II

GCRIS

The EZINEX® Process for Secondary Zinc Bearing Materials

Massimo Maccagni and Edoardo Guerrini

Abstract The problem of zinc production from secondary sources is not yet solved despite a lot of different alternatives were presented and some of them are under evaluation. The environmental pressure and the new concept of circular economy are asking for viable solutions for waste or secondary material. The EZINEX® Process is not a new technology but, industrially applied to EAF in the last decade of the last century and dormant for a long time, is newly generating some interest. Engitec started revising the old process and found and applied some modifications in order to revitalize it submitting each unit to a revision work finalized to optimize the process and to the eliminate the problems we have got in the above mentioned industrial plant experience. These new solutions were tested during an extensive work done in a demo plant. The revised process is more flexible and easy to run.

Keywords Zn · Secondary · EAFD · Electrolysis · Ammonium chloride

Introduction

Zinc is a very important metal used in a wide variety of applications throughout our society. Zinc is the 24th most abundant element in the Earth's crust. It naturally exists in the air, water, soil, and the biosphere. Most rocks and many minerals, as well as humans, plants, and animals, contain zinc in varying amounts. In fact, approximately 5.8 million tons of zinc are naturally cycled through the environment annually by plant and animal life, rainfall, natural phenomena, and other activity. Zinc is also common and essential to all life. All living things from the tiniest micro-organisms to humans require zinc to live as it helps with specific metabolic processes. Additionally, zinc is found in a number of products we use daily such as cosmetics, tires, cold remedies, baby creams to prevent diaper rash, treatments for sunburns, and sunscreens. In fact,

M. Maccagni (✉) · E. Guerrini
Engitec Technologies S.p.A, Via Borsellino e Falcone, 31, 20026 Novate Milanese, MI, Italy
e-mail: m.maccagni@engitec.com

E. Guerrini
e-mail: e.guerrini@engitec.com

© The Minerals, Metals & Materials Society 2020

A. Siegmund et al. (eds.), *PbZn 2020: 9th International Symposium on Lead and Zinc Processing*, The Minerals, Metals & Materials Series,
https://doi.org/10.1007/978-3-030-37070-1_68

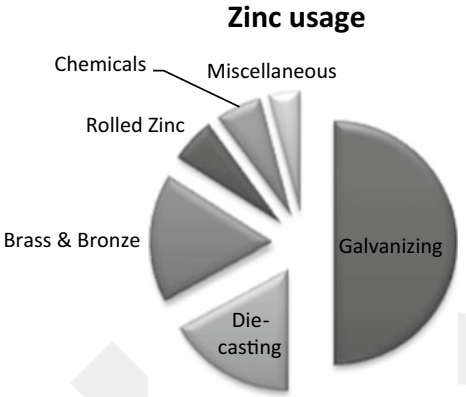

Fig. 1 Zinc usage

zinc oxide blocks more UV rays than any other single ingredient used in sunscreen. The use of zinc in construction is one of the most common and oldest. For more than 150 years, zinc has been used to protect steel from corrosion, and in particular through hot-dip galvanizing and other forms of zinc coatings. In recent years, even pure zinc metal sheets are also occasionally used in roofing and paneling systems.

The most common use of zinc is galvanizing for corrosion protection of steel structures. About 50% of produced zinc is consumed in galvanizing operations, which include galvanized steel used in automobile and appliance production (Fig. 1).

At the end of its consumer life, galvanized steel is recycled to the electric-arc furnace (EAF) to be converted back into steel products. In the EAF, zinc is first reduced and vaporized, and then oxidized and dispersed in the gas phase along with some iron oxides and the oxides of other minor elements. This dust, called electric-arc furnace dust (EAFD), is captured in the baghouse filters. This recovered EAFD contains zinc along with other elements such as iron, nickel, copper, cadmium, lead, and manganese all in the form of oxides. Zinc, in particular, is found in two main forms: zinc oxide and zinc ferrite. EAFD is considered an environmentally hazardous waste due to the heavy metals content, but it also can be considered a type of zinc rich ore. Most mined ores contain only a few percent of zinc, but in the EAFD the zinc concentration is usually over 20%. Some chlorides are also present produced by the combustion of some plastics and lacquers present on the scrap.

Numerous studies have been done to find a definitive treatment for this dust. Most of the resulting processes start with a pyrometallurgical treatment [1] where the dust is upgraded to what is called a Crude Zinc Oxide (CZO) in which the zinc concentration is raised to 55–65%. The classic example is the Waelz oxide [2] coming from the Waelz Process, the most used and known technology for this upgrading, which is based on the use of a long kiln similar to the one used in the cement industry. This CZO is an intermediate product that must be transformed into commercial zinc salts or zinc metal product. Currently, CZO conversion to zinc metal is done through two main processes: the sulphate leaching and electrowinning system and the Imperial Smelting Process (ISP). ISP is facing some critical technical and economic issues

that have led to the closing of most of the existing plants. But even with these long-standing treatment processes, one critical technical issue remains: this CZO cannot be fed untreated in these processes. It contains elements that make it difficult to be used both in the ISP and in the sulphate electrowinning. In fact, the CZO must be treated to eliminate or reduce some of the contained impurities before being fed to one of these two processes.

Chlorides and fluorides are the most harmful elements to these processes. And EAFD is not the only zinc containing feed with this issue. Many potential CZO sources, such as galvanizing ashes, brass foundry, and converters fumes, contain recoverable zinc. But, as with EAFD, they also contain halides that will be transferred to the CZO and must be removed. Chlorides fed into the zinc sulphate electrowinning (EW) system cause anodic chlorine evolution, which is a major personnel health concern. It also increases the lead anode corrosion rate impacting costs and compromising zinc quality. Even a low concentration of a few hundred ppb of fluorides seriously impacts the stripping of the Zn cathodes.

The presence of these halides also causes problems in the condenser unit of the ISP. In recent years, processes to avoid these issues for CZO treatment have been studied and installed. These systems are based on the use of a water wash solution, better if it contains Na_2CO_3, but they are not without their own difficulties. In fact, some were introduced [3] at the beginning of the twenty-first century but they were unsuccessful. For these reasons, a chloride-based recovery system that directly produces metallic Zn would be valuable [4–6]. The major drawback in zinc chloride EW is the Cl_2 anodic evolution and its management versus the typical O_2 evolution in the sulphate EW system [7, 8].

At the beginning of the 1990s, Engitec developed the EZINEX® Process [9] capable of directly treating zinc bearing materials such as EAFD. In 1993, a 500 t/y zinc cathode pilot plant treating EAFD was erected and operated. After one year of operation, an industrial plant producing 2000 t/y of zinc cathode was designed, erected, and operated. During the industrial plant operation, a thermal pilot plant for the conversion of zinc bearing materials to CZO was also built and operated. This thermal process, known as INDUTEC®, is a modification of induction furnace technology. EZINEX® [10] is a hydrometallurgical process based on an NH_4Cl electrolyte and capable of producing metallic zinc directly from CZO without any further pre-treatment. The first industrial scale EZINEX® plant [11] was designed to produce zinc directly from EAFD. During operation, several campaigns replacing the EAFD feed with a CZO feed were conducted producing very good results.

Engitec recently received inquiries from steel producers that have a scrap pre-heater installed in front of their furnace. This furnace feed design produces an EAFD that is quite different from that without the pre-heating. The zinc concentration in this case reaches 40–45% and also has a strong reduction in iron concentration. Engitec realized that this EAFD is suitable for direct treatment in the EZINEX® Process.

The EZINEX® Process

The EZINEX® Process, described through the block diagram shown in Fig. 2, is a chloride-based leaching and electrowinning system able to process oxidized zinc bearing materials. We have modified a little bit of the process and we are submitting a patent to protect these new modifications that, for these reasons, we are not going to be introduced in this paper.

The process now consists of four main operations:

- Leaching of Zn bearing materials
- Solution purification
- Zinc electrowinning
- Evaporation/crystallization.

We will now go into more detail on each operating unit, discuss the chemistry, and define the potential issues.

The Leaching

The leaching solution, the zinc depleted electrolyte returning from electrolysis, is a neutral pH solution of alkali and alkaline-earth chlorides containing significant concentrations of ammonium chloride. In the leaching reactor, Zn oxide and other heavy metal oxides and chlorides are taken into solution together with alkali chlorides and a portion of the alkali earth salts. In the leaching reactor, the following reactions take place:

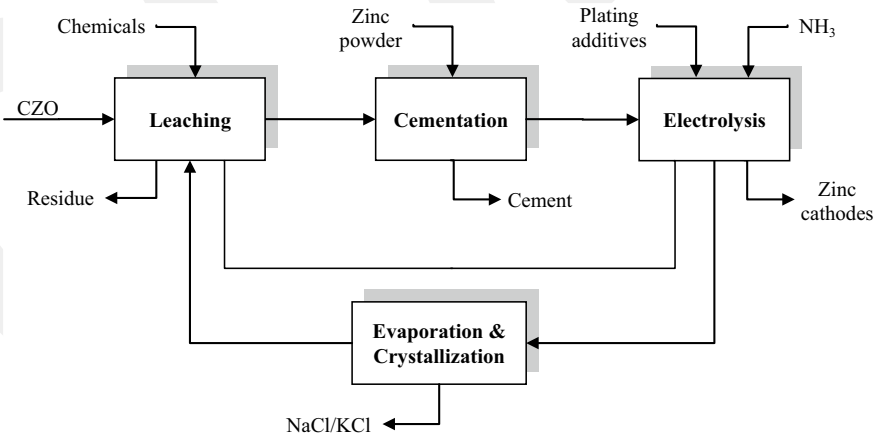

Fig. 2 The EZINEX® Process—block diagram

$$\mathrm{MeO}_{n/2} + n\mathrm{NH_4Cl} \rightarrow \mathrm{Me(NH_3)}_n\mathrm{Cl}_n + n/2\,\mathrm{H_2O}$$
$$\left(\mathrm{Me} = \mathrm{Zn^{2+}}, \mathrm{Cd^{2+}}, \mathrm{Cu^{2+}}, \mathrm{Cu^{+}}, \ldots\right) \quad (1)$$

$$\mathrm{PbCl_2} + n\mathrm{XCl} \rightarrow (\mathrm{X})_n\mathrm{PbCl}_{(2+n)} \quad \left(\mathrm{X} = \mathrm{Na^{+}}, \mathrm{K^{+}}, \mathrm{NH_4^{+}}\right) \quad (2)$$

$$\mathrm{PbO} + n\mathrm{XCl} \rightarrow (\mathrm{X})_n\mathrm{PbCl}_{(2+n)} + \mathrm{X_2O} \quad \left(\mathrm{X} = \mathrm{Na^{+}}, \mathrm{K^{+}}\right) \quad (3)$$

These reactions are very quick and virtually all the zinc contained as zinc oxide is leached while the zinc ferrite remains unleached. Due to the relatively low solubility of zinc amino-chloride, the leaching is operated at a moderately high temperature (>70 °C). The significant advantage of this neutral leaching is that iron is essentially not leached. Calcium tends to build up in solution and is particularly problematic for zinc deposition because it seems to interfere with zinc migration to the cathodic surface. To avoid this problem as well as unwanted crystallization, Ca is precipitated by Na_2CO_3/$NaHCO_3$ addition according to the reactions (4) and (5) below:

$$\mathrm{NaHCO_3} + \mathrm{CaCl_2} \rightarrow \mathrm{CaCO_3} + \mathrm{NaCl} + \mathrm{HCl} \quad (4)$$

$$\mathrm{Na_2CO_3} + \mathrm{CaCl_2} \rightarrow \mathrm{CaCO_3} + 2\mathrm{NaCl} \quad (5)$$

Of course, some other chemicals can be used. Both in EAFD and in CZO, we commonly see a measurable amount of fluorides, which must be kept under control. Due to the presence of calcium, we do not see a build up of fluorides in solution. They are precipitated during leaching according to the following reaction (6):

$$\mathrm{Ca^{2+}} + 2\mathrm{F^{-}} \rightarrow \mathrm{CaF_2} \quad (6)$$

The leaching residue is recycled back to the EAF or thermal generating system to fully recover the unleached zinc remaining as zinc ferrite.

The Leachate Purification

Among the leached elements, metals more noble than Zn that must be removed ahead of the electrowinning cell because they could co-deposit with Zn decreasing its quality. Their removal is achieved through their precipitation by contacting the solution with zinc powder or granules according to the following well-known cementation or displacement reaction (7):

$$\mathrm{Me^{n+}} + n/2\,\mathrm{Zn} \rightarrow \mathrm{Me} + n/2\,\mathrm{Zn^{2+}} \quad \left(\mathrm{Me} = \mathrm{Pb^{2+}}, \mathrm{Cd^{2+}}, \mathrm{Cu^{2+}}, \mathrm{Ag^{+}}, \ldots\right) \quad (7)$$

The competing reaction of zinc dissolution, as shown in reaction (8) below, oxidized by the presence of dissolved air in the solution, is also possible. But at the neutral operating pH, it is kinetically very slow and is therefore not a serious competitive reaction for the cementation.

$$Zn + 1/2\,O_2 + 2NH_4Cl \rightarrow Zn(NH_3)_2Cl_2 + H_2O \tag{8}$$

The complete precipitation of all impurities is fundamental for the chemical purity of the deposited zinc. The design of this unit is very important when a high purity zinc cathode is desired. A multistage unit design is essential for high removal efficiency while optimizing the zinc consumption. A multistage design is also appropriate when notable quantities of valuable metals, such as Ag and Cu, are contained in the treated feed and need to be recovered separately in a relatively pure form.

The purified solution resulting from this operation is ready to be fed to the EW unit.

The Zinc Electrowinning

The EZINEX® EW unit is the core of this process. As already mentioned, one of the problems of conventional chloride EW is the anodic evolution of chlorine that requires a complex cell design and a complex system for the chlorine handling. With the EZINEX® Process, the chloride EW is highly simplified. It occurs in a conventional open cell with permanent titanium cathode blanks and graphite anodes. As with the leaching unit, the electrolysis unit needs to be run at temperatures higher than 60 °C due to zinc solubility. Because of the low concentration of zinc in solution, the electrolysis is assisted by an air sparging system in order to optimize and increase the diffusion rate to a point that the electrolysis can be run at relatively high current densities (>300 A/m^2) even with relatively low zinc concentrations (5–6 g/l).

At the titanium cathode, the zinc deposition occurs according to the reaction (9) below:

$$Zn(NH_3)_2Cl_2 + 2e^- \rightarrow Zn + 2NH_3 + 2Cl^- \tag{9}$$

At the graphite anode, the chemistry is slightly more complicated because the electrochemical reaction (10):

$$2Cl^- \rightarrow Cl_2 + 2e^- \tag{10}$$

is followed by a very quick chemical reaction:

$$Cl_2 + 2/3\,NH_3 \rightarrow 2HCl + 1/3\,N_2 \tag{11}$$

which leads to the following overall anodic reaction

$$2Cl^- + 2/3\,NH_3 \rightarrow 2HCl + 1/3\,N_2 + 2e^- \quad (12)$$

The electrolyte pH is buffered by the effect of amino complexes and is very stable and resistant to change. It must be maintained in the range of 6–7 to avoid the formation of chloro-amine. As shown by reaction (10), ammonia is consumed by chemical reaction and must be added for this make-up as well as consideration for any other reactions or additions that can lower the pH. The overall cell reaction, obtained summing reactions (9) and (12), is shown in reaction (13):

$$Zn(NH_3)_2Cl_2 + 2/3NH_3 \rightarrow Zn + 1/3N_2 + 2NH_4Cl \quad (13)$$

The Zn concentration in the cell is maintained in the range of 5–15 g/l, and the current density is in the range of 300–400 A/m^2. The deposition time is in the range of 24–48 h. At the cathode, the competition for cathodic H_2 evolution is greatly minimized. In fact, the cathodic current efficiency is in the range of 94–98% and the co-deposition of other metals having a low hydrogen overvoltage is not nearly as dramatic as in the case of sulphuric Zn EW. At neutral pH, the hydrogen evolution potential is quite far from that of zinc deposition. When compared to sulphuric EW, the EZINEX® cell voltage is lower, which carries through to lower energy consumption. However, the benefit of this energy savings is not fully realized due to the ammonia consumption. Ammonia and all vapors from the process are collected, scrubbed, and recycled back to the process.

The Electrowinning Unit

Having provided a short explanation above of the process units, we will now go into more detail on the cell design [12] and its electrochemistry. This unit represents the real innovation of the process. The industrial cell is an undivided cell equipped with titanium cathodes, graphite anodes, and a sparging system feeding air under the electrodes. The electrolyte is fed to the cell in a traditional flow-through electrowinning circuit design.

The tank house installed at the Ferriere Nord facility was the first industrial application in the world of zinc amino-chloride electrolysis producing zinc cathodes as an alternative to traditional zinc sulphate electrowinning. During more than three years of operation, the system underwent many changes. The optimization of the operating conditions was reached through the variations of some parameters including cell temperature, electrolyte zinc content, current density, and electrolyte impurity loading. The process demonstrated good operational reliability even at extreme conditions. The process was shown to operate successfully at elevated temperatures up to 80 °C, at very low electrolyte zinc concentrations of 5 g/l, with high impurities concentrations up to 500 mg/l and with Ni and Co concentrations >5 mg/l. Even in these unfavorable conditions, the current efficiency was only affected by short circuits between cathodes and anodes. These shorts circuits were due to both accidental misalignment of the electrodes and premature detachment of the zinc deposit caused

by high cell temperatures (>75 °C). It is significant to note that the high contamination of the electrolyte, caused by a period of poor purification, did not affect the current efficiency even in presence of elements like Sb, Ni, and Co. These elements, which are disastrous in acidic sulphate electrolyte, did not disturb the EZINEX® Process. The only consequence was the co-deposition of the metals into the zinc cathodes creating a lower quality product.

There was never any competition with hydrogen evolution. In the zinc aminochloride electrolysis, the operating pH of the cell is around 6. In this condition, the hydrogen competition is practically impossible even in the presence of elements that normally lower the hydrogen overvoltage and prevent zinc deposition. Figures 3 and 4 represent the cathodic and anodic polarization curves obtained with a synthetic EZINEX® electrolyte. Figure 3 shows that at the operational current density of 300 A/m^2, the potential difference between hydrogen evolution and zinc deposition is at least 250 mV and that 5 g/l of zinc is sufficient to support the electrolysis up to a cathodic current density of 500 A/m^2. This last issue was fully demonstrated during the plant operation.

In Fig. 4, we can see that the anodic potential is basically unaffected by the addition of ammonia/ammonium salts. There is only a small depolarization measured. This likely means that the anodic reaction is not changing but the rate determining step is probably being influenced by the chemical reaction.

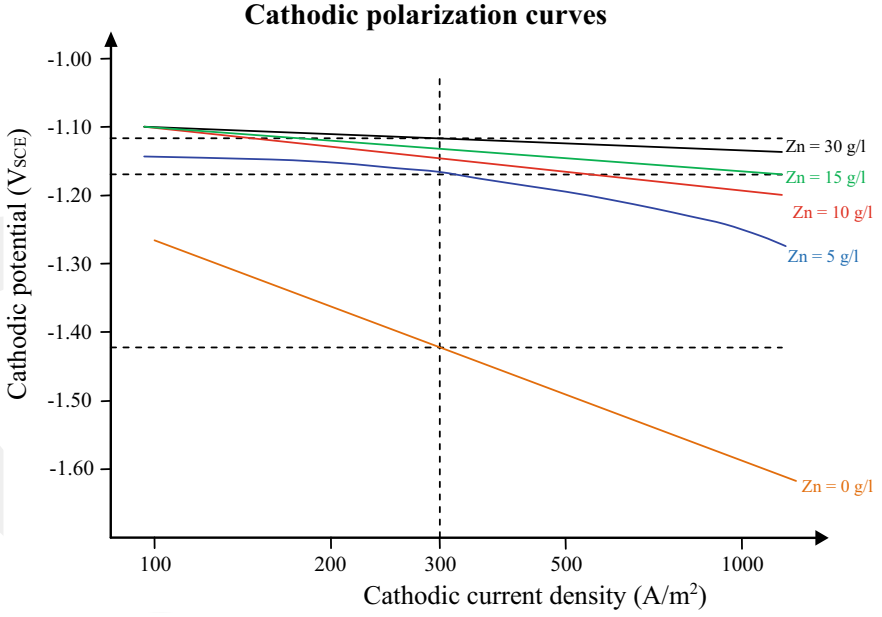

Fig. 3 Cathodic polarization curves

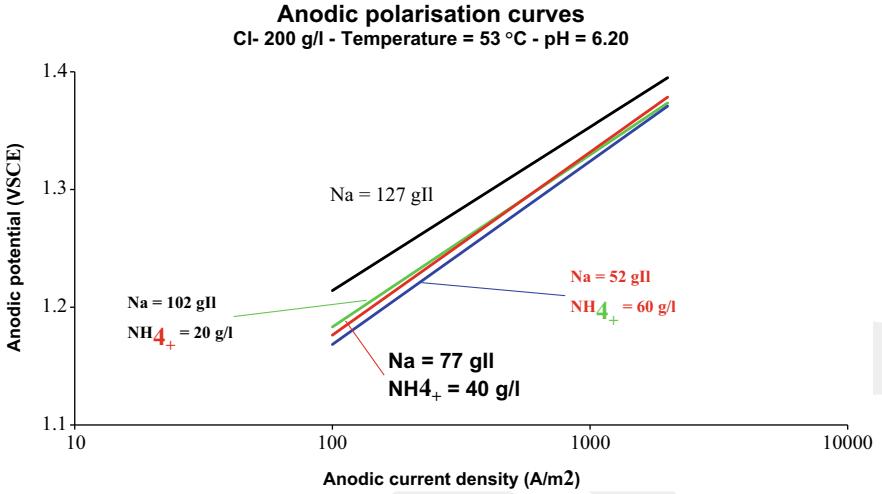

Fig. 4 Anodic polarization curves

The Evaporation/Crystallization

In both the EAFD and CZO feeds, there is a high ratio of (NaCl + KCl)/Zn. These impurity salts build up in the electrolyte and although they may slightly increase the electrolyte conductivity, they also create problems related to their solubility. They must to be controlled and removed to avoid unwanted crystallization in the process.

The operation of this evaporation/crystallization unit is very important for the overall process. We obtain two benefits: the removal of alkaline chlorides from the electrolyte and water balance control. The alkaline salts are not considered a product for economic calculations but can be used for a variety of applications including road treatment and process fluxes. Water entering the plant with reactants make-up, electrochemical additives, residue cake washing and cathode washing is evaporated while the mother liquor, containing concentrated zinc amino complex and ammonium chloride, is recycled back to the plant.

Demo Plant

In the last year, Engitec installed and operated a skid mounted demo plant to recover zinc directly from the EAFD produced at Cape Gate Mini-mill in South Africa. This company is using a scrap pre-heating system that caused a tremendous change of the composition of the EAFD. Instead of the usual 20–25%, the dust has an average zinc content of 35–45% and this was seen as an interesting opportunity for the EZINEX® Process.

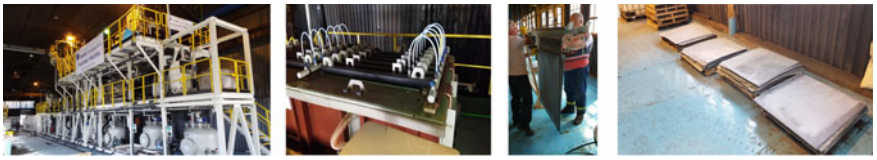

Fig. 5 Pictures of the EZINEX® demo plant

The plant, shown in Fig. 5, is based on a couple of cells equipped with five cathodes.

The plant was operated in campaigns and each one of it was characterized by the introduction of modification trying to further improve the performances of the process. These modifications are including the impurities management and some modification of the cell design that are going to be patented and for this reason they are not going to be mentioned in this paper.

The performance of the last campaign is summarized here below:

- EAFD feed (41% Zn average): 27,000 kg
- Residue (19% Zn average): 14,000 kg
- Operating current density: 300–380 A/m^2
- Plated cathodes: 8250 kg
- Plating efficiency: >96%
- Power consumption (d.c.): 2550–2700 kWh/t Zn

The cathodes were stripped every 25 h and they were smooth and consistent. The zinc purity was in the range of 99.988–99.993%. These campaigns demonstrated the viability of the process that also demonstrated to be easy to be operated.

The Integrate INDUTEC®/EZINEX® Process

Engitec also developed the INDUTEC® Process [13], a proprietary system to convert EAFD to CZO, that is based on a unique induction furnace design. Coupling the EZINEX® Process with INDUTEC® or any fuming process producing CZO creates a powerful system able to handle a variety of wastes and/or secondaries in a very simple system. Figure 6 shows a conceptual plant flowsheet with diverse feeds coming from different industries. Most of these materials are very difficult to process or to dispose, and subsequently, their treatment is very expensive.

With limited or no modifications to the flowsheet, this block diagram can be adapted to other potential feeds to be included in the loop. A careful evaluation can be done to examine each feed and the process requirements. Engitec has also investigated the possibility of converting zinc concentrate into zinc cathode without any pyrometallurgical operation. The combination of EZINEX® and ammonium chloride pressure leaching has promise, and it is a very attractive technology because

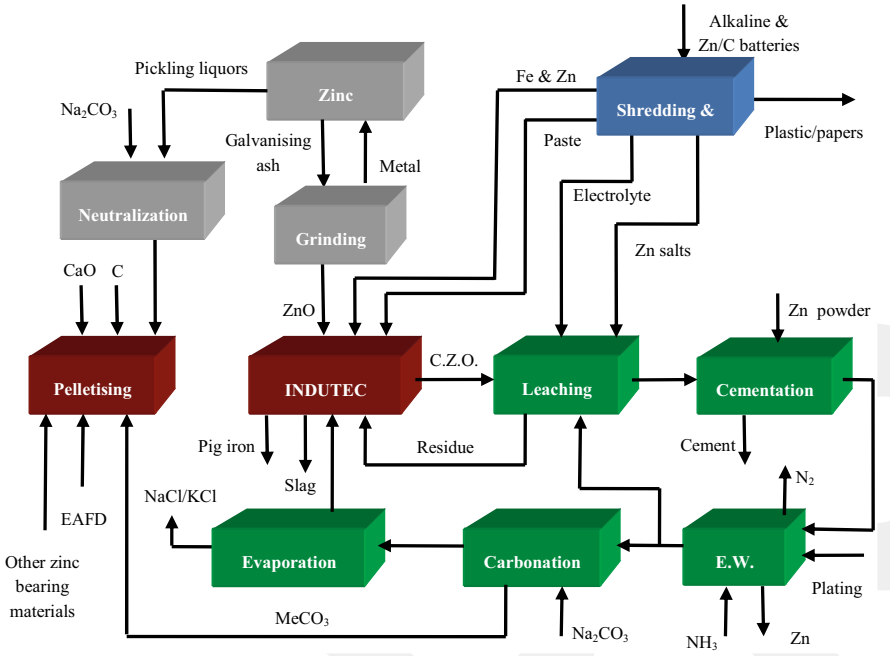

Fig. 6 Integrated INDUTEC®/EZINEX® Process—conceptual block diagram

it allows examination of virtually all potential zinc bearing raw materials in one system. Additional investigation needs to be made to prove the viability of this concept.

Conclusion

The EZINEX® Process to directly produce zinc metal from secondary zinc bearing materials is a very attractive and versatile alternative to ISP and classic sulphuric EW. The overall system is simplified, and the main drawbacks of these traditional technologies are solved within the EZINEX® system.

Combing EZINEX® with a thermal zinc fuming process makes it particularly suitable to accept a wide variety of materials that are currently either landfilled or only partially recovered, even though they contain significant metal values. This system directly produces a commodity product rather than an intermediate, such as CZO. This avoids any technical and economic concerns with transitional product marketing. In fact, some CZO producers are currently attempting to improve the quality of their product by pre-washing the material, but these systems are facing some technical and economic issues as well.

EAFD produced using a scrap pre-heating system is a particularly attractive feed. The high zinc content and low ferrite concentration make in very close to CZO without the added conversion step.

The EZINEX® Process has already been proven on an industrial scale. The INDUTEC® thermal fuming process has been extensively tested, and it is based on well-known steel industry smelting procedures. Other thermal fuming systems are already in operation treating EAFD and their CZO product has been shown to be an excellent feed for EZINEX®.

Acknowledgements We would like to thank Cape Gate for giving us the opportunity to test once again the EZINEX® technology giving us the opportunity to improve the process introducing some innovations.

References

1. Zunkel AD (2000) Recovering zinc and lead from electric arc furnace dust: a technology status report. In: Stewart DL Jr, Daley JC, Stephens RL (eds) Fourth international symposium on recycling of metals and engineered materials, Pittsburgh, Pennsylvania, U.S.A., pp 227–236
2. Palumbo FJ, Marsh RL, Gabler RC (1985) Recovery of metal values from copper converter flue gas. USBM report of investigation 8995
3. Ralston OC (1921) Electrolytic deposition and hydrometallurgy of zinc, chap 7. McGraw-Hill Book Co., New York
4. Burrows WH (1974) Zinc oxide recovery process. U.S. Patent No. 3.849.121, 19 Nov 1974
5. Grontoft F (1979) Electrowinning metals from chloride solutions. U.S. Patent No. 4.155.821, 22 May 1979
6. Prado FG, Prado FL (1992) Dezincing galvanised steel using a non corrosive low energy hydrometallurgical system. In: Proceedings EDP Congress, TMS annual meeting, San Diego, CA, USA, pp 1337–1344
7. Fray DJ, Thomas BK (1981) Zinc chloride electrolysis. U.S. Patent No. 4.292.147, 29 Sept 1981
8. Mackinnon DJ (1983) The electrowinning of metals from aqueous chloride electrolysis. In: Ossed-Asare K, Miller JD (eds) Proceedings of 3rd international symposium on hydrometallurgy. The Metallurgical Society of AIME, pp 659–677
9. Olper M, Maccagni M (2000) Electrolytic zinc production from crude zinc oxide with the EZINEX® process. In: Stewart Jr DL, Daley JC, Stephens RL (eds) Fourth international symposium on recycling of metals and engineered materials, Pittsburgh, Pennsylvania, U.S.A., pp 379–396
10. Olper M (1996) Zinc extraction from EAF dust with the EZINEX process. In: United Nations Economic Commission for Europe (ed) Working party on steel, seminar on the processing, utilisation and disposal of waste in steel industry, Balatonszèplak, Hungary
11. Olper M (1998) The EZINEX process—five years of development from bench scale to a commercial plant. In: Dutrizac JE, Gonzalez JA, Bolton GL, Hancock P (eds) Zinc and lead processing CIM, Calgary, Alberta, Canada, pp 545–560

12. Robinson DJ, MacDonald SA, Olper M (2001) Design details of Engitec "EZINEX" electrowinning plant. In: Gonzalez JA, Dutrizac JE, Kelsall GH (eds) Electrometallurgy 2001, CIM conference, Toronto, Canada, pp 45–56
13. Olper M, Maccagni M (2003) Electrolytic zinc production from crude zinc oxide with the EZINEX process. In: International congress for battery recycling, Lugano, Switzerland

GCRIS

Technologies for Treatment of Zinc-Containing Waste from Metallurgy in KCM AD

Stefan Stoychev, Emil Minchev, Aleksander Kyurkchiev and Georgi Radonov

Abstract The zinc plant in KCM AD started in 1961. The current annual capacity of the plant is 75,000 tons of zinc. The technological scheme is classic—Roasting, Leaching, and Electrowinning. Hydroxide cakes, generated during the leaching, are treated in the Waelz plant. In the period 2009–2011, different options for development of the company were considered with the main goals being increasing the profitability and competitiveness and minimizing quantity of the wastes for landfill. KCM decided to invest with priority in increasing the capacity of the Waelz kilns and realizing a technological line for treatment of zinc-containing secondary materials and wastes, mainly EAF dusts and lead slag from the lead plant. With the realized investments and implemented technologies, the share of treated secondary materials and wastes reached 25% of the total zinc plant input, including 10% EAFD. The circle of the recycles and residues between the two plants in KCM was closed.

Keywords Waelz process · EAF dusts · Lead slag · Oxides washing

Zinc Plant

The zinc plant in KCM AD started in 1961. The current annual capacity of the plant is 75,000 tons of zinc, 74,000 tons of which are SHG. The technological scheme is classic:

- roasting of concentrates in a fluid bed roaster;
- neutral leaching and acid leaching in a sulphuric acid solution;
- precipitation of iron;
- purification of the solution;
- electrolysis;
- melting and casting;
- Waelz kilns—four pcs.

S. Stoychev · E. Minchev · A. Kyurkchiev · G. Radonov (✉)
KCM 2000 Group, Asenovgradsko Shose, 4009 Plovdiv, Bulgaria
e-mail: georgi.radonov@kcm.bg

© The Minerals, Metals & Materials Society 2020

A. Siegmund et al. (eds.), *PbZn 2020: 9th International Symposium on Lead and Zinc Processing*, The Minerals, Metals & Materials Series,
https://doi.org/10.1007/978-3-030-37070-1_69

Choosing a Path for Development

In the period 2009–2011, different options for the development of the company were considered with the main goals being:

- increasing the profitability and competitiveness;
- minimizing the quantities of wastes for landfill by maximizing the treatment of generated residues and recycles in both plants.

KCM decided to invest with priority in:

1. increasing the capacity of the Waelz kilns;
2. realizing a technological line for the treatment of zinc-containing materials and wastes:
    - electric arc furnace dusts (EAFD) from the steel industry;
    - lead slag—generated from the new Ausmelt furnace in KCM.

Stages of Investment Realization

06.2012—Commissioning of the reconstructed Waelz kiln №4, including

- increasing the external diameter from 2.5 to 3.1 m;
- increasing the size of the associated facilities—dust chamber, coolers, and exhaust fans;
- reconstruction of the transport system for Waelz oxides.

08.2013—Commissioning of the "Installation for washing and leaching of Waelz oxides" with an annual capacity of 25,000 tons of Waelz oxides.
08.2015—Commissioning of the reconstructed Waelz kiln №1—identical to Waelz kiln №4.
09.2016—Increasing the capacity of the "Installation for washing and leaching of Waelz oxides" up to 50,000 tons of Waelz oxides per year.
2016–2017—Increasing the capacity of the feeding equipment.

Figures 1, 2, 3, and 4 show some of the milestones during the realization of the investment.

Fig. 1 Reconstruction of Waelz kiln №4

Fig. 2 Reconstruction of Waelz kiln №1

Fig. 3 Installation for washing and leaching of Waelz oxides—filtering department

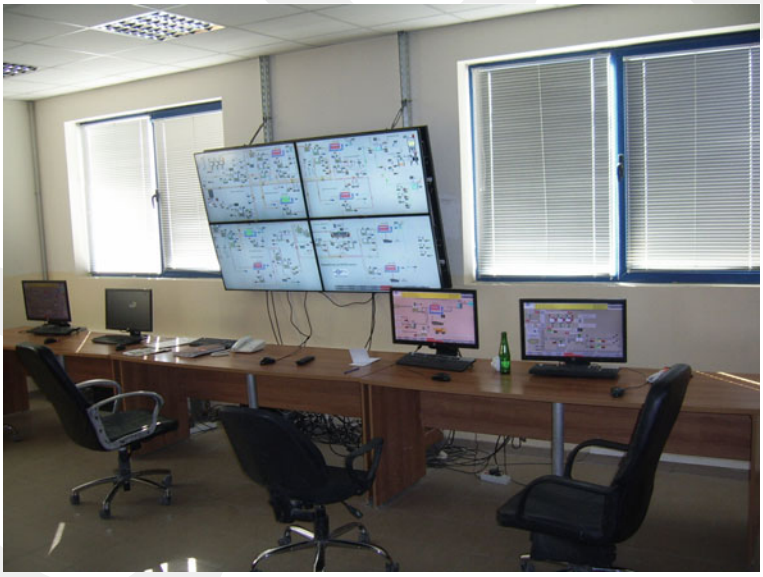

Fig. 4 Installation for washing and leaching of Waelz oxides—control room

Technological Line for Treatment of Secondary Materials

Capacity of the Waelz kilns

The capacity of the Waelz kiln is shown in Fig. 5.

Main materials for the Waelz kilns

In general, we use four types of secondary materials for the Waelz kilns:

- Own cakes—from iron precipitation in the leaching process.
- EAF dusts.
- Slag from the Ausmelt furnace in the lead plant.
- Other oxide materials.

The chemical composition of the feed materials is shown in Table 1.

Types of Waelz feed and obtained Waelz oxides

Three types of feed are prepared for the Waelz kilns:

- Feed from own cakes—based on own cakes with the addition of other oxide materials in order to optimize the zinc content in the feed.

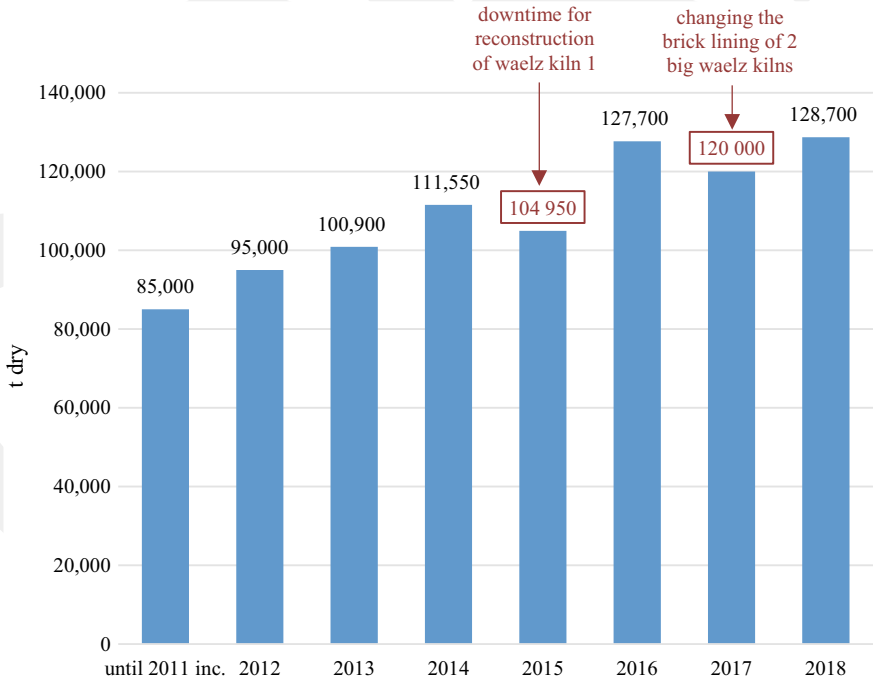

Fig. 5 Capacity of the Waelz kilns

Table 1 Chemical composition of treated materials

Material	Zn (%)	Fe (%)	Pb (%)	SiO_2 (%)	Al_2O_3 (%)	CaO (%)	MgO (%)	Cl (%)	F (%)
Own cakes	17–20	25–30	3.7–5.2	4.9–6.7	0.7–1.3	1.5–2.8	0.3–0.6	0.01–0.02	0.006–0.017
Oxide materials	40–80	1–7	0–5	0–5		0.01–5	0.01–3	0–6	0.004–0.025
EAF dusts	22–45	15–25	0.5–3.0	1.5–5.0	0.38–0.90	3.7–6.8	1.5–3.7	0.8–5.7	0.12–0.50
Lead slag	17–19	17–20	4–6	17–20	2–3	10–14	1.2–2.7	0.01–0.10	0.01–0.05

Table 2 Chemical composition of treated feeds

Material	Zn (%)	Fe (%)	Pb (%)	SiO_2 (%)	CaO (%)	MgO (%)	Cl (%)	F (%)
Own cakes feed	22–24	19–26	2–4	4–6	5–7	0.7–1.2	0.1–0.9	0.01–0.02
EAF dusts feed	20–22	14–17	1–2	2.5–5	13–18	1.5–2	2–3.5	0.1–0.35
Lead slag feed	19–22	14–18	2–5	12–15	13–18	1.5–2.2	0.1–0.9	0.01–0.02

- Feed from EAF dusts—based on EAF dusts.
- Feed from lead slag—based on lead slag with the addition of other oxide materials in order to optimize the zinc content in the feed.

The chemical composition of the feed materials is shown in Table 2.
Changing the working regimes (feeds) of each kiln in the right time allows

- optimal control of the impurities in the system—the feeds of the different working regimes contain different impurities, both as type and as quantity;
- reducing the accretions formation—the materials in each regime are different in nature and because of that they form accretions in different parts of the Waelz kiln, respectively, and they clean accretions in different parts of the Waelz kiln;
- Increasing the lifetime of the bricks—some materials (in our case EAF dusts) begin the accretion formation with a thin uniform layer, which, if properly controlled, protects the bricks without interfering with the Waelz kiln performance.

The chemical composition of the Waelz oxides (WO) obtained from the different feeds varies and is shown in Table 3.

Share of zinc from treatment of secondary materials

We started developing a technology for treatment of the lead slag in the Waelz kilns systematically. Table 4 shows how we managed to increase the treated quantities of lead slag and EAF dusts with the realization of the abovementioned investments—reconstruction of Waelz kilns №4 and Waelz kiln №1, commissioning and expansion of the "Installation for washing and leaching of Waelz oxides". Figure 6 displays the annual processed Waelz feed from EAF dusts and lead slag.

Table 3 Chemical composition of obtained Waelz oxides (WO)

Material	Zn (%)	Fe (%)	Pb (%)	Cl (%)	F (%)
WO (cakes feed)	58–66	1.4–3.4	7–14	0.2–0.5	0.01–0.02
WO (EAF dusts feed)	54–62	1.5–5	5–8	2–6	0.15–0.3
WO (lead slag feed)	56–64	0.5–3	8–15	0.6–1.6	0.03–0.09

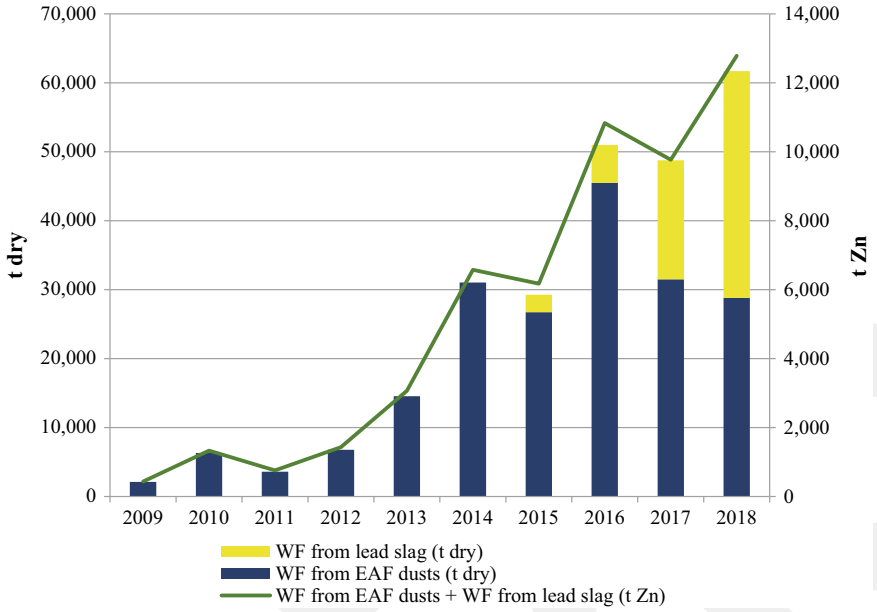

Fig. 6 Processed Waelz feed from EAF dusts and lead slag

Table 4 Share of zinc from treatment of secondary materials

Year	Share of secondary materials—Waelz (%)	Share of oxide materials (%)	Share of EAF dusts (%)	Share of lead slag (%)
2006	**7.77**	7.01	0.76	
2007	**8.03**	7.19	0.84	
2008	**6.81**	6.31	0.50	
2009	**6.67**	6.06	0.61	
2010	**10.28**	8.52	1.77	
2011	**10.48**	9.49	0.99	
2012	**11.53**	9.67	1.86	
2013	**10.99**	7.06	3.94	
2014	**14.91**	6.69	8.22	
2015	**15.10**	7.47	7.27	0.36
2016	**21.14**	8.27	12.32	0.55
2017	**20.88**	9.02	9.05	2.81
2018	**23.51**	9.63	8.16	5.71

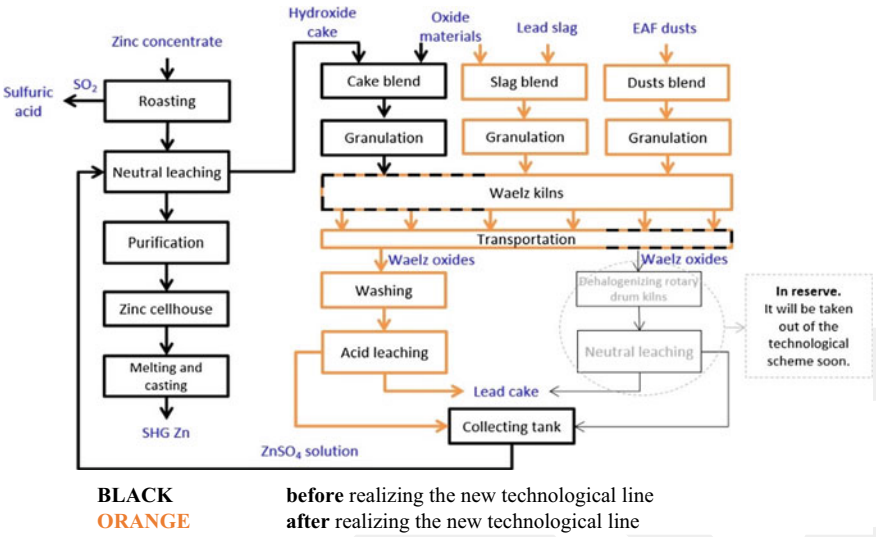

Fig. 7 Scheme for the treatment of EAF dusts and lead slag

Realized scheme for treatment of EAF dusts and lead slag in KCM AD

The uniqueness of every plant and technological line is defined by quality and quantity of the processed raw and secondary materials, type of the technological scheme, equipment level, geographic location, etc. Therefore, each plant has a unique technology for micro-impurities management and process management.

Increasing the share of a new material—EAF dusts, leads to a significant increase in the fluorine and chlorine input in the technological scheme. The main problem is the fluorine, because its content in the EAF dusts is high, and its removal is more problematic. Figure 7 displays the realized technological scheme for the treatment of EAF dusts and lead slag in KCM AD.

Technological line for treatment of Waelz oxides to SHG zinc

We had information about two successfully realized schemes for fluorine removal—a hydrometallurgical process, carried out by washing of the oxides, and a pyrometallurgical process, carried out by high-temperature roasting of the oxides in rotary dehalogenation furnaces.

KCM AD chose the hydrometallurgical method for fluorine removal through two stages of high-temperature washing with sodium carbonate (Na_2CO_3) as a reagent, which does not include a stage for under pressure washing (autoclave).

The absence of an autoclave in our technological scheme is compensated with a flexible management of both the input of fluorine-containing materials and the Waelz oxides obtained from them.

Figure 8 displays the flowsheet and basic operation parameters of the installation for washing and leaching of Waelz oxides.

FLOW		Zn [%]	Pb [%]	F [%]	Cl [%]
Waelz oxides for wetting	Range	59 - 63	7 - 10	0.07 - 0.13	2 - 6
	Average value	61.51	8.01	0.09	3.3
Cake after PW	Range	60 -65		0.02 - 0.09	0.1 - 0.5
	Average value	64.41		0.05	0.29
Cake after HW1	Range	60 - 65		0.02 - 0.04	0.04 - 0.1
	Average value	63.58		0.03	0.06
Cake after HW2	Range	60 - 65		0.008 - 0.02	0.005 - 0.015
	Average value	63.64		0.01	0.01
ZnSO4 solution	Range	130 - 150		40 - 50	250 - 400
	Average value	135 g/l		47 mg/l	322 mg/l
Lead cake	Range	5 - 10	40 - 47		
	Average value	7.00	44.00		

Na_2CO_3 consumption	90 - 140	kg/t WO
Final acidity (after AL)	10 - 20	g/l H_2SO_4
Fluorine in solution for Zinc cellhouse	~ 35	mg/l

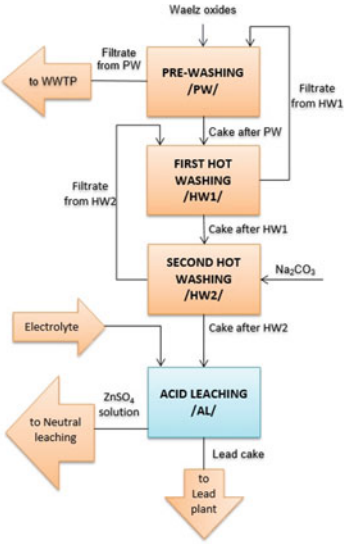

Fig. 8 Installation for washing and leaching of Waelz oxides flowsheet

The installation for washing includes three sections, which allow the flow of oxides with a counter current flow of the filtrate. Each of the sections includes interconnected reactors and a filter press. The filtrate from the pre-washing is sent to our wastewater treatment plant.

The sodium carbonate consumption varies, depending of the fluorine and chlorine content in the Waelz oxides (90–140 kg/t WO).

The acid leaching of the washed Waelz oxides is done with spent electrolyte. The process ends at final acidity 15–20 g/l H_2SO_4.

After settling and filtration of the acidic pulp, lead cake is generated.

Thanks to the realized technological scheme and the flexible management of the flows, the fluorine is successfully removed to the levels, which allow treatment of the resulting zinc sulphate solution to SHG zinc. The current system parameters ensure fluorine levels in the neutral solution, sent to the electrolysis, up 35 mg/l.

Summary

With the investments made and technologies implemented by KCM AD, the circle of the recycles and residues between the zinc plant and the lead plant was closed, as displayed in Fig. 9. This increases profitability and competitiveness of the company and contributes to the circular economy.

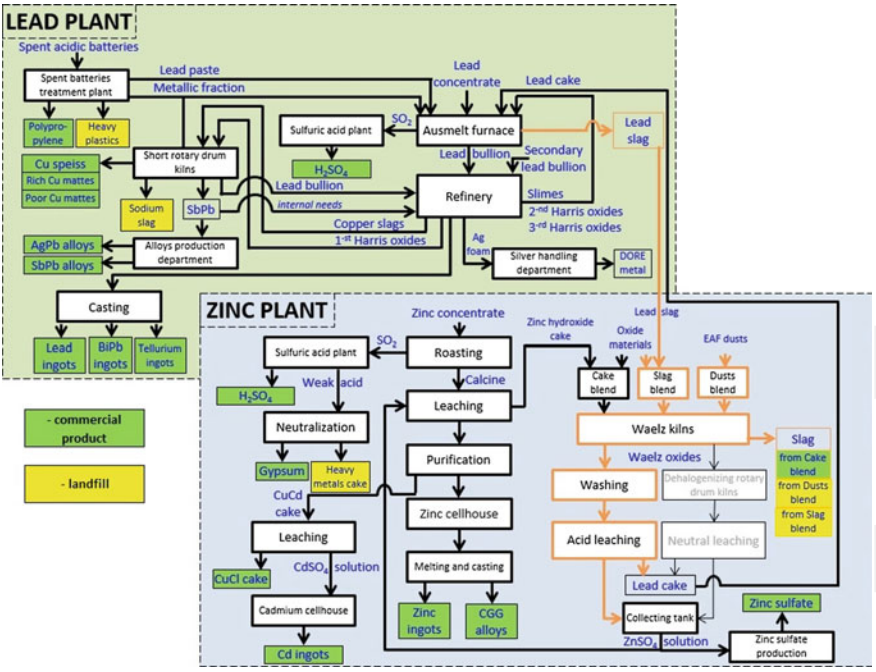

BLACK **before** realizing the new technological line
ORANGE **after** realizing the new technological line

Fig. 9 Integrated flowsheet of KCM AD

Zinc Reduction/Vaporisation Behaviour from Metallurgical Wastes

Timothy Kerry, Alexander Peters, Evangelos Georgakopoulos, Ashkan Hosseini, Erik Offerman and Yongxiang Yang

Abstract The steelmaking industry produces large quantities of zinc-bearing wastes of varying forms that cannot be treated through integrated steelmaking processes. Simultaneously, by-products of the zinc industry containing great amounts of iron and zinc are stored or landfilled. The amount of zinc in these materials is generally below that which is of value to be recycled directly to the zinc smelter, consequently a method of concentration is required. Tata Steel owns and operates the pilot HIsarna ironmaking plant which, due to its high raw materials flexibility, is attractive for the purpose of processing secondary iron sources. Furthermore, it can facilitate the simultaneous recovery of a zinc-enriched flue dust. The high temperature behaviour of various waste materials will be presented with regards to their recyclability in the HIsarna furnace. Blast furnace (BF) sludge and basic oxygen furnace (BOF) sludge from Tata Steel IJmuiden have been studied along with 'goethite' waste produced by Nyrstar. The various input materials have been comprehensively characterised and their reduction/vaporisation behaviour recorded. Mixed samples have been produced and tested in order to define the most appropriate form of delivery of these materials to the HIsarna furnace.

Keywords Recycling · Zinc · Dusts · Self-reduction · HIsarna

Introduction

Zinc is present within iron ore and coal; furthermore, it is widely applied as a protective coating in the production of galvanised steel. Consequently, within steelmaking processes, there is the potential looping and accumulation of zinc. This material can generally be found in the dusts and sludges produced from the high temperature operations taking place on these sites, whether from a sinter plant, blast furnace, electric arc furnace, etc. Moreover, along with concentrated zinc in the flue dusts of these

T. Kerry (✉) · A. Peters · E. Georgakopoulos · A. Hosseini · E. Offerman · Y. Yang
Materials Science and Engineering, TU Delft, Mekelweg 2, 2628 CD Delft, The Netherlands
e-mail: t.j.kerry@tudelft.nl

© The Minerals, Metals & Materials Society 2020

A. Siegmund et al. (eds.), *PbZn 2020: 9th International Symposium on Lead and Zinc Processing*, The Minerals, Metals & Materials Series,
https://doi.org/10.1007/978-3-030-37070-1_70

plants, there are also valuable quantities of other materials such as iron, flux, and carbon. As such, when it is possible, they are returned to the process. However, at high levels of Zn, operational problems can occur in the integrated steelmaking process. The most detrimental effect is the undermining of the walls of the furnaces through Zn penetration, this can lead to localised oxidation [1]. Consequently, the amount of Zn present in the cycle has to be limited, dusts that contain high concentration of Zn are stored or even landfilled [2, 3].

Zn smelters face fluctuating markets for the procurement of zinc ores and can thus face high prices. This leads to the search for secondary sources of zinc at reasonable prices. The zinc-containing residues from steelmaking have a wide variance in zinc concentrations with the maximum being found in EAF dust (up to 43 wt%) [3]. From the integrated steelmaking process, however, values are much more likely to be a maximum of a few percent with a maximum of 8–10% [4, 5]. In general, from any of these sources, concentration of the zinc is required before it can be used within zinc production. Furthermore, the mineralogical form of zinc is of great importance to the zinc recovery. These dusts most commonly contain zinc in the form of ZnO or $ZnFe_2O_4$ [6–8]. Industrially, the former can be readily treated both through hydro- and pyrometallurgical processes, whereas the latter is much more stable and requires harsher, more costly treatment [9].

Commonly, thermal treatment is applied to these secondary materials with the industry standard being a pyrometallurgical technique, the Waelz process [5]. Here, a carbon-based reducing agent (generally in the form of coal) and temperatures of over 1200 °C are utilised to volatilise the zinc [10], the produced vapour can then be condensed and collected. Despite the prevalence of the Waelz kiln, there are several negatives associated with the process such as high amount of newly generated residues and the potential loss of other valuable material [5]. Consequently, alternative approaches for managing these industrial by-products are required. One potential approach is through recycling within the HIsarna furnace. This is an ironmaking route composed of two units, a cyclone converter furnace (CCF) and smelting reduction vessel (SRV). A pilot scale facility has been operating at Tata Steel Ijmuiden since 2010, in which time it has been shown that the process is highly suited to heavy metal recovery. There is no limit on the quantity of zinc that can be input to HIsarna and indeed the process has extremely high raw materials flexibility [11]. HIsarna is capable of recycling ironmaking waste dusts, galvanised steels scrap, and moreover waste materials from other industries, such as zinc production residues. With Zn concentrations of 50% or more in the HIsarna produced dust, it can be sold directly to Zn smelting operations [12]. Not only does this enable the reuse of a valuable resource and therefore contribute towards a circular economy but it also contributes to a positive environmental impact.

Investigations have been taking place into the pyrometallurgical behaviour of some of these industrial by-products. Blast furnace (BF) dust and basic oxygen furnace (BOF) dust along with ‘goethite’ waste from the zinc industry have all been studied. Through an understanding of how to maximise the zinc vaporisation efficiency, the concentration of zinc in the HIsarna off-gas system can be increased. Furthermore, secondary material that is also rich in iron can be added to the process and from this its

reduction behaviour can be investigated. Consequently, the behaviour of individual dusts and also proposed mixtures have been studied to optimise the delivery of the zinc-containing material to the furnace cyclone.

Experimental

Blast furnace dust and basic oxygen furnace dust were received from Tata Steel Europe and goethite from Nyrstar (Fig. 1). The material was dried overnight in a furnace at 120 °C. The elemental compositions of these starting materials were determined using an Axios Max WD-XRF (in oxides mode) and LECO C/S 744 analysis, the results are displayed in Table 1. X-ray diffraction studies were conducted using a Bruker D8 Advance diffractometer for investigating mineralogy of the samples.

Experiments were conducted in a Carbolite STF 16/50/450 horizontal furnace. A flow (2 SLPM) of inert gas (N_2 or Ar) was maintained across the reaction tube. Dust samples were introduced to the furnace in alumina boat crucibles. These could be held in a water-cooled flange prior to introduction to the hot zone at appropriate temperature. After the desired retention time (ranging from 1 to 60 min) had been completed samples could be quenched through pushing the crucible back into the water-cooled flange. Weight measurements were recorded before and after heating. Off-gas analysis was conducted using a Hiden Analytical HPR-20 R&D mass spectrometer.

Fig. 1 As-received material in the wet form, from left-to-right BF dust, BOF dust, and goethite

Table 1 Initial composition of received dusts after drying. C and S calculated with LECO, rest with XRF

Sample	Wt%													
	C	S	Fe_2O_3	ZnO	SiO_2	CaO	MgO	Al_2O_3	MnO	P_2O_5	PbO	K_2O	CdO	As_2O_3
BF dust	41.3	2.32	33.3	4.8	5.3	2.3	0.9	2.8	0.1	0.2	1.1	0.9	0.029	–
BOF dust	2.4	0.09	84.1	0.6	1.3	8.5	1.4	0.1	0.9	0.1	–	–	–	–
Goethite	0.21	12.06	52.1	9.4	4.1	9.3	–	2	0.7	–	3.3	0.1	0.043	0.6

Results and Discussion

Weight loss measurements for the individual dusts were measured over an hour-long residence time at 1000 °C in inert atmosphere (Fig. 2). In the case of BOF dust and goethite, a stable mass was achieved after 5 min indicating that no further reactions were taking place. This reduction equated to 7 and 22% loss of initial mass, respectively. In the case of BF dust, the loss was observed to be higher (30%) and achieved after a 30-min time period (Fig. 2). It can be seen that these values are all much higher than the contained quantity of zinc in the materials, consequently other components must also be lost at this temperature. Off-gas analysis shows the release of carbon monoxide and carbon dioxide from each material and in the case of goethite, an additional release of sulphates. This indicates the desulphurisation from compounds within the goethite sample. In the case of the carbon oxides it shows the reaction of carbon (which makes up 41.3% of BF dust) as a reductant of other material within the sample whilst being oxidised itself.

Over longer retention times, sintering of the BOF dust and goethite was observed leading to the production of strong agglomerates. Blast furnace dust appeared to remain in a similar form throughout the tests, the minimal sintering can be explained through reduced quantities of CaO and iron oxides. The colour of the materials was also noted to become much darker, particularly in the case of goethite. This change from a lighter red/orange colour to a darker brown suggests the reduction of iron to lower oxidation states.

Elemental investigations of the dusts showed minimal reduction in zinc concentration within the goethite sample (Table 2). Conversely, in the BF and BOF dusts, a majority of the zinc was removed. In the latter case, this was from a very low starting point (0.6 wt%). However, it was deemed valuable to study the general BOF dust behaviour as other sources will contain appreciable zinc levels. Focusing on the case of the BF dust, it can be seen that a substantial amount of carbon was also

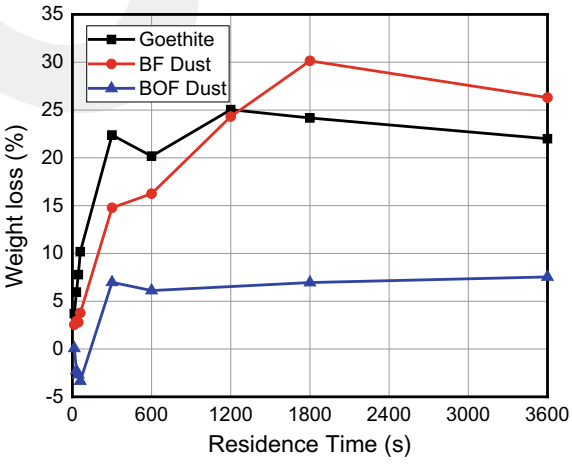

Fig. 2 Weight loss of industrial waste dusts after incremental residence times at 1000 °C under an inert atmosphere

Table 2 Weight loss of zinc and carbon from individual dust samples

		Goethite		BF dust		BOF dust	
Element	Residence time (min)	Mass of element (g)	Weight loss (%)	Mass of element (g)	Weight loss (%)	Mass of element (g)	Weight loss (%)
Zn	0	0.12	8.33	0.06	96.67	0.007	71.43
	30	0.11		0.002		0.002	
C	0	0.0007	57.14	0.4	27.5	0.023	95.65
	30	0.0003		0.29		0.001	

lost in this time indicating the self-reducing behaviour of the dust. On the contrary, in goethite, there is extremely low quantity of carbon to facilitate the zinc reduction reaction. Zinc will be present in the varying industrial waste dusts in different mineralogical forms but primarily as zinc oxide (ZnO) and franklinite ($ZnFe_2O_4$) [6–8]. These compounds will undergo simultaneous reduction and vaporisation at the temperatures studied in the presence of a reducing agent [8].

The reduction of ZnO primarily takes place through the mechanism described by reactions 1–3. The overall mechanism is given by 1 which is mediated by reactions 2 and 3 [13].

$$ZnO(s) + C(s) \leftrightarrow CO(g) + Zn(g) \tag{1}$$

$$C(s) + CO_2(g) \leftrightarrow 2CO(g) \tag{2}$$

$$ZnO(s) + CO(g) \leftrightarrow CO_2(g) + Zn(g) \tag{3}$$

In the case of franklinite, it has been shown that at 1000 °C franklinite decomposes into zinc oxide and hematite through reaction 4 [14]. Concurrently, direct reaction with carbon can lead to the release of zinc vapour (reaction 5 as mediated by reaction 2) [14].

$$ZnFe_2O_4(s) \leftrightarrow ZnO(s) + Fe_2O_3(s) \tag{4}$$

$$3ZnFe_2O_4(s) + 4C(s) \leftrightarrow 3Zn(g) + 2Fe_3O_4(s) + 4CO(g) \tag{5}$$

In the case of reaction 4, this is obviously followed by the previously described reduction process given by reactions 1–3. It can be seen that by increasing the carbon content of the material the reduction and hence, vaporisation of zinc can be realised and kinetics increased. However, excess carbon should be accounted for when looking at the carbon balance of the process.

The reducing behaviour of carbon also has an impact on the oxidation states of iron found in the various materials. XRD analysis has shown the starting and final

mineralogy (Table 3) indicating the reactions taking place. It has been shown that there is enough carbon present in the BF dust to fully reduce the iron from hematite to the metallic form. Similarly, in BOF dust, the magnetite present has been reduced leaving metallic iron and wüstite. It is apparent that there was insufficient carbon within the sample to fully reduce the iron. In the case of goethite, limited reduction has been observed with some hematite being formed, this is due to the minimal carbon within the sample. The ability of the material to undergo self-reduction is of interest as it can potentially minimise use of virgin carbon sources within the process.

In order to volatilise the remaining zinc and investigate the reducing effect on iron within the sample, it was decided to mix materials. Goethite and BOF dust were both mixed in 60:40 ratios with BF dust, a material rich in carbon (41.3 wt%). The ratio was chosen to allow enough carbon for the theoretical complete reduction of Zn and Fe. The accentuated effect of the reductant on the sample weight loss is shown in Fig. 3. After 30 min, there is roughly an extra 10 and 20% weight loss in the BOF/BF dust and goethite/BF dust mixtures, respectively, when compared to a calculated cumulative value of the two individual dusts. This can be accounted for by reduction of iron and zinc and loss of zinc vapour and carbon oxides. Table 4 shows the loss of carbon and zinc from the material. It can be seen that in both mixtures, the zinc vaporisation is mostly complete. Similarly, a large proportion of the carbon present has also been lost from the sample through reduction reactions.

Table 3 Fe-bearing phases present in industrial waste dusts before and after heating in inert atmosphere at 1000 °C

	Initial Fe-bearing phases	30 min Fe-bearing phases
Goethite	FeOOH	Fe_3O_4, Fe_2O_3
BF dust	Fe_2O_3	Fe
BOF dust	Fe, FeO, Fe_3O_4	Fe, FeO

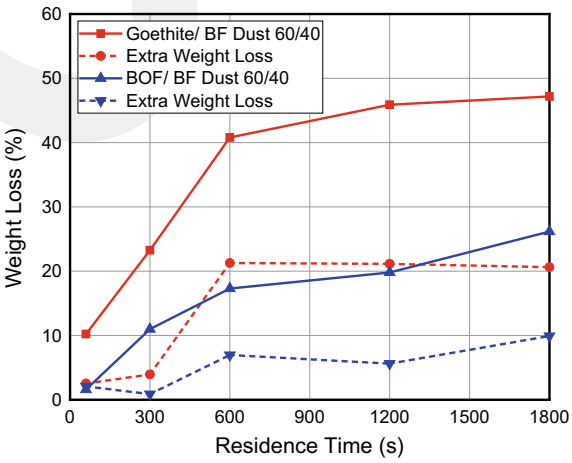

Fig. 3 Weight loss of mixed dusts and the extra weight loss calculated compared to the behaviour of individual dusts

Table 4 Weight loss of Zn and C from mixed dust samples

		Goethite/BF dust (60:40)		BOF/BF dust (60:40)	
Element	Residence time (min)	Mass of element (g)	Weight loss (%)	Mass of element (g)	Weight loss (%)
Zn	0	0.1	90.00	0.04	97.50
	30	0.01		0.001	
C	0	0.18	61.11	0.18	44.44
	30	0.07		0.1	

Table 5 Fe-bearing phases present in mixed waste dusts before and after heating in inert atmosphere at 1000 °C

	Initial Fe-bearing phases	30 min Fe-bearing phases
Goethite/BF dust (60:40)	FeOOH, Fe_2O_3	Fe
BOF/BF dust (60:40)	Fe, FeO, Fe_2O_3, Fe_3O_4	Fe

Once again, over the longer time periods of the experiment, a darker colour could be observed. However, compared to the individual BOF dust and goethite samples, the mixed material showed little sign of sintering. XRD analysis was used to investigate the reduction of iron within the mixed dusts and in both cases, it was seen that the only phase remaining was metallic iron (Table 5). This is indicative of the fact that there is sufficient carbon within the sample to reduce both the iron and zinc. In fact, it is in great excess based on the residual carbon in the mixed dusts (Table 4). The morphology of this material is comparable to that of direct reduced iron (DRI) and allows both resource recovery and reduction of coal usage [15].

By mixing industrial waste dusts with carbon-rich blast furnace dust, it has been shown that both reduction/vaporisation of zinc and complete reduction of iron can be achieved. This confirms their appeal for usage with the HIsarna furnace as a means of resource recovery. It is clear that carbon is in considerable excess in the 60:40 ratios tested in this study, consequently work needs to be made on finding optimal concentration. Furthermore, studies of briquette/-pellet formulation should be undertaken to define the most appropriate composition.

Conclusions

The behaviour of industrial waste dusts at 1000 °C in inert atmosphere has been undertaken. The potential of BF dust, BOF dust, and goethite for recycling within the HIsarna furnace has been considered with respect to contained iron and zinc. It was found that by mixing the latter two materials with BF dust in a 60:40 ratio produced a mixture that showed very promising behaviour for zinc recovery and iron

reduction. Whilst almost all of the zinc was lost from the samples within the 30 min of experimentation, the iron was completely reduced to its metallic form. The product resembles DRI and as such can offer a material to the steel industry which can lower costs and allow for the recycling of valuable material, reducing coal consumption.

References

1. Besta P et al (2013) The cycle and effect of zinc in the blast-furnace process. Metalurgija 52:197–200
2. Lanzerstorfer C, Angerbauer A, Gaßlbauer M (2018) Feasibility of air classification in dust recycling in the iron and steel industry. Steel Res Int 89:1–6
3. Lanzerstorfer C (2018) Electric arc furnace (EAF) dust: application of air classification for improved zinc enrichment in in-plant recycling. J Clean Prod 174:1–6
4. Kuwauchi Y, Barati M (2012) Model for the carbothermic reduction of dust-carbon composite agglomerates. AISTech Iron Steel Technol Conf Proc 53:143–152
5. Antrekowitsch J, Rösler G, Steinacker S (2015) State of the art in steel mill dust recycling. Chem Ing Tech 87:1498–1503
6. Suetens T, Guo M, Van Acker K, Blanpain B (2015) Formation of the ZnFe2O4 phase in an electric arc furnace off-gas treatment system. J Hazard Mater 287:180–187
7. Veres J (2014) Determination of zinc speciation in metallurgical wastes by various analytical methods. Int J Chem Environ Eng 5(5)
8. Pickles CA (2003) Reaction of electric arc furnace dust with molten iron containing carbon. Miner Process Extr Metall 112:81–89
9. De Buzin PJWK, Heck NC, Vilela ACF (2017) EAF dust: an overview on the influences of physical, chemical and mineral features in its recycling and waste incorporation routes. J Mater Res Technol 6:194–202
10. Wu CC, Chang FC, Chen WS, Tsai MS, Wang YN (2014) Reduction behavior of zinc ferrite in EAF-dust recycling with CO gas as a reducing agent. J Environ Manage 143:208–213
11. Meijer K et al (2014) The HIsarna ironmaking process 1. Eur Steel Environ Energy Congr 23
12. Ma NY (2011) On in-process separation of zinc from EAF dust. Epd Congr 947–952
13. Colbert D, Irons GA (2006) Electric arc furnace dust injection into iron and steel melts. Can Metall Q 45:1–8
14. Lee J-J, Lin C-I, Chen H-K (2001) Carbothermal reduction of zinc ferrite. Metall Mater Trans B 32:1033–1040
15. Mombelli D, Di Cecca C, Mapelli C, Barella S, Bondi E (2016) Experimental analysis on the use of BF-sludge for the reduction of BOF-powders to direct reduced iron (DRI) production. Process Saf Environ Prot 102:410–420

Recycling of Zinc from Galvanized Steel Scrap

Shafiq Alam, V. I. Lakshmanan and R. Sridhar

Abstract A process flowsheet for zinc recovery from galvanized steel scrap in alkaline media has been studied. The process includes leaching of zinc by sodium hydroxide followed by solvent extraction using organic extractants containing oxine derivatives, such as Kelex 100, LIX-26. Zinc was stripped from the loaded organic by sulphuric acid, which was then recovered by precipitation as zinc carbonate.

Keywords Zinc · Recycling · Leaching · Solvent extraction · Steel scrap · EAF dust

Introduction

About 80% of world's zinc is used for galvanizing steel, which is used for making car body. New scrap from auto sector and old scrap from auto junk go to steelmakers as they are cheap source of feedstock for steel manufacturing industries. During making steel from galvanized steel scrap, zinc is volatilized that goes to air as electric arc furnace (EAF) dust, which is collected in the baghouse and landfilled. According to the US Environmental Protection Agency (EPA), this zinc containing dust is classified as hazardous material. In this work, a hydrometallurgical process has been developed and patented for recovery of zinc from galvanized coatings [1]. The process flowsheet includes leaching of zinc from galvanized steel scrap. The zinc-free scarp called black steel was ready for feedstock to steelmakers for clean steel making. Zinc in the pregnant leach solution (PLS) was solvent extracted and precipitated as zinc carbonate to recover zinc as a value added product.

S. Alam (✉)
Department of Chemical and Biological Engineering, University of Saskatchewan, 57 Campus Drive, Saskatoon, SK S7N 5A9, Canada
e-mail: shafiq.alam@usask.ca

V. I. Lakshmanan · R. Sridhar
Process Research ORTECH Inc., 2395 Speakman Drive, Mississauga, ON L5K 1B3, Canada

© The Minerals, Metals & Materials Society 2020

A. Siegmund et al. (eds.), *PbZn 2020: 9th International Symposium on Lead and Zinc Processing*, The Minerals, Metals & Materials Series,
https://doi.org/10.1007/978-3-030-37070-1_71

Experimental

Leaching of Zinc

Leaching tests were carried out batch wise in a 4 L stainless steel container at 90 °C, where a 500 g galvanized steel scrap was added to 1 L of 200 g/L sodium hydroxide solution. Peroxide was used as an oxidizing agent. After 30 min of agitation, scrap was removed and a fresh 500 g scrap was added to this leach liquor and leaching was continued. At every stage, sample was collected for analysis. Percentage of zinc recovered in leach was found to be 92.45%, and the zinc was leached as sodium zincate, $Zn(ONa)_2$ in the PLS.

Solvent Extraction (SX) of Zinc

A series of SX tests were carried out to recover zinc from PLS using different kinds of organic extractants containing oxine derivatives (e.g. Kelex 100, LIX-26). Initially Kelex 100 was tested for zinc recovery from alkaline media. Scoping tests showed that Kelex 100 extracts zinc from caustic solution; however, since the production of Kelex 100 was stopped, a similar kind of extractant named LIX-26 has been used. Extraction test was carried out at 40 °C using different concentrated extractants at different organic/aqueous (O/A) ratio. In all cases, 5 vol% EXXAL 13 alcohol was used as a modifier and NORPAR 13 was used as a diluent. As shown in Table 1, it was found that at 1:1 O/A ratio, 15 vol% LIX-26 can extract about 25% Zn from its alkaline solution containing about 200 g/L NaOH and 35 g/L Zn.

Kinetics of zinc extraction was very fast and the equilibrium reached within 5 min. Scrubbing of loaded organic was carried out with water at room temperature followed by stripping of zinc at room temperature with different concentrated sulphuric acid. As shown in Table 2, sulphuric acid with a pH of 1 was found to be the most suitable stripping agent for zinc recovery from loaded LIX-26.

Table 1 Extraction of zinc

Type of extractant	Extractant concentration (M)	Zn loading in org. (g/L)	% Extraction of Zn (@ 1:1 O/A ratio)
Kelex-100	0.168	3	7
Kelex-100	0.8	14	25
LIX-26	0.168	4	10
LIX-26	0.5	10	25
LIX-26	0.8	15	30

Table 2 Stripping of zinc

Organic feed (loaded LIX-26)	Aqueous feed (H_2SO_4)	% Stripping of Zn
11.25 g/L Zn	pH = 1	90
10.08 g/L Zn	pH = 1.5	20
10.08 g/L Zn	pH = 2	8.38
10.08 g/L Zn	pH = 3	0.11

Precipitation of Zinc

Zinc was precipitated from strip solution as zinc carbonate. Precipitation test was carried out at room temperature. A 100 mL of stripped solution containing 4.958 g/L Zn was stirred with 1.3 g sodium carbonate powder for about 30 min. Complete precipitation (99.92%) of zinc was taken place as zinc carbonate.

Reaction Scheme

Based on the experimental results the following reaction mechanism was derived, where HQ represents the hydroxyquinoline extractant.

Leaching:

$$Zn + 2NaOH + 1/2O_2 \rightarrow Zn(ONa)_2 + H_2O$$

Extraction:

$$Zn(ONa)_2 \rightarrow {ZnO_2}^{2-} + 2Na^+$$

$${ZnO_2}^{2-} + 2HQ \rightarrow ZnQ_2 + 2OH^-$$

$$2Na^- + 2OH^- \rightarrow 2NaOH$$

Stripping:

$$H_2SO_4 + ZnQ_2 \rightarrow 2HQ + ZnSO_4$$

Precipitation:

$$ZnSO_4 + Na_2CO_3 \rightarrow ZnCO_3 + Na_2SO_4$$

Conclusion

A sustainable process has been developed for zinc and steel scrap recycling where zinc was leached in an alkaline media as sodium zincate followed by solvent extraction of zinc with LIX-26 and precipitation as zinc carbonate as a value added product. Caustic leaching of zinc had an added benefit that avoided dissolution of iron as impurity in the PLS. De-zinced black steel ensured zinc-free feedstock for steelmakers. This allowed sustainable development by eliminating hazardous zinc dust production in the steel making plants. Recycling of zinc allowed a decrease of environmental damage from primary zinc production. It also decreases greenhouse gas production.

Reference

1. Lakshmanan VI, Sridhar R, Alam MS (2005) Recovery of zinc from galvanized coatings. Canadian Patent, Serial No. CA 2347552 (Issued on April 19, 2005)

GCRIS

Part XX
Zinc Leaching and Fe-Control II

GCRIS

A New Route for Treating Neutral Leaching Residue

Caio César Spindola de Oliveira, Daniel Dayrell Pereira, Felipe Ramos Pereira Mendes and Mateus Felipe Louredo Araujo

Abstract In the zinc smelter process, more specifically in the acid leaching step, sulfuric acid is added to the neutral leach residue until 45–60 g/L free acidity is reached, usually retrieving 92% of the zinc contained in the residue. However, it also makes iron and other impurities soluble. Because of that, the solution must go to some iron removal step (jarosite, for example). In this work, we compared this method to the sulfatation process. By simulating a roaster gas outlet (8% of SO_2), at 650 °C, in a fluidized bed reactor (2 kg/h), we were able to solubilize 96.6% of the zinc and only 2.9% of the iron. That means, no excess acid was required in order to obtain the zinc, and less acid was spent with iron (less residue was obtained as well because hematite occupies 67% less mass than jarosite). With these results, we may improve acid balance, residue reduction, and raw materials consumption in a zinc plant.

Keywords Sulfatation · Neutral underflow · Zinc recovery

Introduction

Conventional Leaching Process

In the traditional zinc RLE (roasting, leaching, and electrowinning) process, after roasting the zinc sulfide concentrate, the obtained zinc calcine (zinc oxide) is mixed

C. C. S. de Oliveira (✉) · D. D. Pereira · F. R. P. Mendes · M. F. L. Araujo
Nexa Resources, BR040, km 284, Tres Marias/MG 39206-000, Brazil
e-mail: caio.oliveira@nexaresources.com

D. D. Pereira
e-mail: daniel.pereira@nexaresources.com

F. R. P. Mendes
e-mail: ext.felipe.mendes@nexaresources.com

M. F. L. Araujo
e-mail: mateus.araujo.ma1@nexaresources.com

© The Minerals, Metals & Materials Society 2020

A. Siegmund et al. (eds.), *PbZn 2020: 9th International Symposium on Lead and Zinc Processing*, The Minerals, Metals & Materials Series,
https://doi.org/10.1007/978-3-030-37070-1_72

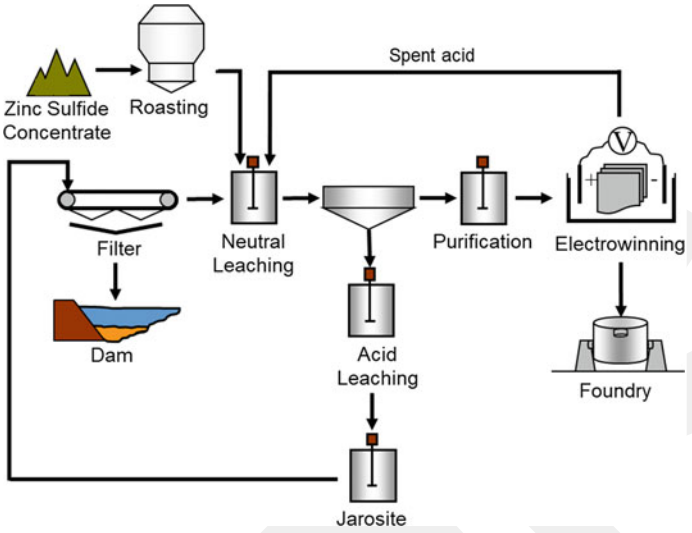

Fig. 1 Simplified flowsheet of a conventional zinc RLE process

with the spent acid from the Electrowinning process (enriched with concentrated new sulfuric acid), producing a neutral concentrated solution of zinc sulfate (Eq. 1). Because this solution must be close to a neutral pH, not all zinc from the calcine is solubilized. Usually, 85% of the zinc is recovered in the neutral leaching phase, and most of the remaining zinc is obtained in the following acid leaching phase (Fig. 1).

Neutral leaching reaction

$$ZnO(s) + H_2SO_4(aq) \rightarrow ZnSO_4(aq) + H_2O(l) \quad (1)$$

In the second phase, concentrated sulfuric acid is added to the neutral leach residue/underflow until 45–60 g/L of free acidity is reached, retrieving 92% of the zinc contained in the residue, resulting in an overall global leaching recovery of approximately 98.8%. This extreme acidity is necessary due to the formation of zinc ferrites in the roaster, which are much more stable than zinc oxide and require a more aggressive leaching process (Eq. 2).

Roaster reactions

$$2ZnS(s) + 3O_2(g) \rightarrow 2ZnO(s) + 2SO_2(g)$$

$$4FeS_2(s) + 11O_2(g) \rightarrow 2Fe_2O_3(s) + 8SO_2(g)$$

$$ZnO(s) + Fe_2O_3(s) \rightarrow ZnFe_2O_{4(S)}$$

Acid leaching reaction

$$ZnFe_2O_4(s) + 4H_2SO_4(aq) \rightarrow ZnSO_4(aq) + Fe_2(SO_4)_3(aq) + 4H_2O(1) \quad (2)$$

Unfortunately, the final acidity is not suitable for the following processes, and besides that, it makes iron and other undesirable impurities soluble (like germanium, arsenic, among others). Because of that, the resulting flow must go to a neutralization (usually with the calcine) and iron removal step, commonly, jarosite (Eq. 3).

Jarosite reaction

$$3Fe_2(SO_4)_3(aq) + (NH_4)_2SO_4(aq) + 12H_2O(l) \rightarrow 2(NH_4)Fe_3(SO_4)_2(OH)_6(s) + 6H_2SO_4(aq) \quad (3)$$

In this operation, iron is precipitated in this mineral form called jarosite, and while forming, drag the mentioned impurities with it. Unluckily, some of the zinc is lost as well. Spite the formation of sulfuric acid in the reaction, the jarosite mineral includes some sulfate, removing sulfuric acid from the process. This reaction requires strict pH control; otherwise, the mineral will not form. Because of that, calcine is usually used to control de pH, yielding a compatible flow to be incorporated in the neutral leaching (after some solid/liquid separation process).

Alternative to Conventional Leaching Process

Looking for improvements in the RLE process, this work evaluated the sulfatation process as an alternative for the neutral leaching residue treatment. As it can be seen in Eq. 1, the roasting process releases SO_2, and at the right conditions (around 650 °C), the zinc ferrite from the neutral leaching residue reacts with this gas producing zinc sulfate and hematite (Eq. 4) [1–8].

Sulfatation reaction

$$2ZnFe_2O_4(s) + 2SO_2(g) + O_2(g) \rightarrow 2ZnSO_4(s) + 2Fe_2O_3(s) \quad (4)$$

Regarding Eq. 4, an acid phase would not be needed, meaning that no extra acid would be required in order to obtain the zinc from the ferrite form. Besides that, the jarosite step becomes unnecessary as well, as the impurities are not solubilized (and no zinc would be lost). Adding Eqs. 2 and 3 and comparing with 2 and 4, it was possible to look for further assumptions (Eq. 5):

Sulfuric acid overall balance in the conventional process

$$6ZnS(s) + 30H_2O(1) + 12Fe_2(s) + 57O_2(g) + 2(NH_4)SO_4(aq) \rightarrow 18H_2SO_4(aq) + 4(NH_4)Fe_3(SO_4)_2(OH_6(s) + 6ZnSO_4(aq)$$

$$H_2SO_{4re} = 1.5$$

Sulfuric acid overall balance in the sulfatation process

$$2ZnS(s) + 4FeS_2(s) + 19O_2(g) + 8H_2O(l) \rightarrow 8H_2SO_4(aq) + 2ZnSO_4(s) + 2Fe_2O_3(s)$$

$$H_2SO_4 : Fe = 2.0 \quad (5)$$

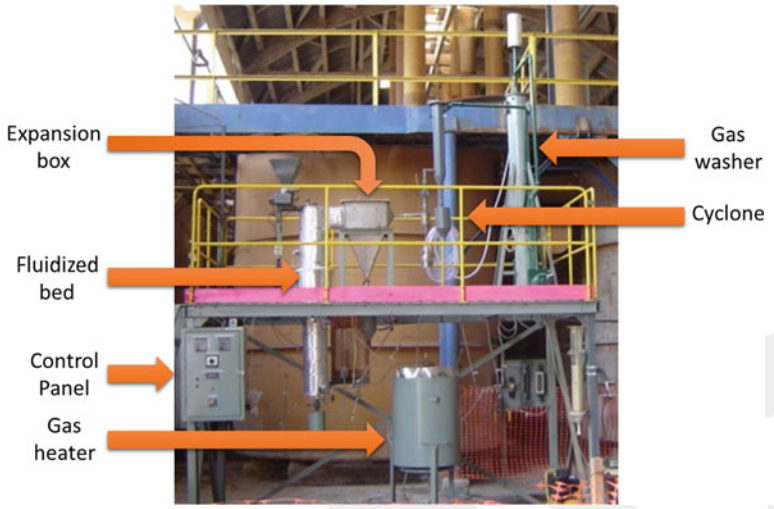

Fig. 2 Fluidized bed reactor (2 kg/h)

As it can be seen in Eq. 5, the theoretical sulfatation process would produce 1/3 more acid than the common process, relatively to the iron content in the zinc concentrate. It requires 2/3 less oxygen and water, does not consume ammonium sulfate, would increase the zinc overall recovery rate, (as no zinc would be lost to the jarosite), and produces a residue with 1/2 of the mass per mol of iron.

In order to evaluate these advantages, a theoretical model was tested in the HSC Outotec Software®. Besides that, samples from the neutral leaching underflow from the Tres Marias smelter process were collected, dried at 105 °C until stable weight was reached, and tested in a pilot fluidized bed reactor (Fig. 2). The input and output from the pilot sulfatation process were analyzed in an ICP spectrometer. Samples were dissolved with aqua regia solution and diluted; each result was compared with its respective standard.

Results and Discussion

After collecting the underflow from Tres Marias neutral leaching process and drying until constant weight, this material was analysed as described previously, and the results are shown in Table 1.

As it can be seen in Table 1, the underflow from the neutral leaching in Tres Marias still contains some zinc Oxide. It also carries zinc sulfate from the neutral leaching. Only a third of it is zinc ferrite. In order to evaluate if this composition is suitable for the sulfatation process, this composition was theoretically evaluated in the HSC Outotec Software®, obtaining the following result (Fig. 3).

Table 1 Composition of the dried underflow from Tres Marias neutral leaching process

Specie	Percentage (%)
ZnO	10.01
$ZnSO_4$	23.41
$PbSO_4$	4.33
$ZnFe_2O_4$	29.44
$MgSO_4$	2.13
$CaSO_4$	18.28
SiO_4	6.40
H_2O	6.00

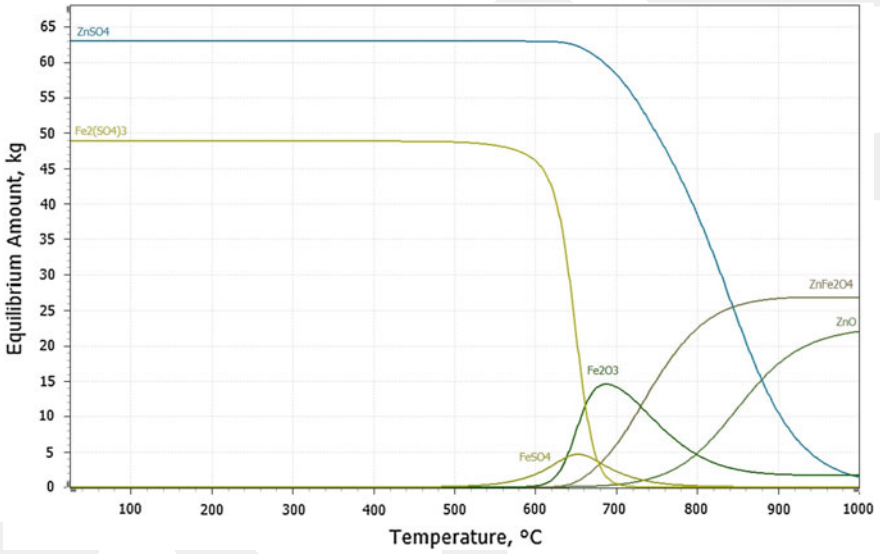

Fig. 3 Theoretical equilibrium composition from 0 to 1000 °C, of Tres Marias neutral leaching residue, under sulfatation conditions (1000 Nm^3, air enriched with 8.25% of SO_2)

The theoretical evaluation for Tres Marias neutral leaching residue under sulfatation conditions (Fig. 3) showed that below 600 °C all zinc and iron would be in the sulfate form. This would not give any gain in acid production, and besides that, all contaminants would also be soluble. Above 700 °C, significant amount of zinc ferrite would be formed, requiring an acid leaching phase. That means the best condition of sulfatation for the Tres Marias underflow is between 600 and 700 °C. In this range, most of the zinc is in the sulfate form, and the majority of iron stays in the hematite form. Sulfates of Ca, Mg, Pb, and SiO_2 do not change in the process.

With the theoretical results, a fluidized bed reactor (Fig. 2) was used to evaluate the hypothesis. Table 2 shows the conditions and results for these experiments: the gas flow was determinate for minimum fluidization, 20 L/min; this flow was enriched

Table 2 Experimental conditions and results for Tres Marias neutral underflow sulfatation

Test	Mass (kg)	Gas flow (L/min)	Temperature	Time	Zn recovery	Iron solubilization
1	1.0	20	650	1.0	96.6	2.9
2	0.3	5.0	550	1.0	96.2	24.2
3	2.0	20	750	1.0	72.1	0.4

Zn recovery calculates the percentage of zinc that is solubilized after the sulfatation process (solubilization was accomplished by simple washing the solid with water or with slight acid conditions, with significant results improvement with acid condition—final pH 3.8)

with liquid SO_2 in order to obtain a constant flow with 8% of this gas (simulation a roaster gas outlet). Besides that, calculating the SO_2 demand, 1 kg of Tres Marias neutral underflow would need 0.16 g of SO_2. In the test, it was provided 274 g. This huge stoichiometric excess was necessary in order to not change the SO_2 outlet concentration; otherwise, the sulfatation process would drop this gas concentration significantly; interfering in the sulfuric acid plant, diminishes its efficiency.

Test number 1 showed a very good zinc recovery and little iron solubilization. Test number 2 has shown also very good zinc recovery, but because the temperature is lower, it favors the formation of iron sulfate (even with the gas flow reduction, but still excessive). The drop in zinc recovery at test number 3 was due formation of zinc ferrites.

Regarding the fluidized bed reactor, some sulfatation was observed at the walls, even after just few tests. This would require constant maintenance in the fluidized bed reactor. Other operations have to be tested, like rotating oven, or Wedge furnace, in order to evaluate performance and prevent wall sulfatation.

Conclusion

The sulfatation process was evaluated as an alternative for acid leaching plus jarosite process. Regarding the zinc recovery, it has shown the same or even better performance. The iron solubilization was diminished, but further investigation regarding other impurities must be performed. The process requires special attention for temperature control, especially because it is extremely exothermic. A minimum flow is required for fluidization of the reactor, as well to not alter significantly the SO_2 concentration, preventing significant alterations in the rest of the process. Further investigations are required to achieve the overall balance of the plant and to choose the right equipment. Sulfatation was observed in the walls of the reactor, and in an industrial scale fluidized bed reactor, this would require constant maintenance.

References

1. Li Y, Liu H, Peng B, Min X, Hu M, Peng N, Yuang Y, Lei J (2015) Study on separating of zinc and iron from zinc leaching residues by roasting with ammonium sulphate. Hydrometallurgy 158:42–48
2. Guler E, Seyrankaya A, Cöcen I (2008) Effect of sulfation roasting on metal extraction from cinkur zinc leach residue. The J Ore Dress 10:1–10
3. Yu D, Utigard TA, Barati M (2013) Fluidized bed selective oxidation-sulfation roasting of nickel sulfide concentrate: part II. Sulfation roasting. Metall Mater Trans B 45:653–657
4. Zhao YM, Hou YN, Cui YG, Liang HW, Li LN (2015) Recovery of copper from copper sulfide concentrate by sulfation roasting. Int J Nonferrous Metall 4:9–13
5. Lund RE, Warnes DE (1957) Selective sulfation for cadmium recovery at Josephtown Smelter. J Metals 9:608–611
6. Frankiewicz TC (1976) Selective sulfation of non-ferrous metals in a salt-moderated roast. Proc Electrochem Soc 6:478–493
7. Ozer M, Acma E, Atesok G (2017) Sulfation roasting characteristics of copper-bearing materials. Asia-Pac J Chem Eng 12:365–373
8. Morris DR (1994) Technological assessment of alternative processes: the processing of sulphide minerals. Can Metall Q 33:297–304

GCRIS

Study of a Novel Chloride Volatilization Process for the Treatment of Jarosite Residue

H. B. Wang, C. Z. Zheng and S. C. Qin

Abstract A novel chloride volatilization process for the treatment of jarosite residue stored in Serbia has been developed. In this process, valuable metals such as lead, zinc, copper, silver, and indium are chlorinated and volatilized with the addition of chlorinating agent. Iron is enriched in the slag and used in iron making systems after magnetic separation or other methods. Sulfur combines with calcium and forms a stable calcium sulfate to avoid the production of sulfur dioxide. The influence of reducing agent, chlorinating agent, and temperature on the volatilization rate of zinc, lead, copper, silver, and indium is investigated. The results show that the addition of chlorinating agent, reducing agent, and temperature has an effect on the metal volatilization rate; the addition of chlorinating agent improves the volatilization rate of lead, zinc, copper, silver, and indium; and the addition of reducing agent further improves the metal recovery rate. Under the recommended conditions, the volatilization rate of each element is zinc 98.26%, lead 99.88%, copper 97.32%, indium 58.73%, and silver 95.22%, respectively. The chloride volatilization process not only transforms jarosite residue into general solid waste, but also comprehensively recovers valuable metals such as lead, zinc, copper, silver, indium, and iron. The process completely solves the potential pollution of jarosite residue and has good economic benefits.

Keywords Jarosite residue · Chloride volatilization · Comprehensive utilization

H. B. Wang (✉) · C. Z. Zheng · S. C. Qin
BGRIMM Technology Group, Beijing 100070, China
e-mail: whaibei_01@163.com

C. Z. Zheng
e-mail: zhengchaozhen123@163.com

S. C. Qin
e-mail: qshuchen@163.com

C. Z. Zheng
University of Science and Technology Beijing, Beijing 100083, China

© The Minerals, Metals & Materials Society 2020

A. Siegmund et al. (eds.), *PbZn 2020: 9th International Symposium on Lead and Zinc Processing*, The Minerals, Metals & Materials Series,
https://doi.org/10.1007/978-3-030-37070-1_73

Introduction

Jarosite residue is a solid waste slag produced in the process of iron removal in hydrometallurgical zinc plants [1, 2]. It usually contains valuable metals such as iron, lead, zinc, and copper and contains high value-added metals such as indium and silver, which have certain economic recovery value. Jarosite residue can exist stably under certain acidic conditions but it will decompose or hydrolyze and dissolve heavy metal ions under conditions of environmental pH or temperature rises, resulting in soil and water pollution [3, 4]. Therefore, jarosite residue is not easy to be piled up for a long time. It should be treated and utilized in time, otherwise causes waste of resources and brings potential pollution risks to the surrounding environment. There are millions of tons of jarosite residue stored in Serbia [5]. The slag storage facilities for storing jarosite residue are very simple. There are no anti-seepage measures and no obvious dam construction and protection embankment. The slag reservoir is a local river and nearby water bodies. The residents face huge potential threats. Next to the slag bank is a river which poses a huge potential threat to the water area and residents.

The main purpose of comprehensive treatment of jarosite residue is to solidify and treat priceless substances harmlessly while extracting valuable metals from jarosite residue. There are two kinds of processes: pyrometallurgy and hydrometallurgy. Pyrometallurgy mainly includes high temperature roasting-magnetic separation method and chlorination roasting method. For example, the roasting-magnetic separation process proposed by Lu et al. [6] after high temperature reduction roasting and magnetic separation resulted in an iron grade magnetic separation concentrate reaching 58.99–58.72%, and the sulfur content is low. Hydrometallurgy mainly uses sodium hydroxide or ammonia water to decompose jarosite residue. For example, the ammonia water decomposition jarosite residue process is proposed by Beijing General Research Institute of Mining and Metallurgy. Ammonia water can decompose 95% jarosite residue, about 60% zinc and copper enter the solution, and 75% silver remains in the slag. In addition, there is a method of leaching jarosite residue with concentrated sulfuric acid or hot acid and a combination of pyrometallurgical and hydrometallurgical treatment. For example, Lan et al. [7] proposed the iron slag acid leaching–roasting–acid leaching process. The medium–low temperature roasting–NH_4Cl leaching–alkali leaching process was proposed by Xue et al. [8]. The pyrometallurgy–hydrometallurgical combined process can select the combination of processes according to the composition and properties of the materials to achieve effective leaching of valuable metals.

Jarosite residue is a kind of pollutant and a resource. It adopts an environmentally friendly treatment method to recover the associated rare precious metals such as lead, zinc, copper, indium, and bismuth and realizes the resource utilization of valuable elements. Fixed disposal of invaluable and harmful elements is the trend of jarosite residue treatment. A new process of calcification, chlorination, and volatilization of jarosite residue has been developed in this paper. It can not only convert jarosite residue into general solid waste, but also comprehensively recovers valuable metals

Table 1 Jarosite residue chemical element analysis results

Element	Fe	Zn	Pb	Cu	As	Sb	F	Cl	Si	S
Content	28.35	5.2	9.61	0.65	0.29	0.039	0.005	0.01	1.5	8.5
Element	Cd	Ca	Mg	Al	Na	Ag (g/t)	Ga (g/t)	Ge (g/t)		In (g/t)
Content	0.04	0.2	0.025	0.48	0.12	356	86	38		240

such as lead, zinc, copper, silver, indium, and iron. The slag can further recover iron and carbon comprehensively, completely solve the potential pollution of jarosite residue, and has good economic benefits.

Experimental

Raw Material

The jarosite residue raw material is from Serbia and is supplied by the University of Belgrade, Serbia. The jarosite residue is yellowish in color and contains 24.27% water. The specific surface area of iron slag is 3.9 m^2/g, the average surface area is 1.537 μm, the volume average particle size is 3.714 μm, the material <20 μm is 99.6%, and <25 μm is 100%. The chemical element analysis of the jarosite residue was carried out, and the results are shown in Table 1. Zn, Pb, Cu, and other valuable metals are high in content and contain valuable metals such as Ga, Ge, Ag, and In, which have high economic value of recovery.

The XRD analysis results of jarosite residue are shown in Fig. 1. It can be seen from Fig. 1 that the phases contained in the jarosite residue are mainly jarosite, silica, and a small amount of hematite and Mn_3O_4.

In order to find out the changes of the jarosite residue in the process of thermal decomposition, the thermogravimetry–differential thermal analysis (TG–DTA) was carried out, and the analysis results are shown in Fig. 2. It can be seen from the TG–DTA of the jarosite residue has two endothermic valleys at 401 and 601 °C, and there are different degrees of weight loss, indicating that the jarosite residue is decomposed twice at this temperature.

Apparatus and Procedure

Comprehensive resource utilization and harmless use of jarosite residue are mainly high temperature calcification chlorinated jarosite residue to obtain metal chloride volatile soot. Extraction of sponge indium is by leaching–extraction–displacement of volatile soot. Lead–silver slag is leached by chlorination—lead powder replaces silver—iron filings replace lead to obtain sponge silver and sponge lead. The indium

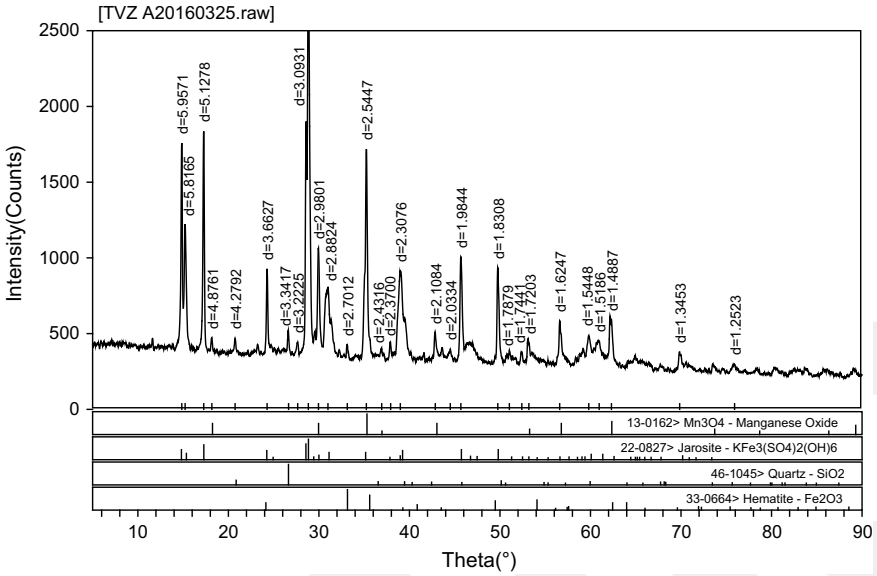

Fig. 1 XRD pattern of jarosite residue

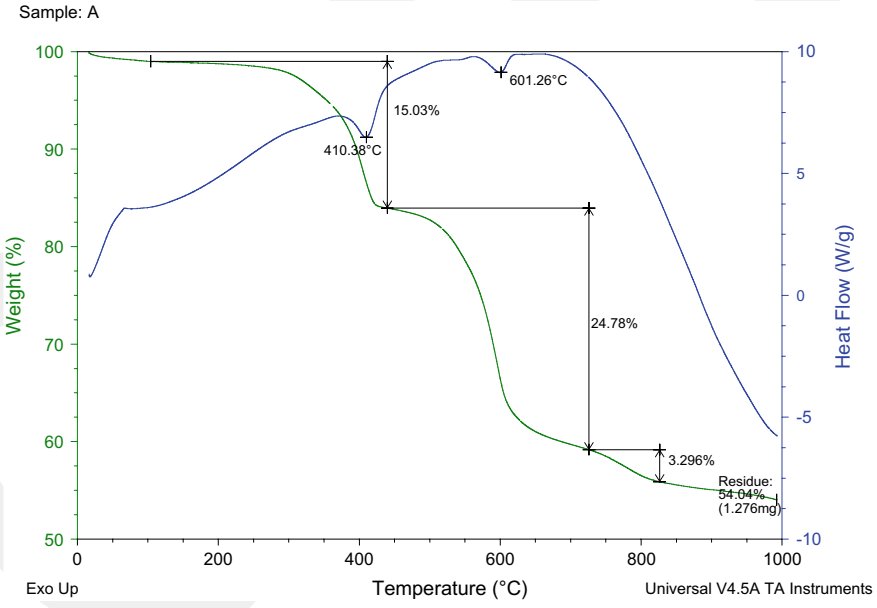

Fig. 2 TG–DTA of the jarosite residue

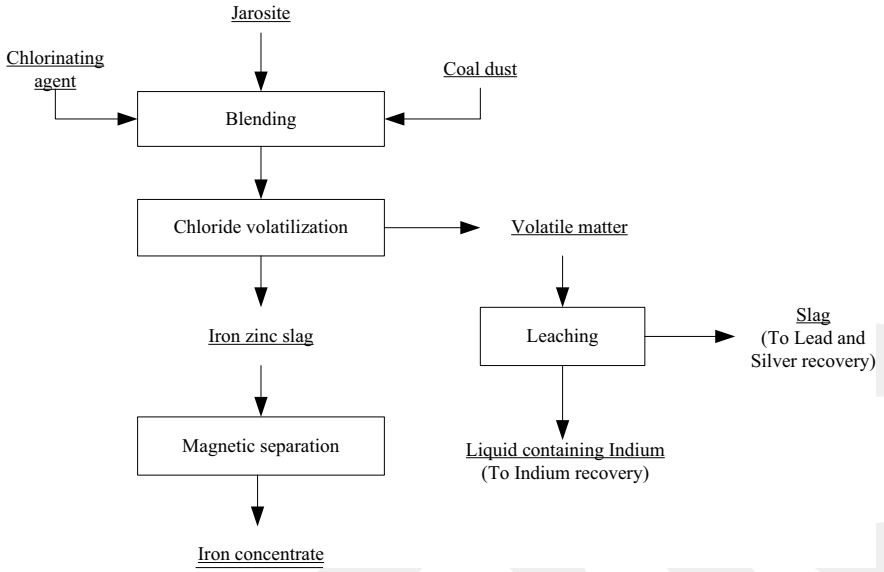

Fig. 3 Flowchart of slag calcification and chlorination of jarosite residue

raffinate is extracted by copper extraction—electrowinning to obtain cathode copper. Zinc chloride products obtained by indium replacement post solution purification and remove impurities evaporation crystallization. It realizes the effective separation of lead, zinc, copper, silver, and silver elements. It can be made into a saleable product realizing the comprehensive utilization of jarosite residue. The process flowchart is shown in Fig. 3.

Reagents: jarosite residue, calcium chloride, coal powder. Instruments: X-ray diffractometer, thermogravimetric analyzer, inductively coupled plasma optical emission spectrometer. The elemental composition of jarosite residue was analyzed by inductively coupled plasma optical emission spectrometry (ICP-OES). The new technology of calcification and chlorination volatilization of jarosite residue is mainly to study the chlorination volatilization of valuable metals such as lead, zinc, copper, silver, and indium under the action of chlorinating agent. Also, the enrichment of iron elements in the slag can be used in ironmaking system after magnetic separation or other enrichment.

Results and Discussion

Effect of Chlorinating Agent Content Under No Pulverized Coal

The effect of chlorinating agent content on the volatilization rates is investigated under no pulverized coal. The content of chlorinating agent was varied from 12 to 24% using roast temperature of 1100 °C, roast time of 2 h, and total feed amount of 50 g. The effects of the volatilization rates of copper, silver, and indium are shown in Table 2 and Fig. 4.

It can be seen from Fig. 4 that under the condition of no addition of pulverized coal, with the increase of the content of calcium chloride, the volatilization rate of zinc, lead, indium, and silver metal increases greatly, and the increase rate of copper volatilization rate is small. During the increase of calcium chloride from 12 to 24%, the volatilization rate of zinc, lead, indium, silver, and copper increased from 29% to 85.53%, from 30.21% to 85.33%, from 55.67% to 91.42%, from 37.46% to 68.18%, and from 11.12% to 32.98%, respectively.

Table 2 Metal volatilization rate under no pulverized coal

Chlorinating agent content (%)	Volatilization rate/%				
	Zn	Pb	Cu	In	Ag
12	29.00	30.21	11.12	55.67	37.46
16	44.87	32.67	21.29	80.88	41.46
20	65.87	50.24	23.69	88.05	48.41
24	85.53	85.33	32.98	91.42	68.18

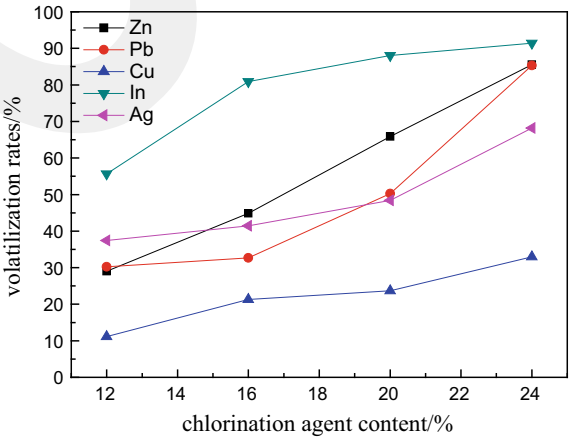

Fig. 4 Effect of chlorinating agent on volatilization

Increasing the content of calcium chloride added has a significant effect on the increase of the volatilization rate of zinc, lead, indium, and silver. When the addition amount is 24%, zinc, lead, and indium can obtain better volatilization results, and the volatilization rate almost all reached more than 85%.

Effect of Chlorinating Agent Content Under Pulverized Coal

The effect of chlorinating agent content on the volatilization rates is investigated under pulverized coal. The content of chlorinating agent was varied from 12 to 28% using a roast temperature of 1100 °C, calcination time of 2 h, total feed amount of 50 g, and pulverized coal addition amount of 3%. The effects of the volatilization rates of copper, silver, and indium are shown in Table 3 and Fig. 5.

It can be seen from Fig. 5 that under the condition of 3% addition of pulverized coal, the volatilization rates of five metals, such as zinc, lead, copper, indium, and silver, increases to different degrees with the increase of calcium chloride addition. Among them, the volatilization rate of zinc, copper, and indium metal

Table 3 Metal volatilization rate under pulverized coal

Chlorinating agent content (%)	Volatilization rates/%				
	Zn	Pb	Cu	In	Ag
12	26.33	93.20	15.38	17.77	86.62
16	51.70	99.02	34.91	41.79	95.21
20	74.23	99.61	56.36	58.05	96.83
24	98.26	99.88	97.32	58.73	95.22
28	99.43	99.86	97.90	75.91	97.34

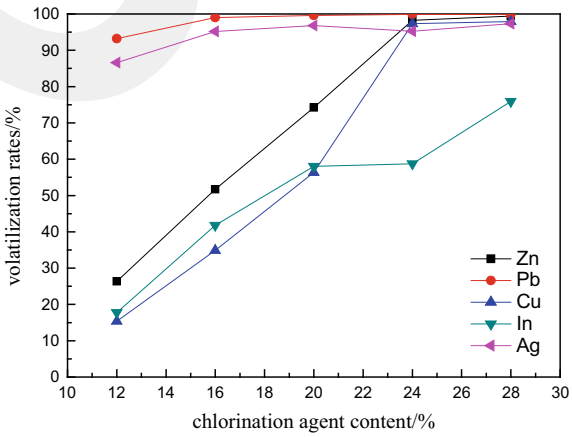

Fig. 5 Effect of chlorinating agent content on metal volatilization rate

increases greatly. When the amount of calcium chloride increased from 12 to 28%, the volatilization rate of zinc, copper, and indium increased from 26.33% to 99.43%, from 15.38% to 97.90%, and from 17.77% to 75.91%, respectively. The volatilization rate of lead and silver increased slowly under the content of calcium chloride of 12%, but both maintained a high volatilization rate, which reached 93.2% and 86.62%, respectively.

The volatilization rate of lead and silver is relatively high, which is less affected by the addition amount of calcium chloride. The volatilization rate of zinc, copper, and indium metal is greatly affected by the addition of chlorinating agent. When the content of calcium chloride added is of 24%, zinc, lead, and copper can obtain better volatilization results, which are 99.43%, 99.86%, and 97.90%, respectively. If only lead and silver are recovered, the chlorinating agent is added in an amount of 16%, and the volatilization rate can reach 99.02% and 95.21%, respectively. If multiple elements are recovered in the same process, the chlorinating agent content should be increased to 24%.

By comparing Figs. 4 and 5, it can be found that under the condition of 3% addition of reducing agent pulverized coal, the volatilization rates of lead, zinc, copper, and silver are all increased, and the evaporation rate of lead and silver is particularly significant. The volatilization rate of lead and silver increases from 30.21% to 93.20% and from 37.46% to 86.62%, respectively, under the content of calcium chloride added of 12%. This is supposed to be the addition of pulverized coal to create a CO reducing atmosphere, which can accelerate the reduction in lead and zinc and increase the volatilization rate. However, the volatilization rate of indium is significantly reduced from 55.67 to 17.77% under the same conditions. So, the addition of pulverized coal is not conducive to the volatilization of indium.

Effect of Roasting Temperature Under Pulverized Coal

The effect of roasting temperature on the volatilization rates is investigated under pulverized coal. The roast temperature was varied from 800 to 1200 °C using calcination time of 2 h, chlorinating agent content of 24%, total feed amount of 50 g, and pulverized coal addition amount of 3%. The effects of the volatilization rates of copper, silver, and indium are shown in Table 4 and Fig. 6.

It can be seen from Fig. 6 that the influence of roasting temperature on the volatilization rate of different metals is obviously different. The temperature has little effect on the volatilization rate of lead and indium, and the degree of influence on the volatilization rate of zinc, copper, and silver is large. During the roast temperature increase from 800 to 1200 °C, the volatilization rate of lead element is almost always maintained at a high volatilization rate of 96–99%. The volatilization rate of indium element is only maintained in the range of 52–58%. The volatilization rate of zinc, copper, and silver element increased from 58.68% to 98.26%, from 21.84% to 94.78%, and from 12.03% to 97.31%, respectively.

Table 4 Metal volatilization rate under different roasting temperature

Roast temperature (°C)	Volatilization rates/%				
	Zn	Pb	Cu	In	Ag
800	58.68	96.19	21.84	52.11	12.03
900	80.90	99.17	42.55	52.99	27.02
1000	85.80	99.61	74.50	54.79	87.24
1100	98.26	99.88	97.32	58.73	95.22
1200	98.26	99.96	94.78	54.48	97.31

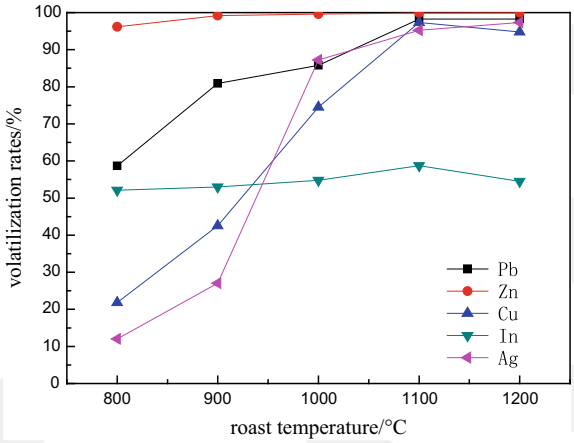

Fig. 6 Effect of roasting temperature on metal volatilization

The elevated temperature can significantly increase the volatilization rate of zinc, copper, and silver. When the temperature reaches 1100 °C, the volatilization rates of zinc, copper, and silver can reach 98.26%, 97.32%, and 95.22%, respectively, and the lead volatilization rate can reach 99.88%. Meanwhile, lead, zinc, copper, and silver metals have obtained a good volatilization rate, so the recommended temperature is 1100 °C.

Slag Sample Analysis

In order to determine the phase composition of the slag sample after roast, XRD analysis was carried out, and the analysis results are shown in Fig. 7.

According to the analysis of slag phase, the slag sample mainly contains hematite and calcium sulfate, indicating that in the process of calcification and chlorination, sulfur is fixed in the form of calcium sulfate, and iron is converted into hematite. In

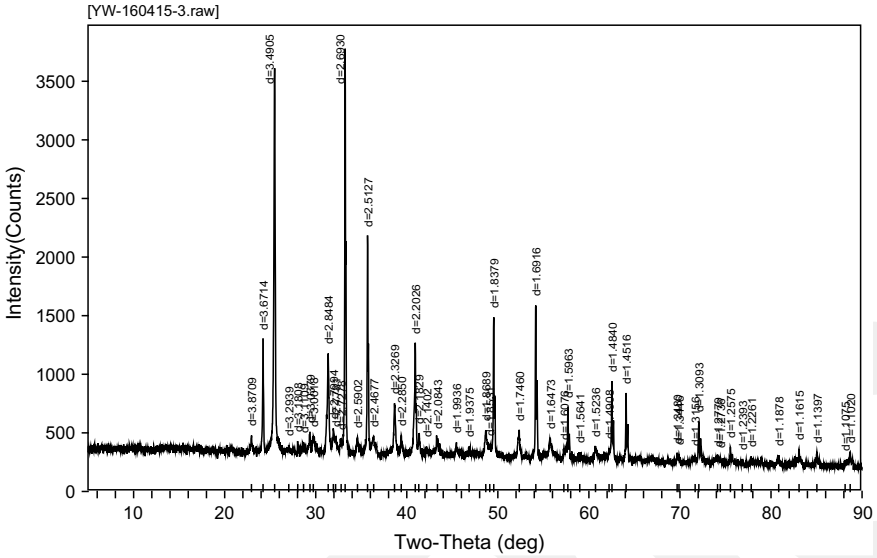

Fig. 7 Slag phase analysis

the experiment, a magnet was used for the test, it was observed that the magnetism was remarkable, and the slag was recovered by magnetic separation or the like.

Conclusion

According to the above test, the addition amount of chlorinating agent, pulverized coal, and temperature influences the metal volatilization rate. The addition of chlorinating agent can increase the volatilization rate of lead, zinc, copper, silver, and indium, and the addition of pulverized coal can further improve the metal recovery rate. Considering the chlorination recovery of the same process in a variety of metals, the optimum process conditions are 24% calcium chloride, 3% pulverized coal, 73% jarosite residue, roasting temperature of 1100 °C, and roasting time of 2 h. The volatilization rate of zinc, lead, copper, indium, and silver are 98.26%, 99.88%, 97.32%, 58.73%, and 95.22%, respectively.

Acknowledgements This work was supported by National Key Research and Development Plan of China (2018YFC1900401) and National Natural Science Foundation of China (51434001).

References

1. Jha MK, Kumar V, Singh RJ (2001) Review of hydrometallurgical recovery of zinc from industrial wastes. Resour Conserv Recycl 33(1):1–22
2. Pelino M (2000) Recycling of zinc-hydrometallurgy wastes in glass and glass ceramic materials. Waste Manag 20(7):561–568
3. Dutrizac JE, Jambor JL (2000) Jarosites and their application in hydrometallurgy. Rev Mineral Geochem 40(1):405–452
4. Rathore EN, Patil MP, Dohare ED (2014) Utilization of jarosite generated from lead-zinc smelter for various applications: a review. IJCIET 5(11):192–200
5. Manojlović VD, Kamberović ŽJ, Gajić NM (2019) An alternative route for valorization of valuable metals from jarosite residue. Tehnika 74(3):388–393
6. Lu DK, Jin ZN, Xie F (2013) Research on magnetite preparation by reductive baking of jarosite residue. Copp Eng 1:6–11
7. Lan BB, Liu XY, Liu LH (2013) Research on comprehensive utilization technology of jarosite residue. Multipurp Util Miner Resour 6:54–58
8. Xue PY, Ju SH, Zhang YF, Wang XW (2011) Recovery of valuable metals by leaching of roasted jarosite residue. Chin J Process Eng 11(1):56–60

GCRIS

Magnetic Separation of Iron Ion from Leaching Solution by Magnetic Seeding in Hydrometallurgy

Tong Yue, Haisheng Han, Wei Sun, Yuehua Hu, Zhiyong Gao, Runqing Liu, Li Wang, Lei Sun and Honghu Tang

Abstract Millions of tons of hazardous iron oxide residues are produced during the iron purification process of sulphate leaching solutions in nonferrous metals hydrometallurgy industry per year. The generated iron oxide residues, which mainly contain goethite and gypsum precipitates adsorbing the hazardous elements of arsenic, sulfur, zinc, and germanium, pose a great threat to the local ecological environment and human health. A novel method for the treatment and recovery of goethite and gypsum by synthetic magnetic nanoparticles (MNPs) such as α-Fe_3O_4 and γ-Fe_2O_3 are proposed to treat the residues efficiently and cost-effectively. MNPs serve as the magnetic crystal nuclei of the goethite precipitates during the iron purification process, and the goethite and gypsum precipitates formed under this condition can be separated in magnetic field. Subsequently, the magnetic crystal nuclei were treated using a rod milling and magnetic collecting to obtain goethite precipitates in order to minimize costs. Both precipitates can be digested as raw materials of iron making and building materials, respectively. Additionally, we found that the separation efficiency of the goethite and gypsum precipitates was much higher when γ-Fe_2O_3 was used as the crystal nuclei, indicating that the surface of γ-Fe_2O_3 was more favorable for the formation of goethite particles than α-Fe_3O_4.

Keywords Magnetic separation · Goethite precipitates · Gypsum precipitates · Hydrometallurgy

Tong Yue and Haisheng Han contributed equally to this work.

T. Yue · H. Han · W. Sun (✉) · Y. Hu (✉) · Z. Gao · R. Liu · L. Wang · L. Sun · H. Tang
School of Minerals Processing and Bioengineering, Central South University, Changsha 410083, China
e-mail: sunmenghu@csu.edu.cn

Y. Hu
e-mail: hyh@csu.edu.cn

© The Minerals, Metals & Materials Society 2020

A. Siegmund et al. (eds.), *PbZn 2020: 9th International Symposium on Lead and Zinc Processing*, The Minerals, Metals & Materials Series,
https://doi.org/10.1007/978-3-030-37070-1_74

Introduction

For the green production and sustainable development of environment, the treatment of industrial hazardous solid waste has received more and more attention. In non-ferrous metals hydrometallurgy industry, millions of tons of hazardous iron oxide residues are produced during the iron removal process in sulphate leaching solutions. Iron is present as an undesirable constituent in zinc, copper, and nickel concentrates, and the solubilisation of the desired metals during the leaching process also leads to dissolution of iron into the solution. Iron constitutes an impurity in leaching solutions, which must be removed before electrolysis.

In most existing hydrometallurgy plants, iron is removed by its precipitation as jarosite and goethite. Impounding large amounts of residues from the jarosite process in tailings ponds incurs high operating cost. The exposure of these residues to atmospheric conditions will cause severe environmental problems, due to the presence of heavy metals and/or hazardous elements, such as Zn, Ge, In, Pb, Se, and S. Furthermore, it is difficult to use jarosite residue because the Fe content in jarosite is lower than 30% with high fluctuation in the content of other undesired elements. Compared with jarosite residue, goethite residue has a lower volume and a higher Fe content (more than 40%), and contain a small amount of impurity elements. At the same time, it is possible to use this residue as an iron source in iron making after suitable treatments. Most electrolytic zinc plants use calcium hydroxide or calcium carbonate as neutralizer in the goethite process, which introduces no impurity into the solution and has a relatively low cost. However, using calcium carbonate or calcium hydroxide led to co-precipitation of calcium sulfate with goethite precipitates, resulting in the difficulty in utilizing these residues. As a result, the residues have to be impounded in tailings ponds which pose great threat to local soil, water, and atmosphere by contained heavy metals and/or hazardous elements in the residue, such as Zn, Ge, As, and S.

To treat these progressively expanding hazardous residues, a novel method is developed in this study to convert these hazardous residues into secondary resources. To accomplish this objective, maghemite fine particles are introduced first into the goethite process as the nucleus seeds to promote goethite precipitation, imposing the required magnetism of goethite precipitates from the attached maghemite fine particles. The magnetically responsive goethite precipitate-maghemite composite particles are separated from calcium sulfate precipitates using a magnetic drum separator. After appropriate treatment to remove the hazardous impurities, the produced goethite-maghemite composite particles and the separated calcium sulfate can be used as ironmaking raw material and building material, respectively. This paper reports the results of addressing a long-term impoundment problem of the hazardous iron residues in smelters with our novel method.

Magnetic Separation of the Goethite and Gypsum Precipitates

Maghemite fine particles were used in the laboratory test under the industrial production conditions of iron removal by the goethite process. In brief, 1 L of sulfuric acid leachate of zinc oxide dust was introduced into a 2-L jacketed pilot plant reactor and heated to keep at 85 °C by water bath. High temperature is known to benefits the formation of goethite precipitates. Added into the leachate were 1–7 g/L of maghemite fine particles, with the mixture being kept under stirring by a mechanical mixer at 200 rpm. Substituting for oxygen-enriched air environment applied in the industry, 10 mL H_2O_2 solution (6 wt%) as the oxidant (representing a 22.9% excess) was pumped into the vessel and reacted for 60 min to oxidize all the ferrous ions to ferric ions in solution as shown in Eq. (1). The fraction of hydrogen peroxide that contributed to oxidation was 67.1%. The pH during the reaction was maintained between 4.0 and 4.5 by pumping 50 g/L $Ca(OH)_2$ slurry into the system. In the goethite process, a large amount of calcium sulfate dihydrate ($CaSO_4{\cdot}2H_2O$, gypsum) and goethite (α-FeOOH) precipitates were generated as shown by Eq. (2) and Eq. (3), respectively.

$$2Fe^{2+} + H_2O_2 \rightarrow 2Fe^{3+} + 2H_2O \tag{1}$$

$$Ca(OH)_2 + {SO_4}^{2-} + 2H_2O \rightarrow CaSO_4 \cdot 2H_2O + 2OH^- \tag{2}$$

$$Fe^{3+} + 3OH^- \rightarrow \alpha\text{-}FeOOH + H_2O \tag{3}$$

After crystallization by the goethite process, the suspension was pumped into a 30 × 30 cm magnetic drum separator to separate the magnetic particles from the suspension. The flow of the suspension was 100 ml/min. The magnetic drum separator uses electromagnets to generate magnetic field and its magnetic field strength can be adjusted from 0 to 3000 Gs. After the magnetic separation, the magnetic concentrate and non-magnetic tailings were obtained after solid–liquid separation by filtration. Both products were soaked in pH 3.0 sulfuric acid solution for 30 min under vigorous stirring at the solid-liquid mass ratio of 1:5 to remove the adsorbed zinc ions from particles surfaces. It should be noted that the zinc co-precipitated inside goethite and gypsum cannot be removed by this acid washing. After filtration and drying at 80 °C for 12 h, goethite (the concentrate) and gypsum (the tailings) particles were obtained that could be potentially used as raw materials for value-added products.

Finally, reduction roasting was used to remove the impurity elements such as S and As from goethite. Figure 1 is a schematic illustration of the entire process.

The recoveries of Fe and Ca in the concentrates and tailings with different dosages of α-Fe_3O_4 or γ-Fe_2O_3 NPs are shown in Fig. 2a. The Fe recovery in the concentrates increased from 15.01 to 52.43%/29.29 to 96.29% with increasing the dosage of α-Fe_3O_4/γ-Fe_2O_3 from 1 to 7 g/L, which indicated that the amount of goethite

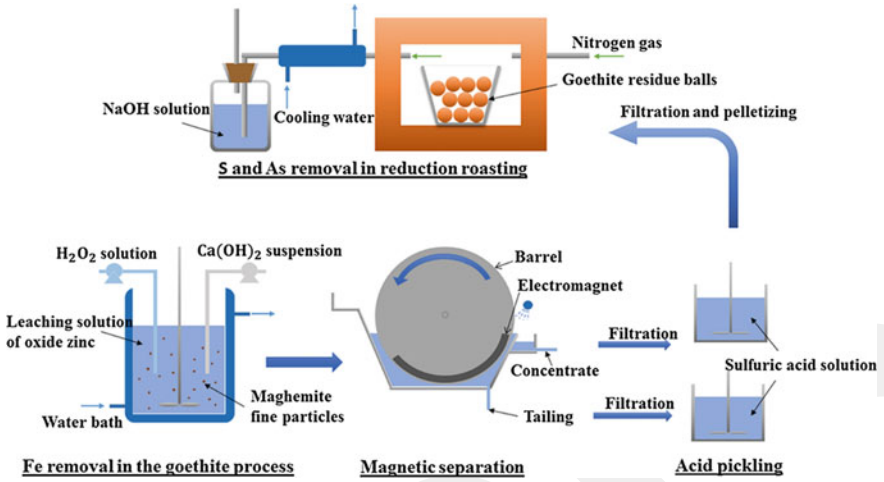

Fig. 1 Schematic illustration of magnetic separation and production of desired goethite and gypsum product

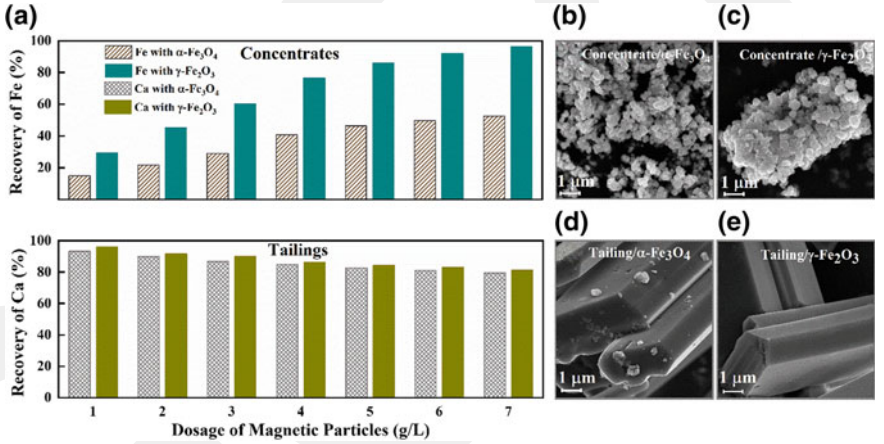

Fig. 2 Recovery of Fe and Ca (**a**) in the concentrate and tailing after magnetic separation, respectively; SEM images (**b–e**) of the concentrate and tailing with 7 g/L MNPs

precipitates formed on the surface of γ-Fe_2O_3 was much larger than that on α-Fe_3O_4 surface. It can be also observed that the losses of Ca in the concentrates were almost the same with different MNPs addition and increased slightly with increase in the dosage of the MNPs, suggesting that gypsum precipitates lost in the concentrates were not affected by the MNPs. The slight increase in the loss of Ca in the concentrates would be attributed to the entrainment of gypsum by the magnetic particles in the magnetic separation.

The microtopography of the concentrates and tailings with the two MNPs is shown in the SEM images (Fig. 2b–e). In the concentrates, the goethite particles with α-Fe_3O_4 as the crystal nuclei were dispersive and less than 1 μm in diameter, while the goethite particles with γ-Fe_2O_3 as the crystal nuclei aggregated into large particles. The newly formed goethite precipitates on the surface of the MNPs have low crystallinity and can be used as the flocculants between different goethite precipitates. Hence, it is hard for the α-Fe_3O_4 particles with a small amount of goethite attached on the surface to aggregate with each other. As can be seen from the SEM image of tailing for α-Fe_3O_4, there were many goethite particles on the surface of the gypsum particles. These goethite particles, which were formed in the solution rather than on the α-Fe_3O_4 surface, were non-magnetic and therefore could not be collected during magnetic separation. Instead, those non-magnetic goethite particles entered the tailings with gypsum particles. Only gypsum particles appeared in the tailing for γ-Fe_2O_3, which suggested that almost all the goethite particles were collected into the concentrate for γ-Fe_2O_3.

In order to reduce the cost of the magnetic nanoparticles, the recovery of the two magnetic nanoparticles from the concentrates and the cycle use efficiency of the MNPs as the magnetic seeds in the goethite process was investigated. Figure 3a, b shows the magnetic collection yield of the concentrates for α-Fe_3O_4 and γ-Fe_2O_3 under different milling time and magnetic fields. 5 min of the milling time and 750 Gs of the magnetic field intensity were optimum for collecting the magnetic nanoparticles from the concentrates. The obtained magnetic nanoparticles were reused as the magnetic seeds for a new iron removal process and their performance was investigated. The recovery of Fe and loss of Ca in the multiple cycle use of the α-Fe_3O_4 or γ-Fe_2O_3 are shown in Fig. 3c and 3d, respectively. For γ-Fe_2O_3, the recovery of Fe was around 99% during the 5 cycles, which is much higher than that of α-Fe_3O_4 (around 60%), while the loss of Ca for both magnetic nanoparticles maintained at around 15–20%. These results indicated the feasibility of recycling magnetic seeds in the iron removal process, which would effectively reduce the cost of magnetic seeds in the industrial application.

Conclusion

The residues of the goethite process in the zinc oxide dust hydrometallurgy contain toxic and heavy metallic elements. Impounding these residues in tailings ponds causes serious environmental concerns. In this study, a novel and robust method based on the addition of maghemite fine particles as the crystal nucleus of goethite precipitates in the goethite process was proposed and tested. The goethite precipitates formed on the surface of maghemite particles became magnetic that can be separated into goethite concentrate and calcium sulfate tailings by magnetic separation. The calcium sulfate (gypsum) tailings generated with a small quantity of goethite can be used in cement and building materials production. The technology developed in this

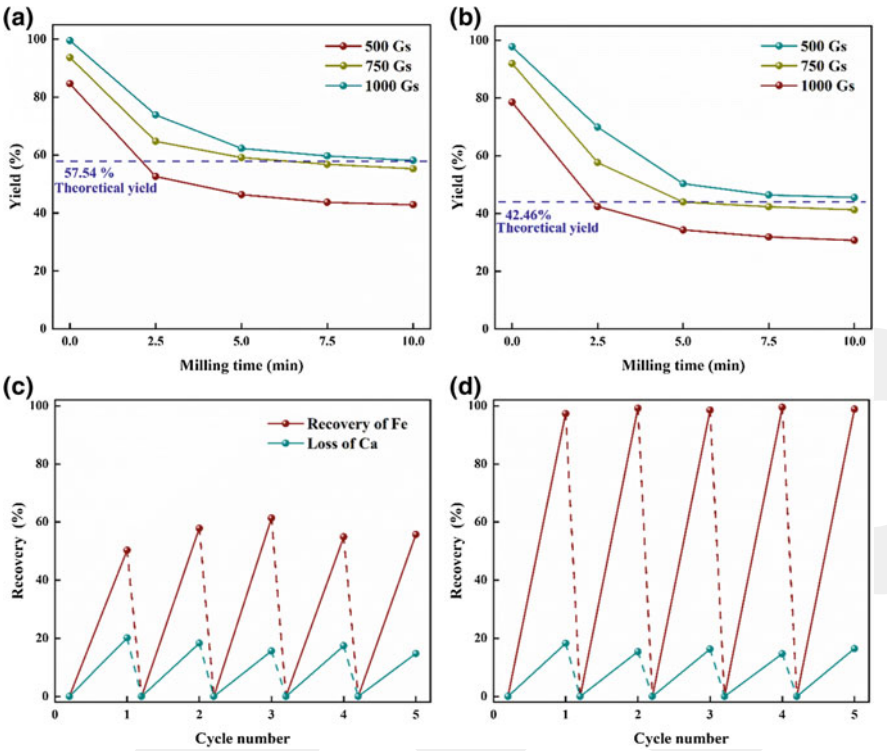

Fig. 3 Magnetic recovery of α-Fe_3O_4 (**a**) and γ-Fe_2O_3 (**b**) from the concentrates after rod milling; and recovery of goethite precipitates in the cycle use of α-Fe_3O_4 (**c**) and γ-Fe_2O_3 (**d**)

study provides a feasible way to convert a hydrometallurgy waste of zinc hydrometallurgy to value-added raw materials for the ironmaking and production of building materials. An array of techniques has been used to characterize the goethite formation on MNPs and the results showed that γ-Fe_2O_3 is superior to α-Fe_3O_4 for the formation of goethite particles on its surface.

Experimental Study on Pressure Leaching of Zinc Sulfide Concentrate and Discussion on the Latest Relevant Progress

Haibei Wang, Shuchen Qin, Kaixi Jiang and Bangsheng Zhang

Abstract In this paper, a typical zinc sulfide concentrate has been studied in detail by process mineralogy. Its main mineral composition and occurrence state of elements were identified. In addition, the effects of technological conditions such as temperature and acidity on the pressure leaching were investigated. The phase transformation of iron was analyzed and the related mechanism was explained. At the same time, the latest experimental progress in the field of zinc pressure leaching, such as leaching process, leaching kinetics, elemental behavior, and phase transformation in the process of pressure leaching, is also introduced.

Keywords Pressure leaching · Zinc sulfide concentrate · Latest relevant progress

Introduction

The most commonly used process in the smelting of zinc sulfide concentrate is roasting-leaching-electrodeposition [1], during which a large amount of SO_2 is generated in the roasting process, resulting in environmental pollution. In the process of pressure leaching of zinc sulfide, elemental sulfur is generated, avoiding the generation of SO_2, and iron resources can be recycled by forming hematite. Therefore, pressure leaching is a method of high reaction efficiency and is environmental friendly [2–4]. The total reaction of zinc sulfide concentrate in pressure acid leaching process is as follows: $2ZnS + 2H_2SO_4 + O_2 = 2ZnSO_4 + 2H_2O + 2S$. The iron ion produced

H. Wang (✉) · S. Qin · K. Jiang · B. Zhang
BGRIMM Technology Group, Beijing, China
e-mail: whaibei_01@163.com

S. Qin
e-mail: qshuchen@163.com

K. Jiang
e-mail: jiangkx@bgrimm.com

B. Zhang
e-mail: zbsvictory@163.com

© The Minerals, Metals & Materials Society 2020

A. Siegmund et al. (eds.), *PbZn 2020: 9th International Symposium on Lead and Zinc Processing*, The Minerals, Metals & Materials Series,
https://doi.org/10.1007/978-3-030-37070-1_75

by the dissolution of iron contained in minerals is a good oxygen-transporting agent [5]. Its reaction is: $ZnS + Fe_2(SO_4)_3 = ZnSO_4 + 2FeSO_4 + S$, $4FeSO_4 + 2H_2SO_4 + O_2 = 2Fe_2(SO_4)_3 + 2H_2O$. High temperature oxidation leaching of sphalerite is direct leaching, and oxidation of sphalerite by iron ions is indirect leaching, both of which contribute to the high efficient leaching of sphalerite.

In the leaching process, temperature and acidity are the key influencing factors. This study uses zinc sulfide concentrate from a smelter in Sichuan as raw material, which contains 55.46% Zn, 2.44% Fe, and 29.28% S. The mineralogy research of the zinc concentrate was carried out. The effects of temperature and acidity on the leaching process were studied in detail. The phase transformation was analyzed by the XRD analysis of the residue sample and the S and Fe behavior is elaborated. In addition, the latest experimental progress in the field of zinc pressure leaching is introduced.

Process Mineralogy Research

Mineral Composition and Relative Content of Mineral Samples

The composition of the mineral was analyzed through optical microscope, scanning electron microscope, and other instruments and methods, such as ICP and titrimetric analysis. The result shows that the majority of metal minerals in the ore sample are sphalerite(Zn·Fe)S, along with a small amount of galena(PbS), chalcopyrite($CuFeS_2$), pyrite(FeS_2), trace amounts of tetrahedriter ($Cu_{12}Sb_4S_{13}$), covelline(CuS), arsenopyrite(FeAsS), and smithsonite($ZnCO_3$). Nonmetallic minerals are mainly quartz(SiO_2), along with dolomite ($xCaCO_3 \cdot yMgCO_3$), a small amount of chlorite, muscovite($KAl_2[Si_3AlO_{10}](OH,F)_2$), traces of apatite($Ca_5(PO_4)_3(F,Cl,OH)$), vermiculite($CaTi[SIO_4]O$). The mineral composition and relative content of the ore samples are shown in Table 1.

Table 1 Mineralogical composition of ore and relative content

Minerals	Content/%	Minerals	Content/%
Sphalerite	85.10	Dolomite	2.29
Chalcopyrite	1.85	Chlorite	0.96
Pyrite	1.45	Muscovite	0.94
Galena	1.87	Others	0.83
Quartz	4.71	Total	100.00

Characteristics of Main Minerals in Ore Samples

Sphalerite

The majority of sphalerite are produced in the form of irregular shaped monomers. Part of sphalerite is encapsulated with particles of chalcopyrite, galena, and pyrite. Sometimes, sphalerite and gangue minerals are produced together. Occasionally, particles of sphalerite are encapsulated in the gangue minerals or minerals such as tetrahedriter and arsenopyrite are embedded in the sphalerite. According to energy dispersive spectroscopy, main impurities of sphalerite are Fe and Cd. The iron content varies from 0.45 to 2.85%, while the Cd content is relatively low, generally less than 1%. In addition, it is occasionally that Cu is detected in sphalerite with a low content (Figs. 1, 2, 3 and 4).

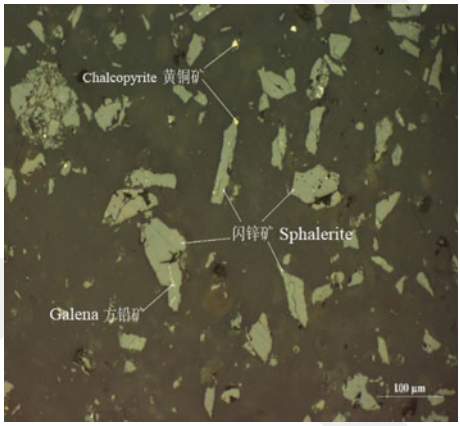

Fig. 1 Sphalerite

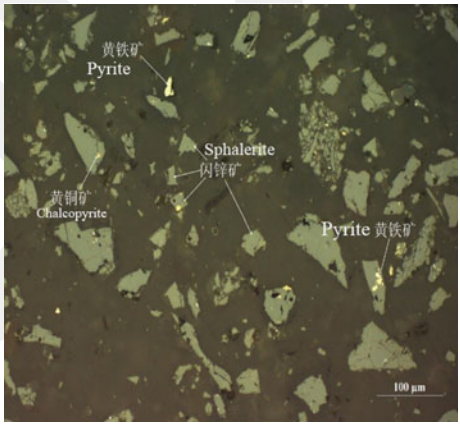

Fig. 2 Sphalerite, chalcopyrite, and pyrite

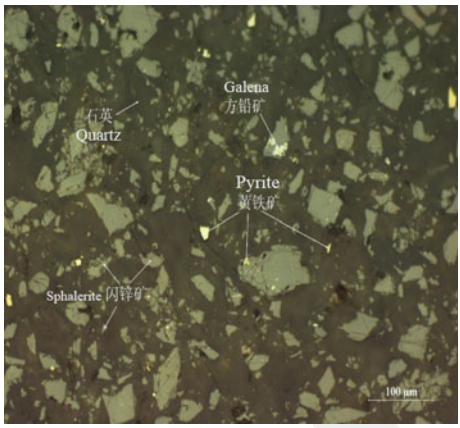

Fig. 3 Sphalerite, pyrite, and galena

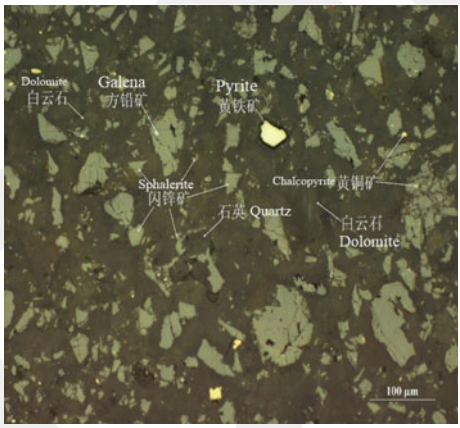

Fig. 4 Sphalerite, quartz, and dolomite

Chalcopyrite

Chalcopyrite is mainly produced in the form of irregular monomers. Part of chalcopyrite is encapsulated in sphalerite in the form of particles. It is occasionally observed that chalcopyrite is produced with sphalerite, pyrite, and galena. Occasionally, chalcopyrite is produced with copper sulfide minerals such as tetrahedriter and covelline. The size of the chalcopyrite is fine with the particle size of below 0.043 mm (Figs. 5 and 6).

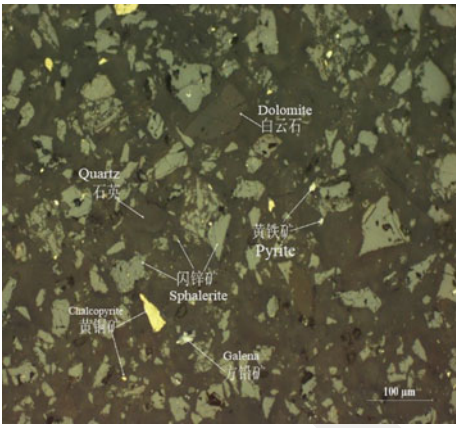

Fig. 5 Chalcopyrite and sphalerite

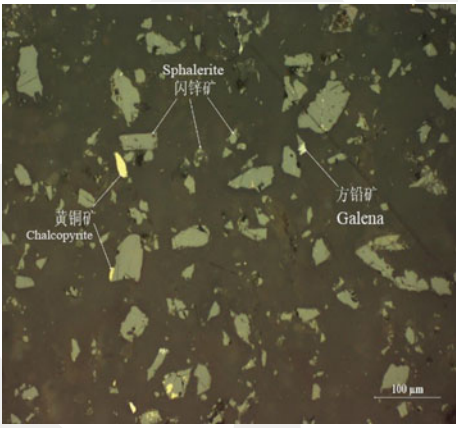

Fig. 6 Chalcopyrite and sphalerite

Pyrite

Pyrite is mainly produced in the form of irregular monomers. Sometimes, it can be seen that pyrite is embedded in sphalerite with finely granules. Occasionally, pyrite can be produced with sphalerite and chalcopyrite. The particle size of pyrite is also relatively fine, mainly concentrating in the range of 0.010–0.043 mm (Figs. 7 and 8).

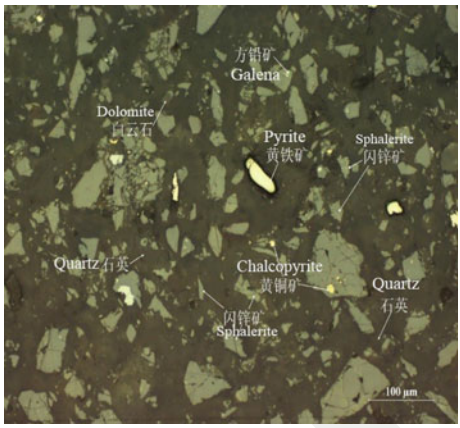

Fig. 7 Pyrite

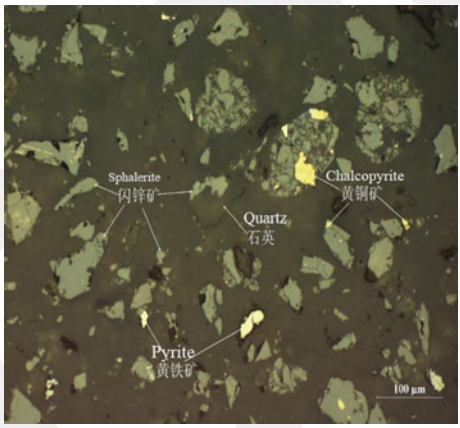

Fig. 8 Pyrite and sphalerite

Occurrence State of Iron in Mineral Samples

The iron content in the ore sample is 2.44%. The iron is mainly present in the sphalerite in the form of isomorphism. The distribution rate of iron in sphalerite is 45.72%. Secondly, the iron exists in the form of pyrite and chalcopyrite with the distribution rate of 27.68% and 23.16%, respectively. 1.95% of iron exists in the form of silicates such as chlorite and muscovite. In addition, 1.49% of iron is present in

Table 2 Balance sheet of iron

Minerals	Relative content of minerals containing Fe/%	Content of Fe in minerals/%	Distribution rate of Fe/%
Sphalerite	85.10	1.31	45.72
Chalcopyrite	1.85	30.52	23.16
Pyrite	1.45	46.55	27.68
Dolomite	2.29	1.59	1.49
Chlorite	0.96	3.89	1.53
Muscovite	0.94	1.07	0.42

the dolomite in the form of carbonate. The calculation results of the element balance of iron in the ore sample are shown in Table 2.

Leaching Test

Effect of Temperature on Leaching

Under the conditions of oxygen pressure 0.5 MPa, time 2 h, L/S ratio 5:1, and initial acid concentration 183.9 g/L, the effect of temperature on the leaching rate of Fe and Zn during the pressure leaching of zinc sulfide concentrate was investigated. The leaching temperatures are 105 °C, 120 °C, 130 °C, 140 °C, 150 °C, and 160 °C, respectively. The test results are shown in Fig. 9.

It can be seen from Fig. 9 that the zinc leaching rate increases with the temperature. The iron leaching rate first increases with temperature and then decreases when the temperature exceeds 150 °C. When the temperature is below 150 °C, the leaching reaction is accelerated due to the increased dissolution of iron, which is the dominant behavior of iron. When the temperature exceeds 150 °C, the dominant behavior of iron changes to forming a precipitate by hydrolyzation, resulting in the lower iron leaching rate. At this time, the large difference between the leaching rate of zinc and iron is beneficial to the separation of zinc and iron.

Effect of H_2SO_4 on Leaching

Under the conditions of temperature 150 °C, oxygen pressure 0.5 MPa, time 2 h, and L/S 5:1, the effect of acidity on the leaching rate of iron and zinc during the pressure leaching of zinc sulfide concentrate was studied. The acidity is changed by using different ratio of the H_2SO_4/Zn as follows: 0.9:1, 1:1, 1.1:1, 1.15:1, 1.2:1, and 1.25:1, respectively. The test results are shown in Fig. 10.

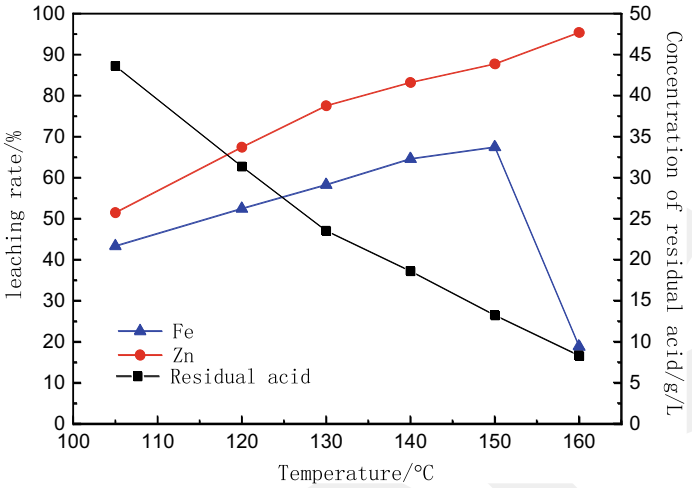

Fig. 9 Effect of leaching temperature on leaching rate of Zn and Fe

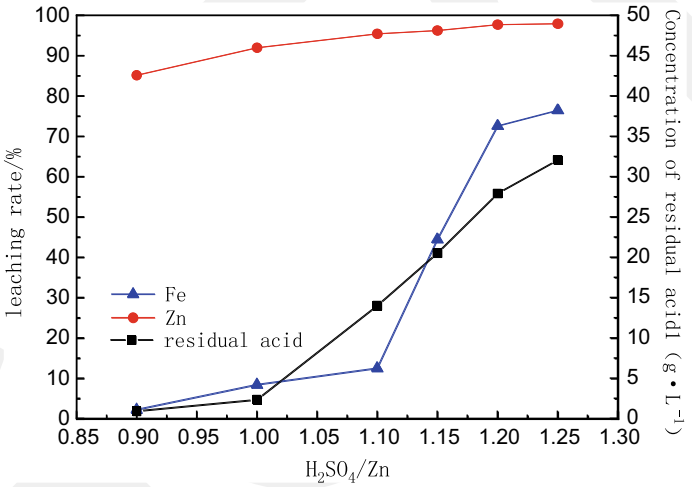

Fig. 10 Effect of H_2SO_4/Zn on leaching rate of Zn and Fe

It is obvious in Fig. 10 that the zinc leaching rate increases with the ratio of H_2SO_4/Zn. When the ratio of H_2SO_4/Zn increases to 1.2:1, the zinc leaching rate curve tends to be gentle and the increment became smaller. The zinc leaching rate reaches 97.7%. Therefore, the best ratio of H_2SO_4/Zn for zinc leaching rate is 1.2:1. The iron leaching rate also increases with the H_2SO_4/Zn ratio, but in a different way. When the H_2SO_4/Zn ratio increases from 0.9 to 1.1, the iron leaching rate gradually increases and reaches 12.5%. When the H_2SO_4/Zn ratio continues to increase, the iron leaching rate is enhanced dramatically to 72.6%. Since the zinc leaching rate is

close to the limit in the H_2SO_4/Zn ratio range, excessive acid is going to leach the iron-containing mineral, resulting in the largely increased iron leaching rate. When the H_2SO_4/Zn ratio continues to increase, the iron leaching rate tends to be the same.

Residue Phase Analysis

Figures 11 and 12 exhibit XRD patterns of the raw materials and the leaching slag, respectively. It can be seen from the figure that the raw materials mainly contain various types of sulfides and quartz, while the leaching slag mainly contains residual sulfides, elemental sulfur, and Pb-jarosite. Comparatively, the peak of sulfide in the

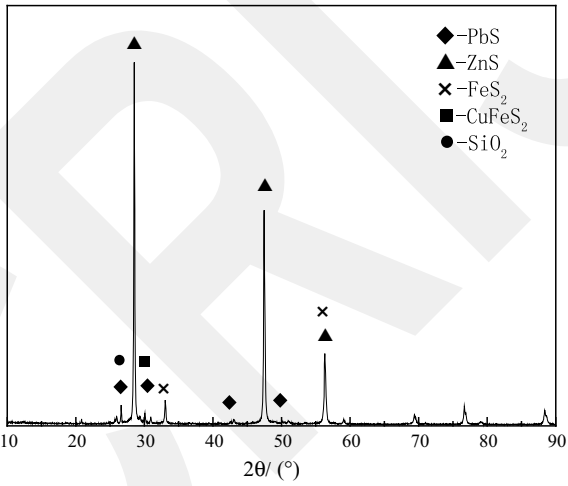

Fig. 11 XRD pattern of the ZnS concentrate

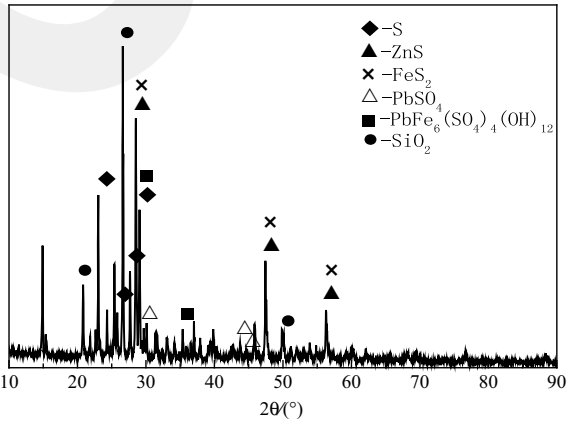

Fig. 12 XRD pattern of the leaching residue

leaching slag is lower than that in the raw materials, which is due to the decrease of sulfide after leaching. Meanwhile, the elemental sulfur and Pb-jarosite are observed in the slag sample after leaching. The appearance of elemental sulphur is due to that the sulphide is leached in the oxygen enriched and pressurized system. The Pb-jarosite phase comes from the precipitate formed by the hydrolyzation of iron ions produced by the leaching process.

Other Recent Relevant Experimental Studies

In the process of pressure leaching, sulfur is recycled in the form of elemental sulfur, which avoids the problem of SO_2 pollution. However, this process has the disadvantages of large equipment investment and high operational safety requirements. The oxygen enriched atmospheric direct leaching technology can avoid the aforementioned disadvantages. The Outokumpu smelter in Finland realized the oxygen enriched atmospheric pressure leaching by increasing the leaching pressure through increasing the pulp height, which has been gradually industrialized [6, 7]. Although the oxygen enriched atmospheric pressure direct leaching has certain advantages, the leaching rate is slow and the process is time-consuming. In order to solve this problem, Xu et al. [8] used zinc concentrate as the research object and compared the leaching kinetics of zinc concentrate by combining atmospheric leaching and pressure leaching. It is pointed out that in the oxygen enriched atmospheric pressure leaching of zinc sulfide concentrate, the zinc leaching process is controlled by the interface chemical reaction both in the upper and the bottom of the leaching tank, and the leaching kinetic equation follows the unreacted shrinkage nucleus model. For the zinc leaching at the bottom of the leaching tank, the leaching rate is significantly enhanced due to the large pulp pressure at the bottom of the tank. They also found that the influence of temperature on the leaching rate is significantly greater than that of the slurry pressure.

Zhu et al. [9] conducted a series of studies on the dissolution behavior of oxygen and pointed out that moderately increasing the temperature in the range of 90–160 °C contributes to the increase of oxygen dissolution rate and the dissolution and transportation of oxygen in aqueous solution. The extension of the oxygen pipe is beneficial to the oxygen dissolution rate. In addition, multiple air intake modes are better than the single air intake mode.

Gu et al. [10] from Northeast University used synthetic sphalerite as the research object, and carried out kinetic studies. Their study demonstrated that the leaching process of sphalerite is controlled by surface chemical reaction, of which the kinetics follows the “unreacted shrinkage nuclear model”.

Xu et al. [11] studied the behaviors of zinc, sulfur, and iron during the low temperature pressure leaching of iron sphalerite. It was pointed out that the main chemical reaction in the early stage of leaching is the acid dissolution of iron sphalerite. In the later stage of leaching, dissolution of iron and the hydrolysis and precipitation

of dissolved iron proceed simultaneously. The precipitation form of iron can be regulated.

Tian [12] from Northeastern University systematically studied the basic process of oxygen enriched pressure leaching of sphalerite from the perspectives of mechanical activation, different catalytic leaching systems, and oxygen bubble behavior. The study pointed out that mechanical activation caused the variation of crystallite size and the distortion of lattice, resulting in reduced sphalerite particle size and increased specific surface area of the sphalerite. All of these lead to the enhanced reaction kinetics, leading to an increase in the oxidation rate of the sphalerite and a reduction of the acid leaching reaction order. During the reaction, the variations of sulfur conversion rate and the indium leaching rate with the change of the reaction conditions are consistent, both of which are kinetically controlled by the interface chemical reaction. In addition, it was also pointed out that the leaching process is effectively promoted by the self-precipitation redox mechanism of Fe. In their study, the variation of bubble refinement and gas holdup during the reaction was explored, and the phenomenological equations of gas holdup and diameter were obtained.

Conclusion

The majority of the metal minerals in this ore sample are sphalerite, along with a small amount of galena, chalcopyrite, and pyrite. Non-metallic minerals are mainly quartz, along with dolomite, a small amount of chlorite and muscovite. The iron content in the ore sample is 2.44%. The iron is mainly present in the form of isomorphism. The distribution rate of iron in sphalerite is 45.72%. Secondly, the iron exists in the form of pyrite and chalcopyrite with the distribution rate of 27.68% and 23.16%, respectively. 1.95% of iron exists in the form of silicates such as chlorite and muscovite. In addition, 1.49% of iron is present in the dolomite in the form of carbonate.

Temperature and acidity have a large effect on the leaching rate of zinc and iron. The zinc leaching rate increases with temperature and acidity. The change trend of iron leaching rate with temperature and acidity is different. The iron leaching rate increases to the highest value of 67.5% with the temperature of 150 °C, and then decreases to the lowest value of 18.9%. The iron leaching rate increases with the acid-zinc ratio. The rate of increase is slightly different for certain range of acid-zinc ration.

Acknowledgements This work was financially supported by the National Natural Science Foundation of China (Key Project No. 51434001) and National Key Research and Development Plan of China (2018YFC1900401).

References

1. Souza AD, Pina PS, Leão VA (2007) Bioleaching and chemical leaching as an integrated process in the zinc industry. Miner Eng 20(6):591–599
2. Buban KR, Collins MJ, Masters IM, Trytten LC (2000) Comparison of direct pressure leaching with atmospheric leaching of zinc concentrates. In: DUTRIZAC J E. Proceedings of lead-zinc 2000. Pittsburg: The Minerals, Metals & Materials Society, pp 727–738
3. Berezowsky RMGS, Collins MJ, Kerfoot DGE, Torres N (1991) The commercial status of pressure leaching technology. JOM 43(2):9–15
4. Ding-fan QIU (1994) Process chemistry and industrial practice of pressure hydrometallurgy. Min Metall 3(4):55–67
5. Jikun Wang, Ying Dong, Tingxi Zhou (2005) Industrial test and industrialization of high-iron zinc sulfide concentrate pressurized leaching. China Eng Sci S1:202–206
6. Svens K, Kerstien B, Runkel M (2003) Recent experiences with modern zinc processing technology. Erzmetall 56:94–103
7. Takala H (1999) Leaching of zinc concentrates at Outokumpu Kokkola plant. Erzmetall 52:37–42
8. Xu Z, Zhu H, Wang C (2013) The direct pressure leaching kinetics of zinc sulfide concentrate in oxygen-enriched sulfuric acid system. The Chin J Nonferrous Metals 23(12):3440–3447
9. Zhu H (2014) Study on oxygen dissolution behavior of zinc sulfide concentrate under pressure leaching conditions. Jiangxi University of Science and Technology
10. Gu Y, Zhang T, Lu G, Liu Y, Yan W, Dou Z (2011) Kinetics of oxygen pressure acid leaching of synthetic low-iron sphalerite. In: Proceedings of 2011 AASRI conference on artificial intelligence and industry application (AASRI-AIIA 2011 V4)
11. Xu Z, Jiang Q, Wang C (2012) The behavior of zinc, sulfur and iron in low temperature pressure leaching process of iron sphalerite. Nonferrous Metals (Smelt) (07):6–11
12. Tian L (2017) Basic research on oxygen-enriched pressure leaching process of sphalerite. Northeastern University

Recent Operational Improvements of Hematite Plant at Akita Zinc Co., Ltd.

Dai Matsuura, Yasuo Usami and Kenji Ichiya

Abstract AKITA ZINC Co., Ltd. (Iijima Zinc Refinery), jointly owned by DOWA METALS & MINING Co., Ltd. (DMM) and another non-ferrous metal company, has used the company's own hematite process for iron control since the beginning of operations in 1971. The amount of zinc leach residue for the hematite plant has been increasing recent years due to the increase of iron content and decrease of zinc grade in concentrate .In addition, some quality issues of by-product have been occurred recently. The following solutions were carried out to stabilize hematite operation.

1. Zinc leach residue treatment increase
   - Renewal of SO_2 leaching autoclave
   - Improvement of cake-washing method
2. By-product quality improvement
   - Modification of filter for de-arsenic process.

Keywords Hematite plant · Autoclave renewal · Cake-washing method improvement · Filter modification

Introduction

DMM carries out mining and smelting activities for precious metals, PGMs, rare metals, and base metals such as copper, lead, and zinc. It owns KOSAKA SMELTING & REFINING Co., Ltd., producing copper and lead, and the AKITA ZINC Co., Ltd. (AZC) in Akita Prefecture. DOWA is a unique smelting company which has established a metallurgical complex for copper, lead, and zinc, combining with a recycling business.

AZC was established in 1971 with design capacity of 72,000 t/y zinc; it is jointly owned by DMM and another non-ferrous metal company. AZC has increased its

D. Matsuura (✉) · Y. Usami · K. Ichiya
Akita Zinc Co., Ltd., 217-9 Shimo-Kawabata Furumichi Iijima, Akita 011-8555, Japan
e-mail: matsuurd@dowa.co.jp

© The Minerals, Metals & Materials Society 2020

A. Siegmund et al. (eds.), *PbZn 2020: 9th International Symposium on Lead and Zinc Processing*, The Minerals, Metals & Materials Series,
https://doi.org/10.1007/978-3-030-37070-1_76

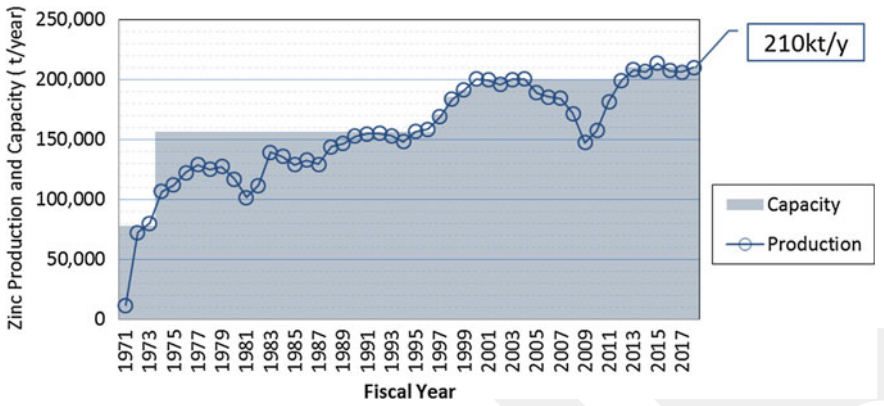

Fig. 1 Annual electrolytic zinc production and capacity at AZC

capacity continuously and reached 210,000 t/y of zinc now. Figure 1 shows the changes of actual production and capacity in zinc [1].

In order to achieve maximum recoveries of valuable metals, AZC has adapted the original hematite process for residue treatment since the start of operations. At the leaching stage, the almost iron in the zinc concentrates is precipitated as zinc leach residue, together with a most of valuable metals. Therefore, iron control is one of the key steps in the hydrometallurgical zinc process operation. There are several hydrometallurgical methods for zinc leach residue treatment, such as the jarosite process, the goethite process, and the hematite process. AZC is the only refinery in the world which presently operates the hematite process. The iron in the zinc leach residue is separated as hematite. The hematite process is generally perceived to be high cost process and difficult to operate, but we have improved in order to overcome those difficulties. Those modifications enabled a recent increase in production and recovery.

Figure 2 shows the changes in the amount of zinc leach residue generated. The amounts of zinc leach residue for the hematite plant has increased recent years due to the expansion of zinc production and elevation of iron content in concentrate. In this situation, hematite plant was required the higher performance than before.

Figure 3 shows the schematic flow sheet of AZC. The other operations—roasting, leaching, purification, electrolysis—are typical processes.

The iron in the zinc concentrate changes chemically into the zinc ferrite during the roasting process. The major portion of the zinc leach residue is zinc ferrite. Also, lead sulfate and silica exist. Through the hematite process, zinc leach residue is decomposed and is formed to various by-products. Table 1 shows the components of those by-products.

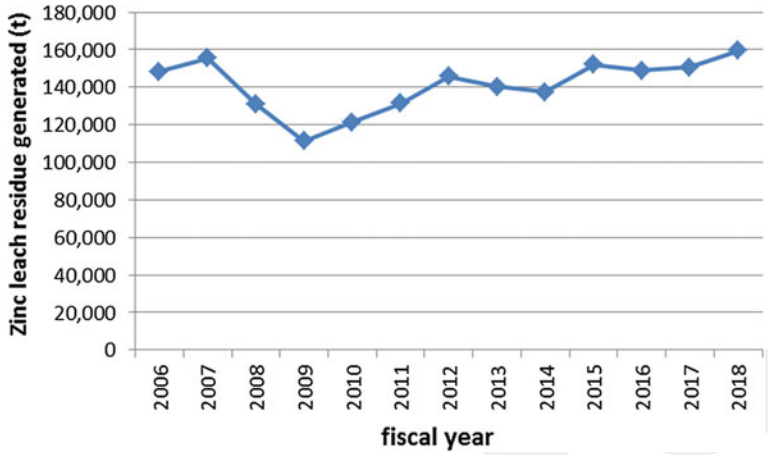

Fig. 2 Annual zinc leach residue generated

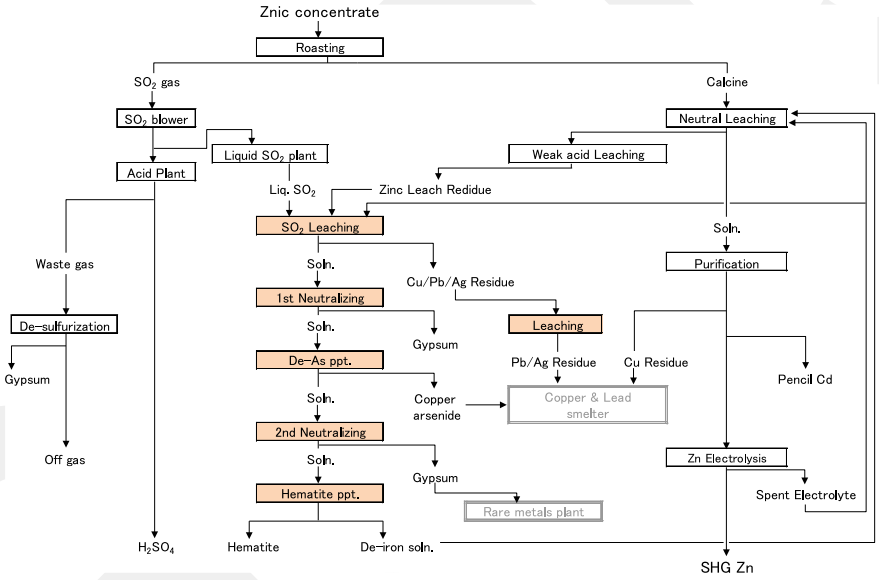

Fig. 3 Schematic flow sheet of the AZC operation

Recent Improvements of the Hematite Process

Renewal of SO_2 Leaching Autoclaves

In the SO_2 leaching process, iron is leached from zinc leach residue through autoclaves. These autoclaves are constructed of steel shell with lead lining, and acid-resistant porcelain bricks on the inside which are commonly used at high temperature

Table 1 Components of the by-products

	Components					
	Fe	Zn	Pb	SiO_2	Cu	As
	%	%	%	%	%	%
Zinc leach residue	23.1	23.2	6.0	6.6	0.7	0.4
Pb/Ag residue	1.8	3.0	23.2	25.3	0.2	–
First neutralizing gypsum	–	0.2	–	–	–	–
Copper arsenide	–	0.5	–	–	63.2	27.3
Second neutralizing gypsum	–	–	–	–	1.0	–
Hematite	54.1	0.6	–	–	–	–

Photograph 1 State of partition wall in autoclave

and high concentration of acid. The decrepitude by operating 40 years caused some problems. Photograph 1 shows the state of the partition wall inside the vessel [2].

Due to repairs by aging, zinc leach residue treatment was reduced by about 800 tons every year. Figure 4 shows the opportunity loss in treatment of zinc leach residue.

From the above, we decided to renew the leaching autoclaves.

We also considered renewing two units at the same time. On the renewal of leaching autoclaves, we examined the suitable material for our process with high endurance. Considering the risk of defects, we decided to renew only one unit first. After confirming no fatal problems, we decided to renew another unit.

Then, the test was focused on the material change because we concerned the shortage of welding technicians for lead lining and the cost enlargement of repair bricks.

Durability Performance

The test piece was attached on the six blades of the agitator installed at leaching autoclave using a welding material with same composition. Photograph 2 shows the installation status.

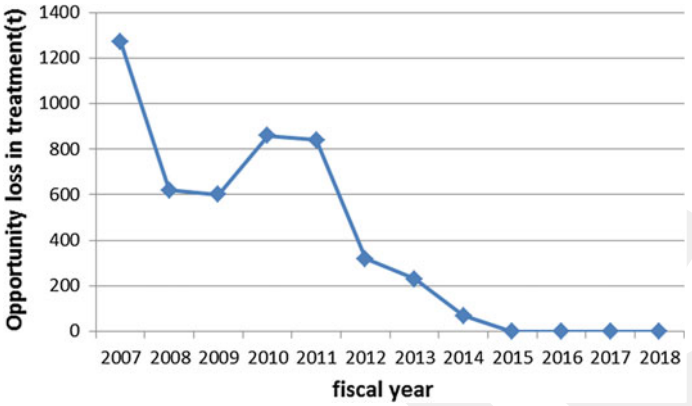

Fig. 4 Opportunity loss in treatment of zinc leach residue due to repairs by aging

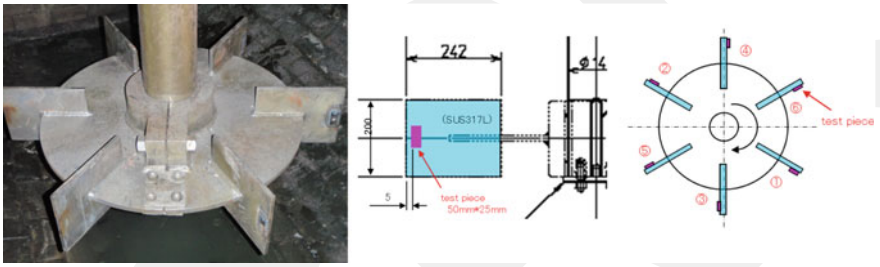

Photograph 2 Installation of sample materials

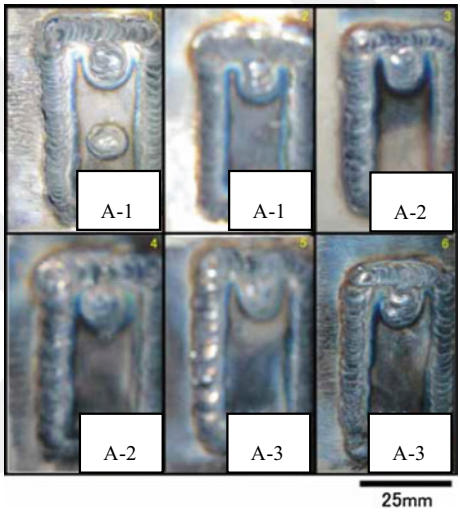

Photograph 3 Appearance immediately after installation

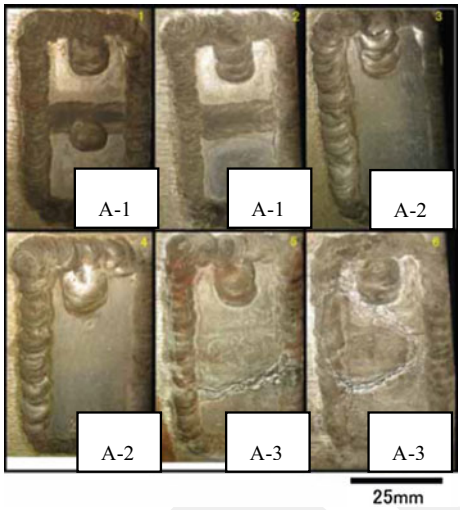

Photograph 4 Appearance after two years

The test was conducted for two years. Photograph 3 shows the starting test pieces and Photograph 4 shows after two years.

Material

A-1: Initial state is a machined surface. The surface has become white due to the overall erosion, and scratches of grinding have become thinner.

A-2: Initial state is a machined surface. The metallic luster is slightly lost, and scratches of grinding remain.

A-3: The surface is clearly eroded, and both specimens were deeply damaged. Under this environment, erosion resistance is insufficient.

Welded parts

A-1: The erosion is clearly observed on the welded part. The weld is more eroded than the specimen itself.

A-2: Slight erosion is observed. The erosion is minimum among test.

A-3: Severe erosion is observed.

Crevice Corrosion Test

A test was preparing in the gaseous zone and liquid zone. The test device is attached to the actual equipment shown in Photograph 5.

The test was conducted for eight months. There was no change in the weight and thickness of the sample pieces. Corrosion rate is calculated to less than 0.1 mm/year.

The results imply that A-2 shows excellent corrosion resistance and abrasion resistance in this condition. Therefore, A-2 was decided to adopt in new equipment.

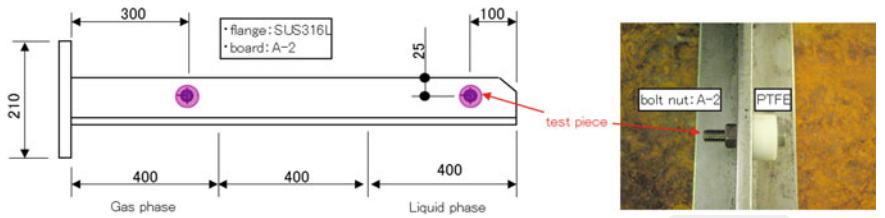

Photograph 5 Sample condition

One vessel was renewed in August 2012 and another one was renewed in August 2015. As a result, the opportunity loss of zinc leach residue treatment by repairing the leaching autoclaves was eliminated.

Improvement of Cake-Washing Operation

A large amount of solution always circulates in the hydrometallurgical process systems of AZC. Figure 5 shows the schematic diagram of the plant water balance. The total water volume is approximately 30,000 m^3. Fresh water input to the system along with additives and washing water used for the by-products. Washing procedure through the hematite filtration has been improved.

Several patterns have been tested (Table 2). The conventional centrifuge time cycle is in pattern 1. The pattern 2, 3, and 4 were tested. The total washing time was adjusted for all patterns. Test results are shown in Fig. 6. In this test, low zinc content indicates a suitable washing pattern. As a result, it was found that the pattern 4 with the three-step washing showed most effective.

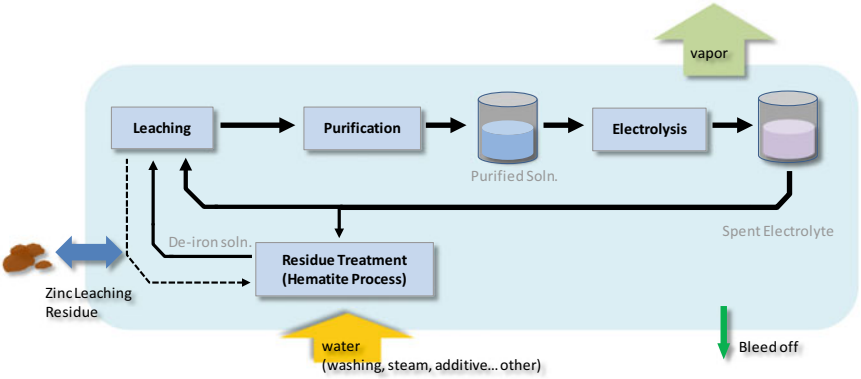

Fig. 5 Schematic diagram of the water balance

Table 2 Test patterns

	Time cycle	Total time
Pattern 1	Slurry feed ⇒ 300 s dehydration ⇒ 120 s washing ⇒ 30 s dehydration 120 s	570 s
Pattern 2	Slurry feed ⇒ 300 s dehydration ⇒ 120 s washing ⇒ 10 s dehydration ⇒ 30 s washing ⇒ 20 s dehydration 120 s	600 s
Pattern 3	Slurry feed ⇒ 300 s dehydration ⇒ 120 s washing ⇒ 5 s dehydration ⇒ 20 s washing ⇒ 25 s dehydration 120 s	590 s
Pattern 4	Slurry feed ⇒ 300 s dehydration ⇒ 120 s washing ⇒ 5 s dehydration ⇒ 20 s washing ⇒ 5 s dehydration ⇒ 20 s washing ⇒ 20 s dehydration 120 s	610 s

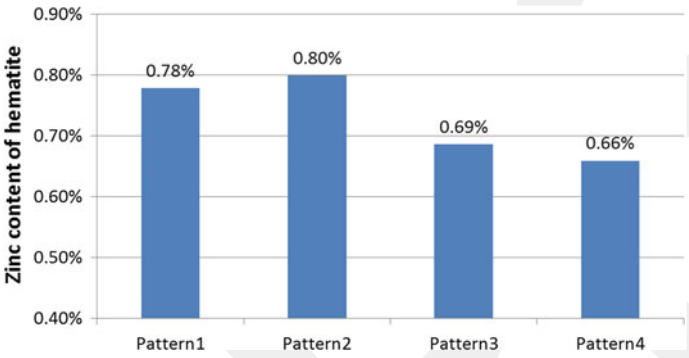

Fig. 6 Results of zinc content of hematite

Figure 7 shows the relationship between the amount of washing water and the zinc content in actual operation. Blue plot shows before improvement and red plot shows after improvement. This improvement reduced 23 m^3/D of washing water. In other words, this brought the 1500 t/year increase of zinc leach residue treatment.

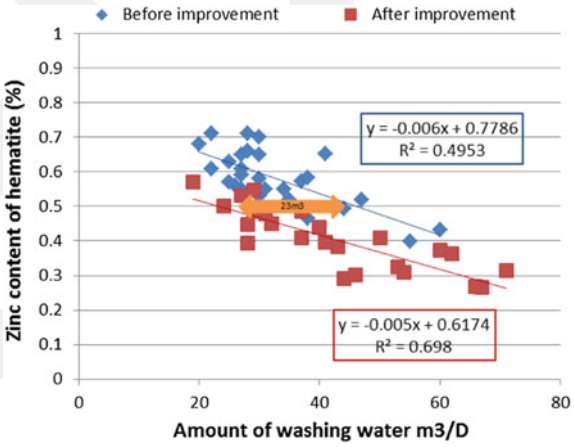

Fig. 7 Relationship between the amount of washing water and the zinc content in hematite

Modification of Filter for De-Arsenic Process

Copper and arsenic are co-precipitated by zinc powder. The chemistry of the arsenic removal step is shown in Eq. (1).

$$6Cu^{2+} + 2As^{3+} + 9Zn \rightarrow 9Zn^{2+} + 2Cu_3As \quad (1)$$

This process was introduced in 2003 to improve the quality of the hematite. A filter press was used for separating copper arsenide residue from de-arsenic slurry. From the start of de-arsenic process operation, copper arsenide residue had some problems in the quality.

The one of them is the agglomeration of the residue. Photograph 6 shows normal residue and agglomerated residue. The zinc sulfate existing in adhesion water acts like glue when drying. Once the residue agglomerates, it causes some problems at the next process.

Another one is residue liquefaction. Photograph 7 shows the liquefied residue.

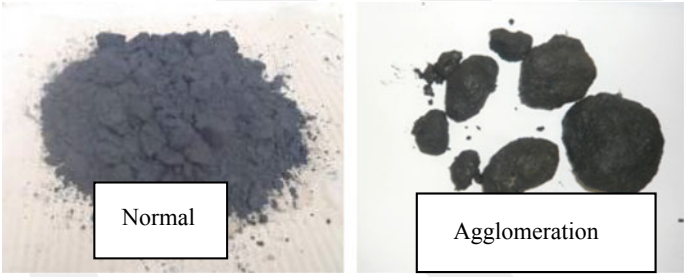

Photograph 6 Normal residue and agglomerated residue

Photograph 7 Liquefied residue

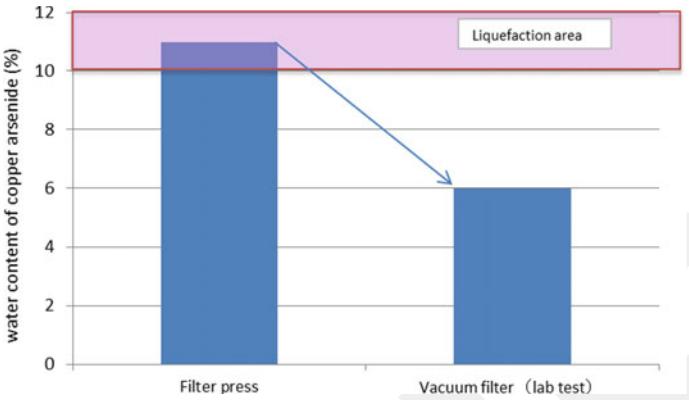

Fig. 8 Water content comparison by different filter

Filtration with a filter press has a high water content of about 10–15%, and a phenomenon of liquefaction due to vibration was observed. If liquefaction occurs during transportation, it may cause deterioration of handling during unloading. For this reason, shipments were required staying a few days at the yard and draining.

Several attempts were carried out to improve the filtration process to solve those problems. There are two requirements: the ability to wash the residue (prevent agglomeration), and the ability to reduce water content (prevent liquefaction). The filtration test was carried out to reduce water content for copper arsenide residue with vacuum filter. Figure 8 shows the water content of cake filtered through present filter press comparing with laboratory test by vacuum filter [3]. A vacuum filter performed the water content reducing to about 6%. In addition, washing equipment can be installed easily compared with filter press. Therefore, we introduced a horizontal vacuum filter.

Figure 9 shows changes in zinc content of residue. The average zinc content was reduced to 0.5% from 1.7% due to modification. Then, agglomeration problem has eliminated.

It is seen that water content of 11.2% is improved to 8.8% in Fig. 10. Of course, liquefaction phenomenon has not detected.

Conclusions

1. The amount of zinc leach residue treatment was increased by renewal of leaching autoclaves.
2. The fresh water input was decreased by modification of hematite washing procedure.

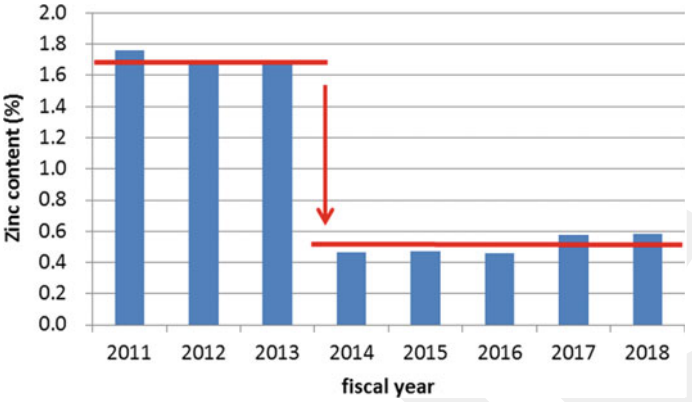

Fig. 9 Zinc content transition

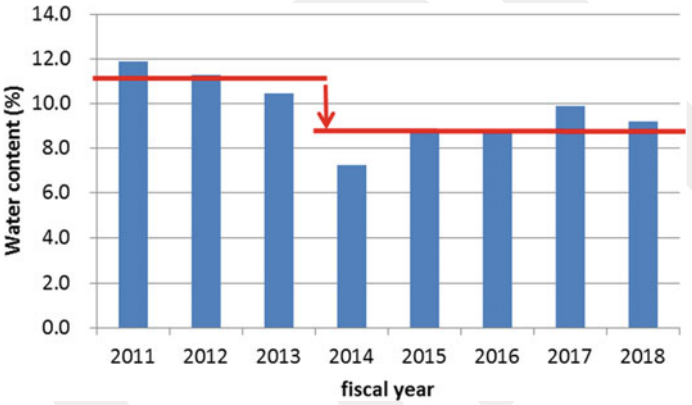

Fig. 10 Water content transition

3. The de-arsenic process filter was renewed from filter press to vacuum filter in order to solve the quality problems of liquefaction and agglomeration of copper arsenide residue.

These improvements led to stable operation of hematite process and then securing of stable zinc production.

In order to increase zinc production in the future, further increase in zinc leach residue treatment will be required, so we will continue to work on it as a continuing issue.

Acknowledgements I greatly thank Akita Zinc Co., Ltd. and Dowa Mining Co., Ltd. for granting permission to publish this paper. And I also would like to express appreciation to Mr. Togashi and Mr. Kanno. Their assistance was critical to this paper.

References

1. Kanno M, Horiuchi A, Aichi T, Sato S (2016) Recent operation and improvements of hematite process at Akita Zinc Co., Ltd. Iron Control 2016, Quebec
2. Tashita H, Horiuchi A, Usami Y, Kanno M (2014) Installation and operation of a new autoclave for leaching zinc residue. J MMIJ 130(6):331–334
3. Matsuura D, Aoki D (2015) Improvement of RT copper residue quality. J MMIJ 131(6):403–406

GCRIS

The Analysis of Fe Behavior in Zinc Pressure Leaching

Longyi Chen

Abstract In the process of Zinc hydrometallurgy, the behavior of Fe determines the length of the process and has a direct effect on Zinc leaching efficiency, the comprehensive recovery methods as well as the recovery effect of rare metals such as Ga, Ge, In, and so on, which is one of the most important factors to be considered in process selection for Zinc smelting enterprises. This paper analyzes the behavior of Fe under different leaching temperature, acidity, and pressure in Zinc pressure leaching from zinc sulphide concentrate to provide a reference and theoretical basis of process selection for different comprehensive recovery as required.

Keywords Pressure leaching · Goethite · Jarosite · Hematite · Iron removal

Introduction

Zinc sulfide concentrate mainly contains zinc and iron, of which the iron content is about 5–15%. During Zn hydrometallurgy, the iron in the concentrate is one of the key concerns in the selection of Zn metallurgical process as it will determine the length of the process, and will directly affect the zinc leaching rate and the comprehensive recovery methods and effect of the siderophile scattered metals such as gallium, indium, and germanium. During the oxygen pressure leaching of the zinc sulfide concentrate, pressure leaching is conducted under the control of different temperatures, acidity, and oxygen partial pressure in the autoclave to control the iron behavior that correspondingly affects the siderophile elements, such as gallium, germanium, and indium.

L. Chen (✉)
CINF Engineering Co., Ltd., Changsha 410019, Hunan, China
e-mail: 180242539@qq.com

© The Minerals, Metals & Materials Society 2020

A. Siegmund et al. (eds.), *PbZn 2020: 9th International Symposium on Lead and Zinc Processing*, The Minerals, Metals & Materials Series,
https://doi.org/10.1007/978-3-030-37070-1_77

Mechanism of Oxygen Pressure Leaching of Zinc and Iron from Zinc Sulfide Concentrate

Oxygen pressure leaching of zinc sulfide concentrate is an intensive leaching process. Currently, the pressure leaching of Zn sulfide concentrate is mainly based on the two-stage countercurrent pressure leaching. In primary pressure leaching, different reaction conditions are controlled based on different raw material composition. The leaching pressure, temperature, and final acid of sulfide concentrate rich in siderophiles such as gallium, germanium, and indium are controlled at 4.5 kPa, 110 °C, and 15 g/l, respectively, while the leaching pressure, temperature, and final acid of sulfide concentrate free of siderophiles is controlled at 11 kPa, 150 °C, and 10 g/l, respectively. In the secondary pressure leaching, the leaching pressure is basically controlled at 11 kPa, the temperature is controlled at 150 °C, and the final acid is controlled at 50–70 g/l.

Zinc sulfide concentrate reacts in the autoclave under given temperature, acidity, and partial pressure of oxygen. The sulfur in the concentrate as sulfide is oxidized into elemental sulfur and goes to the leached residue. In the Secondary leaching process, most of zinc and Fe in the sulfide concentrate as ZnS·FeS and Fe_7S_8 as well as the scattered metals like gallium, germanium, indium, and copper can be dissolved out of sulfide concentrate, and will go to the leachate as soluble sulphate, before going back in countercurrent way to the primary oxygen pressure leaching, while only little pyrite (FeS_2) and chalcopyrite ($CuFeS_2$) can be dissolved. The main chemical reaction formulas of oxygen pressure leaching of zinc sulfide concentrate are as follows:

$$\mathrm{ZnS \cdot FeS + 4H^+ + O2 \rightarrow Zn^{2+} + Fe^{2+} + 2H_2O + 2S^0 \downarrow} \quad (1)$$

$$\mathrm{2Fe_7S_8 + 42H^+ + 11.5O_2 \rightarrow 14Fe^{3+} + 21H_2O + 16S^0 \downarrow} \quad (2)$$

$$\mathrm{ZnS \cdot FeS + 2Fe^{3+} \rightarrow Zn^{2+} + 3Fe^{2+} + 2S^0 \downarrow} \quad (3)$$

During the reaction, iron acts as a medium to transfer oxygen and promotes the reaction. Meanwhile, gallium, germanium, and indium are simultaneously leached into the solution.

Analysis of Fe Behavior Under Different Oxygen Pressure Leaching Conditions

Iron ions are stable only under high acid, while under certain acidity and temperature, iron is liable to combine with water or other ions in water to generate precipitation.

In the process of oxygen pressure leaching of zinc sulfide concentrate, the iron reported to the solution in the secondary oxygen pressure leaching returns to the primary oxygen pressure leaching. The iron can be selectively retained in the solution or precipitated into the residue. By controlling the conditions of the primary oxygen pressure leaching in the autoclave, the iron is mainly precipitated in three forms: namely as goethite, jarosite, and hematite. When the iron is precipitated into the residue, the siderophiles like gallium, germanium, and indium will also report to the residue with the precipitation of Fe.

Iron Precipitation as Goethite During Oxygen Pressure Leaching

In the Fe_2O_3–SO_3–H_2O system, the control temperature of iron precipitation as goethite is generally above 90 °C, and the high temperature is favorable for accelerating the iron precipitation speed and increasing the iron precipitation rate. In primary oxygen pressure leaching, some goethite will be precipitated under the controlled acidity [1, 2]. The reaction formula is as follows:

$$Fe^{2+} + H_2O + 0.5O_2 \rightarrow FeOOH \downarrow + 2H^+ \tag{4}$$

$$Fe^{3+} + 2H_2O \rightarrow FeOOH \downarrow + 3H^+ \tag{5}$$

Normally, the formation of goethite requires a lower acidity, and the formation of the stable goethite requires the pH value of >2. Therefore, the goethite formation reaction is not the main reaction of iron precipitation in autoclave during oxygen pressure leaching of zinc sulfide concentrate.

Iron Precipitation as Jarosite During Oxygen Pressure Leaching

Under certain temperature, acidity, and in the presence of monovalent cation (A^+), ferric ions in the sulfuric acid system will form the jarosite minerals [3]. The reaction formula for the formation of jarosite is as follows:

$$Fe^{3+} + H_2O + {SO_4}^{2-} \rightarrow Fe(OH)SO_4 + H^+ \tag{6}$$

$$2Fe(OH)SO_4 + 2H_2O \rightarrow Fe_2(OH)_4SO_4 + 2H^+ + {SO_4}^{2-} \tag{7}$$

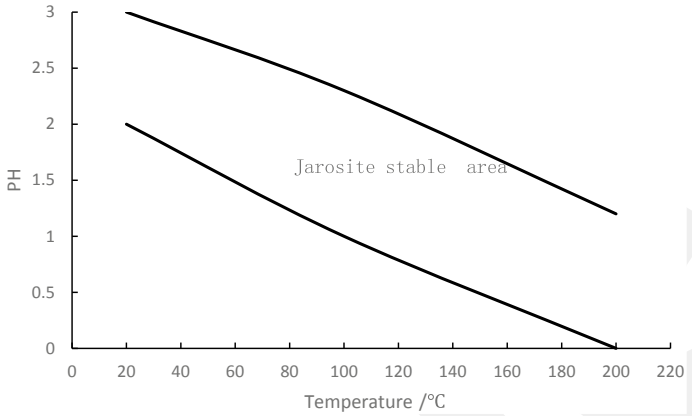

Fig. 1 Temperature-pH relationship of stable area of jarosite

$$2Fe(OH)SO_4 + 2Fe_2(OH)_4SO_4 + 2A^+ + 2H_2O \rightarrow A_2Fe_6(SO_4)_4(OH)_{12} \downarrow + 2H^+ \quad (8)$$

It can be seen from the reaction formula (6) to (8) that acid is produced during the jarosite formation, and the acid is to be neutralized to continue the jarosite formation, therefore, the acidity of jarosite formation should not be too high.

Moreover, the formation of jarosite minerals is an endothermic process, so its formation rate is slow at low temperature, and the formation rate of jarosite accelerates with the increase of temperature [3]. However, when the temperature exceeds 180 °C, jarosite starts to decompose and is turned into hematite [3]. The temperature-pH relationship in the stable region of jarosite is shown in Fig. 1.

It can be seen from the temperature-pH relationship of jarosite stable area that the region between the two curves is the jarosite stable area. When the autoclave temperature is controlled at 110 °C, the jarosite stable region is at about pH value: 0.8–2.3, that is, when the sulfuric acid concentration is ≥8 g/l, jarosite will be dissolved and cannot exist stably. When the autoclave temperature is controlled at 150 °C, the jarosite stable region is at about pH: 0.4–1.7, that is, when the sulfuric acid concentration is ≥20 g/l, jarosite will be dissolved and cannot exist stably.

Therefore, when the leaching pressure is controlled at 4.5 kPa, the temperature is controlled at 110 °C and the final acid is controlled at 15 g/l, iron cannot be precipitated as jarosite. When the leaching pressure is controlled at 11 kPa, the temperature is controlled at 150 °C, and the final acid is controlled at 10 g/l, the iron is in the stable area of jarosite, and most of the iron will be precipitated as jarosite.

Iron Precipitation as Hematite During Oxygen Pressure Leaching

During the pressure leaching, when the temperature of Fe_2O_3–SO_3–H_2O system is 50 °C, relatively stable goethite (α-FeOOH) starts to exist in the system. When the temperature is increased to 120 °C, Fe_2O_3 is precipitated out of the solution, and the stability of Fe_2O_3 phase is gradually improved with the increased temperature [4]. Moreover, goethite and jarosite will generate Fe_2O_3 from the hydrolysis reaction with the increased temperature. The reaction formula of iron precipitation as hematite is presented as follows:

$$2Fe^{2+} + 0.5O_2 + 2H_2O \rightarrow Fe_2O_3 + 4H^- \tag{9}$$

$$2Fe^{3+} + 3H_2O \rightarrow Fe_2O_3 + 6H^+ \tag{10}$$

At high temperature, α-FeOOH hydrolysis reaction formula is as follows:

$$2\alpha - FeOOH \rightarrow Fe_2O_3 \downarrow + H_2O \tag{11}$$

At high temperature, jarosite hydrolysis reaction formula is as follows:

$$A_2Fe_6(SO_4)_4(OH)_{12} \rightarrow 3Fe_2O_3 \downarrow + 2A^+ + 6H^+ + 4SO_4^{2-} + 3H_2O \tag{12}$$

In the autoclave, when the temperature reaches 140 °C and the solution contains less than 15 g/l acid, the iron is precipitated mostly as jarosite and goethite with some hematite. With the increase of temperature in the autoclave, hematite increases continuously, and at 155 °C or higher, iron is precipitated mainly as hematite [5].

Conclusions

(1) Analysis is made of the behavior of Fe in the oxygen pressure leaching process of zinc sulfide concentrate under different control conditions of the autoclave to provide a reasonable process selection reference and theoretical basis for different comprehensive recovery requirements of various zinc sulfide concentrates.

(2) The behavior of iron during oxygen pressure leaching is theoretically analyzed. When the pressure, temperature, and final acid in the primary oxygen pressure leaching is controlled at 11 kPa, 150 °C, and 10 g/l, respectively, the iron is precipitated as jarosite into the residue mainly with some precipitated as hematite. Moreover, a small amount of iron is precipitated as goethite into the residue. When the pressure, temperature, and the final acid of primary oxygen pressure leaching is controlled at 4.5 kPa, 110 °C, and 10 g/l–15 g/l, respectively, most

of the iron is leached and kept in the solution, while the iron existing as pyrite ($FeS_{2)}$ and chalcopyrite ($CuFeS_2$) in the zinc sulfide concentrate is basically not leached out.

(3) The control range of the final acid and temperature of two different oxygen pressure leaching processes is obtained to provide the theoretical backup for the control conditions of oxygen pressure leaching process of zinc sulfide concentrate and to guide the production practice to some extent.

References

1. Wu Y (2014) Iron removal by precipitation as goethite and its application in hydrometallurgy. Hydrometallurgy 33(2):86–89
2. Dan Y, Yang Y, Gong Q et al (2011) New mechanism of goethite formation. In: Proceedings of Cu–Ni hydrometallurgical technology exchange and application promotion conference of China Nonferrous Metal Academic Association
3. Wang C, Ma S, Lu A et al (2005) Study on formation conditions of jarosite and its environmental significance. J Petromineralogy 24(6):607–611
4. Koerker FW, Calderwood HN (1938) The system ferric oxide-sulfur trioxide-water. The J Phys Chem 42(9):1151–1155
5. Lu J, Dreisinger D (2013) Pressure oxidation of ferrous ions by oxygen and hematite precipitation from concentrated solution of calcium, copper and iron chlorides. Hydrometallurgy 140(11):59–65

GCRIS

Part XXI
Zinc Hydrometallurgy

GCRIS

Development of the New Zinc-Separation Process for the Blast Furnace Dust

Mariko Shinoda, Toyoshi Yamaguchi, Ryota Murai, Goro Okuyama and Ikuhiro Sumi

Abstract Blast furnace dust has been recycled as iron source in the sintering process. However, dust-recycling rate is limited due to the zinc content; therefore, it is necessary to remove zinc from the dust. In this study, laboratory-scale experiments were conducted. The hydrometallurgical process is composed of acid leaching, leachate purification, and zinc recovery. By acid leaching, 68 wt% of zinc and 6.4 wt% of iron were selectively leached under the pH value of 2.0. By the addition of hydrogen peroxide, the iron was completely separated from leachate under the pH value of 5.0. Zinc was finally recovered as zinc hydroxide at alkali condition (pH value of 9.0). The zinc concentration in the sludge was 42.6 wt%. Based on the experimental results, the blast furnace dust can be potentially used as zinc and iron source.

Keywords Blast furnace · Dust-recycling · Zinc-separation · Hydrometallurgy

Introduction

Utilization of by-products such as dust and slag generated in the iron-making process is one of the resource-saving technologies in steel works. In particular, the blast furnace dust is used as iron source because the main components of the dust include iron and carbon. However, the blast furnace dust contains zinc, which is deposited on the blast furnace wall the causing deterioration of ventilation and liquid permeation. Therefore, the recycling rate of the blast furnace dust is limited by the amount of zinc. In order to further promote the recycling of the dust, it is necessary to separate zinc from dust.

M. Shinoda (✉) · T. Yamaguchi · R. Murai · G. Okuyama
Environmental Process Research Department, JFE Steel Corporation, 1-1, Minamiwatarida-cho, Kawasaki-ku, Kawasaki 210-0855, Japan
e-mail: m-shinoda@jfe-steel.co.jp

I. Sumi
Corporate Planning Department, JFE Holdings, Inc., 2-2-3, Uchisaiwai-cho, Chiyoda-ku, Tokyo 100-0011, Japan

© The Minerals, Metals & Materials Society 2020

A. Siegmund et al. (eds.), *PbZn 2020: 9th International Symposium on Lead and Zinc Processing*, The Minerals, Metals & Materials Series,
https://doi.org/10.1007/978-3-030-37070-1_78

The practical zinc-separation includes dry [1, 2] and hydrometallurgical (wet) processes. In the dry process, the dust is heated at temperature of approximately 1000 °C in order to remove zinc in a gas phase. Nevertheless, construction cost of the dry process tends to be rather high. Therefore, the dry process is suitable for large-scale treatment, and application in the small plants is not economically feasible. In fact, all plants in Japan are large-scale facilities with 100,000 ton/year production capacity.

On the other hand, hydrometallurgical zinc-separation process has not been practically used in Japan. In Italy, hydrometallurgical process called EZINEX® method [3] is applied. After zinc oxide separation from the electric furnace dust, a high-purity metallic zinc is recovered by hydrometallurgical process and electrolysis. However, it is not economical to apply this method for the blast furnace dust because of very high electric power consumption (approximately 900 kWh/t-dust) and too low zinc content.

In the previous studies, zinc in the blast furnace dust was removed by using organic acids (dicarbonic acid and amine carboxylic acid) [4, 5]. These methods have enabled selective leaching of zinc from the blast furnace dust. However, organic acids were more expensive than inorganic (e.g., sulfuric acid, hydrochloric acid, etc.), therefore, the practical use of this method was rather difficult.

In order to improve the recycling rate of the blast furnace dust, a new zinc-separation process by using of hydrometallurgical route is introduced in this study.

Experimental

Blast furnace dust was collected as the slurry at Chiba Works of JFE Steel Corporation. This slurry was dried at 105 °C for 12 h and used in the experiment. The dried dust was analyzed by ICP-AES. It contained 1.04 wt% of zinc and 35.7 wt% of iron.

Acid Leaching

During the treatment, 50 g of blast furnace dust was suspended in 500 mL of distilled water. The suspension was stirred at 500 rpm at room temperature. The pH value of the suspension was between 2.0 and 5.0, and it was controlled by addition of sulfuric acid. Due to increased content of leached iron, the test below pH value of 2.0 was interrupted. After 1 h, the pH-controlled suspension was filtrated to separate leachate and residue. Zinc and iron in the leachate were analyzed by ICP-AES.

The percentage of metal-leached was calculated by Eq. (1).

$$y = \frac{x_{sol}}{x_{ini}} \times 100[\text{wt\%}] \tag{1}$$

x_{sol} metal in the leachate after acid leaching [g]
x_{ini} metal in blast furnace dust before acid leaching [g]
y percentage of metal-leached [wt%].

Purification of the Leachate After Acid Leaching

During the treatment described in the previous chapter, not only zinc but also other metals such as iron were leached. When alkaline reagent was added to this leachate, zinc and other metals were co-precipitated, however, this precipitate had a low content of zinc. In order to increase the zinc content, it was necessary to purify leachate.

A 500 mL of the leachate after acid leaching was stirred at 500 rpm at room temperature. The pH of this solution was controlled from 4.0 to 6.0 in order to remove iron. For further purification of the leachate, 35% of hydrogen peroxide solution was added. Then, the leachate was filtrated and analyzed by ICP-AES.

Alkaline Treatment

A 500 mL of purified leachate was controlled at pH value of 9.0 by sodium hydroxide. The reaction temperature and reaction time were the same as in the previous chapter. After the treatment, the leachate was filtrated to recover zinc concentrated sludge and then dried at temperature of 105 °C to remove water and analyzed by ICP-AES.

Results and Discussion

Effect of pH on Acid Leaching

The pH effect on percentage of metal-leached during the acid leaching is shown in Fig. 1 [6]. The amount of leached zinc was increased with decreased pH value. At the pH value of 2.0, 68 wt% of zinc was leached. In contrast, the amount of leached iron was slightly increased at lower pH (i.e., only 6.4 wt% of iron was leached at pH value of 2.0).

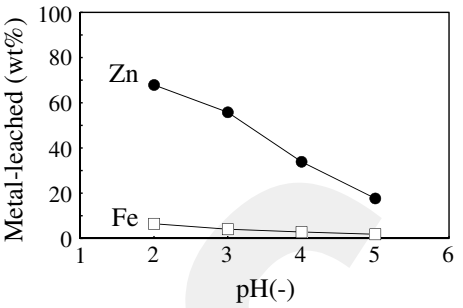

Fig. 1 Effect of pH on percentage of metal-leached in acid leaching [6]

Effect of pH and Influence of Hydrogen Peroxide Addition on the Purification of the Leachate

The effect of pH on percentage of metal remained in the leachate after the purification process is shown in Fig. 2 [6]. By controlling the pH value between 4.0 and 5.0, most of zinc in leachate remained. In contrast, remained iron tended to decrease with increase in pH. It was found that high pH value was necessary to precipitate iron. Therefore, the pH value of 5.0 seems to be most suitable for the purification process.

At pH value of 5.0, iron was completely precipitated by adding hydrogen peroxide; no iron remained in the leachate (Fig. 2 [6]). On the other hand, the percentage of zinc remained slightly changed after hydrogen peroxide addition.

The effect of hydrogen peroxide addition on iron precipitation could be explained by the potential-pH diagram in the Zn–Fe–O–H system (Fig. 3 [6, 7]). At the pH value of 5.0 without hydrogen peroxide, the oxidation-reduction potential was 0.39 V *versus* standard hydrogen electrode (SHE), so that the solution condition became the boundary between Fe^{2+} and $Fe(OH)_3$. The iron precipitation was incomplete, and 54 wt% of iron remained in the leachate (Fig. 2 [6]). By hydrogen peroxide addition, the oxidation-reduction potential was 0.6 V versus SHE. The iron was precipitated as $Fe(OH)_3$ and completely removed from the leachate.

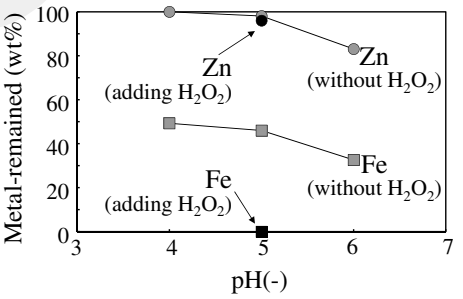

Fig. 2 Effect of pH on percentage of zinc and iron remained in the leachate [6]

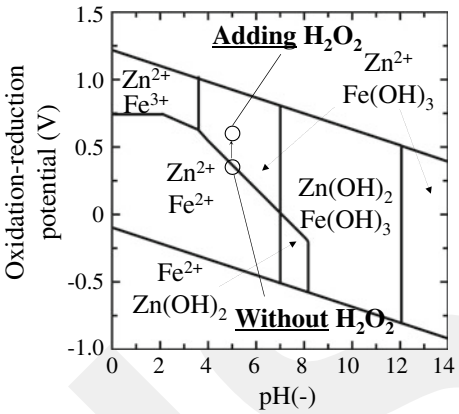

Fig. 3 Potential-pH diagram of Zn–Fe–O–H system [6, 7]

Recovery of Zinc by Alkali Treatment

Zinc was recovered from the leachate obtained from the purification process. The concentration of zinc and iron were 42.6 wt% and 0.03 wt%, respectively.

Conclusions

In this study, a new process/technology for zinc leaching from the blast furnace dust by sulfuric acid and recovery of high-purity leached zinc were introduced. The separation process consists of three steps, namely acid leaching, leachate purification, and alkali treatment. Following results can be summarized:

By acid leaching, 68 wt% of zinc and 6.4 wt% of iron were selectively leached under the pH value of 2.0.

By the addition of hydrogen peroxide, the iron was completely separated from leachate under the pH value of 5.0. After the alkali treatment, the zinc concentration in the sludge was 42.6 wt%.

References

1. Sun X, Hwang JY, Huang X (2008) The microwave processing of electric arc furnace dust. JOM 60(10):35–39
2. Hara Y, Ishiwata N, Itaya H, Matsumoto T (2000) Smelting reduction process with a coke packed bed for steelmaking dust recycling. ISIJ Int 40(3):231–237
3. Olper M, Maccagni M (2008) From C.Z.O. to zinc cathode without any pretreatment. The Ezinex process. Paper presented at the international symposium on lead and zinc processing, lead & zinc 2008, Durban, South Africa, 25–29 Feb 2008

4. Zhang D, Zhanf X, Yang T, Rao S, Hu W, Liu W, Chen L (2017) Selective leaching of zinc from blast furnace dust with mono-ligand and mixed-ligand complex leaching systems. Hydrometallurgy 169:219–228
5. Steer JM, Griffiths AJ (2013) Investigation of carboxylic acids and non-aqueous solvents for the selective leaching of zinc from blast furnace dust slurry. Hydrometallurgy 140:34–41
6. Shinoda M, Yamaguchi T, Murai R, Sumi I (2019) Development of zinc-separating process of blast furnace dust using hydrometallurgical system. Tetsu-to-Hagané 105(8):847–853
7. Pourbaix M (1966) Atlas of electrochemical equilibria. Pergamon Press, Oxford, p 312, 419

GCRIS

Outotec Gypsum Removal Circuit and Outotec Cooling Tower Performance in Neutral Solution Cooling

Tuomas Hirsi and Björn Saxen

Abstract In a gypsum removal process, a solution which is saturated with calcium is cooled to lower temperature with solution cooling towers to precipitate calcium as gypsum ($CaSO_4 \cdot 2H_2O$) and remove it before the next process step. In zinc refineries, gypsum removal is part of the solution purification step before electrowinning. Gypsum removal after leaching is important to control the maintenance load of the downstream equipment. Outotec gypsum removal plant was started in 2018 as a part of the zinc Direct Leaching plant in Torreón, Mexico. The plant utilizes Outotec cooling towers for solution cooling and Outotec high rate thickener for solid particle separation from the solution flow. First operation results are showing efficient gypsum removal from the solution flow. In this paper is presented the Outotec gypsum removal process and shows results from operation and discusses the importance of efficient operation and low emissions from the solution cooling.

Keywords Gypsum removal · Cooling tower · Cooling efficiency

Introduction

Outotec has delivered a gypsum removal circuit to Met-Mex Peñoles site in Torreón, Mexico, as part of the expansion based on concentrate Direct Leaching plant. More information on the Direct Leaching plant can be found in a separate paper published in PbZn 2020 [2], having more detailed presentation of the whole process and achieved improvements. The gypsum removal circuit installed is the final part of the solution purification before the solution goes to zinc electrowinning and spent electrolyte cooling circuit.

T. Hirsi (✉)
Outotec (Finland) Oy, PO Box 1000 02231 Espoo, Finland
e-mail: tuomas.hirsi@outotec.com

B. Saxen
Outotec (Finland) Oy, PO Box 69 28101 Pori, Finland
e-mail: bjorn.saxen@outotec.com

© The Minerals, Metals & Materials Society 2020

A. Siegmund et al. (eds.), *PbZn 2020: 9th International Symposium on Lead and Zinc Processing*, The Minerals, Metals & Materials Series,
https://doi.org/10.1007/978-3-030-37070-1_79

Fig. 1 Gypsum removal circuit in Torreon. 2pcs of Outotec cooling tower 6000 and an Outotec high rate thickener

In the zinc electrowinning, where the zinc is recovered, new neutral solution is added constantly to the circulation, whilst spent electrolyte is bled from the circulation. The solution heats in the electrowinning and is cooled in forced draft cooling towers. If there is high enough concentration of calcium in the solution, it precipitates in the spent electrolyte cooling towers and subsequent launders and electrolyte cells. Before the solution comes to the circulation, it goes through a solution purification, which also includes a gypsum removal plant unit. The purpose of this plant unit is to bring the calcium content in the solution below the saturation point of the lowest temperature point of the cooling circuit (Fig. 1).

In this paper, gypsum removal from neutral solution before zinc electrowinning circuit is discussed. Outotec has delivered gypsum removal cooling tower to other process applications such as gypsum removal before copper solvent extraction [1].

Basic Principle of Gypsum Removal

Gypsum is a solid precipitate of calcium, sulphate, and water ($CaSO4 * H_2O$), and it is white in its natural form. Some other metals and impurities precipitate with the

gypsum, depending on the solution composition. More information about gypsum is presented in our paper from 2013 [1]. In this paper, the discussion is constrained to gypsum properties in Zinc refinery neutral and spent electrolyte solutions. Calcium is soluble in the water solutions, and the solubility changes slightly depending on the water temperature. When the solutions contain acid and other sulphates, the solubility of the calcium increases with raising temperature in a clear trend. In the zinc plant, the temperature range where the gypsum containing solutions are processed is generally between 30 and 75 °C. In the graph of Fig. 2 is presented the solubility of the calcium in Neutral zinc solution coming to the tower as derived from two different sources.

The article by Azimi et al. [7] was made using a solution with slightly lower concentration of zinc, 120 g/l, but still close to the actual process conditions and can be utilized as a reference. The internal Outotec values have been measured on site to give reference for the calcium solubility.

The neutral solution comes in a temperature of about 70–75 °C to the gypsum removal circuit. First it is cooled in the cooling towers where the temperature is dropped to 34–28 °C depending on the site. Then, the solution is directed towards the thickener where the precipitating gypsum is removed through underflow. With seed recirculation from the thickener underflow, the gypsum precipitation to the equipment surfaces can be reduced and gypsum settling in the thickener improved.

Figure 3 is presented a generalized temperature profile and process steps on gypsum removal for neutral solution and spent solution circulation. As the calcium solubility in the spent electrolyte circulation is higher than in the neutral solution [3 and 4], the neutral solution can be added in higher temperature to the circulation if needed. Due to the nature of the cooling process utilized, the solution going out of

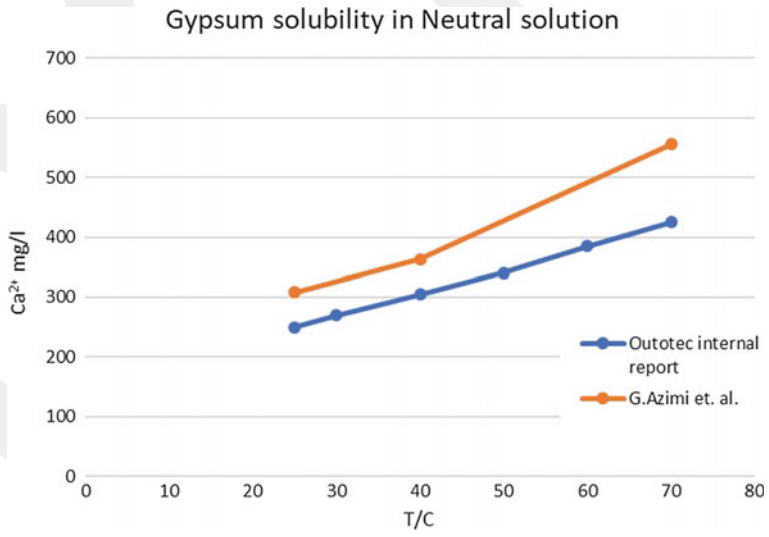

Fig. 2 Solubility of gypsum in neutral solution in literature

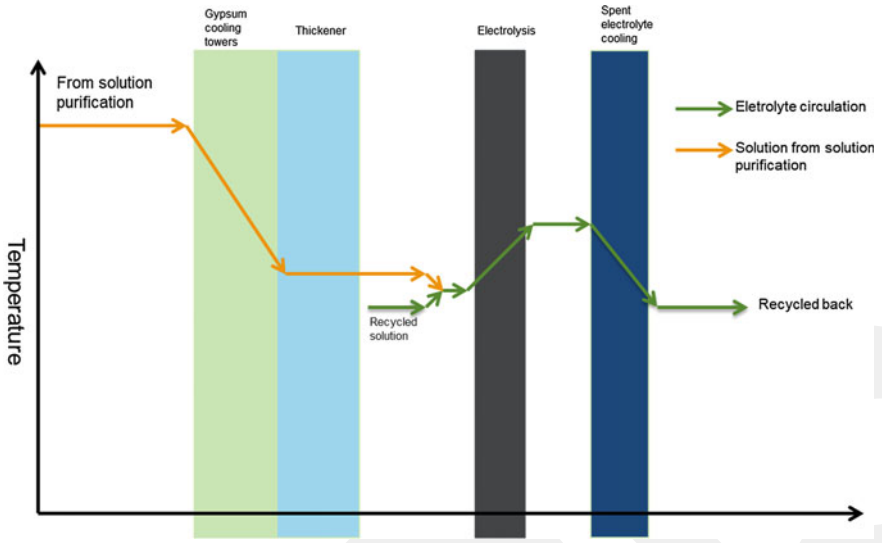

Fig. 3 Generalized temperature profile in the gypsum removal and spent electrolyte circulation

the process step is slightly less in volume compared when going in, caused by the evaporation of water from the solution due to cooling by air.

The main reason to utilize a gypsum removal circuit in zinc production chain is to reduce the need for cleaning work and to avoid unnecessary maintenance costs. Solubility of calcium in the spent electrolyte circuit is strongly dependent on the temperature [3] of the solution and any excessive calcium is most probably precipitated as gypsum in the spent circulation cooling towers and in the launders after the towers where the temperature of the solution is coolest in the circulation.

Cooling Tower Efficiency, Emissions, and Effect on Product Losses

The integral part of the gypsum removal circuit is the solution cooling tower utilized to bring down the solution temperature to precipitate the gypsum out of solution. The cooling gradient of the solution temperature is controlled by controlling the fan speed. This enables adjusting the tower operation to the prevailing weather conditions, avoiding using excessive air inside the tower, thus reducing emissions and maintenance needs. The performance of the Outotec cooling tower has been presented in multiple articles, most notably [1, 5, 6]. In the reference site in Zambia [1], clear benefits of the cooling removal utilization before solvent extraction were shown, resulting in over six metric tons of gypsum removed each day.

The main source of emissions and product losses from the process is the solution exiting through the cooling tower gas outlets. The fan pushes the gas in from the lower part of the tower, from where it flows upwards, whilst solution to be cooled is sprayed from the top part of the tower counter currently to the air. The cooling is mainly based on the evaporation of the solution, with some conductive heat transfer involved. The gas outlets are equipped with demisters removing solution droplets from the gas flow. Most commonly used demisters are the vaned (or chevron) type demisters. Also, in Outotec cooling tower these demisters are utilized, but the specialty is usage of patented horizontal gas outflow (Fig. 4), instead of conventional vertical outflow.

In 2017, a result from site measurements was published showing on the fifth of emissions of generally utilized vertical cooling tower and a possibility for even lower emissions by installing more stringent emissions control by more effective demisters. However, this would reduce the cooling efficiency [5].

Table 1 shows estimated product losses of the zinc from the cooling process. The cooling efficiency here has been estimated to be 1.5 times of the conventional tower, in some instances this has been over 2.5 times [6].

Fig. 4 Outotec cooling tower horizontal flow outlet

Table 1 Generic product losses from a cooling tower circuit

	Flow	Zinc concentration	Drift loss		
	m^3/h	g/l	%	g/h	kg/a
Outotec cooling tower	200	180	0.0002	72	576
Traditional vertical outflow tower	200	180	0.001	360	5760

It is assumed in average 1.5 more conventional towers are required to achieve same cooling capacity as one Outotec tower

Gypsum Removal Efficiency in Torreón

For the efficiency estimations for this article, multiple measurements for gypsum content in solution were performed. However, due to difficulties of obtaining representative samples from the solution, there is, at this point, no large array of results to present. The sampling campaign shall be continued in the future to obtain more accurate results. In the results shown in Table 2, we have calculated removed gypsum from the process by utilizing process values from the sampling date.

In a previous article, it has been discussed a gypsum removal circuit in copper solvent extraction circuit in the Chambishi Plant, Zambia. Also, in this paper, the efficiency of the circuit was found to be excellent and led to huge savings in required gypsum removal from the solvent extraction during maintenance as crud removal was almost eliminated [1].

By comparing the measurement results to the previously presented solubility data, it can be seen (Fig. 5) that the concentration level of calcium is not saturated in the incoming solution. The non-saturation levels in the incoming solution can be caused by temperature changes before the gypsum removal in the solution purification process where part of the gypsum has already precipitated and made errors in the measurements. The slight difference in the lower temperature Ca result is probably caused by differences in solution in each measurement case or in sampling errors. For example, the amount of zinc in the solution affects the calcium solubility: higher amount of zinc tends to lower the solubility [3].

Table 2 Removed gypsum with gypsum removal process based on measurements and samples taken one day in September 2019

Flow	108	m^3/h
Ca_{in}	366	mg/l
Ca_{out}	313.9	mg/l
Removed Ca	6	kg/h
Removed $mCaSO_4 * 2H_2O$	24	kg/h
	587	kg/d
	4.1	t/wk

Note the plant was not working on full capacity on this date

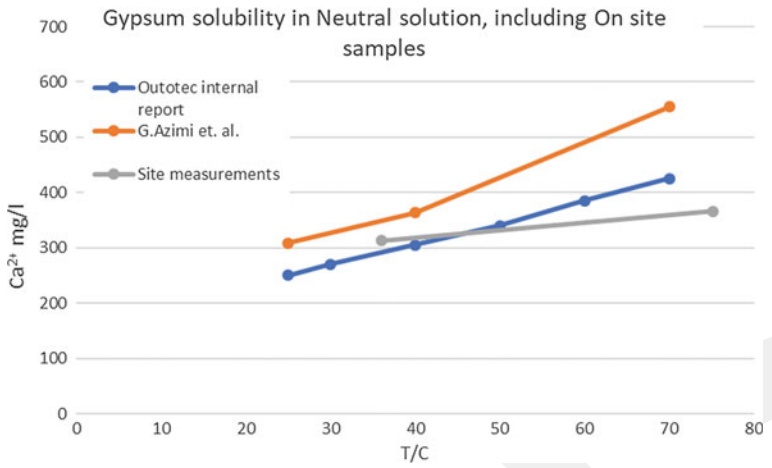

Fig. 5 Solubility of gypsum in neutral solution in literature compared to the measurements from site

Conclusions

The operation of gypsum removal is integral in ensuring lower maintenance costs and less disturbed process on the later process steps. Gypsum removal circuit operating at Met-Mex Peñoles in Torreon, Mexico, has been able to show achievement of gypsum reduction in line with previous literature data and Outotec experience. With the Outotec gypsum removal circuit, the reduction of gypsum is achieved, and it is in line with previous literature data and Outotec experience. Outotec cooling tower has also proven high efficiency in the operation, and the emissions can be estimated to be considerably lower than in operations utilizing conventional cooling tower.

In the future, further development shall be made to optimize the gypsum removal efficiency through optimized cooling tower operation and process control such as underflow circulation optimization.

The results in this paper show similar benefits in utilizing gypsum removal circuit as were found in the previous paper Outotec has published. The patented horizontal outflow towers bring a unique way of minimizing emissions from the gypsum removal plant.

Acknowledgements The authors would like to acknowledge Met-Mex Peñoles in Torreón, Mexico, for providing access to the process data utilized in this publication.

References

1. Hirsi T, Salonen P, Vaarno J (2013) Outotec® cooling towers provide cooling efficiency and low emissions in gypsum removal in SX plants. In: The Southern African Institute of Mining and Metallurgy Base Metals Conference, 2013
2. Björn S, Florentino E, Maciej W. Zinc plant expansion and modification for increased metals recovery. PdZn2020
3. Dutrizac JE (2002) Calcium sulphate in simulated zinc processing solutions. Hydrometallurgy 65(2):109–135
4. Outotec Internal Research Report
5. Hirsi T (2017) Outotec developments in reducing emissions from solution cooling towers. Proceedings of EMC
6. Hirsi T, Ritasalo T, Saarikoski A, Vaarno J, Lahtinen M, Larragoitia SAC (2013) Outotec® cooling towers provide higher efficiency and decreased emissions. Proceedigns of EMC
7. Azimi G, Papangelakis VG, Dutrizac JE Development of chemical model for the solubility of calcium sulphate in zinc processing solutions

GCRIS

Purification and Comprehensive Recovery Metal Values from Zinc Hydrometallurgical Solution

Yue Yang, Shaole Song, Honghu Tang, Li Wang, Wei Sun and Yuehua Hu

Abstract The cost of removing impurities from zinc hydrometallurgy solution by zinc replacement is expensive. Moreover, valuable metals, such as copper and cobalt, are difficult to be recovered when they enter into the zinc slag in the zinc replacement. In this study, a novel process for purification and comprehensive recovery metal values from zinc hydrometallurgical solution has been developed. A slow-release precipitator has been designed. Copper in zinc leaching solution has been selectively separated by a slow-release mineralization process based on differences in solubility of zinc and copper sulfide. Almost 100% copper can be removed and the copper grade of precipitate can reach about 20%. We also designed a precipitator with –CSS–group for selectively recovering cobalt from zinc leaching solution after copper removal. It indicated that cobalt removal efficiency is almost 100% with little zinc loss. The cobalt grade of precipitate can reach almost 14%. All the above results show that the developed approach can effectively remove copper and cobalt from zinc hydrometallurgy solution, significantly reduce zinc powder dosage and realize the comprehensive recovery of copper and cobalt, and thus improve the economic efficiency of zinc smelting.

Y. Yang · S. Song · H. Tang · L. Wang · W. Sun (✉) · Y. Hu (✉)
School of Minerals Processing and Bioengineering, Central South University, Changsha 410083, China
e-mail: sunmenghu@csu.edu.cn

Y. Hu
e-mail: hyh@csu.edu.cn

Y. Yang
e-mail: yangyue18@csu.edu.cn

S. Song
e-mail: 784808988@qq.com

H. Tang
e-mail: honghu.tang@csu.edu.cn

L. Wang
e-mail: li-wang@csu.edu.cn

© The Minerals, Metals & Materials Society 2020

A. Siegmund et al. (eds.), *PbZn 2020: 9th International Symposium on Lead and Zinc Processing*, The Minerals, Metals & Materials Series,
https://doi.org/10.1007/978-3-030-37070-1_80

Keywords Zinc hydrometallurgical solution · Zinc smelting · Copper removal and recovery · Cobalt removal and recovery

Introduction

Hydrometallurgy is currently the main method of zinc smelting in the world, and more than 80% of zinc is obtained by hydrometallurgy. It mainly consists of four basic processes: roasting, leaching, purification, and electrowinning. When leaching zinc with sulfuric acid, other impurity ions, such as iron, copper, and cobalt, inevitably enter the leachate along with zinc. These impurity ions will cause serious harm to the electrowinning process of zinc, so they must be removed. Meanwhile, copper and cobalt are considered as important metals because of their vast applications in various fields. Take cobalt for example, cobalt is applied in the field of aviation, aerospace, electronics, batteries, and alloys. In China, cobalt consumption has sharply increased. By contrast, the cobalt content is scarce (only 0.001%) in the earth's crust. The price of cobalt is rapidly rising due to the large demand but low content. Currently, copper and cobalt in zinc leaching solution are removed by replacement reaction with zinc powder. Because the replacement reaction occurs on the surface of zinc powder, it is inefficient, and easily encapsulation and passivation can occur, which means excess zinc powders are needed, resulting in high-cost. Moreover, due to incomplete reaction, the grades of copper and cobalt in zinc slag are low, and recovering these metals from zinc slag is difficult and expensive. Therefore, how to reduce the consumption of zinc powder, reduce the smelting cost, and realize the comprehensive utilization of valuable components (copper and cobalt) has become one of the most important problems for zinc hydrometallurgical process.

In this study, precipitators replacing zinc powder for removal and recycling of copper and cobalt have been developed. With the help of selective precipitation, not only copper and cobalt in zinc hydrometallurgy solution can be effectively removed, but also the comprehensive recovery of copper and cobalt can be accomplished, and thus significantly reducing zinc powder dosage and improving the economic efficiency of zinc smelting.

Slow-Release Mineralization for Copper Removal and Recovery

Figure 1 shows the process of slow-release mineralization for copper removal and recovery. The slow-release agent has high surface activity and is full of activated sulfur components. When it enters the zinc acid leaching solution, the activated sulfur will slowly be released from the surface of the agent into solution. When the sulphur enters the solution and has stabilized as S^{2-}, it can react with copper to form CuS. Since sulfur is released into the solution slowly, there is no excess

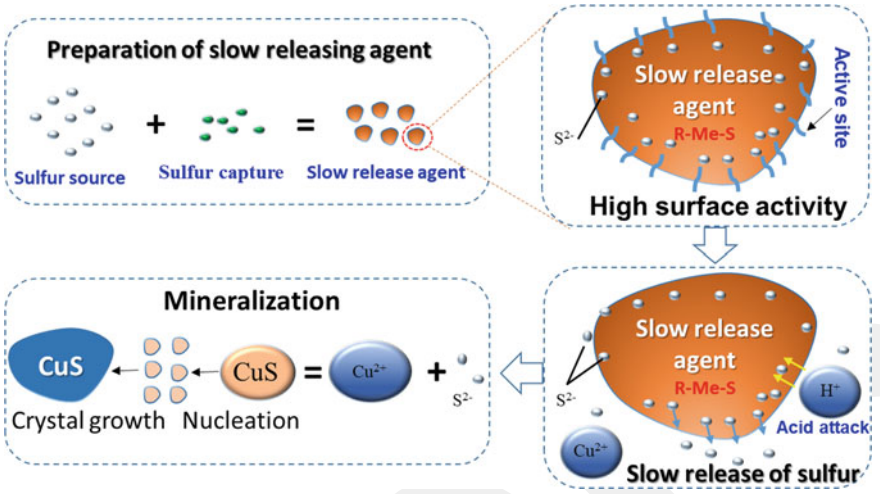

Fig. 1 Schematic illustration of slow-release mineralization for copper removal and recovery

sulfur in the solution. Sulfur preferentially combines with copper to form copper sulphide. Figure 2 shows the results of effect of copper removal from typical zinc leaching solution. The removal efficiency of copper can reach almost 100% when the conditions remain at pH = 2–4, $T = 70$ °C, 3 h, and the amount of precipitant is 2 times of the theoretical amount.

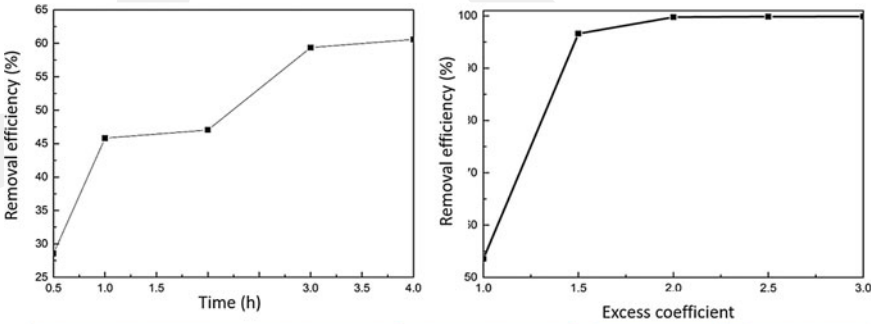

Concentration mg/L Items	Co	Ni	Cu
K_{sp}	5×10^{-22}	4×10^{-20}	6×10^{-37}
Before purification	11	20.2	785
After purification	11.3	21	--
Removal efficency (%)	-	-	100%

Fig. 2 Effect of copper removal from zinc leaching solution

Cobalt Removal and Recovery

Group –CSS– has introduced a precipitator for cobalt removal. The optimized structures of designed binding with metal ions included a similar four-membered ring (–C–S–M–S–). This clearly indicates the chelation between the designed precipitator anion and these specific metal ions. Both sulfur-metal (S–M) bonds in the same molecule were nearly the same, which suggested that both sulfur atoms in the designed precipitator were equivalent. In most cases, a shorter bond length suggests a better affinity. Mean bond lengths of the two S–M bonds are given in Table 1. The mean bond lengths between Ni/Co and designed precipitator show the shortest/second shortest bond being at 2.165/2.213 Å. The further calculated changes in the ΔG of these chelation reactions suggest that the designed precipitator can more strongly bind with Ni^{2+}, Fe^{3+}, and Co^{2+} with strong binding energies of −604.54, −604.05, and −291.19 kJ/mol, respectively. It was found that the designed precipitator reagent prefers to interact with Fe^{3+}, indicating that Fe^{3+} must be removed from the lixivium in advance. After Fe^{3+} and Cu^{2+} removal, the cobalt can be selectively recovered from zinc solution. Figure 3 shows the effect of cobalt removal

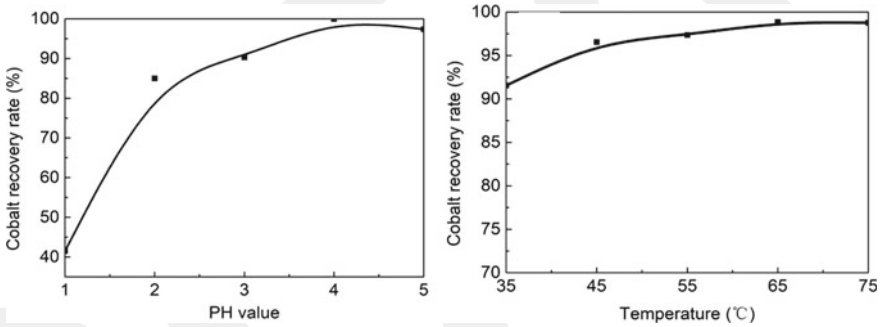

Fig. 3 Effect of cobalt removal from zinc leaching solution

Table 1 Mean bond lengths of two M–S bonds in $(–CSS–\cdots M)^{n+}$ structure

Structure		Mean bond length/Å	ΔG/(KJ/mol) T = 298.15 K
络合产物	Ni^{2+}	2.165	−604.54
	Fe^{3+}	2.428	−604.05
	Co^{2+}	**2.213**	**−291.19**
	Fe^{2+}	2.374	−267.68
	Cu^{2+}	2.355	−235.34
	Zn^{2+}	2.405	−205.96

from zinc leaching solution. It indicates that the removal efficiency of cobalt is almost 100% when the mass of added agent/the total mass of cobalt metal in solution = 10, pH > 4, $T = 75$ °C. The amount of metals in precipitated slag is tested by ICP, and the results shows that the zinc grade is 0.1%, and cobalt grade is 13.63%.

Conclusion

In summary, a novel process for purification and comprehensive recovery metal values from zinc hydrometallurgical solution has been developed. Copper in zinc leaching solution has been selectively separated by a slow-release mineralization process based on differences in solubility of zinc and copper sulfide. Almost 100% copper can be removed and the copper grade of precipitate can reach about 20%. –CSS– group has been designed as precipitator for selectively recovering cobalt from zinc leaching solution. It indicated that cobalt removal efficiency is almost 100% with little zinc loss. The cobalt grade of precipitate can reach almost 14%. With the help of selective precipitation, not only copper and cobalt in zinc hydrometallurgy solution can be effectively removed, but also the comprehensive recovery of copper and cobalt can be realized, thus significantly reducing zinc powder dosage and improving the economic efficiency of zinc smelting.

Refining of Zinc Chloride by the Combination of Cementation Reaction and Vacuum Distillation

Gen Kamimura and Hiroyuki Matsuura

Abstract In order to develop an efficient recycling process of zinc from electric arc furnace (EAF) dust, several refining methods of crude zinc chloride, which can be produced through selective chlorination and evaporation process of EAF dust, were investigated. In the experiments with cementation reaction using metallic zinc at 723 K, the removal of cadmium from 40 mol%$ZnCl_2$-KCl-NaCl melt was focused on, which standard electrode potential is close to that of zinc. Cadmium chloride was effectively removed from molten salt when KCl was added to $ZnCl_2$ rather than NaCl. With two steps of cementation reaction, cadmium was removed to about 10 massppm with adding fewer metallic zinc. In the experiments with vacuum distillation at 800 K, the separation of $ZnCl_2$ from impurities with lower vapor pressures was investigated using a laboratory-scale electric furnace with wide temperature distribution.

Keywords Zinc · Electric arc furnace dust · Recycling · Vacuum distillation · Cementation

Introduction

Electric arc furnace (EAF) dust is one of the by-products generated in EAF steelmaking process. The raw materials for EAF steelmaking process are steel scraps, which usually contain used zinc-coated steel plates. Through EAF process, most of zinc evaporates and moves to dust through gas phase and is concentrated as oxide. A part of iron also moves to the EAF dust mainly due to burst of carbon monoxide bubble at the surface of the liquid steel bath [1]. That is why EAF dust is mainly composed of zinc oxide, iron oxide, and zinc ferrite. EAF dust is considered as a

G. Kamimura (✉)
Graduate School of Frontier Sciences, The University of Tokyo, 5-1-5 Kashiwanoha, Kashiwa, Chiba 277-8561, Japan
e-mail: kamimura02@pyromet.k.u-tokyo.ac.jp

H. Matsuura
School of Engineering, The University of Tokyo, 7-3-1 Hongo, Bunkyo-Ku, Tokyo 113-8656, Japan

© The Minerals, Metals & Materials Society 2020

A. Siegmund et al. (eds.), *PbZn 2020: 9th International Symposium on Lead and Zinc Processing*, The Minerals, Metals & Materials Series,
https://doi.org/10.1007/978-3-030-37070-1_81

secondary resource for zinc, but cannot be recycled with hydrometallurgical process using leaching with acid or alkali solution, and electrolysis of the aqueous solution, since the leaching speed is very small, and the leaching selectivity of zinc is not good. Thus, EAF dust must be processed with pyrometallurgical process such as Waelz kiln process. The process uses carbothermic reduction reaction of zinc in EAF dust with coke in rotary kiln at about 1473 K. Despite zinc is reduced to metallic state under such high temperature, the exhaust gas must be oxidized again to recover zinc as a form of crude zinc oxide. The crude zinc oxide must be processed with the Imperial Smelting Process (ISP) for the recovery of metallic zinc. Another problem exists in the residue generated in Waelz kiln process. Some of zinc in EAF dust is not reduced and remains in clinker because zinc oxide tends to dissolve in wüstite produced during reduction and stabilize thermodynamically [2]. If the clinker is contaminated with zinc oxide, it cannot be used as ironmaking materials. For example, zinc content in clinker of Waelz kiln process is about from 0.24 to 6.0 mass% [2, 3], while the upper limit of zinc content in raw materials of ironmaking and steelmaking is 0.1 mass% [2]. Actually, most of the clinker remains piled up. Therefore, more efficient recycling process is needed and should be better for the recovery of both zinc and iron.

Our group has worked on the development of recycling process using chlorination reaction of zinc in EAF dust with various chlorinating agents [4–7]. In this process, zinc can be recovered as chloride through gas phase, while most of iron remains in EAF dust as oxide under high oxygen partial pressure atmosphere. Next, the recovered zinc chloride ($ZnCl_2$) is electrolyzed in molten salt state. Metallic zinc can be collected as liquid phase in this electrolysis and peeling of the electrodeposit is not necessary [8]. However, EAF dust is the multicomponent system, and the impurities can contaminate the evaporated $ZnCl_2$ in chlorination process and further the electrodeposited zinc in molten salt electrolysis process. Especially, many heavy metals in EAF dust are easier to be chlorinated with zinc thermodynamically and are nobler than zinc electrochemically. This study focuses on the purification processes of $ZnCl_2$ in order to prevent the purity of electrodeposited zinc from lowering. One is vacuum distillation process, and another is cementation process.

Vacuum Distillation

Figure 1 shows vapor pressure of some chlorides [9]. $ZnCl_2$ has higher vapor pressure than many chlorides of heavy metals. Therefore, $ZnCl_2$ is expected to be separated from molten salt composed of chlorides with low vapor pressure in vacuum at high temperature. Purification of crude $ZnCl_2$ with atmospheric distillation under inert atmosphere and oxidizing atmosphere has been investigated [8, 10]. This study investigated purification of crude $ZnCl_2$ with vacuum distillation.

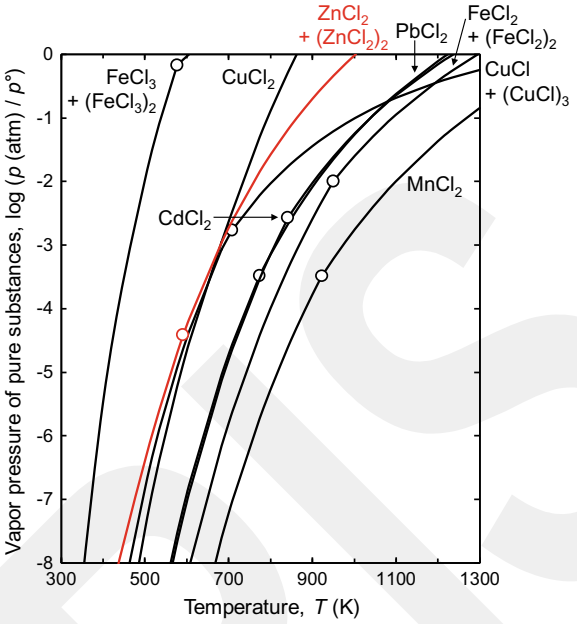

Fig. 1 Vapor pressure of chlorides: $p^{\circ} = 1$ atm, white circles show melting points of chlorides [9]

Experimental

Vacuum distillation experiments of $ZnCl_2$ containing chloride impurities were conducted in a laboratory-scale electric furnace providing wide temperature distribution. Five grams of crude $ZnCl_2$ sample were placed in an alumina crucible or a quartz crucible, and the crucible was placed in the end of a closed quartz reaction tube (O.D. 50 mm × I.D. 46 mm × L. 500 mm) after drying in vacuum for more than 72 h at 393 K. The sample was heated to 700 or 800 K, and vacuum distillation was started at the temperature under about 5 Pa total pressure achieved with rotary pump. After prescribed time, the reaction tube was immediately pulled out from the furnace and cooled down in air. Weights of deposits and residue were measured and concentrations of zinc, iron, and lead in these samples were analyzed by ICP-OES.

Results and Discussion

Figure 2 shows the results of vacuum distillation of $ZnCl_2$ containing iron (II) chloride ($FeCl_2$) and lead chloride ($PbCl_2$) (Fe: 2.2 mass%, Pb: 3.7 mass%) for 4 h at 800 K. Figure 2a shows the temperature distribution of the reaction tube. Figure 2b shows the weight of zinc, iron, and lead in the initial sample, deposit, and residue. As shown in Fig. 2, $FeCl_2$ and $PbCl_2$ were concentrated in residue at 800 K and deposit in 490–710 K temperature zone, and purified $ZnCl_2$ (Fe: 0.066 mass%, Pb: 2.0 mass%)

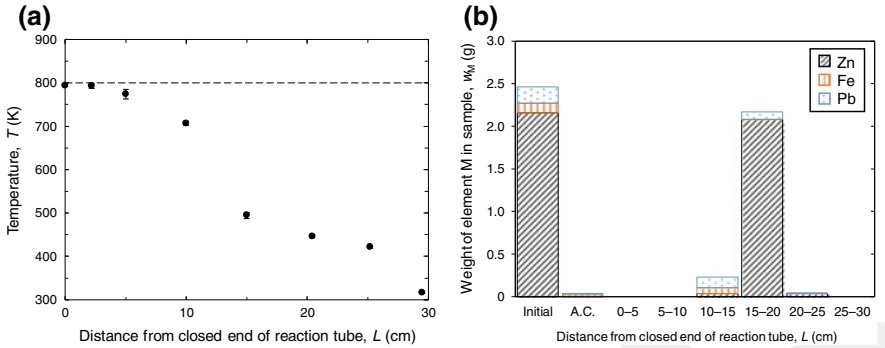

Fig. 2 Results of vacuum distillation experiment for 4 h at 800 K: **a** temperature distribution and **b** weight of zinc, iron, and lead in initial sample, deposit, and residue. A.C. shows residue in the alumina crucible

were recovered from 450–490 K temperature zone. Vapor pressure of the chlorides shown in Fig. 1 supports this deposition trend. Figure 3 shows the results of vacuum distillation of $ZnCl_2$-$FeCl_2$-$PbCl_2$ sample (Fe: 2.2 mass%, Pb: 3.7 mass%) for 4 h at 700 K. Figure 3a shows the temperature distribution of the reaction tube. Figure 3b shows the weight of zinc, iron, and lead in initial sample, deposit, and residue. As shown in Fig. 3, $FeCl_2$ and $PbCl_2$ were concentrated in residue at 700 K and deposit in 620–690 K temperature zone, and purified $ZnCl_2$ (Fe: 0.11 mass%, Pb: 3.8 mass%) was recovered from 460–620 K temperature zone. The concentrations of iron and lead were larger than those after vacuum distillation at 800 K. It is because the temperature range where purified $ZnCl_2$ deposited in vacuum distillation at 700 K is wider than that during the vacuum distillation at 800 K. This means that the utilization of soaking area for deposition of $PbCl_2$ in high temperature zone is preferable for efficient separation of $PbCl_2$ and $ZnCl_2$.

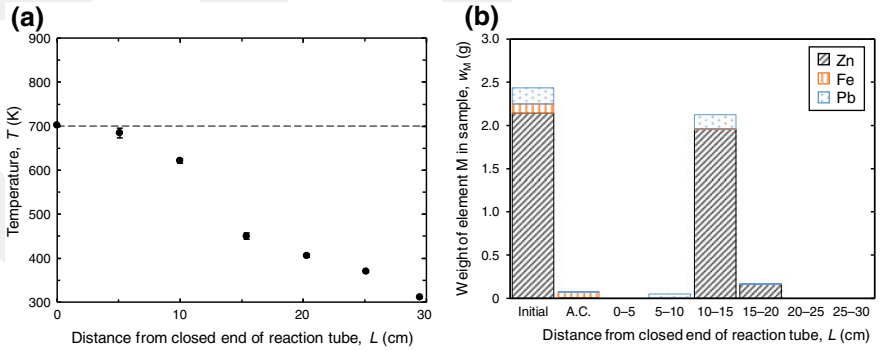

Fig. 3 Results of vacuum distillation experiment for 4 h at 700 K: **a** temperature distribution and **b** weight of zinc, iron, and lead in initial sample, deposit and residue. A.C. shows residue in the alumina crucible

In another experiment, copper (I) chloride (CuCl), cadmium chloride ($CdCl_2$), and manganese (II) chloride ($MnCl_2$) were considered as minor impurities in crude $ZnCl_2$. CuCl has relatively high vapor pressure as a form of trimer $(CuCl)_3$ and is expected to contaminate recovered $ZnCl_2$. However, some of CuCl remained in a crucible and high temperature area, and the concentration of copper in purified $ZnCl_2$ was lower than prediction based on the vapor pressure. $CdCl_2$ has the almost same vapor pressure with $PbCl_2$, and the deposition behavior of $CdCl_2$ is similar to that of $PbCl_2$. $MnCl_2$ is difficult to remove in cementation process thermodynamically, and vacuum distillation process is considered as the only route for separation of $ZnCl_2$ from $MnCl_2$. The result showed that most of manganese remained in the crucible.

Cementation

Pioneering investigation on purification of molten salt containing $ZnCl_2$ by cementation with zinc was conducted by Devilee et al. [11]. In their experiments, the concentrations of iron, lead, and copper in molten salt containing $ZnCl_2$, KCl, and NaCl (31.0 mol% $ZnCl_2$-40.0 mol% KCl-29.0 mol% NaCl) decreased to about 20 massppm, below 1 massppm and 6 massppm with slightly excess zinc at 673 K, respectively. However, the concentration of cadmium in such melt decreased only to 130 massppm, which agreed with the results of rough thermodynamic calculation. Although the possibility of cementation process for refining of molten salt containing $ZnCl_2$ was proven by them, this process has not been optimized in terms of thermodynamic parameters such as temperature, composition of solvent, and so on. This study focuses on the effect of composition of solvent on removal of $CdCl_2$ by cementation with zinc.

Experimental

Equilibrium experiments of cementation reaction (1) were conducted in $ZnCl_2$-KCl-NaCl melt at 723 K [9, 12].

$$\begin{aligned} &CdCl_2(s) + Zn(l) \rightarrow ZnCl_2(l) + Cd(l) \\ &\Delta G^\circ = -31,260\,\mathrm{J/mol} \quad \text{at } 723\ \mathrm{K} \end{aligned} \tag{1}$$

Ten grams of 40 mol% $ZnCl_2$–KCl–NaCl sample containing 0.50 mol% $CdCl_2$ were placed in a PYREX glass crucible (O.D. 19.8 mm × I.D. 17.9 mm × H. 80 mm), and the crucible was then placed in the bottom of separable flask after drying in vacuum for more than 72 h at 393 K. Addition of alkali chloride drastically decreases the activity of $ZnCl_2$ in molten salt phase, which is advantageous to the promotion of cementation reaction (1) forward. The sample was heated to 723 K in

argon atmosphere, and a zinc grain was added into the melt. After prescribed time, the crucible was taken out and cooled down in argon. After separating metal phase with chloride phase, the concentrations of zinc and cadmium in both phases were analyzed by ICP-OES.

Results and Discussion

Figure 4 shows the equilibrium mole fraction of $CdCl_2$ in 40 mol%$ZnCl_2$-KCl-NaCl melt coexisting with liquid zinc-cadmium alloy at 723 K with concentration of KCl in chloride. The mole fraction of cadmium in the alloy was from 0.132 to 0.164. When the mole fraction of KCl in chloride is larger than 0.2, the equilibrium mole fraction of $CdCl_2$ in chloride is from 1.2×10^{-4} to 1.6×10^{-4}, which is smaller than that when the mole fraction of KCl in chloride is smaller than 0.2. With these data, the ratio of activity coefficients of $ZnCl_2$ and $CdCl_2$ was calculated. Each activity coefficient cannot be determined, but the ratio serves as the indicator showing thermodynamic lower limit of $CdCl_2$ concentration in molten salt by cementation reaction.

Further, the second-step cementation experiments were conducted by remelting the refined chloride sample above and adding zinc metal again. One of the second-step purification experiments decreased the concentration of cadmium in molten salt from 190 massppm to 13 massppm. Second-step cementation process can save the amount of added zinc compared to the case adding at one time.

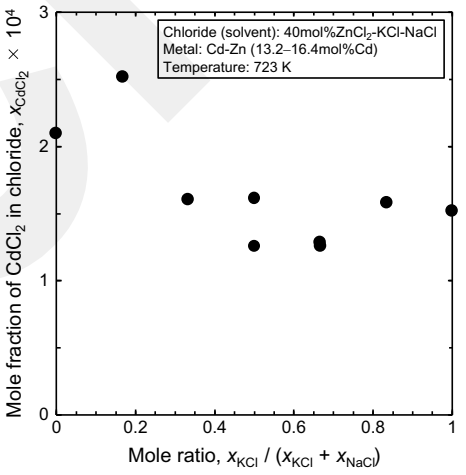

Fig. 4 Equilibrium mole fraction of $CdCl_2$ in chloride with mole ratio of KCl to (KCl + NaCl) in chloride (mole fraction of $ZnCl_2$ in chloride: 0.392–0.400)

Summary

In order to develop the purification process of $ZnCl_2$ recovered by chlorinating EAF dust, vacuum distillation process and cementation process were investigated. In the vacuum distillation experiments, deposit in low temperature zone was purified $ZnCl_2$. The concentration of iron in purified $ZnCl_2$ was below 0.1 mass%, but the concentration of lead in purified $ZnCl_2$ depended on the temperature range of deposition zone. Some of CuCl remained in a crucible or deposited in high temperature zone. $CdCl_2$ showed the similar tendency of deposition to $PbCl_2$. Most of $MnCl_2$ remained in a crucible. In the cementation experiments, the equilibrium mole ratio of $CdCl_2$ in 40 mol% $ZnCl_2$-KCl-NaCl melt coexisting with liquid zinc-cadmium alloy at 723 K was determined. By using these data, the ratio of activity coefficients of $ZnCl_2$ and $CdCl_2$ was calculated. The second-step purification experiments demonstrated the further decrease of cadmium concentration in molten salt from 190 massppm to 13 massppm. From the above results, the ideal practice for refining of $ZnCl_2$ should be as follows; the purification process of crude $ZnCl_2$ starts with vacuum distillation process without adding alkali chloride in order to utilize the high vapor pressure of $ZnCl_2$, and then the cementation process is conducted after adding alkali chlorides into $ZnCl_2$ melt to decrease the activity of $ZnCl_2$. Addition of alkali chloride also decreases the vapor pressure and the viscosity of molten salt, which is preferable for practical operation. Refining the limit of cementation reaction is better than that of vacuum distillation. However, these processes must be combined in order to reduce the necessary amount of added zinc in cementation process. Finally, pre-electrolysis should be used before electrowinning of zinc. These processes can make the purity of electrodeposited zinc much higher.

References

1. Guézennec AG, Huber JC, Patisson F, Sessiecq P, Birat JP, Ablitzer D (2005) Dust formation in electric arc furnace: birth of the particles. Powder Technol 157(1–3):2–11
2. Nagasaka T, Yamaguchi K, Mizuno H (2017) Method for processing iron and steel dust, method for producing zinc, method for producing starting material for iron and steel, and starting material for iron and steel. WO 2017/187973, 2 November 2017
3. Nakamura T, Shibata E (2009) Roles of high temperature furnaces on resource recovery from dusty waste. J High Temp Soc 35(1):21–25
4. Matsuura H, Hamano T, Tsukihashi F (2006) Removal of Zn and Pb from Fe_2O_3–$ZnFe_2O_4$–ZnO–PbO mixture by selective chlorination and evaporation reactions. ISIJ Int 46(8):1113–1119
5. Sun G, Matsuura H, Tsukihashi F (2016) Chlorination reaction of EAF dust by $MgCl_2$. CAMP-ISIJ 29:661
6. Sun G, Matsuura H, Tsukihashi F (2017) Chlorination reaction of EAF dust by $CaCl_2$. CAMP-ISIJ 30:245
7. Yoshiyama K, Matsuura H (2016) Effect of aluminum and copper on the selective chlorination and evaporation reaction of electric arc furnace dust. Proc MMIJ Autumn Meet 3:2410
8. Kinotech Solar Energy Corporation (2015) Zinc production method using electric furnace dust as raw material. WO 2015/030235, 5 March 2015

9. Knacke O, Kubaschewski O, Heseelmann K (1991) Thermochemical properties of inorganic substance, 2nd edn. Springer Verlag, Heidelberg
10. Wang C, Hu X, Matsuura H, Tsukihashi F (2007) Evaporation kinetics of the molten $PbCl_2$-$ZnCl_2$ system from 973 to 1073 K. ISIJ Int 47(3):370–376
11. Devilee RA, Sandwijk AV, Reuter MA (1999) Selective removal of iron contaminations from zinc-chloride melts by cementation with zinc. Metall Mater Trans B 30B(4):607–611
12. Barin I (1995) Thermochemical data of pure substances, 3rd edn. VCH, Verlagsgesellschaft mbH, Weinheim

GCRIS

Advanced Concept "Poly Metallurgical Refinery" Developed by Cobre Las Cruces

Carlos Frias, Joaquin Gotor, Francisco Sanchez, Jorge Blanco, Natalia Moreno and Edward Vera

Abstract Cobre Las Cruces has developed a novel and advanced concept named "Poly Metallurgical Refinery (PMR)" able to treat efficiently polymetallic bulk concentrates and low-grade and dirty concentrates that cannot be processed in conventional refineries. For instance, metal content of treated bulk concentrates range: 2–4% Cu, 5–10% Zn, 3–5% Pb, and 100–200 ppm Ag. The "PMR" concept is based on smart and suitable integration of innovative hydrometallurgical technologies including leaching, purification, and metals winning, aiming to produce on-site several refined or added value metals such as Cu, Zn, Pb, and Ag. Integrated hydrometallurgical technologies developed by Cobre Las Cruces has been tested and validated at pilot plant scale, feeding 300–400 kg/h of bulk concentrates; gathered results have been very positive and new PMR Technologies present many advantages versus conventional technologies, e.g. increased mineral resources efficiency, higher metals recovery, and minimum environmental footprint. In short, PMR Technologies represent a great technological breakthrough for the twenty-first century mining-metallurgical industry aiming to develop a more robust and sustainable business to benefit efficiently complex and polymetallic ores.

Keywords Polymetallic ores · Copper · Zinc · Lead · Silver · Atmospheric leaching

Introduction

There are worldwide many smelters or refineries of copper, zinc, or lead metal, dealing with selective concentrates containing Cu, Zn, or Pb sulfides [1]; it can be said that those mentioned factories are "Mono Metallurgical Refineries" recovering just one of those metals as main product and may be other minor metals as byproducts.

C. Frias (✉) · J. Gotor · F. Sanchez · J. Blanco · N. Moreno · E. Vera
Cobre Las Cruces SA, Ctra. SE-3410, Km 4.100, Gerena, 41860 Seville, Spain
e-mail: carlos.frias@fqml.com

© The Minerals, Metals & Materials Society 2020

A. Siegmund et al. (eds.), *PbZn 2020: 9th International Symposium on Lead and Zinc Processing*, The Minerals, Metals & Materials Series,
https://doi.org/10.1007/978-3-030-37070-1_82

Table 1 Composition of bulk concentrates treated in CLC pilot plant

Component	Range (%)
Cu	2–4
Zn	5–10
Pb	3–5
Ag	100–200

There are also "Imperial Smelting Furnace" (ISF) smelters [2] dealing with mixed concentrates containing Zn and Pb sulphides and producing refined Zn and Pb metals and likely other byproducts such as silver.

However, there is not any industrial refinery to date capable of efficiently treating polymetallic bulk concentrates and low-grade and dirty concentrates containing the four metals: Cu, Zn, Pb, and Ag, and producing in situ those refined metals or added value metals. That is the main objective of this project developed by Cobre Las Cruces (CLC) named "Poly Metallurgical Refinery (PMR)". The "PMR" notion is well aligned with "Mine-to-Metal" approach aiming at extracting and refining the valuable metals in the mine site. The "PMR" advanced concept is based on smart and suitable integration of innovative hydrometallurgical technologies including bulk flotation, concentrate atmospheric leaching, purification, and metals winning that were tested and validated in a pilot plant facility designed, build, and operated by CLC, having a capacity of 300–400 kg/h of bulk concentrate.

Produced pilot plant results and achievements after two years continuous operation have been very successful, and newly developed PMR Technologies present many advantages versus conventional technologies, including:

- Ability and flexibility to deal with low-grade and dirty and polymetallic concentrates that cannot be treated in conventional smelters. Table 1 shows composition range of treated bulk concentrates in CLC pilot plant yielding 90–95% metals extraction.
- Higher efficiency of the mineral resources, allowing over 90% recovery of the valuable metals Cu, Zn, Pb, and Ag contained in polymetallic and complex ores applying bulk flotation while conventional selective flotation typically recovers 40–70% of those metals.
- Producing in situ refined metals ("commodities") rather than selling concentrates, which raises mining business profitability and, in addition, environmental footprint is minimised because it is not necessary to transport the concentrates to far locations, avoiding spillage or airborne contamination, and any generated waste is confined in the mine site and disposed of under most safer conditions.
- A more robust and sustainable mining-metallurgical business is developed, opening the way to exploit lower grade and difficult deposits containing for instance high arsenic, mercury, bismuth, thallium, etc., which are very detrimental impurities to deal with in conventional smelters [3].

Summarising, the PMR Technologies represent a great technological breakthrough for the twenty-first century mining-metallurgical industry and it is the result

of a huge R&D work performed by CLC team during five years, covering the three levels of development: laboratory, bench scale, and continuous pilot plant. The most relevant PMR Project outcomes and achievements are outlined in this paper.

The SICAL Process

Since 2009, CLC operates its hydrometallurgical copper refinery producing over 73,000 tpa "five-nines" copper cathodes applying atmospheric leaching process to secondary copper sulphide (mainly chalcocite) ores, which are leached in ferric sulphate media, injecting oxygen, running at 90 °C, and yielding 92–97% copper extraction in daily operations [4]. Secondary copper ores will be exhausted in 2020, and therefore, CLC is developing the PMR Project to treat their reserves of primary polymetallic ores beyond 2030.

Thus, CLC is extracting copper very efficiently from chalcocite ores through atmospheric leaching in ferric sulphate media. However, it is well known that ferric sulphate leaching of chalcopyrite minerals according to next Reaction 1 is difficult due to formation of a layer of elemental sulphur covering the mineral surface, which behaves as a diffusion barrier slowing down and stopping that oxidation reaction.

$$CuFeS_2 + 2\,Fe_2(SO_4)_3 = CuSO_4 + 5\,FeSO_4 + 2\,S \quad (1)$$

Some authors found that silver ions have positive catalytic effect to enhance the prior reaction because elemental sulphur layer seems to become more conductive and oxidation reaction goes to end, fully leaching chalcopyrite minerals [5, 6].

To date, silver catalytic effect has been proposed just to leach chalcopyrite in copper concentrates. Take in mind the current state of the art and also its broad industrial experience in ferric sulphate atmospheric leaching, Cobre Las Cruces has developed the Silver Catalysed Atmospheric Leaching (SICAL) Process [7] to apply silver catalytic concept to leach both chalcopyrite and also sphalerite minerals contained in polymetallic bulk concentrates according to Reactions 2 and 3:

$$CuFeS_2 + 2\,Fe_2(SO_4)_3 + \left[\mathrm{Ag\,Catalyser}\right] = CuSO_4 + 5\,FeSO_4 + 2\,S \quad (2)$$

$$ZnS + Fe_2(SO_4)_3 + \left[\mathrm{Ag\,Catalyser}\right] = ZnSO_4 + 2\,FeSO_4 + S \quad (3)$$

Following is described the interesting results that were obtained after application of SICAL Process to different types of bulk concentrates having the average composition presented in Table 2.

Copper and zinc bearing minerals are chalcopyrite and sphalerite, respectively, in prior concentrate samples that were leached at 90 °C during 16 h according to Reactions 2 and 3, without any silver addition in one case, and adding 2000 ppm

Table 2 Composition of bulk concentrate samples checked by SICAL Process

Concentrate type	Cu (%)	Zn (%)	Pb (%)	Ag (ppm)	Fe (%)	S (%)
A	3.6	4.6	1.6	45	33	40
B	1.9	4.8	2.0	43	34	42

Table 3 Leaching efficiency of Cu and Zn metals with and without Ag catalyser

	Ag addition = 0 ppm		Ag addition = 2000 ppm	
Concentrate type	Cu (%)	Zn (%)	Cu (%)	Zn (%)
A	54.8	98.7	97.8	93.9
B	55.6	96.9	96.6	82.6

of silver (as silver sulphate) in another case; the percentages of copper and zinc extraction are shown in Table 3.

- It is observed that both concentrates A and B have similar positive behaviour in regard Cu leaching enhancement after adding Ag catalyser, e.g. raising copper recovery from 55 to 97–98%.
- However, the concentrates A and B have different behaviour in regard Zn recovery after adding Ag catalyser; for instance, in concentrate A, Zn leaching rate is slightly reduced, while in concentrate B, Zn leaching efficiency decreases substantially from 96.9 to 82.6%.
- In consequence, it is remarkable that Ag catalytic effect applied to bulk concentrates containing chalcopyrite and sphalerite minerals present different behaviour in regard Cu and Zn metals: usually, Cu metal extraction is enhanced when silver catalyser is added; however, Zn metal extraction may be negatively affected by the presence of silver catalyser.

To overcome the above-mentioned negative Zn leaching behaviour in some polymetallic bulk concentrates, e.g. concentrate B case, CLC has developed a suitable solution consisting on performing the SICAL Process in two sequential stages:

- Stage 1. The bulk concentrate sample is leached under atmospheric leaching conditions without silver addition aiming to maximise Zn leach extraction.
- Stage 2. After Zn metal has been effectively leached, silver catalyser is added to the reactor, and then Cu metal is efficiently extracted from chalcopyrite mineral thanks to silver catalytic effect.

See below how Cu and Zn metal extraction is maximised running in two process stages: first, with no Ag addition, and second, adding 2000 ppm Ag as catalyser (Table 4).

Table 4 Cu and Zn metals extraction adding Ag catalyser just in the second stage

	STAGE 1 Ag addition = 0 ppm		STAGE 2 Ag addition = 2000 ppm	
Concentrate type	Cu (%)	Zn (%)	Cu (%)	Zn (%)
B	55.6	96.9	95.0	97.0

PMR Process Design

Taking in mind CLC accumulated experience after operating very successfully its copper hydrometallurgical refinery for more than 10 years and a deep knowledge of SICAL technology, the PMR Process has been designed and developed by CLC to treat its reserves of primary polymetallic ores aiming to achieve next objectives:

1. Capability and flexibility to deal with diverse bulk concentrates such as polymetallic, low-grade, and dirty (high impurities content) concentrates.
2. To reuse the existing facilities at CLC factory to minimise Capex of new Poly Metallurgical Refinery "PMR", including the areas: crushing and milling, atmospheric leaching, and copper SX and EW.
3. Producing in situ the four metals: Cu, Zn, Pb, and Ag as refined metals (commodities) or added value metals to enhance business profitability.
4. To minimise production costs; with that objective, Ag catalyser will be fully recovered and recycled to atmospheric leaching reactors.
5. To utilise proven commercial technologies, such as Cu SX-EW and Zn SX-EW to extract copper and zinc metals, respectively. To develop simple technologies to extract lead and silver metals; with that objective, cementation techniques were chosen.

Figure 1 shows the PMR Process conceptual scheme, well aligned with prior objectives, and including the existing facilities at CLC factory as well as the new facilities to be installed. The main process stages are briefly described.

– *Conminution and Flotation*. The primary polymetallic ores are crushed and milled and then fed to flotation circuit producing a bulk concentrate with maximum Cu, Zn, Pb, and Ag metals recovery.
– *Atmospheric Leaching Catalysed by Silver*. The bulk concentrate goes to atmospheric leaching process catalysed by silver addition (SICAL Process). A portion of silver cement is recycled as Ag catalyser. Cu and Zn are efficiently leached according to Reactions 2 and 3 and those metals are released to the pregnant leach solution. On the other hand, Pb and Ag metals are deported to the leached residue in form of solid sulphates.
– *Copper SX and EW*. The pregnant solution passes to Cu SX and EW areas to produce high purity "five-nines" copper cathodes for selling.
– *Zinc SX and EW*. Copper raffinate is conditioned and next fed to Zn SX and EW areas to yield high purity SHG zinc cathodes for selling.

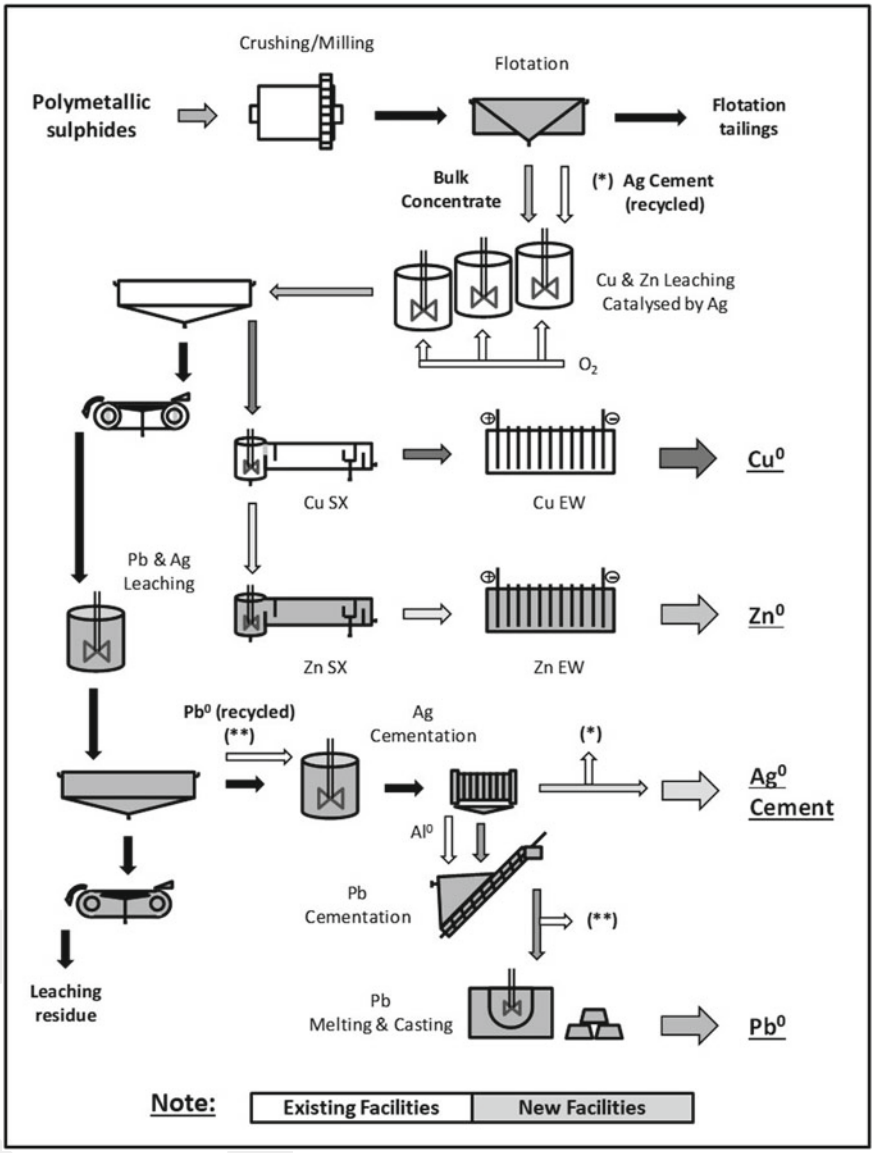

Fig. 1 Conceptual scheme of developed PMR Process

– *Lead and Silver Leaching in Chloride Media*. The leached residue from prior atmospheric leaching stage is treated in hot brine solution to leach efficiently Pb and Ag according to Reactions 4 and 5:

$$PbSO_4 + 4\,NaCl \rightarrow PbNa_2Cl_4 + Na_2SO_4 \quad (4)$$

$$Ag_2SO_4 + 4\,NaCl \rightarrow 2\,AgNaCl_2 + Na_2SO_4 \quad (5)$$

– *Silver Cementation*. Lead and silver pregnant solution goes to Ag cementation using recycled lead metal according to Reaction 6. Silver is fully precipitated. A portion of Ag cement is recycled to the SICAL Process as Ag catalyser, while remaining Ag cement is sold.

$$2\,AgNaCl_2 + Pb^0 \rightarrow 2\,Ag^0 + PbNa_2Cl_4 \quad (6)$$

– *Lead Cementation*. The pregnant solution, free of silver, passes to Pb cementation using aluminium metal according to Reaction 7. The lead is fully cemented and produced metal cement is compacted to yield lead briquettes, which are further melted and casted to obtain high purity lead ingots for selling.

$$3\,PbNa_2Cl_4 + 2\,Al^0 \rightarrow 3\,Pb^0 + 2\,AlCl_3 + 6\,NaCl \quad (7)$$

PMR Pilot Plant

Cobre Las Cruces designed and built a pilot plant having a capacity of 1 t/h of primary polymetallic sulphides and yielding about 300–400 kg/h of bulk concentrate to feed hydrometallurgical circuit [8]. The main objective of the pilot plant was testing and validating the developed PMR Technologies; thus, the pilot plant was designed based on next principles:

– It was not necessary to install in the pilot plant commercially proven technologies such as Cu SX-EW and Zn SX-EW.
– Installed technologies in the pilot plant included: milling and bulk flotation; atmospheric leaching reactors (SICAL Process) and associated solid/liquid separation equipment; hot brine leaching reactors and associated solid/liquid separation equipment; silver cementation and solid/liquid separation; and lead cementation and solid/liquid separation. Additional works were performed in external laboratories: lead cement compacting and lead melting tests.

Below is depicted some photographs of CLC pilot plan facilities in Fig. 2.

Relevant results gathered in CLC pilot plant after two years continuous operation and more than 5,000 tonnes of treated polymetallic ores is summarised in Table 5.

Fig. 2 General views of CLC pilot plant

Conclusions

Cobre Las Cruces has developed successfully the "Poly Metallurgical Refinery (PMR)" Project that represents a great technological breakthrough for the twenty-first century mining-metallurgical industry aiming to develop a more robust and sustainable business to benefit efficiently polymetallic, complex, and low-grade ores.

The developed PMR Technologies have been tested and validated at pilot plant scale and produced results and achievements have been very positive after two

Table 5 Pilot plant relevant results after two years of continuous operation

Section: Bulk flotation	Results
Polymetallic ores grade (%, ppm)	Cu = 1.2; Zn = 3.3; Pb = 2.8; Ag = 70
Bulk concentrates range (%, ppm)	Cu = 2–4; Zn = 5–10; Pb = 3–5; Ag = 100–200
Metals recovery range (%)	Cu = 80–90; Zn= 90–95; Pb = 70–80; Ag = 70–75
Section: Atmospheric leaching	Results
Bulk concentrate feeding (kg/h)	300–400
Silver catalyser addition (ppm)	100–1000
Metals leaching efficiency (%)	Cu = 90–95; Zn = 92–97
Section: Chloride Leaching	Results
Atm. leach residue feeding (kg/h)	100–200
Metals leaching efficiency (%)	Pb = 95–97; Ag = 96–99
Section: Silver Cementation	Results
Produced Ag cement (kg/h)	1–2
Ag cementation efficiency (%)	98–99
Section: Lead cementation	Results
Produced Pb cement (kg/h)	15–20
Pb cementation efficiency (%)	98–99

years of continuous operation. PMR Technologies present many advantages versus conventional technologies, such as:

– Higher efficiency of the mineral resources, allowing over 90% recovery of the valuable metals Cu, Zn, Pb and Ag contained in polymetallic and complex ores applying bulk flotation while conventional selective flotation typically recovers 40–70% of those metals.
– Producing in situ refined metals ("commodities") rather than selling concentrates, which raises mining business profitability and, in addition, environmental footprint is minimised because it is not necessary to transport the concentrates to far locations, avoiding spillage or airborne contamination, and any generated waste is confined in the mine site and disposed of under most safer conditions.

– A more robust and sustainable mining-metallurgical business is developed, open the way to exploit deposits containing for instance high As, Hg, Bi, Sb, Tl, etc., which are very detrimental impurities in conventional smelters.

Acknowledgements This project has received funding from the European Union's Horizon 2020 research and innovation programme under grant agreement No: 689515.

The authors wish to express their gratitude to Cobre Las Cruces company for authorising publication of this paper regarding Poly Metallurgical Refinery (PMR) Project developed in its pilot plant facilities located near Seville city, in Spain.

References

1. Cusano G et al (2017) Best available techniques (BAT), Reference document for the non-ferrous metals industries, industrial emissions directive 2010/75/EU integrated pollution prevention and control. Publications of the European Union. Chapters 3, 5 and 6. ISBN 9789279696558
2. Buschow KHJ et al. (2001) Encyclopedia of materials: science and technology, 1st edn. Elsevier. ISBN 9780080431529 (2001)
3. Alvear G, Löbbus M (2018) Arsenic management for the copper smelting industry. Int Semin Impurities Copper Raw Mater Japan Oil, Gas and Metals National Corporation (JOGMEC), October 17 (2018)
4. Delgado E, Frias C, Gotor J (2013) Las Cruces copper plant start-up: beyond design performance through process improvements implementation. In: Proceedings of Copper'2013 International Conference, Santiago, Chile, 1–4 December, pp. 25–42
5. Miller JD, McDonough PJ, Portillo HQ (1981) Electrochemistry in silver catalysed ferric sulfate leaching of chalcopyrite. In: Kuhn MC (ed) Process and fundamentals considerations of selected hydrometallurgical systems. SME-AIME, 27, pp 327–338
6. Cordoba EM, Muñoz JA, Blazquez ML, Gonzalez F, Ballester A (2009) Comparative kinetic study of the silver-catalyzed chalcopyrite leaching at 35 and 68 °C. Int J Min Process 92:137–143 (Elsevier)
7. Frias C, Vera E, Romero A, Blanco J (2015) Flotation and hydroprocessing of bulk concentrates from Las Cruces Mine. In: Lead and zinc 2015 international symposium, Dusseldorf, Germany, pp 549–560, 14–17 June
8. Frias C, Blanco J, Vera E, Romero A, Gotor J, Sanchez F (2017) Polymetallic ores hydroprocessing at Cobre Las Cruces. Flotation pilot plant outcomes. In: European metallurgical conference EMC'2017, Leipzig, Germany, 25–28 June, pp 715–726

Part XXII
Environmental and Safety Practices II

GCRIS

A New Lead Cementation Equipment and Lead Recovery Process in Chloride Media Developed by Cobre Las Cruces

Carlos Frias, Juan Pedro Soler, Jorge Blanco, Luis Pastor and Natalia Moreno

Abstract A new lead cementation equipment and lead cementation process with aluminium metal in chloride media have been developed by Cobre Las Cruces. Lead-bearing material is leached in hot brine solution; next, pregnant solution is purified to remove certain impurities; finally, lead metal is cemented onto rotating aluminium discs. That way, lead is produced in form of lead powder that is further compacted and melted to yield lead ingots. Cobre Las Cruces operated along one year new cementator prototype feeding 20 kg/h of lead and producing at the end more than 25 tonnes of lead metal powder. Compaction tests on lead powder were also undertaken. The lead cementator prototype includes a few rotating aluminium discs where lead particles are deposited on aluminium surface and detached in continuous applying variable rotational speed. Achievements of developed lead cementation project are very valuable and are outlined in this paper.

Keywords Lead · Cementation · Chloride media · Rotating disc · Aluminium

Introduction

Usually, metals cementation equipment is formed by tanks or vessels containing therein a solution loaded of a noble metal, and the objective of which is to achieve chemical reduction and recovery of said noble metal by means of using another less noble metal, in metallic form, that comes into contact with the solution.

Different contacting pathways are used in cementation processes, including:

- Conventional copper cementation [1] with fragments or bits of iron or iron scrap deposited in channels, rotating drums, or vibrating screens, through which the copper-loaded solution is circulated to yield cemented copper metal.
- Cementation with metal powder in stirred tanks [2], which is typical, for instance, to purify zinc electrolytes prior to zinc electrodeposition process.

C. Frias (✉) · J. P. Soler · J. Blanco · L. Pastor · N. Moreno
Cobre Las Cruces SA, Carretera SE-3410, Km 4.100, Gerena, 41860 Seville, Spain
e-mail: carlos.frias@fqml.com

© The Minerals, Metals & Materials Society 2020

A. Siegmund et al. (eds.), *PbZn 2020: 9th International Symposium on Lead and Zinc Processing*, The Minerals, Metals & Materials Series,
https://doi.org/10.1007/978-3-030-37070-1_83

– Cementation in fluidized bed or fixed bed columns used sometimes to cement copper metal in contact with iron particles or granulates.

In general, prior methods and equipment used in the metallurgical industry for metals cementation present certain drawbacks, such as:

– Regardless of the type or shape of the less noble metal used, i.e., fragments, granules, powder, as the more noble metal is cemented on the surface of the less noble metal, said surface is coated by a layer of cemented metal and gradually becomes smaller, and consequently, the kinetics of the cementation or chemical reduction reaction decreases slowly.
– Moreover, as a result of the metal cementing particle being coated with the cemented metal as the cementation reaction progresses, an unreacted less noble metal core will usually remain, contaminating the more noble cemented metal.
– Aiming to achieve high cementation reaction efficiency, the less noble metal is frequently added in high excess over stoichiometry, giving rise to a large contact surface. In any case, using the cementing metal in excess entails extra cost on one hand and a disadvantage on the other hand because the unreacted portion of the cementing metal adheres to the cemented metal and contaminates it.
– Furthermore, many existing cementation processes are usually discontinuous or batch processes; i.e., once the added amount of the less noble metal is depleted, the equipment must be stopped and emptied in order to extract the produced cemented product containing the more noble metal. It means operating time losses.

Summarisig, all the above drawbacks generate lower productivity and higher operating costs. This paper deals with a novel continuous cementation concept on rotating aluminium discs that solves mentioned drawbacks.

Lead(II) ions are highly soluble in hot brine solutions forming lead chloro-complexes, particularly at temperature ranging 60–90 °C [3]. In next reaction (1) is shown how lead sulphate reacts with sodium chloride solutions to form stable Pb(II) sodium chloro-complexes:

$$PbSO_4 + 4\,NaCl \rightarrow PbNa_2Cl_4 + Na_2SO_4 \quad (1)$$

Many projects were developed in the last years to recover lead in chloride media [4, 5], and even more, the first industrial scale plant was built at Horsehead's Mooresboro factory in North Carolina (USA) to produce 5600 tpa Pb as lead carbonate [6].

As an alternative to recover lead as Pb-carbonate concentrate, Cobre Las Cruces did an extensive research and pilot demonstration project to recover lead in the form of cemented lead metal onto rotating aluminium discs. Cobre Las Cruces operated along one year a new cementator prototype feeding 20 kg/h of lead in hot brine solution and producing at the end several tonnes of lead metal powder, which was further compacted to yield lead metal briquettes.

Thus, a new lead cementation equipment and lead cementation process with aluminium metal in chloride media have been developed by Cobre Las Cruces leaching lead-bearing material in hot brine solution; next, lead pregnant solution is purified to

remove certain impurities; finally, lead metal is cemented onto rotating aluminium discs having variable rotational speed. Achievements of developed lead cementation project are very valuable and are outlined in this paper.

Laboratory Study

A detailed laboratory study was undertaken to know the behaviour and performance of lead metal cementation onto rotating aluminium discs. Chemical reaction that takes place to reduce Pb(II) in brine solution to Pb(0) in contact with aluminium metal is as follows:

$$3\,PbNa_2Cl_4 + 2\,Al^0 \rightarrow 3\,Pb^0 + 2\,AlCl_3 + 6\,NaCl \quad (2)$$

Laboratory lead cementation tests were performed in batch conditions, and contained lead in brine solution was depleted along the time when cementation reaction did progress.

In next Table 1 is shown the variability of main components contained in the brine solutions used in laboratory lead cementation tests according to the targets.

Aluminum discs having 100 cm^2 active surfaces were coupled to an agitator shaft and introduced into a glass filled with 2 L of the preceding solutions to be completely covered by liquid, and said discs were rotated at different revolutions. The cementation reaction of the lead onto the aluminum disc surface begins immediately, forming a cemented lead product which looks like a spongy powder.

The cemented lead powder detaches from the aluminum disc surface when running at proper revolutions, such that the kinetic of the cementation process reaches optimum values with a maximum percentage of cemented noble metal recovery in a given time because aluminium surface may remain totally free of cemented lead just controlling discs rotational speed. Besides, cemented lead product contains minimum aluminium as a contaminant.

Table 1 Composition of brine solutions used in laboratoty lead cementation tests

Component	Content (g/l)
Pb	1–15
Al	0–10
Na	80–100
Cl	120–160

Table 2 Effect of aluminium disc rotational speed to detach cemented lead powder

Rotational speed of aluminium disc (rpm)	Surface of aluminium disc free of cemented lead powder (%)
0	0
100	80
200	97
300	100

Aluminium Discs Rotational Speed

Table 2 shows the percentage of effective surface of the aluminium discs which are free of cemented lead powder as the rotational speed of the disc increases.

It is observed that tested aluminum discs have a rotational speed above 200 rpm which yields 100% free aluminium surface maximising lead cementation efficiency.

Lead Cementation Kinetic

Next Table 3 shows the percentage of lead metal cemented after 15 min of reaction time depending on aluminium discs rotational speed.

It is remarkable that lead cementation reaction presents the faster kinetic when aluminium discs are rotating over 200 rpm.

Based on gathered positive laboratory results regarding lead metal cementation onto rotating aluminium discs, Cobre Las Cruces passed to next project development stage to design and demonstrate the new lead cementation process at pilot plant scale.

Lead Cementation Equipment Design

The philosophy to design the new lead cementation equipment is based on the next targets:

Table 3 Effect of aluminium discs rotational speed on lead cementation reaction kinetic

Rotational speed of aluminium disc (rpm)	Cemented lead after 15 min reaction time (%)
0	52
100	95
200	99
300	100

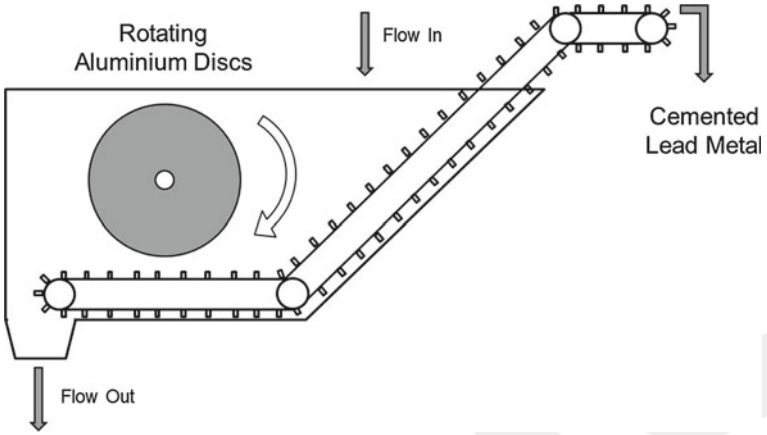

Fig. 1 Conceptual scheme of developed lead cementation equipment

- Continuous operation. Including continuous lead cementation process and besides continuous extraction of produced lead powder.
- Process maximum efficiency. Aluminium discs will run at proper revolutions to allow full detachment of cemented lead powder. As a result, 100% of alumnium surface will be always free and ready to react with Pb(II) ions in solution.
- High purity product. Cemented lead powder will have minimum contamination with aluminium.
- Minimise aluminium consumption. Running conditions will be adjusted and controlled, e.g. temperature, concentrations, timing, etc.

Taking in mind the above statements, in the Fig. 1 is shown a conceptual scheme of developed lead cementation equipment.

Lead Cementator Prototype

A lead cementator prototype was built and tested at pilot plant scale. The lead cementator includes the next main components:

- Vessel. Shape of cementation vessel is similar to Fig. 1 tank, having a capacity of 2000 L. See photo below.
- Lead powder extraction system. Different extraction systems were checked to take out, in continuous, the cemented lead from cementation vessel. For instance, belt conveyor provided good performance.
- Alumnium discs driving system. A motor attached to a gear moves a shaft where 1–6 aluminum discs can be placed. Different aluminium discs were checked by varying metal composition, morphology, size, etc.

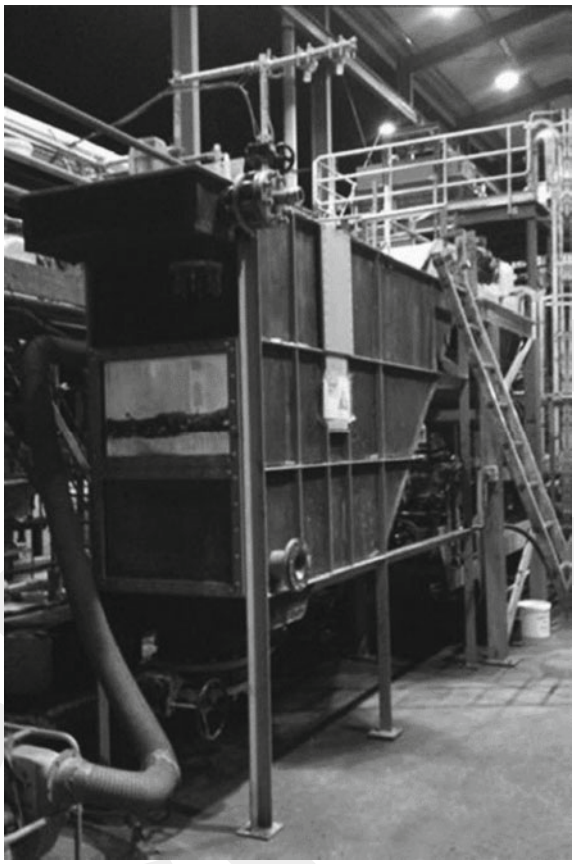

Fig. 2 General view of the lead cementator prototype

– Instrumentation. Main process parameters that were monitored includes: flowrate, temperature, pH, redox potential, discs revolutions, etc.

A photograph of the lead cementator prototype installed in the pilot plant is depicted in the Fig. 2.

Cementation Pilot Plant Design and Operation

A pilot plant having a capacity of 20 kg/h Pb metal in brine solution feeding the cementation process was designed and operated along one year at Cobre Las Cruces premises in Spain.

A simplied flowsheet of the lead cementation pilot plant is presented in Fig. 3, and next, main process stages are briefly described.

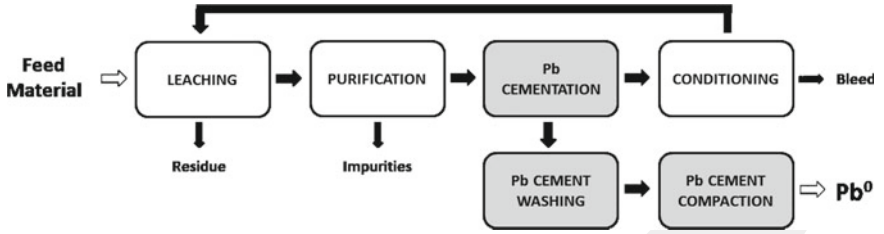

Fig. 3 Simplified flowsheet of lead cementation pilot plant

- Leaching. Feed material usually containing lead sulphate is leached in hot brine solution according to reaction (1) releasing Pb(II) ions to the media in form of stable chloro-complexes.
- Purification. Some impurities such as Cu, As, Bi, etc., are removed through cementation with lead metal. Precipitated impurities are then separated, and purified lead pregnant solution goes to cementation process.
- Pb Cementation. Lead is cemented onto rotating aluminium discs according to reaction (2). Produced lead metal powder is extracted in continuous and sent to washing.
- Conditioning. Depleted lead brine solution is conditioned to adjust proper concentrations. A bleed solution is taking out to keep stable the water balance.
- Pb Cement Washing. Produced lead powder is washed with hot water in a belt filter. Recovered filtrate containing some chlorides is recycled to the main circuit.
- Pb Cement Compaction. Washed lead powder is compacetd using a press compactor to yield lead briquettes ready to be subsequently melted and casted, yielding finally lead ingots.

Pilot Plant Relevant Results

In next Table 4 is summarised the process conditions to operate the lead cementation.

In total, the lead cementation pilot plant produced more than 25 tonnes of cemented lead metal. In next Table 5 is shown relevant results of some representative operating campaings.

Lead briquettes after cemented lead compaction is shown in Fig. 4.

Table 4 Lead cementation process operating conditions

Parameter	Target
Temperature, °C	60–80
Residence time, h	0.5–2.0
Brine solution, N	4.0–5.0
Pb feed rate, kg/h	15–20

Table 5 Relevant results of lead cementation pilot plant

Campaign C-05	Results
Produced Pb cement, kg	1420
Pb cementation efficiency, %	98.7
Al excess over stoichiometric, %	4.2
Campaign C-07	Results
Produced Pb cement, kg	1136
Pb cementation efficiency, %	98.9
Al excess over stoichiometric, %	1.1
Campaign C-10	Results
Produced Pb cement, kg	2029
Pb cementation efficiency, %	97.0
Al excess over stoichiometric, %	2.3

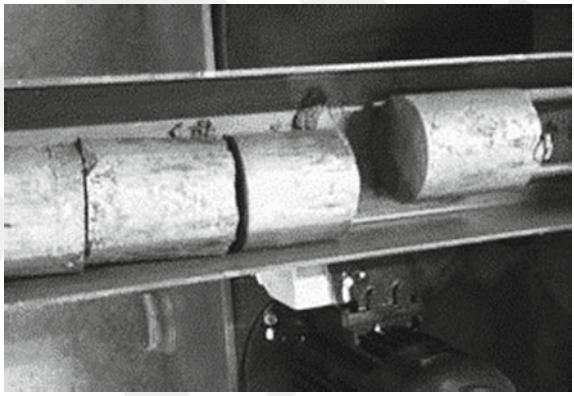

Fig. 4 Lead briquettes leaving the compaction machine

Conclusions

Cobre Las Cruces has developed a new lead cementation equipment and lead cementation process with aluminium metal in chloride media, which has been successfully demonstrated and validated at pilot plant scale.

Project results after producing more than 25 tonnes of cemented lead metal have been very positive, and new developed cementation technologies present a lot of technical and economic advantages in comparison with traditional cementation techniques.

Main conclusions of this project are as follows:

– In conventional cementation, the surface of the less noble metal is coated by a layer of more noble cemented metal and reaction kinetic gradually decreases; however, in this new development, such a drawback is overcome using rotating aluminium discs running at proper revolutions to allow full detachment of cemented lead

powder; in consequence, 100% of aluminium surface is always free and ready to cement continuously lead metal keeping constant (and maximised) the kinetic rate.

– On the other hand, in conventional cementation processes, as a result of the less noble metal particle being coated with the more noble cemented metal as the cementation reaction progresses, an unreacted less noble metal core will usually remain, contaminating the produced cemented metal; the new developed cementation technique on rotating discs solves that limitation because lead metal reacts and cements onto aluminium surface and is immediatelly detached by discs rotational speed; as a result, lead contamination with aluminium is minimum.
– Many existing cementation processes are usually discontinuous or batch processes; i.e., once the added amount of the less noble metal is depleted, the equipment must be stopped and emptied in order to extract the produced cemented product containing the more noble metal, and it means operating time losses; the new developed lead cementation process operates in continuous, and produced lead cement is extracted continuously from the cementation tank, e.g. by means of a belt conveyor. No loosing time happens.
– Gathered results confirm that new lead cementation process onto rotating aluminium discs is fast and efficient, consuming just 2–4% of aluminium excess over stoichimetric amount. Therefore, this is a very efficient and cost-effective cementation process. In addition, produced lead metal presents high purity.

Acknowledgements The authors wish to express their gratitude to Cobre Las Cruces company for authorising the publication of the achievements of this research and development project carried out in pilot plant facilities located near Seville city, in Spain.

References

1. Frias C, Delgado E (2018) Hydrometallurgy in the Iberial Pyrite Belt: past, present and future. In: 14th international congress on energy and mineral resources, Seville, Spain, 10–13 April
2. Chunhua Y, Hongqiu Z, Yonggang L, Weihua G (2018) Modelling, optimization, and control of solution purification process in zinc hydrometallurgy. IEEE/CAA J Automatica Si 5(2):564–576
3. Tan, K.G., Bartels, K., Bedard, P.L.: Lead Chloride Solubility and Density Data in Binary Aqueous Solutions. Hydrometallurgy Journal 17, Issue 3, pp. 335–356, March (1987)
4. Frias C, Frades M, Pecharroman E, Diaz G (2010) Pilot plant demonstration of the PRIMALEAD process confirms the viability to get green lead product from mine lead. In: Lead an zinc 2010 international symposium, Vancouver, Canada, pp 1135–1144
5. Frias C, Diaz G, Martin D, Sanchez F, Mejias A, Garcia Quismondo E (2011) Integrated plant to recover zinc, lead and silver from crude zinc oxides applying ZINCEX and PLINT technologies. TMS 2011, chloride 2011: practice and theory of chloride-based metallurgy, San Diego, CA, USA, February 27–March 3, pp 433–442
6. Pecharroman E, Alvarez C, Frades M, Pinedo MT, Diaz G, Staley A, Pusateri J, Johnson E (2015) ECOLEAD process: a clean technology to recover lead and silver from residues. In: Lead an zinc 2015 international symposium, Dusseldorf, Germany, 14–17 June, pp 171–184

Performance and Mechanism of Chlorine Removal in Wastewater by Combination of $CuSO_4$ and Zero-Valent Copper

Yongguang Luo, Hongtao Qu, Yunhao Xi, Jingtian Zou, Te Zhang, Jing Li, Libo Zhang and Tianqi Liao

Abstract In this study, we examined effect and mechanism of removal of chlorine ion in wastewater by combination of $CuSO_4$ and copper. Experimental studies have shown that $CuSO_4$ combined with copper completely removes chlorine from wastewater with an initial chlorine concentration of 1300 mg/L within only 30 min at the optimum experimental conditions. The optimum experimental conditions are that $CuSO_4$ concentration is 10 g/L, copper concentration is 8.6 g/L, and the reaction temperature is 35 °C. The products such as CuCl and copper are characterized by XRD analyses. The $CuSO_4$ added to the wastewater ionizes to form Cu^{2+}, which reacts with the copper to form Cu^{+}. Then a large amount of Cu^{+} reacts with chloride ions in the wastewater to produce CuCl precipitate. This leads to a decrease in the concentration of chlorine in the wastewater. This study demonstrates that the combination of $CuSO_4$ and copper can quickly and efficiently remove chlorine from waste water.

Keywords Chlorine · Waste acid · CuCl precipitate · $CuSO_4$ and copper

Y. Luo · Y. Xi · J. Zou · J. Li (✉) · L. Zhang (✉) · T. Liao
Faculty of Metallurgical and Energy Engineering, Kunming University of Science and Technology, Kunming 650093, China
e-mail: lijingkind@163.com

Y. Xi · J. Zou · J. Li · L. Zhang · T. Liao
Kunming Key Laboratory of Special Metallurgy, Kunming University of Science and Technology, Kunming 650093, China

State Key Laboratory of Complex Nonferrous Metal Resources Clean Utilization, Kunming University of Science and Technology, Kunming, Yunnan 650093, China

National Local Joint Laboratory of Engineering Application of Microwave Energy and Equipment Technology, Kunming, Yunnan 650093, China

Key Laboratory of Unconventional Metallurgy, Ministry of Education, Kunming 650093, China

Y. Luo · H. Qu · T. Zhang
Yunnan Chihong Zn and Ge CO., LTD, Qujing, Yunnan 655011, China

© The Minerals, Metals & Materials Society 2020

A. Siegmund et al. (eds.), *PbZn 2020: 9th International Symposium on Lead and Zinc Processing*, The Minerals, Metals & Materials Series,
https://doi.org/10.1007/978-3-030-37070-1_84

Introduction

Chlorine (Cl) is widely exists in natural environments, such as in seawater, in solid waste, and in industrial or domestic wastewater, it is one of essential micronutrient for plant and animal survival [1, 2]. In industrial or domestic wastewater, free chlorine is predominant form of chloride ions, and free chlorine mainly includes dissolved chlorine (Cl_2), hypochlorous acid (HClO), hypochlorite (ClO^-) ions and salt (NaCl) [3]. Generally, the chlorine dissolved in the water and hypochlorous acid (HClO) is injected into industrial or domestic wastewater at a sufficient concentration to control the growth of microorganisms by destroys target organism [1, 4]. Even if chloride concentration is at a lower concentration level in the aqueous solution, it is still highly corrosive and causes serious poisoning to humans and aquatic organisms [5–7]. When contact with liquid chlorine in the human eye and skin, it could cause eye and skin burns. If the human body is directly exposed to 500 ppm chlorine, it may cause death within 30 min [8]. When exposed to 1000 ppm chlorine, it may cause death in minutes [4, 9, 10]. Therefore, developing and applying a fast and efficient method to remove free chlorine from water is still worthful.

In order to resolve the problems caused by chlorine pollution control, various methods have been proposed to treat chlorine-containing wastewater. Now, the popular techniques for treatment chlorine-containing wastewater are as follow: activated carbon adsorption, membrane technology, electrochemical, chemical precipitation and ion exchange [11]. Coal-based activated carbon has the strongest reaction with free chlorine due to its high phenol and iodine numbers. Prolonging the contact time, increasing the initial influent free chlorine concentration and lowering the pH of the solution can effectively increase the chlorine removal rate [12, 13]. Membrane technology has received extensive attention in the field of wastewater treatment due to its flexibility, cleanliness and environmental friendliness, convenience and high efficiency [4, 14, 15]. Use ion exchange resin (Chelex-100) to react with chlorine to remove chloride interference, ensuring the accuracy of detecting chlorite ion concentration in drinking water. In addition, regeneration by the removal of chloride ions adsorbed by the ion exchange resin (Chelex-100) proved to be unsuccessful [11]. Iron anode reactor, Ti/RuO_2 anode reactor and the effective chlorine removal reactor formed combinatorial electrochemical system (CES), which can effectively treat organic wastewater containing nitrogen and chlorine ion [16]. In addition, free chloride ions can be reacted with metals such as copper, lead, zinc, and iron to remove chlorine from solution [17]. Copper fibers were made from copper rods and applied to remove chlorine from chlorine-containing solution. Experimental studies have shown that 1.0 g of copper fibers can remove about 1.0 mg/L (100 mL) of chlorine within 60 min [18].

The objective of this paper to study the effect and the removal mechanism of copper powder combined with $CuSO_4$ to remove chlorine from solution. The effects of different copper to chlorine molar ratios (Cu/Cl), different $CuSO_4$ concentration,

different reaction times and different reaction temperatures on chlorine removal efficiency were investigated. The precipitate obtained after chlorine removal were characterized by applying SEM-EDS, XRD spectroscopy. The mechanism of chlorine removal was analyzed by using techniques such as SEM-EDS and XRD. The results of this research may provide valuable suggestions for improving the arsenic removal technique.

Materials and Methods

Materials and Reagents

The wastewater in the experiment was taken from Yunnan, China through a smelter process of zinc, which was produced in the process of smelting flue gas for sulfuric-acid production and has been treated with arsenic removal. The initial pH of wastewater was 2.2, and the main element components are shown in Table 1. All the chemicals used in the experiment were of reagent grade, and glass reactor was rinsed in 15% HCl and washed with deionized (DI) water before use. In addition, commercial copper (Cu > 98%) was purchased from Tianjin Ruijinte Chemical Reagent Co., Inc., China, and sulfate pentahydrate ($CuSO_4 \cdot 5H_2O > 99\%$) was provided by Tianjin Zhiyuan Chemical Reagent Co., Inc., China. Experiments were conducted using DI water, and the reagents used in this study were of analytical grade purity.

Experimental Methods

All wastewater chlorine-removal experiments were systematically carried out in a 250 mL glass reactor. 100 mL wastewater added into 250 mL glass reactor, then which the reaction solution was placed in a magnetic stirrer (Shanghai, DF-101S) for heating. A temperature-controller probe was also inserted into the reactor to observe the reaction temperature.

The wastewater chlorine-removal experiments mainly studied the effects of the molar ratio of copper to chlorine, $CuSO_4$ concentration, reaction temperature, and reaction time on the efficiency of chlorine removal. When one factor changed, the other factors were fixed. To investigate the influence of copper addition on the chlorine removal, different quality of copper (the molar ratio of copper to chlorine) was added into 100 mL of wastewater, which ranges from 0.17 to 0.5. To investigate the effects

Table 1 Compositions of wastewater samples used in this study

Composition	Cl	As	Pb	Cd	F	Cu	Fe	Zn
Concentration (mg/L)	1145	1.04	2.320	8.633	819	8.633	1005	414.6

of $CuSO_4$ concentration on the chlorine removal, different $CuSO_4$ concentration was added into 100 mL of wastewater, which ranges from 8 to 40 g/L. To determine the effects of reaction temperature on the chlorine removal, which ranges from 25 to 80 °C. To study the effects of reaction time on the chlorine removal, which ranges from 5 min to 40 min. Chlorine concentration of the filtrate was analyzed through ion chromatography (IC 25, Dionex equipped with an IonPacAS15/AG15). The precipitates after chlorine removal were dried at 50 °C for 6 h, and characterized through SEM, XRD.

Results and Discussion

Effects of Reaction Temperature on Chlorine Removal

As shown in Fig. 1, reaction temperature has a negative impact on chlorine removal. The experiment was carried out at different reaction temperature ranging from 20 to 80 °C.

Experimental results show, the chlorine concentrations in waste water was decreased from 1300 to 104 mg/L at reaction temperature was 20 °C. As reaction temperature increases from 20 to 35 °C, the chloride concentration in the wastewater decreases from 104 to 94 mg/L, and the chloride removal rate reaches a maximum of 92.46 wt%. Then, as the reaction temperature increases, the chloride concentration in the wastewater was gradually rises. The chlorine concentrations in waste water was

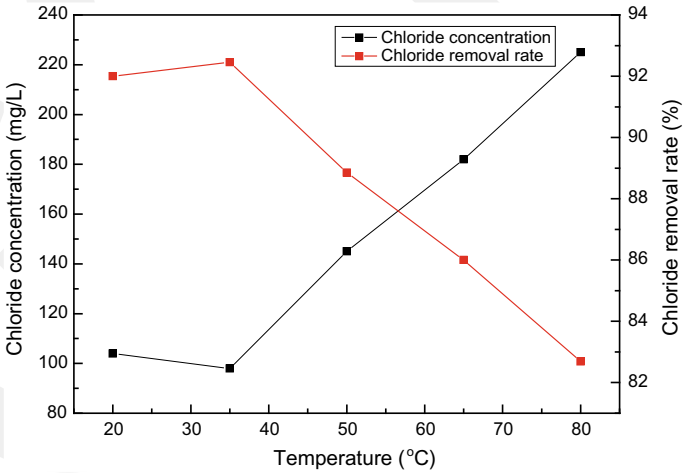

Fig. 1 Effect of reaction temperature on chlorine removal (Experimental condition: zero-valent copper concentration was 6.4 g/L, $CuSO_4$ concentration was 9 g/L, reaction time was 30 min, and stirring speed was 300 rpm)

increased from 94 to 145 mg/L at reaction temperature ranging from 35 to 50 °C, and the chloride removal rate was decreased from 92.46 to 88.85%. When the reaction temperature was 80 °C, the chlorine concentration in waste water reaches a maximum value of 225 mg/L, and the chloride removal rate reaches a minimum of 82.69%. Based on the above results, when the temperature was 35 °C, the chloride removal rate reaches the maximum; therefore, the optimum reaction temperature was 35 °C.

Effects of Reaction Time on Chlorine Removal

Figure 2 indicates that reaction time has significant effect on chlorine removal, the experiment was conducted at different reaction time ranging from 5 to 40 min.

Quantitatively, the chlorine concentrations in waste water was decreased from 1300 to 826 mg/L at reaction time was 5 min. When the reaction time was 10 min, the chlorine concentration in the wastewater was reduced to 255 mg/L, and the chlorine removal rate was 80.38%. Then, reaction time was extended to 30 min, the chlorine concentration in the wastewater was reduced to 88 mg/L, and the chlorine removal rate was 93.23%. However, as the reaction time was extended from 30 to 40 min, the chlorine removal rate was slightly increased, the chlorine concentration in waste water was decreased from 88 to 78 mg/L, and the chlorine removal rate increased from 93.69 to 94.00%. The chlorine removal rate was increased by only approximately 0.31% when the reaction time was extended by 10 min. Therefore, based on these results, we conclude that the best chlorine—removal effect was obtained with a

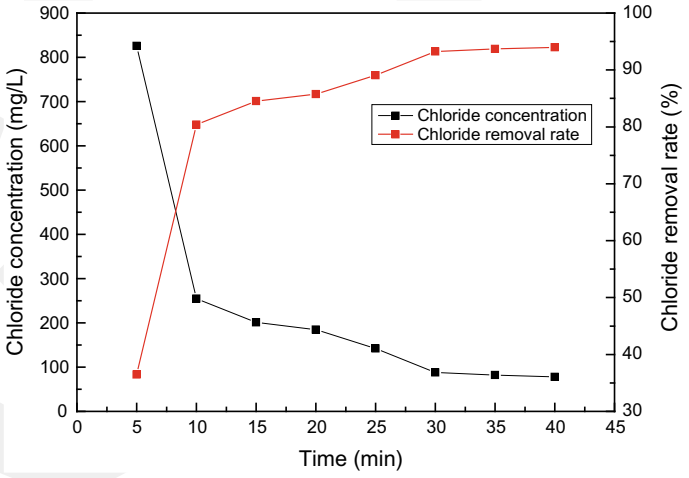

Fig. 2 Effect of reaction time on chlorine removal (Experimental condition: zero-valent copper concentration was 6.4 g/L, $CuSO_4$ concentration was 9 g/L, reaction temperature was 35 °C, and stirring speed was 300 rpm)

reaction time of 40 min, but considering economic and production efficiency, 30 min was chosen as the best reaction time.

Effects of Zero-Valent Copper Concentration on Chlorine Removal

The experiment about the effect of zero-valent copper concentration on chlorine was carried out, the result is shown in Fig. 3. At a zero-valent copper concentration range of 4.3–12.8 g/L, the chlorine concentration decreased rapidly and reached a minimum at a zero-valent copper concentration of 6.4 g/L. As shown in Fig. 3, the chlorine concentration in waste water decreased from 1300 to 168 mg/L at zero-valent copper concentration is 4.3 g/L, and the chlorine removal rate is 87.08%. Continue to increase zero-valent copper concentration to 8.6 g/L, the chlorine concentration in waste water is 78 mg/L, and the chlorine removal rate is 94%. However, as zero-valent copper concentration was increased from 8.6 to 12.8 g/L, the chlorine removal rate was slightly increased, the chlorine concentration in waste water was decreased from 78 to 74 mg/L, and the chlorine removal rate increased from 94 to 94.31%. The chlorine removal rate was increased by only approximately 0.31% when zero-valent copper concentration was increased 4.2 g/L. Therefore, based on these results, we conclude that the best chlorine-removal effect was obtained with zero-valent copper concentration was 12.8 g/L, but considering economic and production efficiency, zero-valent copper concentration was 8.6 g/L was chosen as the best zero-valent copper concentration.

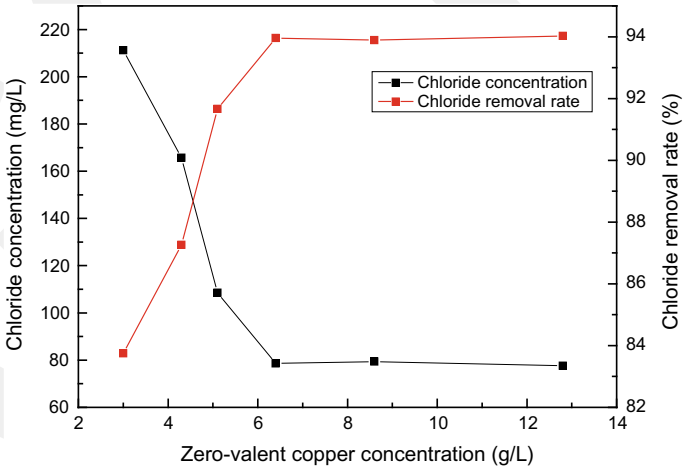

Fig. 3 Effect of zero-valent copper concentration on chlorine removal (Experimental condition: $CuSO_4$ concentration was 9 g/L, reaction time was 30 min, reaction temperature was 35 °C, and stirring speed was 300 rpm)

With the increase of zero-valent copper concentration, a large amount of Cu^{+} produced by the reaction of Cu^{2+} with Cu. A large amount of Cu^{+} reacts with chloride ions in the wastewater to produce CuCl precipitate, which leads to the decrease of chlorine concentration decreased in wastewater. The reaction equation of Cu^{2+}, Cu and chloride in wastewater shown in Eqs. 1 and 2.

$$Cu^{2+} + Cu = 2Cu^{+} \tag{1}$$

$$Cu^{+} + Cl^{-} = CuCl \tag{2}$$

Effects of $CuSO_4$ Concentration on Chlorine Removal

As shown in Fig. 4, the effect of $CuSO_4$ concentration on chlorine removal was examined. With $CuSO_4$ concentration range from 8 to 40 g/L, the chlorine concentration decreased rapidly.

The chlorine concentrations in waste acid decreased from 1300 to 470 mg/L at $CuSO_4$ concentration is 4.3 g/L, and the chlorine removal rate is 63.85%. Then, with the increased of $CuSO_4$ concentration, the chlorine concentration decreased. Continue to increase $CuSO_4$ concentration from 8 to 10 g/L, the chlorine concentration in waste water is decreased from 470 to 61 mg/L, the chlorine removal rate increased from 63.85 to 95.31%. With the increase of $CuSO_4$ concentration, a large

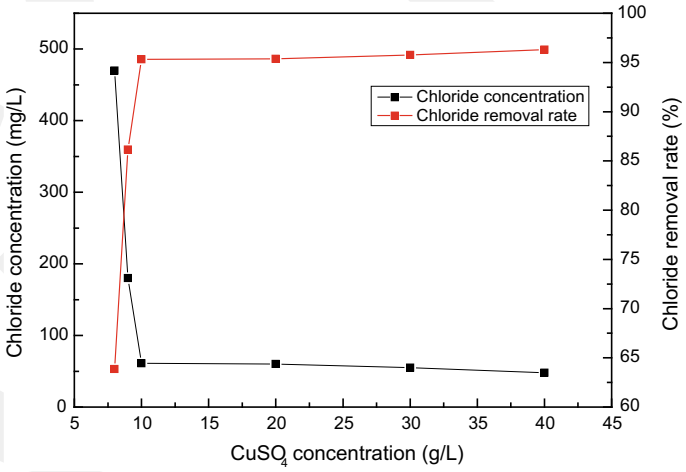

Fig. 4 Effect of $CuSO_4$ concentration on chlorine removal (Experimental condition: zero-valent copper concentration was 8.6 g/L, reaction time was 30 min, reaction temperature was 35 °C, and stirring speed was 300 rpm)

amount of Cu^{+} produced by the reaction of Cu^{2+} with Cu. Then, Cu^{+} reacts with chloride ions in the wastewater to produce CuCl precipitate. However, as $CuSO_4$ concentration was increased from 10 to 40 g/L, the chlorine removal rate was slightly increased, the chlorine concentration in waste water was decreased from 61 to 45 mg/L, and the chlorine removal rate increased from 95.31 to 96.31%. The chlorine removal rate was increased by only approximately 1%, and $CuSO_4$ concentration was increased 40 g/L. Based on these results, the best chlorine-removal effect was obtained with $CuSO_4$ concentration was 40 g/L, but considering economic and production efficiency, $CuSO_4$ concentration was 10 g/L was chosen as the best condition.

Characteristics of Precipitate After Chlorine Removal Reaction

The experiment was carried out under the optimal experimental conditions for chlorine removal, and the filter residue was dried. The precipitate after chlorine removal reaction was analyzed using SEM, XRD. SEM images of precipitate after chlorine removal reaction and EDX elemental maps of Cu, Cl are shown in Fig. 5a, b and c, respectively. As shown in Fig. 5a, SEM images of precipitate after chlorine removal reaction showed a remarkable granule shape, and the particles were tightly bonded together. Combined with the SEM-EDS element maps of Cu and Cl, as shown in Fig. 5b and c. The main components of the precipitate after chlorine removal reaction are copper and chlorine. In the precipitation, the chlorine content was 64.73% and the copper content was 35.27%. This indicates that the main phase in the precipitate is a copper chloride compound and elemental copper. The proposed mechanism for the rapid and effective removal of chlorine from wastewater by combination of $CuSO_4$ with zero-valent copper is shown in Fig. 7.

Figure 6 shows the XRD patterns of precipitate after chlorine removal reaction for 30 min. As shown in Fig. 6, few sharp peaks are observed on XRD patterns of

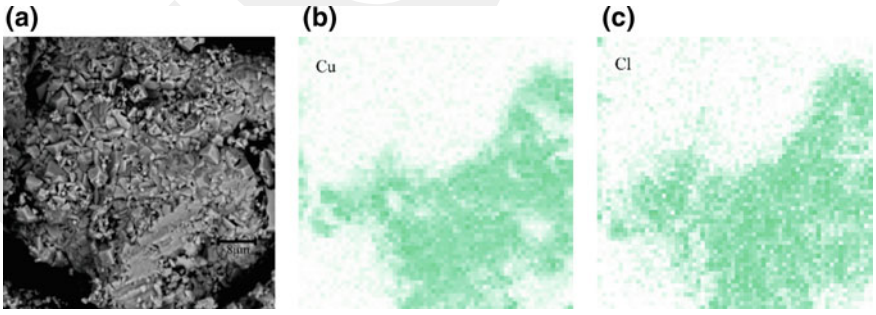

Fig. 5 **a** SEM image of precipitate after chlorine removal reaction; **b** SEM-EDS elemental maps of Cu; **c** SEM-EDS elemental maps of Cl. Composition of Cu is 76.69 wt% and that of Cl is 23.31 wt%

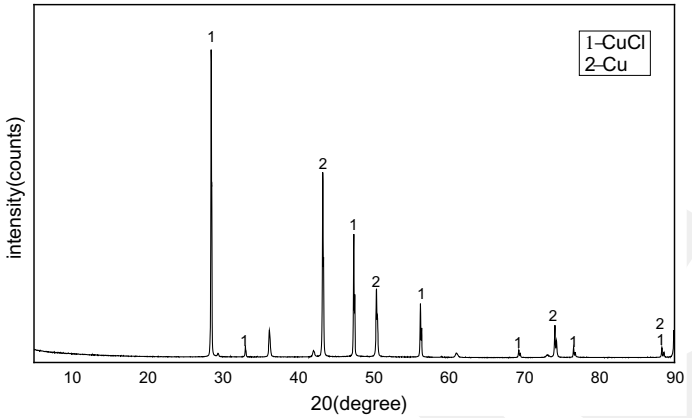

Fig. 6 XRD pattern of precipitate after chlorine removal reaction for 30 min

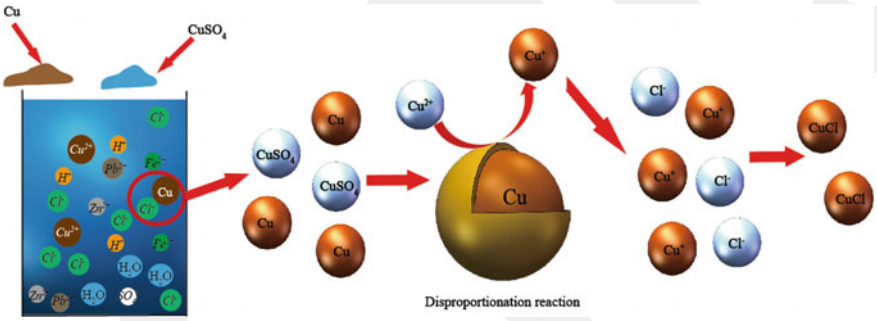

Fig. 7 The proposed mechanism for the rapid and effective removal of chlorine from wastewater by combination of $CuSO_4$ with zero-valent copper

precipitate after chlorine removal which correspond to crystalline forms of copper and CuCl. This is in agreement with the SEM-EDS elemental map showing that the main elements of the precipitate are copper and chlorine. The $CuSO_4$ added to the wastewater ionizes to form Cu^{2+}, which reacts with the copper powder to form Cu^{+}. A large amount of Cu^{+} reacts with chloride ions in the wastewater to produce CuCl precipitate. The reaction equation of Cu^{2+}, Cu and chloride in wastewater shown in Eqs. 1 and 2. Which leads to the decrease of chlorine concentration decreased in wastewater.

Conclusions

Based on our experimental investigations, the following conclusions can be drawn: the combination of $CuSO_4$ and copper can quickly and efficiently remove chlorine from waste water. The optimum experimental conditions are that $CuSO_4$ concentration is 10 g/L, copper concentration is 8.6 g/L, the reaction temperature is 35 °C and stirring speed is 300 r/min. The $CuSO_4$ added to the wastewater ionizes to form Cu^{2+}, which reacts with the copper to form Cu^{+}. Then Cu^{+} reacts with chloride ions in the wastewater to produce CuCl precipitate. Lead to the decrease of chlorine concentration in the wastewater. Under optimal experimental conditions, the chlorine concentration in waste water decreased from 1300 to 61 mg/L in 30 min, and the removal rate of chloride was as high as 95.31%.

Acknowledgements This work was supported by a Yunnan Provincial Science and Technology Key Project (No. 2017FA026). The authors are grateful to the Kunming Key Laboratory of Special Metallurgy, Kunming Academician Workstation of Advanced Preparation for Superhard Materials Field, and Kunming Academician Workstation of Metallurgical Process Intensification.

References

1. Rahmati NO, Pourafshari Chenar M, Azizi Namaghi H (2017) Removal of free active chlorine from synthetic wastewater by MEUF process using polyethersulfone/titania nanocomposite membrane. Sep Purif Technol 181:213–222
2. Addink R, Altwicker ER (2001) Formation of polychlorinated dibenzo-p-dioxins/dibenzofurans from residual carbon on municipal solid waste incinerator fly ash using Na37Cl. Chemosphere 44:1361–1367
3. Gunjal DB, Naik VM, Waghmare RD, Patil CS, Shejwal RV, Gore AH, Kolekar GB (2019) Sustainable carbon nanodots synthesised from kitchen derived waste tea residue for highly selective fluorimetric recognition of free chlorine in acidic water: A waste utilization approach. J Taiwan Inst Chem Eng 95:147–154
4. Greenlee LF, Lawler DF, Freeman BD, Marrot B, Moulin P (2009) Reverse osmosis desalination: water sources, technology, and today's challenges. Water Res 43:2317–2348
5. Kist LT, Rosa EC, MachadoÊL, Camargo, ME MoroCCJET (2013) Glutaraldehyde degradation in hospital wastewater by photoozonation 34:2579–2586
6. Emmanuel E, Keck G, Blanchard J-M, Vermande P, Perrodin Y (2004) Toxicological effects of disinfections using sodium hypochlorite on aquatic organisms and its contribution to AOX formation in hospital wastewater. Environ Int 30:891–900
7. Watson K, Shaw G, Leusch FDL, Knight NL (2012) Chlorine disinfection by-products in wastewater effluent: bioassay-based assessment of toxicological impact. Water Res 46:6069–6083
8. Yongqiang D, Geli L, Nana Z, Ruixue W, Yuwu C, Guonan CJAC (2012) Graphene quantum dot as a green and facile sensor for free chlorine in drinking water 84:8378–8382
9. Suryanarayanan A (2014) Chlorine. In: Wexler P (ed) Encyclopedia of toxicology, 3rd edn. Academic Press, Oxford, pp 860–863
10. Judd S (1999) Process Saf Environ Prot 77:251–252
11. Bhindi AK, Chiswell B (1992) Method based on Chelex-100 ion-exchange resin for the removal of chlorine interference in the determination of chlorite ion. Anal Chim Acta 265:117–126

12. Zhang H, Liu W, Li B, Wei Z, Chang Q, Ying W, Liu YJEP (2008) Control, activated carbon treatment for removing residual free chlorine in water
13. Li B, Zhang H, Zhang W, Huang L, Duan J, Hu J, Ying W (2010) Cost effective activated carbon treatment process for removing free chlorine from water 5:714–720
14. Rahmanian B, Pakizeh M, Maskooki A (2010) Micellar-enhanced ultrafiltration of zinc in synthetic wastewater using spiral-wound membrane. J Hazard Mater 184:261–267
15. Dahe GJ, Teotia RS, Bellare JR (2012) The role of zeolite nanoparticles additive on morphology, mechanical properties and performance of polysulfone hollow fiber membranes. Chem Eng J 197:398–406
16. Zhou J, Lou Z, Yang K, Xu J, Li Y, Liu Y, Baig SA, Xu X (2019) Electrocatalytic dechlorination of 2,4-dichlorobenzoic acid using different carbon-supported palladium moveable catalysts: adsorption and dechlorination activity. Appl Catal B 244:215–224
17. Liu B, Wang X, Tian Y, Shi Y, Gou Y, Kang B (2010) Hygienic quality of drinking water in Zhouqu county: an investigation after the flood and the mud-rock flow disaster
18. Asada T, Omichi M, Yamada M, Yamada A, Oikawa K (2005) Study on a removal mechanism for residual chlorine by copper fiber 15:42–48

GCRIS

A Review on Recycling Technologies and Product Life Cycle Issues of Zinc and Lead

Syeda Afsara

Abstract Secondary lead mainly refers to the lead recovered from discarded lead–acid battery, lead dust, and slag from lead smelting process. The pyrometallurgical process of spent lead involves direct smelting of lead or the desulphurization at lower temperatures followed by smelting. In electrowinning, lead was desulphurized by Na_2CO_3 and NaOH. The paste was leached, and lead compounds were dissolved in acid for electrowinning. Zinc can be recovered by leaching its compounds with ammonia, hydrochloric acid, and sulphuric acid. Various processes like solvent extraction and cementation can be employed to remove impurities. There are certain problems related to the production of zinc and lead: (i) Distribution of mineral dust particles in the area of grinding and screening. (ii) The presence of acid vapors in the areas of leaching, purification, and electrolysis causes the pollution of the water, soil, and loss of green space. (iii) Gas and diesel fuel release greenhouse gases.

Keywords Lead · Zinc · Leaching

Introduction

Secondary sources of lead are lead–acid battery, lead dust, and slag from lead smelting process while the primary sources are galena (PbS), cerussite ($PbCO_3$), and sulfuric acid galena ($PbSO^4$) [1]. The global lead consumption keeps rising as it is used for automotive, backup power, and energy storage for renewables [1]. Zinc is another important metal that is used in acidic or alkaline Zn–Mn batteries because of the versatility, low maintenance, and reduced cost [2]. The extraction of lead and zinc from their ores cannot meet the ever-increasing demand for their uses. This is why the secondary extraction of lead and zinc from batteries and dust is quickly replacing the primary production from ores. Moreover, lead is a toxic metal and causes lead contamination in landfills. Zinc batteries contain mercury, manganese and other heavy metals which pose an environmental threat if dumped in landfills. The storage

S. Afsara (✉)
Bangladesh University of Engineering and Technology, 1000 Dhaka, Bangladesh
e-mail: syedaafsara734@gmail.com

© The Minerals, Metals & Materials Society 2020

A. Siegmund et al. (eds.), *PbZn 2020: 9th International Symposium on Lead and Zinc Processing*, The Minerals, Metals & Materials Series,
https://doi.org/10.1007/978-3-030-37070-1_85

capacity of landfills is limited, and disposal costs of batteries are high [2]. Recycling of lead and zinc thus reduces the environmental concern and the depletion of ores.

Pyrometallurgical methods such as the Waelz process recycles zinc from zinc dust while the Isasmelt amongst other technologies can recover lead from batteries. Pyrometallurgical methods produce toxic gases such as SO_2 and require high temperature. This is why hydrometallurgical processes are being developed. Process such as the LEADCLOR process, the PLACID process, and the Ezinex process recovers the metal by leaching in acids and electrowinning in an electrolytic cell.

Recovery of Lead and Recycling

The Isasmelt Process

Before being treated in a pyrometallurgical vessel, the scrap batteries need to be broken apart into components in a battery breaking facility. The hammer mill in CX plant reduces the feed size and deposits it onto a vibrating washing screen that allows the fine lead paste to pass through and be collected in a stirred tank prior to desulfurization. The paste slurry that contains lead oxide and lead sulfate is partially dewatered and pumped into the reaction vessels with collected battery acid and liquid caustic soda.

$$H_2SO_4 + 2NaOH \rightarrow Na_2SO_4 + 2H_2O$$

$$PbSO_4 + 2NaOH \rightarrow Na_2SO_4 + H_2O + PbO$$

Desulfurized paste from the CX plant, together with reductant, is continuously fed into a bath of molten battery paste. The submerged combustion lance agitates the bath and produces a soft bullion that is intermittently tapped into a launder and pot system. At the end of each complete cycle, the furnace slag is conditioned and reduced to produce a high-antimony bullion and a discard slag [3] (Fig. 1).

LEADCLOR Process

The leachant in this case is a dilute solution of ferric chloride, which reacts with lead sulfide to form ferrous chloride and elemental sulfur. The cementation process precipitates the impurities in an oxydo-reduction reaction so that they are removed and do not interfere with the deposition of lead during electrolysis. Electrolysis dissociates the residual lead chloride into its elements, and the chlorine is collected and used to oxidize the ferrous chloride, thereby reforming ferric chloride for re-use

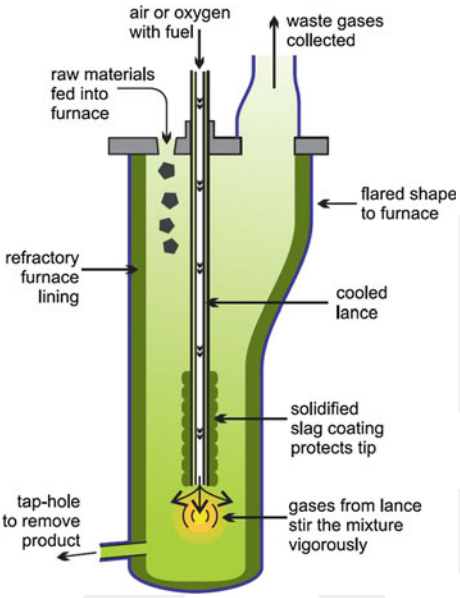

Fig. 1 Isasmelt process [4]

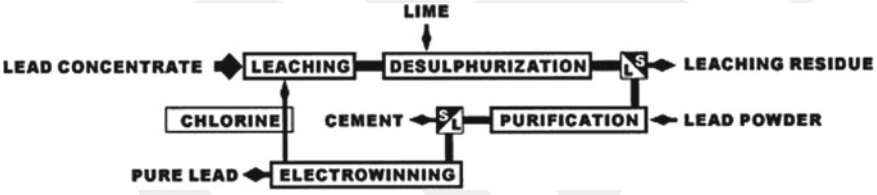

Fig. 2 Block diagram of LEADCLOR process [5]

as leachant. The process has a purification step enabling lead of 99.99% or higher purity [5] (Fig. 2).

Placid Process

The Placid process is a development of the LEADCLOR process. As can be observed in Fig. 3, the former PLACID process is simple and consists of four main stages [6]:

- Secondary lead raw material is leached using a hot hydrochloric acid brine to form a lead chloride solution.
- Sulfate is removed from the lead pregnant solution by adding lime to create gypsum for such commercial applications as cement additives and plaster manufacturing.

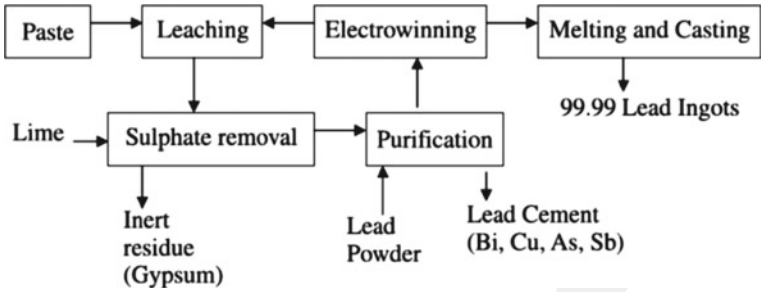

Fig. 3 Placid process [1]

- Metallic impurities in the lead pregnant solution are cemented using lead powder, producing a metallic cement containing mainly residual lead and copper, bismuth, tin, etc.
- The obtained solution can be processed by electrowinning, producing a high-quality lead product (>99.99% lead). The very low content of bismuth is remarkable and unique to PLACID lead. The anodic reaction evolves oxygen and regenerates hydrochloric acid, which is sent back to the leaching step. Thus, net reagent consumption is very low.

A single PLACID and also LEADCLOR electrowinning cell are illustrated diagrammatically in Fig. 4. The electrolytes for the two electrodes—the anode and the cathode—are different and are separated by a membrane that is permeable only by proton ions H^+. On the cathode, lead chloride is stripped of its lead atom, which leaves two chlorine atoms that are 'negatively charged' having additional electrons. These negatively charged chlorine atoms combine with protons passing through the membrane to reform hydrochloric acid, which is returned to the leaching bath for re-use [5].

The lead chloride is then recovered through electrowinning procedure as shown in Fig. 2 [1].

$$PbO + 2HCL = PbCl_2 + H_2O$$

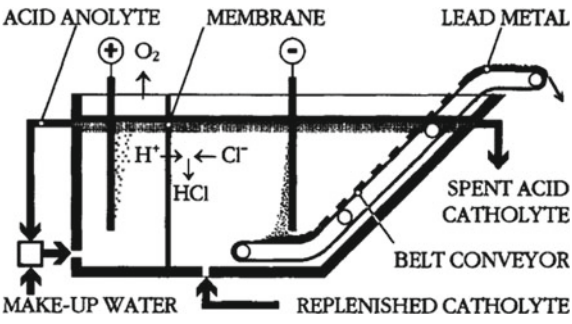

Fig. 4 Placid electrowinning cell [5]

$$Pb + PbO_2 + 4HCl = 2PbCl_2 + 2H_2O$$

$$PbSO_4 + 2NaCl = 2PbCl_2 + Na_2SO_4$$

Hydrogen-Lead Oxide Fuel Cell

Hydrogen gas is fed into the anode, where it undergoes electro-oxidation with the OH^- ions to form water and releases electrons. The electrons pass through the external circuit, carry out electric work, and then arrive at the cathode. The refined PbO dissolved in heated aqueous NaOH forms $HPbO_2^-$ ions, which are then pumped into the cathode, where the $HPbO_2^-$ ions combine with the electrons from the anode and water to produce metallic Pb and OH^- ions. The produced OH^- ions combine with the Na^+ ions migrating from the anolyte through the sodium-ion exchange membrane to form NaOH. The involved reactions including the complexation dissolution of PbO in NaOH are given below (Fig. 5):

Anode: $H_2 + 2OH^- \rightarrow 2H_2O + 2e^-$ (electro-oxidation $E^\circ = -0.828$ V)
Cathode: $PbO(s) + OH^- \rightarrow HPbO_2^-$ (complexation reaction)
$HPbO_2^- + 2e^- + H_2O \rightarrow Pb(s) + 3OH^-$ (electro-reduction $E^\circ = -0.531$ V).

The overall reaction of the fuel cell is as follows:
$H_2 + PbO(s) \rightarrow H_2O + Pb(s)$ ($E^\circ = -0.531 - (-0.828) = 0.297$ V) [7].

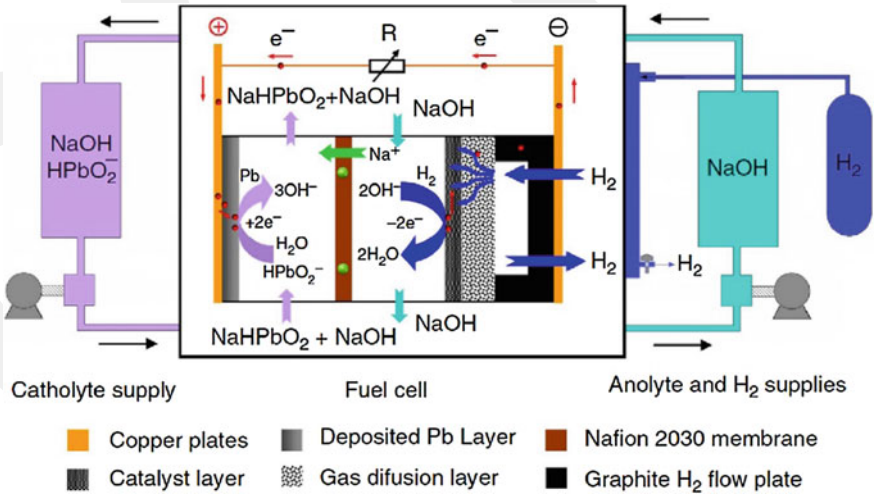

Fig. 5 Schematic of a H_2–PbO fuel cell [1]

Recovery of Zinc and Recycling

The Waelz Process

The Waelz process is a method of recovering zinc from metallurgical waste and other recycled materials. It consists of a rotary tubular furnace, zinc-bearing wastes, and a solid reducing agent which are charged into the inclined rotary furnace. Coke breeze is used as the reducing agent. The modern version of the Waelz process includes preliminary agglomeration of the charge. The charge travels through the furnace in the opposite direction of the flue gases. The products of oxidation of the sublimates (oxides of zinc and lead and other volatile elements) are removed from the furnace together with the flue gases and deposited in filters. The final product of the technology is crude zinc oxide with a high content of impurities (compounds of Pb, Cd, etc.) that is subsequently used in zinc production. The Waelz oxides are washed with the addition of sodium carbonate. This is done in two or three stages and is designed to remove halogens (Cl, F) and reduce the concentration of alkali metals. The resulting product contains up to 68% Zn [8] (Fig. 6).

The Modified Zincex Process

The Modified Zincex Process is a hydrometallurgical process to obtain high-quality zinc slabs from secondary raw materials. The process has the following conceptual steps:

(1) Direct and atmospheric leaching, in mild conditions, of the raw material in a diluted sulphuric aqueous acid solution:

$$ZnO + 2H^{+} = Zn^{2+} + H_2O$$

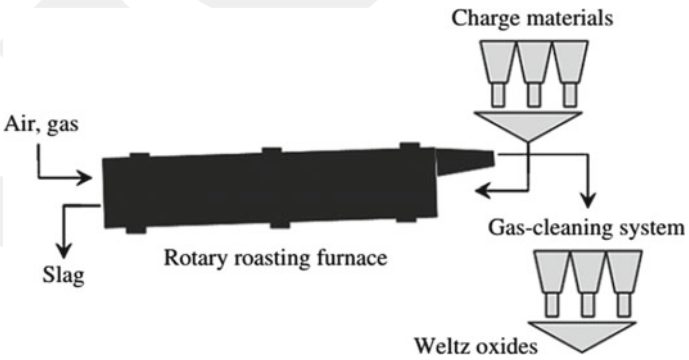

Fig. 6 Diagram of a unit designed to recycle dust by the Waelz process [8]

This aqueous acid solution is mainly recycled from the solvent extraction section.

(2) Purification of some impurities of the leached liquor, principally iron and aluminium, by precipitation. The precipitation residue is mainly gypsum and hydroxides. Depending on the raw material, this stage is optional.
(3) Selective zinc extraction from the pregnant liquor by a liquid cationic exchanger (D2EHPA) resulting in an organic extract containing all the leached zinc from the previous step and an acid aqueous raffinate depleted of zinc, which is mostly used in the leaching step (with the organic phase underlined) is as follows:

$$2\,\mathrm{RH} + \mathrm{Zn}^{2+} \rightarrow \mathrm{R_2Zn} + 2\,\mathrm{H}^{+}$$

A small fraction from this aqueous circuit is bled-off in order to remove soluble impurities such as cadmium, chloride, fluoride, and magnesium.

(4) The next step is the zinc stripping from the organic extract by means of the high acidity of the zinc spent electrolyte:

$$\mathrm{R_2Zn} + 2\mathrm{H}^{+} \rightarrow 2\mathrm{RH} + \mathrm{Zn}^{2+}$$

(5) The last step of the process is the electrodeposition of zinc on aluminium cathodes from the loaded electrolyte, with the production of an acidic spent electrolyte which is recycled back to the previous stripping step [9] (Fig. 7):

$$\mathrm{Zn}^{2+} + \mathrm{H_2O} = \mathrm{Zn} + 2\,\mathrm{H}^{+} + 1/2\mathrm{O_2}$$

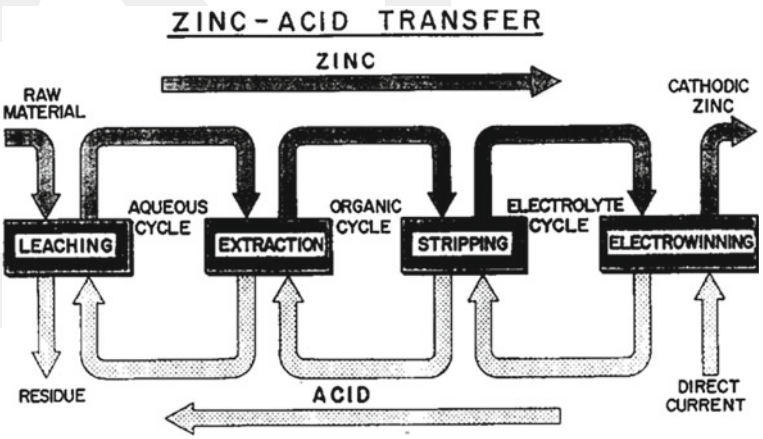

Fig. 7 Conceptual process diagram of modified Zincex process [9]

The EZINEX Process

The zinc-bearing materials are usually submitted to a thermal treatment in which the zinc is vaporised and reoxidised producing crude zinc oxide (C.Z.O.). The EZINEX process is a chloride based leaching and electrowinning system which can deal with materials based on oxidised zinc and consists of five main operations:

- Leaching of Zn bearing materials: In the leaching reactor, Zn and the other heavy metals contained are dissolved together with alkaline chlorides.

$$MeO_{n/2} + n\,NH_4Cl \rightarrow Me(NH_3)_nCl_n + n/2\,H_2O \quad (Me = Zn^{2+},\ Cd^{2+}, Cu^{2+}, Cu^{+}, \ldots)$$

$$PbCl_2 + nXCl \rightarrow (X)_nPbCl_{(2+n)} \quad \left(X = Na^{+},\ K^{+},\ NH_4^{+}\right)$$

- Solution purification

The most problematic impurities for the E.W. are the metals more noble than Zn that could be co-deposited together with Zn into the cathode. This operation is run adding some zinc powder or granules that causes the removal of such impurities because of the following cementation or displacement reaction:

$$Me^{n+} + n/2\,Zn \rightarrow Me + n/2\,Zn^{2+} (Me = Pb^{2+}, Cd^{2+}, Cu^{2+}, Ag^{+}, \ldots)$$

- Zinc electrowinning: The EZINEX E.W. occurs in a conventional open cell with permanent titanium blank cathodes and graphite anodes. The electrolysis, for the zinc solubility problems, has to be run at high temperature too (70–75 °C) and assisted by an air sparging system that optimises the diffusion rate to a point that the electrolysis can be run at relatively high current densities (300 A/m^2) even with relatively low zinc concentrations (5 g/l).

At the titanium cathode,

$$Zn(NH_3)_2Cl_2 + 2\,e^{-} \rightarrow Zn + 2\,NH_3 + 2\,Cl^{-}$$

At the graphite anode,

$$2\,Cl^{-} + 2/3\,NH_3 \rightarrow 2\,HCl + 1/3\,N_2 + 2\,e^{-}$$

- Evaporation/crystallisation unit:

The impurities usually building up in this system are essentially alkali chlorides, fluorides, calcium, and magnesium. They can slightly modify the electrolyte conductivity but, in any case, they have to be removed to avoid unwanted crystallisation somewhere in the plant.

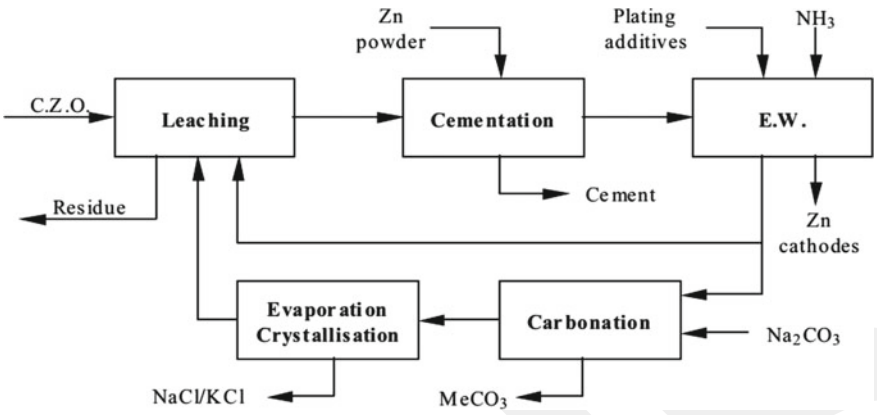

Fig. 8 EZINEX process block diagram [10]

- Carbonation: Calcium and magnesium which are less noble than zinc tend to build up in solution and can be removed by precipitation by $Na_2CO_3/NaHCO_3$ [10] (Fig. 8).

$$NaHCO_3 + MeCl_2 \rightarrow MeCO_3 + NaCl + HCl$$

$$Na_2CO_3 + MeCl_2 \rightarrow MeCO_3 + 2\,NaCl$$

$$Ca^{2+} + 2\,F^- \rightarrow CaF_2$$

Product Life Cycle Issues of Zinc and Lead

The severe effects of zinc and lead mining include destruction of vegetation and pasture areas for mineral exploration, development of residential townships near the mine in a protected area, and the effect on regional climate and ecosystems [11].

Environmental problems within the factory are as follows [11]:

- Distribution of mineral dust particles in the area of grinding and screening area;
- The industrial wastewater in the flotation unit that is the most important pollution of the plant;
- Low grade ore fines which are discharged on the tailing dam crest and back of them, and the strong wind disperses the particles in the surface water, villages, and downstream farms. These particles contain heavy metals

The environmental problems in the zinc smelter unit include

- The presence of acid vapors in the areas of leaching, purification, and electrolysis causes the pollution of the water, soil and loss of green space.
- The solid waste is filter press cake of the leaching and purification units. Filter press cake of the leaching unit depot is in the open area. This cake has no valuable materials.

The production of zinc and lead causes release of greenhouse gases such as are CO_2, NO_2, and CH_4, and depletion of water resources, air, and ozone. Pyrometallurgical smelting produces SO_2 and emission of other heavy metals.

Conclusion

Production of lead and zinc from secondary resources is starting to dominate the market. Even though in smaller quantities, pyrometallurgical smelting still releases some SO_2, particulates of lead, and other heavy metals into the atmosphere. The particulates and gaseous pollutants can be removed by technologies such as wet scrubbers and electrostatic precipitators. The SO_2 can be used to produce sulphuric acid. Hydrometallurgical processes are greener and recover 99.99% of metals. They separate metals from unwanted substances by leaching and remove sulphur by producing compounds that are eliminated by leaching. Recovery of elemental sulfur from zinc and lead concentrates can be carried out by direct leaching residue (DLR) using atmospheric distillation [12]. Hence, there are ways of controlling emissions of gaseous and particulates. The processes discussed result in significant recovery of lead and zinc from batteries and dust and also greatly reduce our dependence on ores from which zinc and lead are obtained. These processes are also a useful means of recycling valuable metals, acids, and plastics from spent batteries which cause disposal problems in landfills.

References

1. Zhang Wei, Yang Jiakuan, Wu Xu, Hu Yuchen, Yu Wenhao, Wang Junxiong, Dong Jinxin, Li Mingyang, Liang Sha, Hu Jingping, Kumar Ramachandran (2016) A critical review on secondary lead recycling technology and its prospect. Renew Sustain Energy Rev 61:108–122. https://doi.org/10.1016/j.rser.2016.03.046
2. Sayilgan, E, Kukrer T, Civelekoglu G, Ferella F, Akcil A, Veglio F, Kitis M (2009) A review of technologies for the recovery of metals from spent alkaline and zinc–carbon batteries. Hydrometallurgy 158–166. https://doi.org/10.1016/j.hydromet.2009.02.008
3. Ramus K, Hawkins P (1993) Lead/acid battery recycling and the new Isasmelt process. https://doi.org/10.1016/0378-7753(93)80159-M
4. http://www.essentialchemicalindustry.org/metals/copper.html
5. Andrews D, Raychaudhuri A, Frias C (1999) Environmentally sound technologies for recycling secondary lead. J Power Sources 88:124–129 (2000). https://doi.org/10.1016/S0378-7753(99)00520-0

6. Diaz Geomayra, Martín D, Frías C, Sánchez F (2001) Emerging applications of ZINCEX and PLACID technologies. JOM 53:30–31. https://doi.org/10.1007/s11837-001-0009-8
7. Pan Junqing, Sun Yanzhi, Li Wei, Knight James, Manthiram Arumugam (2013) A green lead hydrometallurgical process based on a hydrogen-lead oxide fuel cell. Nat Commun 4:2178. https://doi.org/10.1038/ncomms3178
8. Doronin IE, Svyazhin AG (2011) Commercial methods of recycling dust from steelmaking. Metallurgist 54(9–10):673–681
9. Diaz G, Martin D (1994) Modified Zincex Process: the clean, safe and profitable solution to the zinc secondaries treatment. Resour Conserv Recycl 10:43–57. https://doi.org/10.1016/0921-3449(94)90037-X
10. Olper M, Maccagni M (2008) From C.Z.O. to zinc cathode without any pretreatment. The Ezinex process. Lead and Zinc 85–98
11. Nazari S, Gharabaghi M (2015) Investigation on life cycle assessment of lead and zinc production 49:245–252
12. Li H, Yao X, Wang M, Wu S, Ma W, Wei W, Li L (2013) Recovery of elemental sulfur from zinc concentrate direct leaching residue using atmospheric distillation: a pilot-scale experimental study. J Air Waste Manage Assoc 64(1):95–103. https://doi.org/10.1080/10962247.2013.827605

GCRIS

Part XXIII
Poster Session

GCRIS

Reaction Mechanism on a Novel Enhanced Smelting Technique for Lead-Acid Battery Paste Recycling

Wei Jin, Shenghai Yang, Yongming Chen, Yafei Jie, Shufeng Liu, Xinjie Deng, Yan Xi, Di Chang, Fang Hu and Yun Li

Abstract Lead-acid batteries contain a lot of valuable metals, such as lead, tin, copper, antimony, as well as waste plastic shells, and other harmful substances. Cleaner and efficient recycling of waste lead-acid batteries is of significance in environmental protection and comprehensive recycling of resources. In this study, oxygen-enriched side-blow pool smelting technique was developed and innovatively employed to recycle lead battery paste. This study investigated the reaction mechanism of lead recycling in lead paste–CaO–FeO–SiO_2–C reaction system. Therefore, the phase transformation and evolution of lead paste in oxidizing atmosphere were described in detail. XRD and SEM-EDS analysis results indicated that the whole reaction evolution can be summarized as follows: PbO and PbS were formed from $PbSO_4$ in a weak oxidizing atmosphere through the thermal decomposition and reduction reactions. Then, the lead oxide formed was combined with slag-forming components (CaO, SiO_2, and $FeC_2O_4 \cdot 2H_2O$) to generate new oxides phase. As the temperature increases, metallic lead was extracted and recycled through the reactions between lead sulfide and the new-formed oxide phase.

Keywords Oxygen-enriched enhanced smelting · Lead battery recycling · Secondary lead materials · Phase transformation · Lead extraction

Introduction

As one of the basic metal materials, lead has been widely used in lead-acid batteries, chemical anti-corrosion, communication equipment, and other fields. Currently, 80–85% of global refined lead was used in lead-acid batteries production [1–3]. With

W. Jin · S. Yang · Y. Chen (✉) · Y. Jie · S. Liu · X. Deng · Y. Xi · D. Chang · Y. Li
School of Metallurgy and Environment, Central South University, Changsha 410083, Hunan, China
e-mail: csuchenyongming@163.com

F. Hu
School of Chemistry and Chemical Engineering, Central South University, Changsha 410083, Hunan, China

© The Minerals, Metals & Materials Society 2020

A. Siegmund et al. (eds.), *PbZn 2020: 9th International Symposium on Lead and Zinc Processing*, The Minerals, Metals & Materials Series,
https://doi.org/10.1007/978-3-030-37070-1_86

the increase in the amount of car ownership and communication equipment in recent years, the demand for metal lead has been increasing. At present, based on the current mining scale, the expected exploitation years of the confirmed lead mineral resources are only ten years [4]. The lead mineral resources were rapidly depleted. Therefore, lead extraction from the recycled lead resources is of increasing significance for the lead production industry.

The main raw material for producing recycled lead is waste lead-acid battery, which mainly contained two types of batteries: PP battery and ABS battery [5, 6]. The lead-acid battery typically comprises the lead grid, lead sulfate paste, waste plastic, and other components [7]. The lead content in the lead paste of the two types of batteries accounts for more than 65% of the lead in the whole waste lead-acid battery. Processing the lead acid paste has become the key to a cleaner and efficient lead production. Typically, the lead acid paste consists of four components: $PbSO_4$ (50–55%), PbO_2 (25–30%), about PbO (5–10%), and Pb (3–8%) [8, 9]. The traditional lead smelting of raw material is lead sulfide concentrate, due to the large difference in physical and chemical properties between raw materials; the traditional lead smelting processes are not suitable for the production of recycled lead. Recycled lead smelting mainly used pyrometallurgy and hydro-pyrometallurgy combined processes to treat lead sulfate [10]. The hydrometallurgical process of lead sulfate paste mainly adopts two processes: "pre-desulfurization-leaching-electrolytic deposition" and "solid phase electrolytic reduction". However, many problems existed in the two technological routes, such as long process, high consumption of reagents, low production efficiency, high investment, and operation cost [11–13]. The pyrometallurgical treatment of lead paste is mainly divided into two technical routes: individual smelting and combined smelting of lead-containing wastes. However, the current pyrometallurgy cannot get rid of high energy consumption, low-metal lead recovery rate, and poor product quality [14–17]. The hydro-pyrometallurgy combined processes were generally firstly performed a lead paste pre-desulfurization process, and then, the desulfurized lead paste was subjected to the pyrometallurgical reduction smelting. However, the temperature in the furnace changed greatly due to the intermittent operation, the service life of the refractory in the furnace was short, and the productivity efficiency was low, which limited its development.

At present, the promising process for treating lead paste is an oxygen-enriched double-side-blow pool smelting process. With the advantages of high automation degree, clean and environmental friendly production process, stable product quality, and remarkable energy saving effect, it will gradually be the development trend of recycled lead smelting technology. However, the basic theoretical research on the lead paste oxidation smelting reaction mechanism in the oxygen-rich atmosphere is limited. In this study, X-ray diffractometer (XRD, D/Max 2550PC, Rigaku, Japan) and scanning electron microscopy equipped with a energy-dispersive spectrometer (SEM, TESCAN MIRA3 LMU; EDS, Oxford X-Max20) were used to determine the phase transformation mechanism of lead paste in oxidizing atmosphere.

Experimental Materials and Methods

Experimental Materials

The experimental raw material of lead paste was provided by a non-ferrous metal smelter. X-ray fluorescence spectrometry was used to analyze its main chemical composition. The results are given in Table 1. Chemical phase analysis of the lead paste is given in Table 2. It indicates that the lead paste contained 69% lead and 4.5% sulfur. Furthermore, it was found that 43.6% of the total lead was $PbSO_4$. PbO_2 and PbO accounted for 34.1% and 21.2%, respectively. XRD and SEM-EDS were used to analyze the phase of lead paste. The corresponding results are presented in Figs. 1 and 2.

Table 1 Chemical composition of lead paste, wt%

Element	Pb	S	Fe	CaO	SiO_2
Contents	69.09	4.46	0.50	0.91	10.31

Table 2 Chemical phase composition of lead paste, wt%

Element	$PbSO_4$	PbO_2	PbO	Pb	Pb_T
Contents	30.13	23.53	14.67	0.76	69.09
Ratio	43.61	34.05	21.23	1.11	100.00

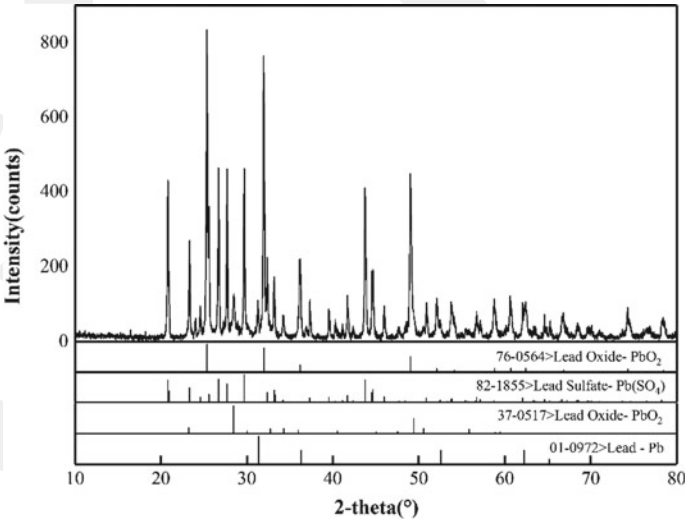

Fig. 1 X-ray diffraction pattern of lead paste

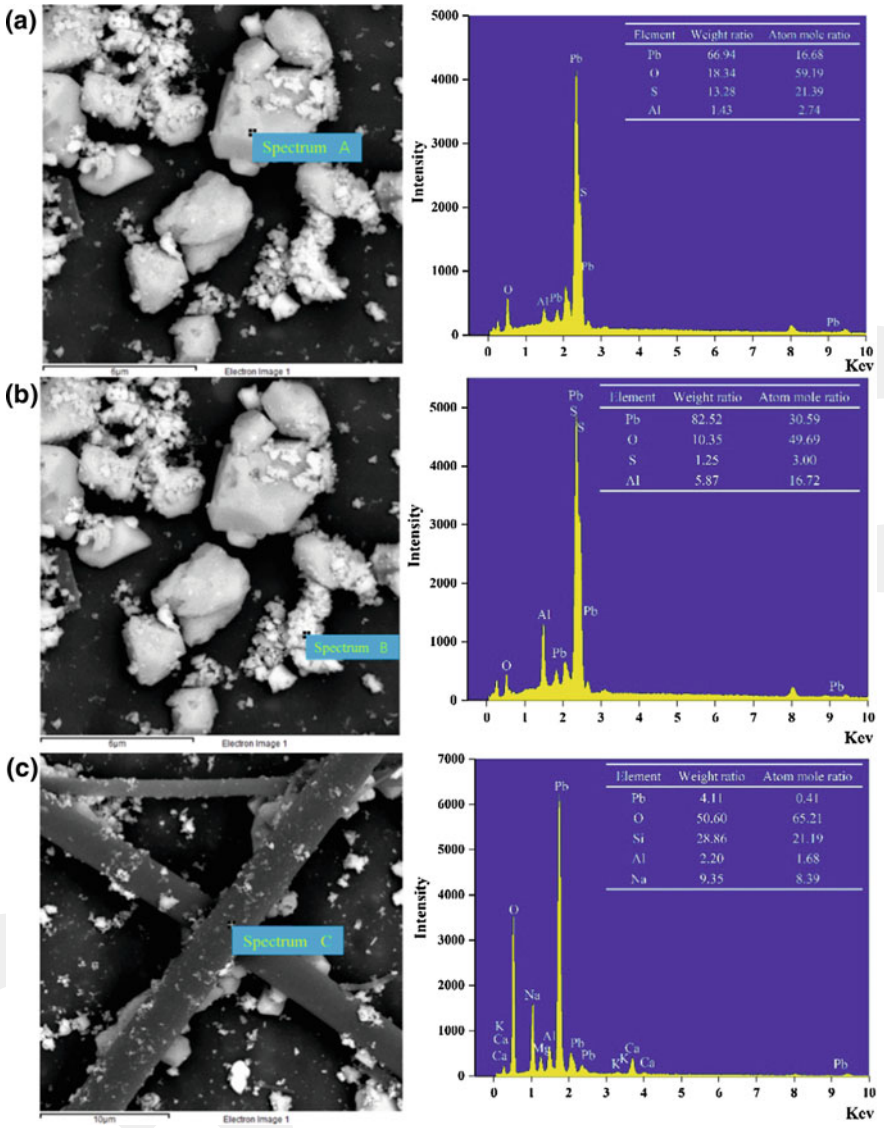

Fig. 2 SEM microstructure and corresponding EDS spectra of lead paste

Figure 1 shows the XRD patterns of lead paste. It is observed that $PbSO_4$, PbO_2, Pb, and a small number of gangues are the major components. As shown in Fig. 2, lead paste is mainly composed of three main elements: lead, oxygen, and sulfur. The big particle at point A was $PbSO_4$, and the small particles at B were PbO_2 and PbO. A large number of fibrous strips were detected in lead paste. It is highly probable

Na_2SiO_3 residue through the EDS analysis of point C, which remained in the crushing and sorting process of lead-acid batteries.

Experimental Methods and Equipment

The SiO_2, CaO, and $FeC_2O_4 \cdot 2H_2O$ chemical reagents used in this study were of analytical purity. After drying for 24 h, it was uniformly mixed with the lead paste according to the dosing principle and placed in the alumina crucible for smelting. The gas used was a O_2 and Ar mixed gas, and the gas flow rate was controlled at 140 ml/min and 60 ml/min, respectively. The reaction mechanism investigation was carried out in a horizontal tube furnace equipped with a gas mixing chamber, as shown in Fig. 3.

A thermocouple in an alumina sheath was positioned over the specimen to measure the experimental temperature. The right end of the alundum tube was connected with mixing chamber, and the left end was connected with NaOH solution to absorb SO_2 and SO_3 tail gas.

In this paper, systematic smelting tests were processed at different temperatures and times. The mixture was pushed slowly into the central heating zone of the furnace at preset temperature, after flushed with mixture gas, and held there for a preset time. The alumina crucible was taken out rapidly and quenched in water. The solid products were carefully separated and crushed for analysis preparation.

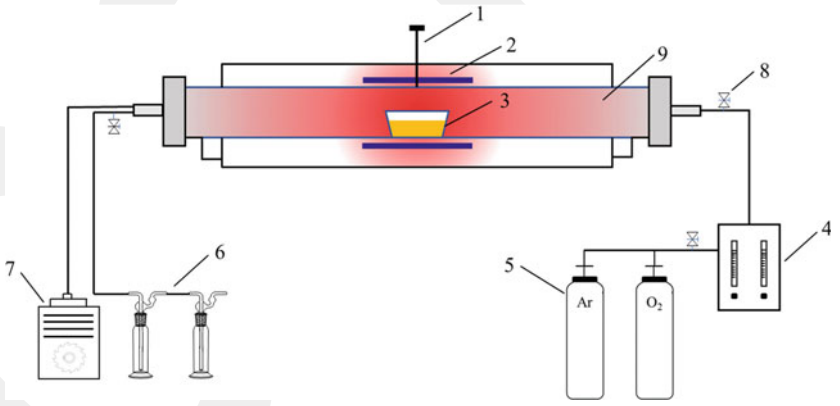

Fig. 3 Schematic of the experimental apparatus. 1. Thermocouple; 2. high-temperature alloy resistance wire; 3. specimen; 4. mixing chamber; 5. high-pressure tank; 6. NaOH solution; 7. vacuum pump; 8. valve; 9. alundum tube

Results and Discussion

Figure 4 shows the XRD pattern of solid smelting products generated from lead paste–CaO–FeO–SiO_2–C mixed reaction system at different temperatures and different reaction times. It was found in Fig. 4a that after reaction at 700 °C for 15 min, the PbS diffraction peak appeared, indicating that the reduction of $PbSO_4$ has been

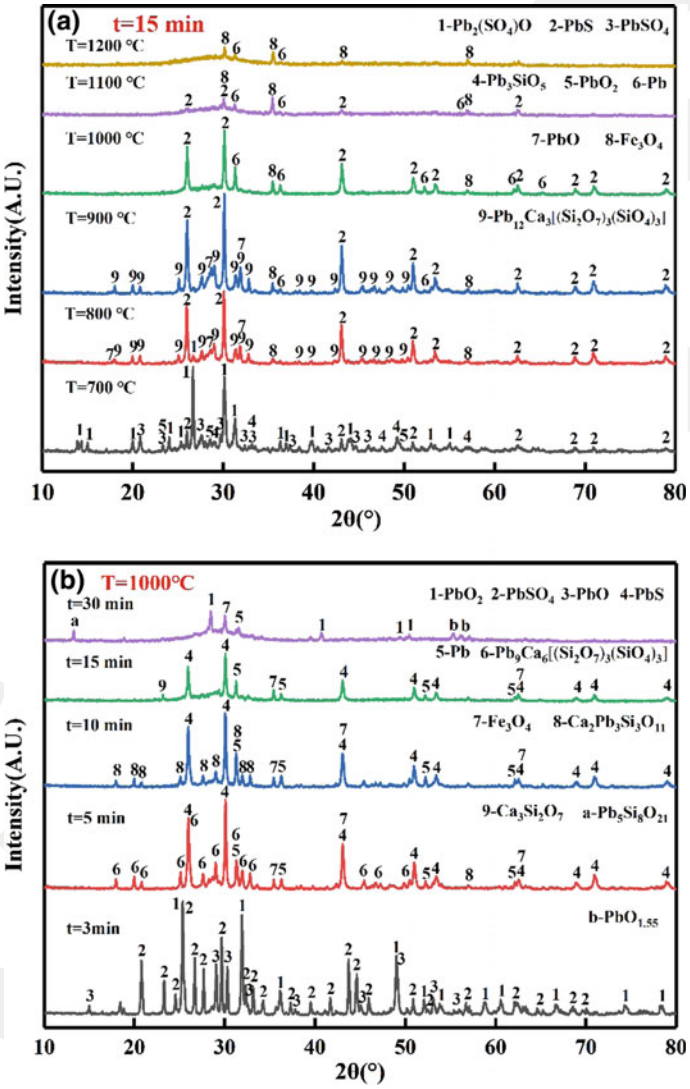

Fig. 4 The XRD pattern of solid products in lead paste–CaO–FeO–SiO_2–C mixture at different temperatures and different reaction times

carried out. At the same time, PbO combined with SiO_2 to form Pb_3SiO_5, and $PbSO_4$ decomposed to $Pb_2(SO_4)O$. With increased temperature, the PbS diffraction peak intensity enhanced. This indicated that the PbS content increased. Furthermore, it was observed that the Fe_3O_4 began to appear due to the gradual oxidization of FeO. When the temperature increased to 900°C, more PbO was combined with slag components compared with the low temperature. The main reactions in the system were the combination between lead, calcium, and silicon oxides, forming a new $Pb_{12}Ca_3[(Si_2O_7)_3(SiO_4)_3]$ mixture. The metallic Pb appeared illustrated that the exchange reactions between PbS and PbO occured at this temperature range. After 15 min of reaction at temperature exceeded 1000 °C, the solid products are comprised of PbS, Pb, and Fe_3O_4. The exchange reactions between PbS and PbO were completed. Metallic Pb was produced in large quantities as small particles. As the reaction continued, metallic Pb beads gathered and separate from the mixture. As a result, the diffraction peaks intensity of Pb weakened when temperature exceeds 1000 °C.

As shown in Fig. 4b, the reactions in the lead paste–CaO–FeO–SiO_2–C mixture were not obviously carried out before 3 min of reaction at 1000 °C. When the reaction time was extended to 10 min, PbS was detected. This suggested that the reduction reaction of $PbSO_4$ took place firstly in a relatively short time. At the same time, metallic Pb was also detected. This indicated that the PbO initially immobilized in the $Pb_9Ca_6[(Si_2O_7)_3(SiO_4)_3]$ and $Ca_2Pb_3Si_3O_{11}$ reacted with PbS. When the reaction time was extended to 15 min, the individual PbO disappeared. The exchange reactions between PbS and PbO were completed, and the final products were PbS, Pb, Fe_3O_4, and slag components. A large number of lead beads formed and concentrated into liquid lead and separated from the solid products; therefore, the diffraction peaks intensity of Pb became weak in the XRD patterns at the reaction time of 15 min and 30 min. Finally, the elemental lead in the solid product was present as metallic lead and lead oxide after 30 min of reaction at 1000 °C. At the same time, PbS disappeared, which indicated that the lead oxide was more stable in oxidizing atmosphere.

In order to further investigate the formation path of metallic Pb, SEM-EDS analysis was subjected to characterize the exchange reactions between PbS and PbO. Figure 5 illustrated the results of the product in the lead paste–CaO–FeO–SiO_2–C mixture at 900 and 1000 °C after 10 min of reaction time.

As shown in Fig. 5a, the main reactions in the system at 900 °C before 10 min of reaction were the combination between lead, calcium, silicon, and iron oxides. The lead-iron-silicon oxides existed as two phases which were different from the lead content. The transformation regions of $PbFe_{0.13}Si_{0.38}O_{1.88}$ to $PbCa_{0.58}SiO_3$ were clearly divided into three parts. The lead content in each region was analyzed by EDS. The results showed that the lead content decreased from 81.24 to 67.03 wt.% from the light region to the black region. This indicated that PbS reacted with PbO to convert it to metallic Pb, resulting in a gradual decrease of lead content in mixed oxides near the metallic Pb phase. It was further observed in Fig. 5c, d that metallic Pb inserted in the intersection of PbS and PbO-containing oxide mixture, which also confirmed that the metallic Pb was formed by the exchange reactions between PbS and PbO.

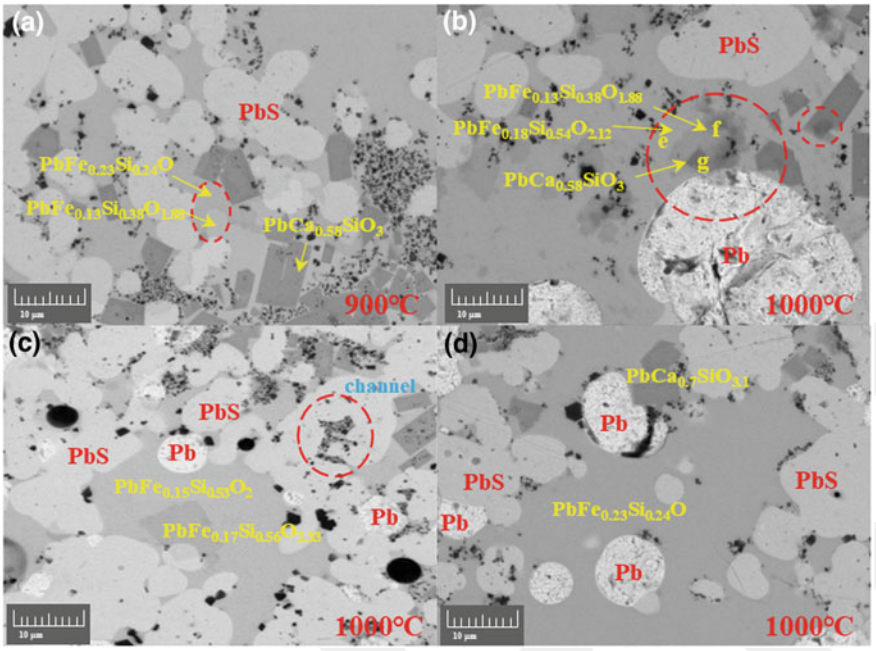

Fig. 5 SEM micrographs of products in the lead paste–CaO–FeO–SiO_2–C mixture at 900 and 1000 °C for 10 min of reaction

Conclusions

A novel lead paste recycling process by oxygen-enriched side-blow pool smelting technique was experimentally confirmed to be feasible. The phase transformation mechanisms were clarified. The thermal decomposition reactions and reduction reactions of lead paste in a weak oxidizing atmosphere took place. Lead oxide and lead sulfide formed, respectively. The reaction mechanism was summarized as follows: $PbSO_4 = 1/2\ PbO \cdot PbSO_4 + 1/2SO_2(g) + 1/4O_2(g)$; $PbSO_4 + 4C = PbS + 4CO(g)$. As temperature increased, the main reactions in the system were combination between lead oxides, calcium oxides, and silicon oxides, forming a $Pb_{12}Ca_3[(Si_2O_7)_3(SiO_4)_3]$ mixture. Then, the PbO immobilized in the $Pb_9Ca_6[(Si_2O_7)_3(SiO_4)_3]$ and $Ca_2Pb_3Si_3O_{11}$ reacted with PbS to generate metallic Pb. The reaction path was briefly summarized as follows: $PbS + 2PbO \cdot Ca_xSi_yFe_zO_h = 3Pb + SO_2(g) + 2Ca_xSi_yFe_zO_h$. The reaction mechanism regarding the lead extraction from the spent lead-acid battery paste in the oxygen-enriched smelting process provides a theoretical guidance for the secondary lead recycling and production.

Acknowledgements We are grateful to Hunan Provincial Science Fund for Distinguished Young Scholars, China, grant number 2018JJ1044, for providing financial support.

References

1. Liu W, Tian J, Chen L, Guo Y (2017) Temporal and spatial characteristics of lead emissions from the lead-acid battery manufacturing industry in China. Environ Pollut 220:696–703
2. Zhang W, Yang J, Wu X, Hu Y et al (2016) A critical review on secondary lead recycling technology and its prospect. Renew Sustain Energy Rev 61:108–122
3. Zhang L, Xu Z (2016) A review of current progress of recycling technologies for metals from waste electrical and electronic equipment. J Clean Prod 127(19–36)
4. Wang J, Meng L, Hu X (2018) Analysis of lead pollution and lead resources in lead battery industry chain. Chinese Battery Ind 4(16)
5. Ellis TW, Mirza AH (2010) The refining of secondary lead for use in advanced lead-acid batteries. J Power Sources 195:4525–4529
6. Li M, Liu J, Han W (2016) Recycling and management of waste lead-acid batteries: a mini-review. Waste Manage Res 34(4):298–306
7. Pavlov D (2017) Lead-acid batteries: science and technology, Elsevier
8. Ning P, Pan J, Li X, Zhou Y, Chen J, Wang J (2016) Accelerated desulphurization of waste lead battery paste in a high-gravity rotating packed bed. Chem Eng Process 104:148–153
9. Lin D, Qiu K, Recycling of waste lead storage battery by vacuum methods. Waste Manag 31(7):1547–1552
10. Li Y, Yang S, Taskinen P, He J, Liao F, Zhu R, Chen Y et al (2019) Novel recycling process for lead-acid battery paste without SO_2 generation—reaction mechanism and industrial pilot campaign. J Clean Prod 217:162–171
11. Pan J, Zhang X, Sun Y, Song S, Li W, Wan P, Preparation of high purity lead oxide from spent lead acid batteries via desulfurization and recrystallization in sodium hydroxide. Ind Eng Chem Res 55(7):2059–2068
12. Singh A, Karandikar PB, Review on desulfation of lead-acid battery for HEV. Int J Curr Eng Sci Res 2(9):85–96
13. Jeong K-P, Kim JG, Lead acid battery recycling and material flow analysis of lead in Korea. J Mater Cycles Waste Manag 20:1348–1354
14. Kreusch MA, Ponte MJJS et al, Technological improvements in automotive battery recycling. Res Cons Recycl 52(2):368–380
15. Tang C, Tang M et al, Pilot test of reduction-matting smelting of jamesonite concentrate with short rotary furnace. Min Metal Eng 24(1):51–53
16. Li Y, Tang C, Chen Y, Yang S, Guo L, He J, Tang M, One-step extraction of lead from spent lead-acid battery paste via reductive sulfur-fixing smelting: thermodynamic analysis. In: Hwang JY et al (eds), 8th international symposium on high-temperature metallurgical processing. The minerals, metals & materials series. Springer, Cham, pp 767–777
17. van der Kuijp TJ, Huang L, Cherry CR, Health hazards of China's lead-acid battery industry: a review of its market drivers, production processes, and health impacts. Environ Health 12(1):61

Author Index

A
Abadías Llamas, A., 351
Abe, S., 593
Afsara, Syeda, 947
Alam, Shafiq, 821
Antrekowitsch, J., 309, 437
Araújo, Mateus Felipe Lourêdo, 247, 827

B
Bai, Hua, 301
Balgimbaeva, U. A., 429
Bartie, N. J., 351
Bauer, Ino, 739
Baxter, Ken, 135
Behrmann, Dirk, 187
Bergs, Alexander, 683
Blanco, Jorge, 913, 925
Blanpain, Bart, 237
Breuer, Thomas, 187
Brooks, Geoffrey, 173

C
Cao, Jian, 633
Cau, Tony, 135
Chang, Di, 961
Chen, Cui, 301
Chen, Longyi, 877
Chen, Mao, 539
Chen, Pan, 633
Chen, Song-xuan, 51
Chen, Xiangqiang, 275
Chen, Xue-gang, 51
Chenyang, 633
Chen, Yongming, 961
Chintinne, Mathias, 237
Chou, Kuo-Chih, 51
Chung, Kyeong Woo, 253
Close, R., 165
Cooper, Tom, 135
Crivits, Tijl, 173
Cui, Kaihui, 707
Cui, Wenzhao, 539
Cybulski, Andrzej, 729
Czettl, Christoph, 661

D
Dahlstrom, James, 695
Davis, Boyd, 41
Degel, Rolf, 683
Deng, Xinjie, 961
Deschênes, Jean-Michaël, 767
Dias, Maria José, 247
Doganov, Georgi, 321
Dong, Ze-shang, 31
Dreisinger, David, 135
Drezdzon, Mark A., 777, 551

E
Ebner, Tamara, 661
Elias, F., 605
Ellis, Timothy, 777
Ellis, Timothy W., 551
Estrada, Florentino, 365

F
Filho, Tone Takayama, 101
Filzwieser, Andreas, 683

© The Minerals, Metals & Materials Society 2020

A. Siegmund et al. (eds.), *PbZn 2020: 9th International Symposium on Lead and Zinc Processing*, The Minerals, Metals & Materials Series,
https://doi.org/10.1007/978-3-030-37070-1

Fleuriault, Camille, 557
Fonseca, D., 605
Fraser, Alex, 767
Frias, Carlos, 913, 925

G
Gao, Zhiyong, 633, 847
Genderen van, Eric, 491
Georgakopoulos, Evangelos, 811
Gonçalves, G., 605
Gonzales, Gian Piero Pajuelo, 101
Gotor, Joaquin, 913
Gou, Hai-Peng, 51
Gregurek, D., 19, 557
Grogan, Joseph, 41, 695
Grund, Sabina, 491
Guerrini, Edoardo, 581, 785
Gül, Erkan, 447
Guo, Muxing, 237

H
Hammerschmidt, Jörg, 377
Hanel, Martina, 683
Han, Haisheng, 633, 847
Hanke, G., 309, 437
Hasegawa, N., 593
Hassall, Claire, 615
Haus, Steffen, 377
Hayes, P. C., 337
Heegaard, Bror Magnus, 391
He, Xingmin, 301
He, Y., 291
Heibeck, M., 351
Hesterberg, Travis, 551, 777
Hidayat, T., 337
Hirata, Koichiro, 519
Hirsi, Tuomas, 891
Hosseini, Ashkan, 811
Hu, Fang, 961
Hughes, Stephen, 63
Hussaini, Shokrullah, 447
Hu, Yuehua, 625, 633, 847, 899
Hymer, Timothy, 111

I
Ichiya, Kenji, 865
Imris, Matej, 391
Ito, S., 593

J
Jak, E., 337
Jiang, Kaixi, 853
Jiang, Tao, 673
Jie, Yafei, 961
Jin, Wei, 961

K
Kamimura, Gen, 905
Kaya, Muammer, 447
Kerry, Timothy, 811
Kim, Jonghyun, 253
Kim, Min-seuk, 253
Körbler, Nadine, 661
Krassnig, Hans-Jörg, 683
Kubota, N., 91
Kudo, T., 91
Kurniawan, 253
Kursunoglu, Sait, 447
Kyurkchiev, Aleksander, 799

L
Lahtinen, Marko, 365
Lakshmanan, V. I., 821
Lan, Dailong, 653
Lebel, Trevor, 41
Lee, Jae-chun, 253
Leite, Thiago O. N., 231
Liao, Tianqi, 707, 935
Li, Dong-bo, 31
Li, Guanghui, 673
Li, Jing, 707, 935
Lima de, Juliano Alves, 101
Li, Ming-chuan, 51
Li, Peng, 31
Liu, A., 165
Liu, Cheng, 31
Liu, Runqing, 625, 633, 847
Liu, Shufeng, 961
Li, Yun, 961
Luidold, Stefan, 661
Luo, Yongguang, 707, 935
Lux, Timm, 683

M
Maccagni, Massimo, 581, 785
Margraf, Rüdiger, 187
Martins, Eder Lucio, 101, 231
Martins, Júlia M., 231
Ma, Shaobin, 265
Matsuura, Dai, 865

Matsuura, Hiroyuki, 905
Mendes, Felipe Ramos Pereira, 827
Minchev, Emil, 799
Miwa, K., 759
Moats, Michael, 111, 123
Moreno, Natalia, 913, 925
Murai, Ryota, 885

N
Nagraj, Samant, 237
Nakano, H., 593
Nicol, Stuart, 41
Ni, Zhangyuan, 625
Nyberg, Jens, 391

O
Offerman, Erik, 811
Okajima, Nobuaki, 531
Okuyama, Goro, 885
Oliveira de, Caio César Spindola, 247, 405, 827

P
Pastor, Luis, 925
Pei, Zhong-Ye, 51
Penchel Jr., Sérgio A., 231
Peng, Zhiwei, 673
Pereira, Daniel Dayrell, 247, 405, 827
Peters, Alexander, 811
Pina, Pablo S., 231
Pusateri, John F., 75

Q
Qin, S. C., 835
Qin, Shuchen, 853
Qi, Zhen, 479
Qu, Hongtao, 707, 935

R
Radonov, Georgi, 799
Raiford, Matthew, 721
Rao, Mingjun, 673
Reed, M. E., 165
Reemeyer, L., 507
Reinharter, K., 19, 557
Reuter, M. A., 351
Rhamdhani, Akbar M., 173
Roberts, Huw, 3
Rodrigue, Benjamin, 695
Runkel, Marcus, 377

S
Sakata, Yusuke, 569
Salminen, Justin, 391
Sanchez, Francisco, 913
Satoh, S., 759
Sato, Ryosuke, 519
Saxén, Björn, 365, 891
Schiemann, Robert, 377
Schmidl, J., 19
Scott, Margaret, 123
Shang, Wenxing, 673
Sharipov, R. Kh., 429
Shevchenko, M., 337
Shibata, Etsuro, 285
Shinoda, Mariko, 885
Shishin, D., 337
Soler, Juan Pedro, 925
Song, Shaole, 899
Song, Yan, 275
Souza de, Adelson Dias, 247
Spanring, A., 19, 557, 605
Sridhar, R., 821
Starev, Nikolay, 321
Stelter, M., 351
Storf, Christian, 661
Stoychev, Stefan, 799
Suleimenov, E. N., 429
Sumi, Ikuhiro, 885
Sun, Lei, 633, 847
Sun, Wei, 625, 633, 847, 899

T
Takayama, Tone, 231
Takaya, S., 91
Takei, Takuma, 531
Tanaka, Fumito, 519
Tang, Honghu, 847, 899
Tang, Kaile, 469
Taylor, Patrick R., 419
Teixeira, Fabiana M., 231
Thompson, L., 165
Tirpak, Brandon, 75
Tu, Fubing, 469

U
Usami, Yasuo, 865
Usui, Shojiro, 531

V
Vanparys, Robin, 173
Vera, Edward, 913

W
Wang, Changtao, 625
Wang, Haibei, 835, 853
Wang, Jianming, 327
Wang, Jie, 673
Wang, Li, 847, 899
Wang, Liancheng, 673
Watanabe, H., 91
Waters, Nick, 135
Weber, Peter, 187
Wei, Junyan, 653
Wet de, J. R., 75
Wilson, David, 63
Wood, Jacob, 63
Worland, Andrew, 135
Wrobel, Maciej, 365
Wu, Weiguo, 275, 327, 653
Wu, Xiaosong, 201

X
Xin, Pengfei, 327, 653
Xi, Yan, 961
Xi, Yunhao, 707, 935
Xu, Liang, 265, 275, 653

Y
Yamaguchi, E., 759
Yamaguchi, Takuhiro, 221
Yamaguchi, Toyoshi, 885
Yang, Lei, 673
Yang, Shenghai, 961
Yang, Yongxiang, 811
Yang, Yue, 633, 899
Yao, Xin, 31
Yuan, Zhang Fu, 479
Yue, Tong, 847

Z
Zhang, 633
Zhang, Bangsheng, 853
Zhang, Ge, 275
Zhang, L., 291
Zhang, Leru, 469
Zhang, Libo, 707, 935
Zhang, Ling, 291, 469
Zhang, Te, 707, 935
Zhang, Wanjia, 633
Zhao, Baojun, 539
Zheng, C. Z., 835
Zheng, Leixia, 673
Zou, Jingtian, 707, 935
Zschiesche, Christoph, 739

GCRS

Subject Index

A
Acid leaching, 886
Actual ore flotation tests, 637
Additives, 20, 111, 115, 118, 123–126, 128, 130, 195, 448, 793
Adsorption coprecipitation, 707, 711, 713, 716
Adsorption work, 479, 481, 485, 486
Advanced automotive lead batteries, 723
Advanced fuels and reductants, 70
Alkaline, 123, 124, 126, 253, 254, 256, 260, 261, 431, 448, 524, 626, 788, 793, 887
Alkaline leaching, 254, 255, 262
Alkaline treatment, 887
Aluminium, 511, 687, 729, 919, 925–929, 931–933, 953
Aluminium discs rotational speed, 928
Ammonium chloride, 582, 583, 788, 793, 794
A method of lead decoppering and production of metallic Al-Cu foam and Al-Cu drosses, 731
Analysis of Fe behavior under different oxygen pressure leaching conditions, 878
Analysis of the volume fraction of oxygen in melt, 37
Analysis results and countermeasures, 602
Antimony, 4, 5, 285, 286, 305, 306, 329–331, 369, 534, 554, 593, 653–655, 657, 660, 674, 695, 697, 700, 703, 704, 746, 748, 750, 752, 765, 948, 961
Antimony smelting, 214
Antimony smelting slag, 653, 654, 656–660
Application of CSC technology, 205, 217
Applications of Pb in energy harvesting, 780
Ascorbic Acid (AA) leach, 465
Assessment of metal bearing by-products, 314
Atmospheric leaching, 84, 914–919, 921
Ausmelt smelting, 6, 321
Autoclave renewal, 865, 867, 868, 874
AZR flame reactor on-site EAF dust recycling process, 82
AZR history, 76

B
Base metals recovery, 285
Battery, 3, 5–15, 19, 21, 26, 84, 147, 166, 168, 275, 421, 545, 551–554, 557, 558, 569–573, 575, 577, 579–582, 585, 586, 589, 591, 593, 594, 601, 602, 606, 695, 696, 707, 708, 711, 713, 716, 721–725, 731, 734–736, 777–781, 900, 947, 948, 961, 962, 968
Blast furnace, 20, 71, 165–168, 170, 171, 173–177, 183, 184, 207, 214, 237, 291, 423, 519, 520, 558, 569, 570, 573, 574, 576, 885–887, 889
Blast furnace and sinter plant operation, 166
Bleed treatment, 159
Blood Lead (Pb's), 551–553, 594, 597, 741
Bottom blowing reduction smelting, 330
Bottom-blown bath, 31
Boundary conditions, 36, 473
Broad operation temperature range, 688
Burtite synthesis, 521
Business segments of JX nippon mining & metals group, 531

© The Minerals, Metals & Materials Society 2020

A. Siegmund et al. (eds.), *PbZn 2020: 9th International Symposium on Lead and Zinc Processing*, The Minerals, Metals & Materials Series,
https://doi.org/10.1007/978-3-030-37070-1

By-products, 312

C

Cake-washing method improvement, 865
Capacity of the Waelz kilns, 803
Cathode starter sheet fabrication, 159
Cellhouse parameters, 118
Cementation, 85, 103, 253–255, 259–262, 369, 584, 674, 704, 789, 790, 905, 906, 909–911, 917, 919, 921, 925–933, 947, 948, 954
Cementation pilot plant design and operation, 930
Cemented carbide, 662, 663, 666, 670, 671
Chalcopyrite, 856
Challenges, 394
Characteristics of main minerals in ore sample, 855
Characteristics of precipitate after chlorine removal reaction, 942
Characterization, 315, 438
Characterization of the slags, 42
Charge transfer, 112
Chemical analyses, 564
Chemical reactions, 471
Chinese zinc market, 620
Chloride media, 918, 925, 926, 932
Chloride volatilization, 835
Chlorine, 537, 709, 807, 808, 935–944, 948, 950
Choosing a path for development, 800
Circular economy, 310, 352, 499, 502, 503, 581, 785
Circularity, 363, 392, 492, 495, 497
Citric acid ($C_6H_8O_7$) leach in absence of NaCl, 455
Citric acid ($C_6H_8O_7$) leach in presence of NaCl, 461
Climate change, 492, 502
Closed circuit flotation index, 630
Closed mine monitoring, 593, 594
Closing comments and outlook for secondary lead production, 14
Cobalt, 275, 277, 286, 369, 662–664, 670, 671, 673, 674, 676, 678–680
Cobalt removal and recovery, 902
Coke, 173–184
Collective concentrate, 431, 432
Collector, 206, 207, 209–211, 294, 317, 627, 628, 630, 631, 633–641, 643–647
Commissioning of the new lead refinery in 2014, 740
Comparison with box fuming process, 71
Comparison with plasma process, 72
Comparison with side blowing process, 71
Comparison with Waelz kiln process, 70
Compiled operational experience, 754
Comprehensive utilization, 306, 328, 329, 333, 839
Concentrate leaching, 365, 366
Concentrate mineralogy, 154
Construction and start-up of the new No. 3 electrowinning plant, 225
Construction materials, 275
Contact angle measurement, 637, 641
Continuity equation, 471
Continuous removal of copper in crude lead, 330
Contrast of indexes of zinc residues treatment, 272
Cooling elements, 67
Cooling tower control, 89, 193, 226, 227
Cooling tower efficiency, emissions and effect on product losses, 894
Copper, 21, 32, 65, 67, 68, 71, 118, 168, 191, 201, 203–206, 209, 210, 213, 216, 217, 237, 239, 292, 309, 311, 313, 314, 357, 359, 440, 442–444, 448, 494, 519–521, 569, 570, 572, 576, 622, 629–631, 685, 687, 691, 786, 848, 878, 899–901, 903, 913, 915–917, 925, 926
Copper smelter, 287, 534–536, 539–543, 545, 546, 594
Copper smelting, 285, 287, 288, 344, 531, 534, 538–540, 759, 761
Copper smelting waste treatment, 216
Corrosive damage on the CF water cooling jacket, 577
Co—Zn phases, 661, 663, 665–668, 670, 671
Crude lead, 321, 329, 540, 740, 742, 746, 748, 750, 751, 753, 761
Crystallization, 113
CSC smelting furnace, 203, 204, 207, 209, 212, 213, 216
CSC technology commercial experimental research, 212
CuCl precipitate, 935, 941–944
Current challenges about tin metal production, 766
Current efficiency, 85, 103, 111, 115, 116, 119, 122, 575, 585, 791, 792
$CuSO_4$ and copper, 935, 944

D
Decoppering, 729–733, 735, 736
Definitive feasibility methodology, 153
Definitive feasibility study, 147
Demonstrative lead-zinc smelting process, 301
Demo plant, 793
Description of oxygen-enriched air side blown furnace, 292
Design criteria for the new lead refinery, 749
Design of green smelting project, 301
DFT calculation and wavefunction analysis of simplified coordination model, 638
DFT calculations, 643
Digital evolutions in the process industry, 379
Digitalization, 378–380, 386
Digital know-how, 384, 386
Digital process know-how and its usage in advanced plant operation, 382
Direct leaching, 392, 405, 408
Direct leaching processes, 408
Discrete phase model, 471
Disturbance analysis of gas jet on equipment in furnace operation, 38
Dust-recycling, 885
Dusts, 6, 231, 232, 285, 303, 515, 533, 539–541, 545, 546, 594, 596, 759, 799, 800, 803–807, 811–813, 815–818

E
EAF dust, 20, 63, 66, 75–79, 81–83, 91–93, 95–97, 288, 289, 494, 812, 905, 906, 911
Effective use of lead smelters, 288
Electrowinning, 289
Electric Arc Furnace Dusts (EAFD), 70, 458, 786, 787, 789, 793, 794, 796
Economic considerations, 317, 444
Economics, 7, 507, 514, 589, 723
Economics of lead and zinc mine production in North America, Europe and Australia, 514
Effect of adhered sulfuric acid, 577
Effect of chlorinating agent content under no pulverized coal, 840
Effect of chlorination agent content under pulverized coal, 841
Effect of H_2SO_4 on leaching, 860
Effect of leaching time, 256
Effect of NaOH concentration, 256
Effect of oxidation of zinc powder on purification of high-cobalt zinc sulfate solution, 678
Effect of pH and influence of hydrogen peroxide addition on the purification of the leachate, 888
Effect of pH on acid leaching, 887
Effect of pulp density, 257
Effect of roasting temperature under pulverized coal, 842
Effect of temperature, 257, 261
Effect of temperature on leaching, 859
Effect of the quantity of Zn powder, 260
Effect of time on the cementation of lead, 260
Effects of $CuSO_4$ concentration on chlorine removal, 941
Effects of reaction temperature on chlorine removal, 938
Effects of reaction time on chlorine removal, 939
Effects of zero-valent copper concentration on chlorine removal, 940
Effects on economic, 361
Effects on society, 360
Effects on the environment, 360
Electric arc furnace dust, 231
Electric furnace, 205, 206, 440, 469, 886
Electrochemical leaching, 429
Electrogalvanizing, 123
Electrolysis, 112, 115, 227, 248, 249, 393, 406, 500, 570, 572, 575, 576, 582, 585, 788, 790–792, 848, 886
Electrolyte temperature drop and piping blockage, 226
Electrolytic refining, 331
Electrowinning, 77, 84, 89, 101, 102, 111, 113–115, 117, 135, 136, 140, 141, 143, 148, 151, 153–159, 221–225, 228, 229, 231, 253, 277, 304, 351–353, 357, 358, 365–367, 369, 393, 405, 408, 582, 584, 589, 780, 786–791, 799, 827, 839, 891, 892, 900, 911, 947, 948, 950, 954
Electrowinning and cathode handling, 157
Electrowinning process, 351, 827, 900
Electrowinning unit, 791
Emissions and their associated environmental impact, 357
Employment and operations along the value chain, 501
Energy and climate resilience, 500
Energy storage systems for grid services, 724

Environmental management in smelting operations, 552
Equipment design improvements, 745
E-scrap, 287, 289
Estimated capital cost, 161
Evaporation/crystallization, 793
Exergy, 351, 355, 356, 361, 363
Existing flotation concentrator modifications, 148
Expansion by atmospheric direct Leaching, 367
Experimental materials, 709, 963
Experimental methods and equipment, 965
EZINEX® process, 788, 954

F
Factory configuration, 328
FactSage, 237, 240, 244
Fast Pb process, 582
Features and technologies of non-ferrous smelters in Japan, 287
Feed preparation, leaching and solid/liquid separation, 156
Ferro alloy, 26
Filter modification, 865, 873
Filter technology, 195
First operational results, 371
Flash smelting, 469–471, 473
Flotation, 248, 295, 396, 402, 437, 442–445, 447, 448, 451, 452, 457, 459, 468, 625–643, 645–647, 914, 917, 919, 921
Flotation process development, 141
Flotation tests, 442
Flue dust, 811
Fluorine wastewater treatment, 602
Formic Acid (FA) leach, 465
Fuming, 20, 64–68, 70–73, 79, 207–214, 237–244, 291, 293, 294, 296–299, 351, 354, 356–362, 391, 395, 397–402, 794–796
Fuming Furnace (FF), 41, 265–267, 270, 271, 305, 327, 330, 332, 333, 335, 653–660
Fuming furnace blowing smelting, 330
Fuming stage, 296
Fundamental studies to improve lead battery performance, 724
Furnace body, 191
Furnace hearth, 191
Future application of CSC technology, 217

G
Galena, 419, 425, 430, 560, 625–631, 633, 635–643, 645–647
Galena-pyrite bulk flotation, 627
Galena-pyrite separation, 628
Gas-liquid mixing, 31, 33, 39
General, 189
General application overview for iltec in metallurgical plants, 690
Geometry and mesh, 470
Germanium, 268, 275, 303, 673, 674, 676, 678–680
Global growth of secondary lead production since 1990, 6
Goethite, 66, 352, 392, 394, 408, 409, 437, 438, 452, 847–852, 879, 881
Gypsum removal efficiency in Torreón, 896

H
Hardware, 689
Health and wellbeing, 499
Heat balance control, 68, 396, 414
Heat recovery, 691
Heat removal and specific heat capacity, 688
Hematite, 352, 409, 413, 414, 827, 829, 831, 879–881
Hematite plant, 865, 866
High Alkaline Preferential Process (HAPP), 625, 626, 630–632
High electrical conductivity, 688
High soda supply, 29
HIsarna, 811, 812, 818
Historical operation, resources and challenges, 137
History and milestones of ILTEC, 684
Hull cell, 123, 125–130
Hull cell testing, 125
Hydrogen-lead oxide fuel cell, 951
Hydrometallurgical facility, 151
Hydrometallurgical facility design basis, 153
Hydrometallurgy, 430, 847, 848, 851, 852, 877, 899, 900, 903
Hydrometallurgy process development, 142
Hydroxide precipitation (lime slaking), 700

I
Identifiers, 767, 768, 774
ILTEC, 683–685, 689–691
Implementation, 369
Implementation in customer plant level, 383
Importance of ISP, 288

Improved Pb materials for lead batteries, 553
Improvement in zinc recovery rate, 95
Improvement of cake-washing operation, 871
Improvement of hoods of short rotary furnaces, 596
Improvement of occupational health and safety and environmental protection, 742
Improvement of the nighttime power rate, 228
Improvement of working environment around furnaces, 594
Improvements of separation work of waste lead-acid battery, 602
Impurities, 20, 71, 85, 86, 89, 111, 114–118, 120–122, 124, 254, 259, 261, 262, 309, 377, 393, 397, 399, 406, 407, 421, 444, 448, 453, 463, 468, 519, 584, 787, 790, 791, 794, 827, 829, 832, 848, 899, 914, 917, 922, 925, 927, 931
Impurities in Zn concentrates, 406
Impurity removal and electrolyte preparation, 156
Increased furnace availability, 693
Increasing oxygen enrichment, 68
Increasing safety, 690
Increase of Sn Input, 761
Industrial scale application, 691
Industrial treatment technologies, 696
Industry structure, 512
Influence of metallic elements, 575
Influence of minor elements, 575
Influence of organic substances (separator), 579
Inorganic acid leach (HCl, H_2SO_4, and HNO_3), 453
İnorganic acids, 447–449, 453–455
Integrate INDUTEC®/EZINEX® process, 794
Integration, 772
Introduction of new granulation process, 93
Ionic liquid, 683–688, 690, 691
Iron co-precipitation, 697
Iron oxide attack, 25
Iron precipitation as goethite during oxygen pressure leaching, 879
Iron precipitation as hematite during oxygen pressure leaching, 881
Iron precipitation as jarosite during oxygen pressure leaching, 879
Iron removal, 249, 393, 408, 412, 827, 829, 848, 849, 851
Isasmelt process, 948

J
Jarosite, 66, 70, 314, 352–363, 365–368, 371–373, 375, 391–394, 396, 397, 399, 402, 419, 437–445, 827, 829, 830, 832, 837, 848, 861, 866, 879–881
Jarosite residue, 372, 835–839, 844
Jarosite treatment, 356, 359, 360, 437

K
Kiln temperatures & reaction zone control, 79
Kosaka flow, 759
Kuettner thermodynamic process model, 197

L
Laboratory tests, 196, 559, 563, 568
Lance, 43, 265, 268, 269, 287, 321, 753, 948
Largest scale, 327
Laser marking, 767–769, 771–775
Laser marking process, 768
Latest relevant progress, 853
Leachate purification, 789
Leaching, 20, 52, 63, 64, 86, 101, 102, 107, 108, 118, 135, 136, 141–143, 151, 153–156, 159, 160, 201, 209, 212, 213, 221, 247–251, 253–259, 265–268, 277, 286, 303, 304, 306, 328, 353–357, 365–369, 371–373, 375, 392–395, 397–399, 401, 402, 405, 406, 408, 412, 419–421, 423, 425, 429–431, 433, 434, 437, 438, 441, 443, 447–449, 452, 453, 455–468, 521, 522, 535, 539–541, 545, 546, 583, 585, 586, 589, 618, 654, 673, 674, 677, 759, 762, 764, 786, 788–790, 799, 800, 802, 803, 805, 807, 808, 821–824, 827–832, 836, 837, 847, 848, 853, 854, 859–863, 865–868, 871, 874, 877, 878, 880, 885–889, 891, 899–903, 906, 913, 915, 916, 918, 919, 921, 926, 931, 947, 948, 950, 952–954, 956, 962
Leaching of zinc, 822
Leaching test, 859

Lead, 3–15, 19–23, 25, 26, 29, 41–49, 51, 52, 58, 63, 65, 66, 71, 76, 91, 103, 104, 135–138, 140–143, 147, 148, 151, 153–159, 162, 163, 165–169, 187–189, 191, 192, 201, 203, 207–214, 231, 237, 253–255, 258, 260–262, 265–270, 272, 274, 275, 277–279, 285–289, 291–299, 301–307, 309–311, 313, 314, 316, 317, 321–325, 327–331, 333, 335–338, 341–347, 355, 357, 359, 365–367, 371, 372, 374, 380, 381, 399, 419–421, 423, 425, 426, 429–434, 437–444, 447, 469, 470, 473, 474, 479–486, 507–516, 519, 521–523, 529, 536, 537, 539, 540, 543, 545, 546, 551–554, 557–560, 562, 563, 567–586, 589, 591, 593, 594, 597, 598, 601, 602, 605–609, 611, 612, 617, 622, 625–632, 654–660, 662, 667, 671, 674, 684, 690, 695–698, 701, 703, 704, 709, 721–725, 729–736, 739–741, 744–746, 748, 750–754, 756, 759–762, 764, 765, 767–772, 774, 777–780, 786, 787, 799, 803, 808, 812, 816, 835–837, 839–844, 862, 865–868, 907–909, 911, 913, 917–919, 921, 925–933, 936, 944, 947–952, 955, 956, 961–968
Lead-acid batteries, 3–5, 7, 10, 11, 13–15, 321, 514, 593, 594, 601, 602, 606, 961, 965
Lead and zinc metallurgy, 20
Lead battery recycling, 543
Lead bullion production at Zhuzhou smelter, 302
Lead cementation equipment design, 928
Lead cementation kinetic, 928
Lead cementator prototype, 929
LEADCLOR process, 948
Lead continuous smelting, 209
Lead extraction, 163, 962, 968
Lead hydrometallurgical technology, 140
Lead melting and casting, 158
Lead melting/cathode handling ventilation, 159
Lead production, 3–6, 9, 153, 508, 509, 514, 605, 740, 962
Lead recycling, 4, 14, 695, 961
Lead reduction, 267
Lead refinery, 5, 739, 740, 742, 744, 747–751, 754, 756
Lead refining, 328, 333, 336, 729, 733, 740–742, 757
Lead slag, 41, 42, 46, 303, 329, 332, 341, 342, 347, 799, 800, 804–807
Lead smelter and refinery, 740
Lead smelting, 41, 42, 71, 158, 165, 166, 168, 171, 174, 201, 207, 209, 217, 268, 285, 287, 288, 301, 321, 327, 328, 333, 335, 337–339, 341, 345, 348, 469, 470, 514, 520, 544, 552, 557, 569, 593, 597, 602, 654, 657, 759–761, 947, 962
Lead smelting furnace, 470
Lead smelting with treatment of lead and zinc slag, 207
Lead–zinc deposit types, 509
Lead–zinc ore, 626
Life Cycle Assessment (LCA), 496
Lime, 81, 85, 397, 399, 442, 519, 583, 586, 625–631
Lithium ion, 12, 13, 15, 553, 601, 725, 779
Location, 137
Low grade concentrates, 231–233, 235, 236
Low grade lead-zinc oxide ore, 51–56, 59, 268

M

Macroscopic overview, 564
Magnesia-chromite brick, 563
Magnetic separation of the goethite and gypsum precipitates, 849
Main equipment, 201, 203, 207, 209, 211, 297
Main materials for the waelz kilns, 803
Main process and production management, 302
Main techno-economic indicators, 297
Major equipment, 656
Major production data and process data, 657
Malic Acid (MA) leach, 465
Management of Hosokura mines, 601
Manganese in zinc electrolysis, 104
Manganese reduction in electrolyte, 106
Mass transfer, 113
Material recovery and losses and residue production, 354
Materials, 232, 328, 674
Materials and methods, 52, 232, 635, 937
Materials and reagents, 635, 937
Material stewardship, 492, 493, 495, 496, 498, 503
Mathematical model, 33

Mathematics model, 471
Matte formation, 191
Mechanism of oxygen pressure leaching of zinc and iron from zinc sulfide concentrate, 878
Metal extraction, 453, 461, 916
Metallo's fuming process, 239
Metal recovery, 275, 285, 653, 740, 812, 835, 844
Metal recycling, 317
Metal-speiss equilibria, 344
Methane reduction, 47
Methane reduction set up, 43
Methane sulfonic acid, 135
Micro-flotation tests of artificial mixed minerals and batch-flotations tests of actual ore, 639
Micro-flotation tests of single mineral, 638
Micro-flotation tests of single mineral and artificial mixed minerals, 636
Microstructure, 19, 21–23, 26, 28, 29, 115, 123, 565, 567, 568, 768
Mineral composition and relative content of mineral samples, 854
Mineralogical investigation, 565
Mineralogy, 137, 143, 153, 155, 163, 232, 813, 817, 853, 854
Mineral processing, 441
Minimize side reactions (secondary reactions), 105
Minor element distributions, 342
Minor elements, 339, 343, 540, 740
Minor elements (Ca, Sb, Sn), 354, 569, 570, 572, 574, 575, 579, 778
Minor elements in the waste lead battery, 570, 572
Mist spraying system around blast furnace, 596
Model assumptions, 33
Model framework, 240
Model predictions, 241
Model validation, 473
Modification of filter for de-arsenic process, 873
Modifications for improved metals recovery, 371
Modified Zincex process, 952
Mooresboro process overview, 84
Mooresboro restart project, 85
Multi-component fluxing diagrams, 345

N

Neutral underflow, 832
New cooling options, 690
New processes, equipment and instruments, 691
No altering, non-consumable, 689
Non corrosive, 687
Non-cyanide, 123, 124
Non explosive, 686
Non-ferrous metals, 65, 430, 770
Non-ferrous smelter, 285, 321
Non-flammable, 687
Non-oxide infiltration, 26
Non-toxic, not harmful, 688
Novel cooling options, 684, 691
Numercial models and boundary conditions, 470
Numerical calculation model, 33
Numerical simulation, 31, 32, 36, 37, 39, 469

O

Occurrence state of iron in mineral samples, 857
Off-gas treatment, 187, 192, 193, 197, 199, 440
Operating cost estimate, 162
Operational experience during first years of operation, 751
Operations, 4–6, 10–12, 14, 101, 154, 302, 306, 338, 366, 509, 512, 531, 543, 551, 552, 696, 740, 749, 750, 811, 812, 865, 866, 897, 954
Optimal conditions for tin leaching, 522
Optimising fuming process stages, 67
Optimization of granulation conditions, 94
Optimization of roasting plant operation, 378
Organic acids, 447–450, 453, 457, 463, 467, 886
Organic substance, 579
Orthogonal array experimental design, 709
Orthogonal experiment, 707, 708, 716
Outline of research techniques, 339
Outlook for next 40 years, 515
Outotec, 19, 21, 63–66, 68, 70, 166, 167, 171, 377, 384, 385, 409, 521, 830
Outotec ausmelt process development, 64
Overall interest on zinc oxidized ores, 248
Overview of Annaka zinc refinery, 221
Overview of the new no. 3 electrowinning plant, 224
Oxalic Acid (OA) leach, 462
Oxidation mechanism, 51, 52
Oxidation reduction, 168, 169, 171, 202, 888

Oxidation stage, 294
Oxides washing, 800, 802, 805, 807
Oxidized Pb–Zn flotation tails, 448
Oxygen, 6, 12, 43, 45, 47, 55, 103, 143, 266–269, 272, 277–279, 303–306, 321, 327–331, 333, 335, 336, 348, 367, 372, 541, 545, 546, 733, 734, 736, 751, 753, 811–813, 854, 859–862, 906, 950, 961, 962, 964, 968
Oxygen-enriched air side blown, 291, 292, 296, 297, 299
Oxygen-enrichment & productivity, 81
Oxygen-enriched enhanced smelting, 961

P
Parameters impacting polarization, 118
Paroo station - operating history, 137
Pb recovery in JX nippon mining & metals, 535
Pb recovery in Saganoseki copper smelter, 535
Pb recovery in the HMC, 536
Pelletizing, 81, 94, 388
Percentages of mass loss, 56
Perovskite, 777, 781
Phase equilibria, 45, 337–342, 347
Phase equilibria in high-PbO slag systems in air, with Pb metal and with Pb–Cu metal alloy, 341
Phase evolution, 51, 52
Phase transformation, 853, 854, 961, 962, 968
Φ-pH diagram of Zn-H, 677
Physical characterization, 126
Physical model, 32
Pilot plant relevant results, 931
Placid process, 949
Plant A, 170
Plant B, 171
Plant expansion, 365, 367
PMR pilot plant, 919
PMR process design, 917
Polarization, 111–122, 792, 793
Polymetallic, 280, 739
Polymetallic ores, 309, 913, 915, 917, 919, 921
Post combustion transition zone, 192
Post mortem study, 563, 568
Power and steam generation, 161
Power usage pattern of electrowinning plant in Annaka refinery, 224
Practical guide to zinc deposits, 117
Practical problems of lead decoppering with the application of aluminum, 733
Precipitation of zinc, 823
Pre neutralization, 249–251
Pressure leaching, 248, 277, 303, 304, 794, 853, 854, 859, 860, 862, 877–879, 881, 882
Pretreatment of waste lead acid accumulator, 329
Previous treatment of wastewater containing fluorine at high concentration, 598
Primary lead, 6–8, 507, 551, 605
Principle of gypsum removal, 892
Principle of the smelting process, 294
Principles of ScanArc plasma process, 395
Problems in the working environment around furnaces, 594
Process control improvements, 748
Process copper-nickel ore to produce low-grade matte nickel, 205
Process description of Hosokura smelter, 594
Process development and product quality, 315
Process flow, 268, 269
Process flow for processing of lead-bearing polymetallic materials, 293
Process gas treatment (filter), 194
Process mechanism, 201, 202
Process mineralogy research, 854
Process modelling, 166, 169, 345
Process principle, 202
Process simulation, 357, 363, 385
Process theory, 654
Production indicators, 270
Production process control, 303
Product life cycle issues of zinc and lead, 955
Progress of zinc leach slag recovery and recycling, 278
Progress of zinc smelting slag recovery and recycling, 277
Project execution, 86
Properties of the cooling medium IL-B2001, 686
Pure jarosite process, 371
Purification, 102, 103, 107, 140, 148, 159, 277, 365, 368–371, 534, 537, 673, 674, 676–680, 740, 759, 761, 762, 764, 766, 799, 866, 891, 892, 896, 906, 909–911, 947, 949, 953, 954, 956
Purification of the leachate after acid leaching, 887

Pyrite, 388, 412, 430, 625–631, 633–643, 645–647, 856, 878, 882
Pyrometallurgical recovery, 539
Pyrometallurgical refining, 167, 169
Pyrometallurgy, 41, 51, 52, 166, 214, 317, 340, 341, 540, 541, 836, 962

R

Range analysis, 710
Rationalization of the closed dam monitoring, 601
Raw material management, 302
Raw materials in Europe, 311
Reaction, 113
Reaction principle of zinc residues smelting, 266
Reaction scheme, 823
Read a deposit, 119
Realized scheme for treatment of EAF dusts and lead slag in KCM AD, 807
Recent improvements in the Ausmelt process for zinc fuming, 67
Recent improvements of the hematite process, 867
Recovery, 64, 65, 67, 71, 85, 86, 92, 188, 201, 206, 207, 209, 213–215, 217, 247, 249–251, 253, 254, 258–260, 263, 291, 293–295, 299, 310–312, 316, 317, 351–356, 359, 391–393, 397, 406, 408, 414, 419–421, 423, 426, 431, 434, 437–440, 442, 443, 445, 447, 448, 458, 500, 502, 503, 522, 558, 581, 586, 589, 616–618, 626–632, 637, 639, 641, 645, 646, 688, 691, 692, 787, 828, 830, 832, 847, 849–852, 877, 881, 885, 889, 899–903, 913, 914, 916, 917, 921, 925, 927
Recovery of lead and recycling, 948
Recovery of zinc and recycling, 952
Recovery of zinc by alkali treatment, 889
Recycling, 3, 5–7, 9–12, 14, 64, 75–77, 82, 84, 91, 97, 215, 277, 285, 286, 288, 289, 307, 309–317, 329, 337, 338, 348, 352, 353, 357, 419–421, 423, 448, 486, 491–495, 497, 502, 503, 514, 519, 520, 531, 538, 540, 551–554, 557, 575, 581, 582, 586, 589, 591, 594, 601, 606, 669, 695, 696, 722, 740, 812, 818, 819, 824, 851, 865, 885, 886, 900, 905, 906, 948, 956, 961, 968
Reducing feed moisture, 68
Reduction, 41–43, 45–49, 101–104, 106–108, 173, 174, 181–184, 231, 234, 267, 268, 270, 306, 307, 321, 323, 324, 327, 329, 330, 333, 335, 365, 372, 537, 539–541, 543, 545, 546, 552, 653–655, 658, 667, 701–704, 729, 735, 761, 762, 811–813, 815–819, 836, 842, 863, 897, 906, 948, 951, 961, 962, 966–968
Reduction/Red-Ox phenomena, 28
Reduction stage, 295
Refined zinc demand, 615, 619
Refined zinc production, 615, 618, 619, 622
Refining, 4, 5, 12, 135, 285, 286, 288, 306, 327, 330, 331, 339, 341, 344, 348, 512, 514, 515, 531, 533, 534, 537, 540, 554, 593, 653, 730, 732–734, 736, 739, 741, 746, 748–753, 756, 759, 766, 865, 905, 909, 911
Refractories, 20, 21, 80, 558, 684
Refractory corrosion, 605, 607
Refractory material, service life & construction, 80
Regulation of fluorine in Hosokura wastewater treatment, 597
Remote monitoring camera system, 601
Removal of arsenic and selenium, 527
Residue phase analysis, 861
Resistance, 114
Resource circulation, 285, 286, 288, 289
Resource consumption - thermoeconomics, 355
Responsible sourcing, 492, 495, 497, 501–503
Restart, 87
Reverberatory furnace, 23, 215, 419, 423, 558, 563, 567
RLE process, The, 405
Roaster feed pre-treatment system, 372
Roaster optimizer as part of a digital solution concept, 382
Roasting, 19, 20, 76, 91–93, 101, 102, 221, 248, 253, 268, 277, 356, 365–367, 372–375, 377–379, 381–383, 385–388, 392, 393, 405, 408, 413, 414, 420, 539, 673, 799, 807, 827, 829, 836, 842–844, 849, 853, 866, 900
Role of the HMC in copper smelting, 534
Rotating disc, 933
RSKS furnace, 331
RSKS smelting technology, 327

S

Safe cooling, 683, 684
Safety, 82, 119, 165, 191, 312, 378–380, 383, 386, 502, 618, 626, 683–685, 688, 690–693, 772, 777
Safety aspects, 685
Sample preparation and characterisation, 177
Sb recovery in the HMC, 537
Secondary, 19, 21, 22, 29, 64, 72, 77, 85, 128, 168, 187, 189, 191, 207–214, 226, 237, 239, 248, 254, 262, 294–296, 298, 309–314, 316, 317, 407, 419, 423, 448, 494, 557, 558, 569, 581, 582, 589, 634, 689, 774, 777, 785, 795, 848, 878, 879, 915
Secondary lead, 3–9, 11–15, 41, 136, 324, 551, 593, 605, 606, 612, 695–697, 701, 704, 947, 949, 968
Secondary lead materials, 328
Secondary lead production in china, 11
Secondary lead smelting, 593
Secondary raw materials, 285–289, 740, 952
Selenium, 286, 695, 701, 703, 704
Selenium removal in conventional secondary lead iron co-precipitation systems, 701
Self-reduction, 817
Separation of particulate matter, 195
Share of zinc from treatment of secondary materials, 805
SICAL process, The, 915
Side Blowing Furnace (SBF), 187, 189
Side-submerged combustion, 265, 266, 278–280
Silicate, 22, 25, 64, 247–251, 394, 419, 448, 562, 564, 565, 567
Silicate leaching process, 248
Silver, 65, 71, 103, 188, 209, 210, 213, 214, 253, 254, 263, 265, 266, 268, 272, 277, 303, 305–307, 317, 328, 329, 331, 354, 355, 357, 359, 365–367, 371, 372, 374, 431, 437–445, 507, 510, 514, 515, 540, 569, 570, 573, 593, 594, 622, 626, 750, 760, 761, 835–837, 839–844, 914–919, 921
Simulation, 31–33, 36, 37, 39, 237, 241, 242, 351, 353–355, 357–360, 363, 386, 405, 412, 414, 471, 473, 474, 577, 638, 832
Simulation-based evaluation of the resource efficiency of the zinc production, 353
Simulation of the considered zinc production flowsheets, 353
Single nozzle simulation, 474
Single series, 327
SKS furnace, 331
SKS lead smelting technology, 327
SKS smelting, 329
SKS technology, 168
Slag, 173–179, 181–184
Slag and coke preparation, 176
Slag attack and forsterite bursting, 21
Slag cleaning, 41, 539
Slag granulation, 193
Slag-matte equilibria, 341
Slag reduction, 71, 187
Slag sample analysis, 843
Slag test, 605, 609, 610
Slow-release mineralization for copper removal and recovery, 900
Smelting, 6, 12, 136, 265–268, 275, 277, 278, 280, 285–289, 301–307, 321, 323–325, 327–331, 333, 335, 337, 342, 347, 507, 511, 512, 514, 515, 531–535, 537–541, 543, 551, 552, 554, 606, 653, 654, 696, 701, 707–709, 729, 740, 759, 761, 762, 764, 766, 812, 853, 865, 906, 937, 947, 956, 961, 962, 965, 966, 968
Smelting tests of Boliden Kokkola residues using ArcFume plasma reactor, 396
Sn recovery system, 762
Solar cells, 777, 781
Solution implementation steps, 385
Solvent extraction, 286, 511, 821, 822, 824, 892, 894, 896, 947, 953
Solvent extraction (SX) of zinc, 822
SO_2 – removal, 195
Source of information in digital systems, 380
Species distribution, 474
Speiss formation, 344
Sphalerite, 253, 430, 625–627, 630, 631, 633, 635–643, 645–647, 855, 915, 916
SSC FF technology, 266
Stable burtite synthesis, 523
Stages of investment realization, 800
Standard k-e turbulence model, 34
Steel making, 691
Steel scrap, 821, 822, 824
Structure of the waste lead battery and the disassembling line, The, 570
Submerged Combustion Furnace (SSC), 270

Sulfatation, 405, 408, 409, 413, 414, 827, 829–832
Sulfatation, Leaching and Electrowinning (SLE), 408
Sulfide precipitation, 698
Sulfur corrosion, 23
Sulfur-graphite electrode, 431
Sulfuric acid, 171, 206, 210, 249, 250, 253, 295, 383, 387, 406, 408, 413, 421, 521, 569–574, 577–580, 625, 626, 629, 632, 827–829, 832, 849, 879, 880, 886, 889, 900
Surface roughness, 479–484, 486
Surface roughness measurements of alumina substrate, 480
Surface roughness of alumina substrate, 481
Sustainability, 66, 359, 361, 362, 380, 491, 498, 499, 777, 778
Sustainability evaluation, 361
Sustainable cities and circular economy, 502
Sustainable development, 358–360, 491, 492, 497, 498, 502, 503, 848
Systematic acid equilibrium, 303
Systematic analysis of Pb–Cu–Fe matte/slag equilibria, 344

T
Tailings disposal, 160
Tartaric acid (TA) leach, 467
Technical and economic index, 333
Technical characteristics, 201, 203
Technological challenges, 275
Technological line for treatment of secondary materials, 803
Technological line for treatment of waelz oxides to SHG zinc, 807
Technological process, 329
Technology alternatives, 167
Technology trends, 338
Temperature field, 474
Test conditions and technical indexes, 213
Test parameters, 232
Thermodynamic considerations for new process to treat copper smelter dust, 543
Thermodynamic modelling, 338, 339
Thermodynamic simulation, 44
Thermoeconomics, 355, 363
Thermoelectric, 781
Thermogravimetric and differential thermal analysis, 53
Three-continuous furnace bath smelting technology, 301
Tin leaching, 521
Tin smelting (reduction), 762
Tin (Sn), 286–288, 337, 338, 340, 344, 531, 533, 534, 536, 537, 732, 734, 740, 748–750, 752, 756, 761, 762, 764, 765
Top submerged lance technology, 167
Top Submerged Lance (TSL), 6, 41, 265, 266, 268, 272, 273, 287, 288, 321, 322, 324, 759, 761
Traceability, 381, 767, 774
Treatment of lead and zinc oxide ore, 213
Treatment of wastewater containing fluorine at high concentration, 597
Treatment of zinc leaching residue, 212
Treatments of secondary raw materials and associated problems in non-ferrous smelters, 286
Troubles in the start-up stage, 226
Tungsten, 286, 661–671
Two-way transformation, 307
Types of waelz feed and obtained waelz oxides, 803
Typical cases of industrial application of CSC technology, 205

U
UN SDG roadmap, 491, 503
Upgrading of main equipment, 304
Upper furnace, 191
Urban mine, 531
Utilities and reagents, 160
Utilization, 273, 275, 277, 305, 307, 321, 367, 553, 729, 733, 742, 743, 836, 837, 894, 908

V
Vacuum distillation, 905–909, 911
Velocity field, 473
VOF model, 32–34

W
Waelz Kiln feed preparation & control, 81
Waelz kiln process, 70, 77, 79, 91
Waelz kiln process improvements, 77
Waelz process, 231, 232, 812, 948, 952
Waste acid, 707–709, 712, 716, 941
Waste heat boiler/quench, 192
Waste lead battery recycling, 569
Waste treatment, 288

Waste water, 52, 148, 302, 695, 697, 698, 701, 704, 808, 935, 938–942, 944
Wastewater containing fluorine at high concentration in lead smelting, 597
Water-free cooling, 683
Wear mechanism, 21, 557
Wear phenomena, 19–21, 29
Wet Electrostatic Precipitators (WESPs), 552
Wetting, 22, 195, 196, 479–484, 486
Wetting measurements of lead drop, 481
Wetting of lead drop on alumina substrates with different roughness, 482
Worldwide applications, 386

X
XRD analyses, 56
XRD and SEM, 128

Z
Zero Valent Iron (ZVI) reduction of selenate, 701
Zeta potential measurement, 637, 642
Zinc (Zn), 4–6, 19–21, 23, 26, 29, 41, 45, 47, 51, 52, 63–68, 70–73, 75–79, 81–87, 86, 89, 91, 93, 95–97, 101–108, 111–126, 128–130, 171, 189, 191, 201, 203, 207–214, 217, 221, 223, 224, 228, 231, 232, 234–241, 244, 247–251, 253–262, 265–272, 274–280, 285, 286, 288, 289, 291, 294, 296, 298, 299, 301, 303–305, 307, 309–311, 313, 314, 316, 321–323, 327, 328, 330, 335, 337, 351–359, 361–363, 365–369, 371–375, 377, 378, 380, 383, 386, 388, 391–395, 397–399, 401, 402, 405–414, 419–421, 423, 425, 429–432, 434, 437, 438, 440, 442–445, 447–449, 452–468, 491, 493–503, 507–516, 540, 545, 569, 571, 582, 593, 615–622, 625–632, 635, 636, 639, 641, 645, 647, 654–661, 663–668, 670, 671, 673–675, 677–680, 707, 709, 750, 759, 761, 767–772, 774, 785–796, 799, 800, 803, 805, 806, 808, 811–813, 815–819, 821–824, 827–832, 835–837, 839–844, 847–849, 851–854, 859, 860, 862, 863, 865–869, 871–875, 877–879, 881, 882, 885–889, 891–896, 899–903, 905–911, 913–917, 919, 921, 925, 936, 937, 947, 948, 952–956
Zincate, 124, 126, 128
Zinc concentrate with high in iron percentage, 409
Zinc content increase in electrolyte, 105
Zinc contributes to the UN SDGs, 498
Zinc electrodeposition vs. hydrogen evolution, 114
Zinc electrometallurgy, 102
Zinc electrowinning, 790
Zinc electrowinning cellhouse, 304
Zinc flotation, 630
Zinc fuming process benchmarking, 70
Zinc-oxygen pressure leaching, 301
Zinc plant, 799
Zinc plant residue, 253, 254, 262
Zinc powder, 369, 371, 673–680, 873, 954
Zinc process, 304, 661, 663, 669–671, 866
Zinc production, use and recycling, 493
Zinc recovery, 64, 75, 78–80, 82, 83, 91–93, 95–97, 209, 247, 249, 251, 405, 408, 409, 414, 630, 832
Zinc recycling, 75, 76, 97, 494
Zinc rejection from sulfur concentrate, 629
Zinc residue, 265
Zinc residue treatment technology, 265
Zinc-separation, 886
Zinc slag, 268, 274, 275, 280
Zinc smelting process, 221
Zinc smelting slag and zinc leach residue, 277
Zinc sulfate solution, 102, 104, 673, 674, 678, 679
Zinc sulfide concentrate, 853, 854, 859, 860, 862
Zn extraction, 257, 407, 458, 459, 461
ZnO, 27, 95, 237–245, 253, 256, 405, 406, 412, 421, 441, 449, 455
$ZnSO_4$ crystal adhesion to cooling fan casing, 226
ZVI, 701–704